QUESTION 111

QUESTION 111

QUESTION

111

EARTHQUAKE PERFORMANCE AND SAFETY OF DAMS

1. Static, seismic and post-seismic monitoring of dams.
2. Feedback from earthquake failures, including tailings dams and levees.
3. Importance of multiple features of earthquake hazard (e.g., ground shaking, surface fault movements, mass movements).
4. Seismic design and performance criteria for dam structure, reservoir rim and impacted area.
5. Earthquake safety evaluation of all types of dams and safety-critical elements (e.g., spillway, low-level outlets)

PERFORMANCE SISMIQUE ET SÉCURITÉ DES BARRAGES

1. Surveillance statique, sismique et post-sismique des barrages.
2. Retour d'expérience des ruptures par séismes, y compris les barrages de stériles miniers et les digues.
3. Importance du caractère multifactoriel du risque sismique (par exemple, secousses du sol, mouvements des failles de surface, mouvement de masse).
4. Critères de conception et de performance sismique pour le corps du barrage, les berges de la retenue et le bassin versant.
5. Évaluation de la sécurité sismique des barrages existants et des éléments critiques pour la sécurité (par exemple les évacuateurs de crues, les pertuis de fond)

QUESTION

111

TABLE OF CONTENTS OF PAPERS

TABLE DES MATIÈRES DES RAPPORTS

PAPERS ON QUESTION 111

RAPPORTS SUR LA QUESTION 111

Taylor & Francis
Taylor & Francis Group
http://taylorandfrancis.com

COMMISSION INTERNATIONALE DES
GRANDS BARRAGES

VINGT-HUITIEME CONGRES DES
GRANDS BARRAGES
CHENGDU, MAI 2025

EMPIRICAL SEISMIC DATA INTERPRETATION FOR EMBANKMENT DAMS (*)

DongSoon PARK
Head Researcher, K-WATER Research Institute

SOUTH KOREA

SUMMARY

This paper presents a statistical analysis of strong motion data recorded on existing embankment dams. The study aims to enhance our understanding of the seismic response of these structures, providing valuable insights for the design of new dams and the seismic evaluation of existing ones. Utilizing the JCOLD 2014 strong motion database, we examined 190 shaking events from 54 earthquakes recorded on 60 dams. The database, spanning from 1978 to 2012, includes tri-directional strong motion records at both dam foundations and crests. Multivariate analysis and linear/nonlinear fit modeling were employed to investigate seismic response characteristics and their pairwise correlations. The focus was on seismic amplification and fundamental periods, and their relationships with shaking intensity, dam geometry, and input motion frequency content. Nonlinear fit prediction equations and curves were developed, incorporating uncertainty (RMSE) and R-square values in three directions. Despite significant data scatter, these equations offer practical utility in estimating seismic response during preliminary design or seismic assessment phases.

Interprétation des données sismiques pour les barrages en remblai

DOI: 10.1201/9781003642428-105

RÉSUMÉ

Cet article présente une analyse statistique des données de mouvements forts enregistrées sur des barrages en remblai existants. L'étude vise à approfondir notre compréhension de la réponse sismique de ces structures, fournissant ainsi des informations précieuses pour la conception de nouveaux barrages et l'évaluation sismique de ceux existants. En utilisant la base de données JCOLD 2014 sur les mouvements forts, nous avons examiné 190 événements sismiques provenant de 54 tremblements de terre enregistrés sur 60 barrages. Cette base de données, couvrant la période de 1978 à 2012, comprend des enregistrements de mouvements forts tridirectionnels à la fois au niveau des fondations et de la crête des barrages. Une analyse multivariée et une modélisation d'ajustement linéaire/non linéaire ont été employées pour étudier les caractéristiques de la réponse sismique et leurs corrélations par paires. L'accent a été mis sur l'amplification sismique et les périodes fondamentales, ainsi que sur leurs relations avec l'intensité des secousses, la géométrie du barrage et le contenu fréquentiel des mouvements d'entrée. Des équations et des courbes de prédiction d'ajustement non linéaire ont été développées, intégrant l'incertitude (RMSE) et les valeurs R-carré dans trois directions. Malgré une dispersion significative des données, ces équations offrent une utilité pratique pour estimer la réponse sismique lors des phases préliminaires de conception ou d'évaluation sismique.

1. INTRODUCTION

Embankment dams constitute a significant portion of large dams worldwide, with their seismic safety under strong excitation being a critical concern. Recent earthquakes have highlighted the complexity of embankment dam responses, often exceeding predictions and emphasizing the need for a deeper understanding. This paper focuses on empirically investigating the seismic response characteristics of embankment dams by analyzing strong motion data recorded by the Japan Commission on Large Dams (JCOLD) [1].

While modern embankment dams have demonstrated resilience to significant seismic shaking, uncertainties remain due to the multi-hazard nature of seismic events [2,3]. Numerous factors influence dam response, including dam geometry, material properties, foundation conditions, and input motion characteristics [4]. However, limited field data and the complexities of these interactions make comprehensive understanding challenging.

This study aims to analyze JCOLD strong motion data to gain insights into acceleration response characteristics and fundamental periods of embankment dams. By examining the relationships between various seismic parameters, we seek to contribute to the development of advanced seismic design and evaluation methodologies.

The JCOLD dataset, comprising acceleration time histories recorded at dam foundations, ground, and crests from 1978 to 2012, forms the basis of this analysis. The data, sorted by motion components (stream, dam axis, vertical), was re-analyzed using multivariate methods and linear/nonlinear fit modeling.

Key Correlations Investigated are:

- Amplification of motion based on peak acceleration at the dam foundation and crest.
- Fundamental periods of dams and their correlations with other parameters.

This research leverages real, recorded strong motion data over several decades, providing valuable insights into the seismic behavior of embankment dams. The findings are expected to contribute to the refinement of seismic design and evaluation approaches for these structures.

2. JCOLD STRONG MOTION DATABASE

2.1. Strong motion data used in the study

The dataset utilized in this research comprises acceleration records collected from 60 embankment dams across Japan, spanning 34 years (1978-2012) [1]. Accelerograms were recorded at both the dam foundation and crest, capturing motions in three orthogonal directions: stream, dam axis, and vertical. The dataset encompasses a total of 190 shaking events originating from 54 earthquakes, with the 2011 Tohoku and 2004 Niigata earthquakes each contributing 20 events. The dams within the database are categorized as either rockfill (R) or earthfill (E), with

Table 1
Summary of strong motion data used in the study
Résumé des données des mouvements forts utilisées dans l'étude

			PGA (g)					
	H (m)	**L (m)**	**STREAM**	**DAM AXIS**	**VERTICAL**	**M**	**DEPTH (km)**	**RE (km)**
Min.	19.0	90	0.012	0.011	0.004	2.3	0	0.56
Med.	48.9	310	0.044	0.047	0.026	6.1	19.8	37.9
Max.	176.0	1,597	1.044	0.917	0.705	9.0	111.7	460
STD	32.5	270	0.113	0.095	0.069		25.2	94.2

Note, H = dam height, L = dam crest length, PGA = peak ground acceleration, M = earthquake magnitude, Re = epicentral distance, Min. = minimum, Med. = median, Max. = maximum, STD = standard deviation.

118 (62%) and 72 (38%) events recorded on rockfill and earthfill dams, respectively. Table 1 provides a summary of the dams included in the study.

Table 2 shows the statistical distribution of data analysis depending on the direction of each direction of strong motion. The median dam heights and lengths are 51.7 m and 318 m, which yields the median ratio of L/H as 5.6. Cases for significant intensity (e.g., PGA greater than 0.1g) shows relatively lack of data. The range of PGA is large, but the very large majority of the data are for less than 0.1g. For example, the 75% quartile values of PGA in the direction of dam axis, stream, and vertical are 0.092g, 0.082g, and 0.061g, respectively. All other parameters such as I_a, T_p, and T_n contains the majority of smaller value range in a similar fashion. Case histories of significantly large earthquake shaking are rare, but a few cases in this database set gives insightful seismic aspects of embankment dams subjected to very high PGA. The minimum and maximum values of each parameter indicate a clear range of applicability of curve fit equation per case, which will be shown later.

2.2. Fundamental periods calculation

The general definition of a fundamental period (or natural period) is the period at which a system tends to oscillate in the absence of any driving or damping force [4]. The important physical implication is that when the forcing period is close to the fundamental period of a system, resonance occurs. In other words, one of the important influencing factors on the dynamic response of a dam (e.g., crest amplification) is the frequency content of the excitation relative to the natural frequency of the dam [5,6].

The fundamental period of a dam is particularly defined as the corresponding period which leads to the maximum spectral amplification from the dam foundation to the crest, i.e., the period where the maximum transfer function between dam foundation and the crest is found. Thus in this study, the fundamental period was obtained by searching for the period which produces the maximum acceleration response amplitude ratio (of motions between the crest and foundation) in the frequency domain.

There have been many approaches to obtaining the fundamental periods of dams, e.g., using the acceleration amplification ratio of FFT analyses, using the acceleration response spectra ratio, or using forced vibration experiments [7–11]. The fundamental periods of embankment dams (with a height of 30 to 130 m) are known to be approximately from 0.2 to 0.8 s [12–14].

Two types of response amplitude ratios were independently computed by (1) FFT (fast Fourier transform)-based and (2) ARS (acceleration response spectrum)-based analyses. For FFT-based Tn computation, it is searched for the peak ratio of

Table 2
Statistical distribution of recorded strong motion data on dams
Distribution statistique des données de mouvements forts enregistrées sur les barrages

INDEX	UNIT	DAM AXIS				STREAM			
		MIN	MED	MAX	STD	MIN	MED	MAX	STD
$a_{p.f}$	g	0.011	0.047	0.917	0.095	0.012	0.044	1.044	0.113
$a_{p.c}$	g	0.020	0.125	0.528	0.116	0.022	0.119	1.495	0.179
$a_{p.r}$		0.2	2.3	9.3	1.5	0.5	2.7	13.7	2.0
$I_{a.f}$	m/s	0.0002	0.02	5.07	0.51	0.0005	0.02	5.12	0.56
$I_{a.c}$	m/s	0.0011	0.11	18.11	1.96	0.0032	0.13	16.33	2.86
$I_{a.r}$		0.02	7.1	77.1	11.0	0.15	9.9	129.2	18.3
$T_{p.f}$ (ars)	sec	0.036	0.152	1.299	0.179	0.039	0.161	1.438	0.243
$T_{p.c}$ (ars)	sec	0.042	0.193	0.725	0.155	0.056	0.284	1.408	0.214
T_n (ars)	sec	0.042	0.388	0.867	0.151	0.039	0.394	0.781	0.151
$T_{p.f.v}/T_{p.f.h}$		-	0.969	3.902	0.688	0.1	0.8	4.8	0.7

The glossary of each symbol used in this study is defined as below.
M: moment magnitude of earthquake
R_e: epicentral distance
E: earthfill type dam
R: rockfill type dam
H: height of dam
L: crest length of dam
$a_{p,f}$: peak acceleration at the dam foundation (in g) (= PGA in this study)
$a_{p,c}$: peak acceleration at the dam crest (in g)
$a_{p,r}$: the ratio of peak acceleration at the dam crest and the foundation
$I_{a,f}$: Arias intensity of acceleration time history at the dam foundation (in m/s)
$I_{a,c}$: Arias intensity of acceleration time history at the dam crest (in m/s)
$I_{a,r}$: the ratio of Arias intensity at the dam crest and the foundation
$T_{p,f}$ (fft): FFT-based predominant period measured at the dam foundation (in sec)
$T_{p,c}$ (fft): FFT-based predominant period measured at the dam crest (in sec)
T_n (fft): FFT-based fundamental period of the dam embankment (in sec)
$T_{p,f}$ (ars) or $T_{p.f}$: ARS-based predominant period measured at dam foundation (in sec)
$T_{p,c}$ (ars) or $T_{p.c}$: ARS-based predominant period measured at dam crest (in sec)
T_n (ars) or T_n: ARS-based fundamental period of the dam embankment (in sec)
$T_{p.f.v}$: Predominant period at the foundation in a vertical direction of motion (in sec)
$T_{p.f.h}$: Predominant period at the foundation in a horizontal direction of motion (in sec)
Min: the minimum value of given data
Max: the maximum value of given data
Med: the median value of given data
STD: standard deviation of given data
RMSE: The square root of the MSE (i.e., the average of the squares of the errors of each value) that estimates the standard deviation of the random error. Simply it means standard deviation of data
SE: standard error, which measures the amount of variability in the sample mean, i.e., standard deviation of sampling distribution
R^2: A value estimating the proportion of variation in the response that can be attributed to the model rather than to random error. The model with the R-square value closest to one is the better fit.

the magnitude of Fourier Amplitude spectra between crest and foundation motion. For ARS-based Tn computation, peak ratio of the spectral acceleration of response spectra between crest and foundation is obtained with the condition of the 5% damped response spectra for all motions. Fig. 1 illustrates a computation procedure of T_n using either FFT-based or ARS-based response amplitude ratio between the dam crest and foundation.

Theoretically, the FFT-based fundamental period is more reasonable to use because it directly accounts for the real frequency content. However, FFT based analysis has a disadvantage in that outliers or noisy spikes in the motion hinder the correct computation of the real peak amplification ratio; hence, a smoothing technique is essentially applied in many cases. In this study, the FFT-based fundamental period calculation used a median smoothing function with the appropriate window width since it is least likely to be affected by spurious data points. The median smoothing technique yields a smoothed vector by replacing values with the median of the window width (typically the value of 31), which is contracted near the ends of the vector.

ARS-based analyses compute the maximum response ratio of a single degree of freedom, and it generally yields a more stable result. In this study, both methods were used in the preliminary stage. Based on the results, both methods produced a reasonable similarity in terms of the proximity and the range of fundamental periods in most cases. But, sometimes those values are not close each other mainly because FFT-based one significantly depends on both the degree of smoothing and the shape of the transfer function. Smoothing function makes a significant difference of peak ratio and its corresponding period search. Also, there is no clear peak ratio in some cases that, for example, almost the same multiple peaks are shown or unclear peak ratio is shown, or sometimes unreasonable high-frequency peak component is obtained. Considering a typical range of computed T_n is thought to be as 0.05 to 1.5 sec (mostly being $0.1 \sim 1.0$ sec), alternative reasonable peak value was searched for within typical range of 0.05 to 1.5 sec when there are spurious peaks in the high-frequency range less than 20 Hz. When multiple peaks of similar values are observed, T_n is manually obtained by comparing ARS-based values using engineering judgement. Even though appropriate smoothing was taken for FFT-based T_n computation, multiple spikes of similar ratios were shown in the amplitude ratio plot, so we needed to carefully judge which T_n computed is actually significant in an engineering sense. When there is no apparent amplification ratio, those data were not included in the final analyses.

Thus, in reality, FFT-based Tn computation could be erroneous much more than we expected because of spurious, momentary peaks and its dependency on the degree of smoothing. In some cases, there could be several other noticeable apparent higher amplification ratios at specific periods, which means T_n can be not a single value, but multiple. In any case, it was believed to be useful to compare both FFT-based T_n and ARS-based T_n values to make a decision using engineering judgement. Hence, in this study, ARS-based T_n computation is believed to give more stable and reasonable results.

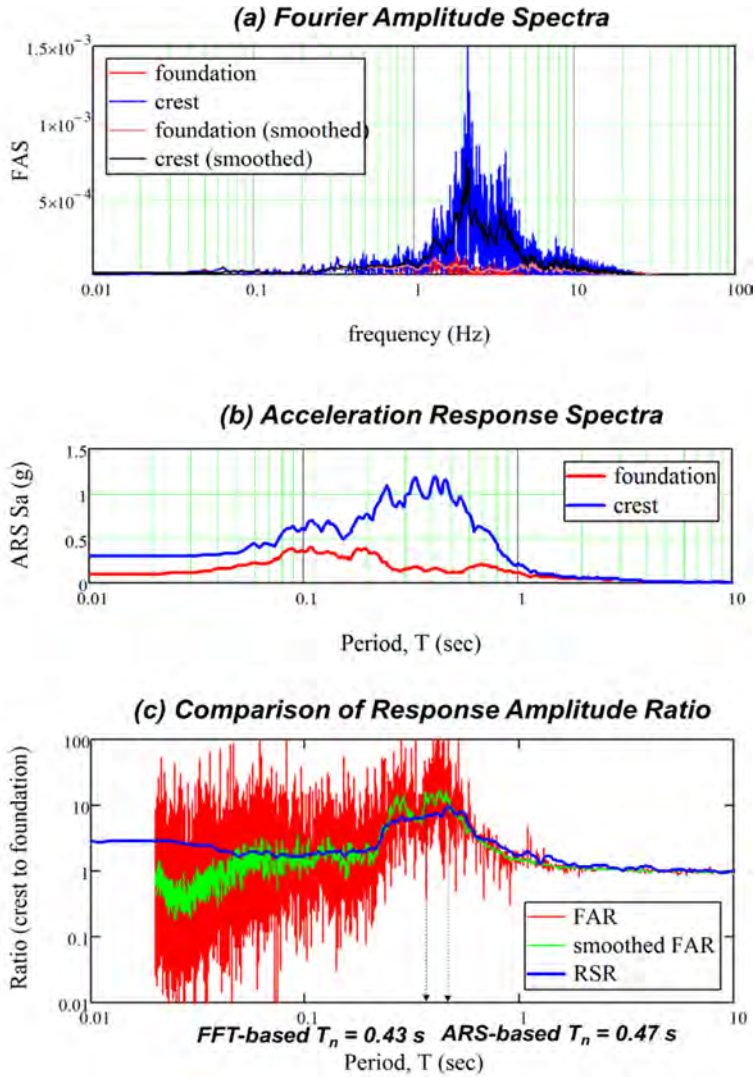

Fig. 1
An example of computation procedure of Tn recorded at Aratozawa dam during 2011 Tohoku earthquake (FAR = Fourier amplitude ratio)
Un exemple de procédure de calcul de Tn enregistré au barrage d'Aratozawa lors du séisme de Tohoku en 2011 (FAR = rapport d'amplitude de Fourier)

2.3. Multivariate analysis and nonlinear fit

Multivariate analysis was taken to find any statistically significant correlation among many seismic parameters. Multivariate analysis enables to observe relationships and patterns between variables. It identifies dependencies, outliers, and clusters using the scatterplot matrix, correlations report, and pairwise correlations. Pairwise correlations list the Pearson product-moment correlations for each pair of variables, also indicates significance probabilities. The *p*-value corresponds to a test of the null hypothesis that the true correlation between the variables is zero. It is a test of no linear relationship between the two response variables [15]. The *p*-value as a probability value ranging from 0 to 1 indicates how likely it is that a result occurred by chance alone. The small *p*-values for the pairs indicate evidence of correlation. If the *p*-value is small, it indicates the result was unlikely to have occurred by chance alone, which means statistically significant. Based on pairwise correlations, higher correlations that show small *p*-values less than 5% for pairs are searched for. A total of 20 different parameters were used in the analysis – H, L, L/H, $a_{p.f}$, $a_{p.c}$, $a_{p.r}$, $I_{a.f}$, $I_{a.c}$, $I_{a.r}$, $T_{p.f}$ (fft), $T_{p.c}$ (fft), T_n (fft), $T_{p.f}$ (ars), $T_{p.c}$ (ars), T_n (ars), $T_{p.f.v}$, $T_{p.f.v}$ / $T_{p.f.h}$, M, depth, and R_e.

In overall, it is observed that there is significant scatter among each trial correlation, but there exists relatively higher correlation for some variables. Fig. 2 shows an example scatterplot matrix for some important variables. According to the result of the multivariate analysis, T_n is believed to correlate H, L, PGA, $a_{p.c}$, $I_{a.f}$, $I_{a.c}$, $T_{p.c}$, and source depth. The peak acceleration at the crest, $a_{p.c}$ may be correlated to PGA, $T_{p.c}$, T_n, and M. Similarly, $I_{a.c}$ may be correlated to $I_{a.f}$, $T_{p.f}$, $T_{p.c}$, T_n, and M.

It is valuable to make a series of fitting equations and curves among highly correlated variables for use in engineering practice. Linear fit can be considered for some correlations such as H – T_n, $a_{p.f}$ – $a_{p.c}$, and $T_{p.f}$ – $T_{p.c}$, but the conceivable best-fit linear equations have problematic physical meaning in the sense that there is a non-zero value for zero x variable. Therefore, nonlinear fitting equations were used to provide more appropriate equations. For approximately proportional relationships, the fitting curve equations are given in the form of Michaelis-Menten as,

$$\mathrm{f(x)} = \frac{ax}{b+x} \tag{1}$$

where a = (is called) maximum reaction rate, b = inverse affinity.

For inversely proportional relationships, the exponential power function is adopted as either

$$\mathrm{F(x)} = ae^{bx} \tag{2}$$

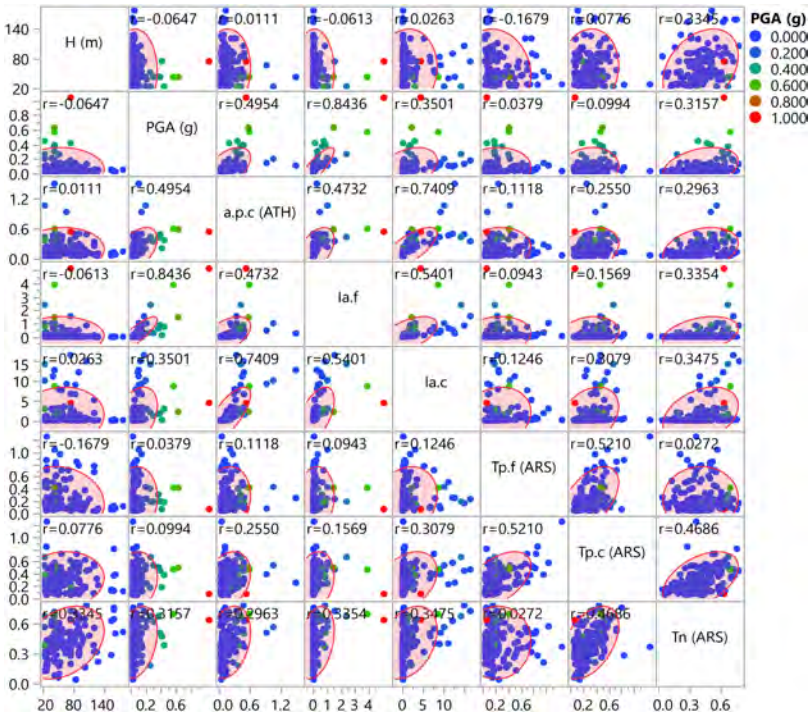

Fig. 2
A partial example scatterplot matrix in a dam stream direction by multivariate analysis
Un exemple partiel de matrice de nuages de points dans la direction du flux du barrage par analyse multivariée

where a = scale, b = growth rate.

$$\text{or} \qquad f(x) = a + be^{cx} \tag{3}$$

where a = asymptote, b = scale, c = growth rate.

3. SEISMIC RESPONSE CHARACTERISTICS

3.1. PGA-BASED CORRELATION

The seismic amplification of motion was revisited using the peak acceleration. First, nonlinear fitting curve equations of peak acceleration between dam foundation and crest are proposed in Table 3 in the form of Michaelis-Menten model depending on the direction of motion and the dam type. Fig. 3 shows the plot of peak acceleration at the dam foundation and the crest, and the plot of residuals between predicted versus observed data. In spite of scattering in nature, there is a sort of nonlinearly proportional correlation each other. Higher peak acceleration at the foundation yields higher peak acceleration at the dam crest, but the ratio is gradually attenuated.

The direction of motion does not make any significant difference in the shape of fitting curves (Fig. 3). But the dam type produces a moderate difference in a fitting curve shape (Fig. 4). For two horizontal components of motions in terms of fitting curves, rockfill dam tends to show a little higher crest peak acceleration for lower PGA (e.g., < 0.3g) and less crest peak acceleration for higher PGA. Note should be taken that the majority of data is in the smaller PGA regime so that larger PGA gives some degree of uncertainty. Based on the residual plot, there seems not have any noticeable bias in data analysis.

Standard deviation from RMSE values shows that the stream direction data contains more uncertainty than the other two direction data. Dam type does not exhibit any noticeable difference in the degree of standard deviation. From the value of R-squared, the correlation of proposed nonlinear fit seems at the reasonable level in overall.

Table 3
Nonlinear fitting of peak acceleration between dam crest and foundation for embankment dams
Ajustement non linéaire de l'accélération maximale entre la crête et la fondation pour les barrages en remblai

DIRECTION	DAM TYPE	NONLINEAR FITTING OF $a_{p.f} - a_{p.c}$ IN THE FORM OF $f(x) = ax / b+x$			
		a	b	RMSE	R^2
Dam axis	E	0.886	0.401	0.062	0.716
	R	0.543	0.118	0.067	0.657
	E+R	0.593	0.163	0.071	0.634
Stream	E	0.864	0.318	0.104	0.630
	R	0.616	0.116	0.158	0.269
	E+R	0.664	0.152	0.143	0.376

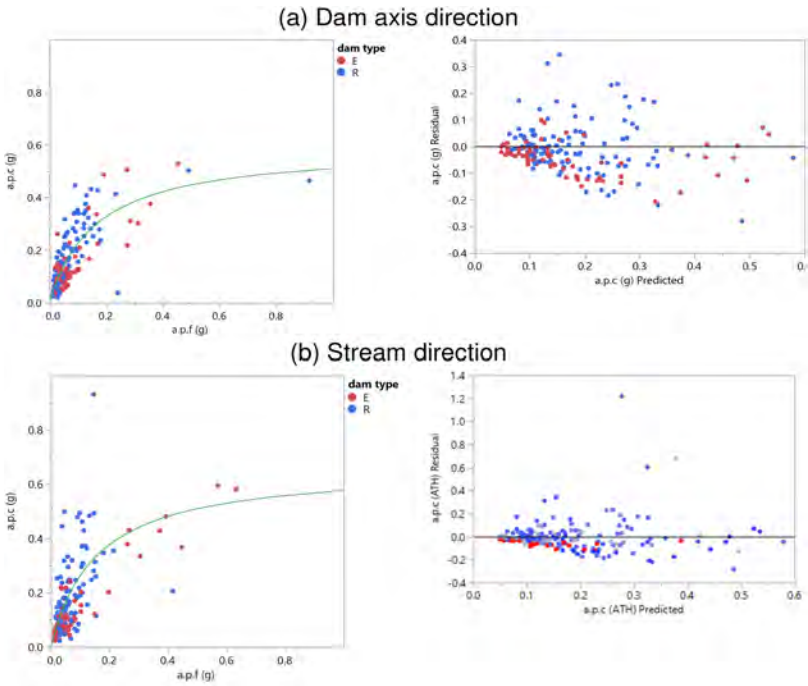

Fig. 3
Nonlinear fitting and residual analysis of peak acceleration between dam crest and foundation depending on the direction of motion for embankment dams
Ajustement non linéaire et analyse des résidus de l'accélération maximale entre la crête et la fondation des barrages en remblai en fonction de la direction du mouvement

One of the different angle to look at the amplification characteristics of dam body is to study the inversely proportional relationship of PGA and $a_{p.r}$ as shown in Fig. 5. With some exceptions, the seismic motion mostly amplifies (Fig. 5). However, amplification of motion gets weaker at a higher PGA. The peak acceleration ratio ranges from 0.4 to 8 mostly. Peak acceleration ratio between the dam crest and the foundation ranges by 0.2 – 9.3, 0.5 – 13.7, and 0.6 – 11.1 in a dam axis, stream, and vertical direction respectively. Median peak acceleration ratio is 2.3, 2.7, and 2.3 with the same order of direction. The 75% quartile values are 3.4, 3.8, and 3.2

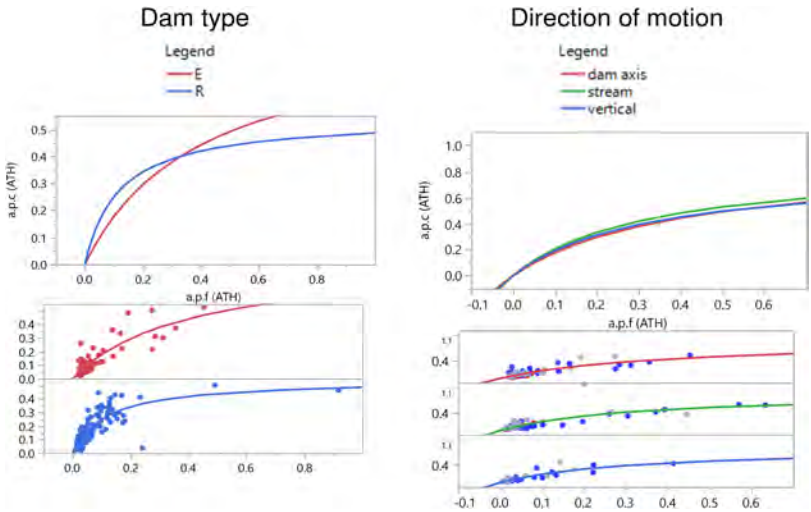

Fig. 4
Comparison of peak acceleration between dam crest and foundation depending on the dam type and the direction of motion
Comparaison de l'accélération maximale entre la crête et la fondation du barrage en fonction du type de barrage et de la direction du mouvement

respectively. Obviously, $a_{p.r}$ varies a lot in small PGA values and decays rapidly as PGA increases, which is associated with energy dissipation and increased non-linearity induced stiffness decay and damping increase as shaking intensity become higher (Albano et al. 2015; Kim et al. 2012; Yuan et al. 2014). At a PGA higher than about 0.3 g, the amplification ratio of the peak acceleration is typically around 1.0, and even de-amplification is observed. There is almost no difference in the trend between rockfill and earthfill dams, between the direction of motions.

Table 4 shows the result of nonlinear regression fit. Since majority of points is in PGA less than 0.2 g, major scatter comes from lower PGA region. In overall, large scatter exist based on the low value of R-squared. A nonlinear fitting prediction model was established in the exponential form of f(x) = a + b Exp(cx), where a is an asymptote, b is scale, and c is growth rate. The nonlinear fit constants are given in Table 4 depending on the direction. The direction of shaking components and/or dam type does not exhibit a distinct difference in the shape of fitting curves. On this plot, stream direction data yields relatively higher RMSE than dam axis and vertical direction data.

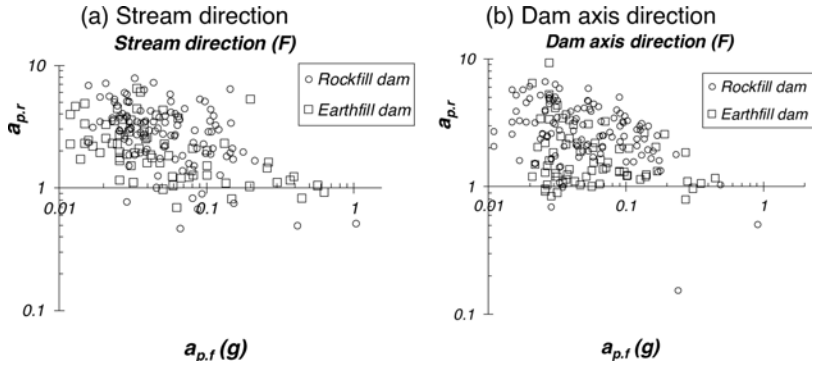

Fig. 5
A plot of the peak acceleration amplification of motion (analyzed with data from JCOLD 2014)
Un graphique de l'amplification de l'accélération maximale du mouvement (analysé avec les données de JCOLD 2014)

Table 4
Nonlinear fitting of peak ground acceleration and peak acceleration ratio between dam crest and foundation
Ajustement non linéaire de l'accélération maximale du sol et du rapport d'accélération maximale entre la crête et la fondation du barrage

DIRECTION	DAM TYPE	NONLINEAR FITTING OF $a_{p.f} - a_{p,r}$ IN THE FORM OF f(x) = a + b Exp(cx)				
		a	b	c	RMSE	R^2
Dam axis	E+R	0.714	2.661	−5.330	1.375	0.123
Stream	E+R	0.620	3.197	−4.360	1.938	0.087
Vertical	E+R	0.989	2.024	−4.738	1.439	0.046

3.2. Fundamental period of embankment dams

3.2.1. *The effect of PGA on the fundamental period of dams*

It is known that fundamental periods increase with increasing intensity of the shaking. Since PGA representative parameter of shaking intensity, it is useful to

study the correlations between PGA and fundamental period from measured data. Peak ground acceleration at dam foundation is plotted with the fundamental period obtained from ARS-based method depending on the direction of shaking and the dam type (Fig. 6). The simple nonlinear fitting curve is plotted together with the equation in the form of $f(x) = a\ x^b$, where a and b are obviously different per case as seen in Table 5. The values of *a* and *b* were determined by analytic Gauss-Newton method. The scatter is significant and the majority of data are for less than 0.2 g, accordingly, the RMSE of the relative error was given as well in order for end users to be able to quantify the related uncertainty.

In spite of scattering, Fig. 6 shows that the fundamental period of the dam increases with peak acceleration in overall. The two horizontal components of motion (in dam axis and stream direction) do not make any big difference in the plot, but the vertical component of motion apparently a lot lower fundamental period than the horizontal components. The fitting curve of vertical direction has less RMSE than horizontal direction data because the vertical ones are concentrated within the relatively narrower band of fundamental period computed. The RMSE of earthfill dam data in the stream direction is greater than other cases, which implicates the uncertainty of earthfill data in the stream direction is larger.

The effect of dam type on the fundamental period is not obvious, rather they are distributed in a similar fashion. The fitting constants from separate dam type classification do not produce a significant difference from those of combined dataset of each dam type.

Table 5
Nonlinear fitting of peak ground acceleration at dam foundation and fundamental period of embankment
Ajustement non linéaire de l'accélération maximale du sol à la fondation du barrage et de la période fondamentale du remblai

DIRECTION	**DAM TYPE**	**NONLINEAR FITTING OF $a_{p.f} - T_N$ IN THE FORM OF $f(x) = a\ x^b$**		
		a	**b**	**RMSE**
Dam axis	E	0.509	0.118	0.148
	R	0.540	0.114	0.147
	E+R	0.525	0.113	0.147
Stream	E	0.668	0.199	0.279
	R	0.599	0.114	0.143
	E+R	0.641	0.154	0.139
Vertical	E	0.450	0.210	0.089
	R	0.226	0.027	0.090
	E+R	0.303	0.110	0.092

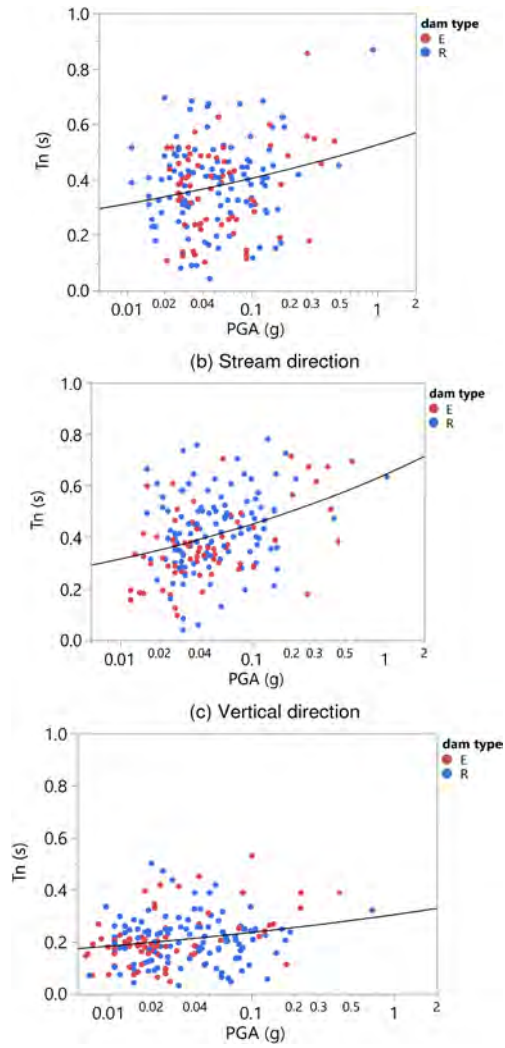

Fig. 6
Nonlinear fitting of peak acceleration at foundation and fundamental period of dam
Ajustement non linéaire de l'accélération maximale à la fondation et de la période fondamentale du barrage

3.2.2. *The effect of dam height and length on the fundamental period of dams*

There is an expectation the dam stream direction is affected by the dam height and the dam axis direction is affected by the crest length (or the valley width) and so should be its fundamental period of vibration. Quite possibly the crest length over dam height ratio could play a role. Thus, it is useful to check (1) firstly, if there is any statistical significance between H or L and T_n, and (2) secondly, if so, what kind of correlations exist.

To do so, the multidimensional behavior of variables was explored using the multivariate analysis to see how many variables relate to each other. Among many variables, the correlations between H and T_n, and L and T_n in both directions are statistically significant. The correlation coefficients using the Pearson product-moment correlation (which measures the strength of the linear relationship between two variables) of H – T_n and L – T_n are 0.287 and 0.219 in the dam axis direction, and 0.343 and 0.281 in the stream direction, respectively. The strength of the correlation is not very high. If there is an exact linear relationship, the correlation (r) is 1 or -1, in opposite case, the correlation becomes toward zero.

One of the traditional approaches to explaining T_n of embankment dams is to use a simple variable, H. Typical correlation fit of H versus T_n is to utilize a linear regression fit, but it is more like the nonlinear format, and moreover, linear fit can have a problematic non-zero T_n value at zero height. Thus, in this study, Michaelis-Menten model was adopted as shown in Table 6 and Fig. 7.

Though there is a broad trend for the proportionality between the fundamental period and dam height, there is significant scatter in the data. It means conversely that there is no single dominant factor such as dam height that controls the seismic response of an embankment dam as stated by Albano et al. [16]. Most of the fundamental periods of the embankment dams range from 0.1 to 1.0 sec. There is some uncertainty about high earthfill dams because the height of most earthfill dams is less than 50 m. T_n in a vertical direction is much less than T_n in two horizontal directions. Data distribution and the fitting shape of dam axis and stream directions are virtually in reasonable agreement each other. As seen in the residual plot in Fig. 7, no apparent bias is observed.

From the RMSE values, nonlinear fit in the two horizontal directions shows a similar level of scattering, but the fit in the vertical direction shows a lot less scatter. This is because data in the vertical direction is distributed in a densely populated narrow region of T_n.

Among many correlations of seismic parameters, the dam height versus a fundamental period of dams is a traditionally well-known correlation. Thus, a comparison was made to aid in the validation of the proposed fitting equations and to enhance its reliability for use in practice. Table 7 and Fig. 8 show a comparison of H – T_n fitting data in this study with any of the existing pertinent equations and

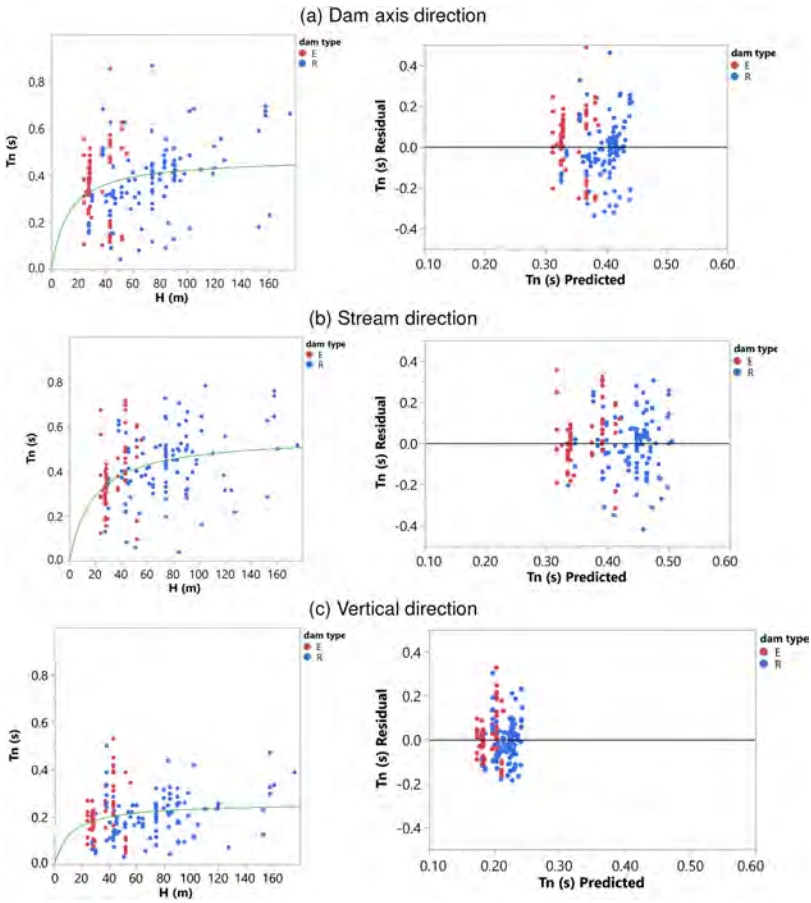

Fig. 7
Nonlinear fitting and residual analysis of dam height versus fundamental period of dam
Ajustement non linéaire et analyse des résidus de la hauteur du barrage par rapport à la période fondamentale du barrage

Table 6
Nonlinear fitting of dam height and fundamental period of embankment dams
Ajustement non linéaire de la hauteur du barrage et de la période fondamentale des barrages en remblai

DIRECTION	DAM TYPE	NONLINEAR FITTING OF H – T_N IN THE FORM OF *f(x) = ax/b+x*			
		a	***b***	**RMSE**	**R^2**
Dam axis	E	0.435	6.352	0.151	0.009
	R	0.592	35.942	0.141	0.126
	E+R	0.474	12.496	0.147	0.055
Stream	E	0.967	53.682	0.133	0.173
	R	0.564	20.688	0.141	0.085
	E+R	0.558	18.315	0.139	0.133
Vertical	E	0.453	38.014	0.096	0.100
	R	0.317	35.633	0.085	0.106
	E+R	0.259	11.883	0.092	0.045

corresponding plots in the literature. Based on the combined plot of analyzed data and fitting, proposed nonlinear fitting equations in this study shows more reasonable match with observed data relatively. Specifically, at higher dams, previous fitting formula generally over-predicts. Because the height of earthfill dams is less than 60 m, a fitting curve for combined earthfill and rockfill dams is closely following the curve of rockfill dams. Considering the large degree of scattering in data, more sample data need to be added in the future in order to obtain more reliable trend line and fitting formula.

Table 7
Comparison of H – T_n fitting equations of this study and in the literature
Comparaison des équations d'ajustement H – T_n de cette étude et de la littérature

REFERENCE	TYPE	DIRECTION	FIT EQUATION	REMARK
This study	E+R	Stream	$T_n = 0.558H / (18.315+H)$	
	E	Stream	$T_n = 0.967H / (53.682+H)$	
	R	Stream	$T_n = 0.564H / (20.688+H)$	
Papadimitriou et al. [11]	E	Stream	$T_n = 0.024\ H^{0.75}$	Elastic T_n
Sasaki [17]	E	Stream	$T_n = 1.101/100*H \pm 0.094$	
	R	Stream	$T_n = 0.542/100*H \pm 0.148$	

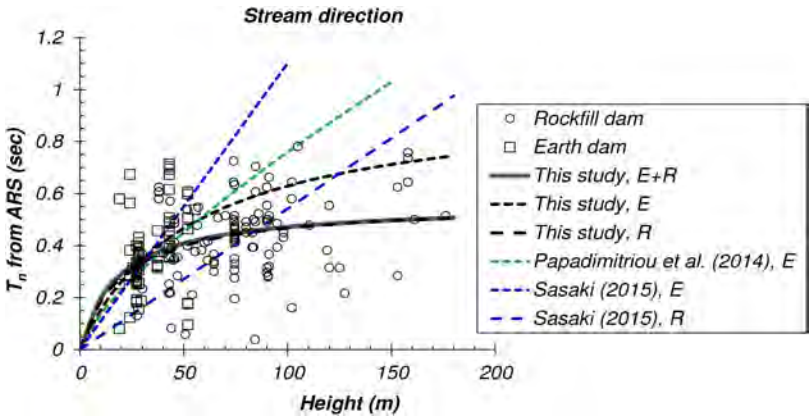

Fig. 8
Comparison of H – Tn fitting plots of this study and in the literature
Comparaison des graphiques d'ajustement H – Tn de cette étude et de la littérature

4. CONCLUSION

It is important to collect and analyze strong motion data measured on existing dams to understand the seismic response of embankment dams and to properly design or evaluate dams under seismicity area. In this study, the JCOLD strong motion database published in 2014 was visited (JCOLD 2014) and analyzed for 190 earthquake events (of 54 earthquakes) obtained from 60 embankment dams measured from 1978 to 2012. The paper presents a statistical analysis of the strong motion data recorded at the dam foundation and the crest in two horizontal and vertical directions.

The purpose of this paper is to study the seismic response characteristics in view of various seismic parameters and their pairwise correlations using multivariate analysis and linear/nonlinear fit modeling. Some conclusions have been drawn.

Based on the multivariate analysis and pairwise correlations of 20 seismic parameters (dam height and length, peak acceleration, Arias intensity, predominant period, and fundamental period in the three components of directions), T_n is correlated to H, L, PGA, $a_{p.c}$, $I_{a.f}$, $I_{a.c}$, and $T_{p.c}$. The peak acceleration at the crest, $a_{p.c}$ is correlated to PGA, $T_{p.c}$, T_n, and M. Similarly, $I_{a.c}$ may be correlated to $I_{a.f}$, $T_{p.f}$, $T_{p.c}$, T_n, and M.

Nonlinear fit prediction equations and curves between correlation parameters are proposed with the degree of uncertainty (RMSE) and R-square values in three directions. Admitting significant scattering of data, the proposed equations could be useful in practice for estimating seismic response at a preliminary stage of design or seismic evaluation.

Seismic response analyses in terms of the peak acceleration between foundation and crest show that seismic motions are mostly amplified through the embankment; however, de-amplification is also observed for some cases. The amplification ratio decreases as the PGA increases which becomes more apparent (ratio around 1.0 or below) for a PGA greater than 0.3 g.

A majority of the fundamental periods (T_n) of the embankment dams range from 0.1 to 1.0 s. Even with the scatter, it is confirmed that there is a broad proportionality between T_n and the dam height, PGA, and predominant period at dam crest. The proposed $H - T_n$ is believed to be a more reasonable match with field data comparing to literature fits. T_n in the vertical components is typically less than those in the two horizontal components.

In most proportional correlations, the two horizontal components show virtually no difference each other. In many cases, pairwise correlations in the stream direction yielded relatively a more uncertainty than other directions.

These empirical findings contribute to the seismic evaluation of existing embankment dams and to the seismic design of new embankment dams.

ACKNOWLEDGMENT

This study is funded by the K-water Research Institute, “Innovative digital informatics technology for water infrastructures safety.” Research Project, January 2023 – December 2025. The acceleration time histories used for the analyses in this study were from the “Acceleration records on dams and foundations No. 3 published by the Japan Commission on Large Dams in 2014. The author recognizes their pioneering work and appreciates the JCOLD, for their contribution and allow for the use of the data. Anonymous reviewers gave valuable review comments and are greatly appreciated.

REFERENCES

[1] JCOLD 2014. Acceleration records on dams and foundations No. 3. Japan Commission on Large Dams, Tokyo, Japan.

[2] USSD 2014. Observed performance of dams during earthquakes, Volume III. United States Society on Dams, Denver, CO, USA.

[3] WIELAND, M. 2012. Seismic design and performance criteria for large storage dams. In 15th World Conference on Earthquake Engineering, Lisboa, Portugal.

[4] PARK, D.S., AND KISHIDA, T. 2019. Seismic response of embankment dams based on recorded strong motion data in Japan. *Earthquake Spectra*, 35(2): 955–976.

[5] CHUGH, A.K. 1985. Estimation of the fundamental period of large earthfill and rockfill dams. 土質工学会論文報告集, 25(3): 146–150.

[6] UDDIN, N., AND GAZETAS, G. 1995. Dynamic response of concrete-faced rockfill dams to strong seismic excitation. *Journal of Geotechnical Engineering*, 121(2): 185–197.

[7] AHLBERG, J.E., FOWLER, J., AND HELLER, L.W. 1972. Earthquake Resistance of Earth and Rock-fill Dams: Analysis of Response of Rifle Gap Dam to Project RULISON Underground Nuclear Detonation. Report 2.

[8] BRAY, J.D., AND TRAVASAROU, T. 2007. Simplified procedure for estimating earthquake-induced deviatoric slope displacements. *Journal of Geotechnical and Geoenvironmental Engineering*, 133(4): 381–392.

[9] GAZETAS, G. 1987. Seismic response of earth dams: some recent developments. *Soil Dynamics and Earthquake Engineering*, 6(1): 2–47.

[10] ONER, M. 1984. Estimation of the fundamental period of large earthfill and rockfill dams. 土質工学会論文報告集, 24(4): 1–10.

[11] PAPADIMITRIOU, A.G., BOUCKOVALAS, G.D., AND ANDRIANOPOULOS, K.I. 2014. Methodology for estimating seismic coefficients for performance-based design of earthdams and tall embankments. *Soil Dynamics and Earthquake Engineering*, 56: 57–73.

[12] ABDEL-GHAFFAR, A.M., AND SCOTT, R.F. 1979. Analysis of earth dam response to earthquakes. *Journal of the Geotechnical Engineering Division*, 105(12): 1379–1404.

[13] MAKDISI, F.I., AND SEED, H.B. 1979. Simplified procedure for evaluating embankment response. *Journal of the Geotechnical Engineering Division*, 105(12): 1427–1434.

[14] MEJIA, L.H., SEED, H.B., AND LYSMER, J. 1982. Dynamic analysis of earth dams in three dimensions. *Journal of the Geotechnical Engineering Division*, 108(12): 1586–1604.

[15] JMP 2016. JMP 13 Multivariate methods. In JMP user manual. JMP A Business Unit of SAS, SAS Institute Inc., Cary, NC, USA.

[16] ALBANO, M., MODONI, G., CROCE, P., AND RUSSO, G. 2015. Assessment of the seismic performance of a bituminous faced rockfill dam. *Soil Dynamics and Earthquake Engineering*, 75: 183–198.

[17] SASAKI, T. 2015. Tentative report - analysis on acceleration data of dams collected by JCOLD. In ICOLD 25th Congress / 83rd Annual Meeting, Stavanger, Norway.

COMMISSION INTERNATIONALE DES
GRANDS BARRAGES

VINGT-HUITIEME CONGRES DES
GRANDS BARRAGES
CHENGDU, MAI 2025

DYNAMIC ANALYSIS OF COMBINED EMBANKMENT DAM FOR THE HEIGHTENING OF AN EXISTING TAILINGS STORAGE FACILITY (*)

Ljupcho PETKOVSKI
Full professor, Chair of Hydraulic Structures
Ss Cyril and Methodius University, Civil Engineering Faculty – Skopje

Stevcho MITOVSKI
Associate Professor, Chair of Hydraulic Structures
Ss Cyril and Methodius University, Civil Engineering Faculty – Skopje

REPUBLIC OF NORTH MACEDONIA

SUMMARY

The need to provide an additional volume for depositing tailings material, necessary for the regular operation of mines in conditions of spatial limitation, actualizes the heightening of the tailings storage facilities. The upgrade of the existing tailings storage facilities, with the upstream construction method of a new tailing sandy dams over the existing waste lagoon, is a heterogenic geo environment that is susceptible to liquefaction during dynamic (cyclic) loading and therefore they are the civil engineering structures with the highest stability risk.

This heightening is characterized by detailed geotechnical in-situ investigations, sophisticated structural analyses (static, nonsteady seepage, and dynamic), and necessary modification of the geometry of the embankment. That is illustrated by the results of the dynamic analysis and seismic resistance assessment of a

Analyse dynamique d'un barrage en remblai combiné pour la surélévation d'une installation de stockage de résidus existante

DOI: 10.1201/9781003642428-106

heightening of the existing upstream combined diverting dam and modification of the previous rockfill dam with clay core, with tailings sandy dam above the waste lagoon of the tailings storage facility Toranica, Kriva Palanka, Republic of North Macedonia.

RÉSUMÉ

La nécessité de fournir un volume supplémentaire pour le dépôt des résidus, nécessaire à l'exploitation régulière des mines dans des conditions de limitation spatiale, actualise la surélévation des installations de stockage des résidus. La mise à niveau des installations de stockage de résidus existantes, avec la méthode de construction en amont d'un nouveau barrage de sable à résidus au-dessus de la lagune à déchets existante, constitue une structure hétérogène susceptible de se liquéfier lors d'un chargement dynamique (cyclique) et ce sont donc des ouvrages de génie civil. avec le risque de stabilité le plus élevé.

Ce rehaussement est caractérisé par des investigations géotechniques détaillées in situ, des analyses structurelles sophistiquées (statiques, infiltrations instables et dynamiques) et une modification nécessaire de la géométrie du remblai. Cela est illustré par les résultats de l'analyse dynamique et de l'évaluation de la résistance sismique d'un rehaussement du barrage de dérivation combiné en amont existant et de la modification du précédent barrage en enrochement à noyau d'argile, avec un barrage de sable à résidus au-dessus du bassin à déchets de l'installation de stockage de résidus de Toranica, Kriva Palanka en République de Macédoine du Nord.

1. INTRODUCTION – HEIGHTENING OF TAILINGS STORAGE FACILITIES WITH TAILINGS SAND DAMS ABOVE EXISTING WASTE LAGOONS

The tailings storage facilities (TSF) are complex engineering structures, composed of starter dam with tailings sand dam and/or diversion embankment dam, waste lagoon, drainage system, water conveyors for taking out of the cleared water and structures for protection in case of inflow (external) water. In case of tailings dams the lowest safety is obtained by upstream method of construction. In such case, for each subsequent stage, the dam crest is displaced upstream apropos the sandy dams are founded on the deposited tailings silt. The heterogeneous medium – tailings dam over waste lagoon or tailings dam with upstream method of construction is subjected to liquefaction under static and dynamic (cyclic) loading. Therefore, the heightening of the tailings facility with tailings dams over waste lagoons are treated as hydraulic structures of highest risk and are not recommended in seismic active regions.

Logical question arises – from where comes the need of the mining companies to initiate solutions with heightening over existing waste lagoons? It is obvious that they are embankments structures with highest risk and for confirmation of their safety are necessary detail geotechnical investigations and sophisticated structural (static, seepage, dynamic) analysis apropos high financial investment. The explanation, in our opinion, is as follows [1]. On one hand, the space for survival, development and growth of mining companies, essential for the existence of the population in certain regions (which rely on the mining complex), due to the imposition of increasingly strict environmental and sociological criteria, is becoming more and more limited. On other hand, obtaining permission to expand the concession area (or increase the industrial scope) from a huge number of agencies/institutions, in countries that are heavily bureaucratized and, unfortunately, corrupt, for mining companies is prolonged in a long-term exhausting administrative process with the highly uncertain outcome. Therefore, mining companies are more and more often opting for solutions for hydraulic engineering facilities with highest risk level, i.e. heightening with cycloned sand over the existing waste lagoons of water-saturated tailings mud.

The heightening of the existing TSF, with the construction of a new tailings sand dam over existing waste lagoon (a method similar to the upstream advancement of tailings dam facilities), is a heterogeneous geo-environment that is subjected to liquefaction under static and dynamic (cyclic) loading and therefore they are hydraulic engineering structures with greatest safety risk. The analysis of the stability of these heterogeneous geo-environments confirmed that the critical loading state by comparing: (a) the long-term static (with the highest required safety coefficient 1.5), (b) the short-term static (with the lower required safety coefficient 1.3), (c) the seismic resistance during earthquake action (where short excursions are tolerated with a safety factor less than 1.0), and (d) incidental loads during the occurrence of liquefaction (with a required safety factor of 1.1) is precisely the occurrence of liquefaction. Therefore, we believe that the occurrence of liquefaction (static and dynamic) must become a mandatory loading condition of the TSF, because the commonly adopted geometry and composition of the cross-section (the arrangement of local materials) which guarantees the required stability depends on this loading condition.

2. OCCURRENCE OF LIQUEFACTION AT TSF

The liquefaction phenomena occur in water-saturated and loose (insufficiently compacted) sands, which are represented in certain zones of the TSF. When liquefaction occurs, regardless of whether it is static or dynamic, the structure of the granules is destroyed and the shear strength of the material rapidly decreases to steady-state strength.

In the context of Critical state line (CSL) and Collapse surface (CS) in the (q-p`) stress space we distinguish static and dynamic liquefaction, fig 1. Where q = (σ1 - σ3) is a deviator stress and represents the shear of the soil material and p' = (σ'1 + σ'2 + σ'3) / 3 is mean effective stress, which is defined in terms of effective principal stress. Static liquefaction [2] is possible in the following two cases: (a) with additional external loading causing an increase in shear stress, and (b) with additional water saturation and reduction of effective normal stresses. Dynamic liquefaction [3] occurs during the action of an earthquake, where cyclic loading causes a continuous increase in pore pressure, which conditions a decrease in effective stresses.

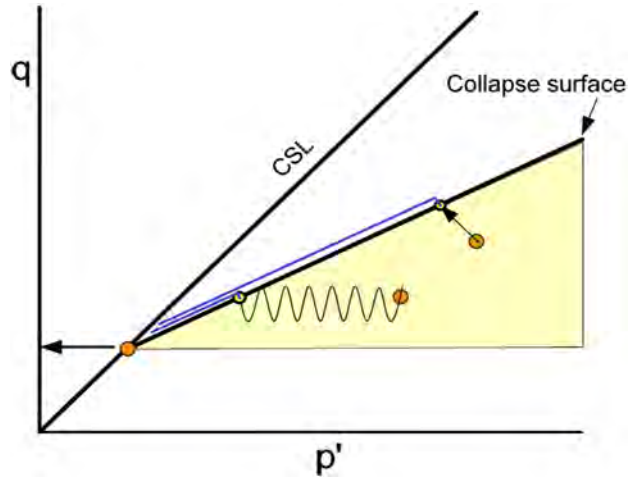

Fig. 1
Static and cyclic stress path to the collapse surface in the potentially liquefiable region (yellow shaded region)
Cheminement des contraintes statiques et cycliques jusqu'à la surface d'effondrement dans la région potentiellement liquéfiable (région ombrée en jaune)

3. TSF TORANICA – BASIC PARAMETERS

Toranica mine of mining company Bulmak, near Kriva Palanka, in the eastern part of North Macedonia (fig. 2), currently operates with an ore production of about 320,000 t/year, and for the needs of that production, the existing tailings dam facility Toranica 1 is in operation. The waste lagoon of the tailings dam is created with upstream (upper) and downstream (lower) dam, fig. 3. The upstream (diversion or

retention) dam is a conventional dam (earth fill dam with a clay facing), with crest elevation at 977.5 masl. The downstream dam is a tailings dam with a downstream construction of cycloned tailings sand.

Fig. 2
Location in Europe and map of Republic of North Macedonia
Situation en Europe et carte de la République de Macédoine du Nord

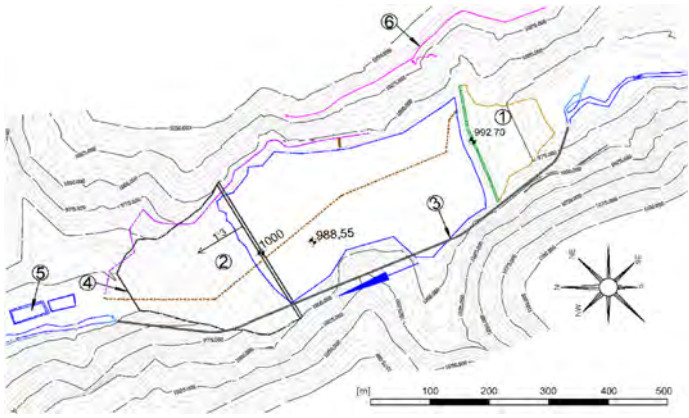

Fig. 3
Layout of TSF Toranica 1', according to the geodetic survey from September 2023. (1) upstream or retention or diversion dam, (2) downstream or tailings dam, (3) diversion tunnel, (4) gabion wall to protect the exit structure of the tunnel, (5) sedimentation tanks for drained and treated water, (6) pulpline
Implantation du TSF Toranica 1', selon le levé géodésique de septembre 2023. (1) barrage amont ou barrage de rétention ou de dérivation, (2) barrage aval ou barrage à résidus, (3) tunnel de dérivation, (4) mur de gabions pour protéger l'ouvrage de sortie du tunnel, (5) bassins de décantation pour eaux drainées et traitées, (6) pulpline

4. TSF TORANICA – MODIFICATIONS TO THE HEIGHTENINGS

The existing 'Toranica 1' TSF, so far has been heightened twice above elevation 977.5 masl. The first heightening was up to crest elevation of 990.0 masl. The retention dam was heightened by a tailings dam with a central construction method, but with a crest displaced from the conventional dam, i.e. founded on the waste lagoon, at position "A" (fig. 4). The second heightening, which is in the construction stage, was designed up to an elevation of 1,000 masl, in accordance with the technical documentation for the 'Toranica' mine TSF, prepared by Geing - Skopje, in 2018. With this project, it was foreseen that the retention dam would be heightened by a tailings dam with a crest at 1,000 masl, made from cycloned sand with a central construction method, founded on the waste lagoon at position "B".

An alternative solution for the heightening of the upstream dam up to the elevation of 1,000 masl, analyzed in Annex 1, prepared by DIPKO – Skopje in 2022, fig. 5, is with a cyclone location near "A", apropos displaced upstream by 47.25 m compared to "B". By comparing variants "B" (2018) and "A" (2022), at same level of technical investigation of the stability, with limit equilibrium method and shear strength in undrained conditions in the existing waste lagoon, it was confirmed that the variant "A" poses higher degree of stability.

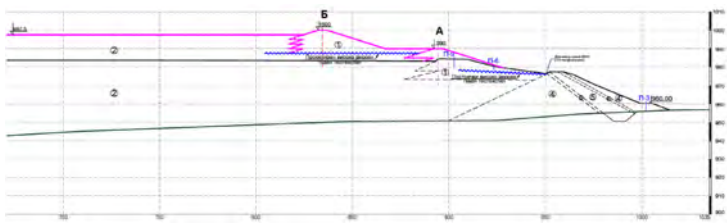

Fig. 4
Schematic display of the heightening of the upstream dam at TSF Toranica, according to annex 3 of Basic Design from 2018-09-12
Représentation schématique du rehaussement du barrage amont du TSF Toranica, selon l'annexe 3 du Basic Design du 2018-09-12

In October 2023, the heightening of the upstream (retention) dam (Fig. 6) till elevation 1,000.0 masl was carried out according to Annex 2, prepared by DIPKO - Skopje, in 2023, using data from SPT and CPT field geotechnical investigations from March 2023. With the dynamic analysis in Annex 2 for the solution of the cross-section according to Annex 1, a stability factor lower than 1.0 was obtained for the post-earthquake condition with the occurrence of liquefaction in the waste lagoon. A variant was adopted with a minimum amount of embedded mine rockfill

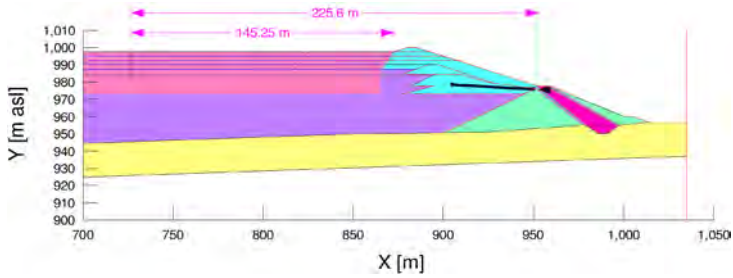

Fig. 5
Model for heightening of the upstream dam of the tailings dam Toranica, according to Annex 1 from 2022-08-30
Modèle de rehaussement du barrage amont du barrage à résidus Toranica, selon l'annexe 1 du 2022-08-30

and which provides a stability factor (F) at least as much as is permitted for the condition after an earthquake at occurrence of liquefaction (Fper), that is value of F=1.152>Fper=1.1. That form of "supported drainage" has the following dimensions: a berm width of 4.0 m and a height of 12 m, that is, from the crest elevation of the original diversion dam at 977.5 masl (with a crown width of 6.9 m) till elevation 990 masl.

Taking into account the long period for obtaining the Approval for the construction of the new Toranica_2 TSF, (downstream of 'Toranica, for which geotechnical investigations and a reviewed Basic Design have been prepared), which due to numerous administrative bureaucratic difficulties can be extended to 4-5 years, the Client 'Bulmak, Probishtip' approved the continuation of the exploitation of the existing Toranica, with a new heightening at 1,005 masl.

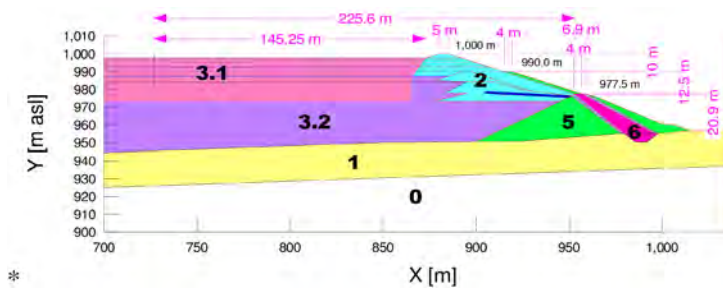

Fig. 6
Model for the heightening of the upstream dam up to 1,000 masl, according to Annex 2, 2023.07.03
Modèle pour le rehaussement du barrage amont jusqu'à 1 000 m d'altitude, selon l'annexe 2, 2023.07.03

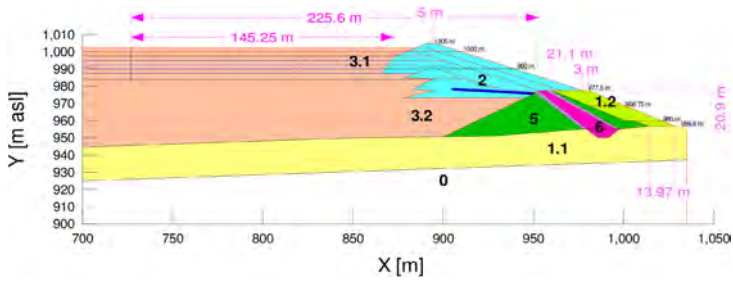

Fig. 7

Model of the heightening to 1,005 masl of the upstream (retention) dam Toranica_1, 0 – bedrock, boundary seepage and deformable condition, 1.1 - gravelly mixture, alluvium in the base below the dam, 1.2 - gravelly mixture, fill above the aerial slope of the earth-rock dam, 2 – cycloned tailings sand, dam, 3 - tailings mud, sedimentary lake (3.1 shallow zone and 3.2 deep zone), 5 - stone, retaining body of retention dam, 6 - clay, inclined core of retention dam, 7 - sand, filter transition zones of retention dam

Modèle de surélévation à 1 005 m d'altitude du barrage amont Toranica_1, 0 – substrat rocheux, suintement limite et état déformable, 1.1 - mélange graveleux, alluvions dans la base en dessous du barrage, 1.2 - mélange graveleux, remblai au-dessus de la pente aérienne de la terre- barrage rocheux, 2 – sable de résidus cycloné, barrage, 3 - boue de résidus, lac sédimentaire (zone peu profonde 3.1 et zone profonde 3.2), 5 - pierre, corps de retenue du barrage de rétention, 6 - argile, noyau incliné du barrage de rétention, 7 - sable, filtrer les zones de transition du barrage de retention

By the heightening till 1,000 masl with the central method in position "A" was exhausted the stability of the retention dam (Annex 2) and therefore it was adopted that the heightening from 1,000 to 1,005 masl should be made with progression in the opposite direction from the waste lagoon (toward the aerial slope of the retention dam). For this purpose, the inclined layers of tailings sand (with slope V:H = 1:3) should be supported on widened crest of the retention dam (earth rock) at elevation of 977.5 masl, fig. 7. The modified geometry of the upstream dam in the preliminary analysis (compared with Annex 2) made according to the perception and concept of the technical feasibility of heightening by 5.0 m at the Toranica TSF prepared by HEI – Skopje in 2023) was obtained with a slope of tailings sand of V:H = 1:3, a berm at an elevation of 977.5 masl wide 3.0 m and a slope of alluvium ballast V:H = 1:2.3. Backfilling with gravel mix (alluvium) at a height of 977.5 - 956.6 = 20.9 m and variable width, filled in horizontal layers of 30 cm and with moderate compaction, should be carried out before disposal on the downstream slope of tailings sand with a slope of V: H = 1:3, higher from the heightening at elevation of 1,000.0 masl.

5. DYNAMIC ANALYSIS OF COMBINED EMBANKMENT DAM FOR THE TSF HEIGHTENING TO 1005 MASL

The structural (static, filtration and dynamic) analysis of the heightening of the upstream (diversion) dam up to 1.005 masl at the tailings dam Toranica 1 was made according to the latest recommendations of ICOLD, i.e. with one mathematical model for different loading stages, where each subsequent stage is with initial state of stresses determined by the previous stage. The adoption of the physical, mechanical, strength, deformable and water-permeable characteristics of the materials is based on the large number of field and laboratory tests, primarily in the past period for the tailings dam Toranica, but also with a comparison of the values for the new tailings dam Toranica_2.

To determine the values for the undrained shear strength of tailing mud in static conditions Su(yield)/σ`v and in liquefaction conditions Su(liq)/$\sigma$`v, which were determined by in-situ SPT and CPT, data from the latest field geotechnical investigations in 2023-03-16 were used. The field investigations consisted of boring of two boreholes at a distance from the upstream edge of the original conventional retention dam (crest at elevation 977.5 masl) ID-1 at 55.6 m and ID-2 at 72.5 m to a maximum depth of about 40 m, at the maximum cross-section (approximately in the middle of the river bed). Two series of standard (dynamic) penetration tests (SPT) and one cone (static) penetration test with pore pressure measurement (CPT) were carried out in the boreholes in ID-1. In borehole ID-1, liquefaction potential was estimated at a depth of about 16.1 m, with SPT, and the lowest strength parameters with CPT were obtained approximately in that zone.

With the CPT results in ID-1, for the critical depth of 15 to 25 m, fig. 8, values for CPT were estimated and using expressions from the technical literature for the calculation of undrained shear strength [4], [5], [6], [7], [8], [9] the values of Su(yield)/σ`v and Su(liq)/$\sigma$`v were determined. For further analysis, the following values Su (yield)/σ`v = 0.21 and Su(liq)/$\sigma$`v = 0.04 were adopted. The values of the residual strength of liquefied local materials Su(liq) and φ(liq), were determined using the data of the initial effective vertical stresses S'y =300 kPa (for shallow lagoon) and S'y =600 kPa (for deep lagoon) and φ(liq) = 10^o. The initial state of stresses before the beginning of the heightening is determined by approximating the pore pressure distribution according to the measured data with piezometers, with the type of "Insitu" analysis, thus simulating the initial state of total stresses (initial state for the next stage of loading) and effective stresses.

With the initial stress state of the tailings dam for the waste lagoon at an elevation of 984 masl, heightening was simulated in 7 load stages, for the following elevations in the lagoon: 987.5, 990.0, 992.5, 995.0, 997.5, 1,000.0 and 1,002.5 masl, so that the dam crest of the from cycloned sand is always 2.5 m higher than the waste lagoon. Each stage (layer) of the waste lagoon and sand dam with a height of 2.5 m has a duration of 180 days and was calculated by consolidation

analysis in 10 load increments with an exponential increase, because the dissipation of excess pore pressure is most intense in the initial period. The construction of the alluvium embankment along the aerial slope of the retention dam begins after reaching the crest elevation of the sand dam at 1,000.0 masl. The alluvium embankment is simulated in 3 load cases up to elevations 960.0, 968.75 and 977.5 masl with a duration of 15, 30 and 30 days each (or a total of 75 days), with consolidation analysis in 5 load increments with exponential raise. With the described approach, the pre-earthquake state of stresses was obtained, Figure 6, for which a dynamic analysis was carried out.

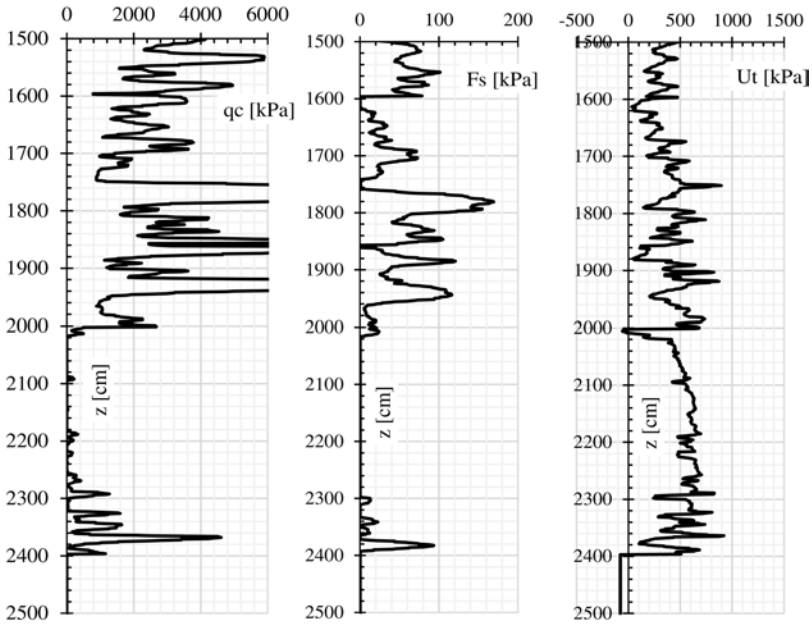

Fig. 8
(1) qc - CPT cone resistance, (2) Fs - CPT sleeve friction, (3) Ut - Total pore pressure during penetration, measured behind the tip
(1) qc - Résistance du cône CPT, (2) Fs - Frottement du manchon CPT, (3) Ut - Pression interstitielle totale lors de la pénétration, mesurée derrière la pointe

In this research, having in mind the size and importance of the tailings storage facility Toranica, as well as the available dynamic material parameters, it is adopted the dynamic behavior of the dam to be determined by the application of Equivalent Linear (EL) Analysis [10]. The dynamic response of the geo-environment, during SEE with PGAx = 0.36 g and PGAy = 0.25 g, duration of t =20 s, with synthetic

accelerogram T=10,000_1, is displayed in fig. 9. A visual control that the dynamic response is correct is the diagram of the relative horizontal displacements, fig. 10.

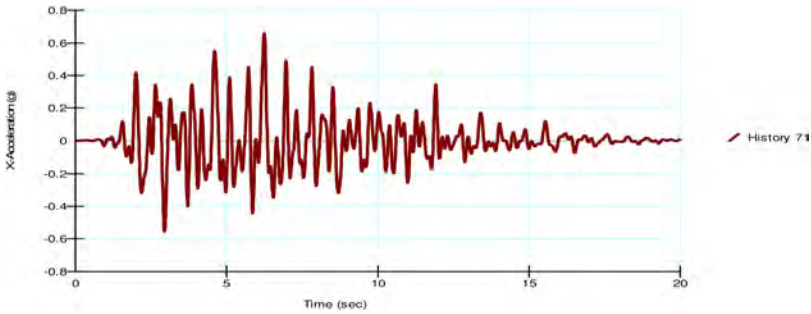

Fig. 9
Absolute accelerations a[g] ÷ t[s] in horizontal direction, at the crest of retention dam Toranica „1“ with heightening at 1,005 masl (response), at history point (71)
Accélérations absolues a[g] ÷ t[s] dans le sens horizontal, à la crête du barrage de rétention Toranica « 1 » avec surélévation à 1 005 m d'altitude (réponse), au point historique (71)

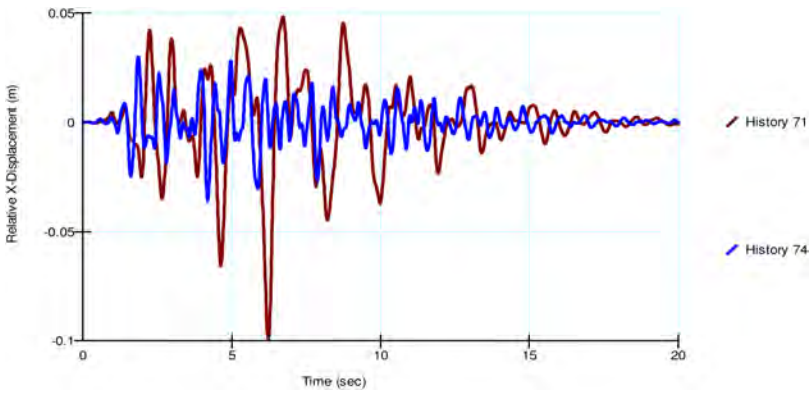

Fig. 10
Relative displacements, horizontal x[m] ÷ t[s], in the berm of the embankment of retention dam “74” at 977.5 masl (response) and in the crest of the heightened retention dam “71” at 1.005 masl (response)
Déplacements relatifs, horizontaux x[m] ÷ t[s], dans la berme du remblai du barrage de rétention “74” à 977,5 m d'altitude (réponse) et dans la crête du barrage de rétention surélevé “71” à 1,005 m d'altitude (réponse)

The permanent vertical displacement, caused by the inertial forces during the excitation, which is relevant for the assessment of the seismic resistance of the dam crest at 1.005 masl is the crest settlement, value of 65 cm, calculated by the Dynamic Deformation (DD) method, fig. 11. DD analysis is successive non-linear redistribution of the stresses. By such method, for geomedium discretized by finite elements (FE), are calculated deformations caused by forces in nodes, calculated by the incremental stresses in the elements. Thus, by application of non-linear model, for each time step of the dynamic response of the structure is obtained new state of the total stresses and pore pressure. By the differences of the effective stresses in two successive time steps are obtained incremental forces, resulting in deformations, in accordance with the chosen constitutive law for dependence stress – strain. So, for each loading case during the dam's dynamic response are produced elastic and eventual plastic strains. If dynamic inertial forces cause plastic strains, then in the geomedium will occur permanent deformations. The permanent displacements, at any point in the dam and at end of the seismic excitation, are cumulative sum of the plastic deformations.

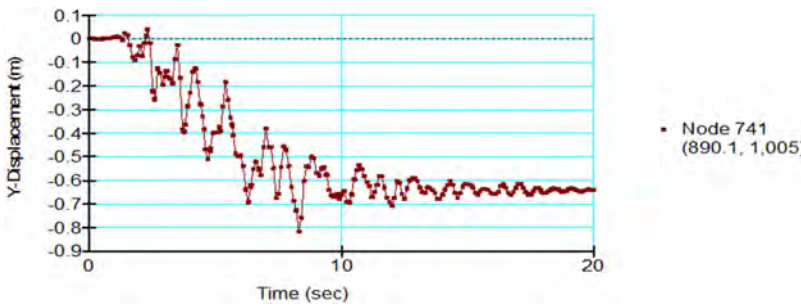

Fig. 11
Permanent vertical settlements of 65 cm, determined by the DD method in the upstream edge of the dam crest at elevation of 1.005 masl, at history point (71) or FE mesh node 741
Tassements verticaux permanents de 65 cm, déterminés par la méthode DD dans le bord amont de la crête du barrage à une altitude de 1,005 m d'altitude, au point historique (71) ou au nœud de maillage FE 741

During the earthquake, there is an increase in the pore pressure, which creates a liquefaction zone after the earthquake action. At the q/p´ stress state, the q/p´ ratio is the deviator stress divided by the mean effective stress and liquefiable zone is where q/p´ ratio is between the critical state line (CSL) and the collapse surface (CS), fig. 12.

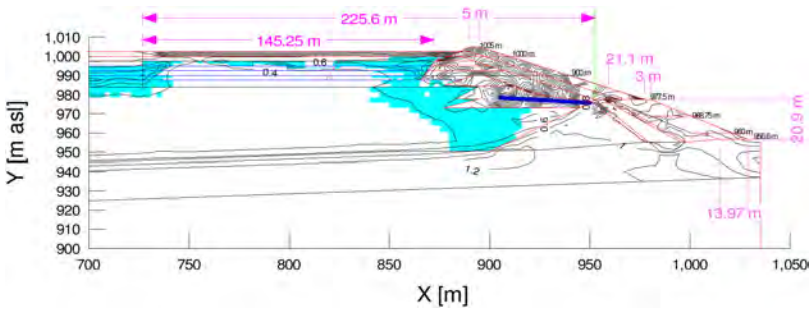

Fig. 12
Distribution of the q/p' ratio [-] with a liquefied zone (blue shaded region), for the state of stresses at the end of the earthquake action (dynamic liquefaction)
Distribution du rapport q/p' [-] avec une zone liquéfiée (zone grisée en bleu), pour l'état des contraintes à la fin de l'action sismique (liquéfaction dynamique)

For the state of dynamic liquefaction is obtained minimum stability of the slope of the Toranica retention dam with a crest at 1.005 masl in the post-earthquake stage, fig. 13. The occurrence of liquefaction will cause a redistribution of the effective stresses, which will result in post-earthquake displacements in the geo-environment, horizontal and vertical, fig. 14, with crest settlement approximately 0.5 m.

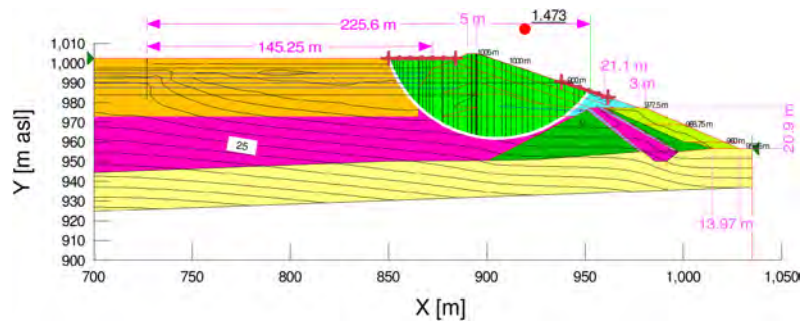

Fig. 13
Critical slope slip surface, in the post-earthquake stage with a regular beach length of 150 m
Surface de glissement de pente critique, en phase post-séisme avec une longueur de plage régulière de 150 m

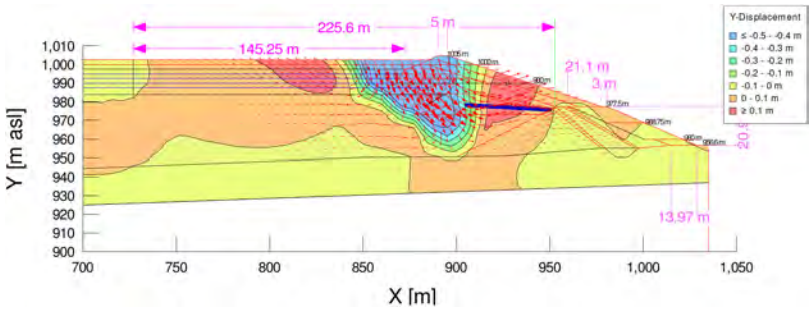

Fig. 14
Distribution of additional vertical Y displacements and XY displacement vectors after earthquake action, with dissipation of liquefaction excess pore pressure
Répartition des déplacements verticaux supplémentaires Y et des vecteurs de déplacement XY après l'action sismique, avec dissipation de l'excès de pression interstitielle de liquéfaction

6. CONCLUSIONS

The general conclusion that with the heightening of the upstream (retention) dam of the Toranica TSF, according to the adopted geometry and layout of the local materials, satisfactory static stability and seismic resistance is provided, according to the applicable design regulations, is based on the following facts.

For the critical slip surface for the downstream slope in the pre-earthquake stage, with shear strength in liquefied zones (under static liquefaction conditions), a high stability factor of 1.801 is obtained, significantly higher even than that allowed for permanent stability with Fper = 1.5.

The dynamic response of the geoenvironment, determined by ELA, during SEE with peak ground acceleration PGA = 0.36 g and PGAy = 0.25 g, duration of t = 20 s, with synthetic accelerogram T=10,000_1, for standard state and regular scenario with beach length of approximately 150 m, with peak crest acceleration PCA = 0.65 g (at crest elevation 1.005 masl), i.e. dynamic amplification factor DAF = PCA/PGA = 1.8. The visual control that the dynamic response is correct is the diagram of the relative horizontal displacements, in range +5 to -10 cm.

The permanent vertical displacement, caused by the inertial forces during the excitation, which is relevant for the assessment of the seismic resistance of the dam crest at 1,005.0 masl is the crest settlement, value of -0.65 m, is calculated by the Dynamic Deformation (DD) method. During the earthquake excitation, the average acceleration did not exceed the yield acceleration (where the stability factor is equal

to 1.0), that is, the permanent deformations, calculated by the Newmark Method (NM) are equal to zero.

During an earthquake, there is an increase in pore pressure, which creates widened liquefaction zone after the earthquake. For the state of dynamic liquefaction, the minimum stability of the slope of the Toranica retention dam with a crest at 1.005 masl is obtained. For the critical sliding surface, it is value of 1,473, that is, it is greater than the one allowed for an incident extreme load Fper = 1.1.

The occurrence of liquefaction will cause a redistribution of effective stresses, which will result in post-earthquake displacements in the geoenvironment, both horizontal and vertical, with vertical settlement in the crest at elevation 1.005 masl of 50 cm. The total permanent settlement in the crest are 65+50=115 cm. They are lower than the protective height from the normal water level to the dam crest of 2.5 m apropos there is no danger of a rapid and uncontrolled emptying of the tailings mud from the waste lagoon.

REFERENCES

[1] PETKOVSKI L., “EMBANKMENTS ABOVE EXISTING WASTE LAGOONS – GEO ENVIRONMENTS WITH THE HIGHEST POTENTIAL HAZARD”, UDK: 627.824, Original scientific paper, Water-economy, ISSN 0350-0519, Vol. 54 (2022), No. 317-318, p. 109-121, Beograd, Serbia, 2022.

[2] PETKOVSKI L., MITOVSKI S., “Application of SPT Results On Liquefaction Phenomenon Modelling Of Tailings Dam”, 3-rd International Symposium on Dams and Earthquakes, organized by WGDE-EC-ICOLD and PCOLD, ISBN: 978-972-49-2308-6 Proceedings, p.209-220, (6-8).05.2019, Lisbon, Portugal, 2019.

[3] PETKOVSKI L., MITOVSKI S., “ASSESMENT OF SEISMIC RESISTANCE OF COMBINED TAILINGS DAMS”, 26. Congress on Large Dams, ICOLD, 1–7 July 2018, Vienna, Austria, CD Proceedings Q.101-R.58, p.978-991, 2018.

[4] CAMPANELLA, R. G., GILLESPIE, D., AND ROBERTSON, P. K. “Pore pressures during cone penetration test-ing.” Proc., 2nd European Symp. on Penetration Testing, ESPOT II, Balkema, Rotterdam, The Netherlands, 507–512, 1982.

[5] CAMPANELLA, R. G., *ET AL.* “Recent Developments in In-situ Testing os Soils, XI ICSMFE San Francisco”, 1985.

[6] OLSON, S.M., AND STARK, T.D. “Yield strength ratio and liquefaction analysis of slopes and embank-ments”, *Journal of Geotechnical and Geoenvironmental Engineering, ASCE*, 129(8): 727–737, 2003.

[7] ROBERTSON, P.K. “Evaluation of flow liquefaction and liquefied strength using the cone penetration test”, *Journal of Geotechnical and Geoenvironmental Engineering, ASCE*, 136(6): 842–853, 2010.

[8] ROBERTSON, P.K. “Cone penetration test (CPT)-based soil behaviour type (SBT) classification system — an update”, *Canadian Geotechnical Journal*, 53 (12): 1910–1927, 2016.

[9] ROBERTSON, P.K., “Evaluation of flow liquefaction and liquefied strength using the cone penetration test: an update”, *Canadian Geotechnical Journal*. 00: 1–5 (0000), 2020.

[10] GeoStudio v8, Quake “Dynamic Modeling”, Sigma ‘‘Stress/deformation analysis”, Slope “Stability modeling”, GEO-SLOPE International Ltd., Calgary, Alberta, Canada, 2018.

COMMISSION INTERNATIONALE DES
GRANDS BARRAGES

VINGT-HUITIEME CONGRES DES
GRANDS BARRAGES
CHENGDU, MAI 2025

A GUIDELINE FOR DYNAMIC ANALYSIS AND LIQUEFACTION PREDICTION OF EMBANKMENT DAMS: CASE STUDY OF SANTA RITA DAM, COLOMBIA (*)

Narjes SOLTANI
Universitat Politècnica de Valencia, Valencia, Spain

Camilo Andrés CARDONA VILLA, Daniel Eduardo TOSCANO PATIÑO &
Alejandro VELÁSQUEZ PÉREZ
EPM, Medellín, Colombia

Sergio AMOEDO-FERNÁNDEZ
iPresas Risk Analysis, Valencia, Spain

Ignacio González TEJADA
Universidad Politécnica de Madrid, Madrid, Spain

Ignacio ESCUDER-BUENO
Universitat Politècnica de València, Valencia, Spain
iPresas Risk Analysis, Valencia, Spain

SPAIN

SUMMARY

In this article, a methodology for the dynamic analysis of embankment dams has been presented, with a focus on liquefaction prediction. The Santa Rita Dam in Colombia has been used as a case study. The proposed methodology involves

**Un guide pour l'analyse dynamique et la prédiction de la liquéfaction des barrages en remblai – cas du barrage de Santa Rita en Colombie*

DOI: 10.1201/9781003642428-107

generating a 2-dimensional numerical model using the finite difference method, implementing static and dynamic boundary conditions, a damping model, preparing accelerograms, and calibrating the material constitutive model. The traditional method of the Mohr-Coulomb and the advanced model of PM4Sand/Silt are compared to highlight the progression in dynamic analysis techniques of embankment dams.

The results show considerably more plastic displacement and pore pressure in the PM4Sand/Silt model than in the Mohr-Coulomb model. Moreover, the modes of displacement are different in the two models. The crest displacement for the Mohr-Coulomb model is toward the downstream, while the PM4Sand/Silt model is toward the upstream. This is because of excess pore pressure generation on the upstream surface during the earthquake, which leads to washing down the upstream face and a bit of crest.

Nevertheless, the maximum Normalized Crest Relative Permanent Settlement (NCRPS) of the Santa Rita dam is 0.5%. According to Pells & Fell (2022) and Swaisgood (2014) studies, an NCRPS of less than 1% is considered as a minor damage level to the dam body. Furthermore, neither constitutive model has indicated a potential for liquefaction under the given seismic conditions, even in the case of PM4Sand/Silt with increased excess pore pressures.

Finally, the crest settlement in the numerical models has been compared with data from other case histories. The results highlight the remarkable preciousness of the PM4Sand/Silt model in predicting permanent deformations.

RÉSUMÉ

Dans ce rapport, une méthodologie pour l’analyse dynamique des barrages en remblai est présentée, avec un accent particulier sur la prédiction de la liquéfaction. Le barrage de Santa Rita en Colombie a été utilisé comme étude de cas. La méthodologie proposée implique la génération d’un modèle numérique bidimensionnel en utilisant la méthode des différences finies, la mise en œuvre de conditions aux limites statiques et dynamiques, un modèle d’amortissement, la préparation des accélérogrammes et la calibration du modèle constitutif des matériaux. La méthode traditionnelle de Mohr-Coulomb et le modèle avancé de PM4Sand/Silt sont comparés pour mettre en évidence les progrès des techniques d’analyse dynamique des barrages en remblai.

Les résultats montrent des déplacements plastiques et des pressions interstitielles considérablement plus importants dans le modèle PM4Sand/Silt que dans le modèle Mohr-Coulomb. De plus, les modes de déplacement sont différents dans les deux modèles. Le déplacement de la crête pour le modèle

Mohr-Coulomb est vers l'aval, tandis que le modèle PM4Sand/Silt est vers l'amont. Cela est dû à la génération d'un excès de pression interstitielle sur la surface amont pendant le séisme, ce qui entraîne le lessivage de la face amont et de la crête. Le tassement relatif permanent normalisé de la crête (NCRPS) maximum du barrage de Santa Rita est de 0,5 %. Selon les études de Pells & Fell (2022) et Swaisgood (2014), un NCRPS inférieur à 1 % est considéré comme un niveau de dommage mineur pour le corps du barrage. De plus, aucun des modèles constitutifs n'a indiqué un potentiel de liquéfaction dans les conditions sismiques données, même dans le cas du PM4Sand/Silt avec des pressions interstitielles excessives accrues. Enfin, le tassement de la crête dans les modèles numériques a été comparé aux données réelles. Les résultats mettent en évidence la remarquable précision du modèle PM4Sand/Silt dans la prédiction des déformations permanentes.

1. INTRODUCTION

Embankment dams, crucial components of global hydropower and water supply systems, account for 70-80% of all dams worldwide (the International Commission on Large Dams [1]). Their versatility in different site conditions and using locally sourced materials make them a preferred choice. However, they also account for most dam failures compared to other types of dams [1]. Earthquakes, a significant cause of these failures, often lead to a substantial decrease in soil stiffness and strength due to liquefaction. This underscores the need for expert engineering practices, including comprehensive dynamic analysis and advanced material constitutive models, to ensure their safety and reliability under cyclic loading conditions.

This study presents a methodology for the dynamic analysis of embankment dams. This methodology, which is illustrated in Fig. 1 and explained in detail in the following sections, includes:

(I) Generation of a 2-dimensional numerical model of the dam and foundation
(II) Application of static boundary conditions and static constitutive models
(III) Application of static loads, including self-weight of the dam and foundation (considering the construction process of the dam body), hydrostatic, and pore pressure loads
(IV) Controlling the static stability of the dam
(V) Selecting, scaling, and modifying (i.e., Deconvolution, Baseline Correction, and Filtering) the accelerograms
(VI) Changing static boundary conditions with the dynamic ones
(VII) Using a proper damping model reflecting the energy dissipation due to plastic deformations

(VIII) Choosing a proper constitutive model representing the cyclic response of the materials, excess pore pressure generation/dissipation mechanism (liquefaction phenomena)

(IX) Calibration of the constitutive model parameters according to the in-situ o laboratory data

(X) Controlling the dynamic results like horizontal and vertical displacements in upstream and downstream surfaces and the crown, minimum effective stresses, and maximum pore pressure contours in the whole model.

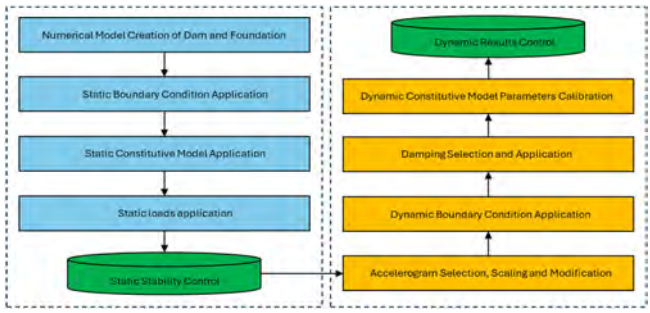

Fig. 1
Flowchart of static and dynamic numerical analysis of embankment dams

To achieve the goals of the article, the Santa Rita embankment dam is used as a case study. A 2-dimensional geometry of the dam is constructed using a finite difference numerical model, and the static stability of the earthdam is analyzed with the Mohr-Coulomb material model. In this step, the dam's construction process is also simulated. Subsequently, the model is adapted for dynamic analysis, involving preparing accelerograms, applying dynamic boundary conditions calibrating dynamic material parameters, including damping. To show the importance of using sophisticated material constitutive models in the dynamic analysis of embankment dams, especially those prone to liquefaction, first, results for the Mohr-Coulomb model are presented, and then the PM4Sand/Silt models are applied, and the results are compared.

2. LIQUEFACTION: FROM EMPIRICAL TO ADVANCED MODELS

Over recent decades, the methods for predicting the dynamic response of embankment dams have evolved from simple, practical approaches to more

sophisticated, expert constitutive models. Traditional methods such as Mohr-Coulomb, UBCTOT [2], Finn [3], and the Roth model [4] have been widely used for their simplicity and practicality. However, these methods are gradually being replaced by advanced models like PM4Sand [5], PM4Silt [6], and UBCSAND [7], which offer improved simulations of plastic deformations and liquefaction phenomena. Each method has strengths and limitations, making it crucial to understand their specific applications and constraints. This study compares the traditional Mohr-Coulomb method with the advanced PM4Sand/Silt method to highlight the progression in modeling techniques and their capacity to account for more complex phenomena.

The Mohr-Coulomb soil-model is a widely used constitutive relationship [8], [9], [10], [11]. It is a simple, linear, elastic-perfectly plastic model based on the Mohr-Coulomb failure criterion. However, it has significant limitations in the cyclic analysis of soils. First, the model lacks strain hardening/softening, which means it cannot simulate progressive changes in soil strength with increased deformation [8]. Second, it does not inherently include mechanisms to simulate excess pore pressure build up during cyclic loading. In practice, additional empirical methods are often used to estimate pore pressure changes. These simple methods are based on relating the excess pore pressures to changes in vertical stress or soil volume. For a 2-dimensional saturated media, the pore pressure can be approximated to half of the deviatoric stress defined by $q = \sigma_1 - \sigma_3$ [12].

In contrast to the Mohr-Coulomb model, PM4Sand/Silt is a bounding surface plasticity model, based on the critical state theory, developed specifically for sand and low-plasticity silts and clays subjected to earthquake loading [5], [6]. The capability of this model to simulate plastic deformations under cyclic loading and, consequently, pore pressure build up under undrained conditions makes it ideal for seismic response and liquefaction potential assessments. In PM4Sand/Silt, the shear modulus G is defined as a function of mean stress and the current stress ratio:

$$G = G_0 P_A \left(\frac{P}{P_A}\right)^{n_G} C_{SR} \tag{1}$$

where P_A is the atmospheric pressure and C_{SR} is a factor that accounts for the stress ratio history. In this formula, G_0 and n_G are constant parameters that need to be calibrated. In PM4Sand/Silt, the plastic deformations are controlled by stress ratio and can accumulate during repeated loading cycles. In an analysis, when the plastic volumetric strain increments are positive, contraction happens. The Contraction phenomena in undrained conditions (typical of fast loading cycles like earthquake loading) can produce high excess pore pressures, reducing effective stresses and loss of shear strength, ultimately resulting in liquefaction. In the PM4Sand/Silt models, the contraction is controlled by the contraction rate parameter hp0, another fundamental constant that requires calibration.

In engineering practice, it is essential to note that using highly complex models for liquefaction analysis is often unjustified due to the many uncertainties regarding model parameters and the numerous approximations required. This article proposes a methodology for calibrating PM4Sand/Silt to predict embankment dams' dynamic response and liquefaction potential, mainly when limited in situ or laboratory tests are available. The calibration strategy will be discussed in detail in section 7.

3. SANTA RITA DAM

The Santa Rita Dam is a compacted earth-fill dam in Antioquia, Colombia, constructed between 1967 and 1976 [13]. The reservoir of the dam has a total volume of 1,147.55 hm^3, which makes it the fourth-largest reservoir in the country (Fig. 2). The dam body is constructed of different materials with a maximum height of 59.5 m and a crest length of 360m (Fig. 3). A summary of the material properties is listed in Table 1.

Fig. 2
The Santa Rita Dam

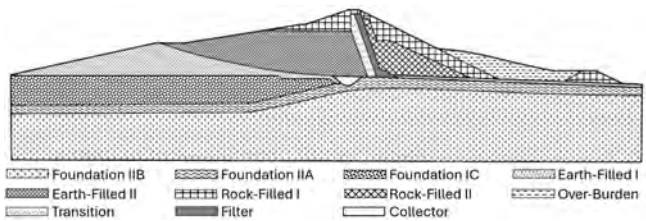

Fig. 3
Different materials used in the dam body of Santa Rita

Table 1

Material parameters of Santa Rita dam

ZONE	UNIT WEIGHT (KN/M^3)	ELASTIC MODULUS (MPA)		POISON RATIO	COHESION (KPA)	FRICTION ANGLE (°)	POROSITY
		STATIC	DYNAMIC				
Foundation IIB	25.0	127.8	Refer to Fig. 8	0.30	-	-	0.38
Foundation IIA	22.0	30.4		0.30	-	-	0.38
Foundation IC	18.8	12.8		0.33	15.0	30.0	0.35
Earth-Filled I	20.0	12.7		0.30	12.3	32.0	0.35
Earth-Filled II	20.0	13.0		0.31	12.5	34.0	0.37
Rock-Filled I	20.0	15.8		0.31	0.0	35.0	0.36
Rock-Filled II	21.0	20.0		0.30	0.0	35.0	0.38
Over-Burden	20.0	11.7		0.32	0.0	36.0	0.38
Transition	20.0	15.8		0.31	0.0	35.0	0.36
Filter	21.5	16.4		0.30	0.0	35.0	0.36
Collector	21.5	16.4		0.30	0.0	35.0	0.36

4. THE STATICAL NUMERICAL MODEL

Fig. 4 shows the 2-dimensional numerical model of Santa Rita dam in FLAC2D software, an explicit finite difference numerical program. The statical boundary conditions for the bottom of the model are fixed displacements in X and Y, while for the vertical boundaries, just the displacement in the X (horizontal) direction is limited.

The static loading is done in a step-by-step process; first, the foundation is analyzed under its self-weight and full pore water pressure. Then, the dam body layers will be added in 10 stages until the final elevation is 1891 m. At the end of each stage, the whole model will be statically run under the former loads and the self-weight of the new layers. In the end, the hydrostatic pressure and the groundwater surface will be defined. The groundwater surface (shown in the dashed line in Fig. 5(b)) is examined through a separate steady-state pore

pressure analysis and is calibrated by piezometric data. In this step, it is assumed that the maximum water level is 1887 m and the materials below the groundwater surface are fully saturated.

The constitutive models in the static analysis for the foundation and the dam body are linear-elastic and Mohr-Coulomb, respectively. Fig. 5 shows the contours of vertical displacement, pore pressure, and pore pressure ratio (pore pressure/ total vertical stress). According to Fig. 5(a), the maximum settlement is 1.3 m.

The pore pressure ratio, which may vary between 0 and 1, is crucial in recognizing the liquefiable areas. A pore pressure ratio of 0 indicates an effective stress equal to total vertical stress (zero pore pressure), while a value of 1 shows zero effective stress, which is the point of liquefaction. According to Fig. 5(c), except for the shallow areas on the upstream surface, the pore pressure ratio in the dam body is less than 0.65.

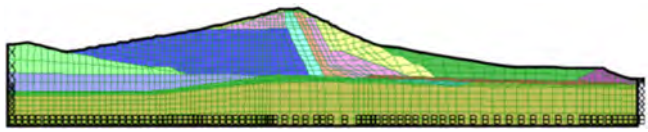

Fig. 4
The 2-dimensional numerical model of the Santa Rita dam

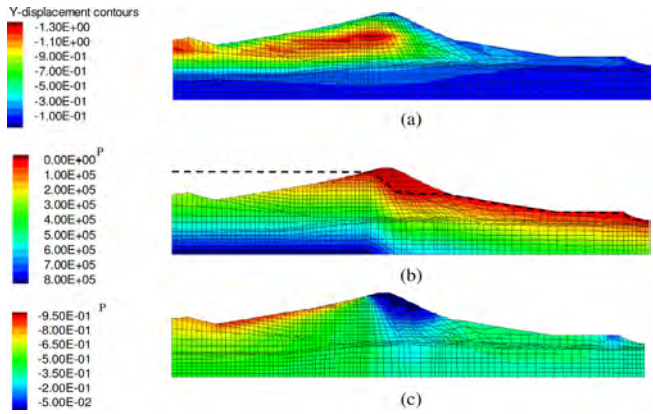

Fig. 5
The contours of a) vertical displacement in meters, b) pore pressure in Pascal. The dashed line is the water surface line, and c) pore pressure ratio (pore pressure/ total vertical stress)

5. ACCELEROGRAM PREPARATION

Fig. 6 shows the Design Response Spectrums (DRS) of the Santa Rita dam´s site for four different Return Periods (RP) of 475, 2500, 5000, and 10000 years, extracted from site hazard analysis. Each DRS is characterized by factors such as magnitude, epicentral distance, and ground shear wave velocity. These characteristics are the primary criteria for selecting accelerograms, i.e., the earthquake records that closely match the parameters outlined in the DRS will be selected. The NGA-West2 library, available on the PEER website, is used to find earthquake records with specific characteristics [14]. According to FEMA (2005) guidelines [16], three different accelerograms are selected for each DRS (Table 2).

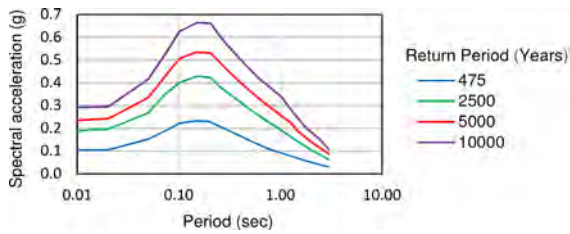

Fig. 6
Design response spectrums of the Santa Rita dam´s site

Table 2
The Selected Accelerograms for the probabilistic dynamic analysis of Santa Rita

RP[1]	RSN[2]	STATION	MAGNITUDE	EPICENTRAL DISTANCE (KM)	SHEAR WAVE VELOCITY (M/S)
475	68	San Fernando	6.61	22.77	316.46
	284	Irpinia_ Italy-01	6.9	9.55	476.62
	108	Oroville-02/Up & Down	4.79	12.65	377.25
2500	6	Imperial Valley-02	6.95	6.09	213.44
	985	Northridge-01	6.69	29.88	297.07
	148	Coyote Lake	5.74	7.42	349.85
5000	6	Imperial Valley-02	6.95	6.09	213.44
	8057	Christchurch	6.2	41.08	336.98
	15	Kern County	7.36	38.89	385.43
10000	139	Tabas_ Iran	7.35	13.94	471.53
	719	Superstition Hills	6.54	17.03	208.71
	1636	Manjil_ Iran	7.37	49.97	302.64

[1]Return Period
[2]Record Sequence Number

The next step involves scaling the Accelerations' Response Spectrum (ARS) to the DRS. To reach this objective, the Abrahamson scaling method [17] is employed. After the scaling process, three modifications are made to the accelerogram´s time histories: Deconvolution, Baseline Correction, and Filtering. Deconvolution analysis is necessary when the earthquake time histories are applied to the bottom of the foundation rather than to the bottom of the dam, and the density of the foundation is included in the dynamic solution. This process involves a reverse calculation to determine the depth motions that will accurately reproduce the objective ground motion when they reach the surface. The baseline correction is the second modification for removing the unrealistic residual displacements at the end of the time histories, which may be produced as a consequence of the scaling process. Last but not least, modification filters the unnecessary high frequencies of accelerograms' time history to achieve a coarser mesh requirement. The three mentioned modifications are done through iDATA software (*iPresas Deconvolution Analysis of Target Acceleration)*.

6. THE DYNAMIC BOUNDARY CONDITION AND DAMPING

In the numerical dynamic analysis, the free-field and viscous boundary conditions are used for the lateral and vertical boundaries, and the foundation's base, respectively. The damping mechanism of the dam-foundation system is simulated by Hysteretic damping because of its ability to capture energy dissipation resulting from material plasticity. This damping in the model is activated by defining the strain-dependent shear modulus, as illustrated in Fig. 7. A small amount of 0.2% stiffness-proportional Rayleigh damping is accompanied by Hysteric damping to provide the minimum energy dissipation at the beginning of the dynamic analysis, where plastic deformations are still low.

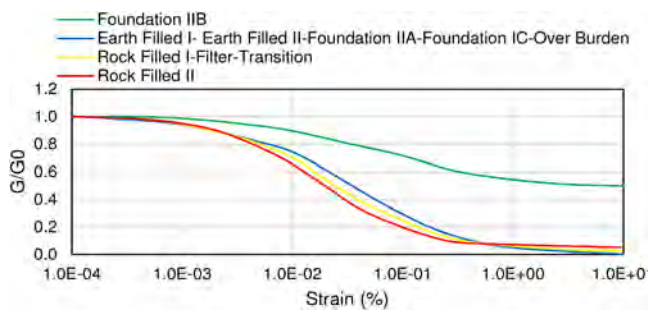

Fig. 7
Strain-dependent shear modulus used for Hysteric damping definition

7. CONSTITUTIVE MODELS PARAMETERS

In this article, to evaluate the importance of using advanced constitutive models in the dynamic analysis of embankment dams, the analysis will be done considering two cases: 1) Mohr-Coulomb and 2) the PM4Sand/Silt Constitutive model. For the former case, Earth-Filled I, Earth-Filled II, and Over-Burden zones are simulated by the PM4Silt model, and Filter and Collector zones are modeled by the PM4Sand model. The remaining zones will be kept with the Mohr-Coulomb criteria as they are mainly filled by coarse rock and, as a result, are unlikely to be liquefiable. For the Mohr-Coulomb models, the parameters listed in Table 1 and Fig. 8 are used.

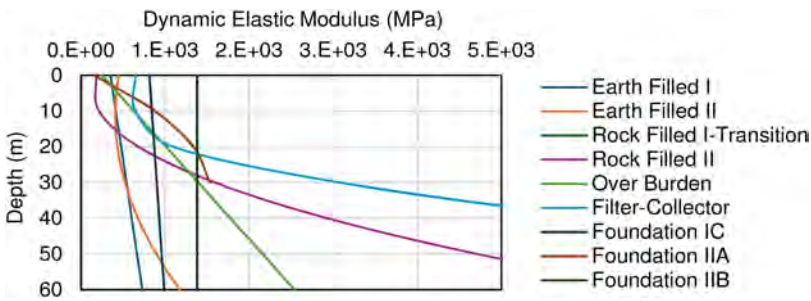

Fig. 8
Dynamic Elastic modulus for different zones of Santa Rita dam derived from the shear wave velocity test

In the PM4Sand/Silt model, the material parameters can be classified into two groups: 1) general parameters and 2) case-sensitive parameters. Usually, the default values proposed by the model´s developers can be used without modifications for the general parameters [5], [6]. It has been shown that the sensibility of the results to these parameters is neglectable [5], [6]. Conversely, the case-sensitive parameters should be chosen and calibrated carefully for each parameter. These parameters are listed in Table 3. The unit weight and porosity of different zones of the dam can be found in Table 1. The relative density, which shows the compressibility of soil, can be derived from the Standard Penetration Test (SPT) and with the help of an empirical formula expressed by:

$$D_r = 0.147\sqrt{(N_1)_{60}} \tag{2}$$

where $(N_1)_{60}$ is the corrected number of blows in SPT. However, the other four parameters need special effort for calibration. In Fig. 9, the strategy for the calibration of these parameters is shown. Su_{factor} is the first parameter that should be calibrated. This parameter can be calculated according to Fig. 10, where the Mohr-Coulomb shear strength ratio is calculated for a representative unit element located in the depth of Z in the dam body under undrained 2-dimensional confinement. This calculation, which is needed for the PM4Silt model, should be repeated for three representative points located in Earth-Filled I, Earth-Filled II, and Over-Burden zones. Su_{factor} calculated for these zones are listed in Table 5.

Table 3

The case-sensitive parameters of PM4Sand/Silt

PARAMETER	SYMBOL	SAND	SILT
Density	ρ_d	✓	✓
Porosity	n	✓	✓
Relative Density	D_r	✓	-
Shear Modulus Coefficient	G_0	✓	✓
Shear Modulus Power	n_g	0.5	✓
Shear Strength Ratio	Su_{factor}	-	✓
Contraction Rate	h_{p0}	✓	✓

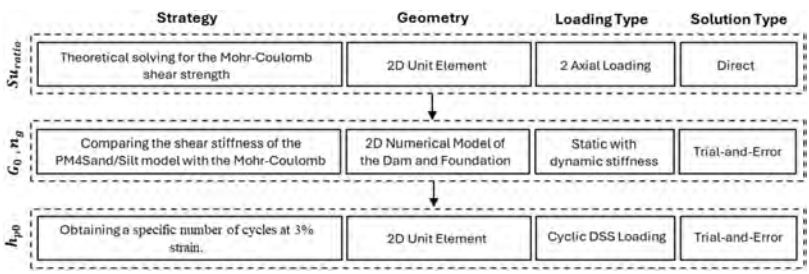

Fig. 9

The flowchart of PM4Sand/Silt parameters calibration

In the second step, G_0 and n_g should be calibrated. These two coefficients control the shear stiffness of the materials. It is worth mentioning that in PM4Sand, n_g is constantly 0.5 and does not need to be modified. A practical way to estimate these

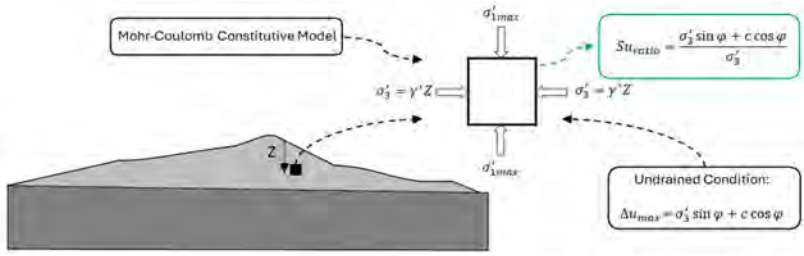

Fig. 10
The methodology for calculating Su_{factor}

two parameters for each material is by changing them in a trial-and-error process until the shear stiffness of the different zones in a dry model using PM4Sand/Silt and at the beginning of the dynamic analysis is equivalent to the shear stiffness in the Mohr-Coulomb model. This method also prepares a fair comparison between the two mentioned models. The final calibrated values are shown in Table 5.

Table 4
Criteria for calibration of h_{p0}

ZONE	CONSTITUTIVE MODEL	CRR	CRR/ Su_{factor}	OBJECTIVE STRAIN	OBJECTIVE NUMBER OF CYCLE	REF.
Earth-Filled I	PM4Silt	0.23	0.44	3%	100-120	[6]
Earth-Filled II	PM4Silt	0.21	0.43	3%	100-120	[6]
Over-Burden	PM4Silt	0.25	0.53	3%	30-100	[6]
Filter	PM4Sand	0.18	-	3%	15	[5]
Collector	PM4Sand	0.18	-	3%	15	[5]

Table 5
Final calibrated parameters of PM4Sand/Silt model for Santa Rita dam

ZONE	CONSTITUTIVE MODEL	Su_{factor}	G_0	n_g	h_{p0}
Earth-Filled I	PM4Silt	0.52	1100	0.5	7
Earth-Filled II	PM4Silt	0.49	792	0.75	30
Over-Burden	PM4Silt	0.47	1800	0.75	15
Filter	PM4Sand	-	700	0.5	1.3
Collector	PM4Sand	-	1350	0.5	0.45

The last and most challenging parameter is h_{p0}. This parameter can be calibrated by numerical simulation of a cyclic Direct Simple Shear (DSS) test on a unit element. In this approach, a unit element with a constitutive model of PM4Sand/Silt and confined by the in-situ stress (similar to Fig. 10) is analyzed under a cyclic horizontal strain with a constant rate of 0.05. In this analysis, the maximum loading value for each cycle is limited to the Cyclic Resistance Ratio (CRR). CRR can be calculated based on the cyclic strength correlations by Boulanger and Idriss (2007) and Dahl (2011). In this method, the value of h_{p0} is changed in a trial-and-error to obtain a specific number of cycles (Table) at 3% strain as recommended in [6].

8. DYNAMIC ANALYSIS RESULTS

Some studies have shown that the damage level of an embankment dam can be predicted by monitoring its Normalized Crest Relative Permanent Settlement (NCRPS) [18], [19], [20]. Fig. 11 shows the NCRPS (normalized to the dam height and relative to the dam's base settlement) and crest absolute settlement of Santa Rita dam for Mohr-Coulomb and the PM4Sand/Silt models. As shown in the figure, both NCRPS and absolute settlement are more in PM4Sand/Silt than in the Mohr-Coulomb model. Furthermore, the settlement differences between these two models increase with the PGA value, reaching 0.45% differences in NCRPS for a PGA = 0.32. The maximum NCRPS of the Santa Rita dam is 0.5%. According to Pells & Fell (2002) and Swaisgood (2014) studies, an NCRPS of less than 1% is considered as a minor damage level to the dam body [21], [22].

In Fig. 12, the NCRPS of Santa Rita dam for both PM4Sand/Silt and Mohr-Coulomb is compared with the earthquake-induced settlement of 82 embankment dams around the world gathered by [22]. It is seen that the PM4Sand/Silt model likely reflects the cyclic response of embankment dams more precisely than the Mohr-Coulomb model. The crest horizontal permanent displacement of Santa Rita dam for the models Mohr-Coulomb and PM4Sand/Silt are compared in Fig. 13. As seen from this figure, in the Mohr-Coulomb model, the crest is displaced toward the downstream (positive values), while the displacement in the PM4Sand/Silt model is toward the upstream (negative values).

This different reaction to the seismic loads can be associated with the increased excess pore pressure in the dam upstream surface simulated by the PM4Sand/Silt model. To highlight that, the contours of excess pore pressure for the input earthquake of RP10000-RSN1636 and at the end of the dynamic analysis are shown in Fig. 14. According to this figure, the maximum excess pore pressure in the Mohr-Coulomb and PM4Sand/Silt model is 50 and 100 kPa, respectively. Also, it

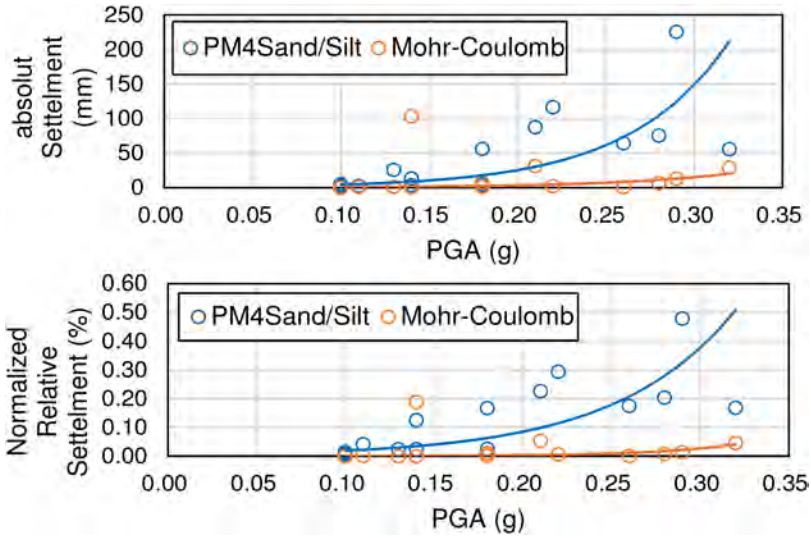

Fig. 11
Comparison of crest permanent settlement of Santa Rita dam with Mohr-Coulomb and PM4Sand/Silt model

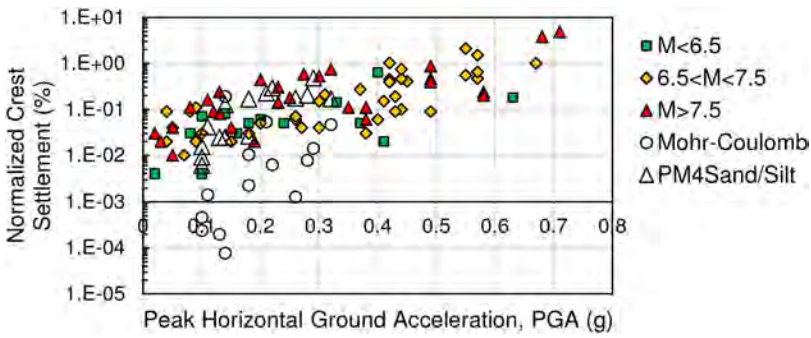

Fig. 12
Comparison of NCRPS of Santa Rita dam in Mohr-Coulomb and PM4Sand/Silt model, and with the earthquake-induced settlement of 82 embankment dams around the world gathered by [22]

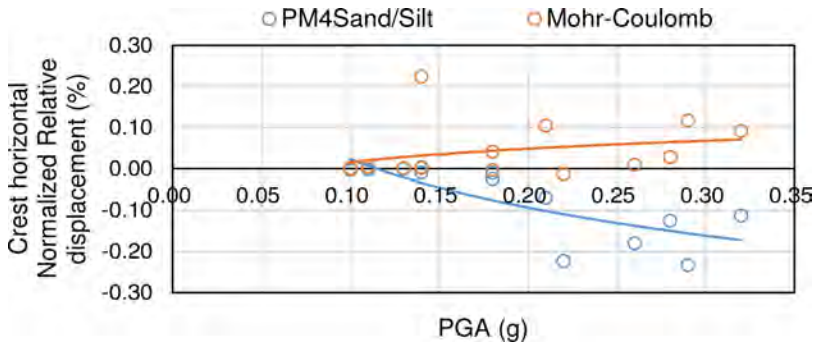

Fig. 13
Comparison of crest horizontal permanent displacement of Santa Rita dam with Mohr-Coulomb and PM4Sand/Silt model

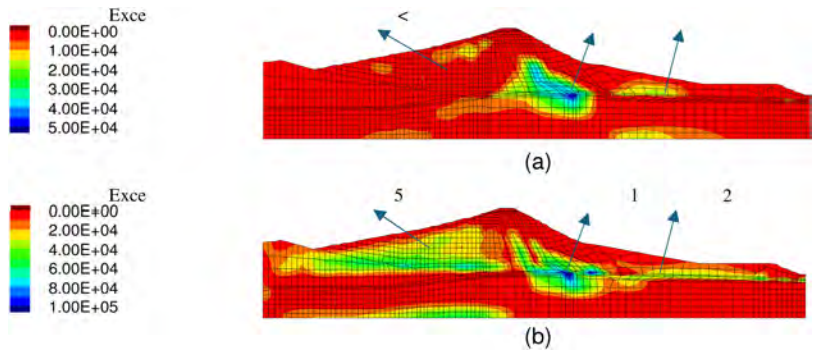

Fig. 14
Comparison of excess pore pressure of Santa Rita dam with Mohr-Coulomb and PM4Sand/Silt model at the end of dynamic analysis with RP10000, RSN1636

can be seen that the excess pore pressure in the upstream section of the dam (zones Earth-filled I and II) for the PM4Sand/Silt model is considerably more than in the Mohr-Coulomb model, which is the reason for the crest upstream displacement. However, the contours of the maximum excess pore pressure ratio (the ratio of excess pore pressure to the total vertical stress) show no liquifiable area, even when the PM4Sand/Silt model is applied (Fig. 15). The maximum excess pore pressure ratio in the Santa Rita dam is 0.35, which, in addition to the static pore pressure ratio of 0.5 in this zone (Over-Burden), is still below the liquefaction limit of 1.

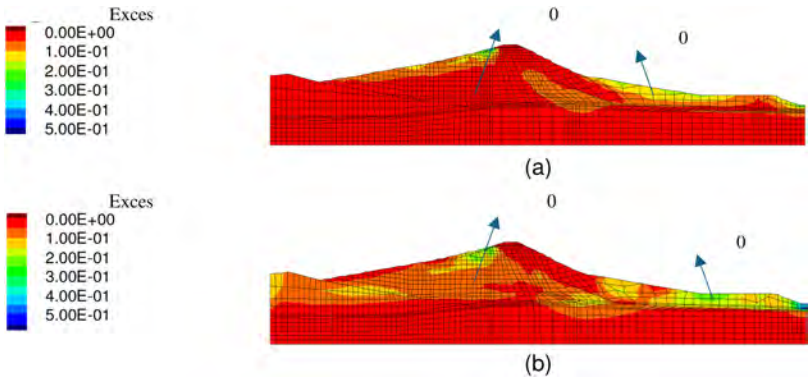

Fig. 15
Comparison of maximum excess pore pressure ratio of Santa Rita dam with Mohr-Coulomb and PM4Sand/Silt model during the dynamic analysis with RP10000, RSN1636

REFERENCES

[1] ICOLD, “Incident database, Bulletin 99 update: Statistical analysis of dam failures,” 2019.

[2] T. D. STARK *ET AL.*, “Seismic deformation analysis of tuttle Creek dam,” *Canadian Geotechnical Journal*, vol. 49, no. 3, pp. 323–343, 2012.

[3] J.-C. CHOU, H.-T. YANG, AND D.-G. LIN, “Calibration of finn model and ubcsand model for simplified liquefaction analysis procedures,” *Applied Sciences*, vol. 11, no. 11, p. 5283, 2021.

[4] E. M. DAWSON, W. H. ROTH, S. NESARAJAH, G. BUREAU, AND C. A. DAVIS, “A practice oriented pore-pressure generation model,” in *FLAC and Numerical Modeling in Geomechanics-2001*, CRC Press, 2020, pp. 47–54.

[5] R. W. BOULANGER AND K. ZIOTOPOULOU, “PM4Sand (Version 3): A sand plasticity model for earthquake engineering applications,” *Center for Geotechnical Modeling Report No. UCD/CGM-15/01, Department of Civil and Environmental Engineering, University of California, Davis, Calif*, 2015.

[6] R. W. BOULANGER AND K. ZIOTOPOULOU, “PM4Silt (Version 1): A silt plasticity model for earthquake engineering applications,” *Report No. UCD/CGM-18/01, Center for Geotechnical Modeling, Department of Civil and Environmental Engineering, University of California, Davis, CA, 108 pp.*, 2018.

[7] M. H. BEATY AND P. M. BYRNE, “UBCSAND constitutive model version 904aR,” *Itasca UDM Web Site*, vol. 69, no. 3, 2011.

[8] A. H. BHUTTO *ET AL.*, “Mohr-Coulomb and hardening soil model comparison of the settlement of an embankment dam,” *Engineering, Technology & Applied Science Research*, vol. 9, no. 5, pp. 4654–4658, 2019.

[9] D. RAKIĆ, M. ŽIVKOVIĆ, S. VULOVIĆ, D. DIVAC, R. SLAVKOVIĆ, AND N. MILIVOJEVIĆ, “Embankment dam stability analysis using FEM,” in *3rd South-East European Conference on Computacional Mechanics*, 2013, pp. 12–14.

[10] P. VAHDATI, S. LEVASSEUR, H. MATTSSON, AND S. KNUTSSON, “Inverse Mohr-Coulomb soil parameter identification of an earth and rockfill dam by genetic algorithm optimization,” *The Electronic journal of geotechnical engineering*, vol. 18, no. X, pp. 5419–5440, 2013.

[11] J. SADREKARIMI AND M. KIA, “Performance of a large dam, field measurements and analytical approach,” in *Proceedings of the 16th International Conference on Soil Mechanics and Geotechnical Engineering*, IOS Press, 2005, pp. 1115–1118.

[12] S. HANSBO, “Experience of consolidation process from test areas with and without vertical drains,” in *Elsevier Geo-Engineering Book Series*, vol. 3, Elsevier, 2005, pp. 3–49.

[13] EPM, “Información técnica de soporte de la presa Santa Rita,” 2021.

[14] PEER, “PEER NGA West2 Database,” University of California, Berkeley. [Online]. Available: http://peer.berkeley.edu/ngawest2/

[15] P. FEMA, “Federal Guidelines for Dam Safety, Earthquake Analyses and Design of Dams,” 2005, *FEMA Washington, DC*.

[16] P. FEMA, “Federal Guidelines for Dam Safety, Earthquake Analyses and Design of Dams,” 2005, *FEMA Washington, DC*.

[17] L. AL ATIK AND N. ABRAHAMSON, “An improved method for nonstationary spectral matching,” *Earthquake spectra*, vol. 26, no. 3, pp. 601–617, 2010.

[18] R. FELL, D. S. BOWLES, L. R. ANDERSON, AND G. BELL, “The status of methods for estimation of the probability of failure of dams for use in quantitative risk assessment,” in *Transactions of the International Congress on Large Dams*, 2000, pp. 213–236.

[19] J. R. SWAISGOOD, “Seismically-induced deformation of embankment dams,” in *Proc. US National Conference on Earthquake Engineering*, 1998.

[20] J. HE AND E. M. RATHJE, “Seismic capacity models for earth dams and their use in developing fragility curves,” *Earthquake Spectra*, p. 87552930241243070, 2024.

[21] S. PELLS AND R. FELL, *Damage and cracking of embankment dams by earthquakes and the implications for internal erosion and piping*. University of New South Wales, School of Civil and Environmental Engineering, 2002.

[22] J. R. SWAISGOOD, “Behavior of embankment dams during earthquake,” *Journal of Dam Safety*, pp. 35–44, 2014.

Q.111 - R.5

COMMISSION INTERNATIONALE DES
GRANDS BARRAGES

VINGT-HUITIEME CONGRES DES
GRANDS BARRAGES
CHENGDU, MAI 2025

MONITORING AND INTERPRETATION OF THE DYNAMIC BEHAVIOR OF CONCRETE DAMS (*)

Jorge Pereira GOMES & José V. LEMOS
LNEC, National Laboratory for Civil Engineering, Lisbon

Sérgio PEREIRA & Álvaro CUNHA
Construct-ViBest, Faculty of Engineering (FEUP), University of Porto

PORTUGAL

SUMMARY

Evaluating the dynamic response of works and monitoring the evolution of their behaviour during the different phases of their life are very important and form part of structural safety monitoring activities.

In recent years, systems have been implemented to monitor the dynamic behaviour of several recent concrete dams and forced vibration tests have also been carried out to determine their modal parameters at the end of construction. Numerical models were developed for each dam, incorporating the dam-foundation-dam set and calibrated with experimental results. This communication presents some results of the numerical models developed for various levels of the reservoir, comparing them with monitoring during normal operation and the occurrence of seismic events.

The combination of numerical models and observed results of the behaviour of dams is a fundamental tool for supporting the safety control of large construction projects.

**Auscultation et interprépation du comportement sismique des barrages en béton*

 DOI: 10.1201/9781003642428-108

RÉSUMÉ

L'évaluation de la réponse dynamique des ouvrages et le suivi de l'évolution de leur comportement au cours des différentes phases de leur vie sont très importants et font partie des activités de contrôle de la sécurité structurelle.

Ces dernières années, des systèmes ont été mis en place pour observer le comportement dynamique de plusieurs barrages récents en béton, et des essais de vibration forcée ont également été réalisés pour déterminer leurs paramètres modaux à la fin de la construction. Des modèles numériques intégrant l'ensemble barrage-fondation-barrage ont été développés pour chaque barrage et calibrés avec les résultats expérimentaux. Cette communication présente quelques résultats des modèles numériques développés pour différents niveaux du réservoir, en les comparant avec la surveillance pendant l'exploitation normale et l'occurrence d'événements sismiques, montrant une bonne concordance.

La combinaison des modèles numériques et des résultats observés du comportement des ouvrages est un outil fondamental pour soutenir le contrôle de la sécurité des grands ouvrages.

1. INTRODUCTION

Monitoring the behavior of structures whose operation involves significant risks is essential to detect anomalies and intervene promptly to prevent any structural accidents. Periodic evaluation of the dynamic behavior of structures is an important tool because it allows the detection of corresponding structural modifications over that period based on changes in dynamic behavior. These changes can pertain solely to the evolution of the mechanical characteristics of the material (favorable or unfavorable), variability of actions, or significant structural changes, particularly related to cracking. For implementing this methodology, it is useful to determine the dynamic behavior of the structures for reference states and, from that point on, monitor its evolution. Over the past years, techniques for conducting forced vibration tests on concrete dams and other structures have been developed at LNEC to characterize their dynamic behavior. These testing methodologies are part of a continuous evolution process, with considerable improvements implemented over time, particularly in the control of dynamic actions applied to the dam, the reliability of the records obtained concerning structural behavior, and their processing to identify the structure's dynamic parameters.

In recently constructed dams, systems that allow monitoring the dam's dynamic behavior over time have been implemented. These systems can be divided into two types: (i) seismic monitoring systems (SMS) that allow recording the action

imposed on the structure and the corresponding structural response during seismic events, and (ii) continuous dynamic monitoring systems (CDMS) that, based on dynamic response records due to ambient actions (noise, traffic, wind, plant operation, etc.), can determine dynamic parameters and verify possible behavior changes over time. To support the structural safety assessment of the dam, numerical models representing the dam-reservoir-foundation system were developed and calibrated with experimental results. The models incorporate the discretization of the reservoir to simulate the water effect without resorting to numerical simplifications, such as the consideration of the Westergaard's added mass method, frequently used in modeling the dynamic behavior of concrete dams, which overestimates the water effect, requiring correction by a coefficient without any objective criterion for its selection. The developed numerical models eliminate this subjective factor since they incorporate the geometric discretization of the reservoir, water behavior, and water-dam interaction. The reservoir uses a macro-element technique with mixed discretization for its representation, already validated through comparisons with analytical solutions. Determining the dynamic response of structures and monitoring the evolution of their behavior over various lifetime stages is fundamental and is part of the structural safety control activities. The combination of experimental and numerical methods is an indispensable tool for supporting the safety assessment of structures. This communication describes the methodology applied in evaluating the dynamic behavior of dams, which includes forced vibration tests, the monitoring systems implemented in the dams, and the numerical models developed for behavior interpretation. The numerical results are compared with the experimental ones, showing excellent agreement.

2. DYNAMIC BEHAVIOR MONITORING

2.1. General aspects

Dynamic behavior monitoring of concrete dams over time is part of the safety control activities for these structures. The methodology implemented at LNEC starts with determining the modal parameters of the structures, preferably at the end of construction or a certain operational phase, considering this as the reference situation, and later evaluating its evolution over time, checking for any changes that may indicate damage to the dam. The reference situation is obtained at the end of construction by performing two tests: one with the reservoir empty and the other when it reaches full storage level during the first filling of the reservoir. Monitoring the dynamic behavior over time is carried out using records obtained from continuous dynamic monitoring systems (CDMS) and seismic monitoring systems (SMS). The following sections briefly describe the methodology used in forced vibration tests and the configurations of the dynamic monitoring systems recently implemented.

2.2. Forced vibration tests

Forced vibration testing consists in the application to the structure of a load with a perfectly known sinusoidal variation. This action usually causes a forced vibration movement with the same frequency as the one of the applied loads (but out of phase) and with amplitudes that, apart from the load intensity, depend on the applied frequency and on the natural frequencies of the structure. For applying the dynamic action to the structures, an eccentric mass vibrator was developed at LNEC, which has been improved and automated over time. One of the major problems associated with the identification of the structural dynamic response involves the level of measured values, which should allow the identification in the records of the component related with the structural dynamic response. The forced vibration test presents advantages comparatively with other techniques, because, on the one hand, it increases the measured values of the dynamic response (hence ensuring a greater reliability of results), and, on the other hand, it overrides other noise sources “forcing” the structure to respond only to the imposed excitation. The natural frequencies are associated with well-defined vibratory structural movements. Recently, the continuous frequency sweep methodology was applied, replacing the traditional discrete frequency sweep, with excellent results. This methodology consists in the application to the structure of a sinusoidal dynamic action, by continuously varying the frequency between two previously defined values (initial and final frequency, Fig. 1). This procedure was validated against the results obtained by the previous methodologies. Moreover, an extremely relevant and conditioning factor of results is the velocity of variation in the frequency imposed to the structure during testing. The test must be slowly performed so that the whole structure will be able to respond within the same frequency. The determination of the structural dynamic response is achieved by the calculation of FRF (Frequency Response Function), between series recorded in the sensors installed on the body of the dam, and by the record of the load generated by the vibrator and applied to the structure. The natural frequencies of the structure are expected to be close to the maximum FRF values occurring in the frequency interval in which the structure was subject to excitation and which correspond to vibration shapes of the dam. The continuous sine sweep methodology is sometimes used in shaking table tests to determine the dynamic parameters of the physical models [1] and is a powerful way to achieve good results. In some cases, the evaluation of the dynamic behavior of the specimens is made with the application of white noise, but this procedure is not viable in real structures.

Hence, a good characterization of the movement during the forced vibration test, by properly positioning the measuring equipment, conjugated with a numerical model, will provide valuable information about the structural behavior. The calibrated numerical model can later be used to determine the structure’s response to other dynamic actions, particularly seismic actions. However, the force intensity applied during the forced vibration test should not cause damage to the structure. When the calibrated mathematical model during the test is used to assess the structure’s response to actions that cause high stress levels, its structural parameters should be suitably adapted.

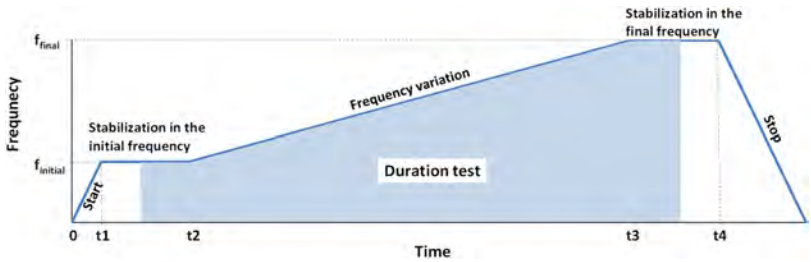

Fig. 1
Methodology used to frequency variation in the forced vibration test by continuous frequency scanning (sine sweep)
Méthodologie utilisée pour la variation de fréquence dans les essais de vibrations forcées par balayage de fréquence continu (balayage sinusoïdal)

2.3. Continuous dynamic monitoring systems (CDMS)

The purpose of continuous monitoring systems for the dynamic behavior of dams is to measure vibrations at various points on the dam body, in auxiliary structures, and potentially at the foundation level, for different types of excitation. Based on the accelerations measured under ambient/operational/exceptional excitation, it is possible to automatically identify the modal parameters of the dam-foundation-reservoir system (natural frequencies, modal configurations, and modal damping's) throughout the structure's life. Due to the high stiffness of dams, the structure's response to environmental actions is reduced. Therefore, uniaxial accelerometers are typically installed in the radial direction (the direction with the greatest movement amplitude). The distribution of sensors across the structure should be done to evaluate modal configurations, placing them in locations with higher amplitudes to increase measurement reliability. Hence, it is natural to place sensors only in the upper galleries, as for lower levels, the values observed for environmental actions are of the same order of magnitude as the equipment noise and thus insignificant. The system is usually configured to record time series of accelerations lasting 30/60 minutes from all instrumented points. The duration is defined according to the amplitudes of the recorded signals and the techniques used in their processing, which can be adjusted if necessary. For each record, automatic processing is performed to determine the modal parameters, allowing up to 48/24 daily values for each parameter. The central system, consisting of a computer, manages and stores the records. Automatic record processing can be performed on the system's central unit or a remote computer that receives the data and processes it. This task division can be beneficial for the system's reliability and longevity.

In these systems, “output-only” modal identification methods are used due to the unknown excitation imposed on the structure. The most used methods include Frequency-Domain Decomposition (FDD), Enhanced Frequency-Domain Decomposition (EFDD), Covariance driven Stochastic Subspace Identification (SSI–Cov), and poly-Least Squares Complex Frequency Domain (p-LSCF). LNEC has partnered with ViBest from FEUP in developing methodologies for automatic modal identification applied to concrete dams in this area [2][3][4]. Along this research line, methodologies are being developed and tested for the automatic detection of structural behavior changes and identifying the area and damage associated with said modification. As an example of this type of system, the description of the one implemented at the Baixo Sabor dam is presented. The continuous dynamic monitoring system implemented at the dam consists of three subsystems connected by optical fiber, totaling 20 uniaxial accelerometers installed in the radial direction (Fig. 2). Each subsystem has a digitizer that later sends the information to an Intel® NUC (Next Unit of Computing) compact computer. To ensure good synchronization of the data recorded by all digitizers, a GPS (Global Positioning System) antenna was installed in each subsystem. Additionally, the NUC computer is connected to the fiber optic network between the dam and the plant, allowing remote access. All-time records are automatically transmitted via a dedicated VPN (Virtual Private Network) connection to LNEC and FEUP facilities, where they are subsequently processed and analyzed.

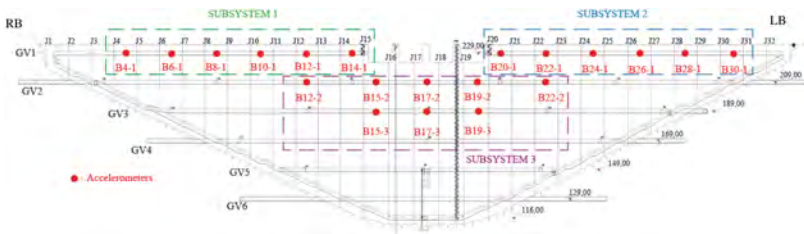

Fig. 2
Position of measuring points and subsystem components of Baixo Sabor continuous dynamic monitoring system
Position des points de mesure et des composants du sous-système du système de surveillance dynamique continue de Baixo Sabor

2.4. Seismic monitoring systems (SMS)

According to the Portuguese dam safety regulations, it is necessary to install a Seismic Monitoring System (SMS) to monitor the dynamic response of the structure during seismic events. Consequently, this type of system has been installed in recently constructed dams. The SMS aims to analyze the dynamic behavior of dams under seismic actions. For this purpose, active systems are used, which are permanently operational to ensure the measurement and recording of the structure's response during earthquakes. Additionally, these systems facilitate the accurate characterization of the dynamic action applied to the dam and, when deemed useful, the propagation in the soil along the reservoir. Given the importance of the structure and the area where it is located, two types of SMS have been defined:

1. Installation of sensors on the dam alone, to observe the dynamic behavior of the structure and characterize the seismic action imposed by the foundation.
2. Installation as indicated in the previous point, plus remote stations along the reservoir to determine the characteristics of the seismic event (location, magnitude, moment, etc.).

These systems must be on constant "alert" so that when a seismic event occurs, they can activate the automatic mechanisms for collecting, storing, and transmitting information. When a pre-established acceleration level is exceeded at any measurement point, the system should automatically collect records from the entire network of stations. Each monitoring point consists of a tri-axial accelerometer with local digitization and recording, for subsequent transmission to the central system. The records from the SMS are stored in the computer integrated into the central unit, and it is crucial to develop applications for the remote management and exploration of the system, automatic processing of records related to the structural response, and integration with the dam monitoring database. As an example of such a system, the description of the implementation at the Baixo Sabor Hydroelectric scheme is presented, which includes the Baixo Sabor and Feiticeiro dams. A seismic monitoring system was installed to measure and record the structures' response during seismic events. This system also allows for the characterization of the actions and their propagation in the rock mass, comprising three subsystems with the following general composition:

- External subsystem: 6 remote stations, installed directly in the rock mass, along the reservoir (Fig. 3).
- Upstream subsystem: 6 interior stations, installed in the Baixo Sabor dam (Fig. 4).
- Downstream subsystem: 2 interior stations, in the Feiticeiro dam.

Fig. 3
General layout with the location of remote seismic stations and internal subsystems of the Baixo Sabor hydroelectric scheme
Schéma général avec l'emplacement des stations sismiques à distance et des sous-systèmes internes de l'aménagement hydroélectrique de Baixo Sabor

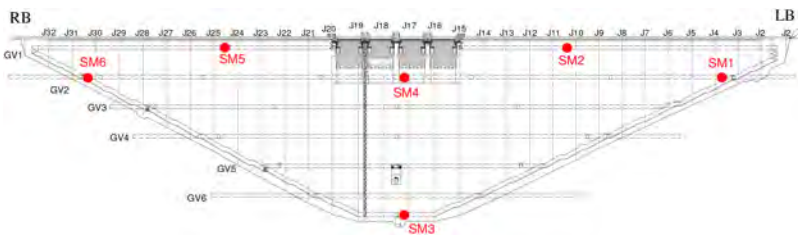

Fig. 4
Location of seismometers in the upstream subsystem at the Baixo Sabor dam
Localisation des sismomètres dans le sous-système amont du barrage de Baixo Sabor

Figure 5 shows an aspect of the remote stations and the installation inside the dams.

Fig. 5
Views of the seismic stations: a) remotely installed directly in the rock mass; and b) inside the dams
Vues des stations sismiques: a) installées à distance directement dans la masse rocheuse ; et b) à l'intérieur des barrages

2.5. Final remarks

Dynamic monitoring of the behavior of concrete dams allows us to support the assessment of the safety of works in an expeditious and global way. Dynamic behavior observation systems have been implemented in all new dams recently built. Table 1 shows the systems installed in Portuguese dams, as well as the forced vibration tests carried out. The forced vibration tests are carried out for two situations, the first with an empty reservoir and the second when the full storage level is reached, during the first filling of the reservoir. In this way, it is possible to determine the dam's behavior for two reference situations and check the overall quality of the work. LNEC was responsible for carrying out the forced vibration tests and defining and configuring the dynamic observation systems, and currently manages and operates these systems.

Table 1
Dams in Portugal with seismic monitoring systems (SMS), continuous dynamic monitoring systems (CDMS) and forced vibration tests performed (FVT)

DAM	YEAR OF CONSTRUCTION	TYPE	MAXIMUM HEIGHT (M)	OWNER	FVT	SMS		CDMS
						TYPE 1	TYPE 2	
Alqueva	2002	Arch	96.0	EDIA	2		X	-
Alto Ceira II	2014	Arch	41.0	EDP	2	X		-
Alto Tâmega	2023	Arch	106.5	Iberdrola	2	X		-
Baixo Sabor	2015	Arch	123.0	Engie	2		X	X
Cabril	1954	Arch	136.0	EDP	2			X

(Continued)

Table 1
Continued

DAM	YEAR OF CONSTRUCTION	TYPE	MAXIMUM HEIGHT (M)	OWNER	FVT	SMS		CDMS
						TYPE 1	TYPE 2	
Daivões	2020	Gravity-Arch	77.5	Iberdrola	2	X		-
Feiticeiro	2015	Gravity	45.0	Engie	-		X	-
Foz Tua	2017	Arch	108.0	Engie	2		X	X
Ribeiradio	2015	Gravity-Arch	83.0	EDP	-	X		-

SMS:
- Type 1 – Accelerometers only on the dam
- Type 2 – Accelerometers on the dam and along the reservoir

3. NUMERICAL MODELS FOR BEHAVIOR INTERPRETATION

3.1. General aspects

To monitor the evolution of the dynamic behavior of concrete dams, numerical models are developed with the modeling of the dam-foundation-reservoir system. The model was built with the code 3DEC [5], a discrete element code widely used in the field of rock mechanics. This code has been extensively used in the safety assessment of concrete dams, given its ability to take into consideration the failure modes through a jointed rock foundation, under static or dynamic loads. In the various models developed in the present work, the discontinuities related to the dam's contraction joints, the dam-foundation joint, and the dam-reservoir interface are represented, while the rock mass is assumed to be an equivalent continuum. The models incorporate the discretization of the reservoir to simulate the effect of water without resorting to numerical simplifications, such as the Westergaard added masses method [6], which is often used in modeling the dynamic behavior of concrete dams. It is recognized that in arch dams, the Westergaard added masses overestimate the mass value that should be added to the nodal points of the dam's upstream face [7][8]. Due to this, it is usually necessary to scale the associated masses with a factor that can vary between 0.5 and 1.0, with no objective criterion for its selection. The developed numerical models eliminate this subjective factor by incorporating the geometric discretization of the reservoir and the behavior of the water. The models are initially calibrated with the results of forced vibration tests, considering a linear elastic behavior of the dam's concrete. This is because the level of vibrations imposed on

the structure is low, not inducing high stresses for which non-linear material behavior would need to be considered. However, the constitutive model of the contraction joints allows for the consideration of non-linear structural behavior in case the joints become open.

3.2. Modeling of hydrodynamic interaction with the 3DEC program

The explicit representation of the reservoir requires the inclusion of elements in the calculation mesh that adequately simulate the dynamic behavior of the fluid and its interaction with the dam and the foundation rock mass, as well as the application of appropriate dynamic boundary conditions. The standard deformable blocks in 3DEC are discretized into first-degree tetrahedrons, used for representing the rock mass, and into 20-node finite elements, used for discretizing the arch. These standard elements cannot simulate the behavior of a fluid, which is treated as an elastic material with zero shear modulus, as they generate spurious deformation modes without physical meaning. To avoid this problem, 3DEC employs a numerical technique known as mixed discretization, as described by Cundall. This technique essentially replaces the volumetric strain in an element with the average of the volumetric strains in a set of adjacent elements, which are assumed to have the same volumetric strain and, consequently, the same pressure [9]. In 3DEC, there are two types of mixed discretization: one based on parallelepiped macro-elements and another that can be applied to an arbitrary tetrahedral mesh. In this case, the first option was adopted, with the reservoir being divided into a mesh of 8-node blocks (or macro-elements) bonded together to simulate a continuous medium. To obtain a symmetrically responding parallelepiped, two layers of 5 tetrahedrons each are superimposed, averaging their stiffnesses and stresses. The mixed discretization technique is applied separately to each layer, taking an equal volumetric strain as the average of the 5 tetrahedrons. The use of macro-elements with mixed discretization for representing the reservoir was tested by comparing it with the analytical solution developed by Westergaard, which accurately simulates the hydrodynamic interaction for the case of a rigid dam with a vertical face subjected to uniform acceleration [10]. These tests demonstrated that the formulation approximates well the known parabolic pressure distribution diagram exerted by the fluid on the dam. The dam-reservoir interface is represented by an elastic joint with zero tangential stiffness, considering only normal stresses on the upstream face. Similarly, an interface of the same type was introduced at the base of the reservoir. The zero tangential stiffness of the joint allows the fluid to slide over the rock mass without generating shear stresses. At the far end of the reservoir, boundary conditions are introduced to simulate the radiation of energy to the part of the reservoir not included in the model, using a formulation of viscous boundaries typically employed in 3DEC for this purpose.

3.3. Developed models

The reservoir modeling using this new approach has already been applied to interpret the results of the forced vibration tests conducted on the Baixo Sabor [11] (Fig. 6a,b) and Foz Tua dams [12](Fig. 6c,d) dams, where very satisfactory results were obtained. In addition to these dams, similar numerical models have been developed for all projects where forced vibration tests were performed. However, since the projects belong to different owners, this joint methodology is exemplified using the Baixo Sabor and Foz Tua dams.

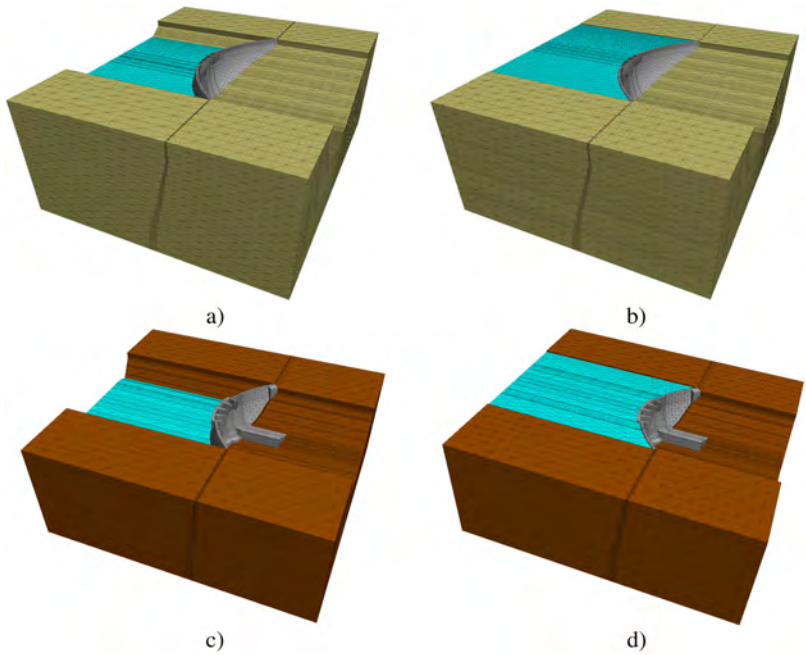

Fig. 6
Numerical models, Baixo Sabor: a) reservoir level a 195,5 m; b) reservoir level a 234,0 m; Foz Tua: c) reservoir level a 123,0 m; and d) reservoir level a 168,9 m
Modèles numériques, Baixo Sabor: a) niveau du réservoir a 195,5 m; b) niveau du réservoir a 234,0 m; Foz Tua: c) niveau du réservoir a 123,0 m; et d) niveau du réservoir a 168,9 m

4. COMPARISON OF RESULTS

4.1. Forced vibration tests

Table 2 show the experimentally determined natural frequencies based on the results of the forced vibration tests, the natural frequencies calculated using the numerical models and the differences between the two methodologies for the Baixo Sabor and Foz Tua dams. Checking the correspondence between the experimental and numerical modes can initially be done by visually comparing the modal configurations, which gives a direct idea of the correlation between the shapes of the vibration modes. However, modal configurations are generally quite complex, which is why it is advisable to use the MACij (Modal Assurance Criterion) coefficient matrix [13]. There was excellent agreement between the experimental values and the numerical values, with a maximum difference of 1.33% for Baixo Sabor and 7.43% for Foz Tua, and it can be concluded that the numerical models developed reproduce the site conditions when the tests were carried out. For Foz Tua, the average difference was around 2.33%, which is an acceptable value.

4.2. Continuous dynamic monitoring systems (CDMS)

The numerical models calibrated with the forced vibration tests make it possible to monitor the evolution of the dynamic behavior of the construction site over time, taking into account the variation in actions, particularly the height of the reservoir. To this end, various models are developed with different reservoir levels and the results are compared with those of the continuous dynamic monitoring systems installed. Fig. 7 shows the values of the first six eigenfrequencies, determined for different reservoir levels, from the numerical model (NUM), the forced vibration test (FVT) and the average curve obtained from continuous dynamic monitoring systems (CMDS). The observed results cover the period from 2016 to 2022. The average CMDS curve was determined from the multiple linear regression coefficients applied to the respective parameters. For elevation 234 m, there is excellent agreement between the 3 methodologies for practically all frequencies, with the exception of the last one, where the forced vibration test shows a small difference of 1.3%, which is perfectly acceptable. The results of the numerical model and the observed results are in good agreement, and it can be concluded that there was no change in behavior over the observation period.

Table 2
Comparison of the natural frequencies determined experimentally in the forced vibration tests and through the numerical models, for the empty and full reservoir situations of the Baixo Sabor [11] and Foz Tua [12] dams

	MODE	NATURAL FREQUENCY (HZ)		MAC	DIFFERENCE	
		FORCED VIBRATION	NUMERICAL MODEL		(HZ)	(%)
Baixo Sabor	Model for the empty reservoir situation (195.5 m)					
	1	2.75	2.75	0.82	0	0.00%
	2	2.95	2.95	0.96	0	0.00%
	3	3.87	3.92	0.91	0.05	1.29%
	4	4.46	4.43	0.78	-0.03	-0.67%
	5	5.26	5.33	0.88	0.07	1.33%
	6	5.88	5.92	0.84	0.04	0.68%
	Model for the full reservoir situation (234.0 m)					
	1	2.44	2.44	0.96	0.00	0.00%
	2	2.57	2.56	1.00	-0.01	-0.39%
	3	3.34	3.31	0.96	-0.03	-0.90%
	4	3.93	3.92	0.90	-0.01	-0.25%
	5	4.78	4.75	0.88	-0.03	-0.63%
	6	5.37	5.44	0.84	0.07	1.30%
Foz Tua	Model for the empty reservoir situation (123.0 m)					
	1	3.66	3.65	0.99	-0.01	-0.27%
	2	3.88	3.90	0.98	0.02	0.52%
	3	5.09	5.32	0.96	0.23	4.52%
	4	6.81	6.81	0.94	0.00	0.00%
	5	7.87	8.24	0.86	0.37	4.70%
	Model for the full reservoir situation (168.9 m)					
	1	3.05	3.05	0.99	0.00	0.00%
	2	3.25	3.23	0.98	-0.02	-0.62%
	3	4.30	4.42	0.96	0.12	2.79%
	4	5.64	5.88	0.94	0.24	4.26%
	5	6.90	7.41	0.86	0.51	7.39%

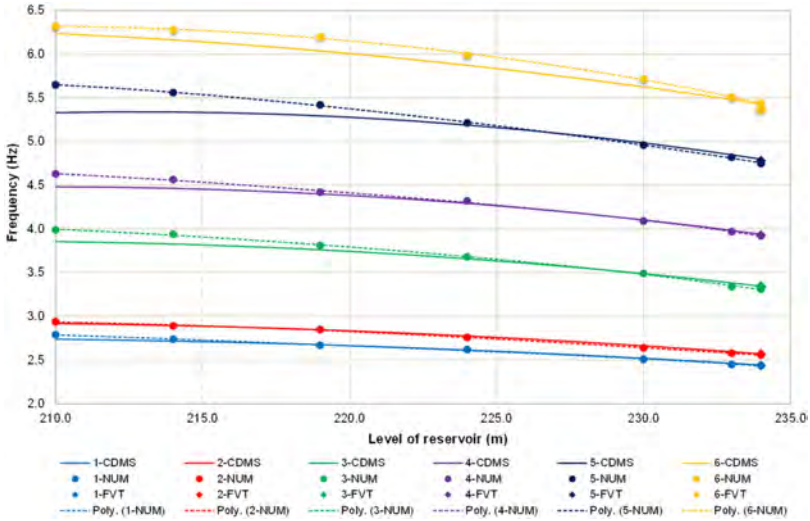

Fig. 7
Natural frequencies determined with the numerical model (NUM), FVT and average curve for CDMS, for different elevations of the Baixo Sabor reservoir
Fréquences naturelles déterminées avec le modèle numérique (NUM), FVT et courbe moyenne pour CDMS, pour différentes élévations du réservoir de Baixo Sabor.

4.3. Seismic monitoring systems (SMS)

For the analysis of the dam's dynamic behavior to small earthquakes, the numerical model calibrated with the experimental results was adopted, considering absorbent boundaries to simulate the continuity of the foundation massif. Due to the finite size of the numerical model, the reflection of seismic waves at the boundaries where there is continuity of the rock mass would affect the dynamic behavior of the dam. Therefore, free field conditions were imposed, based on the model proposed in 3DEC [2] (Fig. 8a), for the absorption of seismic waves, thus simulating their propagation beyond the finite boundary of the numerical model (Fig. 8b). The seismic monitoring system (SMS) implemented at the Baixo Sabor dam has recorded the occurrence of several low-intensity earthquakes. The event of 2020/10/03 at 12:29 was chosen, whose epicenter was located about 8 km from the dam and had a magnitude of approximately 2.0. Based on the records of the seismometers installed along the dam's foundation, the velocities to be applied to the base of the numerical model were determined. These velocities were converted into dynamic stress histories based on the characteristics of the rock mass (specific mass and propagation

velocities of the shear and pressure waves), for application in the numerical model. Fig. 9 shows the velocities obtained in the foundation (SM3) and near the crown (SM2) in the numerical model and in the SMS. There is good agreement between the peak values obtained with the numerical model and the observed values [6].

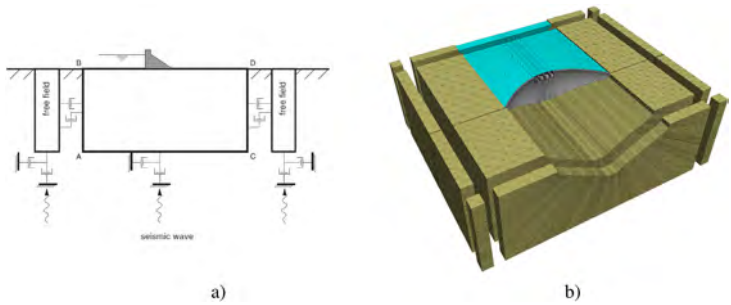

Fig. 8
Numerical model for the study of seismic action: a) schematic of the adopted boundary conditions (free field); and b) view of the numerical model
Modèle numérique pour l'étude de l'action sismique : a) schéma des conditions aux limites adoptées (champ libre) ; et b) vue du modèle numérique

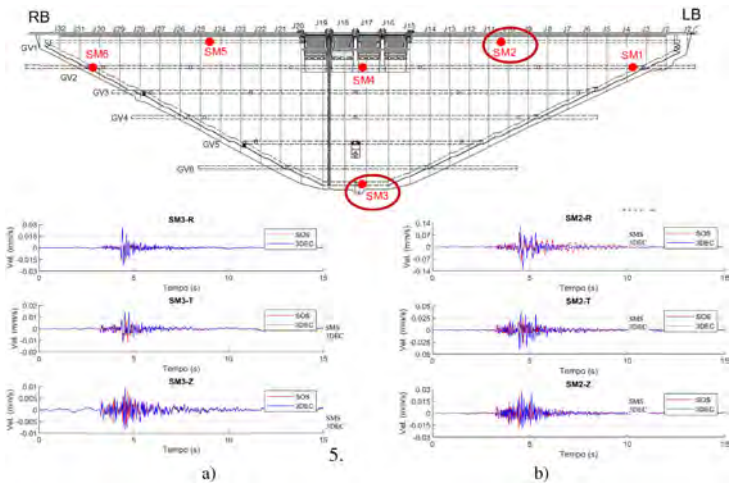

Fig. 9
Comparison of the velocities obtained from the numerical model with the values observed at the Baixo Sabor dam: a) point SM3; and b) point SM2
Comparaison des vitesses obtenues à partir du modèle numérique avec les valeurs observées au barrage de Baixo Sabor : a) point SM3 ; et b) point SM2

6. CONCLUSIONS

Evaluating the dynamic behavior of structures is an important tool because it makes it possible to detect the structural changes that have occurred during this period, based on the change in the dynamic behavior of the work. The performance of forced vibration tests on concrete dams to determine dynamic behavior continue to be one of the most reliable techniques in this area. Complementing these results with the installation of continuous dynamic and seismic monitoring systems provides a robust experimental methodology for monitoring structural behavior. To interpret the results of the dynamic monitoring, a numerical model is used, representing the foundation rock mass, calibrated with the results of the forced vibration test. In this model, the reservoir is discretized with finite elements, which makes it possible to simulate the effect of the interaction of the water with the dam and the foundation more accurately. With regard to Westergaard's method of added masses, which is widely used in practice, the model adopted makes it possible, on the one hand, to eliminate the subjectivity of considering the correction factor relating to the added masses and, on the other, to better simulate the dynamic behavior of the dam-reservoir-foundation set. For this model, various discretizations of the reservoir were made, corresponding to different water levels. The values of the eigenfrequencies determined numerically and experimentally show a good agreement.

ACKNOWLEDGEMENTS

The authors would like to acknowledge the Portuguese National Laboratory for Civil Engineering (LNEC), through its research program DAM_AGE (0402/1101/19817), and to Movhera/ENGIE for allowing us to present some of the results of the study and monitoring of the dynamic behavior of the Baixo Sabor and Foz Tua dams.

REFERENCES

[1] LILHANAND, K.; TSENG, W.S., (1987). Generation of synthetic time histories compatible with multiple-damping design response spectra. Wittman, F.H; p. 105-112; ISBN 90-6191-771-9; 1987; A.A. Balkema Publishers; Accord, MA (USA); SMIRT 9: international conference on structural mechanics in reactor technology; Lausanne (Switzerland).

[2] PEREIRA, S.; MAGALHÃES, F.; GOMES, J.P.; CUNHA, A.; LEMOS, J.V. (2018) Dynamic monitoring of a concrete arch dam during the first filling of the

reservoir. *Engineering Structures*, Volume 174, pag. 548–560, (https://doi.org/10.1016/j.engstruct.2018.07.076).

[3] PEREIRA, S., MAGALHÃES, F., GOMES, J.P., CUNHA, Á., (2022) Modal tracking under large environmental influence. *Journal of Civil Structural Health Monitoring*, Volume 12, pag. 179–190, (https://doi.org/10.1007/s13349-021-00536-2).

[4] PEREIRA, S.; GOMES, J.P.; MAGALHÃES, F.; CUNHA, A.; LEMOS, J.V. (2023) Seven years of continuous dynamic monitoring of baixo sabor dam. 9th International Conference on Computational Methods in Structural Dynamics and Earthquake Engineering, COMPDYN 2023, Atenas, Grécia, junho.

[5] ITASCA (2017). 3DEC, 3-Dimensional Distinct Element Code, Version 5.2, User's Manual. Itasca Consulting Group. Minneapolis.

[6] WESTERGAARD, H.M. (1933) Water pressures on dams during earthquakes. Trans. ASCE, vol. 98, paper nº 1835.

[7] Chinese National committee for Large Dams (CHINCOLD) (2014) Seismic safety of dams in China.

[8] PRISCU, R.; POPOVICI, A.; STEMATIU, D.; STERE, C. (1985) *Earthquake engineering for large dams*. John Wiley & Sons.

[9] MARTI, J.; CUNDALL, P. (1982). Mixed discretization procedure for accurate modelling of plastic collapse. *Int. Journal Numerical and Analytical Methods in Geomechanics*, vol. 6, pp. 129–139.

[10] LNEC, (2008). Numerical modeling of fluid-structure interaction through a finite element formulation in displacements (in Portuguese). Relatório 54/2008.

[11] GOMES, J.P.; LEMOS, J.V. (2020) Characterization of the dynamic behaviour of a concrete arch dam by means of forced vibration tests and numerical models. *Earthquake Engineering & Structural Dynamics*. Volume 49, Issue 7, pág. 679–694. (https://doi.org/10.1002/eqe.3259).

[12] GOMES, J.P.; LEMOS, J.V., (2020) Evaluation of the dynamic behavior of Foz Tua dam based on experimental and numerical methods (in Portuguese). Congresso Nacional Reabilitar & Betão Estrutural, Lisboa.

[13] ALLEMANG, R. J., (2003). The Modal Assurance Criterion – Twenty years of use and abuse. Sound and Vibration, pp, 14-21.

Q.111 - R.6

COMMISSION INTERNATIONALE DES
GRANDS BARRAGES

VINGT-HUITIEME CONGRES DES
GRANDS BARRAGES
CHENGDU, MAI 2025

A STUDY ON THE POTENTIAL EFFECTS OF SPECTRAL MATCHING ON SIMULATED SEISMIC RESPONSE OF ARCH DAMS (*)

Amin ASKARINEJAD
Coordinator of Dam Safety Technical Bases, SWISS FEDERAL OFFICE OF ENERGY – SFOE

Anton D. TZENKOV, Federico GALSTER & Thomas MENOUILLARD
Dam Safety Specialist, SWISS FEDERAL OFFICE OF ENERGY – SFOE

Milaine CÔTÉ
Dam Safety Commissioner, SWISS FEDERAL OFFICE OF ENERGY – SFOE

SWITZERLAND

SUMMARY

A critical requirement outlined in modern seismic safety codes for dams when selecting natural earthquake records is to ensure compatibility between the average and individual elastic response spectrum of the input acceleration time series and the normative spectrum. The design spectrum may also be derived from site specific seismic hazard analysis. It is generally expected that within a specific period range, which depends on the dynamic properties of the dam, the average elastic spectrum should not deviate from the design spectrum by more than a certain percentage of tolerance. Given the considerable variability present

(*) *Une étude sur les effets potentiels de l'adaptation spectrale sur la réponse sismique des barrages-voûtes*

 DOI: 10.1201/9781003642428-109

in natural earthquake records, two primary approaches have been employed to ensure their compatibility with the spectrum specified by the seismic safety codes: linear scaling and spectral matching. Spectral matching, in particular, involves the application of modulating functions, often in the form of wavelet transforms, strategically applied in the time (or frequency) domain to align the response spectrum of the ground motion with the required code-specific spectrum. While spectral matching methods can adjust records to match design spectra, there is a scarcity of research exploring how this modification technique may impact the simulated response of concrete arch dams. This paper aims to investigate the variations in the dynamic response of an arch dam subjected to scaled and spectrally matched natural earthquake records. The height of the hypothetical dam is set at 150 meters located in a narrow V-shaped valley, and three normative spectra defined by the new Swiss Federal Office of Energy (SFOE) directive on seismic safety verification of dams are utilized. Each target spectrum reflects the seismic demand of an earthquake zone in Switzerland. The hypothetical dam is subjected to testing using six sets of ground motions in three dimensions, with each set composed of 11 records. Three of these sets include linearly scaled natural earthquake records, while the other three consist of the corresponding spectrally matched input motions.

RÉSUMÉ

Une exigence essentielle des codes modernes de sécurité sismique pour les barrages lors de la sélection des enregistrements sismiques naturels est d'assurer la compatibilité entre le spectre de réponse élastique moyen et individuel des séries temporelles d'accélération et le spectre normatif. Le spectre de conception peut également être dérivé d'une analyse de l'aléa sismique spécifique au site. En général, il est attendu que, dans une plage de périodes spécifique, qui dépend des propriétés dynamiques du barrage, le spectre élastique moyen ne s'écarte pas du spectre de conception de plus qu'un certain pourcentage de tolérance. Étant donné la variabilité considérable présente dans les enregistrements sismiques naturels, deux approches principales ont été employées pour assurer leur compatibilité avec le spectre spécifié par les codes de sécurité sismique : la mise à l'échelle linéaire et l'ajustement spectral. L'ajustement spectral, en particulier, implique l'application de fonctions modulantes, souvent sous la forme de transformations en ondelettes, appliquées stratégiquement dans le domaine temporel (ou fréquentiel) pour aligner le spectre de réponse du mouvement du sol avec le spectre requis par le code. Bien que les méthodes d'ajustement spectral puissent adapter les enregistrements pour correspondre aux spectres de conception, il existe peu de recherches explorant comment cette technique de modification peut affecter la réponse simulée des barrages-voûtes en béton. Cet article vise à étudier les variations de la réponse dynamique d'un barrage-voûte soumis à des

enregistrements sismiques naturels mis à l'échelle et ajustés spectralement. La hauteur du barrage hypothétique est fixée à 150 mètres et il est situé dans une vallée étroite en forme de V. Trois spectres normatifs définis par la nouvelle directive de l'Office fédéral de l'énergie (OFEN) sur la vérification de la sécurité sismique des barrages en Suisse sont utilisés. Chaque spectre cible reflète la demande sismique d'une zone sismique en Suisse. Le barrage hypothétique est soumis à des essais utilisant six ensembles de mouvements de sol en trois dimensions, chaque ensemble étant composé de 11 enregistrements. Trois de ces ensembles incluent des enregistrements sismiques naturels mis à l'échelle linéairement, tandis que les trois autres se composent des mouvements correspondants ajustés spectralement.

1. INTRODUCTION

The process of defining seismic input for the nonlinear dynamic analysis of arch dams has evolved significantly over the years. Traditionally, artificially produced earthquakes were used for this purpose. However, modern seismic safety codes have shifted away from this approach due to the fact that artificially generated earthquakes often lack the complex characteristics of natural seismic events, such as frequency content, temporal energy distribution, and strong motion duration which are critical for accurate seismic analysis of arch dams. Consequently, the current best practice involves using either simulated acceleration time series derived from physics-based numerical simulations or natural earthquake records, with a preference for the latter. The seismic safety verification of arch dams necessitates ground motions that align with the specific seismic hazards of the site. This involves ensuring that the selected ground motions meet several critical criteria of:

- *Hazard Compatibility: Ground motions must be representative of the seismic hazard at the dam site. This is determined by factors such as the tectonic regime, fault depth, the magnitude of relevant potential earthquakes and the distance to the seismic source, based on disaggregation data. This ensures that the selected ground motions reflect realistic seismic loads on the structure.*
- *Intensity Measures: Ground motions should adhere to prescribed ranges of important intensity measures like significant duration and Arias intensity, which are essential for capturing the number of loading cycles and the seismic energy that will impact the dam structure.*
- *Elastic Response Spectrum Compliance: The average elastic response spectrum of the chosen ground motions must closely match the target response spectrum specified by seismic safety codes. This compatibility ensures that the spectral characteristics of the ground motions are suitable for the dynamic behaviour of the dam.*

Due to the inherent variability in natural earthquake records, engineers often employ two main techniques to adjust ground motions to meet these criteria:

(i) **Linear Scaling:** This method involves uniformly scaling the amplitude of a ground motion record. While it is easy to implement, it may not adequately capture the required spectral features;

(ii) **Spectral Matching:** This method involves modifying the frequency content and phase of ground motion records through the application of modulating functions, such as wavelet transforms, to achieve enhanced compatibility with the target spectrum. While effective, excessive application of this approach can significantly alter the inherent characteristics of the ground motion records, potentially leading to substantial deviations in the simulated structural response from realistic outcomes.

Both of these methods have their advantages and disadvantages. Previous studies have highlighted that spectrally-matched records tend to reduce response variability but may slightly overestimate or underestimate structural responses due to their smoother response spectra. Researchers such as Bazzurro and Luco (2006), Heo et al. (2011), and Baker et al. (2023) have explored these impacts, underscoring the importance of careful application of spectral matching techniques.

The primary objective of this research is to evaluate whether spectral matching techniques introduce significant biases in the seismic response of arch dams. By comparing responses obtained from real, amplitude-scaled, and spectrally matched records, the study seeks to quantify the extent of these biases and their implications for seismic safety assessments. For this purpose, a hypothetical 150-meter arch dam situated in a narrow V-shaped valley is subjected to six sets of ground motions, each comprising 11 acceleration time series with three components. Three of these sets consist of linearly scaled natural earthquake records, selected based on the disaggregation of seismic hazard across three distinct locations in Switzerland, representing varying levels of seismic activity. The remaining three sets consist of the same records, spectrally matched, providing a basis for comparison.

In Chapter 2, the geometry of the dam, concrete properties, rock type, assumptions regarding interfaces, and hydrodynamic loads are detailed, alongside the results of the modal analysis of the structure. Chapter 3 presents the target normative spectra and a statistical analysis of the effects of spectral matching on the relevant intensity measures of the records. In Chapter 4, the results of the 3D analysis of the arch dam are discussed, with a focus on the maximum horizontal acceleration at the crest and the maximum tensile stresses within the dam body, comparing the responses between linearly scaled and spectrally matched input motions. Chapter 5 provides a quantitative analysis of the impacts of spectral matching on the seismic response of the simulated arch dam, offering recommendations on the application of this technique. Furthermore, the applicability of the Demand Capacity Ratio as a function of the Cumulative Overstress Duration is

examined for seismic performance evaluation of the arch dam. The chapter also discusses the suitability of Acceleration Spectrum Intensity (ASI) as a relevant intensity measure for the seismic safety assessment of arch dams.

The findings of this paper are intended to offer some insights for researchers, regulators and engineers contributing to the advancement of practices in the seismic design and assessment of arch dams.

2. SIMULATED CASE OF ARCH DAM

2.1. Geometry, material properties, and hydrodynamic loads

For the purposes of this study, it has been deemed appropriate to analyse an example of a 150 m high concrete arch dam located in a narrow V-shaped valley. The geometry of the dam has been defined on the bases of USACE (1994) recommendations and the authors' experience. A symmetrical valley has been assumed and its width has been chosen to be twice the height of the dam at the crest of the dam and 0.2 times at the base of the dam (Fig. 1). The cross-section of the central cantilever of the dam and the line of centres are shown in the same figure. The arches of the dam have been defined with parabolic functions.

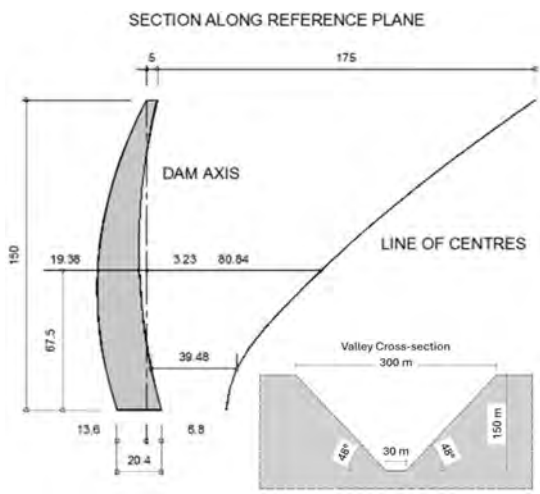

Fig. 1
Cross-section of the central vertical section of the dam and the valley with line of centres
Coupe transversale de la section centrale du barrage et de la vallée avec ligne des centres

The response of the dam to the investigated seismic impacts has been simulated by means of a 3D FEM model of the dam-foundation system, (**Error! Reference source not found.**). The model is built with hexahedral and tetrahedral elements with linear interpolation of the shape functions. The dimensions of the modelled part of the foundation are 600 m, 390 m, and 345 m in the cross-stream, along-stream, and the vertical direction respectively.

The dam-reservoir interaction is represented by Westergaard added masses (Westergaard 1931) at the upstream face nodal points. The viscous damping of the dam-foundation system is simulated by means of the Rayleigh method by setting the proportionality constants so as to give a modal damping ratio of 5% in the first and the fourteen vibration modes. A time step of 0.01 seconds is used in the $\alpha-$method of Hughes, Hilbert and Taylor (Hughes 1987) with α =-0.3 for direct integration of the equations of motion of the system. A criterion of 0.01 is set for displacement and force convergence. The foundation has been modelled as massless and both rock and the concrete are modelled with linear elastic constitutive laws (table 1).

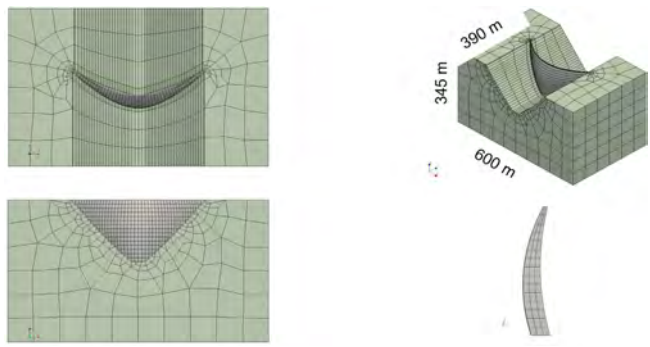

Fig. 2
3D FEM mesh of the dam-foundation system.
Maillage MEF 3D du système barrage-fondation

Table 1
Properties of the concrete and the foundation
Propriétés du béton du barrage et de la fondation

MATERIAL	DENSITY (KG/M^3)	YOUNG'S MODULUS (STATIC / DYNAMIC) (GPA)	TENSILE STRENGTH (STATIC / DYNAMIC) (MPA)	POISSON'S RATIO (-)
Concrete	2500	25 / 31.25	3.5 / 4	0.20
Rock	0	27 / 33.75	-	0.25

2.2. Static analysis and eigenperiods of the dam

The static analysis takes into account the dam's self-weight and the hydrostatic pressure exerted by the water in the dam's reservoir on the upstream face of the dam. No silt pressure and no thermal effects have been considered in the current study. In order to obtain realistic values for self-weight stresses, it has been applied by considering five construction stages, each 30 m high. It is assumed that at the end of each stage, the joints between the dam blocks are grouted. The hydrostatic pressure has been applied for the full supply water level, which has been assumed to be two meters below the dam crest level.

The dynamic behaviour of the arch dam has been analysed by determining its natural modes of vibration (eigenperiods and mode shapes). These are essential for understanding how the dam will respond to seismic activity and other dynamic loads. The first seventy modes of free vibration of the dam-foundation-reservoir system have been evaluated. The first thirty-seven eigenperiods and the corresponding effective masses activated in each of the three global directions are given in the Table 2.

Table 2
Eigenperiods and effective masses for dam with full reservoir
Périodes propres et masses effectives pour le barrage avec réservoir plein

		X DIRECTION (CROSS-STREAM)			Y DIRECTION (ALONG-STREAM)			Z DIRECTION (VERTICAL)		
MODE	PERIODS	EFF. MASS MNs^2/m	%	CUM. %	EFF. MASS MNs^2/m	%	CUM. %	EFF. MASS MNs^2/m	%	CUM. %
1	0.55	208	10.73	10.73	0	0.00	0.00	0	0.00	0.00
2	0.51	0	0.00	10.73	994	29.51	29.51	4	0.27	0.27
3	0.36	0	0.00	10.73	308	9.14	38.65	1	0.05	0.32
4	0.29	0	0.00	10.73	515	15.30	53.95	43	2.91	3.23
5	0.27	15	0.75	11.49	0	0.00	53.95	0	0.00	3.23
6	0.23	199	10.28	21.77	0	0.00	53.95	0	0.00	3.23
7	0.21	0	0.00	21.77	27	0.82	54.77	1	0.07	3.29
8	0.19	0	0.00	21.77	53	1.57	56.34	23	1.57	4.87
9	0.17	12	0.64	22.41	0	0.00	56.34	0	0.00	4.87
10	0.17	0	0.00	22.41	186	5.53	61.87	65	4.43	9.29
11	0.15	19	0.97	23.37	0	0.00	61.87	0	0.00	9.29
12	0.14	0	0.00	23.37	7	0.21	62.08	1	0.05	9.34
13	0.13	294	15.14	38.51	0	0.00	62.08	0	0.00	9.34
14	0.13	0	0.00	38.51	87	2.58	64.66	673	45.63	54.97

(Continued)

Table 2
Continued

		X DIRECTION (CROSS-STREAM)			Y DIRECTION (ALONG-STREAM)			Z DIRECTION (VERTI-CAL)		
MODE	PERIODS	EFF. MASS MNs^2/m	%	CUM. %	EFF. MASS MNs^2/m	%	CUM. %	EFF. MASS MNs^2/m	%	CUM. %
15	0.13	0	0.00	38.51	18	0.52	65.18	62	4.20	59.18
16	0.12	253	13.03	51.55	0	0.00	65.18	0	0.00	59.18
17	0.12	94	4.83	56.38	0	0.00	65.18	0	0.00	59.18
18	0.12	0	0.00	56.38	18	0.54	65.72	3	0.21	59.38
19	0.10	4	0.23	56.60	0	0.00	65.72	0	0.00	59.38
20	0.10	0	0.00	56.60	73	2.17	67.89	1	0.08	59.47
21	0.10	0	0.00	56.60	29	0.85	68.74	1	0.06	59.53
22	0.10	7	0.36	56.96	0	0.00	68.74	0	0.00	59.53
23	0.09	5	0.24	57.20	0	0.00	68.74	0	0.00	59.53
24	0.09	0	0.00	57.20	9	0.28	69.02	1	0.07	59.60
25	0.09	0	0.00	57.20	0	0.00	69.02	0	0.00	59.60
26	0.09	0	0.00	57.20	17	0.50	69.52	0	0.03	59.63
27	0.08	38	1.95	59.15	0	0.00	69.52	0	0.00	59.63
28	0.08	0	0.00	59.15	5	0.14	69.66	0	0.01	59.64
29	0.08	0	0.01	59.16	0	0.00	69.66	0	0.00	59.64
30	0.08	0	0.00	59.16	0	0.00	69.66	0	0.00	59.64
31	0.07	4	0.21	59.38	0	0.00	69.66	0	0.00	59.64
32	0.07	0	0.00	59.38	0	0.01	69.67	113	7.69	67.33
33	0.07	0	0.00	59.38	54	1.60	71.27	1	0.09	67.43
34	0.07	0	0.00	59.38	14	0.40	71.67	3	0.23	67.66
35	0.07	0	0.00	59.38	48	1.42	73.09	6	0.38	68.04
36	0.07	2	0.09	59.47	0	0.00	73.09	0	0.00	68.04
37	0.07	11	0.57	60.04	0	0.00	73.09	0	0.00	68.04

3. TARGET NORMATIVE SPECTRA AND INPUT MOTIONS

3.1. TARGET SPECTRA

Three hypothetical dams are assumed to be located in different earthquake zones in Switzerland, namely, Z1a (e.g., Canton of Tessin), Z2 (e.g., Canton of

Grisons) and Z3b (e.g., Canton of Valais). All dams are founded on site class R as defined in the directive on seismic safety of dams in Switzerland (SFOE 2021)[†]. The return period used for the safety earthquake is set to 10'000 years for a Category I dam under the Swiss regulations. The 3 normative target spectra are presented in Fig. 3.

Vertical target spectra are derived from horizontal spectra using a linear scaling factor of 0.7. When records are scaled linearly, the vertical component of the corresponding earthquake is also adjusted with the same factor as the one for the geometric mean of the two horizontal components. When necessary, the scaling factors for individual vertical component spectra are adjusted to prevent an undershoot of 50% or more relative to the vertical target spectrum. Additionally, the mean spectral acceleration of the vertical components at the period of the dam's first vertical vibration mode is verified to be at least 90% of the target value. For spectrally matched sets, the vertical components of all records are adjusted to be compatible with the vertical target spectrum.

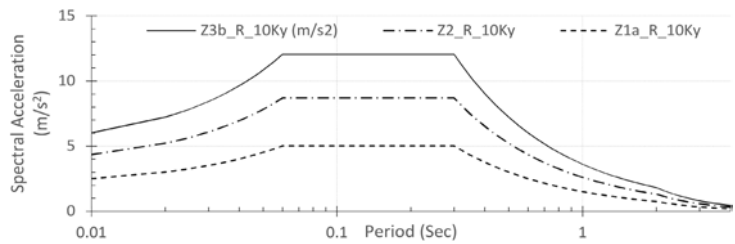

Fig. 3
Target normative spectra for 3 locations in Switzerland for site class of R and earthquake return period of 10'000 years.
Spectres normatifs cibles pour 3 sites en Suisse pour une classe de sol R et une période de retour de tremblements de terre de 10'000 ans.

3.2. Input motions

In order to check the seismic performance of the dam, three sets of 11 recorded earthquakes are scaled and spectrally matched to be compatible with the normative target spectra for each earthquake zone. In total 33 records were treated to satisfy the compatibility requirements with the normative spectra. The results of the variation of 4 intensity measures of the dominant horizontal component relevant for the seismic performance of the arch dams are presented in Fig. 4.

[†]Site Class R: Massive rock without significant local weaknesses, weathering, or loose rock inclusions; comprehensively and quantitatively investigated with $V_{s30} > 1100$ m/s.

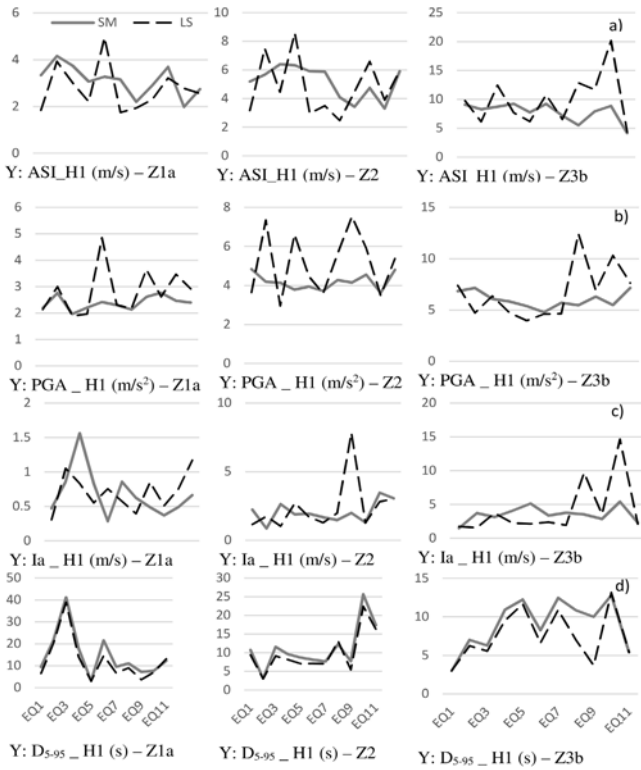

Fig. 4

Summary of comparisons between the Intensity measures for the dominant horizontal component of linearly scaled (LS) and spectrally matched (SM) records. Row a) Acceleration Spectrum Intensity (ASI) for the vibration period range of T1 = 0.05 sec to T2 = 0.5 sec as defined in Equation 1. Row b) Peak Ground Acceleration (PGA). Row c) Arias Intensity (Ia) and row d) Significant duration (D5-95). Left to right columns show the data for the dams located in three earthquake zones of Z1a, Z2, and Z3b.

Résumé des comparaisons entre les mesures d'intensité pour la composante horizontale dominante des enregistrements Linéairement mis à l'échelle (LS) et ajustés spectralement (SM). Ligne a) Intensité du spectre d'accélération (ASI) pour la plage de périodes de vibration de T1 = 0,05 s à T2 = 0,5 s comme défini dans l'équation 1. Ligne b) Accélération maximale au sol (PGA). Ligne c) Intensité d'Arias (Ia) et ligne d) Durée significative (D5-95). De gauche à droite, les colonnes montrent les données pour les barrages situés dans les trois zones sismiques Z1a, Z2 et Z3b

3.3. Statistical analysis of the intenstiy measures (IM)

In total 33 linearly scaled earthquake records were spectrally matched using the method proposed by Al Atik and Abrahamson (2010). In this approach a cosine wavelet tapered with a Gaussian function is used. This wavelet adjusts the initial time series to match the target spectrum while preserving the nonstationary characteristics.

Among various metrics, the Acceleration Spectrum Intensity (ASI) (Von Thun 1988) may be considered as a simple but relevant intensity measure. ASI quantifies the severity of an earthquake's acceleration response over a specified period range, reflecting the energy imparted to the structure at relevant frequencies. This analysis explores the ASI values from earthquake simulations, examining the differences between linearly scaled and spectrally matched seismic records. ASI is defined as the integral of the acceleration response spectrum over a specified period range, typically chosen to capture the significant modal contributions of the structure.

$$\mathrm{ASI} = \int_{T_2}^{T_2} S_a(T)dT \tag{1}$$

where $S_a(T)$ is the acceleration response spectrum at period T.

For the hypothetical dam selected for this study, the period range was set from T_1=0.05 sec seconds to T_2=0.5 seconds, covering more than 70% of the modal mass under natural vibration in all three orthogonal directions (Table 2). This measure provides insight into the structure's response characteristics and potential vulnerabilities under seismic loading (e.g., Chopra and Goel, 2001, Akkar and Bommer, 2010, Shome and Cornell, 1999, Priestley et al., 2007).

Summary statistics (Fig. 4a) indicate notable differences between the scaled and matched records. When comparing ASI trends across various earthquake records, it is evident that the ASI values of the scaled records exhibit significant variability, characterized by several pronounced peaks. In contrast, the ASI values of the spectrally matched records demonstrate lower variability. However, the average ASI values for each set, regardless of whether the records were linearly scaled or spectrally matched, are comparable. This observation extends to the other tested intensity measures as well. The only exception is the significant duration ($D_{5\text{-}95}$), which generally exhibits slightly higher values for the spectrally matched records compared to the scaled records.

4. RESULTS OF DYNAMIC ANALYSIS OF ARCH DAMS

In this chapter the results of 66 three-dimensional FEM simulations are presented in two categories: namely, the response spectra at the crest of the dam and the maximum vertical tensile stresses.

4.1. The response spectra at the crest of the dam

The response spectra at the crest of the arch dam indicate significant peaks in spectral accelerations, highlighting the dam's natural frequencies (Fig. 5). Major peaks occur at periods of approximately 0.11s, 0.17s, 0.24s, 0.28s, and 0.35s, corresponding to frequencies of about 9.09 Hz, 5.88 Hz, 4.17 Hz, 3.57 Hz, and 2.86 Hz respectively. The highest peak at 0.28s suggests the dominant natural frequency. These values correspond to the theoretical and simulated values of natural frequencies of the dam (Table 2).

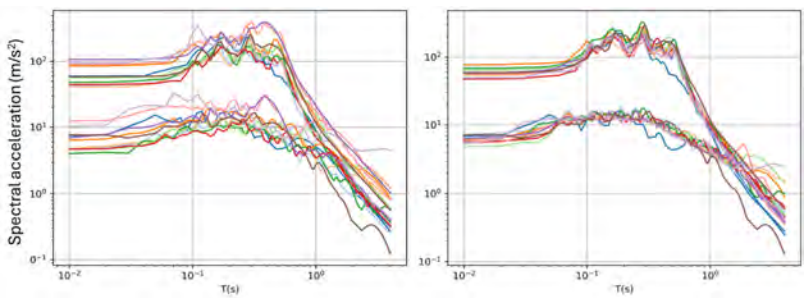

Fig. 5
Comparison of the elastic response spectra of the dominant horizontal acceleration at the dam crest and the dam base for 11 records of earthquake zone Z3b, (left: linearly scaled records, right: Spectrally matched records).
Comparaison des spectres de réponse élastique de l'accélération horizontale dominante au couronnement et à la base du barrage pour 11 enregistrements de tremblement de terre de la zone sismique Z3b (à gauche : enregistrements linéairement amplifiés, à droite : enregistrements spectrale ajustés).

Comparing the two sets of responses, i.e., LS vs SM, it can be observed that the plot for the linearly scaled records shows significant variability in spectral accelerations across different periods. There is also a broader range of acceleration

values, indicating a less uniform response across the different records. Whereas, for the spectrally matched records, peaks are more pronounced and concentrated, indicating a more predictable and controlled response. The spectrally matched response spectra provide a more consistent and clear identification of the arch dam's natural frequencies, with less variability compared to the linearly scaled records. The linearly scaled records, on the other hand, highlight the potential range of responses, offering a broader perspective on the dam's behaviour under different seismic scenarios. Both sets of records could be valuable for comprehensive seismic assessment and ensuring the dam's seismic safety.

4.2. Vertical tensile stresses in the dam

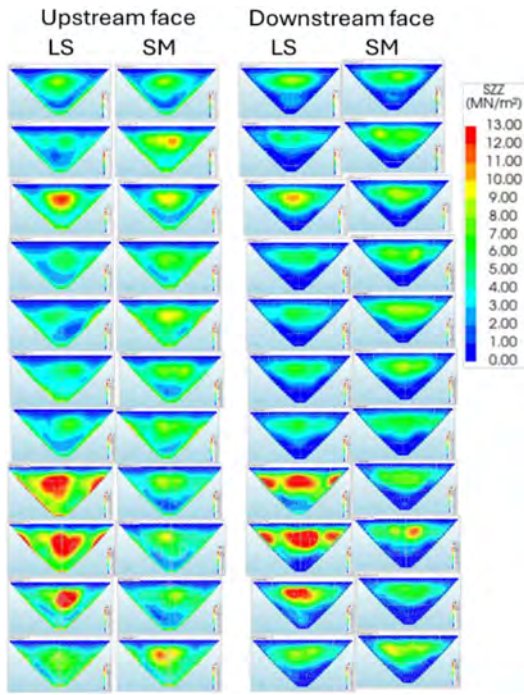

Fig. 6
Comparison of the envelope of vertical tensile stresses on the upstream (left column) and downstream (right column) faces of the dam for 22 earthquakes in zone Z3b.
Comparaison de l'enveloppe des contraintes de traction verticales sur les faces amont (colonne de gauche) et aval (colonne de droite) du barrage pour 22 séismes dans la zone Z3b

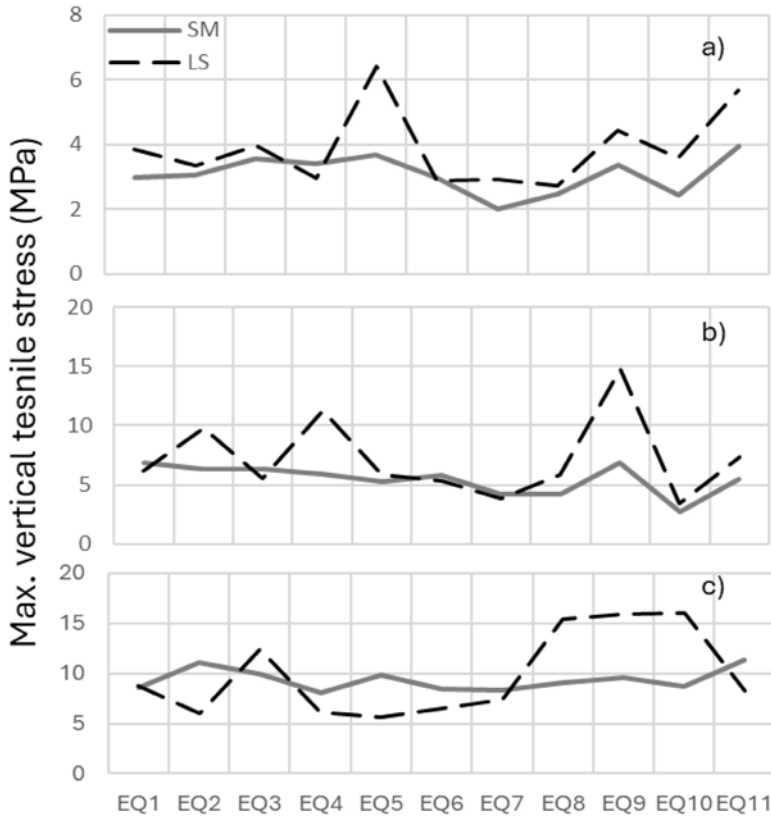

Fig. 7
Comparison of the maximum vertical tensile stress in the dam body for 11 earthquakes (EQ1 to EQ11) in three different earthquake zones in Switzerland; a) Z1a, b) Z2, and c) Z3b.
Comparaison de la contrainte de traction verticale maximale dans le corps du barrage pour 11 tremblements de terre (EQ1 à EQ11) dans trois zones sismiques différentes en Suisse ; a) Z1a, b) Z2, et c) Z3b.

The distribution of the envelope of the vertical tensile stresses on both faces of the dam and the maximum values for each input motion are presented in Fig. 6 and Fig.7, respectively. The results show that the maximum values and the variation of stresses for the linearly scaled records is higher than that for the spectrally matched ones. The maximum vertical tensile stresses generally occur on the upstream face of the dam.

4.3. Acceleration spectrum intensity and correlation with imposed seismic structural demands

The ASI, PGA, PGV, $D_{5\text{-}95}$, Arias Intensity for three components (H1, H2, and V), as well as the geometric mean of ASI of each earthquake were calculated for both treatment procedures and the correlation of these IMs has been calculated with the maximum vertical tensile stress in the dam. The results (Fig. 8) indicate that for these analyses, the ASI_H1 and PGA_H1 show the highest correlation with the structural demand. It should be noted that the duration of the records does not exhibit a strong correlation with the maximum tensile stress as these simulations were done assuming a linear elastic behaviour for the material. In case of use of other constitutive laws, particularly, non-linear elastoplastic material models, the correlation with Arias Intensity and the significant duration of the earthquake are expected to be higher.

Fig. 8

Correlation between the maximum vertical tensile stress in the dam body (SZZ_Max) and 16 different intensity measures (IM); ASI: the acceleration spectral intensity, PGA: peak acceleration, PGV: Peak ground velocity, Ia: Arias intensity, D5-95: Significant duration.

Corrélation entre la contrainte de traction verticale maximale dans le corps du barrage (SZZ_Max) et 16 différentes mesures d'intensité (IM) ; ASI : l'intensité spectrale d'accélération, PGA : l'accélération maximale, PGV : la vitesse maximale au sol, Ia : l'intensité d'Arias, D5-95 : la durée significative.

4.4. Demand capacity ratio and cumulative inelastic duration

To compare the response of the dams across the three earthquake zones and assess the behaviour within each zone as a function of the input motion treatment approach, the Demand Capacity Ratio (DCR) and the corresponding tensile stress exceedance duration relative to the tensile strength of the concrete are calculated and analysed. This comparison provides a detailed evaluation of the dam's performance under varying seismic conditions and input motion treatments. The performance levels of a concrete arch dam are classified based on the maximum DCR and the extent of overstressed regions: minor or no damage is expected if the DCR

remains below 1, indicating an elastic response; if the DCR exceeds 1 but stays below 2, with overstressed areas limited small portion of the cross-sectional area and the cumulative inelastic duration within acceptable limits (Fig. 6), the damage is considered acceptable; otherwise, the damage is classified as severe. It can be observed that the average DCR values for the spectrally matched input motions across all three zones are lower than those for the linearly scaled inputs. Although some individual records, primarily the linearly scaled ones, exceed the threshold, the mean DCR curves remain below the thresholds, except for the records in zone Z3b (Fig. 9c). However, it should be noted that for a more realistic estimate of the dam's dynamic performance, the assumptions of linear elastic behaviour for the material, a massless foundation, a monolithic structure, rigid contact interfaces, and hydrodynamic loads based on the Westergaard method may need to be revised.

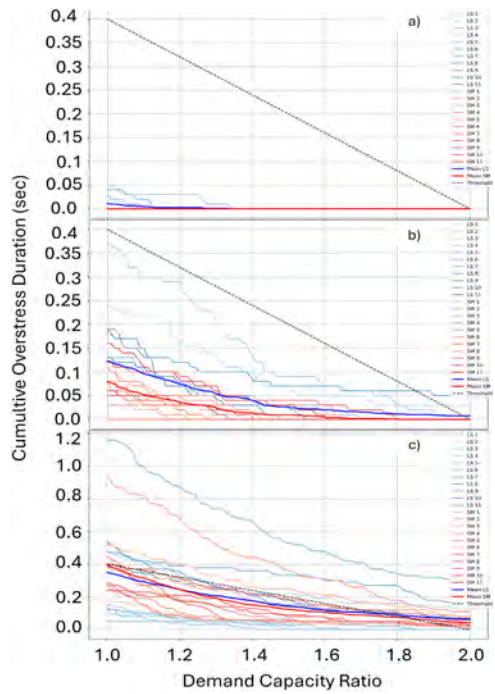

Fig. 9

Demand capacity ratio and the cumulative overstress duration for the maximum vertical tensile stress for zones Z1a (a), Z2 (b) and Z3b (c). The assumed dynamic tensile strength is 4 MPa. The threshold for arch dams is defined based on Ghanaat (2004).

Le rapport demande-capacité et la durée cumulative de surcontrainte pour la contrainte de traction verticale maximale dans les zones Z1a (a), Z2 (b) et Z3b (c). La résistance dynamique en traction supposée est de 4 MPa. Le seuil pour les barrages-voûtes est défini selon Ghanaat (2004).

5. CONCLUSIONS

Table 3 presents a comparison of the average maximum tensile stresses and the normalized standard deviation of maximum tensile stresses for three earthquake zones (Zone 1a, Zone 2, and Zone 3b) under two record treatment approaches: linearly scaling (LS) and spectrally matching (SM). In Zone 1a, the average maximum tensile stresses are slightly higher for the SM records (3.09 MPa) compared to the LS records (3.03 MPa), with the normalized standard deviation being marginally lower for the SM records (0.28) than for the LS records (0.31). In Zone 2, the average maximum tensile stresses are lower by 12.5% for the SM records (5.51 MPa) compared to the LS records (6.30 MPa), however, the normalized standard deviation is significantly reduced in the SM records (0.16) compared to the LS records (0.35). In Zone 3b, the average maximum tensile stresses for the SM records (9.37 MPa) are less 5% lower than those for the LS records (9.86 MPa), with a marked decrease in the normalized standard deviation for the SM records (0.11) compared to the LS records (0.41). This data indicates that while the average maximum tensile stresses between the two treatments are relatively comparable, the use of spectrally matched records (especially for Zones 1a and 3b) tends to result in lower variability in tensile stress distribution across all zones.

Table 3
Comparison of the average maximum tensile stresses and the corresponding normalised standard deviation
Comparaison des contraintes de traction maximales moyennes et de l'écart-type normalisé correspondant.

EARTHQUAKE ZONE	RECORD TREATMENT METHOD	AVE. ASI_H_1 (M/S)	AVE. PGA_H_1 (M/S^2)	IA_H_1 (M/S)	$D_{5\text{-}95}\_H_1$ (S)	AVE. SZZ_MAX (MPA)	NORMALISED STD. SZZ_MAX
Zone 1a	LS	3.89	2.82	0.7	12.44	3.03	0.31
	SM	3.08	2.38	0.68	14.76	3.09	0.28
Zone 2	LS	7.16	5.14	2.41	9.83	6.30	0.35
	SM	5.47	4.18	2.04	11.13	5.51	0.16
Zone 3b	LS	9.88	6.70	4.16	7.52	9.86	0.41
	SM	7.81	6.01	3.52	9.02	9.37	0.11

Moreover, the results indicate that the average values of PGA, and Arias Intensity (Ia) generally slightly decrease from Linearly Scaled (LS) to Spectral Matched (SM) records across different earthquake zones. Whereas the average value of significant duration (D_{5-95}) slightly increases when transitioning from LS to SM.

These observations highlight that in areas with moderate earthquakes (Zones 1b and 2), spectral matching (SM) might result in slightly longer shaking durations but slightly lower Arias Intensities, ASI and PGA potentially resulting in lower values of tensile stresses in arch dams compared to linearly scaled (LS) records by more than 12%. Therefore, it is advised not to use spectral matching for these areas.

In Zone 3b the difference between the maximum tensile stresses for LS and SM records is less than 5%. Additionally, there is a scarcity of records that can be treated with linear scaling to be compatible with the target spectra. Therefore, the necessity of using spectral matching arises. It is suggested to check values of ASI, Arias Intensities and significant durations of all spectrally matched records and compare them to expected values based on established prediction equations (e.g., Afshari and Stewart 2016, Travasarou et al. 2003, Campbell and Bozorgnia 2012) and the hazard disaggregation parameters of the site. Moreover, considering the slightly lower values of the average tensile stresses, it is recommended that the maximum allowable undershoot of the spectrally matched records be set to 95% of the target spectrum as a compatibility criterium.

It should be noted that a more accurate assessment of the dynamic performance of concrete arch dams may necessitate revising the modelling assumptions of this current study, which include linear elastic behaviour of the materials, massless foundation, monolithic structure, rigid contact interfaces, and hydrodynamic loads as defined by the Westergaard method.

REFERENCES

[1] AFSHARI, K., & STEWART, J. P. (2016). Physically parameterized prediction equations for significant duration in active crustal regions. *Earthquake Spectra*, 32(4), 2057–2081.

[2] AKKAR, S., & BOMMER, J. J. (2010). Empirical equations for the prediction of PGA, PGV, and spectral accelerations in Europe, the Mediterranean region, and the Middle East. *Seismological Research Letters*, 81(2), 195–206.

[3] AL ATIK, L. AND ABRAHAMSON, N. (2010). An improved method for non-stationary spectral matching. *Earthquake spectra*, vol. 26, no 3, p. 601–617.

[4] BAKER, J. W., HASELTON, C. B., LUCO, N., STEWART, J. P., & ZIMMERMAN, R. B. (2023). Updated ground motion spectral matching requirements in the 2015 NEHRP recommended seismic provisions.

[5] BAZZURRO, P., & LUCO, N. (2006). Do scaled and spectrum-matched near-source records produce biased nonlinear structural responses. In 8th US National Conference on Earthquake Engineering (pp. 18-22).

[6] CAMPBELL, K. W., & BOZORGNIA, Y. (2012). A comparison of ground motion prediction equations for Arias intensity and cumulative absolute velocity developed using a consistent database and functional form. *Earthquake Spectra*, 28(3), 931–941.

[7] CHOPRA, A. K., & GOEL, R. K. (2001). Direct displacement-based design: use of inelastic vs. elastic design spectra. *Earthquake spectra*, 17(1), 47–64.

[8] GHANAAT, Y. (2004). Failure modes approach to safety evaluation of dams. In Proceedings of the 13th World Conference on earthquake engineering.

[9] HEO, Y., KUNNATH, S. K., & ABRAHAMSON, N. (2011). Amplitude-scaled versus spectrum-matched ground motions for seismic performance assessment. *Journal of Structural Engineering*, 137(3), 278–288.

[10] HUGHES, T. (1987). *The Finite Element Method – Linear Static and Dynamic Finite Element Analysis*. Prentice-Hall, Inc.

[11] PRIESTLEY, M. J. N., CALVI, G. M., & KOWALSKY, M. J. (2007, March). Direct displacement-based seismic design of structures. In NZSEE conference (Vol. 30, pp. 1-23).

[12] SHOME, N., & CORNELL, C. A. (2000, July). Structural seismic demand analysis: consideration of collapse. In 8th ASCE Specialty Conference on Probabilistic Mechanics and Structural Reliability (pp. 1-6).

[13] Swiss Federal Office of Energy SFOE (ed.) (2021). Directive on the Safety of Water Retaining Facilities, Part C3: Seismic safety. Bern, Switzerland.

[14] TRAVASAROU, T., BRAY, J. D., & ABRAHAMSON, N. A. (2003). Empirical attenuation relationship for Arias intensity. *Earthquake engineering & structural dynamics*, 32(7), 1133–1155.

[15] U.S. Army Corps of Engineers (USACE) (1994). *Engineering and Design: Arch Dam Design (EM 1110-2-2201)*. Washington, DC: USACE.

[16] VON THUN, J. L. (1988). Earthquake ground motions for design and analysis of dams. Earthquake engineering and soil dynamics II-recent advances in ground-motion evaluation.

[17] WESTERGAARD, H.W. (1993). *Water pressures on dams during earthquakes*. American Society of Civil Engineers (ASCE), Proceedings.

Q.111 - R.7

COMMISSION INTERNATIONALE DES
GRANDS BARRAGES

VINGT-HUITIEME CONGRES DES
GRANDS BARRAGES
CHENGDU, MAI 2025

DAM SAFETY ANALYSIS CONCEPT FOR FREQUENT CHANGES OF SEISMIC LOADS (*)

Martin WIELAND
Chairman, ICOLD Committee on Seismic Aspects of Dam Design, AFRY SWITZERLAND LTD., Zurich

SWITZERLAND

SUMMARY

Due to the ongoing progress in the field of probabilistic seismic hazard analysis, the results of seismic hazard analysis are still improving, resulting, in general, in increased seismic hazard values at dam sites. Therefore, one would assume that due to the new results a seismic re-evaluation of a dam would always be required. However, one should be aware of the fact that the seismic safety analysis of dams includes various uncertainties which are comparable with those of the seismic hazard. Therefore, simply improving the seismic hazard analyses will not improve the quality of the seismic safety assessment if the other uncertainties remain unchanged. As a result, new safety analyses are not necessary. A new “beyond the SEE ground motion” load combination is proposed as an additional seismic load combination, which provides information on the seismic safety reserves of a dam. This is very useful, in view of the frequent changes of the seismic hazard.

**Concept d’analyse de la sécurité des barrages en cas de changement des charges sismiques*

 DOI: 10.1201/9781003642428-110

RÉSUMÉ

En raison des progrès constants dans le domaine de l'analyse probabiliste de l'aléa sismique, les résultats de l'analyse de l'aléa sismique continuent de s'améliorer, ce qui se traduit, en général, par une augmentation des valeurs de l'aléa sismique sur les sites des barrages. Par conséquent, on pourrait supposer qu'en raison des nouveaux résultats, une réévaluation sismique d'un barrage serait toujours nécessaire. Cependant, il faut savoir que l'analyse de la sécurité sismique des barrages comprend diverses incertitudes qui sont comparables à celles de l'aléa sismique. Par conséquent, le simple fait d'améliorer les analyses du risque sismique n'améliorera pas la qualité de l'évaluation de la sécurité sismique si les autres incertitudes restent inchangées. Par conséquent, de nouvelles analyses de sécurité ne sont pas nécessaires. Une nouvelle combinaison de charges « au-delà du mouvement du sol SEE » est proposée comme combinaison de charges sismiques supplémentaire, qui fournit des informations sur les réserves de sécurité sismique d'un barrage. Ceci est très utile, compte tenu des changements fréquents de l'aléa sismique.

1. INTRODUCTION – UNCERTAINTIES IN THE SEISMIC ANALYSIS OF DAMS

The uncertainties in the seismic analysis of dams have increased substantially since the change from the pseudo-static seismic analysis to a more realistic dynamic analysis of dam-reservoir-foundation systems. In the pseudo-static analysis, the seismic loads (inertia forces and hydrodynamic pressures) were represented by a seismic coefficient. The uncertainties in the seismic safety analysis were related to (i) the material properties (e.g., the tensile strength of mass concrete or residual strength properties to be used in sliding stability analyses of concrete and embankment dams), (ii) the seismic coefficient (usually a value of 0.1 was used, almost independently of the seismic hazard at the dam site), (iii) the seismic load combinations, and (iv) the combination of the horizontal and vertical earthquake components. As the seismic loads were generally low, the seismic load combinations did not govern the design of most dams. Therefore, it was possible to use the most unfavorable set of parameters to assess the seismic safety of the dam.

With the change of the methodology towards a dynamic analysis, several additional factors have to be considered. Because of the new seismic safety criteria for dams, requiring the dam to resist the worst ground motion at the site, the seismic load combinations became the decisive design factor for most storage dams with large damage potential. The uncertainties in the dynamic analysis of dams are as follows (Wieland et al., 2005):

1. Uncertainties in the earthquake ground motion represented by spectrum-matched acceleration time histories in which the duration of strong ground

shaking is a key parameter when used as input for nonlinear dynamic analyses (Wieland, 2018; Wieland, 2022b).

2. Uncertainties in the dynamic analysis models of dam-reservoir-foundation systems: The water in the reservoir can be modelled as a compressible or an incompressible fluid and the foundation as either massless or with mass. The dynamic interaction of the dam with the foundation and the reservoir is the main concern, which has also implications on how the seismic ground motion is applied. Separate numerical models are used for deformation and stress analyses and for dynamic stability analyses. Depending on the type of nonlinearities, other types of dam models are used.
3. Uncertainties in dynamic material properties of the dam and foundation materials: In large concrete dams, the damping ratio has the greatest impact on the dynamic response. The material models used in inelastic seismic analyses are quite complex, as these models use parameters which are not readily available, therefore, comprehensive sensitivity studies are necessary to investigate their effect on the dynamic response.
4. Uncertainties in the definition of acceptable or allowable deformations and stresses (e.g., tensile stresses exceeding the dynamic tensile strength and the resulting tension cracks are accepted, whereas compressive stresses which exceed the compressive strength of mass concrete cannot be accepted except at locations of stress singularities, such as sharp corners).

Moreover, for large storage dams, the seismic hazard is a multi-hazard: Besides ground shaking, it includes the effects of mass movements at the dam site and into the reservoir or even in the catchment area, the effects of active faults or discontinuities in the footprint of the dam, which can be activated during strong earthquakes, and other site-specific and project-specific hazards (Wieland, 2009). However, in this paper the emphasis is on ground shaking. For the other seismic hazards, different analysis methods may be required.

From the above list, it is evident that due to the shift towards a dynamic analysis of dams, additional uncertainties have appeared. The first development, which has led to the improvement of the numerical analysis of dam-reservoir-foundation systems, is the finite element method. Significant progress was achieved in this field, and there exist several general-purpose finite element programs for linear and nonlinear dynamic analysis of dams. The analysis methods have reached a satisfactory level, which means that further improvements in the analysis methods do not necessarily improve the accuracy of the dynamic response of a dam during a strong earthquake as long as the uncertainties in other fields remain unchanged.

As already pointed out, the damping ratio is the key unknown factor in the dynamic analysis of concrete dams.

For embankment dams, the inelastic dynamic analysis methods have not progressed much since the 1970s.

The situation is different for the seismic hazard analysis, which started with the construction of the first commercial nuclear power plants. As the safety of these power plants is determined by a probabilistic safety analysis, a probabilistic description of the seismic hazard was required, which led to the development of the probabilistic seismic hazard analysis (PSHA). However, as the database of strong earthquakes was very limited at that time, the attenuation laws required for seismic hazard analyses were quite simple. With an increased number of strong motion data, it was possible to develop better attenuation laws. The present attenuation laws, called NGA-West2, developed over the last 10-15 years, represent the current state-of-the-art. As these attenuation laws (also referred to as ground motion prediction equations) were calibrated for strong earthquakes recorded worldwide, are suitable for the seismic hazard analysis of large dams. In seismic guidelines for dams (ICOLD, 2016) a return period of the ground motion parameters of up to 10,000 years is required.

It is often argued that attenuation laws developed from data recorded in the region where a dam project is located should be used in the seismic hazard analysis. Although this would be desirable, it is not feasible at the present time, as the number of strong earthquake records is too small; furthermore, the calibration of region-specific attenuation laws is inadequate, especially in the range of seismic motions that are relevant for dams. This can lead to incorrect estimates of the ground motion parameters of very strong earthquakes; such site-specific attenuation laws cannot be used for large dams, but may be correct in the range of the return periods typically used in seismic building codes.

There are major uncertainties in the dynamic material properties of mass concrete, embankment dam materials and the foundation rock. These uncertainties may be accounted for by sensitivity analyses. If earthquake records or ambient vibration data are available for a concrete dam, then the elastic material parameters of mass concrete and the foundation rock can be determined by calibration of the dam model. However, the calibrated material properties of concrete dams may differ substantially from the measured ones, therefore, confidence in calibrated models is limited.

Finally, there is a major question of how to use the results of dynamic analyses and how to determine the acceptable dynamic response of a dam. The main results of an inelastic dynamic analysis are the dam deformations at the end of an earthquake. However, the main result from a linear-elastic analysis of concrete dams is the maximum dynamic deformation and the maximum static and dynamic principal stresses.

The refinement of the numerical model reveals higher stresses at kinks and corners in the dam-foundation model. From the theory of elasticity, we know that stress singularities with theoretically infinite tensile and compressive stresses occur at sharp corners. Therefore, cracks may develop at such locations during an earthquake.

This short qualitative discussion shows that with increasing demand for accuracy, the complexity of the dynamic analysis increases. A major problem are the material parameters needed in some of the soil, rock and concrete models, as some of them

may be difficult to obtain. Moreover, acceleration time histories are required as the seismic input for the dynamic analysis. A large number of seismologists are working on the improvement of the seismic hazard analysis methods and new results are published almost daily. Therefore, the question arises on how often a seismic re-analysis of a dam must be made, as the dam safety assessment should be based on the current state-of-the-art. Accordingly, any change in parameters or input data relevant for the analysis of a dam-reservoir-foundation system would require a re-analysis, which is not practicable. This problem is the main subject discussed in this paper.

2. NEED FOR THE SEISMIC SAFETY RE-ANALYSIS OF DAMS

There are a number of reasons for carrying out seismic safety evaluations of large water dams as well as tailings dams: These are as follows (Wieland, 2022a):

- New information on the seismic hazard (ground shaking, mass movements) and/or seismotectonics is available;
- A dam has been subjected to strong earthquake shaking;
- New seismic design criteria are introduced;
- New seismic performance and safety criteria are introduced;
- New dynamic methods of analysis are introduced, such as nonlinear dynamic analysis methods;
- Certain dam types and poorly designed, constructed and maintained dams are vulnerable to earthquakes.
- The seismic vulnerability of a dam has increased due to dam modifications, ageing, etc.
- Changes in the risk classification of dams; and
- The seismic risk has increased, e.g., due to the increased number of people living downstream of a dam and/or due to economic development, etc.
- It is obvious from this extensive list that there are various reasons why the seismic safety of a dam has to be reassessed. Changes in the seismic hazard are only one of these reasons. Besides these important reasons, there are other reasons discussed in the previous section that are related to various types of uncertainty in the dynamic analysis of dams.

3. ASSUMPTIONS FOR THE SEISMIC SAFETY ANALYSIS OF DAMS

The following assumptions and recommendations are usually made for the seismic analysis of large concrete dams:

1. Uniform ground motion along boundaries of the dam foundation.
2. Use of three spectrum-matched, statistically independent acceleration time histories of the horizontal and vertical earthquake components (ICOLD, 2016).

These records must have a long duration of strong ground shaking and include an extension to account for possible aftershocks (Wieland, 2022b). This feature is relevant for nonlinear seismic analyses including dynamic stability analyses.

3. The dam foundation is massless.
4. The water in the reservoir is incompressible.
5. For nonlinear dynamic analyses, simplified post-cracking models can be used in which sliding along lift joints, the dam-foundation contact and/or sliding surfaces in the foundation rock may be assumed. For arch dams, block joint opening and sliding may be assumed, ignoring e.g., the effect of shear keys. For the sliding of detached blocks, residual strength properties of concrete and rock should be used (zero cohesion).
6. Best estimate dynamic material properties should be used and much attention must be paid to the selection of the damping ratio, which is often over-estimated (5% damping is the maximum allowed in the Swiss earthquake guidelines for concrete dams).
7. The critical seismic load combination includes permanent static loads without temperature effects, full reservoir and the worst-case seismic ground motion that is called the safety evaluation earthquake (SEE) ground motion.

These assumptions and recommendations simplify the dynamic analysis and the resulting dynamic response is generally conservative. Therefore, if a dam is safe based on such an analysis, no more sophisticated dynamic analyses are required. This relatively simple analysis case should always serve as a reference for more comprehensive analyses, especially when dynamic interaction effects of the dam with the compressible reservoir and the mass of the foundation are accounted for, which, in general, result in a smaller dynamic response as the reference case. There are still questions about the dynamic interaction effects of the dam with the foundation because of the local topography and the behavior of the different foundation rocks, joint systems and other discontinuities including shear zones, anisotropic material behavior, etc., which cannot be modelled and analyzed properly. Therefore, the radiation damping in the foundation may be greatly overestimated if homogeneous and isotropic foundation conditions (e.g., half-space or layered half-space) are assumed.

For the dynamic analysis of embankment dams, the assumptions are similar to those for concrete dams. The main differences are in the selection of the static and dynamic material laws of the different embankment materials. Most data are for shear strain dependent shear moduli and damping ratios of different soil types. These dynamic analyses are carried out by the linear equivalent analysis method, developed in the late 1960s. The results are then used as input for a Newmark-type sliding block analysis of critical dam and abutment slopes. Again, this is the simplest dynamic analysis of embankment dams, which should be carried out as a reference for more sophisticated dam analyses. Moreover, due to the flat upstream face of embankment dams, the hydrodynamic pressure can be neglected. Also for dams founded on rock with stiffness ratios between the foundation rock and the fill material

that may be generally in the range of 10 to 100 or more, the dynamic interaction effects play a much smaller role than in the case of concrete dams, especially when the stiffness ratio is 100 or more.

These assumptions and recommendations made for the reference dynamic analyses of concrete and embankment dams may overestimate the dynamic response considerably, if records of strong earthquakes taken from well-instrumented dams were to be re-analyzed. Unfortunately, only few records exist for moderate earthquakes recorded in well-instrumented dams. More observational data of strong earthquakes will become available in the near future, which will allow an improvement of the dam analysis models; however, generalization of such dynamic analysis results will be difficult, as each dam project is unique.

This rather lengthy discussion was necessary in order to put into perspective the importance of a seismic re-analysis, due to new or updated findings. It is a misconception to believe that the improvement of seismic analysis methods improves the seismic safety assessment of a dam, when the uncertainties in the other fields remain unchanged. Improving the reliability of safety assessments would need a simultaneous improvement in the seismic hazard, the methods of dynamic analyses, and the behavior of different dam and foundation materials under seismic actions. The basis of any safety assessment is the identification and analysis of the seismic failure modes and the definition of the corresponding limit states.

4. PROPOSED CONCEPT FOR AVOIDING FREQUENT CALLS FOR THE SEISMIC RE-ANALYSIS AND SAFETY ASSESSMENT OF LARGE DAMS

The ICOLD Committee on Seismic Aspects of Dam Design has called for the seismic safety assessment of existing dams since 1999, when the author became Chairman of that committee. Since then, a number of countries and dam owners have taken up this recommendation and carried out such safety assessments and others are planning to do it. This slow process could be accelerated if the dam safety authorities in all countries would require that seismic safety evaluations be carried out in order to check if their dams satisfy the current seismic safety guidelines of ICOLD (ICOLD, 2016) or their own dam safety guidelines. The objective of the seismic safety assessment is to verify that all dams satisfy the current seismic safety criteria. This was and still is necessary, because most dams built before the 1990s were designed to resist earthquakes using the now outdated and obsolete pseudo-static analysis concept, which sometimes is also called the limit-equilibrium method. It turned out that the peak ground acceleration (PGA) at some dam sites determined from site-specific seismic hazard analyses is up to a factor of 5 or even 10 times higher than the typically used pseudo-static acceleration of 0.1 g. In dams built before the mid-1930s, earthquakes were not among the standard load cases for the dam design and this was still the case until recently in some regions of low seismicity.

Although the earthquake load case with a seismic coefficient of 0.1 did not govern the dam design, most well designed, constructed, maintained and operated dams had considerable seismic safety reserves and satisfy todays seismic safety criteria. Seismic strengthening measures were mainly required in dams which had already other types of structural and safety deficiencies. Therefore, the process of seismic safety evaluation of existing water dams is still progressing and now it is adapted for tailings dams, which belong to the most vulnerable dams during earthquakes.

At present, the main drive behind the seismic safety checks is the rapid development in the field of the probabilistic seismic hazard analysis, as an increased number of records of strong earthquakes have become available and the number of records is growing rapidly.

In recent years, significant progress was made in the field of probabilistic seismic hazard analysis. The focus of these analyses was on the development of seismic hazard maps for earthquake building codes using return periods of 475 years and 2475 years. However, for high consequence dams the ground motion parameters are required for return periods of up to 10,000 years. Such seismic hazard maps are usually unavailable; therefore, site-specific seismic hazard analyses are required for large dams, which may be quite costly. Moreover, due to the ongoing research on seismic hazard assessment, the seismic hazard for a specific project may change from year to year or even faster. This is an unfortunate situation for dam engineers, as they cannot wait for the latest results announced by researchers, as it is necessary to decide upon the seismic design criteria in order to be able to go ahead with the design of the different structures and components of a large dam project. It may happen that during or shortly after completion of dam construction, new seismic hazard analysis results are provided by seismic hazard analysts implying that a seismic re-analysis should be carried. Of course, this can be done but is not in the interest of any dam owner as such analyses require a considerable effort. In order to avoid frequent seismic safety analyses, the following options are possible:

1. To check the seismic safety of a dam for a ground motion that exceeds the anticipated ground motion at the dam site.
2. To check the ultimate seismic capacity of a dam and the corresponding failure modes.
3. To check the seismic safety of the dam for SEE acceleration records which are scaled by factors of 1.5 or 2.0.
4. To check the safety of dams for horizontal ground motions with a minimum PGA of 0.3 g. This requirement is similar to the concept of a seismic coefficient of 0.1 used almost worldwide for the seismic design of dams in the past.

In general, a moderate change in the seismic hazard would not require a new seismic safety analysis of well-designed, well-constructed and well-maintained dams (ICOLD, 2001). In terms of PGA a moderate change is a value of about 30%

of the horizontal PGA of the SEE exceeding 0.3 g. For PGA values of less than 0.3 g, 0.1 g may be considered as a moderate change.

Option 1 is feasible for the safety check of well-designed and well-constructed small consequence dams at locations with low to moderate seismicity. For example, by checking the seismic safety of a dam for an earthquake with a PGA of 0.5 g in a region where little information on the seismic hazard exists and the seismic hazard is estimated as about 0.2 g or less, the analysis of an expensive site-specific seismic hazard study can be avoided.

Option 2 would be the best option, but it will be very time consuming to calculate the seismic reserves of a dam, as various failure modes must be analyzed. It is obvious that such analyses include major uncertainties.

Options 3 and 4 are the recommended options and require the analysis of an additional load combination, called “beyond the SEE ground motion” load combination.

According to option 3, if the PGA of any future seismic hazard analyses is less than the PGA of the “beyond the SEE ground motion” load combination, then the seismic safety criteria are satisfied.

According to option 4, if the updated PGA of the SEE is less than 0.3 g, then the seismic safety criteria are satisfied.

Therefore, by analyzing an additional “beyond the SEE ground motion” load combination, future dam safety re-assessments can be minimized. However, these options only apply to changes in the seismic hazard. As much research is carried out on the seismic hazard analysis, the seismic hazard is the parameter that may undergo the greatest changes in the near future.

In the above discussion, the seismic hazard is represented by the PGA as a single parameter. A better engineering representation of the seismic hazard is by means of acceleration response spectra. It is assumed that in the “beyond the SEE ground motion” load case all spectrum values are scaled by the same factor as the PGA.

Moreover, in nonlinear dynamic analyses the duration of strong ground shaking, or the number of significant load cycles, is more important than the PGA of a short earthquake. For example, sliding movements depend almost linearly on the duration of strong ground shaking, a parameter, which needs further attention by the seismologists.

If increased seismic hazard values are published and the above additional load case has not been analyzed, then the seismic safety of dams will always be questioned. Unfortunately, the dam owners are usually not in a position to reply to

such concerns. Therefore, a pro-active approach would be of great advantage. The concept of “beyond the SEE ground motion” load case is not new and is recommended in the nuclear industry, where a beyond-seismic-design load case is specified, whereby the worst ground motion is multiplied by a factor of 1.3. This is a useful concept, which is also recommended for other hazards like floods, which may change due to climate change, etc. It is known that several natural and especially man-made hazards are changing with time. Furthermore, the design and safety criteria are also changing, therefore knowing the safety reserves of dams is very useful.

5. FREQUENCY OF SEISMIC SAFETY CHECKS OF DAMS

It is important to know that seismic safety checks have to be carried out repeatedly during the long economic life of large dams, which can easily exceed 100 years if they are well maintained. As discussed in the previous sections, one could find several reasons for improving the seismic safety assessment of dams and even more reasons could be found if the complexity of seismic analysis is increased. It would be a nightmare if dam engineers would have to upgrade the seismic analysis frequently, e.g. every year. To avoid such situations, two measures are recommended as follows:

1. To include the “beyond the SEE ground motion” load combination in the seismic safety evaluation of a dam.
2. To carry out detailed dam safety inspections and evaluations (e.g., every five years) in which the seismic design and safety criteria are reviewed. If there are major changes, a safety re-assessment is recommended.

As the information on the seismic hazard and the seismic design and safety criteria are not changing frequently, it is expected that seismic safety evaluations are only required every 20 to 40 years or even less frequently in Europe. The main candidates for a seismic re-analysis are dams which have shown signs of unusual behavior. These are also the dams that may require seismic upgrading.

As pointed out earlier, eventually the seismic safety of all existing dams, especially older ones, must be reconfirmed on the basis of current safety criteria.

Some problems may arise if the number of dams that have to be checked is very high. In this case, a ranking system in which several factors like seismic hazard, dam type, age of dam, condition of the dam, consequences of dam failure, etc. are considered, is recommended.

Another problem may arise if a revised seismic hazard analysis has shown an increased seismic hazard shortly after completion of a comprehensive seismic

safety assessment of dams. If the seismic hazard expressed in terms of PGA does not increase by more than about 0.1-0.2 g, then a re-analysis would only be recommended for borderline projects, i.e. projects which according to the present analysis could satisfy the seismic safety criteria only with the help of sophisticated dynamic analyses or by making optimistic assumptions. In general, a moderate increase in the seismic hazard does not really change the seismic safety of the dam, as there are numerous other “uncertain” factors, which have an equal effect on the seismic response of the dam. Therefore, the accuracy of seismic safety assessment does not change by improving only a single factor.

Seismic reassessment should only be done when they are really needed and not when non-experts in seismic safety evaluations push for a re-analysis. Of course, nothing is wrong in doing re-analyses, but when the benefits are marginal, there is little use for it.

However, a change of the seismic hazard should be used as a chance to request the dam owners to check the “beyond the SEE ground motion” load combination, which would be beneficial to the dam owners, if the result is positive. This should be the case for well-designed and well-constructed dams in countries of moderate to high seismicity.

6. SEISMIC SAFETY CRITERIA FOR LARGE DAMS

Today’s seismic safety criteria are quite general and allow much room for interpretation. A dam subjected to the SEE ground motion must satisfy the following safety criteria (Wieland, 2022a):

- retaining the reservoir and protecting people from the catastrophic release of water from the reservoir,
- controlling the reservoir level after an earthquake, as a dam could be overtopped and destroyed if the inflowing water into the reservoir cannot be released through damaged spillways or low-level outlets, and
- lowering the reservoir level after an earthquake (a) for repair works or (b) for increasing the safety of a damaged dam or when there are doubts about the safety of a dam; this requires the construction of low-level outlets in storage dams.

More specifically, the SEE safety criteria for the dam body and safety-critical components and equipment are as follows:

- Dam body: Structural damage (cracks, deformations, leakage etc.) is accepted as long as the stability of the dam is ensured and there is no uncontrolled release of large quantities of water from the reservoir.

- Safety-critical components and equipment: These components and equipment must be fully operable during and after the SEE. Minor distortions are accepted as long as they have no impact on the proper functioning of the components and equipment (Wieland, 2017).
- Abutment rock (important for arch dams): All potential abutment wedges must be safe.
- Reservoir slopes: No mass movements into the reservoir which could block intakes of the spillway or low-level outlets or create large impulse waves in the reservoir that could cause overtopping of the dam crest, are accepted. This requirement is very important for embankment dams, as overtopping may cause dam failure.
- Catchment area: Earthquakes may cause landslide dams, debris flows along rivers or glacier lake outburst flows that may create large floods transporting huge amounts of sediment; these events, observed in mountainous regions like the Himalayas, are a threat to run-of-river power plants, diversion structures and storage dams with small reservoir and embankment dams, which could be overtopped and fail; sliding stability failure could also be due to the overtopping of small concrete dams.

Moreover, any seismic safety analysis of a dam must include a comprehensive failure mode analysis. The failure modes depend on the dam type, the safety-critical elements, local site conditions and the multiple hazards created by strong earthquakes.

7. CONCLUSIONS

The main conclusions of the qualitative assessment of the factors and uncertainties in the seismic safety assessment of dams, which may require a safety re-assessment of dams, are as follows:

1. The seismic hazard is a multi-hazard for most dam projects. Ground shaking is the main hazard considered in all earthquake guidelines for dams and other structures, but the other hazards such as fault movements in the footprint of dams or large mass movements may be even more important than ground shaking.
2. A failure mode analysis of a dam is required, in which all hazards associated with strong earthquakes are considered.
3. The seismic safety analysis of dams – a time history analysis is today's state-of-practice – including different types of uncertainties related to the seismic input (usually ground shaking), the numerical modelling of the dam-reservoir-foundation system, the static and dynamic material properties and the quantification of the dam safety criteria (usually deformations) is needed.
4. As a reference case, a simplified dynamic analysis should be carried out in which the foundation rock is assumed massless; other assumptions are necessary for any dynamic analysis.

5. There are several reasons for performing seismic safety analyses of large dams and one of them is related to changes in the seismic input. By means of periodic safety reviews (e.g. every 5 years), which include the review of the seismic design and safety criteria, a recommendation for a seismic re-analysis could be made.
6. Minor changes in the seismic hazard in the order of 0.1-0.2 g in regions of moderate to strong seismicity do not require any re-analysis of well-designed, well-constructed and well-maintained dams.
7. A “beyond the SEE ground motion” load combination, in which the ground motion of the safety evaluation earthquake is multiplied by a factor of 1.5 or 2.0, is recommended as an additional seismic load combination. This load combination can be used to determine the seismic safety reserves of a dam project. At the same time, there will be no need for a seismic re-analysis of dams, when the increased seismic hazard is less than that of this extreme load combination.
8. As the seismicity at a dam site does not change drastically with time – but the seismic hazard analysis methods are being improved continuously – and since the dam design and safety criteria are also not changing frequently, it is expected that a comprehensive seismic safety evaluation of a dam may only be required approximately every 20 to 40 or even 50 years, unless a dam shows signs of unusual behavior or its risk classification is increased.
9. It is a well-known fact that in view of the different types of uncertainty in the seismic safety analysis of dams, the ongoing improvement of the seismic hazard analysis methods do not necessarily result in an improvement of the dam safety assessment, when the other uncertainties are not reduced. Therefore, frequent seismic safety evaluations due to improvements in the seismic hazard analysis are generally not required.
10. A similar load combination such as “beyond the SEE ground motion” could also be used for other hazards, which show the tendency to increase, e.g. the flood hazard.

The concept of the “beyond the SEE ground motion” load combination is very useful, as dam owners would be able to answer immediately any public concerns regarding the seismic safety of dams, whenever new seismic hazard values are announced, which happens quite frequently. Therefore, this load combination should be included in future seismic guidelines of ICOLD.

ACKNOWLEDGEMENTS

The opinions expressed in this paper are those of the author, which are not necessarily those of ICOLD or AFRY.

REFERENCES

[1] ICOLD (2001) *Design Features of Dams to Effectively Resist Seismic Ground Motion, Bulletin 120, Committee on Seismic Aspects of Dam Design*, ICOLD, Paris, 2001.

[2] ICOLD (2016) *Selecting Seismic Parameters for Large Dams, Guidelines, Bulletin 148, Committee on Seismic Aspects of Dam Design*, ICOLD, Paris, 2016.

[3] WIELAND M., GUIMOND R., MALLA S. (2005) Uncertainties in seismic analysis of concrete and embankment dams, *Proc. Symposium on Uncertainty Assessment in Dam Engineering, Paper No. 015-S1, 73rd Annual Meeting of ICOLD*, Tehran, Iran, May 1-6, 2005.

[4] WIELAND M. (2009) The many features of the seismic hazard in large dam projects and strong motion monitoring of large dams, *Proc. 2nd Int. Conf. on Long-term Behaviour of Dams*, Graz, Austria, Oct. 12-13, 2009.

[5] WIELAND M. (2017) Seismic aspects of safety relevant hydro-mechanical and electro-mechanical elements of large storage dams, *Proc. Symposium, 85th Annual Meeting of ICOLD*, Prague, July 3-7.

[6] WIELAND M. (2018) Models of earthquake ground shaking used in seismic design and safety checks of large dams, *Int. Journal of Civil Engineering*, https://doi.org/10.1007/s40999-018-0339-3, June 2018.

[7] WIELAND M. (2022a) The urgent need for the seismic safety evaluation of existing dams, *Proc. International Dam Safety Conference*, Jaipur, Rajasthan, India, Oct. 10-12, 2022.

[8] WIELAND M. (2022b) Importance of duration of strong ground shaking on seismic safety assessment of dams and infrastructure projects, *Proc. 3rd European Conference on Earthquake Engineering & Seismology (3ECEES)*, Bucharest, Romania, Sep. 4-9, 2022.

Q.111 - R.8

COMMISSION INTERNATIONALE DES
GRANDS BARRAGES

VINGT-HUITIEME CONGRES DES
GRANDS BARRAGES
CHENGDU, MAI 2025

COMPARISON OF EARTHQUAKE DAM SAFETY EVALUATION OF LARGE EMBANKMENT DAMS WITH EARTHFILL CORE IN DIFFERENT PARTS OF THE WORLD (*)

Stefan EHLERS
Section Head Dam Engineering, AFRY Switzerland Ltd.

SWITZERLAND

SUMMARY

A comparison of the methodologies considered for earthquake dam safety evaluation of five large embankment dams with earthfill core, located on three different continents, is presented. The comparison focuses on the determination of the seismic loads and highlights the importance of national guidelines to reach consistency regarding the level of safety.

The study further comprises the analyses methods used (pseudo-static method, simplified deformation analyses, sliding block analyses, non-linear deformation analyses, post-earthquake stability analyses) and the performance criteria applied. Each method is evaluated in terms of advantages, limitations and disadvantages regarding the accuracy and reliability of the analyses results. Additionally, the requirements for budget, time and computational resources are discussed. Explanation is given why analyses methods developed in the 1960s are still attractive compared to sophisticated non-linear analyses.

Comparaison de l'évaluation de la sécurité au séisme des grands barrages en remblai avec noyau en terre dans différentes parties du monde

 DOI: 10.1201/9781003642428-111

RÉSUMÉ

Une comparaison des méthodologies utilisées pour l'évaluation de la sécurité sismique de cinq grands barrages en remblai à noyau en terre, situés sur trois continents différents, est présentée. La comparaison se concentre sur la détermination des charges sismiques et souligne l'importance des directives nationales pour assurer une cohérence en matière de niveaux de sécurité.

L'étude porte également sur les méthodes d'analyse utilisées (méthode pseudo-statique, analyses simplifiées de déformation, analyses de blocs glissants, analyses de déformation non-linéaire, analyses de stabilité post-séisme) et les critères de performance appliqués. Chaque méthode est examinée en termes d'avantages, de limitations et d'inconvénients concernant la précision et la fiabilité des résultats d'analyse. De plus, les exigences en termes de budget, de temps et de ressources informatiques sont discutées. Une explication est fournie pour expliquer pourquoi les méthodes d'analyse développées dans les années 1960 restent attrayantes par rapport aux analyses non-linéaires sophistiquées.

1. INTRODUCTION

This article covers the earthquake safety evaluation of the five large embankment Dams A to E with an earthfill core as sealing element. The dams are located on three different continents (Table 1). All dams are large dams according to the definition of the International Commission on Large Dams. Embankment Dam D is 15 m high and connected to a 47 m high gravity dam. As the reservoir volume exceeds by far 1 million m^3, Dam D is clearly a large dam according to the definition of ICOLD (ICOLD, 2016).

For Dams B and C national dam safety guidelines exist and the national dam hazard classification applies. Dam B impounds a reservoir with a volume of about 424 million m^3 at Maximum Operation Level. Thus, Dam B is allocated to group A+ as structure of great importance according to the guidelines of Mexico, because its failure would cause the loss of life and would lead to serious ecological, economic, and social loss (IIE-CFE, 2008). Dam C is a large dam of category I according to the geometrical criteria of the Swiss dam safety directive (SFOE, 2016). Thus, all Dams A to E belong to the highest hazard category according to ICOLD and applicable national guidelines.

The earthquake safety of Dams A to E has been evaluated in the years 2015 to 2020. The analyses and evaluations have been carried out according to the directives and guidelines applicable at the time of project execution. The present comparison includes some simplifications and concentrates on aspects, which are relevant for the comparison.

Table 1
Earth core embankment dams

DAM		HEIGHT	GUIDELINE SEISMIC CRITERIA	PGA[1)]
A	Philippines	131 m	ICOLD[2)]	0.89g
B	Mexico	47 m / 15 m	Mexico[3)] / ICOLD[4)]	0.21g / 0.42g
C	Switzerland	91 m	Swiss Guideline[4)]	0.27g
D	Armenia	77 m	ICOLD[2)]	0.62g
E	Colombia	230 m	ICOLD[2)]	0.61g

[1)]horizontal Peak Ground Acceleration
[2)]Earthquake with return period 10,000 years or deterministically determined (84th percentile level)
[3)]Earthquake with return period 2,450 years
[4)]Earthquake with return period 10,000 years

2. SEISMIC LOADS AND PERFORMANCE CRITERIA

2.1. Introduction to seismic loads and performance criteria

Earthquakes are multiple hazard events and include ground shaking, displacements along potentially active faults, landslides, rockfalls, and other site-specific and project-specific hazards. Only the direct impact of ground shaking on the dams is covered in this article.

2.2. ICOLD Bulletin 148

In projects A, B, D and E, the seismic loads had to be determined according to “international guidelines” due to the Client’s request. In these projects, ICOLD Bulletin 148 (ICOLD, 2016) was the accepted reference for determination of the design criteria. Thus, the large storage dams A, B, D and E have to withstand the worst ground motion at the dam site, meaning to retain the reservoir and to protect people from the catastrophic release of water from the reservoir. This means that a dam should be analyzed for the Safety Evaluation Earthquake (SEE), which, for the extreme or high consequence Dams A, B, D and E, should be estimated at the 84th percentile level if developed by a deterministic approach, and needs not have a mean annual exceedance probability (AEP) smaller than 1/10,000 if developed by a probabilistic approach.

2.3. Dam A (Philippines) seismic loads

A site specific Probabilistic and Deterministic Seismic Hazard Assessment Study was conducted. For the SEE the maximum horizontal Peak Ground Acceleration on the rock surface was determined to PGA = 0.89 g. Three sets of spectrum-matched acceleration records were considered, each set with acceleration time histories in x-, y- and z-direction. The time histories were generated based on recorded time histories, which were scaled and matched to the site-specific response spectrum.

2.4. Dam B (Mexico) seismic loads

The seismic loads to be considered in the stability and safety analyses of dams in Mexico are defined by the Mexican Guideline for seismic design of civil structures (CFE, 2008). Thus, Dam B needs to be analyzed for the Failure Limit State (FLS) and the corresponding earthquake with a return period of 2,450 years. As requested by the Client, Dam B had also to be evaluated according to international guidelines. For Dam B it was decided additionally to evaluate for an earthquake of 10,000 years return period, following the probabilistic design criteria for the SEE according to ICOLD Bulletin 148.

The earthquake load for the FLS as well as for the SEE was determined with the software Prodisis provided by the Mexican authorities (IIE-CFE, 2014). Thus, the Peak Ground Acceleration (PGA) on the rock foundation at Dam B site for the group A+ structure is 0.21 g for the FLS and 0.42 g for the SEE. Three sets of acceleration time history records for the FLS as well as for the SEE were considered, which were generated with the software Prodisis.

2.5. Dam C (Switzerland) seismic loads

For Dam C, the seismic load of an event with a statistical return period of 10,000-years had to be considered for the class I dam. Based on the seismic hazard map (FOWG, 2003), for the location of Dam C a MSK intensity of 8.6 and horizontal Peak Ground Acceleration of 0.27 g was determined. For analysis three sets of acceleration time histories were considered, each set with a horizontal and a vertical time history. The minimum duration of the time histories was calculated to 18.5 s (according to FOWG, 2003). The time histories were generated based on time histories given by the Swiss Dam Safety authority FOWG, which were scaled and matched to the site-specific response spectrum.

2.6. Dam D (Armenia) seismic loads

For Dam D a site-specific Probabilistic and Deterministic Seismic Hazard Assessment Study was prepared. The deterministically determined Most Credible Earthquake (MCE) was considered as the Safety Evaluation Earthquake (SEE) for earthquake analysis. The maximum horizontal peak ground acceleration on the rock surface for dam D was determined to be PGA = 0.62 g. Two sets of artificial spectrum matched acceleration time histories were provided by the Client for dam analysis.

2.7. Dam E (Colombia) seismic loads

A site-specific Probabilistic and Deterministic Seismic Hazard Assessment Study was prepared for Dam E. For the SEE the horizontal Peak Ground Acceleration on the rock surface was determined to be PGA = 0.89 g. The time histories were prepared by a third-party consultant.

2.8. Comparison and discussion of seismic loads and performance criteria

ICOLD Bulletin 148 (ICOLD, 2016) is the accepted reference for seismic design criteria in the international dam business. Thus, for extreme to high consequence dams, the probabilistically determined 1/10,000-year earthquake event or the deterministically determined earthquake at 84th percentile level, shall be considered. This seems to be the upper boundary in many countries of moderate to high seismicity. However, in some areas of low seismicity, e.g. in UK and Ethiopia, return periods of 30,000 years have been considered for very large dam projects (Wieland, 2024).

For Dams A, D and E, a site-specific seismic hazard analysis study was carried out. Although there seems to be a common understanding about the general methodology for such a study, e.g. as formulated in Kramer, 1996 or Studer *et al.*, 2007, the input ground motions determined from Seismic Hazard Assessment Studies for seismic analysis of a specific dam are not consistent when prepared according to different national guidelines or by different Consultants. The reason is that an earthquake hazard is one of the least known hazards and strong earthquakes are rare events. The estimation of the ground motion at the dam site for the strongest earthquakes with a very low probability of occurrence is associated with major uncertainties (Wieland, 2024).

In Table 1 the Peak Ground Acceleration of the earthquake loads is shown to provide an indication about the earthquake load for the different dam projects.

However, with regards to embankment dams with an earthfill core, it is highlighted that inelastic deformations, the build-up of pore pressure in the earthfill core and other damage mechanisms depend on the duration of strong ground shaking. Therefore, the duration of the acceleration time histories plays also an important role in earthquake dam safety engineering.

3. EARTHQUAKE ANALYSIS OF DAMS A TO E

3.1. DAM A (PHILIPPINES)

In 2015 AFRY Switzerland Ltd. (Pöyry Energy Ltd. at the time of project execution) carried out a Rehabilitation Study for Dam A, which included the safety evaluation and earthquake analysis of the existing dam. Beside the Main Dam A, two saddle dams of similar design and heights of 130 m and 20 m have been evaluated with the same methodology.

Dam A is a 131 m high rockfill dam with an inclined earthfill core. The dam's typical cross-section is shown in Fig. 1. The upstream slope has an inclination of 1 (v):2.5(h) with a steeper section near the dam crest (1(v):1.4(h)). The downstream slope has an inclination of 1(v):1.4(h). The earthfill core material consists of silty clayey sand with some gravel. Upstream and downstream of the core three filter zones were designed, each with a width of 3 m. The rockfill shells of the dam consist of hard to very hard, fresh to slightly weathered quarried basalt. The largest particle size is about 100 cm, but smaller in large parts of the dam.

There is no specific guideline for earthquake safety analysis of large dams in the Philippines. Thus, the approach for earthquake dam safety evaluation was proposed by AFRY and discussed with the Dam owners and operators from the Philippines and South Korea. In general, the approach follows the ICOLD guidelines. Details of the project and the earthquake safety evaluation have been published previously (Ehlers *et al.*, 2016).

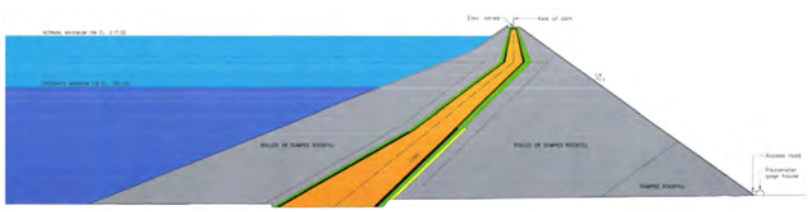

Fig. 1
Cross-section of Dam A

Numerical analysis was carried out by means of a two-dimensional finite element model for the highest cross-section of the dam. The software package GeoStudio was used (Geo-Slope Int., 2012). The results of the static stress analysis served as initial state for the dynamic stability analyses.

The geotechnical parameters considered for the analyses were mainly determined based on geotechnical investigations and laboratory testing. Noteworthy is that cyclic / dynamic triaxial tests and resonant column tests were carried out on the earthfill core material establishing reliable input parameters for the seismic analysis of the dam. The cyclic triaxial tests provided important information on the built-up of pore water pressure during earthquake ground shaking, while the resonant column test provided information on the strain-dependency of shear modulus, G, and the damping ratio, D (as input for the equivalent-linear method).

The earthquake response due to the SEE was calculated in dynamic response analyses using the equivalent-linear method (Seed et al., 1970). The earthquake analyses showed that the effective stresses within the earthfill core are decreased with respect to the static condition, as a result of the seismic excess pore pressures generated during earthquake shaking. Calculations of permanent displacements of slopes have been carried out using the Newmark sliding block analysis (Newmark, 1965). A considerable sensitivity analysis was carried out, considering maximum, mean and minimum values for relevant parameters such as shear modulus, G, and damping ratio, D.

The sequential kinematics of slip circle development and sliding during an earthquake is shown in Fig. 2. Thus, a cumulative effect can be assumed on the vertical displacement of the crest region, caused by the alternating nature of the earthquake ground shaking leading to alternate sliding of the upstream and downstream slopes. The strict application of this mechanism, considering the critical slip circles of the upstream and downstream shoulders due to the SEE, leads to the deformation of the crest region of Dam A as shown in Fig. 3. The densification of the dam body was considered according to Bureau, 1997.

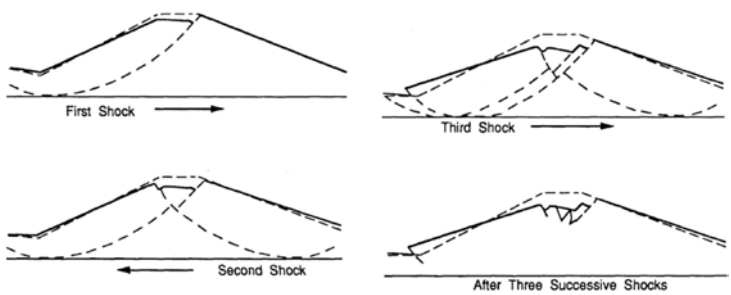

Fig. 2
Crest settlement due to upstream and downstream slope sliding (according to N. Ambraseys, reproduced by Yan, 1991)

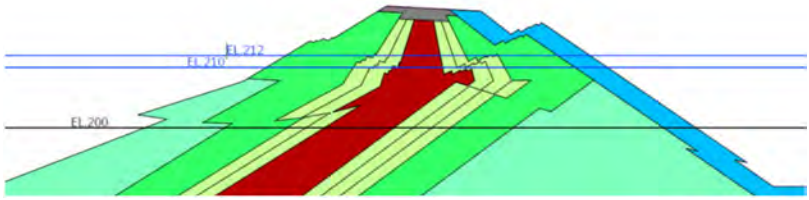

Fig. 3
Crest area of Dam A after the SEE, deformation kinematics according to N. Ambraseys

Earthquake safety of Dam A was evaluated on the basis of the failure modes (i) overtopping, due to crest settlement, and (ii) internal erosion due to offset of the filter zones (according to Fig. 3). In addition, (iii) post-earthquake slope stability was analyzed. The excess pore pressures produced in the core and the filter layers during the earthquake reduce the effective stresses in these zones. In the static post-earthquake stability analyses of the slopes it was demonstrated that the global factors of safety are reduced after the SEE, compared to the results of the static stability analysis carried out for the non-seismic load cases.

3.2. Dam B (Mexico)

Dam B comprises mainly of a gravity masonry dam structure with a height of 47 m. At the right abutment the gravity dam is complemented by an embankment dam section of 15 m in height. After dam construction was completed in 1930, the dam was later heightened two times to its final height of 47 m.

The embankment dam has a masonry core, which was heightened in the second stage with a concrete block, and in the third stage the dam's core was heightened with plastic clay. Filter layers of sand and gravel, 1 m thick, are located upstream and downstream of the clay core. The dam shell consists mainly of gravel. The dam slopes are covered with rockfill and have an inclination of 2.0(h):1(v); Fig. 4.

In 2017 AFRY was awarded with the safety evaluation of Dam B including stability and earthquake analyses. Details of the project and the dam analysis have been published previously (Ehlers et al., 2021). The analyses and assessments have been carried out according to Mexican standards as well as according to international guidelines.

In a first step, and as requested by the Mexican guidelines (CFE, 2008), a pseudo-static earthquake analysis was performed based on the two-dimensional

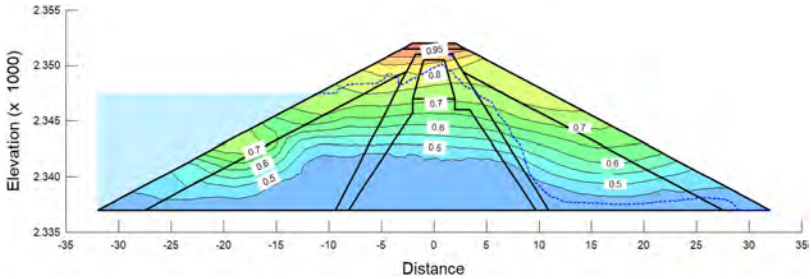

Fig. 4
Cross-section of Dam B with peak values of horizontal acceleration due to earthquake ground shaking (Ehlers et al., 2021)

finite element model (GeoStudio; Geo-Slope Int., 2012), which was already used for the static analysis. With the pseudo-static factor according to the Mexican regulations, the required factor of safety was reached. The geotechnical parameters for the static and pseudo-static stability analyses were taken mainly from investigations carried out in 2007.

To complete the earthquake analyses in accordance with international guidelines, deformations were calculated by considering the acceleration time histories. Therefore, the equivalent-linear method (Seed et al., 1970) was used with subsequent Newmark sliding block analysis (Newmark, 1965). The parameters for the earthquake analyses were assumed based on available literature.

A considerable sensitivity analysis has been carried out, considering maximum, mean and minimum values for relevant parameters such as shear modulus, G, and damping ratio, D. The cumulative effect of slip circle sliding at the upstream and downstream slopes was considered according to Ambraseys (see Fig. 2). In addition, the densification of the dam body was considered according to Bureau, 1997.

Earthquake safety of Dam A was evaluated on the basis of the failure modes (i) overtopping, due to crest settlement, and (ii) internal erosion due to offset of the filter zones (according to Fig. 3). In addition, (iii) post-earthquake slope stability was analysed.

3.3. Dam C (Switzerland)

Dam C is a 91 m high embankment dam with central earthfill core. The dam shell consists of sandy gravel with a low fines content. There is one filter layer

between the moraine material of the earthfill core and the dam shell. The crest width is 12 m. The upstream slope has an inclination varying from 1(v):2.1(h) to 1(v):3.4 (h), while the downstream slope has an inclination of 1(v):1.63(h) to 1(v):2.6(h) plus berms. Within the framework of a dam heightening study in 2023, AFRY Switzerland carried out the review of the existing documentation to evaluate the impact of dam heightening on the earthquake safety of Dam C.

Earthquake analysis and earthquake safety evaluation was performed in accordance with the Swiss regulations valid at the time of earthquake safety evaluation (SFOE, Version 2.0, 2016). The Swiss regulation was revised in 2021 (SFOE, Version 2.1, 2021) and is currently again under revision. It is assumed that the methodology and the requirements for earthquake analysis will not change with the upcoming revision, but the earthquake hazard, meaning the seismic load to be considered, is expected to change.

Three different cross-sections of Dam C have been analyzed, covering the highest dam section as well as the different foundation conditions. A two-dimensional finite element model was used. The results of the static stress analysis served as initial state for the dynamic dam analysis. The dynamic response of the dam was calculated with the equivalent-linear method (Seed et al., 1970). Calculations of permanent displacements of slopes have been carried out using the Newmark sliding block analysis (Newmark, 1965). The densification of the dam body was considered according to Bureau, 1997. In addition, the reliability of the analysis results was evaluated on the basis of a comparative calculation using the method of Makisi & Seed (Makisi et al., 1978; in combination with Sarma, 1979).

The static geotechnical parameters are taken from the comprehensive geotechnical investigations, which were carried out before and during dam construction. The maximum shear modulus Gmax, a dynamic key parameter for calculating the dam's earthquake response, was determined on the basis of in-situ geophysical investigations. The reduction of the shear modulus and the increase of the damping ratio with shear strain was considered based on an intensive literature review, which was assumed to form a sound basis for analysis. Laboratory tests for determining the dynamic soil parameters have not been carried out as the success of this was questioned: i) it is difficult to take representative soil samples from the dam, ii) their remoulding in the laboratory is a potential source of error, and iii) only the smaller fraction of soil material can be tested in the laboratory, which means that the test results do not reflect the real material properties. A considerable sensitivity analysis was carried out in relation to the dynamic soil parameters.

Earthquake safety of Dam C was evaluated on the basis of the failure modes; (i) overtopping, due to crest settlement and (ii) internal erosion due to offset of the filter zones. Additionally, (iii) post-earthquake slope stability was analyzed.

3.4. Dam D (Armenia)

In 2020 AFRY Switzerland Ltd. (Pöyry Energy Ltd. at that time) carried out dam safety evaluation of the 77 m high Dam D in order to evaluate the need for dam rehabilitation and strengthening (Fig. 5). Beside Dam D, two other earth core rockfill dams of similar design and heights of 65 m and 43 m, located in the same river cascade, have been evaluated according to the same methodology. Dam analyses and safety evaluation was carried out according to international guidelines.

Dam D is a 77 m high embankment dam with a slightly to upstream inclined earthfill core. The shoulder slopes have inclinations of 1(v):2.5(h; upstream) and 1 (v):1.65(h) to 1(v):2.15(h; downstream). The dam body consists mainly of gravel-cobble soil. The core material is called “clay loam core”. Upstream and downstream of the core there is a filter and transition zone.

Fig. 5
Upstream face of Dam D

Numerical analysis was carried out by means of a two-dimensional finite element model of the highest dam section using the GeoStudio software package (Geo-Slope Int., 2012). The results of the static stress analysis served as initial state for the dynamic stability analysis. The earthquake response due to the SEE was calculated in a dynamic response analysis using the equivalent-linear method (Seed et al., 1970). The static geotechnical parameters were taken from previous investigation campaigns. The geotechnical parameters for the earthquake analysis were assumed based on available literature.

Calculations of permanent displacements of the slopes were carried out using the Newmark sliding block analysis (Newmark, 1965). A considerable sensitivity analysis has been carried out, considering maximum, mean and minimum values for relevant parameters such as shear modulus, G, and damping ratio, D. The cumulative effect of slip circle sliding at the upstream and downstream slopes was considered according to Ambraseys (see Fig. 2). In addition, the densification of the dam body was considered according to Bureau, 1997.

The earthquake safety of Dam D was evaluated for the failure modes; (i) overtopping, due to crest settlement and (ii) internal erosion due to offset of the filter zones. In addition, (iii) post-earthquake slope stability was analyzed.

3.5. Dam E (Colombia)

Dam E was designed as a 232 m high Earth Core Rockfill Dam with a central earthfill core. The slopes have inclinations of 1(v):2.0(h; upstream) and 1(v):1.4(h; downstream). The dam body consists mainly of different zones of rockfill (zones 3B and 3C). Three filter and transition zones are located between the earthfill core and the rockfill dam shell. Dam E has a volume of about 20.5 million m3. Due to an incident during dam construction in 2018, the dam design had to be modified in its upper part. AFRY was awarded to provide opinion on the safety of the dam, based on available documentation and analyses.

The original dam design was analyzed with a two-dimensional finite element model, including i) the pseudo-static method, ii) the equivalent-linear approach plus subsequent Newmark sliding block analysis, and iii) non-linear analyses. Further non-linear time history analysis was carried out with a 3D-model. After the incident and the modification at the top part of the dam, dam analyses under consideration of the mentioned methods were repeated, plus additional analyses with numerical models covering only parts or specific areas of the dam were carried out in addition. For the non-linear analyses linear elastic, elasto-plastic, Modified Cam-Clay and Hardening Soil small strain models were considered.

Geotechnical parameters for the dam analyses were gained from soil testing, which was carried out before and during dam construction. The parameters were calibrated based on the results from the monitoring instruments, e.g. form settlement gauges. The parameters for the earthquake analyses were modified based on available literature.

The earthquake safety of Dam E was evaluated on the basis of the failure modes (i) overtopping, due to crest settlement, and (ii) internal erosion due to offset of the filter zones. In addition, (iii) post-earthquake slope stability was analysed.

3.6. Summary earthquake analysis dams A to E

A summary of the earthquake analyses methods used, and the applied safety evaluation criteria, is provided in Table 2.

Table 2
Earthquake analysis methodology and safety criteria

DAM		METHODOLOGY	SAFETY CRITERIA
A	Philippines	equiv.-lin. Method + Newmark Superposition + Bureau	1) freeboard 2) internal erosion 3) post-eq. stability
B	Mexico	1) pseudo-static 2) equiv.-lin. Method + Newmark	1) freeboard 2) internal erosion 3) post-eq. stability
C	Switzerland	1) equiv.-lin. M. + Newmark + Bureau 2) Makdisi - Seed (for plausibility check)	1) freeboard 2) internal erosion 3) post-eq. stability
D	Armenia	equiv.-lin. Method + Newmark Superposition + Bureau	1) freeboard 2) internal erosion 3) post-eq. stability
E	Colombia	1) pseudo-static 2) equiv.-lin. Method + Newmark 3) non-linear analysis (2d & 3d)	1) freeboard 2) internal erosion 3) post-eq. stability

4. EVALUATION OF EARTHQUAKE ANALYSIS METHODS

4.1. Pseudo-static method

The pseudo-static analysis method for seismic slope stability analysis was proposed in 1936 by Mononobe (Mononobe *et al.*, 1936). The earthquake load (ground shaking) is represented by the horizontal inertia load acting in the most unfavorable direction in the center of gravity of the sliding mass (Fig. 6). All seismic loads were considered as static loads and, therefore, they could be analyzed in the same way as the other static loads, which made this analysis quite simple. The simplicity of this method and thus its attractiveness might be the reason, why its application survives today, at least to some extent.

The selection of the appropriate pseudo-static coefficient is the most important, and most difficult aspect of a pseudo-static stability analysis. In recognition of the fact that dam slopes are not rigid and that the peak acceleration exists for only a very short time, the pseudo-static coefficients used in practice generally correspond to acceleration values well below the Peak Ground Acceleration (PGA; Kramer, 1996). Seismic coefficients in the range of 0.1 to 0.4 have been proposed by Terzaghi in 1950 (Terzaghi, 1950), and factors between 0.1 and 0.4 by Seed in 1966 (Seed et al., 1966). Nevertheless, in practice, for a long time, typically a seismic coefficient of 0.1 was used, almost irrespective of the seismic hazard at the dam site (Wieland, 2024). In national guidelines of countries in Western Europe the seismic coefficient is in the range of 0.5 to 0.67 times the Peak Ground Acceleration (SwissCOLD, 2010). For Dam B, the seismic coefficient was calculated to 0.44 for the SEE and to 0.61 for the FLS according to the Mexican Guideline (CFE, 2008).

In pseudo-static analysis, usually the dam is assumed to be sufficiently earthquake resistant, when the factor of safety of 1.0 was reached. However, ICOLD questioned in 1983 in their Bulletin 46 “Seismicity and Dam Design” the meaning of a Factor of Safety when applied to structures, which suffer considerable permanent deformation before failure, and particularly when the applied loads result from natural hazards, such as earthquakes (ICOLD, 1983). The pseudo-static approach is known to not adequately reflect the oscillating nature of the earthquake load (Smoltczyk, 2002). Further, the pseudo-static method is unable to reliably evaluate the stability of slopes susceptible to weakening instability. Especially at embankment dams with earthfill core the build-up of pore-water pressure, combined with the reduction of effective stress and strength, plays an important role in dam stability analysis, which cannot be neglected. Thus, in many places the pseudo-static method is considered outdated. It should not further be used, as it does not provide meaningful results (Wieland, 2018).

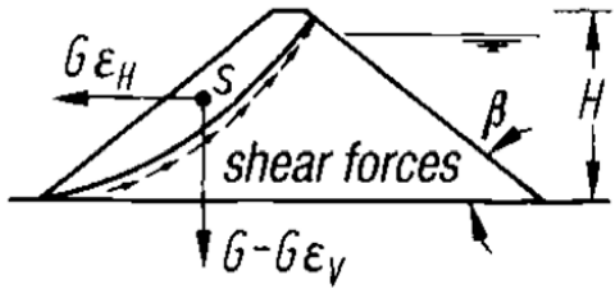

Fig. 6
Arrangement of earthquake forces according to the pseudo-static method (Smoltczyk, 2002)

4.2. Equivalent-linear method

The equivalent-linear method was developed by Seed & Idriss (Seed et al., 1970) and is carried out on the basis of acceleration time histories. It belongs to the group of elastic soil models, with the result that no permanent deformations can be calculated. The equivalent-linear analysis consists of an iterative computational procedure to adjust the shear strain-dependent damping ratio and the dynamic shear modulus of each finite element until these dynamic properties are compatible with the dynamic shear strains (Fig. 7, left figure).

In the equivalent-linear analysis the material properties are only adjusted at the end of each pass through the earthquake record. The excess pore-pressures are calculated based on the peak dynamic shear stresses, which are not known until the end of the dynamic analysis. This means that the excess pore-pressures can only be calculated at the end of the dynamic analysis. This is one of the shortcomings of the equivalent-linear analysis method. The extent of excess pore water pressure build-up is relevant in earthquake dam analyses, as it reduces the effective stress with direct implication on the reduction of strength and increase of deformation.

The equivalent-linear method is widely used in geotechnical earthquake engineering (Studer *et al.*, 2007), i.a. for the analysis of the seismic response of embankment dams. A great amount of information is available in the soil dynamics literature on the material properties required for this analysis. It is therefore assumed that the dynamic soil parameters for this method can be determined with a high degree of reliability. Further, the method is relatively simple and does not require large computational resources. Sensitivity analysis is practicable, even to large extent, as carried out for Dams A to D.

4.3. Newmark analysis

Newmark proposed the sliding block analysis for the calculation of permanent deformation of the dam's slopes due to earthquake ground shaking (Newmark, 1965). Thus, the permanent displacement is calculated for relevant slip circles at the upstream and downstream slopes by integrating the time history of the relative sliding velocity produced by the acceleration pulses exceeding the yield level (Fig. 7, right figure). The result of the Newmark analysis is dam deformation, meaning that performance criteria have to be applied for dam safety evaluation. The Newmark method only considers shear deformations and does not account for volume change and crest settlements resulting from the dynamic compaction of soils (sand, gravel & rockfill) during earthquake shaking, which for example is explicitly stated to be the case in ICOLD Bulletin 148 (ICOLD, 2016).

The method is quite simple, and the Newmark analysis tool is integrated in common software packages used for slope stability analysis, e.g. in the module Quake/w of GeoStudio (Geo-Slope Int., 2012). This might be one reason why this method is widely used.

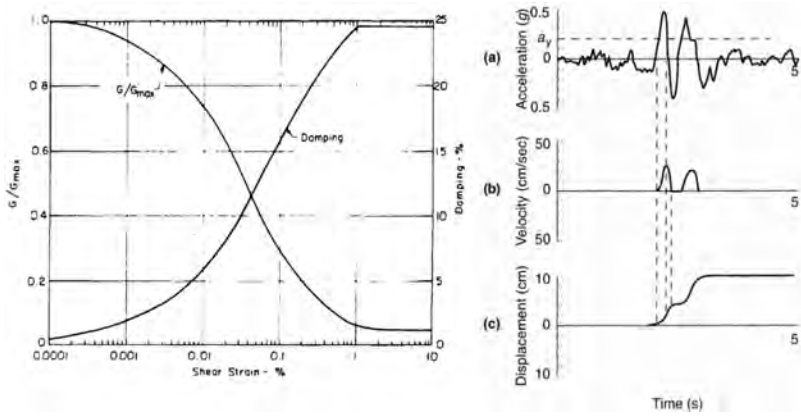

Fig. 7
Shear modulus G and Damping ratio D in relation to shear strain g (Makdisi & Seed; 1978; left); Development of permanent slope displacements; Kramer, 1996; right)

4.4. Non-linear dynamic analysis

Soil tends to behave in a highly non-linear manner under load. Therefore, a more realistic non-linear numerical model seems to be the right choice for earthquake analysis. The fully coupled dynamic numerical analysis method performs the direct integration of the non-linear stress-strain performance equations after each time step, to truly capture the non-linear behavior of soil. The analysis is based on effective stresses and the potential build-up of excess pore water pressure, which can have significant impact on effective stress and hence deformation, is considered after each time step of the analysis. The method derives direct calculation of permanent deformations.

The number of model parameters increases with the level of sophistication. The parameters for the soil models, such as Hardening Soil (HS), Hardening Soil with small-strain stiffness (HSS or HSsmall) or Modified Cam-Clay (MCC), require calibration based on laboratory test results, construction history, dam performance monitoring data etc. In practice, large uncertainties remain regarding the material properties due to a lack of information and/or difficulty in calibration. Therefore, a large number of sensitivity analyses are required, which are usually not carried out due to the limitations of the computational resources. The reliability of the analyses results is therefore limited.

4.5. Method of G. Bureau

Guiles Bureau developed an empirical method to estimate crest settlement due to earthquake ground shaking (Bureau, 1997). The method does not consider slope failure or slip circle sliding, respectively. Thus, the method is assumed to estimate earthquake-induced dam crest settlement due to densification of the embankment fill. Parameters considered are the local intensity of shaking (peak ground acceleration and earthquake magnitude), expressed in terms of the Earthquake Severity Index (ESI), and the friction angle of the dam's fill material. The method considers the results from physical model tests, the recorded seismic performance of several rockfill dams founded on rock, and numerical studies using elasto-plastic material models.

4.6. Method of Makdisi & Seed

Makdisi and Seed developed an analytically based correlation to estimate the permanent deformation of the slopes of an embankment dam (Makdisi *et al.*, 1978). The method uses the work of Sarma for calculation of the natural frequency and the earthquake amplification of the dam (Sarma, 1979). Based on the yield acceleration of a specific slip circle, its permanent deformation is calculated. The graphs for deformation estimation were developed on the basis of numerous calculations, considering the shear modulus, G, and the damping ratio, D, in a range which is common for dam projects. The method was introduced into the Swiss dam safety directive as suitable method for earthquake safety evaluation of medium size dams (dam class II; FOWG, 2003). The method is simple and quick to use.

5. CONCLUSION

ICOLD Bulletin 148 is considered to be the internationally accepted reference for the seismic design criteria and the determination of seismic loads for large dams. National directives and guidelines, as existent in Switzerland or Mexico, provide a sound basis to ensure that the dams within those countries have an equal level of safety. Seismic Hazard Assessment Studies might not provide comparable results for the same site when carried out according to different national guidelines or by different Consultants.

The comparison of the earthquake analyses methods reveals that the most commonly applied method to calculate the earthquake response of large earth core embankment dams is still the equivalent-linear method. The reason might lie in the

good data base for analysis input parameters and due to the simplicity of the method. In general, such analyses consider total stresses and do not allow for the calculation of permanent deformations. For many large embankment dams no project-specific geotechnical investigation campaigns are carried out to determination the geotechnical soil parameters for the equivalent-linear method (such as dynamic triaxial testing or resonant column test).

Frequently the Newmark sliding block analysis is used for computation of permanent deformations, eventhough this method was developed almost 60 years ago. Its popularity might be founded in the simplicity of the method. The fact, that the Newmark method only considers shear deformations and does not account for volume change and crest settlements resulting from the dynamic compaction of soils (sand, gravel & rockfill) during earthquake shaking, does not always seem to be adequately reflected in the analyses' methodologies. Further the superposition of upstream and downstream slope deformation does not seem to be commonly considered.

More sophisticated non-linear dynamic analysis is rarely used. The advantages of such analyses are obvious, as the stress-strain characteristic is modified after each time step to capture the non-linear behavior of the soil. If foreseen, a suitable and comprehensive geotechnical investigation campaign should be foreseen at an early stage of the project to increase the reliability on the large number of geotechnical soil parameters required. Nevertheless, an extensive sensitivity analysis is required to ensure accurate and reliable analyses results. For consultants this is an almost impossible task, as the analyses are expensive and large computation capacity is required. Thus, one can come to the conclusion that non-linear analyses have little value for practical application and cannot be used for seismic safety assessments of real dam projects. A general change in the models used by dam engineers is not expected in the near future (Wieland, 2024). The tendency seems to be to carry out non-linear analysis in the case the earthquake safety requirements of a dam analyzed with the equivalent-linear method are not met. This development is observed with apprehension, as the requirements for sound geotechnical information and sensitivity analysis still apply and are even more difficult to fulfill when non-linear analysis was not planned from the start.

Simple methods are still widely used in the international dam business. For a consultant, sometimes dealing with tight time schedule and tight budget, simple methods are appreciated to obtain early information of the relevance of the seismic load case for a specific project. The method of Makdisi & Seed seems to be widely used and accepted. For all simple methods it is of great importance to evaluate whether the selected method is suitable and within the limits of applicability.

The principle to always attempt simplified procedures before using more detailed and complex methods reaches its limit when it comes to the pseudo-static analysis of embankment dams with earthfill core. Pseudo-static analysis considers neither the oscillating nature of an earthquake nor the reduction in stiffness and

strength during earthquake ground shaking. The build-up of excessive pore water pressure associated with the reduction of effective stress and strength, requires attention and cannot be neglected. For embankment dams with earthfill core the pseudo-static analysis method is not suitable. The opinion that this method is outdated, at least for embankment dams with earthfill core, seems to become generally accepted.

The evaluation criteria of the earthquake safety on the failure modes (i) overtopping, (ii) internal erosion, and (iii) post-earthquake slope failure seem to be established.

REFERENCES

[1] BUREAU G. (1997), Evaluation Methods and Acceptability of Seismic Deformations in Embankment Dams, *Proceedings of the 19th Congress on Large Dams*, Florence, Italy.

[2] EHLERS S, GOLTZ M. (2021), Safety evaluation of Mexico's Tepuxtepec dam, Hydropower & Dams, Issue Six.

[3] EHLERS S, WIELAND M, PARK Y, HAN G, FALLAH H, ROSHANOMID H. (2016), Stability Analysis of Angat Rockfill Dam and Dykes, including dynamic stability and deformation analysis, *Hydro 2016: Int. Conference and Exhibition*, Switzerland.

[4] Geo-Slope International Ltd. (2012), *Modelling with SEEP/W 2012, SLOPE/W 2012, SIGMA/W 2012, and QUAKE/W 2012, an engineering methodology*, Calgary, Alberta, Canada.

[5] ICOLD Bulletin 46 (1983), *Seismicity and Dam Design, Guidelines*, International Commission on Large Dams.

[6] ICOLD Bulletin 72 (1989), *Selecting Seismic Parameters for Large Dams, Guidelines*, International Commission on Large Dams.

[7] ICOLD Bulletin 148 (2016), *Selecting Seismic Parameters for Large Dams, Guidelines*, International Commission on Large Dams.

[8] Instituto de Investigaciones Eléctricas de México, Comisión Federal de Electricidad (IIE-CFE, 2008), Manual de diseño de obras civiles, diseño por sismo, sección 3.12 estructuras tipo 9 presas.

[9] Instituto de Investigaciones Eléctricas de México, Comisión Federal de Electricidad (IIE-CFE), PRODISIS versión 2.0 (2014) and versión 4.1.1 (2017).

[10] KRAMER L. S. (1996), *Geotechnical Earthquake Engineering*, Prentice-Hall International Series in Civil Engineering and Engineering Mechanics, New Jersey, USA.

[11] MAKDISI F I, SEED H B. (1978), Simplified procedure for estimating dam and embankment earthquake-induced deformations. *Journal of the Geotechnical Engineering Division, ASCE*, Vol. 104, No. GT7, pp 849–867, 1978.

[12] MONONOBE, N., TAKATA, A. AND MATUMURA, M. (1936) *Seismic stability of the earth dam, Trans. 2nd Congress on Large Dams*, Washington, D.C. Q. VII, pp. 435–44.

[13] NEWMARK N. M. (1965), Effects on Earthquakes on Dams and Embankments, *Geotechnique*, Vol. 15, No. 2, pp. 139–160.

[14] SARMA, S K. (1979), Response and stability of earth dams during strong earthquakes. miscellaneous papers, GL-79-13, US Army Engineer WES, CE, Vicksburg, Miss.

[15] SEED H B, IDRISS I. M. (1970), Soil Moduli and Damping Factors for Dynamic Response Analysis, Report No. EERC 70- 10, Earthquake Engineering Research Center, University of California, Berkeley, USA.

[16] SMOLTCZYK U. (2002), Geotechnical Engineering Handbook, Volume 1 Fundamentals, Ernst & Sohn.

[17] STUDER J A, LAUE J, KOLLER M G. (2007), Bodendynamik – Grundlagen, Kennziffern, Probleme und Lösungsansätze, 3. Auflage, Springer Verlag.

[18] Swiss Federal Office for Water and Geology (FOWG, 2003), Safety of Water Retaining Facilities, Basis document for earthquake safety evaluation, report of the FOWG, water series.

[19] Swiss Federal Office of Energy (SFOE), Supervision of Dams Section, Directive on the Safety of Water Retaining Facilities, Part C3: Earthquake Safety, Version 2.0 (2016) and Version 2.1 (2021).

[20] Swiss Federal Office of Energy (SFOE), Supervision of Dams Section, Directive on the Safety of Water Retaining Facilities, Part C1: Design and construction, Version 2.0 (2017).

[21] Swiss Committee on Dams (SwissCold, 2010), Comparison of the Swiss guideline for Seismicity on Dams with guidelines in Germany, Austria, France and Italy, Technical Committee “Seismic Safety on Dams”.

[22] TERZAGHI (1950), MECHANISMS OF LANDSLIDES, ENGINEERING GEOLOGY (BERKEY) VOLUME, GEOLOGICAL SOCIETY OF AMERICA.

[23] WIELAND M. (2018), Application of pseudo-static sliding stability analysis in seismic design and safety evaluation of embankment dams, *16th European Conference on Earthquake Engineering*, Thessaloniki, Greece.

[24] WIELAND M. (2024), *92nd ICOLD Annual Meeting & International Symposium on "Dams for People, Water, Environment and Development"*, New Delhi, India.

[25] YAN L. (1991), Seismic deformation analysis of earth dams: a simplified method. Report No. SML 91-01. California Institute of Technology, Soil Mechanics Laboratory, Pasadena, California, USA.

COMMISSION INTERNATIONALE DES
GRANDS BARRAGES

VINGT-HUITIEME CONGRES DES
GRANDS BARRAGES
CHENGDU, MAI 2025

SEISMIC FRAGILITY ASSESSMENT OF CONCRETE GRAVITY DAM DUE TO BASE SLIDING AS A POTENTIAL MODE OF FAILURE (*)

Bikram Kesharee PATRA
PhD student, Dept. of Building, Civil & Environmental Engineering, Concordia University

Ashutosh BAGCHI
Professor, Dept. of Building, Civil & Environmental Engineering, Concordia University

CANADA

SUMMARY

The risk-based approach has become the contemporary standard for evaluating the safety of existing dams, facilitating the effective planning of rehabilitation measures, and efficiently utilizing limited resources. This approach comprehensively considers various potential failure modes and estimates their failure probabilities from all plausible causes. In this context, this study aims to evaluate the seismic vulnerability of a concrete gravity dam, with a specific focus on the base sliding failure mode. The case study uses a coupled 2D Dam-Foundation-Reservoir (DFR) model developed using Abaqus software and accounts for the effects of both contact and material, nonlinearity. Material non-linearity is implemented using the Concrete Damage Plasticity (CDP) model, contact nonlinearity is implemented through the Cohesive Zone Model (CZM). Structural elements are incorporated in the dam and foundation, while acoustic elements represent the reservoir, and infinite elements are employed at the

**Évaluation de la fragilité sismique d'un barrage-poids en béton : le glissement de la base est un mode de défaillance potentiel.*

DOI: 10.1201/9781003642428-112

foundation periphery. The dam is subjected to gravity, hydrostatic, uplift, and hydrodynamic loads alongside the combined effect of horizontal and vertical ground motions. A suite of 55 ground motion records was selected, utilizing the Conditional Mean Spectrum (CMS) encompassing a range of five return periods extending from 475 to 10000 years. A comprehensive set of 330 nonlinear simulation systems was conducted to investigate the impact on crest displacement when comparing tied versus cohesive interactions at the dam foundation interface. Additionally, the simulations examined specific conditions, such as with and without uplift pressure, to determine which scenario base sliding becomes a critical risk factor. System response parameters, such as relative base and crest displacement were used to develop the fragility curves for the defined limit states and damage indices. The fragility curves based on relative crest displacement and base sliding under various seismic intensities provide a probabilistic perspective on the likelihood of the dam experiencing different levels of damage. It has been observed that models with cohesive contact at the dam foundation interface exhibit reduced peak crest displacement values compared to tied models, resulting in lower fragility estimates. Additionally, there is a noticeable difference in base displacement at the heel and toe of the dam, with higher values observed at the heel. To study the base sliding behavior, the model parameters are chosen such that the base sliding failure mode is more dominant than the displacement-based failure mode. Lastly, the study's findings offer valuable insights into how model assumptions, contact simulation, and consideration of uplift pressure influence the overall seismic vulnerability assessment of concrete gravity dams.

RÉSUMÉ

L'approche basée sur le risque est devenue la norme contemporaine pour évaluer la sécurité des barrages existants, facilitant ainsi la planification efficace des mesures de réhabilitation et l'utilisation efficiente des ressources limitées. Cette approche prend en compte de manière exhaustive les divers modes de défaillance potentiels et estime leurs probabilités de défaillance pour toutes les causes plausibles. Dans ce contexte, cette étude vise à évaluer la vulnérabilité sismique d'un barrage-poids en béton, en se concentrant spécifiquement sur le mode de défaillance par glissement à la base. L'étude de cas utilise un modèle couplé 2D Barrage-Fondation-Réservoir (DFR) développé avec le logiciel Abaqus, en tenant compte des effets de la non-linéarité à la fois des contacts et des matériaux. La non-linéarité des matériaux est implémentée à l'aide du modèle de Plasticité avec Endommagement du Béton (CDP), et la non-linéarité des contacts est implémentée à travers le Modèle de Zone Cohésive (CZM). Les éléments structuraux sont intégrés dans le barrage et la fondation, tandis que des éléments acoustiques représentent le réservoir ; des éléments infinis sont utilisés à la périphérie de la fondation. Le barrage est soumis à des charges

gravitationnelles, hydrostatiques, de soulèvement, et hydrodynamiques, en plus de l'effet combiné des mouvements du sol horizontaux et verticaux. Une série de 55 enregistrements de mouvements sismiques a été sélectionnée, en utilisant le spectre moyen conditionnel (CMS) couvrant une gamme de cinq périodes de retour s'étendant de 475 à 10 000 ans. Un ensemble complet de 330 simulations non linéaires a été réalisé pour étudier l'impact sur le déplacement du couronnement lors de la comparaison entre les interactions liées et cohésives à l'interface barrage-fondation. De plus, les simulations ont examiné des conditions spécifiques, comme avec et sans pression de soulèvement, afin de déterminer dans quel scénario le glissement à la base devient un facteur de risque critique. Les paramètres de réponse du système, tels que le déplacement relatif à la base et au couronnement, ont été utilisés pour développer les courbes de fragilité pour les états limites définis et les indices de dommage. Les courbes de fragilité basées sur le déplacement relatif du couronnement et le glissement à la base sous diverses intensités sismiques offrent une perspective probabiliste sur la probabilité que le barrage subisse différents niveaux de dommages. Il a été observé que les modèles avec contact cohésif à l'interface barrage-fondation présentent des valeurs de déplacement au sommet inférieures par rapport aux modèles liés, entraînant des estimations de fragilité plus faibles. De plus, une différence notable de déplacement à la base, au niveau du talon et de la pointe du barrage, a été observée, avec des valeurs plus élevées au niveau du talon. Pour étudier le comportement du glissement à la base, les paramètres du modèle sont choisis de manière que le mode de défaillance par glissement à la base soit plus dominant que le mode de défaillance basé sur le déplacement. Enfin, les résultats de l'étude offrent des informations précieuses sur la manière dont les hypothèses du modèle, la simulation des contacts et la prise en compte de la pression de soulèvement influencent l'évaluation globale de la vulnérabilité sismique des barrages-poids en béton.

1. INTRODUCTION

There are over 61,000 large dams worldwide, many of which have been in service for more than 50 years and are now approaching or exceeding a century of operation. The safety of these national infrastructures poses a significant challenge for owners, operators, and policymakers due to their high hazard potential. Furthermore, operational hazards have been revised upward, and there have been significant changes in downstream infrastructure development and population settlement since the construction of these dams. According to the International Commission on Large Dams (ICOLD), concrete gravity dams account for about a quarter of the global portfolio of large dams, which includes more than 61,000 dams [1]. The risk-based safety assessment approach

requires contemporary standards for effective safety evaluation of existing dams, rational planning for rehabilitation measures, and effective utilization of limited resources. This approach considers the various plausible failure modes and estimates the likelihood of exceeding threshold values for various possible failure modes. This exceedance probability conditioned on an intensity measure such as PGA, and return periods, acts as an important input for planning remedial measures and assessing consequences. The key potential failure modes for concrete gravity dams include sliding, overturning, and structural cracking. These structures must withstand these potential failure modes, especially during seismic events. One of the primary failure modes during an earthquake is extensive cracking and deformation between the base of the dam and the foundation rock, known as base sliding displacement. Historical examples highlight the significance of this failure mode, the 1981 Even Plum Dam failure in China, experienced base sliding-induced failure due to seismic activity, [2], similarly, the 1911 Austin Dam failure in the USA, provides another example of sliding failure [3]. These events highlight the importance of considering base sliding as a critical failure mode in concrete dams. Further, the accurate modeling of coupled Dam-Foundation Reservoir (DFR) systems involves complex interactions between the dam, foundation, and reservoir, which significantly influence the system's response to static and dynamic loads. Traditional modeling approaches often rely on assumptions such as linear material properties and simplified contact simulations, potentially leading to inaccurate estimations of the dam's behavior. These models may not fully capture the nonlinearity associated with geometry, contact, and material properties, thus inaccurately estimating the system response. The development of mathematical models for predicting the seismic response of concrete gravity dams, including interface zone deformation, is a complex problem due to the interaction between the dam, compressible water, and the foundation rock [4].

To this end, this study adopts a comprehensive approach to evaluating the seismic vulnerability of a concrete gravity dam using a coupled 2D DFR model. The model considers fluid and soil structure interactions and is subjected to both static and dynamic loading. Material and contact non-linearity are incorporated through the Concrete Damage Plasticity (CDP) model and the Cohesive Zone Model (CZM) at the dam-foundation interface, respectively. Non-reflecting boundary conditions are employed at the foundation periphery and reservoir end to accurately represent the infinite extent of these domains. To develop fragility curves, multiple damage indices based on crest displacement and base sliding are defined for three limit states: minor, moderate, and significant damage. The study compares crest displacement-based fragility curves for models using tied conditions versus those with cohesive interaction at the dam-foundation interface. Additionally, it presents fragility curves for base sliding under similar conditions. By adopting a probabilistic assessment framework, this research highlights the importance of understanding variations in system response due to different contact modeling practices. This approach is crucial for informed decision-making in

risk-based safety assessments, ultimately enhancing the resilience and safety of concrete gravity dams.

2. LITERATURE REVIEW

The base sliding failure mode is particularly critical as it can significantly alter the system response and potentially destabilize the structure. The impact of joint opening and sliding at the dam foundation interface on the seismic performance of concrete gravity dams has been a topic of interest in various studies. Léger et al. [5] investigated the stability of concrete gravity dams by modeling sliding at the interface using gap-friction elements. Their findings indicated that the nonlinear deformation at the dam-foundation rock interface effectively reduces the seismic response of the dam. Chopra et al. [6] investigated the sliding response of a gravity dam on rigid rock using a simplified model. Their findings indicated that base sliding plays a more significant role than the rocking motion of the dam about its toe or heel. Hall et al. [7] examined the nonlinear response of Pine Flat Dam, focusing on crack initiation and propagation along the dam-foundation interface using a smeared crack approach. The foundation was modeled using frequency-independent impedance coefficients. The study revealed that although uplift could occur over part of the base, the rocking of the dam about the base was not significant. Instead, a permanent slip due to sliding at the base was observed. Chávez and Fenves [4] developed a comprehensive model for base sliding, incorporating dam-water interaction with considerations for water compressibility, reservoir bottom absorption, and dam-foundation interaction. Using a hybrid time-frequency domain procedure, their results indicated that sliding can occur even during a moderate earthquake. Wang et al. [8] focused on XFEM-based seismic potential failure mode analysis of concrete gravity dam-water-foundation systems through incremental dynamic analysis. Bernier et al. [9] evaluated the seismic fragility of a concrete dam with spatial variation of the friction angle, providing insights into modeling parameters, spatial variation significance, and overall vulnerability to failure modes. Liang et al. [10] conducted a probabilistic seismic analysis for the deep sliding stability of a concrete gravity dam-foundation system, obtaining seismic fragility curves for vulnerability assessment under earthquake hazards. The deformability of the rock bases on which concrete dams are built is typically compatible with the dam deformability, leading to the consideration of the “dam-base” system in stress-strain analyses [11]. The natural frequencies of the vibrations of this system play a significant role in seismic stability analyses, with the dimensions of the rock base impacting the results [11]. Various methods, such as considering noninertial bases or forming rigidity matrices for the dam-base system, have been explored to account for base heterogeneity in numerical analyses [11]. In the context of seismic stability, the sliding safety of concrete gravity

dams along the dam-foundation interface is a critical consideration [12]. The stability against sliding at the interface between the dam base and the foundation rock is essential for ensuring the structural integrity of concrete gravity dams during seismic events [13]. The evaluation of numerical models and input parameters, including the interface along the dam base allowing sliding and overturning of the dam, is crucial for accurate analyses of concrete gravity dams [14]. The evaluation of the probability of failure by sliding in concrete gravity dams is a key aspect of ensuring the safety and stability of these structures [15]. The seismic fragility assessment of concrete gravity dams considers limit states such as sliding at the concrete-to-rock interface at the base of the dam, highlighting the importance of understanding and mitigating potential failure modes [16]. The effect of AAR and aging-induced effects can impact the system response and sliding at lift and base joints [17,18]. Despite these advancements, limitations in current studies remain. These include assumptions regarding material homogeneity, boundary conditions, and simplifications in modeling contact interactions. Furthermore, many studies rely on specific case studies, limiting the generalizability of their findings. This research aims to address these limitations by employing a comprehensive modeling approach that includes both material and contact non-linearity, non-reflecting boundary conditions, and a detailed probabilistic assessment framework. Doing so provides a more accurate and holistic understanding of the seismic vulnerability of concrete gravity dams, particularly focusing on the critical failure mode of base sliding.

3. CASE STUDY

The Pine Flat Dam concrete gravity was considered here as a case study due to existing data on detailed investigation and extensive documentation of its geometric, dynamic, and material properties in the scholarly community [19]. Situated in California, USA, the dam plays a crucial role in fulfilling several vital functions such as water storage, hydroelectric power generation, and flood control. These functions highlight the dam's importance in the region's infrastructure ecosystem. This study employs a two-dimensional DFR model of the Pine Flat Dam to investigate the impact of various factors on dam safety and performance, particularly in the context of seismic vulnerability and resilience, while considering the impact of base sliding failure mode. The model incorporates the dam's cross-section of block 16, as shown in Fig. 1 (a) and (b). The dam's height from the deepest foundation block is 130 meters, and its crest length is 561 meters. The structure comprises 36 monoliths, each with a width of 15.25 meters, and an additional block measuring 12.2 meters in width. This detailed modeling approach, which captures the dam's geometrical layout and structural components, provides a firm foundation for the investigation.

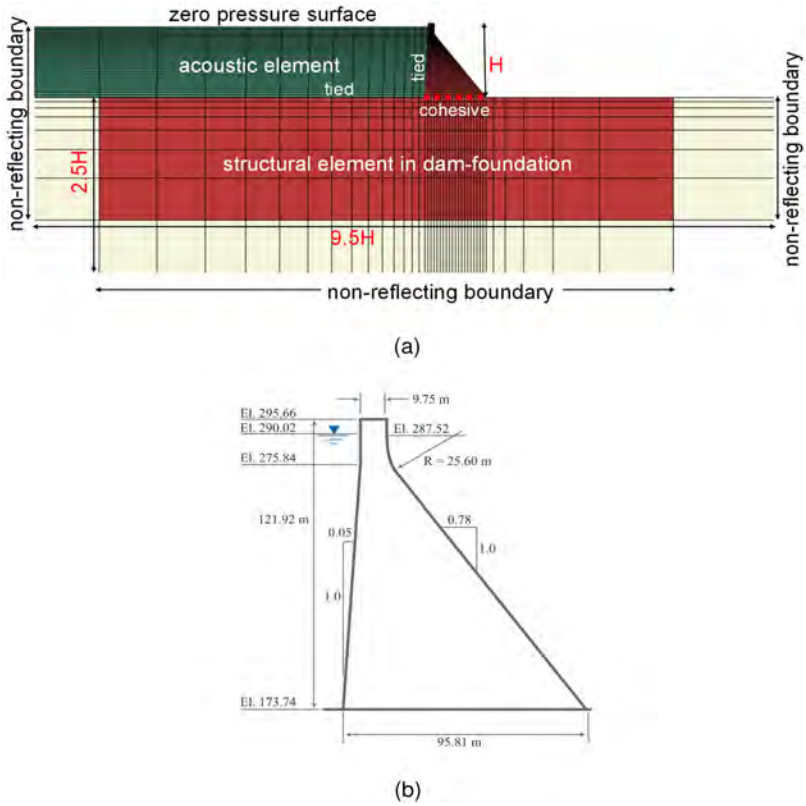

Fig. 1
(a) Considered Abaqus DFR model (b) Dam Cross-section
(a) Modèle Abaqus DFR considéré (b) Section transversale du barrage

3.1. Methodology

Fig. 2 shows the methodology adopted for assessing the seismic performance of the coupled Dam-Foundation-Reservoir (DFR) system of Pine Flat Dam is outlined as follows. Initially, a two-dimensional finite element model of the DFR system is developed using Abaqus 2022 to simulate the dam's response to static and dynamic forces. Ground motions for five return periods are selected using the Conditional Mean Spectrum (CMS) method, ensuring alignment with the dam's seismic hazard profile. Nonlinear time history analyses are performed on the model, considering material and contact nonlinearity, and incorporating fluid-structure and

soil-structure interactions. The model evaluates three different contact scenarios at the dam foundation interface: tied contact, cohesive interaction with uplift, and cohesive interaction without uplift, under combined loading conditions. This comprehensive analysis provides critical structural responses, including normalized crest displacement (NCD) and normalized base displacement (NBD). Subsequently, limit state functions defining minor, moderate, and severe damage thresholds are established. Fragility curves, derived from a lognormal distribution, are then developed to quantify the failure probabilities at various seismic intensities. These curves visually demonstrate the dam's performance thresholds, highlighting the impact of material properties, contact simulations, and uplift pressure on seismic vulnerability.

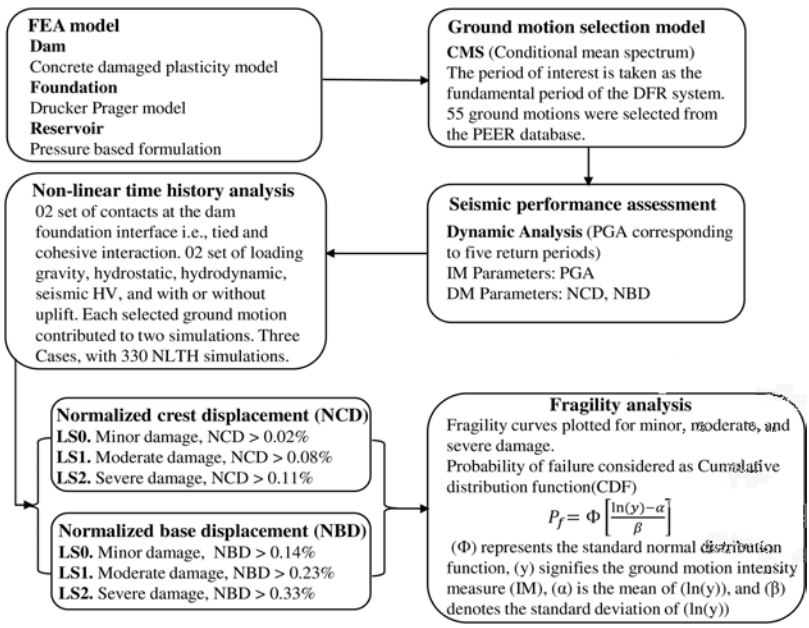

Fig. 2
Outline of methodology adopted for seismic fragility assessment
Aperçu de la méthodologie adoptée pour l'évaluation de la fragilité sismique

3.2. Ground motion selection

The selection of ground motion significantly affects the system response, making careful selection across various return periods and methods crucial for accurate system response and fragility estimations [20]. A comprehensive seismic hazard analysis for Pine Flat Dam in California, USA, was performed using the

USGS tool [21]. Spectral accelerations for return periods of 475, 975, 2475, 5000, and 10,000 years were determined, and ground motions were selected from the Pacific Earthquake Engineering Research Center (PEER) database. This analysis focused on a 0.50-second spectral period with a shear wave velocity (Vs_{30}) of 760 m/s at the B/C boundary. The uniform hazard spectrum (UHS) was generated using the USGS's conterminous U.S. 2014 (v4.2.0) model, which provided disaggregation for 11 attenuation equations, essential for developing the target spectrum and selecting ground motions via the Conditional Mean Spectrum (CMS) method. The disaggregation data, particularly from the Campbell & Bozorgnia [22] attenuation equation aligned the PEER database's target spectrum with the UHS. Parameters included a 5% damping ratio, global/California region specification, a magnitude of 6.42, and R_{jb} of 46.13 km, favoring strike-slip fault types. The fundamental period of the DFR system, 0.551 seconds, guided the selection of 55 ground motions across the five return periods, ensuring their alignment with the site's seismic profile. Fig. 3 illustrates the mean CMS, standard deviation range, and spectra of the selected ground motions for return period 1 in 5000 years, confirming their adherence to the defined seismic parameters and validating their applicability for the analysis.

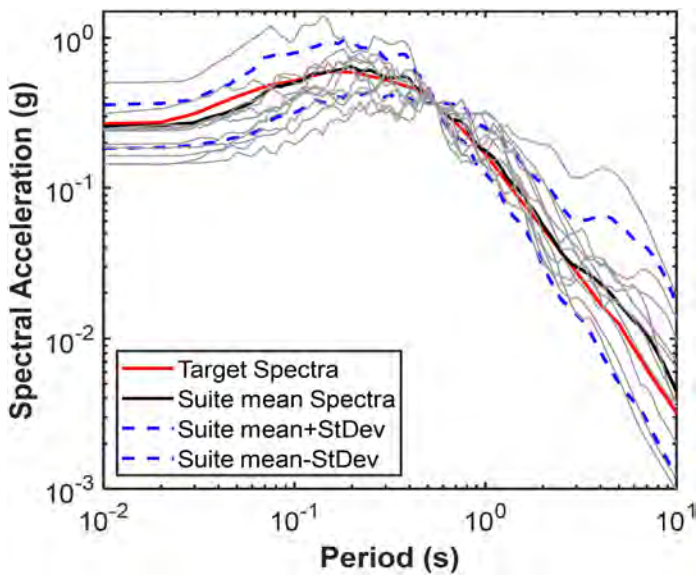

Fig. 3
Ground Motion Suite based on CMS 1 in 5000 years
Suite de mouvements de terrain basée sur le CMS 1 sur 5000 ans

3.3. Numerical model

The numerical simulation for the two-dimensional Dam-Foundation-Reservoir (DFR) model was conducted using Abaqus 2022, incorporating fluid-structure interaction (FSI) and soil-structure interaction (SSI). The reservoir's fluid dynamics were modeled with acoustic elements (AC2D4), while the dam and its rock foundation were represented using plane stress elements (CPS4R). Non-reflecting boundary conditions were applied at the foundation periphery and reservoir end to accurately represent the infinite extent of these domains, and infinite elements (CINPE4) were used for the surrounding foundation to capture seismic wave propagation effects accurately. The top surface of the reservoir was defined as a zero-pressure surface, and Rayleigh viscous damping was utilized to simulate the material damping properties. The base material properties used across all models are detailed in Table 1. Material and contact nonlinearity were incorporated through the Concrete Damage Plasticity (CDP) model for the dam and the Cohesive Zone Model (CZM) at the dam-foundation interface. The CZM model in this study was used to simulate mode-I (opening) and mode-II (sliding) at the dam foundation interface under seismic loading, as illustrated in Fig. 4. The simulation considered different contact simulation approaches and uplift pressure, with specific parameters and variations detailed in Table 2. A thorough nonlinear dynamic

Table 1
Material properties for Pine Flat DFR system (Patra et al., 2024a)

MATERIAL PROPERTIES	CONCRETE	FOUNDATION	RESERVOIR
Density	2482 kg/m^3	2640 kg/m^3	1000 kg/m^3
Bulk modulus (K)	-	-	2070 MPa
Poisson's ratio	0.2	0.333	-
Rayleigh damping Alpha (α)	-	1.64	-
Rayleigh damping Beta (β)	0.004333	0.00668	-

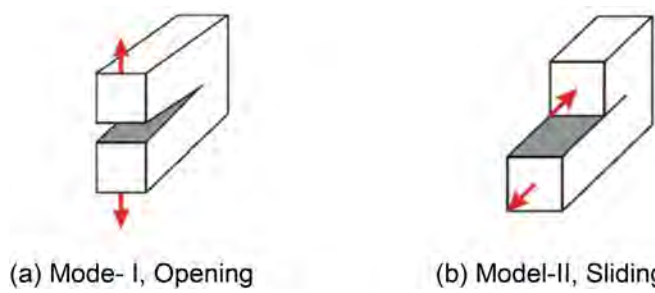

Fig. 4
Dam-Foundation Interface opening and sliding
Interface barrage-fondation ouverture et glissement

analysis was conducted to examine the dam's response under various loading scenarios, including self-weight, hydrostatic thrust from the reservoir water, hydrodynamic effects during seismic events, uplift pressure from fully choked drains, and varying seismic impacts. Seismic loads, including horizontal and vertical components (H_1V or H_2V), were applied to replicate the multidirectional nature of seismic forces. A total of 330 simulations were grouped into three cases based on the type of contact at the dam-foundation interface (tied or cohesive interaction) and the consideration of uplift force. Ground motions were applied at the dam's base, with the potential for deconvolution and application to the foundation's base [23]. The simulation outcomes provided displacement histories at the dam crest and the dam foundation interface.

3.4. Material and contact nonlinearity

In analyzing the seismic performance of concrete gravity dams, both material and contact nonlinearity play crucial roles in capturing the complex behaviors under seismic loads. Material nonlinearity in the dam concrete is modeled using the Concrete Damage Plasticity (CDP) model. The CDP model considers the inelastic behavior of concrete, including the effects of tensile cracking and compressive crushing. It is defined by parameters such as the dilation angle, flow potential eccentricity, and the ratio of biaxial to uniaxial compressive strength, among others. The constitutive equations governing the CDP model include the damage variable (d) and the effective stress (σ') shown in Eq. 1:

$$\sigma = (1 - d)\sigma' \tag{1}$$

Where (σ) is the nominal stress, and (σ') is the effective stress. The evolution of the damage variable (d) reflects the degradation of material stiffness due to cracking and crushing. The CDP properties used in this study are ψ_c: dilatation angle 36.31°; σ_{co}: compressive initial yield stress 12.08 MPa; σ_{cu}: compressive ultimate yield stress 22.41 MPa; σ_{to}: tensile failure stress 2.24 MPa; e: flow potential eccentricity 0.1 and R: ratio of the initial equibiaxial to the uniaxial compressive yield stress 1.16.

Contact nonlinearity is addressed using the Cohesive Zone Model (CZM), which simulates the interaction between the dam and its foundation. The CZM captures the processes of debonding and sliding along the dam-foundation interface under seismic loads. The model is characterized by a traction-separation law that defines the relationship between the normal and shear tractions (T_n) and (T_s) and the corresponding separation displacements (δ_n) and (δ_s) shown in Eq. 2 and Eq. 3:

$$T_n = K_n\left(\delta_n - \delta_{n,0}\right) \tag{2}$$

$$T_s = K_s\left(\delta_s - \delta_{s,0}\right) \tag{3}$$

Where (K_n) and (K_s) are the stiffness coefficients in the normal and shear directions, and ($\delta_{n,0}$) and ($\delta_{s,0}$) are the initial separation displacements. The CZM can simulate mode-I (opening) and mode-II (sliding) failures, providing a comprehensive understanding of how the dam interface behaves under seismic excitation. The fracture parameters for interface cracks as reported in [24] for Normal stiffness, K_{nn} = 3.07x10^5 MPa, Shear stiffness, K_{ss} = 1.30x10^{7}MPa, Coefficient of friction, μ = 0.5, tensile strength 0.827 MPa, cohesive strength 2.20 MPa, angle of internal friction 51°, fracture energy G_F^I 0.038 N/m, G_F^{II} 0.038 N/m was used in this study.

4. SEISMIC PERFORMANCE ASSESSMENT

The seismic performance assessment involves nonlinear dynamic analysis, evaluation of cumulative damage processes, and assessment against defined limit states to ensure the dam's safety and functionality during and after seismic events. A key aspect of this evaluation is the displacement of the dam crest, which is a critical indicator of the dam's structural health. Determining displacement limit states requires analyzing their impact on essential operational components within the dam, such as gates and gantry cranes, whose continuous operation is vital. Excessive displacement can lead to the malfunction or failure of these components, necessitating the establishment of displacement thresholds to maintain their functionality and safety. Furthermore, significant displacements at the dam foundation interface could result in opening and sliding, potentially leading to overturning. Integrating limit states with ground motion return periods allows for the development of fragility curves, providing probabilistic insights into the likelihood of certain damage states occurring. This study defines limit states for crest displacement and base sliding, with displacement values normalized against the dam's height and base width to compute the Normalized Crest Displacement (NCD) and Normalized Base Displacement (NBD), as shown in Eq. 4 and 5.

$$NCD = \frac{crest\ displacemnt(m)}{height\ of\ the\ dam(m)} \tag{4}$$

$$NBD = \frac{base\ displacemnt(m)}{base\ width\ of\ the\ dam(m)} \tag{5}$$

The analysis incorporates three defined limit states (LS_0, LS_1, and LS_2) to represent varying degrees of damage within the concrete gravity dam, consistent with performance-based earthquake engineering (PBEE) principles. LS_0, indicating minor damage, involves minimal impact on the dam's integrity, characterized by superficial issues such as hairline cracks or minor surface defects. Although these initial signs of wear do not threaten the dam's stability, they require monitoring to prevent further escalation. Advancing to LS_1, or moderate damage, the dam exhibits more significant structural stress, with visible cracks and deformation that go beyond

minor aesthetic concerns. At this stage, while the dam's functionality is not immediately compromised, corrective measures are necessary to maintain safety. The most critical state, LS_2, denotes severe damage, where extensive damage compromises the dam's structural integrity, presenting a risk of instability. This level of damage necessitates urgent and extensive repair work to mitigate the risk of failure. These limit states provide a structured approach to evaluating and managing the dam's condition across escalating levels of seismic-induced distress, as outlined in Table 2. This facilitates preemptive intervention strategies to enhance seismic resilience.

Table 2
Damage limit states

LIMIT STATE		
LS_0 Minor damage	NCD $>$ 0.02%	NBD $>$ 0.14%
LS_1 Moderate damage	NCD $>$ 0.08%	NBD $>$ 0.23%
LS_2 Severe damage	NCD $>$ 0.11%	NBD $>$ 0.33%

4.1. Fragility curves

The fragility curves presented in Fig. 5 illustrate the probability of exceedance for Normalized Crest Displacement (NCD) and Normalized Base Displacement (NBD) under various seismic conditions, contact simulations, and with or without uplift pressure. Fig. 5 (a) and Fig. 5 (b) compare the fragility curves of the dam with tied contact at the foundation interface without uplift and cohesive interaction without uplift, respectively. Fig. 5 (c) and Fig. 5 (d) show the fragility curves for the dam with cohesive interaction at the foundation interface, considering scenarios without uplift (NBD-WU) and with uplift (NBD-U). From the curves, it is evident that the probability of exceedance increases with the return period, indicating higher risks of failure as the seismic intensity grows. The tied contact condition shows a higher probability of exceedance compared to cohesive interaction for the same limit state, suggesting that the cohesive interaction provides a better estimation of system response and resistance to seismic forces. Additionally, the inclusion of uplift pressure in the analysis Fig. 5 (d) significantly increases the probability of exceedance, highlighting the destabilizing effect of uplift forces when the drains fully choked on the dam's seismic performance. Overall, the fragility curves provide valuable insights into the impact of different contact conditions and uplift pressures on the dam's seismic resilience, guiding strategies for improving dam safety under seismic loading.

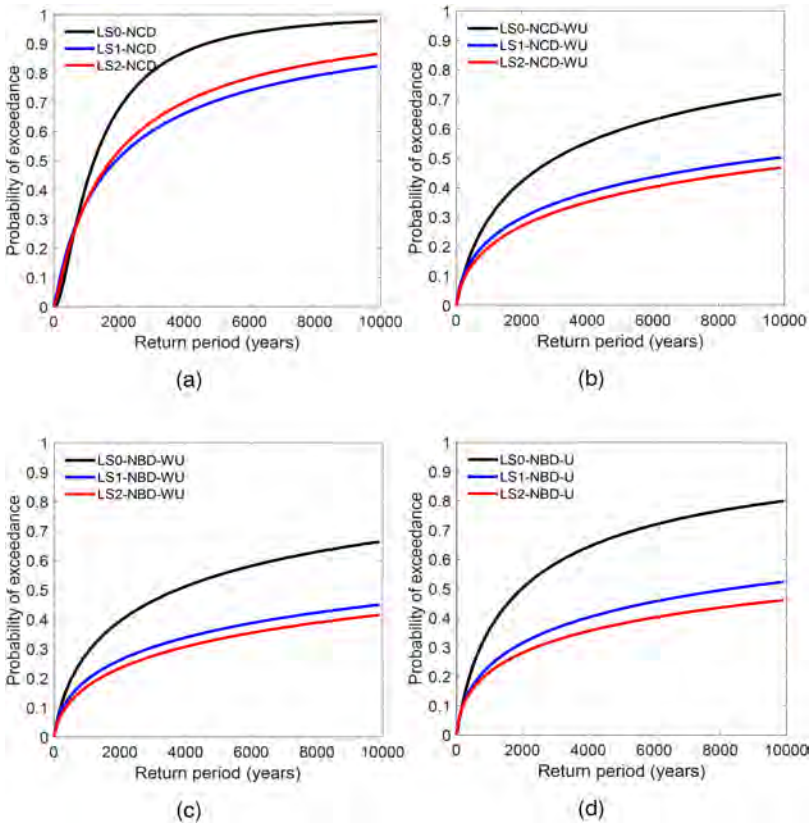

Fig. 5
Fragility curves (a) NCD, (b) NCD-WU, (c) NBD-WU (d) NBD-U
Courbes de fragilité (a) NCD, (b) NCD-WU, (c) NBD-WU (d) NBD-U

Fig. 6 provides a comparative analysis of the impact of uplift pressure and the type of dam-foundation interface on the fragility estimations of the DFR system. In Fig. 6 (a), the comparison between NCD and NCD-WU both models without uplift shows that the cohesive interaction at the dam-foundation interface results in lower probabilities of exceedance compared to the tied interface, indicating that the type of foundation interface significantly affects the dam's seismic performance. Similarly, Fig. 6 (b) compares NBD without uplift (NBD-WU) and NBD with uplift (NBD-U), showing that the inclusion of uplift pressure increases the fragility estimate for the dam, particularly for LS_0.

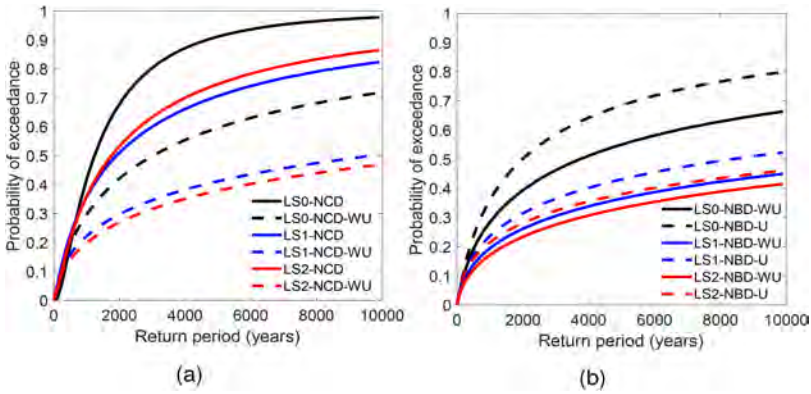

Fig. 6
Fragility curves comparison (a) NCD vs NCD-WU, (b) NBD-WU vs NBD-U
Comparaison des courbes de fragilité (a) NCD vs NCD-WU, (b) NBD-WU vs NBD-U

Overall, these fragility curves emphasize the importance of considering both the type of contact at the dam foundation interface and the presence of uplift pressure in seismic safety assessments. The higher probabilities of exceedance in scenarios with cohesive interaction and uplift pressure suggest that these factors can substantially impact the structural integrity and seismic resilience of concrete gravity dams. Additionally, the curves reflect the variation in ground motion impact on the dam's response, highlighting the necessity for comprehensive seismic risk management strategies that account for different interaction conditions and uplift effects.

5. CONCLUSION

The present study evaluates the seismic vulnerability of concrete gravity dams, with a particular focus on the critical failure mode of base sliding. By employing a coupled 2D Dam-Foundation-Reservoir (DFR) model and considering both material and contact non-linearity, the research provides a nuanced understanding of the interactions between the dam, foundation, and reservoir. The choice of contact interaction i.e., tied versus cohesive, incorporation of uplift, and variations of ground motions within and across the return periods significantly influence the system response, introducing variations in the dam's response that impact the dam's seismic vulnerability assessment. The key findings and implications that emerge from this investigation are listed below.

1. Tied models generally overestimate failure probabilities compared to models with cohesive interaction at the dam foundation interface. This overestimation is especially pronounced in crest displacement-based fragility (NCD). The tied models present a more conservative failure probability estimation. This difference underscores the importance of accurately modeling the dam-foundation interface to avoid over-conservative safety assessments.
2. Incorporating uplift affects the outcome of the analysis significantly impacting the base sliding-based fragility (NBD). The failure probability increases markedly when uplift is taken into account, highlighting the critical role of uplift forces in the seismic stability of dams. This finding emphasizes the necessity of including uplift in comprehensive seismic assessments.
3. Employing multiple damage indices (NBD and NCD) in fragility assessments offers a more detailed and nuanced understanding of the dam's seismic performance. This approach enables a better evaluation of different failure modes and their associated risks, providing a holistic view of potential vulnerabilities.
4. Considering multiple return periods (475, 975, 2475, 5000, and 10,000 years) and a range of ground motions helps account for record-to-record (RTR) variability. This comprehensive approach ensures that the analysis captures the variations in seismic demand across different scenarios, thereby offering a robust probabilistic assessment framework.
5. This research addresses some of the limitations of previous studies by incorporating non-reflecting boundary conditions and a probabilistic assessment framework.

The study's comprehensive approach and detailed modeling provide a robust foundation for future research and practical applications in dam safety management. Future studies should delve into parametric analyses of the variation of Cohesive Zone Model (CZM) parameters to gain deeper insights into their influence on dam behavior. Incorporating contact interactions at lift joints and exploring alternative contact interaction models, such as the Virtual Crack-Closure Technique (VCCT) based on Linear Elastic Fracture Mechanics (LEFM) and the Extended Finite Element Method (XFEM), would enhance the accuracy and realism of the models. Extending the current methodology to three-dimensional (3D) models is essential to include contact interactions at the dam-foundation interface, between blocks, and at lift joints comprehensively. Additionally, future research should incorporate layered foundations instead of a uniform foundation to further refine the seismic vulnerability assessments. These advancements will provide a more robust and detailed understanding of the seismic performance of concrete gravity dams.

ACKNOWLEDGMENT

Support of the Natural Sciences and Engineering Research Council of Canada (NSERC) is gratefully acknowledged.

REFERENCES

[1] ALTAREJOS-GARCÍA, L., ESCUDER-BUENO, I., SERRANO-LOMBILLO, A., DE MEMBRILLERA-ORTUÑO, M.G. Methodology for estimating the probability of failure by sliding in concrete gravity dams in the context of risk analysis. *Structural Safety 36–37*, 1–13, 2012. https://doi.org/10.1016/j.strusafe.2012.01.001

[2] BERNIER, C., PADGETT, J.E., PROULX, J., PAULTRE, P. Seismic Fragility of Concrete Gravity Dams with Spatial Variation of Angle of Friction: Case Study. *Journal of Structural Engineering* 142, 05015002, 2016. https://doi.org/10.1061/(ASCE)ST.1943-541X.0001441

[3] CAMPBELL, K.W., BOZORGNIA, Y. NGA-West2 Ground Motion Model for the Average Horizontal Components of PGA, PGV, and 5% Damped Linear Acceleration Response Spectra. *Earthquake Spectra* 30, 1087–1115, 2014. https://doi.org/10.1193/062913EQS175M

[4] ČERVENKA, JAN., CHANDRA KISHEN, J.M., SAOUMA, V.E. Mixed mode fracture of cementitious bimaterial interfaces: ; Part II: numerical simulation. *Engineering Fracture Mechanics* 60, 95–107, 1998. https://doi.org/10.1016/S0013-7944(97)00094-5

[5] CHÁVEZ, J.W., FENVES, G.L. Earthquake analysis of concrete gravity dams including base sliding. *Earthquake Engineering & Structural Dynamics* 24, 673–686, 1995. https://doi.org/10.1002/eqe.4290240505

[6] CHÁVEZ, J.W., FENVES, G.L. Earthquake analysis and response of concrete gravity dams including base sliding, 1993.

[7] CHOPRA, A.K., ZHANG, L. Base sliding response of concrete gravity dams to earthquakes, in: Eleventh World Conference on Earthquake Engineering. Acapulco, Mexico, p. 9, 1996.

[8] GROSHEV, M.E., OLIMPIEV, D.N. Seismic stability of concrete gravity dams operating jointly with their bases. *Hydrotechnical Construction* 25, 232–240, 1991. https://doi.org/10.1007/BF01423642

[9] HALL, J.F., MICHAEL J, D., BAHAA, E.-A. Defensive Design of Concrete Gravity Dams. California Institute of Technology, 1991.

[10] ICOLD. World Register of Dams [WWW Document], 2024. URL https://www.icold-cigb.org/GB/world_register/general_synthesis.asp (accessed 9.29.23).

[11] LÉGER, P., KATSOULI, M. Seismic stability of concrete gravity dams. *Earthquake Engineering & Structural Dynamics* 18, 889–902, 1989. https://doi.org/10.1002/eqe.4290180611

[12] LIANG, H., GUO, S., TIAN, Y., TU, J., LI, D., YAN, C. Probabilistic Seismic Analysis of the Deep Sliding Stability of a Concrete Gravity Dam-Foundation System. *Advances in Civil Engineering* 2020, 8850398, 2020. https://doi.org/10.1155/2020/8850398

[13] MARTT, D.F., SHAKOOR, A., GREENE, B.H. Austin Dam, Pennsylvania: The Sliding Failure of a Concrete Gravity Dam. *Environmental & Engineering Geoscience* 11, 61–72, 2005. https://doi.org/10.2113/11.1.61

[14] PATRA, B.K., BAGCHI, A. Assessment of seismic resilience of aging concrete gravity dams, in: Symposium "Dams for People, Water and Environment and Development." Presented at the 92nd ICOLD Annual Meeting, 29 Sept. - 03 Oct. 2024, ICOLD, New Delhi, India, 2024.

[15] PATRA, B.K., SEGURA, R.L., BAGCHI, A. Modeling Variability in Seismic Analysis of Concrete Gravity Dams: A Parametric Analysis of Koyna and Pine Flat Dams. *Infrastructures* 9, 10, 2024a.

[16] PATRA, B.K., SEGURA, R.L., BAGCHI, A. Impact of uncertainty associated with ground motion selection on fragility assessment of dams. *Presented at the 18th World Conference on Earthquake Engineering (WCEE2024)*, Milan, Italy, 2024b.

[17] RUGGERI, G. Sliding Safety of Existing Gravity Dams - Final Report, 2004.

[18] SARKAR, A., PATRA, B.K., BAGCHI, A A. A simplified thermo-mechanical model for damage assessment in concrete gravity dams due to Alkali-Aggregate-Reaction (AAR). *Presented at the Canadian Society for Civil Engineering (CSCE) Annual Conference*, Niagara Falls, Ontario, 2024.

[19] SEGURA, R.L., BERNIER, C., MONTEIRO, R., PAULTRE, P. On the Seismic Fragility Assessment of Concrete Gravity Dams in Eastern Canada. *Earthquake Spectra* 35, 211–231, 2019. https://doi.org/10.1193/012418EQS024M

[20] SOOCH, G.S., BAGCHI, A. A new iterative procedure for deconvolution of seismic ground motion in dam-reservoir-foundation systems. *Journal of Applied Mathematics* 2014, 1–10, 2014. https://doi.org/10.1155/2014/287605

[21] USGS. Unified Hazard Tool [WWW Document]. Earthquake Hazards Program, 2023. URL https://earthquake.usgs.gov/hazards/interactive/ (accessed 10.29.23).

[22] USSD. Evaluation of Numerical Models and Input Parameters in the Analysis of Concrete Dams, A Summary Report of the USSD Workshop, Miami, May 3, 2018. USSD, 2018.

[23] WANG, G., WANG, Y., LU, W., ZHOU, C., CHEN, M., YAN, P. XFEM based seismic potential failure mode analysis of concrete gravity dam–water–foundation systems through incremental dynamic analysis. *Engineering Structures* 98, 81–94, 2015. https://doi.org/10.1016/j.engstruct.2015.04.023

[24] ZUO, C.Z. The Seismic Influence on Uplift-Sliding of Arch Dam, in: Proceedings of the China-US Workshop on Earthquake Behavior of Arch Dams. Presented at the China-US Workshop on Earthquake Behavior of Arch Dams, Bejing, China, 1987.

Q.111 - R.10

COMMISSION INTERNATIONALE DES
GRANDS BARRAGES

VINGT-HUITIEME CONGRES DES
GRANDS BARRAGES
CHENGDU, MAI 2025

IMPACT OF EARTHQUAKE SEQUENCES ON EARTHEN EMBANKMENT SYSTEM PERFORMANCE: A NUMERICAL STUDY (*)

Trevor J CAREY
Department of Civil and Mineral Engineering, University of Toronto, Canada

Tyler J OATHES
Department of Civil and Environmental Engineering, Rutgers University, United States of America

CANADA

SUMMARY

The 2023 Kahramanmaras earthquake sequence in Türkiye, starting with a 7.8 magnitude earthquake, led to extensive damage and has been followed by continuous aftershocks. Despite the rapid succession of seismic loading, there were no catastrophic failures of dam infrastructure. This is crucial as aftershocks, being dependent events, are usually not directly accounted for in standard seismic hazard assessments. This paper presents a numerical study investigating the effects of an initial earthquake, followed by aftershocks, on an idealized embankment system. The dynamic response of the zoned embankment is modeled using critical state compatible, stress ratio-based, bounding surface plasticity constitutive models, PM4Sand and PM4Silt. Sequential earthquake motions from the same sequence were applied to the model, with varying reconsolidation times between individual events. Findings from this study demonstrate how the intensity of both the main-shock and aftershock produce different performances and the dissipation of excess porewater pressures will affect system performance during an aftershock.

Impact des séquences sismques sur la performance des systèmes des remblais en terre : une étude numérique

 DOI: 10.1201/9781003642428-113

Conclusions are drawn on how study findings may be expanded for analyses during the design or retrofit of embankment dams to earthquake sequences, leading to safer, more cost-efficient designs.

RÉSUMÉ

La séquence sismique de 2023 à Kahramanmaraş en Turquie, débutant par un tremblement de terre de magnitude 7,8, a causé d'importants dommages et a été suivie de répliques continues. Malgré la succession rapide des charges sismiques, il n'y a eu aucune défaillance catastrophique des infrastructures de barrages. Cela est crucial car les répliques, en tant qu'événements dépendants, ne sont généralement pas directement prises en compte dans les évaluations standard des risques sismiques. Ce rapport présente une étude numérique qui examine les effets d'un séisme initial suivi de répliques sur un système de remblai idéalisé. La réponse dynamique du remblai zoné est modélisée en utilisant des modèles constitutifs de plasticité à surface limite compatibles avec l'état critique, basés sur le rapport de contraintes, PM4Sand et PM4Silt. Des séquences de secousses sismiques issues de la même série ont été appliquées au modèle, avec des temps de reconsolidation variables entre les événements individuels. Les résultats de cette étude montrent comment l'intensité du séisme principal et de la réplique produisent des performances différentes et comment la dissipation des pressions interstitielles excédentaires affectera les performances du système lors d'une réplique. Des conclusions sont tirées sur la manière dont les résultats de l'étude peuvent être élargis pour les analyses lors de la conception ou de la réhabilitation des barrages en remblai pour des séquences sismiques, conduisant à des conceptions plus sûres et plus rentables.

1. INTROUDCTION AND BACKGROUND

Earthquake aftershocks pose a significant hazard to earthen dams, a risk often underestimated or neglected in design or retrofit where commonly only mainshock events are considered. Aftershocks may have greater local intensities than preceding mainshocks due to the complexities in earthquake source, site, and path conditions. The potential for cumulative damage from successive seismic events is heightened by soil's susceptibility to fatigue failures and the temporal effects of excess porewater pressure drainage [1]. This differentiates soils from other structural systems, where damage from repeated events can typically be assessed by reductions in stiffness and force-based analysis approaches [2].

The 2023 Kahramanmaraş (Türkiye-Syria) earthquake sequence consisted of a M_w 7.8 mainshock followed by a series of aftershocks in the following days and

weeks, with the strongest aftershock being a M_w 7.5 event 9 hours after the mainshock [3]. Fig. 1 presents the magnitude and timing of the aftershocks following the initial M_w 7.8 event. Within 24 hours of the main event, five aftershocks greater than a M_w 6.0 occurred and within 72 hours approximately thirty aftershocks larger than M_w 5.0 occurred. Despite this unprecedented number of large aftershocks coupled with a significant amount of lower magnitude events, there were no observations of catastrophic failures in earthen dams [4].

Earthquake aftershocks are well-documented in geological and historical records, with recent sequences included in ground motion databases. Predicting aftershocks is straightforward, as it has been observed that more earthquakes typically follow larger events. However, the exact magnitude, timing, and location within a seismic source cannot be precisely predicted for aftershocks, like mainshocks. Forecasting aftershocks relies on statistical models developed in the 1980s [5], which have remained robust as datasets have expanded and community understanding of earthquakes has improved.

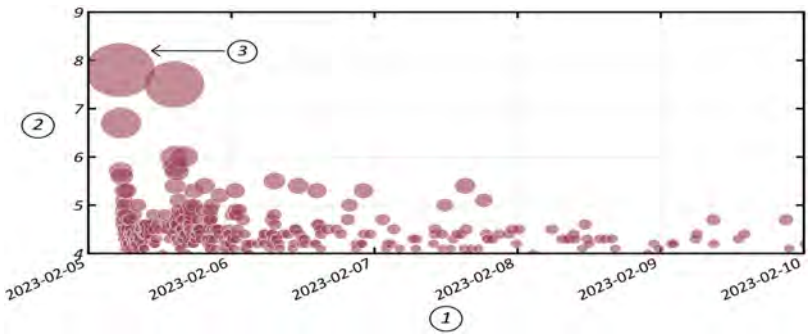

Fig. 1
Timeline and magnitude of the earthquakes from the February 2023 Kahramanmaras earthquake sequence. (Data from USGS)
Chronologie et magnitude des séismes de la séquence sismique de Kahramanmaras de février 2023. (Données de l'USGS)

1. Date
2. Earthquake magnitude
3. Earthquake events

1. Date
2. Magnitude du séisme
3. Événements sismiques

Earthquake sequences present a unique set of questions critical to reducing seismic risk for dams. Key considerations include accurately representing seismic demands from multiple events of varying intensities and understanding how earthquake-induced damage accumulates in earthen dam systems. Additionally, it is important to explore whether soils exhibit self-healing behaviors that could

mitigate the impacts of repeated seismic events. This paper does not aim to determine if current designs are overly conservative but rather understand how earthquake sequences affect the deformation performance of dams. Decisions by dam owners, operators, and regulators regarding design conservatism rely on precise predictions of both seismic demand and system behavior.

Prior research has examined the effects of aftershocks on engineered systems [2]. For structural systems, this includes adapting structural design to accommodate aftershock hazards and evaluating the collapse performance of buildings due to mainshock and aftershock interactions. Generally, these studies focus on the life safety performance of structures during a complete earthquake sequence. In dam engineering, many studies have concentrated on concrete gravity dams due to their high stiffness and limited ability to accommodate strains [6] and have shown that aftershocks increase damage in concrete gravity dams. While prior research provides insights into potential risks, the complex soil and system-level effects controlling earthen dams during earthquakes requires more advanced analysis methods and constitutive models that many of these past research studies did not utilize.

Numerical modeling is a powerful tool for analyzing dam performance across earthquake sequences. Advanced constitutive models can capture the effects of damage from repeated events, accurately simulating the evolution of soil and system behaviors over time including reconsolidation between events. These models can assess the system response to an earthquake sequence or focus on the impact of specific aftershock scenarios, as illustrated in Fig. 1. Such models include PM4Sand [7] and PM4Silt [8] which belong to a family of stress ratio controlled, critical state compatible, bounding surface plasticity models formulated for use in dynamic applications that have been shown to reasonably approximate sand and plastic soil behavior, along with dam dynamic performance [9].

This paper presents a framework for numerically modeling the effects of earthquake sequences on a prototypical earthen dam system. It includes a description of the dam geometry, numerical approach, and constitutive models. The framework also outlines the ground motion sequence, and the underlying assumptions used to evaluate responses. Using two earthquake sequences, the study demonstrates the framework under various conditions. The paper concludes with findings, recommendations for future research, and practical implications.

2. NUMERICAL METHODS AND APPROACH

The goal of this study was to systematically develop a general understanding of how the magnitude and timing of aftershocks might impact the deformation of earthen dams during earthquake sequences. To this end, this study utilized a hypothetical dam geometry and soil properties typical of those found in practice and

the numerical approach follows similar studies on earthen dams [10] rather than simulating a specific case history. A 20 m tall earthen dam with 2.5:1 H:V sandy upstream and downstream shells and an internal clay core was modeled. Fig. 2 presents a schematic of the hypothetical dam geometry and soil profile. The dam is underlain by a 20-meter-thick sand foundation layer, which is underlain by competent bedrock. A reservoir was 16 meters above the ground surface leaving 25% of the dam to exist as free board and the water table was assumed to linearly decrease to the ground surface near the downstream toe. The clay core was embedded two meters into the foundation layer.

The soil layers were assumed to have properties that are generally consistent with earthen dams in practice. Additionally, the analysis aimed to avoid having zones that are typically engineered (dam shell and core) control the deformation mechanisms and instead have accumulation of deformations in the underlying foundation, which is often unaltered and native. The dam shells were a dense sand with a relative density (D_r) of 75% and a bulk density (ρ_b) of 1900 kg/m^3. The foundation was a medium dense sand with a D_r of 55% and a ρ_b of 1800 kg/m^3. The compacted clay core was assigned a peak undrained strength ratio of 0.3 (minimum undrained strength of 50 kPa) and a ρ_b of 1900 kg/m^3. The bedrock was competent, with a shear wave velocity of 960 m/s and a ρ_b of 2300 kg/m^3.

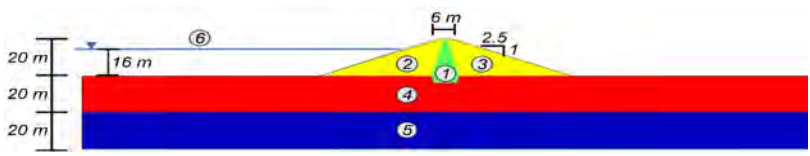

Fig. 2
Geometry of the idealized earthen dam system
Géométrie du système barrage en remblai idéalisé

1. Core
2. Upstream shell
3. Downstream shell
4. Foundation
5. Bedrock
6. Water level

1. *Noyau*
2. *Recharge amont*
3. *Recharge Aval*
4. *Fondation*
5. *Soubassement*
6. *Niveau hydraulique*

The numerical analysis was conducted using the finite difference program FLAC 8.1, which has over three decades use simulating the static and dynamic performance of geosystems. The mesh contained 1 m tall X 1 m wide elements, except in the bedrock layer where elements were 5 m tall. FLAC's automatic meshing scheme adjusted the mesh sizes as needed to fit the geometry of the slope and internal core. The model extended 150 m beyond the dam structure on both sides to limit edge effects and the base of the model was compliant.

The soils were modeled using PM4Sand (shell and foundation) or PM4Silt (core) and the bedrock was assumed to be linear elastic. The PM4 models track damage and pore pressure generation across a range of dynamic loading conditions. Both models have three required input parameters and roughly 20 additional parameters which are assigned default values for sand-like (PM4Sand) and fine grained-like (PM4Silt) soils or can be adjusted for soil-specific analyses. Table 1 presents the model parameters; all secondary parameters retained their recommended default values. Model parameters for the shell, core, and foundation were selected based on parameters presented in [7,8] for the baseline calibrations with the same relative density or similar undrained strengths. The bedrock was modeled with the elastic material model with a shear wave velocity of 960 m/s and a bulk density of 2300 kg/m^3.

Table 1
PM4Sand and PM4Silt constitutive model parameters

	SHELL	**FOUNDATION**	**CORE**
Constitutive model	PM4Sand	PM4Sand	PM4Silt
Go	785	677	660
hpo	0.57	0.4	30
Dr	0.75	0.55	—
su,ratio / su	—	—	0.3 / 50 kPa

Fig. 3a presents the monotonic stress-strain responses for the different materials under constant volume direct simple shear (DSS) loading with σ'_{vc} = 1 atm and K_o = 0.5. The shell and core have peak strengths of approximately 77 kPa and 50 kPa, respectively, that mobilize at approximately 2% shear strain. The shell undergoes slight strain-softening after peak strength mobilization. The foundation has a peak strength of approximately 19 kPa which is mobilized at 1% shear strain. The foundation material is the weakest material as it was assumed to be a native soil. Fig. 3b illustrates the cyclic strength curves from stress reversal cyclic DSS loading with σ'_{vc} = 1 atm and K_o = 0.5 for the shell, core, and foundation soils. At ten cycles the foundation, shell, and core have cyclic resistance ratios of approximately 0.16, 0.32, and 0.34, respectively. The cyclic strength of the foundation is much lower than the shell and core (consistent with the monotonic responses) and is expected to control the system performance during shaking.

3. GROUND MOTIONS AND TESTING SEQUENCE

Simulating the earthquake sequence was achieved using the three steps outlined in Fig. 4. First, a mainshock earthquake was applied to the dam, with a peak ground acceleration (PGA) of either 0.275 g or 0.125 g, these are termed ‘High PGA’

and ‘Low PGA’ events, respectively. The two intensities were selected to provide a range of initial seismic energies and damage to the earthen dam, ultimately providing a spectrum of responses. Following the mainshock, the dam underwent different degrees of uniform reconsolidation (0%, 50%, and 100%) throughout the entire system as a proxy for different time intervals between mainshocks and aftershocks. This work focuses on understanding the cumulative nature of multiple events and does not yet account for void redistribution or transient groundwater flow and their associated deformations. After reconsolidation, the dam was subjected to aftershocks of either high (0.275 g) or low (0.125 g) PGA, to provide a range of potential responses. For each base sequence, 12 combinations of loading and reconsolidation states were tested. All ground motions were applied as a shear stress time series to a compliant base.

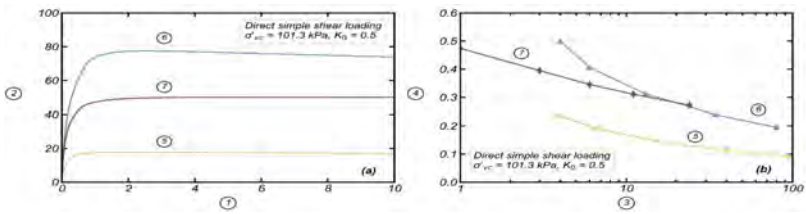

Fig. 3
Material behavior expressed as (a) monotonic response under DSS loading and (b) as number of cycles versus CSR for cyclic DSS loading
Comportement du matériau exprimé comme (a) réponse monotone sous chargement DSS et (b) nombre de cycles en fonction du CSR pour chargement DSS cyclique

1. Shear strain (%)
2. Shear stress (kPa)
3. Number of uniform cycles
4. Cyclic stress ratio (CSR)
5. Foundation
6. Upstream shell & downstream shell
7. Core

1. *Deformation relative cisaillement*
2. *Contrainte de cisaillement*
3. *Nombre de cycles uniformes*
4. *Rapport de contrainte cyclique*
5. *Fondation*
6. *Recharge amont & recharge aval*
7. *Noyau*

Two earthquake sequences were selected for the analysis. This approach was inspired by the 2023 Türkiye earthquakes, where earthen dams experienced multiple large loading events due to their proximity to multiple epicenters [3]. However, ground motion time series from these events are unavailable. Instead ground motions were selected from the NGAWest2 database [11] to have PGAs similar to the target high (0.275 g) and low (0.125 g) PGAs, minimizing the magnitude of the scale factor and preserving the motions natural characteristics. Fig. 5 shows the scaled time normalized acceleration traces and response spectra. Further details on the sequences and ground motions are discussed below and

summarized in Table 2. The Cumulative Absolute Velocity (CAV) is an evolutionary intensity parameter that accounts for both motion duration and amplitude. CAV has been used in other geotechnical applications to evaluate the level of damage in a system. The CAV in Table 2 was calculated from the scaled motion.

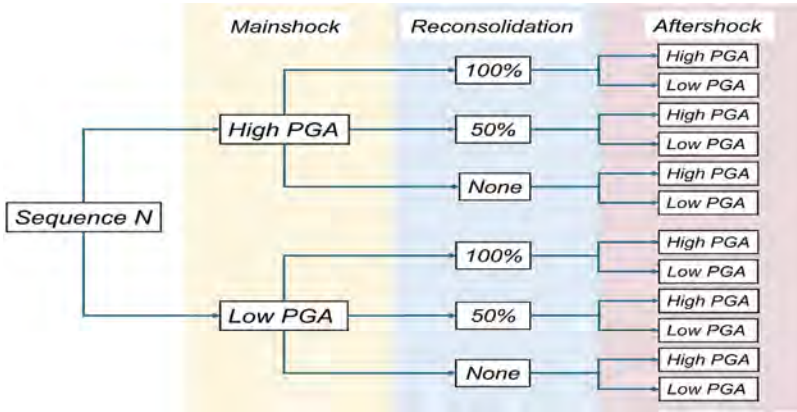

Fig. 4
Analysis flow chart for each sequence
Diagramme de flux d'analyse pour chaque sequence

3.1. Sequence 1: Landers – Big Bear

The first earthquake sequence consists of ground motions from the 1992 Landers earthquake as the mainshock and the aftershock was the 1992 Big Bear earthquake, which occurred 3 hours later. The 1992 Landers earthquake was a M_w 7.3 event with ground motion recordings with RotD50 PGAs ranging from 0.1 to 0.72 g. The Big Bear earthquake was a M_w 6.5 event with RotD50 PGAs ranging from 0.02 to 0.52 g. Details on the selected recordings can be found in Table 2. The selected high and low intensity mainshocks have peak spectral accelerations of 0.67 g and 0.44 g at periods of 0.68 sec and 0.36 sec, respectively. The selected aftershocks have peak spectral accelerations of 1.0 g and 0.43 g at periods of 0.43 sec and 0.2 sec for the high and low intensity events respectively.

The Landers and Big Bear earthquakes do not constitute a true mainshock-aftershock sequence on the same fault system [12]. Big Bear was an independent event, making this a regional sequence. While the distinction between traditional and regional earthquake sequences is important in seismology, it is less significant when considering the impact on dam systems, as their performance is affected more by ground motion characteristics than by the type of earthquake sequence.

3.2. SEQUENCE 2: DARFIELD – CHRISTCHURCH

The second sequence uses the 2010 Darfield event as the mainshock and the 2011 Christchurch event for the aftershock. The 2010 Darfield earthquake was a M_w 7.1 event with ground motion recordings with RotD50 PGAs ranging from 0.001 to 0.73 g. The 2011 Christchurch earthquake was a M_w = 6.1 event with recorded RotD50 PGAs ranging from 0.0004 to 1.39 g at the different recording stations. The selected high and low intensity mainshocks have peak spectral accelerations of 1.02 g and 0.51 g at periods of 0.55 sec and 0.43 sec, respectively. The selected aftershocks have peak spectral accelerations of 0.86 g and 0.41 g at periods of 0.57 sec and 0.44 sec for the high and low intensity events, respectively.

Table 2
Ground motion time histories details for both sequences

SEQUENCE	EVENT	EARTHQUAKE	M_w	PGA	RECORDING STATION	SCALE FACTOR	DURATION (S)	CAV (M/S)
1	Mainshock	1992 Landers	7.3	High	Yermo Fire Station	1.12	44	10.8
				Low	Desert Hot Springs	0.73	50	7.8
	Aftershock	1992 Big Bear	6.6	High	Desert Hot Springs	1.22	60	8.7
				Low	San Bernadino - 2nd & Arrowhead	1.12	46.7	6.1
2	Mainshock	2010 Darfield	7.1	High	Christchurch Resthaven	1.05	150	19.2
				Low	Christchurch Botanical Gardens	0.80	150	8.7
	Aftershock	2011 Christchurch	6.2	High	Riccarton High School	0.95	22	7.3
				Low	TPLC	0.99	44.1	3.7

4. RESULTS

A total of twenty-four analysis combinations for the two sequences were performed following the framework discussed above. The results are first presented for the baseline case (Sequence 1 – High PGA Mainshock) with no reconsolidation between the mainshock and aftershock to investigate how deformations and strains accumulate across subsequent earthquakes. Additional high and low PGA mainshocks (and their associated aftershocks) are then used to evaluate the deformation accumulation without reconsolidation from different ground motion characteristics and intensities. Finally, reconsolidation between mainshocks and aftershocks is induced to demonstrate how the timing between events may influence a dam's dynamic performance.

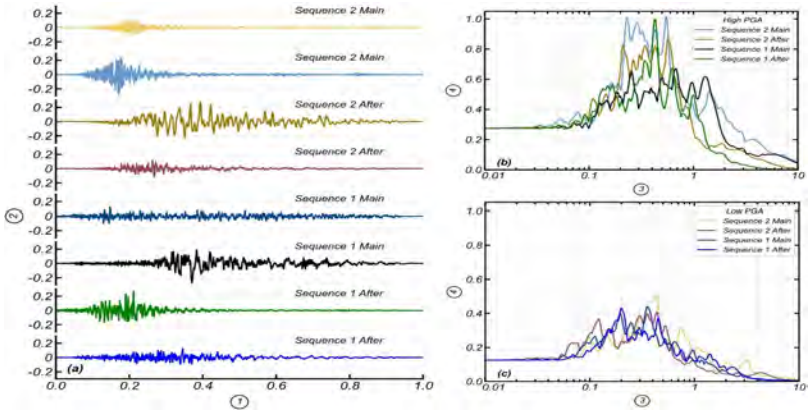

Fig. 5
Selected ground motion (a) acceleration time series and response spectra for the (b) high PGA and (c) low PGA events
Mouvement sismique sélectionné (a) séries temporelles d'accélération et spectres de réponse pour les événements (b) à haute PGA et (c) à basse PGA

1. Normalized time
2. Acceleration (g)
3. Period (s)
4. Spectral acceleration (g)

1. *Temps Normalisé*
2. *Acceleration (g)*
3. *Période (s)*
4. *Accélération Spectrale (g)*

4.1. Baseline condition: sequence 1 – high PGA mainshock – no reconsolidation

Figure 6 shows the horizontal and vertical crest displacements for the mainshock (Fig. 6a) and aftershock (Fig. 6b) versus normalized time. The mainshock causes 0.64 m of crest settlement, primarily occurring in the last two-thirds of the motion due to lower shaking intensity in the first part of the motion (as shown in Fig. 5). This settlement aligns with a significant horizontal displacement pulse. The high-intensity aftershock results in an additional 0.41 m of settlement, while the low-intensity aftershock adds 0.29 m, totaling 1.05 m and 0.93 m of settlement, respectively. The high PGA aftershock causes 41% more settlement than the low PGA aftershock, consistent with its CAV being 43% greater.

The total crest settlement is helpful in estimating the loss of freeboard at the dam's crest but does not show how displacements are distributed throughout the dam. Figures 7 and 8 present horizontal and vertical displacement contours, and Fig. 9 shows shear strain contours for the high PGA mainshock only (top), high PGA aftershock only (middle), and the high PGA mainshock and aftershock combined

(bottom). Horizontal displacements (Fig. 7) are largest beneath the upstream and downstream toes of the dam, with approximately 0.6 to 0.7 meters of displacement during the mainshock. The maximum displacement is more widespread at the upstream toe due to increased demand and lower effective stresses from the reservoir. The aftershock displacement is larger on the downstream side (∼0.6 m) compared to the upstream side (∼0.4 m), resulting in greater cumulative displacement downstream.

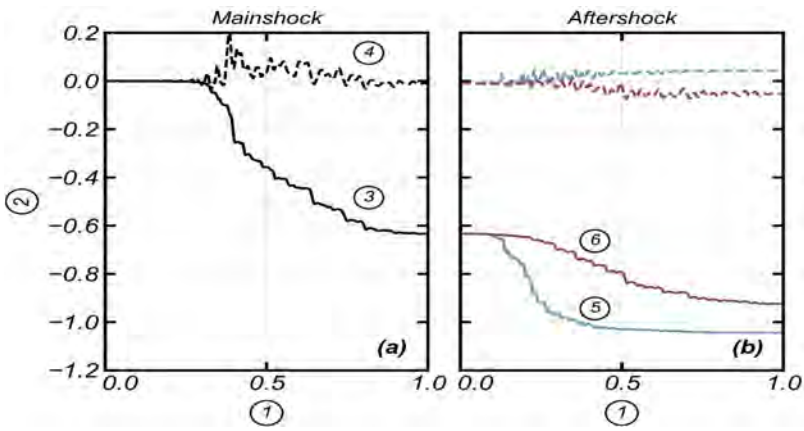

Fig. 6
Vertical and horizontal crest displacement versus time for Sequence 1 High (a) mainshock and (b) aftershocks
Déplacement vertical et horizontal du sommet en fonction du temps pour la Séquence 1 Haute (a) séisme principal et (b) répliques

1. Normalized time
2. Displacement (m)
3. X-Displacement (m)
4. Y-Displacement (m)
5. Low PGA (g)
6. High PGA (g)

1. *Temps Normalisé*
2. *Deplacement (m)*
3. *X- Deplacement (m)*
4. *Y- Deplacement (m)*
5. *Faible PGA (g)*
6. *Haute PGA (g)*

The vertical displacements in Fig. 8 are largest at the dam's crest for the mainshock and aftershock, as horizontal displacements at the toe cause slumping at the crest. During the mainshock, the crest settles approximately 0.64 m. The upstream shell settles about 0.5 m, while the downstream shell settles about 0.3 m, with the difference driven by the reservoir load. Just beyond both toes, there is positive horizontal displacement, indicating potential rotational failure surfaces. This pattern is repeated in the aftershock, but with lower magnitudes of settlement.

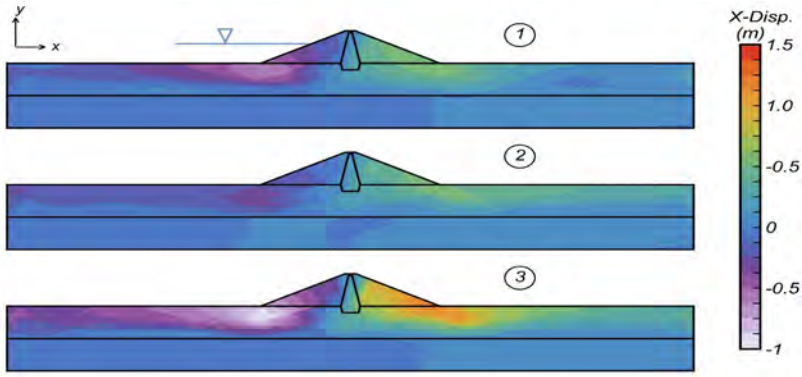

Fig. 7
Contour of x-displacements for Sequence 1 high PGA mainshock and high PGA aftershock
Contour des déplacements en x pour le séisme principal et les répliques à haute PGA de la Séquence 1

1. Mainshock
2. Aftershock
3. Main and Aftershock

1. *Séisme principal*
2. *Séisme réplique*
3. *Séisme principal & réplique*

The shear strain contour in Fig. 9 shows greater deformation in the upstream shell during the mainshock, with localized shear bands in the foundation layer reaching 15%. Complementary shear bands develop through the core, constraining the conical settlement pattern at the crest. A slip surface resembling a circular displacement pattern forms, connecting shear bands in the foundation with those through the core. An approximately 25 m long horizontal shear band forms beneath both toes at the bedrock-foundation interface. It is more pronounced under the downstream toe, where settlements are smaller, suggesting potential stress damping in this area.

During the aftershock, additional horizontal shear bands of strains develop upstream of the dam, with limited strain accumulating in the foundation where it developed during the mainshock, indicating potential stress damping of the transmitted shear stresses during shaking. Strain increases left of the downstream shear band, but the band does not propagate downstream, contributing to smaller displacements compared to the upstream side.

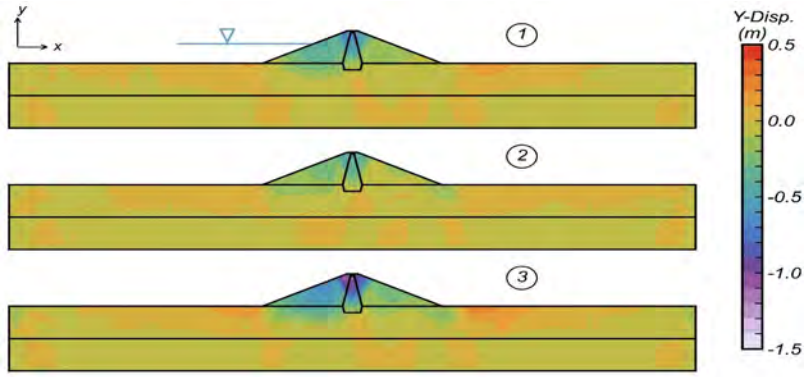

Fig. 8
Contour of y-displacements for Sequence 1 high PGA mainshock and high PGA aftershock
Contour des déplacements en y pour le séisme principal et les répliques à haute PGA de la Séquence 1

1. Mainshock
2. Aftershock
3. Main and Aftershock

1. *Séisme principal*
2. *Séisme réplique*
3. *Séisme principal & réplique*

4.2. Alternative sequences – no reconsolidation

To evaluate the sensitivity of the previous observations, the analysis was repeated for a second independent sequence (high and low PGA mainshocks) and a lower PGA mainshock from Sequence 1. Figure 10 shows the horizontal and vertical crest displacements versus normalized time for these sequences, and Table 3 lists the crest settlements for each motion. For Sequence 2, the high PGA mainshock resulted in 1.18 m of crest settlement, nearly double that of Sequence 1, which aligns with the increased CAV of the motion. The high and low PGA aftershocks caused additional crest settlements of 0.39 m and 0.13 m, respectively. The damage from the high PGA aftershock is similar to that of Sequence 1, reflecting the similar CAVs, while the low PGA aftershock resulted in significantly less settlement, consistent with its lower CAV.

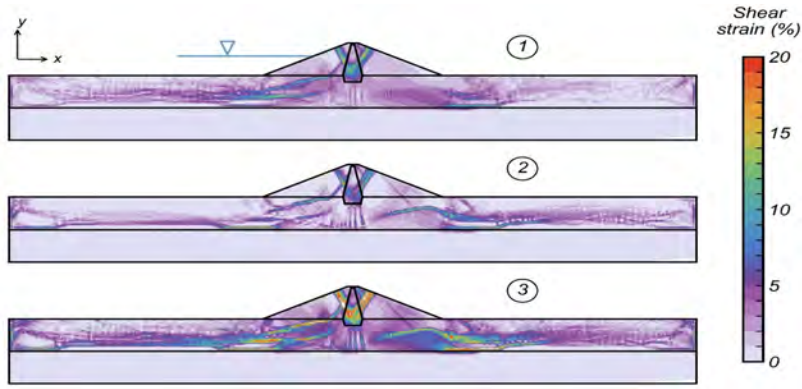

Fig. 9
Contour of shear strain for Sequence 1 high PGA mainshock and high PGA aftershock
Contour de la déformation de cisaillement pour le séisme principal à haute PGA de la Séquence 1 et le séisme secondaire à haute PGA.

1. Mainshock
2. Aftershock
3. Main and Aftershock

1. *Séisme principal*
2. *Séisme réplique*
3. *Séisme principal & réplique*

S1 and S2 Low PGA mainshocks had similar CAVs (7.8 m/s versus 8.7 m/s) which produce nearly identical crest settlements, 0.14 m versus 0.16 m. For both mainshocks, the settlements due to the aftershocks are a function of the CAV of the ground motion record, with increasing CAV correlated with larger crest settlements. To further investigate this trend, the total crest settlement for each sequence was plotted against the cumulative input CAV in Fig. 11. All sequences generally followed a linear trend which can be described as:

$$Total\ Settlement(m) = 0.104 \times Total\ CAV(m/s) - 1.1 \quad (1)$$

which fits the data with an R^2 of approximately 0.92. Further work is needed to investigate the robustness of this apparent trend and identify other factors which might influence it.

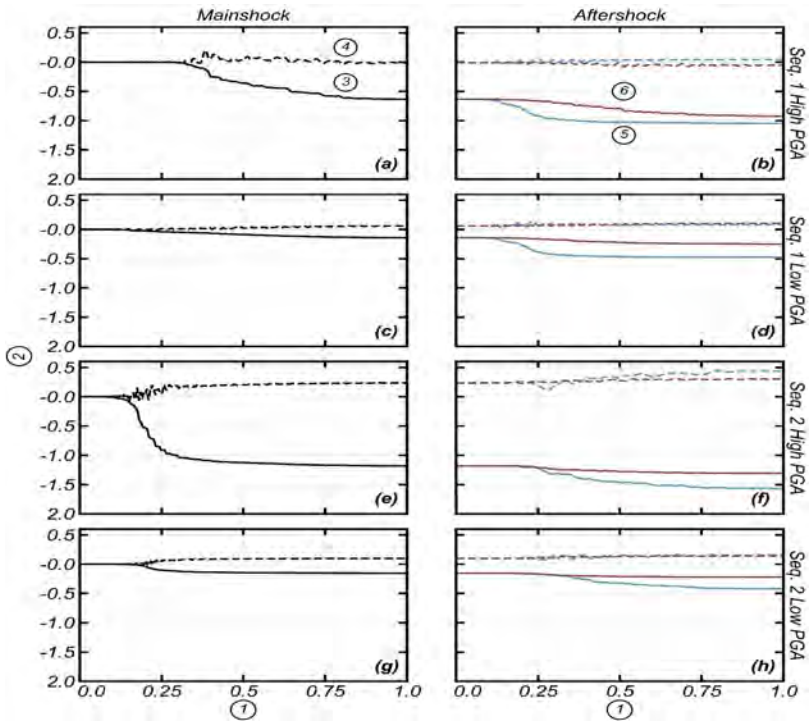

Fig. 10

Horizontal and vertical crest displacements for all four sequences for the mainshock (a,c,e,g) and aftershocks (b,d,f,h) shocks.

Déplacements horizontaux et verticaux des crêtes pour les quatre séquences, pour le séisme principal (a, c, e, g) et les répliques (b, d, f, h)

1. Normalized time
2. Displacement (m)
3. X-Displacement (m)
4. Y-Displacement (m)
5. Low PGA (g)
6. High PGA (g)

1. *Temps Normalisé*
2. *Deplacement (m)*
3. *X- Deplacement (m)*
4. *Y- Deplacement (m)*
5. *Faible PGA (g)*
6. *Haute PGA (g)*

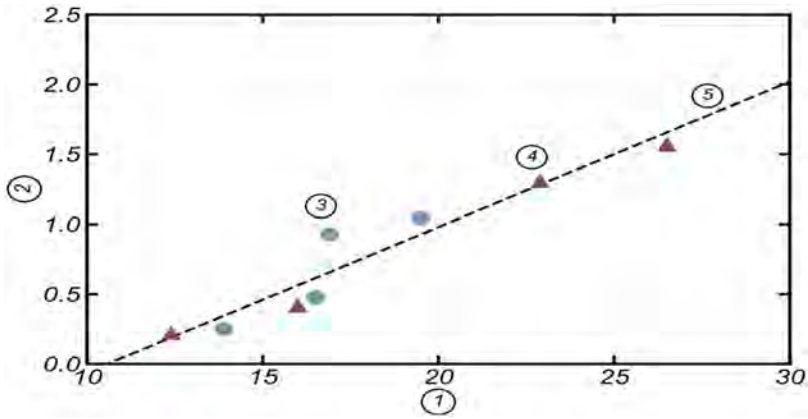

Fig. 11
Total crest settlement from earthquake sequences without reconsolidation versus total cumulative absolute velocity.
Affaissement total des crêtes des séquences sismiques sans reconsolidation par rapport à la vitesse absolue cumulative totale.

1. Cumulative Absolute Velocity (m/s)
2. Displacement (m)
3. Sequence 1
4. Sequence 2
5. Equation 1

1. *Vitesse Absolue Cumulative (m/s)*
2. *Deplacement (m)*
3. *Séquence 1*
4. *Séquence 2*
5. *Équation 1*

4.3. Impact of reconsolidation

The generation of pore pressures during the mainshock changes the effective stress state and alters how the material behaves during the subsequent event. To investigate the impact of the pore pressures at the initiation of the aftershock, the excess pore pressures were manually reduced to represent reconsolidation levels of 50% and 100% (return to initial pore pressure conditions). The pore pressures were reduced in small increments and mechanical equilibrium was established within each increment. Minimal deformations (less than 1 cm) were observed. Figure 12 presents the crest settlement time histories for the Sequence 1 High PGA mainshock with the different reconsolidation magnitudes and aftershock intensities while Table 3 presents the crest settlements for all the sequences. Reconsolidation was shown to not influence the observed crest settlements for all low PGA mainshock sequences. For Sequence 2 High PGA aftershock sequences, reconsolidation does not influence the crest settlement due to the aftershock either. However, for Sequence 1 High PGA aftershock sequences, reconsolidation increases the magnitude of crest settlement (see Fig. 12b blue) observed during the aftershock, with

the magnitude of the increase being most significant increasing from 0% to 50% compared with 50% to 100%. Further work is needed to understand the physics behind which conditions might lead to reconsolidation increasing the settlements during the aftershock.

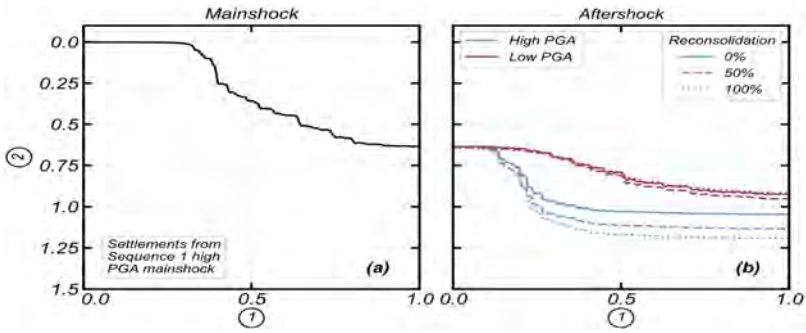

Fig. 12
Impact of different magnitudes of reconsolidation on settlement of dam crest for Sequence 1 high PGA mainshock
Impact des différentes magnitudes de reconsolidation sur l'affaissement de la crête du barrage pour le séisme principal à haute PGA de la Séquence

1. Normalized time
2. Displacement (m)

1. *Temps Normalisé*
2. *Deplacement (m)*

Table 3
Crest displacements for the main and aftershocks with different degrees of reconsolidation

	MAINSHOCK		AFTERSHOCK			
			CREST ΔY (M) AT RECONSOLIDATION OF:			
Sequence	PGA	Crest Δy (m)	PGA	0%	50%	100%
1	High	0.63	High	1.05	1.13	1.19
			Low	0.93	0.95	0.92
	Low	0.14	High	0.48	0.5	0.51
			Low	0.25	0.25	0.25
2	High	1.18	High	1.57	1.58	1.58
			Low	1.31	1.33	1.31
	Low	0.16	High	0.42	0.42	0.43
			Low	0.22	0.22	0.22

5. DISCUSSION

The framework herein provides a range of dam deformations and displacements that resulted from earthquake sequences of mainshocks and aftershocks with varying ground motion intensities. Additional aftershocks, such as those from smaller magnitude events seen in the Turkey earthquake sequence in Fig. 1, can be included, along with more modeling complexities, dam geometries, or material heterogeneity. As long as the seismic hazard remains constant and failure mechanisms do not change, these refinements will reduce uncertainties in dynamic performance but will likely still be within the range seen in this analysis.

A limitation of this analysis is the lack of direct modeling of seepage during reconsolidation. Instead, excess porewater pressures were uniformly reduced to 50% and 100% of their maximum value to decrease computational time, which could take up to a week per analysis. This simplification means reconsolidation strains and delayed dam failures, like void redistribution, are not directly considered. However, for the zoned earthen dam in this study, delayed failures are unlikely due to the absence of long lateral extents of permeability contrasts, and reconsolidation strains are not expected to control crest deformation.

This study demonstrates the importance of incorporating “pre-damage” or the sequence of earthquakes in modeling. For instance, in Fig. 10, Sequence 1 with no reconsolidation shows that a high PGA aftershock caused about 0.42 m of crest settlement following a high PGA mainshock, but only 0.34 m after a low PGA mainshock. This indicates that deformation is not interchangeable forward and backward; a high PGA mainshock followed by a low PGA aftershock result in different deformations than the reverse. In this analysis, a high PGA mainshock (like the Kahramanmaraş sequence) generally caused more deformation, highlighting the need to model the complete earthquake sequence using models like PM4Silt and PM4Sand, which can account for repeated loading events and loading history. Accurately predicting seismic hazards for both the mainshock and aftershock is crucial, as errors can significantly alter simulation outcomes.

The analysis utilizes ground motion intensity parameters that capture the amplitude and duration of motions (CAV). The two sequences in Table 3 had the same PGAs for the mainshocks and aftershocks and originated from similar magnitude events, yet they produced different deformations. CAV’s predictive power has been seen in other geotechnical and structural applications.

After shaking, reconsolidation and dissipation of excess porewater pressures begin immediately, with time to dissipation depending on system geometry and soil permeability. Figure 12 shows that reconsolidation leads to greater settlements during aftershocks under certain conditions, with the most significant settlements after 100% reconsolidation. While the reasons for larger settlements in reconsolidated cases are beyond this paper’s scope, the working theory is that the

reestablished stiffness decreases the dam's natural period, aligning better with ground motion frequency and energy. This theory is consistent with the fact that the increased settlement was only observed for Sequence 1 which may have spectral characteristics that align better with the new natural period.

6. CONCLUSIONS

This paper presents a numerical investigation into how earthquake sequences and reconsolidation affect the dynamic performance of a hypothetical earthen dam. Using FLAC 8.1 with PM4Sand and PM4Silt, 2 earthquake sequences with varying intensities and reconsolidation levels were simulated. Key findings include:

- The framework utilized herein provides a roadmap for assessing the impact of earthquake sequences on different earthen systems and provides a baseline that can be modified to incorporate additional controlling physics as needed.
- Reconsolidation was found to increase the magnitude of crest settlement under certain dynamic conditions, which conflicts with the traditional view that reconsolidation increases the strength of material and reduces subsequent deformations. Further work is needed to fully identify the conditions under which this may occur.
- The total CAV of an earthquake sequence was shown to be a good proxy for estimating the total crest settlements across all earthquake sequences investigated.
- Shear band development at the interface between the bedrock and the foundation material was shown to potentially provide stress damping and reduce the observed deformations within the system.
- Damage during the mainshock can provide a pathway for further deformations to occur, however it can also result in a change in system stiffness which alters the stress propagation and potentially altering the observed deformation.

While this study offers initial insights into the effects of aftershocks and reconsolidation, it only considered a single dam geometry, a limited set of ground motions, and did not account for transient flow deformations. Therefore, caution is advised in extending these conclusions beyond the studied conditions.

REFERENCES

[1] IDRISS IM, BOULANGER RW. *Soil liquefaction during earthquakes*. Oakland, CA: Earthquake Engineering Research Institute (EERI); 2008.

[2] RIBEIRO FLA, BARBOSA AR, NEVES LC. Application of Reliability-Based Robustness Assessment of Steel Moment Resisting Frame Structures under Post-Mainshock Cascading Events. *J Struct Eng* 2014;140:A4014008.

[3] GOLDBERG DE, TAYMAZ T, REITMAN NG, HATEM AE, YOLSAL-ÇEVIKBILEN S, BARNHART WD, *ET AL*. Rapid Characterization of the February 2023 Kahramanmaraş, Türkiye, Earthquake Sequence. *The Seismic Record* 2023;3:156–67.

[4] LASHGARI A, MOSS RES. Displacement and damage analysis of earth dams during the 2023 Turkiye earthquake sequence. *Earthquake Spectra* 2024;40:939–76.

[5] HARDEBECK JL, LLENOS AL, MICHAEL AJ, PAGE MT, SCHNEIDER M, VAN DER ELST NJ. Aftershock Forecasting. *Annual Review of Earth and Planetary Sciences* 2024;52:61–84.

[6] ZHANG S, WANG G, SA W. Damage evaluation of concrete gravity dams under mainshock–aftershock seismic sequences. *Soil Dynamics and Earthquake Engineering* 2013;50:16–27.

[7] BOULANGER R, ZIOTOPOULOU K. PM4Sand (Version 3.2): A sand plasticity model for earthquake engineering applications. Center for Geotechnical Modeling Report No UCD/CGM-22/02, Department of Civil and Environmental Engineering, University of California, Davis, Calif 2022.

[8] BOULANGER RW, ZIOTOPOULOU K. PM4Silt (Version 2): A silt plasticity model for earthquake engineering applications. Report No UCD/CGM-22/03, Center for Geotechnical Modeling, Department of Civil and Environmental Engineering, University of California, Davis, CA, 108 Pp 2022.

[9] KIERNAN M, MONTGOMERY J. Numerical Simulations of Fourth Avenue Landslide Considering Cyclic Softening. *J Geotech Geoenviron Eng* 2020;146:04020099.

[10] BOULANGER RW, MONTGOMERY J. Nonlinear deformation analyses of an embankment dam on a spatially variable liquefiable deposit. *Soil Dynamics and Earthquake Engineering* 2016;91:222–33.

[11] ANCHETA TD, DARRAGH RB, STEWART JP, SEYHAN E, SILVA WJ, CHIOU BS-J, *ET AL*. NGA-West2 Database. *Earthquake Spectra* 2014;30:989–1005.

[12] HAUKSSON E, JONES LM, HUTTON K, EBERHART-PHILLIPS D. The 1992 Landers Earthquake Sequence: Seismological observations. *J Geophys Res* 1993;98:19835–58.

Q.111 - R.11

COMMISSION INTERNATIONALE DES
GRANDS BARRAGES

VINGT-HUITIEME CONGRES DES
GRANDS BARRAGES
CHENGDU, MAI 2025

PRACTICAL CONSIDERATIONS TO ASSESS THE STABILITY OF AGING CONCRETE DAMS IN A SEISMIC ZONE IN EASTERN CANADA (*)

Bevin HSIEH
Eng, M.Eng, AtkinsRéalis

Sylvain RENAUD
Eng., Ph.D, AtkinsRéalis

Idris FODIL
Eng., M.Sc.A., AtkinsRéalis

Siamak OHADI
CEP, M.Sc.A., AtkinsRéalis

Eugenia GEORGIADES
Eng., AtkinsRéalis

Kritam MAHARJAN
CEP, M.Sc.A., AtkinsRéalis

Guy HÉNAULT
Eng. M.Sc.A., Rio Tinto

CANADA

SUMMARY

Dam owners must regularly assess and monitor the safety of concrete retaining structures, which are often aging. The outcomes of the stability analyses

Considérations pratiques pour évaluer la stabilité des barrages en béton vieillissants dans une zone sismique de l'est du Canada

 DOI: 10.1201/9781003642428-114

may not satisfy the safety criteria for seismic load combinations. As a result, engineers must increasingly refine their simulation approaches to provide more realistic predictions. In 2022, a new probabilistic seismic hazard assessment conducted for the Rio Tinto's Isle-Maligne dams (built in 1926 and located in Québec), resulted in much higher spectral accelerations than in previous stability studies. This paper presents the various approaches adopted to optimize the seismic safety assessment of Isle-Maligne dams. A progressive three-level approach, combining the gravity method and temporal dynamic rigid body analyses, is developed, and applied to the 54 sections of the Isle-Maligne dams. An original bilinear shear strength criterion is developed for unbonded dam joints, including an apparent cohesion. An in-depth analysis of on-site boreholes is also carried out to better estimate the bedrock level beneath the structures and to reject unfavourable dam-rock interface dips. Through the presentation of various results, this work illustrates the challenges faced by dam engineers, and suggests some best practices to optimize seismic analyses in future projects.

RÉSUMÉ

Les propriétaires de barrages doivent régulièrement évaluer la sécurité de leurs ouvrages de retenue en béton bien souvent vieillissants. Les résultats des analyses de stabilité peuvent ne pas satisfaire les critères de sécurité pour les combinaisons de charge sismique. Par conséquent, les ingénieurs doivent de plus en plus raffiner leur approche de modélisation afin de fournir une prédiction plus réaliste. En 2022, une nouvelle évaluation probabiliste du risque sismique menée pour les barrages d'Isle-Maligne, propriété de Rio Tinto (construits en 1926 et situés au Québec), a mené à l'obtention d'accélérations spectrales beaucoup plus importantes que pour les précédentes études de stabilité. Ce travail présente les différentes solutions adoptées afin d'optimiser la vérification de la sécurité sismique des barrages d'Isle-Maligne. Ainsi, une approche progressive, en trois niveaux, combinant la méthode gravitaire et des analyses dynamiques temporelles de corps rigide, est développée et appliquée aux 54 sections de l'aménagement d'Isle-Maligne. Un critère original de résistance au cisaillement bilinéaire est aussi développé pour les joints de barrage non-liés en incluant une cohésion apparente. Une analyse approfondie des forages sur site est aussi menée pour mieux estimer le niveau du roc sous les ouvrages et écarter des pendages d'interfaces barrage-fondation défavorables. Au travers de la présentation de différents résultats, ce travail illustre les défis rencontrés par les ingénieurs, et souligne plusieurs considérations pratiques adoptées afin d'optimiser les analyses sismiques pour de futurs projets.

1. INTRODUCTION

Dam owners must regularly assess the safety of their often ageing concrete dams. Assessing the seismic stability of these structures has been a major concern for researchers and engineers for several decades (Tinawi *et al.* 1998, USACE 2007, Miquel and Bouaanani 2010, Bernier *et al.* 2016, Segura *et al.* 2019). However, successive refinements and updates of the seismic hazard models have resulted in more severe seismic demands in eastern Canada (Rosset *et al.* 2023). Concrete lift joints and dam-rock interfaces are often considered as weakness planes along which cracking, rocking and sliding can occur during an earthquake (Nuss *et al.* 2012). To analyze these weakness planes, a progressive four-level approach can be adopted (Ghrib et al. 1997): 1st level, pseudo-static analysis; 2nd level, pseudo-dynamic analysis; 3rd level, linear dynamic analysis; and 4th level, non-linear dynamic analysis. The 3rd and 4th levels require advanced numerical methods such as the finite element method (FEM). Several studies demonstrate the relevance of conducting nonlinear dynamic stability analyses using FEM (e.g. Alliard and Léger 2008, Renaud *et al.* 2015, Bernier *et al.* 2016). However, many of these works were part of advanced research projects, generally well ahead of engineers' everyday uses.

It is common to restrict seismic analyses to the use of pseudo-static and pseudo-dynamic methods combined with the gravity method and the Mohr-Coulomb failure criterion (USACE 1995; CDA 2007; FERC 2016). Yet, these methods present several limitations, as they cannot account for: the transient nature of earthquakes; the 3D effects of the geometry of a dam monolith; and the geometric irregularities of the dam-rock interface. Moreover, uncertainties remain in the choice of Mohr-Coulomb parameters (EPRI 1992), which can significantly affect the outcomes of stability analyses (Renaud *et al.* 2015, Bernier *et al.* 2016). Several standards recommend assuming an unbonded, cohesion-free dam-rock interface (ICOLD 2004; CDA 2007; FERC 2016). However, previous works demonstrate the major role of roughness on the shear strength of concrete-rock contacts (Mouzannar *et al.* 2017, Renaud *et al.* 2020). The effect of such roughness along an unbonded contact can be considered through non-linear failure criteria (Barton and Choubey 1977, Renaud *et al.* 2020) that can be approximated by the Mohr-Coulomb model by using an apparent cohesion (Rullière et al. 2018).

Therefore, engineers are faced with numerous challenges when selecting assumptions and methods to assess the seismic stability of dams. The outcomes of these analyses can have a direct impact on decisions regarding rehabilitation strategies. Such decisions need to be considered against field observations indicating a relatively good seismic behaviour of concrete dams, which may reflect the conservatism of some analysis approaches (Nuss *et al.* 2012).

This paper presents the various solutions adopted to optimize the seismic stability analyses of the Isle-Maligne dams. A new progressive approach is developed and applied to the 54 sections of the hydroelectric development. At levels I and II, pseudo-static and pseudo-dynamic analyses are carried out using the gravity method. At level III, time-dynamic rigid-body analyses are conducted to assess the residual sliding displacement of each section. The calculated displacement is compared with damage thresholds to predict the dam seismic performance. An original bilinear shear strength criterion is also developed for unbonded dam joints. This criterion incorporates an apparent cohesion determined by combining experimental results from site contact specimens with a nonlinear failure envelop model. An in-depth analysis of on-site boreholes is also conducted to better estimate the bedrock level beneath the structures and reject unfavorable dam-rock interface inclinations. Through the presentation of the different results of a real engineering project, this work illustrates the challenges encountered by dam experts, and emphasizes some best practices to optimize seismic analyses in future projects.

2. STUDY CASE: ISLE-MALIGNE DEVELOPMENT

The Isle-Maligne hydroelectric development, owned by Rio Tinto, was built between 1923 and 1926 and is located in the Saguenay region of Québec, where the homonymous magnitude 6 earthquake occurred in 1988. In 2022, a new probabilistic seismic hazard assessment resulted in much higher spectral accelerations As than in previous stability studies (Nanometrics 2022). In 2023, AtkinsRéalis was commissioned by Rio Tinto to assess the impact of implementing its internal D5 standard (RT 2021) for the Isle-Maligne hydroelectric development. The D5 standard requires that the Isle-Maligne dams meet the provincial dam safety requirements (LSBQ 2023) and the CDA guidelines (CDA 2007) since Rio Tinto considers the CDA guidelines to be the federal requirements in Canada. A return period of 1/5000 years was used to assess the stability of north lateral dam, water intake, spillway 1 and spillway 4 of Isle-Maligne, as required by the CDA (2007). In fact, the LSBQ (2023) only requires the use of the maximum design basis earthquake (MDE) corresponding to a return period of 1/2500 years. This paper presents the developed approach and methods illustrated by several results extracted from the study conducted by AtkinsRéalis.

The Isle-Maligne hydroelectric development is quite unique since it consists of several geographically dispersed retaining structures on the Grande and Petite Décharge of Lac St-Jean, as shown in Figure 1. This paper focuses on the seismic stability analyses of spillway 4 and Isle-Maligne main dams. The Isle-Maligne main

dams consist of north lateral dam, water intake and spillway 1 which are all concrete gravity structures. Rehabilitation work were carried out between 1991 and 2004 and led to: the addition of post-tensioning anchors on spillways 1 and 4, and on the north lateral dam; and the drilling of a drainage system within the water intake. As shown in Figure 1, the seismic stability assessment of these retaining structures requires the analysis of 54 sections. This high number stems from the variation of the following properties: quantity of post-tensioning anchors; elevation of dam-rock interface; and shape of ogees and dam crests.

In Québec, the Dam Safety Regulations allow the use of seismic hazard values from the Geological Survey of Canada to assess the stability of dams subjected to seismic loads. However, more accurate seismic parameters were developed as part of a site-specific probabilistic seismic hazard assessment for the Isle-Maligne development (Nanometrics 2022). Thus, the ground seismic demand was quantified for various return periods using a probabilistic regional model. The target seismic spectra resulting from this study, for a soil of Category A (rock of good quality), with a damping of ξ = 5%, for a return period of 1/5000 years, are depicted in Figures 2 (a) and (b), for the horizontal and vertical components, respectively.

A suite of 11 triaxial seismic records (2 horizontal components and one vertical) was also selected and calibrated by Nanometrics (2022). Two scenarios contribute to the seismic hazard of the Isle-Maligne site: (1) moderate to high magnitude earthquakes ($M \geq 5$) at short epicentral distances (less than 100 km); and (2) high magnitude earthquakes ($M \geq 7$) at epicentral distances comprised between 100 and 200 km. It is noteworthy that Eastern North American (ENA) earthquakes have much higher frequency content than Western North American (WNA) earthquakes. However, records of ENA earthquakes with high magnitudes remain rare. Therefore, hybrid accelerograms were employed. These time histories were constructed by McGuire *et al* (2001) by modifying historical WNA records to match ENA frequency characteristics. Since the natural period T of a 30 m high gravity dam is around 0.1 s, the accelerograms in the database were calibrated so that the geometric mean of the response spectra of their two horizontal components is equal to or greater than the target spectrum shown in Figure 2 (a), corresponding to 1/5000 years and ξ = 5%, on soil A, for $0.05s \leq T \leq 1s$. Then, the 11 best matches were kept as the selected triaxial records. A final calibration factor was applied so that the horizontal mean response spectrum of all accelerograms is always greater than 90% of the target spectrum for $0.05s \leq T \leq 1s$. The proportionality initially observed between the horizontal and vertical components is preserved after calibration. Figures 2 (a) and (b) illustrate the response spectra of the horizontal and vertical components, respectively, of the selected accelerograms.

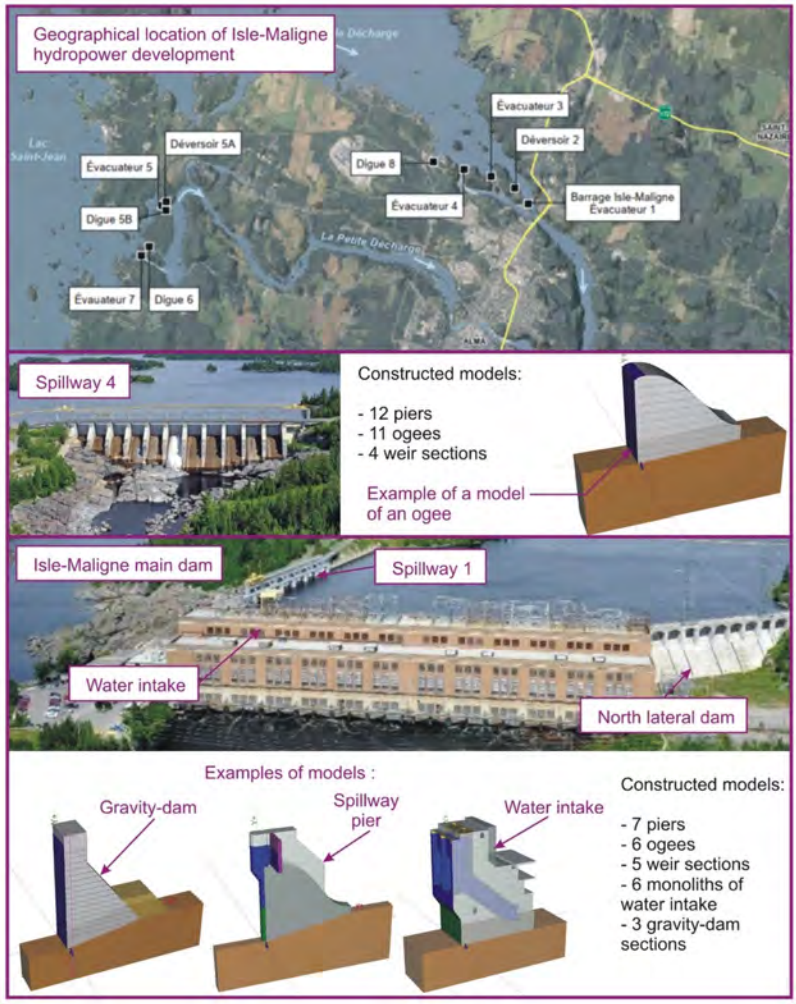

Fig. 1
Geographical location of the Isle-Maligne retaining structures whose sections were analyzed: spillways 1 and 4, north lateral dam, and water intake.

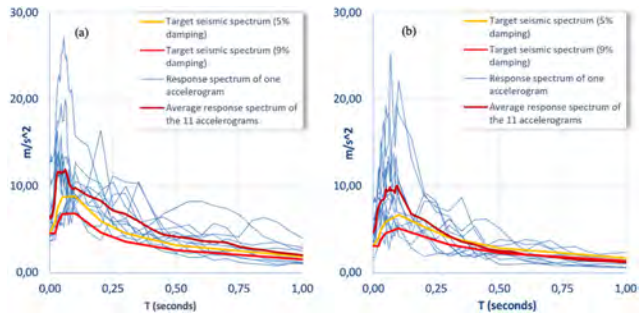

Fig. 2
Seismic spectra of the Isle-Maligne site (target spectra and accelerogram response spectra), for soil A, for a return period of 1/5000 years, for the following components: (a) horizontal; and (b) vertical.

Probabilistic seismic hazard assessment (Nanometrics 2022) has led to fairly large spectral accelerations on the rock (soil A) for the Isle-Maligne site for 1/5000 years (greater than 0.9 g for the horizontal component, for ξ = 5%). In this context, it seems reasonable to anticipate that cracking, openings and sliding will occur along dam joints under such ground motions. For seismic demands larger than the MDE (1/2500 years), some damage can be tolerated as long as the structure is able to retain the reservoir. In this case, USACE (2007) specifies that a damping ξ of up to 10% can be employed for linear elastic analyses of dam-reservoir-foundation systems. Thus, Figures 2 (a) and (b) present the two horizontal and vertical seismic spectra, corresponding to ξ = 9%, constructed from the target spectra (ξ = 5%) using the method of Atkisons and Pierre (2004). The value of ξ = 9% has been selected based on engineer judgement, as it is more conservative than ξ = 10%, and more favorable than ξ = 5%, as allowed by USACE (2007).

Finally, a detailed review of the available documentation and experimental tests carried out at the Isle-Maligne dam site has been conducted to assess various mechanical parameters. Denoting C and EC the density and the dynamic modulus of elasticity of concrete, the following properties are considered hereafter: C = 2330 kg/m3 and EC = 27.9 GPa for the north lateral dam; C = 2410 kg/m3 and EC = 25 GPa for the water intake; C = 2380 kg/m3 and EC = 30 GPa for spillway 1; C = 2440 kg/m3 and EC = 31.9 GPa for spillway 4. It should be noted that the Isle-Maligne dams rest on a competent anorthosite foundation of excellent quality. Experimental tests led to a rock compressive strength higher than 100 MPa, and a rock density of 2800 kg/m3. The modulus of elasticity of the rock ER is assessed between 36 and 80 GPa, depending on the state of cracking of the foundation. As discussed in Section 4 of this paper, a detailed review and analysis of the shear strength properties has also been conducted.

3. PROGRESSIVE APPROACH

3.1. Level I: Pseudo-static method

The new progressive approach developed throughout this paper, with the corresponding acceptability criteria, is presented in Figure 3. This progressive approach is based on three levels of analysis, ranked from the simplest to the most sophisticated. Analyses always start with level I (pseudo-static method). Although based on highly simplified assumptions, the easy-to-check level I is essential to guarantee the robustness of the seismic assessment. Levels II and III correspond to the pseudo-dynamic and Newmark methods, respectively. If, at a given level, the assumptions are judged to be too simplistic, or if one of the acceptability criteria is not met, then the seismic evaluation must move on to a higher level of analysis. Thus, the conservatism of certain assumptions in Levels I and II can be nuanced by the results of Level III, without having to employ more advanced numerical models that would be too complex and time-consuming to implement for the 54 sections of Isle-Maligne.

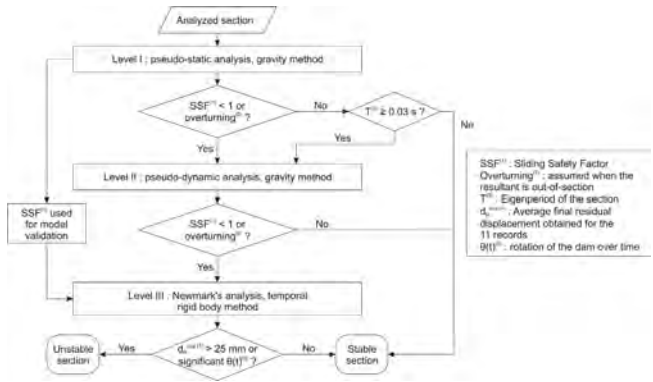

Fig. 3
New progressive approach for seismic stability analyses and corresponding acceptability criteria

The level I of the adopted progressive approach (pseudo-static method) is applied using the gravity method with the CADAM3D software (Technologie MLT Inc. 2024). The seismic demands are modeled as equivalent static inertia forces applied to the structure. The magnitude of these inertia forces are calculated by multiplying the mass by the seismic accelerations. A pseudo-static analysis is divided into two stages. In the first stage, a stress analysis is carried out using the Peak Ground Acceleration (PGA) to assess the normal stress distribution and crack length. A very

brief acceleration is sufficient to initiate a crack. The PGA is obtained horizontally and vertically as the spectral accelerations for T = 0 s in Figures 2 (a) and (b) and do not depend on ξ. However, a longer acceleration is required to trigger dam sliding or rocking (CDA 2007). In the second stage, a stability analysis using a sustained acceleration equal to FR*PGA is conducted to determine the sliding safety factor (SSF) and the position of the resultant along the weakness plane, which can be a lift joint or the dam-rock interface. A resultant out of the weakness plane can imply an overturning instability. FR = 1/2 and FR = 2/3 for ENA and WNA earthquakes, respectively (Tinawi *et al.* 1998). This difference is due to the higher frequency content of ENA earthquakes. As a result, for the Isle-Maligne dam site, FR = 1/2. The pseudo-static method accounts for fluid-structure interaction via Westergaard's added masses. However, it does not account for the flexibility of the structure, which can substantially amplify the seismic demands. For this reason, pseudo-dynamic analyses (level II) are required for structures with a natural period $T \geq 0.03$ s.

3.2. Level II: Pseudo-dynamic method

The pseudo-dynamic method (level II) uses the modal characteristics of the structure (periods and mode shapes) and the characteristics of the target spectra corresponding to the seismic hazard. Seismic spectra with damping of ξ = 9%, shown in Figure 2, are used for the Isle-Maligne dam site, as explained above. Two pseudo-dynamic methods are available in CADAM3D. The method of Fenves and Chopra (1987) is highly effective and recognized for typical gravity dams, but is associated with certain limitations for structures with geometric irregularities, such as water intakes. The method of Miquel and Bouaanani (2010) is suitable for sections with irregular geometry, such as water intakes, since it estimates the mode shapes using FEM. These methods account for the interaction between the concrete dam, the rock-foundation and the reservoir through specific analytical formulas as it can affect the dynamic behaviour of the structure.

It should be noted that CADAM3D can account for the damping effects due to the sedimentation at the base of the reservoir when the method proposed by Fenves and Chopra (1987) is selected, but not with the method of Miquel and Bouaanani (2010). Like the pseudo-static method, the pseudo-dynamic method is divided into two stages. In the first stage, a stress analysis is conducted with a peak acceleration equal to the seismic spectral acceleration corresponding to the vibration period T of the section. In the second stage, a stability analysis is carried out using a sustained acceleration equal to half the peak acceleration used previously, i.e. FR = 1/2. The pseudo-dynamic method accounts for the dynamic amplification of the seismic demands within the structure due to its flexibility. Yet, it cannot consider the transient nature of seismic loads. Although it can identify possible sliding or overturning risks, it is unable to quantify the magnitude of theses instabilities.

3.3. Level III: Newmark method

The level III of the adopted progressive approach is applied using the Newmark method with the RSDAM software (Leclerc *et al.* 2002). This level consists of a dynamic time-history analysis that calculates the permanent dam displacements resulting from sliding or rocking, triggered by the ground motion, along the weakest contact plane. This weakest plane is generally either the dam-rock interface (DRI), or the lowest concrete lift joint (CLJ). Sliding along contact is calculated by assuming the moving part of the dam as a rigid block. The principle of the analytical calculation is based on a critical acceleration threshold at which the rigid block starts to slide. The relative acceleration is defined as the difference between the ground acceleration at time t and the critical acceleration. The relative displacement of the dam in respect to the rock foundation at each time increment is determined by integrating the relative acceleration twice. Block sliding ends when the velocity returns to zero and the ground acceleration is less than the critical acceleration. The use of RSDAM allows to conduct Newmark analyses while accounting for the effect of the vertical seismic component on the sliding response of the dam monolith. RSDAM is also able to quantify the rotation of the dam monolith over time to investigate a possible overturning risk. The fluid-structure interaction is modeled through Westergaard's added masses, thus ignoring water compressibility. The residual displacement dR is defined as the residual sliding displacement of the dam obtained at the end of the time-history analysis.

Analyses conducted with RSDAM are associated with certain limitations. First, the dynamic amplification of the seismic demand within the dam, due to structural flexibility, is ignored. This assumption can be justified as non-linearities (uplifting or sliding) along the weakest joint act as a seismic isolator, causing the upper part of the dam to behave like a rigid body. Furthermore, the analyses conducted with RSDAM cannot provide the stress distribution along the analyzed weakness plane and cannot account for the ratio EC/ER unlike the FEM. However, these limitations are compensated by various conservative assumptions. During an earthquake, cracking occurring along higher lift joints results in the dissipation of seismic energy, thus reducing the shear forces acting along the analyzed weakness plane. Such effect is neglected by RSDAM. Beneficial effects of rock foundation damping is also ignored by RSDAM. Finally, the Newmark method requires the weakest joint to be defined as fully cracked, thus neglecting the initial presence of chemical or apparent cohesion.

Analyses are conducted with RSDAM in the 2D upstream-downstream plane, with only one horizontal and one vertical components. As noted before, 11 triaxial records were selected and calibrated by Nanometrics (2022) according to target spectra with ξ = 5%, as shown in Figure 2. Each record has two horizontal and one vertical components, each of which can be positive or negative. However, only one horizontal component can be implemented in the RSDAM model. This leads to 8 possible load combinations for each record and for each section. To avoid 4752 time-history analyses for the Isle-Maligne development, one section was selected

and analyzed to identify the critical load combination which results in the maximum dR among the 8, for each of the 11 records. This reduced the maximum number of analyses to 594. Note that the horizontal component which provides the maximum dR generally corresponds to the highest Arias intensity. It is noteworthy that the value of ξ does not affect the PGA (spectral acceleration for T = 0s). Yet, a dam assumed as a rigid body is supposed to have a theoretical vibration period of T = 0s. Theoretically, the spectral damping used to calibrate the suite of records has no impact on the PGA. In practice, the use of a target spectra with ξ = 5% leads to a certain conservatism which can partially compensate the effects of some simplifying assumptions of the Newmark method (see section 5.5).

Denoting dRavg as the average of the 11 dR obtained for the 11 accelerograms, if dRavg $>$ 25 mm upon completion of level III, the section is assumed unstable, as shown in Figure 3 and 4. No maximum threshold is set for one residual displacement dR obtained with one single time history. Indeed, the 11 response spectra can demonstrate substantial variability in the Figure 2 due to the calibration process. Furthermore, the use of an average value limits the impact of many uncertainties that may affect the prediction of the seismic behaviour of dam monoliths. The engineer's judgment is proven sufficient to effectively assess whether the rotation θ(t) of the dam over time might cause a risk of overturning (see section 5.5). The threshold value of 25 mm is based on the damage scale shown in Figure 4, inspired from Bernier *et al.* (2016), and adapted specifically for the Isle-Maligne dam site.

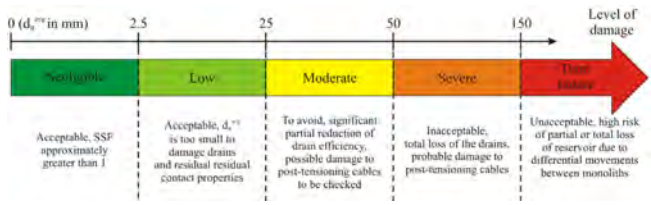

Fig. 4
Damage scale as a function of dRavg adapted to the Isle-Maligne dam site

4. SHEAR STRENGTH OF INTERFACES

This section presents the detailed review and analysis conducted to assess the shear strength properties of the Isle-Maligne dam joints. The shear strength of an interface is commonly characterized by the Mohr-Coulomb criterion. An interface is considered bonded when there is a chemical link corresponding to a non-zero tensile strength f_t. The peak shear strength τ_p of the interface is then given by:

$$\tau_p = \sigma_n \tan(\varphi) + c \tag{1}$$

in which σ_n is the normal stress, φ is the friction angle along the interface, and c is the chemical cohesion, i.e. the shear strength of the chemical link for $\sigma_n = 0$. It is noteworthy that c can be related to f_t through Griffith's criterion, i.e. $c/f_t = 2$. $f_t = c = 0$ when an interface is unbonded. The shear strength of an unbonded interface is called residual and is given by $\tau_r = \sigma_n \tan(\varphi_r)$ where φ_r is the residual friction angle.

In 1990, an investigation campaign was carried out at the Isle-Maligne dam site. Two types of unbonded interfaces were observed within the boreholes: (1) lift joints; and (2) cracks within the concrete. Dam-rock interface shear strength is assumed to be controlled by cracks within the concrete directly above the concrete-rock contact. Indeed, the 1990 campaign suggested that the concrete-rock contact is in very good condition and partially bonded. In addition, the numerous large asperities observed on the rock foundation surface in the vicinity of the structures indicate a probably highly rough dam-rock interface with a foundation of excellent quality. Several contact specimens were subjected to direct shear tests in laboratory. These tests provide the shear stress τ along the contact specimen as a function of shear displacement δ_s for a constant normal stress σ_n. Most of the curves $\tau(\delta_s)$ do not vary much with δ_s. Thus, the plateau of $\tau(\delta_s)$ can be identified as the residual shear strength $\tau_r(\sigma_n)$. Figure 5 shows all the couples $(\sigma_n; \tau_r)$ obtained experimentally for DRI (shear tested cracks within concrete) and CLJ. Based on these results, the shear strengths of DRI and CLJ were characterized by a friction angle of $\varphi_r = 45^\circ$ by performing a linear regression through the origin, i.e. $c = 0$, as the contact specimens were unbonded. Such unilinear failure envelop is found suitable for high normal stress levels. However, this may lead to a significant underestimation of the experimental shear strength when $\sigma_n \leq 1$ MPa, as shown in Figure 5. Yet, it has been estimated in the past that $\sigma_n \leq 1$ MPa for most of the Isle-Maligne dam monoliths. This emphasizes the limitations of Mohr-Coulomb criterion to model the residual shear strength of rough contacts, i.e. with substantial asperities, like those drilled from the Isle-Maligne dam site. Such unbonded rough contacts are better characterized by a non-linear failure envelop $\tau_r(\sigma_n)$, which may be difficult to simplify into a single straight line (Barton and Choubey 1977).

Therefore, two bilinear criteria are developed to approximate the non-linear failure envelopes of CLJ and DRI. The envelope of these bilinear criteria shown in Figure 5 consists of two segments joining at a transition normal stress $\tilde{\sigma}_n = 300$ kPa. Their equation is given by:

$$\tau_r = \begin{cases} \sigma_n \tan(\varphi_0) & \text{if } \sigma_n \leq \tilde{\sigma}_n \\ \sigma_n \tan(\varphi_{ap}) + c_{ap} & \text{otherwise} \end{cases} \quad (2)$$

in which φ_0 is the initial friction angle considered for $\sigma_n \leq \tilde{\sigma}_n$, and φ_{ap} and c_{ap} are the apparent friction angle and cohesion, respectively. The values of these parameters are shown in Table 1 for CLJ and DRI. It is interesting to note that $c_{ap} \neq 0$ while the contacts are unbonded, i.e. $f_t = 0$. Therefore, these criteria present several advantages: (1) the uncertainty related to the presence of chemical cohesion is eliminated;

(2) SSF are assumed to be assessed with the residual shear strength of the joints; and (3) c_{ap} can reappear as soon as $\sigma_n \geq \tilde{\sigma}_n$ even if cracking or sliding already occurred along the weakness plane (this is very practical in the case of a recompressed interface in post-seismic conditions).

Table 1
Shear strength parameters obtained for the Isle Maligne dam site

	φ_0	φ_{ap}	c_{ap}	φ_b^r	JRC	JCS
CLJ (lift joints)	53,2°	40°	150 kPa	32°	12.5	13 MPa
DRI (dam-rock interface)	58°	43°	200 kPa	32°	12.5	30 MPa

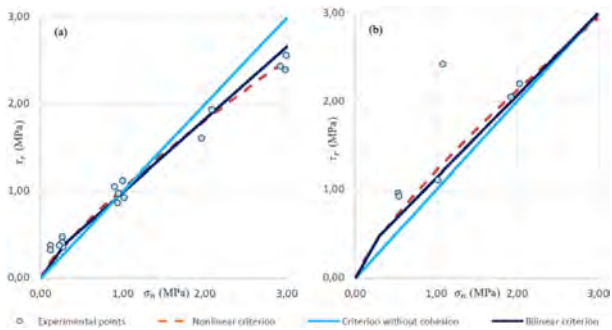

Fig. 5
Shear strength criteria and experimental pairs $(\sigma_n;\tau_r)$: (a) concrete lift joints (CLJ); and (b) dam-rock interface (DRI)

The non-linearity of the failure envelope $\tau_r(\sigma_n)$ is explained by the combination of asperities shearing and loss of contact interlock. As a result, the curve $\tau_r(\sigma_n)$ will exhibit gentler slopes for higher values of σ_n. The shear strength of unbonded rough contacts can be characterized using the model JRC - JCS (Barton and Choubey 1977) given by:

$$\tau_r = \sigma_n \tan\left(\varphi_b^r + JRC \log\left(\frac{JCS}{\sigma_n}\right)\right) \tag{3}$$

in which JRC is the joint roughness coefficient, varying from 0 (planar joint, no roughness) to 20 (very rough joint); JCS is the joint compressive strength; and φ_b^r is related to the basic friction angle (corresponding to a smooth planar interface) while accounting for contact weathering. Reminding that all shear tested joints were concrete-concrete contacts, the values of φ_b^r, JRC and JCS shown in Table 1 are back calculated from the experimental pairs $(\sigma_n;\tau_r)$ using Eq.(3). It is important to note that the values found in Table 1 are specific to the Isle-Maligne dam site.

Values of JRC and JCS are consistent with some observations from the 1990 campaign which indicate that concrete cracks exhibit fairly rough and clean contacts, while lift joints are often weathered . Thus, two non-linear envelops, based on Eq.(3), are obtained for CLJ and DRI, as shown in Figure 5. These non-linear envelops can be simplified through a linear regression into an equivalent Mohr-Coulomb criterion given by (Rullière *et al.* 2020):

$$\tau_r = \tan(\varphi_{ap}) + c_{ap} \tag{4}$$

Therefore, the apparent cohesion c_{ap} is a mathematical parameter which account for the non-linearity of the failure envelop of a rough unbonded joint while using the Mohr-Coulomb criterion. Nevertheless, the shear strength of an unbonded joint remains zero for $\sigma_n = 0$. Thus, Eq. (4) may overestimate the shear strength for low values of σ_n since $c_{ap} \neq 0$. For this reason, a bilinear criteria is introduced using a transition normal stress $\tilde{\sigma_n} = 300$ kPa which is visually identified. These bilinear failure envelops provide a reasonable approximation of the JRC - JCS model, while being conservative for low values of σ_n.

However, applying Eq.(2) remains challenging in the case of a fully cracked interface, or when the distribution of σ_n is not provided, for instance when the Newmark method is used. In such circumstances, another shear strength criterion is specifically adopted with a friction angle $\varphi_r = 45°$ considered without cohesion. Such criterion corresponds to the original linear regression passing through the origin and using the experimental pairs $(\sigma_n; \tau_r)$. It is noteworthy that Newmark method necessarily assumes the occurrence of a sliding mechanism. As the dam starts to slide, the weakness plane is automatically fully cracked. Thus, it seems reasonable to assume that asperities are sheared, leading the non-linearity of $\tau_r(\sigma_n)$ observed under low normal stresses to fade.

5. RESULTS EXAMPLES

5.1. Comparison between the gravity method and the FEM

This section presents various examples of results from this engineering project to illustrate the relevance of the solutions carried out to optimize the seismic stability analyses. First, the gravity method (CADAM3D) and the FEM are compared. Some finite element (FE) models of the Isle-Maligne water intake monoliths were constructed for previous studies using the Abaqus software. At the time, the FEM was chosen as it enabled better consideration of the 3D effects of the irregular geometry of the water intake and its penstock, as well as the effects of the E_C/E_R ratio, to determine the stress distribution within the monoliths. However, the FE analyses were only conducted with the pseudo-static method combined with Westergaard's added masses. It would have been too complex and time-consuming

to adapt these FE models to conduct the pseudo-dynamic analyses required by this study. On the contrary, CADAM3D allows to quickly modify the analysis methods, geometrical parameters (e.g. lift joint levels), or mechanical parameters (e.g. shear strength properties). Nevertheless, such simplicity can result in a certain loss of accuracy. To better understand the extent of this, CADAM3D models were specially constructed and analyzed using the same properties and analysis assumptions as existing FE models. It is important to note that these models consider very conservative assumptions and acceleration values, which are not representative of the seismic behaviour of the structure, and differ from those used in this study. Their results are compared in Table 2 for normal (N) and seismic (ED) load combinations. A fair agreement is found between SSF obtained by CADAM3D and Abaqus in Table 2. This comparison is important since the acceptability criterion for Levels I and II is based on SSF (Figure 3). Despite this good matching, the cracking length along the joints predicted by Abaqus and CADAM3D can substantially differ (not shown in Table 2). Unlike CADAM3D, Abaqus accounts for the local flexibility of the structure, which enables a much more accurate prediction of the stress distribution. That said, this flexibility has no impact on the normal and shear forces acting along the joints when the pseudo-static method is employed. This comparison has therefore allowed us to better understand the limitations of CADAM3D, while validating its use to conduct extensive analysis campaigns and to assess corresponding SSF as part of this project. This also demonstrates the relevance of comparative studies for engineers to ensure the validity of numerical results and save time, when a choice has to be made between an accurate, complex and time-consuming method and a simplified, fast and easy method.

Table 2
Comparison between FEM (Abaqus) and gravity method (CADAM3D) using the pseudo-static method

	WATER INTAKE MONOLITH 2			**WATER INTAKE MONOLITH 5**		
	DEAD WEIGHT	**SSF(N)**	**SSF (ED)**	**DEAD WEIGHT**	**SSF (N)**	**SSF (ED)**
FEM (Abaqus)	589 MN	1,65	0,52*	627 MN	3,36	0,86*
CADAM3D	591 MN	1,65	0,55*	630 MN	3,02	0,85*

*SSF obtained with a fictitious acceleration, not representative of the seismic behaviour of the structure.

5.2. Effect of the inclination of the dam-rock interface

This section presents the in-depth analysis of on-site boreholes conducted to better estimate the bedrock level beneath the structures and to reject unfavourable dam-rock interface inclinations. It is noteworthy that the elevations of the upstream heel and downstream toe of the dam monoliths read from available drawings are

quite uncertain as these drawings depicted information from the construction period (1923 to 1926) which may not reflect the as-built state. Due to these uncertainties, the inclination of the dam-rock interface was often selected as negative in the previous studies to ensure the conservatism of the analyses, as illustrated in red in Figure 6 (a) for the water intake of Isle-Maligne. Moreover, it can be seen in Figure 6 (b) that the elevations of the heel and the toe can substantially vary from one monolith to another, thus increasing the uncertainty. That said, rehabilitation work from 1991 to 2004 led to drill two upstream and downstream injection curtains, a drainage curtain, and to install several piezometers, as shown in Figure 6 (a). Most of these boreholes reach the rock foundation. Thus, these drilling operations allowed to measure the elevation of the concrete-rock contact for several points with varying coordinates along the upstream-downstream X-axis, as shown in Figure 6 (a). An in-depth analysis of the measurements obtained from these on-site boreholes enables a better identification of the likely concrete-rock profile under each monolith of the water intake, as illustrated in blue in Figure 6 (a). Sliding along the unfavorable inclined dam-rock profile shown in red in Figure (a) would require shearing good quality anorthosite or mass concrete associated with substantial cohesion and tensile strength. The dam monolith is more likely to slide along a horizontal unbonded weakness plane such as an open lift joint. Following this logic, it is possible to assume a more favorable inclination of the dam-rock interface, as indicated in Figure 6 (a) (in green) and (c). Drainage and injection curtains also provide an accurate measurement of the concrete-rock profile under the dam monoliths along the bank-to-bank Y-axis, as depicted by Figure 6 (b). These concrete-rock profiles highlight the existence of a substantial macro-roughness of the rock foundation surface underneath the structure. The shear keys due to roughness will significantly increase the shear strength of the dam-rock interface. This confirms that the weakness plane will most likely occur along a horizontal crack within the concrete rather than along the highly rough irregular contact between the dam and its foundation despite its general negative inclination.

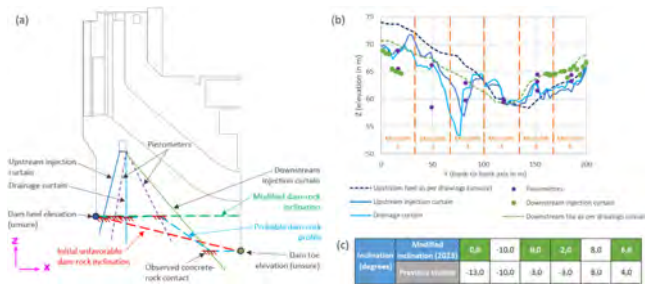

Fig. 6
Investigation of the dam-rock interface profile under the water intake: (a) upstream-downstream section with the various boreholes; (b) measured concrete-rock profiles along the bank-to-bank axis; and (c) optimization of the inclination of the dam-rock interface

Table 3 presents the results of the stability analyses of 4 sections. It should be noted that the dips of the dam-rock interfaces used in previous studies (Section 0) were -13° for the water intake monolith 1 (denoted M1), +5° for pier 1 of spillway 1, -6.6° for pier 5 of spillway 4, and 1.6° for ogee 6 of spillway 4. Analyzing the data obtained from the various boreholes drilled since 1991 (including, for spillway 4, the installation of post-tensioning anchors) the dips of the dam-rock interface are modified more favorably to 0° for water intake M1, +10.2° for pier 1 (spillway 1), and 0° for pier 5 (spillway 4). The dip of ogee 6 (spillway 4) remains unchanged. Table 3 compares the SSF of each section obtained for the seismic load combination with the pseudo-static method along the dam-rock interface with the former dip (section 0) and the modified dip. It is shown that SSF obtained with the modified dips are significantly higher.

Table 3
Effect of various model optimizations on the seismic stability along the dam-rock interface

METHOD GEOMETRY CRITERIA FOR τ_r[(1)] COMPRESSIBILITY[(2)]	PSEUDO-STATIC			PSEUDO-DYNAMIC[(3)]		NEWMARK	
	SECTION 0	MODIFIED DIP		MODIFIED FIP		MODIFIED DIP	
	FORMER INC.	FORMER INC.	NEW INC.	NEW INC.	COMP.	NEW INC.	
	SSF	SSF	SSF	SSF	SSF	d_R^{moy}	Max (θ(t))
Water intake M1	0.83	1.15	1.15	1.19	O.S.[(4)]	4.2 mm	0°
Pier 1 (spill. 1)	1.23	1.56	1.82	1.34	1.18	3.4 mm	0°
Pier 5 (spill. 4)	1.23	1.51	1.51	1.52	1.36	1.0 mm	0°
Ogee 6 (spill. 4)	0.96	0.96	1.36	1.17	0.72	11.5 mm	0°

[(1)]Former (φ_r = 45° and c = 0 kPa) and new (Section 4) criterion of τ_r;[(2)] Incompressible or compressible water;
[(3)] Method of Miquel and Bouaanani (2010);[(4)] Out-of-section resultant, unstable model on overturning.

5.3. Effect of shear strength properties

This section discusses the benefits of the new residual shear strength criterion τ_r developed in section 4 of this paper, compared with the former criterion. As a reminder, the new criterion is bilinear as shown in Eq.(2), except when the interface is 100% cracked (which is assumed for the analyses conducted with RSDAM). In the latter case, the new criterion corresponds to the former one which was found adequate at high normal stress levels, i.e. $\varphi_r = 45°$ and $c = 0$ kPa. Table 3 compares SSF obtained, for the seismic load combination, along the dam-rock interface of the 4 sections, with the pseudo-static method, with the modified dips, with the former and new shear strength criteria. It is shown that the SSF of the water intake

M1 and the pier 5 (spillway 4) is not affected by the change of criterion. The dam-rock interfaces of these two monoliths are in fact 100% cracked, corresponding to the case where $\varphi_r = 45°$ *and* $c = 0$ kPa, regardless of the employed criterion (former or new). However, for pier 1 (spillway 1), SSF = 1.82 with the new criterion, while SSF = 1.56 with the former criterion. Furthermore, for ogee 6 (spillway 4), SSF = 1.36 with the new criterion, while SSF = 0.96 with the former criterion. These results clearly illustrate the relevance of the developed bilinear criterion, which can substantially increase SSF at low normal stress levels when little cracking occurs.

5.4. Pseudo-dynamic analysis and water compressibility

This section discusses the contribution of pseudo-dynamic versus pseudo-static analyses, which correspond to Levels II and I of the proposed progressive approach, respectively. Table 3 compares SSF obtained along the dam-rock interface of the 4 sections for the seismic load combination with the pseudo-static and pseudo-dynamic methods while the modified dips and the new criterion of τ_r are considered. CADAM3D is used to obtain these results with the gravity method. For convenience, all the pseudo-dynamic results in Table 3 are determined using the method of Miquel and Bouaanani (2010). It should be noted that the method of Fenves and Chopra (1987) can also be used for spillway piers and ogees in CADAM3D. It is shown in Table 3 that the results are generally more conservative when the pseudo-dynamic method is used. In fact, this method considers the dynamic amplification of the seismic demand within the dam resulting from structural flexibility, as opposed to the pseudo-static method. Furthermore, the method of Miquel and Bouaanani (2010) and Fenves and Chopra (1987) account for the effects of the mode shapes of the structure on the distribution of the hydrodynamic pressures, and the reservoir water can be considered compressible or incompressible. Usually, the estimation of hydrodynamic pressures is conservative when the compressibility of water is considered. Nevertheless, when the vibration period of the dam-reservoir system get closer to the fundamental period of the reservoir, the calculation of the hydrodynamic pressures may become unrealistic, as the structure and reservoir start to resonate together. This is because the method of Miquel and Bouaanani (2010) does not account for damping at the base of the reservoir in CADAM3D. By assuming an incompressible reservoir, the risk of resonance is eliminated, but hydrodynamic pressures might potentially be less conservative.

Table 3 compares SSF obtained with the pseudo-dynamic method, considering compressible or incompressible water. The results are more conservative when the water compressibility is considered. For ogee 6 (spillway 4), SSF = 1.17 and SSF = 0.72, respectively, depending upon whether the water is considered incompressible or compressible. Nevertheless, these values must be nuanced in the light of the vibration periods of the dam-reservoir system and of the reservoir alone. For example, the shear force at the dam-rock interface of ogee 6 (spillway 4)

is 77 MN when the water is incompressible, and 106 MN when the water is compressible. However, the vibration period of the dam-reservoir-foundation system for this section is 0.065 s, while the vibration period of the reservoir alone is 0.08 s. It is therefore possible that the structure of ogee 6 (spillway 4) and the reservoir resonate together. Since unsatisfying behaviours of water intake M1 and ogee 6 (spillway 4) are obtained in Table 3 when the water compressibility is considered, the stability of these monoliths cannot be proved at Level II (pseudo-dynamic analyses). Nonetheless, this conclusion is not definitive, as SSF > 1 for these two monoliths with an incompressible reservoir. This demonstrates the relevance of Level III (Newmark analyses) to clarify results of pseudo-dynamic analyses which fail to demonstrate the stability of a given section. Overall, this paper suggests to conduct pseudo-dynamic analyses with an incompressible reservoir when the dam is found unstable while considering water compressibility. This helps to provide a more nuanced understanding of the conservatism of certain results. Unfavorable results obtained with compressible water should not be ignored though.

5.5. The benefits of Newmark analyses

This section discusses the benefits of using Newmark analyses with RSDAM, and more generally of using a progressive approach. First, it should be noted that models of dam monoliths are constructed in RSDAM using the default shape of a typical gravity-dam. However, this typical shape may substantially differ from an irregular cross-section of an water intake or a spillway pier. These geometric irregularities can be considered in RSDAM by adding or removing volumes, as depicted in Figure 7 for the water intake. These volumes are defined by their mass, the position of their center of gravity, and their mass inertia. Some forces must also be manually implemented, such as sediment pressures or hydrostatic and hydrodynamic pressures on the gates. A pseudo-static analysis can be carried out using RSDAM by defining a time-constant accelerogram corresponding to the horizontal and vertical accelerations used in CADAM3D analyses. As indicated in Figure 3, this paper strongly recommends comparing the SSFs obtained by pseudo-static analyses on CADAM3D and RSDAM in order to validate the constructed models. The defined shear strength properties and weakness plane must be the same in both models. Seismic load combination factors, generally 1 and 0.3 for the horizontal and vertical components, must be included in pseudo-static analyses with RSDAM. However, these factors must not be considered for temporal dynamic analyses as the accelerograms already vary in time. Indeed, these factors allow the consideration of the non-simultaneity of horizontal and vertical peak accelerations when such information is unavailable, i.e. for pseudo-static and pseudo-dynamic analyses. Figure 8 (a) shows that a fair agreement is found between SSF obtained by the pseudo-static analyses conducted with CADAM3D and RSDAM with the 54 analyzed sections.

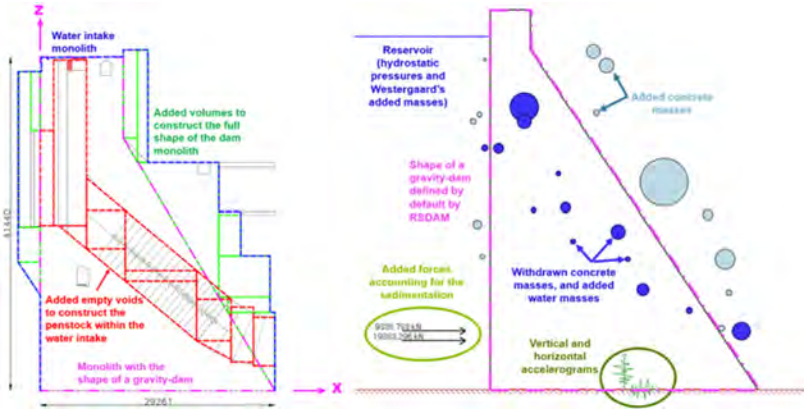

Fig. 7
Construction of the irregular geometry of a water intake monolith using RSDAM

As a reminder, d_R^{avg} is the average of the 11 residual displacements d_R obtained with the 11 ground motions through a dynamic time-history analysis. Figure 8 (b) shows the values of d_R^{avg} as a function of the SSF obtained with RSDAM using the pseudo-static method for all 54 analyzed sections. It can be observed that, for numerous sections, $d_R^{avg} < 25$ mm, i.e. d_R^{avg} is below the acceptable limit, while SSF < 1. This result emphasizes the relevance of the Newmark analyses (Level III). Newmark analyses are also conducted with RSDAM since this software can consider the effects of the vertical seismic component and quantify the rotation over time θ(t) of the dam monolith. Analyses conducted in parallel with this project have shown that the vertical component can substantially affect the non-linear behaviour of dam monoliths. Thus, for one of the accelerograms used with a section of the north lateral dam, d_R = 34 mm and d_R = 21 mm, with and without the vertical component, respectively. This result illustrates that neglecting the effect of the vertical component on dam sliding can lead to unconservative results that can hamper damage estimate. The quantification of θ(t) enables the assessment of the overturning risk. For instance, an out-of-section resultant is found in Table 3 for water intake M1 by pseudo-dynamic analysis with water compressibility, suggesting a potential risk of overturning. However, the rotation of this section is found by RSDAM to remain null over time. In fact, RSDAM results proved that the risk of overturning identified in the pseudo-dynamic analyses (Level II) is negligible for all sections of the Isle-Maligne dam site. This discrepancy is due to the transient, fast nature of the ground motions used in the temporal analyses. It should be noted that, at the end of Level III, the stability of water intake M1 and ogee 6 (spillway 4) is demonstrated in Table 3. These results highlight the relevance of Newmark analyses with RSDAM, as they remove doubts and uncertainties raised by pseudo-dynamic analyses. Finally, as shown in Figure 8 (b),

several sections present $d_R^{avg} > 0$ while SSF > 1. It can be seen, in Figure 2, that the mean response spectrum of the 11 accelerograms substantially exceeds the target seismic spectrum with ξ = 5%. Thus, the PGA of the mean response spectrum is approximately 30% higher than the PGA of the target spectrum, for both the horizontal and vertical components. This can be attributed to a certain conservatism inherent to the employed calibration method. This conservatism is kept to partially compensates the inability of RSDAM to account for the dynamic amplification of the seismic response within the structure. Overall, sliding displacement obtained from rigid-body time-history analyses should always be discussed in the light of the potential conservatism of the accelerograms used and their response spectrum.

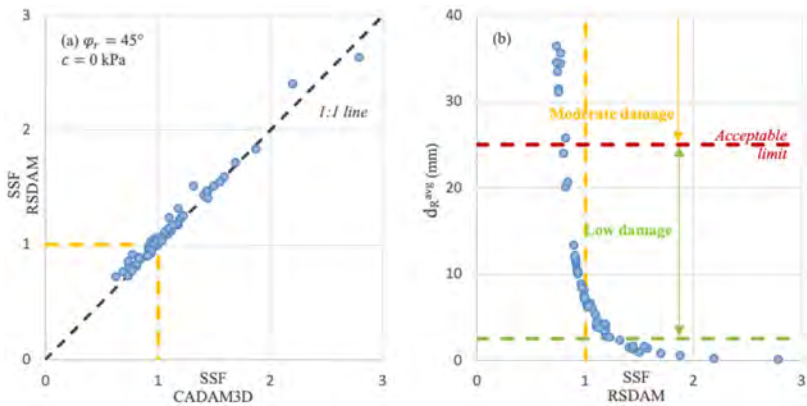

Fig. 8
Results of the Newmark method (RSDAM) for each analyzed dam monolith: (a) validation with CADAM3D (SSF obtained with the pseudo-static method, $\varphi_r = 45°$ and $c = 0$ kPa); and (b) dRavg as a function of SSF

Figures 9 (a) and (b) respectively show the sliding displacement and SSF curves obtained over time for water intake M1 with the 11 ground motions with RSDAM (considering both horizontal and vertical components). It can be observed that the SSF curves are regularly below 1. However, the resulting sliding displacement remains limited to a few millimeters, which is relatively insignificant on the scale of the dam monolith. This emphasizes the relevance of using a sustained acceleration with the pseudo-static and pseudo-dynamic analyses. Indeed, a sustained acceleration implies that SSF must be long enough below 1 to induce a substantial sliding. That said, the instant at which the dam slides matches well with the lowest peaks of the SSF curve for which SSF < 1. Figure 9 (a) also shows a certain variability of the residual sliding displacements d_R depending on the ground motions. Thus, 9 out of 11 ground motions lead to $d_R < 5$ mm. Despite an identical selection and calibration procedure, the 11 records present variable temporal

properties (number of peak accelerations, duration, ratio of vertical to horizontal PGA) which can explain these discrepancies. As in any sampling process, it is difficult to justify that the analysis leading to d_R = 23 mm is less valid than the analysis leading to d_R = 2 mm. However, ignoring all results outside the maximum of d_R = 23 mm would be far too conservative regarding the overall behaviour of the structure. For instance, SSF = 1.15 and SSF = 1.19 in Table 3 with pseudo-static and pseudo-dynamic analyses with an incompressible reservoir. Therefore, it is preferable to consider the average d_R^{avg} of the final residual displacements d_R as the main indicator. It is also essential to select enough accelerograms to obtain d_R^{avg} as representative as possible. Finally, it is noteworthy that the final interpretation of the seismic stability of the water intake M1 is inferred by considering all the results of the three levels of analysis. The proposed progressive approach enables the adoption of various optimization strategies to assess the dam seismic stability while ensuring their validity through the comparison and verification of various results. While remaining quite straightforward, the proposed progressive approach provides a comprehensive and robust vision of the structure's seismic behaviour, as opposed to a more classical analysis procedure which would be limited to a few indicators and would not investigate the effects of the considered simplifications.

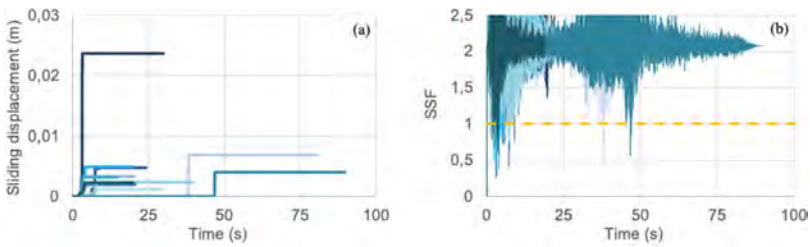

Fig. 9
Results obtained over time for the water intake M1 with the 11 ground motions using the Newmark method (RSDAM): (a) sliding displacement; and (b) SSF

6. CONCLUSION

This paper presented the various solutions adopted to optimize the seismic stability assessment of the Isle-Maligne dams. A progressive approach was developed and applied. This approach included three levels of analysis: levels I and II, pseudo-static and pseudo-dynamic analyses using the gravity method, respectively; and level III, Newmark analyses providing residual sliding displacement. This paper underlined several best practices to be followed at the start of a project to ensure the validity while optimizing the seismic stability analyses. For instance, a thorough analysis of boreholes from previous rehabilitation work has enabled the reassessment of numerous dam-rock interface inclinations. Better dam stability indicators

were obtained with the modified inclinations while keeping a satisfactory degree of confidence. This paper also highlighted that dam engineers must adopt a critical mindset regarding the shear strength properties inferred from investigations conducted several decades ago. In this work, the development and the adoption of a new bilinear failure criterion has led to higher SSF along slightly cracked joints. The relevance of using a progressive approach for seismic analyses was also demonstrated. It was shown that Newmark analyses efficiently removed the doubts and uncertainties raised by pseudo-dynamic analyses. Pseudo-static analyses provided a preliminary assessment of the seismic behaviour of structures. Pseudo-static analyses were also easy to check, which made them extremely efficient to validate the models constructed for Newmark analyses. Finally, pseudo-dynamic analyses were used to nuance the possible non-conservatism of some assumptions considered by the other levels of analysis. Thus, the proposed progressive approach enabled the adoption of various optimization strategies to assess the dam seismic stability while ensuring their validity through the comparison and verification of various results. The final interpretation of all the results from all the levels of analysis provided the engineer with a comprehensive and robust understanding of the seismic behaviour of the dam monoliths.

REFERENCES

ALLIARD, P. M., AND LÉGER, P. 2008. “Earthquake safety evaluation of gravity dams considering aftershocks and reduced drainage efficiency.” *Journal of Engineering Mechanics (ASCE)*, Vol. 134: pp 12–22.

ATKINSON, G. M., AND PIERRE, J. R. 2004. “Ground-motion response spectra in eastern North America for different critical damping values.” *Seismological Research Letters*, Vol. 75(4): 541–545.

BARTON, N., AND CHOUBEY, V. 1977. “The shear strength of rock joints in theory and practice.” *Rock mechanics*, Vol. 10: pp 1–54.

BERNIER, C., PADGETT, J. E., PROULX, J., AND PAULTRE, P. 2016. “Seismic fragility of concrete gravity dams with spatial variation of angle of friction: case study.” *Journal of Structural Engineering*, Vol. 142(5): 05015002.

CDA (Canadian Dam Association). 2007. Dam Safety Guidelines.

EPRI (Electric Power Research Institute). 1992. Uplift pressures, shear strengths and tensile strengths for stability analysis of concrete gravity dams. EPRI TR-100345, Vol. 1.

FENVES, G., AND CHOPRA, A.K. 1987. “Simplified earthquake analysis of concrete gravity dams.” *Journal of Structural Engineering*, Vol. 133: pp 1688–1708.

FERC (Federal Energy Regulatory Commission). 2016. *Engineering guidelines for the evaluation of hydropower projects. Chapter III: Gravity Dams*.

GRIFFITH, A. A. (1920). “The phenomena of flow and rupture in solids.” *Philosophical transactions of the Royal Society of London*, A221, 163–198.

ICOLD (International Commission on Large Dams). 2004. Sliding Safety of Existing Gravity Dams - Final Report.

LECLERC, M., LÉGER, P., AND TINAWI, R. 2002. RSDAM, User Manual.

LSBQ. 2023. Loi sur la sécurité des barrages au Québec (updated on January 1st, 2023).

MCGUIRE, R. K., W. J. SILVA, AND C. J. COSTANTINO. 2001. Technical Basis for Revision of Regulatory Guidance on Design Ground Motions: Hazard- and Risk-consistent Ground Motion Spectra Guidelines, NUREG/CR-6728, U.S. Nuclear Regulatory Commission, Washington, DC.

MIQUEL, B., AND BOUAANANI, N. 2010. “Simplified evaluation of the vibration period and seismic response of gravity dam-water systems.” *Engineering Structures*, Vol. 32: pp 2488–2502.

MOUZANNAR, H., BOST, M., LEROUX, M., AND VIRELY, D. 2017. “Experimental study of the shear strength of bonded concrete-rock interfaces: surface morphology and scale effect.” *Rock Mechanics and Rock Engineering*, Vol. 50: pp 2601–2625.

Nanometrics. 2022. Probabilistic Seismic Hazard Assessment for Rio Tinto Developments in Quebec: Isle Maligne Site. Technical Report, January 2022.

NUSS, L. K., MATSUMOTO, N., AND HANSEN, K. D. 2012. “Shaken, but not stirred - Earthquake performance of concrete dams.” 32nd Annual USSD Conference, New Orleans, Louisiana.

RENAUD, S., BOUAANANI, N., AND MIQUEL, B. 2015. “Efficiency and limits of the progressive approach to assess the stability of gravity dams: case study of a stepped foundation.” CDA Annual Conference, Mississauga, Ontario.

RENAUD, S., BOUAANANI, N., AND MIQUEL, B. 2020. “Numerical simulation of experimentally shear-tested contact specimens from existing dam joints.” *Computers and Geotechnics*, Vol. 125: 103630.

RT (RIO TINTO). 2021. Group standard - HSEC-B-23 - D5 - Management of tailings and water storage facilities, January 2021

ROSSET, P., LONG, X., AND CHOUINARD, L. 2023. “Influence of the 2020 Seismic Hazard Update on Residential Losses in Greater Montreal, Canada.” *GeoHazards*, Vol. 4(4): pp 406–420.

RULLIÈRE, A., RIVARD, P., PEYRAS, L., AND BREUL, P. 2020. “Influence of roughness on the apparent cohesion of rock joints at low normal stresses.” *Journal of Geotechnical and Geoenvironmental Engineering*, pp 146(3): 04020003.

SEGURA, R., BERNIER, C., MONTEIRO, R., AND PAULTRE, P. 2019. “On the seismic fragility assessment of concrete gravity dams in eastern Canada.” *Earthquake Spectra*, Vol. 35(1): pp 211–231.

USACE (US Army Corps of Engineers). 1995. Gravity Dam Design. EM-1100-2-2200.

USACE (US Army Corps of Engineers). 2007. Earthquake Design and Evaluation of Concrete Hydraulic Structures, EM-1100-2-6053.

Technologie MLT Inc. 2024. CADAM 3D, User Manual.

TINAWI, R., LÉGER, P., LECLERC, M., AND CIPOLLA, G. 1998. “Shake table tests for the seismic response concrete gravity dams.” Proceedings of the 11th European Conference on Earthquake Enginering, Paris, France.

COMMISSION INTERNATIONALE DES
GRANDS BARRAGES

VINGT-HUITIEME CONGRES DES
GRANDS BARRAGES
CHENGDU, MAI 2025

SEISMIC RESILIENT DESIGN OF WAIMEA COMMUNITY DAM (*)

Brian BENSON & David CAMERON-ELLIS
Technical Director, Damwatch Engineering Limited

Peter AMOS
Managing Director, Damwatch Engineering Limited

NEW ZEALAND

SUMMARY

Situated at the convergence of tectonic plates, New Zealand experiences frequent, large seismic events. The country is seismically active and faces unique challenges due to its tectonic setting. Being the first large dam to be constructed in New Zealand in 30 years, the design of the 52 m high Concrete Faced Rockfill Waimea Community Dam incorporated a contemporary approach to ensuring seismic resilience.

For dam safety, the Safety Evaluation Earthquake (SEE) earthquake is a 1:10,000 annual exceedance probability (AEP) probabilistic ground motion from an earthquake with a moment magnitude (Mw) of 7.1, a peak ground acceleration (PGA) of 0.64g and maximum spectral acceleration of approximately 1.65g. The NZ Dam Safety Guidelines require that the design must include one aftershock within a day following the mainshock. The design aftershock for Waimea Dam has an Mw of 6.5 and PGA of 0.58g.

**Conception sismique résiliente du barrage communautaire de Waimea*

DOI: 10.1201/9781003642428-115

Key elements of its design include:

- An erosion-resistant and flexible rockfill embankment, allowing controlled movement during earthquakes. The overarching embankment design performance requirements were the accommodation of earthquake deformations and conveyance of post-earthquake leakage which would have reduced embankment stability to an unsafe level.
- A reinforced concrete facing slab with appropriate slab dimensions, joint details and reinforcing.
- Constructable pre-cast upstream crest wall elements.
- Flexible waterproofing elements connecting the facing slab to the crest walls, as well as between wall elements with appropriate capability for accommodating large movements, and post-seismic flooding.

This paper discusses the contemporary approach to the designs of the components of the dam mentioned above.

It includes a discussion on the geotechnical approach to ensuring appropriate seismic performance and internal stability of the supporting embankment materials, including a comprehensive understanding of the movement of the various components of the embankment during an earthquake. It covers the structural configuration of the upstream zone of the structure, including all rockfill and concrete components, in resisting earthquake effects, with an emphasis on ensuring dam safety during and after an earthquake.

RÉSUMÉ

Située à la convergence des plaques tectoniques, la Nouvelle-Zélande connaît des événements sismiques fréquents et importants. Le pays est sismiquement actif et fait face à des défis uniques en raison de son contexte tectonique. Étant le premier grand barrage construit en Nouvelle-Zélande depuis 30 ans, la conception du barrage communautaire de Waimea en enrochements à face en béton de 52 m de haut a intégré une approche contemporaine pour assurer la résilience sismique.

Pour la sécurité des barrages, le tremblement de terre d'évaluation de la sécurité (SEE) est un mouvement du sol probabiliste de probabilité de dépassement annuel (AEP) de 1/10 000 d'un tremblement de terre avec une magnitude de moment (Mw) de 7,1, une accélération maximale du sol (PGA) de 0,64 g et accélération spectrale maximale d'environ 1,65 g. Les directives de sécurité des barrages néo-zélandais exigent que la conception comprenne une réplique dans la

journée suivant la secousse principale. La réplique de conception pour le barrage de Waimea a un Mw de 6,5 et un PGA de 0,58 g.

Les éléments clés de sa conception comprennent :

- Un remblai en enrochement flexible et résistant à l'érosion, permettant un mouvement contrôlé lors des tremblements de terre. Les principales exigences de performance de conception du remblai étaient la prise en compte des déformations sismiques et la transmission des fuites post-séisme qui auraient réduit la stabilité du remblai à un niveau dangereux.
- Une dalle de parement en béton armé avec des dimensions de dalle, des détails de joints et des armatures appropriés.
- Des éléments de mur de crête amont préfabriqués constructibles.
- Des éléments d'étanchéité flexibles reliant la dalle de parement aux murs de crête, ainsi qu'entre les éléments de mur avec une capacité appropriée pour s'adapter aux mouvements importants et aux inondations post-sismiques.

Ce rapport discute de l'approche contemporaine de la conception des composants du barrage mentionnés ci-dessus.

Il comprend une discussion sur l'approche géotechnique visant à garantir des performances sismiques appropriées et la stabilité interne des matériaux de support du remblai, y compris une compréhension globale du mouvement des différents composants du remblai lors d'un tremblement de terre. Il couvre la configuration structurelle de la zone amont de la structure, y compris tous les composants en enrochement et en béton, pour résister aux effets sismiques, en mettant l'accent sur la sécurité du barrage pendant et après un tremblement de terre.

1. INTRODUCTION

Waimea Dam is a 53m high, Concrete Faced Rockfill Dam (CFRD) completed in early 2024 for the primary purpose of providing irrigation and community water supply. The dam is located in the northwest part of New Zealand's South Island. This region lies on the boundary of the Australian and Pacific tectonic plates, in the tectonic transition between the Hikurangi Subduction zone to the north and the strike-slip Alpine Fault to the south. It is a high seismicity region. Several regional active faults lie within 12 km of the site in different directions. An aerial photo of the dam from a downstream perspective in April 2024 is presented in Fig. 1 below.

Fig. 1
Waimea Dam

Beside the embankment, Waimea Dam's main components include:

- A reinforced concrete face slab.
- A precast concrete parapet wall at the dam crest.
- A concrete free-overflow spillway.
- A reinforced concrete low-level diversion outlet.
- Grout curtain.
- Flexible waterproofing elements connecting the facing slab to the parapet wall, as well as between wall elements with appropriate capability for accommodating large movements, and post-seismic flooding.

From a practical perspective, two significant design limitations constrained the evolution of the design of the embankment:

1. Review of the detailed design of the embankment occurred after the site was established by the contractor. With construction underway, this constrained the dam footprint to that set by the preceding stages of design. Both the upstream and downstream embankment design slopes were 1.5H:1V slopes.
2. Rock materials from the spillway cut were to be utilised for the bulk of the earthfill and rockfill used on the project. On exposure, these materials were found to be prone to breakdown during the extraction and placement process in the dam.

2. DAM SAFETY PERFORMANCE REQUIREMENTS

Waimea Dam has a 'High' Potential Impact Classification (PIC), i.e., hazard rating. This is the highest hazard rating for dams in New Zealand. The New Zealand Dam Safety Guidelines (NZDSG) [1] stipulate there is to be 'no uncontrolled release of the impounded contents' under extreme seismic load conditions, which is referred to as the Safety Evaluation Earthquake (SEE). They also state that under unusual seismic loading, referred to as the Operating Basis Earthquake (OBE), there should be no more than minor, repairable damage. The NZDSG also states that at least one aftershock should be considered with the SEE.

3. SITE GEOLOGY

Geologically, the Waimea Dam basin is dominated by metamorphosed sandstone, siltstone and mudstone. The rock mass consists of a sequence of slightly weathered, moderately strong to strong, light grey to grey, jointed fine sandstone (greywacke) and finely laminated dark grey to black siltstone and mudstone (argillite). Argillite comprises the majority of the rock mass beds and is commonly fissile.

The tectonic history of the rock formation has resulted in a complex occurrence of both macroscopic and microscopic scale defects. These defects include at least four prominent joint sets with bedding ranging between 10 mm and 1 m and crushed and sheared zones varying from 20 mm to $\sim$2 m in thickness that are characterised as shattered rock containing clay-filled seams. The argillite typically splits along micro fractures parallel to the bedding. Bedding and joints are generally closely spaced and tight.

4. SEISMIC HAZARD

Given Waimea Dam's 'High' PIC rating, the NZDSG recommends the following design ground motions:

- Operating Basis Earthquake, OBE: Typically represented by the probabilistic ground motions at 1 in 150 Annual Exceedance Probability (AEP).
- Safety Evaluation Earthquake, SEE: Represented by the 84th percentile level of the Controlling Maximum Earthquake (CME) if developed by a deterministic approach, and need not exceed the probabilistic ground motions for the mean 1 in 10,000 AEP.

- Aftershock: Consider at least one aftershock event at one magnitude less than the CME within one day of the SEE.

GNS Science [2] developed the design ground motions for Waimea Dam. The ground motions were developed based on the foundation bedrock having a time averaged shear wave velocity over the top 30 m of the ground profile (V_s30) of 800 m/s. Table 1 lists the Peak Ground Accelerations (PGAs) corresponding to the OBE, probabilistic SEE and aftershock. The corresponding horizontal acceleration response spectra are presented below in Figure 2.

Table 1
Design seismic parameters

DESIGN GROUND MOTION	PGA (G)	EARTHQUAKE MAGNITUDE, M_W	EARTHQUAKE SCENARIO
OBE	0.15		1 in 150 AEP
SEE	0.64	7.1	Mean 1 in 10,000 AEP
After-shock SEE	0.44	6.8	84th percentile of Alpine Kaniere-Tophouse and Waimea South fault aftershock; Representative of SEE aftershock where mainshock M_w 7.8 response spectra is similar to 1 in 10,000 AEP
	0.58	6.5	84th percentile CME (Waimea Central and Southern fault) aftershock

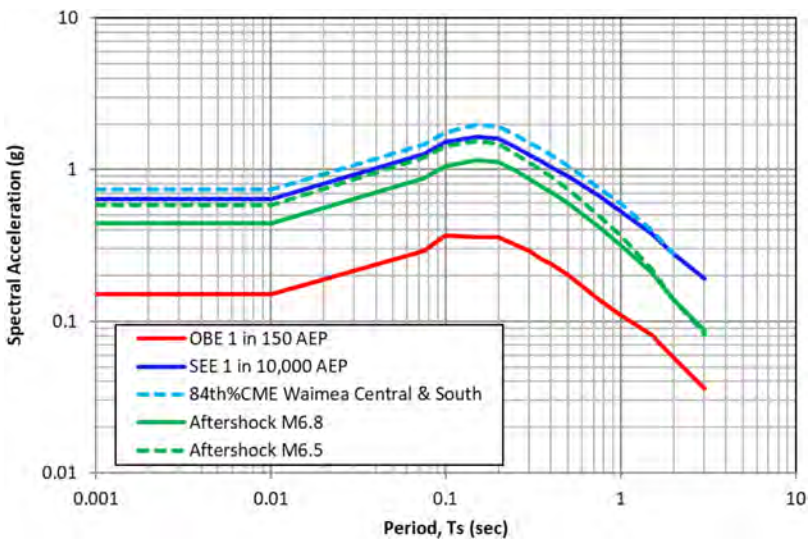

Fig. 2
Design horizontal acceleration response spectra
Accélérations spectrales sismiques horizontales

5. PREDICTED EMBANKMENT SEISMIC DEFORMATIONS

Dynamic numerical analysis was performed to estimate seismic deformations for embankment design. A two-dimensional model of the maximum embankment section was developed for this numerical analysis. The model represented the cross-section general arrangement illustrated in Fig. 3. The characteristics of the various material zones are discussed later in this paper.

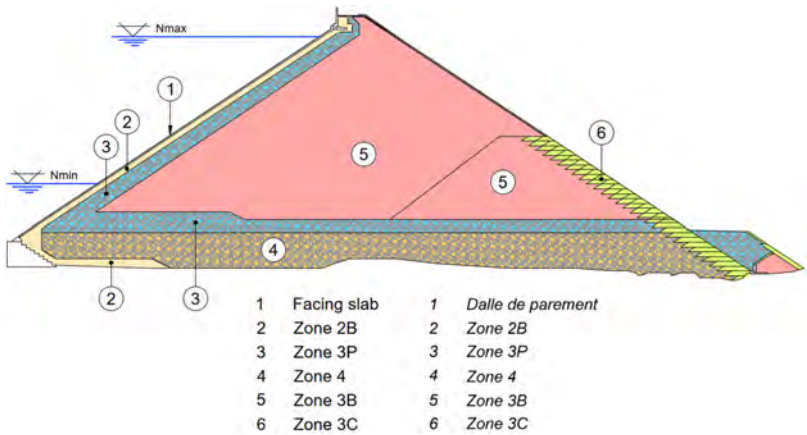

Fig. 3
Maximum cross section of Waimea Dam
Section transversale maximale du barrage de Waimea

Because planned operation of the Waimea Reservoir cycled between the normal maximum operating level (Nmax) and normal minimum operating level (Nmin) annually, both conditions were modelled and analysed. Analyses were performed for three sets of time histories for the 1 in 10,000 AEP and three sets for the aftershock.

Table 2 summarises pertinent dynamic numerical analysis results. The highest permanent displacements from the three sets of time histories were selected for design and are shown in Table 2. Crest centreline settlement, crest centreline horizontal displacement, downstream side of crest displacement, and upstream and downstream slope displacements for SEE and SEE + aftershock ground motions are included in Table 2.

Table 2
Predicted SEE deformations from numerical analysis for embankment design

RESERVOIR LEVEL / DIRECTION	*MAINSHOCK*	MAINSHOCK PLUS AFTERSHOCK	NORMALISED CREST SETTLEMENT (%)
Crest centreline settlement (mm)			
Nmax	290	370	0.72
Nmin	630	790	1.49
Crest centreline horizontal displacement (mm)			
Nmax	300	430	n/a
Nmin	480	620	n/a
Maximum deformations along downstream slope at Nmax (mm)			
Horizontal	900	1230	n/a
Vertical	750	1000	n/a
Maximum horizontal deformations along embankment slopes at Nmin (mm)			
Upstream slope	700	950	n/a
Downstream slope	800	1100	n/a
Maximum vertical deformations along embankment slopes at Nmin			
Upstream slope	360	480	n/a
Downstream slope	580	780	n/a
Maximum vertical deformations at crest downstream side (mm)			
Nmin	1100	1450	n/a

Understanding the distribution and patterns of predicted seismic deformations is essential for design to meet seismic performance expectations. Fig. 4 displays contours of SEE induced displacements, horizontal and vertical separately in the two graphic insets, shown on a two-dimensional cross-section of the embankment dam for Nmin conditions. A two-dimensional embankment dam crest cross-section plot of SEE displacement vectors is presented in Fig. 5. Each vector represents the summed horizontal and vertical displacements at each node in the mesh. A concentration of vectors, visible as high saturation of red colour in Fig. 5, generally indicates the concentrations and patterns of displacements. The maximum vector length is approximately 1.1 m in Fig. 5.

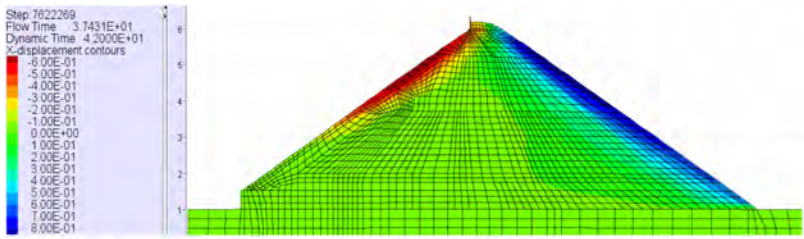

(a) Horizontal displacements/ Déplacements horizontaux

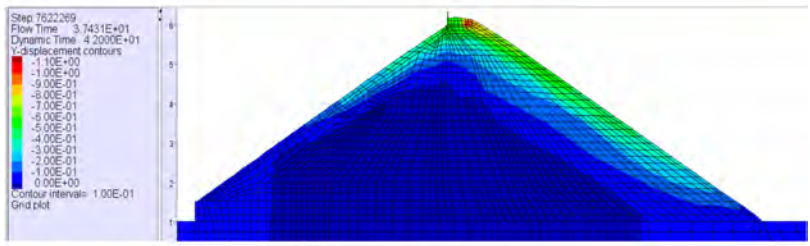

(b) Vertical displacements / Déplacements verticaux

Fig. 4
Contours of seismic displacements for Safety Evaluation Earthquake at normal minimum operating level. [scale in metres]
Courbes de déplacement sismique pour l'évaluation de la sécurité du séisme au niveau minimum normal d'exploitation. [échelle en mètres]

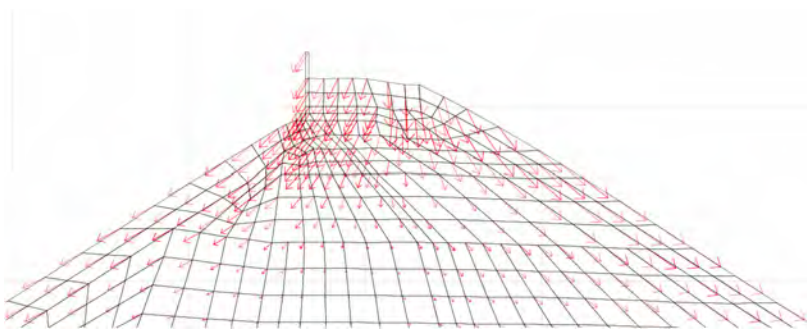

Fig. 5
Crest area displacement vectors for Safety Evaluation Earthquake at normal minimum operating level.
Vecteurs de déplacement pour l'évaluation de la sécurité des tremblements de terre au niveau de fonctionnement minimum normal

There is a significant difference in predicted seismic deformation patterns between the reservoir at normal maximum (Nmax) and minimum (Nmin) operating levels. At Nmax, the reservoir water provides a large degree of inertial restraint of the upstream slope during seismic ground shaking; i.e. the water restrains the upstream slope. At Nmax conditions, the crest settles and tends to rotate downstream with the downstream slope displacing downward towards the lower slope. Under Nmin conditions, both the upstream and downstream slope experience seismic displacements, which results in greater crest deformations and settlement compared to that exhibited along the slopes. The upstream slope displacements do not extend as far down the slope because of the reservoir water's restraint below Nmin.

SEE seismic deformations would severely damage the crest area and upstream slope. Severe deformation to the precast parapet wall units and uppermost embankment would be expected. Such deformations would likely result in joint opening and cracking of the concrete facing, especially in the uppermost portion of the dam. This is discussed further in Section 11 below.

6. EMBANKMENT DAM SEISMIC POTENTIAL FAILURE MODES

Post-earthquake overtopping is considered very unlikely because of the ample estimated post-earthquake freeboard. Crest settlement up to approximately 0.8 m shown in Table 2 result in metres of freeboard between the top of the embankment behind the parapet wall and the reservoir maximum operating level (Nmax).

Significant to major damage of the upstream concrete facing above waterline is expected in a SEE event. This could result in post-earthquake leakage discharge large enough to pose a risk of unravelling of the downstream toe. Were toe erosion to initiate, it could progressively erode the embankment backward towards the reservoir. If intervention failed or erosion did not self-arrest, a breach could result.

Earthquake damage to the upstream concrete facing would result in leakage into the embankment. Seepage pressures could develop in the semi-pervious, dirty rockfill, reducing embankment stability. If seepage pressures were high enough, global instability of the embankment could occur, resulting in breach.

7. EMBANKMENT DAM SEISMIC MITIGATION DESIGN

Two embankment design principles were used to reduce the risk of post-earthquake embankment dam failure: 1) limit the post-earthquake leakage; and 2) collect and convey leakage safely out the downstream toe of the dam.

The maximum embankment cross-section shown in Fig. 2 illustrates the zones discussed below. To limit post-earthquake leakage, a cohesionless sandy transition zone was constructed directly downstream of the concrete facing. Directly downstream of the sandy transition zone, a compatible inclined drain extends behind the entire concrete facing, as illustrated in Fig. 2. This inclined drain is contiguously joined with a blanket drain that extends from behind the upstream plinth to the downstream toe of the embankment dam. The post-SEE design case assumes the concrete facing becomes an ineffective water barrier. The drainage system collects leakage through the upstream facing and safely conveys it out the downstream toe of the dam. Positive seepage pressures are prevented in the downstream portion of the dam, maintaining adequate post-earthquake stability. With low permeability Zone 2B supporting the concrete face and Zone 3P and 4 drainage zones present, the excavated spillway rock could be used to constitute Zone 3B as a “dirty” rockfill.

8. ZONE 2B CONCRETE FACE SUPPORT MATERIAL

The concrete face support zone is designated Zone 2B at Waimea Dam. In addition to the stiffness required to support the concrete facing, post-earthquake performance dictated that it survives the SEE intact to serve as a crack-stopping, flow limiter.

Zone 2B design requirements are summarised as:

- Be stiff enough to adequately support the concrete facing.
- In the event of a crack or rupture of the upstream concrete facing, collapse in to limit the flow through the opening.
- Have a permeability low enough to limit post-earthquake through-leakage in the event of major damage to the concrete facing.
- Be fine enough to be a no-erosion filter where Zone 2B lies directly upon foundation rock defects.
- Be internally stable; i.e. non-suffusive, to retain its stiffness, low permeability and filtering characteristics.
- Be coarse enough to be compatible with the adjacent drainage materials.

The first decision faced for the design of the Zone 2B material was “one material and zone, or two separate materials and subzones?” Zone 2B is not a filter in its position directly beneath the upstream concrete face, although it must perform several similar functions such as being collapsible for crack stopping, internally stable and having adequately low permeability. Additional constraints consisted of maintaining the preceding stage of design’s geometrical envelope and, of course, cost. The large, predicted crest and slope seismic deformations and damage indicated that narrow widths for two stages of Zone 2B would result in one or both stages potentially being truncated. This would result in not meeting the post-earthquake design criteria

above. Constructing two narrow stages would also add considerable cost and schedule to construction.

It was decided to trial Zone 2B as a single stage. In conjunction with internal drainage zones, drainage design dictated a target design permeability for Zone 2B of 1 x 10^{-5} m/s.

The base material available for Zone 2B was site-won processed alluvium. A typical grading is shown in Fig. 6. Some of this material had low plasticity. Its typical grading is sand deficient and empirically determined to be potentially susceptible to internal instability. Given post-earthquake hydraulic gradients as high as 20 across Zone 2B are expected, internal stability was deemed essential. A large permeameter constant head permeability test of the site-won, minus 38 mm processed alluvium yielded hydraulic conductivity of 2.3 x 10^{-4} m/s. It was concluded the site-won, processed alluvium would not meet the post-earthquake performance requirements of Zone 2B.

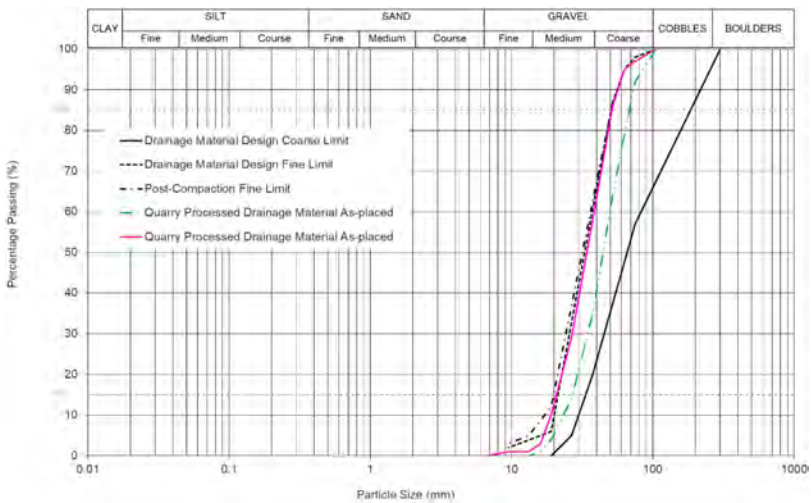

Fig. 6
Drainage Material Gradings
Classification des matériaux de drainage

Blending the site-won processed alluvium with clean sand was considered to improve its permeability, collapsibility, and internal stability. Geologic search in the damsite area for exploitable sand sources was unsuccessful, so blending the site-won, processed alluvium with commercially available sand from off-site was

pursued. Several products were theoretically blended by combining their particle size distributions. The grading of washed concrete sand proved most promising. By adding a minor fraction of concrete sand to the site-won, processed minus 38 mm alluvium, the grading became internally stable and its permeability was lowered. The first permeability test of the theoretically blended Zone 2B material for the coarse limit grading yielded a hydraulic conductivity of 7.7×10^{-6} m/s. The embankment trial showed four overlapping passes with a vibratory steel drum compactor yielded adequate density without excessive fines generation. It was concluded that, by this blending process, a single material and zone for Zone 2B could meet all the design performance criteria, and this was carried through construction of the embankment.

Controlling the moisture content of the materials to be blended and an experienced operator performing the blending were essential to success. A single operator did nearly all the blending of materials for Zone 2B. In all eight lab permeability tests were performed with results in the range between 4.4×10^{-7} m/s to 7.9×10^{-5} m/s. This was considered very good quality control of the blended material.

Zone 2B was designed to nominally be 2 m wide beneath the upstream concrete facing. A custom-made spreader box was built to place the material uniformly and safely. The spreader box included a guide rail that rode along the upstream concrete curbing to maintain alignment. Zone 2B was placed in nominal 400 mm lifts and compacted with four passes of a 4T dual steel drum, vibratory compactor.

Zone 2B wraps around the lower upstream face behind the plinth and extends along the cleaned and treated rock foundation as a filter. It extends for a distance downstream of the plinth equal to half the reservoir water height up to the Inflow Design Flood (IDF). Refer to Fig. 5.

9. INTERNAL DRAINAGE OF THE EMBANKMENT DAM

Post-earthquake conditions for internal drainage design assumed the concrete facing could be an ineffective water barrier and seepage would be controlled by Zone 2B underlying the concrete facing. Post-earthquake internal drainage design took the reservoir level to be at normal maximum operating level (Nmax). For these conditions, the total post-earthquake leakage was calculated on a per metre width basis across the embankment and summed. The embankment's internal drainage system is required to discharge this summed total leakage without saturating the bulk of the embankment composed of relatively poorly drained, fine, dirty rockfill.

Given the seismic performance requirements, an upstream inclined drain adjoining Zone 2B contiguously connected to a blanket drain was selected as the

internal drainage general arrangement. ICOLD CFRD guidance [3] includes placing an underdrain of coarse rock within the valley section to enhance drainage (Zones 3P & 4). Refer to Figure 5. Design of the inclined drain relies on efficiently using gravity to convey all upstream face leakage laterally and down to the blanket drain located in the original river channel at the base of the dam.

The key design criteria for the internal drainage zones were:

- The combined drainage system must convey upstream face leakage out of the dam without significant pressures developing in the embankment above the top of the blanket drain.
- The as-placed drain material needs high permeability.
- The drain material interfacing with Zone 2B needs to be compatible with Zone 2B material.

The grading of the drainage material was designed to meet permeability and material compatibility requirements. The design target permeability was 10^{-1} m/s. To meet compatibility with Zone 2B, the nominal minimum particle size wa determined to be 19 mm. To maintain high permeability, a strict limit to undersize particles, i.e. fraction $<$ 19 mm, was set for stockpile gradings (6% $\leq$ 19mm) and as-placed gradings (12% $\leq$ 19 mm). Gradings showing the drainage material design envelope, i.e. stockpile gradings, and the as-placed fine limit are presented in Fig. 6.

A series of drainage material processing and embankment trials was conducted to ensure that as-placed drainage materials would meet the stringent grading requirements while being adequately compacted. First, processing and embankment trials of site-won rockfill for drainage material were performed. Site-won rockfill was successfully processed. However repeated trials experienced excessive particle breakdown. A post-compaction grading from the site-won rockfill drainage material trials is presented in Figure 6. After several trials, it was concluded adequate drainage material could not be produced from site-won rockfill. Site-won, processed alluvium produced excellent drainage material, but its quantity was much less than needed.

The drainage materials volume was substantial; on the order of 144,000 as-placed cubic metres. The contractor's stockpile of site-won processed alluvium drainage material was soon exhausted. All additional drainage material was obtained from the contractor's quarry 8 km from the dam site. The quarry consists of hard, massive greywacke and limestone. Both rock types were trialled by crushing, screening and constructing an embankment. Both were deemed acceptable. Subsequently, all remaining drainage material was sourced from the hard greywacke at the contractor's quarry. An as-placed (post-compacted) grading of quarry-processed drainage material is presented in Fig. 6.

10. REINFORCED CONCRETE FACING SEISMIC DESIGN

The reinforced concrete facing slab at Waimea Dam provides the primary water barrier of the rockfill embankment. Only slightly changed from the preceding stages of design, the final empirical configuration of the facing slab was based on precedent designs, with thicknesses and reinforcing provisions reflecting contemporary ICOLD and international criteria. As such, the slab was designed as a series of 300mm thick, 15m wide panels intended to be slip-formed on the upstream Zone 2B embankment surface. The slab supporting intake pipework was 400mm thick.

Aside from the slabs along the lower perimeter and the thicker slab supporting intake pipework, reinforcing was centrally placed to contain cracking. The vertical joints between the strips were unreinforced and provided with a single waterstop at the base of the slab. The settlements predicted in the embankment analysis discussed above were utilised to estimate potential joint openings that could ensue following an earthquake to size the waterstop. While initially designed as a looped copper waterstop, this was changed to a large profile PVC waterstop at the request of the contractor. The selected XStop PVC RF345X/25 waterstop from X-Calibur Construction Chemistry features a large centre bulb and tear strip capable of accommodating 100 mm opening or translation.

11. PRE-CAST PARAPET WALL SEISMIC DESIGN

Waimea Dam is provided with a parapet wall at its crest to reduce the overall embankment volumes. The parapet wall is intended as a water barrier and effectively provides a vertical extension of the upstream facing slab to the crest of the dam. It comprises 3m wide pre-cast wall elements with shear key joints between elements.

The base of the wall is located approximately 1.5m above the normal top water level of the dam (Nmax), and the joint between the facing slab and the parapet wall was configured to facilitate vertical movements in line with contemporary design guidelines. To achieve the vertical joint configuration, the top part of the facing slab was provided with a vertical upstand wall at a constant elevation. The precast parapets were installed on the design embankment camber, allowing for embankment settlements of up to 300mm over the life of the dam as indicated in Fig. 7 below.

The vertical joint allows for the settlement of the crest of the dam, both under normal settlement conditions, as well as under seismic conditions. The sealing systems between the different elements must accordingly not only allow for vertical

movements under settlement, but also accommodate opening of the joints under seismic conditions. Critically, the joints need to remain intact following potential significant upheaval caused by earthquakes in order to provide the required security against water level rises. The expanded joint can be exposed to modest flooding and accordingly needs to be configured to continue to perform its water-retaining function in the long term. This is especially important in a post-earthquake situation where settlements will be far larger, and remedial work may only be possible, some weeks or months after the event.

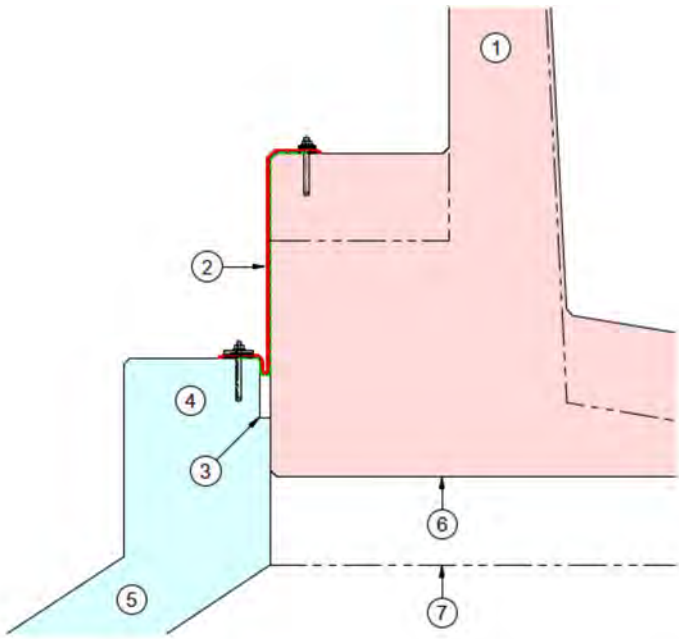

1	Parapet wall	1	*Mur de parape*
2	Geocomposite external waterstop	2	*Waterstop extérieur géocomposite*
3	Slot for loop in waterstop	3	*Emplacement pour boucle dans le waterstop*
4	Vertical upstand wall	4	*Mur vertical*
5	Facing slab	5	*Dalle de parement*
6	Parapet wall with camber	6	*Mur de parapet avec cambrure*
7	Parapet wall without camber	7	*Mur de parapet sans cambrure*

Fig. 7
Embankment Facing Slab – Parapet Wall Joint
Joint entre dalle de parement et mur de parapet

Fig. 8 below depicts the anticipated crest deformation configuration following an earthquake from the numerical analysis undertaken as part of the embankment design, including the facing slab upstand and parapet wall superimposed on the numerical model mesh. While crest movement varies under different levels of impoundment as previously discussed, the vertical joint between the parapet wall and face slab upstand can be expected to open with the two elements also translating vertically relative to each other.

The strategy for the sealing systems between the parapet wall and face slab was aimed at providing a configuration that will ensure that the joint can accommodate the expected seismic movements while retaining its ability to seal against flood rise. To this end, following a review of various sealing systems, an external waterstop system comprising a waterproofing liner, geotextile support layer and anchorage system was developed.

The waterproofing liner is made of a geocomposite Sibelon® CNT 4440 (3mm thick PVC geomembrane heat bonded to a 500 g/m^2 non-woven geotextile) supplied and installed by Carpitech BV. The liner is anchored to the concrete surfaces of the parapet wall units and facing slab upstand wall using stainless-steel battens plates, epoxy resin, rubber gaskets and chemical anchors. A loop in the geocomposite liner was provided to allow a sufficient length of material to span the longitudinal joint, and to accommodate for the potential separation of the structures during an earthquake. As shown in Fig. 7, a slot was formed in the upstand wall to house the loop of excess geocomposite provided. To avoid excessive stress on the geocomposite liner during a succeeding flood event, a geotextile support layer was designed and installed directly below the liner.

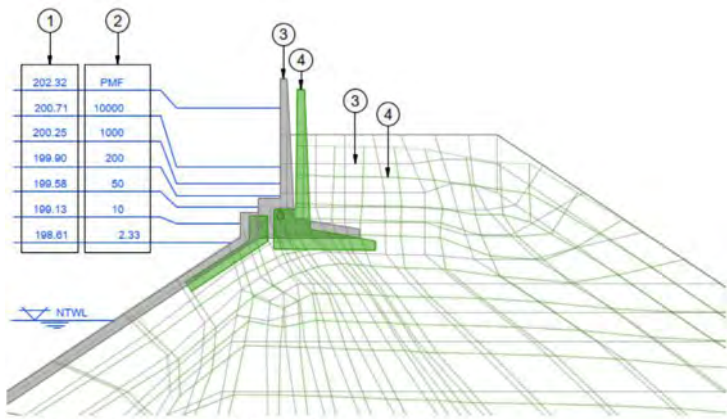

a) Normal top water level / *Niveau d'eau supérieur normal*

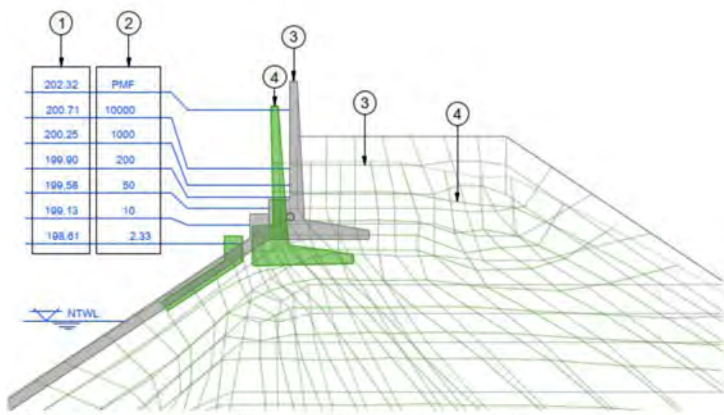

b) Minimum operating level / *Niveau de fonctionnement minimum*

5	Level (m)	*5*	*Niveau (m)*
6	AEP (year)	*6*	*Probabilité de dépassement annuel (année)*
7	Design geometry (grey)	*7*	*Géométrie de conception (gris)*
8	Post Earthquake geometry (green)	*8*	*Géométrie post-séisme (vert)*

Fig. 8
Post-earthquake deformations - facing slab/parapet wall opening
Déformations post-séisme - ouverture dalle de parement/mur parapet

At connections to the cast-in rear-guard PVC waterstops between the facing slab joints, a special connection capable of three-dimensional movement was developed as shown in Fig. 9. The Sibelon® geocomposite was factory-welded to a short length of rearguard waterstop which was then site-welded to the main facing slab waterstop before the final concrete pour of the nib wall.

Fig. 9
Special three-dimensional connection between internal and external waterstops
Connexion tridimensionnelle spéciale entre les joints d'étanchéité internes et externes

A simple variation of a flat external waterstop across the joints between successive precast wall elements was provided to ensure relative movements between elements in an earthquake can be accommodated with acceptable elongation of the geocomposite liner.

12. CONCLUSIONS

High seismic loads from the Safety Evaluation Earthquake (SEE) are predicted to induce large deformations and damage to the crest and slopes of the Waimea Dam embankment. The performance requirement is to safely retain the reservoir after the earthquake despite the damage. Post-earthquake conditions predict the concrete facing would be an ineffective water barrier. The necessity of using site-won, friable, highly fractured rock as the bulk embankment fill presented an unacceptable risk that lack of drainage capacity in the rockfill would lead to potential instability and failure of this high hazard dam.

Potential for post-earthquake instability necessitated defensive seismic design measures. Therefore, internal drainage was incorporated into the embankment design. The internal drainage system consisted of three main components:

1. A flow-limiting, collapsible, internally stable upstream face support zone (Zone 2B).
2. An inclined drain adjoining downstream and compatible with Zone 2B.
3. A high permeability blanket drain at the base of the dam contiguous with the inclined drain.

Seismic deformations of the concrete facing slab and parapet walls were analysed and appropriate provisions for joint opening and translation of elements were provided in their internal and external waterproofing elements.

ACKNOWLEDGEMENTS

The authors are grateful to Waimea Water Limited, owner of Waimea Dam, for their support throughout design and construction, and permission to write this paper. The authors are grateful to New Zealand Society on Large Dams (NZSOLD) for review of this paper.

REFERENCES

[1] New Zealand Society on Large Dams. *New Zealand Dam Safety Guidelines*. 2015.

[2] GNS Science. *Seismic Hazard Assessment for Proposed Waimea Dam. Consultancy Report 2017/150, September*. 2017.

[3] ICOLD. *Bulletin 141 - Concrete Face Rockfill Dams: Concepts for Design and Construction*. 2010.

COMMISSION INTERNATIONALE DES
GRANDS BARRAGES

VINGT-HUITIEME CONGRES DES
GRANDS BARRAGES
CHENGDU, MAI 2025

THREE-DIMENSIONAL EXTENSION OF UBCHYST CONSTITUTIVE MODEL: IMPLEMENTATION AND VERIFICATION (*)

Kuntan CHANG, Nicolas LABANDAA & Riccardo FANNI
[a]*WSP, Pertiams, Perth*

Alfredo ARENAS
ATC Williams, Perth

AUSTRALIA

SUMMARY

This paper introduces a three-dimensional (3D) formulation of a simple and practical constitutive model designed to capture the nonlinear hysteretic damping characteristics of non-liquefiable materials under earthquake loading. This model is a 3D extension of the two-dimensional (2D) UBCHyst model, developed at the University of British Columbia [1], which has been extensively employed for modelling of soils typically used in embankment dams such as compacted clays, dense and unsaturated rockfill, or stiff foundation and weathered bedrock. This paper presents the 3D formulation followed by a comparison with the classical UBCHyst model for monotonic and cyclic direct simple shear tests. The model is then verified against experimental data for rockfill and gravelly materials in both static and cyclic triaxial stress paths. Finally, a seismic response analysis is carried out by applying a seismic record at the base of a one-dimensional (1D) column. The results of the conventional UBCHyst model are compared to the 3D extended UBCHyst model.

Extension tridimensionnelle du modèle constitutif UBCHyst : mise en œuvre et vérification.

DOI: 10.1201/9781003642428-116

RÉSUMÉ

Ce rapport présente une formulation tridimensionnelle (3D) d'un modèle constitutif simple et pratique conçu pour déterminer les caractéristiques de l'amortissement hystérétique non linéaire de matériaux non liquéfiables sous chargement sismique. Il s'agit d'une extension en 3D du modèle bidimensionnel UBCHyst (2D) développé à l'Université de la Colombie-Britannique [1] qui a été largement utilisé pour la modélisation des sols généralement utilisés dans les barrages en remblai tels que les argiles compactées, les enrochements denses et non saturés ou les fondations rigides et le substrat rocheux altéré. La formulation 3D présentée dans l'article est suivie d'une comparaison avec le modèle UBCHyst classique utilisé dans les tests de cisaillement simple direct monotones et cycliques. Le modèle est ensuite vérifié par rapport aux données expérimentales de matériaux d'enrochement et gravillonneux avec des chemins de contraintes triaxiaux statiques et cycliques. Enfin, la réponse sismique est analysée par application d'un enregistrement sismique à la base d'une colonne unidimensionnelle (1D). Les résultats du modèle UBCHyst conventionnel sont comparés à ceux du modèle UBCHyst 3D étendu.

1. INTRODUCTION

The seismic performance of embankment dams heavily depends on the reliability of the earthquake-induced deformations estimated in numerical analyses. Over recent decades, numerical nonlinear deformation analyses have gained significant recognition for providing deeper insights into a dam's seismic response compared to traditional screening methods[2]. The effectiveness of these numerical methods largely hinges on the selection of constitutive models capable of accurately representing complex soil behavior under dynamic loading.

Naesgaard et al. [1] proposed a relatively simple model called UBCHyst for dynamic analyses of soils, intended to be used with undrained strength in low permeability materials and effective stress parameters in highly permeable granular soils, where excess pore water pressure would dissipate almost instantaneously. Originally, this model was formulated and implemented in the 2D space, taking into consideration the hysteretic nature of the material, the shear modulus variation as a function of the stress ratio, limiting this ratio by a Mohr-Coulomb yield surface criterion.

In this paper, the authors proposed a 3D UBCHyst formulation, extending the definitions of the shear stress ratio in a general 3D principal stress space. This 3D formulation has been implemented as a user-defined model in FLAC2D/3D version

9.0 for application in boundary value problems. The developed 3D model retains the primary features of the 2D model, including the reduction of the shear secant modulus with greater strain and the emulation of ratcheting when loaded with a static shear bias (defined as the ratio between the horizontal shear stress and the vertical effective stress). Additionally, it introduces the dependency of the shear modulus reduction on the initial static stress ratio and extends its application to triaxial stress paths.

The developed model is first compared with the classical UBCHyst model for monotonic direct simple shear (MDSS), and cyclic direct simple shear (CDSS). The model is then calibrated using experimental data for rockfill materials in both static and cyclic triaxial tests [3][4] to examine the new features added in the 3D formulation. Finally, a 1D seismic response analysis is carried out, comparing the results with the conventional model.

2. UBCHYST3D CONSTITUTIVE MODEL

2.1. Overview of the 2D formulation

UBCHyst original formulation assumes that the degradation of the shear modulus occurs solely due to the horizontal shear stress τ_{xy} in 2D (plane strain) problems, a condition that is often defined as simple shear (SS) loading. This simplification provides the model a straightforward implementation and mathematical structure, avoiding complex numerical integration algorithms used for others more sophisticated models [5][6]. However, when stress paths deviate from SS, predictions become problematic. Attempts have been made to extend the model to 3D application by replacing τ_{xy} with τ_{xz} or τ_{yz} along the loading direction of interest [7]. Unfortunately, this approach still falls to account for the effect of shear stress generated simultaneously in other directions. Studies from multi-directional CDSS tests suggest that the shear stresses in other directions contribute to the degradation of the shear modulus [8], highlighting the need for a generalized 3D model to capture this effect. Nonetheless, the original UBCHyst has various advantages that the authors believe it is worth to be empowered by a 3D extension, especially considering the following features:

1. Increasing hysteresis and reduction in secant modulus with strain (see Fig. 1a).
2. Plastic strains bias resulting from the ratcheting when loaded with a static bias (see Fig. 1b).

Comportement caractéristique des sols sous chargement cyclique reproduit par UBCHyst.

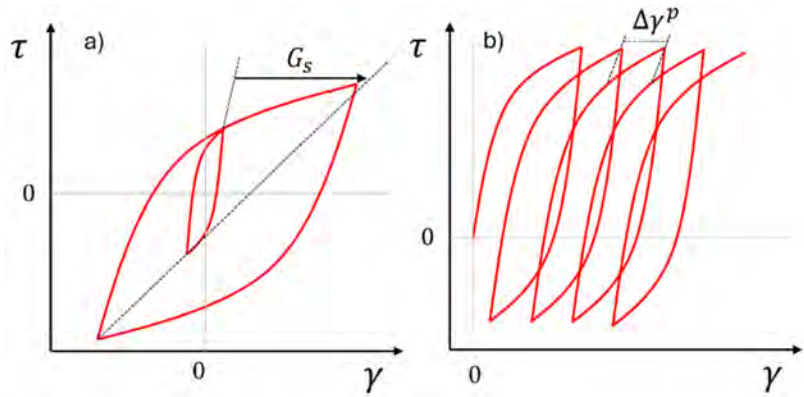

Fig. 1
Characteristic behaviour of soils under cyclic loading reproduced by UBCHyst.
Comportement caract ristique des sols sous chargement cyclique reproduitpar UBCHyst.

2.2. 3D MODEL FORMULATION

The UBCHyst 3D model uses the Mohr-Coulomb yield surface generalised in 3D principal stress space. The formulation of the surface can be expressed in the space of maximum shear stress (t) versus average effective stress (s') as given below in Eq. (1) and illustrated in Fig. 1:

$$t = c'\cos\phi' + s'\sin\phi' \tag{1}$$

Where $t = (\sigma'_1 - \sigma'_3)/2$, $s' = (\sigma'_1 + \sigma'_3)/2$, defined from the maximum principal effective stress (σ'_1) and minimum principal effective stress (σ'_3). Noted the intermediate principal stress does not influence the yield surface in 3D stress space. c' is the cohesion of the soil, ϕ' is the effective frictional angle of the soil. It is recognised that this formulation inherits the same 3D hexagon yield surface in the deviatoric plane as the standard Mohr-Coulomb model and may be a conservative representation of the strength of soils in plane strain (e.g. Jefferies and Shuttle [9]). This feature could be improved in future version of the 3D extended UBCHyst constitutive model.

It is important to note that while the classical UBCHyst model [1][10] refers to the 2D Mohr-Coulomb failure criterion $\tau_f = c' + \sigma' \tan\phi'$ in the definition of the stress ratio, it was implemented based on the stranded algorithm of Mohr-Coulomb model in FLAC2D/3D so that the ultimate strength is still determined by the 3D Mohr-Coulomb failure criterion in a principal stress space, equivalent to Eq. [1].

The 3D formulation uses the original mathematic structure that defines the tangent shear modulus (G_t) as a function of small strain shear modulus ($G_{\max}$) times reduction factors function of the developed stress ratio and the change in stress ratio to failure, which are defined based on the generalised 3D principal stress space. The function is presented in Eq. (2) below:

$$G_t = G_{\max}\left(1 - R_f \quad \eta_1 \backslash \eta_{1f}\right)^n Mod_1 Mod_2 \tag{2}$$

where the followings are defined for the 3D model, with comparisons with the original model being summarised in Table 1.

- $\eta =$ developed stress ratio $= t/s' = \frac{\sigma_1' - \sigma_3'}{\sigma_1' + \sigma_3'}$, this is also termed as mobilised friction angle in UBCSand3D model [11].
- $\eta_1 =$ change in stress ratio η since last reversal $= \eta - \eta_{\max}$
- $\eta_{\max} =$ maximum stress ratio at last reversal
- $\eta_{1f} =$ change in stress ratio to reach the failure envelope in the direction of loading $= \eta_f - \eta_{\max}$
- $\eta_f =$ ultimate stress ratio $= \sin\phi' + c'\cos\phi'/s'$
- R_f and n are calibration parameters
- $\mathrm{Mod}_1 =$ a reduction factor for first $-$ time or virgin loading
- $\mathrm{Mod}_2 = 1 - |(h\eta_{\max} - \eta_{ini})/\left(\eta_f - \eta_{ini}\right)|^{rm} d_{fac} \geq 0.2$ = optional function to account for permanent modulus reduction with large strain, where $h\eta_{\max}$ is the maximum past shear stress ratio, η_{ini} is the initial stress ratio, and rm and d_{fac} are calibration parameters. Note that the value of Mod_2 decreases with the amplitude of maximum past shear stress ratio and the reduction also applies to all subsequent cycles even if they are much smaller in amplitude. Setting d_{fac} to 0 turns off Mod_2(i.e. it sets Mod_2 to 1).

Building upon the original features outlined in previous sections, our 3D extension addresses several limitations of the original model, with the following key improvements:

1. Redefinition of the stress ratio and ultimate strength in terms of principal stresses, by using the maximum shear stress (t) instead of the horizontal shear stress (τ). This definition is consistent with the generalized 3D Mohr-Coulomb failure criterion. This modification allows the model to handle stress paths beyond the DSS mechanism and account for shear stresses in multi directions. Additionally, it accommodates dependence on the initial stress state before shearing when stress paths do not start from the isotropic line (i.e. earth pressure at rest coefficient $K_0 < 1$).
2. Redefinition of the permanent reduction function Mod_2 to prevent shear modulus reduction during the model initialisation caused by non-zero initial shear stress before applying shear loadings.
3. Redefinition of the change in loading direction, which is detected by either a sign flip in the principal stress angle α, or a change in the direction of major

principal stress where α transitions from 0 to 90 or vice versa. The former occurs in cyclic DSS conditions, while the later occurs in cyclic triaxial conditions. Fig. 3 and Fig. 4 illustrate the definition of different loading conditions, and the associated calculation of η_1 and η_{1f}.

Refer to Table 1 for a detailed comparison of the main changes between the classical UBCHyst model and the proposed UBCHyst 3D.

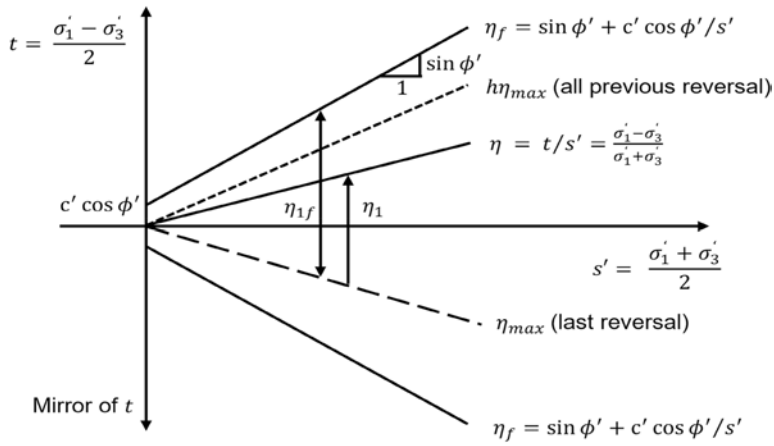

Fig. 2
UBCHyst 3D model key variables
Variables clés du modèle UBCHyst en 3D

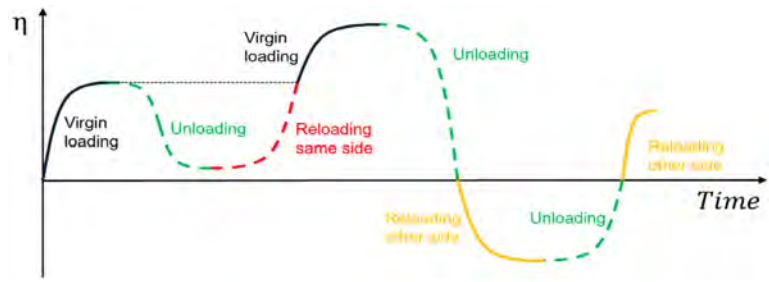

Fig. 3
Stress ratio history including loading, unloading and reloading stress paths.
Historique du rapport de contrainte comprenant les chemins de contrainte de chargement, de déchargement et de rechargement.

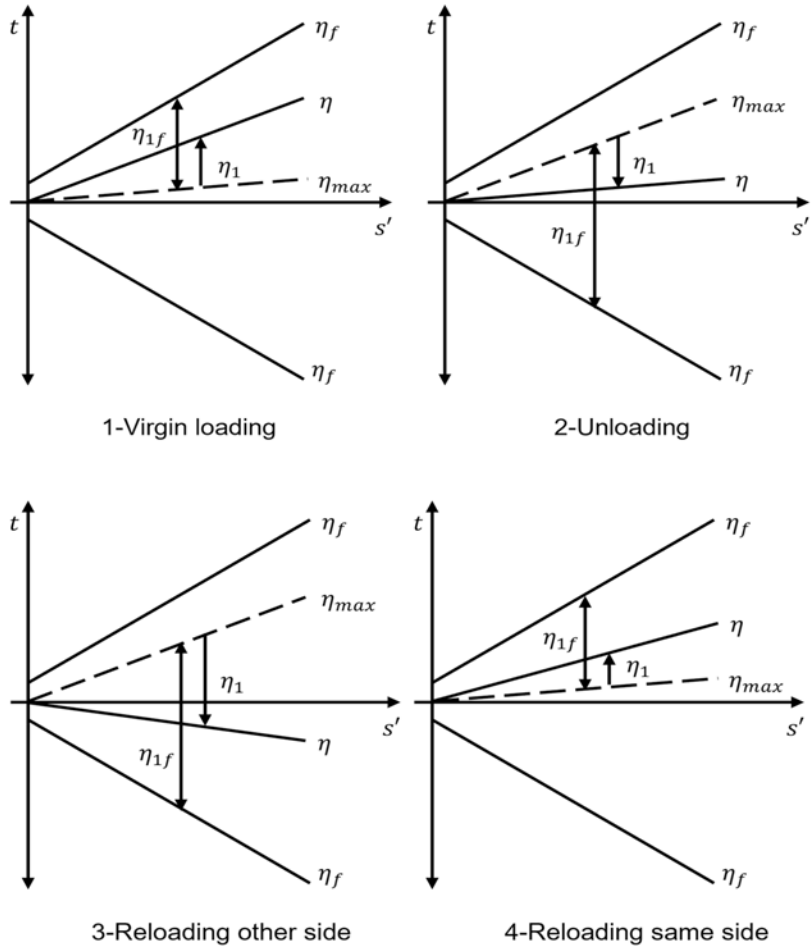

Fig. 4
Definition of η_1 and η_{1f} in varying loading conditions
Définition de η_1 et η_{1f} dans des conditions de chargement variables

Table 1
Comparison between 2D and 3D formulation for UBCHyst
Comparaison entre formulations 2D et 3D pour le modèle UBCHyst

2D	**3D**
Yield surface for stress ratio definition	
$\tau_f = c' + \sigma' \tan\phi'$	$\frac{\sigma'_1 - \sigma'_3}{2} = c' \cos\phi' + \frac{\sigma'_1 + \sigma'_3}{2} \sin\phi'$
Stress ratio	
$\eta = \tau_{xy}/\sigma'_v$	$\eta = \frac{\sigma'_1 - \sigma'_3}{\sigma'_1 + \sigma'_3} = \sin\phi'_{mob}$
Ultimate strength	
$\eta_f = \sin\phi' + c'/\sigma'_v \cos\phi'$	$\eta_f = \sin\phi' + \frac{2 \quad c' \cos\phi'}{\sigma'_1 + \sigma'_3}$
Permanent modulus reduction function	
$Mod_2 = 1 - \left\lvert \frac{h\eta_{\max}}{\eta_f} \right\rvert^{rm} d_{frac} \geq 0.2$	$Mod_2 = 1 - \left\lvert \frac{h\eta_{\max} \quad -\eta_{ini}}{\eta_f - \eta_{ini}} \right\rvert^{rm} d_{frac} \geq 0.2$
Change of loading direction	
Sign flip of τ_{xy}	Either sign flip of principal stress angle α or change of direction of σ'_1 (where α changes from 0 to 90 or vice versa)

3. NUMERICAL EXPERIMENTS

3.1. PARAMETERS SUMMARY

Table 2 summarizes the parameters used for the numerical experiments presented in this paper:

- Set A parameters are used for the MDSS tests presented in section 3.2, and the strain controlled CDSS simulations presented in section 3.3.1.
- Set B parameters are used for the stress controlled CDSS simulations presented in section 3.3.2. These parameters are based on the Itasca implementation of UBCHyst 2D in FLAC2D by Cheng [10].
- Set C parameters are used for the triaxial tests calibration presented in section 3.4.
- Set D parameters are used for the 1D column simulation under plane strain earthquake loading presented in section 3.5. These parameters are based on the simulation presented by Cheng [10].

Table 2
Summary of model parameter used in this study.
Résumé des paramètres du modèle utilisés dans cette étude.

PARAMETER	SYMBOL	UNIT	VALUE			
			SET A	SET B	SET C	SET D
Bulk modulus	K	kPa	G_{max}	G_{max}	$2.2G_{max}$	G_{max}
Small strain shear modulus	G_{max}	kPa	$80p_a(p'/p_a)^{0.7}$	53400	$2000p_a(p'/p_a)^{0.4}$	$701p_a(p'/p_a)^{0.5}$
Friction angle	ϕ'	°	30	30	$70.4 - 4.1\ln p'$	33
Cohesion	c'	kPa	0	0	0	1
Tensile strength	σ_t	kPa	0	0	0	0
Dilation angle	ψ	°	0	0	0	0
Exponent-stiffness	n	-	1.2	2	1.55	2
Failure-ratio	R_f	-	1	0.8	0.95	0.98
Factor-reduction	d_{fac}	-	0.8	0.5	0	0.5
Exponent-reduction	$r\,m$	-	1.6	2	-	2
Factor-first	Mod_1	-	1	0.65	0.5	0.65
Reference pressure	p_a	kPa	100	100	100	100

3.2. Monotonic direct simple shear (MDSS)

Fig. 5 shows the development of maximum shear stress t (normalized by the effective mean stress at consolidation s'_c or effective vertical stress at consolidation σ'_{vc}) with horizontal shear strain Υ in a MDSS test, comparing the results between the classical UBCHyst and the proposed UBCHyst 3D for different values of $K_0 = 0.5,\ 0.7,\ 1.0$. The following can be observed:

- In the isotropic consolidation state ($K_0 = 1.0$), both models yield equal results since under this stress condition t is coincident with τ. This good agreement validates the accuracy of the present 3D development and its implementation.
- In the anisotropic consolidation state ($K_0 < 1.0$), the two models deviate at larger strains where the classical UBCHyst reaches the peak strength earlier, which indicates less shear modulus reduction compared to the UBCHyst 3D. The difference arises from the distinct stress ratio definitions in the two models and the fact that under this stress condition τ is smaller than t, which dictates the ultimate stiffness reduction.
- Stresses normalized by s'_c converge to the same value, consistent with the adopted Mohr-Coulomb yield surface.

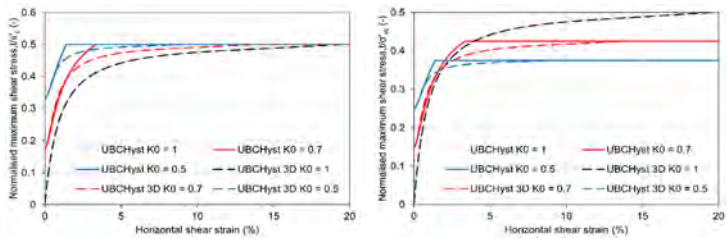

Fig. 5
UBCHyst and UBCHyst 3D comparison. Normalized maximum shear stress versus shear strain, $K_0 = 0.5,\ 0.7,\ 1$.
Comparaison entre modèles UBCHyst et UBCHyst 3D. Contraintes de cisaillement maximales normalisées par rapport à la déformation de cisaillement, $K_0 = 0.5,\ 0.7,\ 1$.

3.3. Cyclic direct simple shear (CDSS)

3.3.1. *Strain controlled*

Fig. 6 presents the results of a strain controlled CDSS test in terms of shear modulus reduction curve and stress-strain hysteretic loops using $K_0 = 1$. The figure compares the classical UBCHyst model with the proposed UBCHyst 3D. Here, it again confirms the identical behaviour from the two models under the isotropic stress state, which confirms the accuracy of the 3D implementation in cyclic applications.

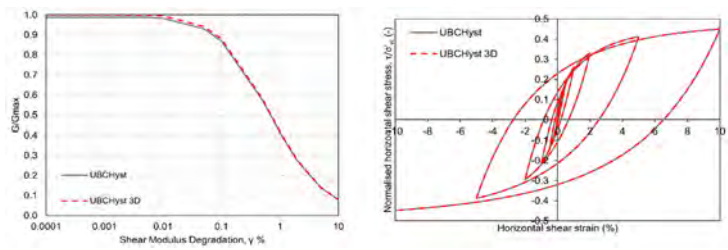

Fig. 6
UBCHyst and UBCHyst 3D comparison. Shear modulus degradation versus shear strain and normalized shear stress versus shear strain, $K_0 = 1$.
Comparaison entre modèles UBCHyst et UBCHyst 3D. Dégradation du module de cisaillement par rapport à la déformation de cisaillement et contrainte de cisaillement normalisée par rapport à la déformation de cisaillement, $K_0 = 1$.

Fig. 7 illustrates a parametric study of the 3D model and how the model response varies for different K_0 values in a CDSS stress path. Tests with $K_0 < 1$ start to show stiffness reduction at a strain one order of magnitude later but with a higher degradation rate, eventually converging to a similar stiffness degradation curve at large strain. The difference implies that calibration should be conducted under a specific K_0 condition that is more representative to the boundary value problem under consideration. It is worth noting that in the classical UBCHyst model, the shear modulus degradation is independent on K_0.

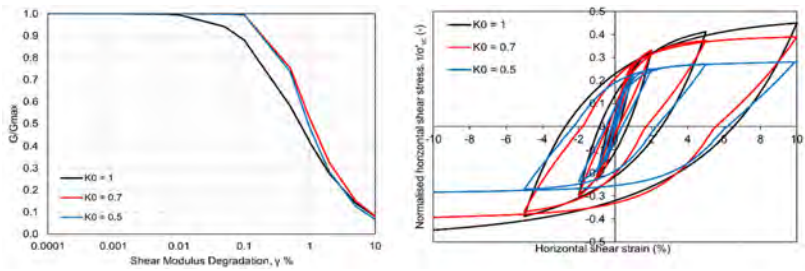

Fig. 7
UBCHyst 3D parametric study. Shear modulus degradation versus shear strain and normalized shear stress versus shear strain, $K_0 = 0.5,\ 0.7,\ 1$.
Étude paramétrique selon le modèle UBCHyst 3D. Dégradation du module de cisaillement par rapport à la déformation de cisaillement et contrainte de cisaillement normalisée par rapport à la déformation de cisaillement, $K_0 = 0.5,\ 0.7,\ 1$.

3.3.2. *Stress controlled*

Fig. 8 shows the results from a stress controlled CDSS test, illustrating the development of η and normalised τ with Υ under the condition of $K_0 = 1$. Consistent with the observations in the previous cases, both models exhibit identical behaviour under this isotropic stress state. As expected, when $K_0 < 1$, the classical UBCHyst maintains the same stress-strain curve. In contrast, the proposed 3D model indicates a reduction in number of cycles to reach the same shear strain, confirming more shear modulus reductions, refer to Fig. 9 and Fig. 10 for $K_0 = 0.7$ and $K_0 = 0.5$ respectively.

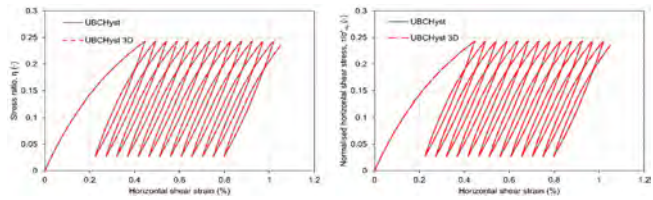

Fig. 8
UBCHyst and UBCHyst 3D comparison. Stress ratio versus shear strain and normalized shear stress versus shear strain, $K_0 = 1$.
Comparaison entre modèles UBCHyst et UBCHyst 3D. Rapport de contrainte par rapport à la déformation de cisaillement et contrainte de cisaillement normalisée par rapport à la déformation de cisaillement, $K_0 = 1$.

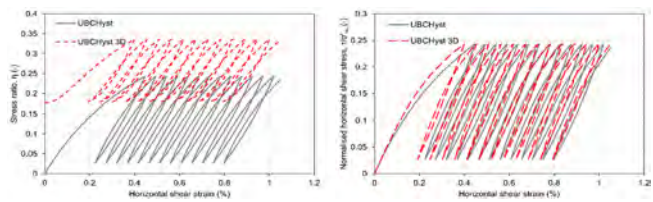

Fig. 9
UBCHyst and UBCHyst 3D comparison. Stress ratio versus shear strain and normalized shear stress versus shear strain, $K_0 = 0.7$.
Comparaison entre modèles UBCHyst et UBCHyst 3D. Rapport de contrainte par rapport à la déformation de cisaillement et contrainte de cisaillement normalisée par rapport à la déformation de cisaillement, $K_0 = 0.7$.

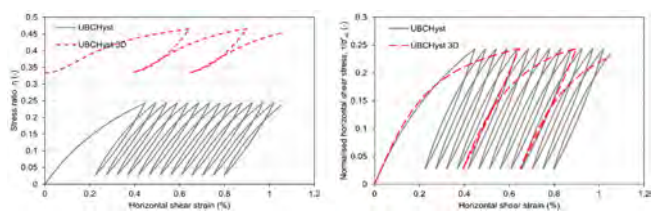

Fig. 10
UBCHyst and UBCHyst 3D comparison. Stress ratio versus shear strain and normalized shear stress versus shear strain, $K_0 = 0.5$.
Comparaison entre modèles UBCHyst et UBCHyst 3D. Rapport de contrainte par rapport à la déformation de cisaillement et contrainte de cisaillement normalisée par rapport à la déformation de cisaillement, $K_0 = 0.5$.

3.4. Calibration with static and cyclic triaxial tests on rockfill

A key improvement in the 3D model is its capability to capture the shear modulus reduction that occurs in the cyclic triaxial stress paths. This feature is validated in this section by comparing the predictions of the 3D model with experimental data on rockfills and gravelly materials from the literature. Fig. 11 shows the simulation of static and cyclic triaxial tests, compared to the experimental results of Liu et al. [3]. Subsequently, Fig. 12 plots the shear modulus degradation curves from strain controlled cyclic triaxial tests against the results from Rollins et al. [4]. All these simulations were conducted using the same set of parameters as listed in Table 2. The following observations were made:

- As showed in Fig. 11 left, the simulation and measurement show a good agreement in the stress strain profiles from all the three static tests with varying confinement pressures of $\sigma_3' = 200,\ 500,\ 800\ \mathrm{kPa}$.
- For the cyclic triaxial test, the model can reasonably reproduce the overall response observed in the experiment test, particularly the stiffness during virgin loading and unloading. The model captures well the stiffness at the initial stage of reloading but overestimates it as reloading approaches the maximum stress during the cycles. In addition, the model does not include the effect of cyclic densification that is typical for dilative materials. As a result, the number of cycles obtained in the simulation is lower than the one shown in the experimental data. Although it is challenging to achieve a good fitting for static and dynamic tests using the same set of parameters, the authors believe that this issue can be solved by introducing additional features to this simple model, such as the effect of number of cycles (i.e. densification rule). This remains an area for future developments.
- As shown in Fig. 12, the model seems to be in good agreement with the shear modulus degradation curves of the experimental results.

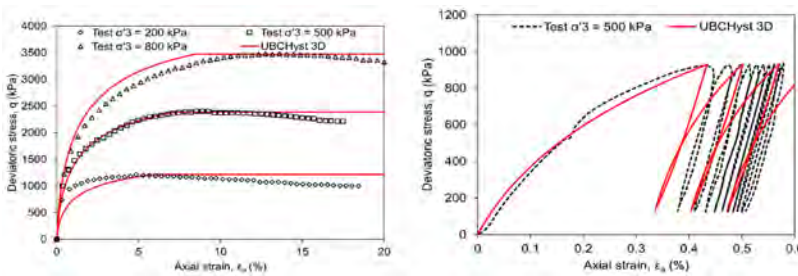

Fig. 11
UBCHyst 3D calibration with static and cyclic triaxial tests on rockfill [3].
Calibrage du modèle UBCHyst 3D à l'aide de tests triaxiaux statiques et cycliques sur des remblais en enrochement [*3*].

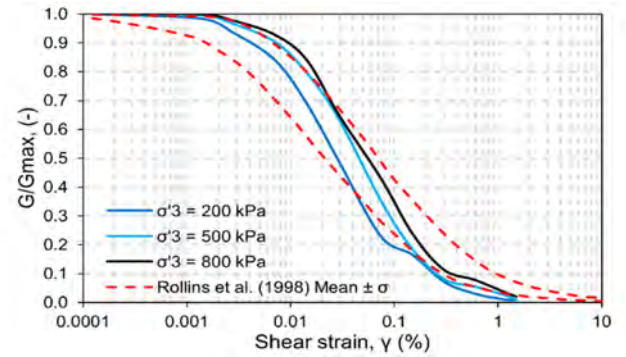

Fig. 12
UBCHyst 3D shear modulus calibration with experimental tests [4].
Calibrage du module de cisaillement du modèle UBCHyst 3D à l'aide de tests expérimentaux [*4*].

3.5. 1D Site response analysis

This section evaluates the performance of the UBCHyst 3D model in a 1D column site response analysis commonly adopted as the initial step of an embankment seismic deformation analysis. The column is modelled with the same geometry and conditions from the study reported by Cheng [10], i.e. fully saturated conditions, 30m height and discretised with evenly sized 1m elements. The input motion chosen for the analysis is also from Cheng [10], and is shown in Fig. 13.

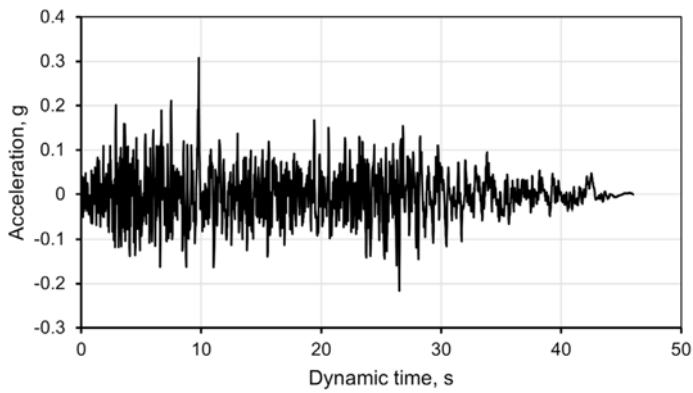

Fig. 13
Seismic record used for the one-column site response example.
Enregistrement sismique utilisé pour l'exemple de réponse du site à une colonne.

Four cases were conducted, namely, UBCHyst and UBCHyst 3D for $K_0 = 1$ and 0.5. Fig. 14 compares the profiles of maximum Cyclic Stress Ratio (CSR), which is the ratio between the horizontal shear stress and the effective vertical stress at consolidation, experienced during the earthquake event, and post-seismic residual displacements along the column. The results indicate that for $K_0 = 1$ the outcomes are identical between the original and extended UBCHyst models. For $K_0 = 0.5$, the UBCHyst model, compared to the isotropic condition, exhibits smaller CSR and displacements along the whole column, with the same maximum displacements located at the top. Whereas the UBCHyst 3D model exhibits distinctly higher CSR and displacements concentrated on the top of the column, and smaller magnitude in the middle of the column. This is believed reasonable as more energy had been dissipated at the top, and thus less stress had been transferred to the middle soil column. Fig. 15 and Fig. 16 further compares the four analysed cases in terms of the normalized horizontal shear stress versus shear strain, and the displacement time histories recorded during the seismic event from the top element of the column. Again, the results consistently confirm that for $K_0 = 1$ both models produce practically identical stress-strain loops, and the same displacement time histories. Conversely, results for $K_0 = 0.5$ tend to diverge, showing a higher CSR, larger strains and larger residual displacements in the UBCHyst 3D model. Fig. 17 displays the response spectrum of the acceleration extracted from the top of the column of both models with varying K_0, and comparisons with the input signal. It is shown that for $K_0 = 1$, outcomes are again identical, but for $K_0 = 0.5$ the 3D constitutive model indicates a higher amplification throughout the spectrum. In summary, modelling using the extended 3D model suggests that soils under a $K_0 < 1$ condition would mobilise higher CSR, larger residual displacements, more plastic strains during the cycle, and more amplification of the signal. This analysis highlights the important of adopting the proposed UBCHyst 3D model in seismic analysis not just for 3D problems but also for properly accounting for the K_0 condition, which represents the typical in situ condition.

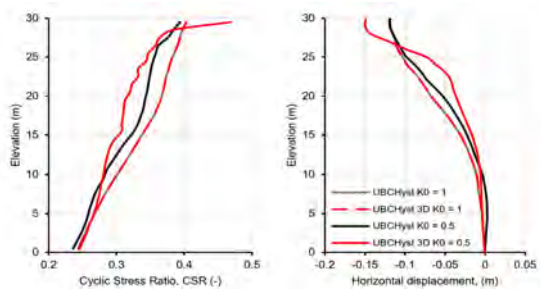

Fig. 14
UBCHyst and UBCHyst 3D comparison: depth profiles of cyclic stress ratio and horizontal displacement for different K_0.
Comparaison entre modèles UBCHyst et UBCHyst 3D : profils de profondeur du rapport de contrainte cyclique et du déplacement horizontal pour différents K_0.

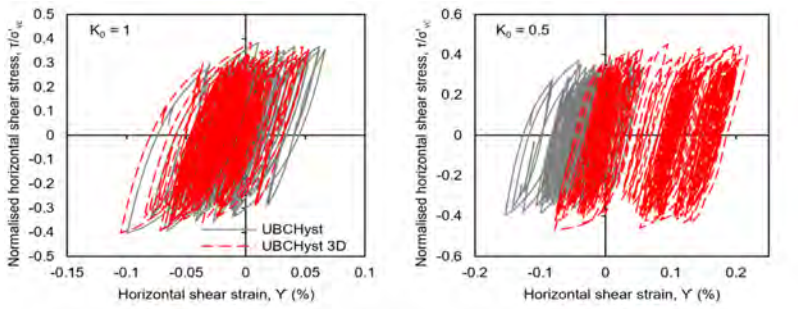

Fig. 15
UBCHyst and UBCHyst 3D comparison: Horizontal shear stress vs horizontal shear strain at the top of the column.
Comparaison entre modèles UBCHyst et UBCHyst 3D : contrainte de cisaillement horizontale par rapport à la déformation de cisaillement horizontal au sommet de la colonne.

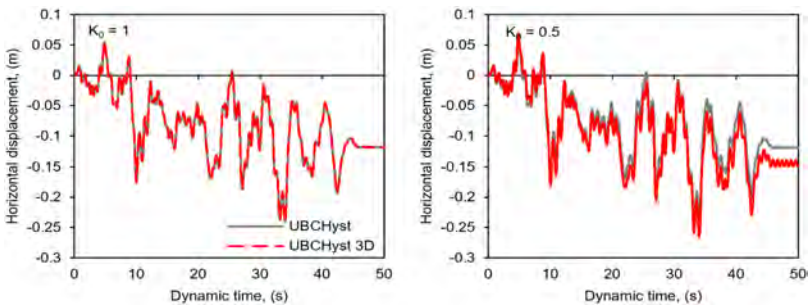

Fig. 16
UBCHyst and UBCHyst 3D comparison: Time history of horizontal displacement at the top of the column.
Comparaison entre modèles UBCHyst et UBCHyst 3D : historique temporel du déplacement horizontal au sommet de la colonne.

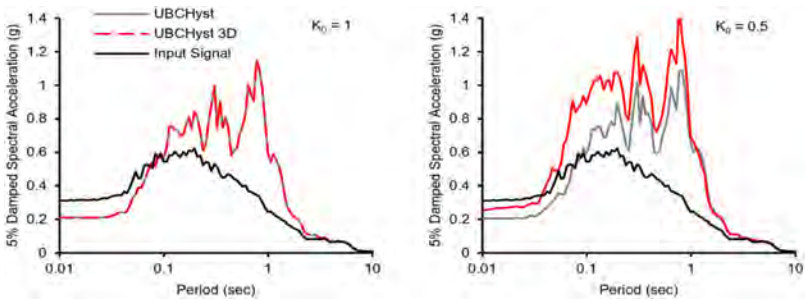

Fig. 17
UBCHyst and UBCHyst 3D comparison: Acceleration spectrum and comparison with input signal.
Comparaison entre modèles UBCHyst et UBCHyst 3D : spectre d'accélération et comparaison avec le signal d'entrée.

4. CONCLUSIONS

This paper presented the formulations of a 3D extension of the widely used 2D constitutive model UBCHyst, and validations though DSS numerical experiments and comparisons with triaxial experimental results on rockfills and gravelly materials. This extension holds the main advantages of the original model, i.e., the mathematical and implementation simplicity, the reduced number of parameters, and the capability to reproduce stiffness degradation with cycles and loading amplitude, and the development of plastic strain under bias stress conditions. A key element in the 3D extension is the redefinition of the stress ratio and ultimate strength in terms of principal stresses, by using the maximum shear stress instead of the horizontal shear stress. This modification allows the 3D model to avoid the limitations of the original 2D model like the stress state generalization, the stress ratio insensitivity to K_0, and that it is no applicable beyond the SS stress paths.

The developed 3D model was compared to the original UBCHyst model in several MDSS and CDSS tests, showing that the extended UBCHyst 3D model is identical to the original model when the test starts from an isotropic stress condition where the horizontal shear stress is coincident with the maximum shear stress, while differs for anisotropic stress conditions as the horizontal shear stress differs from the maximum shear stress. Moreover, the developed 3D model is capable to reasonably reproduce the overall response observed in laboratory static and cyclic triaxial tests on rockfills, which confirms the extensions beyond the SS stress paths. Finally, the performance of the developed model was examined through a 1D seismic response analysis, which suggested higher CSR and displacements when

soils are under K_0 stress conditions, indicating that predictions using the original UBCHyst model are unable to capture the effect of initial static stresses conditions different than isotropic, a limitation that the extended UBCHyst model has overcome.

This paper represents a first approach to a UBCHyst generalization for 3D modelling purposes, addressing some of the limitations known from the previous 2D version. Future studies are recommended to thoroughly evaluate the model performance in 2D and complex 3D boundary value problems such as a valley embankment.

We note that UBCHyst has been developed to simulate shear induced deformation of rockfills, gravelly materials and dilative cohesive soils under cyclic loading. However, in its current form the model is not capable to capture other mechanisms that may cause permanent deformations such us particle degradation causing a reduction of the effective strength properties, and seismic compaction, among others. Future updates of the model will be implemented focusing on these limitations.

REFERENCES

[1] NAESGAARD E., BYRNE P.M., AMINI A. Hysteretic Model for Non-liquefiable Soils (UBCHyst5d). *ITASCA UDM Library*, 2011.

[2] USSD Committee on Earthquakes, *Analysis of Seismic Deformations of Embankment Dams*. 2022.

[3] LIU H., ZOU D., LIU J. Constitutive modeling of dense gravelly soils subjected to cyclic loading. *International Journal of Numerical and Analytical Methods in Geomechanics*, 2014.

[4] ROLLINS K., EVANS M.D., DIEHL N.B., Daily W.D. Shear modulus and damping relationships for gravels. *Journal of Geotechnical and Geoenvironmental Engineering*, 1998.

[5] BOULANGER R.W., ZIOTOPOULOU K. PM4Sand (Version 3): *A Sand Plasticity Model for Earthquake Engineering Applications*. *Center for Geotechnical Modeling REPORT* NO.UCD/CGM-15/01, 2015.

[6] YANG M., TAIEBAT M., DAFALIAS Y. F. SANISAND-MSf: a sand plasticity model with memory surface and semifluidized state. *Géotechnique*, 2020.

[7] ARENAS A. Hysteretic model implemented in FLAC3D based in UBCHyst. *Numerical modelling workshop at Golder Associates*, 2018.

[8] ISHIHARA K. AND YAMAZAKI F. Cyclic simple shear tests on saturated sand in multi-directional loading. *Soils and Foundations*, 1980, 20(1), pp.45–59.

[9] JEFFERIES M. AND SHUTTLE D. On the operating critical friction ratio in general stress states. *Géotechnique*, 2011, 61(8), pp.709–713.

[10] CHENG Z. *Implementation of UBCHyst model as a user-defined model in FLAC2D v9*. Technical Memo Ref. UDM-UBCHYST-FLAC2Dv9, 2023.

[11] TSEGAYE A. *Plaxis liquefaction model*. Report no. 1. PLAXIS knowledge base, 2010.

Q.111 - R.14

COMMISSION INTERNATIONALE DES
GRANDS BARRAGES

VINGT-HUITIEME CONGRES DES
GRANDS BARRAGES
CHENGDU, MAI 2025

INFLUENCE OF WATER COMPRESSIBILITY IN EARTHQUAKE ANALYSES OF CONCRETE GRAVITY DAMS (*)

Michael MCKAY
Senior Associate Engineer, SMEC Australia Pty. Ltd.

Francisco LOPEZ
Chief Technical Principal, SMEC Australia Pty. Ltd.

Sam LALLI
Senior Engineer, SMEC Australia Pty. Ltd.

Stella HARRISON
Engineer, SMEC Australia Pty. Ltd.

AUSTRALIA

SUMMARY

Finite Element Analysis (FEA) of concrete dams is becoming increasingly more complex in order to better capture their behaviour under both static and seismic loading. One paramount aspect of this is the modelling of the dam-foundation-reservoir interaction during earthquakes, as the generated hydrodynamic pressures against the dam wall have a significant impact on the total response of the system. Historically, hydrodynamic pressures have been estimated assuming that the water of the reservoir is an incompressible fluid. However, several studies have shown that ignoring the compressibility of water can either underestimate or overestimate

L'importance de la compressibilité de l'eau dans les analyses sismiques des barrages-poids en béton

 DOI: 10.1201/9781003642428-117

the seismic response of concrete dams. Compressibility of fluids is often neglected in FEA without an understanding of the implications of such an assumption.

This paper presents a practical 4-step procedure for assessing the influence of water compressibility on the seismic response of a concrete gravity dam. The procedure can be followed to make an initial assessment on whether compressible water should be used in the time-history FEA or whether the more simplistic incompressible water approach could be used without significantly impacting the seismic response.

A worked example of a generic concrete gravity dam illustrated the use of the 4-step procedure, demonstrating that the influence of water compressibility was relatively minor. Through a sensitivity analysis it was found that the influence of compressibility of water on gravity dams is most significant in dams with a low ratio of the fundamental frequency of the reservoir to that of the dam alone (Ω_r), in relatively flexible dams, dams in relatively rigid foundations, dams in narrow valleys and FE models considering a massless foundation.

RÉSUMÉ

Afin de mieux appréhender le comportement des barrages en béton par rapport aux charges statiques et sismiques, l'analyse par éléments finis (AEF) de ces barrages devient de plus en plus complexe. L'un des aspects primordiaux de cette complexification est la modélisation des interactions barrage-fondations-réservoir lors des séismes, les pressions hydrodynamiques générées contre la paroi du barrage ayant un impact significatif sur la réponse globale du système. Jusqu'à présent, les estimations des pressions hydrodynamiques se sont fondées sur l'hypothèse que l'eau du réservoir est un liquide incompressible. Cependant, plusieurs études ont démontré que le fait d'ignorer la compressibilité de l'eau pouvait conduire soit à une sous-estimation, soit à une surestimation de la réponse sismique des barrages en béton. La compressibilité des liquides est souvent négligée dans les analyses par éléments finis, sans que les implications d'une telle hypothèse soient comprises.

Cet article présente une méthode pratique en quatre étapes permettant d'évaluer l'influence de la compressibilité de l'eau sur la réponse sismique d'un barrage-poids en béton. Cette méthode peut servir à effectuer une première évaluation afin de déterminer s'il est nécessaire de prendre en compte la compressibilité de l'eau dans l'analyse temporelle par éléments finis ou si l'approche plus simpliste d'une eau incompressible peut être utilisée sans impact significatif sur la réponse sismique.

L'exemple concret d'un barrage-poids en béton illustre le recours à la méthode en quatre étapes en démontrant que l'influence de la compressibilité de l'eau est relativement mineure. Une analyse de sensibilité révèle que l'influence de la compressibilité de l'eau sur les barrages-poids est plus significative pour les barrages avec un faible rapport entre la fréquence fondamentale du réservoir et celle du barrage seul, les barrages relativement flexibles, les barrages construits sur des fondations relativement rigides, les barrages situés dans des vallées étroites et les modèles d'éléments finis prenant en considération des fondations sans masse.

1. INTRODUCTION

Finite Element Analysis (FEA) of concrete dams is becoming increasingly more complex in order to better capture their behaviour under both static and seismic loading. One paramount aspect of this is the modelling of the dam-foundation-reservoir interaction during earthquakes, as the generated hydrodynamic pressures against the dam wall have a significant impact on the total response of the system. Historically, hydrodynamic pressures have been estimated assuming that the water of the reservoir is an incompressible fluid modelled as hydrodynamic added masses or as incompressible fluid elements. However, several studies have shown that ignoring the compressibility of water can either underestimate or overestimate the seismic response of concrete dams [1,2]. While compressible fluid elements are becoming more common in Finite Element (FE) packages, their use greatly increases the complexity of a model in terms of set up, calibration, running times and required computing power. As a result, compressibility of fluids is often neglected in commercial FE software and analysts frequently decide to model the reservoir as an incompressible fluid, without understanding the implications of such an assumption.

This paper presents a proposed step-by-step methodology that can be used at a preliminary level to estimate the difference in the seismic response of a concrete dam using both compressible and incompressible fluid elements. The benefit of the proposed method is that it provides an early identification of whether the dam can be analysed and provide accurate enough results using the simpler incompressibility approach; or whether the compressibility of water is significant and should be included in the analysis. The paper then follows the method to examine the impact of water compressibility on the seismic response of a generic concrete gravity dam. Furthermore, a comprehensive sensitivity analysis was conducted for an array of scenarios which included variation of parameters such as mass or massless foundation, variation of the modulus of elasticity of the dam and the foundation, variation in valley shape and variation in dam height, amongst others.

2. DESCRIPTION OF INCOMPRESSIBLE AND COMPRESSIBLE FLUID ELEMENTS

By definition, water is a compressible material that increases its density as it is pressurised. However, the compressibility of water is considered negligible when compared to other materials and states of matter such as gases. For that reason and for simplicity in many calculations, water is often assumed to be an incompressible fluid. Hydrodynamic pressures have been traditionally modelled using Westergaard's added masses approach [3], which was developed based on an incompressible reservoir for a straight gravity dam with a vertical upstream face in a wide valley. In an incompressible water approach, the speed of the hydrodynamic pressure waves (C) is infinite and the fluid elements compute a frequency independent hydrodynamic added mass on the upstream face of the dam, assuming that the reservoir bottom is rigid [4]. Incompressible fluid elements that are based on Westergaard's approach but consider the shape of the reservoir and the geometry of the dam are available in current commercial FEA packages.

Consideration of water compressibility in seismic analysis introduces a frequency-dependent component to the response of the reservoir. Compressible fluid elements more accurately model the transmission of pressure waves through the reservoir with finite velocity (C = 1,440 m/s) and allow for consideration of pressure absorption at the reservoir bottom. The water compressibility can drastically increase or reduce the seismic response of a dam in the following ways:

- The hydrodynamic force on a dam due to a seismic load can increase under certain frequency ranges due to the propagation of hydrodynamic pressure waves through the compressible fluid reservoir in the upstream-downstream direction [1].
- The demand can decrease due to the consideration of reservoir bottom absorption [4]. Modelling of the alluvium and sediments at the bottom of the reservoir results in a more realistic representation of the dissipation of hydrodynamic pressure waves and leads to a reduction in hydrodynamic force on the dam [1].

As such, depending on the frequency content of the seismic load, the geometry of the dam, the material properties of the dam and foundation, and the reflectiveness of the reservoir bottom material the seismic response of a dam can either increase or decrease. Previous studies have demonstrated that FE models that account for water compressibility (along with other improvements in accuracy such as foundation mass) result in good agreement between computed results and recorded results at five real dams [2,5]. While it has been widely recommended to account for compressibility of the reservoir when undertaking seismic analyses of concrete dams [1,2,6], this paper examines whether in some cases the use of a simplified incompressible approach is acceptable.

Alluvium and sediments at the bottom of the reservoir can have an influence on the dam's response to seismic loading as they can partially absorb hydrodynamic pressure waves [1]. The interaction between the water and the reservoir bottom is represented by a boundary condition at the base of the compressible fluid elements. The amount of absorption or reflection is based on the "α" coefficient, which represents the ratio of the amplitude of the reflected pressure wave to the amplitude of the incident pressure wave. A value of α=1 indicates full reflection of the pressure wave and α=0 indicates full absorption [4]. It has been previously demonstrated that the seismic response of concrete dams is highly sensitive to "α", and its appropriate selection is critical to accurately represent the response of a dam to seismic loading [1,7].

3. METHOD OF ASSESSING THE INFLUENCE OF WATER COMPRESSIBILITY

A practical procedure has been developed by the Authors in collaboration with DIANA FEA BV, which may assist engineers in determining the influence of water compressibility on the seismic demand of a concrete dam prior to undertaking a time-history analysis. The results of the method will help determine whether a simplistic incompressible water approach may be appropriate for a seismic FEA in lieu of the more complex water compressibility approach. The proposed procedure comprises of four steps as follows:

Step 1: The first step estimates the frequency ratio Ω_r as per the method in Proulx and Paultre [6], described as follows:

- Create a linear FE model of the dam, including the foundation but excluding the reservoir.
- Undertake a frequency (eigenvalue) analysis of the model to determine f_1 (the fundamental frequency of the dam alone/empty reservoir).
- Calculate f_1^r (the fundamental frequency of the reservoir) idealised as a fluid of constant depth and infinite length, using the following empirical formula:

$$f_1^r = \frac{C}{4H} \tag{1}$$

where C = wave propagation velocity in water; and H = average reservoir depth.

- Calculate the frequency ratio Ω_r using the following formula:

$$\Omega_r = \frac{f_1^r}{f_1} \tag{2}$$

where f_1^r = fundamental frequency of the reservoir; and f_1 = fundamental frequency of the dam alone.

- If Ω_r is less than 1.5 the compressibility of water may have a significant influence on the response of the dam, and the assessment should move to Step 2.
- If Ω_r is greater than 1.5 it is unlikely that the influence of water compressibility would be significant and hence the incompressible fluid approach may be suitable for the time-history analysis.
- Previous studies have demonstrated that there is a correlation between the effects of water compressibility and the Ω_r value. Compressibility of water has been shown to be insignificant in the response of gravity dams for systems where $\Omega_r > 1.5$ [6].

Step 2: A u*nit* l*oad* f*requency* a*nalysis (linear analysis)* is undertaken as follows:

- Develop two linear FE models of the dam, where one contains compressible fluid elements with reservoir bottom absorption and the other incompressible fluid elements.
- Undertake a frequency response analysis of each model subject to a unit load (e.g., constant acceleration of 1.0 m/s^2 for a range of frequencies of interest such that the resonant frequencies for the dam are covered). The frequency step size needs to be fine enough to capture the peak responses and the range large enough to capture the range of frequencies the dam will respond to. A frequency analysis can be undertaken to determine what frequencies contribute the most mass.
- Chart the results of the analysis in terms of frequency vs acceleration, displacements or stresses at various points on the dam (e.g., accelerations at several locations along the dam crest) for each model. The results will show the response of the dam along the range of frequencies of interest for each model. It is expected that for frequencies with a large mass participation, such as the fundamental frequency, the response of the dam would be greater.
- The influence of water compressibility should be checked at all frequencies of interest and the outcome of the assessment determined as follows:
    - If both frequencies and magnitudes of the peak responses are similar for the compressible and incompressible approaches, the influence of the water compressibility is deemed to be insignificant, and hence the incompressible fluid approach would be suitable for the time-history analysis.
    - If the magnitudes of the peak responses for the compressible approach are either consistently higher or consistently lower than the

incompressible approach for all frequencies of interest, the influence of water compressibility should be accounted for in the time-history analysis. Noting that if the compressible approach is consistently lower, an incompressible approach could be conservatively adopted.

- If the frequencies of the peak responses are different between the approaches and/or the magnitudes of the compressible approach vary between above and below that of the incompressible approach at several frequencies of interest, then the impact of water compressibility is inconclusive and Step 3 of the method is warranted.

Step 3: An earthquake load frequency analysis (linear analysis) is undertaken as follows:

- Step 3 follows a similar process to Step 2, however, a Fourier amplitude spectrum in terms of amplitude and phase angle is applied to the models rather than a unit load. In this step, the earthquake record, which is typically presented as an acceleration time-history, is converted into a Fourier amplitude spectrum using a Fourier transformation. This step is considered more accurate than Step 2 as it requires the input of a site-specific ground motion time-history, from which the frequencies are calculated. The same model, frequency step size and frequency range as per Step 2 are used.
- Chart the results of the analysis as per Step 2. The results of the analysis will show the response of the dam for the range of frequencies specific to the earthquake for each model.
- The influence of water compressibility should be checked at all frequencies of interest and the outcome of the assessment should be determined based on the descriptions provided as part of Step 2.
- As an additional comparison as part of Step 3, stresses in the dam concrete at key frequency steps can be assessed and compared to understand the influence of fluid compressibility at locations of interest (e.g., understand the influence of compressibility on tension at the upstream heel or stress concentrations at locations of known deficiencies).
- Repeat this step for all ground motions the dam will be assessed for (typically 3 to 5 ground motions).
- If it is unclear that compressibility of water will have a significant influence on the demand on the dam, move to Step 4.

Step 4: An equivalent linear analysis is undertaken, as follows:

- Perform an inverse Fourier transformation of the displacement, acceleration or stress results from Step 3 to convert the results from the frequency domain to the time domain, generating the results for an equivalent linear analysis.
- Chart the results of the analysis in terms of time vs displacements, accelerations or stresses.

- The equivalent linear analysis gives an indication of both the significance of water compressibility and the expected influence on increasing or decreasing the demand on the dam.
- While the outcome should be the same as Step 3, Step 4 allows the user to assess the results in the time domain, which is more intuitive than in the frequency domain.
- Note as the equivalent linear analysis is only based on steady-state results of the frequency response analysis, it does not account for transient effects or other applied loads (e.g., gravity, hydrostatic loads, uplift forces etc.) and should be used as a comparison tool only.
- If the influence of water compressibility is found to be insignificant, it may be appropriate to undertake the analysis using incompressible fluid elements as part of a transient seismic analysis (time-steps) as it is simpler to implement and analyse.

If water compressibility is found to be significant and is to be included in the time-history analysis, the analysis must be run in a solver that is able to account for water compressibility. Options for analysis with compressible fluid elements vary between software packages, but it is likely that it will require the analysis to be executed in the frequency domain. Solvers such as a hybrid frequency-time domain (HFTD) implemented in DIANA® [8] can be used to perform nonlinear seismic analysis including the compressibility of water; other programs with similar capabilities may also be used, however, each solver has specific capabilities and limitations that need to be carefully considered and may require validation before proceeding with the analysis.

4. WORKED EXAMPLE

A worked example of the 4-steps procedure to determine the influence of water compressibility on a generic concrete gravity dam is presented herein. The details of the model and the results of each step of the assessment are provided below. In addition, sensitivity analyses of different model parameters were undertaken to identify any trend in the results that may help determine in what particular circumstances the influence of water compressibility is likely to be significant. The FEA was undertaken with a linear 3D FE model using commercial package DIANA®. The generic concrete gravity dam model is presented in Fig. 1 and has the following geometry: a 50 m high and 200 m long concrete gravity dam with 0.7(H):1 (V) downstream slope and vertical upstream face, symmetrical valley with a flat 90 m wide valley floor, steep dam abutments and gentle abutment slopes above crest level, reservoir level 5 m below the dam crest and foundation dimensions determined as per USBR [4].

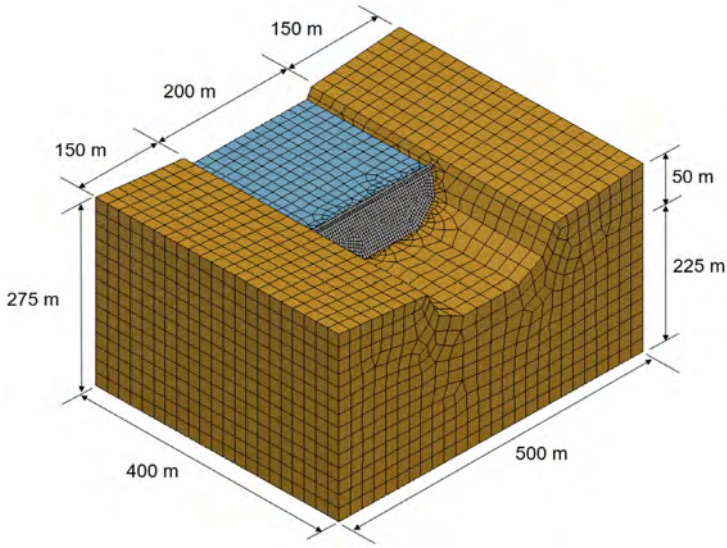

Fig. 1
FE model geometry
Géométrie du modèle par EF [éléments finis]

Typical material properties were adopted for the model, which are summarised in Table 1 below. The foundation was assumed to be a homogenous rock foundation with a Youngs Modulus equal to the adopted concrete modulus (Ec/Er=1.0).

Table 1
FE model adopted material properties
Propriétés des matériaux adoptées pour le modèle par EF [éléments finis]

LOCATION	PROPERTY	VALUE
Dam Concrete	Density (γ_c)	2,400 kg/m^3
	Poisson's Ratio (ν)	0.2
	Youngs Modulus (E_c)	25 GPa
Rock Foundation	Density (γ_r)	Massless
	Poisson's Ratio (ν)	0.25
	Youngs Modulus (E_r)	25 GPa
Reservoir	Density (γ_w)	1,000 kg/m^3
	Reservoir Bottom Absorption Coefficient (α)	0.7

Other key features of the model are:

- The model is linear elastic.
- The foundation was considered massless. Note that a sensitivity case considered massed foundation.
- Two models were developed, one with incompressible fluid elements, and one with compressible fluid elements with reservoir bottom absorption.
- The relationship defined in Hall et al [9] was used to select a reservoir bottom absorption coefficient of 0.7.
- A Rayleigh damping of 5% was adopted for both the foundation rock and dam concrete.
- The first two fundamental modal shapes and frequencies in the upstream-downstream direction are presented in Fig. 2.
- The element sizes for the different components were developed based on USBR [4] such that the model running times were minimised while accuracy of results was preserved.

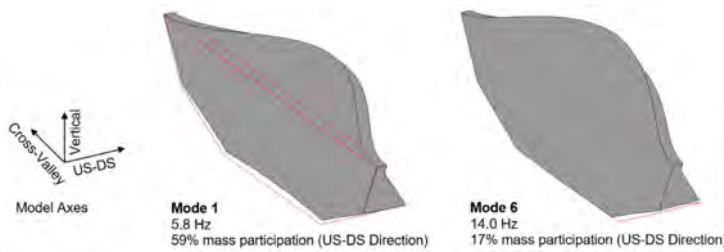

Fig. 2
First two fundamental modal shapes (upstream-downstream direction)
Les deux premières formes modales fondamentales (direction amont-aval)

4.1. Seismic loads

For the worked example a spectrally scaled version of the Loma Prieta (Gilroy Array 1) earthquake was adopted as the generic seismic load for the example model (Steps 3 and 4 of the proposed methodology). The ground motion time-history is reproduced in Fig. 3. The peak ground accelerations are 5.1 m/s^2 (at 4.23 s) in the upstream-downstream direction, 4.4 m/s^2 (at 3.43 s) in the cross-valley direction and 2.3 m/s^2 (at 1.79 s) in the vertical direction.

For input into the frequency response analysis in Step 3, a Fourier Transformation of the acceleration time-history was undertaken. The Fourier

amplitude spectra are shown in Fig. 4, which shows that the dominant frequencies of the input earthquake are in the range of 1 to 5 Hz for all three components of the earthquake.

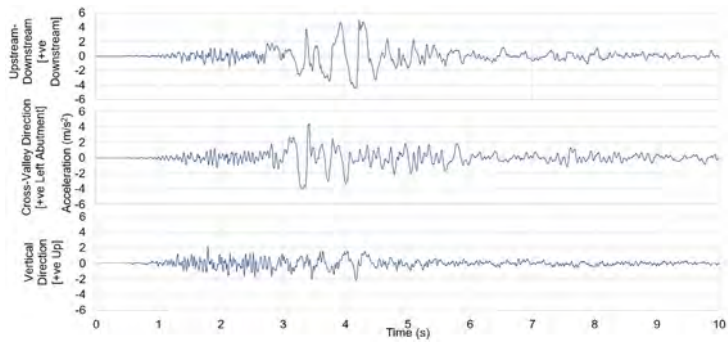

Fig. 3
Time-history of Loma Prieta (Gilroy Array 1)
Accelerogramme de Loma Prieta (station de Gilroy Array 1)

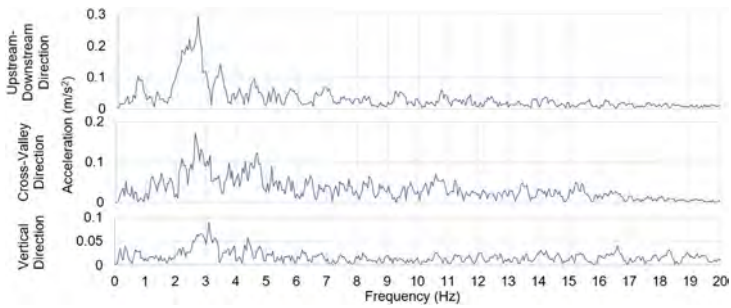

Fig. 4
Fourier transformation of Loma Prieta (Gilroy Array 1)
Transformation de Fourier de Loma Prieta (station de Gilroy Array 1)

4.2. Worked example results

The four steps outlined in this paper were followed for the worked example dam and the results of each step are presented below.

Step 1: The fundamental frequency of the dam without the reservoir was 6.7 Hz based on a frequency (eigenvalue) analysis of the dam-foundation system. The fundamental frequency of the reservoir alone was calculated as 8.1 Hz using Eq. [1]. The ratio between the fundamental frequencies of the reservoir alone and the dam alone (Ω_r), was calculated using Eq. [2] and found to be 1.20. Since $\Omega_r <$ 1.5, the compressibility of water may have a significant influence on the response of the dam and cannot be disregarded based on the results of this step. The assessment was therefore continued to Step 2.

Step 2: A frequency (eigenvalue) analysis of the dam-foundation-reservoir system was undertaken which showed that the fundamental frequency is 5.8 Hz, and that 90% of the mass participation is accounted for by 18.5 Hz. Therefore, Step 2 of the analysis was undertaken using a unit input acceleration of 1.0 m/s^2 across the range of 0 Hz to 20 Hz. A comparison of the dam's response in the upstream-downstream, cross-valley and vertical directions is shown in Fig. 5., for both the compressible and incompressible approaches.

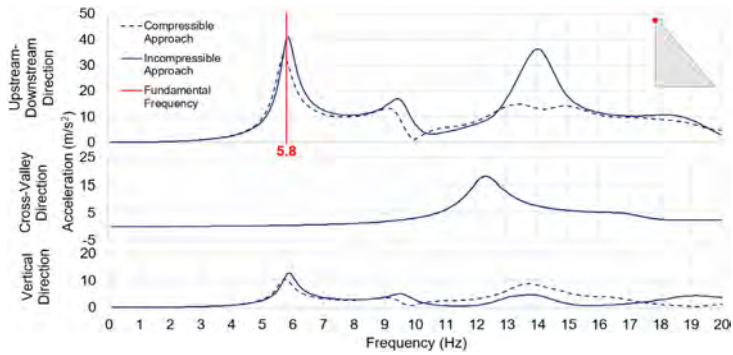

Fig. 5
Step 2 results – comparison of accelerations at dam crest node
Résultats de l'étape 2 – comparaison des accélérations au nœud de la crête du barrage

The results show that the compressibility of water generates a significant decrease in the seismic response around the dam's fundamental mode at 5.8 Hz and second fundamental mode at 14.0 Hz for the upstream-downstream direction and the fundamental mode in the vertical direction. This difference is caused by the influence of water compressibility on the seismic response due to the linear elastic deformation of the dam, a difference in the propagation of hydrodynamic pressure waves through the fluid medium and the influence of reservoir bottom absorption. The crest accelerations at the fundamental frequency in the upstream-downstream direction are

approximately 18% less for the compressible approach in comparison to the incompressible approach. It is noted that the results of both approaches are identical in the cross-valley direction. As water has no shear strength, the hydrodynamic force from the reservoir is only applied in the normal direction to the upstream face of the dam. Given the worked example is a straight concrete gravity dam with a vertical upstream face; there is no hydrodynamic effect observed in the cross-valley direction.

The results in the upstream-downstream and vertical directions show for the that the influence of water compressibility on the demand on the dam is in general as follows: negligible for frequencies less than 4 Hz, slightly increased between 4 Hz and 5.5 Hz and slightly reduced between 5.5 Hz and 10.5 Hz. At frequencies higher than 10.5 Hz the results indicate that compressibility may significantly reduce the demand in the upstream-downstream direction but increase the demand in the vertical direction. Therefore, the influence of water compressibility for the example dam could result in either an increased or decreased demand on the structure, depending on the frequency content of the earthquake signal and the amplitude of each component of the earthquake. As the results of Step 2 are inconclusive, Step 3 of the assessment was undertaken.

Step 3: In Step 3 the analysis input the Fourier amplitude spectrum of the earthquake time-history for Loma Prieta (Gilroy Array 1), shown in Fig. 4. A comparison of the dam's response for the compressible and incompressible water approaches is shown in Fig. 6 for the upstream-downstream, cross-valley and vertical directions. The amplification of the signal through the dam body can be appreciated by comparing the outcrop acceleration at the base of the dam in Fig. 4 with the response at the crest in Fig. 6 (i.e. at the fundamental frequency of 5.8 Hz the amplification from base to crest is 2.9 m/s^2 and 3.9 m/s^2 for the compressible and incompressible approaches, respectively).

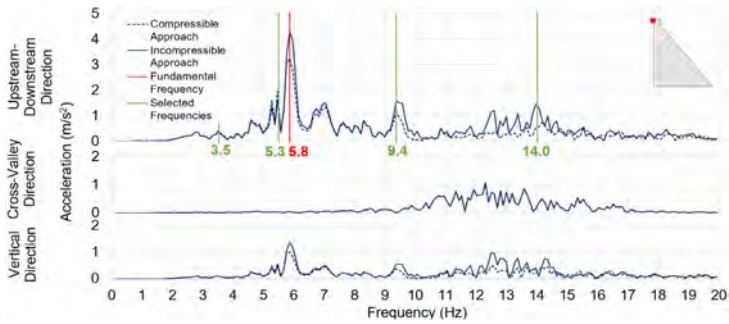

Fig. 6
Step 3 results – comparison of accelerations at dam crest node
Résultats de l'étape 3 – comparaison des accélérations au nœud de la crête du barrage

As predicted in Steps 1 and 2, Step 3 results indicate that some influence on the demand on the dam can be expected due to water compressibility in both the upstream-downstream and vertical directions. As for Step 2, the influence of water compressibility on the dam's response is: negligible for frequencies less than 4 Hz, slightly increased between 4 Hz and 5.5 Hz, decreased at approximately 5.8 Hz (the dam's first fundamental frequency), and slightly decreased between 5.5 Hz and 9 Hz. For frequencies higher than 9 Hz, the Step 3 results indicate that water compressibility is expected to reduce the demand on the structure. The results of Steps 2 and 3 shown in Fig. 5 and Fig. 6 give an indication of the dam's response across a range of frequencies for strategically selected nodes in the dam (e.g., a node at the crest in the centre of the valley as per this worked example). However, to detect areas of the structure where the influence of compressibility could be more significant, the stresses on the dam wall were assessed. The stresses developed in the dam wall were assessed for a selection of frequencies that presented different levels of impact on the seismic response when comparing the compressible and incompressible approaches, as follows: at 3.5 Hz (a frequency that shows no significant difference between the two approaches); at 5.3 Hz (a frequency where the compressible response is larger than the incompressible response); at 5.8 Hz (the fundamental frequency where the incompressible response is notably larger than the compressible response); at 9.4 Hz (a second peak where the incompressible response is notably larger than the compressible response); and 14.0 Hz (the second fundamental frequency where the incompressible response is notably larger than the compressible response). The stress assessment for the selected frequencies was conducted in terms of vertical stress on the upstream face of the dam, as presented in Fig. 7.

The following observations were made while comparing the stress results:

- At 3.5 Hz: No meaningful difference in the stresses between the compressible and incompressible approaches.
- At 5.3 Hz: A minor increase of 0.05 MPa in the tensile stress at the upstream heel when considering water compressibility.
- At 5.8 Hz (first fundamental frequency): A decrease in the tensile stress at the upstream heel when considering water compressibility. As 5.8 Hz is indicated to be the peak of the dam's response from the accelerations at the crest node, the stresses observed at the upstream heel for the incompressible approach are likely to be the largest across all frequencies for both approaches and would have the largest influence on the overall seismic demand on the structure. The decrease in tensile stress between the models at 5.8 Hz is 0.1 MPa, which is more significant than the increase observed at 5.3 Hz, as there is more mass associated with the fundamental frequency, but is still considered minor.
- At 9.4 Hz and 14.0 Hz (second fundamental frequency): There is a decrease in tensile stresses on the upstream face of the dam when considering water compressibility, although as the magnitudes are small, they are unlikely to significantly contribute to the overall seismic demand on the structure.

The comparison shows that the influence of water compressibility on the dam indicated by the dam crest node accelerations is consistent with the state of stresses in the dam wall. Based on the comparison of the stress results and the dam crest accelerations for this particular worked example, the influence of water compressibility is expected to be minor. However, to get a full understanding of the influence of compressibility in the time domain, Step 4 of the assessment was undertaken.

It is noted in this case and for this specific earthquake, that adopting incompressible fluid elements would be conservative. Should this occur, the modeller should recognise that it may not be justified to include the effects of water compressibility, given it can be difficult to implement, particularly if earthquake loading is not the critical load case.

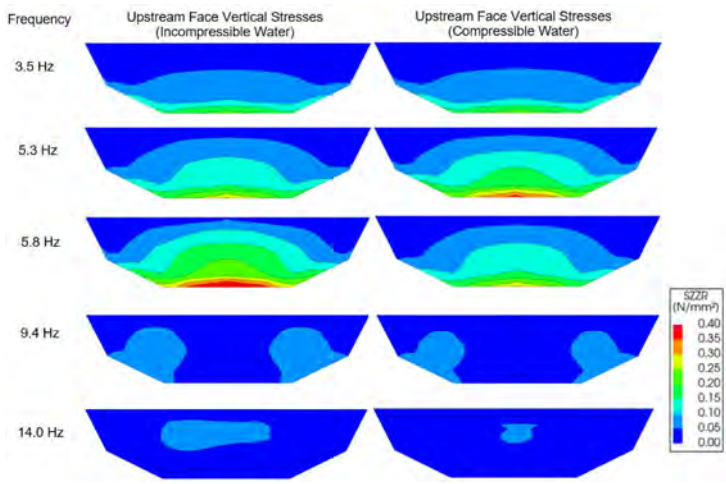

Fig. 7
Step 3 results – comparison of vertical stresses on the upstream face of the dam
Résultats de l'étape 3 – comparaison des contraintes verticales sur la face amont du barrage

Step 4: This step of the analysis involves an inverse Fourier Transformation of the Step 3 results to convert the results to the time domain. A comparison of the dam's response in terms of displacements at a node on the dam crest is presented in Fig. 8. It should be noted that the displacements shown are based on steady-state results from the frequency analysis and are therefore only due to the seismic load. The influence of other applied loads such as uplift forces or hydrostatic loads are not accounted for. Step 4 results show that the displacements between the compressible

and incompressible approaches in terms of crest displacements are similar, with slightly larger displacements for either approach at different time steps, although the highest peaks of displacement are for the incompressible approach. This indicates that the incompressible approach slightly overestimates the response of the dam. As the displacements are similar, Step 4 indicates that it would be reasonable to conservatively adopt incompressible water for preliminary earthquake analysis of the dam.

As a verification of the Step 4 process, the displacements from the incompressible fluid approach were compared to a linear time-history analysis of the earthquake in the time domain also using incompressible fluid elements. The results are expected to be similar as both models account for the same input load, albeit in different forms. Fig. 9 shows that the results of the two assessment methods are very similar, indicating that the Fourier Transform approach is valid.

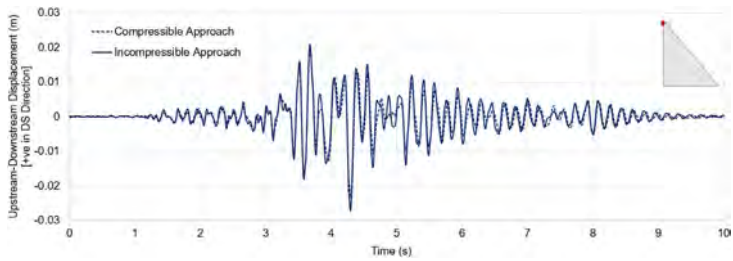

Fig. 8
Step 4 results – comparison of displacements at dam crest node
Résultats de l'étape 4 – comparaison des déplacements au nœud de la crête du barrage

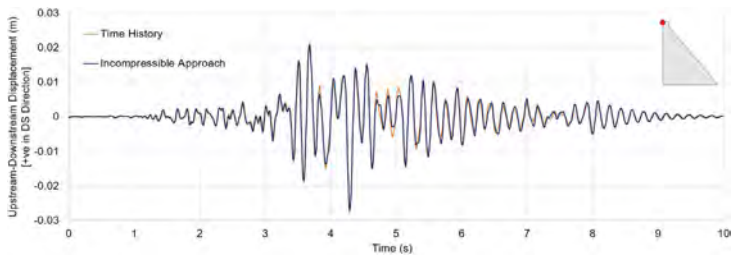

Fig. 9
Step 4 results – comparison of displacements at dam crest node for incompressible approach and linear time-history analysis
Résultats de l'étape 4 – comparaison des déplacements en crête du barrage avec l'approche incompressible et l'analyse linéaire de l'historique temporel

5. SENSITIVITY ANALYSIS

A sensitivity analysis was undertaken to demonstrate how different geometries, material parameters and other model options affect the influence of water compressibility on the seismic response of the dam. The sensitivity of the following items was assessed:

- Ratio of the dam concrete and foundation rock modulus of elasticity (E_c/E_r)
- Dam height
- Valley width
- Reservoir bottom absorption "α" coefficient
- Consideration of mass in the foundation

A summary of the changes to the 'base case model' are presented in Table 2.

Table 2
Sensitivity case summary
Résumé des cas de sensibilité

SENSITIVITY CASE	FOUNDATION YOUNGS MODULUS	CONCRETE YOUNGS MODULUS	DAM HEIGHT	CREST LENGTH	"α" COEFFICIENT	FOUNDATION DENSITY
1 (Base Case)	25 GPa	25 GPa	50 m	200 m	0.7	Massless
2	41.7 GPa	25 GPa	50 m	200 m	0.7	Massless
3	17.9 GPa	25 GPa	50 m	200 m	0.7	Massless
4	25 GPa	15 GPa	50 m	200 m	0.7	Massless
5	25 GPa	35 GPa	50 m	200 m	0.7	Massless
6 ("Short" dam)	25 GPa	25 GPa	25 m	200 m	0.7	Massless
7 ("Tall" dam)	25 GPa	25 GPa	100 m	200 m	0.7	Massless
8	25 GPa	25 GPa	50 m	100 m	0.7	Massless
9	25 GPa	25 GPa	50 m	300 m	0.7	Massless
10	25 GPa	25 GPa	50 m	200 m	0.5	Massless
11	25 GPa	25 GPa	50 m	200 m	0.6	Massless
12	25 GPa	25 GPa	50 m	200 m	0.8	Massless
13	25 GPa	25 GPa	50 m	200 m	0.9	Massless
14	25 GPa	25 GPa	50 m	200 m	0.7	2,700 kg/m^3

The results, a table of the peak accelerations at the fundamental frequencies in the upstream-downstream direction based on the results of Step 1 and 2 of the method, are presented in Table 3. The fundamental frequency in the upstream-downstream direction was selected for comparison as it generally exhibits the largest response which highly influences the stress demand on the dam wall. Note that "Difference" in Table 3 refers to the difference between the fundamental frequency accelerations at the dam crest node for the compressible water approach relative to the incompressible water approach.

The key findings of the sensitivity analysis were:

- For all sensitivity cases the inclusion of water compressibility reduced the demand on the structure in comparison to water incompressibility.
- For all sensitivity cases, there is a correlation between increasing frequency ratio (Ω_r) and decreasing significance of water compressibility. This is illustrated in Fig. 10, which shows the frequency ratio with the difference in accelerations between the compressible and incompressible approaches at the fundamental frequency for sensitivity cases 1 to 9. These results are consistent with Proulx & Paultre [6] who quoted a value of Ω_r

Table 3
Sensitivity results
Résultats de sensibilité

SENSITIVITY CASE	E_C/E_R	Ω_R	INCOMPRESSIBLE WATER		COMPRESSIBLE WATER		DIFFERENCE
			FUNDAMENTAL FREQUENCY	DAM CREST ACCELERATION	FUNDAMENTAL FREQUENCY	DAM CREST ACCELERATION	
1 (Base Case)	1	1.20	5.8 Hz	40.9 m/s^2	5.7 Hz	33.4 m/s^2	-18%
2	0.6	1.11	6.2 Hz	42.6 m/s^2	6.1 Hz	34.1 m/s^2	-20%
3	1.4	1.28	5.2 Hz	36.9 m/s^2	5.1 Hz	31.2 m/s^2	-15%
4	0.6	1.44	4.9 Hz	39.3 m/s^2	4.9 Hz	35.7 m/s^2	-9%
5	1.4	1.08	6.5 Hz	40.5 m/s^2	6.3 Hz	30.1 m/s^2	-26%
6	1	1.55	10.9 Hz	32.9 m/s^2	10.8 Hz	30.5 m/s^2	-7%
7	1	0.84	3.8 Hz	46.2 m/s^2	3.6 Hz	26.4 m/s^2	-43%
8	1	0.90	8.0 Hz	40.6 m/s^2	7.7 Hz	26.7 m/s^2	-34%
9	1	1.29	5.4 Hz	38.8 m/s^2	5.3 Hz	32.2 m/s^2	-17%
10	1	1.20	5.8 Hz	40.9 m/s^2	5.7 Hz	29.4 m/s^2	-28%
11	1	1.20			5.7 Hz	31.2 m/s^2	-24%
12	1	1.20			5.7 Hz	36.4 m/s^2	-11%
13	1	1.20			5.7 Hz	39.3 m/s^2	-4%
14	1	1.20	5.8 Hz	11.6 m/s^2	5.6 Hz	10.9 m/s^2	-6%

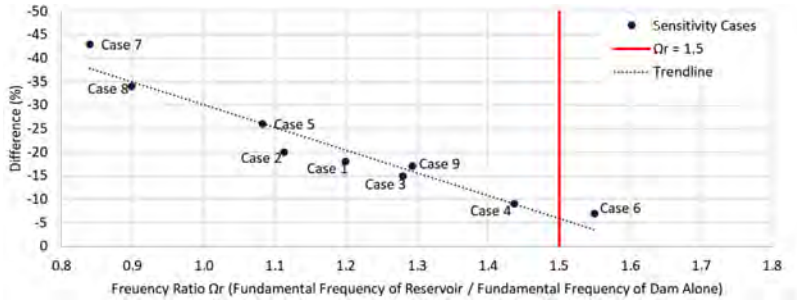

Fig. 10
Frequency Ratio Ω_r Comparison
Comparaison des rapports de fréquence Ωr

greater than 1.5 as the ratio where the compressibility of water becomes insignificant.

- The influence of water compressibility was less significant for dams on flexible foundations and more significant for dams on rigid foundations, in line with similar studies [1,10].
- The influence of water compressibility was less significant for rigid dams and more significant for more flexible dams, in line with similar studies.
- The influence of water compressibility was more significant for "tall" dams and less significant for "short" dams, in line with similar studies [10].
- The influence of water compressibility was more significant for dams in narrow valleys.
- As the "α" coefficient tends towards 1 (rigid reservoir bottom and full reflection), the response at the fundamental frequency of the dam gets closer to that of the incompressible approach (i.e., the influence of water compressibility is less significant).
- Inclusion of mass in the foundation significantly reduced the influence of water compressibility on the seismic response of the dam.

The full sensitivity analysis and discussion is provided in Lalli et al [11].

6. CONCLUSIONS

Previous studies have demonstrated that ignoring the influence of water compressibility in finite element modelling of concrete dams can lead to inaccurate results. However, due to the complexity of the compressible fluid elements, the use of incompressible fluid elements has been accepted by the industry as a

compromise between the accuracy of the results and the limitations of FEA software. More recently several commercial packages have started accounting for the compressibility of water, although with limitations.

This paper presented a practical 4-step procedure for assessing the influence of water compressibility on the seismic response of a concrete gravity dam. This linear-elastic procedure may be used by dam engineers to make an initial assessment on whether compressible water should be included in a time-history FEA, or whether the more simplistic incompressible water approach can be used without significantly impacting the seismic response.

A worked example of a generic gravity dam illustrated the use of the 4-step procedure, demonstrating that the influence of water compressibility was relatively minor, noting that the analysis was conducted for a single ground motion.

A sensitivity analysis was also undertaken to determine the influence of material parameters and geometry changes on the seismic response of the worked example with compressible and incompressible water, showing varying effects on the results. The influence of compressibility was shown to be the most significant for dams with a low frequency ratio (Ω_r), relatively flexible dams, dams in relatively rigid foundations, dams in narrow valleys and FE models considering a massless foundation. The trends observed and findings of the sensitivity analysis were consistent with previous studies, validating that the 4-step assessment process presented in this paper gives a strong indication of the influence of water compressibility related to concrete gravity dam analysis.

Further investigations would be beneficial to keep advancing the understanding of the influence of water compressibility in concrete gravity dams. This could include additional variations to the combinations of materials and geometries performed in this study, as well as an extension of the methodology to concrete gravity-arch dams and double curvature arch dams.

REFERENCES

[1] FENVES, G. L. & CHOPRA, A. K., 1984. *Earthquake analysis and response of concrete gravity dams*, Berkeley: Earthquake Engineering Research Center, University of California.

[2] CHOPRA, A. K., 2020. *Earthquake Engineering for Concrete Dams: Analysis, Design, and Evaluation*. 1st ed. Berkeley: John Wiley & Sons Ltd.

[3] WESTERGAARD, H. M., 1933. *Water pressures on dams during earthquakes*. *Transactions of the American society of Civil Engineers*, 98(2), pp. 418–433.

[4] USBR, 2006. *State-of-Practice for the Nonlinear Analysis of Concrete Dams at the Bureau of Reclamation*. U.S. Department of the Interior Bureau of Reclamation.

[5] CHOPRA, A. K. & WANG, J., 2012. *Comparison of recorded and computed earthquake response of arch dams*. In 15th World Conference on Earthquake Engineering, Lisbon, Portugal.

[6] PROULX, J. & PAULTRE, P., 1997. *Experimental and numerical investigation of dam reservoir foundation interaction for a large gravity dam*. *Canadian Journal of Civil Engineering*, 24(1), pp.90–105.

[7] HALL, J. F. & CHOPRA, A. K., 1980. *Dynamic response of embankment, concrete-gravity and arch dams including hydrodynamic interaction*, Berkeley: Earthquake Engineering Research Center, University of California.

[8] DIANA, 2022. *DIANA Finite Element Analysis Software*, Version 10.6 Release 06/12/2022. Delftechpark 19a, 2628 XJ Delft, The Netherlands: DIANA FEA BV.

[9] HALL, R. L., DE BEJAR, L., SJOSTROM, K. J. & MATHEU, E. E., 1998. *Effect of reservoir-subbottom energy absorption on hydrodynamic forces on dams*. NIST SPECIAL PUBLICATION SP, pp. 116-129.

[10] CHAVEZ, J. W. & FENVES, G. L., 1993. *Earthquake analysis and response of concrete gravity dams including base sliding*, Berkeley: Earthquake Engineering Research Center, University of California.

[11] LALLI, S., LOPEZ, F., MCKAY, M. and Harrison, S., 2023. *The importance of water compressibility in seismic analyses of concrete gravity dams*. ANCOLD 2023 Conference Proceedings, Cairns.

COMMISSION INTERNATIONALE DES
GRANDS BARRAGES

VINGT-HUITIEME CONGRES DES
GRANDS BARRAGES
CHENGDU, MAI 2025

OPTIMIZATION OF THE CROSS-SECTIONAL DESIGN OF TRAPEZOIDAL CSG DAMS (*)

Nario YASUDA
Head of Eng. Division 1,
JAPAN DAM ENGINEERING CENTER

Zengyan CAO
Senior Advisor, Engineering Department
J-POWER BUSINESS SERVICE CORPORATION

Taku NAKAMURA
River Division, Dept. of Prefectural Land Development,
MIE PREFECTURAL GOVERNMENT

JAPAN

SUMMARY

In this study, via numerical analyses, the effects of the elastic modulus of the CSG and the upstream and downstream slopes of the dam on the seismic performance of the dam were clarified. To improve dam safety and reduce construction costs, the upstream face was adjusted to a steeper slope in the analysis, and it was revealed that the internal stability was less satisfactory. In addition, it was also found that seismic safety can be improved by increasing the unit cement content in a limited area near the upstream and downstream ends of the dam base. That is, the construction cost of a dam can be significantly reduced through rational improvement of the cross-sectional shape and arrangement of the unit cement content.

**Optimisation de la conception en section transversale des barrages CSG trapézoïdaux*

DOI: 10.1201/9781003642428-118

RÉSUMÉ

Dans cette étude, des analyses numériques ont permis de clarifier les effets du module d'élasticité du CSG et des pentes en amont et en aval du barrage sur la performance sismique des barrages de type CSG. Pour améliorer la sécurité du barrage et réduire les coûts de construction, la face amont a été ajustée à une pente plus raide dans l'analyse, et il a été révélé que la stabilité interne était moins satisfaisante. En outre, il a également été constaté que la sécurité sismique peut être améliorée en augmentant la teneur en ciment unitaire dans une zone limitée près des extrémités amont et aval de la base du barrage. En d'autres termes, le coût de construction d'un barrage peut être considérablement réduit grâce à une amélioration rationnelle de la forme de la section transversale et de la disposition de la teneur unitaire en ciment.

1. INTRODUCTION

The cross-sectional design of trapezoidal cemented sand and gravel (CSG) dams [1], [2] differs from that of other types of dams in that the strength and elastic modulus of the CSG using locally available rocky raw materials are assumed and the finite element method (generally a two-dimensional model) is used to satisfy internal and external stability requirements. Four dams have been completed, and one is under construction in Japan as of June 2024. Regardless of the design seismic intensity, dam height, and rock raw material used, the slopes of the upstream and downstream faces of these trapezoidal CSG dams are all 1:0.8. The unit cement content is also determined by the relationship between the stress generated and the strength of the CSG. During the 2018 Hokkaido Eastern Iburi Earthquake, an acceleration of up to 450 cm/s^2 was recorded in the bottom inspection gallery of the Apporo Dam, a 47.2 m-high trapezoidal CSG dam located only 8.6 km from the epicenter. The dam was not damaged by the earthquake, and using a three-dimensional model to simulate the behavior of the dam during the earthquake, a reproduction analysis [3] confirmed that dam safety was unaffected. Nevertheless, it is necessary to verify whether the earthquake resistance of the trapezoidal CSG dam is sufficient or whether its design is reasonable from an economic point of view.

In this study, numerical analyses were carried out to examine the possibility of optimizing the cross-sectional design. In the analyses the elastic modulus of the CSG was varied within the range considered on the basis of the actual data of existing trapezoidal CSG dams. The upstream and downstream slopes of the dam were varied in several patterns, not only for the current pattern of 1:0.8. Moreover, the changes in the seismic performance of the dam under each condition were examined. As a result, the influence of these parameters on the seismic

performance of the dam was clarified. It was revealed that the dam has sufficient seismic resistance against strong seismic motion of the “lower limit acceleration response spectrum for seismic performance verification of dams” [4] when the dam slope in the current design is 1:0.8 and the elastic modulus of the CSG is within the normal range of possibility. In addition, with respect to construction cost reduction, more economical dam construction is possible by making the slope of the dam steeper and adjusting the unit cement content used in the cross section to conform to the stress generated during the earthquake.

2. EXAMINATION OF THE FACTORS AFFECTING THE SEISMIC STABILITY OF TRAPEZOIDAL CSG DAMS

A coupled analysis of the dam-reservoir-foundation was conducted assuming the maximum cross section of a typical trapezoidal CSG dam. The effects of the upstream and downstream slopes of the dam and the elastic modulus of the CSG on the internal and external stability of the dam were considered in the dynamic analysis. Although the setting of the CSG strength is important in evaluating the stability of a dam, the CSG strength was assumed to be a constant value (two types for two unit cement contents) in this study to focus on the level of influence of the above-mentioned parameters.

In the design of a trapezoidal CSG dam, the internal and external stability evaluation of the dam must be conducted using the stresses obtained under each of the conditions of design seismic motion, verification seismic motion, and the maximum credible earthquake (hereinafter referred to as MCE) in Japan, in addition to the normal conditions, as described below, and the required safety criteria must be met under all conditions. However, to investigate the factors affecting the stability of a dam, only the MCE ground motion assumed for a certain existing dam is used in this section.

The dam analysis program “UNIVERSE “ [5] was used for the linear analysis.

2.1. Model for analysis

Considering the existing trapezoidal CSG dams in Japan, the height of the model dam was set to a constant value of 50 m, and the upstream and downstream slopes of the dam were varied as a parameter. Specifically, four patterns of 1:0.5, 1:0.6, 1:0.7, and 1:0.8 were set for both the upstream and downstream slopes, and four patterns of 1:0.4, 1:0.5, 1:0.6, and 1:0.7 were set for the upstream face with the downstream face fixed at 1:0.8, for a total of eight models. Figure 1 shows a model

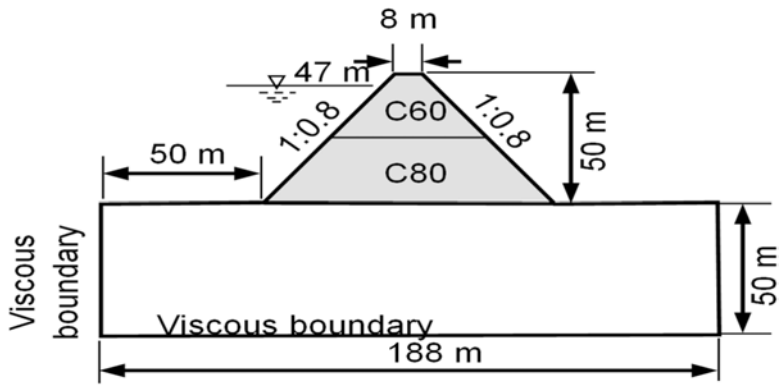

Fig. 1
Analysis model
Modèle d'analyse

with upstream and downstream slopes of 1:0.8 as an example. The reservoir was modelled via the finite difference method with a depth of 47 m in all the models and a length that is three times the depth in the upstream direction (the coupling between the reservoir and foundation was not considered, and the lengths of the reservoir and foundation were different). The wave equation for the reservoir and the equation of motion for the dam-foundation were solved separately, and the coupled conditions (hydrodynamic pressure condition and kinetic velocity condition) at the upstream face of the dam were used to account for the effects of the dam and reservoir interaction. Viscous boundary conditions [6] were used at the bottom and lateral boundaries of the foundation model to account for the influence of the vibration of the surrounding ground on the analytical model and for the dissipation of scattered waves due to vibration of the dam and foundation. At the upstream end of the reservoir, a complete absorption boundary condition [7] of wave energy was applied, and at the bottom of the reservoir, a partial reflection condition [7] (impedance ratio of 1.5 between sediment and water at the reservoir bottom) was set. At the reservoir surface, the effects of surface gravity waves were considered.

2.2. Physical properties

2.2.1. *Elastic modulus of the CSG*

Table 1 summarizes the elastic modulus of the CSG used in the design of trapezoidal CSG dams, including dams under construction or planned in Japan. The elastic modulus of the CSG varied over a relatively large range because of the

different CSG materials and mixtures. In addition, pressure-meter tests in the borehole of the Apporo Dam revealed that the actual elastic modulus of the dam body is much larger than the design value [3]. Furthermore, a dynamic reproduction analysis revealed that the dynamic elastic modulus is approximately 1.3 times the static modulus [3]. Considering the experience of trapezoidal CSG dams in Japan, the unit cement content of the CSG in this study was set to 60 kg/m^3 for the upper half of the model (hereinafter referred to as C60) and 80 kg/m^3 for the lower half (hereinafter referred to as C80). The elastic modulus of the CSG was set to the range of values shown in Table 2 (in actual dam design, the elastic modulus of the whole dam body was assumed to be constant, and the elastic modulus of C80 was adopted). The elastic modulus of the foundation was set to a constant value of 12,000 N/mm^2 on the basis of the example of Apporo Dam.

Table 1
Elastic modulus of CSG used in design

DAM NAME	ELASTIC MODULUS (N/mm^2)
Tobetsu	4,000
Kim	2,000
Sanru	2,700
Apporo	2,000
Naruse	3,500
Chokai	3,000
Honmyogawa	5,000
Narusegawa	3,000

Table 2
Variables set in analysis

SLOPE		ELASTIC MODULUS OF CSG (N/mm^2)*				
		1,300	2,700	4,000	5,300	6,700
UPSTREAM	DOWNSTREAM	2,000	4,000	6,000	7,500	9,000
1:0.5	1:0.5	○	○	○	○	○
1:0.6	1:0.6	○	○	○	○	○
1:0.7	1:0.7	○	○	○	○	○
1:0.8	1:0.8	○	○	○	○	○
1:0.4	1:0.8	○	○	○	○	○
1:0.5	1:0.8	○	○	○	○	○
1:0.6	1:0.8	○	○	○	○	○
1:0.7	1:0.8	○	○	○	○	○

Note*: The upper row shows the elastic modulus of C60, and the lower row shows that of C80

2.2.2. *Density, Poisson's ratio and damping ratio of the CSG*

The density, Poisson's ratio, and damping ratio of the CSG and foundation were obtained from the results of material tests [3] of the Apporo Dam. The physical properties shown in Table 3 were used. In the analysis, the damping of the dam and foundation was evaluated as Rayleigh damping.

Table 3
Material properties used in analysis

ITEMS	ELASTIC MODULUS (N/mm^2)	DENSITY (g/cm^3)	POISSON'S RATIO	DAMPING RATIO
CSG	Showed in Table 2	2.1	0.25	5%
Foundation	12,000	2.5	0.3	3%

2.2.3. *CSG strength and frictional resistance of the dam base*

The strength of the CSG required to evaluate the internal stability of the dam was obtained via uniaxial compression tests [8], and the test results are shown in Fig. 2. The CSG strengths of C60 and C80 are assumed to be 1.55 N/mm^2 and 2.30 N/mm^2, respectively, on the basis of these results. The frictional resistance coefficient at the dam-foundation interface used in the external stability study was set to 1.0.

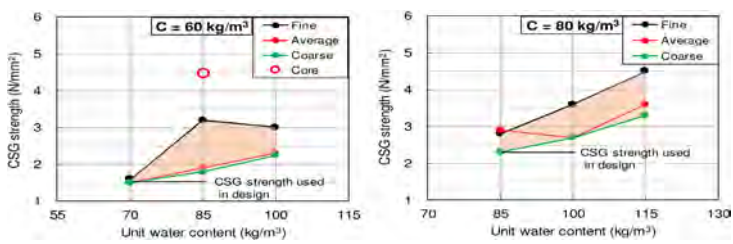

Fig. 2
Uniaxial compression test results of CSG
Résultats des tests de compression uniaxiale du CSG

2.3. Input ground motion

Here MCE ground motion was defined and used as the seismic motion at the dam base. To eliminate the influence of the frequency characteristics of the input ground motion on the analysis results to the fullest extent, the input ground motion was created

to conform to “the lower limit acceleration response spectrum for seismic performance verification” (shown in Fig. 3(b)) specified in the “Guidelines for Verification of Seismic Performance of Dams against Large Earthquakes (Draft) [4]” for the earthquake records obtained at Apporo Dam. Figure 3(a) shows the acceleration time history of the ground motion. The maximum acceleration is 320 cm/s^2. To ensure that the seismic motion at the base of each model dam is the same, the seismic motion shown in Fig. 3(a) was pulled back to the bedrock bottom of each analytical model and then input with a time increment of 0.01 s in the stream direction. The response of the coupled dam-reservoir-foundation system was analysed via the direct integration method.

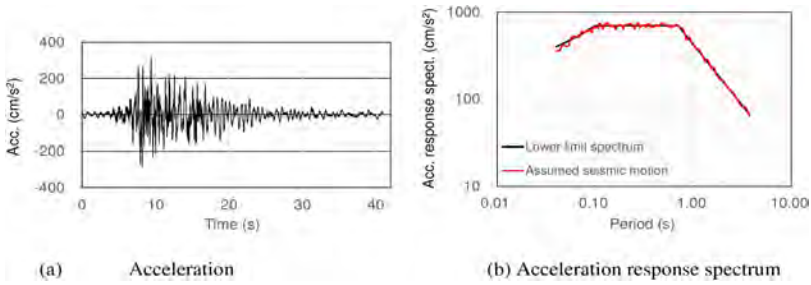

Fig. 3
Input ground motion
Mouvement imposé du sol

2.4. Effects of the slope and elastic modulus of the CSG on the seismic stability of dams

2.4.1. *Internal stability*

Since the tensile strength of the CSG is approximately 1/7 of the compressive strength according to laboratory tests [10], [11], the safety factor for each element in the analysis is the ratio of the CSG strength to the maximum stress generated during the earthquake, which is the larger value obtained by comparing the maximum tensile stress multiplied by 7 and the maximum compressive stress (including the static stress). That is, the safety factor F_e is calculated for each element, by using Eq. (1).

$$F_e(t) = \frac{\sigma_c}{\sigma_b(t)} \tag{1}$$

where σ_c is the CSG strength from the uniaxial compression test and is set separately for C60 and C80, as described in Section 2.2.3, and σ_b is the maximum stress generated during an earthquake, including the static stress for each element as described above.

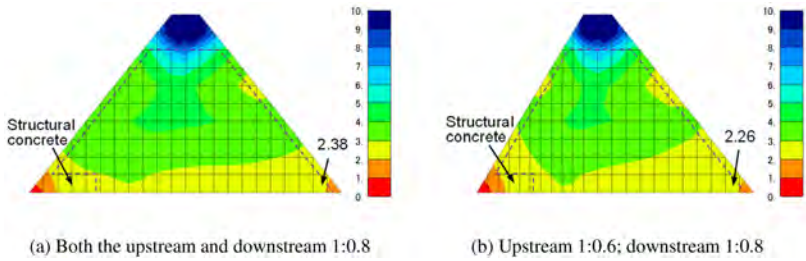

(a) Both the upstream and downstream 1:0.8 (b) Upstream 1:0.6; downstream 1:0.8

Fig. 4
Example of the distribution of the minimum safety factor (Elastic modulus of CSG (C60): 4,000 N/mm^2)
Exemple de répartition du facteur minimum de sécurité (Module élastique du CSG (C60): 4,000 N/mm^2)

As an example of the analysis results, Fig. 4 shows the distribution of the minimum safety factor of the dam body with an elastic modulus of 4,000 N/mm^2 and slopes of 1:0.8 for both the upstream and downstream faces and 1:0.6 for the upstream face and 1:0.8 for the downstream face. The lower the elevation is, and the closer to both the upstream and downstream faces at the same elevation the elements are, the smaller the safety factor becomes. At the upstream end of the dam base, the safety factor is less than 1 (the required safety factor is $F_e \geq 1.0$ when subjected to MCE ground motion). In trapezoidal CSG dams, structural concrete or watertight concrete is usually provided near the upstream end. The length of the structural concrete in the stream direction is assumed to be 1/6 of the width of the dam base from the upstream end, referring to the existing dams. Considering that protection concrete is placed on the upstream and downstream faces of the dam and that structural concrete is placed near the dam crest, no internal stability assessment was performed outside the area enclosed by the dashed line in Fig. 4. In most cases, the minimum value of the safety factor occurs at the downstream or upstream end of the dam base because of tensile stresses. The relationship between the minimum safety factor and the slope of the dam body in each case is shown in Fig. 5. In Fig. 5(a), the safety factor increases with the gentle slopes and the larger elastic modulus of the CSG, although the variation is rather large. The safety factor is maintained above 1.0 except for the case where the upstream and downstream slopes are both 1:0.5. In Fig. 5(b), almost the same trend can be found, but the effect of the upstream slope is diminished. This is presumably because the minimum safety factor occurs mostly at the downstream end of the dam base, except for the area of structural concrete. On the other hand, the distribution of the minimum safety factor in Fig. 4 shows that the safety factor is approximately 1 in a very limited range at the upstream and downstream ends of the dam base, whereas a safety factor of 2 or higher is obtained over a wide range. This suggests the possibility of increasing the unit cement content within a certain range at the

upstream and downstream ends of the dam base and conversely reducing the unit cement content used in the inner and upper areas of the dam body. Figure 5 shows that if the elastic modulus of the CSG is greater than 4,000 N/mm^2 and the slope is less than 1:0.6, the change in the safety factor due to the change in the elastic modulus of the CSG is not significant. In other words, if the elastic modulus of the CSG is greater than 4,000 N/mm^2, then there is no need to increase the unit cement content further. Figure 5(b) also shows that the increase in the safety factor is not significant even if the upstream slope is gentler than 1:0.6. In other words, an elastic modulus of the CSG of approximately 4,000 N/mm^2 and an upstream slope of 1:0.6 are considered optimal for both dam stability and economic efficiency.

From the internal stability mentioned above, it is considered possible to reduce the volume of the dam body and the total amount of cement used while ensuring the internal stability of the dam by flexibly adjusting the slope and the arrangement of the unit cement content.

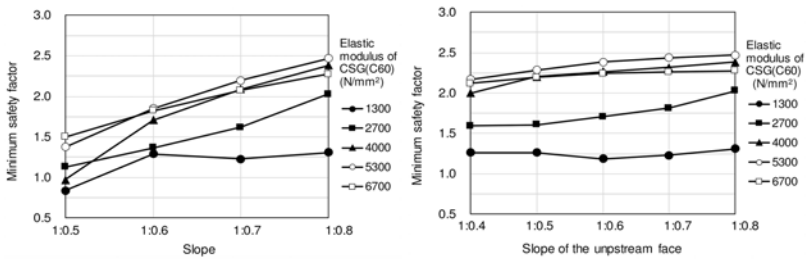

(a) Both the upstream and downstream slopes are changed

(b) Only the upstream slope is changed (Downstream slope 1:0.8)

Fig. 5
Relationship between the minimum safety factor and slopes
Relation entre le minimum facteur de sécurité et pentes

2.4.2. *External stability*

The external stability of the dam is evaluated via the vertical and shear stresses that are generated from time to time at the dam base during earthquakes by using the compressive condition of the dam base reaction force (to check stability against overturning) and sliding stability.

The compressive condition of the base reaction force is verified by checking the distribution of the vertical stresses at the time when the shear force on the dam base is at its maximum during an earthquake while considering the uplift pressure. The uplift pressure coefficient at the foundation drain hole (assumed to be 1/6 of the dam base from the upstream end) is 0.2, and at the downstream toe is 0. The vertical stresses at the dam base were analysed for each slope and elastic modulus

of the CSG. Figure 6 shows the results when the slope ratio is 1:0.8 as an example. For the same slope, the distribution of vertical stress on the dam base does not vary greatly with changing elastic modulus of the CSG, and tensile stress is generated in a very limited range at the upstream end. The tensile stress in this range is due mainly to the uplift pressure, but it is within the range of the structural concrete and is not expected to affect the external stability of the dam because the structural concrete and bedrock are unified, and adhesion of the dam base is expected. Figure 7 shows the relationship between the slope and the maximum tensile stress at the upstream end of the dam base. The figure shows that the gentler the slope is, the smaller the maximum tensile stress at the upstream end of the dam base. The maximum tensile stress at the upstream end of the dam base is inversely proportional to the slope. Nevertheless, the range of elastic modulus of the CSG and the range of slope variation considered do not pose a problem for the compressive condition of the dam base reaction force. Therefore, the dam slope and the elastic modulus of the CSG can be adjusted.

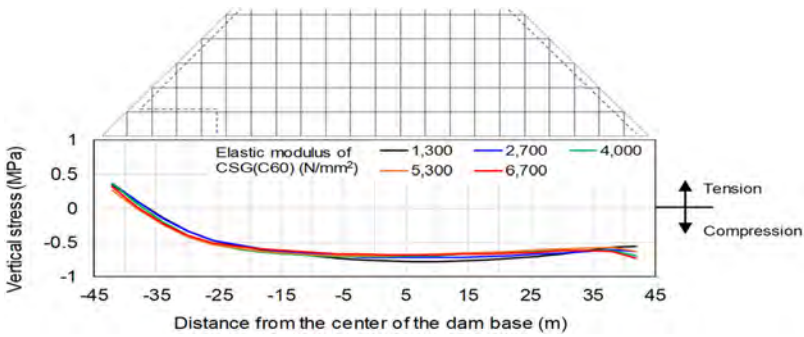

Fig. 6
Distribution of vertical stress at the dam base (Slope: 1:0.8)
Répartition des contraintes verticales à la base du barrage (Pente : 1:0,8)

Next, the sliding stability of the dam base was evaluated via the safety factor according to Eq. (2).

$$F_s(t) = \frac{\sum f(\sigma_{ni}(t) - u_i)l_i}{\sum \tau_i(t)l_i} \quad (2)$$

where f is the frictional resistance coefficient of the dam base, which is set to 1.0 on the basis of the results of shear tests [12] in an investigation audit in the dam foundation. $\sigma_{ni}(t)$ and $\tau_i(t)$ are the vertical stress and shear stress of each element of the dam base, respectively. l_i is the length of element i at the dam base in the stream direction, and u_i is the uplift pressure. However, when $\sigma_{ni}(t) - u_i$ is tensile, its

contribution to the resisting force is not included. Figure 8 shows an example of the sliding safety factor of the dam base (1:0.8 for both the upstream and downstream slopes) calculated via Eq. [2]. Figure 9 shows the relationship between the slope and the minimum sliding safety factor of the dam base. This figure reveals that the sliding safety factor of the dam base is maintained above 1.0 for all elastic moduli of the CSG and slopes set in this study (the required safety factor for MCE ground motion is Fs $\geq$ 1.0). Except for the cases of slopes steeper than 1:0.6 for the upstream slope, the sliding safety factor generally tends to be higher for the cases with gentler slopes and higher elastic moduli of the CSG. When both the upstream and downstream slopes are gentler than 1:0.6 or when the upstream slope is gentler than 1:0.6 with a downstream slope of 1:0.8, the minimum sliding safety factor is greater than 1.4. On the basis of above, the cross section of trapezoidal CSG dams can be designed more flexibly from the sliding stability of the dam base, with more emphasis on the reducing the construction cost.

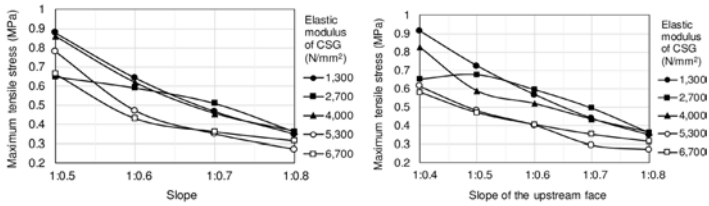

(a) Both the upstream and downstream slopes are changed

(b) Only the upstream slope is changed (Downstream slope 1:0.8)

Fig. 7
Relationship between the maximum tensile stress at the dam base and slopes
Relation entre le maximum contrainte de traction à la base et aux pentes du barrage

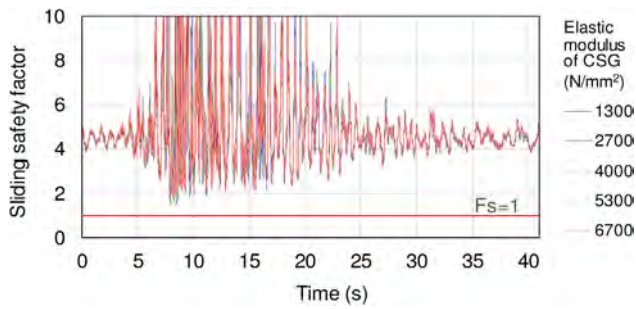

Fig. 8
Example of the sliding safety factor(Slope: 1:0.8)
Exemple du facteur de sécurité de glissement (Pente : 1:0,8)

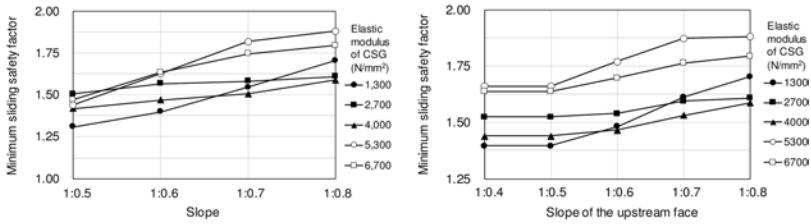

(a) Both the upstream and downstream slopes are changed

(b) Only the upstream slope is changed (Downstream 1:0.8)

Fig. 9
Relationship between the minimum sliding safety factor and slopes
Relation entre le minimum coefficient de sécurité de glissement et pentes

3. PROPOSAL AND VERIFICATION OF THE OPTIMIZED CROSS-SECTIONAL DESIGN

The slope of existing trapezoidal CSG dams in Japan thus far is 1:0.8 on both the upstream and downstream sides, and the unit cement content is divided according to elevation considering the generated stress. Among these dams, the Apporo Dam was undamaged despite being subjected to a large earthquake equivalent to the assumed MCE ground motion. On the basis of the investigations of the previous sections, the volume of the dam body can be reduced by adopting a steeper slope from the external stability in the cross-sectional design of a trapezoidal CSG dam. In terms of internal stability, the safety factor is small in a narrow area at the upstream and downstream ends of the dam base and near the surface of the upstream and downstream sides. This possibly addresses these issues by increasing the unit cement content within a limited area; conversely, it is possible to reduce the unit cement content in the inner or upper portions of the dam body. Thus, more economical construction of a trapezoidal CSG dam will be possible to ensure the safety of the seismic design by adjusting the arrangement of the slope and unit cement content in an appropriate manner. Referring to Figs. 4, 7, and 9, as an example, a dam is assumed with a downstream slope of 1:0.8, an upstream slope of 1:0.6, and an arrangement of the unit cement content in the cross section, as shown in Fig. 10, for ease of construction. The seismic stability and economic efficiency of the assumed dam are verified below.

3.1. Conditions for verification

3.1.1. *Validation items*

As in the current seismic design of trapezoidal CSG dams, the internal stability of the dam according to Eq. [1], the external stability according to Eq. [2], and the compressive condition of the dam base reaction force were evaluated. The conditions for calculating the stresses and the method for using the stresses in Eqs. [1] and [2] are as follows, with a safety factor of 1.0 or greater to satisfy the stability requirements.

(1) Calculate the static stresses at the normal water level and multiply them by 2.0.
(2) Multiply the stresses generated by the design seismic motion (equivalent to a maximum acceleration of 120 cm/s^2) by 1.5 (including the static stresses, without a foundation in the analytical model).
(3) Multiply the stresses generated by the verification seismic motion (equivalent to a maximum acceleration of 250 cm/s^2) by 1.2 (including the static stresses, without a foundation in the analytical model).
(4) Multiply the stresses generated by MCE ground motion by 1.0 (including the static stresses, with a foundation in the analytical model)

3.1.2. *Analytical model*

Figure 10 shows the analytical model of the dam body. However, as described in Section 3.1.1, the foundation shown in Fig. 1 is added to the model depending on the items considered. Table 4 shows the physical properties of the linear elastic material, including the protection and structural concrete as well as the foundation. The strength values of the CSG with unit cement contents of 60 kg/m^3 and 80 kg/m^3 are 1.55 N/mm^2 and 2.3 N/mm^2, respectively, whereas the CSG with a cement content of 100 kg/m^3 is 3.8 N/mm^2 based on the same type of material test.

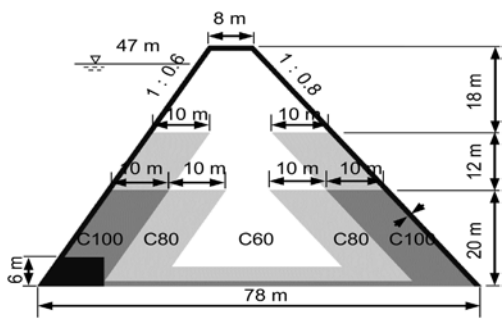

Fig. 10
Analysis model of the proposed CSG distribution
Modèle d'analyse de la répartition proposée de la CSG

For the boundary conditions of the model, the dam base was fixed (excitation plane) for the model without a foundation, and the side and bottom of the foundation were used as the viscous boundary (excitation position) for the model with a foundation.

Table 4
Material properties used in analysis

ITEMS	ELASTIC MODULUS (N/mm^2)	DENSITY (g/cm^3)	POISSON'S RATIO	DAMPING RATIO	STRENGTH (N/mm^2)
CSG	C60:4,000 C80:6,000 C100:7,500	2.1	0.25	5%	1.55 2.30 3.80
Protection and structural concrete	35,000	2.4	0.2	5%	5.00
Foundation	12,000	2.5	0.3	3%	–

3.1.3. *Input seismic motions*

The design seismic motion (Fig. 11(a)) and verification seismic motion (Fig. 11 (b)) were created by normalizing the maximum acceleration to 120 cm/s^2 and 250 cm/s^2 using the earthquake records at an existing trapezoidal CSG dam base as the earthquake ground motions at the base of the model dam. The MCE ground motions are those mentioned above in Fig. 3.

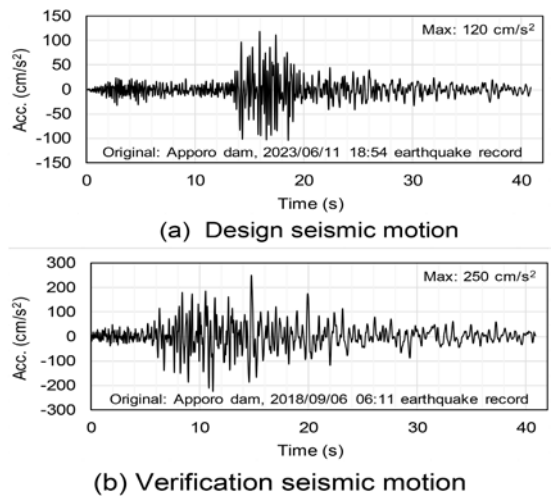

Fig. 11
Design and verification seismic motions
Conception et vérification des mouvements sismiques

3.2. Internal stability of the dam

The safety factors of the dam under the four conditions described in Section 3.1.1 are shown in Fig. 12. The model dam with the proposed slope and unit cement content (Fig. 10) exhibits a minimum safety factor of 1.12 for MCE ground motion but meets the internal stability requirement ($\geq$1.0) for all conditions.

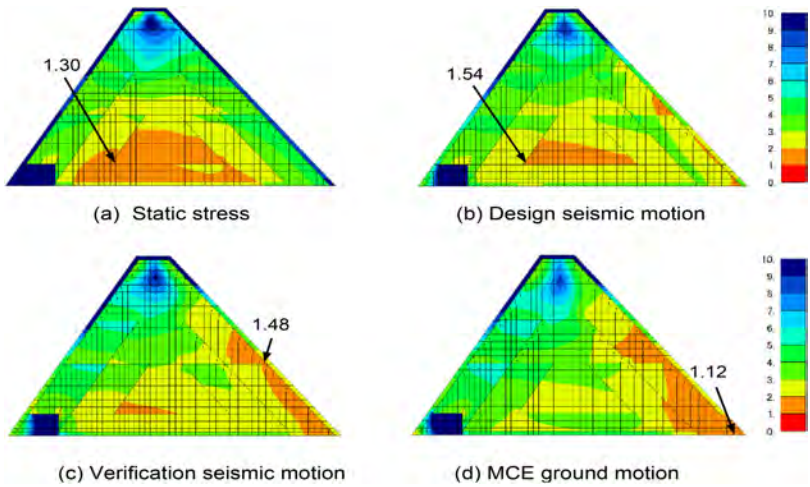

Fig. 12
Distribution of the minimum safety factor under specified conditions
Répartition du minimum facteur de sécurité dans des conditions spécifiées

3.3. External stability

The compressive condition of the dam base reaction force (to confirm stability against overturning) and sliding stability of the proposed model dam under four conditions set via the external stability evaluation method described in Section 2.4 were evaluated. Figure 13 shows the distribution of the vertical stress on the dam base obtained under each condition. The maximum tensile stress values are 0.49 N/mm^2, 0.91 N/mm^2, 1.20 N/mm^2, and 1.26 N/mm^2, in that order of static stress, design seismic motion, verification seismic motion, and MCE ground motion, although tensile stress occurs in a very narrow area near the upstream end of the dam base. Since the area near the upstream end is within the range of structural concrete, these tensile stress values are less than the dynamic tensile strength of dam concrete based on crack tension tests (up to 5 N/mm^2 can be expected) [13], and there are no problems

with dam stability. In addition, as shown in Fig. 13, the vertical stress changes abruptly from a tensile state to a compressive state along the dam base directly under the structural concrete. The structural concrete is assumed to be unified with the protection concrete in the analytical model, and the water pressure received upstream generates a clockwise rotational moment in the structural concrete, as well as the effect of a large change in uplift pressure. All the CSG behind the structural concrete is in compression, and there is no problem with the compressive condition of the dam base reaction force. Figure 14 shows the time history of the sliding safety factor of the dam base. The minimum sliding safety factor under the condition of MCE ground motion is 1.37, and conclusively, the sliding stability of the dam base is maintained under all conditions.

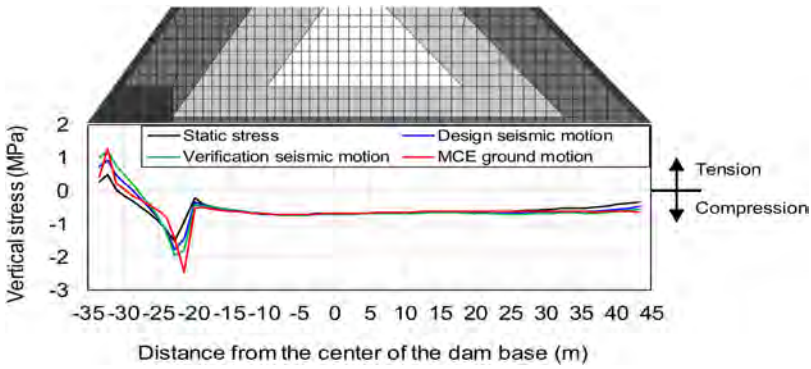

Fig. 13
Vertical stress distribution on the dam base
Répartition verticale des contraintes sur la base du barrage

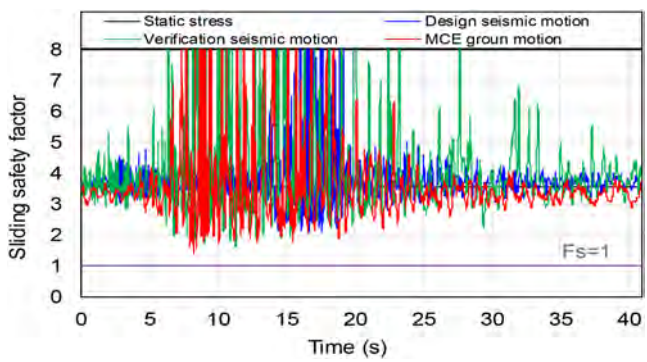

Fig. 14
Sliding safety factor of the dam base
Coefficient de sécurité de glissement de la base du barrage

3.4. Economic evaluation

The economic feasibility of the proposed model dam is discussed by comparing the dam volume and cement consumption with those of the current design, assuming that the dam is the same size as the existing trapezoidal CSG dams in Japan. Typically, the dam height is assumed to be 50 m, and the width of the crest is assumed to be 8 m. In the current design, the slope is 1:0.8 for both the upstream and downstream faces, and the unit cement content for the CSG is set as shown in Fig. 1. In the proposed model dam, the upstream and downstream slopes are 1:0.6 and 1:0.8, respectively, and the unit cement content in the cross section is shown in Fig. 10. The total volume of the dam is reduced by approximately 10.4%, and the total amount of cement used is reduced by approximately 11.3%. Although this is only an example, sufficient economic efficiency can be expected while ensuring dam safety through flexible design of the cross-sectional shape and unit cement content.

The above is an example of a rational cross-sectional design of a trapezoidal CSG dam. Via this model, a more economical dam construction that is adapted to the actual conditions of the dam site is proposed on the premise that the safety of the dam is ensured. On the other hand, in the model of the dam shown in Fig. 10, the construction width for placing the CSG with the same unit cement content is set at 10 m. However, in Japan, the minimum construction width of existing and currently constructed trapezoidal CSG dams is 20 m, so further study is needed from the viewpoint of rational construction.

4. CONCLUSIONS

The conclusions of this study are summarized as follows:

1) Seismic response analysis and evaluation of the seismic stability of a trapezoidal CSG dam with different slopes and different elastic moduli of the CSG against MCE ground motion were conducted. It was clarified that ensuring internal stability is relatively difficult. However, it was also confirmed that the cross-sectional design of current trapezoidal CSG dams ensures sufficient stability. Therefore, the dam volume and the total amount of cement used may be reduced while ensuring the seismic stability of the dam by flexibly adjusting the slope and the arrangement of the unit cement content.
2) As an example of a rational cross-sectional design, by appropriately setting the slope of the upstream and downstream faces to 1:0.6 and 1:0.8, respectively, and the unit cement content from 100 kg/m^3 to 60 kg/m^3 from the outside to the inside, from the base to the crest, the seismic stability of the dam can be maintained under the specified MCE ground motion. Moreover,

the dam volume can be reduced by approximately 10%, and the total amount of cement can be reduced by approximately 11%.

Although the rationalization of the design was examined from the perspective of analysis in this study, it is necessary to further investigate whether it is rational from the perspective of actual construction.

REFERENCES

[1] TADAHIKO FUJISAWA, HITOSHI YOSHIDA, NARIO YASUDA, TAKASHI SASAKI, ATSUMI HIGUCHI, TOSHIHARU FUETA. Trapezoidal CSG dam, *Dam Engineering*, Vol. 240, pp. 4–24, 2006 (in Japanese)

[2] TAKETO UOMOTO. Potential and issues of trapezoidal CSG dams, *Dam Engineering*, 21(4), pp. 232–241, 2011 (in Japanese).

[3] NARIO YASUDA, ZENGYAN CAO, SHUNPEI ANDO. Material properties and seismic evaluation of trapezoidal CSG dam based on actual seismic behavior, *Journal of JSCE*, A1, Vol.78, No.2, pp.254–268, August 2022

[4] RIVER BUREAU, MINISTRY OF LAND, INFRASTRUCTURE, TRANSPORT AND TOURISM (NILM). Guidelines for Seismic Performance Verification of Dams against Large-Scale Earthquakes (Draft) and its Commentary, March 2005 (in Japanese)

[5] HIROYUKI WATANABE, YOSHIAKI ARIGA, ZENGYAN CAO. Earthquake resistance of a concrete gravity dam evaluated with 3-D nonlinear analyses, *Proceedings of Japan Society of Civil Engineers*, No.696/I-58, pp.99–110, 2002 (in Japanese).

[6] FUSANORI MIURA, HIROSHI OKINAKA. Dynamic analysis method for 3-D soil-structure interaction systems with the viscous boundary based on the principle of virtual work, *Proceedings of Japan Society of Civil Engineers*, No.404/I-11, pp.395–404, 1989 (in Japanese).

[7] TADASHI HATANO. Examination of resonance of hydrodynamic pressure during earthquakes due to elasticity of water, *Proceedings of Japan Society of Civil Engineers*, No. 129, pp. 1–5, May 1966 (in Japanese).

[8] YUMITO NAKASE, JUNICHI SUGIMOTO, MASAAKI KONNO, TORU KAWAMURA. Stability of Apporo Dam against the 2018 Hokkaido Eastern Iburi Earthquake: Analysis of the behavior during the earthquake, *Dam Engineering*, Vol.415, pp.41–52, 2021 (in Japanese).

[9] JAPAN DAM ENGINEERING CENTER (JDEC). Trapezoidal CSG Dam Design, *Construction and Quality Control Technical Document*, June 2012 (in Japanese).

[10] TADAHIKO FUJISAWA. CSG Note No. 9 -Mechanical Properties of CSG-, *Dam Engineering*, No. 364, pp. 31–45, Japan Dam Engineering Center, January, 2017. (in Japanese).

[11] MASASHI KONDO, TAKASHI SASAKI, MASUHIRO BEPPU. Tensile Strength and Tension Softening Properties of CSG including Loading Rate Effect, *Journal of Japan Society of Civil Engineers*, E2, Vol.70, No.2, pp.232–251, 2014 (in Japanese)

[12] NARIO YASUDA, SEIZO MACHIYA, TAKASHI MIURA. In-Situ measurement of the friction resistance coefficient of the foundation rock of the Narusegawa Dam, *9th International Symposium on Roller Compacted Concrete (RCC) Dams and Cemented Material Dams*, Guangzhou, China, 2023.12

[13] YASUSHI ENOMURA, MASASHI KONDO, *ET AL.* Experimental study on dynamic tensile strength, fracture characteristics of dam concrete, *Technical memorandum of Public Works Research Institute*, No. 4326, 2016 (in Japanese).

Q.111 - R.16

COMMISSION INTERNATIONALE DES
GRANDS BARRAGES

VINGT-HUITIEME CONGRES DES
GRANDS BARRAGES
CHENGDU, MAI 2025

SEISMIC ANALYSIS AND REINFORCEMENT METHOD FOR SMALL GRAVITY DAM WITH HORIZONTAL CRACKS (*)

Hideaki KAWASAKI
Head Principal Engineer, JAPAN DAM ENGINEERING CENTER

Naoki IWATA
General Manager of Technical Headquarters, CHUDEN ENGINEERING CONSULTANTS

Teruo SUGA
Head of River and Erosion Control Department, CIVIL ENGINEERING CONSULTANTS

Ryouji KIYOTA
Manager of Analytical Solutions Department, CHUDEN ENGINEERING CONSULTANTS

JAPAN

SUMMARY

In Japan, guidelines outline the seismic performance criteria that dams must meet to withstand the maximum earthquake motion at their location in the future (maximum possible earthquake motion). For concrete gravity dams, these guidelines recommend evaluating seismic performance through nonlinear dynamic analysis, which accounts for the initiation and propagation of tensile cracks within the dam's body concrete, using an FEM model that assumes the dam body is initially

Analyse sismique et méthode de renforcement pour un petit barrage-poids avec des fissures horizontales

 DOI: 10.1201/9781003642428-119

crack-free. However, for small dams, this approach often fails to detect tensile cracks, as the stress induced by seismic activity is minimal. However, older dams, especially those with open horizontal construction joints, may not be as safe as they appear when the deterioration of the dam body is taken into account.

In this study, a two-dimensional FEM model is developed for the Senbon Dam (16 m high, 109 m long, Matsue City Waterworks Bureau), which exhibits leakage along its horizontal construction joints. The model incorporates continuous horizontal cracks as joint elements to simulate these conditions. Seismic response analysis was conducted by inputting the maximum possible earthquake motion into the model, aiming to evaluate the impact of horizontal cracks on the behavior during an earthquake. In addition, the effectiveness of PS anchors, installed to reduce the tensile stress within the dam body, was evaluated.

The results showed that even if the sliding safety factor for the block above the cracks is high enough to prevent sliding, rocking motion could still induce displacement along the horizontal cracks. This rocking motion also generates significant acceleration due to the impact. However, introducing compressive stresses into the cracks via PS anchors was found to nearly eliminate displacement along the horizontal cracks.

RÉSUMÉ

Au Japon, des lignes directrices définissent les critères de performance sismique que les barrages doivent respecter pour résister au mouvement sismique maximal à leur emplacement dans le futur (mouvement sismique maximal possible). Pour les barrages-poids en béton, ces directives recommandent d'évaluer la performance sismique par une analyse dynamique non linéaire, qui tient compte de l'apparition et de la propagation de fissures de traction dans le béton du corps du barrage, à l'aide d'un modèle FEM qui suppose que le corps du barrage est initialement exempt de fissures. Cependant, pour les petits barrages, cette approche ne permet souvent pas de détecter les fissures de traction, car la contrainte induite par l'activité sismique est minime. Cependant, les barrages plus anciens, en particulier ceux dont les joints de construction horizontaux sont ouverts, peuvent ne pas être aussi sûrs qu'ils le paraissent lorsque la détérioration du corps du barrage est prise en compte.

Dans cette étude, un modèle FEM bidimensionnel est développé pour le barrage de Senbon (16 m de haut, 109 m de long, Matsue City Waterworks Bureau), qui présente des fuites le long de ses joints de construction horizontaux. Le modèle incorpore des fissures horizontales continues comme éléments de joint pour simuler ces conditions. L'analyse de la réponse sismique a été effectuée en introduisant le mouvement sismique maximal possible dans le modèle, afin d'évaluer l'impact des fissures horizontales sur le comportement lors d'un tremblement de terre. En outre,

l'efficacité des ancrages installés pour réduire la contrainte de traction dans le corps du barrage a été évaluée.

Les résultats ont montré que même si le facteur de sécurité de glissement pour le bloc au-dessus des fissures est suffisamment élevé pour empêcher le glissement, le mouvement de basculement peut toujours induire un déplacement le long des fissures horizontales. Ce mouvement de basculement génère également une accélération significative due à l'impact. Cependant, l'introduction de contraintes de compression dans les fissures par le biais d'ancrages a permis d'éliminer presque totalement le déplacement le long des fissures horizontales.

1. INTRODUCTION

In Japan, the seismic performance of dams is typically assessed using governmental guidelines [1], which are designed to ensure that dams can withstand the maximum earthquake motion expected at their location in the future (referred to as the maximum possible earthquake motion). For concrete gravity dams, this seismic evaluation is conducted using nonlinear dynamic analysis by the finite element method (FEM). This method considers the formation and propagation of tensile cracks in the dam concrete, though it does not take into account pre-existing cracks within the dam body. The analysis results indicate that even if tensile cracks develop on the upstream face of the dam, the dam's overall stability and water storage capability are likely to be preserved, as long as the cracks do not extend through to the downstream face.

However, when horizontal gaps are present in the dam due to open horizontal construction joints, temperature-induced shrinkage, voids around aggregates, or tensile stresses from load action, these gaps can become vulnerable points during seismic events, potentially compromising the stability of the blocks above them. Kondo et al. [2] conducted a study simulating the behavior of a concrete gravity dam with a detached upper block using the discrete element method, informed by shaking table experiment results. The study demonstrated that the upper block tends to slip due to its rocking motion, which involves repeated rotational motion. Despite these findings, a method for evaluating the behavior and stability of dams with horizontal gaps has yet to be established.

This study evaluates the seismic performance of the Senbon Dam (height 16 m, length 109 m, operated by the Matsue City Waterworks Bureau), which exhibits leakage along its horizontal joints, by applying the maximum possible earthquake motion. The continuous horizontal gaps between the upper and lower faces of the dam body were modeled using joint elements, conservatively assuming complete separation.

For small dams, FEM-based dynamic analysis under maximum possible earthquake motion typically does not predict the formation of tensile cracks, as the stress generated by the earthquake is generally low. Preliminary analysis of the Senbon Dam, which did not account for existing cracks, indicated no significant seismic performance issues However, given the presence of horizontal gaps within the dam body, further analysis was conducted to assess the potential for horizontal cracks under seismic loading. Additionally, the study examined the effectiveness of PS anchor reinforcement in mitigating the development of these horizontal gaps.

In Japan, all dams must meet the seismic stability requirements outlined in the cabinet order on river structures [3]. Consequently, PS anchors were installed at the Senbon Dam to reinforce the dam body and ensure compliance with the mandated stability standards.

2. OVERVIEW OF THE SENBON DAM

The Senbon Dam, built in 1918, is a masonry concrete gravity dam, standing 16 m high and stretching 109 m in length. It was built to serve as a water source for Matsue City's water supply system. Fig. 1 shows a downstream view of the dam, where the left side is the overflow section, and the right side, featuring an intake tower, serves as the non-overflow segment. The intake tower, a semi-cylindrical structure, extends from the upstream face of the dam. The dam is founded on bedrock with a uniaxial compressive strength ranging from 10–30 N/mm^2. The concrete of the dam body, now approximately 100 years old, has a uniaxial compressive strength between 16 and 30 N/mm^2 and a unit weight of 20.3–23.2 kN/m^3. In some areas, this is slightly lower than the typical uniaxial compressive strength of ordinary unreinforced concrete.

As shown in Fig. 1(a), many leakages line by much efflorescences were observed on the high position downstream face of the non-overflow section. Additionally, within the intake tower's shaft, free lime deposits were observed at the same depth, indicating potential issues. A borehole investigation revealed low water tightness in the dam evidenced by the movement of pore water during drilling and browning in the borehole core, suggesting possible leakage pathways 5–7 meters below the dam's crest.

The cabinet order [3] regulates that no tensile stress should be generated on the upstream face of the dam body when seismic inertia forces are applied. However, at the Senbon Dam, tensile stresses were detected near the dam's base on the upstream face. To address this, reinforcement using PS anchors was implemented between 2019 and 2020, with a required design anchor force of 439.6 kN/m at the main section and a PS anchor pitch of 2.5 meters [4,5]. Though this

reinforcement significantly reduced the leakage in the non-overflow section, leakages still slightly remain 5–7 m below the dam's crest like as Fig. 1(b).

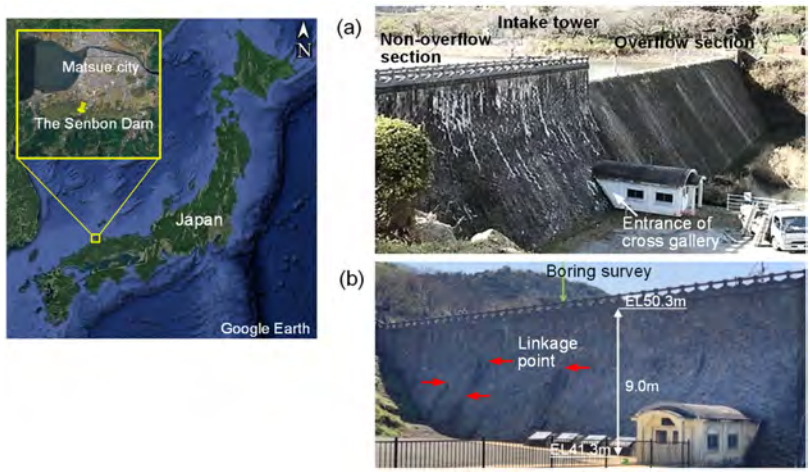

Fig. 1
Appearance of the downstream face of the Senbon Dam and leakage area in the non-overflow section
Aspect de la face aval du barrage de Senbon et de la zone de fuite dans la section sans débordement

3. ANALYSIS METHOD

The seismic performance of the dam prior to reinforcement with PS anchors was evaluated using dynamic two-dimensional FEM (2-D FEM) analysis following the guidelines [1] and applying the maximum possible earthquake motion. Initially, a 2-D FEM model of the dam was created, assuming an intact dam body without horizontal cracks (referred to as the no-crack model). This model did not include PS anchors. Seismic response analysis was conducted by subjecting this model to the maximum possible earthquake motion, and the resulting acceleration response of the dam body, as well as the sliding safety factor at the dam bottom, were calculated. In addition, stresses at the locations of horizontal cracks were evaluated, and the sliding safety factor was determined to assess the possibility of crack propagation.

Next, a second model was developed, incorporating horizontal cracks (the horizontal crack model). Joint elements were used to simulate slip and separation within the previously intact model. Horizontal cracks were conservatively assumed to be completely separated prior to the earthquake and assumed to have zero tensile strength. The earthquake response analysis for this model included calculating the extent of crack opening due to the rocking motion of the upper block along the horizontal crack, as well as determining the sliding safety factor and displacement along the crack. The acceleration response and tensile stresses at the dam bottom for the horizontal crack model were then compared with those of the no-crack model, enabling an evaluation of the effect of horizontal cracks on the behavior of the dam.

Furthermore, to evaluate the effect of hydrodynamic pressure from the reservoir on the behavior of the horizontal crack model, a separate analysis was performed with the reservoir removed. This allowed for an investigation into how hydrodynamic pressure affects the sliding safety factor and displacement along the horizontal cracks.

At the Senbon Dam, PS anchors were installed as a countermeasure to prevent tensile stress from developing at the upstream end of the dam body, using the seismic intensity method. The effectiveness of this PS anchor reinforcement was also examined.

4. ANALYSIS CONDITIONS

4.1. Analysis model

A 2-D FEM model was created for the non-overflow section on the right side of the dam, where leakage was observed, as shown in Fig. 2. The analysis area extended about twice the dam's height upstream and downstream and reached about the height of the dam below the anchor tips, with the foundation rock assumed to be uniformly distributed bedrock.

The analysis process consists of three steps: the first step is to set the initial stresses by calculating the self-weight; the second step is to apply the normal hydrostatic and sediment pressures to the dam's surface; and the third step is to perform a dynamic analysis using the maximum possible earthquake motion. The hydrodynamic pressure during the earthquake was automatically accounted for by modeling the reservoir with fluid elements during the seismic response analysis. When assessing the reinforcement effects of PS anchors, an additional step was included after the application of hydrostatic and sediment pressures. This step

involved simulating the installation and tensioning of the PS anchors, applying the tightening force to the horizontal cracks.

For the model's boundary conditions, Steps 1 and 2, where static loads are applied, utilized only the main body of the FEM model, excluding the free ground on either side. The bottom boundary was fixed, and the lateral boundaries were treated as vertical rollers. In Step 3, where seismic forces are dynamically applied, free-ground models were added on both sides, connected by dashpots to suppress the reflection of seismic motion at the lateral boundaries of the model. At the bottom boundary, dashpots were also installed to reduce seismic wave reflections.

The dam and bedrock were modeled using plane strain elements, the reservoir with fluid elements, and the anchor with truss elements. Horizontal cracks were represented using joint elements, allowing for slippage and separation.

The PS anchor, represented by truss elements, shared nodes with the plane strain elements in the ground at the anchor head and the bond length, ensuring that the dam, rock mass, and PS anchor acted as a cohesive unit. The design anchor force was applied as a concentrated load at the anchor head and as a distributed load along the bond length, as shown in Fig. 3.

The design anchor force was applied through concentrated and distributed loads, as shown in Fig. 3. Specifically, a concentrated downward load was applied at the anchor head, while an upward distributed load was applied along the bond length. This combination of forces generated compressive stress between the anchor head and the bond length.

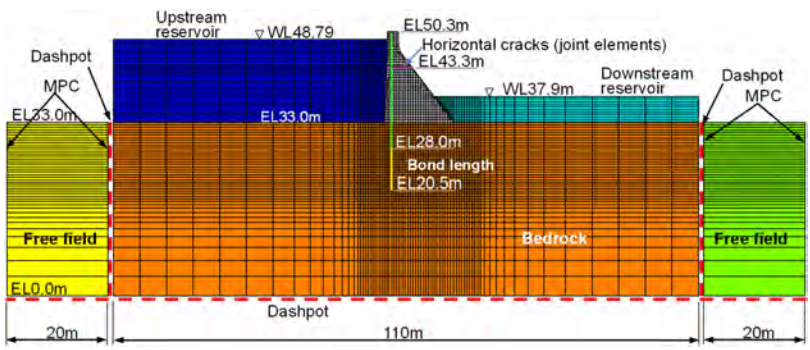

Fig. 2
2-D FEM analysis model for earthquake response analysis
Modèle d'analyse FEM 2-D pour l'analyse de la réponse aux tremblements de terre

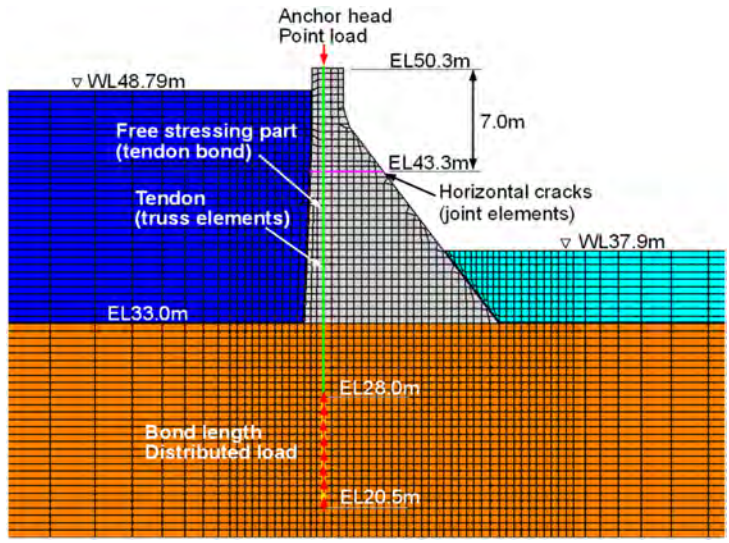

Fig. 3
Enlarged view of the 2-D FEM analysis model near the dam and PS anchor
Vue agrandie du modèle d'analyse FEM 2-D près du barrage et de l'ancrage PS

4.2. Physical properties for analysis

The physical properties used in the analysis of the dam concrete and foundation rock are shown in Table 1. The uniaxial compressive strength of the dam concrete ranges from 16 to 30 N/mm^2, and its unit weight ranges from 20.3 to 23.2 kN/m^3. The unit weight and Poisson's ratio for the dam concrete are based on average values from uniaxial compression tests, and the Young's modulus is derived from horizontal loading tests conducted downhole. The Young's modulus of the foundation rock mass was obtained from seismic surveys and uniaxial compression tests of rock cores. Damping ratios used in the analysis are standard values commonly employed in previous research.

Since horizontal cracks are represented using joint elements, it is necessary to define parameters such as shear strength, internal friction angle, tensile strength, and both vertical and shear spring stiffnesses. The shear strength was set to 1/10 (1.6 N/mm^2) of the minimum uniaxial compressive strength for the dam concrete. The internal friction angle was set to 30° [6], while the tensile strength was assumed to be zero, reflecting the potential separation of the joint surfaces.

The spring stiffness connecting the horizontal cracks was chosen to be as high as feasible to prevent overlap of dam elements on either side of the crack, but excessive stiffness can cause impact loads in the event of separation. Therefore, the spring stiffness of 1.0×10^6 kN/m^3 was selected based on rock discontinuity test results [7].

The PS anchor has a design anchor force of 1104 kN, with an anchor pitch of 2 m and a cross-sectional area of 11.096 cm^2. The Young's module for the anchor is 1.94×10^8 kN/m^2. In the FEM analysis model, the cross-sectional area and tension force, distributed according to the 2-meter pitch, were incorporated.

Table 1
Physical properties for analysis of dam concrete and bedrock

	DAM CONCRETE	BEDROCK
Unit volume weight γ (t/m3)	2.23	2.62
Poisson's ratio ν_d	0.26	0.33
Dynamic Young's Modulus E_d (MPa)	18,000	15,700
P-wave velocity V_p (m/s)	3,600	3,000
S-wave velocity V_s (m/s)	1,800	1,500
Damping constant h	0.05	0.05
Shear strength τ_0 (MPa)	1.6 (crack)	0.657
Friction angle φ (°)	30 (crack)	40

4.3. Input seismic motion

During the Western Tottori Prefecture Earthquake (M7.3) on October 6, 2000, which affected the area near the Senbon Dam, maximum horizontal and vertical accelerations of 5.29 m/s^2 and 4.85 m/s^2, respectively, were recorded at the base of Kasho Dam (a 46.4 meter high concrete gravity dam). These recorded accelerations exceeded the seismic motions defined in the governmental guidelines [1] and were therefore used as the reference seismic motions for the foundation of the Senbon Dam. Seismic motions for the model's foundation were derived through deconvolution analysis using a 2-D model and then input to the analytical model. The acceleration time history and acceleration response spectrum of the input earthquake motion are shown in Fig. 4.

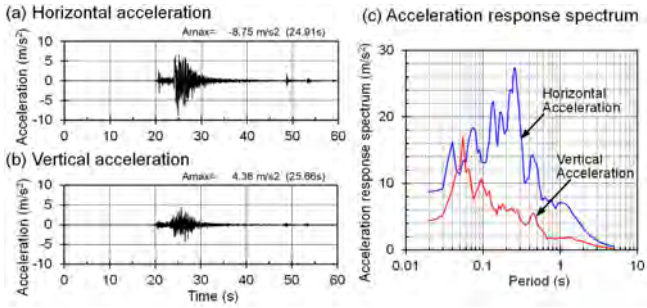

Fig. 4
Acceleration time history and acceleration response spectrum of input earthquake motion
Historique de l'accélération et spectre de réponse à l'accélération du mouvement sismique d'entrée

5. SEISMIC RESPONSE ANALYSIS RESULTS

5.1. Seismic behavior of a dam body without horizontal cracks

The distribution of the maximum horizontal and vertical accelerations of the dam body is shown in Fig. 5. The maximum horizontal acceleration at the dam's summit reaches 21.05 m/s^2, showing significant amplification as it progresses toward the top, with a sharp increase observed near the upper section, as shown in Fig. 5(a). The highest vertical acceleration recorded is 7.85 m/s^2, with greater values noted at the upstream face of the dam, as shown in Fig. 5(b). This increase is likely attributable to the rocking motion affecting the entire dam structure, including the foundation bedrock.

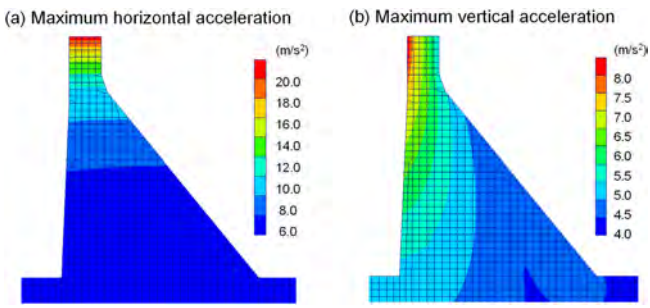

Fig. 5
Maximum acceleration distribution in the no-crack model
Distribution de la contrainte de traction maximale dans le modèle sans fissure

The distribution of maximum principal stress (maximum tensile stress) within the dam body is shown in Fig. 6. Seismic response analysis was performed for scenarios with and without hydrodynamic pressure to compare the effects on tensile stress development. At the dam's base, the maximum tensile stress is 1.13 MPa at the upstream end and 0.42 MPa at the downstream end. Tensile stress is present throughout nearly all of the dam's base, except for an element located 5 m from the upstream face near the center. However, these tensile stress levels are lower than the tensile strength of 1.6 MPa, which is 1/10 of the uniaxial compressive strength of the dam concrete, and thus are insufficient to cause cracking. In the absence of hydrodynamic pressure, the tensile stress at the upstream end reduces to 0.82 MPa, about 70% of the stress observed with hydrodynamic pressure. Tensile stress is absent in the range between 9 and 11 m from the upstream face of the dam. The minimum sliding safety factor for the foundation rock at the dam base is 2.10, ensuring stability against sliding.

At a horizontal crack located 10.3 m above the dam bottom, the maximum tensile stress recorded is 0.42 MPa at the upstream end and 0.27 MPa at the downstream end. No tensile stress is observed within 2–3 m from the upstream dam face. When hydrodynamic pressure is not applied, the tensile stress at the upstream end is 0.37 MPa, representing only a 10% reduction due to the shallow water depth relative to the horizontal crack location. For scenarios without horizontal cracks, the tensile stress remains well below the tensile strength, with a safety factor exceeding 4. However, when horizontal cracks are present, stress concentrations at the crack tips lead to significantly higher tensile stresses, which could potentially cause crack extension.

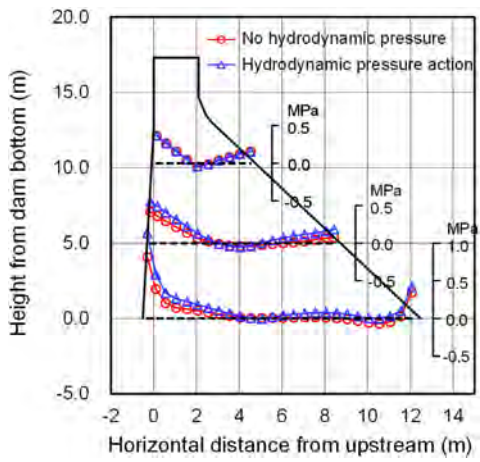

Fig. 6
Maximum tensile stress distribution in the no-crack model
Distribution de la contrainte de traction maximale dans le modèle sans fissure

5.2. Seismic behavior of dams with horizontal cracks

Fig. 7 shows the maximum horizontal and vertical acceleration distribution throughout the dam body, as well as the time history of acceleration at various points. The rocking motion of the block above the horizontal crack generates extremely high horizontal and vertical accelerations, exceeding 20 m/s^2 in the upper block. The maximum horizontal acceleration distribution shows a significant spike at the top of the horizontal cracks, likely due to the separation and impact resulting from the rocking motion. Similarly, the maximum vertical acceleration is notably high at both ends of the horizontal cracks, suggesting that the upper block edge experiences substantial impact during the rocking motion.

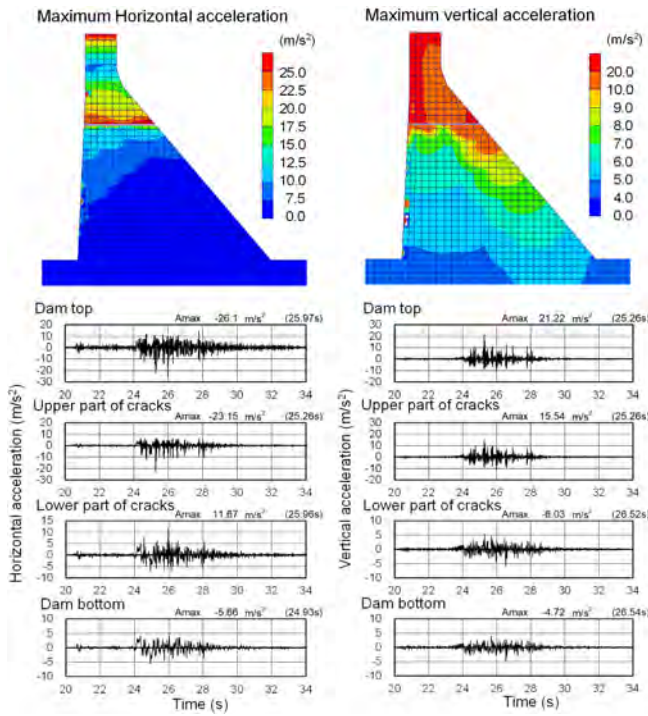

Fig. 7
Maximum acceleration distribution and acceleration time history in horizontal crack model
Distribution de l'accélération maximale et historique de l'accélération dans un modèle de fissure horizontale

When comparing the horizontal acceleration time histories at the top and bottom of the crack, there is a pronounced increase in acceleration at the top of the crack, with differing response waveforms. The time history of vertical acceleration also shows a sharp amplification at the top of the crack, there is a pronounced increase in a positive peak. This suggests that the load impacts the crack, causing significant amplification of acceleration at the top.

Fig. 8 shows the time histories related to horizontal displacement, sliding safety factor, and separation of the horizontal crack. As shown in Fig. 8(a), intermittent displacement was observed in the horizontal cracks between 24.4 and 29.2 s, culminating in a final displacement of 64.8 mm. Fig. 8(c) shows the aperture width at the upstream end of the crack, indicating that separation-induced apertures appeared between around 24.5 and 29.0 s. Despite the significant aperture width, the displacement during this period was relatively small. Fig. 8(d) through 8(f) compare the normal and shear forces acting on the entire horizontal crack and the detachment tip position for the internal from 24.4 to 27.0 s, when the displacement was observed. In Fig. 8(f), the detachment tip position represents the distance downstream from the upstream end of the crack. When separation occurs at the upstream end, the detachment tip position starts at 0.0 m and increases. Conversely, the separation at the downstream end begins at 4.77 m and decreases.

The time histories of the displacement shown in Fig. 8(e) and (f) exhibit a staircase pattern. This pattern corresponds to the upstream end separation caused by the rocking motion of the upper block, with shear forces generally exceeding 0.2 MPa. At 25.98 s, the maximum separation at the upstream end reaches 4.66 m, with only a minimal contact at the downstream end, resulting in negligible displacement at that time. Following this, a significant displacement occurs as the separation length decreases. Conversely, around 24.9–25.0 s, although the separation length is short, the displacement increases due to intermittent separation events.

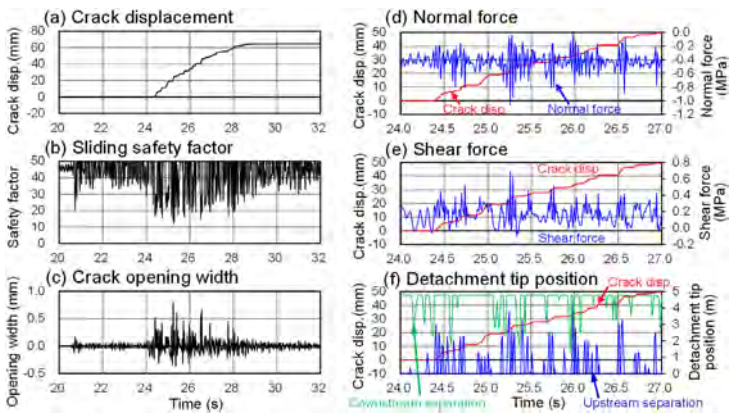

Fig. 8
Time history of crack behavior in horizontal crack model
Historique du comportement des fissures dans un modèle de fissure horizontale

Fig. 9 illustrates how shear force along the crack correlates with separation length, highlighting changes in displacement over 0.01 s intervals. Here, separation length is measured just before each 0.01-second mark of displacement to assess the impact of motion reversal. As shown in Fig. 9(a), displacement generally increases when the shear force is larger than 0.2 MPa. Figure 9(b) shows that larger separation lengths, indicative of larger rocking motion, result in greater displacement. Instances where displacement occurs despite zero separation length indicate that motion reversal and inertia continue to influence displacement even after the separation has closed.

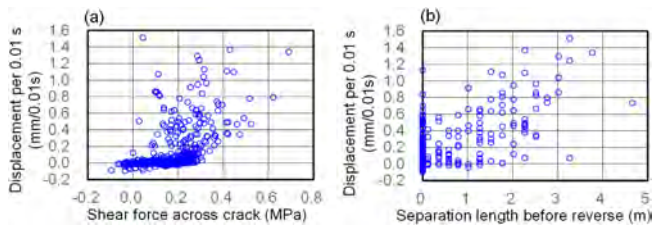

Fig. 9
Relationship between displacement every 0.01 s and shear force and separation length
Relation entre la quantité de déplacement toutes les 0,01 s, la force de cisaillement et la longueur de separation

The sliding safety factor measures the ratio between the shear resistance force, which is derived from vertical stress, and the shear force acting along the entire length of the horizontal crack. With an assumed shear strength of 1.6 MPa at the contact surface, the minimum sliding safety factor for the horizontal crack is 11.9. However, if the horizontal cracks are open, shear strength cannot be expected. If 50% of the horizontal cracks are open, i.e., if the shear strength is 50%, the minimum sliding safety factor decreases to 6.4. When the close contact is less than 28%, the safety factor drops below 4, and if there is no contact at all, i.e., zero shear strength, the safety factor falls below 1. This demonstrates that sliding safety is highly dependent on the degree of contact in the horizontal cracks. Given that the final displacement of 64.8 mm suggests that the cracks are mostly open, this indicates a significant loss of stability.

5.3. Impact of hydrodynamic pressure from the reservoir

To evaluate the effect of hydrodynamic pressure from the reservoir on the seismic response of the horizontal crack model, a dynamic response analysis was

conducted without incorporating reservoirs upstream and downstream of the horizontal crack model. Fig. 10 shows the acceleration response at the dam top, the displacement of horizontal cracks, and the time history of the detachment tip position. In the absence of hydrodynamic pressure, horizontal and vertical accelerations significantly decrease to about 12 m/s^2, and the sharp spikes in acceleration caused by the impacts of the upper block are removed. Crack displacement is also reduced to 23.0 mm because the number and size of upstream crack separations, which cause crack displacement, are reduced. These results indicate that rocking motion can still cause displacement along horizontal cracks in the dam with horizontal cracks, even with the reduction of reservoir water levels to prevent hydrodynamic pressure acting on the upper block above the cracks.

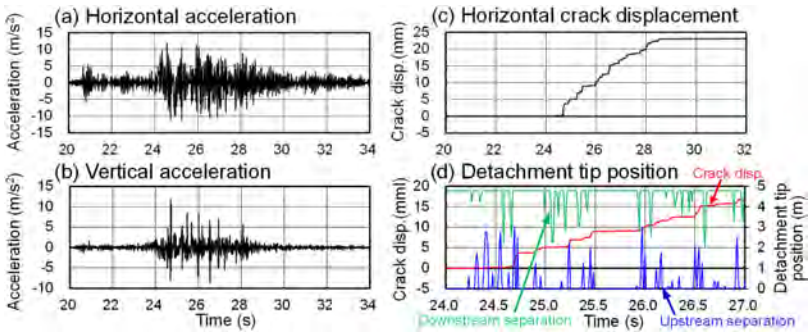

Fig. 10
Seismic response of dam top and cracks without hydrodynamic pressure
Réponse sismique du sommet du barrage et des fissures sans pression hydrodynamique

5.4. Effectiveness of PS anchor measures

By introducing compressive stress into the dam body through the use of PS anchors, the normal stress within the horizontal cracks increases, which helps to reduce rocking motion and prevent separation. To evaluate this effect, a seismic response analysis was conducted by incorporating the compressive forces from the PS anchors. Fig. 11 shows the maximum acceleration distribution in the dam body, the acceleration response at the dam top, horizontal crack displacement, and the time history of separation positions. The analysis shows that previously observed large spikes in acceleration, caused by rocking of the upper block above the crack, are significantly diminished, and the horizontal accelerations exceeding 20 m/s^2 near the crack are no longer present.

However, the maximum vertical acceleration distribution shows that while accelerations at the upstream face and top of the dam are reduced to about 10 m/s^2, a peak acceleration exceeding 20 m/s^2 is observed at the downstream end of the crack. This increased acceleration at the downstream end is attributed to separations occurring there. Since the PS anchors were placed upstream to alleviate tensile stress on the upstream side, they introduced significant compressive forces, effectively minimizing separations upstream. As shown in Fig. 11(f), separation at the upstream side of the crack was minimal, with only a 0.24 mm separation occurring around 25.24 s, followed by no further significant displacement or separation at the upstream side.

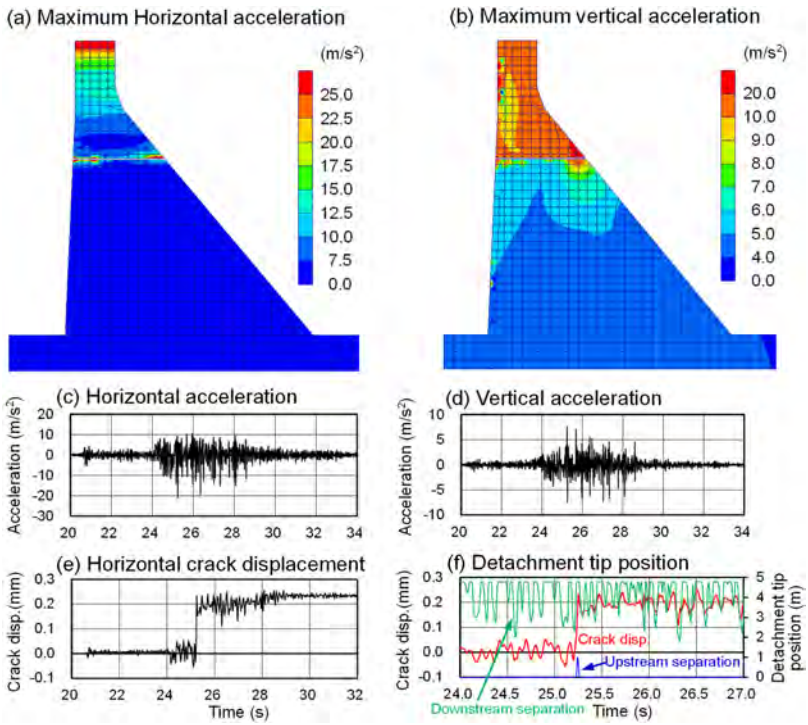

Fig. 11
Seismic response of dam body and cracks considering the effect of countermeasures by PS anchors
Réponse sismique du corps du barrage et des fissures en tenant compte de l'effet des contre-mesures par les ancrages PS

6. CONCLUSIONS

A 2-D FEM seismic response analysis was conducted on the Senbon Dam, which was considered to have developed horizontal cracks due to deterioration of horizontal joints, to assess the impact of these cracks on earthquake behavior. The analysis also evaluated the effectiveness of PS anchors installed to mitigate tensile stress in the dam body. As a result, the following findings were obtained.

(1) Even with a high sliding safety factor and no sliding displacement, continuous horizontal crack can still experience displacement due to rocking motion.
(2) The upper block generated extremely high accelerations during separation and impact caused by rocking motion.
(3) Displacement along horizontal cracks due to rocking motion occurs when the upstream separation length is significant and the shear force acting on the entire crack is relatively high.
(4) Lowering the reservoir water level to eliminate hydrodynamic pressure on the upper block reduces the displacement caused by rocking motion, although some displacement still occurs.
(5) Introducing compressive stress into the horizontal cracks using PS anchors effectively suppress upstream separation, resulting in minimal crack displacement.

The results of this study are considered conservative due to the assumption that the horizontal cracks were completely separated. Future research should focus on assessing the current degree of opening in these horizontal joints and determining whether these cracks might extend during earthquakes. In addition, this study did not take into account uplift pressure caused by water seepage into the cracks. The presence of uplift pressure could decrease the stability of the blocks, increase separation length, and potentially lead to greater displacement. It is necessary to evaluate the impact of uplift pressure from water infiltration during earthquakes, and to develop analytical methods that include this method. Furthermore, in cases of significant displacement, such as those in studied here, small deformation theory in FEM analysis may not be able to properly evaluate the displacement. Therefore, incorporating discontinuous continuum analysis could provide a more accurate evaluation.

Generally, small concrete gravity dams are less susceptible to seismic motion, however, many old dams often have horizontal gaps in the dam bodies. This study demonstrates that they may still pose risks due to crack-induced deterioration, when horizontal gaps are assumed in an old small concrete gravity dam. In these cases, it is quite important to check the seismic performance considered horizontal cracks, as this method does.

ACKNOWLEDGEMENTS

We would like to thank the Matsue City Waterworks Bureau for providing us with valuable materials for conducting this study.

REFERENCES

[1] RIVER BUREAU, MINISTRY OF LAND, INFRASTRUCTURE, TRANSPORT AND TURISM, JAPAN. Guidelines for seismic performance evaluation of dams against large earthquakes (draft). 2005. (in Japanese)

[2] KONDO M., KIRINASHIZAWA T., KOJIMA H. & YAMAGUCHI Y. Seismic performance evaluation of concrete dams considering ultimate stability of detached upper block. *Inter. Sympo. On Dams for a Changing World*, 2012.

[3] RIVER BUREAU, MINISTRY OF CONSTRUCTION, JAPAN, Cabinet Order on River Management Facilities and Structures. 1978. (in Japanese)

[4] KAWASAKI H., IWATA N., SUGA T. & FUKUMOTO H. Static Analysis on Senbon Dam Seismic Reinforcement by Post-tensioned Anchor. *Journal of Japan Society of Dam Engineers*, Vol.31(1), 2021. (in Japanese)

[5] TOKUNAGA A., OTA C., NAKAKUMA T. & KAWASAKI H. Refurbishment of the historically valuable masonry dam using prestressed anchors. *Symposium "Management for Safe Dams" - 91st Annual ICOLD Meeting*, 2023.

[6] PUL S., GHAFFARI A., OZTEKIN E., H*Ü*SEN M. & DEMIR S. Experimental Determination of Cohesion and Internal Friction Angle on Conventional Concretes. *Materials Journal*, Vol.114(3), 2017.

[7] YOSHINAKA R., YOSHIDA J., SASAKI T. & SASAKI K. Evaluation of mechanical design parameters of rock discontinuities considering scale effect. *Japanese Journal of JSCE*, C Vol.62(2), 2006.

Q.111 - R.17

COMMISSION INTERNATIONALE DES
GRANDS BARRAGES

VINGT-HUITIEME CONGRES DES
GRANDS BARRAGES
CHENGDU, MAI 2025

NONLINEAR ANALYTICAL MODELING OF DAM GATED PIER BASED ON EARTHQUAKE RECORDS (*)

Yoshiki MATSUOKA, Yusuke OTSUBO & Tsuyoshi ARIMITSU
Hydropower Engineering Center
THE KANSAI ELECTRIC POWER CO., INC
JAPAN

SUMMARY

The frequent occurrence of large scale earthquakes in recent years has necessitated the seismic evaluation of dams, spillway gate, and dam gated pier. In the seismic evaluation of dam gated piers, it is necessary to evaluate the contact behavior between dam gated pier and spillway gate during earthquakes, but conventional analytical modeling methods ignore the effects of overflow shape and stiffness of the dam body, and are not rational. Therefore, in this study, the effects of the overflow shape and stiffness of the dam body on the dam gated pier were evaluated, and appropriate restraint conditions were considered. The applicability was confirmed through a replicated analysis using seismic observation records of the actual dam, and a reasonable analytical model was proposed.

**Modélisation analytique non linéaire des piles inter-vannes de barrage basée sur des enregistrements sismiques*

 DOI: 10.1201/9781003642428-120

RÉSUMÉ

La fréquence de tremblements de terre majeurs ces dernières années a rendu nécessaire l'évaluation sismique des barrages, des vannes de déversement et des piles entre vannes. Dans l'évaluation sismique de ces piles, il est nécessaire d'évaluer le comportement de contact entre la pile et la vanne de l'évacuateur de crues pendant les tremblements de terre, mais les méthodes de modélisation analytiques conventionnelles ignorent les effets de la forme du débordement et de la rigidité du corps du barrage, et ne sont pas rationnelles. L'applicabilité a été confirmée par une analyse répétée utilisant les enregistrements d'observation sismique du barrage réel, et un modèle analytique raisonnable a été proposé.

1. INTRODUCTION

Among the structures attached to the dam, the spillway gate and the dam gated pier for supporting the gate play an important function in properly controlling the volume of flowing water in the reservoir. The dam gated pier is an integral of the main body of the dam and is a reinforced concrete (RC) structure with a slender profile in the dam axis direction. Many dam gated piers constructed before around 1955 used round rebar as the main rebar. The rebar ratio of the main rebar is designed to satisfy the standard at the time of installation. Moreover, the rebar ratio tends to be small because the concrete section needs to be large to install the gate opening/closing mechanism at the top end of the dam gated pier. The value is lower than the rebar ratio of 0.2 % specified in the current standard [1], and it's an "ultra-low rebar ratio". In addition, the base of the dam and dam gated pier have a characteristic overflow shape that hangs from the upstream side to the downstream side. Seismic evaluation of these facilities is necessary against the backdrop of the frequent large-scale earthquakes that have occurred in recent years [2]. In the seismic evaluation, it is necessary to evaluate not only the components of the dam gated piers and the spillway gates alone, but also the effects of contact behavior between the dam gated piers and the spillway gates during earthquakes. In the seismic evaluation of the dam gated piers, there is a method using a model with beam elements having M-φ characteristics. And using a model with three-dimensional solid elements has also been proposed [3], [4]. This proposal is intended solve problems in modeling using the M-φ model, such as the behavior of bending capacity drops rapidly after concrete cracks, and the adhesion stress-slip characteristics of round rebar, because dam gated pier is an RC structure consisting of using round rebar and ultra-low rebar ratio. On the other hand, in the seismic evaluation of spillway gates, there is a method using a model with shell elements [5]. However, these proposals are only intended for the evaluation of dam gated piers and the spillway gates as individual components, and not for the evaluation of contact behavior. For example, it is not impossible to model dam gated piers and the spillway gates simultaneously using a solid model and evaluate their

contact behavior during earthquakes, but the model becomes complicated and the calculation cost increases. In the seismic evaluation of the contact behavior between dam gated piers and spillway gates during earthquakes, a method using a model in which dam gated piers and spillway gates are coupled by means of beam and fiber elements with M-φ characteristics has been proposed [6]. However, the dam gated pier is considered to be affected by the characteristic overflow shape and the stiffness of the dam body, and these effects must be appropriately taken into account in the modeling, which have not been discussed in the previously proposed methods. In this study, a modeling method was validated to properly evaluate the contact behavior between the dam gated piers and spillway gates during an earthquake. In the verification, the effects of the overflow shape and the stiffness of the dam body on the load-bearing capacity of the dam gated piers were evaluated, and the conditions of the model restraints were examined. The applicability of the conditions of restraints was evaluated trough analysis using seismic observation records of the actual dam. This article is based on a study first reported in the proceedings of the Japan Society of Civil Engineers, Vol.70A [7].

2. CONSIDERATION OF THE RESTRAINT CONDITIONS OF THE BASE

The existing method of modeling dam gated pier with the M-φ model does not take into account the effects of overflow shape and stiffness of the dam body because the lower end is fully fixed. The solid model and M-φ model were used to study the effects of the overflow shape and the stiffness of the dam body on the load-bearing capacity of the dam gated pier. Note that the M-φ model is a model that sets nonlinear characteristics for beam elements that approximate the relationship between the bending moment and curvature of RC structures. Therefore, as a modeling method that incorporates these effects, the foundation springs utilized for calculating the natural period as outlined in the Technical Standards for Road Bridges [8] were established as the conditions of restraints, and the outcomes were evaluated through a comparison with a solid model. In this study, static nonlinear incremental loading analysis and nonlinear seismic response analysis were performed. The analysis programs used were DIANA for the solid model and TDAPIII for the M-φ model.

2.1. Static nonlinear incremental loading analysis

2.1.1. *Analysis model*

The analysis case is shown in Table 1, and the analytical model is shown in Fig. 1 and 2. The dam gated pier is 9.1 m in height, 1.5 m in width, and have a rebar ratio of 0.04 %. Three cases of solid models were used by changing the modeling

range and the condition of the base in order to grasp the influence of the overflow shape and the stiffness of the dam body. In Case 1, the dam gated pier is modeled using nonlinear element, and the dam body is modeled using linear element to account for the stiffness of the dam body. Furthermore, the base is a basic case in which the overflow shape is considered. Case 2 represents a variation of Case 1, wherein the overflow shape differs. Case 3 is a fully constrained model of the dam embankment portion of Case 2. The concrete was modeled as a solid element (primary element) and the rebar was modeled as a BAR-type embedded rebar element, with perfect adhesion between the rebar and concrete. For the nonlinear properties of concrete, the Maekawa-Fukuura Concrete Model [9] as a distributed cracking model was used for the cracking model. The elasto-plastic fracture model by Maekawa et al. [10] was used for the compressive properties before the concrete cracks, and after cracking the stress-strain relationship and tensile properties were set based on the Standard Specifications for Concrete [1]. For shear transmission characteristics on the cracking surface, a model was created, in which stiffness reduction obtained using the ratio between the shear strain on the cracking surface and cracking opening strain as a parameter was considered [11]. Conversely, the nonlinear characteristics of the rebar were set using a proposed equation for the skeletal curve of a single rebar calculated from the tensile test shown in the Standard Specification for Concrete [1] was used. The M-φ model was constructed using beam elements with nonlinear M-φ characteristics above the top of the overflow. Two cases of base restraint we employed a fully fixed configuration and a foundation spring. In this verification, the effects of the overflow shape and the stiffness of the dam body are modeled as foundation springs between the foundation structure and the ground. In particular, the model assumes that the dam gated pier (concrete frame), which is reinforced concrete above the overflow top elevation, is directly supported by the dam body (solid ground), which is dam concrete below the overflow top elevation (Fig. 3). In other words, the dam gated piers (concrete frame) are not rooted in, and the vertical, shear, and rotational springs from the dam body (solid ground) are assumed to exist at the lower end of the M-φ model. The foundation springs were calculated using the dynamic ground reaction coefficient formulas Eq.[1] and [2] and the foundation-structure-to-ground spring formulas Eq.[3], [4] and [5] for the bottom of the direct foundation, ignoring the rooting in of the surrounding ground.

Table 1
Analysis case

CASE	MODEL	SHAPE	CONDITION OF THE BASE	MODEL
Case 1	Solid	Overflow	Dam body (Linear elements)	Fig. 1 (a)
Case 2	Solid	No Overflow	Dam body (Linear elements)	Fig. 1 (b)
Case 3	Solid	No Overflow	Fully fixed	Fig. 1 (c)
Case 4	M-φ	-	Fully fixed	Fig. 2 (a)
Case 5	M-φ	-	Foundation spring	Fig. 2 (b)

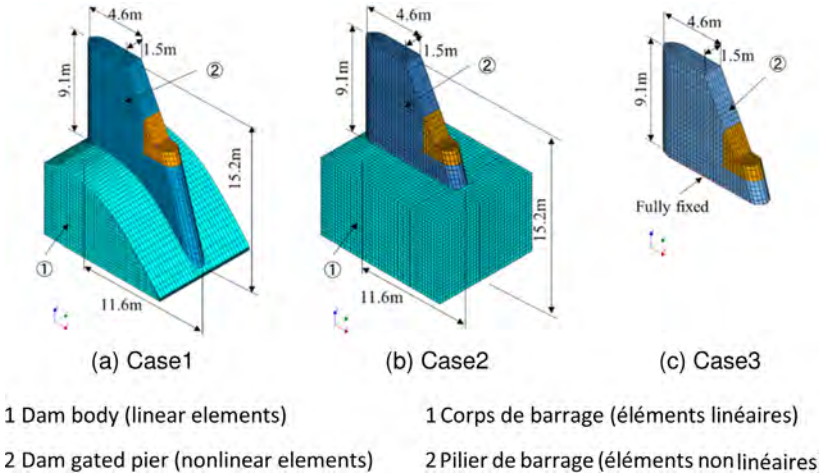

Fig. 1
Analysis model (Solid)
Modèle d'analyse (Solide)

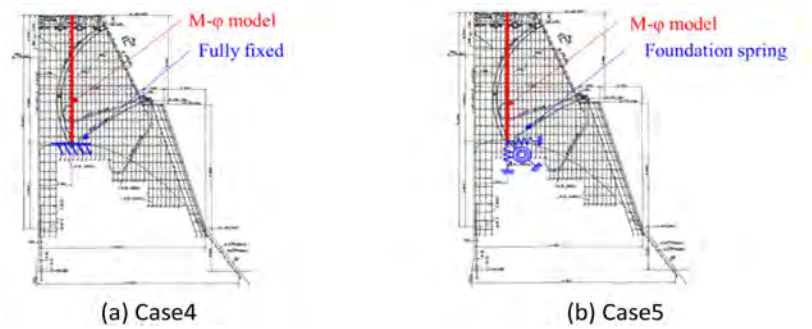

Fig. 2
Analysis model (M-φ)
Modèle d'analyse (M-φ)

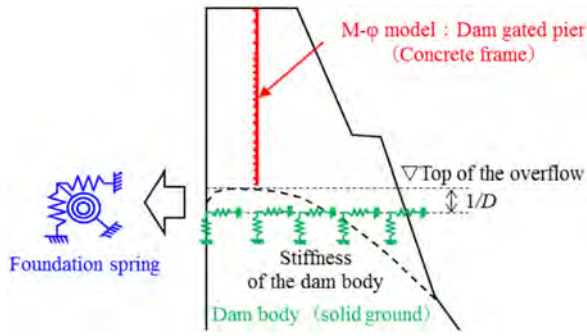

Fig. 3
Modeling overview of base foundation spring
Aperçu de la modélisation des ressorts de fondation.

$$K_{v0} = E_D / 0.3 \tag{1}$$

k_{v0}: Standard value of coefficient of vertical ground reaction (kN/m^2)

E_D: Dynamic deformation coefficient (kN/m^2)

$$K_v = k_{v0}(B_v/0.3)^{-3/4} \tag{2}$$

k_v: Coefficient of vertical ground reaction (kN/m^3)

B_v: Converted loading width of the foundation (m), which is calculated by Bv =$A_v^{1/2}$.

A_v: Loading area of foundation (m^2)

$$K_v = k_v \cdot A_v \tag{3}$$

K_v: Vertical spring (kN/m)

$$K_s = k_s \cdot A_v \tag{4}$$

K_s: Shear spring (kN/m)

k_s: Horizontal shear spring coefficient (kN/m^3), calculated by $\lambda \cdot k_v$.

λ: Ratio of 1/3 to the vertical ground reaction coefficient k_v.

$$K_\theta = k_v \cdot I \quad (5)$$

K_θ: Rotational spring (kN · m)

I: Sectional secondary moment (m^4)

The values and parameters used to calculate the foundation springs are shown in Table 2. In establishing the foundation spring, it is reasonable to consider a cross-section of the foundation shape situated between the top of the overflow section and the bottom of the overflow section. In this verification, the cross-section was set at a distance of D/10 downstream from the top of the overflow section, in accordance with the design method for overhanging piers [12]. D represents the width of the dam body in both the upstream and downstream directions.

Table 2
Values and the parameters

PARAMETER	UNIT	VALUES
Dynamic deformation coefficient	$\times 10^6$ kN/m^2	32.8
Standard value of coefficient of vertical ground reaction	$\times 10^6$ kN/m^2	190.3
Width (Dam axis)	m	1.524
Length (Upstream/downstream axis)	m	9.886
Loading area of foundation	m^2	15.066
Sectional secondary moment	m^4	2.916
Converted loading width of the foundation	m	3.882
Coefficient of vertical ground reaction	$\times 10^3$ kN/m^3	16,027
Horizontal shear spring coefficient	$\times 10^3$ kN/m^3	5,342
Vertical spring	$\times 10^3$ kN/m	241,461
Shear spring	$\times 10^3$ kN/m	80,487
Rotational spring	$\times 10^3$ kN·m/rad	46,734

The cyclic behavior of dam gated pier has been demonstrated in model tests simulating dam gated pier, wherein the yield bending strength (My) is found to be smaller than the crack bending strength (Mc) [13]. Obtaining a force balance in the analysis is challenging when the flexural capacity of concrete rapidly decreases after cracking occurs. Consequently, a provisional M-φ curve was employed for the M-φ model, without accounting for the capacity of cracks to bend (Fig. 4) [14]. The resilience model utilized in this analysis was the Takeda model [15], which is a widely used approach in the analysis of RC structures.

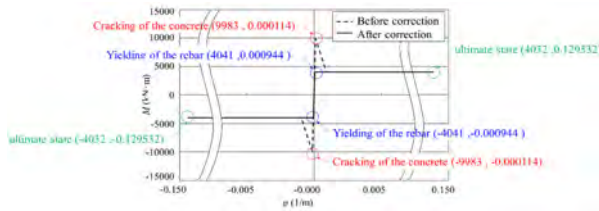

Fig. 4
Provisional M-φ curve
Courbe M-φ provisoire

The material properties of concrete and rebar are shown in Tables 3 and 4. The compressive strength, tensile strength, Young's modulus, and unit volume mass of the concrete were obtained from tests conducted on specimens extracted from actual dam gated pier and these are static values. Tensile fracture energy was calculated using Eq. [6] proposed by Horii et al [16]. The physical properties of the rebars were set to the values specified in JIS G 3112, and the strain hardening initiation strain was set to twice the strain value of deformed rebar specified in the Standard Specifications for Concrete [1] based on the trend of the material test results of SR235 round rebar R13 and SD345 deformed rebar D13 conducted in this research.

Table 3
Material properties of concrete

PARAMETER	UNIT	VALUES
Compressive strength	N/mm^2	37.167
Tensile strength	N/mm^2	3.727
Young's modulus	N/mm^2	3.22×10^4
Tensile fracture energy	N/mm	0.326
Unit volume mass	kN/m^3	23.83

Table 4
Material properties of rebar

PARAMETER	UNIT	VALUES
Yield strength	N/mm^2	235
Tensile strength	N/mm^2	380
Young's modulus	N/mm^2	2.00×10^5
Strain hardening initiation strain	-	0.028

$$G_f = (0.79\, d_{max} + 80) \times (f_c/10)^{0.7} \quad (6)$$

G_f: Tensile fracture energy (N/mm)

d_{max}: Maximum size of coarse aggregate (63.5mm in actual dam)

f_c: Compressive strength (N/mm^2)

2.1.2. *Loading conditions*

In the analysis, the weight of the dam gated pier and the hydrostatic pressure acting on the dam gated pier and the spillway gate were applied, and then the stress state was taken over. Thereafter, the seismic inertia force and seismic hydrodynamic pressure of the dam gated pier were gradually increased in accordance with the static seismic intensity. The seismic hydrodynamic pressure was incorporated into the model as an additional mass in the direction of the dam axis. The overburden loads on operating bridges, etc., were considered as additional mass at the top of the dam gated pier.

2.2. Analysis results

2.2.1. *Stress distribution at base of the dam gated pier*

The stress distribution at the base of the dam gated pier in Cases 1, 2 and 3 (kh = 0.4 before crack initiation) is shown in Fig. 5 and the maximum stress values are shown in Table 5. In all cases, stresses are observed in in the dam piers and in the entire cross-section at the base of the dam body. The neutral axes of compressive and tensile stresses in the axial direction of the dam are generally constant, and the cross-section resisting the load is uniform regardless of the overflow shape or the stiffness of the dam body. The reason for the wider compressive region downstream is that the fixed portion of the gate, where hydrostatic pressure acts is located on the downstream side. In all cases, the maximum compressive and tensile stresses are located on the upstream side. This phenomenon is believed to be a consequence of the dam gated pier's center of gravity being situated upstream, coupled with the fact that the upper load, such as the operating bridge, exerts its influence on the upstream side. Conversely, the maximum stress values for compression and tension exhibited notable differences among the cases (Table 5). This can be attributed to the differing stress values resulting from the varying vertical stresses at the base of the dam, which are influenced by the overflow shape and the stiffness of the dam body.The overflow shape and the stiffness of the dam body exert a minor influence on the stress distribution at the base, whereas they exert a significant impact on the maximum stress. Consequently, it is imperative to

incorporate this phenomenon into the M-φ model, taking into account the specific conditions of the base.

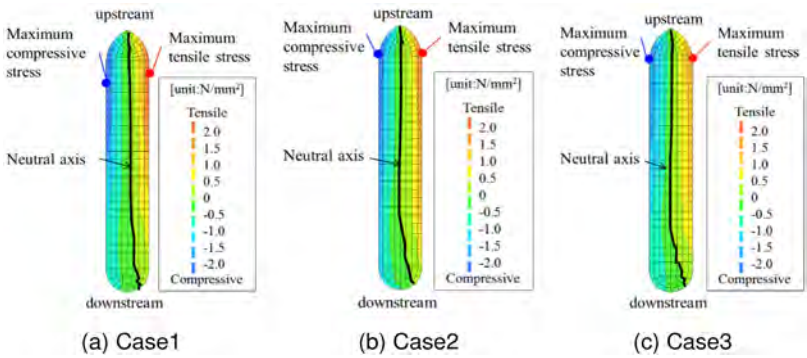

Fig. 5
Stress distribution at the base of the dam gated pier
Distribution des contraintes à la base du pilier de la digue

Table 5
Maximum stress value (N/mm^2)

CASE	COMPRESSIVE	TENSION
Case 1	3.09	2.40
Case 2	2.82	2.23
Case 3	2.03	1.62

2.2.2. *Horizontal seismic intensity-displacement relationship*

The relation between horizontal seismic intensity and displacement at the dam gated pier top position is shown in Fig. 6. A comparison of the stiffness up to displacement of δ=2 mm between Case 1 and Case 2 reveals that stiffness of Case 2 is larger than that of Case 1. This discrepancy can be attributed to the disparate impact of the overflow shape. The overflow shape is not represented in Case 2, resulting in a shorter effective height on the downstream side of the dam gated pier in comparison to Case 1. Furthermore, a comparison between Case 2 and Case 3 reveals that stiffness of Case 3 is larger than that of Case 2. This is attributable to the discrepancy in the impact of the stiffness of the dam body. In Case 3, the base is entirely fixed and thus not influenced by the stiffness of the dam body, resulting in increased stiffness. Moreover, a comparison of Case 4 and Case 5 reveals that

stiffness of Case 4 is larger than that of Case 5. This is due to the fact that Case 4 has the base constraint condition fully fixed, thus rendering the overflow shape and the stiffness of the dam body inconsequential. When comparing the solid model and the M-φ model cases, Case 5 is analogous to Case 1, and Case 4 is analogous to Case 3. In other words, the foundation spring situated at the base in the M-φ model is capable of simulating the impact of the overflow shape and the stiffness of the dam body. When the load-bearing capacity was defined as the maximum horizontal seismic intensity in a linear region, Case 1 and Case 2 exhibited a value of kh = 0.9 and kh = 1.0, respectively, and a gradual increase in displacement was observed following the attainment of the load-bearing capacity. In contrast, Case 3 had a value of kh = 1.2, resulting in a rapid increase in deformation following the attainment of the load-bearing capacity. This is due to the fact that the fissures at the base of the dam gated pier, which were caused by the bending deformation, spread rapidly across the entire cross-section in the absence of an overflow geometry. In other words, the load-bearing capacity and the extent of crack initiation are contingent upon the presence or absence of the overflow geometry. In contrast, the values for Case 4 and Case 5 are both 0.3, which are less than that observed in Cases 1, 2, and 3. This is due to the fact that the bending capacity is set at a uniquely low level in the provisional M-φ curves for Cases 4 and 5.

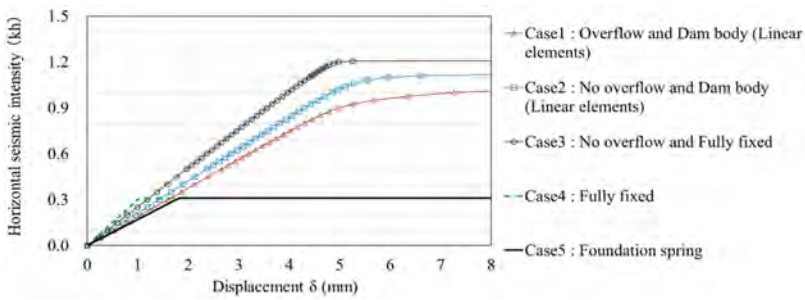

Fig. 6
Relation between horizontal seismic intensity and displacement
Relation entre l'intensité sismique horizontale et le déplacement

2.3. Nonlinear seismic response analysis

2.3.1. *Analysis model*

In order to confirm the effect of the foundation spring on dynamic behavior, a nonlinear seismic response analysis was conducted. The analysis models were constructed based on three cases. Case1 of the solid model and Case4 and 5 of the

M-φ model, as outlined in Section 2.1, were selected for analysis. The conditions, including material properties and nonlinear characteristics, remained unaltered. In the analysis, the permanent load of the dam pier's self-weight and the hydrostatic pressure acting on the dam pier and the flood discharge gate were applied, and the resulting stress state was inherited. Subsequently, seismic motion (in the dam axis direction) was input at the lower end of the model. In order to account for the dynamic water pressure, the range of water in contact with the side of the dam gated pier in the dam axis direction is applied as an added mass. The time step employed during the analysis was 0.005 seconds, and the Newmark β method (β = 1/4) was utilized for numerical integration. Moreover, Rayleigh damping was employed as the damping mechanism (Fig. 7).

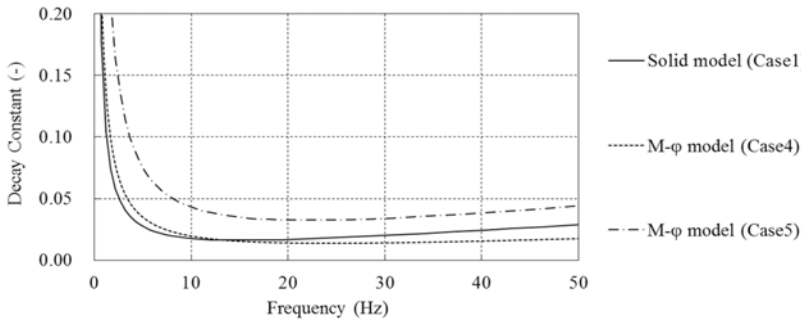

Fig. 7
Rayleigh-type damping
Amortissement de type Rayleigh

2.3.2. *Input seismic motion*

The acceleration time history waveforms of the input seismic motion used in the nonlinear seismic response analysis were prepared with reference to the lower limit spectrum for verification given in the Guidelines for Seismic Performance Verification of Dams against Large-scale Earthquakes (Draft) and its Commentary [2]. The phase characteristics are based on records of the Southem Hyogo prefecture earthquake in 1995 at the Hitokura dam. In order to verify the validity of the spectra for multiple earthquake ground motions, the entire spectrum was multiplied by a constant so that the maximum values of the acceleration response spectra were 500, 700, 850, and 1000 cm/s^2 (Fig. 8). The maximum acceleration of the input seismic motion at the lower end of the dam pier was 247, 346, 420, and 494 cm/s^2 , respectively. In this study, the input seismic motion was applied only in the direction of the dam axis, where the seismic behavior of the dam gated pier is dominant during an earthquake. The input seismic motion (maximum acceleration of 247 cm/s^2 as an example) is shown in Fig. 9.

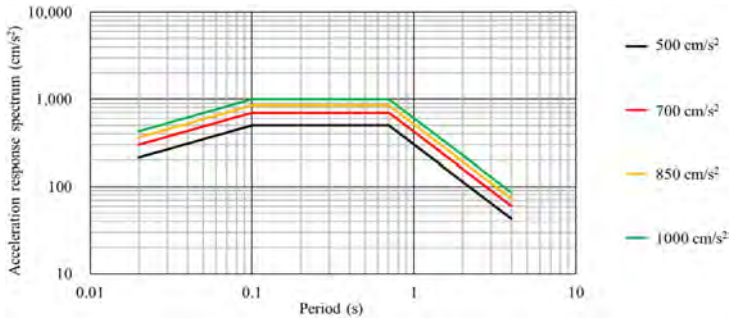

Fig. 8
The acceleration response spectra
Les spectres de réponse à l'accélération

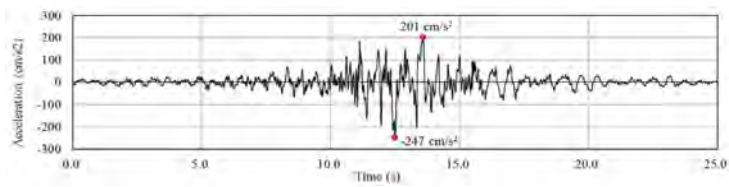

Fig. 9
The input seismic motion (maximum acceleration of 247 cm/s^2)
Le mouvement sismique d'entrée (accélération maximale 247 cm/s^2)

2.4. Analysis results

The relation between the maximum acceleration of the earthquake motion and the maximum response displacement (horizontal direction) of the dam gated pier top edge is shown in Fig. 10. Case 1 is in a linear state even at a maximum acceleration of 494 cm/s^2. On the other hand, Cases 4 and 5 are in a linear state up to a maximum acceleration of 247 cm/s^2 and then in a nonlinear state. This is because Cases 4 and 5 primarily set the bending strength to be small using the provisional M-φ curves, while Case 1 accurately models the nonlinear properties of the material, and the effects of the modeling differences are apparent. Focusing on the response displacement at the maximum seismic acceleration of 247 cm/s^2, there is a difference in initial stiffness between Cases 1 and 4. On the other hand, the initial stiffness of case 5 and case1 is almost the same. In other words, the foundation spring is able to reproduce a behavior that takes into account the effects of the overflow shape and the stiffness of the dam body.

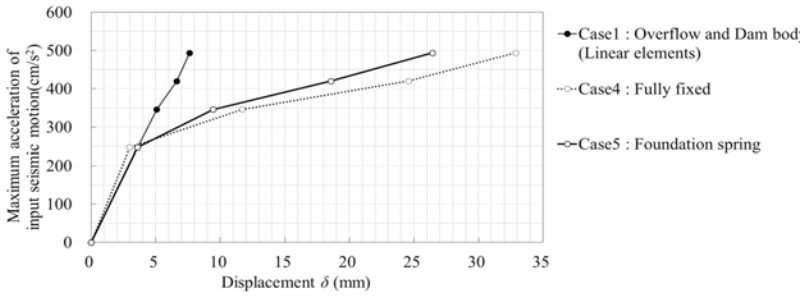

Fig. 10
Relation between the maximum acceleration of the seismic motion and the maximum response displacement of the dam pier top edge
Relation entre l'accélération maximale du mouvement sismique et le déplacement maximal de la réponse de l'arête supérieure de la pile du barrage

3. APPLICABILITY VERIFICATION USING EARTHQUAKE OBSERVATION RECORDS

In this verification, a reproduction analysis was performed using earthquake observation records of an actual dam to verify the applicability of the foundation spring. Note that the actual dam gated pier used in this verification is different from the actual dam gated pier used in Chapter 2.

3.1. Earthquake observation records

The dam subjected to seismic observation is a 32.2 m high gravity concrete dam located in Nagano Prefecture, Japan. Seismographs were installed on the dam body, dam gated pier, and the spillway gate for earthquake observation. The arrangement of the seismographs is shown in Fig. 11. The earthquakes used in the reproduction analysis were those in which a greater seismic response was confirmed at the dam gated pier than at the dam body (inspection gallery). The maximum accelerations recorded by each seismograph are shown in Table 6. The earthquake studied was a magnitude 5.6 earthquake that occurred in southern Nagano Prefecture at 7:02 a.m. on June 25, 2017. At the dam gated pier, accelerations of up to 342 cm/s^2 in the dam axis direction and up to 197 cm/s^2 in the upstream and downstream directions occurred, and the responses were approximately 4.9 and 2.7 times larger than those of the dam embankment (inspection gallery), respectively.

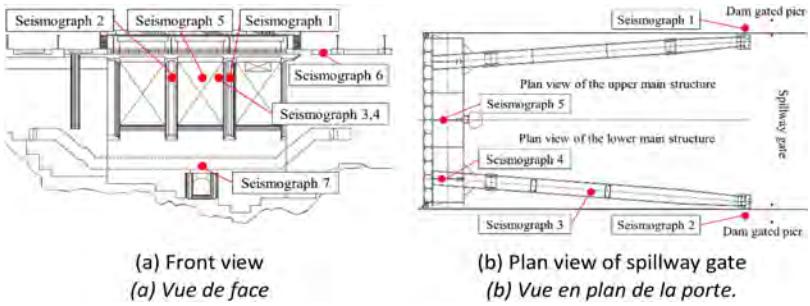

Fig. 11
Arrangement of the seismographs
Disposition des sismographes

Table 6
Maximum accelerations (cm/s^2)

SEISMOGRAPH LOCATION	DIRECTION		
	UPSTREAM AND DOWNSTREAM	DAM AXIS	VERTICAL
1 Dam gated pier (right bank)	170	309	119
2 Dam gated pier (left bank)	197	342	106
3 Gate pillar center	479	291	481
4 Gate main girder end	480	471	437
5 Gate main girder center	471	470	480
6 Dam body (top)	233	199	115
7 Dam body (inspection gallery)	72	70	77

3.2. Conditions for reproduction analysis

In this verification, the dam gated pier and the spillway gate were modeled using a previously proposed method [6]. The reproduction analysis model is shown in Fig. 12(a). The dam gated pier was modeled using beam elements with nonlinear M-φ characteristics to take into account the nonlinear characteristics of RC structures, as in Chapter 2. The dam gated pier has an operating bridge on its top edge, and there are a hoist and an operation panel to operate the spillway gate. In this verification, these were modeled as additional masses at the top of the dam gated pier. On the other hand, the spillway gate was modeled using nonlinear fiber elements. The steel material used for the spillway gate was elastoplastic material, and

the nonlinear characteristics were given a bilinear stress-strain relationship as shown in Fig. 12(b). A bilinear moving hardening law [17] was used for the restoring force model.

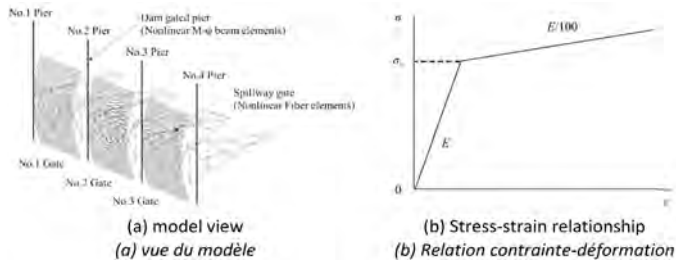

Fig. 12
Reproduction analysis model
Modèle d'analyse de la reproduction

The boundary conditions of the reproduction analysis model are shown in Fig. 13. Nonlinear springs were set on the sides of the spillway gate, taking into account 5mm of free space between the gate and the dam gated pier. Nonlinear springs were also set at the lower end of the spillway gate.

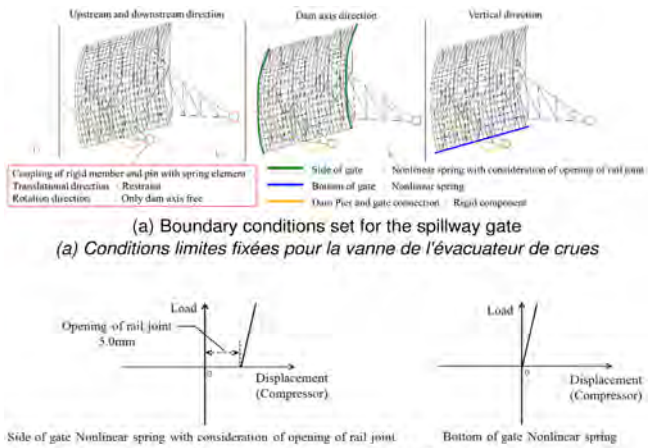

Fig. 13
Boundary conditions of the reproduction analysis model
Conditions limites du modèle d'analyse de la reproduction

The load conditions are shown in Fig. 14. The dam gated pier was set up with hydrodynamic pressure in the upstream and downstream directions and in the dam axis direction as additional masses. The spillway gate was set up with hydrodynamic pressure in the upstream and downstream direction only as an additional mass. The hydrodynamic pressure in the upstream and downstream directions acting on the spillway gate takes into account the effect of the gate door body is setback on the downstream side [14]. Waveforms observed at the dam body (inspection gallery) were input to the dam gated pier base to evaluate the response of the dam gated pier.

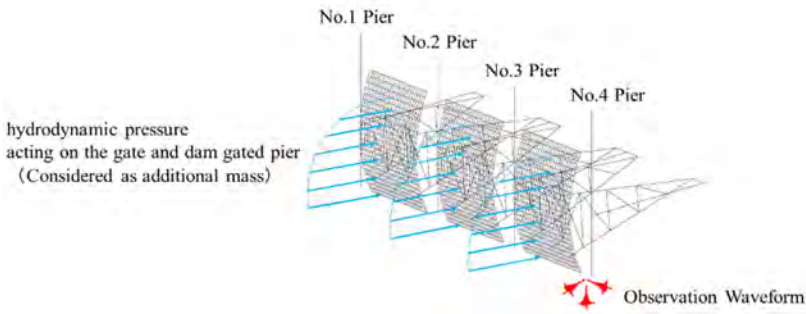

Fig. 14
Boundary conditions of the reproduction analysis model
Conditions limites du modèle d'analyse de la reproduction

The material properties of concrete and rebar for the dam gated pier are the same as in Chapter 2. The material properties of steel for the spillway gate are shown in Table 7. These values were obtained from past tests using cores taken from the structures in question or from general values given in the specifications for road bridges [8].

Table 7
Material properties of steel for the spillway gate

	UNIT	COMPONENT	
		ENGINE FRAME	PRESSURE RECEIVER
MATERIAL	**-**	**SS400**	**SM400**
Unit volume mass	kN/m^3	91.0	
Young's modulus	N/mm^2	2.06×10^5	
Poisson's ratio	-	0.206	
Yield strength	N/mm^2	235	

The analysis program used was TDAP III. The analytical cases were a case with fully fixed restraint conditions at the base of the dam gated pier (Case 1) and a case with foundation springs (Case 2). The values and parameters used to calculate the foundation springs are shown in Table 8.

Table 8
Values and the parameters

PARAMETER	UNIT	VALUES	
		DAM AXIS	UPSTREAM DOWNSTREAM
Dynamic deformation coefficient	$\times 10^6$ kN/m^2	26.7	26.7
Standard value of coefficient of vertical ground reaction	$\times 10^6$ kN/m^2	89.0	89.0
Dimensions (Dam axis)	m	2.5	2.5
Dimensions (Upstream/downstream axis)	m	23.317	23.317
Loading area of foundation	m^2	58.293	58.293
Sectional secondary moment	m^4	30.361	2,641
Converted loading width of the foundation	m	7.635	7.635
Coefficient of vertical ground reaction	$\times 10^3$ kN/m^3	7,855	7,855
Horizontal shear spring coefficient	$\times 10^3$ kN/m^3	2,618	2,618
Vertical spring	$\times 10^3$ kN/m	457,867	457,867
Shear spring	$\times 10^3$ kN/m	152,622	152,622
Rotational spring	$\times 10^3$ kN · m/rad	238,472	20,744,500

3.3. Analysis results

The time history waveform of response acceleration and the frequency response characteristic obtained by seismograph 1 (right bank of dam gated pier) are shown in Fig. 15. The main motion in the observation record occurs around 10-12 sec, while the main motion in Case 1 also occurs around 10-12 sec. However, the peak acceleration tends to be smaller than that of the observation record. On the other hand, the peak of acceleration in Case 2 tends to improve compared to Case 1.The dominant frequency in the observed record occurs around 19 Hz, while Case 1 has a dominant frequency around 22 Hz. On the other hand, the dominant frequency in Case 2 occurs around 19 Hz, which is

reproduced better by foundation springs. In the observation record, a large amplification occurs around 10 Hz. On the other hand, in the replicated analysis, the amplification occurs around 5 Hz in both Case 1 and Case 2. This is due to the location of the seismograph installed at the dam gated pier, which is close to the fixed pin of the spillway gate. The frequency response characteristics of the spillway gate in the observation records show that the dominant frequency occurs around 11 Hz (Fig. 16). In addition, the result of past vibration excitation experiments have confirmed that the frequency of the spillway gate is dominant at around 10 Hz [18]. The results suggest that the foundation springs improve the reproducibility of the actual seismic behavior and are applicable. These results were obtained for an earthquake of approximately 70 cm/s^2 at the dam base (inspection gallery). It is desirable to continue the seismic observation in the future, and to revalidate the results when further records of large scale earthquakes are obtained.

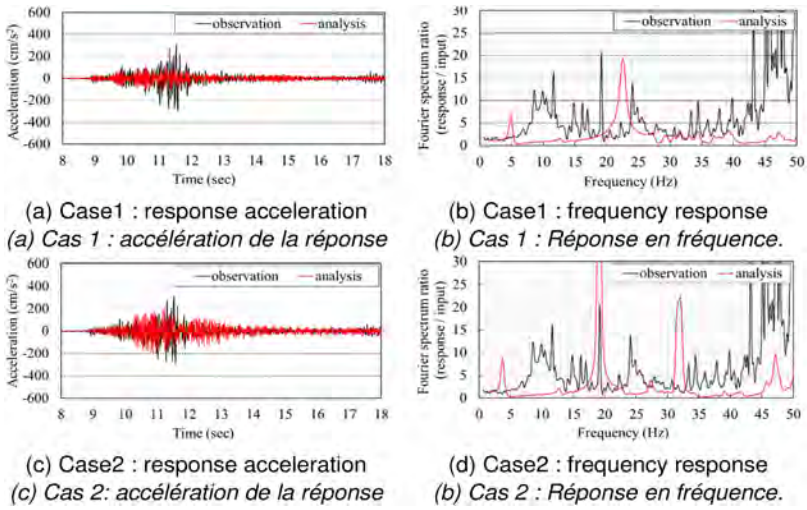

Fig. 15
Time history waveform of response acceleration and the frequency response characteristic at seismograph 1 (right bank of dam gated pier)
Forme d'onde de l'accélération de la réponse et réponse en fréquence du sismographe 1 (rive droite de la pile du barrage)

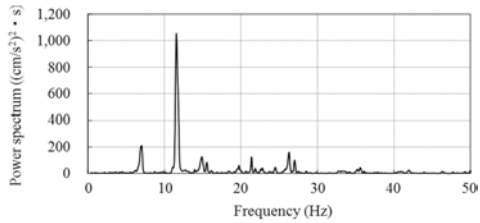

Fig. 16
Frequency response characteristics of the spillway gate
Réponse en fréquence des vannes de l'évacuateur de crues

4. CONCLUSIONS

This study was conducted to examine the modeling of the dam gated pier with the aim of developing an analytical model to appropriately evaluate the contact behavior between between the dam gated pier and the spillway gate. The following is a conclusion of the findings and proposed modeling methodology.

The results of the static nonlinear incremental loading analysis and nonlinear seismic response analysis using a solid model show that the overflow shape and the stiffness of the dam body affect the bearing capacity, stiffness, and generated stress of the dam gated pier.

The foundation springs for calculating the natural period as shown in the road bridge specifications can reproduce the behavior considering the effects of overflow shape and stiffness of dam body.

The results of the analysis using seismic observation records of the actual dam showed that the foundation springs improved the reproducibility of the seismic behavior of the dam gated pier.

In the evaluation of the contact behavior between the dam gated pier and spillway gate, setting the foundation spring as a constraint condition at the base of the M-φ model of the dam gated pier enables a reasonable evaluation, taking into account the effects of the overflow shape and stiffness of the dam body.

ACKNOWLEDGEMENTS

We would like to express our sincere appreciation to Professor Nakamura of the Graduate School of Nagoya University, Dr. Nishiuchi and Dr. Sugimoto of the

Central Research Institute of the Electric Power Industry, and Dr. Uchida and Dr. Nakanishi of the NEWJEC Co., Ltd. for their invaluable cooperation in this research.

REFERENCES

[1] JAPAN SOCIETY OF CIVIL ENGINEERS. *Standard Specification for Concrete Structures [Design]*, 2017(in Japanese).

[2] RIVER BUREAU, MINISTRY OF LAND, INFRASTRUCTURE, TRANSPORT AND TOURISM. *Guidelines for Seismic Performance Verification of Dams against Large-Scale Earthquakes (Draft) and its Commentary*, 2005(in Japanese).

[3] FUJITA M., SATO N., TOMIDA N., KUKIDOME T. Application of Nonlinear Dynamic Analysis Method of 3D Solid Model for Seismic Performance Verification of Dam Columns, *Dam Engineering, 27*(3), pp. 185–194, 2017(in Japanese).

[4] TAKAGI Y., TANAKA Y., UCHIDA S. Comparative study of three-dimensional nonlinear analysis models for dam gated pier seismic resistance evaluation, *Electric Power Civil Engineering Association*, No.406, pp.19–23, 2020(in Japanese).

[5] NUCLEAR AND INDUSTRIAL SAFETY AGENCY, Ministry of Economy, Trade and Industry. *Manual for Seismic Performance Verification of Hydroelectric Power Generation Facilities*, 2012(in Japanese).

[6] OTSUBO Y., TAKAHASHI M., UCHIDA S. Analytical Study on Interaction between Dam gated pier and Spillway Gate during Earthquake, *Electric Power Civil Engineering Association*, No. 367, pp. 54–58, 2013(in Japanese).

[7] MATSUOKA Y., OTSUBO Y., ARIMITSU T., UCHIDA S., NAKANISHI Y., NAKAMURA H. Nonlinear analytical modeling of dam gated pier based on earthquake records, *Proceedings of the Japan Society of Civil Engineers*, Vol.70A, pp.229–240, 2024(in Japanese).

[8] JAPAN ROAD ASSOCIATION. *Specifications for highway bridges [Seismic Design V],* 2017(in Japanese).

[9] MAEKAWA K., PIMANMAS A., OKAMURA H. *Nonlinear mechanics of reinforced concrete*, *Spon Press*, London, 2003.

[10] JAPAN SOCIETY OF CIVIL ENGINEERS. *Standard Specification for Concrete Structures [Structural Performance Verification]*, 2007 (in Japanese).

[11] JAPAN CONCRETE INSTITUTE. *Fundamentals, Applications and Examples of Nonlinear Finite Element Methods for Structural Engineers, Report of the Research Committee on the Use of Nonlinear Finite Element Analysis*, 2008 (in Japanese).

[12] JAPAN ROAD ASSOCIATION. *Specifications for highway bridges [Substructure IV]*, 2012(in Japanese).

[13] MATSUOKA Y., AOSAKA Y., OTSUBO Y., ARIMITSU T., SUGIMOTO K., SHIBAYAMA A., NISHIUCHI T., UCHIDA S., NAKANISHI Y., NAKAMURA H. Cyclic behavior of RC structures using round bars with very low reinforcement ratio and applicability of bond - slip model of round bar, *Proceedings of the Japan Society of Civil Engineers*, Vol.69A, pp.215–230, 2023(in Japanese).

[14] NAKAYAMA Y., OMACHI T., INOUE S. Practical evaluation of hydrodynamic pressures on dam-gates during eathquakes, *Proceedings of the Japan Society of Civil Engineers*, Vol.64A, No.4, pp.959–969, 2008(in Japanese).

[15] JAPAN ROAD ASSOCIATION. *Specifications for highway bridges [Seismic Design V]*, 2002(in Japanese).

[16] HORII H., UCHIDA Y., KASHIWAYANAGI M., KIMATA H., OKADA T. Study on Tensile Softening Characteristics for Evaluation of Bearing Capacity of Concrete Dam, *Electric Power Civil Engineering Association*, No.286, pp.113–119, 2000 (in Japanese).

[17] JAPANESE SOCIETY OF STEEL CONSTRUCTION. *Current Status and Reli ability Improvement of Dynamic Seismic Analysis of Steel Bridges Using Fiber Models*, 2011(in Japanese).

[18] DOI H., TANAKA Y., OTSUBO Y., NAKANO A., NAKANISHI Y., ARIGA Y. Study on Dynamic Analysis Model of Spillway Gate Using Actual Observation Results, *Journal of JSCE A1 (Structural and Earthquake Engineering)*, Vol. 69, No. 4 (Earthquake Engineering Journal, Vol. 32), I_601-I_608, 2013. (in Japanese)

Q.111 - R.18

COMMISSION INTERNATIONALE DES
GRANDS BARRAGES

VINGT-HUITIEME CONGRES DES
GRANDS BARRAGES
CHENGDU, MAI 2025

EARTHQUAKE ENGINEERING FOR CONCRETE DAMS (*)

Anil K. CHOPRA
Structural Engineering Consultant and Professor Emeritus, University of California, Berkeley

UNITED STATES OF AMERICA

SUMMARY

The present practice for defining design earthquakes and corresponding performance requirements for concrete dams are presented, limitations identified, and improvements proposed. The traditional assumption of a service life of 100 years is questioned and arguments presented for reevaluating this assumption. The features of dam—water—foundation interaction that must be included in dynamic analyses are identified based on the results of such analyses of four dams.

RÉSUMÉ

La pratique actuelle pour définer les séismes de conception et les exigences de performance correspondantes pour les barrages en béton sont présentées, les limites identifiées, et les améliorations proposées. L'hypothèse traditionnelle d'une durée de vie de 100 ans est remise en question et des arguments sont présentés pour réévaluer cette hypothese. Les caractérisitiques de l'interaction barrage-eau-fondation qui doivent être incluses dans les analyses dynamiques sont identifiées sur la base des résultats de ces analyses de quatre barrages.

(*) *Ingénierie sismique pour les barrages en béton*

 DOI: 10.1201/9781003642428-121

1. INTRODUCTION

Earthquake-resistant design of new concrete dams and seismic safety evaluation of existing dams consists of four phases: (1) select design earthquakes; (2) define design ground motions; (3) compute stress and deformation demands by dynamic analysis of the dam—water—foundation system; and (4) evaluate seismic performance of the dam. This paper addresses the first three topics.

Presented in the first part of this paper are the ICOLD definitions of the Operating Basis Earthquake (OBE) and Safety Evaluation Earthqu8ake (SEE) or Maximum Design Earthquake (MDE), and the associated performance requirements for the dam. Several issues related to these definitions and criteria are discussed, their limitations identified, and improvements suggested.

Design earthquakes for concrete dams are based on specified probabilities of exceedance over 100 years, the assumed service life of the project. Based on the age of major and important existing dams, it is argued that the traditionally assumed service life may not be realistic. The implications of assuming a longer service life are presented in Section 3 of the paper.

Presented subsequently are methods for selecting and scaling ground motions (GMs) consistent with the seismic hazard—e.g., a mean return period of 10,000 years—for the design of concrete dams. This subject has been a popular research topic since the early 2000s, but the focus has been on a single component of GM in the context of multistory buildings. We will present an extension of these procedures to all three components—two horizontal and one vertical—that should be considered in three-dimensional dynamic analysis of dams.

It is now widely recognized that several factors must be included in dynamic analysis of concrete dams subjected to earthquake excitation: (1) the semi-unbounded extent of the impounded water and foundation domains; (2) dam–foundation interaction considering mass, flexibility, and damping of rock; (3) dam–water interaction considering compressibility of water and the sediments that invariably deposit at the reservoir bottom; and (4) spatial variations in ground motion around the canyon. However, these factors are not always included because many commercial finite-element analysis programs do not lend themselves to include them. As a result, it became popular to ignore the mass and material damping of rock as well as compressibility of water. It is demonstrated in Section 5 that this practice results in excessive over-estimation of stresses that would lead to over-conservative and, hence, expensive design of new dams, and to the erroneous conclusion that an existing dam is unsafe, thus requiring retrofit at enormous cost.

2. DESIGN EARTHQUAKES

It is common to consider two levels of ground motion (GM) with corresponding performance requirements in the seismic design of a new dam or service evaluation of an existing dam. We first summarize terminology and definitions in the publications of the International Commission on Large Dams (ICOLD) [1].

The Operating Basis Earthquake (OBE) is the event that produces GM at the site that can reasonably be expected during the service life of the project. This statement has usually been interpreted as the GM that has a 50% probability of exceedance (PE) in 100 years, the commonly assumed life of concrete dams. The corresponding mean return period is 144 years (calculated assuming a Poisson model for occurrence of events). The OBE should be determined by Probabilistic Seismic Hazard Analysis (PSHA). At this level of ground shaking, the facility—dam, appurtenant structures, equipment, powerhouse, etc.—should experience little or no damage and continue to function without interruption; this performance requirement implies that the dam remains essentially within the linear range of behavior.

The Safety Evaluation Earthquake (SEE) or Maximum Design Earthquake (MDE) is the earthquake event that produces GM at the site that is rare. Factors to consider in selecting the intensity of this GM are the consequences of failure of the dam, criticality of project function (power generation, water supply, flood control, etc.), and turnaround time to restore the facility to be operational after the earthquake event. The MDE represents ground shaking at the site associated with a long mean return period: 10,000, 3000, or 1000 years for dams where the consequences of dam failure are high, moderate, or low, respectively. Mean return periods of 10,000 (precisely 9950) years and 1000 (precisely 949 years) represent ground shaking associated with a 1% and 10% PE in 100 years, respectively. The MDE should also be determined by PSHA. At this level of ground shaking, there should be no catastrophic failure, such as the uncontrolled release of the impounded water, although significant damage or economic loss may be tolerated. This performance requirement implies that the dam is allowed to deform significantly into the nonlinear range.

The ICOLD document also defines a Maximum Credible Earthquake (MCE). This represents the GM during the largest magnitude earthquake along a recognized fault or within a particular seismo-tectonic province. A deterministic approach is used to determine the MCE ground motions at the site. For each identified fault, the largest magnitude earthquake is used as input to a ground motion prediction model (GMPM) to provide the probability distribution of the GM intensity. The 84^{th} percentile value is defined as the deterministic-based MCE-level motion.

At sites close to major faults with high-slip rates (e.g., the San Andreas and Hayward faults in California), the earthquake event that produces the MCE-level GM

may have a relatively high annual rate of occurrence, e.g., 0.015[*] for the Hayward fault in California. Combining the annual rate of 0.015 with a GM with a 16% probability of being exceeded results in a return period of 416[†] years, a much, much shorter return period than the 10,000 years for the MDE. This implies that when the next large earthquake occurs on a major fault in California, the MCE-level GM would, on average, be exceeded at 16% of the dams. This does not seem to be prudent, suggesting that the MCE-level (84^{th} percentile deterministic) GM is not intense enough. However, in other parts of the world where the slip rates on active faults are low, the MCE-level GM may be much more intense than the GM with a 10,000-year return period. Therefore, for safety evaluation of high-consequence dams, the more intense of two GMs should be selected: (1) GM from MCE on known active faults; and (2) GM associated with 1% PE in 100 years or return period of 10,000 years [2].

2.1. Comments and observations

The performance requirement that a facility should continue to function without interruption during the OBE seems to have been introduced to minimize economic losses during "frequent" earthquakes. However, it appears that the definition of the OBE has been based on tradition instead of extensive studies on life-cycle cost (economic) analysis. For a portfolio of 100 dams, the present definition of OBE-level GM and performance requirement implies that, on average, 50 dams would experience more intense GM during their lifetime, and, hence, may not remain functional. This number would, most likely, seem excessively large to many engineers and policymakers. To investigate this and related issues, systematic research on life-cycle cost analysis of concrete dams should be undertaken to develop a basis for making rational decisions on the choice of OBE-level GM. Such investigations would likely suggest that the ground motion should be associated with a probability of exceedance that is significantly lower than 50%, implying a return period much longer than 144 years. Some organizations have chosen a return period of 475 years [2].

Turning to the MDE, the performance requirement of no catastrophic failure during MDE-level GM—a rare, intense GM—seems appropriate. However, it is not clear that the definition of the MDE is appropriate. Consider a portfolio of 100 concrete dams and a 100-year service life; the overall probability of at least one dam experiencing an MDE ground motion is

---

[*] *The Hayward fault has a 31.7% chance of rupturing in a 6.7 or larger magnitude earthquake in the next 26 years http://seismo.berkeley.edu/hayward/hayward_hazards.html. The associated annual rate of occurrence is 0.015.*

[†] *Return period = $(0.015 \times 0.16)^{-1}$ = 416 years.*

1 – Prob (no dam experiences MDE during service life)

$= 1 – (1 – 0.01)^{100}$

$= 0.63$

where the exponent refers to the number of dams. This means that the probability of at least one dam experiencing this intense (or more intense) GM over a 100-year period is 63%. Will those dams all meet the performance requirement of no catastrophic failure? It is not possible to answer this question with confidence because of limitations in our current (2025) ability to determine the extent of cracking in concrete, sliding at joints and interfaces in the dam and the foundation rock, or operability of equipment and appurtenant structures necessary to lower the level of impounded water in case of emergency after a major earthquake. Various reasons underlying these limitations were presented in Section 11.12 of Chopra [2020]. This unfortunate state of affairs suggests that until nonlinear modeling and dynamic analysis of concrete dams and their foundations improve to develop a high degree of confidence in the results, the design criteria should be made more stringent.

Major dams where the consequences of failure are unacceptable should be designed more conservatively. This conservatism can be achieved by two initiatives taken individually or together. First, the intensity of the OBE-level ground motion is increased by lowering the probability of exceedance, i.e., lengthening the return period. Shown in Fig. 1 are the Uniform Hazard Spectra (UHS) for several values of probability of exceedance (PE) over 100 years—50%, 10%, 5%, 2%, and 1%—for the Pine Flat Dam site in California. Obviously, the forces to be considered in the linearly elastic design or evaluation of the dam, consistent with performance requirements for the OBE-level ground motion, increase as the PE decreases. The second initiative could be to control more stringently the damage permitted during the MDE to a threshold much lower than what is envisaged in the current requirement of “no uncontrolled release of the impounded water.”

3. ASSUMED SERVICE LIFE

Design earthquakes for concrete dams are based on specified probabilities of exceedance—50% in the case of the OBE and 1% in the case of the MDE—over 100 years, the assumed service life of the project. However, the choice of 100 years may not be realistic. Consider two examples: it is difficult to imagine that the iconic Hoover Dam built in 1933, will be abandoned in 2033, which is less than ten years from the time of this writing. The Aswan Low Dam (also known as Old Aswan Dam)

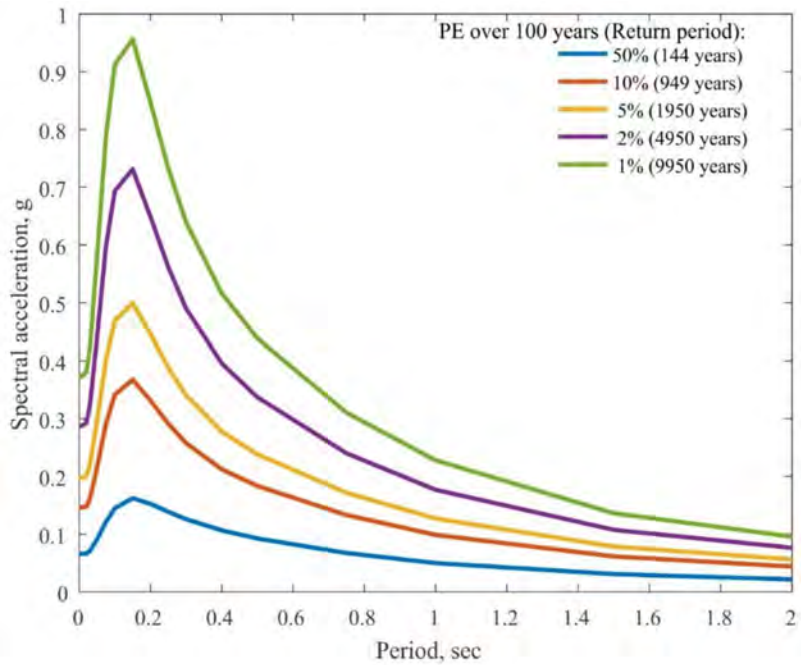

Fig. 1
Uniform hazard spectra for several values of probability of exceedance over 100 years for the Pine Flat Dam site in California; corresponding return periods are noted (from Chopra [3]).
Spectres de danger uniformes pour plusieurs valeurs de probabilité de dépassment sur 100 ans pour le site de Pine Flat Dam en Californie; les périodes de retour correspondantes sont notées (d'après Chopra [3]).

on the Nile River in Egypt was constructed between 1899 and 1902, and continues (2024) to serve as a critically important facility in support of the power generation needs of Egypt. Having already existed for 122 years, most likely this dam will continue to remain functional for many more years to come.

Suppose we consider a service life of 200 years. For the same probability of exceedance, the ground motion will now be more intense. This is illustrated in Fig. 2 where the UHSs are plotted for PE = 1% and 10% over 100 and 200 years. Note: the spectral ordinates and design forces are increased by about 30% to 40% for a service life of 200 years over the values for a 100-year service life.

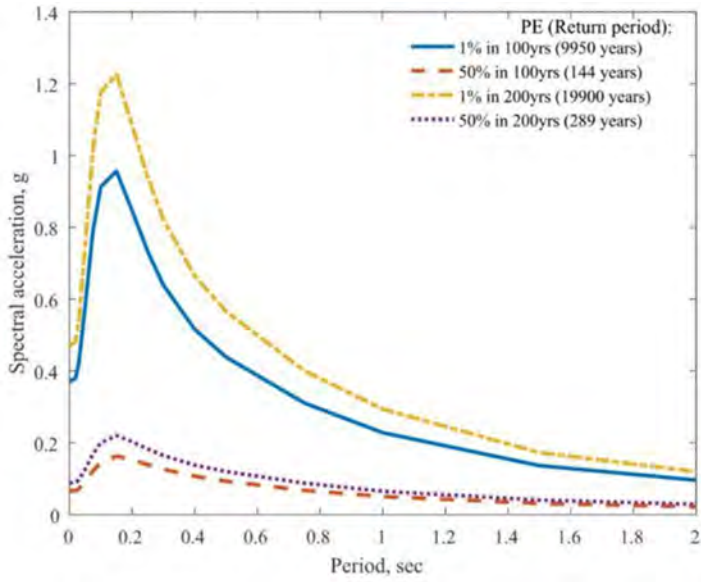

Fig. 2
Uniform hazard spectra for the Pine Flat Dam site, California, corresponding to a probability of exceedance = 1% and 10% over 100 and 200 years; corresponding return periods are noted (from Chopra [3]).
Spectres d'aléa uniformes pour le site de Pine Flat Dam en Californie, correspondant à une probabilité de dépassement = 1% et 10% sur 100 et 200 ans; les délais de retour correspondantes sont notés (d'après Chopra [3]).

4. GROUND-MOTION SELECTION AND MODIFICATION

Presented in this section is an overview of this topic that is fully developed in Chapter 13 of Chopra [3].

4.1. TARGET SPECTRUM

4.1.1. *Single horizontal component*

The goal of dynamic analysis of a concrete dam is to estimate seismic demands that may be imposed by unknown ground shaking at the site caused by

future earthquakes. Because the ground motion (GM) cannot be defined uniquely, we are interested in the statistics of structural response to an ensemble of GMs. These GMs should, in some sense, be consistent with the seismic hazard at the site, usually characterized by the uniform hazard spectrum (UHS). Although the UHS is a candidate for the user-specified target spectrum (TS), researchers have demonstrated that the UHS is over-conservative and is not representative of individual GM spectra associated with an earthquake of magnitude equal to the mean value occurring at the mean distance. Thus, the UHS is not an appropriate target for selecting GMs to be used in dynamic analysis of concrete dams.

Figure 3 shows the UHS with a 1% probability of exceedance in 100 years for the Pine Flat Dam site in California (119.3°W and 36.8°N). This exceedance probability corresponds to a return period of 9950 years; this is the mean time between occurrences of the specified hazard, assuming that the exceedances follow a Poisson random process. A return period of 10,000 years is often selected for critical facilities such as major dams and nuclear power plants.

The conditional mean spectrum (CMS) has been developed by Baker [4] as a TS that overcomes the drawbacks of the UHS. The CMS is constructed for a selected value of the conditioning period, denoted by T^*, where the spectral acceleration is specified. Typically, T^* is selected as the fundamental vibration period of the structure and $A(T^*)$ as the UHS value. Shown in Fig. 3 is the CMS for the Pine Flat Dam site and $T^* = 0.5$ sec. It has a (slight) hump near the conditioning period of 0.5 sec where it matches the UHS and then drops off on both sides. Shown to be representative of recorded GMs, the CMS may be appropriate as a TS for dynamic analysis of structures.

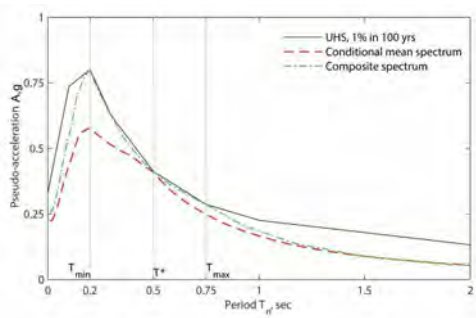

Fig. 3
Uniform hazard spectrum (UHS), conditional mean spectrum (CMS), and CMS–UHS composite spectrum for the Pine Flat Dam site (from Chopra [3]).
Spectre de danger uniforme (UHS), spectre moyen conditionnel (CMS), et spectre composite CMS-UHS pour le site du barrage Pine Flat (d'après Chopra [3]).

Researchers have demonstrated several concerns with using the CMS as the TS to select and modify GMs. First, the CMS conditioned on a single period, T^*, almost always underestimates significantly the demand because the nonlinear dynamics of a complex structure depend on many more features of the GM besides spectral acceleration at a single period. Second, the demands from an intensity-based assessment with a single CMS vary with the choice of T^*.

The most promising proposal for the target spectrum is a composite spectrum that combines features from both the CMS and the UHS [3; Chapter 13]. The CMS–UHS composite spectrum is identical to the UHS at periods between T_{min} and T_{max}—the shortest and longest structural periods of interest—but less intense than the UHS outside of this period range. At periods shorter than T_{min}, it is identical to the CMS with $T^* = T_{min}$, whereas at periods longer than T_{max}, it is identical to the CMS, with $T^* = T_{max}$; see Fig. 3.

4.1.2. *Two horizontal components*

Researchers have demonstrated that it is appropriate to define the target spectrum as a pair of identical spectra for the two horizontal components of GM [Chopra 2020; Chapter 13]. This is the CMS–UHS composite spectrum presented in Fig. 3.

4.2. Ground-Motion selection and amplitude scaling

The simplest goal of ground-motion selection and modification (GMSM) procedures is to estimate the median (or mean) values of seismic demands. For this purpose, we want to select GMs whose response spectra are similar to the target spectrum in amplitude and shape. The number of recorded GMs that satisfy both requirements simultaneously is often insufficient. For example, the large majority of recorded GMs are weaker than the intensity represented by the UHS and CMS in highly seismic regions. Furthermore, the response spectra for many of the records with the desired intensity $A(T^*)$ may not be similar in shape to the TS. Given this background, selection of GMs usually proceeds in two stages. First, every record in the database is scaled to make its spectral amplitude(s) similar to the target amplitude(s). Second, the scaled records whose response spectra are similar in shape to the target spectrum over a specified period range are selected. This period range for selecting GMs should include the vibration periods of all vibration modes that are significant in the response of the structure.

The first step of scaling GMs to an intensity similar to that of the TS can be achieved in various ways, e.g., scale each GM so that the selected scale factor (SF) minimizes the difference between the response spectrum of the scaled GM and TS

over the selected period range. A good metric for this “difference” is the sum of the squared differences (SSD) between the two spectra over the selected period range. To preserve the relative intensity of the two horizontal components in the original recorded GM, both components are scaled by the same factor. Once all the GMs in a large database have been scaled appropriately, the SSD between the response spectra pair for each GM and the TS pair is computed and the GMs with the smallest SSD are selected. Figure 4 shows the CMS (chosen, for example, as the TS) and the response spectra for 11 GMs selected for similarity to the CMS. Presented for illustration, this figure is restricted to one component of GM.

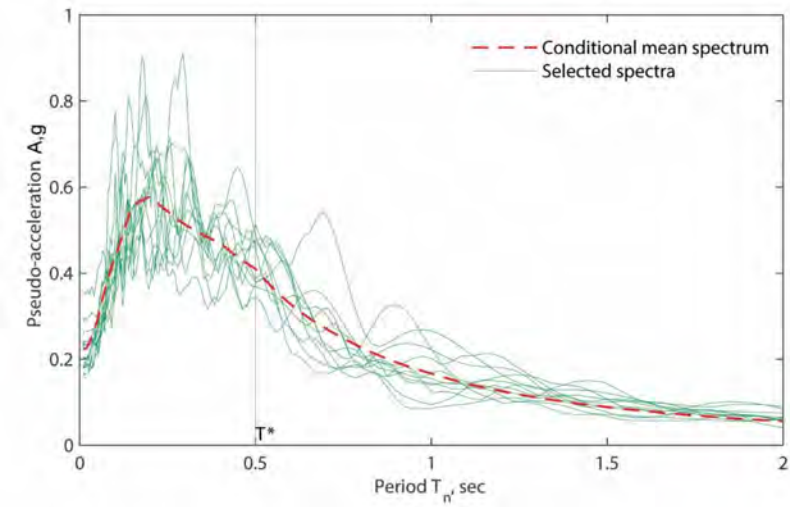

Fig. 4
Response spectra for 11 scaled GMs selected for similarity with the CMS; the period range for matching of GMs is 0.05–10 sec (not shown in the figure) (from Chopra [3]).
Spectres de résponse pour 11 GM à l’échelle sélectionnés pour leur similarité avec le CMA, la plage de périodes pour l’appariement de GM est de 0.05 à 10 secondes (non illustrée sur la figure) (d’après Chopra [3]).

4.3. Three components of ground motion

The methodology to develop target spectra for two horizontal components of GM, and then to select and scale GMs to match the TS outlined above, was presented in Chapter 13 of Chopra [2020]. This methodology has been extended to three components of GM. Derived was a theory to develop the target spectrum for

the vertical component of the GM and the GMSM method was extended to consider simultaneously the vertical component. This methodology requires the user to specify the relative importance of the horizontal and vertical components of GM in the response of the structure.

Since horizontal GMs are usually much more important in the response of concrete dams, a simpler approach is to first select these two components without considering the vertical component. The target spectrum for the horizontal components of the GM defined by Fig. 3 remains valid, and a TS for the vertical component is not required. The vertical component accompanying a selected record is scaled by the same SF that was applied to the horizontal components. [3; Chapter 13].

5. ESSENTIAL FACTORS IN EARTHQUAKE ANALYSIS

A comprehensive presentation of this topic is available in Chopra [5] and Chapters 6 and 9 of Chopra [2] and only a brief overview is included herein. Research conducted during 1984–1996 demonstrated that several factors must be included in dynamic analysis of concrete dams subject to earthquake excitation: (1) the semi-unbounded extent of the impounded water and foundation domains; (2) dam–foundation interaction considering mass, flexibility, and damping of rock; (3) dam–water interaction considering compressibility of water and the sediments that invariably deposit at the reservoir bottom; and (4) spatial variations in GM around the canyon.

Starting in 1996, the U.S. Bureau of Reclamation embarked upon a major program to evaluate the seismic safety of their dams. This investigation included earthquake analysis of several arch dams. Results presented herein are for four dams: Hoover Dam, a 221-m-high, thick arch dam, Deadwood Dam, a 50-m-high single curvature dam; Monticello Dam, a 93-m-high double curvature dam; and Morrow Point Dam, a 142-m-high double curvature dam. Ground motions consistent with the seismic hazard for each of the four dam sites were selected. All analyses were implemented by the EACD-3D-96 computer software[‡] [6; 7; 8; 9' 10].

5.1. Implications of ignoring mass of rock

Compared are the earthquake-induced stresses in each of the four dams computed for two cases: (1) including all effects of dam–foundation interaction; and (2) ignoring the mass of foundation rock, i.e., considering foundation flexibility only

[‡]*Developed by Tan and Chopra [1996].*

(Figs. 5–8). For these two cases, the largest arch stress on the upstream or downstream face of the dam is 3.3 MPa (476 psi) versus 5.8 MPa (844 psi) for Deadwood Dam; 5.0 MPa (730 psi) versus 9.7 MPa (1410 psi) for Monticello Dam; 4.6 MPa (665 psi) versus 9.2 MPa (1336 psi) for Morrow Point Dam; and 5.2 MPa (758 psi) versus 15.2 MPa (2204 psi) for Hoover Dam. These results demonstrate that if the mass of foundation rock is ignored, stresses are overestimated by a factor of about 2 for the first three dams and by a factor of about 3 for Hoover Dam. Because such overestimation of stresses may lead to overly conservative designs of new dams and to the erroneous conclusion that an existing dam is unsafe and thus requires upgrading, it is imperative that mass of rock be included in earthquake analysis of concrete dams.

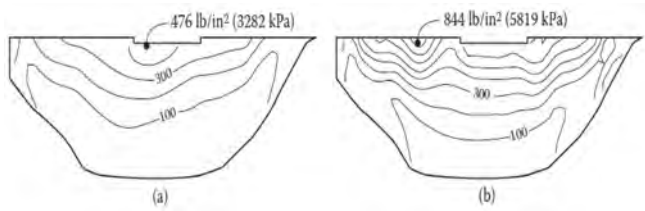

Fig. 5
Peak values of tensile arch stresses in Deadwood Dam for two cases: (a) including all effects of dam–foundation interaction, and (b) ignoring the mass of foundation rock (from Chopra [3]).
Valeurs maximales des contraintes de traction de la voûte dans le barrage Deadwood pour deux cas: (a) incluant tous les effets de l'interaction barrage-fondation, et (b) ignorant la mass de la roche de foundation (d'après Chopra [3]).

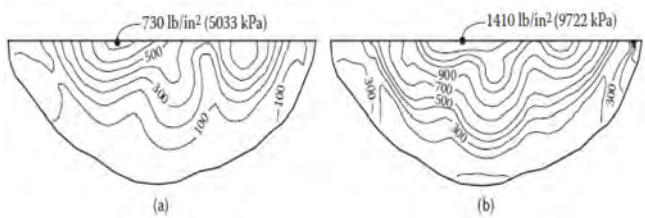

Fig. 6
Peak values of tensile arch stresses in Monticello Dam for two cases: (a) including all effects of dam–foundation interaction, and (b) ignoring the mass of foundation rock (from Chopra [3]).
Valeurs maximales des contraintes de traction de la voûte dans le barrage Monticello pour deux cas: (a) incluant tous les effets de l'interaction barrage-fondation, et (b) ignorant la mass de la roche de foundation (d'après Chopra [3]).

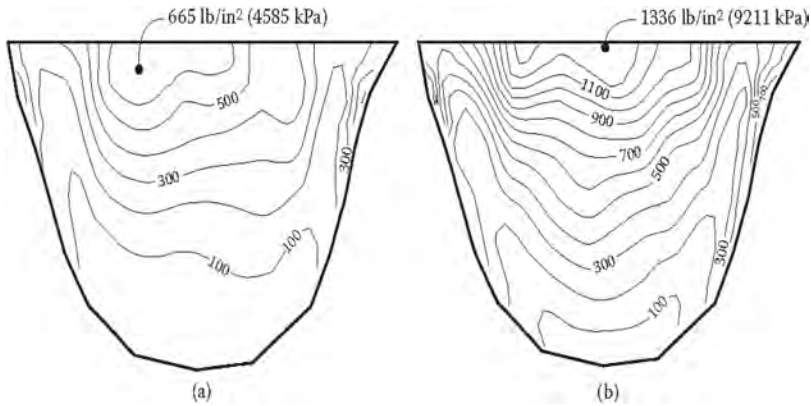

Fig. 7
Peak values of tensile arch stresses in Morrow Point Dam for two cases: (a) including all effects of dam–foundation interaction, and (b) ignoring the mass of foundation rock (from Chopra [3]).
Valeurs maximales des contraintes de traction de la voûte dans le barrage de Morrow Point pour deux cas: (a) incluant tous les effets de l'interaction barrage-fondation, et (b) ignorant la mass de la roche de foundation (d'après Chopra [3]).

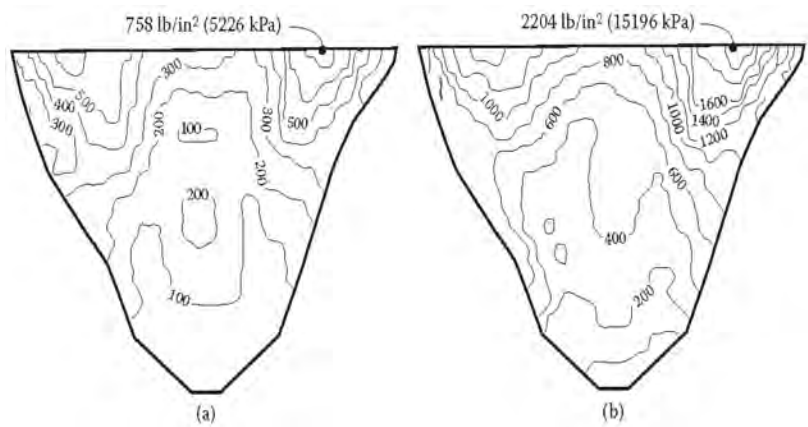

Fig. 8
Peak values of tensile arch stresses in Hoover Dam for two cases: (a) including all effects of dam–foundation interaction, and (b) ignoring the mass of foundation rock (from Chopra [3]).
Valeurs maximales des contraintes de traction de la voûte dans le barrage Hoover pour deux case: (a) incluant tous les effets de l'interaction barrage-fondation, et (b) ignorant la mass de la roche de foundation (d'après Chopra [3]).

5.2. Implications of ignoring water compressibility

Compared are the earthquake-induced stresses in two of the four Reclamation dams computed under two conditions: (a) including compressibility of water; and (2) ignoring water compressibility; in the latter case, reservoir boundary absorption effects are implicitly ignored. By neglecting water compressibility and reservoir boundary absorption, the stresses may be significantly underestimated, as in the case of Monticello Dam (Fig. 9), or considerably overestimated as in the case of Morrow Point Dam (Fig. 10); observe that these discrepancies vary with the location on the dam surface. Thus, hydrodynamic effects should *not* be modeled by an added mass of water vibrating with the dam—a model that ignores water compressibility—in dynamic analysis.

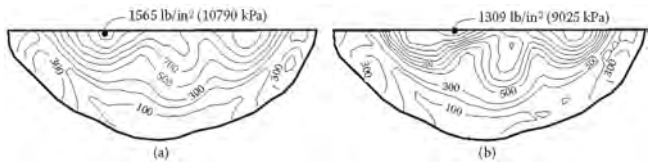

Fig. 9
Peak values of tensile arch stresses in Monticello Dam computed under two conditions: (a) water compressibility included, and (b) water compressibility ignored (from Chopra [3]).
Valeurs maximales des contraintes de traction de la voûte dans le barrage Monticello pour deux conditions: (a) compressibilité de l'eau incluse, et (b) compressibilité de l'eau ignorée (d'après Chopra [3]).

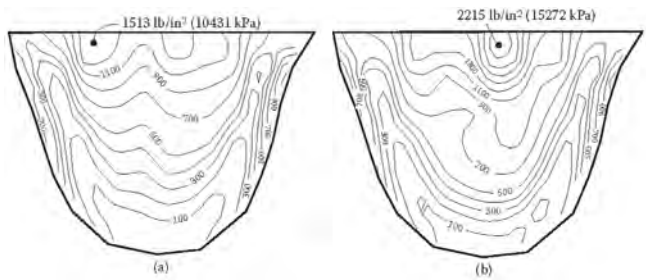

Fig. 10
Peak values of tensile arch stresses in Morrow Point Dam computed under two conditions: (a) water compressibility included; and (b) water compressibility ignored (from Chopra [3]).
Valeurs maximales des contraintes de traction de la voûte dans le barrage Morrow Point pour deux conditions: (a) compressibilité de l'eau incluse, et (b) compressibilité de l'eau ignorée (d'après Chopra [3]).

REFERENCES

[1] ICOLD*, Selecting seismic parameters for large dams, Bulletin 148, International Commission on Large Dams, Paris, France*, 2016.

[2] ANCOLD, *Guidelines for Design of Dams and Appurtenant Structures for Earthquakes*. Australian National Committee on Large Dams, Inc., Tasmania, Australia, 138 pgs. 2019.

[3] CHOPRA A.K. (2020). *Earthquake Engineering for Concrete Dams*, 297 pgs., John Wiley and Sons, Chichester, United Kingdom.

[4] BAKER J.W., Conditional mean spectrum: Tool for ground-motion selection. *ASCE J. Struct. Eng.*, 137 (3): 322–331, 2011.

[5] CHOPRA A.K., Earthquake analysis of arch dams, Factors to be considered*. ASCE J. Struct. Eng.* 138 (2): 205–214, 2012.

[6] TAN H.-C., CHOPRA A.K., EACD-3D: A computer program for three-dimensional earthquake analysis of concrete dams, *Report No. UCB*/*SEMM-96*/*06*, University of California, Berkeley, Calif., 131 pgs., 1996.

[7] BUREAU OF RECLAMATION, Linear elastic dynamic structural analysis including mass in the foundation for Hoover Dam, *Technical Memorandum HVD-MDA-D8110-97-2*, Denver, Colorado, 1998.

[8] BUREAU OF RECLAMATION, Linear elastic analysis addressing structural issues for the modification decision analysis for Deadwood Dam, *Technical Memorandum DEA-D8110-MDA-TM-98-1*, Denver, Colorado. 1998.

[9] BUREAU OF RECLAMATION, Executive summary of the static and dynamic stability studies of Hoover Dam, Modification design analysis, *Technical Memorandum No. HVD-MDA-D8110-97-1*, Denver, Colorado, 1998.

[10] BUREAU OF RECLAMATION, Linear elastic static and dynamic structural analysis of Monticello Dam, *Technical Memorandum No. MONT-IE-D8110-99-2,* Denver, Colorado, 1999.

COMMISSION INTERNATIONALE DES
GRANDS BARRAGES

VINGT-HUITIEME CONGRES DES
GRANDS BARRAGES
CHENGDU, MAI 2025

SSHAC EVALUATION OF THE SEISMIC FRAGILITY FOR AN EMBANKMENT DAM (*)

Martin W. MCCANN, JR., PHD
Jack R. Benjamin & Associates, Inc., President

Zach RUBY, PE
Grant County Public Utility District, Chief Dam Safety Engineer

Michael BEATY, PHD, GE
Beaty Engineering LLC; Principal Engineer

Thomas WESTOVER, PE, MBA
Cornforth Consultants, Inc., Vice President

Gonzalo CASTRO, PHD, PE, GE, NAE
Consultant

Bo LUNDQVIST
Jack R. Benjamin & Associates, Inc., Engineer

UNITED STATES OF AMERICA

SUMMARY

The Wanapum Left Embankment seismic fragility analysis has adapted and implemented the SSHAC process to assess the aleatory and epistemic uncertainties in the estimate of conditional probability of URR. The study was motivated by the desire of Grant County Public Utility District to develop a realistic, detailed

**Évaluation par un processus SSHAC de la fragilité sismique d'un barrage en remblai*

DOI: 10.1201/9781003642428-122

estimate of the risk of URR and downstream consequences to support a risk-informed decision about the seismic safety of the Wanapum Left Embankment. The SSHAC process has provided a structure to make a detailed assessment of the sources of aleatory and epistemic uncertainty in the characterization of the embankment (e.g., subzone blowcounts, CRR, V_s, and S_r). This formal process allowed a detailed identification and quantitative understanding of many aleatory and epistemic uncertainties, particularly those related to assessing CRR and S_r. The sources of epistemic uncertainty that have been identified have been incorporated in a logic tree format that provides the structure for estimating the uncertainty in the seismic fragility. In this context, the aggregate impact of uncertainties in the embankment characteristics and seismic loading on the estimate of embankment deformations and potential for URR are estimated.

RÉSUMÉ

L'analyse de la fragilité sismique de la digue gauche de Wanapum a adapté et implémenté le processus SSHAC pour évaluer les incertitudes aléatoires et épistémiques dans l'estimation de probabilité conditionnelle du URR. L'étude a été motivée par la demande du Grant County Public Utility District de développer un estimé réaliste et détaillé du risque de rupure et les conséquences long terme afin de supporter une décision en connaissance des risques à propos de la sécurité sismique de la digue gauche de Wanapum. Le processus du SSHAC a fourni une structure pour faire une évaluation des sources d'incertitude aléatoires et épistémiques dans la caractérisation de la digue (c'est à dire le décompte des coups en sous zone, les CCR, Vs, er Sr). Ce processus formel permet une identification détaillée et une compréhension quantitative de plusieurs incertitudes aléatoires et épistémiques, surtout en ce qui a trait au CRR et Sr. Les sources d'incertitudes épistémiques qui ont été identifiées ont été incorporées dans un format d'arbre de logique qui fournit la structure pour estimer l'incertitude liée à la fragilité sismique. Dans ce contexte, l'impact agrégé des incertitudes dans les caractéristiques de la digue et du chargement sismique sur l'estimé des déformations de la digue et le potentiel de URR est estimé.

1. INTRODUCTION

As part of its dam safety program, Grant County Public Utility District (GCPUD) is undertaking a risk-informed approach to the seismic safety evaluation of the Left Embankment at its Wanapum hydropower development. The seismic risk analysis will assess the potential for Uncontrolled Release of the Reservoir (URR) and resulting downstream consequences. The project was initiated following questions raised by the Federal Energy Regulatory Commission (FERC), the United

States regulator for hydropower projects. A critical part of the risk analysis is the estimate of the seismic fragility, which is an assessment of the seismic performance of the Left Embankment and the chance of URR as a function of earthquake magnitude and ground motion. The assessment of the seismic fragility for the embankment is a technically complex analysis with considerable uncertainty. GCPUD has applied the SSHAC process (Budnitz, et al, 1997 [1]; USNRC, 2012 [2]; USNRC 2018 [3]) to this engineering analysis. The SSHAC process was developed to provide structure to complex technical evaluations where technical experts must integrate sources of epistemic uncertainty, including consideration of alternative data, models and methods, and where there is often limited data (direct evidence) to estimate model parameters. This paper describes the SSHAC process and its implementation for the Left Embankment seismic fragility analysis.

2. WANAPUM DAM

Wanapum Dam is a part of GCPUD's Priest Rapids Hydroelectric Project which is regulated by the FERC. The dam is located on the mainstem of the Columbia River at River Mile 415. The dam includes left and right earthen embankments, two gravity sections with fish ladders, a gated spillway, and a powerhouse that provides up to 1,125 MW of power from 10 generating units.

2.1. LEFT EMBANKMENT

The Left Embankment spans the historic Columbia River channel, with all concrete structures being built in the dry on the right bank prior to inundation of the reservoir. The dam is underlain by a thick series of Columbia River Basalt flows covered with more recent alluvium. The native alluvium was deposited and reworked by the catastrophic glacial-age Missoula floods as well as more recent Columbia River flooding. The catastrophic floods were very high energy events which likely occurred dozens of times and resulted in a complex scour and depositional environment. These floods deposited relatively uniform gravels and cobbles during the high velocity stage, and then fine sand slackwater deposits when the flood waters formed an enormous temporary lake in Central Washington due to a constriction at the upstream end of the Columbia River Gorge.

The Left Embankment was constructed in two phases. In Phase 1, the embankment on either side of the river channel was constructed concurrent with the right embankment and concrete structures. In Phase 2, a River Closure Section (RCS) diverted river flows through a completed approach channel to the spillway and future unit section of the powerhouse as the full embankment was brought to final grade.

The RCS includes upstream and downstream dumped rock dikes used for the initial diversion. The rockfill was dumped through flowing water in the river channel, resulting in a coarse, relatively low relative density fill. The maximum particle size appears less than about 12 inches in much of the fill and includes a wide range in gradations. The area between the dikes was filled with coarse sand that was vibro-densified below the water table. A bentonite slurry cutoff wall, excavated by dragline, was constructed as a seepage barrier. A zoned embankment with a central sandy silt core, upstream and downstream filters, and coarse granular shells was constructed upon the slurry cutoff, densified fill, and the dumped rockfill dikes.

2.2. Seismic concerns

The dumped rockfill and underlying alluvium are generally coarse sands, gravels, and cobbles with little to no fines. The depositional mechanisms (end dumped through water for the dumped rockfill and deposited during a mega-flood for the alluvium) result in granular materials below the water table at low relative density that are potentially liquefiable. The dam is located in a seismically active region, with both local crustal fault sources and the more distant Cascadia Subduction Zone (CSZ) that is capable of producing magnitude 9+ earthquakes of long duration shaking. Foundation and dumped rockfill liquefaction from a large seismic event could result in deformations leading to overtopping or distress to the seepage barrier triggering a delayed internal erosion failure.

A key characterization issue (and source of considerable uncertainty) is the liquefaction susceptibility and subsequent residual strength (S_r) of gravelly soils. The body of data and models for evaluating liquefaction triggering and S_r have generally been developed for sands, in which Standard Penetration Test (SPT) blowcounts are the key index parameter. Gravelly soils have two complicating differences with sands: i) SPT blowcounts are typically not representative and another method (e.g., Becker blowcounts) must be used to determine an equivalent penetration resistance; and ii) it is unclear from published literature if the approaches developed for sands are directly translatable to gravels and cobbles with no adjustment for particle size or gradation. These key modeling issues, among others in the fragility, are addressed using the SSHAC process as described in the following sections.

3. APPROACH

To address concerns about the potential seismic vulnerability of the Left Embankment, the FERC directed GCPUD to convene a Board of Consultants

(BOC) to oversee the evaluation of its embankments. GCPUD formed a BOC and initiated work on the Left Embankment analysis. However, at the same time, the FERC was moving toward Risk-Informed Decision Making (RIDM). In addition, GCPUD had made early in-roads applying RIDM methods to dam safety issues. Building on this experience and with the FERC's concurrence, GCPUD elected to change directions and take a risk-informed approach to evaluating the seismic safety of the Left Embankment. To specifically address the seismic safety concerns for the Left Embankment, they elected to conduct the seismic fragility assessment using the SSHAC process (Budnitz, et al. 1997 [1]; USNRC, 2012 [2]; USNRC 2018 [3]). The SSHAC process is a formalized, structured approach to conducting expert evaluation projects, that can be carried out at four different levels of analysis. GCPUD elected to conduct a SSHAC Level 3 analysis. With this decision, the members of the BOC were re-assigned to different positions within the project (positions defined in the SSHAC guidelines), and other experts were added to the project team. With the decision to adopt the SSHAC process, GCPUD abandoned the BOC format.

3.1. SSHAC Process

The SSHAC process was developed in the 1990s as a result of conflicting, parallel probabilistic seismic hazard analysis (PSHA) studies that were conducted to estimate frequency of occurrence of earthquake ground motions in the eastern U.S. The two studies, one funded by the federal government and the second by the private sector, relied on expert elicitation from earth scientists (geologists, seismologists, geophysicists, etc.) to estimate the inputs to the PSHA. The two studies used the same data, models and methods to conduct the analysis. However, the projects differed in the manner in which they were organized and in the way they elicited input from the experts. One study took a rather unstructured approach to the elicitation process, whereas the other took a more structured approach. The results of the two studies ended up being vastly different (despite their reliance on the same approach (models) and data to estimate the seismic hazard). In view of these differences a panel was formed to understand the reason for the differences and to establish guidance for future studies that rely on expert elicitation. The conclusion of the panel was that the source of the differences between the two studies was not technical, but rather a result of the processes that were used to work with and elicit input from the scientific experts. The product of the panel's work was the SSHAC process (Budnitz, et al., 1997 [1]). The original SSHAC guidance was updated in 2012 and again in 2018 (USNRC, 2012 [2]; USNRC, 2018 [3]). It is worth noting that while the development of the process grew out of issues in estimating seismic hazard, its foundational basis translates to other problems in engineering and science where assessments must rely on technical evaluations and subjective interpretations of data, models and methods by experts.

3.2. Basic principles

The authors of the SSHAC process found the primary source of differences between the two studies, and more generally the potential pitfalls in executing any successful study of similar complexity that relies on the subject evaluation of experts, are typically procedural rather than technical in nature. Here, procedural relates to the organizational structure of a study and specifically the process of elicitation of expert inputs on technical issues where there is a legitimate range of technically defensible estimates of models and model parameters in the technical community (Budnitz, et al., 1997 [1]). With this finding, the panel developed a structure for studies where there are epistemic uncertainties in data, models, and methods and a need to utilize experts to evaluate complex datasets and develop a quantitative measure of uncertainty.

3.3. Goal of the SSHAC process

Among the procedural features of the SSHAC process involved establishing a clear statement of the study goal. The goal statement has evolved since its early development, however the principles have remained the same (NRC, 2018 [3]). For purposes of the Wanapum seismic fragility study, the wording has been slightly revised to reflect the nature of the current study. The SSHAC seismic fragility study goal is:

> *The fundamental goal of the SSHAC process is to produce a probabilistic seismic fragility analysis that captures the center, body, and range (CBR) of technically defensible interpretations (TDI).*

Based on the process described in the NUREG, this outcome is achieved through faithful execution of the two phases of the SSHAC method. In the first phase, the Technical Integration (TI) Team evaluates available data, models, and methods of potential relevance to the seismic fragility analysis that exists within the larger technical community. In the second phase, the TI Team integrates these data, models, and methods into the inputs to the seismic fragility model that capture the center, body, and range of technically defensible interpretations. In this conceptualization, the center is the best estimate of the resulting interpretations, the body describes the shape of the distribution about the best estimate, and the range encapsulates the upper and lower limits of the TDI.

The concept of center, body and range is illustrated in Figure 1. In this conceptualization, the center is the best estimate of the resulting interpretations, the body describes the shape of the distribution about the best estimate, and the range encapsulates the upper and lower limits of the TDI.

3.4. ELEMENTS

There are four primary elements of the SSHAC process (USNRC, 2012 [2]):

1. Evaluation – Evaluation refers to the "consideration of the complete set of data, models, and methods proposed by the larger technical community that are potentially relevant to the analysis."
2. Integration – Integration refers to the process of "representing the center, body, and range of technically defensible interpretations in light of the evaluation process (i.e., informed by the SSHAC assessment of existing data, models, and methods)."
3. Documentation – This refers to the importance of fully and completely documenting the evaluation and integration that was carried out in the development of the model of aleatory and epistemic uncertainties.
4. Peer Review – The original SSHAC panel strongly recommended participatory peer review (referred to as the PPRP) for SL3 studies. The primary responsibility of the peer review is to ensure the SL3 process is properly implemented.

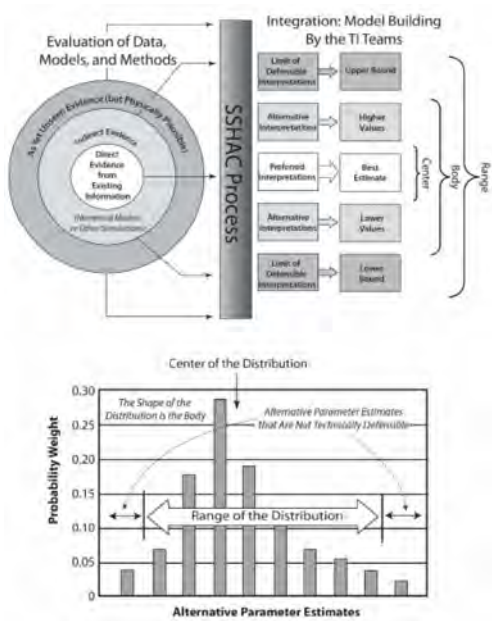

Fig. 1
Illustration of the concept of the center, body and range of technically defensible interpretations (USNRC, 2018 [3]).
Illustration du concept du centre du corps et de la portée des interprétations techniquement défendables (USNRC, 2018 [3]).

In a SL3 study, the analysis is carried out by a Technical Integration (TI) Team. The responsibility of the TI Team is to carry out a process of evaluation and integration (as defined in the SSHAC guidance). The TI Team is responsible for developing the inputs to the seismic fragility analysis and the fragility estimates for the Left Embankment. They carry out these elements of the process described above, following a series of steps identified in the SSHAC guidance. These steps include holding a specific series of workshops and meetings, and interactions with the PPRP (USNRC, 2018 [3]).

4. UNCERTAINTY FRAMEWORK

Probabilistic models of structure performance are representations of the 'real-world'; and thus have limitations and modeling uncertainties. Modeling uncertainties are attributable in part to limitations of data to estimate model parameters, models and methods to simulate an event – in this case the potential for liquefaction and the embankment response. In the seismic fragility analysis, the event of primary interest is the potential (conditional probability) for URR estimated as a function of earthquake magnitude and spectral acceleration (e.g., the seismic fragility of the Left Embankment).

To support a probabilistic analysis, it is useful to establish a framework that identifies, defines, and characterizes the types of uncertainty that affect model predictions. Establishing a framework has several benefits. First, it provides a structure for identifying and characterizing different sources of uncertainty. Secondly, it supports the characterization of these sources as aleatory or epistemic uncertainty. Third, it ensures that sources of uncertainty are clearly and distinctly identified. Lastly, it aids in preventing errors such as double counting or failing to identify and include sources of uncertainty in an analysis. For complex problems such as predicting the potential for large deformations and breach of embankments, there are uncertainties associated with alternative models that could be used, or technically defensible interpretations by experts of available data which may produce very different results (e.g., estimates of embankment deformation). Further, all models, whether analytical or empirical, require parameters to make predictions/ estimates. For analytical models these parameters are often physical attributes of the system (e.g., geometry, material properties), parameters of constitutive models that describe material behavior, etc. In the case of empirical models, these parameters (e.g., regression coefficients) are derived in a statistical analysis. For both empirical and analytical models, the quality and volume of data are important factors in assessing the confidence in the estimate of the model parameters and consequently in the model results (e.g., predictions).

Modeling and parameter uncertainties are different than uncertainties associated with the randomness of events (e.g., frequency of earthquake occurrences), or the stochastic variability in soil material properties, or the time of day when an earthquake occurs. Randomness of events is often referred to as inherent or irreducible – the randomness in nature. The uncertainty in random events is referred to as aleatory uncertainty and is quantified in terms of the frequency or probability of occurrence. In contrast, modeling events include uncertainties in the ability to estimate the frequency or probability of these events with any precision. These uncertainties are attributable to limitations of data, limitations in models and methods to predict events (e.g., seismic response of an embankment), and alternative interpretations of available data, or alternative methods for modeling a particular problem. These uncertainties are referred to as knowledge, or epistemic uncertainties.

An uncertainty framework was used to define the types of uncertainty that affect model predictions: aleatory and epistemic uncertainty. Aleatory uncertainty is attributed to the inherent randomness of events or properties; this is variability that in principle cannot be reduced. Random events are predicted in terms of their frequency of occurrence or the fraction of the time an event or property occurs. Examples of sources of aleatory uncertainty are variations in soil properties within a soil deposit, the spatial variability of soils in the foundation, the frequency or rate of future earthquake occurrences, or the randomness of earthquake ground motions (for an earthquake of a given magnitude that occurs a certain distance from a site), etc.

Epistemic or knowledge-based uncertainty is attributed to lack-of-knowledge about events or physical processes. This lack-of-knowledge may be manifested in terms of alternative models or methods to evaluate problems, or alternative interpretations of available evidence. Alternative models or interpretations must be technically defensible (are consistent with available evidence) but may lead to different results. The differences in models or interpretations represents a component of knowledge or epistemic uncertainty. Another type of knowledge uncertainty is attributed to limitations in available data (both amount and quality) that impacts the assessment of model parameters (parametric epistemic uncertainty). Table 1 shows such a framework/taxonomy for characterizing sources of uncertainty and their type in the context of models and model parameters.

The uncertainty framework in Table 1 suggests aleatory and epistemic uncertainties are modeled separately – they are not combined or conflated. An aleatory uncertainty model quantifies the sources of randomness (aleatory uncertainty) in estimating the seismic response of the embankment and the conditional probability of URR.

The epistemic model quantifies the uncertainty in developing the model inputs. These uncertainties include alternative, but technically defensible interpretations of available evidence (data, models, or methods), including evidence that may be conflicting.

Table 1
Framework for Characterizing Sources of Uncertainty

	TYPES OF UNCERTAINTY	
MODELING ELEMENT	**EPISTEMIC**	**ALEATORY**
Models	Uncertainty about a model and the degree to which it can predict events of interest. Model epistemic uncertainty addresses the possibility that a model may systematically (but not necessarily predictably), over- or under-predict events/results such as deformations. Model epistemic uncertainty may be based on different interpretations of experts about the technical defensibility of alternative models or methods of analysis, different conceptual frameworks, or the applicability of alternative datasets.	Aleatory model uncertainty is the variability not explained by a model. For instance, variability that is attributed to elements of the physical process that are not modeled and therefore represents random differences between model predictions and observations.
Parameter	Parametric epistemic uncertainty is the uncertainty associated with estimating model parameters given available data, indirect measurements, etc.When available data to directly estimate model parameters is limited. This uncertainty may also arise from alternative estimates based on expert assessments.	This uncertainty is similar to aleatory modeling uncertainty. However, this is variability that may be due to factors that are random but have a systematic effect on model results.

5. SEISMIC FRAGILITY ANALYSIS FRAMEWORK

In this section we describe in further detail the aleatory uncertainty model and epistemic uncertainty model. This notion is illustrated in Figure 2.

5.1. Aleatory uncertainty model

The aleatory model produces estimates of the seismic response (deformation) of the embankment to earthquake ground motions and the conditional probability of URR (seismic fragility) due to sources of aleatory uncertainty (randomness, variability) only. The sources of aleatory uncertainty include the randomness in the details of earthquake loading (input ground motion input histories) and in embankment properties such as embankment subzone blowcounts, shear wave velocity, etc. The randomness in the loading and the characterization of the embankment is manifested as randomness in estimates of the embankment response and potential for URR.

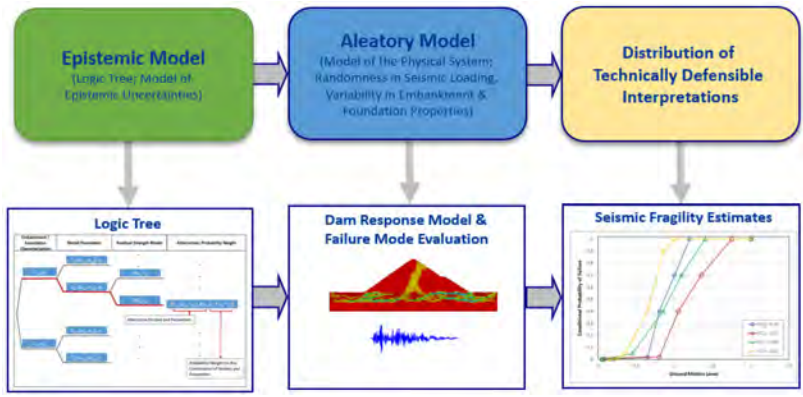

Fig. 2
Illustration of the aleatory and epistemic uncertainty models (the embankment diagram is from Boulanger and Montgomery, 2015 [4]).
Illustration des modèles incertains de l'aléatoire et du épistémique (le diagramme de la digue provient de Boulanger et Montgomery, 2015 [4]).

The result of the aleatory model is an estimate of the conditional probability of URR as a function of a measure of earthquake ground motion (e.g., spectral acceleration) and earthquake magnitude. This result is a seismic fragility curve. In the Left Embankment seismic fragility analysis, results are calculated as a function of earthquake source type (crustal or subduction), reservoir level, earthquake magnitude, and spectral acceleration.

5.2. Epistemic uncertainty model

The epistemic uncertainty model quantifies the uncertainty in the inputs to the aleatory model – that is uncertainty in data, models and methods. The model of epistemic uncertainties must capture the center, body, and range of technically defensible approaches for estimating the seismic performance and the potential for URR.

The result of considering alternative models is different estimates of the seismic fragility of the embankment – considering aleatory and epistemic uncertainties. Figure 3 shows a schematic illustration of multiple fragility curve estimates (also shown in the right side of Figure 2). Each fragility curve is a result of implementing the aleatory seismic fragility model based on alternative model and

parameter inputs. Associated with each fragility curve is a probability weight that is a measure of the degree-of-belief that it is a true measure of the seismic fragility. The set of curves quantifies the uncertainty in the estimate of the seismic fragility.

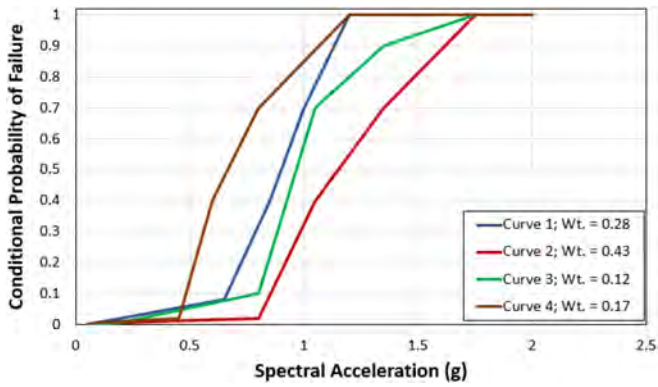

Fig. 3
Illustration of the uncertainty in the estimate of the seismic fragility.
Illustration de l'incertitude dans l'estimé de la fragilité séismique.

A common practice to organize and model sources of epistemic uncertainty is through the use of logic trees. A logic tree is a graphical construct (similar in structure to an event tree) that identifies the uncertain parameters and models that are required in the aleatory model (listed across the top of the tree). For each source of epistemic uncertainty, a series of branches are identified that correspond to technically defensible alternative values of parameters or alternative models. The sources of epistemic uncertainty represented in a logic tree map the uncertainties into a set of alternative inputs (parameters and models) to be used in the aleatory model. Each alternative is assigned a probability weight that is a measure of a technically defensibility alternative (i.e., a degree-of-belief that it is the true state of nature). A path through the logic tree corresponds to a complete set of inputs for the aleatory model (e.g., blowcounts $(N_1)_{60,cs}$, cyclic resistance ratio (CRR) estimates, permeabilities) that is supported by the available data and evidence as interpreted by the TI Team (see the Epistemic Model in Figure 2). The probability weight assigned to a path through the logic tree (see the red line through the logic tree in Figure 2) is the product of the weights for the individual alternatives along the path as estimated by the TI Team.

6. WANAPUM EPISTEMIC UNCERTAINTY MODEL

In the Left Embankment seismic fragility analysis there are two major parts of the epistemic uncertainty model. The first part includes the sources of epistemic uncertainty in the estimation of seismic deformations of the embankment in response to earthquake ground motions. This includes uncertainty in transforming Becker blowcounts to SPT blowcounts, estimates of CRR, alternative models for residual strength, etc. This part of the logic tree has over 400,000 end states, each representing a unique path, a unique set of inputs for modeling the Left Embankment that defines a distribution on estimates of the true state of nature. The second element of the logic tree is associated with the sources of uncertainty in modeling the progression of embankment deformations (damage) to URR for individual failure modes. In aggregate, these parts of the logic tree amount to millions of alternative models of possible embankment performance.

As noted, there are a number of sources of epistemic uncertainty being modeled in the seismic fragility analysis. For this paper, two aspects of the modeling are presented. The first is the uncertainty in estimating SPT blowcounts from Becker soundings. The second is the variation in estimated crest vertical deformations due to the variability in earthquake ground motions and the effect of different Becker blowcount transformations to SPT blowcounts.

6.1. ESTIMATING STANDARD PENETRATION TEST BLOWCOUNTS FOR GRAVELLY SOILS

For the coarse granular materials of the dumped rockfill and alluvium, blowcounts obtained directly from an SPT are unreliable. Becker Penetration Testing (BPT) was therefore used to characterize the material's penetration resistance by converting BPT measurements to equivalent SPT N_{60} values. The conversion of the BPT measurements was conducted using the Harder & Seed Method (H&S) (Harder & Seed, 1986 [5]) as well as the Instrumented Becker method (iBPT) (DeJong et al., 2017 [6]). The equivalent SPT N_{60} derived from the two transformation methods was significantly different. The differences in blowcounts can have a substantial effect on the estimated embankment displacements from non-linear dynamic analyses (discussed later). The interpretation of the raw blowcount and bounce chamber/delivered energy data through the correlation databases is a source of this epistemic uncertainty.

The published correlations for the H&S and iBPT Becker interpretation methods both include a correlation data set of side-by-side BPT/SPT borings. These borings are generally in silty sands, sands, and gravelly materials where the SPT blowcounts were deemed to be representative. They come from a variety of sites with varying depositional characteristics and blowcount profiles. As with many

blowcount-based correlations, there is significant scatter in the data due to in-site variability between adjacent boreholes; site-to-site variability, and potentially from fundamental differences in the response of the soils at different sites.

At the Wanapum site, the BPT blowcounts in the embankment units of interest were generally low with high Delivered Energy Ratios (DER) as measured by the iBPT equipment. The upper embankment materials were compacted in lifts above the water table and are generally dense although underlain by the lower blowcount materials. This stratigraphy of dense over loose soil, combined with high DER/low side friction and the large difference in equivalent SPT N_{60} values estimated by the H&S and iBPT approaches, led the TI Team to evaluate the original sites in each calibration dataset to see if Wanapum-specific insights could be gleaned from the data.

The intent of this review was to determine if either method was more directly applicable to the conditions at Wanapum, or if an alternative interpretation of the calibration datasets would yield a better estimate of the equivalent SPT N_{60}. As a result of this review, a total of nine alternative models were identified by the TI Team and included in the logic tree to model the epistemic uncertainty in the conversion of BPT measurements to SPT N_{60}. Each alternative was assigned a probability weight by the TI Team after significant discussion of the technical evidence supporting the alternatives. The result of evaluating each of the nine branches was an estimate of the distribution on the representative $(N1)_{60,cs}$ to be used in the nonlinear dynamic analysis. The results of this assessment for a dumped rockfill zone are illustrated in Figure 4. The range of the median $(N1)_{60,cs}$ estimates across the nine distributions varies by a factor of 2. The nine alternatives included the original published correlations (with some minor modifications) as well as other interpretations intended to account for i) the high delivered energies encountered at Wanapum; ii) Wanapum-specific BPT/SPT pairs considered as a standalone calibration; iii) Wanapum-specific BPT/SPT pairs considered as part of the larger calibration datasets; and iv) aleatory uncertainty in the correlations predictions derived from the given different potential realizations of the underlying data.

6.2. Seismic response analysis

The seismic response of the Left Embankment was estimated using the analysis program FLAC v8.1 (Itasca, 2019 [7]). Two-dimensional transverse sections were analyzed at 5 locations along the embankment. The FLAC model geometry for the maximum section is shown in Figure 5. Due to the liquefaction potential, the constitutive model PM4Sand was used to simulate the response of most soil units. The effect of epistemic uncertainties were estimated by performing analyses for logic tree branches considering equivalent $(N_1)_{60,cs}$ blowcounts, the percentile for selecting the representative blowcount, CRR and K_s, shear-wave velocity (Vs), transient seepage and permeability, and S_r.

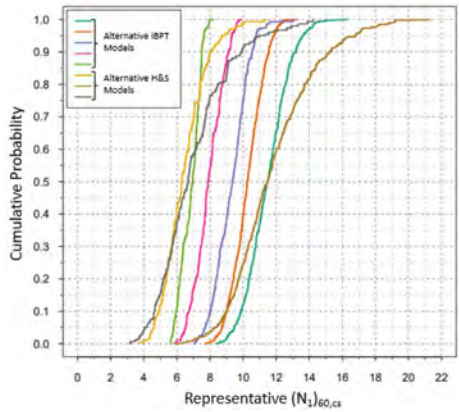

Fig. 4
Illustration of alternative estimates of the distribution on the representative $(N_1)_{60,cs}$ considering alternative methods for processing and transforming Becker blowcount data.
Illustration d'estimés alternatifs de la distribution sur le représentant $(N_1)_{60,cs}$ considérant les méthodes alternatives de traiter et transformer les données du décompte des coups

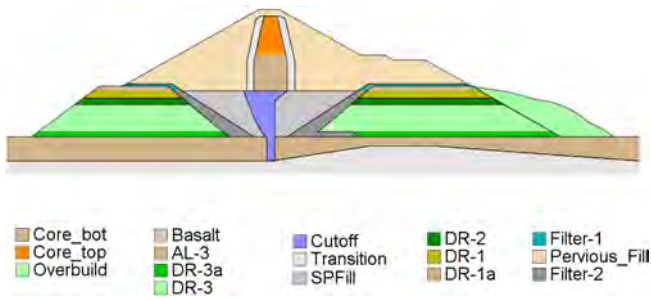

Fig. 5
FLAC model geometry for maximum embankment section.
Modèle de géométrie FLAC pour section endiguée maximale

The variability in seismic loading (earthquake time histories for the same magnitude earthquake and ground motion level) is a substantial contributor to the aleatory uncertainty in estimated embankment deformations. The probabilistic seismic hazard analysis (PSHA) for the site estimated the hazard from both nearby

crustal sources (M_W=5.0-8.0) and the Cascadia Subduction Zone (M_w = 7.5-9.5) with uniform hazard response spectra defined for annual frequencies of exceedance of 10^{-3} to 10^{-6} per year. A dataset of 30 seed ground motions were identified for each source type and 0.5-unit M_w bins (e.g., 5-5.5, 5.5-6, etc.). Linear scaling was used to adjust each ground motion to the target response spectrum over the response period range of most interest (T $\sim$ 0.3-0.8s) to maintain the intrinsic character of each recorded ground motion.

Although the 30 seed motions within each magnitude bin are individually considered representative of the PSHA, each ground motion produces different estimates of displacement due to their non-stationary characteristics and variations in frequency content. To improve the estimate of both median response and aleatory uncertainty, a subset of 5 records was selected for each M_w bin that evenly represent the range in estimated cumulative absolute velocity (CAV) between about median-1.8 standard deviations and median+1.8 standard deviations. Target CAV values consistent with the uniform hazard response spectra were developed using relevant ground motion models (e.g., the conditional CGGM from Macedo et al., 2021 [8]). An example of the estimated variability in vertical crest displacement at the end of shaking as a function of spectral amplitude and M_w is shown in Figure 6. Preliminary estimates of the logarithmic standard deviation of vertical crest deformations vary from about 0.45 to 0.55 for crustal earthquake motions.

Initial estimates of the epistemic uncertainty in vertical crest deformations indicate the median can vary significantly. For instance, if the estimated blow counts are high in critical zones (e.g., from the iBPT approach), deformations can be somewhat limited. Alternatively, if the estimated blow counts are low (e.g., from the H&S approach), the embankment deformations may be significantly greater. An initial comparison of these results is shown in Figure 7.

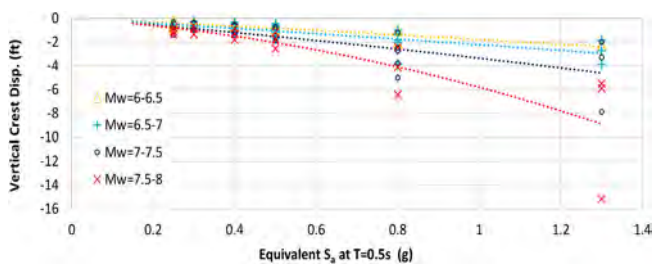

Fig. 6
Example estimates of the median crest settlement at end of shaking for maximum section and the same CRR, V_S and permeability branch as a function M_W and S_a.
Exemples d'estimés du dépôt en crête médiam à la fin du brassage pour section maximale et le même CRR, V_S et branche de perméabilité comme fonction M_W et S_a.

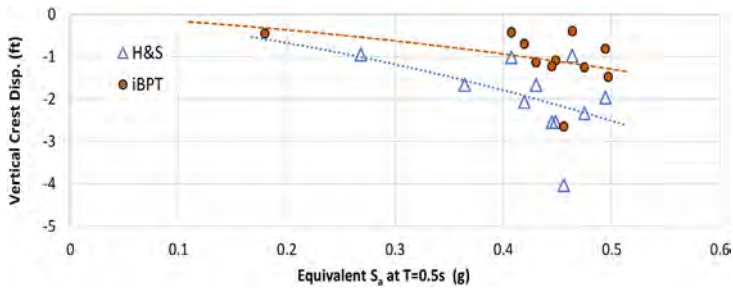

Fig. 7
Example comparison of the median vertical crest settlement at end of shaking for the maximum embankment section and different estimates of blowcounts as a function S_a for M_W = 7-7.5.
Exemple de comparaison du dépôt en crête médian à la fin du brassage pour digue maximale et différents estimés de décompte des coups comme fonction S_a pour M_W = 7-7.5.

7. SEISMIC FRAGILITY ESTIMATES

As described above, the logic tree defines alternative sets of inputs to the seismic fragility quantification. The result are thousands of alternative estimates of the seismic fragility of the Left Embankment. Each fragility estimate has a probability weight associated with it that is defined in the logic tree (it is the product of the probabilities for the various parameters and models on a path through the logic tree). These probabilities define a probability mass function on the estimate of the conditional probability of URR. At each ground motion level, the probability mass function, the estimates of the conditional probability of URR and the associated probability weights, can be rank ordered to determine a cumulative distribution. Repeating this at each ground motion level, percentile (e.g., 5^{th}, 50^{th}, and 95^{th} percentiles) fragility curves can be determined to display the uncertainty and level of confidence in the results. In addition, the mean estimate of the conditional probability of URR can be calculated.

Figure 8 presents an example of the seismic fragility results derived in this project. In Figure 8a the individual seismic fragility estimates derived from the logic tree inputs are shown. As noted, each curve has a probability weight associated with it. In general, the probability associated with the upper and lower estimates of the seismic fragility have very low values, indicating there is a low degree-of-belief (some, but limited technical support) that these are the true estimate. Figure 8b shows the 1^{st}, 5^{th}, 15^{th}, 50^{th}, 85^{th}, 95^{th}, and 99^{th} percentile estimates of the seismic fragility and the mean.

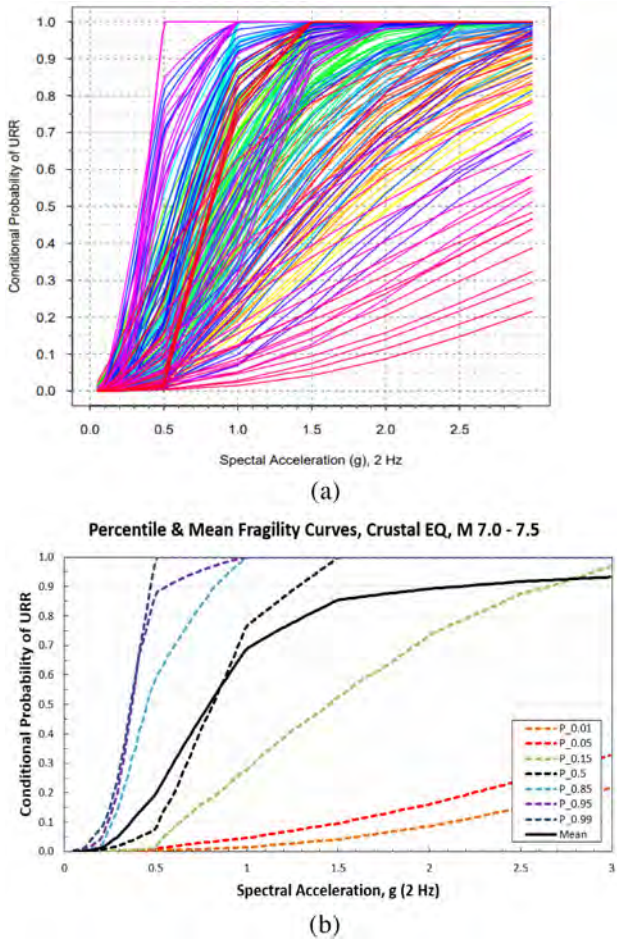

Fig. 8

An example of the results of the seismic fragility analysis, a) display of individual seismic fragility curve estimates based on the inputs defined in the logic tree, and b) 1st, 5th,15th, 50th, 85th, 95th, and 99th percentile and mean estimates of the seismic fragility. The results are shown for crustal earthquakes of M_W = 7-7.5.

Un exemple des résultats de l'analyse de la fragilité seismique, a) démonstration de l'estimé de la courbe basé sur les données définies dans l'arbre de la logique et b) 1er, 5e, 15e, 50e, 85e, 95e et 99e percentiles et estimés de moyens de la fragilité séismique. Les résultats sont démontrés pour séismes de croûte de M_W = 7-7.5.

The results reveal there is considerable uncertainty in estimating the seismic fragility of the Left Embankment. A deaggregation of the results provides the following observations:

- The uncertainty in the estimated blowcounts for critical subzones in the embankment and in the residual strength are critical parameters.
- Often a combination of parameters can collectively lead to alternatively high and low estimates of the seismic fragility; it is not always the extremely low or high values.
- While there are more than 30 failure modes that are evaluated in the embankment, a relatively small number are the primary contributors to the potential for URR.
- The uncertainty in the estimate of the conditional probability of failure is considerable. At some ground motion levels, the range in estimates can vary from nearly 0 to 1.0.

ACKNOWLEDGEMENTS

The project team appreciates the support of numerous professionals who contributed to this study. This includes Jason DeJong, Ian Hunter, Andy Kost, Bo Andre Lundqvist, Kevin Marshall, David Mishalanie, staff of the Federal Energy Regulatory Commission, and the project Participatory Peer Review Panel members: Kevin Coppersmith, Edward Kavazanjian, and Lelio Mejia.

REFERENCES

[1] BUDNITZ, R., APOSTOLAKIS, G., BOORE, D.M., CLUFF, L., COPPERSMITH, K.J., CORNELL, C.A., AND MORRIS, P. (1997). "Recommendations for Probabilistic Seismic Hazard Analysis: Guidance on Uncertainty and Use of Experts," *Prepared by the Senior Seismic Hazard Analysis Committee (SSHAC) for the Nuclear Regulatory Commission, NUREG/CR-6372*, Washington, D.C.

[2] U.S. Nuclear Regulatory Commission (2012). *Practical Implementation Guidelines for SSHAC Level 3 and 4 Hazard Studies*, NUREG-2117, Rockville, MD.

[3] U.S. Nuclear Regulatory Commission (2018). *Practical Implementation Guidelines for SSHAC Level 3 and 4 Hazard Studies*, NUREG-2213, Rockville, MD.

[4] BOULANGER, R.W. AND J. MONTGOMERY (2015). *"Nonlinear Deformation Analyses of an Embankment Dam on a Spatially Variable Liquefiable Deposit,"* 6th International Conference on Earthquake Geotechnical Engineering, Christchurch, New Zealand.

[5] HARDER, L., AND SEED, H. B. (1986). *"Determination of Penetration Resistance for Coarse-grained Soils Using the Becker Hammer Drill,"* University of California, Berkeley, UCB/EERC-86/06.

[6] DEJONG, J., GHAFGHAZI, M., STURM, A., WILSON, D., DEN DULK, J., ARMSTRONG, R., DAVIS, C. (2017). "Instrumented Becker Penetration Test I: Equipment, Operation, and Performance." *J. Geotechnical and Geoenvironmental Eng*. 10.1061/(ASCE)GT.1943-5606.0001717.

[7] ITASCA (2019). FLAC v8.1, *Fast Lagrangian Analysis of Continua*. http:// www.itascacg.com.

[8] MACEDO, J., ABRAHAMSON, N., AND LIU, C. (2021). "New Scenario-Based Cumulative Absolute Velocity Models for Shallow Crustal Tectonic Settings." *Bull. Seism. Soc. of Am.*, 111 (1): 157–172, https://doi.org/10.1785/0120190321.

COMMISSION INTERNATIONALE DES
GRANDS BARRAGES

VINGT-HUITIEME CONGRES DES
GRANDS BARRAGES
CHENGDU, MAI 2025

JUSTIFICATION DE LA STABILITÉ AU SÉISME DE GRANDS CANAUX FRANÇAIS PAR APPROCHES GRADUÉES (*)

Grégory COUBARD, Vinicius ALVES-FERNANDES, Philippe KOLMAYER & Astrid MONDOLONI
EDF

Romain GRANJON, Rachid FELLAG & Jérémy MEYNET
CNR

FRANCE

SUMMARY

The seismic reassessment of large hydraulic scheme with long linear canals raises many organizational and logistical issues. These long linear canals represent several hundred kilometers and are of prime interest for the two main French owners EDF and CNR. Since 2018, a ministerial order defines the mandatory situations for which the dams (and dikes) must be justified. Concerning the seismic justification, the assessment is mandatory in the most severe seismic zones (classified 3 or higher) and conducts EDF and CNR engineerings to develop and apply graded approaches both for liquefaction risk analysis and for dynamic shearing analysis (from pseudo-static to simplified dynamic transient methods).

RÉSUMÉ

Le diagnostic de stabilité au séisme des grandes infrastructures hydrauliques linéaires pose un certain nombre de contraintes d'un point de vue logistique et

Seismic stability analysis of large French canals using graded approaches

DOI: 10.1201/9781003642428-123

organisationnel. Ce type d'ouvrage représente un linéaire non négligeable sur le territoire français, et ce en particulier pour les principaux concessionnaires d'hydro-électricité que sont EDF et CNR. L'apparition d'un arrêté ministériel en 2018 visant à justifier de la stabilité des ouvrages hydrauliques dans le cadre des EDD, établis en zone de sismicité 3 ou plus, a conduit les ingénieries CNR et EDF à favoriser la mise en œuvre de démarches graduées, et ce tant pour l'analyse du risque de liquéfaction que vis-à-vis de la stabilité au cisaillement.

1. INTRODUCTION

En France, la sûreté des grands barrages doit être périodiquement réévaluée au travers d'une analyse de risques spécifique (appelée EDD : Etude de dangers) reposant elle-même sur une étude de stabilité dont les situations sont imposées depuis 2018 par arrêté ministériel [1]. Pour les plus grands ouvrages existants (classés A & B, correspondant globalement à des hauteurs respectives de 20 et 10 m, cf. figure 1) et localisés dans les zones sismiques les plus sévères (zones 3 et plus, cf. figure 1), la vérification de stabilité est requise en situation sismique. Cette démonstration concerne donc les grands canaux hydroélectriques français exploités par EDF et CNR sur le Rhône, le Rhin et la Durance (dont les localisations sont données de manière approchée sur la figure 1). Ces canaux sont des barrages en remblais de conceptions variables sur fondation meuble dont les hauteurs sur terrain naturel peuvent varier de quelques mètres à plus de vingt mètres et retenant des volumes d'eau importants (barrages de classes A & B). Une illustration d'un système d'endiguement type présent sur le Rhône est donnée par la figure 2.

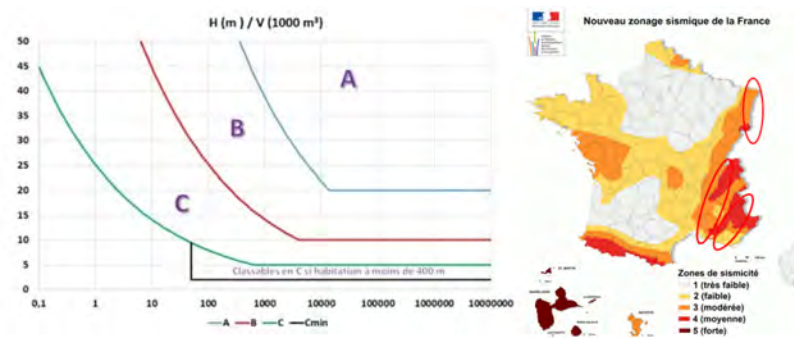

Fig. 1
Classification des ouvrages and zonage sismique français avec localisation du Rhône, du Rhin et de la Durance
French dam classification and seismic zoning with localization of Rhône, Rhin and Durance Rivers

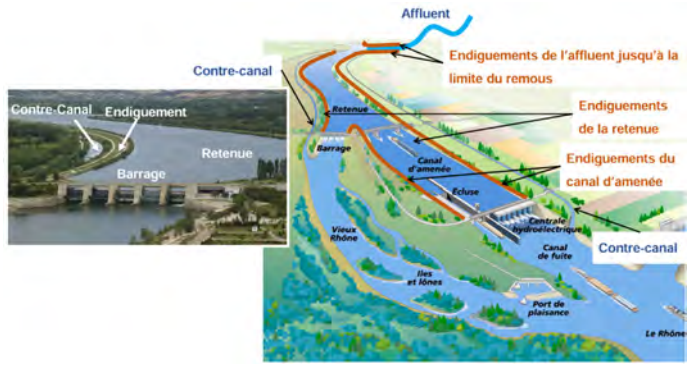

Fig. 2
Aménagement hydroélectrique type et endiguement sur le Rhône
Typical hydroelectric scheme and levees along Rhône River

La manière de démontrer la stabilité au séisme ou les méthodes de calcul sont, quant à elles, définies dans des recommandations françaises publiées par la profession au travers de groupes de travail ([2] & [3]). Dans ces documents et plus particulièrement dans les recommandations concernant spécifiquement le risque sismique [2], la notion d'approche graduée est abordée et préconisée. Elle consiste simplement à augmenter le niveau de complexité des études par étape lorsque l'étape précédente ne permet pas de justifier l'ouvrage étudié. Ce type d'approche a été déclinée à EDF et CNR pour les deux risques principaux que sont la liquéfaction et le cisaillement dynamique.

Le présent article propose d'illustrer la démarche d'approche graduée au travers (i) de la méthodologie globale adoptée à CNR pour les deux risques liquéfaction et cisaillement dynamique ainsi qu'au travers (ii) du développement d'une méthode dynamique transitoire simplifiée développée par EDF vis-à-vis du risque de cisaillement dynamique hors problématique de liquéfaction.

2. METHODOLOGIE PAR APPROCHES GRADUÉES

2.1. Démarche générale

La démarche générale d'approche graduée appliquée aux digues ou barrages latéraux en remblais consiste, en première approche, à analyser de manière

décorrélée le risque de liquéfaction et le risque de cisaillement dynamique. Si le risque de liquéfaction peut être écarté alors le risque de cisaillement dynamique est étudié par approches graduées en partant de méthode simple et en allant vers des méthodes avancées: (i) analyse pseudo-statique, (ii) analyses pseudo-dynamiques, (iii) analyse dynamique transitoire simplifiée. Si le risque de liquéfaction ne peut être écarté, des modélisations plus complexes doivent être envisagées : analyse dynamique transitoire non-linéaire avec couplage hydromécanique.

Cette démarche générale est illustrée dans les paragraphes suivants au travers de la méthodologie globale adoptée à CNR (EDF ayant une méthodologie semblable mais variant à la marge sur quelques points notamment dans l'analyse du risque de liquéfaction).

2.2. Les ouvrages CNR et la methodologie adoptee

Depuis les années 50, la Compagnie Nationale du Rhône (CNR) a aménagé le Rhône pour la production hydroélectrique en construisant des ouvrages en béton et plus de 400 km d'endiguements, afin de créer la retenue en amont du barrage de retenue et de la dérivation vers l'usine. Ces ouvrages ont été édifiés à l'aide des matériaux présents sur site, excavés au droit des futurs endiguements. Plus rarement, ces derniers ont été réalisés à l'aide de matériaux issus de zones d'emprunt toujours situées à proximité. Ces ouvrages sont de classe B au sens de la réglementation française. Ces ouvrages s'établissent dans la vaste vallée alluvionnaire du Rhône, avec un remplissage majoritairement sablo-graveleux (généralement quelques dizaines de mètres d'épaisseur), sous une couche de limons plus ou moins argileux. Ces alluvions reposent sur un substratum de nature variable, allant des terrains Tertiaires (molasses, marnes …) jusqu'aux terrains Primaire (cristallins) à proximité des anciens reliefs existant le long de la vallée. La sismicité de la vallée est généralement considérée comme modérée (1.6 m/s^2) à moyenne (2.4 m/s^2).

On distingue deux grandes catégories de digues en fonction des matériaux qui se trouvaient à disposition lors de l'excavation des emprises des digues de la retenue et du canal:

Les ouvrages dits « digues graviers », constitués de matériaux grossiers (graves sableuses ou sables graveleux), généralement roulés compactés côté amont pour diminuer la perméabilité des matériaux, le reste de l'ouvrage étant généralement constitué de matériaux « déversés». Ces digues sont souvent assises directement sur les alluvions grossières en place, après décapage partiel ou total des faibles épaisseurs de limons en place présents au droit de l'emprise de l'ouvrage.

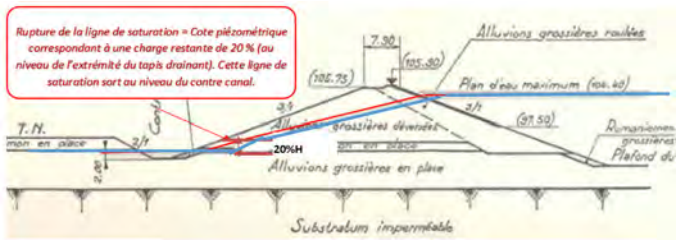

Fig. 3
Coupe type digue graviers
Typical gravel embankment cross-section

Les ouvrages dits « digues mixtes » ou « limons », correspondant à des ouvrages « zonés » dont le cœur est constitué par d'importants volumes de limons, rapportés en partie ou en totalité, du fait de grandes quantités de matériaux fins présents dans l'emprise des terrassements (Fig. 4).

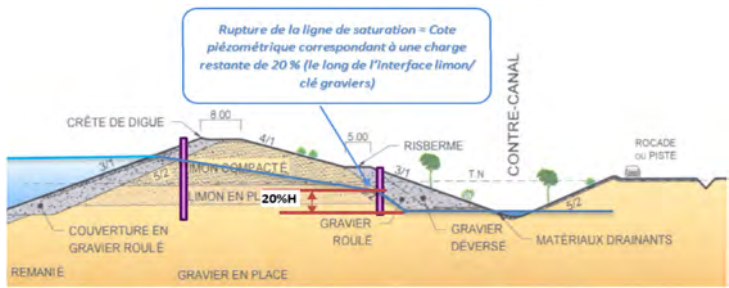

Fig. 4
Coupe type digue mixte/limons
[Typical mixed/silt embankment cross-section]

Au-delà de ces deux grandes typologies, il existe des sous-catégories d'ouvrages que CNR s'est attachée autant que faire se peut d'identifier.

2.2.1. *Démarche CNR*

La démarche porte sur l'analyse conjointe du comportement des ouvrages au glissement sous sollicitations dynamiques (approche pseudo-statique et dynamique

simplifiée) et une analyse graduée du risque de liquéfaction. Les configurations particulières locales relevées le long de la vallée en lien avec le risque de liquéfaction font l'objet d'une analyse plus spécifique.

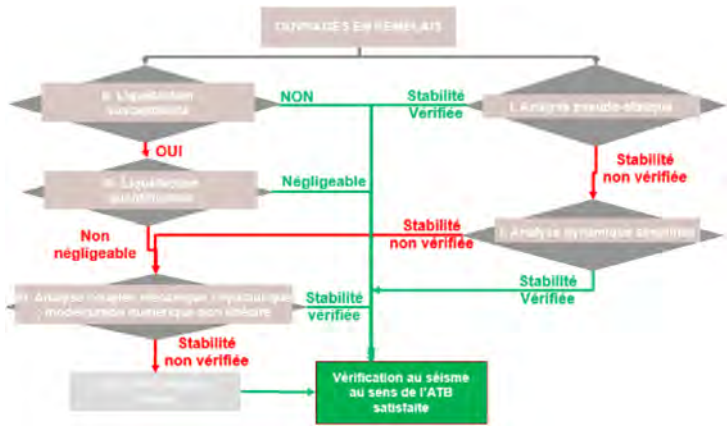

Fig. 5
Logique de progression de l'analyse
Analysis flowchart

L'analyse du risque de liquéfaction est menée en parallèle de l'analyse de stabilité au glissement sous sollicitation dynamique, et ce pour écarter au plus tôt la nécessité d'avoir recours à des modélisations non linéaires du fait de la particularité des mécanismes de rupture par liquéfaction et de leur complexité.

2.2.2. *Logistique et organisation*

L'analyse des grandes infrastructures linéaires nécessite un important travail d'inventaire amont, si tant est que les données d'archives soient facilement accessibles et exploitables. La mise en œuvre de cette démarche propre à CNR a nécessité:

1/ De nombreuses recherches en archive et la conception de bases de données:

La construction du DGO (Dossier Géotechnique des Ouvrages), regroupant les documents relatifs aux données géotechniques, géophysiques et géologiques des ouvrages CNR. Cette mission a représenté pour CNR l'équivalent de 8 mois de

travail en ETP, pour un total de 500 boites d'archives et 2000 dossiers consultés et numérisés,

La construction de la base de données digues (découpage des 400 km d'endiguements en 442 tronçons types différents intégrés dans un SIG avec des caractéristiques de matériaux et géométriques) et qui a nécessité près de 2 ans de travail.

La base de données de sondages compilant et digitalisant l'ensemble des sondages réalisés le long de la vallée du Rhône sur le périmètre de la concession ainsi que les très nombreux essais géotechniques réalisés (*in-situ* ou au laboratoire). Cette tâche a été réalisée sur plusieurs années (travail initié en 2010) pour arriver à quasiment finaliser le travail, ne restant actuellement que deux aménagements de la concession à traiter sur les 18 existants.

2/ Un investissement important de l'ingénierie CNR pendant 2 ans pour déployer les approches pseudo-statique et pseudo-dynamique:

L'analyse des profils représentatifs des 400 km d'endiguements afin d'identifier des profils géométriques types suffisamment enveloppes et représentatifs de la diversité des ouvrages rencontrés le long de la vallée du Rhône (12 profils types dans le cadre de cette étude),

La définition de valeurs suffisamment larges mais réalistes des caractéristiques géologiques et géomécaniques des matériaux rencontrés le long de la vallée du Rhône (tant dans les ouvrages qu'en fondation),

La définition de paramètres complémentaires encadrant (géométrie de la ligne de saturation, amplitude du niveau de la sollicitation sismique (accélération, effet de site potentiel),

Le croisement des différents paramètres pour les différents profils types afin de calculer leur stabilité au séisme : 4320 simulations pour l'approche pseudo-statique, et 3240 simulations pour l'approche pseudo-dynamique.

In fine, l'étude de sensibilité a porté sur une douzaine de profils génériques représentatifs des différentes typologies d'ouvrages rencontrées le long de la concession, à savoir 4 profils de type graviers, et 8 profils de type mixtes limons. Différents scénarii de charges hydrauliques résiduelles internes ont été pris en compte dans les calculs de stabilité, compris entre 0 et 20 % (0, 10 et 20 %).

Différents jeux de caractéristiques mécaniques des sols ont été également considérés. Ces jeux de caractéristiques mécaniques ont été établis sur la base de l'analyse statistique des différentes campagnes de reconnaissances historiques réalisées au droit des différents aménagements et des retours d'expérience au cours de l'histoire de la Compagnie Nationale du Rhône.

3/ Une approche spécifique du phénomène de liquéfaction afin de cibler les secteurs à risque potentiel:

Les bases de données, les recherches en archives et les données comportementales ont permis d'avoir une connaissance fine de nos ouvrages afin de mettre en avant les dispositions constructives et d'exploitation permettant d'exclure le risque de liquéfaction, Pour les secteurs pour lesquels il subsistait un doute, nous avons mené des campagnes de reconnaissances ciblées et des études spécifiques permettant d'écarter le risque de liquéfaction. De la même manière les zones dites « d'incident » où les données d'auscultation indiquent la présence d'une évolution notable des conditions de site (conditions d'écoulement et érosion interne, …) sont traités de manière indépendante et spécifique.

Notre démarche a été formalisée dans une note, qui outre la méthodologie explicitée, démontre la tenue des endiguements de la CNR pour le séisme réglementaire (selon les profils, pas de glissement ou glissement de faible ampleur sans impact sur la tenue globale et absence de risque de liquéfaction). Ces résultats sont utilisés pour la démonstration de conformité à la réglementation dans le cadre des études de dangers des ouvrages CNR.

3. ANALYSE DU RISQUE DE LIQUÉFACTION

3.1. Démarche générale et progression de l'analyse

La méthodologie mise en œuvre par CNR pour l'évaluation du risque de liquéfaction s'articule autour de 3 étapes successives :

Etape 1 : Analyse des dispositions constructives – identification des profils en écart avec les caractéristiques sécuritaires de conception des digues CNR.

Etape 2 : Analyse complémentaire en regard des configurations standards de fonctionnement des ouvrages.

Etape 3 : Etudes des caractéristiques géotechniques des matériaux.

3.1.1. *Analyse des dispositions constructives*

La première étape de l'analyse du risque de liquéfaction des sols de fondations des digues est menée en se basant sur :

a) le type de digue (composition et sols de fondation),

b) les dispositions constructives des profils en travers issus des dossiers conformes à exécution (profils en travers type, d'exécution, localisation des profils ...).

Cette analyse a été réalisée profil par profil sur les digues de retenue et de canaux qui retiennent un niveau d'eau permanent en fonctionnement normal (hors crue). Le premier inventaire consiste donc à vérifier dans quelle mesure l'ensemble des profils d'endiguement le long de la concession répondent bien aux deux exigences de conception suivantes :

Une conception géométrique (en particulier pour les digues dites mixtes/limons, et dans une moindre mesure pour les digues en graviers à « noyaux limons ») en forme de « voûte » venant en appui/ancrage sur les alluvions grossières de fondation de bonne qualité, via d'importantes recharges graveleuses amont et aval. Le confinement global des matériaux laissés en place dans le soubassement de l'ouvrage est assuré par ces éléments de butée et le chargement apporté par les matériaux compactés sus-jacents.

La présence de recharges graveleuses largement dimensionnées de façon à anticiper une faiblesse/rupture éventuelle des limons contenus dans le soubassement des ouvrages du fait d'une montée éventuelle des pressions interstitielles. Le risque de liquéfaction globale du soubassement est alors considéré comme exclu pour les ouvrages à la suite des conclusions des essais d'ébranlement en vraie grandeur réalisés en 1954 par CNR sur Montélimar et de la conception retenue pour la grande majorité du linéaire des ouvrages de la concession. En effet, on retiendra que :

Les alluvions et graviers de fondation ont une perméabilité élevée qui permet de dissiper facilement et rapidement les surpressions d'eau interstitielle qui pourraient se générer lors d'un séisme, rendant par conséquent ces sols difficilement liquéfiables.

Les recharges en alluvions amont et aval, si elles sont ancrées dans les alluvions en place, permettent de limiter le volume de limon en place potentiellement liquéfiable sous la digue. Ces recharges permettent également de favoriser la dissipation des pressions dans les limons tout en assurant le confinement de ces derniers. Pour les profils ayant des configurations identiques/similaires, le risque de liquéfaction est écarté. L'ensemble des écarts à cette conception de base des ouvrages CNR a conduit à retenir une liste de tronçons où une analyse complémentaire est nécessaire, ce qui correspond à la seconde étape.

3.1.2. *Analyse complémentaire*

L'analyse complémentaire vise alors à déterminer si ces écarts ne sont que le reflet d'une adaptation particulière de l'ouvrage aux conditions locales, mais sans

conséquence sur la stabilité globale de l'ouvrage sous sollicitation sismique : absence de saturation des sols, absence de mise en charge à retenue normale (fonctionnement en digue sèche des queues de retenue en particulier, etc …), ou si ces écarts sont a priori préjudiciables pour la stabilité globale de l'ouvrage sous sollicitation sismique.

Si l'analyse complémentaire ne permet pas d'exclure une sensibilité à un scénario de rupture d'ensemble par liquéfaction de l'ouvrage en retenue normale, les tronçons concernés sont étudiés en analysant les caractéristiques géotechniques des matériaux présents en fondation des ouvrages. Cette étude porte alors sur l'analyse de l'ensemble des données géotechniques disponibles à la CNR (granulométrie, essais d'identifications et de laboratoire …), issues :

- Des campagnes de reconnaissances préliminaires à l'aménagement.
- Des campagnes de reconnaissances post travaux.
- Des campagnes de reconnaissances réalisées dans le cadre des diagnostics d'ouvrages.

3.1.3. *Etudes des caractéristiques géotechniques des matériaux*

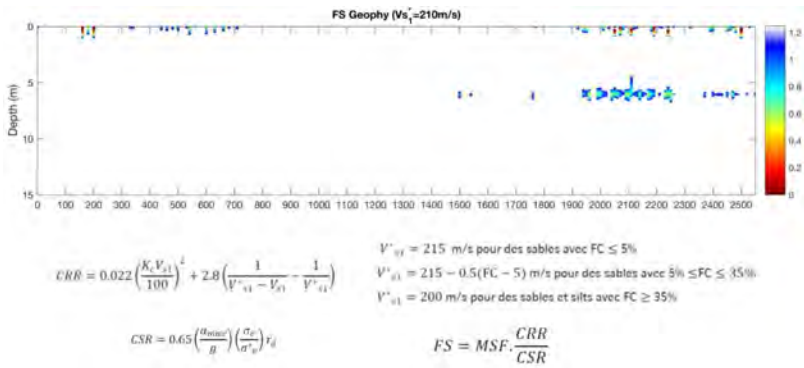

Fig. 6
Exemple de profil de distribution de FS le long de l'aménagement de Vallabrègues calculé à partir des valeurs de Vs issues de la campagne de reconnaissance MASW
Example of the FS distribution profile along the Vallabrègues development, calculated using Vs values from multichannel analysis of surface waves (MASW) testing

Dans le cas où ces dernières données s'avéraient insuffisantes pour conclure, il est fait appel à une analyse spécifique à partir de reconnaissances et analyses complémentaires. L'analyse se réalise le long des systèmes

d'endiguement préalablement identifiés comme étant sensibles à la liquéfaction, et est calculé à partir des profils de valeurs de Vs fournis. La méthode [10] est utilisée compte tenu de son déploiement rapide. Elle a été étalonnée sur d'importantes campagnes de reconnaissances au pénétromètre statique CPTU.

Cet indice (dit d'Iwasaki [6]) permet d'exprimer la sensibilité à la liquéfaction d'un site en considérant le profil de sol dans ses 20 premiers mètres. Le calcul est effectué sur la base de la méthodologie [11] :

$\mathrm{LPI} = \int_0^{20} Fw(z)dz$Aveco°:

- z°: la profondeur
- F°: f(FS_L) avec°:
- FS=1 - FS_L si $FS_L < 1$ et Fs=0 si $FS_L > 1$
- w(z)°: fonction de pondération égale à w(z) = 10 - 0.5z

- pour 0 < LPI<5 => effets mineurs
- pour 5<LPI<15 =>effets visibles
- pour LPI > 15 => effets graves

En pratique, le calcul de l'indice LPI s'effectue sur l'ensemble des couches de sol de 20 m d'épaisseur et découpé en n sous couches, suivant l'expression :

$$\mathrm{LPI} = \sum_{1}^{n} Fi\mathrm{wi(z)Hi}$$

Les calculs sont présentés sous la forme d'un profil LPI le long des différents profils des tronçons étudiés. Le calcul de la valeur de LPI est conduit par intégration le long de profils verticaux de la distribution des coefficients de sécurité vis-à-vis du phénomène de liquéfaction.

3.2. Retour d'experience vis-a-vis du risque de liquefaction le long des amenagements de la cnr

La mise en œuvre de la méthodologie CNR d'évaluation de la sensibilité de ses endiguements en remblai vis-à-vis du risque sismique a permis de démontrer que la quasi-totalité des endiguements CNR ne sont pas sensibles au phénomène de liquéfaction du fait de dispositions constructives favorables (matériaux compactés et drainants, recharges amont et aval en alluvions grossières créant des « effets voûtes » et de la présence de matériaux pas ou peu sensibles (sortant des fuseaux granulométriques des matériaux sensibles à la liquéfaction).

Pour les quelques secteurs potentiellement plus sensibles, l'étude spécifique montre que les sols liquéfiables se présentent de manière diffuse et très peu étendue au sein de la seule formation limoneuse en fondation sous les niveaux de sollicitations à considérer (approche probabiliste). Leur potentiel de liquéfaction peut être considéré comme faible, et n'est pas de nature à remettre en cause la stabilité

des ouvrages dans l'état actuel des connaissances, les critères de sévérité de liquéfaction s'avérant généralement nuls à faibles, et ponctuellement très modérés.

4. ANALYSE DU CISAILLEMENT DYNAMIQUE

4.1. Approche pseudo-statique

L'approche consiste classiquement à analyser la stabilité potentielle d'une masse de sol sous l'effet complémentaire de forces horizontales d'inertie induites par le séisme en plus de la gravité, selon les procédés de calcul classiques de stabilité des pentes mis en œuvre par CNR pour justifier de la stabilité de ces ouvrages (méthode des tranches de type Bishop, surface de rupture circulaire, Fig.7). Cette force horizontale « complémentaire » associée au séisme s'exprime sous la forme:

$$F = k*V*\gamma b$$

Avec:

γb: Masse volumique du sol

V: volume de la masse glissante

k: coefficient pseudo-statique adimensionnel, $k = \alpha*ag*S/g$

α: coefficient sismique adimensionnel, pris égal à 2/3 pour la composante horizontale*

ag: accélération au rocher

S: Coefficient d'amplification de site

g: l'accélération de la pesanteur

4.2. Approche pseudo-dynamique

Les méthodes pseudo-dynamiques permettent de compléter l'analyse pseudo-statique en estimant les déplacements permanents, et ce dans la mesure où:

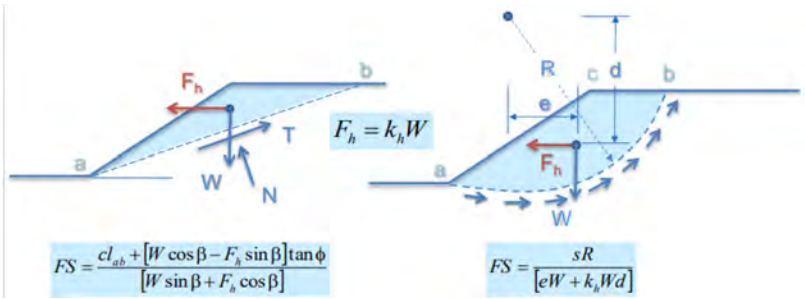

Fig. 7
Approche pseudo-statique
Pseudo-static approach

a) La stabilité des ouvrages vis à vis du cisaillement dynamique ne peut être obtenue via l'approche pseudo-statique
b) les phénomènes de montée de pression interstitielle / liquéfaction peuvent être raisonnablement écartés du fait du niveau de sollicitation sismique et de sa durée, de la nature et sensibilité des matériaux constitutifs des ouvrages et de leurs fondations, ainsi que de la classe des ouvrages.

Bien que de complexité moindre que les approches dynamiques non linéaires, l'approche pseudo-dynamique nécessite néanmoins une démarche d'analyse plus élaborée, qui peut s'avérer très chronophage lorsqu'elle concerne la justification d'ouvrages de grande extension et à profils variés, tels que les ouvrages de retenue ou de canaux des aménagements au fil de l'eau. En effet, la résolution du problème nécessite la réalisation de trois étapes distinctes et indépendantes:

Etape 1: Analyse de la stabilité critique au glissement : on cherche à définir pour chaque masse de glissement l'accélération critique conduisant à un facteur de sécurité égal à 1.

Etape 2: Caractérisation du mouvement sismique du barrage, en particulier l'accélération de la masse potentielle de glissement étudiée. Les travaux d'amélioration de la prédiction de la réponse dynamique des ouvrages sur sols meubles [4] s'avèrent particulièrement faciles d'usage en regard de celles déjà existantes.

Etape 3: Analyse de type Newmark [5], permettant de définir les déplacements irréversibles lorsque l'accélération de la masse de glissement potentielle dépasse l'accélération critique. Dans ce cas, le corps n'est pas considéré comme un bloc rigide mais comme un corps élastique non linéaire.

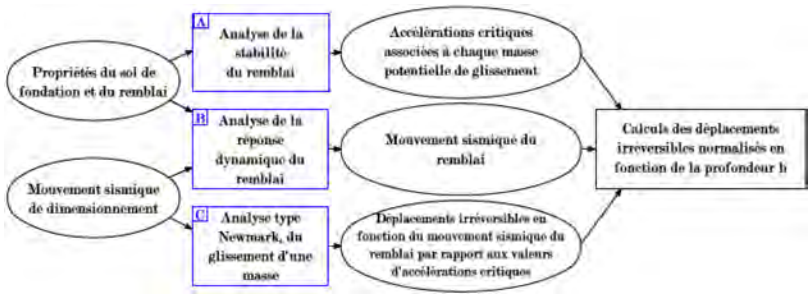

Fig. 8
Méthodologie schématique pour l'estimation des déformations irréversibles
Diagram of the methodology used to estimate permanent deformations

Les différentes étapes du calcul sont présentées dans le logigramme indiqué sur la Figure 8.

L'étape 2 de caractérisation du mouvement sismique du remblai s'avère assez complexe, et fait généralement appel à des processus itératifs, qui sont d'autant plus complexes qu'ils dépendent à la fois des caractéristiques physiques des ouvrages et de sa fondation, en particulier en présence d'une fondation alluviale intercalaire entre celui-ci et le substratum. Il existe peu de méthodes permettant d'apprécier cette interaction.

De manière à alléger la procédure, (cf. étape 2), les travaux de [4] ont été utilisés. Ces derniers consistent en l'établissement d'un outil de calcul simplifié basé sur une étude paramétrique portant sur différentes configurations de géométrie de digues, de conditions de fondation (épaisseur de couche d'alluvions, vitesse Vs des alluvions), de niveaux de sollicitations sismiques calés sur les spectres de réponse réglementaires de chacune des zones de sismicité de la métropole et des DOM TOM) : 0.01 g, 0.1 g, 0.3 g et 0.5 g. Ces situations sont adaptées au besoin de CNR car couvrant le champs des configurations pratiques rencontrées le long de la vallée du Rhône. on pourra se reporter pour plus d'information sur cette méthode aux articles CFBR associés [18] [19].

On utilise en particulier des abaques, qui sont établis sur la base des paramètres suivants :

PGA: accélération au rocher, prise égale à 1.6 en zone sismique 3 ou 2.4 m/s^2 en zone 4,

V_{cmin}: vitesse moyenne des ondes de cisaillement dans la couche de fondation (alluvions grossières du Rhône),

fo: fréquence de résonnance du remplissage alluvionnaire de la vallée du Rhône en fondation des ouvrages. On retiendra que la fréquence fo d'une couche de sol est reliée à son épaisseur H (m) et à la vitesse de propagation des ondes de cisaillement dans la couche (Vcmin : m/s) par la relation suivante : fo = Vcmin / (4 x H),

Vd: Vitesse moyenne des ondes de cisaillement Vs dans le corps de digue.

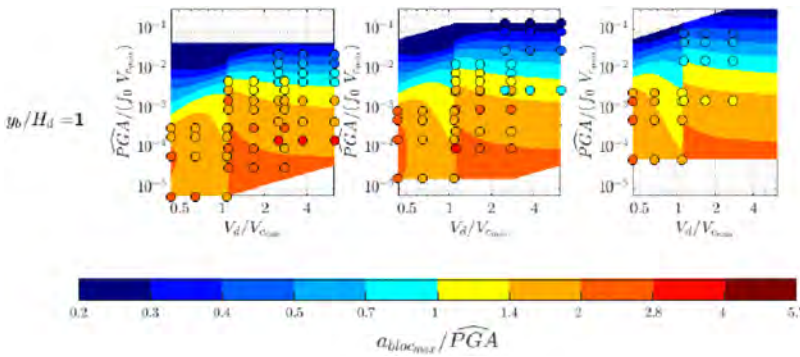

Fig. 9
Abaque associé pour la détermination de l'accélération maximale du bloc pour yb/Hd = 1
Associated chart for determining maximum block acceleration for yb/Hd = 1

Une représentation graphique permet d'exploiter facilement l'évolution de la fonction de forme nouvellement associée aux résultats des simulations.

La valeur de l'accélération du bloc ainsi déterminée pouvant alors être injectée dans les abaques de Seed-Makdisi [9] ou autre approche équivalente pour déterminer le déplacement irréversible associé, moyennant une évaluation réaliste de la période propre du système fondation + ouvrage. La transition abrupte observée pour le rapport Vd/Vcmin = 1 est à mettre en relation avec le choix des configurations choisies pour les simulations numériques.

Le développement de cet outil a permis de simplifier de manière conséquente le processus de cette étape 2, et donc d'obtenir un gain de temps très significatif sur l'analyse générale de sensibilité de la stabilité des ouvrages au cisaillement cyclique via l'approche pseudo-dynamique.

4.2.1. *Retour d'expérience de l'utilisation de l'approche pseudo-dynamique et de la démarche simplifiée proposée pour l'évaluation du mouvement sismique sur les ouvrages CNR*

Concernant la stabilité au glissement en l'absence de risque de liquéfaction, il ressort en particulier que pour les digues graviers, dans les configurations potentiellement sensibles préalablement identifiées par la méthode pseudo-statique, à savoir certaines configurations en zone de sismicité 4, les déplacements irréversibles se révèlent finalement nuls ou restent marginaux et ne sont pas de nature à générer de désordres significatifs engendrant un risque pour la sûreté hydraulique. Ils sont en effet inférieurs à 3 cm, bien en deçà des recommandations [2] fixées à 3 % de la hauteur de l'ouvrage.

Pour les digues dites « limons » ou mixtes, l'approche de calcul dynamique simplifiée permet d'établir que la conception originale des ouvrages CNR contribue à les rendre relativement robustes à la sollicitation sismique. Les calculs de sensibilité conduisent à envisager des déformations irréversibles faibles en zone de sismicité 3, de l'ordre de quelques centimètres (3 cm) tout au plus, et des déplacements horizontaux irréversibles modérés en zone de sismicité 4, de l'ordre de 10 à 20 cm, qui restent en deçà des seuils recommandés (3 % de la hauteur) pour garantir la tenue des ouvrages en cas de séisme.

4.3. Analyse dynamique transitoire simplifiée

L'analyse dynamique transitoire simplifiée présentée ici a été développée par EDF et constitue une gradation supplémentaire vis-à-vis des méthodes pseudo-statique et pseudo-dynamique exposées aux paragraphes précédents. Cette analyse comprend deux grandes étapes : (i) Analyse de la réponse dynamique de l'ouvrage étudié (ou des différents profils type du canal) avec le modèle de comportement d'Iwan ([12] & [13]), (ii) Estimation des déplacements irréversibles induits s'appuyant sur l'évolution temporelle des champs d'accélération calculés à l'étape précédente et sur l'accélération critique des cercles de glissement étudiés. Cette estimation est basée sur la méthode de Newmark ([5] & [14]).

Pour rappel, cette approche dynamique transitoire simplifiée ne peut être appliquée que si le risque de liquéfaction a pu être précédemment écartée (i.e. pas de couplage hydromécanique).

4.3.1. *Modèle d'Iwan*

Le modèle de comportement d'Iwan ([12] & [13]) implémenté dans le logiciel Code Aster, est une loi de comportement 3D élastoplastique multimécanisme

classique pour la description du comportement cyclique déviatorique des matériaux. A chaque surface de charge de type Von Mises est associée un mécanisme d'écrouissage cinématique linéaire, et la règle d'écoulement plastique est associée. Ce modèle peut être interprété par un schéma rhéologique comme un arrangement en série d'un élément de Jenkin (ressort avec patin frottant parfaitement plastique). L'utilisation d'un écrouissage cinématique permet au modèle de considérer la dissipation d'énergie par amortissement hystérétique et d'être directement en adéquation avec les règles de Masing.

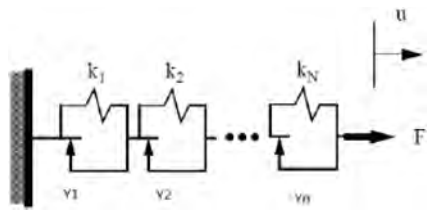

Fig. 10
Schéma rhéologique du modèle d'Iwan implémenté dans Code Aster
Rheological model of Iwan model implemented in Code Aster

Le principal avantage de ce type de modèle est la possibilité de prescrire directement la courbe d'évolution du module de cisaillement sécant G avec la déformation de cisaillement γ. En plus, le fait de considérer un écrouissage cinématique linéaire permet un passage d'une mise en équation tensorielle du modèle 3D à un système d'équations scalaires à résoudre, ce qui permet un cout numérique réduit. Les inconvénients du modèle sont (i) l'impossibilité de directement imposer l'évolution de l'amortissement du matériau avec le niveau de déformation, (ii) la non prise en compte d'un critère de rupture adapté à la mécanique des sols et (iii) l'hypothèse d'un comportement volumique uniquement élastique, sans dilatance.

Sous ces hypothèses, le modèle d'Iwan peut être vu comme une amélioration directe de la méthode linéaire équivalente couramment utilisée dans le domaine de la dynamique des sols.

La calibration des paramètres d'écrouissage cinématique linéaire de chaque surface de charge vise à approcher un modèle hyperbolique pour le comportement en cisaillement, décrit via l'équation suivante:

$$\tau = \frac{G_{\max}\gamma}{1 + \left(\frac{\gamma}{\gamma_{ref}}\right)^{n}} \qquad (1)$$

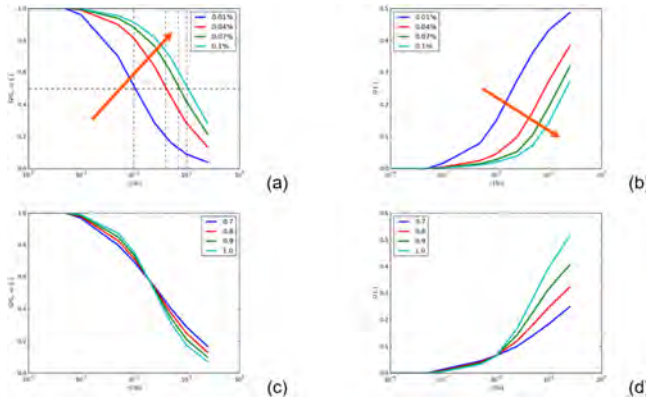

Fig. 11
Effet des paramètres de calibration du modèle sur l'évolution du module de cisaillement sécant G et l'amortissement D. (a) (b) : modification de γ_{ref} et (c), (d) : modification de l'exposant n
Impact of calibration parameters on G(γ) and D(γ) curves. (a) (b): Impact of γ_{ref} parameter and (c) (d): Impact of n parameter

$G_{\max}$ est le module de cisaillement initial du sol (ou module de cisaillement à très faible distorsion). γ_{ref} et n sont les paramètres de calibration de la loi.

Le modèle permet d'approcher cette équation linéairement par morceaux, l'erreur commise dans l'approximation étant donc directement liée au nombre de surfaces de charge. L'implémentation réalisée dans Code Aster considère 12 surfaces, afin d'approcher au mieux l'intervalle de déformations de cisaillement entre 10^{-5} et 10^{-2}.

La figure 14 montre l'impact du choix de paramètres γ_{ref} et n sur les courbes G(γ) et D(γ) décrivant respectivement l'évolution du module de cisaillement et de l'amortissement hystérétique en fonction de la distorsion.

4.3.2. *Estimation des déplacements irréversibles par la méthode de Newmark*

La méthode de Newmark [5] a été implémentée dans le logiciel Code Aster [14]. Elle permet de calculer les déplacements irréversibles liés à la réponse dynamique des remblais le long de différentes surfaces de glissement.

Cette méthode se base sur l'idée que la masse délimitée par la surface de glissement peut être approchée par un bloc glissant sur un plan incliné. Lors d'un

séisme, ce bloc peut glisser dès lors que son accélération moyenne, définie comme le quotient entre la résultante des efforts horizontaux sur cette zone et sa masse, dépasse une accélération critique, définie comme l'effort inertiel qui conduit à un facteur de sécurité unitaire.

L'implémentation actuelle de la méthode dans Code Aster permet deux possibilités : (i) l'utilisateur entre la géométrie des cercles de glissement étudiés et de leurs accélérations critiques associées (estimées par une méthode d'équilibre limite), (ii) l'utilisateur entre seulement la géométrie des cercles étudiés et les accélérations critiques sont déterminées directement par Code Aster.

Les déplacements irréversibles des cercles étudiés sont ensuite obtenus par une double intégration de la partie positive de la différence entre l'accélération moyenne $k_m(t)$ et l'accélération critique k_c.

4.3.3. *Application de l'approche à un grand canal*

L'approche dynamique transitoire simplifiée présentée dans les paragraphes précédents a été appliquée sur un grand canal hydraulique (exploité par EDF) d'une hauteur maximale de 30 m.

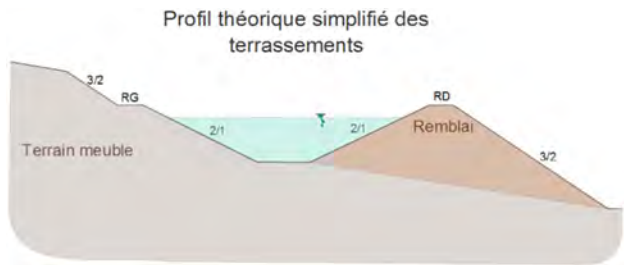

Fig. 12
Allure du canal au niveau des profils étudiés par approche dynamique transitoire simplifiée
Typical cross section profile of the studied canal with the simplified transient dynamic approach (only the right bank is concerned)

Sur ce canal, le risque de liquéfaction a pu être écarté rendant l'analyse du cisaillement dynamique par approche graduée applicable. Le canal a été étudié au travers de 15 profils bidimensionnels représentatifs des variations géométrique et géomécanique le long du linéaire étudié (canal de plusieurs kilomètres de long).

La première étape de l'approche graduée a été un analyse pseudo-statique. En cohérence avec les recommandations [2], les forces d'inertie ont été prises en compte en appliquant un coefficient de 2/3 au PGA dans la direction horizontale.

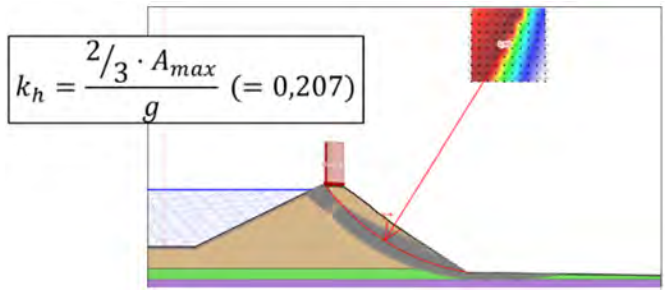

Fig. 13
Illustration de l'analyse pseudo-statique
Illustration of the pseudo-static analysis

Cette analyse n'a permis de justifier aucun des 15 profils étudiés.

La seconde étape de l'approche graduée a été l'analyse pseudo-dynamique. Sur ce canal, cinq méthodes différentes, issues de la littérature, ont été appliquées dont la méthode présentée au §. 4.2, afin de d'estimer les déplacements irréversibles en crête d'ouvrage. Sur cet ouvrage, conformément aux recommandations [2], le déplacement limite requis était de 20 cm correspondant au tiers de la revanche. Ce déplacement limite a été dépassé par une ou plusieurs méthodes pseudo-dynamiques sur 5 des 15 profils étudiés.

La troisième (et dernière étape) a été l'analyse dynamique transitoire simplifiée présentée dans les paragraphes précédents. L'objectif était de justifier les 5 derniers profils non conformes. Les paramètres du modèle d'Iwan ont été calibrés de la manière suivante :

- G_{max} : module de cisaillement estimé pour chaque classe de matériaux des digues et de la fondation à partir des reconnaissances géophysiques (MASW, V_s) et géotechniques (SPT),
- γ_{ref} et n : paramètres d'Iwan calés de manière à reproduire les courbes $G/G_{max}(\gamma)$ et $D(\gamma)$ publiés dans la littérature ([15] & [16]) pour les différents types de classes de matériaux rencontrés (et ayant fait l'objet d'analyses granulométriques).

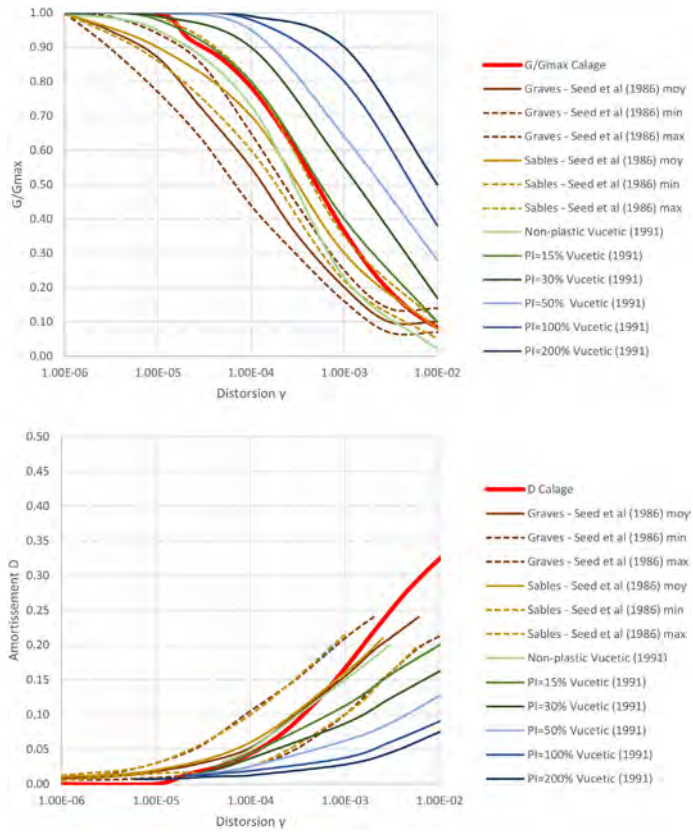

Fig. 14
Illustration du calage des courbes G/G_{max} et D pour les limons et les graves limons ($\gamma_{ref} = 5.10^{-4}$ et n = 0,8)
Illustration of the $G/G_{max}(\gamma)$ and $D(\gamma)$ curves calibrated for the silt and silty gravels materials ($\gamma_{ref} = 5.10^{-4}$ and n = 0,8)

Pour chaque profil étudié, des cercles de glissement ont été définis en talus amont et aval et leurs accélérations critiques k_c associés ont été déterminées en amont de la vérification de la stabilité au séisme.

Remarque : Les cercles sont définis de sorte qu'ils intéressent au moins la moitié de la crête (pour éviter de retenir des cercles de peau non significatifs pour l'analyse de la sûreté de l'ouvrage). Le découplage, de la réponse dynamique et de

l'estimation des déplacements, inhérent à la méthode dynamique transitoire simplifiée présentée ici, ne permet pas de définir les cercles les plus critiques a priori. De ce fait, des cercles sont positionnés à intervalle régulier comme illustrés sur la figure suivante.

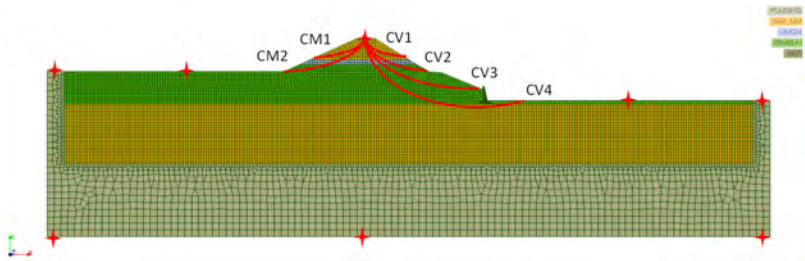

Fig. 15
Définition des cercles de glissement sur un des cinq profils étudiés
Definition of the sliding circles on one of the five studied profiles

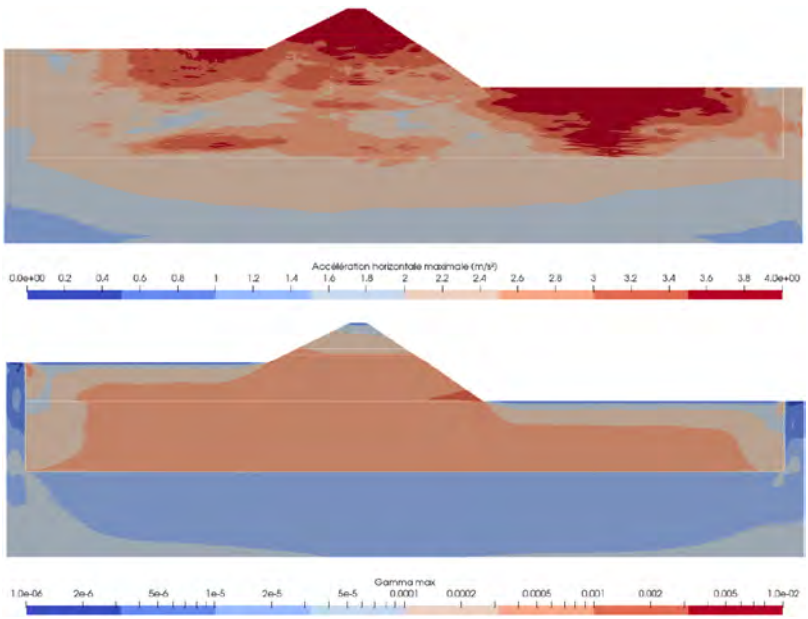

Fig. 16
Accélérations horizontales maximales et distorsion maximales obtenues au cours du séisme sur un des cinq profils étudiés
Maximum horizontal accelerations and maximum shear strain calculated with one of the accelerogram on one of the five studied profiles

L'évolution temporelle des accélérations obtenues par le modèle d'Iwan permet ensuite l'estimation des déplacements irréversibles par double intégration de la différence $k_m(t) - k_c$.

Sur le canal étudié, les déplacements irréversibles ainsi obtenus ont été bien inférieurs au critère requis (glissement inférieur à 20 cm environ) et l'approche dynamique transitoire simplifiée a ainsi permis de justifier les profils restants et de juger l'ouvrage conforme.

L'application de l'approche graduée sur ce grand canal hydraulique (exploité par EDF) illustre parfaitement les gains obtenus à chaque étape ou gradation. L'utilisation de méthodes plus avancées permet de lever les conservatismes initiaux. L'approche graduée et plus particulièrement l'analyse dynamique transitoire simplifiée, développée par EDF, a ainsi permis de justifier l'ouvrage et d'éviter des travaux de confortement non nécessaires.

5. CONCLUSION

La mise en œuvre d'une démarche graduée, tant pour l'analyse de stabilité au cisaillement que pour l'analyse du risque de liquéfaction, permet de graduer l'effort à réaliser en vue de justifier ou non de la stabilité de ces ouvrages, en priorisant les démarches les plus complexes sur les cas pour lesquels les approches les plus simples ne permettent pas d'assurer la bonne tenue des ouvrages. Cette démarche est cohérente avec l'état de l'art actuel. C'est ainsi que peut être réalisées pour différents tronçons d'un même ouvrage différentes analyses, s'enchaînant successivement ou non selon les résultats rencontrés:

- Concernant le risque de liquéfaction, l'analyse de la susceptibilité, et si besoin la quantification, et l'estimation de l'intensité du phénomène permettent d'écarter une grande partie des ouvrages du domaine de sensibilité des ouvrages au phénomène de liquéfaction, et ce sans avoir recours à des approches couplées non linéaires.
- Approche pseudo-statique, pseudo-dynamique et dynamique transitoire simplifiée (classiquement en linéaire équivalent, ou de manière plus raffinée d'un point de vue rhéologique en élasto-plasticité) pour l'analyse de stabilité au cisaillement.

Ces approches ont été utilisées par EDF (Rhin, Durance) et CNR (Rhône) et ont permis de justifier des grands ouvrages linéaires.

RÉFÉRENCES

[1] Journal Officiel de la République Française, Arrêté du 6 août 2018 fixant des prescriptions techniques relatives à la sécurité des barrages. https://www.legifrance.gouv.fr/loda/id/JORFTEXT000037345568

[2] *Ministère de l'Ecologie et du Développement Durable – Direction Générale de la Prévention des risques, Risque sismique et sécurité des ouvrages hydrauliques*. October 2014.

[3] *CFBR (French Committee on Large Dams), Guidelines for the justification of embankment dams and levees*, October 2015.

[4] DURAND, C. (2018), *Stabilité des digues sous chargement sismique : vers une nouvelle génération de méthodes simplifiées*, Thesis Viva completed on the 12th July 2018.

[5] N. M. NEWMARK, Effects of Earthquakes on Dams and Embankments. *Géotechnique* Vol. 15 Issue 2, pp. 139–160, June 1965.

[6] IWASAKI T, ARAKAWA T, TOKIDA K. (1982), Simplified procedures for assessing soil liquefaction during earthquakes. *Proceedings of the Conference on Soil Dynamics and Earthquake Engineering,* 925–939, Southampton.

[7] AFNOR. (2005), NF EN 1997-1, EUROCODE 7.

[8] DARENDELI, M B. (2001), *Development of a New Family of Normalized Modulus Reduction and Material Damping Curves*.

[9] MAKDISI F I, SEED H B. (1978), Simplified procedure for estimating dam and embankment earthquake- induced deformations, *Journal of the Geotech Eng. Div.*, ASCE, 104.

[10] ANDRUS *ET AL*. (2004), Guide for Shear-Wave-Based Liquefaction Potential *Evaluation.*

[11] AFPS. (2021), *Cahier Technique-AFPS CT 45 – Liquéfaction*.

[12] W.D. IWAN, A distributed-element model for hysteresis and its steady-state dynamic response. *ASME*, December 1966.

[13] CODE ASTER DOCUMENTATION R7.01.38, LAW OF IWAN FOR CYCLIC GRANULAR MATERIAL BEHAVIOR.

[14] CODE ASTER DOCUMENTATION U4.84.45, MACRO-COMMAND POST_ NEWMARK.

[15] H. SEED, R. WONG, I. IDRISS ET K. TOKIMATSU, *Moduli and Damping Factors for Dynamic Analyses of Cohesionless Soils, Journal of Geotechnical Engineering*, Vol. 112, Issue 11 (November 1986), November 1986.

[16] M. VUCETIC ET R. DOBRY, *Effect of Soil Plasticity on Cyclic Response, Journal of Geotechnical Engineering*, Vol. 117, Issue 1 (January 1991), January 1991.

[17] MARTIN, R., KOMATITSCH, D., BLITZ, C. ET LE GOFF , N. (2008). *Simulation of seismic wave propagation in an asteroid based upon an unstructured MPI spectral-element method : Blocking and non-blocking communication strategies. In Lecture Notes in Computer Science (including subseries Lecture Notes in Artificial Intelligence and Lecture Notes in Bioinformatics)*, volume 5336 LNCS, pages 350–363.

[18] *Evaluation of embankment dam seismic response by a new generation of simplified and graded methods, ICOLD, Chengdu*, 2025

[19] METHODOLOGIE SIMPLIFIEE POUR LA JUSTIFICATION AU SEISME D'UNE DIGUE SUR FONDATION MEUBLE, *Colloque CFBR : « Justification des barrages : Etat de l'art et Perspectives »*, Chambéry, 27 et 28 novembre 2019

Q.111 - R.21

COMMISSION INTERNATIONALE DES
GRANDS BARRAGES

VINGT-HUITIEME CONGRES DES
GRANDS BARRAGES
CHENGDU, MAI 2025

ARCH DAMS UNDER MODERATE TO HIGH SEISMIC LOADS: REVIEW AND UPDATE OF FAILURE MECHANISMS BASED ON RECENT NUMERICAL ANALYSES (*)

Frédéric ANDRIAN, Maxime VONIÉ, ALAIN YZIQUEL & Bernard TARDIEU
ARTELIA

Emmanuel ROBBE & Nicolas HUMBERT
EDF

FRANCE

SUMMARY

Most arch dams were designed before 1990 without applying modern seismic risk assessment methods. This paper reviews and applies the current practices. Furthermore, it proposes an additional failure mechanism to those usually considered for seismic load cases, based on numerical simulation. It also suggests performance criteria and modeling approaches to assess the related safety factors. The paper then presents the seismic analysis of Enguri dam in a high seismicity context and the feedback from the analysis of six French arch dams constructed in moderate seismicity areas. The paper recalls the practices considered by the authors as the state of the art for evaluating their behavior under moderate to severe earthquakes.

It is generally accepted that an earthquake can only induce vertical (contraction joints) and horizontal (concrete lift joints) cracks in an arch dam. Similarly, relative displacements are also considered possible at the dam/foundation interface.

**Barrages-voûtes sous chargements sismiques modérés à élevés : revue et mise à jour des mécanismes de rupture à l'aide de simulations numériques modernes*

 DOI: 10.1201/9781003642428-124

However, in the absence of excessive compression stress within the concrete, a crack is generally not considered critical. Beyond the analysis of seismic stresses, the sliding of rock volumes and the dynamic overturning of a block toward upstream are part of the failure mechanisms generally verified.

In parallel, physical models and numerical simulations seem to show that the failure mechanisms of arch dams mainly concern the upper part and involve the separation of some parts from the main structure, without a common approach to define and assess the related ultimate limit state.

The seismic analysis of Enguri dam, one of the highest arch dams, which needs to be verified for an earthquake with a PGA close to 1g, revealed high shear stresses within the concrete, remote from the abutments, consistently with the modal shape of the arch. These stresses are not experienced by the dam under static load cases, suggesting a potential failure mechanism involving the projection of portions of the dam toward downstream in case of excessive stress. The paper details the approach for characterizing this failure mechanism and for assessing the related safety factors. Furthermore, it recalls the performance criteria and approaches for assessing the safety factors related to failure mechanisms already analyzed by the state of the art.

In addition to the results presented for an arch dam built in a high seismicity area, the paper also presents a synthesis of seismic analysis results for six arch dams located in France constructed on low to moderate seismicity areas. This synthesis provides useful orders of magnitude for verifying models. it also highlights that for arch dams constructed on moderate seismic areas, it seems unlikely that a failure mechanism in the upper part (by overturning of a block toward upstream or shearing along a surface in the upper part) would be initiated.

RÉSUMÉ

La majorité des barrages-voûtes ont été conçus avant 1990 et sans appliquer les méthodes modernes d'évaluation des risques sismiques. Cet article présente une revue ainsi qu'une mise en pratique des pratiques actuelles et propose un mécanisme de rupture supplémentaire aux mécanismes habituellement considérés en situation sismique, en s'appuyant sur la simulation numérique. Il propose également des critères de performance et des méthodes de modélisation pour évaluer les marges de sécurité qui y sont associées. Dans un second temps, l'article présente la justification au séisme du barrage d'Enguri dans un contexte de forte sismicité et le retour d'expérience de la justification de 6 voûtes françaises soumises à une sismicité modérée. L'article propose un rappel des pratiques considérées par les auteurs comme étant l'état de l'art pour évaluer leur comportement sous séismes modérés à sévères.

Il est généralement admis qu'un séisme peut uniquement induire des fissures verticales (joint entre plots) et horizontales (reprises de bétonnage) dans un barrage-voûte. De même des mouvements relatifs sont également jugés possibles à l'interface barrage/fondation. En revanche, en l'absence d'une sollicitation excessive à la compression du béton, une fissure n'est généralement pas jugée critique dans le comportement. Au-delà de l'analyse des contraintes sismiques, le glissement de volumes rocheux et le basculement dynamique d'un plot vers l'amont font partie des mécanismes de rupture généralement vérifiés lors des analyses.

En parallèle, les modèles physiques et les simulations numériques semblent montrer que les mécanismes de rupture des barrages-voûtes concernent principalement la partie supérieure avec la désolidarisation de partie d'ouvrage sans pour autant qu'il n'existe d'approche commune pour définir et estimer l'état limite ultime associé.

L'analyse sismique du barrage d'Enguri, l'un des plus hauts barrages-voûtes, devant être vérifié pour un séisme dont l'accélération maximale au rocher est proche de 1g, a révélé des contraintes de cisaillement élevées dans le béton, loin des appuis du barrage, cohérentes avec les déformées modales de la voûte. Ce sont donc des contraintes qui ne sont pas subies par le barrage en situation statiques et suggérant un mécanisme de rupture potentiel impliquant la projection de portions du barrage vers l'aval en cas de sollicitation excessive. L'article détaille alors les principes de caractérisation et d'évaluation des marges de sécurité vis-à-vis de ce mécanisme de rupture. Par ailleurs, il rappelle les critères de performance et les méthodes d'analyse des marges de sécurité pour les mécanismes de rupture déjà analysés par la profession.

En complément des résultats présentés pour une voûte construite en zone de forte sismicité, l'article présente également une synthèse des résultats d'analyses sismiques pour 6 barrages-voûtes situés France métropolitaine en zones de sismicité faible à modérée. Cette synthèse fournit des ordres de grandeur utiles à connaitre pour la vérification des modélisations. Elle met en évidence également que pour des voûtes en zone sismique modérée, il apparait peu vraisemblable qu'un mécanisme de défaillance en partie supérieure (par basculement d'un bloc vers l'amont ou cisaillement le long d'une surface en partie supérieure) ne soit initié.

1. INTRODUCTION

Most of arch dams were designed before 1990. Their design often considers only a fixed seismic coefficient (pseudo-static) approach without any site-specific seismic hazard assessment. In France, the seismicity is very low to moderate excepting the French Caribbeans Islands where it is high. Abroad, it is possible to

face very severe earthquake loads to be checked for existing arch dams. For many of the latter, the Safety Evaluation Earthquake (SEE) PGA (Peak Ground Acceleration) to which they need to be assessed may be significantly higher than the design seismic coefficient.

In parallel, the last one to two decades saw a significant progress in the understanding of the seismic behavior of arch dams and the underlying physical and mathematical processes. Hence, a more reliable prediction of their seismic behavior is now allowed by time history analysis including advanced dam/reservoir/foundation interaction and even non-linear effects.

On the other hand, arch dams are reputed to behave well under seismic loadings. Two of them endured moderate earthquakes without any failure [1]:

- Pacoima, 113m high in the USA, subjected to a 0.44g PGA earthquake in 1994 with a reservoir level at 30% of full supply level,
- Shapai, 130m high in China, subjected to a 0.2 to 0.5g PGA earthquake in 2008.

Still, there is not any arch dam subjected to high earthquake load case to date and there are not any super high arch dams (>200m) subjected to high or severe earthquake, limiting the available feedback.

Considering the above, the current paper presents a gradual approach for assessing the behavior of arch dams subjected to two categories of earthquakes:

- Low to moderate earthquakes, based on the feedback of the seismic analyses of 6 arch dams in France (§5),
- High to severe earthquakes, with the example of Enguri arch dam developed in §4.

The authors propose that the threshold between the two categories would be a SEE PGA of about 0.4g for an arch dam as they are reputed behave well under seismic loading compared to the other types of dams.

2. FAILURE MECANISMS AND CRITERIA FOR ARCH DAMS UNDER EARTHQUAKE LOAD

2.1. Current practice

Most of the existing international guidelines for the safety assessment of arch dams under earthquake load case ([2], [3], [4]) assume that the only possible earthquake-induced cracks in arch dams are the following:

- Vertical, by the opening of contraction joints,
- Horizontal, along concrete lift joints,
- Following the dam/foundation interface.

In the French guidelines/practice, it is assumed that the failure mechanisms under static load cases are relevant with a few adjustments which are recalled hereafter.

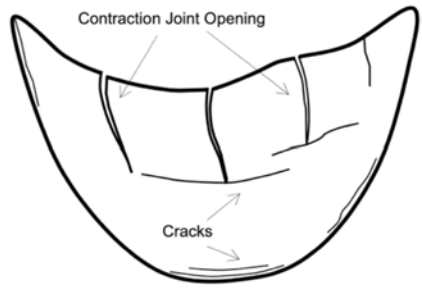

Fig. 1
Illustration of arch dam response under large earthquakes [5]
Illustration de la réponse d'un barrage-voûte sous sollicitation sismique sévère [*5*]

The sliding of rock volumes which is considered acceptable if the dam can accommodate the related stress redistribution without any domino-effect failure. The current guidelines emphasize the role of uplift pressure in the rock volume stability and recommends sensitivity analysis with regards to this parameter.

The excess in compressive stress is addressed with a factor of safety depending on the type of model (linear or non-linear).

The dynamic overturning of a cantilever or of a part of cantilever toward upstream is checked by means of a kinetic approach. The calculations compute the position of rocking concrete block barycenter which is compared to the position of rotation point (§3.5.4).

The overall sliding along the dam/foundation interface is considered unlikely if the arch is well keyed and/or if the bedrock excavation is well designed. On the other hand, local sliding may occur and is believed to generate an increase in pore pressures and in leakage rates.

Finally, an excessive tensile stress is not deemed critical if the dam is able to redistribute the relating stress and if the cracks close back under post-earthquake load case.

But from the authors point of view, based on the literature and feedback from recent numerical analyses on dams under high (§4) and moderate (§5) seismic hazard, an additional failure mechanism should be considered and will be proposed hereafter.

2.2. Attempts to characterize the failure under earthquake load case in the literature

In the absence of common practice for characterizing the failure modes of arch dams in numerical calculations or in physical scale models, the current chapter attempts to summarize the most relevant examples of works dedicated to that topic.

2.2.1. *Physical scale models*

Physical scale models had been often used before numerical analysis became more popular in the early 90s for the seismic analysis of arch dams. They may still be used under some circumstances in specific countries. They consist in building a reduced scale of the dam, the reservoir and maybe some parts of its foundation with materials which respect physical and hydraulic similitude with the real size system. The earthquake loads were applied by means of exciters or by means of shaking tables.

The tests conducted by ISMES [6] in the early 80s show that the typical failure produced by horizontal motion concerns only the upper part of the dam while the lower part remains intact. This failure mode is stated to occur from narrow V-type canyon to U-shape valleys, even when the models include the contraction joints

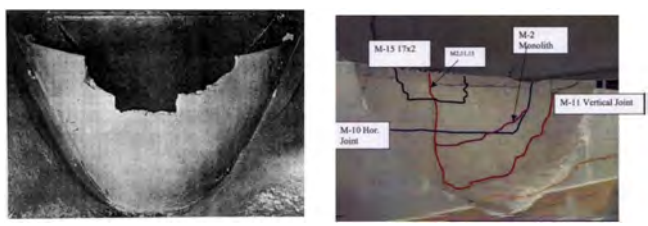

Fig. 2
Typical failure modes of arch dams on physical scale models: ISMES (left) and USBR (right) [6]
Mécanismes de rupture types de barrages-voûtes sur des modèles physiques réduits : ISMES (à g.) et USBR (à dr.) [6]

More recently, in the early 2000s, USBR [6] conducted a series of tests in which the initial joint pattern is stated to significantly influence the failure type of the dam. In this case, the failure state is a push through of the dam toward downstream.

2.2.2. *Numerical analyses*

The seismic analysis of the 249m high Deriner arch dam designed for a SEE PGA of 0.35g is described in [7]. Among the cited papers, only this one does not use non-linear constitutive model for the concrete. At the time of the studies, it is stated that such approach was not still affordable. A linear time history analysis was then conducted with the maximum tensile stress being analyzed to select a few detached blocks considering lift joint opening. Then, the detached blocks were analyzed in a separate 2D time history analysis considering contact elements at the base of the detached blocks. The analysis adopts two strong assumptions:

- There can only be horizontal (lift joints) and vertical (contraction joints) crack opening. The case of diagonal cracks is not addressed,
- The detached block can only move toward upstream due to the shape of the dam.

The following table summarizes the results of the separate 2D analysis of a 20m-high detached block located at the crest of the crown cantilever. The calculated sliding/rocking crack displacements are compared to the detached block base thickness, here 17m. And as they are significantly slower (maximum sliding of 71cm and maximum crack opening of 15cm), they are judged acceptable in the paper.

Table 1

Results of the rocking-sliding analysis of a 20m high detached block in upper central part of Deriner dam as per [7]

Résultats des calculs au glissement/basculement d'un plot détaché de 20 m de haut sur la partie supérieure centrale du barrage de Deriner [7]

EARTHQUAKE GROUND MOTION	EARTHQUAKE DURATION (s)	RESERVOIR (EMPTY/ FULL)	MAX. SLIDING DISPLACEMENT ALONG CRACK AT LIFT JOINT (mm)	MAX. CRACK OPENING DISPLACEMENT AT UPSTREAM EDGE (mm)	MAX. CRACK OPENING DISPLACEMENT AT DOWNSTREAM EDGE (mm)
MCE1	15	empty	272	129	58
MCE2	25	empty	525	149	40
MCE3	32	empty	708	142	76
MCE1	15	full	346	136	96
MCE2	25	full	307	143	86
MCE3	32	full	280	110	30

The seismic design of the 210m high Dagangshan arch dam for which SEE PGA is 0.56g is discussed in [8]. The numerical model uses added mass approach for the dam/reservoir interaction and a sensitivity analysis is made with regards to the bedrock foundation boundary conditions. A damage-plasticity constitutive law is used for the dam concrete and the contraction joints are modelled. The effect of steel rebars in reducing the cracking intensity of the downstream face is assessed by considering cantilever rebars made of 3T40@300mm.

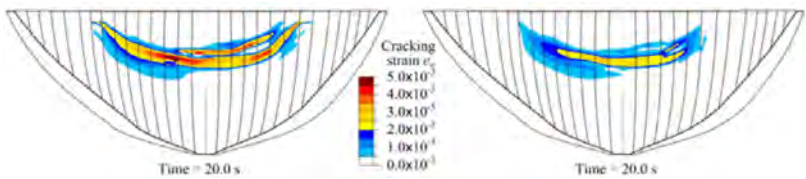

Fig. 3
Calculated cracking strain in the downstream face of Dagangshan dam: without (left) and with (right) the consideration of rebars [8]
Déformation de fissuration calculée sur le parement aval du barrage de Dagangshan : avec (à dr.) et sans (à g.) prise en compte des armatures [*8*]

The results highlight the importance of the use of viscous-spring boundary conditions for the bedrock foundation in reducing the seismic response of the system (25 to 40% reduction). Despite the consideration of contraction joints, the results depict diagonal cracks at the sides of the cracking pattern on the downstream face. Finally, the rebars only allows some reduction in the crack extension and improve the concrete stiffness after damage occurs but cannot prevent the dam from cracking.

The use of Endurance Time Analysis Function (ETAF) for arch dams is introduced in [9]. ETAF is an artificial acceleration history, linearly increasing with time but which is more or less compatible with a scaled site acceleration response spectrum at any specific time. Its purpose is to assess the critical acceleration that an arch dam can withstand. Applied to the case of 4 arch dams with numerical models considering damage plasticity constitutive law for concrete, this approach shows an abrupt increase in crest displacement when failure occurs. Regardless of the critical PGAs, that abrupt increase occurs when the ratio between dynamic and static displacements reaches approximately a value of 4. The critical PGAs range from 0.52g for the tallest dam (111m) to 1.3g for the arch dam located in a narrow V-shape canyon.

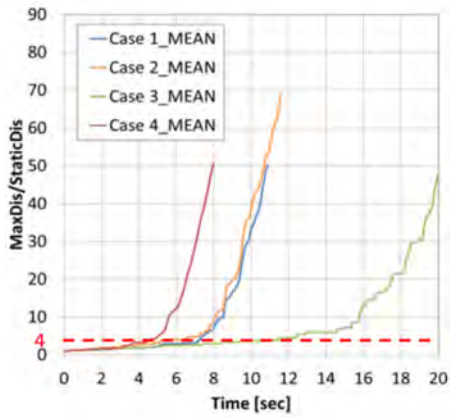

Fig. 4
Evolution of ratio between dynamic and static displacement of the crest of the crown cantilever during ETAF signal as per [9]
Evolution du rapport entre les déplacements dynamiques et statiques en crête de la console de clé pendant le signal ETAF [*9*]

The seismic analysis of an existing 84m-high arch dam is conducted in [10]. A non-linear time history analysis is performed with an increasing level of complexity including:

- A linear elastic constitutive model for all the materials,
- A concrete damage-plasticity constitutive law for the dam concrete,
- A concrete damage-plasticity constitutive law with the removal of an element which has reached a plastic strain of 1.0,
- Pre-defined failure planes (interface elements) to follow the layout of the damaged elements in the previous models.

The model with a linear elastic model in the dam body concrete shows that the ratio between the dynamic crest displacement and the static displacement reaches almost 20.The model with a linear elastic model in the dam body concrete shows that the ratio between the dynamic crest displacement and the static displacement reaches almost 20.

The two intermediate models show the possible loss of the upper portion of the arch. Then the final model with pre-defined failure planes shows that a total loss of the upper portion is not expected but irreversible displacements along the

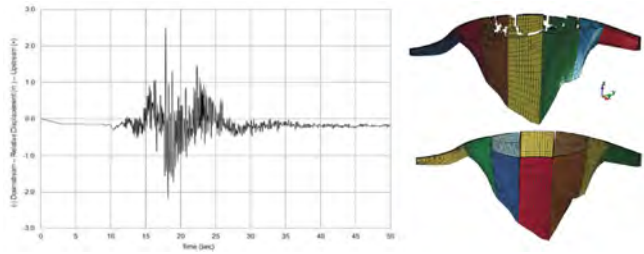

Fig. 5
Relative displacement of crown cantilever crest with dynamic analysis starting at 8.8s (left), concrete damage with elements removed (top right), and dam deformed shape at maximum upstream relative displacement (bottom right)
Déplacement relatif en crête de la console de clé avec les calculs dynamiques démarrant à 8.8s (à g.), endommagement du béton avec suppression des éléments (en haut à dr.), et déformée amplifiée lors du déplacement relatif maximum (en bas à dr.)

pre-defined failures planes may occur. The paper highlights the drawback of the concrete damage-plasticity constitutive law in which the contribution of an element to the dam stiffness is lost after its failure. It is understood that this has motivated the use of interface elements to simulate the crack instead. On the other hand, the last model assumes that the failure planes are or almost horizontal (lift joints) or vertical (along the contraction joints).

The seismic analysis of Cabril (132m high) and Cahora Bassa (170m high) arch dams is conducted in [11]. The calculations consider non-linear models with the contraction joints and concrete damage plasticity constitutive law for the dam body concrete. ETAF earthquake loads is applied to the model and the ultimate state of the dam is considered to be reached when compression crushing occurs so as to generate an uncontrolled release of the reservoir water.

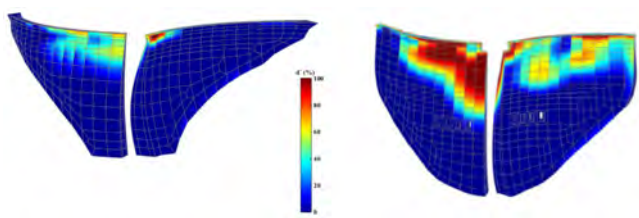

Fig. 6
Calculated compression damage state of Cabril (left) and Cahora Bassa (right) dams at ultimate PGA: US (left half) and DS (right half) faces
Etat d'endommagement à compression calculé des barrages de Cabril (à g.) et de Cahora Bassa (à dr.) à l'accélération maximale au rocher ultime : amont (demi-figure de g.) et aval (demi-figure de dr.)

According to that criterion, the ultimate state of Cabril dam is reached for a PGA equating 1.3g whereas for Cahora Bassa dam, the ultimate PGA is 0.8g.

The above examples show that there is not any consensual approach for assessing the ultimate state or ultimate earthquake for an arch dam. However, the failure mechanisms are believed to involve loss of arch portions, crushing, sliding. Most of the references allow tension damage/cracking as an acceptable behavior of an arch dam.

2.3. Proposing clarifications for seismic failure mechanisms of arch dams

Based on the above examples and the general understanding of arch dam behavior, it can be assumed that the safety of an arch dam is ensured as long as an active arch can develop from a bank to another i.e., the loads are still safely transferred to the abutments.

This load transfer mobilizes compression through the dam body. A few arch dams, most of which being subjected to concrete swelling, endure compressive stress which is close to the compressive strength of concrete under static load case. General experience shows that creep occurs if the loading rate is slow. On the other hand, there is not any arch dam which has been tested under dynamic loading up to such level of compressive stress. Hence, it may be preferable, to keep some safety margin with regards to dynamic strength under dynamic loads, all the more that the effective active arch may be thinner due to tension cracking.

A secondary failure mechanism would be an interruption of the active arch due to an excessive shear stress. A specific attention should be paid to the dynamic modal shape of arch dams which may induce a stress pattern which cannot exist under static load cases and generates high shear stress remote from the abutments. An analysis of the direction of such shear cracking and the magnitude of the resulting irreversible displacement as well as their possible consequences may be required. On the other hand, local shear sliding at the dam/foundation interface may also be analyzed in order to assess the consequential increase in leakage discharge due to dilatancy. The capacity of the existing foundation drains can be checked accordingly.

Finally, it is deemed impossible to critically interrupt an active arch due to an excessive tensile stress as long as the relating cracks close back under post-earthquake load case i.e., the dam is able to redistribute the stress. On the other hand, a specific care should be paid to areas already highly loaded in shear as they require to be able to redistribute the stress due to the tension crack opening.

The above suggestions are to be added to the already assumed failure mechanisms including the dynamic projection of dam upper portions toward the upstream as well as the more conventional failure mechanisms under static load cases.

3. TIME-HISTORY ANALYSES FOR THE SEISMIC EVALUATION OF ARCH DAMS

This chapter recalls the state-of-the art gradual approach for evaluating the seismic behavior of an arch dam.

Several references ([12,15], . . .) show that the consideration of an advanced dam/reservoir/foundation dynamic interaction is preferred for the analysis of arch dams. Many conclusive tests have been conducted by dam stakeholders and this approach can now be considered as state-of-the-art. Such approach includes:

- A massed foundation with boundary conditions accounting for the semi-infinite nature of the medium,
- At least solid incompressible elements for the reservoir water or if possible compressible solid elements (or equivalent formulations) allowing the propagation of pressure waves to the upstream far end of the reservoir,

3.1. Preliminary modal analysis

A preliminary modal analysis usually has two purposes:

- Calibrate the material parameters of the numerical model with the possibly available results from ambient vibration tests or also from any time history data relating to earthquakes for example,
- Assess the possible amplification of the response spectra for the main eigenmodes of the system.

3.2. Linear elastic analysis

The linear elastic analysis allows to preliminary assess the overall behavior of the system:

- Displacements, velocities and accelerations,

- The amplification of the free-field motion at several locations of the system,
- Stresses.

The generation of tensile arch is one of the drawbacks of this approach as it cannot release the tensile stress at the location of contraction joints and the dam/foundation interface. The consequence is an overestimation of the horizontal arch stress but also a possible underestimation of some other parameters including the vertical tensile stress on the downstream face, the accelerations, the velocities and displacement at the crest.

3.3. Non-linear analysis considering the contraction joints and the dam/foundation interface

The next stage considers the effect of the contraction joints as well as the dam/foundation interface. The shear keys or the effect of helical contraction joints can be considered as well.

In addition to the previous stage, this approach provides information about the following parameters at the dam/foundation and contraction joints:

- The possible opening,
- The possible sliding/shear displacement.

This approach is deemed more realistic than the previous one and is recommended if the dam crest is expected to exhibit a displacement toward upstream which is significantly beyond its position with an empty reservoir.

3.4. Non-linear analysis constitutive law for the dam body concrete

If with the previous approach the dam body is still expected to exhibit extensive cracking, then a non-linear constitutive law can be assigned to the concrete.

The objective is to assess if there can be a loss of a portion of the dam which will generate an uncontrolled release of the reservoir.

A specific care should be paid to the choice of the constitutive law. It should be able to simulate a realistic behavior of the crack initiation, propagation as well as the residual post-cracking behavior of the concrete in relation to the applied intensity of earthquake.

An alternative may be the use of interface/joint elements at locations of potential cracks. However, as crack propagation is sensitive to load path, it should

be ensured that the location of the pre-fixed interface/joint elements follows a realistic propagation and that alternative cracking layout have been tested if deemed realistic.

3.5. Supplementary analyses and elements of criteria

The following analyses are conducted based on the results of the numerical analyses and are focused on the actual failure mechanisms of arch dam.

3.5.1. *Performance criteria with regards to compressive stress*

Most of arch dams are designed to exhibit an arch stress of about 3 to 7MPa under usual static load cases. That may reach up to 10MPa for super high arch dams or also very thin arch dams. Hence, they normally have comfortable margin with regards to excessive compressive stress assuming that the concrete compressive strength is higher than 25MPa.

On the other hand, it is deemed necessary to adopt a prudent approach with regards to excessive compressive stress under dynamic loading as such situation was probably never encountered in an arch dam. Moreover, if cracking occurs under earthquake load case, the active arch may be thinner than in a linear elastic numerical model, resulting in a higher actual arch stress.

Hence, if a non-linear analysis which can consider concrete cracking is applied, a factor of safety with regards to compressive strength close to 1 may be justified. Otherwise, a higher factor of safety may be recommended.

3.5.2. *Performance criteria with regards to tensile stress*

The document [3] proposes an approach to analyze the acceptability of excessive tensile stresses. The analysis is based on the results of the linear elastic model and allows to state whether a non-linear analysis is required for more accurate estimate of the damage.

The approach consists in analyzing the overstressed area highlighted by the time history analysis. The level of non-linear response is considered acceptable if:

- The demand-capacity ratio is lower than 2 i.e., the calculated maximum tensile stress is lower than 2 times the uniaxial splitting tensile strength of concrete,
- The overstressed region is limited to 20% of the dam surface, and
- The cumulative inelastic duration of each overstressed model element falls below the performance curve given in Fig. 7.

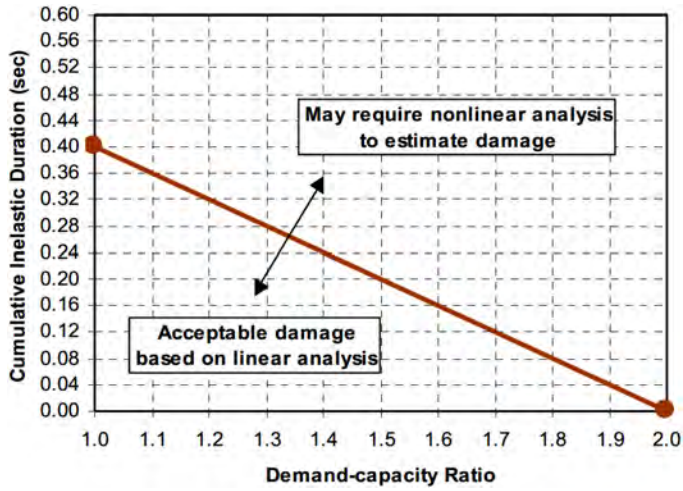

Fig. 7
Performance curve for linear elastic analysis of arch dams as per [3]
Courbe de performance pour les modèles élastiques linéaires de barrages-voûtes [*3*]

3.5.3. *Performance criteria with regards to shear within the concrete*

The modal shapes of arch dams may highlight shearing which is not encountered under static load cases. Are of specific interest those for which shearing is encountered remote from the abutments (Fig. 16).

When the time history analysis highlights similar deformed shape as the one shown in Fig. 16, an analysis of shear state of several model elements at selected critical times can be used to assess the safety margin of the dam body concrete with regards to Mohr Coulomb criterion.

A special care is needed for elements which are already subjected to excessive tensile stress as the shear strength of the element may already be reduced by tension cracking.

The direction of shear crack is of attention in order to assess if this may result in a loss of the natural keying of the blocks toward downstream. Under such condition, an assessment of the cumulative displacement can be undertaken to state about the risk of loss of dam portion.

3.5.4. *Dynamic overturning of a block or a part of a block toward upstream*

The possible tension cracking at several lift joints of individual blocks is already dealt with in §3.5.2. This paragraph addresses the case of the ultimate state of a block or a part of the block which is projected toward upstream and overturns due to an excessive initial velocity i.e., kinetics is at stake instead of stresses and force equilibrium.

The theory behind the approach is detailed in [16] and the application assumptions and modalities are detailed in [4]. Overall, the critical velocity depends on the geometry of the rocking block and on the added mass due to the dam/ reservoir interaction. In practice, the critical velocity is the one for which the center of gravity of the rocking block reaches a vertical alignment with its rotation point.

3.5.5. *Role played by rebars within the concrete*

Arch dams may include rebars within the concrete. Their structural effect mainly depends on the relative cross-sectional area between the concrete and the rebars. If the rebar cross sectional area is lower than the value required to avoid a sudden failure i.e., the rebars are not able to balance the load due to the cracking of some percentage of the concrete area (at least 20 to 25%), then the crack will remain localized. Their opening magnitude may be reduced to a certain extent and possibly some further energy is dissipated through the rebar yielding.

If the rebar cross sectional area exceeds the required value to avoid a sudden failure, then the arch dam can be analyzed as a reinforced-concrete structure and the rebars will at least allow some distribution of the cracks. However, such case may be very rare as a significant quantity of rebars would be needed in a well-proportioned arch dam to reach the required cross-sectional area.

Some arch dams are equipped with a seismic belt made of several horizontal rebars crossing all the blocks near the crest. When crossing the contraction joints, the rebars have an unbonded length. Their main purpose is to avoid an offset of adjacent blocks during the earthquake event. They also provide supplementary energy dissipation through the rebar yielding across the contraction joints. Their efficiency may be checked by including an equivalent stiffness in the numerical model at the contraction joints at the elevation of their installation.

3.5.6. *Shearing at the dam/foundation interface*

The current paper only deals with arch dams for which the bedrock excavation layout prevents from an overall sliding toward downstream. Under such conditions, the earthquake load cases can only generate local shearing at the dam/foundation interface.

Such local shearing, localized at the dam/foundation interface in the numerical model can be further distributed deeper along the natural joint sets of the bedrock. The shearing can generate a loss of efficiency of the foundation grout curtain. Moreover, by dilatancy, a shearing can generate an opening at the joint sets which increases the bedrock permeability. The consequence is an increase in the pore pressure distribution within the foundation bedrock if the drains are not able to evacuate the excess in leakage discharge.

The paper [17] proposes an approach to assess the supplementary leakage discharge due to the shearing within the bedrock by assuming a flow along rough joints. Then, the capacity of the existing drains in evacuating the discharge without reaching saturation can be evaluated in order to state whether an increase in pore pressure distribution is likely to occur or not.

3.5.7. *Stability of rock volumes*

The stability of rock volumes of the abutments can be made by means of three approaches of increasing complexity. The 10th ICOLD benchmark on numerical analysis of dams addresses this aspect in theme C [18].

A pseudo-static approach can be considered assuming that the direction of the earthquake is the most critical for the rock volume stability. The resultant of forces at the dam/rock volume interface is integrated from the numerical model but the stability analysis of the rock volume is conducted with force equilibrium approach e.g., Londe's rock wedge approach [19]. One may consider the amplification of accelerations along the dam's height for the calculation of the resultant of forces applied by the dam.

If the previous approach leads to a sliding factor of safety lower than 1, then a time history of the resultant of forces from the dam can be integrated at the dam/rock volume interface. A rigid-block time-history analysis of the rock volume is then conducted by means of Newmark approach for example and considering the inertial loads from the rock volume itself in order to assess the cumulative irreversible displacement. One can apply the irreversible displacement at the dam/rock volume interface of the numerical model of the dam in order to evaluate the ability of the dam to accommodate accordingly.

A refinement of the above method consists in including the rock volume in the numerical model with interface elements provided with Coulomb friction shear strength parameters at the planes defining the rock volume. A specific care is needed for the choice of the horizontal coefficient of stress within the bedrock as that may significantly influence the results.

4. SEISMIC ASSESSMENT OF ENGURI ARCH DAM UNDER HIGH SEISMIC HAZARD

4.1. BACKGROUND

The 271.5m high Enguri double curvature arch dam is one of tallest arch dams currently under operation. Designed in the 60s, constructed from the 70s, the reservoir reached the full supply level for the first time in 1987.

ARTELIA was appointed by Engurhesi, the dam Owner, to conduct among other assignments the seismic analysis of the dam/reservoir/foundation system according to the current international practice.

The dam includes a pulvino joint with a maximum height of the pulvino base of 50m at the center of the canyon.

The main features of the dam are summarized in the following table.

Table 2
Main features of Enguri dam
Principales caractéristiques du barrage d'Enguri

PARAMETERS	**VALUES**
Maximum height above foundation (m)	271.5
Crest Length / Crest Chord Length (m)	680/550
CL/H - CCL/H	2.5 – 2.03
Crest thickness (m)	10
Maximum base thickness above the pulvino joint/ above the foundation (m)	50 / 90
Bedrock type	Limestone and dolomite

The dam design considers an earthquake PGA of 0.05g and it is understood that at least a physical scale model was used for the seismic analysis of the dam [20]. The dam body includes several rebars which, according to the available documents, intend to balance the excessive stress which could not be withstood by the dam concrete for this design earthquake.

The dam is constructed in a site with very high seismicity. The SEE PGA is 0.965g with a good consistency between the ICOLD Bulletin 148 [21] DSHA and PSHA. The SEE PGA is consequently almost 20 times the one the dam was designed for. Even though arch dams are reputed to behave well under earthquake load cases, a comparison between the crown cantilevers of a few arch dams of

similar dimensions under design or already constructed show that Enguri dam has a rather thin cross section, more specifically for the upper 70m (Fig. 9). The comparison also highlights the total overall damping used in the numerical models of the dam (numerical model described in this paper in the case of Enguri dam).

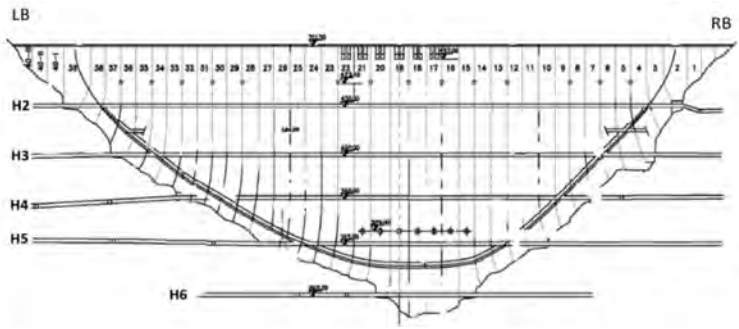

Fig. 8
Upstream elevation of Enguri dam with the block identifications and the dam galleries
Élévation amont du barrage d'Enguri avec l'identification des plots et des galeries

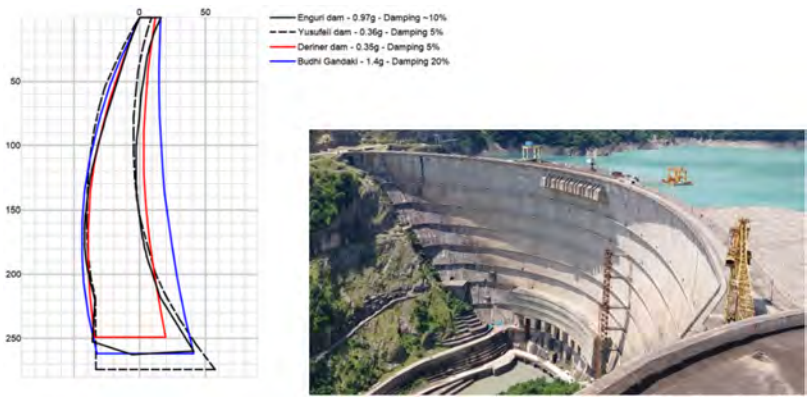

Fig. 9
Comparison of a few crown cantilevers of arch dams (left) including Enguri dam (picture on right)
Comparaison de quelques consoles de clés de barrages-voûtes (à g.) incluant le barrage d'Enguri (photo à dr.)

4.2. Material parameters

The elastic parameters of the bedrock are derived from periodic extensive geophysical surveys of the foundation bedrock which are rare and interesting surveys for arch dam foundation.

For the dam body concrete, they are derived from the calibration of the numerical model with the displacements measured by the dam plumblines. The obtained values are already very high compared to usual values and this is confirmed by previous analyses [22].

The strength parameters for the concrete are based on supplementary surveys and laboratory tests conducted on purpose which highlight values comparable to high-performance concrete.

The strength parameters for the foundation rock mass are assessed by means of a Hoek & Brown approach utilizing existing and new geotechnical surveys as well as the geo-structural outputs from field surveys made on purpose.

The dam/foundation interface shear strength parameters are taken to be the minimum between the dam body concrete and the foundation bedrock parameters.

The material parameters are summarized in the following table where the strength parameters are used only for the non-linear models.

Table 3
Dynamic material parameters for Enguri dam
Caractéristiques mécaniques en situation dynamique pour le barrage d'Enguri

PARAMETERS	**CONCRETE**	**FOUNDATION BEDROCK**	**WATER**	**DAM/FOUNDATION INTERFACE**
Density (kg/m^3)	2570	2700	1000	-
Poisson's ratio	0.2	0.25	-	-
Elastic modulus (GPa)	As per	As per	-	-
Velocity of p-waves (m/s)	-	-	1440	-
Compressive strength (MPa)	78 (dynamic)	-	-	-
Tensile strength (MPa)	3.6 (static) / 5.4 (dynamic)	-	-	-
Equivalent Friction angle (°)	45	-	-	40.5
Equivalent Cohesion (MPa)	16.6 (dynamic)	-	-	1.4

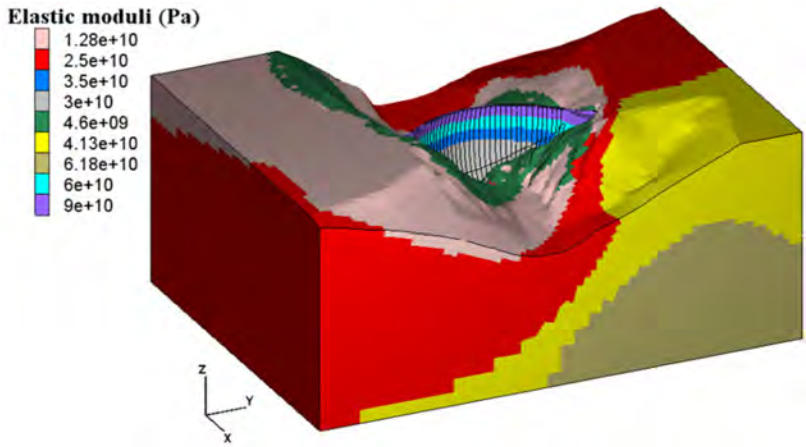

Fig. 10
Distribution of dynamic moduli in the numerical model
Distribution des modules dynamique dans le modèle numérique

4.3. Geometrical model

The geometrical model includes the dam body and truncated foundation and reservoir. The model extends about 2 times the dam height toward all directions from the dam extremities except toward upstream where it extends 2.5 times to allow an accurate simulation of wave propagation within the reservoir.

The geometries were established from the project drawings, including the topography of the reservoir and checked with success by means of a very recent point cloud of the dam and downstream area.

4.4. Preliminary modal analysis

A preliminary modal analysis is conducted by means of ANSYS Mechanical considering a massless foundation and solid incompressible elements for the reservoir. Then a separate modal analysis with compressible acoustic elements with the velocity of waves as per Table 3 is used to identify the eigenmode involving the reservoir.

The results show that the 14 first Eigenmodes have frequencies ranging from 1.25 to 3.46Hz which can be superimposed to the site-specific response spectrum. The mode involving the reservoir has a frequency of 1.45Hz. The analysis of the deformed shapes shows that excepting the Eigenmode involving the reservoir, the system Eigenmodes mobilizes only the upper thinner part of the dam

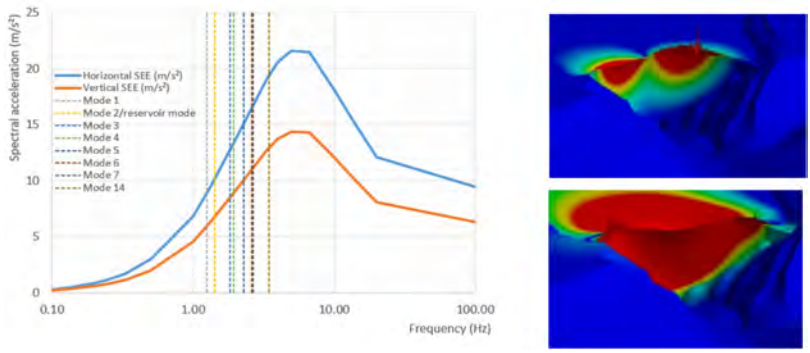

Fig. 11
Superimposition of the Eigenfrequencies with the site-specific response spectra (left), modal shape of 1st Eigenmode (top right) and Eigenmode involving the reservoir (bottom right)
Superposition des fréquences propres avec le spectre spécifique de site, déformée modale du 1er mode (en haut à dr.) et du mode du réservoir (en bas à dr.)

Based on the site-specific response spectrum, the 14 first Eigenmodes of the system avoid the spectral acceleration plateau.

4.5. Time-history analyses

The time-history analysis of the dam is conducted with FLAC3D, an explicit numerical analysis code for geomechanics developed by Itasca.

The model includes about 370,000 mixed discretization elements [23], most of which are hexahedra including about 100,000 in the dam, 167,000 in the foundation and 103,000 in the reservoir. The mesh size is able to solve wave propagation up to 7Hz.

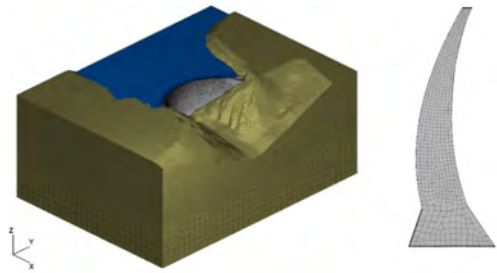

Fig. 12
Numerical analysis and meshing layout for the time history analyses
Modèle numérique et maillage pour les calculs temporels

Five different 3-direction natural acceleration time histories, scaled and matched to the site-specific spectrum are used, two of which: Lexington and Lamont375 are shown in Fig. 13 as they lead respectively to the maximum tension in the concrete and the maximum sliding at the dam/foundation interface.

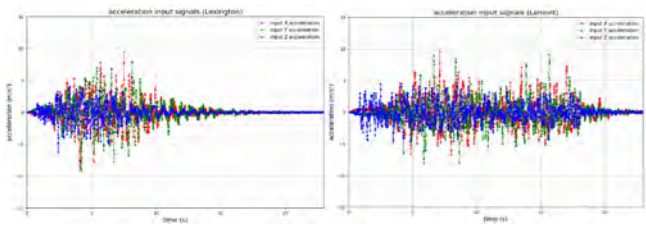

Fig. 13
Scaled and matched Lexington and Lamont375 acceleration input signals
Accélérogrammes Lexington et Lamont375 mis à l'échelle et ajustés

When the concrete uses a linear elastic model, a damping ratio of 5% is applied in the concrete. The linear analysis shows that the maximum tensile stress reaches 20MPa and that the region of the dam overloaded in tension exceeds 20% of the dam surface both on upstream and downstream faces. Consequently, a non-linear analysis considering the contraction joints, the pulvino joint and the dam/foundation interface is conducted. The dam contraction joints are equipped with vertical shear keys and the contraction joints have a helical layout from top to bottom. Hence, in the numerical model, the contraction joints are allowed to open in the normal direction but cannot have any relative tangential displacements. The same assumptions are adopted for the pulvino joint given its layout.

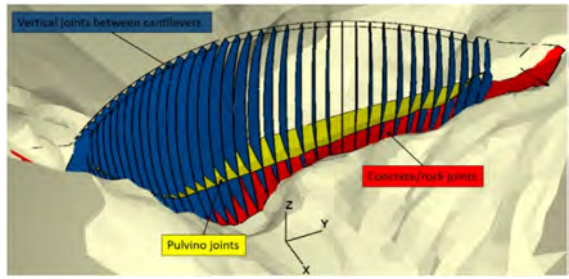

Fig. 14
Interface elements considered in the non-linear models
Eléments d'interface dans le modèle non-linéaire

The non-linear analysis considering the joints shows that the amplification of the SEE PGA is about 8 at the dam crest and that the ratio between the seismic amplitude and the static load displacements at the crest of the crown cantilever is 7 (54cm vs. 7cm). This is very high and based on the literature review in §2.2.2, such value is likely to result in severe damage. As a consequence, if the fictitious tensile arch near the crest in the linear analysis is released by the modelling of the joints, the maximum tensile stress remains very high: 10MPa and 15MPa in the upstream and downstream faces i.e., up to 4.2 times the static strength in a rather wide area. On the other hand, the compressive stress remains below the concrete strength with comfortable margin.

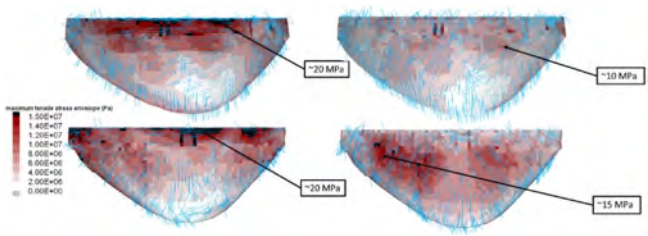

Fig. 15
Envelope and direction of non-concomitant tension principal stresses during the time history analysis: linear model (left), model with interface elements (right), upstream (top) and downstream faces (bottom)
Enveloppe et direction des contraintes principales de traction non concomitantes pendant le calcul temporel : modèle linéaire (à g.), modèle avec les éléments d'interface (à dr.), parements amont (en haut) et aval (en bas)

Given the magnitude of the tensile stresses, the maximum velocities toward upstream is analyzed for 3 detached blocks: one at the center and one on each side of the arch. Three different heights are analyzed from the crest: 50, 70 and 90m. Among all the cases, one 50m-high bank block has a critical velocity of 4.94m/s whereas the average maximum velocity over the block height is 3.4m/s. This value is very high, and it is believed that it is one of the maximum values ever encountered with the application of kinetic block analysis. Still the calculations show that there is some margin before a dynamic projection of the detached block toward upstream occurs.

The behavior of the upper area of the dam draws attention at t=5.55s with the Lexington acceleration series input where a dynamic deformed shape is prone to shearing remote from the abutment i.e., a stress state very different from the static load cases is endured. The analysis of the stress state of selected model elements at this specific time shows that there is an evident overloading in tension. If a residual tensile strength of 0 and a residual cohesion of 5.4MPa is assumed upon tension cracking, the ability of the dam to redistribute the stresses needs to be investigated.

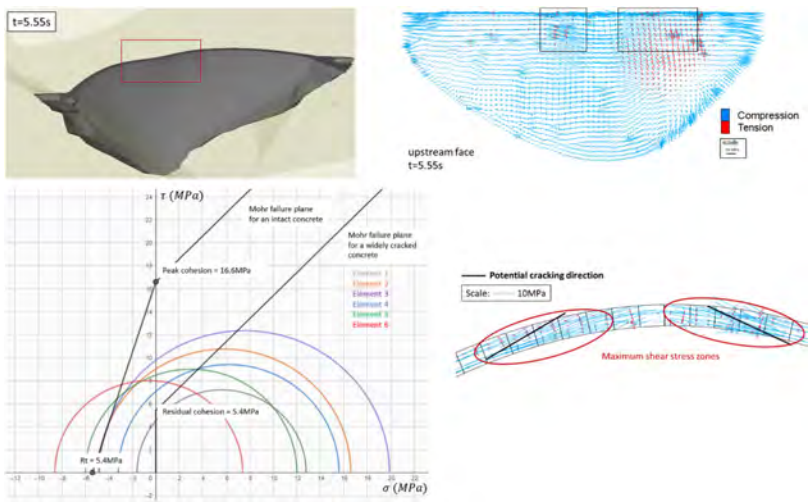

Fig. 16
Envelope and direction of non-concomitant tension principal stresses during the time history analysis: linear model (left), model with interface elements (right), upstream (top) and downstream faces (bottom)
Enveloppe et direction des contraintes principales de traction non concomitantes pendant le calcul temporel : modèle linéaire (à g.), modèle avec les éléments d'interface (à dr.), parements amont (en haut) et aval (en bas)

As several model elements in the area exceed the Mohr Coulomb criterion, a final model is run considering a non-linear constitutive model within the concrete. The selected constitutive law is the Mohr-Coulomb Tension Crack [24] which is an enhancement of Mohr-Coulomb model with an elastic-perfectly fragile behavior with regards to tension and an ability to keep track of the plastic tensile strain and close back a crack. Up to 3 perpendicular cracks are possible per element, each crack being perpendicular to another, and their direction being fixed. The law is elastic-perfectly plastic with regards to shear and the element stiffness with regards to shear is not affected by cracking, making the law behaving as if an interface element is added where tension cracking is expected to occur. This a significant improvement compared to the constitutive laws based on concrete damage as described in §2.2.2 which generate a loss in stiffness at the scale of a damaged element as already stated in [10]. On the other hand, the user may prescribe residual shear strength parameters for cracked elements. This constitutive law was tested with success with the seismic analysis of Pine Flat dam in [25]. One drawback of this constitutive law is that the fracture energy is negligible, leading to an underestimated energy dissipation. Hence, a damping ratio of 10% is considered in the concrete when this constitutive law is used. In the case of Enguri dam, an increased damping ratio is also justified by the severity of the earthquake, by the consideration of an undamped foundation bedrock and by the presence of surface rebars and seismic belt which will yield during the SEE event.

This last model highlights an extensive cracking of the upper 70m of the dam with most of the cracks crossing the entire section of the dam. The average maximum crack opening in the upstream face is about 15cm, peaking locally at 50cm. The cracks delimit small arches i.e., some cracks are diagonal, for which the boundaries are overloaded in shear and which endure sliding toward downstream exceeding 3m and without any stabilisation at the end of the earthquake event. The abovementioned small arches were already found in physical scale models as shown in §2.2.1 but also in other numerical analyses as shown in §2.2.2. The sliding of 3m at the base of detached blocks is very high compared to the values obtained in the case of Deriner dam as shown in §2.2.2 in relation to the thickness of the dam at the location of the crack, which is lower than 20m. In addition, the sliding is toward downstream, which is consistent with the USBR physical scale models described in §2.2.1. The main outcome of this analysis is that there is not any clear active arch anymore in the is upper part of dam under post-SEE load case. The numerical analysis of Enguri dam conducted here is consequently believed to characterize a credible failure mechanism.

For the remaining part of the dam (lower 200m), the cracks are mainly horizontal and do not cross the entire thickness of the dam. They are consequently not critical.

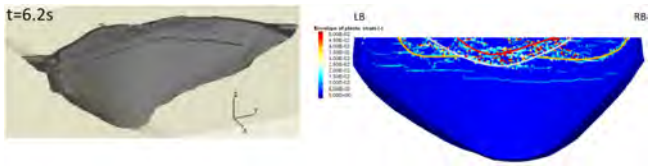

Fig. 17
Crack state on the downstream face at t = 6.2s (left) and envelop of non-concomitant tension plastic strain at the end of SEE (Lexington input)
Etat de fissuration du parement aval à t = 6.2s (à g.) et enveloppe des déformations plastiques de traction à la fin du séisme SES (accélérogramme Lexington)

The analysis of the behavior at the dam/foundation interface highlights a maximum post-earthquake shear displacement after the Lamont375 acceleration input series.

The maximum sliding is localized in the center of the valley with a maximum width of about 85m and the maximum magnitude is about 6cm.

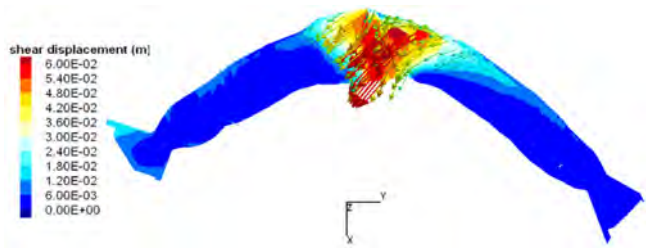

Fig. 18
Maximum post-SEE shear displacement at the dam/foundation interface
(Lamont375 input) Déplacements de cisaillement maximums post-sismiques à l'interface barrage/fondation (obtenu pour l'accélérogramme Lamont375)

The analysis of the increase in leakage discharge assumes that all this shearing occurs in one unique joint. Based on the geo-structural field survey of the foundation, a dilatancy angle between 5 and 10° can be assumed for the bedrock. According to [17], the velocity of water can be expressed as $v = 12.5\sqrt{e.J}$ with e the opening of the joint and J the hydraulic gradient. The velocity is consequently between 1.6 and 2.2m/s and the unit discharge is between 0.008 and 0.02m^3/s/m. Over the 85m-wide sliding, this results in a supplementary post-SEE discharge between 0.7 and 1.7m^3/s. Such value is in the same order of the current leakage

discharge through the dam foundation and can consequently be accommodated by means of supplementary drains drilled at appropriate locations.

The geo-structural field survey of the foundation bedrock allowed to identify a rock wedge on the left abutment which sliding is kinematically compatible with the combined thrust from the dam, the hydrostatic pressure and uplift pressure. The wedge maximum length is about 100 m from upstream to downstream.

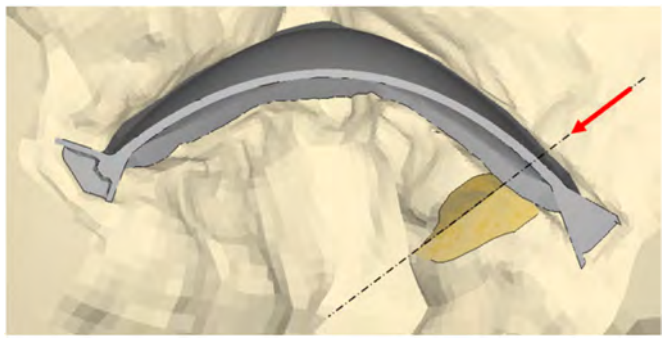

Fig. 19
Rock wedge on the left abutment and direction of the pseudo-static earthquake
Dièdre rocheux sur l'appui rive gauche et direction du séisme pseudo-statique

The stability analysis of the rock wedge under static load cases conducted under the assumptions of Londe's approach shows that the maximum acceptable uplift pressure at the wedge planes is 25% of the reservoir head considered constant at any point of the planes. Given the already very complex behavior of the dam under SEE load case, it is deemed prudent to ensure the safety of this rock wedge by means of a conservative approach. A pseudo-static approach is consequently used with the earthquake direction being the most critical with regards to the wedge sliding.

In the analysis, the thrust from the dam is integrated at the dam/wedge interface and the acceleration profile in the dam body assumes the gradual amplification of SEE PGA toward the crest, in consistency with the results of the time-history analyses.

The analysis shows that a resisting force of 2000MN is required to ensure a stable rock wedge under SEE load case if the uplift pressure at the wedge planes is 25% of the reservoir head. Without any uplift pressure, the required resisting force is 1000MN. The above values are used to design the retrofit works.

5. SEISMIC ASSESSMENT OF ARCH DAMS IN FRANCE WITH A MODERATE SEISMIC HAZARD

The aim of this chapter is to present the main findings regarding the seismic assessment of arch dams in France with a moderate seismic hazard. Focus is made on numerical analyses involving finite-element analyses with time-history approach as described in the §3. For dams located in a low seismic hazard area, such analyses are not mandatory, and the seismic assessment is done using simplified analyses such as pseudo-static method or even considering the validation of the static behavior of the dam. Such analyses are out of the scope of this paper.

This chapter summarizes the results from the seismic analyses on 6 arch dams with PGA from 0.15 to 0.34g. Main assumptions for the analyses are reminded first with the characteristics of the studied dams. The results regarding the failure modes are then compared, and finally a discussion on the interest of such analyses is proposed.

5.1. Main assumptions

Chapter 3 describes the ideal state-of-the-art methodology that should be followed nowadays to perform seismic analyses of arch dams. However, engineers have very often to deal with constraints to perform such analyses, leading sometimes to change in the methodology.

Half of the dams studied involved non-linear analyses exclusively with joint-element at the dam-foundation interface or at the vertical joints between the cantilevers. Such type of non-linearity remains quite reliable and manageable combined with time-history analyses.

For several studies summarized here, combination of advanced soil-fluid-structure interaction and non-linearities led to unacceptable computing time and required to simplify the problem. That's why a few analyses were performed using simplified methods such as Westergaard added masses and/or massless foundation despite the recommended methodology detailed in §3.

For existing arch dams, monitoring of the static displacements allows the calibration of Young modulus of concrete and foundation. This allows to evaluate the static modulus for the evaluation of the static behavior of the dam, required before performing seismic analyses.

Regarding the dynamic properties of the concrete and the foundation, two approaches were chosen:

- If ambient vibration measurements are available, providing the first eigen-frequencies of the system, the dynamic moduli are adjusted by fitting of the computed and measured frequencies. Computed frequencies come from modal analyses considering linear behavior of the dam
- Without any measurements, dynamic moduli are deduced from the static moduli using the following equation: Ed=1.25*Es

Finally, for low to moderate earthquakes, damping of the concrete ranges from 3 to 5: the lower value is generally considered when radiative damping is taken into account. For simplified approach such as massless foundation, 5% damping is considered.

For the safety evaluation of its dams under earthquake, EDF uses a deterministic approach based on historical earthquakes. From the target spectrum, synthetic accelerograms are generated based on the methodology used for the nuclear industry. For linear behavior, analyses are performed using 3 sets of accelerograms; 5 sets are required for non-linear behavior following the French nuclear guidelines [26].

5.2. ARCH DAMS

Table 4 summarizes the arch dams subject of seismic analyses involving time-history analyses with the finite-element software Code_Aster.

Table 4
Summary of arch dams studied
Synthèse des barrages étudiés

DAM	HEIGHT (M)	PGA (G)	CONCRETE DAMPING	SOIL-STRUCTURE INTERACTION	FLUID-STRUCTURE INTERACTION	BEHAVIOR
R	150	0.18	3%	Absorbing boundaries	Added masses	Non-linear at the dam-foundation
L	45	0.23	5%	Massless foundation	Added masses	Non-linear at vertical joints
S	70	0.15	5%	Massless foundation	Added masses	linear
C	101	0.34	3%	Absorbing boundaries	Fluid elements	linear
V	130	0.22	3%	Absorbing boundaries	Fluid elements	Non-linear at the dam-foundation
M	153	0.26	3%	Absorbing boundaries	Fluid elements	linear

Fig. 20 provides a quick overview of the different meshes of the analyzed arch dams.

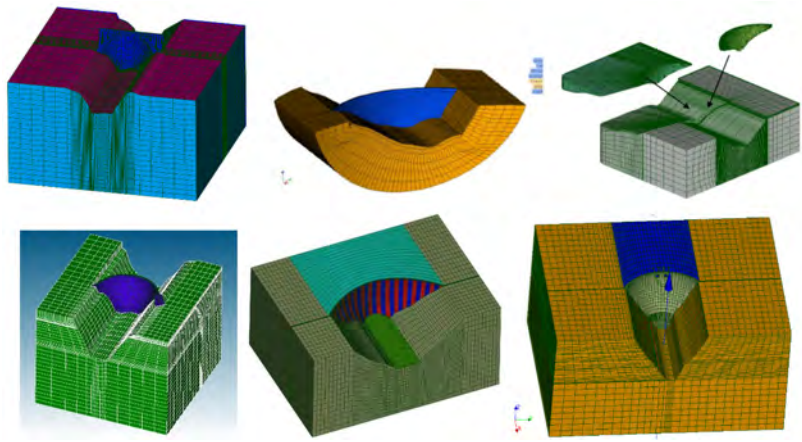

Fig. 20
View of the meshes
Vue des maillages

5.3. General results

Table 5 summarizes the main results from the seismic analyses, providing a good overview of values that can be expected regarding the seismic behavior of arch dams for moderate seismic hazard.

Peak accelerations at the crest are 6 to 12 times the peak ground accelerations. That leads, even for moderate seismic hazard, to quite high accelerations at the crest of the dam from 1.5 g to almost 3 g.

Crest displacements toward downstream under seismic load are generally lower than under hydrostatic load. Nevertheless, 2 dams (M dam and C dam) out of 6 show higher crest displacement under earthquakes for the following reasons:

- M dam is a thick arch dam involving small displacement of the crest under static load while crest displacements under earthquake are driven by the second mode mainly involving the top part of the dam.

- C dam displacements under static load (Fig. 21) show that the maximum displacements are not computed at the crest while the visualization of the first two modes highlights that maximum displacement under earthquake will occur at the crest.
- The other dams are quite slender dams with first symmetric mode shape similar to the deformed shape of the dam under static load. In such case, considering that the earthquake load remains generally lower than the hydrostatic load for moderate seismic hazard (Fig. 22), displacements under earthquake are lower than under hydrostatic load.

The increase in maximum compression stresses due to earthquake load is moderate: from 1.5 MPa to 5 MPa. Regarding these results, two configurations appear:

- Maximum compression stresses under earthquake are located near the abutments where maximum value under static load were already identified as shown on Fig. 23 on the downstream face for V dam: stresses increase from 9.5 MPa to 13.5 MPa with the addition of earthquake load.
- Maximum compression stresses under earthquake are located at the upper part of the dam, under the influence of the deformed shape of higher modes as shown on Fig. 24 on the upstream face of V dam: under static loads only, maximum compression stresses were around 5.5 MPa at the middle elevation of the central cantilevers. With earthquake loads, compression rise up to 10 MPa near the crest of the central cantilever.

Table 5
Main results
Résultats principaux

DAM	1ST FREQUENCY (HZ)	PEAK ACCELERATION (G)		MAX CREST DISPLACMENT TOWARD DOWNSTREAM (MM)		MAX COMPRESSION STRESS (MPA)	
		GROUND	CREST	HYDROSTATIC LOAD	SEISMIC LOAD	HYDROSTATIC LOAD	STATIC +SEISMIC LOAD
R	2.4(*)	0.18	1.5 (x8)	55	40	11	16.1
L	3.3(*)	0.23	2.8 (x12)	59	34	5.6	10.2
S	3.8 (*)	0.15	1.8 (x12)	19	6	8.6	10
C	4.4	0.34	2.0(x6)	7.1	15	4.6	8.6
V	2.3 (*)	0.22	2 (x10)	73.6	29.4	9.4	13.6
M	2.9	0.26	2 (x7.6)	17.9	30.1	7.5	10.6

(*) values calibrated from ambient vibrations measurements

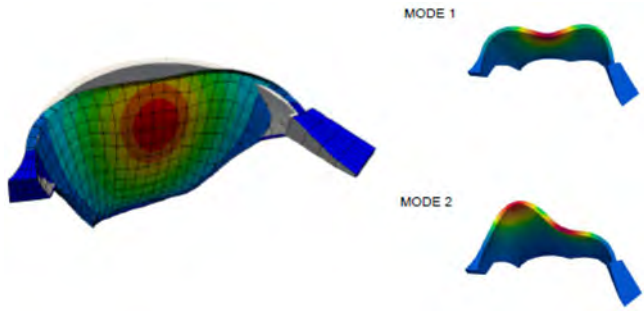

Fig. 21
C dam displacement under hydrostatic load compared to first modes shape
Déformée du barrage sous chargement hydrostatique comparé à la déformée des premiers modes

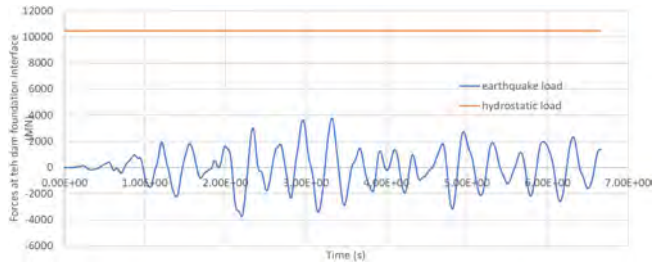

Fig. 22
Comparison between earthquake load and hydrostatic load for M dam
Comparaison entre les efforts sismiques et hydrostatique pour le barrage M

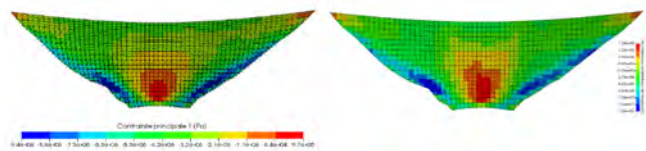

Fig. 23
Maximum principal compression stresses under static (left) and under static + EQ. loads (right) on the downstream face of V dam
Contrainte de compression principale maximale sous chargement statique (g.) et sous chargement statique + sismiques (dr.) sur le parement aval du barrage V

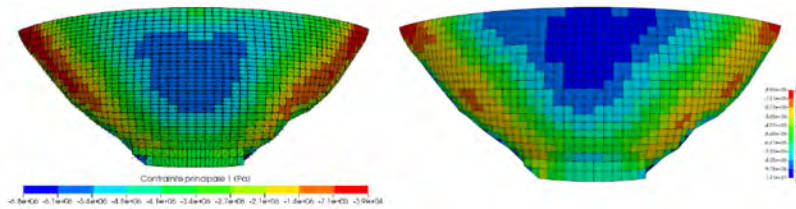

Fig. 24
Maximum principal compression stresses under static (left) and under static + eq. loads (right) on the upstream face of V dam
Contrainte de compression principale maximale sous chargement statique (g.) et sous chargement statique + sismiques (dr.) sur le parement amont du barrage V

5.4. Tensile stresses and demand capacity ratio

Even for moderate earthquake loads, linear analyses compute tensile stresses near the tensile strength of concrete rising the question of the acceptation of such values: will it lead to superficial cracks acceptable for such event or to important damage susceptible to trigger a failure mechanism?

The demand capacity ratio tool, described in §3.5.2, provides an interesting way to answer such question. Fig. 25 shows an example of demand capacity ratio evaluation for the tensile stress at the middle of the central cantilever, on the downstream face. Considering the exceedance of the criteria and that it was mainly vertical tensile stresses leading to horizontal cracks, kinetic blocks analyses were performed (see §5.5) to evaluate the risk of failure triggered by such crack. Similar analyses were performed for two of the analyzed dams considering tensile strength was reached but didn't exceed the defined criteria.

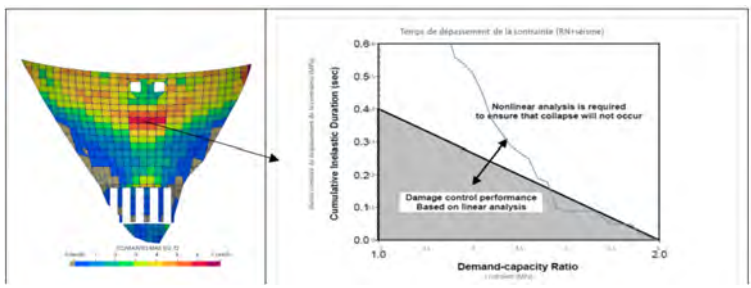

Fig. 25
Demand capacity ratio for M dam
DCR pour le barrage M

In several cases, as proposed in §3.5.3, illustrated in the case of Enguri dam (§4.5) and in Fig. 26, tensile stresses can highlight an embedded small arch within the arch, following one of the modal shape of the structure. For low to moderate earthquakes, similar pattern cannot appear on the upstream face and the shear forces are not sufficient to trigger a failure of this embedded geometry toward downstream.

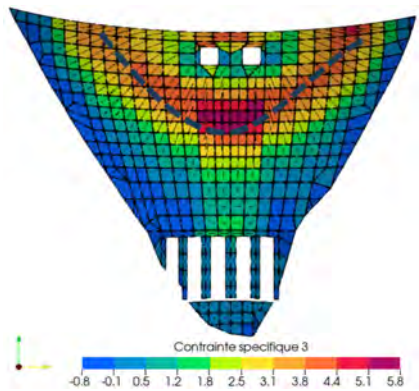

Fig. 26
Tensile stress pattern on the downstream face of M dam at a selected instant of the earthquake
Répartition des contraintes de traction en parement aval du barrage M pour un instant spécifique

5.5. Kinetic blocks analyses

If significant tensile stresses are computed near the crest of the dam in a way to separate a block (opening of joint and horizontal cracks), kinetic blocks analyses can be performed (as described in §3.5.4) to evaluate the risk of dynamic overturning.

Table 6 summarizes the results for the 4 dams for which this kind of analysis was performed. For moderate earthquake, results show that blocks velocities are one order of magnitude lower compared to the velocity required for the block to overturn in the upstream direction.

Table 6
Kinetic blocks analyses results
Résultats des analyses par la méthode 'Kinetic Blocks'

DAM	BLOCK MAX VELOCITY (m/s)	CRITICAL VELOCITY (m/s)
R	0.5	4.1
L	0.4	3.2
C	0.5	
M	0.5	11.9

6 CONCLUSIONS

From the authors point of view, the current practice does not still allow to clearly define dynamic failure mechanisms of arch dams as no arch dam was severely damaged by earthquake. Hence, the existing guidelines suggest that, under seismic load cases, the failure mechanisms for static load case apply also with an additional mechanism related to the overturning of detached upper blocks toward upstream. In the meantime, while there are several attempts in the literature to characterize the ultimate state of arch dams whether from physical scale models or numerical models, there is still not any consensus about their interpretations.

The conducted numerical analysis of Enguri dam with a 0.965g PGA SEE described in the current paper proposes an approach for simulating that ultimate state with increased confidence. Actually, the numerical model uses a non-linear constitutive law which overcomes the main drawback of the current concrete damage plasticity model which may be too much pessimistic and includes unknown parameters.

Furthermore, it shows, in consistency with the results of physical scale models, a failure mechanism involving an upper portion of the dam projected toward downstream. That behavior was often assumed to be impossible due to the arch dam effect, the contraction joint geometry and the simplified consideration of a block delimited by vertical joints and a lift joint. In this spirit, an arch dam is considered safe as long as the active arch is uninterrupted from an abutment to another under post-earthquake load case. However, during dynamic loads, some modal shapes of the system may involve shearing in an area remote from the abutments i.e., which is not encountered under static load cases. For very severe earthquakes, there may be an excessive shear stress for which the related cracks do not follow neither the lift joints nor the contraction joints as usually assumed i.e., there can be diagonal cracks as well. Very likely, small arches on the upper area may be delimited by such cracks for which the layout may generate a loss of the natural keying of the blocks toward downstream and a projection of dam portions toward downstream.

These main findings in the current works need to be tested for other case studies and probably an attempt to elaborate a simplified approach for assessing the stability of the upper small arches can be made in the future.

Having in mind all the failure mechanisms proposed and the results of the analysis of Enguri dam, results of several arch dams under moderate earthquake area (0.15 to 0.34 g) are summarized, providing range of parameter values that can be expected for arch dams under similar load:

- Amplification of the acceleration from the ground to the crest varies from 6 to 12,
- Maximum crest displacement toward downstream due to moderate seismic load is generally lower than under static load but can reach twice the static displacement for particular geometries,
- The increase in maximum compression stresses due to seismic load is moderate for the studied dams: from 1.5 MPa to 5 MPa,
- It seems difficult to trigger any failure mechanisms in the upper part of the dam: velocities are way too small for the overturning mechanism of a block toward upstream while tensile stresses on the upstream face and shear stresses are too small for the mechanism proposed toward downstream.

REFERENCES

[1] USSD, *Observed perfomance of dams during earthquakes*, volume III, February 2014

[2] FERC, *Engineering guidelines for the evaluation of hydropower projects, Chapter 11 – Arch dams*, March 2018

[3] USACE, EM 1110-2-6051, *Time-history dynamic analysis of concrete hydraulic structures*, December 2003

[4] CFBR, *Recommandations provisoires pour la justification du comportement des barrages-voûtes – Octobre 2018*

[5] ICOLD, *Bulletin 206, Technical Committee D on Concrete dams, Arch dam design – Methodologies and criteria – to be published.*

[6] USBR, *Report DSO-06-03, Investigation of the failure modes of concrete dams - Physical model tests*, December 2006

[7] WIELAND ET AL., *Design aspects of Deriner dam, International Waterpower and Dam Construction*, 2008,

[8] CHUHAN ET AL., Seismic safety evaluation of high concrete dams - Part II: Earthquake behavior of arch dams: Case study, *The 14th World Conference on Earthquake Engineering*, Beijing, October 2008

[9] MEGHELLA ET AL., *Endurance Time Analysis for the Seismic, Vulnerability of Arch Dams, 13th ICOLD Benchmark Workshop on the Numerical Analysis of Dams, Lausanne, .* 2015

[10] SOOCH ET AL., *Nonlinear seismic analysis of an existing arch dam under intense earthquake, Sustainable and Safe Dams Around the World* – Tournier, Bennett & Bibeau (Eds), Canadian Dam Association, 2019

[11] ALEGRE ET AL., *Seismic Safety Assessment of Arch Dams Using an ETA-Based Method with Control of Tensile and Compressive Damage, Water .* 2022

[12] CHOPRA A. K, Earthquake Engineering for concrete dams - *Analysis, design, and evaluation*, Wiley-Blackwell, 2020

[13] FRY, J.-J., & MATSUMOTO, N. (Eds.). Validation of Dynamic Analyses of Dams and Their Equipment: Edited Contributions to the International Symposium on the Qualification of Dynamic Analyses of Dams and their Equipments, 31 August-2 September 2016, Saint-Malo, France (1st ed.), 2018

[14] ANDRIAN *ET AL.*, Theme B: Static and seismic analysis of an arch-gravity dam - Synthesis report, *Proceedings of the 14th ICOLD International Benchmark Workshop on Numerical Analysis of Dams*, Stockholm, 2018

[15] ROBBE E., Seismic back analysis of monticello arch dam – Blind prediction workshop and additional analyses, *USSD*, 2017

[16] TARDIEU *ET AL.*, Computational and engineering aspects of aseismic design of arch dams, *Dam Engieneering*, Vol I Issue 1, 1990

[17] TARDIEU *ET AL.*, *Prediction of gravity dams behavior under strong earth-quake, in Validation of Dynamic Analyses of Dams and Their Equipment* - Fry & Matsumoto (Eds), 2018

[18] GUNN R., THEME C “Stability of a dam abutment including seismic loading”, *10th ICOLD International Benchmark Workshop on Numerical Analysis of Dams, Paris*, 2009

[19] LONDE P., *“une méthode d’analyse à trois dimensions de la stabilité d’une rive rocheuse”*, annales des ponts et chaussées, 1965

[20] ICOLD, *Bulletin 27, A review of earthquake resistant design of dams, Technical Committee B on seismic aspects of dam design*, 1974

[21] ICOLD, *Bulletin 148: Selecting Seismic Parameters for Large Dams – Guidelines (Revision of Bulletin 72)* - 2016

[22] BOSSONEY C., Enguri dam Rehabilitation's project, *Proceedings of 9th ICOLD Benchmark Workshop on Numerical Analysis of Dams, Theme C, St-Petersburg*, 2007

[23] MARTI *ET AL.*, Mixed discretization procedure for accurate modelling of plastic collapse, *International Journal of numerical and analytical methos in geomechanics*, vol.6, pp 129–139, 1982

[24] ITASCA SOFTWARE, ITASCA SOFTWARE 9.0 DOCUMENTATION - *Itasca Software Guide - Constitutive Models - Plastic Model group*, 2023

[25] LHERBIER *ET AL.*, Numerical analysis of Pine Flat Dam using finite difference method, *Proceedings of the 15th ICOLD Benchmark Workshop on Numerical Analysis of Dams*, Milano, 2019

[26] GUIDE ASN 2.01*, Prise en compte du risque sismique à la conception des ouvrages de genie-civil d'installation nucléaire de base à l'exception des stockages à long terme des déchets radioactifs*, 2006

COMMISSION INTERNATIONALE DES
GRANDS BARRAGES

VINGT-HUITIEME CONGRES DES
GRANDS BARRAGES
CHENGDU, MAI 2025

EVALUATION OF EMBANKMENT DAM SEISMIC RESPONSE BY A NEW GENERATION OF SIMPLIFIED AND GRADED METHODS (*)

Capucine MASSON, Simon DEMARS, François BROUSSET & Frédéric ANDRIAN
ARTELIA

Pierre LABBE
Ecole Spéciale des Travaux Publics

Ziad KTEICH
ENGIE

Vinicius ALVES FERNANDES
EDF R&D

Pierre-Yves BARD & Emmanuel CHALJUB
Institut des Sciences de la Terre

Romain GRANJON
CNR

Jean-Jacques FRY
JJ Fry Consulting

FRANCE

**Évaluation de la réponse sismique d'un barrage en remblai par des nouvelles méthodes simplifiées et graduées*

DOI: 10.1201/9781003642428-125

SUMMARY

This report proposes simplified and graded approaches for assessing the seismic behavior of embankment structures. It begins by describing a linearization method that considers the effects of pore pressure on the equivalent linear shear modulus. This approach is applied to the Aratozawa dam (PGA 1.04g). Subsequently, a graded approach (static, simplified dynamic, nonlinear time response) is implemented on an embankment dam similar in height to Aratozawa and subjected to very strong seismic loading (PGA 1.22g). Finally, a new simplified method for evaluating the seismic behavior of levees, embankments, and medium-sized dams is presented. This method accounts for the specific geometries and foundation properties of these works in the assessment of their seismic behavior.

RÉSUMÉ

Ce rapport propose des approches simplifiées et graduées permettant d'évaluer le comportement sismique des ouvrages en remblai. Il décrit dans un premier temps une méthode de linéarisation prenant en compte les effets de la pression interstitielle sur le module de cisaillement équivalent. Cette approche est appliquée sur le barrage de Aratozawa (PGA 1.04g). Dans un second temps, une approche graduée (statique, dynamique simplifiée, réponse temporelle non linéaire) est mise en œuvre sur un barrage en remblai, similaire au barrage d'Aratozawa en termes de hauteur et soumis à une très forte sollicitation sismique (PGA 1.22 g). Enfin, une nouvelle méthode simplifiée pour évaluer le comportement sismique des digues, des remblais et des barrages de taille moyenne est décrite. Cette méthode permet de prendre en compte les spécificités de ces ouvrages (en termes de géométries et de propriétés de leur fondation notamment) pour l'évaluation simplifiée de leur comportement sismique.

1. INTRODUCTION

On June 14th, 2008, the Aratozawa dam, in Iwate prefecture, Japan, was hit by the magnitude 7.2 Iwate-Miyagi earthquake. A 1.04 g strong motion PGA was recorded in the bottom gallery. Clearly, interpreting the recorded motion and understanding the response of the dam under such strong input motion requires consideration of the non-linear behaviour of the constitutive materials. In addition, although such high levels of seismic acceleration are seldom observed, they are often postulated in safety analyses of dams under seismic input motion as a consequence of long postulated earthquake return periods (extreme events). It is

therefore necessary, in such situations, to consider non-linear dam responses, even though such phenomena are poorly documented and subjected to large uncertainties.

In the current state of knowledge, only time response analyses are appropriate for modelling the seismic response of dams in such situations. However, current modelling techniques are subject to large uncertainties, as shown by the results of the international benchmark PRENOLIN (PREdiction of Non-LINear soil behavior) [1], which focused only on simple 1D soil profiles. In addition, PRENOLIN clearly showed that the higher the demand (such as that expected under strong input motions), the greater the dispersion between participants.

It is therefore necessary for the engineering community to have at its disposal simplified or graded approaches that, to the best extent, enable taking non-linear effects into account without requiring sophisticated non-linear time-responses calculations. This is the domain of linearisation techniques such as those originally introduced by par Seed et Idriss [2] and developed by numerous authors and now widely used. Meehan and Vahedifard [3] identify 23 such methods in literature for the assessment of post-seismic displacements of embankment dams. However, these methods were not calibrated for extreme events and may encompass very conservative assumptions.

In this contribution, we present developments of simplified and graded approaches, mainly on the basis of PhD research work of Durand [4] and Kteich [5]:

- Development of the conventional linearisation approach by considering the pore pressure build-up effects on linear equivalent shear modulus; computation of the Aratozawa dam seismic response and comparison with in-situ observations.
- Implementation of a graded approach (static, simplified dynamic, non-linear time-response) on an earthfill dam, comparable to Aratozawa dam in terms of height and level of seismic input motion (1.22 g).
- Description of a new simplified method to assess the seismic behaviour of levees, embankments and small to middle height embankment dams.

2. EXTENDED LINEAR EQUIVALENT METHOD FOR THE ANALYSIS OF EMBANKMENT DAMS; APPLICATION TO ARATOZAWA DAM

2.1. INTRODUCTION

When dealing with the seismic response of dry or drained soil profiles, a common engineering practice consists in running, in an iterative process, a series of linear equivalent analyses. At every step, the profile model is updated through the

well-known shear modulus degradation curves, so that the process converges towards computed shear strains that are consistent with the shear moduli and damping ratios of the model. We follow the same approach here, considering the additional effect of the pore pressure build-up on the effective shear modulus.

The proposed method is designed in such a way that it is compatible with the conventional modal spectral analysis. One difficulty is that the modal spectral analysis does not provide any information about the experienced strains or stress cycles, whereas the pore pressure build-up process is highly dependent on the magnitude and number of such cycles. To overcome this difficulty, we consider the seismic response of the soil profile as a gaussian stochastic process. In this approach, in addition to the traditional response spectrum, the strong motion duration of the input motion, T_D, should be provided as an input data.

In a first step, we present the method on a soil profile. The approach is validated by consistency of the results with in-field observations of liquefaction and non-liquefaction. In a second step we extend the method to 2D embankment dam modelling, with application to the Aratozawa dam, which was affected by the 2008 Iwate-Miyagi earthquake.

2.2. Soil profile 1D modelling

2.2.1. *Constitutive relationship*

The focal point of the soil constitutive relationship is about the volumetric strain generated by the seismically induced shear strains. Relationships that are available in literature are derived from tests carried out by Martin et al. [6], interpreted by Sawicki and Swidzinski [7] and by Byrne [8]. Sawicki and Swidzinski's interpretation was adopted by Vincens [9] when dealing with seismically induced settlement of dry profiles. However, in the context of pore pressure analysis, it appears that Byrne's model is more appropriate [10]. On those bases, considering that the conventional normalized shear modulus degradation curve (for dry or drained materials) reads $G/G_{\max} = h(\gamma)$, it is substantiated in [10] that, when considering pore pressure effects, this normalized shear modulus reads as per Eq. (1) where r_u is the pore pressure build-up ratio and σ_v' the effective vertical stress.

$$G' = G_{\max} h(\gamma)(1 - r_u)^n, \text{ avec} r_u = \Delta u/\sigma_v' \tag{1}$$

2.2.2. *Stochastic analysis of the profile response*

At every depth of the soil profile, the shear strain response $\gamma(t)$ is idealized as a zero mean gaussian process, as illustrated in Fig. 1-a. This process is characterized

by its number of cycles, N, and its standard deviation σ_γ. The number of cycles is calculated as the product of the strong motion duration, T_D by the natural frequency of the soil profile. The standard deviation is linked to $\gamma_{\max}$, maximum of $\gamma(t)$ calculated as an output of the modal spectral method, by the peak factor, p, such that $\gamma_{\max} = p\sigma_\gamma$.

Peak factors were extensively studied by Der Kiureghian (1979); they are (not very sensitive) functions of the number of cycles and of the bandwidth. For instance, for a 1 Hz frequency and a 15 % damping ratio, the peak factor varies from 2.24 for T_D=5 s to 2.86 for T_D=10 s.

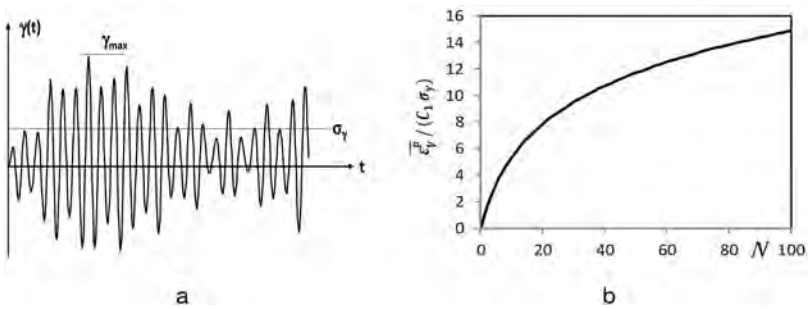

Fig. 1
a) Shear strain response ; b) accumulated strain versus the number of cycles
a) Réponse en cisaillement ; b) déformation cumulée en fonction du nombre de cycles

It is known that cycle amplitudes of a process such as presented in Fig. 1-a are Rayleigh distributed [13]. Therefore, we simulated hundreds of samples of such a process, to derive, based on Byrne's model, an empirical function of the cumulative plastic volumetric strain generated by a shear strain process characterized by its number of cycles and standard deviation. The output is plotted in Fig. 1-b in the form of a non-dimensional cumulative plastic volumetric strain, a numerical representation of which is given by Eq. (2).

$$\bar{\varepsilon_V^p}/\left(C_1\sigma_\gamma\right) = 4.1(\mathrm{Ln}N - 1), \quad 5 \le N \le 100 \tag{2}$$

2.2.3. *Calibration against field observations*

The above-introduced approach enables to evaluate the cumulated effects of the seismic response at the end of the strong motion. At this stage we can update the soil profile model by applying Eq. (1) and iterate the analysis on the updated model according to standard engineering practice. However, since the final value of the pore pressure build-up is not representative of the entire seismic signal, it cannot be directly

used to calculate the updated G' value of the normalized shear modulus. For this reason, we introduce an effective pore pressure build-up, $r_{u,eff} = \chi\, r_u$ which, takes the place of r_u in Eq. (1), where χ is a coefficient that should be calibrated. Based on observations of liquefaction on 12 sites of the Urayasu city at the occasion of the Great East Japan Earthquake (2011), Kteich et al. [10] identified $\chi = 2/3$ as the best estimated value. This χ value results in calculation outputs consistent with the 8 occurrences of liquefaction and 4 occurrences of non-liquefaction observed in Urayazu city.

2.3. The earthquake and dam

2.3.1. *The Iwate-Miyagi 2008 earthquake*

On 14 June 2008, an earthquake of magnitude 7.2 and depth 8 km shook a volcanic mountainous area of northern Japan, causing the death or disappearance of 23 peoples. Damages, including numerous landslides, were reported within a radius of 35 km around the epicentre [14]. A KiK-net station recorded a 3.87g vertical acceleration, the largest acceleration ever recorded [15].

2.3.2. *Aratozawa dam main features*

Several dams were severely shaken by the quake, including the Aratozawa dam located 15 km south of the epicentre of the main event. It is a clay core fill dam, built in 1991, in a semi-elliptical alluvial valley, primarily for irrigation services and flood control. The main geometrical features of the dam are summarized in Table 1.

Table 1
Main features of Aratozawa dam

Height	74.4 m
Crest length	413.7 m
Crest width	10.0 m
Upstream slope	1/2.7
Downstream slope	1/2.1

2.3.3. *Dam response under earthquakes*

The dam is instrumented by accelerometers at three locations of the central core (crest, mid-height, and base) and by fifteen interstitial pressure sensors. During the 2008 Iwate- Miyagi main shock, the dam suffered a settlement of 19.8 cm at the crest of the rockfills and about 40 cm at the crest of the clay core, while the recorded

duration of the strong motion was T_D= 5.36 s. The maximum accelerations in the three directions are presented in Table 2 [16]. We notice that the signal gradually fades in the height of the dam to reach 5.25 m/s^2, about half of PGA recorded at the base (10.24 m/s^2). The response spectrum of the seismic motion recorded in the gallery (upstream-downstream direction) normalized by the PGA is presented in Fig. 2.

A previous earthquake, in 1996, resulted in a significantly lower PGA, 0.28 g, recorded in the bottom gallery. Ohmachi and Tahara [16] calculated and analysed transfer functions between the gallery and the crest for this event. Based on 1996 records, the upstream-downstream fundamental frequency was calculated between 2.85 Hz and 3.03 Hz. Based on the 2008 records, the same frequency was calculated between 0.83 Hz and 1.54 Hz, which corresponds to an equivalent shear modulus divided by a factor of about 5.

Table 2
Peak accelerations recorded in 2008

	UPSTREAM-DOWNSTREAM	DAM AXIS	VERTICAL
Crest	5.25 m/s^2	4.55 m/s^2	6.22 m/s^2
Mid-height	5.35 m/s^2	4.78 m/s^2	4.70 m/s^2
Gallery	10.24 m/s^2	8.99 m/s^2	6.91 m/s^2

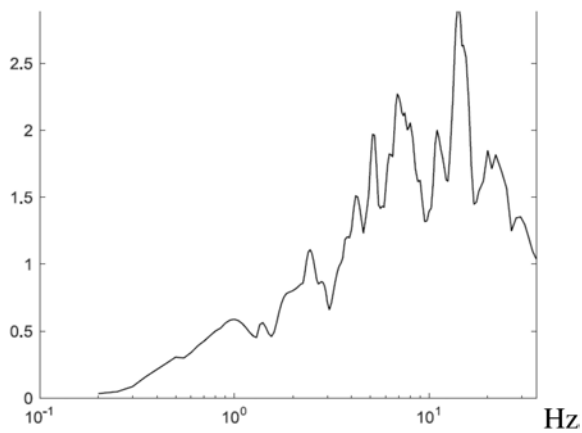

Fig. 2
Response spectrum, divided by PGA, recorded in the gallery
Spectre de réponse, normalisé par le PGA, enregistré en galerie

2.4. 2D approach and application to Aratozwa dam

2.4.1. *General assumptions*

The above introduced 1-D approach can be extended to the 2-D analysis of dikes or dams, where x direction is upstream-downstream and z vertical. The finite element method should be used to construct the 2-D model. As with the 1-D approach, the response can be calculated by modal spectral analysis. For this purpose, the seismic input motion is described by its conventional pseudo-absolute acceleration response spectrum, $S(f,\xi)$.

To implement the proposed approach, it is necessary to calculate the shear strain field $\gamma(x,z)$ at any location of the dam. In practice, depending on the available software, the modal shear strain field for the mode i, $\gamma_i(x,z)$, can be obtained either by derivation of the modal displacement with respect to z, or from the modal strain tensor field. In the context of the modal spectral method, the available output is the set of maximum values $\gamma(x,z)_{\max}$ over the 2-D model.

2.4.2. *Implementation for a 2D dam model*

For the sake of simplicity, we assume that the dam response is controlled by the single predominant mode, of frequency f_1. The following iterative process is adopted: once the dam modal analysis has been updated at iteration j-1, iteration j consists of the following steps:

- Computation of the eigenfrequency ${f_1}^j$, the eigenshape $\varphi_1(x,z)^j$, the modal participation factor ${q_1}^j$, and the modal strain field $\gamma_1(x,z)^j$.
- Computation of the peak strain, at any location in the model:

$$\gamma(x,z)_{\max}{}^j = {q_1}^j \gamma_1(x,z)^j S(f_1,\xi_1)/\left({\omega_1}^j\right)^2.$$

- Calculation of the number of cycles: $N^j = T_D \quad {f_1}^j$.
- Calculation of the peak factor p^j versus N^j in application of Der Kiureghian formulas [14], then computation of $\sigma_\gamma(x,z)^j = \gamma(x,z)_{\max}{}^j / p^j$ at any location.
- Computation at any location of $\varepsilon_V^p(x,z)^j$ in function of $\sigma_\gamma(x,z)^j$ and N^j according to Eq. (2).
- Computation at any location of the pore pressure build-up $\Delta u(x,z)^j$ according to Ziad et al. [10] and computation of $r_u = \Delta u/\sigma'_v$.
- In view of the next iteration, updating G' values according to Eq. (3), where $\gamma_{eff} = 0.65\,\gamma_{\max}$, (usual engineering practice), $r_{u,eff} = 2/3\,r_u$, and $n = 0.5$. Attention is drawn on the fact function $h(\cdot)$ varies, depending on x and z.

$$G'(x,z)^j = G_{\max}(x,z) h\left(\gamma_{eff}(x,z)^j\right)\left(1 - r_{u,eff}(x,z)^j\right)^n \tag{3}$$

In the presented example, convergence is assumed to be achieved when G' varies by less than 5% at any location in the model.

2.4.3. *Aratozawa dam modelling*

A simplified scheme of Aratozawa dam model is presented in Fig. 3. It is composed of three material zones: (A) clayey core, (B) rockfills and (C) very stiff foundation, with a 5000 m/s shear wave velocity. In zones (A) and (B), the shear wave velocity reads $V_s = V_{s0} \quad (z/z_0)^n$ ~~$V_s = V_{s0}\, z^n$ (z in meters)~~, where V_{s0} and n are given in Table 3, and $z_0 = 1\mathrm{m}$. These mechanical characteristics result in a 2.98 Hz fundamental natural frequency, consistent with the year 1996 observations reported above [18].

Computations were carried out with the finite element software of EDF, Code_Aster [17]. The model includes the dam and its foundation and consists of 2364 eight-node quadratic elements, giving 7546 nodes. The model is clamped at the base and has periodicity boundary conditions on the left and right parts of the foundation

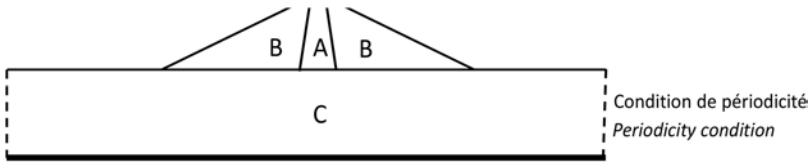

Fig. 3
Scheme of Aratozawa dam 2D model
Schéma du modèle 2D du barrage d'Aratozawa

Table 3
Shear wave velocity in the dam model

ZONE	V_{s0} (M/S)	N
A	200	0.35
B	300	0.20
C	5000	0

To simulate the dam response during the 2008 earthquake, we adopt the degradation curve proposed by Seed et al. [18] for the rockfills, and the one proposed by Vucetic and Dobry [19] for a plasticity index PI=30 for the core. The foundation is assumed to remain in the linear regime.

2.4.4. *Response of Aratozawa dam 2D model*

Our purpose is now to compute the dam model response to the seismic input motion described by the response spectrum presented in Fig. 2. The first iteration is associated to an elastic response, resulting in the number of cycles $N^1 = 16$. Damping is assumed to be 5 %, then derived from degradation curves in subsequent iterations.

The iterative process converges within 5 iterations. The final calculated frequency is f_1^5=1,34 Hz, which is consistent with observations reported Ohmachi and Tahara's [16]. The maximum shear strain developed in the core reaches 3.10^{-3} and the calculated core settlement is 17 cm. As illustrated in Fig. 4, a major interest of the method is that it provides results in terms of pore pressure build-up. Compared to field observations, the discrepancy in the upper part is due to the fact the model regards the core as saturated and undrained, which is certainly not the case. In the middle part, the pore pressure simulation and field observation are in agreement. In the lower part, the discrepancy could be because only the first mode is considered in the calculation of the response. Indeed, it was pointed out by Vincens et al. [9] that the second mode plays a role in a similar situation of seismically induced settlement. However, Vincens et al. were dealing with 1D soil profiles; the case of 2D models requires further investigations.

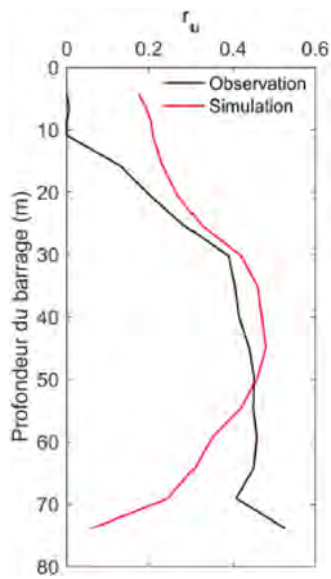

Fig. 4
Pore pressure build-up ratio in the core
Taux de montée de pression interstitielle dans le noyau

3. GRADED APPROACH FOR THE ASSESSMENT OF THE BEHAVIOR OF EMBANKMENT DAMS DURING STRONG EARTHQUAKES

Due to the importance of non-linear effects, the assessment of the seismic behaviour of embankment dams under strong motion is subject to numerous uncertainties. The use of a graded approach improves the confidence that can be placed in the results obtained. In addition, the most basic analyses used in the first steps of the graded approach are very useful for performing sensitivity analysis. This chapter presents the application of the graded approach to “Dam Y”, which is located at 2 km from a major active fault.

3.1. Presentation of the dam (“dam Y”)

The studied dam, referred to as “Dam Y” in this paper, is an earth-fill dam with a clay core. It has a total height of 74 meters and a base width of 404 meters. The upstream and downstream slopes of the dam vary between 1.5H/1V and 3.5H/1V. The crest width is 8 meters.

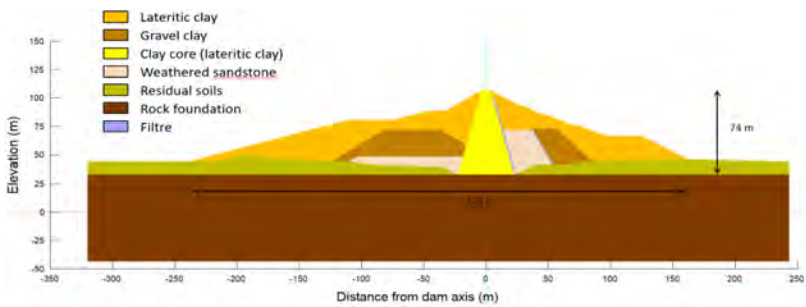

Fig. 5
“Dam Y” cross-section

The main material properties are given in the table below. The undrained shear strength is considered for all seismic calculations.

Table 4
"Dam Y" density and strength material properties

MATERIAL	DENSITY ρ (KG/M^3)	EFFECTIVE FRICTION ANGLE Φ (°)	EFFECTIVE COHESION C' (KPA)	UNDRAINED SHEAR STRENGTH S_u (KPA)	TENSILE STRENGTH R_t (KPA)
Dam core and lateritic clay	2050	25	75	$\max(100;0.25\,\sigma'_v)$	25
Gravel clay	2050	25	65	$\max(100;0.25\,\sigma'_v)$	20
Weathered sandstone	2000	40	0	-	-
Residual soils	2140	36	10	-	3
Rock foundation	2250	35	100	-	30

3.2. Seismic hazard at dam site

A site-specific seismic hazard study has been performed by seismologists from the ISTerre laboratory in Grenoble. Given that the "Dam Y" is located in an area where relatively frequent earthquakes occur at well-identified sources, the determination of the Safety Evaluation Earthquake (SEE) acceleration response spectra is based on a deterministic approach. The considered scenario is a magnitude 7.8 earthquake occurring on a strike-slip fault at very close distance (less than 2 km). The associated ground motion at the dam site is characterized by a peak ground acceleration (PGA) of 1.22 g and the acceleration response spectrum is shown in the Fig 6. Five accelerograms compatible with this response spectrum are considered in the study. They consist in real accelerograms, compatible in terms of magnitude and distance with the deterministic scenario, adjusted to the design response spectrum.

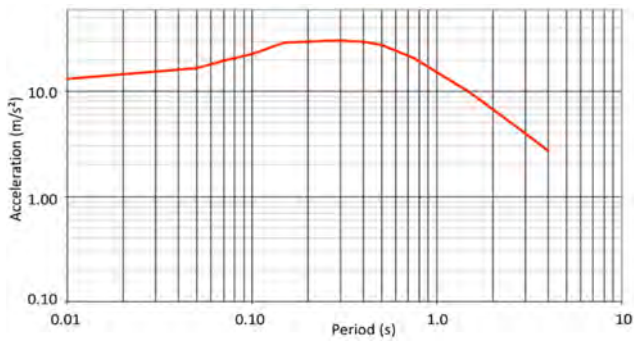

Fig. 6
Acceleration response spectrum at "Dam Y" site

3.3. Pseudostatic analysis

The software SLOPE/W developed by Geostudio is used for this analysis. This software calculates the slip surface by means of a 2D limit equilibrium method and provides the corresponding safety factors. In the present study, Morgenstern & Price's approach is used. The seismic loading is simulated by means of equivalent pseudo-static inertial forces. This approach consists in applying a constant and uniform seismic coefficient k_h corresponding to a horizontal acceleration $a_h = k_h g$ (with $g = 9.81$ m/s^2) to the entire model. A seismic coefficient $k_h = 2/3 * PGA/g = 0.85$ is first considered. The assessed safety factors are: 0.24 for un upstream slope failure and 0.27 for a downstream slope failure. These very low safety factors suggest that a significant sliding of the dam slopes can be expected in the event of such deterministic earthquake.

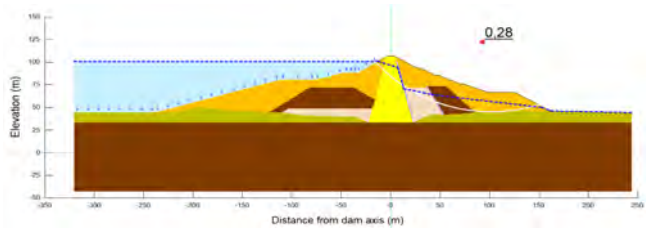

Fig. 7
"Dam Y" – Critical downstream slip surface under SEE loading

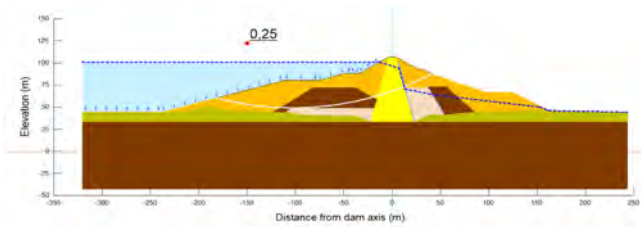

Fig. 8
"Dam Y" – Critical upstream slip surface under SEE loading

3.4. Simplified dynamic analysis

Two types of simplified approaches are considered in order to take into account the different mechanisms that can cause irreversible displacements of "Dam Y" in the event of an earthquake:

- Approaches which model shear deformations of soil leading to a sliding.
- Approaches which model volumetric densification of soil leading to a crest settlement.

In both cases, shear strength degradation of the materials is not considered.

3.4.1. *Shear deformation assessment*

The approach from Makdisi and Seed (1978) is considered. It is a "decoupled" procedure [20], which means that the dynamic response of the dam is evaluated separately from the possible permanent displacements along a slip surface. It is generally based on three main calculation steps:

- Estimation of yield acceleration of a potential sliding mass, i.e. acceleration that leads to a factor of safety equal to 1 when performing a limit equilibrium analysis;
- Estimation of the mean acceleration of the identified potential sliding mass taking into account the dynamic response of the dam;
- Estimation of irreversible displacements along the critical slip surface.

The obtained results are presented in Table 5. As expected, the yield accelerations a_y assessed in the software SLOPE\W for different depths of slip surfaces y_b are relatively small in comparison with the considered PGA at dam site (1.22g). The peak acceleration estimated at the crest $a_{crest\max}$ is 2.01g which corresponds to an amplification of 1.65 of the input PGA. For each potential sliding block, the calculated peak acceleration of the block $a_{block\max}$ is greater than the yield acceleration of the block. The assessed irreversible displacements U along each possible slip surface varies from 2 m to 9 m, which is not acceptable (the allowable displacement is 2.2 m according to French recommendation guidelines). The displacements are generally greater for downstream (downstr.) than for upstream (upstr.) slip surfaces.

Table 5
"Dam Y" – Makdisi and Seed (1978) simplified approach results [20]

	UPPER SLIP SURFACE		**INTERMEDIATE SLIP SURFACE**		**DEEP SLIP SURFACE**	
	UPSTR.	**DOWNSTR.**	**UPSTR.**	**DOWNSTR.**	**UPSTR.**	**DOWNSTR.**
y_b (m)	27.6	22.4	54.4	37.1	61.9	61.3
a_y (g)	0.45	0.52	0.25	0.15	0.17	0.10
$a_{crest\max}$ (g)	2.01					
$a_{block\max}$ (g)	1.45	1.63	0.89	1.25	0.81	0.83
U (m)	2.8	2.7	2.1	9.1	3.1	6.1

3.4.2. *Volumetric densification assessment*

Various empirical methods accounting for volumetric densification of materials in the assessment of crest settlements are described in French reference report “Risque sismique et Sécurité des ouvrages hydrauliques”, including Jansen (1990), corrected by Bureau (2009) to take into account for the height of the dam, Swaisgood (2003), Bureau (1995 and 2002) [21–23]. Jansen’s relationship requires the use of peak acceleration at crest and yield acceleration [21]. The considered values are given in Table 5.

Applying these empirical formulae on “Dam Y” gives the crest settlements presented in Table 6. The estimated settlements differ significatively between the methods. According to Jansen (1990) corrected by Bureau (2009) and Swaisgood (2003), the crest settlement is unacceptable (greater than 1 m). The displacement predicted by Bureau (2012) is significantly lower (around 0.5 m).

Table 6
“Dam Y” – Crest settlements assessed with different empirical approaches

		UPSTREAM	DOWNSTREAM
Jansen (1990) corrected by Bureau (2009) [21]	Upper slip surface	1.82	1.62
	Intermediate slip surface	2.76	3.77
	Deep slip surface	3.50	4.73
Swaisgood (2003) [22]	30.84		
Bureau (2012) [23]	0.47		

3.4.3. *Comments*

All the considered simplified methods except for Bureau (2012) method predict unacceptable irreversible displacements in the dam in case of SEE. The obtained results are consistent with the low factor of safety calculated with the pseudo-static analysis.

The application domain of these simplified approaches, which are either empirical or based on numerical models, is limited by the database used to developed them. This is particularly restrictive when considering extreme solicitation such as in the case of “Dam Y” (PGA: 1.22 g). In particular, when analyzing the data collection used by Swaisgood (2003), one can notice that PGA does not exceed 0.72 g in the case earth fill dams. Therefore, the result provided by Swaisgood (2003) formula for this study (PGA = 1.22 g) is an extrapolation which can explain this unrealistic value of settlement.

3.5. Non-linear analysis in time-domain

3.5.1. *Model assumptions*

The software FLAC developed by Itasca is used for calculations. It is a two-dimensional explicit finite difference program allowing non-linear static and time history dynamic analysis of the dam. The model is extended laterally and vertically to at least one times the height of the dam. It is made of around 36 000 quadrilateral elements distributed equally distributed between the dam body and the foundation (~18 000 elements each). The model mesh size is able to efficiently solve mechanical wave propagation up to 15 Hz. In order to model a representative initial state of displacements and stresses distribution, the construction and the impounding of the dam are modelled.

A linear elastic constitutive law is considered in the rock foundation. The behavior of the dam materials and the residual soils is considered elastoplastic and is modelled using Mohr-Coulomb constitutive law. Due to the short duration of the seismic loading, water is trapped in the dam materials and consequently undrained strengths are considered (Table 4). In the elastic domain, non-linearity is taken into account using Sun et al. (1988) degradation curves [24]. The small strain shear modulus has been determined with V_s measurements. An increasing in modulus with the local depth is taken into account in each element of the model (Fig. 9). The Poisson ratio is 0.4 in the dam core and lateritic clay (undrained behavior), 0.3 in weathered sandstone and residual soils and 0.2 in rock foundation.

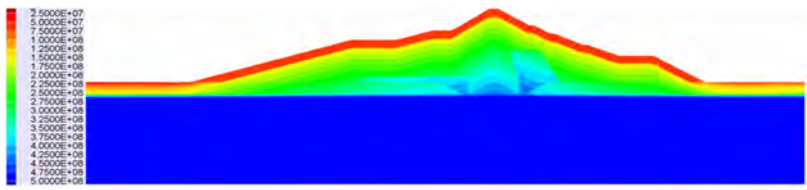

Fig. 9
Small-strain modulus in the model

The lateral boundaries are considered as free-field and the bottom boundary takes into account semi-infinite conditions downward. This means that most of the waves are not reflected back in the model at theses boundaries. Five different horizontal accelerograms are used for the computations. The input motion is introduced as a plane wave with vertical incidence. It is imposed as an equivalent stress at the different elements of the bottom of the model. The polarization of the input motion coincides with the horizontal in-plane direction.

3.5.2. *Main results*

The slip surfaces geometries are similar for all the considered input accelerograms. The amplitude of displacements only differs from one set to another. The detailed results are presented for the input accelerogram that produces the largest displacements in the dam. The Fig. 10 shows the shear strain at the end of the seismic event. Numerous slip surfaces are identified through the dam body. The largest of these starts at the reservoir level on the upstream face and ends at the downstream toe of the dam. Along this slip surface, the shear strains reach 50% in the downstream shoulder and 170% at the dam/residual soils – a criterion of 5% shear strains is usually considered to identify a slip surface.

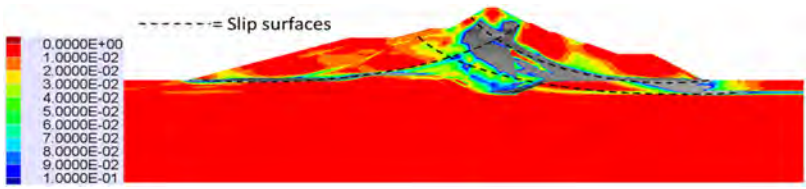

Fig. 10
Post-seismic shear strain (color scale limited to 10%: grey color for higher values)

The following figures (Fig. 11 and Fig. 12) show the final vertical and horizontal displacements in the dam at the end of the seismic event. The maximum settlements are located at the dam crest and reach about 6 m. The maximum horizontal displacement is about 8.5 m located at the downstream toe.

To conclude, the assessed irreversible displacements largely exceed the allowable displacements. This advanced numerical analysis confirms the results obtained from pseudo-static and simplified analyses. All the analyses conducted lead to the conclusion that the dam will fail in the event of the Safety Evaluation Earthquake.

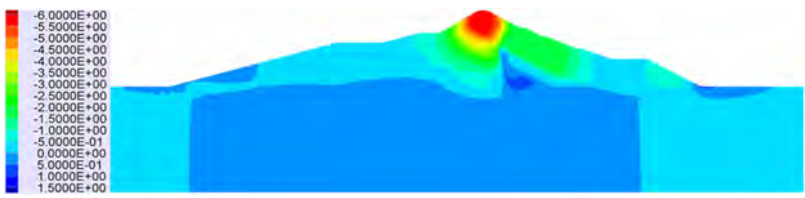

Fig. 11
Post-seismic vertical displacements (in meters)

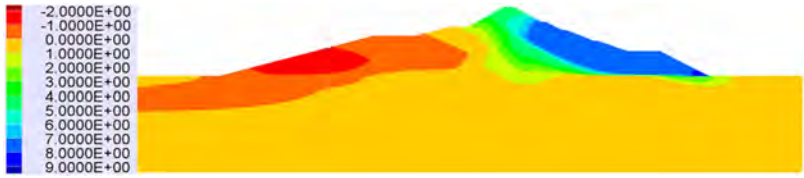

Fig. 12
Post-seismic horizontal displacements (in meters)

4. SEISMIC BEHAVIOR OF LEVEES, EMBAMKEMENTS AND SMALL TO MIDDLE HEIGHT EMBANKMENT DAMS

4.1. Main concerns

Levees, dams and earth embankments of low height (< 20 meters) are strategic structures that must remain stable in the event of an earthquake. However, given the very long length of these structures, it is rarely possible to conduct complex numerical modelling for each section of the embankment in regions of moderate seismicity. It is interesting, if not mandatory, to develop simple tools in order to identify the weakest sections where more complex simulations are needed, saving money and time.

One of the peculiarities of these structures is that they are rarely founded on competent rock (shear wave velocity greater than 800 m/s). It is therefore essential to consider their interaction with the soil foundation, which can have a significant influence on the behaviour of the embankment as shown in Fig. 13.

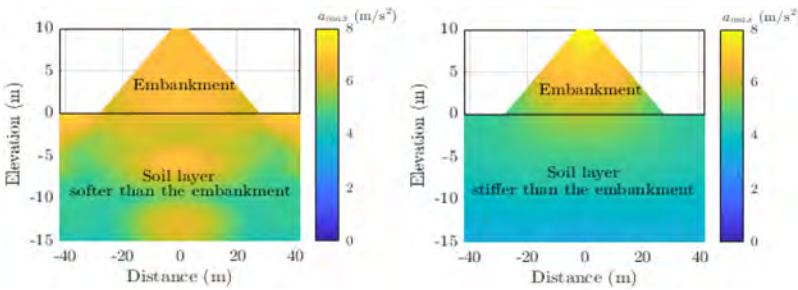

Fig. 13
Influence of soil layer on the seismic response of a ten-meter-high homogenous embankment (left: soil softer than the embankment, right: soil stiffer than the embankment)

Although the influence of the flexibility of a dam's foundation on its seismic movement has been known since the 1960s, very few charts or simplified formulations take it into account. To our knowledge, only two simplified methods for estimating seismic response incorporate the presence of a flexible foundation: the method proposed by Sarma (1979) [26] and the one developed by Papadimitriou et al. (2014) [27]. These methods, have some significant limitations. Specifically, Sarma's method (1979) [26] relies on an outdated resolution (shear beam type) and considers an unrealistic approach to model energy dissipation (uniform rigid rock and viscous damping throughout the model, identical in the dam and the soil, with a very high chosen value (20%) for developing the charts). As for Papadimitriou et al.'s method (2014) [27], it is developed for structures with a height greater than or equal to 20 m (corresponding to the tallest dams) and relies on input parameters poorly suited to engineering context (such as the predominant period of excitation). There is a need for a new simplified method in order to easily verify the embankment and small height dam stability in a French regulatory context.

4.2. Simplified methodology

This proposed simplified methodology can be used to assess the seismic behavior of these specific embankment dams. It is based on the same principal steps as described in §3.4.1: (a) estimation of yield acceleration of potential sliding masses, (b) estimation of the mean acceleration of the identified potential sliding masses and (c) estimation of irreversible displacements along the potential slip surfaces. However, it considers the particularities of small embankments for the assessment of their dynamic response (step (b)), using the results of Durand (2018) [4]. The estimation of yield acceleration of potential sliding block (step (a)) is the same as described in §3.4 for "Dam Y", it is therefore not detailed hereinafter. Steps (b) and (c) are detailed in §4.2.1 and §4.2.2 respectively.

4.2.1. *Use of predictive models from Durand (2018)*

This second step allows for the assessment of the dynamic response of the dam/foundation system and provides:

- Peak acceleration at crest.
- Peak acceleration of potential sliding masses.

The simplified predictive tools, which are the main focus of Durand's thesis (2018) [4], are based on a 2D numerical parametric study to evaluate the seismic response of a set of realistic dams covering a wide range of geometric and mechanical properties. These numerical calculations provide the necessary database for developing straightforward prediction tools. The considered numerical models are both realistic (to account for the main phenomena affecting embankment

movement) and relatively simple (applicable to various situations for deriving a simplified tool). The key characteristics of the numerical models and the chosen parameterization determine the validity domain of the simplified predictive tools.

As illustrated in Fig. 14, each model represents a symmetric trapezoidal-section dam resting on a foundation composed of a horizontal soil layer overlying an elastic rock. The dam is homogeneous, while the soil layer exhibits an increase in shear modulus with depth, reflecting the effect of confinement pressure on mechanical properties. This evolution is described in the models as an increase in the shear wave velocities with depth, following the formula indicated in Fig. 14, where V_a and V_b represent the S-wave velocities at depths $z_a = 0$ m and $z_b = 1000$ m, respectively. This gradient of shear wave velocities has been used, notably by Boudghene-Stambouli et al. [28].

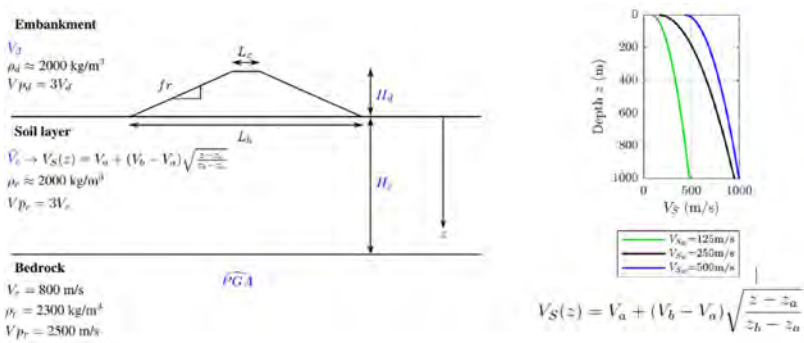

Fig. 14
Numerical parametric study models from Durand (2018)

In total, 540 different numerical models are considered, characterized by five parameters (represented in blue in Fig. 14). The parameter values considered in the study are as follows:

- Embankment height H_d : 4 m – 10 m – 20 m
- S-wave velocity in the embankment V_d : 200 m/s – 300 m/s – 500 m/s
- Thickness of the soil layer H_c : 3 m – 10 m – 30 m – 100 m – 300 m
- S-wave velocity profile in the soil layer $\widehat{V_c}$: 125 m/s – 250 m/s – 500 m/s
- Peak ground acceleration at outcropping bedrock $\widehat{PGA}$: 0.01 – 0.1 – 0.3 – 0.5

For each of the 540 cases, the dynamic response of the dam is characterized by the values of the maximum horizontal acceleration at the crest, denoted as $a_{crest\max}$ (540 values), and the maximum temporal accelerations of five potentially sliding blocks, denoted as $a_{block\max}$ (540 $\times$ 5 = 2700 values). The geometry of these blocks is indicated in the figure below.

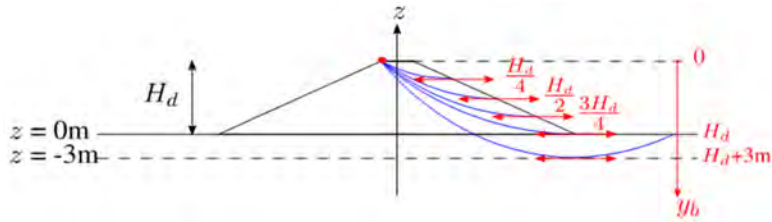

Fig. 15
Geometries of the possible sliding blocks considered by Durand (2018)

The seismic response is calculated for eight different waveforms. Each waveform is derived from real horizontal records from the RESORCE database [29], obtained at rocky sites and adjusted to the design spectra of French regulations using a phase-preserving adjustment technique [30]. The post-processed results represent an average over these eight signals.

The spectral element code SPECFEM2D is used to model the propagation of seismic waves in the 135 dam geometries for the four loading levels and eight waveforms. Nonlinearity is accounted for using an equivalent linear hybrid approach, with mechanical properties specified at each mesh point based on the equivalent 1D linear response of the corresponding soil column (including the dam height, if applicable) for the same loading level. The 2D models are discretized into a sequence of 1D vertical soil columns, each of which underwent equivalent linear analysis using SHAKE91 for eight ground motions at each PGA level at the rock. The evolution of shear modulus and damping is considered based on Darendeli's models (2001) [31] for a plasticity index of 0% (maximum nonlinearity). These curves account for the significant degradation dependence with confinement pressure (i.e., depth) for deep soil columns. For each column, the average equivalent damping and shear modulus profiles derived from the eight input waveforms for a given $\widehat{PGA}$ level are then used in the 2D models where this "local 1D column" is encountered.

The quantities of interest (maximum crest acceleration and maximum acceleration of potential sliding blocks) exhibit a complex and non-linear relationship with the model parameters – namely H_d, V_d, H_c , V_c, $\widehat{PGA}$ (and y_b for sliding blocks). In the pursuit of developing simple prediction tools, the first step is to identify the key parameters (or combinations of parameters) most relevant in controlling these values. The subsequent step involves developing a model to approximate the complex dependence linking these identified relevant parameters to the maximum accelerations. These two steps are carried out using an artificial neural network approach. Detailed analyses and obtained relationships are presented in Durand's thesis (2018) [4]. The obtained relationships are used to generate charts, such as in Fig. 16, for a simpler use of the method.

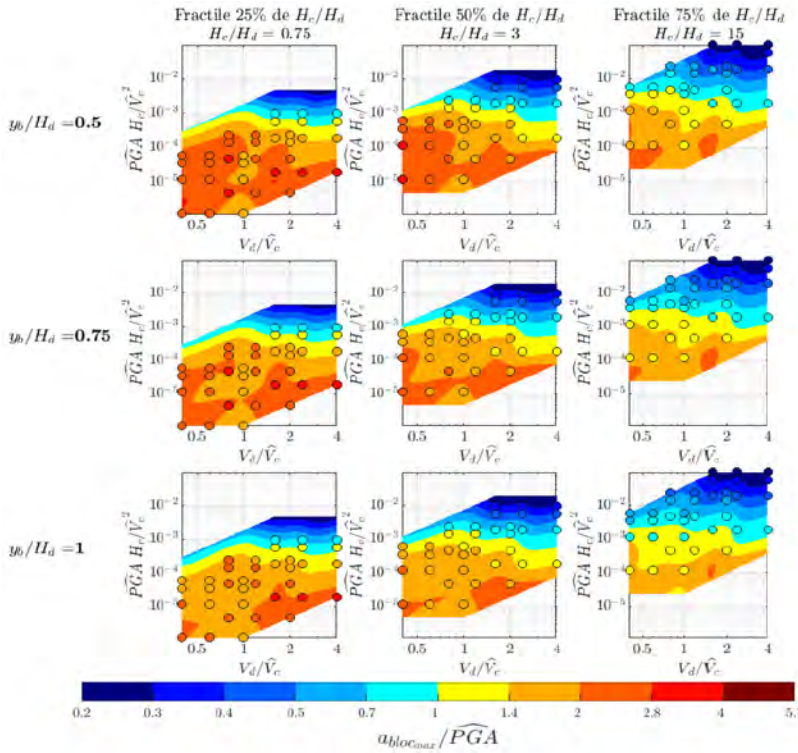

Fig. 16

Charts to assess $a_{block\ max}$ from the different input parameters [4]. The circles o with the same colorscale represents the numerical data from SPECFEM 2D

4.2.2. *Assessment of permanent displacements*

For this final step (step (c)), various existing formulas and charts can be considered. The charts by Makdisi and Seed (1978) [20] and Sarma (1979) [26] are favoured in this study. They require to know the fundamental resonance period of the embankment-foundation system T_0 which can be assessed using the simplified formulation provided by Sarma (1979) [26]. The figure below illustrates a comparison of the displacements they provide. One can notice significant differences between the two simplified methods, especially for low and high values of the ratio $a_y/a_{block\max}$.

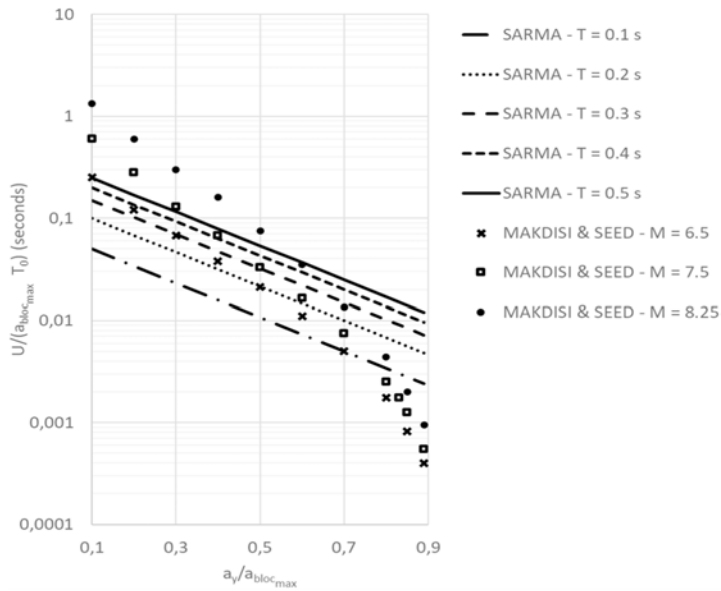

Fig. 17
Comparison of Makdisi and Seed (1978) [20] and Sarma (1979) [26] charts for the assessment of permanent displacements

4.3. Application cases

The use of this simplified methodology is integrated into the Compagnie Nationale du Rhône (CNR) overall process for justifying the seismic stability of the Rhône River embankments [32].

A first comparison with a non-linear numerical model has been performed on an embankment located in the French Pyrenees and presented in [33]: the comparison has shown a good agreement between peak accelerations and permanent displacements assessed by the numerical model and by the simplified method (lower than 5 cm). As a second validation, the methodology is applied on "Embankment G" located in the West Indies and compared to results provided by 2D non-linear computations performed in FLAC3D.

4.3.1. *"Embankment G"*

The studied embankment is 8 meters high and has a slope of approximately 2.5 H/V. Composed of backfill and rockfill, it retains a backfill platform. It is is built on

a 12-meter-thick layer of clayey madrepore sand, resting on tuffite (weathered on the first 10 meters). The considered cross-section is presented on the figure below. The main geotechnical parameters are provided in Table 7.

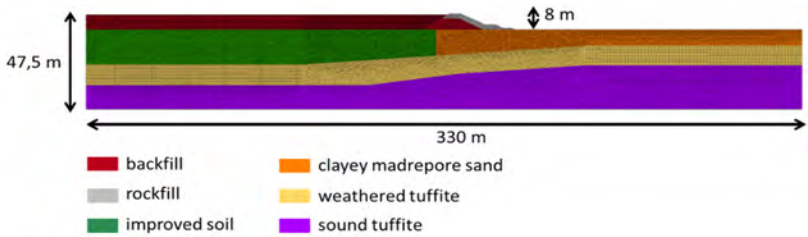

Fig. 18
"Embankment G" cross-section

Table 7
"Embankment G" – Material properties

MATERIAL	DENSITY ρ (KG/M^3)	EFFECTIVE FRICTION ANGLE Φ (°)	EFFECTIVE COHESION C' (KPA)	SHEAR WAVES VELOCITY V_S (M/S)
Backfill	2100	35	0	350
Rockfill	1700	45	5	350
Improved soil	2100	25	3	300
Clayed madrepore sand	1700	25	3	300
Weathered tuffite	1900	26	15	350
Sound tuffite	2000	35	50	450

The embankment is located in the French Antilles, in a high seismicity zone (zone 5). The peak ground acceleration at outcropping rock for an earthquake with a 475-year return period is $\widehat{PGA}$ = 0.306 g. A magnitude of 7.5 is considered for the design. Four accelerograms compatible with the seismic hazard are considered for numerical computations. Under this solicitation the maximum allowed horizontal displacement is 70 cm.

4.3.2. *Application of the simplified methodology*

The critical slip surface calculated in step 1 through a limit equilibrium analysis is characterized by a critical acceleration of a_y = 0.141 g and a depth of

y_b = 8.0 m. The critical slip surface is localized in the downstream part of the embankment, between the middle of the crest and the toe. The following other parameters are considered for the simplified calculations (step 2 and 3): embankment height H_d = 8 m, S-wave velocity in the embankment V_d = 350 m/s, thickness of the soil layer H_c = 22.1 m, S-wave velocity profile in the soil layer $\widehat{V_c}$ = 320 m/s, peak ground acceleration at outcropping rock $\widehat{PGA}$ = 0.306 g, resonance period T_0= 0.33 s, magnitude M = 7.5. The main results are presented in the table below.

Table 8
Embankment G – Results provided the simplified methodology

y_b	a_y	$a_{bloc\max}/\widehat{PGA}$	$a_{bloc\max}$	U MAKDISI	U SARMA
8.0 m	0.141	1.18	0.36 g	11 cm	16 cm

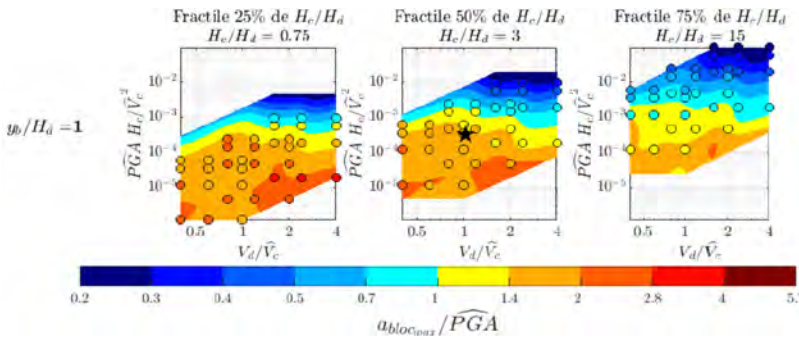

Fig. 19
Position of the considered situation by a black star on Durand (2018) charts

4.3.3. *Comparison with numerical model*

The calculations are performed using the FLAC3D software developed by ITASCA (https://www.itasca.fr/software/flac3d). The model does not exhibit variation in depth (Y direction): a 1 m thick slice is modeled. It thus extends 1 m in the horizontal Y direction, 330 m in the horizontal X direction, and 47.5 m in the vertical Z direction. The mesh contains 37,859 quadratic elements. It allows for the resolution of mechanical wave propagation up to a frequency of 15 Hz.

A linear elastic constitutive law is considered in the sound tuffite. The behavior of the embankment materials and the madrepore clay sand and the weathered tuffite is

considered elastoplastic and is modelled using Mohr-Coulomb constitutive law. A hysteretic Hardin and Drnevich (1972) damping is considered in these materials. Four different horizontal accelerograms are used for the computations. The input motion is introduced in the same manner as for “Dam Y” model (see §3.5.1). The calculated maximum horizontal displacement is between 24,5 cm and 38,3 cm depending on the considered input motion.

Fig. 20
Horizontal displacement at the end of the earthquake (results considering the input motion which maximizes the horizontal displacement in the embankment)

Both approaches lead to horizontal displacements in the same order of magnitude and below the design criteria (70 cm). However, there is a factor 1.5 to 3.5 between the results from the simplified approach and the numerical results. This discrepancy is mainly explained by the effect of the backfill behind the embankment which is not considered in the simplified approach. Additional numerical analyses have been performed without modelling this backfill: the assessed horizontal displacements are divided by two in average in this case.

5. CONCLUSION

This contribution presents developments of simplified and graded approaches, mainly on the basis of PhD research work of Durand [4] and Kteich [5], in order to evaluate the embankment dam seismic response.

The first considered approach is mainly based on the PhD research work of Kteich [5]. The main interest of this approach is that it is compatible with the conventional modal spectral analysis while incorporating the pore pressure build-up effects. For this purpose, the input strong motion duration, T_D, should be provided as input data, in addition to the traditional response spectrum. The approach is first developed for a 1D profile and then extended to a 2D geometry. The application of the 2D-approach to the 74-meter-height core fill Aratozawa dam (PGA 1.04g) shows promising results. It provides engineers with a simplified method that gives an

access to pore pressure build-up through a slight development in the common linearization technique based on degradation curves.

Secondly, a graded approach is considered for the assessment of the seismic behavior of a 74 m high embankment dam ("Dam Y") during a strong earthquake (PGA 1.22g) using successively pseudo-static, simplified dynamic and non-linear analyses. The application domain of the considered simplified approaches, which are either empirical or based on numerical models, is limited by the database used to develop them. This is particularly restrictive when considering extreme solicitation such as in the case of "Dam Y" (PGA: 1.22 g). However, the results provided by the various performed analyses, included the simplified approaches, are quite consistent with each other: except for Bureau's simplified approach (2012), all calculations predict the dam's failure, which provides faith in the obtained results. Due to the ruin of the dam, a post-seismic stability assessment, which is generally part of a complete graded approach, is unnecessary in this case.

Finally, a simplified methodology is proposed to assess the seismic behavior of levees, embankments and small to middle height embankment dams. It is mainly based on Durand (2018)'s results [4]. The main interest of this approach is that it considers the specificities of these facilities – with limited height and generally founded on a soil foundation – in the assessment of their seismic response. The application domain of the approach is restricted to the numerical models considered in the parametric study performed by Durand (2018) [4]: embankment height 4 m to 20 m, S-wave velocity in the embankment 200 m/s to 500 m/s, thickness of the soil 3 m to 300 m, S-wave velocity profile in the soil layer 125 m/s to 500 m/s, peak ground acceleration at outcropping bedrock 0.01 to 0.5. A first application case of this methodology has shown a good agreement of the obtained results with the results provided by more complex numerical model [33]. The comparison presented in this report shows more discrepancies between the simplified approach and the non-linear numerical model: permanent displacements are underestimated by a factor 1.5 to 3.5 by the simplified methodology.

In the long term, the most interesting prospect of this work would be to compare the results given by the simplified and graduated approaches developed in this article to more instrumental data recorded on real embankment sites.

REFERENCES

[1] RÉGNIER J. and 51 co-authors. 2018. PRENOLIN: International Benchmark on 1D Nonlinear Site-Response Analysis—Validation Phase Exercise. *BSSA*.

[2] SEED, H. B. AND IDRISS, I. M. 1970. Soil moduli and damping factors for dynamic response analysis. UCB-EERC 70-10.

[3] MEEHAN, C. L. ET VAHEDIFARD , F. 2013. Evaluation of simplified methods for predicting earthquake-induced slope displacements in earth dams and embankments. *Engineering Geology*, 152(1):180–193.

[4] DURAND C. 2018. Stabilité des digues sous chargement sismique : vers une nouvelle génération de méthodes simplifiées. Thèse de doctorat, *Université Grenoble Alpes.*

[5] KTEICH Z. 2019. Méthodes d'ingénierie pour l'étude du risque de liquéfaction et du tassement sous séisme. Thèse de doctorat, *Université Paris-Est*.

[6] MARTIN, G. R., FINN, W. L., AND SEED, H. B. 1975. Fundamentals of liquefaction under cyclic loading. *Journal of Geotechnical and Geoenvironmental Eng. 101(ASCE# 11231 Proceeding)* :423–438.

[7] SAWICKI, A. AND SWIDZINSKI, W. 1987. Compaction curve as one of basic characteristics of granular soils. *4ième colloque Franco-Polonais de mécanique des sols appliquée*, 1 : 103–115. Grenoble.

[8] BYRNE, P. M. 1991. A cyclic shear-volume coupling and pore pressure model for sand. *International Conference on Recent Advances in Geotechnical Earthquake Engineering and Soil Dynamics*. St Louis, Missouri.

[9] VINCENS, E., LABBÉ, P., AND CAMBOU, B. 2003. Simplified estimation of seismically induced settlements. *International journal for numerical and analytical methods in geomechanics*, 27(8) :669–683

[10] KTEICH Z., LABBÉ P., SEMBLAT J-F., JAVELAUD E., BENNABI A. 2018. Extended Equivalent Linear Method to assess liquefaction triggering: Application to the city of Urayasu during Tohoku 2011 earthquake. *Soils and foundations* 59, 750–763.

[11] WU, G. 2001. Earthquake-induced deformation analyses of the upper San Fernando dam under the 1971 San Fernando earthquake. *Canadian geotechnical journal*, 38(1) :1–15.

[12] DER KIUREGHIAN, A. 1979. On response of structures to stationary excitation. University of California. UCB-EERC 79-32.

[13] PREUMONT, A. 1990. *Vibrations aléatoires et analyse spectrale. PPUR.*

[14] KAYEN, R., COX, B., JOHANSSON, J., STEELE, C., SOMERVILLE, P., KONGAI, K., ZHAO, Y., AND TANAKA, H. 2008. *Geoengineering and seismological aspects of the Iwate Miyagi-Nairiku*, Japan earthquake of June 14, 2008. GEER Web Report, online report.

[15] KAZAMA, M., KATAOKA, S., AND UZUOKA, R. 2012. Volcanic mountain area disaster caused by the Iwate Miyagi-Nairiku earthquake of 2008, Japan. *Soils and Foundations*, 52(1) :168–184.

[16] OHMACHI, T. AND TAHARA, T. 2011. Nonlinear earthquake response characteristics of a central clay core rockfill dam. *Soils and Foundations*, 51(2):227–238.

[17] Code Aster. https://code-aster.org/

[18] SEED, H. B., WONG, R. T., IDRISS, I., AND TOKIMATSU, K. 1986. Moduli and damping factors for dynamic analyses of cohesionless soils. *Journal of Geotechnical Engineering*, 112(11) :1016–1032.

[19] VUCETIC, M. AND DOBRY, R. 1991. Effect of soil plasticity on cyclic response. *Journal of geotechnical engineering*, 117(1) :89–107.

[20] MAKDISI, F. & SEED, H. 1978. Simplified procedure for estimating dam and embankment earthquake induced deformations. *Journal of the Geotechnical Engineering Division*, 107(7):849–867.

[21] JANSEN, R. B. 1990. Estimation of embankment dam settlement caused by earthquakes. Water Power & Dam *Construction*, December 1990.

[22] SWAISGOOD, P.E. 2003. Embankment dam deformations caused by earthquakes. *Pacific conference on Earthquake Engineering*, Paper n°014.

[23] BUREAU, G. 2012. Quick assessment of potential seismic deformations of embankment dams. *Risk Analysis, Dam Safety, Dam Security and Critical Infrastructure Management*. Escuder-Bueno *et al.* (eds) © 2012 Taylor & Francis.

[24] SUN, J. I., GOLESORKHI, R. ET SEED, H. B. 1988. *Dynamic moduli and damping ratios for cohesive soils. Earthquake Engineering Research Center*, University of California Berkeley.

[25] GAZETAS, G. 1987. Seismic response of earth dams : some recent developments. *Soil Dynamics and Earthquake Engineering*, 6(1):2–47

[26] SARMA, S. 1979. Response and stability of earth dams during strong earthquakes. Technical report, U.S. Army Engineer Waterways Experiment Station Geotechnical *Laboratory*.

[27] PAPADIMITRIOU, A. G., BOUCKOVALAS, G. D. ET ANDRIANOPOULOS, K. I. 2014. Methodology for estimating seismic coefficients for performance-based design of earth dams and tall embankments. *Soil Dynamics and Earthquake Engineering*, 56(January):57–73.

[28] BOUDGHENE-STAMBOULI, A., ZENDAGUI, D., BARD, P.-Y. AND DERRAS, B., 2017. Deriving amplification factors from simple site parameters using generalized regression neural networks: implications for relevant site proxies. *Earth, Planets and Space* 69–99.

[29] AKKAR, S. *ET AL.*, 2014. Reference database for seismic ground-motion in europe (RESORCE). *Bulletin of Earthquake Engineering*, 12(1):311–339.

[30] CAUSSE, M., LAURENDEAU, A., PERRAULT, M., DOUGLAS, J., BONILLA, L. F., GUÉGUEN, P. 2014. Eurocode 8-compatible synthetic time-series as input to dynamic analysis. *Bulletin of Earthquake Engineering* 12(2):755–768.

[31] DARENDELI, M. B. 2001. *Development of a new family of normalized modulus reduction and material damping curves. PHD thesis*. The University of Texas at Austin.

[32] COUBARD G, ALVES-FERNANDES V., KOLMAYER, P., MONDOLONI, A., GRANJON, R., FELLAG, R., MEYNET, J., 2025. *Justification de la stabilité au séisme de grands canaux français par approches graduées. 28ème Congrès des Grands Barrages*, Chengdu.

[33] DURAND, C., CHALJUB, E., BARD, P.Y., FRY, J.-J., KOLMAYER, P., TACHKER, P., GRANJON, R., RENALIER, F., 2019. Méthodologie simplifiée pour la justification au séisme d'une digue sur fondation meuble. Colloque CFBR : « Justification des barrages : Etat de l'art et Perspectives », Chambéry.

[34] HARDIN, B. O., & DRNEVICH, V. P. 1972. Shear modulus and damping in soils: design equations and curves. *Journal of the Soil mechanics and Foundations Division*, 98(7), 667–692.

COMMISSION INTERNATIONALE DES
GRANDS BARRAGES

VINGT-HUITIEME CONGRES DES
GRANDS BARRAGES
CHENGDU, MAI 2025

LARGE DAMS AND NEW RULES ON SEISMIC HAZARD IN ALBANIA (*)

Mr. Arjan JOVANI & Mr. Llambro DUNI
ALBCOLD

ALBANIA

SUMMARY

Albania have almost 650 dams, among them 350 are large dams. Almost all the types of large dams in Albania are “earth dams”. Only 4 large dams are concrete dams and 12 of large dams are “rockfill dams”. The height of 10 large dams is more than 60 m and 4 of them are more than 100m. Considering their use, large dams in Albania can be classified different purposes: (i) irrigation, (ii) hydro-energy and solar energy, (iii) water supply, (iv) fishing and (v) Tourist and urban attractions. Most of them have been built for multipurpose.

As in other countries world-wide, in Albania quite all the dams at the time when they were designed, the pseudo-static method of analysis with a seismic coefficient of 0.1, was used, which is considered as absolute today. In Albania up to now we do not have experienced emergencies related to the loss of lives in their downstream section. However, according to the today’s concepts, large dams should be able to resist the effects of the strongest ground shaking to be expected at the dam site, and in this regard, we are conscious of the importance of the modern design and safety rules promoted by ICOLD during the years.

Taken into account the recommendations of ICOLD and the new probabilistic maps describing the seismic hazard in Albania based not on the “Seismic Intensity” as intensity measure, but on the PGA and spectral parameters, there is prepared the Government Decision No. 1162, date 24/12/2020 “For the determination of

Grands barrages et nouvelles règles sismiques en Albanie

DOI: 10.1201/9781003642428-126

procedures and terms to obtain the risk attestation for the subjects which request the construction permission".

Following the new developments in dam design practice, one of the late decisions of the ALBCOLD was the decision on "Dam classification depending on the consequences on the downstream area as result of seismic action". This classification in principe follows the ICOLD classification and divides dams in three main categories: (i) Small risk dams, (ii) Moderate risk dams and (iii) High potential risk dams. Taken into account this classification, the above-mentioned decision of ALBCOLD establishes some "Important Factors" do be applied for the repair of large dams used for irrigation, water supply and energy production which should be applied together with the appliance of the Government Decision No. 1162, date 24/12/2020.

For irrigation purposes dams, important factors of 1; 1.2 and 1.4 are specified for Small risk dams, Moderate risk dams and High potential risk dams, respectively. These importance parameters have to be applied on the 475 years return period of PGA parameter on rock condition.

For large dams with hydroenergy, water supply and urban purposes, the importance parameters have to be applied on the same return period of PGA parameters on rock condition that are given in the original designs or 2000 years return period.

In this Report, the Authors will present new rules on Seismic Hazard in Dams of Albania.

RÉSUMÉ

L'Albanie compte près de 650 barrages, dont 350 grands barrages. Presque tous sont en terre. Seuls 4 grands barrages sont en béton et 12 en enrochement. La hauteur de 10 grands barrages est supérieure à 60 m et 4 d'entre eux font plus de 100 m. Les grands barrages albanais sont destinés à (i) l'irrigation, (ii) l'énergie hydroélectrique et solaire, (iii) l'approvisionnement en eau, (iv) la pêche et (v) les attractions touristiques et urbaines. La plupart d'entre eux ont été construits pour être polyvalents.

Comme dans d'autres pays du monde, en Albanie, presque tous les barrages ont été conçus avec la méthode d'analyse pseudo-statique avec un coefficient sismique de 0,1. Cependant, selon les concepts actuels, les grands barrages devraient être en mesure de résister aux effets des secousses de sol les plus fortes auxquelles on peut s'attendre sur le site du barrage, et à cet égard, nous sommes conscients de l'importance de la conception moderne et des règles de sécurité promues par la CIGB au fil des ans.

Compte tenu des recommandations de la CIGB et des nouvelles cartes probabilistes décrivant l'aléa sismique en Albanie sur la base non pas de l'intensité sismique comme mesure d'intensité, mais de l'accélération au sol et des paramètres spectraux, la décision gouvernementale n° 1162, datée du 24/12/2020 est préparée pour la détermination des procédures et des conditions d'obtention de l'attestation de risques avant construction.

Suite aux nouveaux développements dans la pratique de la conception des barrages, l'une des décisions tardives de l'ALBCOLD a été la décision sur la « Classification des barrages en fonction des conséquences sur la zone en aval à la suite de l'action sismique ». Cette classification suit en principe la classification de la CIGB et divise les barrages en trois catégories principales : (i) les barrages à faible risque, (ii) les barrages à risque modéré et (iii) les barrages à haut risque potentiel. Compte tenu de cette classification, la décision susmentionnée de l'ALBCOLD établit que certains « facteurs importants » doivent être appliqués pour la réparation des grands barrages utilisés pour l'irrigation, l'approvisionnement en eau et la production d'énergie qui doivent être appliqués conjointement avec l'application de la décision gouvernementale n° 1162, datée du 24/12/2020.

Pour les barrages d'irrigation, des facteurs d'importance de 1 à 1,4 sont spécifiés selon le niveau des risques. Ces paramètres d'importance doivent être appliqués sur la période de retour de 475 ans du paramètre PGA.

Pour les barrages hydroélectriqueses ou d'alimentation en eau, les paramètres d'importance doivent être appliqués pour la même période de retour du PGA de la conception originale ou 2000 ans.

Dans ce rapport, les auteurs présenteront de nouvelles règles sur l'aléa sismique dans les barrages d'Albanie.

1. INTRODUCTION

Albania have almost 650 dams, among them 350 are large dams. Almost all the types of large dams in Albania are "earth dams". Only 4 large dams are concrete dams and 12 of large dams are "rockfill dams". The height of 10 large dams is more than 60 m and 4 of them are more than 100m. Considering their use, large dams in Albania can be classified different purposes: (i) irrigation, (ii) hydro-energy and solar energy, (iii) water supply, (iv) fishing and (v) Tourist and urban attractions. Most of them have been built for multipurpose.

As in other countries world-wide, in Albania quite all the dams at the time when they were designed, the pseudo-static method of analysis with a seismic coefficient of 0.1, was used, which is considered as absolute today. In Albania up to now we do

not have experienced emergencies related to the loss of lives in their downstream section. However, according to the today's concepts, large dams should be able to resist the effects of the strongest ground shaking to be expected at the dam site, and in this regard, we are conscious of the importance of the modern design and safety rules promoted by ICOLD during the years.

The old design code which accounts for the seismic effects on the HPP structures in Albania was the Design Technical Codes named KTP-N.2-89.

In Table 1, the importance factors taken into account in regard to the seismic action for the hydro power plants as a whole are presented.

Table 1
Importance factors of the HPP according KTP-N.2-89 design code

HYDRO POWER PLANTS	
CLASS OF THE HYDROPOWER STRUCTURE	**IMPORTANCE FACTOR K_R**
I	1.5
II	1.25
III	1.0
IV	0.75
V	Seismic hazard not considered

As it can be seen from that table, large dams are not specifically mentioned and it is not clear what are the criteria for the classification of the structures in different classes. According KTP-N.2-89, the classification of table 1 above is valid for all the structures under pression of classes II, III and IV, while for class I structures, included large dams, special micro zonation studies have to be carried out for the assessment of seismic hazard that threatens the dam location.

2. NEW RULES ON SEISMIC HAZARD FOR LARGE DAMS

2.1. New classifications of large dams referred risks and consequences on downstream areas

Taken into account the recommendations of ICOLD and the new probabilistic maps describing the seismic hazard in Albania based not on the "Seismic Intensity" as intensity measure, but on the PGA and spectral parameters, there is prepared the Decision of Council of Ministers (DCM) No. 1162, date 24/12/2020 "For the

determination of procedures and terms to obtain the risk attestation for the subjects which request the construction permission".

Also, ALBCOLD is planning to undertake the preparation of the National Standards and Guidelines for the Dam design and monitoring where the methodology for the assessment of seismic hazard at the large dams location will be described in detail.

Following the new developments in dam design practice, one of the ALBCOLD decisions was Decision No. 15, date 15/02/2021 "Dam classification depending on the consequences on the downstream area as result of seismic action".

This classification in principe follows the ICOLD classification and divides dams in three categories:

(i) **Small risk dams** (in case of break no casualties are observed and damages are small, usually circumscribed on the dam's owner property).
(ii) **Moderate risk dams** (in case of break no casualties are observed, but cause economical losses, environmental damage and interruption of infrastructure systems)
(iii) **High potential risk dams** (in case of break cause even one loss of live).

This classification is listed in ascending order of consequence. The hazard classification for a dam can change over time. Factors that can to bring changes are:

- new urban developments in the downstream,
- the increase of the water level in reservoir
- the danger to the plant or animal world,
- The revisions in the various reports of meteorological services.

Based on the above, continuous revision and updating of this classification is needed, in accordance with the frequency of the relevant studies.

2.2. Technical requirements for the risk of seismic actions

ALBCOLD has decided that for the repair of the existing large dams used for irrigation purposes, the Decision of Council of Ministers (DCM) No. 1162, date 24/12/2020 "For the determination of procedures and terms to obtain the risk attestation for the subjects which request the construction permission" to be applied. This includes the use of PGA as seismic hazard parameter according to the maps prepared the National Institute of Geosciences (IGEO) with 475 years of return period (map below).

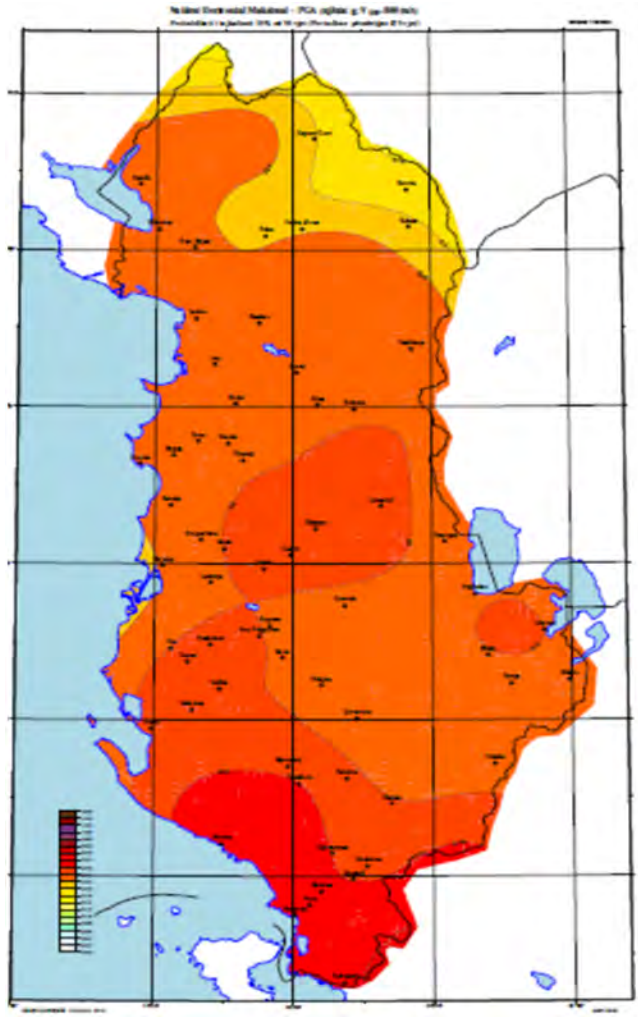

Fig. 1
Map of Peak Ground Acceleration (PGA) for return period of 475 years (source: IGEO)
Carte de l'accélération maximale au sol pour une période de retour de 475 ans (source IGO)

Referred this map and PGA for return period of 475 years, ALBCOLD decided:

- For the existing large dams that are used for irrigation and present a “small risk” according to the above classification, the Safety Coefficient Ks=1.0 should be applied.
- For existing large dams that are used for irrigation and present a “moderate risk” according to the above classification, the Safety Coefficient Ks=1.2 should be applied.
- For the existing large dams that are used for irrigation and present “high potential risk” according to the above classification, The Safety Coefficient Ks=1.4 should be applied.

For the repair of large dams that are part of the energy and water supply infrastructure of Albania and their auxiliary structures, the requirements of DCM No. 1162, dated 24.12.2020, Appendix 2, “Advanced requests in implementation of Albanian design standards and the most advanced international standards for seismic risk assessment”, as well as the specifications of the above requirements for dams with “high potential risk” (Ks=1.4) have to be applied.

For existing large dams with hydroenergy, water supply and urban purposes, the importance parameters have to be applied on the same return period of PGA parameters on rock condition that are given in their original designs.

In recent years design of high dams for energy production is reduced in our country, Actually, in the 30 last years, only a few number of high dams have been constructed in our country, and up to now, the appliance of ICOLD standards, based on the Bulletins No.72, 2010 (Revision) and Bulletin No.148, 2016 “Selecting Seismic Parameters for Large Dams, Guidelines” have been recommended and accepted for the design of this kind of structures. The requirement that are given in Both bulletins will take in the consideration during the design of large dams for energy production, water supply and urban puroposes

The requirements specified for the design of Large Dams are also applied to structures appurtenant to dams and hydro mechanical and electromechanical components of Hydrotechnical works.

3. CONCLUSIONS

Albania is a country with a high level of seismic risks and the results of the recent seismic hazard analysis confirm this evaluation. The actual in force standards for the design of large dams and HPP do not address dams specifically and are based on hazard maps prepared on the early 70s. Accordingly, large dams designed and build in that period are based on those hazard analysis.

Taken in account this situation, and in view of the last event in Durres area with with magnitude M 6.4, surrounded by a number of irrigation facilities, fortunately with no consequences, ALBCOLD is trying to upgrade the design standards, not only of dams for energy production, but for all ones, used for various purposes. To this regard, following the efforts to prepare new technical standards, ALBCOLD has approved some specific requirements in the Decision No. 15, date 15/02/2021 ”Dam classification depending on the consequences on the downstream area as result of seismic action”

This classification in principe follows the ICOLD classification and divides dams in three categories:

- Small risk dams,
- Moderate risk dams and
- High potential risk dams.

Taken into account this classification, the above-mentioned decision of ALBCOLD establishes some “Important Factors” do be applied for the repair of large dams used for irrigation, water supply and hydro energy production which should be applied together with the appliance of the Government Decision No. 1162, date 24/ 12/2020. These importance parameters have to be applied on the 475 years return period of PGA parameter on rock condition.

Following the new developments in dam design practice, one of the late decisions of the ALBCOLD was the decision on ”Dam classification depending on the consequences on the downstream area as result of seismic action”. This classification in principe follows the ICOLD classification and divides dams in three main categories: (i) Small risk dams, (ii) Moderate risk dams and (iii) High potential risk dams.

For irrigation purposes dams, important factors of 1; 1.2 and 1.4 are specified for Small risk dams, Moderate risk dams and High potential risk dams, respectively. These importance parameters have to be applied on the 475 years return period of PGA parameter on rock condition.

Also, It is very important and emergency to prepare the new technical standards for the monitoring of large dams and State technical standards for the Seismic -resistant dams that should be used in the design of new dams as well as in the monitoring, safety and rehabilitation projects of existing large dams. ALBCOLD support this process with experts in the field and through cooperation with research institutions with experience in the field of preparation of technical standards.

For large dams with hydroenergy, water supply and urban purposes, the importance parameters have to be applied on the same return period of PGA parameters on rock condition that are given in the original designs of them or ICOLD Bulletins No. 148, dated 2016.

REFERENCES

[1] Albanian Official Newspaper, (2021), DCM No.1162, date 24.12.2020 “For the determination of procedures and terms to obtain the risk attestation for the subject which the construction permission, Tirana, Albania.

[2] Decision No. 15, date 15.02.2021 “Dam Classification depending on the consequences on the downstream area as result of seismic action”, (2021), Tirana, Albania.

[3] ALBCOLD Website, www.albcold.gov.al (2021), english version, Tirana, Albania

[4] ICOLD Bulletin No.72_revision (2010)

[5] ICOLD Bulletin No.148. (2016), “Selecting seismic parameters for the large dams”.

Q.111 - R.24

COMMISSION INTERNATIONALE DES
GRANDS BARRAGES

VINGT-HUITIEME CONGRES DES
GRANDS BARRAGES
CHENGDU, MAI 2025

SEISMIC MONITORING FOR PALTINU ARCH DAM (*)

Daniel GAFTOI
PhD Engineer, Technical University of Civil Engineering Bucharest

Basarab CHESCA
Namazu Consulting, România
"Ion Mincu" University of Architecture and Urbanism

Radu SARGHIUTA
Professor, Technical University of Civil Engineering Bucharest

Catalin POPESCU
Lecturer, Technical University of Civil Engineering Bucharest

Laurentiu LUNGU
PhD Engineer, Technical University of Civil Engineering Bucharest

ROMANIA

SUMMARY

Paltinu dam is made up of central symmetrical double curvature arch body that rests on a pulvino by means of a peripherical joint and a parabolic wing extending over the left abutment terrace. Over the time it has been subjected to an intensive monitoring program using in situ ambient vibration measurements. As part of this program, a finite element mathematical model was developed and calibrated using data from the initial measurement campaigns and employed to evaluate the structure's safety at each monitoring stage.

Surveillance sismique du barrage-voûte de Paltinu

 DOI: 10.1201/9781003642428-127

To further enhance seismic monitoring capabilities, a new system was installed in 2022 consisting of six accelerometers (one in free field, one on each abutment, one on the foundation – inside bottom gallery and two on the crest of the dam) and one seismometer placed on the west side abutment since this is the quietest area of the dam. Since its installation, the new monitoring system has recorded a series of low-intensity events.

The article briefly presents the initial monitoring program (which is still ongoing), the newly installed seismic monitoring system, and a comparation between them regarding recorded frequencies.

RÉSUMÉ

Le barrage de Paltinu est constitué d'une voûte symétrique à double courbure qui repose sur un pulvino au moyen d'une articulation périphérique et d'une aile parabolique sur la rive gauche. Au fil du temps, il a fait l'objet d'un programme de surveillance intensif utilisant des mesures de vibrations ambiantes in situ. Dans le cadre de ce programme, un modèle mathématique par éléments finis a été développé et calibré à l'aide des données des premières campagnes de mesures et utilisé pour évaluer la sécurité de la structure à chaque étape de la surveillance.

Afin d'améliorer encore les possibilités de surveillance sismique, un nouveau système a été installé en 2022 ; il est composé de six accéléromètres (un en champ libre, un sur chaque culée, un sur la fondation – galerie inférieure intérieure et deux sur la crête du barrage) et un sismomètre placé sur la culée du côté ouest, car il s'agit de la zone la plus calme du barrage. Depuis son installation, le nouveau système de surveillance a enregistré une série d'événements de faible intensité.

Le rapport présente brièvement le programme de surveillance initial (qui est toujours utilisé), le système de surveillance sismique nouvellement installé et une comparaison entre eux en ce qui concerne les fréquences enregistrées.

1. INTRODUCTION

The Paltinu Dam, a structure of exceptional importance in Romania, is subject to a complex monitoring program that combines periodic ambient vibration measurements with data collected by an advanced seismic system recently installed. In

an area prone to seismic activity, such as the one where the dam is located, continuous evaluation of structural integrity becomes essential. The seismic system, implemented in 2022, aims to record seismic events in detail and to supplement the information gathered through biannual ambient measurements.

By correlating data obtained from both sources, this study provides a comprehensive view of the dam's dynamic behavior, thus ensuring a proactive approach in maintaining structural safety and performance. Additionally, this monitoring allows for the early identification of potential degradation related to structural aging, supporting the implementation of appropriate measures to keep the dam in optimal operating condition.

The ambient vibration monitoring method is widely applied globally for both bridges and civil structures [1,2] as well as for hydraulic structures [3–6]. In Romania, this technique has been used, among others, for buttress dams such as Poiana Uzului, Secu, and Gura Râului [7,8], and for arch dams like Paltinu and Cincis [9]. The technique is based on the concept of hybrid models calibrated using the Global Elastic Modulus (GEM), allowing for the evaluation of the evolution of dynamic characteristics and providing a detailed view of the structural condition of dams.

2. AMBIENT VIBRATION MONITORING OF PALTINU DAM

2.1. Paltinu dam

Paltinu Dam, the only double-curvature arch dam with a peripheral joint in Romania, is subject to an intensive monitoring program due to its exceptional importance as a structure – classified as Category A and first-class importance according to Romanian regulations. The dam consists of a central symmetrical double curvature arch body that rests on a pulvino by means of a peripherical joint and a parabolic wing extending over the left abutment terrace.

Its structural height is 108 meters, and the dam is remarkably slender, with a base thickness of 16 meters and a crest thickness of 6 meters. The crest length is 460 meters. The central body of the dam spans 302 meters and is divided into 25 blocks. The parabolic wing is 143 meters long and composed of 13 blocks. Due to the morphological conditions, abutments were required on both banks: the right bank has a gravity-type abutment with a length of 16 meters, while the left bank has a fork-shaped abutment with a length of around 40 meters. The normal retention level is 649.00 meters above sea level, while the crest level is 652.00 meters above sea level. Water discharge from the reservoir is ensured by a glory-type spillway, a mid-level outlet, two bottom outlets, and a hydroelectric plant located at the downstream base of the dam, equipped with two Francis turbines. The reservoir is mainly created for water supply for population and industry, but also for flood routing.

The foundation rock consists of alternating layers of sandstone and schist, with the thickness of sandstone layers varying between 0.5 and 5 meters. There is a well-defined fissure system, particularly evident in the sandstone. The site is intersected by several faults, generally oriented perpendicular to the valley. The permeability of the foundation rock was quite large (2 . . . 8 lugeons) and an extensive grout curtain was provided.

After the dam's commissioning in 1971, during the relatively rapid filling of the last several meters of the reservoir in 1974, significant and asymmetric displacements of the dam were observed, much larger than those predicted by calculations. Based on additional investigations and recalculations, supplementary sealing and drainage works were designed and implemented upstream of the active faults, along with protection and stabilization works on the slopes through concrete covering.

Fig. 1
Aerial photograph of Paltinu dam
Photographie aérienne du barrage Paltinu

2.2. Overview of hybrid model and global elastic modulus

The hybrid model, as defined by various authors such as Abdulamit [8,10,11], Stematiu [12], and Markovic [13], is a combination of in-situ measurements and a mathematical model (typically based on the finite element method), applied to structures like concrete dams. The hybrid model allows the calibration of the mathematical analysis using data from monitoring systems installed on the dam or from mobile labs that can perform regular or special measurements.

A key concept in this approach is the Global Elastic Modulus (GEM). According to the same authors and Sârghiuță [14] and Bugnariu [15], GEM is a

structural parameter specifically used to evaluate the safety and performance of existing concrete dams. The GEM approach assumes certain behaviors: the elastic properties of the materials, the structural continuity of the dam, and the complexity of the mathematical model. Importantly, GEM is not a physical material property, but a parameter tied to the specific mathematical model used in the analysis. It reflects the dam's overall structural behavior, integrating factors such as foundation stiffness and model refinement. GEM becomes meaningless if separated from the calibrated model, as its value is context-specific and dependent on field measurements.

GEM can vary significantly depending on the type of load applied (static vs dynamic), and it is also highly sensitive to seasonal variations. For thin concrete structures like arch or buttress dams, the structural continuity can be affected by joint openings, causing the GEM to differ between colder and warmer seasons. To use GEM effectively, it is essential to ensure that field measurements are taken under similar thermal conditions and with consistent methods and measurement points.

New acquired field measurements are used afterwards for re – calibration of the same mathematical model and the GEM is re – evaluated. If the new value does not significantly differ from the previous ones, it can be concluded that the dam has preserved its structural characteristics. If it is not the case, if discrepancies are encountered, further investigations are required in order to find the cause of the changes.

By combining in-situ measurements with advanced mathematical modeling, the hybrid model and GEM provide a comprehensive framework for tracking the long-term behavior of concrete dams, offering insights into both routine performance and the impacts of extraordinary events, such as earthquakes or heavy surcharges.

2.3. Ambient vibration monitoring campaigns

In parallel with the classical installed monitoring system, an intensive program of ambient vibration measurements was conducted, with the aim of identifying potential structural degradations due to aging of the structure.

The first measurement campaign took place in 2006 (as part of a CEEX research program) and was followed by a pause of approximately 6 years. Starting from 2012, measurement campaigns have been conducted annually or biannually up to the present year. Table 2 shows the fundamental periods obtained for each measurement campaign, along with the reservoir level on the day of the measurements.

Over time, several measurement systems have been used, as presented in Table 1. The initial measurement scheme included plots 4, 9, 13, 17, 21, 25, and 29. Later, starting from 2012, plots 6 and 11 were added to the initial scheme, and this configuration remained consistent over the years (figure 2).

Table 1
Measuring equipment used
Équipements de mesure utilisés

SEISMOMETER ACCELEROMETER	ACQUISITION SYSTEM	SAMPLING FREQUENCY (HZ)	DURATION (MIN)
SS-1 Ranger	VSS-3000 KINEMETRICS	100	10
Brüel & Kjær 8340	Brüel & Kjær 3050 6 channel	100	5
CR4.5-1 H	GEODAS 3/12 channels	100 / 500	5 / 2
VE-51-H	GeoSIG GMSplus	100	5

Table 2
Recorded fundamental periods for all measured blocks (s)
Périodes fondamentales enregistrées pour tous les blocs mesurés

DATE	WATER LEVEL									
[MM-YY]	MASL	BLOCK 4	BLOCK 6	BLOCK 9	BLOCK 11	BLOCK 13	BLOCK 17	BLOCK 21	BLOCK 25	BLOCK 29
10.12	636.00	0.36	0.45	0.43	0.41	0.41	0.45	-	0.45	0.45
06.13	636.00	0.38	0.45	0.45	0.39	0.39	0.45	-	0.40	0.40
10.13	642.00	0.40	0.45	0.45	0.40	0.40	0.45	-	0.40	0.31
05.14	646.00	-	0.42	0.39	0.40	0.40	-	-	0.44	-
10.14	640.00	0.44	0.44	0.45	0.45	0.39	0.44	-	-	-
04.15	641.75	-	-	-	0.46	0.37	0.47	0.49	0.49	0.49
10.15	643.50	0.49	0.45	0.45	0.45	0.40	0.45	0.45	0.26	0.20
04.16	639.25	0.44	0.44	0.44	0.44	0.37	0.44	0.50	0.50	0.50
10.16	643.00	0.47	0.49	0.47	0.47	0.44	0.47	0.47	0.44	0.47
05.17	641.50	-	-	-	0.45	0.50	0.45	-	-	-
10.17	639.00	0.45	0.46	0.46	0.46	0.44	0.45	0.46	0.46	-
05.18	640.50	0.38	0.38	0.43	0.46	0.46	0.45	0.45	0.38	0.38
10.19	640.15	-	0.45	0.46	0.46	0.41	0.45	0.46	0.43	-
06.20	640.00	0.66	0.66	0.66	0.44	0.41	0.44	0.44	0.44	0.44
09.20	639.85	0.45	0.45	0.45	0.46	0.43	0.46	0.46	0.42	0.46
10.21	639.95	0.45	0.46	0.46	0.46	0.38	0.46	0.48	0.50	0.50
06.22	640.00	0.45	0.45	0.45	0.48	0.39	0.45	0.45	0.42	0.45
11.22	639.25	0.37	0.43	0.43	0.45	0.36	0.45	0.43	0.40	0.45
10.23	640.10	0.43	0.44	0.44	0.44	0.49	0.45	0.47	0.40	0.47

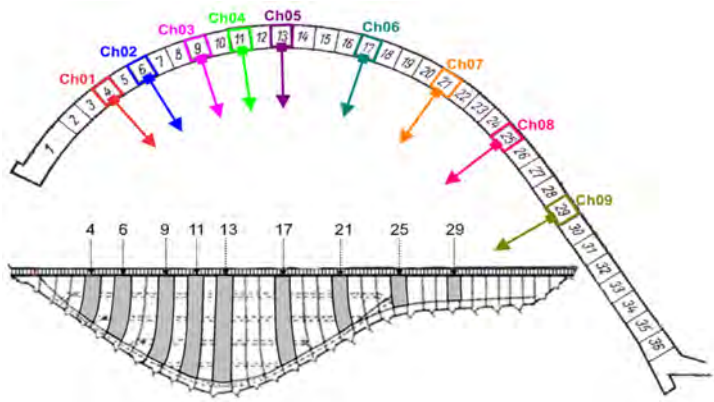

Fig. 2
Measurement scheme adopted for Paltinu dam
Schéma de mesure adopté pour le barrage Paltinu

In figures 3 to 6, the first three measured frequencies for the plots situated in the central area of the arch body (9, 11, 13, 17), the reservoir level recorded on the day of the measurements, and the crest elevation are presented. The absence of some measurement points is mainly due to sensor malfunction at the measured point or the presence of noise signals that could not be processed.

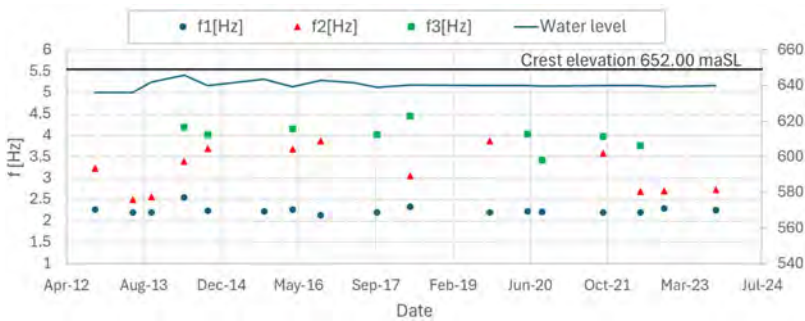

Fig. 3
First 3 frequencies (Hz) recorded and water elevation during measuring campaigns for Block 9
Les trois premières fréquences (Hz) enregistrées et le niveau de l'eau lors des campagnes de mesure pour le bloc 9

Fig. 4
First 3 frequencies (Hz) recorded and water elevation during measuring campaigns for Block 11
Les trois premières fréquences (Hz) enregistrées et le niveau de l'eau lors des campagnes de mesure pour le bloc 11

Fig. 5
First 3 frequencies (Hz) recorded and water elevation during measuring campaigns for Block 13
Les trois premières fréquences (Hz) enregistrées et le niveau de l'eau lors des campagnes de mesure pour le bloc 13

Fig. 6
First 3 frequencies (Hz) recorded and water elevation during measuring campaigns for Block 17
Les trois premières fréquences (Hz) enregistrées et le niveau de l'eau lors des campagnes de mesure pour le bloc 17

The instrumental investigations refer exclusively to the overall behavior of the Paltinu dam in the elastic domain, considering ambient vibrations as the source of vibration, together with vibrations produced by hydromechanics equipment operating in the body of the dam. The frequency of 10.00 Hz produced by the hydromechanical equipment was highlighted on the recorded data.

2.4. Overview of the mathematical model

The mathematical model developed for analyzing the dynamic behavior of the dam employs a 3D finite element approach using ANSYS APDL (figure 7). The interaction between the dam and the foundation is modeled with a “standard” massless foundation system, where only the flexibility of the foundation rock is considered, while its inertia and damping are neglected. The dam is treated as a monolithic structure, discretized using appropriate finite elements, and the dam-water interaction is represented by lumped mass elements that simulate the added hydrodynamic mass according to Westergaard’s method. The foundation is modeled with solid elements, carefully considering the valley’s morphology.

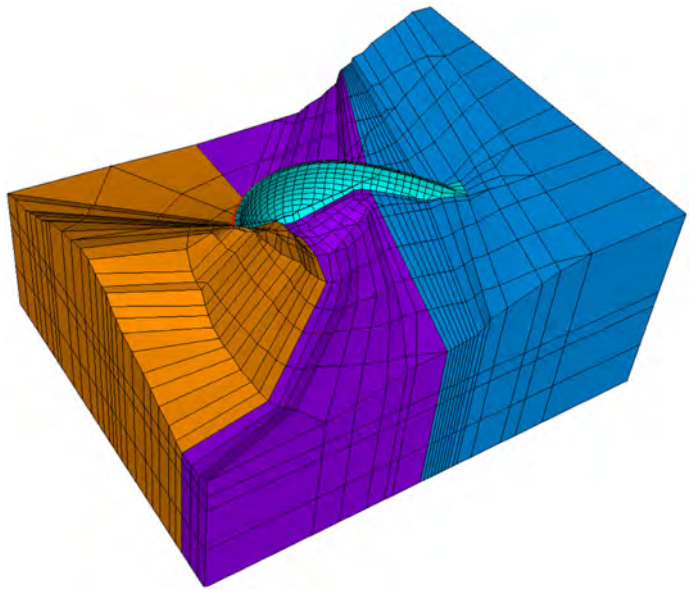

Fig. 7
Mathematical model created for Paltinu dam
Modèle mathématique créé pour le barrage de Paltinu

The sensitivity analysis used to calibrate the model led to a concrete elasticity modulus value of 25 GPa corresponding to the measured fundamental frequency in the first campaign. In figure 8 the deformed shapes and associated frequencies for the first 3 modes are presented.

Fig. 8
Deformed shapes and associated frequencies for the first 3 modes
Formes déformées et fréquences associées pour les trois premiers modes

3. NEW MONITORING SYSTEM

3.1. Short description of the monitoring system

Starting with the end of 2022, a new seismic monitoring system was installed at Paltinu Dam. It consists of six strong motion force balance accelerometers (>160dB sensitivity) and one broadband seismometer (155dB sensitivity). The accelerometers are installed as follows (figure 9 and 10): one in free field, one on each abutment, one on the foundation – inside bottom gallery) and two on the crest/ top of the dam. The main purpose of the system is to record the strong motion events generated by the Vrancea Seismic source (one of the most important seismic source in Romania) located at less the 100km distance. However, considering the high sensitivity of the sensors, it can be used to record smaller earthquakes as well as to compute the eigen frequencies for the points where the sensors are located at the top of the dam. The accelerometers located on the abutments and in free field are aligned along classical North-South directions while the accelerometers placed on the dam (foundation/bottom gallery, crest/top of the dam) are aligned with the main horizontal axis parallel to the radius of the dam. Because the position of the free field station is located near a road, during the installation, the position of the seismometer was changed from the field station to the west side abutment since this is the quietest area of the dam. Each accelerometer has its own digitizer installed in

its proximity. All the digitizers are connected to a main Network Acquisition System using single mode optical fiber. The network acquisition system provides common voting triggering for strong earthquakes. The data is stored on the two SD cards installed in each digitizer as well as in the NAS. For each digitizer a 24h backup battery pack has been installed so that in case of a power failure, the digitizers are able to continuously record the vibrations.

Supplementary, a web based structural health monitoring system connected to the European Seismic Database has been configured allowing requests of seismic records based on database information including weak and medium motion earthquakes.

Commercial names of the Devices and Software: accelerometer- Guralp Fortimus; seismometer – Guralp Certis; digitizer – Guralp Minimus & Minimus+ (for the station with seismometer); Web Based Structural Health Monitoring System – Gempa SHARD".

Fig. 9

Free field station (top left), accelerometer placed on the crest of the dam (top right), accelerometer and seismometer located at block 0 (bottom left) and digital data acquisition system (bottom right).

Station en champ libre (en haut à gauche), accéléromètre placé sur la crête du barrage (en haut à droite), accéléromètre et sismomètre situés au bloc 0 (en bas à gauche) et système d'acquisition de données numériques (en bas à droite).

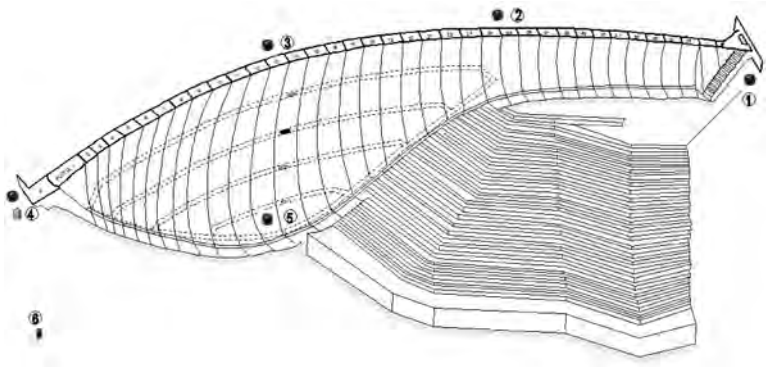

Fig. 10
Position of the accelerometers
Position des accéléromètres

3.2. RECORDED DATA

Below are presented the significant earthquakes starting from December 2023 till September 2024 by the Vrancea Seismic source. The most significant earthquake is the one recorded on September 16th, 2024, 14.40 UTC Time. The below figure presents the records of each sensor on the stream (radial direction) for the accelerometers installed on the dam and on the North-South direction for the accelerometers located on the abutments / free field.

Table 3
Significant recorded earthquakes December 2023 - September 2024
Séismes significatifs enregistrés de décembre 2023 à septembre 2024

DATE AND TIME OF THE EVENT	WATER LEVEL	TEMP	MAG†	DEPTH	EPICENTRAL DISTANCE	STREAM DIRECTION, A3 ACCELERATION
[UTC]	MASL	°C	ML	KM	KM	CM/S^2
2023-12-03 T22:05:48	638.00	8.50	4.8 ml	132.5	68.1	1.03
2023-12-09 T17:08:26	638.00	-1.00	4.0 ml	135.9	60.6	0.08
2023-12-24 T06:06:28	638.00	1.00	4.2 ml	96.8	91.6	0.43

(Continued)

†The values of the magnitudes are computed and reported by the National Institute of Earth Physics, Romania.

Table 3
Continued

DATE AND TIME OF THE EVENT	WATER LEVEL	TEMP	MAG†	DEPTH	EPICENTRAL DISTANCE	STREAM DIRECTION, A3 ACCELERATION
[UTC]	MASL	ºC	ML	KM	KM	CM/S^2
2024-01-15 T09:01:48	637.00	-1.00	4.3 ml	74.0	92.9	0.28
2024-02-05 T21:50:45	636.00	8.50	4.0 ml	15.8	126.4	0.28
2024-02-29 T09:25:45	635.00	7.50	4.2 ml	146.7	67.9	0.27
2024-05-07 T15:32:23	641.00	14.00	4.1 ml	119.8	81.8	0.26
2024-05-22 T09:53:37	642.00	14.00	4.1 ml	90.2	70.6	0.27
2024-08-01 T12:09:01	641.00	22.00	4.5 ml	129.6	87.2	1.44
2024-08-06 T13:04:34	641.00	18.00	4.1 ml	133.3	87.2	0.29
2024-09-16 T14:40:22	638.00	13.00	5.4 ml	126.8	55.6	5.45

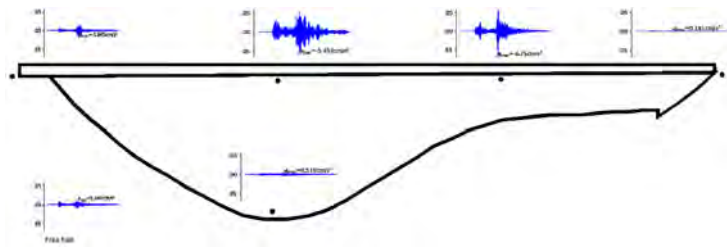

Fig. 11
Recorded motions in the radial direction for the accelerometers installed on the dam and in the North-South direction for the accelerometers located on the abutments / free field for the September 16th, 2024 earthquake. Peak values expressed in cm/s^2 are noted
Mouvements enregistrés dans la direction radiale pour les accéléromètres installés sur le barrage et dans la direction Nord-Sud pour les accéléromètres situés sur les culées / en champ libre pour le séisme du 16 septembre 2024. Les valeurs maximales exprimées en cm/s^2 sont notées

3.3. Measured data – eigen frequencies

For the above-mentioned earthquakes, for each point located on the top of the dam the Fast Fourier Transformation was computed in order to find out the eigen vibration frequency of the corresponding point. In order to get a smooth graph, Konno Ohmachi smoothing techniques was used.

The below combined photo (figure 12) presents the Fast Fourier Spectra for the 9 recorded earthquakes, for the main cross section of the dam – plot no. 13, accelerometer 03.

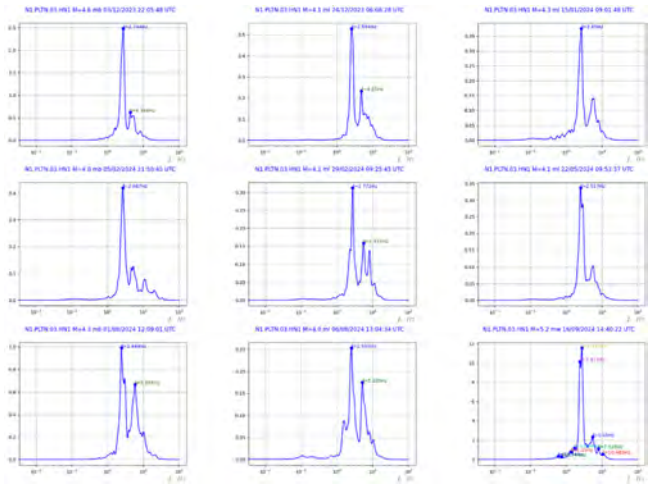

Fig. 12
Fast Fourier Spectra for the 9 recorded earthquakes
Spectres de Fourier rapides pour les 9 séismes enregistrés

Table 4
Fundamental frequencies and periods for block 13 recorded during earthquakes
Fréquences fondamentales et périodes pour le bloc 13 enregistrées pendant les séismes

DATE OF THE EVENT	WATER LEVEL	F1/T1
[YYYY-MM-DD]	MASL	HZ / S
2023-12-03	638.00	2.744 / 0.364
2023-12-24	638.00	2.597 / 0.385
2024-01-15	637.00	2.650 / 0.377
2024-02-05	636.00	2.667 / 0.375
2024-02-29	635.00	2.772 / 0.361
2024-05-22	642.00	2.517 / 0.397
2024-08-01	641.00	2.444 / 0.409
2024-08-06	641.00	2.555 / 0.391
2024-09-16	638.00	2.417 (2.772) / 0.414 (0.361)

As shown in Tables 2 and 4, there is a good correlation between the values measured in the biannual ambient vibration campaigns and the values recorded by the new seismic monitoring system.

4. CONCLUSIONS

Seismic monitoring and annual ambient measurement campaigns have shown that the natural frequencies of the Paltinu Dam remain within normal and constant limits. This indicates that the dam retains its structural integrity without significant long-term degradation.

Data collected over multiple campaigns shows a strong correlation between measured vibration frequencies and those predicted by mathematical models, validating monitoring accuracy. In the context of high seismic activity in the Vrancea region, continuous monitoring is essential for the rapid identification of any deviations that may indicate impending structural degradation.

The implementation of a new seismic monitoring system in 2022 has allowed for precise capture of movements caused by seismic activity in the Vrancea area. This system significantly enhances the capacity to detect seismic events, contributing to a more adaptive preventive maintenance strategy.

Data obtained through the new system enables new assessment of the dam's behavior in response to seismic activity. Integrating this data with existing models greatly improves risk assessments and contributes to proactive structural safety strategies. An essential next step will be developing a new model that incorporates the reservoir to analyze fluid–structure interaction. This approach will enhance the precision of predictions regarding the dam's behavior under extreme conditions, such as seismic events.

ACKNOWLEDGEMENTS

The authors wish to acknowledge Professors Dan STEMATIU, Tudor BUGNARIU and Altan ABDULAMIT, who actively contributed to the development and implementation of the vibration-based structural health monitoring. Our partners, representing the Romanian Waters Authority "Apele Romane", owners of the dam, kindly fed us with information, documentation and directly contributed to in situ dynamic measurements.

REFERENCES

[1] A. ALDEA, S. DEMETRIU, E. ALBOTA, T. KASHIMA "Instrumental response of buildings. Studies within JICA Project in Romania". *Proceedings of ISSRR2007 International Symposium on Seismic Risk Reduction, The JICA Technical Cooperation Project in Romania*, pp.157–170, 2007.

[2] S. DEMETRIU, A. ALDEA, A. UDREA, "Modal parameters of a RC frame structure identified from ambient vibration measurements", *15th World Conference on Earthquake Engineering, Lisbon*, 2012.

[3] G. BUFFI, P. MANCIOLA, L. DE LORENZIS, N. CAVALAGLI, F. COMODINI, A. GAMBI, V. GUSELLA, M. MEZZI, W. NIEMEIER, C. TAMAGNINI, *"Calibration of finite element models of concrete archgravity dams using dynamical measures: the case of Ridracoli"*, Procedia Engineering 199, pg. 110–115, 2017.

[4] S. PEREIRA, F. MAGALHAES, J. P. GOMES, A. CUNHA, J. V. LEMOS, "Vibration-based damage detection of a concrete arch dam", *Engineering Structures* 235, 2021.

[5] J. P. GOMES, J. PALMA, F.MAGALHAES, S. PEREIRA, G. MONTEIRO, D.S. MATOS, *"Seismic monitoring system of Baixo Sabor Scheme for structural dynamic behaviour monitoring and risk management, Commission Internationale des Grandes Barrages, Vingth Sixieme Congres des Grands Barrages, Vienne*, Q. 101 – R. 45, pp 768–788, 2018.

[6] P. MENDES, S. OLIVEIRA, L. GUERREIRO, M.A. BAPTISTA, A. CAMPOS COSTA, *"Dynamic behavior of concrete dams monitoring and modeling"*, Proc. 13th World Conference on Earthquake Engineering, Vancouver, Canada, Paper no. 2126, 2004.

[7] A. ABDULAMIT, S. DEMETRIU, A. ALDEA, C. NEAGU, D. GAFTOI, *"Ambient vibration tests at some buttress dams in Romania"*, X International Conference on Structural Dynamics, EURODYN 2017, Procedia Engineering 199, pp. 2196–2201, 2017.

[8] A. ABDULAMIT, D. STEMATIU, D. GAFTOI, "An alternative method to evaluate the health status for concrete dams". *Environmental Engineering and Management Journal*, Vol. 15, No. 6, pg.1397–1407, June 2016, ISSN: 1582-9596, eISSN: 1843–3707.

[9] D. GAFTOI, A. ABDULAMIT, A. ALDEA, R. SARGHIUTA, C. POPESCU, "Assessing structural safety of an arch dam using in situ vibration tests", *IOP Conf. Series: Materials Science and Engineering 1203*, 2021.

[10] A. ABDULAMIT, R. SÂRGHIUĂ, T. BUGNARIU, “Safety of dam’s assessment using the global elastic modulus”, *Proc. International Symposium “Thirty Years from the Romanian Earthquake of March 4, 1977”*, 2007.

[11] A. ABDULAMIT, D.STEMATIU, I. TOMA, “Identification of Dynamic Elastic Material Properties Using Hybrid Models”, *Proc. New Advances in Modal Synthesis of Large Structures. Non-linear, Damped and Non-deterministic Cases, Lyon, France*, Octobre 5–6 1995.

[12] D. STEMATIU, T. BUGNARIU, I. TOMA, “Global Elastic Moduli for Arch Dams”, *Proc. Conference on Research and Development in the Field of Dams, Crans Montana*, Switzerland, Sept. 7–9 1995.

[13] V. MARKOVIC, S. ZIVKOVIC, J. MARKOVIC, “Global Elastic Modulus Usage for Diagnosing the Mratinje Dam Behavior”, Facta Universitatis, Architecture and Civil Engineering, vol. 2, no. 1, pp. 67–75, 1999.

[14] R. SÂRGHIUĂ, A. ABDULAMIT, T. BUGNARIU, “Safety assessment of arch dams using Global Elastic Modulus concept”, *Proc. International Symposium “Thirty Years from the Romanian Earthquake of March 4, 1977”*, 2007.

[15] T. BUGNARIU, R. SÂRGHIUĂ, A. ABDULAMIT, “The global elastic modulus of buttress dams”, *Proc. International Symposium “Thirty Years from the Romanian Earthquake of March 4, 1977”*, 2007.

COMMISSION INTERNATIONALE DES
GRANDS BARRAGES

VINGT-HUITIEME CONGRES DES
GRANDS BARRAGES
CHENGDU, MAI 2025

ACTIVE FAULT IDENTIFICATION FOR DAM SEISMIC HAZARD ASSESSMENT (*)

Didiek DJARWADI
Director, PT BANYU BIRU SOLUSI GEOTEKNIK

INDONESIA

SUMMARY

Dams built in the highly seismic zone need a proper seismic hazard assessment, since the earthquake shocks may create a substantial permanent deformation on the crest of the dam and sliding on its slopes, and cracks on the concrete dams or permanent deformation that may create a failure to the concrete dam. In order to know the seismotectonic map of the dam which containing the seismic hazard information of the dam as a characteristics condition of the dam location against the seismic hazard, its need to carry out the seismic hazard assessment for far field and near field to the dam location. Far field seismic hazard assessment was carried out according to ICOLD (2016) was in the radius of 100 km but sometimes enlarged to 300 km in case a subduction zone or major fault line which may create big earthquake was found, while the near field seismic hazard assessment was carried out in order to assess in more detail the existence of the fault and its activity, which close to the dam from the far field seismic hazard assessment. The paper discussed the identification of the active fault in the near and far field seismic hazard assessment to the dam. The classification of the active faults, method which can be used to identify the fault such as electric resistivity tomography, geo-radar, seismic refraction and seismic reflection can be used. The paleoseismic trenching and carbon dating on the specific layers on the suspected active faults can enhanced the understanding of the fault and other information that may be obtained such as the recurrence of the earthquake, the last earthquake, interpretation of the geological slip rate. Some examples and results of active fault identification are also presented.

**Identification des failles actives pour l'évaluation de l'aléa sismique des barrages*

DOI: 10.1201/9781003642428-128

RÉSUMÉ

Les barrages construits dans une zone hautement sismique nécessitent une évaluation appropriée de l'aléa sismique, car les chocs sismiques peuvent créer une déformation permanente substantielle sur la crête du barrage et un glissement sur ses pentes ; des fissures sur les barrages en béton ou une déformation permanente qui peut créer une défaillance du barrage en béton. Afin de connaître la carte sismotectonique du barrage qui contient les informations sur l'aléa sismique du barrage en tant que condition caractéristique de l'emplacement du barrage par rapport à l'aléa sismique, il est nécessaire d'effectuer l'évaluation de l'aléa sismique pour le champ éloigné et le champ proche de l'emplacement du barrage. L'évaluation de l'aléa sismique en champ lointain a été réalisée selon la CIGB (2016) dans un rayon de 100 km mais parfois élargie à 300 km en cas de découverte d'une zone de subduction ou d'une ligne de faille majeure pouvant créer un grand tremblement de terre, tandis que l'évaluation de l'aléa sismique en champ proche a été réalisée afin d'évaluer plus en détail l'existence de la faille et son activité, qui se trouve à proximité du barrage à partir de l'évaluation de l'aléa sismique en champ lointain. L'article traite de l'identification de la faille active dans l'évaluation de l'aléa sismique en champ proche et lointain du barrage. La classification des failles actives, la méthode qui peut être utilisée pour identifier la faille telle que la tomographie de résistivité électrique, le géoradar, la réfraction sismique et la réflexion sismique peut être utilisée. Le creusement de tranchées paléosismiques et la datation au carbone sur les couches spécifiques des failles actives suspectées peuvent améliorer la compréhension de la faille et d'autres informations qui peuvent être obtenues telles que la récurrence du tremblement de terre, le dernier tremblement de terre, l'interprétation du taux de glissement géologique. Quelques exemples et résultats de l'identification active des défauts sont également présentés.

1. INTRODUCTION

The source of the earthquakes is a discrete earthquake source, namely an active fault on the earth's plate (intra-crustal fault) and a plate boundary fault such as a megathrust. Active faults will be the main discussion in tracing the source of this earthquake, it will be clearly deciphered and defined in this paper. A fault is a plane or fracturing zone in the earth's crust where the parts on both sides move relative to one another. The two parts of the earth on the fault are generally attached by pressure and frictional force so that when to the two sides it moves slowly but the plane of the fault remains strongly glued together so that the pressure will continue to increase until finally the accumulated pressure on the fault plane exceeds the adhesion force of its friction so that it breaks and moves suddenly releasing the accumulated pressure. This event of rupture and sudden movement on the plane of the fault gives rise to shock waves which then spread in all directions and vibrate the surrounding earth known as

an earthquake event. A fault is called active if it still has the potential to move to produce earthquakes in the future. The characteristic of active faults in general is when indicated to cut or deform morphological formations or soil layers/rocks of Pleistocene–Holocene age (Quaternary Age). Referring to ICOLD [1], faults are defined as active faults if: "there is evidence of movement (earthquake events) during the Holocene Period (from 11,000 years ago), or for large faults showing evidence of movement during the Late Pleistocene Age (from 35,000 years ago), or for major faults main lines showing evidence of movement in the Quaternary Age (from 1.8 million years ago)". However, the definition according to ICOLD [1] can cause confusion due to differences in perception, data acquisition, level of knowledge and interpretation. Therefor an active fault shall be defined in more detail. Active fault needs to be further classified specifically and in detail due to the geological conditions and seismicity in Indonesia which are very specific and different from the rest of the world. The classification of active faults in Japan, the United States, especially the states of California, and New Zealand, which have more likely similar conditions with Indonesia are also different. For example, in New Zealand, active faults are classified by their level of activity based on the recurrent interval as seen in Table 1 below (Kerr & Nathan. [2]).

Table 1
Classification of Active Faults in New Zealand based on the re-period of large earthquakes (Kerr & Nathan. [2])
Classification des failles actives en Nouvelle-Zélande basée sur la re-période des grands tremblements de terre (Kerr & Nathan. [2])

RECURRENCE INTERVAL CLASS	**AVERAGE RECURRENCE INTERVAL OF SURFACE RUPTURE**	**NZ EXAMPLES (FAULTS); CHB EXAMPLES IN BOLD**
I	<2000 years	Alpine, Hope, Awatere, Wellington, **Mohaka**
II	>2000 years to <3500 years	Ostler FZ, Ohariu, Makuri, Rangipo, **Ruahine**
III	>3500 years to <5000 years	Dunstan, Lake Heron, Poutu, Ngakuru, **Poukawa FZ**
IV	>5000 years to <10,000 years	Dalgety, Esk, Karioi, Wheao, **Ruataniwha**
V	>10,000 years to <20,000 years	Pisa, Greendale, Martinborough, **Blackburn FZ**
VI	>20,000 years to <125,000 years	ND

It is very important to understand that the determination of the classification of active faults is not always easy and clear due to field conditions and the limitations of the available data. For example, if in the field it is found that one active fault line is seen not to cut the Holocene sedimentary layer (up to 11,600 years old) does not mean that it is not an active fault, but it can be an active fault but Class III – V, or for example seen in the field the fault path does not cut the Pleistocene Volcanic layer, for example Tufa Toba which is 74,000 years old, then it does not mean that the fault is inactive but it can only be interpreted that the fault is not an active fault Of Classes I - V nor is there any indication of movement until 74,000 years ago, it is still possible

there is movement in the period from 74,000 years to 128,000 years ago or including a Class VI active fault. Conversely, if it is found that the fault cuts through the Tufa Toba Layer then the fault may be included as a Class III active fault, but it could turn out to be Class I or Class II just that there is no fault data that cuts through the Holocene Layer in the region. So, the lower the level of activity of the fault, the more difficult it will be to identify because the tectonic traces of the landscape become more subtle. This is because the rate of motion is lower, it is defeated by the speed of erosion and sedimentation so that the formation of the tectonic landscape is lost to eroding or deposited by sedimentation.

In active fault tracing, in addition to studying the level of activity, it is also necessary to analyze its kinematics or (main) type of movement, namely: strike-slip fault, normal fault, reverse fault.

2. ACTIVE FAULT TRACING PROCEDURE

The results of the analysis of potential earthquake hazards and risks are largely determined by the quality of active fault data input as the source of the earthquake and various earthquake parameters as outlined above. Therefore, there needs to be uniformity in the procedures and methods for obtaining various data and parameters of the source of such earthquakes. In principle, the criteria and procedures for active fault surveys must be in accordance with standards in the international world. Briefly it can be described in the following.

(a) Determine the location of active fault lines, if not yet available, by the method of tectonic landscape analysis, which is to identify various types of landscapes related to fault movement.
(b) Fault identification can be assisted by subsurface geophysical surveys, especially for fault lines that are indicative of non-visible on the surface.
(c) Studi in more detail to analyze the tectonic characteristics and the potential for earthquakes can be done by making trenches for paleo-seismological studies.

An active fault map is the location of a fault path on the earth's surface which is the confluence line between the fault plane and the ground level. Indications of active faults on the surface are characterized by various landscape appearances as a result of interactions between the processes of fault movement and erosion and sedimentation processes, in the form of topographic straightness, fault cliffs, and deflections or shifts from river flows.

Faults can also be boundary planes between two rock formations each characterized by different reliefs and morphological textures (McCalpin, [3]; Yeats et al., [4]). Briefly the active fault is characterized from:

(a) The active fault line intersects young geological deposits, namely the Quaternary Periods layer.
(b) Active faults and their accompanying structures are commonly seen from the morphological formation of fault cliffs that look fresh, the straightness of valleys, rivers and ridges and others.
(c) Indications of movements that occur in the Quaternary Period to the censorship, such as shifts in river flows, river terraces, or human-formed structures.

Figure 1 shows an example of an active fault path (Sumatra Fault) intersecting the landscape of Pleistocene volcanic deposits on the western slopes of Mount Merapi, West Sumatra, which is easily recognized by the straightness of the fault cliffs and narrow elongated valleys.

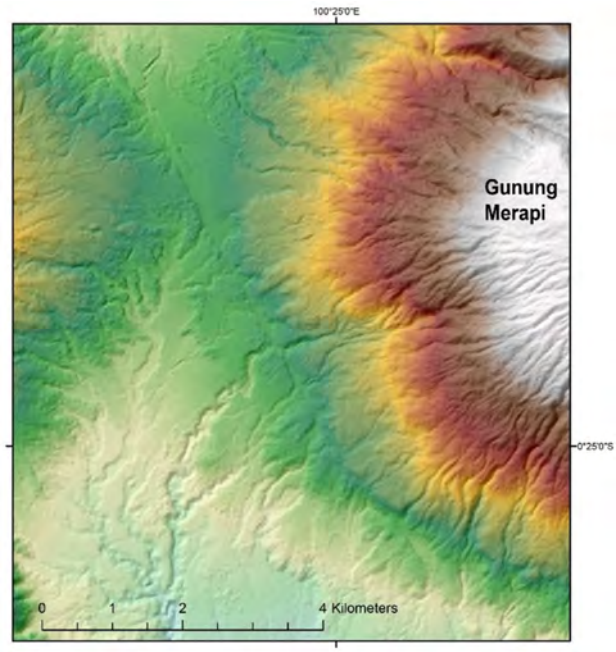

Fig. 1
DEMNAS data summarizes the morphology of Pleistocene volcanic deposits from Mount Merapi. Mount Merapi, West Sumatra. Tectonic landscapes of the Sumatra Fault Line are seen as the straightness of the valleys and cliffs
Les données de DEMNAS résument la morphologie des dépôts volcaniques du Pléistocène du mont Merapi. Mont Merapi, Sumatra occidental. Les paysages tectoniques de la ligne de faille de Sumatra sont considérés comme la rectitude des vallées et des falaises.

But mapping active fault paths is not always easy. For example, in a landscape that consists of all old geological layers, there are no young layers, then identifying the activeness of a fault path is not easy because there is no time reference. Then, landscape formations related to fault movement are also not always visible because it depends on which one is more dominant between the tectonic rate and the speed of erosion and sedimentation. For faults with a low slip rate, the landscape-tectonic formation is not visible on the surface because it has been eroded or sedimented (Burbank and Anderson, [5]). Active fault mapping needs to be done with GIS software to facilitate analysis and also to check its accuracy. The withdrawal of the fault line must be thorough and accurate; Therefore, if the path is clearly visible, a full line can be drawn, if it is not clear so it must be estimated then the line is made dotted, and if it is not visible on the surface because it is buried by young sediment then the line is made dots as shown in the example in Figure 2.

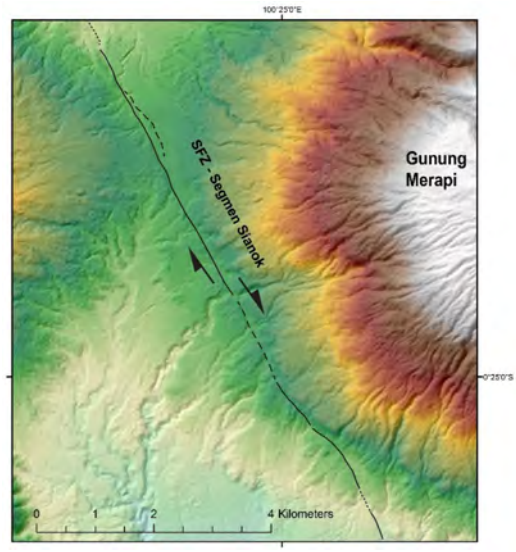

Fig. 2
Sumatra Fault mapping results based on DEMNAS analysis. The full line means that the fault path is clearly visible, the dotted line of the fault path is estimated, the line of the points of the fault path is deposited with young deposits. It can be seen that there is a river flow that has been displaced by a fault.
Résultats de la cartographie des défauts de Sumatra basés sur l'analyse DEMNAS. La ligne pleine signifie que le chemin de faille est clairement visible, que la ligne pointillée du chemin de faille est estimée, que la ligne des points du chemin de faille est déposée avec de jeunes dépôts. On peut voir qu'il y a un écoulement de rivière qui a été déplacé par une faille

2.1. Fault segmentation method

After the active fault map is created, further segmentation-seismic analysis is carried out. The principle of segmentation is that discontinuities of fault lines can limit the process of propagation of earthquake fracturing (fault ruptures). By dividing the fault path into segments constrained by fault discontinuities that are considered impassable by earthquake/fault fracturing propagation, the maximum potential magnitude (M-max) of each segment can be estimated from the empirical relationship of fault length and magnitude (Wells and Coopersmith, [6]). For shear fault systems, for example, fault stepovers that are considered impassable for earthquake fracturing are those that are 4km wide or more (Wesnousky, [7]). So, in shear fault mapping, all stepovers with a width of 4km or more are used as segment barriers. Figure 3. shows an example of segmentation - an extensional stepover between the Sianok and Sumani segments on the Sumatra Fault (Natawidjaja [8]), while Figure 4 shows a Seismotectonic Map (active fault model) created from the map of the active fault in Figure 3.

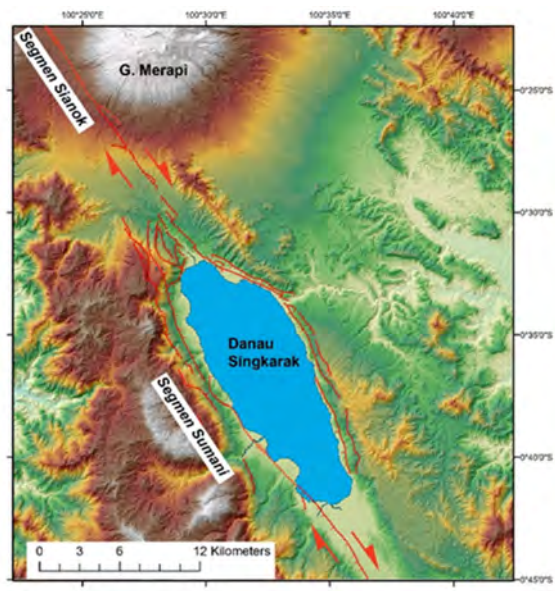

Fig. 3
Example of segmentation - an extensional stepover between the Sianok and Sumani segments on the Sumatra Fault that forms Lake Singkarak. Active fault map data source from Sieh and Natawidjaja [8]
Exemple de segmentation - un enjambement d'extension entre les segments Sianok et Sumani sur la faille de Sumatra qui forme le lac Singkarak. Source de données de carte de faille active de Sieh et Natawidjaja [*8*]

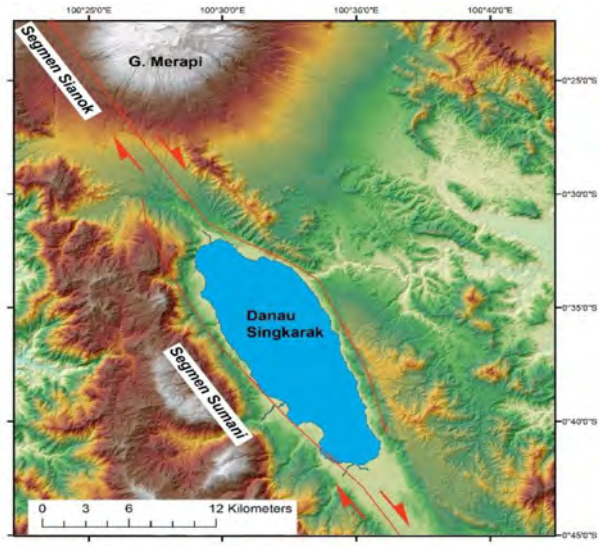

Fig. 4
A Seismotectonic map (active fault model) created from the above active fault map. The Sumatra Fault line in this region is divided into two segments, namely the Sianok Segment and the Sumani Segment. The boundary of the segment is a graben stepover structure that forms Lake Singkarak
Une carte sismotectonique (modèle de faille active) créée à partir de la carte de faille active ci-dessus. La ligne de faille de Sumatra dans cette région est divisée en deux segments, à savoir le segment Sianok et le segment Sumani. La limite du segment est une structure d'enjambement à graben qui forme le lac Singkarak

3. BASIC DATA FOR MAPPING

The thoroughness of active fault mapping is limited by the resolution of the topographic map used. The higher the resolution of the map, the better the active fault mapping because it can see natural formations due to the movement of smaller-dimensional faults. The widely available topographic map data in Indonesia are: 1:50,000 scale topographic map (for outside Java) and 1:25,000 scale Topographic map for Java. The DEM data that is already freely available is:

(a) SRTM-30m Digital Topographic Data (DEM)
(b) DEMNAS Digital Topographic Data from BIG with a grid resolution of 8.5 meters
(c) High-resolution satellite photos available in Google Earth.

Digital topographic data with higher resolution includes 5m IFSAR (DTM and DSM) and the best is LIDAR data that has a resolution below 1m. However commercial LIDAR data is quite expensive but fortunately it can be replaced by drone mapping.

3.1. Map scale

The scale of the Active Fault Map can be divided into two, namely for regional studies and detailed studies in the dam area. For regional scales, active fault maps that can be used to create seismotectonic maps are those whose scale is sufficient to separate the segments of the fault. From experience and many case studies the minimal resolution for basic data is a topographic map is with a scale of 1:50,000 or the equivalent of SRTM-30m digital topographic data. If it is indicated that the location of the dam is at a distance of less than 15-25 km from the active fault line, the mapping accuracy scale used uses a scale of 1:25,000 at least for areas within a radius of 50 km from the location. This should not be a problem because in Indonesia there is now a DEMNAS map with elevation data in the 8.5 m grid which is equivalent even better than the 1:25,000 scale topographic map. So, all it takes is skill to identify the tectonic landscape from the DEMNAS data.

If it is indicated that the location of the dam is in a radius equal to or less than 5 km, the recommended scale of map accuracy is at least 1: 10,000 for areas with a radius of up to 5 km from the location of the dam, depending on field conditions and needs. If it turns out that it is indicated that there is an active fault line that cuts through the body of the dam or other important structures, the mapping needs to be done in more detail up to a scale of 1:1000 for the dam area. In this case, the base map used is not enough to use only DEMNAS map but must be supplemented with topographic maps with higher resolution, such as IFSAR 5m, LIDAR, or assisted by drone mapping. In principle, if the dam is passed by active fault lines, the resulting active fault map needs to be accurate enough to show the location of the active fault line against the dam plan, especially the body of the dam. Active fault studies also need to estimate how high the activeness of each fault segment is, the type of fault, and how much movement can occur during an earthquake so that its damaging effects can be anticipated, especially if passing is important and there are no options to be avoided.

4. ACTIVE FAULT GEOPHYSICAL SURVEY AND INVESTIGATION

Geophysical surveys are needed to help identify or map the fault structures beneath the ground surface, especially when the fault path is not exposed or visible on the surface, so the exact location of the fault is unclear. Survey methods that are often used are *Ground* Penetration *Radar (GPR)* and *Multi-Channel Resistivity*

(MCR) because they are relatively easy to use in all conditions and data processing is simple and fast. Other methods that can also be used are seismic reflection and seismic refraction methods. Each method has its own advantages and disadvantages. The selection of methods depends on the target and geological conditions and field conditions. The logging of the ground cutting sometimes give an advantage in the identification of faults.

4.1. GEO-RADAR METHOD

The geo-radar method or Ground Penetration Radar (GPR) is a subsurface imaging method using electromagnetic wave sources that are often used in the field of geology and civil engineering. GPR uses *microwave* waves (UHF/VHF) with high radio wave frequencies at intervals of 10 Mhz to 2 GHz to detect fields that reflect and/or reflect the waves. Imaging of structures based on areas of reflection/refraction beneath the surface is based on differences in the nature of their *permittivity*, the same principle as geoelectric imaging. The depth of the detected structure is measured from *the time travel* of the wave as is the case in the seismic reflection method. Geo-radar data processing also has many similarities with reflection seismic data. In principle, one point shoot produces a 1D electromagnetic pulse shape that identifies each surface of the plane below the surface. Then from the point-shoot data along the survey lines are integrated (*stacking*) to produce radargram profiles. Geo-radar surveys can create 2D map plan views, 2D profiles, or 3D imaging by combining many 2D profiles. Figure 5 shows the method of implementing *the Ground Penetration Radar* in the field, while Figure 6 shows an examples of *Ground Penetration Radar* results on the fault investigation in Sibolga, North Sumatra.

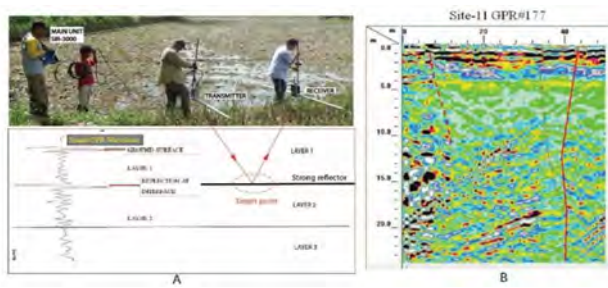

Fig. 5
Ground Penetration Radar (GPR) Method: A. Survey, B. Sample radargram of survey results (Natawidjaja [9]).
Méthode radar à pénétration de sol (GPR) : A. Levé, B. Échantillon de radargramme des résultats de l'arpentage (Natawidjaja [*9*])

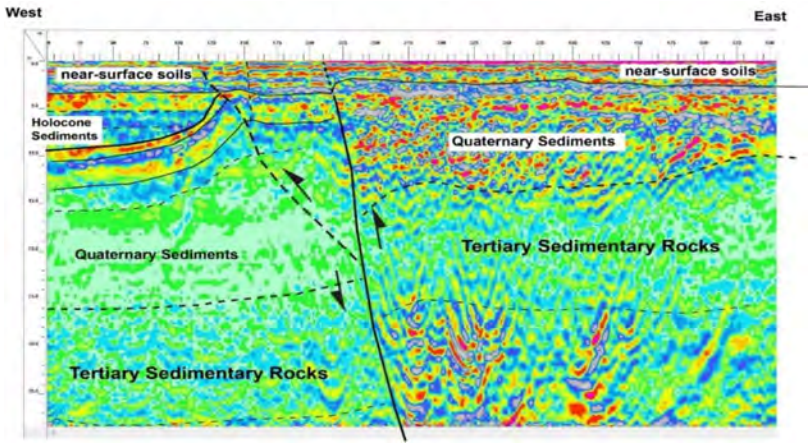

Fig. 6
An example of the results of a GPR survey crossing an active ascending fault line in the northern region of Sibolga. Exhibits the activeness of faults that cut and deform Pleistocene and Holocene sediments (Quaternary)
Un exemple des résultats d'un levé GPR traversant une ligne de faille ascendante active dans la région nord de Sibolga. Présente l'activité des failles qui coupent et déforment les sédiments du Pléistocène et de l'Holocène (Quaternaire)

4.2. Geo-electric method

Geo-electric surveys that typically use Multi-Channel Resistivity (MCR) are part of geophysical tests to scan fault paths and lateral and vertical distributions of rocks based on the physical properties of their electrical conductivity. The principle of scanning is to use an electric current induction source and then record receiving an electric back current that carries a signal containing subsurface structure information. This survey is effective for sites with rock types that have contrasting electrical conductivity values, such as sandstone and clay layering. The use of this tool to find misalignment of layers that indicate the location of the fault is excellent. The resolution and depth of data penetration depend on the spacing of the electrodes used (depending also on geological conditions). There are many geoelectric configuration options, including the Wenner, Schlumberger, and Dipole-dipole methods. The resolution and depth of penetration can be set to match the target and related geological conditions. The arrangement is carried out using different electrode spacing. Generally, the data resolution is half of the electrode space, and the penetration depth is 10 – 15 times the electrode space. Figure 7 shows the results of a geoelectric survey on the Lembang fault.

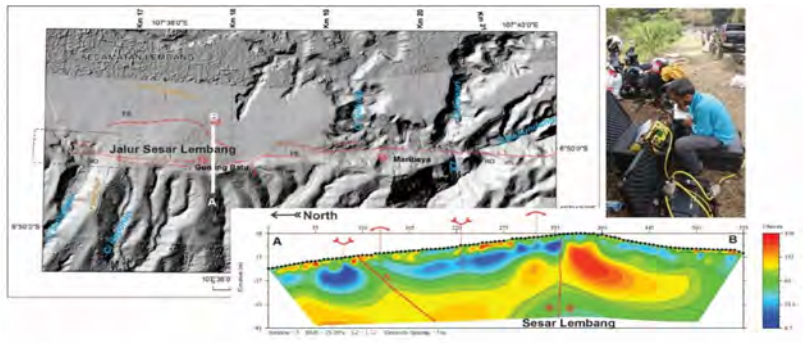

Fig. 7
Multi-Channel Resistivity Survey to see the subsurface structure of the Lembang Fault that has been mapped based on LIDAR and field survey data (Daryono., et al [10]).
Levé de résistivité multi-canaux pour voir la structure souterraine de la faille de Lembang qui a été cartographiée sur la base de données LIDAR et de levés sur le terrain (Daryono., et al [*10*]).

4.3. Seismic refrection and reflection methods

The seismic reflection method is a subsurface scanning method using the principle of wave reflection from a seismic wave source or acoustic wave. Images of subsurface structures are obtained from modeling the reflection of waves reflected by the boundaries of geological structures, either in the form of rock layers or fault planes. The greater the *seismic velocity* contrast of the plane of its structure, the clearer/stronger the field of reflection on the seismic cross section will be seen. The source of seismic waves used can be dynamite explosions, vibration devices, or large hammer *blows*. The reflection seismic survey equipment consists of a main unit (seismograph), a seismic source, a set of geophones *(seismic sensors)* and cables.

Seismic reflection is a geophysical method that is very widely used and developed for a long time for oil and gas exploration. Those used as a seismic source can use dynamite for land or large air guns for the sea so that the penetration is up to thousands of kilometers. On the ground, there is now a strong seismic source but it is safer and easier to permit and use than dynamite, that is, with a blow from a large iron ballast installed under a special truck. This method is now also used for geotechnical purposes but by using smaller seismic sources, such as hammer blows or vibrations. So that the penetration is only tens of meters away. Figure 8 shows the principles of the seismic reflection.

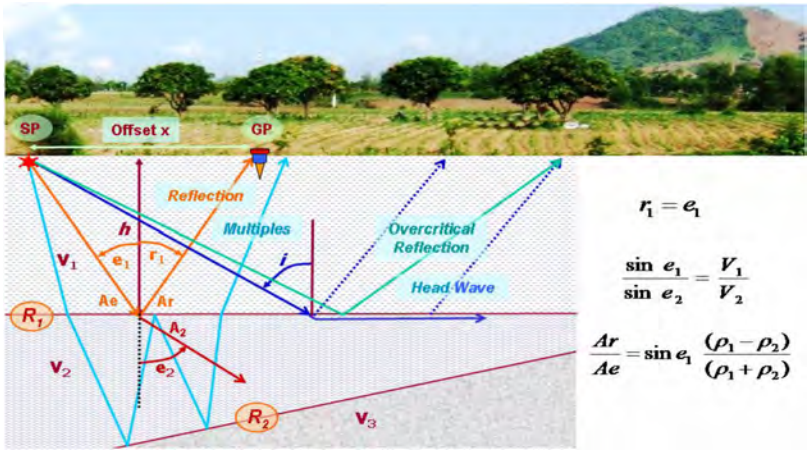

Fig. 8
Principles of Seismic Reflection Method. The equipment consists of a Laptop, Seismograph, a set of Geophone, cables, and seismic sources (dynamite, hammer, vibrator, and others) (source: https://www.wikiwand.com/en/Reflection_seismology).
Principes de la méthode de réflexion sismique. L'équipement se compose d'un ordinateur portable, d'un sismographe, d'un ensemble de géophone, de câbles et de sources sismiques (dynamite, marteau, vibrateur et autres) (source : https://www.wikiwand.com/en/Reflection_seismology).

Another seismic method is seismic refraction. The difference is that this method scans subsurface structures using the principle of wave refraction. Seismic refraction has been developed since the late 1980s to scan the earth's very deep structure (up to the earth's core); But in the past decade it has begun to be widely developed for geotechnical purposes. The most popular method used is referred to as *Seismic Refraction Tomography* (SRT). The function and result are similar to the geoelectric method. Figure 9 shows the principle of the seismic refractive survey method (Terzic et al., [11]).

Another method of fault identification for dam seismic hazard assessment were logging of ground cutting, paleo-seismic trenching and carbon dating. Ground cutting such as road cutting, quarry and others sometimes cut the fault lines or zones. In this condition logging, identifying the stratigraphy of rock unit can also identifying the activity of the fault. Figure 10 and Figure 11 shown an example of fault identification in the road cutting wall toward Batang Toru Power House in North Sumatra (PT Banyu Biru Solusi Geoteknik [12]).

Figure 10 identified some fault in the road cutting walls and clearly indicated the different stratigraphy which indicated the rock types and ages, but some not cut the upper layer rock/soil which have more than 10.000 years in age, that means that the latest earthquake occurred more than the age of the above layers. For dam design, the if the fault has not indicated an activity at the last 10.000 years, it can be justified as an inactive fault.

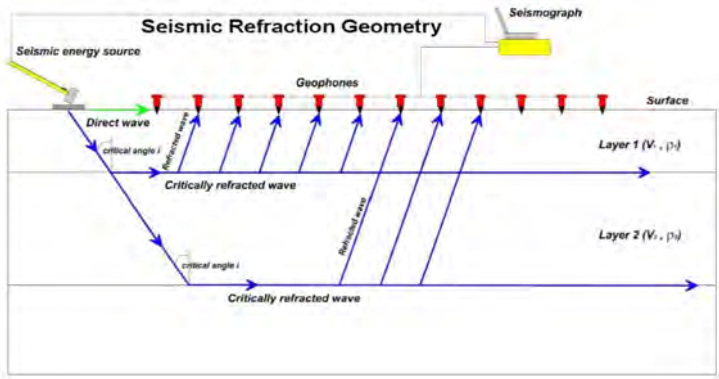

Fig. 9
Principles of seismic refractive survey methods
Principes des méthodes de levés sismiques réfractifs

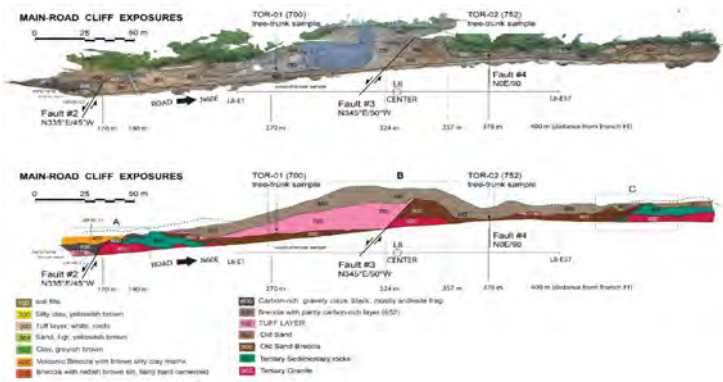

Fig. 10
The result of the 3-D photogrammetric of the road-cliff exposures at the end of the construction road and its geological analysis
Le résultat de la photogrammétrie 3D des expositions route-falaise à la fin de la route de construction et de son analyse géologique

In Indonesia, the paleoseismic trenching and carbon dating shall be carried out in case the geology and seismology site investigation indicated an active fault found within 15 km in distance from the dam location and have a potential earthquake with Mw >7.00 or an active fault found within 10 km in distance from the dam location and have a potential earthquake with Mw >6.00.

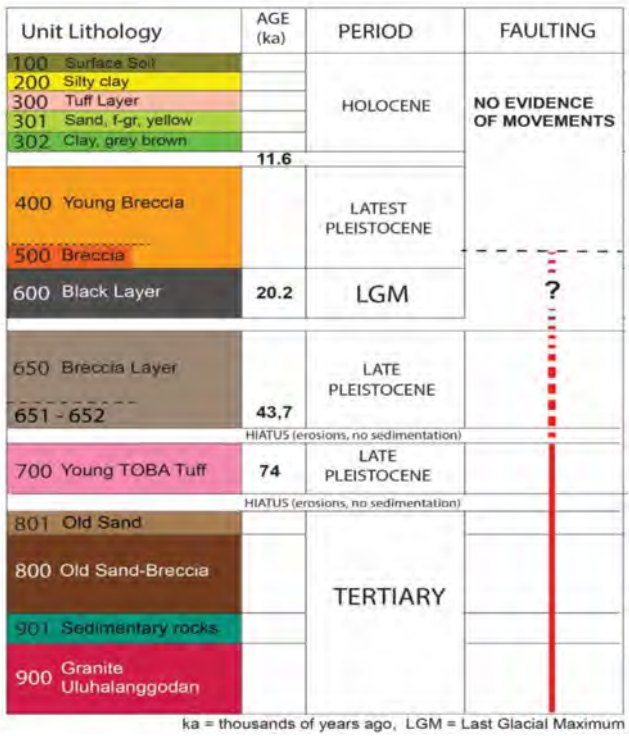

Fig. 11
Summary of Geological History and Fault Activities of road cliff exposure Fig. 10
Résumé de l'histoire géologique et des activités de faille de l'exposition des falaises routières Fig. 10

The carbon dating with AMS (Accelerator Mass Spectrometry) method usually adopted in the prediction of the last earthquake occurred in the fault based on the carbon age which extracting from the soil or sediment layers close to the fault line. Figure 12 shows the soil/rock layers in the paleoseismic trenching, while Figure 13 shows an example of carbon dating result.

The historical record of earthquakes is generally very limited and incomplete. In Indonesia, the history of earthquakes in the past is generally only in the past 100-200 years. Studies relating to historical analysis of earthquakes in the past are commonly referred to as paleo-seismology (McCalpin, [3]., Sieh [12]).

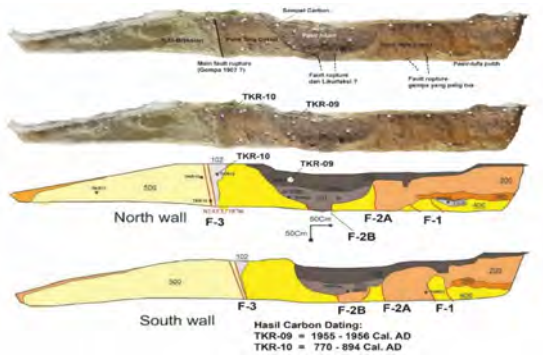

Fig. 12
Paleoseismic trenching result on Sianok Fault in Jambi
Résultat de tranchées paléosismiques sur la faille de Sianok à Jambi

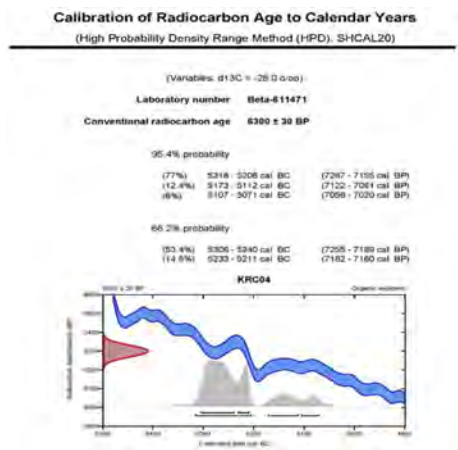

Fig. 13
An example of the carbon dating result using AMS method
Un exemple du résultat de la datation au carbone à l'aide de la méthode AMS

The most widely used method is to make paleoseismic trenches to study the phenomenon and chronology of the magnitude of earthquake events in the past recorded in soil structures and layers (McCalpin, [3]., Yeats et al., [4]). Another function of *trenching* is to ensure the presence of fault lines in important locations if they are not exposed on the surface but have been indicated by indications from landscapes or from subsurface geophysical surveys.

REFERENCES

[1] ICOLD (2016). *Selecting Seismic Parameters for Large Dams*. Guidelines. Bulletin no. 148. Paris, France.

[2] KERR, J., NATHAN, S., VAN DISSEN, R., WEBB, P., BRUNDSON, D., KING, A (2003). *Planning for Development of Land on or Close to Active Faults: A guideline to assist resource management planners in New Zealand*. New Zealand Ministry for The Environment, Wellington, New Zealand.

[3] MCCALPIN, J (1996), *Paleoseismology, International Geophysics Series*, Volume 62, Academic Press, p. 588.

[4] YEATS, R. S., SIEH, K. E., AND ALLEN,C. R (1997). *The geology of earthquakes*. Oxford University Press, New York, 568 p.

[5] BURBANK, D. W., AND ANDERSON, R. S (2001). *Tectonic Geomorphology*. Blackwell Science Inc, 273 p.

[6] WELLS, D. L., AND COOPERSMITH, K. J (1994). *"New empirical relationships among magnitude, rupture length, rupture area and surface displacement"*. Bulletin of the Seismological Society of America, vol. 84, No.4, p. 974–1002.

[7] WESNOUSKY, S. G (2006). "Predicting endpoints of earthquake ruptures." *Journal Nature*, vol. 444, p. 358–360.

[8] SIEH, K., AND NATAWIDJAJA,D. H (2000). "Neotectonics of the Sumatran fault, Indonesia". *Journal of Geophysical Research*. vol. 105, no. B12, p. 295–326.

[9] NATAWIDJAJA, D. H (2018). "Major Bifurcations, Slip Rates, and A Creeping Segment of Sumatran Fault Zone in Tarutung-Sarulla-Sipirok-Padangsidempuan, Central Sumatra, Indonesia". *Indonesian Journal on Geoscience*. Vol. 5, no. 2.

[10] DARYONO, M. R., NATAWIDJAJA, D. H., SAPIIE, B., AND CUMMINS, P (2018). “Earthquake Geology of the Lembang Fault, West Java, Indonesia”. *Tectonophysics*, Vol. 751, p. 180–191.

[11] TERZIG, Z., ERMAKOV, O., AND UROSEVIC, M (2019). “Geophysical Survey as a part of a Multi-tiered Investigation in Fault Characterization and Dam Seismic Hazard Assessment-a case study from South Australia” (online). Available in: http://rayfract.com/pub/TERZIG_ERMAKOV_UROSEVIC_AGS_Paper.pdfAccessed on 24 November 2020.

[12] SIEH, K (1977). *Late Holocene displacement history along the south-central reach of the San Andreas fault*. Ph.D Dissertation. 219 p. Stanford University, Stanford, California.

[13] PT Banyu Biru Solusi Geoteknik (2019). *Active Fault Identification of Batang Toru HEPP Power House, a Field Investigation Report*. 96p.

COMMISSION INTERNATIONALE DES
GRANDS BARRAGES

VINGT-HUITIEME CONGRES DES
GRANDS BARRAGES
CHENGDU, MAI 2025

CURRENT PRACTICE OF SEISMIC HAZARD ASSESSMENT OF DAMS IN INDONESIA (*)

Didiek DJARWADI
Director, PT BANYU BIRU SOLUSI GEOTEKNIK

INDONESIA

SUMMARY

Indonesia is one of the countries in the world with highly seismic activity. Indonesia was surrounded by 4 major subduction zones, namely the subduction of Australian, Asian, Pacific, Philippine to the Indonesia islands potentially create a big earthquake. A major active fault in Sumatra, Java, Sulawesi, Molucca as well in Papua will also contribute to an earthquake. Dam was one of the major structures that must be designed to withstand earthquakes. The knowledge about the magnitude and distance to the earthquake sources shall be well acknowledge to quantify the earthquake shocks and generate the earthquake parameters which can be used in dynamic analysis of the dams with an earthquake loading. The paper discussed the current practice of seismic hazard assessment of the dams in Indonesia. The Guidance of Seismic Hazard Analysis was just finished and wait fot further review before published and available to the public. The Guidance give a guideline to carried out the seismic hazard assessment for dam during the Feasibility Study, Detail Engineering Design and Evaluation during construction, where the foundation and other appurtenant structures excavation may reveal the existence of fault which not encountered during the previous study. The risk of dam failure due to an earthquake as well as the consequence to the downstream area will give influences to the way of seismic hazard assessment which shall be conducted. The dams which have low and moderate risk against failure due to earthquake will have different scope of works compared with dams which have high and extreme risk. The paper also

Pratique actuelle de l'évaluation des risques sismiques des barrages en Indonésie

DOI: 10.1201/9781003642428-129

discussed the result of seismic hazard assessment which called seismotectonic maps which indicated the maximum magnitude of the earthquake generate from a certain active fault, distances of the active faults to the dam, peak ground acceleration and other information which used in the seismic hazard analysis of the dam.

RÉSUMÉ

L'Indonésie est l'un des pays où l'activité sismique est élevée. L'Indonésie était entourée de 4 zones de subduction majeures, à savoir la subduction de l'Australie, de l'Asie, du Pacifique et des Philippines vers les îles indonésiennes qui pourraient créer un grand tremblement de terre. Une faille active majeure à Sumatra, Java, Sulawesi, Moluques ainsi qu'en Papouasie contribuera également à un tremblement de terre. Un barrage est l'une des principales structures qui doivent être conçues pour résister aux tremblements de terre. La connaissance de la magnitude et de la distance par rapport aux sources sismiques doit être bien reconnue afin de quantifier les chocs sismiques et de générer les paramètres sismiques qui peuvent être utilisés dans l'analyse dynamique des barrages avec une charge sismique. Le document traite de la pratique actuelle d'évaluation des risques sismiques des barrages en Indonésie. Le Guide d'analyse des risques sismiques vient d'être terminé et attend un examen plus approfondi avant d'être publié et mis à la disposition du public. Les directives donnent une ligne directrice pour effectuer l'évaluation de l'aléa sismique du barrage au cours de l'étude de faisabilité, de la conception technique détaillée et de l'évaluation pendant la construction, lorsque l'excavation des fondations et d'autres structures annexes peut révéler l'existence d'une faille qui n'a pas été rencontrée lors de l'étude précédente. Le risque de rupture du barrage en raison d'un tremblement de terre ainsi que les conséquences pour la zone en aval auront une influence sur la manière d'évaluer l'aléa sismique. Les barrages qui présentent un risque faible et modéré de défaillance due à un tremblement de terre auront une portée de travaux différente de celle des barrages qui présentent un risque élevé et extrême. L'article discute également du résultat de l'évaluation de l'aléa sismique qui appele des cartes sismotectoniques qui indiquent la magnitude maximale du tremblement de terre généré à partir d'une certaine faille active, les distances des failles actives au barrage, l'accélération maximale du sol et d'autres informations utilisées dans l'analyse de l'aléa sismique du barrage.

1. INTRODUCTION

Seismic hazard assessment for dams in Indonesia was very important, since Indonesia was located in the area with high seismicity. Figure 1 (PuSGeN [1]) shows the earthquake records during period of 1900 up to 2016 for all shocks greater than

Mw 4.5. The maps show the densities of the earthquakes in Indonesia, where only Kalimantan Island has a small seismic activity comparing with another area in Indonesia. The earthquake sources from subduction zone, active faults and Benioff zones almost shock Indonesia every day. This situation leads to the hazard against the structures built in this area shall be accounted. The dam has greater impact to the downstream if the dam was failure due to the earthquake events. The catastrophic damages due to flooding in the downstream of the dam may occur and will impact to the great effort for recovery. ICOLD, 2016 [2] stated that the dams shall be safe with no failure against the maximum credible earthquake based on their seismotectonic, but allow a damage that can be repaired. This statement leads to the condition that the dam was a "site specific" in the seismic hazard, since every dam location has it's own specific against the governing earthquake that may shake the dam.

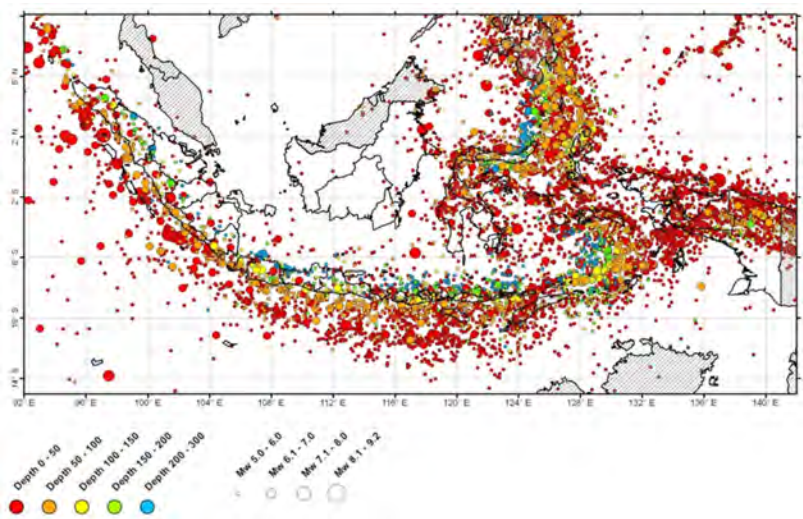

Fig. 1
The Earthquake Records in Indonesia in the Periods of 1990 – 2016 (PuSGeN [1])
Les enregistrements de tremblements de terre en Indonésie dans les périodes de 1990 à 2016 (PuSGeN [1])

In the dam engineering there are two (2) earthquake criteria, namely; OBE (operating basis earthquake) and SEE (safety evaluation earthquake). OBE earthquake is an earthquake shock level that is most likely to occur within the service life of a dam. In the OBE earthquake, the dam body must not be damaged (cracks, deformations, leaks, etc.) that affect the operation of dams and reservoirs. Only small-scale damage is allowed to occur that can be easily repaired. The OBE was determined based on the 145-year earthquake return period based on the

probabilistic analysis (PSHA) approach. SEE is the maximum level of earthquake shock that can occur to the dam. SEE is usually used as a reference to make dam analysis and design. In the SEE earthquake, the dam is allowed to suffer damage (cracks, deformations, leaks etc.) as long as it does not affect the stability of the dam, and should not be uncontrolled leakage of water from the reservoir in large quantities that can cause dam collapse and flooding to the downstream of the dam.

In order to assess the hazard of the dams from an earthquake, it was very important to assess the seismicity of the dam and surroundings. In Indonesia at present there was no official guidelines to carried out assessment of the seismic hazard of the dam, but the draft of the guidelines namely; Guidelines of Seismic Study for Determination the Earthquake Design Parameters, Volume I, Seismic Hazard Assessment has been made and at present waiting for publication from the Indonesian Ministry of Public Works and Housing.

2. INDONESIAN RISK FACTORS OF THE DAMS

In conducting Seismic Hazard Assessment for Dams, the Risk Factors need to be considered and used as a basic to determine the seismic hazard of the dam. Risk factors of the dam collapse due to an earthquake and it's impacted the downstream area also need to be explored in conducting the seismic hazard assessment. As stated in the "Guidelines Dynamic Analysis of Embankment Dam", in the Director General of Water Resources decree no. 27/KPTS/D/2008, dated January 31, 2008, 2 (two) analysis need to be done, namely: a) Risk Class Classification, and b) Earthquake Load Criteria for Seismic Hazard Analysis. Risk classes that should be used in the Seismic Hazard assessment for Dams are presented in Table 1. The four (4) risk factors that should be considered in the seismic hazard assessment for dams are;

(a) Reservoir capacity (10^6 m^3),
(b) Dam height (m),
(c) Evacuation Needs (number of people) and d) Downstream damage risk factor.

Each risk factor is further divided into the following classes; Extreme, High, Moderate, and Low.

The determination of the risk class due to seismic hazard is carried out by calculating the total risk factor (FRtot) which is the sum of the risk factors for the reservoir capacity (FRk), dam height (FRt), evacuation needs (FRe), and the downstream damage risk factor (FRh) using the following equation:

$$FR_{tot} = FR_k + FR_t + FR_e + FR_h \quad (1)$$

where
FR_{tot}: Total risk factor,
FR_k: Risk factors due to reservoir capacity,
FR_t: High risk factors of dam,
FR_e: Factor in evacuation needs,
FR_h: Downstream damage rate factor.

2.1. DAM RISK FACTOR CRITERIA

According to the Total Risk Factors, the risk classes for Seismic Hazard Assessment for Dams as presented in Table 2 are divided into 4 classes namely; Class I (low), Class II (moderate), Class III (high), and Class IV (extreme). The relationship between Total Risk Factors and Earthquake Source and Hazard tracing for Dams is presented in Table 3 below.

Table 1
Risk Factor Criteria for Earthquake Source and Hazard Tracing for Dams
Critères de facteurs de risque pour le traçage des sources et des dangers sismiques pour les barrages

NO	RISK FACTORS	WEIGH				
		EXTREME	HIGH		MODERATE	LOW
1	Reservoir Capacity (106 m^3) (FRK)	> 100 (6)	100 - 1.25 (4)		1,00 - 0,125 (2)	< 0.125 (0)
2	Height of the dam (m) (FRt)	> 45 (6)	45 – 30 (4)		30 – 15 (2)	< 15 (0)
3	Evacuation needs (people) (FRe)	> 1000 (12)	1000 – 100 (8)		100 – 1 (4)	0 (0)
4	Downstream damage risk factor (FRh)	Very high (12)	High (10)	Slightly High (10)	Moderate (4)	None (0)

Table 2
Risk Classes for Seismic Hazard Assessment for Dams
Classes de risque pour l'évaluation de l'aléa sismique des barrages

TOTAL RISK FACTOR	RISK CLASS
(0 - 6)	I (low)
(7 - 18)	II (moderate)
(19 - 30)	III (high)
(31 - 36)	IV (extreme)

Table 3
Relationship between Risk Class and Seismic Hazard assessment for Dams
Relation entre la classe de risque et l'évaluation de l'aléa sismique pour les barrages

DAM RISK CLASS	THE DISTANCE OF THE DAM TO THE NEAREST ACTIVE FAULT THAT CAN PRODUCE EARTHQUAKE MAGNITUDE MW > 7.0	SEISMIC HAZARD ASSESSMENT FOR DAMS
I (Low)	—	Not required
II (Moderate)	—	Not required
III (High)	< 15 km	Needed
IV (Extreme)	< 15 km	Needed

3. SEISMIC HAZARD ASSESSMENT STAGES

The main purpose of seismic hazard assessment for dam is to obtain the most accurate and best possible information from the location of the dam to the sources of earthquakes, active faults, seismicity and potential earthquake hazards with output products in the form of:

(a) Active tectonic maps, seismicity, and seismicity history,
(b) Regional and local scale active fault maps and data on earthquake potential parameters, including slip rate, M-max, recurrent intervals, and their seismic history,
(c) The seismotectonic model contains formulations from maps of active faults and their earthquake parameter tables for earthquake hazard analysis input,
(d) Analysis of the hazard against movement and deformation of an active fault if there is a fault path that crosses the dam foundation. In this proposed guideline of seismic hazard assessment for dam, the study is classified in two stages, namely:
    - During Feasibility Study of the dam, and
    - During Detailed Engineering Design of the dam.

3.1. Seismic hazard assessment at feasibility study

During Feasibility Study, Seismic Hazard Assessment shall be done for all dams regardless the risk class of the dam. The general purpose in this stage is for the selection of the dam site location, in particular the safety of the dam from seismic hazard. The scope of seismic hazard assessment in the feasibility study stage includes:

(a) Desk studies: from scientific publications/literature, reports of previous studies, geological maps, active faults map, seismic catalog data and seismic history,

(b) Preliminary analysis of seismic hazard assessment based on the latest Indonesian Earthquake Source and Hazard Map published by PuSGeN/ Ministry of PUPR [1] to obtain the indication of the PGA (peak ground acceleration) value, and
(c) Evaluating the dam risk level to determine whether required or not a detail seismic hazard assessment in the detail design stage.

3.2. Seismic hazard assessment at detailed engineering design

The seismic hazard assessment at detailed design stage was only for dams with Class III and Class IV risk class. The main purpose of seismic hazard assessment of the dam at this stage is to;

(a) To obtain more complete and accurate information from data on active faults, seismicity, and seismic history on a regional to local scale in relation to earthquake hazard analysis inputs, including ascertaining the position of the dam location and its appurtenant structures to the active fault, and
(b) To obtain complete information of potential earthquake hazards, including the results of *uniform hazard spectra* analysis and *time series* analysis for earthquake-resistant dam designs.

The scope of activities in the detailed stage of dam design includes:

(a) Desk study in more detailed than scientific publications, reports of the results of previous studies, geological maps, maps of active faults, seismic catalog data and seismic history,
(b) Review (and revise) the active fault maps and/or active fault model maps available on a regional scale. The required active fault and seismotectonic fault map data have a minimum accuracy scale of 1:50,000 (equivalent to the results of active fault mapping based on SRTM 30). Active fault maps need to be evaluated and adapted to data/field conditions, then presented in *GIS* digital information, in *hard* and *soft copy* form,
(c) If an active fault map is not yet available or is deemed inadequate or incomplete, it is necessary to mapping the active fault using the standard method, which includes *desk analysis* and field surveys depending on dam site condition and location,
(d) Review and revise the characteristic data and seismic parameters of all active faults identified or mapped from each earthquake sources,
(e) If it is identified that the dam location is at a distance of $\leq$ 15 km from the active fault of Classes 1 to 4 or has a PGA for SEE earthquake $\geq$ 0.5g, it is necessary to conduct a more detailed active fault study by conducting a field survey using a method that is in accordance with the standards, and
(f) Create seismotectonic maps based on the results of regional studies and local-detailed studies (field survey results), including maps of active faults and

their segmentation and descriptions of the characteristics and seismic parameters of all (segments) of active faults that are inputs for seismic hazard analysis.

For dams that have been built, if the detailed design has not included the seismic risk, the seismic hazard assessment may be carried out, and the procedures for implementing seismic hazard assessment was similar with the procedures for the detailed design stage of new dams.

The seismic hazard assessment in the detailed design stage consists of:

(a) far field (regional),
(b) near field seismic hazard assessment. Seismic hazard assessment and active fault identification on a regional scale is recommended to be carried out within a radius of at least 100 km from the dam location and can be carried out up to a radius of 500 km if there a long distant earthquake sources with large magnitude (Mw$>$ 8) are found. Regional seismic hazard assessment is conducted in the Feasibility Study and more detail in the detailed design stage.

3.3. Regional seismic hazard assessment during feasibility study

The seismic hazard assessment at detailed design stage was only for dams with Class III and Class IV risk class. The main purpose of seismic hazard assessment of the dam at this stage is to:

(a) To obtain more complete and accurate information from data on active faults, seismicity, and seismic history on a regional to local scale in relation to earthquake hazard analysis inputs, including ascertaining the position of the dam location and its appurtenant structures to the active fault,
(b) To obtain complete information of potential earthquake hazards, including the results of *uniform hazard spectra* analysis and *time series* analysis for earthquake-resistant dam designs.

The scope of activities in the detailed stage of dam design includes:

(a) Desk study in more detailed than scientific publications, reports of the results of previous studies, geological maps, maps of active faults, seismic catalog data and seismic history,
(b) Review (and revise) the active fault maps and/or active fault model maps available on a regional scale. The required active fault and seismotectonic fault map data have a minimum accuracy scale of 1:50,000 (equivalent to the results of active fault mapping based on SRTM 30). Active fault maps need to be evaluated and adapted to data/field conditions, then presented in *GIS* digital information, in *hard* and *soft copy* form,

(c) If an active fault map is not yet available or is deemed inadequate or incomplete, it is necessary to mapping the active fault using the standard method, which includes *desk analysis* and field surveys depending on dam site condition and location,
(d) Review and revise the characteristic data and seismic parameters of all active faults identified or mapped from each earthquake sources,
(e) If it is identified that the dam location is at a distance of $\leq$ 15 km from the active fault of Classes 1 to 4 or has a PGA for SEE earthquake $\geq$ 0.5g, it is necessary to conduct a more detailed active fault study by conducting a field survey using a method that is in accordance with the standards, and
(f) Create seismotectonic maps based on the results of regional studies and local-detailed studies (field survey results), including: maps of active faults and their segmentation and descriptions of the characteristics and seismic parameters of all (segments) of active faults that are inputs for seismic hazard analysis.

For dams that have been built, if the detailed design has not included the seismic risk, the seismic hazard assessment may be carried out, and the procedures for implementing seismic hazard assessment was similar with the procedures for the detailed design stage of new dams.

The seismic hazard assessment in the detailed design stage consists of:

(a) far field (regional),
(b) near field seismic hazard assessment. Seismic hazard assessment and active fault identification on a regional scale is recommended to be carried out within a radius of at least 100 km from the dam location and can be carried out up to a radius of 500 km if there a long distant earthquake sources with large magnitude (Mw$>$ 8) are found. Regional seismic hazard assessment is conducted in the Feasibility Study and more detail in the detailed design stage.

3.3.1. *Regional seismic hazard assessment during feasibility study*

Regional seismic hazard assessment during feasibility study stage is mainly to collect secondary data for *desk studies* to review, analyze, and formulate regional tectonic conditions, seismicity, earthquake history, and the presence of active fault lines. The main objectives of conducting regional studies in the Feasibility Study Stage are to:

(a) Understanding geology, seismicity, active tectonics, and potential seismicity in particular regarding the existence of active fault lines and their proximity to dam site plans,
(b) Obtaining PGA (peak ground acceleration) values at dam sites are either obtained from deterministic or probabilistic methods,
(c) Evaluate the map of the active faults in regional scale, c) Collect the data that needs includes; previous seismic hazard map. The main reference is the latest Indonesian Earthquake Source and Hazard Map (PuSGeN 2017 [1]),

(d) Review the available geological maps both published and those that have not been published with special notes,
(e) Review tectonic maps, especially active fault maps that have been made, whether they have been published or have not been published with special notes d) Review reports of the previous geological and geophysical studies,
(f) Review seismicity data recorded by earthquake instruments (seismographs) from the best earthquake catalogs or compilations of various earthquake catalog data,
(g) Collect and review historical data of earthquakes from various sources, and
(h) Review the publication of related papers in scientific journals at home and abroad.

Activities that need to be carried out include:

(a) Reviewing the various secondary data above to obtain a comprehensive and up-to-date understanding of geology, seismicity and potential seismic hazards in the dam area, especially with regard to the sources of earthquakes or active faults that are considered significant,
(b) Reviewing the active fault data that is already available, including checking the quality of the map and its validity and feasibility for use in defining significant earthquake sources for the dam site
(c) One of the usual ways to test the quality of active fault maps is to overlay data on active fault lines on DEM maps with GIS software and conduct an inspection of the feasibility of active fault maps using standard morphotectonic analysis methods commonly used in the international world, and
(d) Analyze the earthquake hazard maps that are already available to obtain PGA values at the dam site, and
(e) Making conclusions and recommendations.

3.3.2. *Regional seismic hazard assessment during detailed engineering design*

The difference in regional studies for the Design Phase is in the depth and detail of the data that needs to be obtained and analyzed. All dams with Risk Class III and IV, whether located $\leq$ 15 km or more from the identified Class 1 to 4 active fault lines need to conduct this study. The main objectives of conducting a regional study of seismic hazard assessment are searching for the source and potential of earthquakes in the Dam Design Phase are to:

(a) Provides seismicity and active fault maps with a minimum accuracy scale of 1:50,000 within a radius of at least 100 km from the dam site,
(b) Obtains all the necessary earthquake parameters for earthquake hazard analysis of all its active faults which include; Fault movement type (i.e. normal, shear, strike-slip of combination fault), The length of the fault segment usually measured in kilometers, The maximum earthquake magnitude (Mmax) of each

fault segment, Rate of activity or slip rate or fault shear rate of each fault segment. Earthquake history, earthquake cycle and the last major earthquake, and the recurrent period (recurrent interval) of the earthquake.

(c) Creating a seismotectonic map based on data from points a and b. The data that needs to be collected at least includes: Reviewing the data already collected in the Feasibility Study Phase and supplementing the missing data for a more detailed and comprehensive analysis, Obtain the highest resolution digital topographical or DEM (DTM and/or DSM) data available for active fault study and mapping, where is now widely available now is the 30m SRTM and the 8.5m DEMNAS, DEM data with higher resolution such as 5m IFSAR and LIDAR data.

Activities that need to be carried out in the Design Phase include but not limited on:

(a) Perform regional active fault mapping with a minimum accuracy scale of 1:50,000 (equivalent to mapping based on SRTM 30 data) for dams located more than 15 km from the nearest active fault line or a minimum accuracy scale of 1:25,000 (equivalent to mapping based on 8.5m DEMNAS data) if the dam location is less than 15 km from the Class 1 active fault line to 4. Mapping is done using the Geographic Information System (GIS) method so that the accuracy is clear and easy to check again,
(b) Analyze seismicity data (catalogs) in more detail,
(c) Analyze all active tectonic data, including data from geodesic tectonics (GPS),
(d) Collect historical earthquake data more fully and comprehensively, and
(e) Collect pre-historical or paleoseismic data more detail.

4. NEAR FIELD SEISMIC HAZARD ASSESSMENT

Near field or local seismic hazard assessment and active fault identification needs to be carried out for dams that have a high to extreme level of risk (Class III and IV), if it is indicated or identified that the location of the dam is in an area with high to very high seismicity and/or is near an active fault line, based on existing seismicity and active fault data/maps or on recommendation or following the consultation with competent experts.

The criteria for conducting detailed (near field) seismic hazard assessment and fault identification studies are:

(a) If the location of the dam with risk levels of Class III and IV is indicated to be within a radius of 15 km from the active fault line Class 1 to 4, or has a high earthquake hazard potential level with a PGA value for SEE earthquake equal to or greater than 0.5g according to the latest PuSGeN Map [1]. Active fault

mapping with accuracy equivalent to the scale of 1:25,000 or equivalent using the basic data of DEMNAS 8.5m from the Geographic Information Agency (BIG).

(b) If the location of the dam is indicated to be within a radius of 5 km from active faults Class 1 to 3 in zones with PGA values of SEE earthquakes equal to or greater than 0.7g, it is necessary to study and mapping active faults with a minimum accuracy scale of 1:10,000. The requirement basic data of 1:10,000 topographic maps or DEM data with higher resolution for example IFSAR DSM-DTM 5m and LIDAR is needed. Alternatively, active fault mapping can be assisted by drone surveys.

(c) If it is indicated that there is an active fault line Class 1 to 3 that is suspected of cutting or passing close to the dam foundation or appurtenant structures related to the release of water from reservoirs such as spillway gates, bottom outlet facilities, then an active fault study and mapping with accuracy equivalent up to 1:1000 is needed. In this case, LIDAR data or alternative mapping using a detailed drone survey is needed.

The procedures of near field seismic hazard assessment and faults identification are:

(a) Conducting a desk study of active fault mapping is carried out by morphotectonic analysis of DEM (Digital Elevation Map) data by a standard-appropriate method with resolution and basic map data (DEM) depending on the proximity of fault lines to the dam as described above,

(b) Conducting field surveys for checking and/or further analysis of fault lines that have been identified in the desk study. Those conducted in field surveys include: Direct visual examination in the field related to phenomena, formations and landscapes related to the existence of active fault lines and evidence of movement in the Quaternary Age, especially the late Pleistocene (from 128 thousand years ago until now). Detailed mapping of active faults and related landscapes and their relation to dam locations with the help of drone surveys to create 3D (Ortho-photograph) and DEM aerial photograph is highly detailed. Geophysical (superficial) surveys with appropriate methods, by geo-radar, geo-electric, seismic reflection, and seismic refraction methods, or a combination of methods, according to geological and field conditions and their need to help identify and map fault paths and planes more accurately, including structures below the surface.

It should be noted that this activity is usually carried out by experts who are competent in recognizing morphological phenomena and formations related to fault lines and their movements, both on DEM data and in the field. Sometimes faults found across the road or cutting the rock formations on the road cut slopes. In this case the activity of the fault can be examined. Figure 2 shows the active faults across the main road in North Sumatra. Figure 3 indicated the fault across the road cut slope. It was clearly shown that the fault cut the older rock formation, but on the

top the fault does not cut the younger rock formation. In this case the investigation on the age of younger rock formation can be done to indicate the last rupture of the fault.

In case the tracing of the fault nearby the dam was found using geophysical equipment methods, but no indication of the fault by means of rupture in the surface due to erosion and deposition of the soils, a paleo-seismic method may be done to reveal the activity of the faults found in the near filed seismic hazard assessment and fault identification. The carbon dating also may be done to indicate the activity of the fault

Fig. 2
Active fault with large displacement across the main road in North Sumatra
(D. Djarwadi photo collection)
Faille active avec un déplacement important le long de la route principale dans le nord de Sumatra (collection de photos D. Djarwadi)

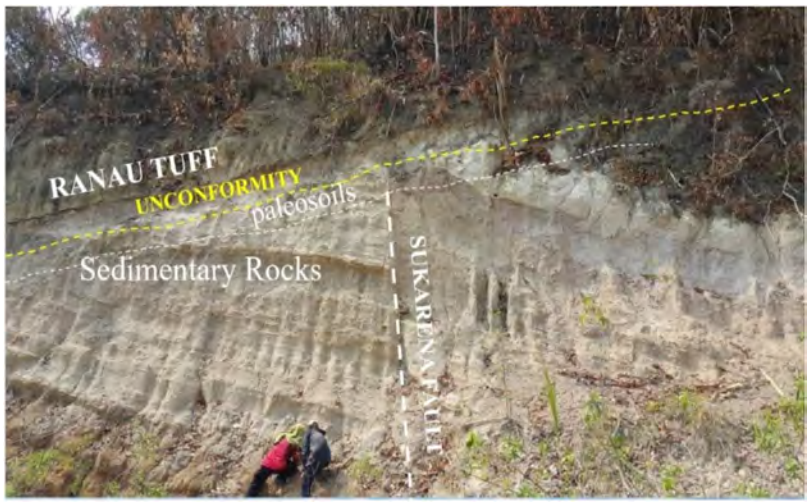

Fig. 3
Fault across the rock formation on the road cut slopes that clearly indicated the rock formation and interpretation of the activity of the fault (Photo and interpretation by Danny Hilman Natawidjaja).
La faille à travers la formation rocheuse sur la route a coupé des pentes qui indiquaient clairement la formation rocheuse et l'interprétation de l'activité de la faille (Photo et interprétation par Danny Hilman Natawidjaja).

Paleo-seismological studies with trenching and carbon dating analysis need to be carried out if:

(a) The location of the dam site is at a distance of less than 5 km from the active fault lines of Classes 1 to 3, or
(b) Earthquake hazard analysis to obtain SEE using deterministic methods and
(c) On the recommendation of a competent expert.

The objectives of paleo-seismological studies and carbon dating analysis are to

(a) Confirming the presence of active fault lines identified from subsurface geo-physical mapping and geological surveys,
(b) Assessing the level of fault activity and classifying its Class 1 to 3,
(c) Study the history of seismicity, including M-max and when was the last major earthquake occur, and
(d) Reviewing earthquake recurrent periods. Figure 4 shows the paleo-seismic trenching on the Siulak fault in Jambi, Sumatra.

5. SEISMIC HAZARD ASSESSMENT RESULT

The main results of seismic hazard assessment are a “seismo-tectonic map” accompanied by another information on the various seismic parameter data from each fault segment, including fault type, fault segment length, M-max, and slip rate. It is usually poured in the form of maps, data and tables. Seismotectonic maps are usually accompanied by a complete description of active tectonic conditions and earthquake characteristics related to each (segment) of its active faults accompanied by completeness of earthquake data including: earthquake event data recorded on seismic instrumental (seismometer), seismicity data from records in history. What is meant by an active fault map to make a seismotectonic map is an original active fault map resulting from the analysis of active fault mapping based on morphological (morphotectonic) analysis, seismic data, geodesy, and geology. In making seismotectonic maps, this active fault map in its segmentation analysis is simplified to a model (segmentation) of active faults.

Fig. 4
a) Aerial view of the paleo-seismic trenching for Siulak fault in Jambi, Sumatra, b) ortho-photo and geological logging of the rock formation which clearly indicated the fault location (photo and logging by Danny Hilman Natawidjaja).
a) Vue aérienne de la tranchée paléo-sismique de la faille de Siulak à Jambi, Sumatra, b) Ortho-photo et diagraphie géologique de la formation rocheuse qui indiquait clairement l’emplacement de la faille (photo et diagraphie de Danny Hilman Natawidjaja).

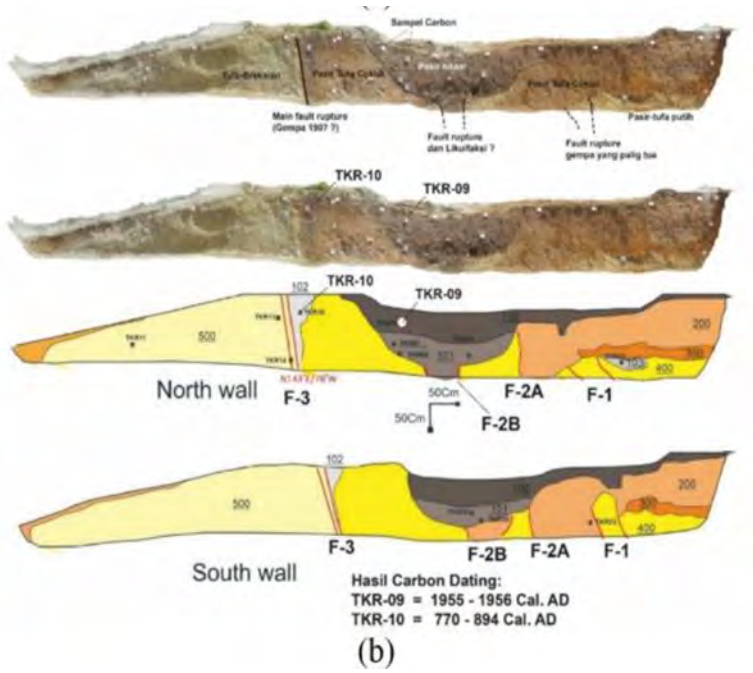

Fig. 4
(Continued)

In principle, the lines (segments) of adjacent active faults can be combined if they are considered to be able to break or move simultaneously when an earthquake occurs; or in other words, earthquake ruptures or fracturing can propagate from one segment to another. For example, in a shear fault path, based on world active fault data, if two segments are separated (referred to as a fault stepover) but less than 4 km wide, the earthquake rupture can still propagate past the stepover to the segment next to it, so that the two segments can be modeled into one line (one earthquake source). Conversely, if the width of *the stepover* is equal to or more than 4 km, the two fault segments are considered to be two sources of the earthquake, each of which has certain seismic parameters, including the maximum potential magnitude of the earthquake. In seismotectonic maps, fault branches that are small in size (less than 10 to15 km) are usually removed. Figure 5 shows the example of seismotectonic map of dam in Jambi.

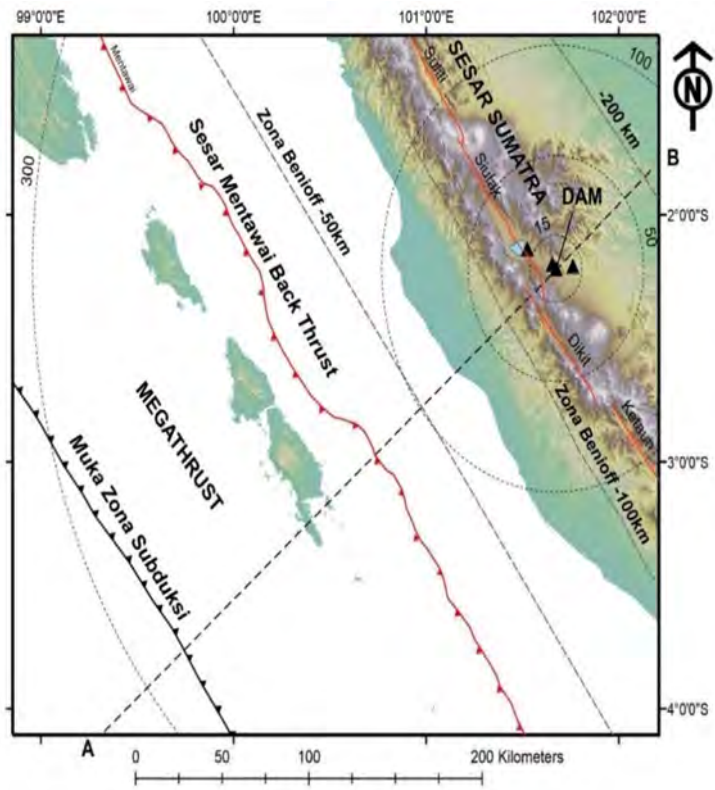

Fig. 5
Example of seismo-tectonic map of dam in Jambi, Sumatra (with permission from PT Banyu Biru Solusi Geoteknik)
Exemple de carte sismo-tectonique du barrage de Jambi, Sumatra (avec l'autorisation de PT Banyu Biru Solusi Geoteknik)

REFERENCES

[1] PUSGEN (2017). Indonesian Earthquake Source and Hazard Map. *Indonesian Ministry of Public Works and Housing* (in Indonesian).

[2] ICOLD (2016). *Selecting Seismic Parameters for Large Dams*. Guidelines. Bulletin no. 148. Paris, France.

Q.111 - R.27

COMMISSION INTERNATIONALE DES
GRANDS BARRAGES

VINGT-HUITIEME CONGRES DES
GRANDS BARRAGES
CHENGDU, MAI 2025

SEISMIC DESIGN OF CONCRETE DAM FOUNDED ON SOFT ROCK OF BATANG TORU HYDROPOWE PROJECT IN INDONESIA (*)

Li ZHISHAN
Deputy Chief Engineer, POWERCHINA Beijing Engineering Corporation Limited

Wang ZHIJIE
Chief Construction Engineer of the Project, SINOHYDRO Bureau 10 Engineering Corporation

CHINA

SUMMARY

Batang Toru dam is situated in the northern region of Sumatra Island in Indonesia near the active Sumatran Fault Zone. It is a concrete gravity dam founded on welded tuff rock in a region of high seismicity, so the seismic performance of the dam is crucial. In order to enhance the seismic performance of the concrete dam, a curved gravity dam with 3 middle-level spillways and a surface spillway is used instead of the original straight gravity dam with 3 surface spillways, the arch action of curved shape can resist a part of the imposed forces caused by the earthquake. The 2-D stability and stress analysis for OBE load condition by seismic coefficient method is adopted in the preliminary selection of dam shape. By means of establishing the 3-D finite-element models of both the dam body and the foundation，the linear response spectrum analysis and nonlinear time-history analysis are applied to assess the dam behavior and dam safety for seismic load cases. The seismic reinforcements are arranged in dam face and some defensive measures are taken to improve the earthquake-resistant performance of the concrete dam. The paper

Conception parasismique du barrage en béton fondé sur roche tendre de la centrale hydraulique de Batang Toru, Indonésie

 DOI: 10.1201/9781003642428-130

presents ways to improve the seismic performance of the concrete dam founded on soft rock and can provide a useful reference for the seismic design of the concrete dam in high seismic regions.

Le barrage de Batang Toru est situé dans la région nord de l'île de Sumatra en Indonésie, près de la zone de faille active de Sumatra. Il s'agit d'un barrage-poids en béton construit sur du tuf soudé dans une zone de forte activité sismique, de sorte que la résistance sismique du barrage est essentielle. Afin d'améliorer la résistance sismique du barrage, un barrage-poids incurvé avec 3 déversoirs intermédiaires et un déversoir de surface a été utilisé à la place du barrage-poids rectiligne initialement envisagé avec 3 déversoirs de surface. Dans le choix préliminaire du type de barrage, une analyse de la stabilité et de la contrainte en 2-D pour la condition de charge OBE a été réalisée par la méthode du coefficient sismique. L'analyse du spectre de réponse linéaire et l'analyse non-linéaire sont appliquées pour évaluer le comportement et la sécurité du barrage en cas de séisme en établissant un modèle aux éléments finis 3-D du corps et de la fondation du barrage. Les renforcements sismiques sont disposés sur la face du barrage et certaines mesures sont prises pour améliorer la résistance sismique du barrage en béton. Ce rapport propose des moyens d'améliorer la résistance sismique des barrages en béton fondé sur des roches tendres et peut fournir une référence utile pour la conception sismique des barrages en béton dans les zones de forte sismicité.

1. INDRODUCTION

Batang Toru dam is situated in the northern region of Sumatra Island in Indonesia, about 80 km south of the famous Lake Toba Caldera, near Sipirok Town (Fig. 1).

Indonesia Island Arc is one of the most active tectonic regions in the world since it is located on the boundaries of three major plates: Eurasia, India-Australia, and Pacific plates. Indonesia sits on the southern edge of the Eurasia Plate, and the island of Sumatra sits atop the Southeast Asian plate, overriding the subduction Indian-Australian plate. With this high relative plate motions and all active fault arrays accommodating the movements, Sumatra ranks is considered as one of the most active seismic region on Earth. In the past few decade's years, numerous major earthquakes ranging from magnitude 6.5 to 9 have occurred in both the

Sumatran fault zone and the megathrust and had destroyed many houses and properties and killed many people.

Fig. 1
Location of the Batang Toru dam in Sumatra, Indonesia
Localisation du barrage de Batang Toru, Sumatra, Indonésie

The Batang Toru dam is a concrete curved gravity dam founded on welded tuff rock. It has a length of 137.44 m and height up to74 m with 3 middle-level spillways and a surface spillway. The dam is divided into 5 dam monoliths with lengths of 10.65 m-39.19 m, and a partial joint evenly divides the central monolith (39.19 m width) only in the upstream 6m section (Fig. 2).

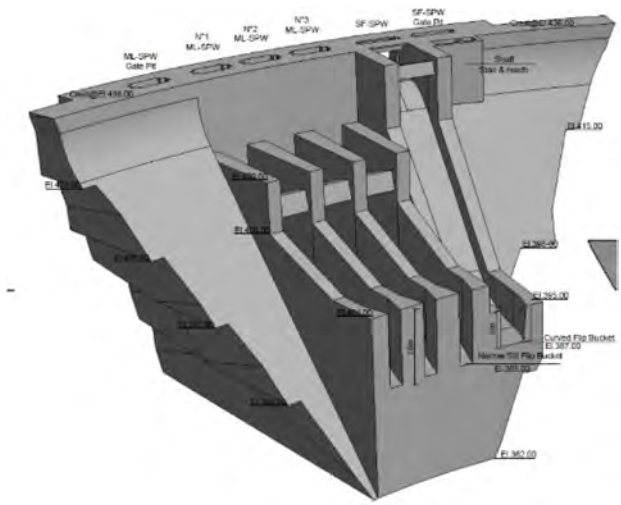

Fig. 2
Illustration of the Batang Toru dam from the downstream view
Vue en aval du barrage Batang Toru

As a concrete gravity dam of 74.0 m high is founded on welded tuff rock near the major active Sumatran Fault Zone, the seismic performance of the dam is crucial in its design. To enhance the seismic performance of the concrete dam, a curved gravity dam with 3 middle-level spillways and a surface spillway is adopted instead of the original straight gravity dam with 3 surface spillways. The two-dimensional (2-D) stability and stress analysis for Operating Basis Earthquake case by gravity method and seismic coefficient method is adopted in the preliminary selection of dam section. By means of establishing the three-dimensional (3-D) finite-element models of both the dam body and the foundation，the linear response spectrum analysis and non-linear time-history analysis are applied to assess the dam behavior and dam safety under seismic loads. The seismic reinforcements are arranged in dam face and some safety measures are taken to improve the earthquake-resistant performance of the concrete dam.

The paper presents ways to improve the seismic performance of the concrete dam founded on soft rock and can provide a useful reference for the seismic design of the concrete dam in high seismic regions.

2. EARTHQUAKE DESIGN PARAMETERS

2.1. Seismic hazard assessment

The Batang Toru dam is located around the major active Sumatran Fault Zone (SFZ) near two major fault segments-Toru and Angkola fault segments. It is a typically high seismic area.

Seismic Hazard Assessment is often used to determine the level of earthquake hazard that may occur in a certain place. Two approaches i.e. Deterministic Seismic Hazard Assessment (DSHA) and Probabilistic Seismic Hazard Assessment (PSHA) were conducted to evaluate the design parameters of earthquake ground motion at the dam site, quantitatively, the corresponding ground motion parameters can be obtained from a deterministic and/or probabilistic seismic hazard analysis. Based on the results of the seismic hazard analysis, it can be obtained using PSHA method that the peak ground acceleration (PGA) generated from all earthquake sources around the location for 50% probability of exceedance (PE) within 100 years of building lifetime or with a return period of 145 years is 0.402 g and with a return period of 10,000 years is 1.275 g. It can also be known using DSHA method that the PGA of maximum credible earthquake (MCE) from 4.02 km controlling earthquake sources (Toru-01B fault) for the 50th percentile and 84th percentile are 0.377 g and 0.648 g respectively.

2.2. Design earthquake

According to ICOLD Bulletin 148 (2016) on the selection of seismic parameters for large dams, two level of earthquakes should be considered in design and analysis of dam: the Operating Basis Earthquake (OBE) and Safety Evaluation Earthquake (SEE). Seismic forces associated with the OBE are considered unusual loads. Those associated with the SEE are considered extreme loads.

The OBE is typically represented by ground motions with the return period of 145 years (that is, a 50 percent probability of occurrence during the service life of 100 years). The OBE ground motion parameters are estimated based on a probabilistic seismic hazard analysis. The SEE may be determined based on the Maximum Credible Earthquake (MCE) which is the largest conceivable earthquake that could occur along recognized faults or tectonic plate boundaries if earthquakes have more frequently occurred or anticipated to occur along such well-identified sources.

Based on the risk or potential hazard classification of the Batang Toru Dam, the 0,402g PGA and ground motion parameters corresponding to the 145 years return period of PSHA method, will be used as OBE, and the 0.648g PGA and ground motion parameters corresponding to the 84th percentile of the DSHA methods will be used as SEE. The acceleration response spectra of OBE and SEE are shown as Fig. 3. The seismic wave of Northern Norcia Italy as the cross and stream river direction modified time histories will be used to do the dynamic analysis for SEE.

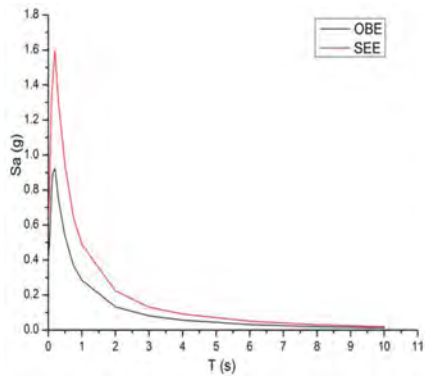

Period(s)	Spectral acceleration (g) for OBE	Period(s)	Spectral acceleration (g) for SEE
0	0.402	0.01	0.648
0.05	0.544	0.05	0.892
0.1	0.805	0.1	1.336
0.135	0.899	0.2	1.598
0.2	0.924	0.3	1.31
0.3	0.751	0.4	1.129
0.4	0.641	0.5	0.943
0.5	0.537	0.75	0.643
0.75	0.37	1	0.489
1	0.285	2	0.224
2	0.133	3	0.13
3	0.081	4	0.091
4	0.057	6	0.05
6	0.031	8	0.03
8	0.019	10	0.019
10	0.012		

Fig. 3
The acceleration response spectra of OBE and SEE
Spectres de réaction en accélération pour OBE et SEE

3. DAMSITE GEOLOGY

The Dam site is located in a V-shape canyon area with a width varying from 15 m to 30 m, where the lithology is dominated by welded tuff, generally rather massive. A comprehensive site investigation and test works have been carried out at damsite area, the average uniaxial saturated compressive strength of the rock is 18.1MPa, which is a relatively soft rock. Based on the UCS value of sound rock and the Rock classification from ISRM, the dam site rock foundation is classified as Soft Rock, but the RQD is mostly above 75%, no fault or weak zones. It is also found that the deformation parameters of tuff rock mass is relatively low from in-situ test results, and the values are only 1.5∼2.0 GPa. The deformation modulus value in the vertical direction is slightly larger than the horizontal direction.

Based on the analyses of several factors: rock strength, weathering, deformation parameter, rock mass quality, and dam height, the D2 rock mass (Fair rock (Class III) and slightly weathered (W2)) has been considered as the dam foundation surface. The bearing capacity of D2 rock mass is not less than 3.6MPa, and D2 rock masses are intact, the φ value is about 40°, and the c value is about 1MPa.

4. SOME CONSIDERATIONS OF SEISMIC DESIGN OF THE DAM

4.1. Selection of dam type

As a dam is built in a region of high seismicity, the earthquake resistance of Batang Toru Dam is crucial. In early design, a concrete straight gravity dam was selected, but it was found that the original section of gravity dam was not massive enough to resist overturning and sliding forces caused by the earthquake. In order to enhance the seismic performance of the concrete dam, an available dam type have to be selected in detailed design. Concrete arch dams are known for their high seismic resistance, and arch dams can transfer the horizontal thrust by arch action to the abutments and is most suitable for narrow canyons. But, as a general rule, an arch dam requires a site with abutments of sufficient strength to support the arch thrust, so it is unsuitable to be applied in site soft rock at the foundation and abutments.

Taking into account of V-shape canyon, welded tuff foundation, and dam height of 74.0m, a curved gravity dam is chosen to replace the straight gravity dam, arching the dam would provide additional margin for dam stability and stress. The arch action of curved shape can be utilized to resist one part of imposed force caused by the water and earthquake. Because it can resist the seismic force by a combination of gravity and arch action, the gravitation force required by the dam is

lessened, which thereby reducing the volume of concrete. Meanwhile, in order to facilitate the thermal control and construction schedule of dam mass concrete, a portion of the conventional concrete in the dam body will be replaced by roller compacted concrete (RCC).

4.2. SELECTION OF DAM SHAPE

As a curved gravity dam founded on soft rock, it can provide some arch action to withstand the seismic load, but the additional margin of arch action should be designed within a reasonable range. The 20%∼30% of total thrust will be considered to transfer to the abutments by arch action based on the economy and safety of dam. Accordingly, the proper shape of the Dam will be selected.

4.2.1. *Dam section*

The basic shape of a dam section controls the shape of the entire dam and, as a result, distribution and magnitude of stresses within the body. Referencing to Gravity Dam Design (USACE EM 1110-2-2200 1995), and the seismic performance of curved gravity dams, the dam section is determined based on the following principles:

- The geometry of dam section will be preliminary selected by finding the optimum cross section that meets the stability and stress criteria for OBE load condition, the Dam must have sufficient weight to withstand the forces caused by OBE case. Two-dimensional (2-D) gravity method and seismic coefficient method are adopted in the preliminary selection of dam section.
- The minimum sliding factor of safety of 1.0 will be used to check the dam section selected for SEE load condition by 2-D analysis method, and the arch action will be considered to resist a part of earthquake load. The final geometry of dam section will meet the stability and stress criteria by a combination of arch and gravity action for each of loading conditions, including SEE load conditions.

The dam section is established at the maximum height section and extends along the rest of the dam to provide a smooth profile. The final geometry of dam section will be verified by 3-D finite-element models analysis. The final geometry of dam section is presented as below:

- The crest elevation: El.436.00m.
- The maximum dam height: 74m.
- The crest width: 7.5m.
- The slope of upstream face: 1V:0.1H ∼1V:0.3H.
- The slope of downstream face: 1V:0.85H.

4.2.2. *Curved shape of dam*

The dam is curved in plan only, the upstream face has a constant radius making it a linear shape face throughout the height of the dam, but the downstream face will reduce the radius as moving down from top elevation to bottom.

Based on topographic and geology condition of dam site, an axis center line in space which is the loci of centers for circular arcs is defined along the middle of river bed, and the arch crown cantilever at the axis center line is defined as the maximum height dam section and the upstream face of dam at the crest will be used as dam axis. In order to transfer the appropriate horizontal thrust by arch action to the abutments, three different arcs alternatives of dam axis among tentative radii of 118m, 200m and 300m, with a single center arc at the axis center line, will be compared for the selection of arcs of dam. Preliminary stable and stress analyses of the dam are carried out by using the arch-cantilever method. After comprehensive evaluation of the abutment stability and deformation, arch effect, constructability, and volume of concrete, the dam axis arcs with 200m radium is chosen as a well-balanced and optimal solution. The maximum center angle of the top arch is 39.39°, obviously, the thrusts transferred to the abutments by arch action is less than normal arch dams， it is advantageous to use a low degree of horizontal curvature for a curved gravity dam founded on soft rock.

4.3. EFFECTS OF OVERFLOW SPILLWAY LAYOUT

The dam crest elevation is EL.436.00 m, and the crest length is 137.44 m (along the dam axis) with maximum height of 74 m. The design flood ($1.5Q_{100}$) for the Dam is 3653 m^3/s, overflow spillways through the dam will be used to flood the water.

To meet the requirement of flood releasing, floating debris discharging, sediment flushing and reservoir empty. Meanwhile, the crest region of dam should be stiffened to resist the earthquake. So, two alternatives of spillways have been studied in detailed design as below：

Alternative 1 is that three surface spillways with radial gates and one bottom outlet through the dam. Each surface spillway has an opening of 9.0 m x 13.8 m (W×H) with the crest elevation at El. 420.50m. The bottom outlet is tentatively 5.0 m x 6.0 m (W×H) with the sill elevation at El. 390.00m. The 3 surface spillways have advantages such as high discharge capacity, it enables to discharge floating debris and provides operation flexibility, and the bottom outlet can be used for the sediment flushing and reservoir empty. The total capacity of overflow spillways is about 3684 m^3/s, which can meet the requirement of design flood. However, the surface spillway would cut the arch effect, the arch action cannot be considered above El.420.50m, and the upper portion of the dam will be weak with respect to seismic resistance.

Alternative 2 is that one lower-wide surface spillway with flap gate and 3 mid-level spillways through the dam. The surface spillway is 9 m wide and 6.3 m high,

with the crest EL.428.00 m, it can keep the floating debris discharging and benefit the small flood releasing. Each mid-level spillway with radial gates has an orifice of 7.0 m x 9.0 m (W×H) with the sill elevation at EL.403.00m， it can meet the flood releasing and benefit the sediment flushing and reservoir empty. Meanwhile, the overflow spillways with lower-wide surface spillway and mid-level spillways can keep an integral belt with the effective arch action on the upper portion of the dam and take advantage of the arch effect to resist the high seismic.

Overall, comparing to alternative 1, the alternative 2 has an advantage of the arched effect to resist the high seismic parameter, meanwhile, it can also meet the requirement of flood releasing, floating debris discharge, empting reservoir, and benefit the sediment flushing capacity, so the alternative 2 is recommended as overflow spillway system though the curved gravity dam located in region of high seismicity.

4.4. Selection of concrete strength of dam body

Selection of concrete strength of dam body is based on the permeability requirements and the results of static and dynamic analysis for OBE case and evaluation for SEE case, the stress during the OBE level must be within acceptable limits, and the demand-capacity ratios are less than 2 which is considered acceptable under SEE case, so the C_{90}14MPa (minimum compressive strength 14MPa at 90 days) of RCC (Roller Compacted Concrete) as Mass Concrete of Dam Body and the C_{90}17.5MPa of GEVR (Grout Enriched Vibrated RCC) as U/S & D/S Impervious Layers will be recommended. For other structures, such as spillway piers and surface, dam crest, etc., the C_{28}24.5 MPa of CVC (Conventional Vibrated Concrete) will be selected.

4.5. Effects of appurtenant structures

For appurtenant structures it is important that their functional and structural integrity is retained in the event of a notable earthquake, their structures and gate system will maintain their normal operating condition after OBE, and following ground motions up to the SEE, they are operable to an extent that the dam is able to pass floods while repairs are carried out. The following factors will be considered for the seismic resistant design of the appurtenant structures:

- Intake tower is located at the right abutment of the river and founded on the fair rock, and the foundation material is capable of withstanding the design loadings of the intake structure. Its design will meet the requirement of seismic resistant of intake structure.

- Three mid-level spillways through the dam and one low–level bottom outlet tunnel (BOT) in the left abutment can all be used to lower and maintain the reservoir level for post-earthquake operation.
- Power supply should be reliable, so one power supply from Powerhouse and one backup power supply from a local diesel generator will be considered for the gate system of spillways and BOT.
- In order to ensure the inspection or operation of dam following an earthquake event, three access roads to dam are considered, one road to the dam is connecting with the right abutment from powerhouse and the others are from the upstream and downstream of left abutments. Three access roads to the dam will remain passable after an OBE event and at least one access road to dam can remain passable after an SEE event.
- The slope protection works of dam abutments and some critical access road will be carried out to prevent rock falls, even in events more frequent than the OBE.

4.6. Seismic instrumentation and monitoring

A seismic monitoring network will be considered to enhance emergency response, contribute to post-earthquake safety assessments, and provide valuable data for advances in earthquake engineering. So, several strong motion sensors will be installed at the crest, base, abutments and downstream of dam to record the earthquake response of the dam site, as following:

- A strong motion sensor will be installed at the base of dam to record the peak ground acceleration.
- A strong motion sensor will be installed at the dam crest to record the amplification of the peak ground acceleration within the structure.
- Two strong motion sensors will be installed at the abutments to record topographic amplifications of the peak ground acceleration
- A strong motion sensor will be installed at the downstream location of the dam to record free-field motions.

Basic requirements for strong ground motion sensors include reliability and sensitivity to measure the three components of ground motion.

Some monitoring Instrumentations for seismic hazards will be laid as following:

- Displacement of dam body, dam foundation, monoliths joints.
- Uplift water pressure of dam foundation, water table of the left bank and right bank of the dam.
- Thermometer of dam base and body.

5. SEISMIC ANALYSIS OF 3D FEM OF DAM

5.1. Methods and 3-D finite-element model

By means of establishing the 3-D finite-element model of both the dam body and the foundation，the linear response spectrum analysis and nonlinear time-history analysis are applied to assess the dam behavior and dam safety under seismic loads. The analysis result of Linear the Response Spectrum under OBE case and Non-linear Time History Analysis under SEE case will be described in this paper.

The 3-D finite-element model included two major components: the foundation and the dam which includes all structural elements like spillway weir, pier, and drainage gallery in the dam. The model still simulated all the dam monoliths and all the joints, dam-foundation interface. The model includes the foundation rock region extend to 2 times of the maximum dam height along 3 directions. The element type includes hexahedron elements and prism elements. There are 678,777 nodes and 644,714 linear solid elements in this model (Fig. 4). Westergaard added mass method will be employed to model the fluid and structure interaction.

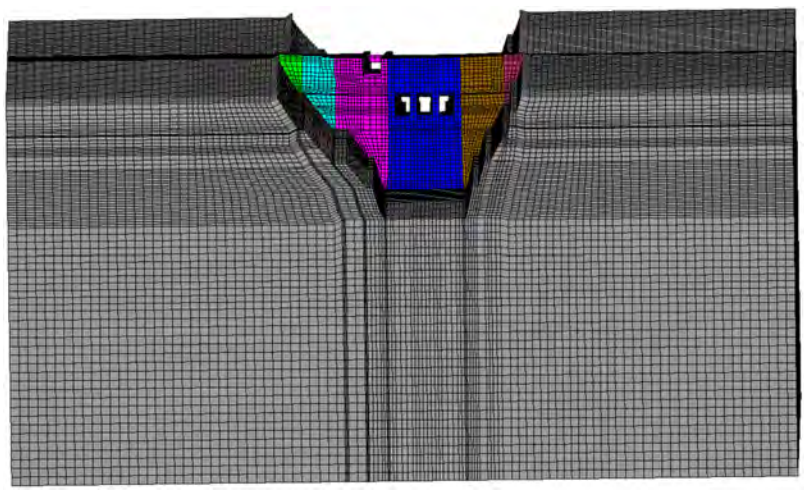

Fig. 4
The finite element mesh of dam-foundation system
Grille d'éléments finis du système de base du barrage

5.2. MATERIALS

The parameters of material used in the FEM-analyses are summarized in table 1. The linear expansion coefficient of concrete is $1.0\times e^{-5}$/ºC. The Linear constitutive laws will be used for concrete and bedrock. Coulomb friction law will be used for Vertical and Dam/foundation contact joints. The fundamental vibration mode of the dam is symmetric vibration mode, with frequency of 3.68Hz. The natural frequency of dam is relatively high due to the thick and solid dam section, the first 10 vibration modes natural frequencies under normal operation case is listed in Table 2, the main vibration shape is along the stream direction (longitudinal axes).

Table 1
The parameters of material

MATERIAL PROPERTY		VALUE	
		STATIC	DYNAMIC
Elastic modulus of concrete(GPa)	$C_{90}14$	17.7	20.41
	$C_{90}17.5$	19.8	22.82
	$C_{28}24.5$	23.5	27.00
Poisson's ratio of concrete		0.167	0.117
Density of concrete(kg/m^3)		2300	2300
Tensile strength of concrete(MPa)	$C_{90}14$	1.4	2.10
	$C_{90}17.5$	1.75	2.63
	$C_{28}24.5$	2.45	3.68
Compressive strength of concrete(MPa)	$C_{90}14$	14	16.10
	$C_{90}17.5$	17.5	20.13
	$C_{28}24.5$	24.5	28.18
Elastic modulus of rock(GPa)		1.5	2.25
Poisson's ratio of rock		0.32	0.30
Density of rock(kg/m^3)		2300	2300
Average friction angle between rock and concrete(degree)		43	29

Table 2
The first 10 vibration modes natural frequencies under normal operation

modes	1	2	3	4	5	6	7	8	9	10
Frequencies (Hz)	4.02	5.56	5.91	6.72	7.27	8.26	8.46	8.98	9.42	10.05

5.3. Linear response spectrum under OBE case

The response spectrum method is usually a required first step in a dynamic analysis for the design and evaluation of dam structures. Loads to be considered as contribution to the loading combinations for the dam are: high water level, uplift, dead load, silt pressure, thermal load, and seismic force under OBE. Linear model with massless foundation model and ANSYS software is used to perform the dynamic analysis with linear behaviors.

The total response can be obtained by a combination of static response and dynamic response (multiplied by +1 and -1), but generally the calculated value differs slightly from the actual value, because the maximum arch and cantilever stresses do not occur at the same time.

5.3.1. *Displacements*

The total response displacements under OBE case are displayed in Fig. 5. The displacement along the dam base is tiny. The maximum displacement occurred in the middle of the dam crest，the maximum value toward the downstream direction is 34 mm, and the maximum value toward the upstream direction is 21 mm.

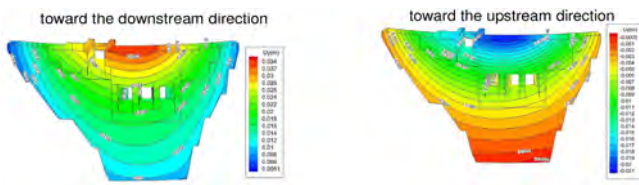

Fig. 5
Displacement contour in stream-river direction
Isoligne de déplacement amont-aval

5.3.2. *Stresses*

There are high response stresses on the upstream and downstream face of dam, which are illustrated in Fig. 6 and Fig. 7.

The maximum tensile stresses occurred in the local stress concentration zones including dam heel and dam toe, and it also occurred at the upstream and downstream face above the mid-level spillway (3.86MPa), and the upstream of surface spillway (2.67MPa), downstream pier (4.34 MPa). Except these localized areas, the tensile stress of the dam in three directions are far less than the values of dynamic tensile strength, which can also meet the design criteria of concrete strength.

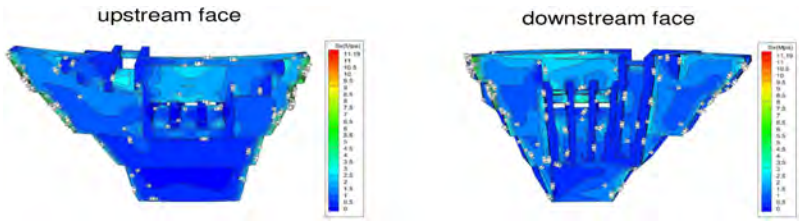

Fig. 6
Total tensile stress contour in cross-river direction
Contraintes de traction de rive à rive

Except the local stress concentration zone including dam heel, dam toe and spillway pier, etc., the compressive stresses of dam are less than concrete compressive strength/2.5, which can meet the design criteria.

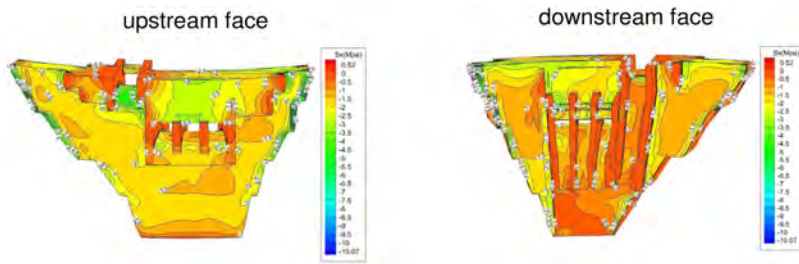

Fig. 7
Total compressive stress contour in cross-river direction
Contraintes de compression de rive à rive

Except stress concentration zone including dam heel, dam toe and spillway pier, etc., the compressive stress is less than concrete compressive strength/2.5, which can meet the design criteria.

5.4. Non-linear time history analysis under SEE case

In this analysis, the dam and the rock mass foundation are considered as an integral system based on the theory of wave propagation. The radiation damping of infinite foundation is taken into account with viscous-elastic artificial boundary method. The contact effects between the transverse joints and the dam-foundation interface are considered using the contact force method.

The seismic waves of *Northern Norcia Italy* record (Fig. 8) will be used as seismic excitation to conduct dynamic analysis. The cross-river direction time history is considered as the vertical direction time history and the vertical direction PGA is scaled to 2/3 of the PGA in horizontal direction.

Moreover, the initial gap values of transverse joint are set as 0mm, 2mm to compare the effect of grouting on seismic response of the dam.

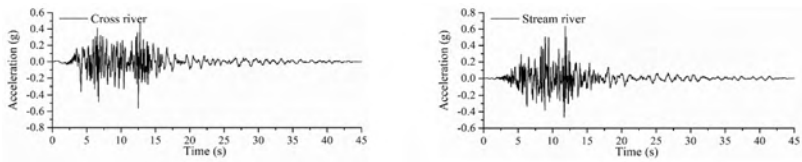

Fig. 8
The modified time histories for dam dynamic analysis of SEE
Spectre modifié de l'analyse dynamique sous SEE

Loads to be considered as contribution to the loading combinations for the dam are: High water level, uplift, dead load, silt pressure, thermal load, and seismic load under SEE. The program used in the research is PSDAP program developed by Department of Earthquake Engineering Research Center of IWHR, China since 1990s.

5.4.1. *Displacements*

Fig. 9 shows the time history of the stream relative displacement with respect to the dam heel of No.4 monolith for initial gap value 0mm and 2mm respectively. The maximum value is about 1.8cm towards upstream. By comparison, the maximum value towards downstream gradually increases from 1.46cm for initial gap value 0mm of transverse joints to 1.57cm for initial gap value 2mm of transverse joints.

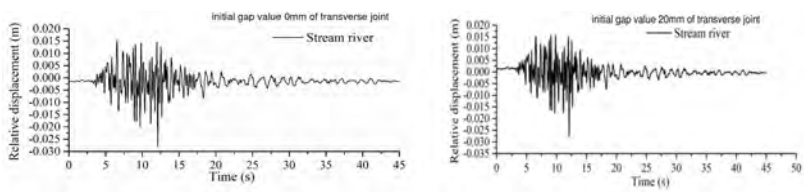

Fig. 9
Time History of the Relative Displacement of dam heel
Evolution du déplacement relatif du pied du barrage

Under the excitation of SEE, although the transverse joints appeared obvious dislocation in stream direction, the values of the dislocation are less than the designed allowable value.

The sliding displacement of dam-foundation interface occurred in all monoliths during the earthquake, the maximum sliding displacement appeared in the No.4 monolith with a value of 2.502cm. The maximum value will increase from 2.502cm for initial gap value 0mm of transverse joints to 3.164cm for initial gap value 2mm of transverse joints.

Based on above results, it indicates that the effect of grouting is small on seismic displacement response for the curved gravity dam.

5.4.2. *Stresses*

The maximum and minimum principle stress contours for initial gap value 0mm are displayed in Fig. 10 and Fig. 11.

The maximum tensile stress occurred in local stress concentration zone including dam heel and dam toe, spillway piers, guide walls. Except for these concentration zones, the tensile stresses of the dam are relatively small and it can be seen that no concrete block along cracks would be formed in the upper part of the dam owing to high vertical tensile stress.

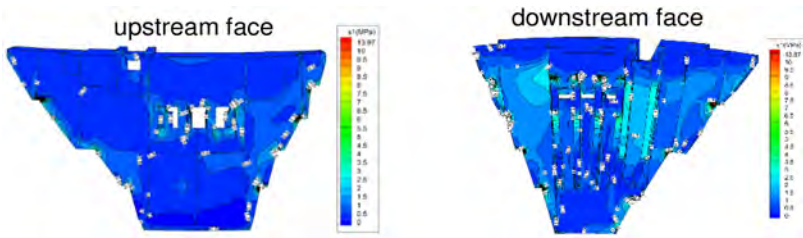

Fig. 10
The maximum principle stress contour (MPa)
Isoligne de contrainte principale maximale (MPa)

For the compressive stress (the minimum principle stress), except stress concentration zone including dam heel, dam toe and downstream pier, the values of compressive stress are less than the allowable compressive strength of concrete.

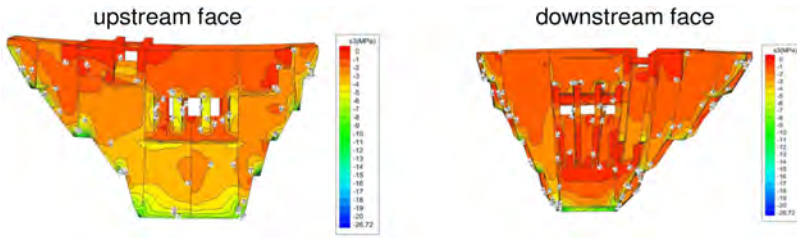

Fig. 11
The minimum principle stress contour (MPa)
Isoligne de contrainte principale minimale (MPa)

In addition, if the initial gap value from 0mm to 2mm of transverse joints, the tensile stress of upstream and downstream face of dam will increase significantly, but the tensile stress of the dam are far less than the values of dynamic tensile strength, which can meet the design criteria, so it also indicates that the effect of grouting is very small on seismic response for the curved gravity dam.

5.4.3. *Earthquake stability*

Post-earthquake stability will be checked by using residual strength parameters of the crack surface and unfavorable distribution of the uplift pressures along the crack. The dam performance for the SEE could be considered satisfactory if the post-earthquake stability meets safety requirements, and the minimum factor of safety of 1.3 will be required for the dam stability along dam-foundation interface.

The post-earthquake uplift pressure distribution is shown in Fig. 12. The water head before the drainage hole is assumed to be H_1, and that after the drainage hole is assumed to be linear distribution from the drainage hole to the dam toe with consideration of the efficiency of the drainage hole. Owing to the fact that the sliding displacement along the dam-foundation interface is far less than the diameter of 15cm drainage hole, the drain is considered to remain operational. The cohesion value on the dam-foundation interface vanishes owing to the dam sliding, and the friction coefficient is 90% of the peak value.

For the Batang Toru dam, the factor of safety of the dam stability (the highest dam monolith) along the dam-foundation interface is 1.36 (less than 1.3), it can meet the requirement of design criteria (EM1110-2200).

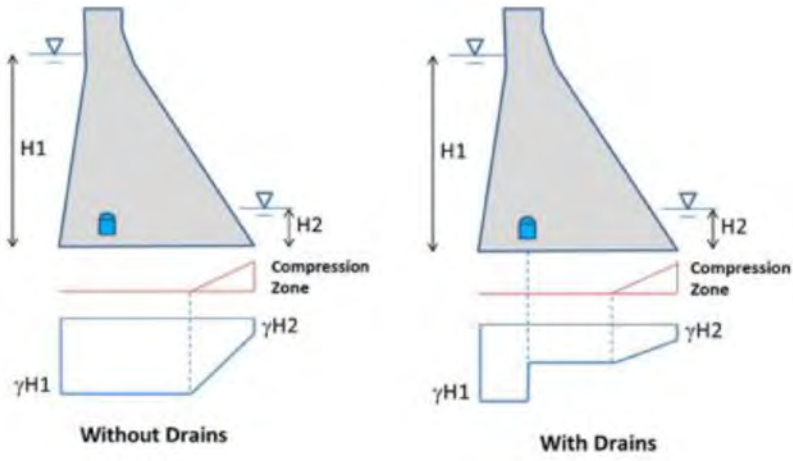

Fig. 12
Post-earthquake uplift pressures with and without drains
Sous-pressions après un tremblement de terre avec et sans drain

6. SOME DEFENSIVE MEASURES OF DAM SEISMIC DESIGN

The following defensive measures will be considered for seismic resistant design of dam:

- Sharp changes of profile and dam alignment will be avoided as far as possible. Any superstructures on the dam crest will be kept to be a minimum.
- Upstream face of dam will be designed to reduce the likelihood of tensile cracking and seepage.
- Typical measures to improve the seismic performance of dam is to arrange seismic reinforcement. So, besides galleries and spillway piles, the steel reinforcement (D25mm@200mm) will be placed at the upstream and downstream face of dam to resist tensile stresses, and the seismic reinforcement can be calculated based on the results of dynamic analysis.
- Failures can also be caused by over-stressing at a sudden change in geometry in the upper part of the dam during a strong earthquake, so the cross section of dam at the narrowing area will be a smooth connection with a circular arc. It also enhances the layout of the placing reinforcements.
- Cracks can also be expected to develop in a concrete dam during a strong earthquake along the contraction and lift joints, so treatments to joint details will be carefully applied, including horizontal lift joints and construction, contraction joints.

- Shear boxes (interlocking) along the contraction joint surfaces will be placed between dam blocks to transfer shear and avoid displacement, especially after earthquake.
- Sufficient drainage facilities for the control of uplift pressures at post-earthquake will be provided. The dimensions of drainage features, location, and orientation will consider foundation displacement during the SEE. The drainage holes are drilled at 3m intervals with a diameter of 100mm, an approximately 60 percent depth of grout curtain and an inclined 15° towards downstream. They will remain operative particularly if some sliding is expected under seismic ground motions.
- Contact faces between rock mass and steep slope foundations of dam will be grouted to ensure the stability of dam monoliths located on abutment slope.
- Foundation defects will be carefully treated to improve the sliding stability.

REFERENCES

[1] ASRURIFAK, M., NATAWIDJAJA, D.H., & DJARWADI, D. Seismic hazard assessment for Batang Toru hydroelectric power plan. Report, 2017.

[2] GUO ZHENSHAN, TU JING, LI DEYU, LI ZHISHAN. Static and Dynamic Analysis of 3D FEM Model for the Batang Toru Dam. Report, 2021.

[3] COMMITTEE ON SEISMIC ASPECTS OF DAM DESIGN. Design features of dams to resist seismic ground motion—guidelines and case histories. Bulletin 120, International Commission on Large Dams (ICOLD), 2001.

[4] COMMITTEE ON SEISMIC ASPECTS OF DAM DESIGN. Selecting seismic parameters for large dams—guidelines (Revision of Bulletin 72). Bulletin 148, International Commission on Large Dams (ICOLD), 2016.

[5] UNITED STATES ARMY CORPS OF ENGINEERS (USACE). Gravity dam design. Engineer Manual, EM 1110-2-2200, USACE, 1995.

[6] UNITED STATES ARMY CORPS OF ENGINEERS (USACE). Time-history dynamic analysis of concrete hydraulic structures. Engineer Manual, EM 1110-2-6051, USACE, 2003.

[7] UNITED STATES ARMY CORPS OF ENGINEERS (USACE). Earthquake Design and Evaluation of Concrete Hydraulic Structures. Engineer Manual, EM 1110-2-6053, USACE, 2007.

[8] NATIONAL ENERGY ADMINISTRATION OF THE PEOPLE'S REPUBLIC OF CHINA. Code for seismic design for hydraulic structures of hydropower projects. Energy Industry Standards, NB 35047, 2015.

[9] CHENG HENG, ZHANG GUOXIN. JIANG CHENFAN1, LIAO JIANXIN, ZHOU QIUJING. Analysis of seismic damage process of high concrete dam-foundation system. IOP Conference Series: Earth and Environmental Science 304, 2019.

[10] MARTIN WIELAND. Seismic design and performance criteria for large dams and methods of dynamic analysis. International Dam Safety Conference, 2019.

[11] THE WORLD BANK. Good practice note on dam safety-technical note 3 seismic risk. *Safety of Dams and Downstream Communities, 2020.*

Q.111 - R.30

COMMISSION INTERNATIONALE DES
GRANDS BARRAGES

VINGT-HUITIEME CONGRES DES
GRANDS BARRAGES
CHENGDU, MAI 2025

RAPID ASSESSMENT OF SEISMIC SAFETY OF CONCRETE DAMS AFTER AN EARTHQUAKE (*)

Houqun CHEN
China Institute of Water Resources and Hydropower Research, Engineering Seismic Research Center, Beijing

CHINA

SUMMARY

China is a seismically active country with many concrete dams located in the western strong seismic zones, where their seismic safety is a significant concern. In the event of a strong earthquake, a rapid assessment of their seismic safety is necessary to promptly report to authorities, issue reassuring notices, and implement appropriate emergency measures. Given that seismic design of engineering is a critical prerequisite for a rapid evaluation of their overall seismic safety, this paper briefly introduces innovative thoughts and concepts in current seismic design for important concrete dams in China, such as rapid determination of site-specific design response spectra, seismic response analysis shifting from a closed vibration system with a massless foundation to an open dynamic system that incorporates foundation mass and energy dissipation, establishing a seismic response analysis model for generalized dam structure that integrates strength and stability, the constitutive analysis of the dam body and its adjacent foundation rock mass shifting from linear elasticity to damage nonlinearity, reasonable handling of residual deformation during damage, taking the inflection point shown on the curve of maximum deformation of key parts of the system under seismic overload as the critical criterion for determining its seismic failure, and application of parallel algorithms and

Évaluation rapide de la sécurité sismique des barrages en béton après un séisme

 DOI: 10.1201/9781003642428-131

cloud computing technologies. Building on the above ideas, this paper proposes concepts and methods for post-earthquake rapid safety assessment, including rapid determination of seismic input of acceleration time history at the dam site, rapidly solving and designing corresponding key displacement response values that characterize the overall seismic safety of the dam system, and clarifying the condition and seismic safety level of the dam after an earthquake.

RÉSUMÉ

La Chine est un pays sismiquement actif, avec de nombreux barrages en béton situés dans la zone sismique forte de l'Ouest, et sa sécurité sismique est un problème majeur. En cas de fort tremblement de terre, il est nécessaire de procéder à une évaluation rapide de sa sécurité sismique afin de pouvoir le signaler rapidement aux autorités, émettre des notifications rassurantes et prendre les mesures d'urgence appropriées. Étant donné que la conception sismique technique est une prémisse clé pour évaluer rapidement sa sécurité sismique globale, cet article présente brièvement des idées et des concepts innovants dans la conception sismique actuelle des barrages en béton d'importance en Chine, tels que la détermination rapide du spectre de réaction de conception pour un site spécifique, la transformation de l'Analyse de la réponse sismique d'un système vibratoire fermé à base non massique à un système dynamique ouvert contenant la masse de base et la dissipation d'énergie, l'établissement d'un modèle d'analyse de la réponse sismique pour une structure de barrage généralisée intégrant force et stabilité, la transformation de l'élasticité linéaire à la non - linéarité des dommages dans l'analyse de la structure du corps du barrage et de sa masse rocheuse de base adjacente, le traitement rationnel de la déformation résiduelle au cours des dommages, en utilisant le point d'inflexion sur la courbedestruction, Application d'algorithmes parallèles et de technologies de Cloud Computing. Sur la base des idées ci - dessus, cet article propose des concepts et des méthodes pour l'évaluation rapide de la sécurité post - sismique, y compris la détermination rapide de l'entrée sismique du calendrier d'accélération du site du barrage, la résolution rapide et la conception des valeurs de réponse de déplacement critiques correspondantes caractérisant la sécurité sismique globale du système du barrage, et la clarification de l'état et du niveau de sécurité sismique du barrage après le séisme.

1. INTRODUCTION

China is a seismically active country with the sources of its major rivers, 80% of its water resources, and many concrete dams concentrated in its western high seismic zones. As the likelihood of strong earthquakes affecting these dams is high,

their seismic safety receives much attention. Once a strong earthquake occurs around a high dam, it is essential to quickly report to authorities so that reassuring notices can be issued accordingly and emergency engineering measures can be considered. Speed is key for decision support in post-earthquake seismic safety evaluation.

As seismic design is a crucial prerequisite for rapidly assessing overall seismic safety, this paper briefly introduces some innovative concepts in modern seismic design for important concrete dams in China, including rapid determination of site-specific design response spectrum of a scenario earthquake, seismic response analysis transitioning from a closed vibration system with massless foundation to an open wave system incorporating foundation mass and energy dissipation, development of a seismic response analysis model integrating strength and stability, the constitutive analysis of the dam body and its adjacent foundation rock mass shifting from linear elasticity to damage nonlinearity, reasonable and simple handling of residual strain in damage analysis, regarding the inflection point on the curve of the maximum displacement of key parts of the system with seismic overload as the critical threshold for determining its seismic failure, and the application of parallel algorithms and cloud computing technologies. For more details, refer to related references.

On the basis of existing seismic design, methods and steps for rapid post-earthquake safety assessment are proposed as follows:

1. Rapid determination of seismic input at the dam site
2. Quick calculation of seismic response parameters reflecting the overall safety of the dam structure
3. Establishing a standard system for assessing the overall seismic safety of the dam structure to clarify its state and safety level under seismic action, providing decision-making basis for determining whether and how to reduce the reservoir water level and other emergency measures. Speed is a crucial factor in the assessment.

2. MAIN BASIS FROM SEISMIC DESIGN FOR RAPID POST-EARTHQUAKE ASSESSMENT

2.1. Rapid determination of seismic input at the dam site

For important dams experiencing strong earthquakes, rapid assessment involves quickly determining the seismic input parameters at the dam site during the earthquake, such as peak acceleration and normalized β response spectrum, to generate the incident acceleration time history $a_d(t)$. Some dam sites lack strong-motion monitoring networks, and even if available, they may not operate correctly

during strong earthquakes. More importantly, even if a so-called “free-field acceleration instrument” is set up hundreds of meters downstream of the dam site, due to the complex geological conditions of the terrain on both sides of the mountain and the foundation below the dam, it is difficult to consider this location as a semi-infinite free-field surface. Consequently, it is challenging to deduce the acceleration time history a_d *(t)* incident from deep within the rock mass towards the dam site using one-dimensional inversion methods.

In China, based on the current internationally accepted seismic hazard probability analysis method [1], the peak ground acceleration a_0 related to an engineering site is determined by the attenuation law calculated from measured strong earthquake acceleration records according to a given exceedance probability value. The site conditions are assumed to be a flat surface of free field bedrock related to the engineering site. The attenuation law is related to the magnitude and epicentral distance, and is statistically analyzed along the long and short axes of the elliptical isoseismic line respectively. Considering that the attenuation law involves many uncertain factors such as mean statistical values, in order to meet the design requirements, the input acceleration a_s of the free-field flat rock stratum should be taken as site-specific design seismic peak ground acceleration a_d, which is a corrected result of a_0 by applying $\pm$ 3 σ (where σ is the standard value) according to a normal distribution.

Given that the attenuation law is a statistical mean and considering many uncertain factors, in order to meet the design requirements, it is necessary to perform uncertainty correction on a_0 according to the normal distribution of $\pm$ 3 σ (where σ is the standard value) before obtaining the site-specific design peak ground acceleration a_d.

The attenuation relation of peak ground acceleration is as follows:

$$lga_0 = A + BM + Clg\left(R + D^{EM}\right) \tag{1}$$

where *M* represents the earthquake magnitude, R the epicentral distance, and *A*, *B*, *C*, *D*, *E* regression coefficients based on regional attenuation relations.

The artificial acceleration time history $a_d(t)$ for the free-field flat rock stratum at the dam site is generated in terms of the design peak ground acceleration a_d and the β response spectrum. Under the assumption of propagation in an ideal undamped homogeneous medium, seismic motion on a flat and free surface of a rock mass superimposes reflected waves equivalent to the incident wave. Therefore, the incident seismic peak ground acceleration a_i can be taken as half of the design value a_d. According to the laws of refraction and reflection of waves propagating in different media in physics, as seismic waves propagate from the deep crust towards the surface, especially the predominant shear waves, their incidence direction gradually approaches vertical to the horizontal surface due to the increasing density of the crust medium with depth.

In generating the seismic acceleration time history $a_i(t)$ required for dam seismic response analysis, in addition to the incident acceleration peak a_i, the normalized statistical average $\beta(T)$ response spectra for various periods T in relation to the incident peak acceleration a_i need to be determined. The response spectrum is related to the magnitude M and epicenter distance R. By selecting from potential seismic sources the set earthquake [2] contributing the most to the design ground acceleration a_s at the engineering site, an innovative approach [3] has been proposed to accelerate the determination of site-specific seismic acceleration response spectrum.

Given that the main seismic safety concerns for high concrete dam projects are the seismic β response spectrum values of the bedrock that may cause damage to the concrete dam, with an epicenter distance R of around 40 km, a magnitude M above 6.0, a periodic component within $(0.2\text{-}1.0)$ seconds, 223 samples within this range were selected from the existing database of strong earthquake accelerations measured in bedrock during intra plate earthquakes. These samples were categorized by magnitude and epicentral distance with bins of $\Delta M=0.5$ and $\Delta R=0.5$ km, respectively. The statistical average acceleration β response spectra were calculated for magnitudes of 6.5, 7.0, 7.5 and epicentral distances of 10 km, 20 km, 30 km, and 40 km. These spectra were used to form the database shown in Fig. 1 [3].

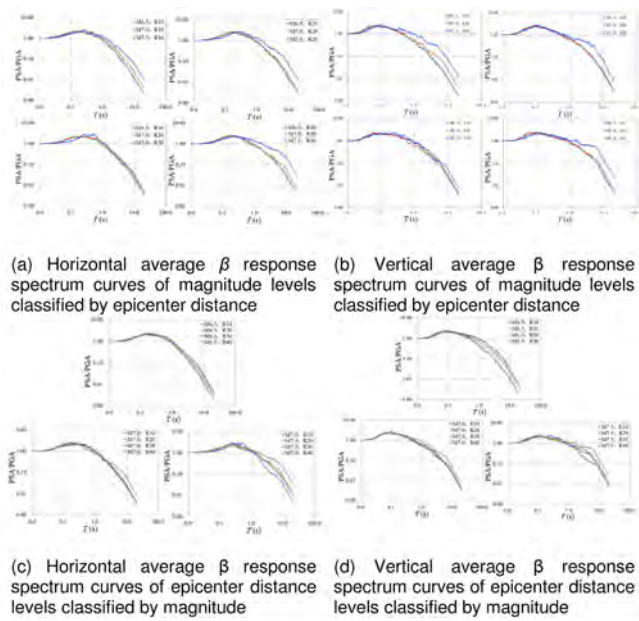

(a) Horizontal average β response spectrum curves of magnitude levels classified by epicenter distance

(b) Vertical average β response spectrum curves of magnitude levels classified by epicenter distance

(c) Horizontal average β response spectrum curves of epicenter distance levels classified by magnitude

(d) Vertical average β response spectrum curves of epicenter distance levels classified by magnitude

Fig. 1
β Response Spectrum Database Categorized by Magnitude and Epicenter Distance
(Cited from Cuiran Zhang)

Based on the magnitude *M* and epicentral distance *R* of the occurring earthquake, the site-specific design β response spectra can be quickly obtained from the database through stepwise interpolation.

The corresponding seismic motion time history can be generated by the site-related peak acceleration and β response spectrum determined by the magnitude *M* and distance *R* of the earthquake.

2.2. Establishing an earthquake response analysis model that integrates strength and stability in an open wave system

In traditional concrete dam seismic design, the calculation model for seismic response analysis is generally performed as a closed vibrational system. As the calculation model is based on the assumption of a massless foundation, obviously the analysis method does not match the actual situation. To overcome this unrealistic traditional approach, it is necessary to shift from a closed vibrational system to an open wave system, taking into account the foundation rock mass, the dissipation of seismic wave energy towards distant areas, and the interaction between the dam body and the foundation rock mass. For this purpose, the foundation needs to be divided into near-field foundation, which takes the actual complex geological structure and dam site topography into consideration, and far-field foundation, which can be treated as homogeneous elastic bodies. The latter is represented by artificial boundaries capable of transmitting or absorbing the escape energy of scattered wave. The dam body and near-field foundation are combined into a generalized dam structure. Besides, in current seismic design, the dam body's strength and stability against sliding are checked separately, regardless of their dynamic coupling effects. Actually, localized overstressed cracking or even upstream-downstream through-cracking may not necessarily mean overall instability. The traditional "rigid body limit equilibrium method" based on numerous assumptions, is entirely unsuitable for dynamic stability check under seismic action. The dynamic coupling effects between dam body strength and sliding stability under seismic action should also be considered. As academician Jiazheng Pan clearly pointed out in his book *Gravity Dam Design,* "How to apply the analysis results of finite element method to verify the sliding stability problem (thus integrating stress and stability requirements into a single problem for comprehensive resolution) is an issue that needs further study." Therefore, it is necessary to establish an earthquake analysis model that integrates strength and stability, as shown in Fig. 2.

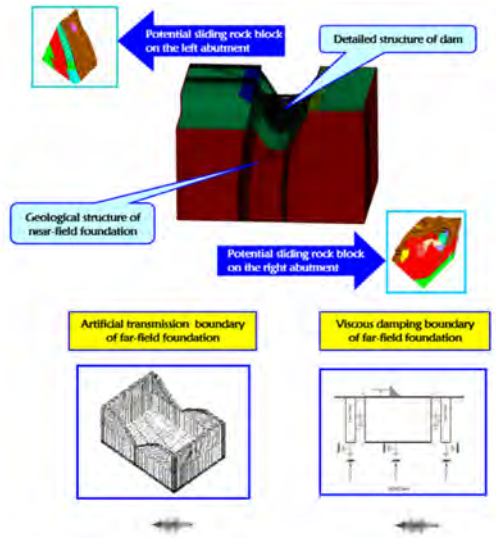

Fig. 2
Analysis model for earthquake response of generalized dam structure as an open wave system

The above model includes the following key points: dynamic interactions among the dam body, foundation, and reservoir water; detailed structures within the dam body such as longitudinal cracks, transverse cracks, flood outlets and pier structures; near-field foundation of dam body representing terrain and various geological structures; sliding blocks of rock mass on both sides of the dam abutment; artificial boundaries (usually viscoelastic and transmissive boundaries) for simulating dissipation of seismic wave energy towards far-field foundation.

For important high dam projects, it is necessary to retain the finite element model and parameters of seismic response analysis so that recheck calculations can be carried out promptly after an earthquake.

2.3. The constitutive relationship of generalized dam structure materials shifting from linear elasticity to cracking damage nonlinearity

To simulate the failure process of broad dam structure composed of concrete and foundation rock mass as quasi-brittle media under earthquake action, it is

advisable to adopt a constitutive relationship based on damage mechanics, that is, to use the damage variable ($0 \leq D \leq 1$) to characterize the strength that continuously declines after surpassing the peak along with the elastic modulus. The residual strain of the dam material is due to its expansion and initiation of microcracks during cyclic loading, which makes it difficult to recover during unloading. Therefore, this residual strain is completely different from the plastic strain characterized by flow and strengthening laws derived from crystal slip and dislocation. Certainly, the damage constitutive behavior of dam material needs to rely on the test results of axial tensile and compressive damage and failure process of concrete under cyclic loading.

The steps for solving the generalized dam material damage process in each time step using the stepwise integration method shown in Fig. 3 are as follows:

1. For the three-dimensional finite element model of the generalized dam material, determine the main tensile and compressive strains ε_t and ε_c, and their weighting factors *r*.
2. The damage surface function *F* is determined by the stress state. When *F* is greater than or equal to 0, the system material enters a nonlinear damage evolution process from linear elasticity.
3. Based on the test results of the material's axial tensile and compressive dynamic cyclic loading, organize the curves of residual strain ε^P, strength σ, and damage variable *D* as functions of deformation *w*, such as *w*-σ and *w*-*D*, to analyze the damage evolution law.
4. According to the tensile and compressive principal strains and weighting factors, the equivalent elastic modulus after damage is comprehensively obtained, and then the finite element model of the three-dimensional system is returned for iterative solution. (For details, see references [4] and [5]).

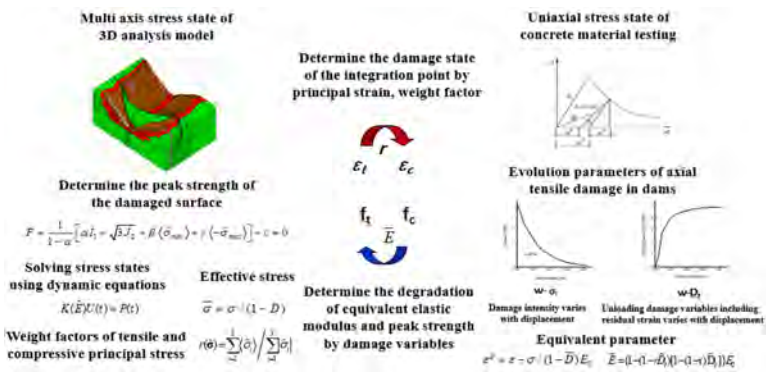

Fig. 3
Schematic diagram of iterative solution for three-dimensional system and uniaxial damage evolution analysis

2.4. Determining the critical criteria for seismic failure of the system

The maximum displacement response u_{max} of the key parts of the dam body is used as the parameter to evaluate the seismic safety of the open wave system which integrates strength and stability. Since engineering dam sites vary in geological and topographical features and dam types, a uniform displacement threshold cannot be established to characterize the overall seismic failure of the system. Therefore, the ultimate state of overall instability of the structural system from quantitative change to qualitative change can only be characterized by the inflection point of the displacement seismic response of each key part of the system during seismic overloading. The overload factor k_e, calculated by the ratio of seismic accelerations at this point to the design seismic acceleration, is used as a quantitative index to measure the overall seismic instability of the dam body.

Fig. 4 illustrates the relationship between the maximum displacement response at critical points of a 300m high arch dam constructed in a strong seismic zone and the seismic overload factor k_e [6].

For important high dam projects, it is necessary to separately calculate the maximum displacement response u_{max} and the seismic overload factor k_e for representative locations at normal water level and dead water level. This is to ensure that after a strong earthquake, the u_{max}-k curve for the water level at the time can be obtained immediately through interpolation.

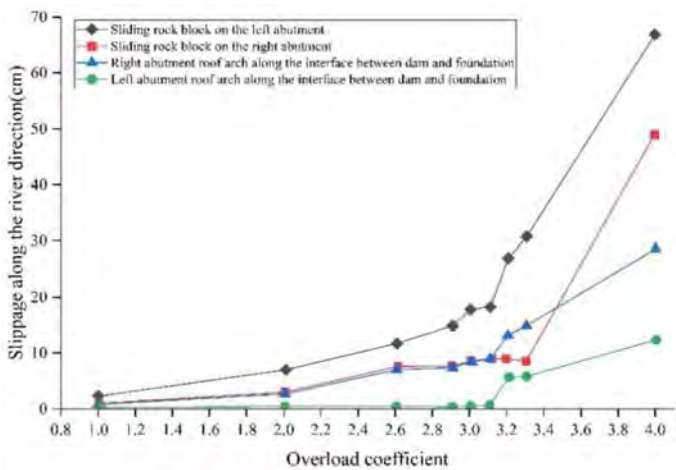

Fig. 4
Relationship curve between maximum displacements of critical points of generalized dam structure and seismic overload coefficients

2.5. Utilizing parallel algorithms and "cloud computing" high-tech

The storage and computing time for nonlinear seismic response analysis of the arch dam-foundation-reservoir system are very large, making conventional serial computing techniques inadequate. Therefore, a finite element parallel algorithm that divides the overall model into several sub-models has been developed (see Fig. 5). By employing a high-performance computing environment with supercomputers and high-speed interconnect networks for software compilation and debugging, environmental variable configuration, job submission, file editing, and result viewing, the "cloud computing" high-tech has been applied in practice (see Fig. 6).

Numerous engineering examples show that parallel cloud computing technology not only significantly accelerates the seismic response analysis of concrete dams but also can reveal the conditions of weak areas of the dam body throughout the earthquake. For example, in a certain project, the finite element mesh had a total of 425,568 elements and 404,090 nodes, with a total of 1,276,704 degrees of freedom, and the unit size of nonlinear parts was only 2 meters. The single-machine running time required 949.4 hours (nearly 40 days), whereas the "cloud computing" high-tech running time was only 18.9 hours, making the processing speed 50.23 times faster than single-machine computation.

Clearly, the above innovative concepts and method of seismic damage analysis for dam body and the application of "cloud computing" create a critical prerequisite for rapid assessment of the overall seismic safety of concrete high dams after an earthquake.

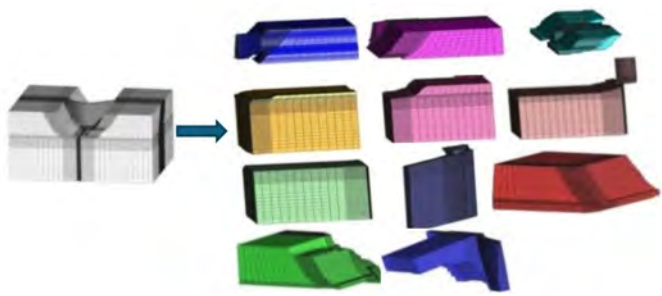

Fig. 5
An example of parallel algorithm that divides the entire model into sub-models

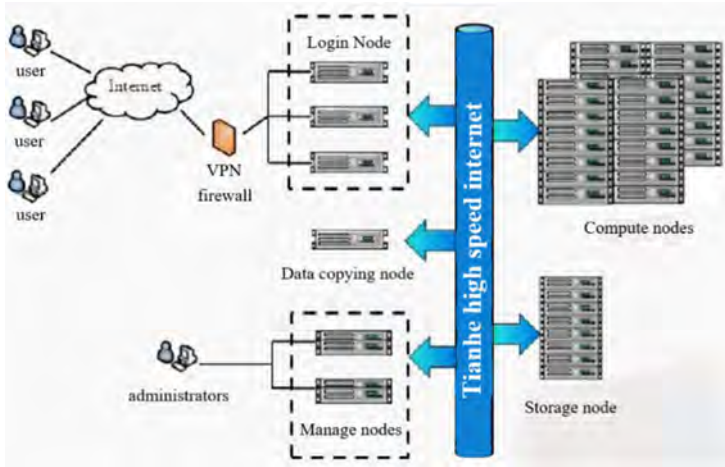

Fig. 6
Application of remote operation cloud computing through high-speed internet

3. METHODS AND STEPS FOR RAPID ASSESSMENT OF SEISMIC SAFETY AFTER AN EARTHQUAKE

3.1. Time history of seismic motion incident at the dam site

In China, earthquake input for engineering seismic resistance is primarily based on point source seismic model [1]. Therefore, it is necessary to promptly obtain the earthquake magnitude *M*, fault orientation, and the estimated center of the most severely damaged area (macro-epicenter) from seismic departments. Under current communication conditions in China, these basic data can be provided by seismic departments in a short time. The following steps determine the time history of seismic motion incident on the dam site.

1. Use the center of the generally most severely damaged area as the macro-epicenter. With its longitude and latitude compared to the dam site, the epicentral distance can be determined by:

$$D(km) = 111.2cos\{1/[sin\varphi_1 sin\varphi_2 + cos\varphi_1 cos\varphi_2(\theta_2 - \theta_1)]\} \quad (2)$$

where θ_1, φ_1 and θ_2, φ_2 are the longitudes and latitudes of the macro-epicenter and the dam site, respectively.

2. Historical earthquake records in China indicate that isoseismic lines, which represent seismic intensity attenuation, are approximately elliptical. When the

fault strike is considered the major axis *X*, and the orthogonal direction is the minor axis *Y*, the coordinates *x* and *y* of the dam site on its isoseismic ellipse, as well as the angle of intersection Ψ between *OD* and the *X*-axis can be determined (see Fig. 7).

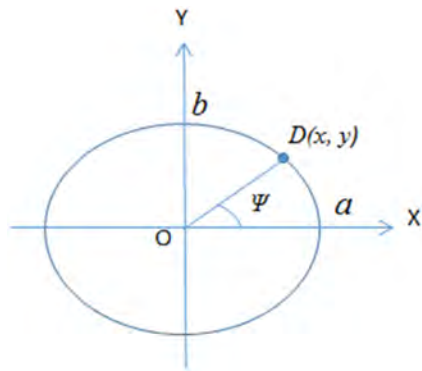

Fig. 7
Schematic diagram of isoseismic elliptical attenuation law

The attenuation law applied now in China is limited to two main axis direction of the isoseismic ellipse only. Therefore, the coordinates distance of the dam site *x* or *y* that causes the maximum acceleration at dam site using the attenuation relationship shown in formula (1) is selected as the macroscopic epicentral distance *R*. Thus, the peak ground acceleration value a_d at the free surface of the dam site and the peak incident seismic acceleration a_i at the base of artificial boundaries can be derived.

According to the earthquake magnitude *M* and distance *R*, the relevant β response spectrum can be quickly obtained using the above database through stepwise interpolation. With the seismic peak ground acceleration a_i and the β response spectrum, the incident seismic peak acceleration time history $a_i(t)$ for the dam site can be generated.

3.2. Seeking parameters for assessing overall seismic safety of dam system after an earthquake

The main parameters and criteria for evaluating concrete dams are: the maximum displacement response of the key parts of the dam under seismic

action, denoted as u_{max}, and the limit seismic overload coefficient k_e, which compares this displacement with the design value a_d when the displacement shows an inflection point as seismic input increases. These serve as quantitative criteria for determining whether the dam faces uncontrolled discharge of reservoir water.

Based on the finite element model and parameters for seismic response analysis of dam body during the design phase, the evaluation parameter u_{max}, which represents the seismic safety of broad dam structure under the occurrence of seismic action, can be obtained using “cloud computing”. The state of the dam body and its weak parts can also be displayed.

3.3. Assessment of overall seismic safety of dam body

3.3.1. *Basis for evaluation*

The main basis for engineering safety evaluation is approved design following current standard and successful completion acceptance meeting design requirements. The performance target for design earthquake is that if there is local damage, the dam should still function normally after repair. For major projects, the performance target against credible earthquakes is to prevent uncontrolled discharge of reservoir water.

3.3.2. *Evaluation system*

For major dam projects, curves of $u_{max} \sim k$ for normal and dead water levels must be provided. Interpolation generates the curve corresponding to reservoir water level during earthquake. In the curve, the overload coefficients k_d, k_c, $(k_c+k_e)/2$, and k_e, represented by the ratios of design earthquake, maximum credible earthquake, mean of maximum credible earthquake and ultimate earthquake, and acceleration of ultimate earthquake to design earthquake acceleration, are used to divide the evaluation system into four levels: I, II, III, and IV. These levels represent the overall seismic safety of generalized dam structure as: meeting the design earthquake requirements, meeting the maximum credible earthquake requirements, having moderate seismic damage, and having severe seismic damage, respectively (see Fig. 8). The seismic safety assessment parameter u_{max} is used to determine the seismic safety level of the dam body. According to the main weak parts of the dam body and their conditions revealed by response analysis results, proposals can be made about whether and how to lower the reservoir water level as emergency measures.

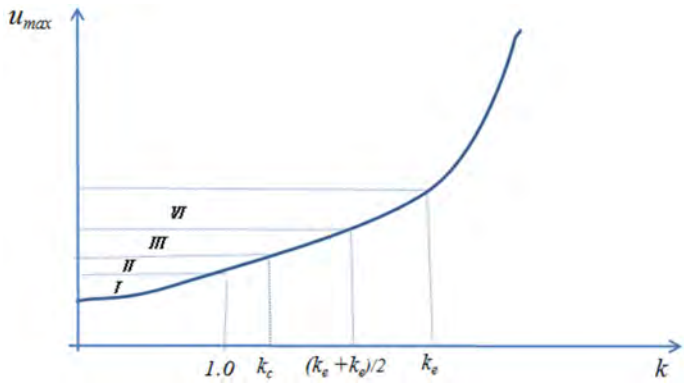

Fig. 8
The overall seismic safety evaluation system based on the seismic overload coefficient k_e by the inflection point of maximum displacement response u_{max}

If water level reduction is necessary, decisions on the required reduction amplitude should consider factors such as seismic conditions, flood conditions, and downstream actual situations. Additionally, based on the dam's post-earthquake actual performance state (including reductions in strength and elastic modulus of damaged units and the dissipation of crack boundary damping), the response of the dam body under static load at different water levels should be calculated so as to select the highest allowable water level that meets the design specifications for safe operation.

4. CONCLUSION

In summary, based on new ideas related to seismic input at the dam site, rapid calculation of the dam structure's seismic response, and assessment of overall seismic safety status of the dam structure, this paper introduces innovative approaches and methods, which include obtaining site-specific β response spectrum by stepwise interpolation based on magnitude and epicentral distance, more rational and straightforward inclusion of residual deformation in material damage analysis, characterizing the dam's critical overall seismic safety with seismic overload coefficient corresponding to the inflection point of maximum displacement response, and the application of parallel algorithms and cloud computing technologies. These innovations represent a significant departure from traditional practices, allowing for a "rapid" assessment of the dam's seismic safety and proposal of post-

earthquake emergency measures. Consequently, engineering operation departments can make scientifically based quantitative evaluations of seismic safety within a very short time after a strong earthquake and promptly implement appropriate measures to ensure the normal and safe operation of the project.

ACKNOWLEDGMENTS

The proposal of the above innovative concepts, ideas, and methods would not have been possible without the collective cooperation of our team and the collaboration of relevant departments. Special thanks are extended to Professor Zhang Cuiran for providing the response spectrum database based on magnitude and epicentral distance, and to senior engineers such as Guo Shengshan, Li Deyu, and Tu Jin for their support for this report.

REFERENCES

[1] GAO M. T. *Seismic ground motion parameter zoning map of China (Implementation Textbook)*. Beijing: China Quality Inspection Press, China Standard Press. 2015.

[2] CHEN H. Q. Overview of the seismic input at dam sites in China, *Earthquake Science*, Vol. 35, pp. 410–425, 2022.

[3] CHEN H. Q., ZHANG C. R. Study on the design response spectra related to seismic site conditions, *Journal of the China Institute of Water Resources and Hydropower Research*, Vol. 21, pp. 307–314, 2023.

[4] CHEN H. Q., LI D.Y., GUO S. S. Damage-rupture process of concrete dams under strong earthquakes, *International Journal of Structural Stability and Dynamics*. Vol. 14, pp. 1450021, 2014.

[5] CHEN H. Q. Seismic safety analysis of tall concrete dams: investigation and insights on critical challenges, *Earthquake Engineering and Engineering Vibration*, Vol.19, pp. 533–539, 2020.

[6] CHEN H. Q., WU S. X., DANG F. N. *Seismic safety of high arch dams*. Elsevier, Amsterdam, 2015.

COMMISSION INTERNATIONALE DES
GRANDS BARRAGES

VINGT-HUITIEME CONGRES DES
GRANDS BARRAGES
CHENGDU, MAI 2025

SHAKING TABLE TEST OF A WHOLE HIGH GRAVITY DAM MODELING DAM RESERVOIR FOUNDATION INTERACTION (*)

Hong ZHONG, Lijun ZHAO & Haibo WANG
State Key Laboratory of Simulation and Regulation of Water Cycle in River Basin, China
Institute of Water Resources and Hydropower Research, Beijing

Chunlei LI & Jin TU
State Key Laboratory of Hydraulics and Mountain River Engineering, College of Water Resource and Hydropower, Sichuan University, Chengdu

CHINA

SUMMARY

The seismic response of a RCC gravity dam with a height of 200m was investigated by shaking table test. All monoliths of the dam including the contraction joints, gate piers, sluice gates and guide walls together with the adjacent intake tower were modelled. The model system also included part of reservoir, partial foundation rock with topographic feature near the dam. A damping boundary made of viscous liquid was used to simulate the radiation damping of the unbounded foundation. The dynamic characteristics and dynamic response of the dam subjected to dynamic loadings including the design earthquake, maximum credible earthquake (MCE) as well as a sequence of overloading conditions with increasing amplitude was investigated. In the presented paper, the response of the dam subjected to design earthquake and MCE is presented. It's found that the natural frequency in the cross-stream direction is hardly influenced by the water

Essai sur table vibrante d'un grand barrrage-poids – modélisation du barrage, du réservoir et de l'interaction avec la fondation

DOI: 10.1201/9781003642428-132

level, while for the case of stream direction, the natural frequency decreased by 23.6% at the most. After all dynamic cases were finished, the fundamental frequency of the highest non-overflow monolith decreased by 10.12%. The effect of valley topography is more significant to the cross-stream acceleration of the dam base as compared to the stream counterpart. The acceleration, displacement, strain, contraction joint opening also differs from monolith to monolith. The research is beneficial to better understand the seismic response of a high gravity dam as a whole.

RÉSUMÉ

La réponse sismique d'un barrage-poids en RCC d'une hauteur de 200 m a été étudiée par un test sur table vibrante. Tous les éléments du barrage, y compris les joints de contraction, les piles de la vanne, les vannes et les murs de guidage, ainsi que la tour de prise d'eau adjacente, ont été modélisés. Le modèle comprenait également une partie du réservoir, une roche de fondation partielle avec des caractéristiques topographiques près du barrage. Une limite d'amortissement faite d'un liquide visqueux a été utilisée pour simuler l'amortissement par la fondation. Les caractéristiques dynamiques et la réponse dynamique du barrage soumis à des charges dynamiques, y compris le séisme de conception, le séisme maximal crédible (MCE) ainsi qu'une séquence de conditions de surcharge avec une amplitude croissante, ont été étudiées. La réponse du barrage soumis à un séisme de conception et à un séisme MCE est présentée. Il a été constaté que la fréquence propre dans le sens transversal du cours d'eau est à peine influencée par le niveau de l'eau, tandis que dans le sens amont-aval, la fréquence propre a diminué de 23,6% au maximum. Une fois tous les cas dynamiques terminés, la fréquence fondamentale du plot sans débordement le plus élevé a diminué de 10,12 %. L'effet de la topographie de la vallée est plus important pour l'accélération transversale de la base du barrag. L'accélération, le déplacement, la déformation, l'ouverture du joint de contraction diffèrent également d'un plot à l'autre. La recherche est bénéfique pour mieux comprendre la réponse sismique d'un grand barrage-poids.

1. INTRODUCTION

With the outburst of several strong earthquakes in recent years, it seems that the earth has come into an era with more strong earthquakes. The majority of high dams are being built or to be built in countries with active seismic activities such as China, Turkey, etc. Considering the possible disastrous results brought about by dam failures caused by strong earthquakes, seismic safety of high dams remains a crucial issue to be solved in dam construction.

As far as can be determined, no large concrete gravity dams with full reservoir have been subjected to extremely intense ground shaking [1]. The closest to such an event was the experience of Koyna gravity dam and Hsinfengkiang buttress dam. Cracks occurred in the dam and the dam remained operational after proper rehabilitation. This testifies the seismic performance of gravity dams, but it remains a great issue how would a high gravity dam perform if an extremely strong earthquake actually take place.

Shaking table test is the most straightforward and robust approach to investigate the performance of a gravity dam under strong earthquake shocks. Most research aims to study the dynamic response and damage process of the dam model during shaking. Tinawi et al. conducted shaking table experiments on four 3.4-m-high plain concrete gravity dam models to study their dynamic cracking and sliding responses [2]. Wang et al investigated the dynamic response, damage mechanism and safety evaluation of a 203 m-high concrete gravity dam on a shaking table [3]. Qiu et al performed shaking table test on the model of a 130-m-high gravity dam and studied its dynamic response as well as failure mode [4]. In order to examine the crack formation and stability of a gravity dam subjected to earthquake shocks, Phansri et al. performed a series of shaking table tests on three small-scale models of a monolith [5]. By including the dam-reservoir-foundation interaction, Mohsin et al. investigated the response of a concrete gravity dam model by shaking model test [6]. In addition to that, there are also research on the seismic reinforcement of gravity dams. For example, Xu et al. compared the seismic failure pattern of a reinforced dam monolith with the unreinforced counterpart by shaking table test to investigate the effect of reinforcement [7].

It's to be noted that in the research mentioned above, a typical monolith was generally chosen from a gravity dam and tested on the table instead of the whole dam. This enables the test to be carried out in a more cost-effective way, and still be representative of the response of the dam that is situated on wide and relatively flat valley. However, it's worthy to bear in mind that the ground motion in the cross-stream direction is ignored, and so is the dynamic interaction of adjacent monoliths. This could cause remarkable error for those dams built on V-shaped valley or when the cross-stream vibration is significant.

In the presented research, the shaking table test of a 200-m-high RCC gravity dam as a whole was performed. All monoliths of the dam together with the adjacent intake tower was modelled including all the contraction joints. The dam-reservoir-foundation interaction was properly modelled by incorporating near-field foundation with river valley topography, radiation damping of far-field foundation as well as a reservoir. The loading cases include excitation of artificial waves corresponding to design earthquake, maximum credible earthquake (MCE) and seismic overloading conditions. The dynamic characteristics of the dam as well as dynamic response under different loading conditions are presented.

2. OUTLINE OF THE TEST

The roller-compacted concrete gravity dam to be investigated is situated in the southwestern part of China, which is known for rich water resources and strong seismic activities. The dam is designed to have a maximum height of 200m and a crest length of 441.8m. The maximum thickness at the dam base is 184.1m. As shown in Figs. 1 and 2, the dam consists of sixteen monoliths, including two monoliths with spillways, two monoliths with bottom outlet, eleven non-overflow monoliths as well as one monolith with fold axis. In addition to that, to the left side of the fold-axis monolith, a row of intake towers is also included.

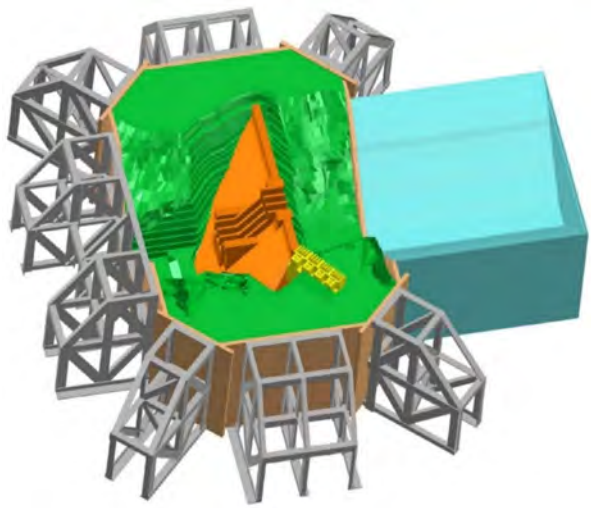

Fig. 1
Sketch of the test

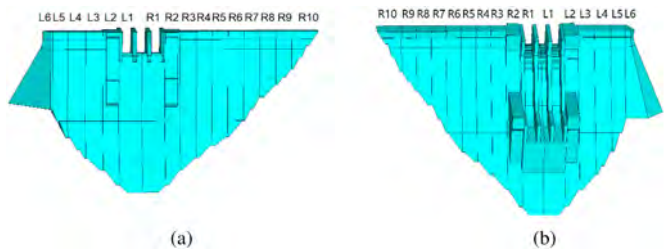

Fig. 2
Geometry of dam and numbering of dam monoliths. (a) and (b) are the upstream and downstream view respectively, L and R in the figure refers to Left and Right respectively.

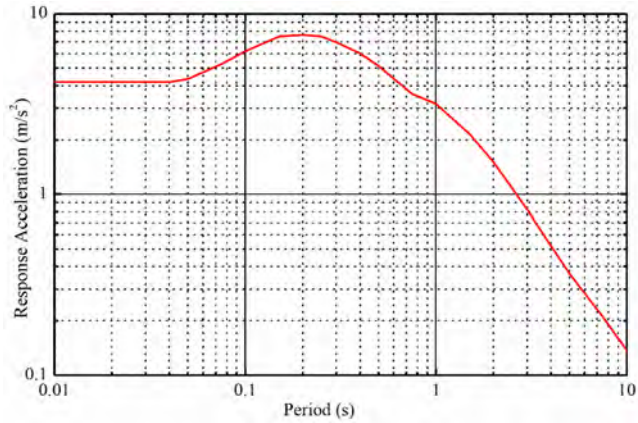

Fig. 3
Response spectrum of ground motion

According to the seismic risk analysis, the design intensity at the dam site is IX. Two levels of earthquake design are adopted for the dam. The peak ground acceleration (PGA) for the design earthquake is 0.43 g, with a return period of 5000 years, and 0.53 g for the MCE with a return period of 10000 years. Shown in Fig. 3 is the response spectrum. In the experiment three sets of acceleration time histories are generated using the response spectrum, the third set (wave 3) is displayed in Fig. 4.

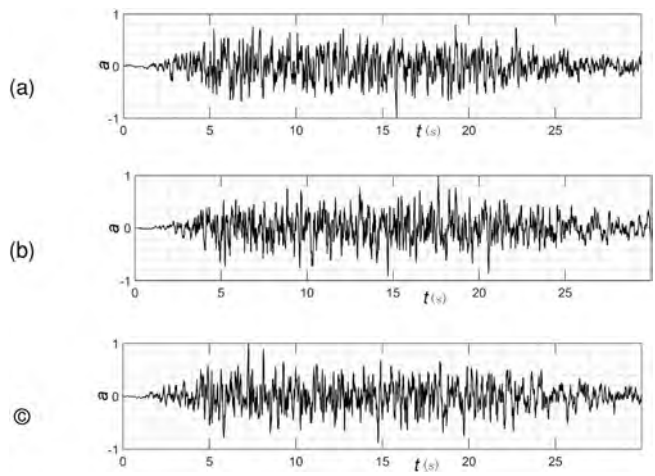

Fig. 4
Normalized acceleration time history. (a), (b) and (c) are the stream component, cross-stream component and vertical component respectively.

2.1. The test facility

The shaking table in China Institute of Water Resources and Hydropower Research (IWHR) is employed to perform the test. The size of the table is 5m×5m and maximum payload is 20000 kg. It provides six controlled degrees of freedom, and the working frequency band ranges from 0.1Hz to 120 Hz. The maximum acceleration, velocity as well as displacement are 1.0 g, ±400mm/s, ±40mm in the horizontal direction respectively, and 0.7 g, ±300mm/s, ±30mm in the vertical direction respectively. Almost all high arch dams built in seismic-active zones in China have been tested on this shaking table [8][9], as well as equipment in nuclear power plants and other industrial facilities.

2.2. Design of the test

The gravity dam together with a reservoir and the near-field foundation are modeled. Considering the size and payload of the shaking table, the ratio scale in geometry is taken as 1/200, resulting in a heigh of 100 cm and crest length of 220 cm for the model dam. The near-field foundation has a maximum height of 133.4 cm, the horizontal extensions are 320 cm and 220 cm in the cross-stream direction and stream direction respectively. A reservoir with a length of 270cm in the stream direction is modeled, which equals 2.7 times the dam height. A waterproof membrane of 0.1 mm thickness is overlayed on the dam, which implies that hydraulic fracture is not investigated.

2.3. Similarity relation

Concerning the similarity relation between the prototype and the model, since the test is performed in the normal gravitational field, the acceleration scale is 1.0. Water is used for the liquid in the reservoir, so the density scale of materials is also 1.0. The selection of elastic modulus of the model material should ensure that the dominant vibration frequencies of the model dam fall within the working frequency of the shaking table, and the material is better to be easily available. In the current study, the strain scale is 1.0, so the elastic modulus scale is equal to the geometry scale, which is 200.0. Based on the four scales mentioned above, the scale of other quantities can be obtained, which are listed in Table 1.

Table 1
Similarity scales of the test

QUANTITY	SCALE	QUANTITY	SCALE
Geometry*	C_l = 200	Frequency	C_f = 0.07071
Density*	C_ρ = 1.0	Deformation	C_δ = 200
Elastic modulus*	C_E = 200	Strain	C_ε = 1.0
Acceleration*	C_a = 1.0	Stress	C_σ = 200
Time	C_t = 14.142		

Note: * represents basic similarity scale.

2.4. Model material for the hydraulic structure

The response of the dam subjected to shaking including elastic response and damage is studied. As it's known that concrete dams suffer damage mainly due to excessive tensile stress in strong earthquakes, so the model material for the dam is expected to reflect tensile cracking of concrete. Since it's very difficult if not impossible to find a model material that fully meets the requirement of similarity for the period beyond yielding point, it's appropriate to use a brittle model material instead that meets the requirement of elasticity similarity, so that the elastic response and crack initiation of the dam can be well modeled.

According to the tensile strength and elastic modulus of mass concrete obtained by material test also performed previously in the lab of IWHR, the mean static axial tensile strength of C20 concrete is 1.71 MPa, and the mean static flexural strength is 2.63 MPa. So the corresponding axial tensile strength and flexural strength for the model material should be around 0.00855 MPa and 0.01315 MPa respectively. The elastic modulus for axial compression and axial tension are 26.9 GPa and 26.4 GPa respectively, so the corresponding values of the model material are 134.5 MPa and 132.0 MPa respectively. The actual elastic modulus of the model material ranges between 110 MPa and 150 MPa.

The model material is a mixture of baritite, lead oxide and talcum powder, from which bricks typically with a size of 10 cm $\times$ 10 cm $\times$ 15 cm are made by compression moulding. The elastic modulus, tensile strength and mass density of the model material is controlled by adjusting the mixing ratio of the mixture and the pressure applied when compressing the mixture into bricks. The bricks are carefully modified to wedges, and then bonded together with adhesives to construct the model dam. For the contraction joints, no adhesive is applied between the bricks to naturally form the joints.

The gate piers, guide walls and intake towers are constructed by reinforced concrete for the prototype, the strength of which is significantly higher than plain concrete. In the presented test, the damage of these structures and elements are not considered, so rubber is used for the model. Concerning the sluice gate, since the dynamic response of the gate is not concerned, and the thickness of the prototype gate is very small, it wouldn't be easy to fabricate a model gate strictly observing the similarity law. So instead, a thin aluminum plate with a thickness of about 3 mm is placed between and glued to the gate piers to retain water.

2.5. Model material for the foundation

The foundation rock is assumed as elastic, and a special rubber is used. According to the geological condition, mainly two kinds of rocks are involved in the project. The slightly-weathered rock has a deformation modulus of 16GPa, and the weakly-weathered rock is 9GPa. So according to the similarity law, the dynamic deformation modulus of the rubber are 72 MPa and 128 MPa respectively. The mass density of the rubber is 2400 kg/m^3. Rubber plates of the size 50 cm $\times$ 50 cm $\times$ 6 cm are produced in the rubber factory, then further machined and spliced with adhesives to form the foundation which contains the topography features in the valley.

2.6. Viscous boundary

To model the radiation damping of the unbounded foundation, a layer of viscous liquid known as methylsilicon rubber is introduced at the outer boundary of the foundation [8][9]. The damping coefficient c_t of the viscous liquid is related to its viscosity by the following relation:

$$c_t = \rho v = \frac{\eta_a}{\Delta L} \tag{1}$$

where $\triangle$L is the thickness of the liquid layer, ρ and v are the mass density and shear wave velocity of the foundation model respectively, where η_a is the viscosity of the viscous liquid and η_a=7000 Pa·S.

2.7. Ground motion input

The bottom of the foundation is fixed to the shaking table, and this differs from the situation of the prototype where the foundation extends to infinity. In the test, with regard to the model, the ground motion is input at the foundation bottom, which is identical to that of the table surface, and the latter is obtained by the motion at the elevation of the prototype foundation corresponding to the table surface. So prior to the test, numerical simulation of the dam-reservoir-foundation system is performed to derive the motion of the foundation by employing the visco-elastic artificial boundary model. It's to be noted that the motion of the foundation at a given elevation is not consistent at different locations, so the average motion at the elevation corresponding to the table surface is used to derive the motion of the shaking table.

2.8. Test instrumentation

Six types of response of the dam are measured, including the acceleration, displacement, strain, contraction joint opening, relative displacement of the gate piers and hydrodynamic pressure. The signal channels for the six types of response are 47, 8, 109, 13, 2 and 10 respectively, which sums up to 189 signal channels.

The accelerometers are mounted at the dam crest of typical monoliths and upstream face of monolith 3# at different elevations. The acceleration at the river valley near the dam toes of typical monoliths as well as foundation top and table surface are also measured. Concerning the intake tower, two triaxial accelerometers are mounted at the top and bottom of the tower respectively. The accelerometers are chosen as light as possible to minimize the influence on the vibration of the dam.

Laser displacement sensors are mounted on the crest of typical monoliths to measure the stream displacement. One additional sensor is used to measure the cross-stream displacement of the gate pier. Since the laser sensors work without contact with the dam, their weight has no influence on the vibration of the dam.

Strain gauges are mounted at the upstream and downstream surfaces of the dam, particularly at the locations characterized by high stress level, including the slope changing area, dam heel and dam toe. The vertical strain near the bottom of the gate piers are also measured. To investigate the strain in the cross-stream direction, several gauges are also mounted near the dam crest and at the upper half of the dam.

Gauges to measure the opening of the contraction joints are also mounted for all the joints of the dam and the joint between the dam and the intake tower.

LVDT is mounted to measure the relative displacement of the gate piers, one between side gate pier and middle pier, and the other one between two adjacent middle piers.

The hydrodynamic pressure at the upstream face at four different elevations of typical monoliths is also measured.

2.9. Loading cases

Shown in Table 2 is a list of the loading cases that have been tested. At the beginning of the test, white noise was input in the system for both empty reservoir and full reservoir. Then the excitation of three sets of artificial waves of design earthquake level was carried out. For the MCE, only one set of artificial waves was tested in order to minimize the accumulative damage to the dam. After that, over-loading cases with increasing amplitude of acceleration were carried out. Right after the test of each artificial wave, white noise was excitated. Totally 21 cases have been tested.

Table 2
Loading cases

CASE	TYPE OF EXCITATION	WATER LEVEL	LOAD LEVEL
1	White noise	Empty reservoir	
2	White noise	Full reservoir	
3	Artificial wave1	Full reservoir	Design earthquake
4	Artificial wave2	Full reservoir	Design earthquake
5	Artificial wave3	Full reservoir	Design earthquake
6	White noise	Full reservoir	
7	Artificial wave	Full reservoir	MCE
8	White noise	Full reservoir	
9	Artificial wave	Full reservoir	1.5 times design earthquake
10	White noise	Full reservoir	
11	Artificial wave	Full reservoir	2.0 times design earthquake
12	White noise	Full reservoir	
13	Artificial wave	Full reservoir	2.5 times design earthquake
14	White noise	Full reservoir	
15	Artificial wave	Full reservoir	3.0 times design earthquake
16	White noise	Full reservoir	
17	Artificial wave	Full reservoir	3.5 times design earthquake
18	White noise	Full reservoir	
19	Artificial wave	Full reservoir	4.0 times design earthquake
20	White noise	Full reservoir	
21	White noise	Empty reservoir	

3. TEST RESULTS

3.1. Dynamic characteristics of the dam

The natural vibration frequency of a monolith can be determined according to the transfer function of the acceleration time histories that have been recorded during the white noise excitation. Listed in Table 3 are the natural vibration frequencies obtained by the acceleration recorded at the dam crest for typical dam monoliths.

It can be seen that the vibration frequencies for different monoliths in the cross-stream direction are close to each other, both for empty reservoir and full reservoir, implying that the integrity of the dam is fairly good under slight amplitude vibration. For empty reservoir and full reservoir, the frequencies of monolith L1# are 30.44 Hz and 30.42 Hz respectively, and it's the lowest among all monoliths. The frequencies of the remaining monoliths range between 31.0 Hz and 31.5 Hz.

Table 3
Fundamental frequency of the dam (Hz)

	MONOLITH	EMPTY RESERVOIR	FULL RESERVOIR	DIFFERENCE
Cross-stream excitation	R9#	30.96	31.06	0.3%
	R6#	31.03	31.05	0.1%
	R3#	31.24	31.27	0.1%
	L1#	30.44	30.42	−0.1%
	L5#	31.42	31.37	−0.2%
	L6#	31.47	31.41	−0.2%
Stream excitation	R9#	31.94	31.89	−0.2%
	R6#	33.36	31.96	−4.2%
	R3#	36.25	31.73	−12.5%
	L1#	39.39	30.11	−23.6%
	L6#	25.79	25.24	−2.1%

For the case of stream direction, the difference in the frequency of different monoliths for empty reservoir is remarkable, and the frequency of the monoliths with spillway is higher than the rest. When the reservoir is filled with water, the frequencies of all monoliths decrease. The frequency of monoliths in the riverbed decreases more than those on the bank slopes. For example, the frequencies of monolith L3# are 36.25 Hz and 31.73 Hz for empty reservoir and full reservoir

respectively, with a decrease of 12.5%. Monolith L1# has the highest frequency for empty reservoir, with is 31.94 Hz. For the case of full reservoir, the frequency has dropped by 23.6% to 30.11 Hz. By comparison, the frequency of monoliths on the bank slopes decreases by less than 5%. Similarly, monolith 6#, which has a very narrow upstream face, is affected by the change in water level only by 2.1%. So for a full reservoir, the frequency of all monoliths tends to get closer.

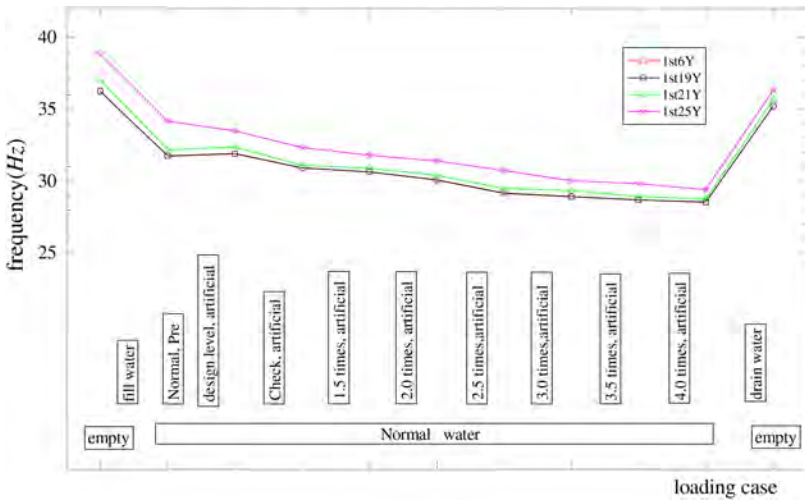

Fig. 5
Fundamental frequency of monolith R3#

Taking monolith R3# as an example, the fundamental equation of the monolith during the whole test is investigated (Fig. 5). The four measuring points are all on the downstream face, in which 6Y is positioned at the dam crest, 19Y at the slope-changing area, 23Y and 25Y at about 2/3 and 1/3 of the dam height. It can be seen that for all loading cases, the fundamental frequency measured increases from the dam crest to downwards, but the variation of the frequency with the loading process is consistent.

From the data measured by 6Y, it's found that the fundamental frequency in the stream direction decreases significantly during the process of reservoir filling. After the shaking of the three sets of artificial waves of design earthquake, the frequency basically doesn't change, implying that the dam remains elastic. After the shaking of the MCE, a decrease of 3.11% in the frequency is observed, reflecting that the dam has suffered damage. For the overloading cases with increasing

acceleration amplitude, the frequency keeps on decreasing but to different degree. After the overloading cases with amplitude 2.0 times and 2.5 times the design PGA, the frequency decreases by 1.89% and 3.00% respectively, which are among the highest during the overloading process. When all the dynamic loading cases have finished, the frequency has decreased by 10.12% as compared to the initial value for a full reservoir.

3.2. Acceleration response of the foundation

Shown in Fig. 6 is the distribution of acceleration amplitudes along the valley for the design earthquake and MCE. It can be seen that the valley topography is significant to the motion of the dam base. For both stream and cross-stream acceleration, the amplitude increases from the riverbed to the bank slopes. Regarding the ratio of acceleration amplitude at the elevation of dam crest to that of the dam base, the maximum value ranges from 1.8 to 2.5 in the stream direction, and 2.7 to 3.1 in the cross-stream direction. The effect of valley topography is more significant to the cross-stream acceleration as compared to the stream counterpart.

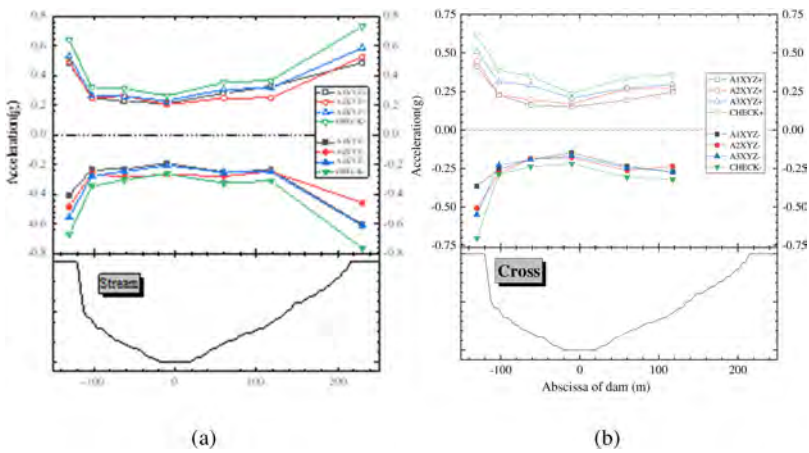

Fig. 6
Acceleration amplitude along the valley. (a) and (b) are the stream and cross-stream component respectively.

3.3. Acceleration response of the dam

Shown in Fig. 7 is the distribution of stream acceleration amplitudes of the dam crest for design earthquake and MCE. It's found that for the design earthquake, the distribution of acceleration amplitudes for the three sets of artificial waves are consistent. The maximum acceleration occurs at monolith R3#, which are 2.000g, 1.976g and 2.071g respectively. The acceleration decreases from the monoliths in the riverbed to those on both slopes. The distribution of acceleration amplitude for MCE is similar, with a maximum value of 2.195g.

Concerning the cross-stream acceleration, the difference in the amplitudes of different monoliths is relatively less significant. The acceleration amplitudes range from 0.4g and 0.9 for the design earthquake and MCE. The maximum acceleration also takes place at monolith R3#, with an amplitude of 0.637g, 0.712g and 0.707g for design earthquake and 0.964g for MCE. The amplitude of monoliths at the left bank is approximately slightly higher than those at the right bank.

Comparing the overall response of the dam under excitation of the three sets of artificial waves, the response of wave 3 is comparable with that of wave 2, and greater than that of wave 1, so in the subsequent overloading test, the acceleration input is obtained by amplifying wave 3 with an amplification factor.

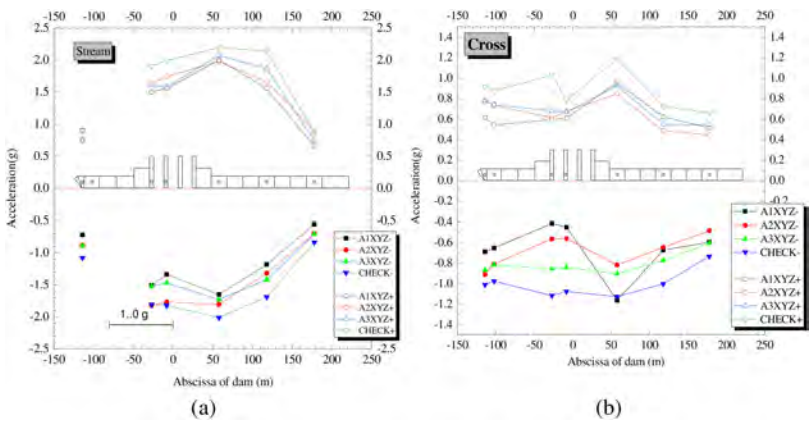

Fig. 7
Acceleration amplitude of the dam crest. (a) and (b) are the stream and cross-stream component respectively.

3.4. Displacement response of the dam

Shown in Fig. 8 is the distribution of displacement amplitude of the dam crest. It can be seen that the displacement towards the upstream and downstream is consistent. The maximum displacement occurs at the monolith R3#, and decreases to monoliths on both slopes. Under design earthquake and MCE, the maximum displacements are 0.378mm and 0.482mm, corresponding to 75.6mm and 96.4mm for the prototype.

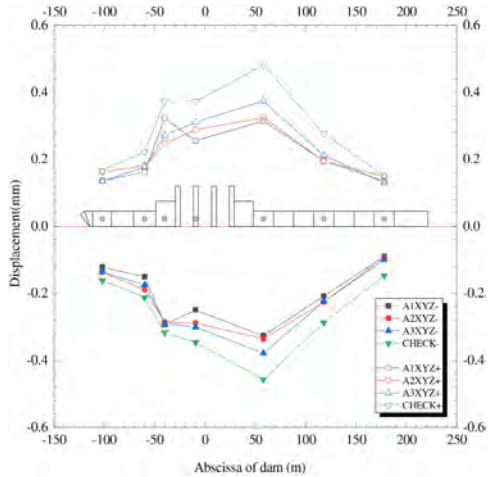

Fig. 8
Displacement amplitude of the dam crest.

3.5. Strain response of the dam

Under the excitation of design earthquake and MCE, Fig. 9 shows the envelope of tensile and compressive strain on the dam surface. It can be seen that the distribution of strain is similar for the load cases presented. High tensile strain takes place at the upper part of both dam surfaces. Under design earthquake, the maximum tensile strain at the upstream and downstream surface are 116.1$\mu\varepsilon$ and 77.7$\mu\varepsilon$ respectively, while under MCE, the tensile strains are 175.4$\mu\varepsilon$ and 70.8$\mu\varepsilon$ respectively. It's to be noted that the strain measured is the dynamic strain, the total strain is a sum of the static strain and dynamic strain. For the case of design earthquake, the total tensile strain is inferred to be slightly greater than the ultimate strain of the model dam material and microcracks might have taken place, however, no crack was witnessed during the test, and the natural frequency of the monolith has not decreased significantly. While for the case of MCE, as the tensile strain

increased, the damage got worse and decrease in the natural frequency of the monolith was significant.

High compressive strain also took place at the upper part of the dam. The envelope of compressive strain at the dam surfaces due to design earthquake and MCE are consistent. Under design earthquake, the maximum compressive strains at the upstream and downstream surface are -96.9$\mu\varepsilon$ and -104.2$\mu\varepsilon$ respectively, while under MCE, the strains are -111.3$\mu\varepsilon$ and -116.0$\mu\varepsilon$ respectively.

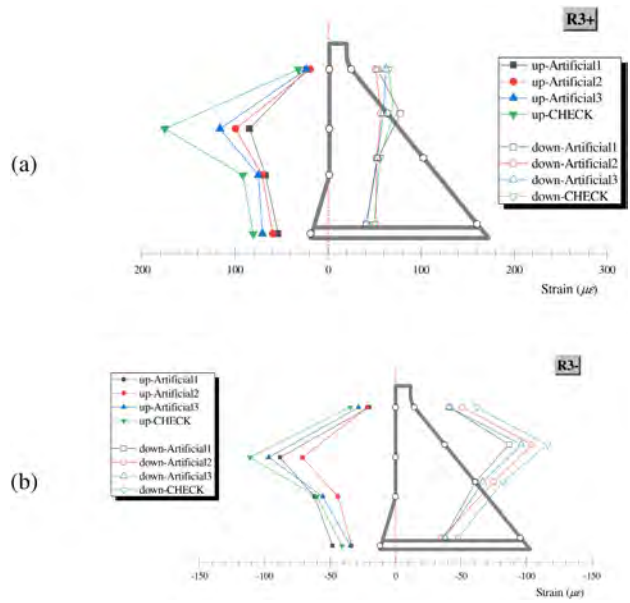

Fig. 9
Strain at dam surfaces of monolith R3#. (a) and (b) are the envelope of tensile and compressive strain respectively.

3.6. Displacement of contraction joints

Fig. 10 shows the displacement of all the contraction joints at the dam crest. In the figure negative value refers to opening, but actually what the gauges measured is a vector sum of opening and slippage. In some cases, the slippage could be greater than the opening. But since it's not possible to differentiate the two, the displacement sum is referred to as opening for convenience in the following.

Under design earthquake, the opening of joints on the left side are generally very small except for the joint between L6# and the intake tower, which is -0.021mm and corresponds to -4.2mm for the prototype. For the joints on the right side, large opening and small opening alternates. Relatively large opening takes place at the joint between monoliths L4# and L5# as well as the one between R6# and R7#, with openings of -0.018mm and -0.029mm, corresponding to -3.6mm and -5.8mm for the prototype.

Under MCE, the opening of all joints increases as compared to the case of design earthquake. But the joints with large openings for design earthquake still outperforms the others for MCE. The one with maximum increase is between monoliths L4# and L5#, which an increase of 50%. The maximum opening took place at the joint between R6# and R7#, which was -0.029mm and corresponded to -5.8mm of the prototype.

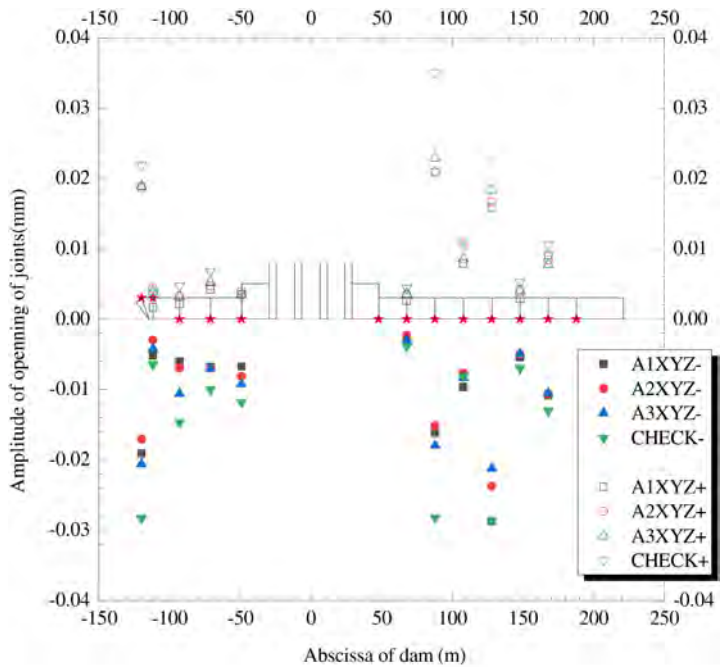

Fig. 10
Displacement of contraction joints

4. CONCLUSIONS

The seismic response of a 200-m-high dam was investigated as a whole by shaking table test. All the monoliths including the contraction joints as well as the adjacent intake tower was modelled. In addition, the near-field foundation with topography, radiation damping of far-field foundation and a reservoir was also modelled. The dynamic characteristics and dynamic response of the dam subjected to excitation of artificial waves corresponding to the design earthquake and MCE was studied. It's found that the response differs for monoliths of different height and different cross section. And the response of the dam in the cross-stream direction is also significant.

ACKNOWLEDGMENTS

The authors are grateful for the financial support from the National Natural Science Foundation of China (No. 51979292).

REFERENCES

[1] CHOPRA A. K. *Earthquake Engineering for Concrete Dams: Analysis, Design, and Evaluation*. Wiley-Blackwell, 2020.

[2] TINAWI R., LEGER P., LECLERC M., *ET AL.* Seismic Safety of Gravity Dams: From Shake Table Experiments to Numerical Analyses. *Journal of Structural Engineering ASCE*, vol. 126, 2000.

[3] WANG M., CHEN J., WEI H., *ET AL.* Experimental investigation of a small-scaled model for overflow section of a high gravity dam on shaking table. *Advances in Mechanical Engineering*, vol. 11, 2019.

[4] QIU J. C., HE W. Q., ZHENG D. J., *ET AL.* Dynamic Failure Experimental Study of a Gravity Dam Model on a Shaking Table and Analysis of Its Structural Dynamic Characteristics. *Sensors*, vol. 24, pp. 1602, 2024.

[5] PHANSRI B., CHAROENWONGMIT S., YOOPRASERTCHAI E., *ET AL.* An experimental study on shaking table tests on models of a concrete gravity dam. *KSCE Journal of Civil Engineering*, vol. 19, pp. 142–150, 2015.

[6] MOHSIN A. Z., OMRAN H. A., AI-SHUKUR A. K. Shaking Table Tests on a Physical Model of a Concrete Gravity Dam. *International Journal of Scientific & Engineering Research*, vol. 6, issue 9, 2015.

[7] XU Q., LIU B., CHEN J., *ET AL.* Shaking Table Test and Numerical Simulation Study of the Reinforcement Strengthening of a Dam. *Buildings*, vol. 12, pp. 1955, 2022.

[8] WANG H. B., LI D. Y. Experimental study of Seismic Overloading of Large Arch Dam. *Earthquake Engineering & Structural Dynamics*, vol. 35, pp. 199–216, 2006.

[9] WANG H. B., LI D. Y. Experimental Study of Dynamic Damage of an Arch Dam. *Earthquake Engineering & Structural Dynamics*, vol. 36, pp. 347–366, 2007.

Q.111 - R.32

COMMISSION INTERNATIONALE DES
GRANDS BARRAGES

VINGT-HUITIEME CONGRES DES
GRANDS BARRAGES
CHENGDU, MAI 2025

STUDY ON THE VERIFICATION OF THE SEISMIC PERFORMANCE OF DAGANGSHAN ARCH DAM DURING LUDING EARTHQUAKE (*)

Jin TU, Hui LIANG, Deyu LI, Cuiran ZHANG & Shaoqing WANG
China Institute of Water Resources and Hydropower Research, Beijing

CHINA

SUMMARY

This study is based on the acceleration records of the dam body and bedrock obtained from the monitoring of the Dagangshan arch dam during the Luding earthquake, as well as other safety monitoring results, to conduct seismic verification analysis between numerical calculations and the dam's seismic performance. In the study, the acceleration records of the free-field measurement points at the dam site were used as the input seismic waves, and the concrete static and dynamic modulus and strength obtained from the dynamic mechanical property test of fully-graded concrete specimens were used as material parameters. Under the conditions of water level during the earthquake and other corresponding loads, the seismic wave response analysis method using viscoelastic artificial boundary to reflect the radiation damping effect of infinite foundation was adopted. The results of the calculation and analysis were verified by the acceleration response of multiple measurement points on the dam body, the opening degree of transverse joints, and the comprehensive stress of static and dynamic stress on the dam body. The results showed that the Dagangshan arch dam withstood the test of strong earthquakes in the Ms6.8 Luding earthquake, and there was no damage to the dam body after the earthquake.

**Vérification du comportement sismiques du barrage de Dagangshan pendant le séisme de Luding*

 DOI: 10.1201/9781003642428-133

The seismic safety performance of the dam-foundation system did not change, and it also verified that the seismic wave response analysis method of the dam-foundation system applied during the design and construction stage of the Dagangshan arch dam could reasonably simulate the seismic response of the dam.

RÉSUMÉ

Cette étude a effectué une analyse de validation sismique des calculs numériques et de la résistance sismique d'un barrage sur la base des enregistrements d'accélération du corps du barrage et du substrat rocheux obtenus par la surveillance du barrage-voûte de Dagangshan pendant le séisme de Luding, ainsi que d'autres résultats de surveillance de la sécurité. Cette étude a utilisé l'enregistrement de l'accélération des points de mesure en champ libre du site du barrage comme onde sismique d'entrée, et le module cinétique, statique et la force du béton obtenus par l'essai de performance mécanique dynamique de l'éprouvette de béton en série complète comme paramètres du matériau. La méthode d'analyse de la réponse aux ondes sismiques utilise des limites artificielles viscoélastiques pour refléter l'effet d'amortissement du rayonnement d'une base infinie dans les conditions de niveau d'eau et d'autres charges correspondantes pendant un séisme. Les résultats des calculs et des analyses ont été validés par la réponse en accélération de plusieurs points de mesure sur le corps du barrage, l'ouverture des joints transversaux et les contraintes statiques du corps du barrage. Les résultats montrent que le barrage-voûte de Dagangshan a résisté à un puissant tremblement de terre de magnitude 6,8 à Luding et que le corps du barrage n'a pas été endommagé après le séisme. La performance de sécurité sismique du système de base du barrage n'a pas changé. On a également vérifié que la méthode d'analyse de la réponse aux ondes sismiques du système de base du barrage appliquée pendant la phase de conception et de construction du barrage de Dagangshan peut raisonnablement simuler la réponse sismique du barrage.

1. INTRODUCTION

At 12:52:00 on September 5, 2022 (Beijing time), a Ms6.8 earthquake occurred in Moxi Town, Luding County, Ganzi Tibetan Autonomous Prefecture (29.59 degrees north latitude, 102.08 degrees east longitude), with a focal depth of 16km. The epicenter was located in Moxi Town, Luding County, Ganzi Tibetan Autonomous Prefecture, 21.0km away from the Dagangshan Dam.In this earthquake, all 21 strong earthquake monitoring points of the Dagangshan Dam were triggered, and strong

earthquake monitoring records of the free field of the bedrock and different parts of the dam body were obtained.

From a global perspective, there are very few important arch dam projects that have experienced strong earthquakes [1], and even fewer that have installed strong motion instruments and recorded seismic responses. The corresponding arch dam seismic damage is also very limited.The Pacoima Arch Dam suffered from the San Fernando earthquake (Ms6.6) on February 9, 1971 and the Northridge earthquake (Ms6.8) on January 17, 1994. The acceleration recorded along the river direction on the left dam abutment during the two earthquakes was 1.25g and 1.58g respectively. The San Fernando earthquake caused a 20cm displacement of the rock mass on the left bank of the dam and a 1cm opening of the structural joint of the buttress. After that, the reinforced Pacoima Arch Dam suffered a 50cm displacement of the rock mass on the left bank during the Northridge earthquake, with a residual opening of 5cm in the left bank buttress structural joint. However, other transverse joints opened during the earthquake and naturally closed after the earthquake. In the following decades, the seismic records and the aseismic performance of Pacoima Arch Dam have become the main data for seismic analysis and calculation verification. However, the 17 channels for strong earthquake monitoring of the Pacoima Arch Dam are located near the dam body or foundation, and there is no real free-field record of the bedrock. In 2008, Shapai Arch Dam withstood the test of the Ms.8.0 Wenchuan earthquake. Post-earthquake investigations showed that the main body of the dam was basically intact[3], but due to the damage of measuring instruments, no valuable seismic records could be detected near the Shapai Arch Dam and the dam site. Therefore, the study had to use the “stochastic finite fault method” [4]based on seismological physical models and empirical statistics to determine relevant parameters, and then calculate the seismic input of the Shapai Dam site during the Wenchuan earthquake. Combined with the seismic performance of the Shapai Arch Dam, a verification study of the earthquake situation during the Wenchuan earthquake was conducted[13].The strong earthquake monitoring records of the bedrock and dam body of the Dagangshan site under the MS6.8 Luding earthquake obtained this time provide extremely valuable information for testing the concepts, methods, and effectiveness of seismic design and research method for a number of high arch dam projects constructed in the strong earthquake areas of southwest and northwest China in the past three decades.

The Dagangshan Arch Dam with a height of 210m，is currently with the highest design seismic input level among the concrete dams higher then 200m in China. After the Luding earthquake, experts conducted on-site inspections and investigations and concluded that “the Dagangshan Dam was not damaged after the earthquake, and the engineering slope and resistance slope were intact; the flood discharge tunnel buildings were intact and could discharge floods normally”[14][15]. This study used acceleration records from the bedrock measurement points at the site as input to conduct a nonlinear seismic wave response analysis and verification of the dam-foundation system.

2. LAYOUT OF STRONG MOTION MONITORING INSTRUMENTS FOR DAGANGSHAN ARCH DAM

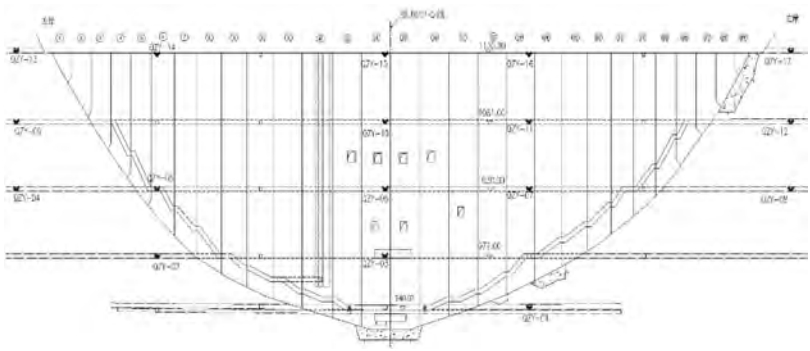

Fig. 1
Locations of seismic monitoring points on the dam body

The strong earthquake monitoring in the Dagangshan dam area is mainly arranged in the grouting adits on the left and right banks, the dam crest, and the dam body gallery.In addition, in order to record the seismic free-field motion in the dam site area, a strong-motion seismograph was installed on the stable bedrock near the access tunnel downstream of the dam.The dam body monitoring points basically consist of “five arches and three beams”, with the focus on the dam crest arch ring and arch crown beams.A total of 21 strong motion instruments are arranged in the dam, the mountains on both sides of the river, and the free field of the bedrock.

3. GROUND MOTION INPUT OF THE DAM SITE IN LUDING EARTHQUAKE

The time-history curve of three-directional acceleration records and the amplification factor spectrum of acceleration in each direction at the QZY21 bedrock free-field measurement poinis are shown in Figure 2. Figures 3 to 5 compare the acceleration response spectra at three directions with the scenario earthquake acceleration response spectra used for design earthquakes.

As shown in Figure 3, from the perspective of the amplification factor spectrum, the acceleration record of the QZY21 bedrock measurement point has a broad spectrum, especially in the period range of 0.5s to 1s along the river and across the river, where the amplification factor spectrum values are greater than that of the corresponding frequency band for the set earthquake. However, as shown in the

comparison of response spectra, the peak acceleration along the flow direction of the dam site bedrock measurement point is 213gal and the peak acceleration across the flow direction is 155gal, while the PGA of the Dagangshan design earthquake is 557.5gal. From Figure 4 to Figure 6, it can be seen that the acceleration response spectrum values of the design earthquake generally envelop the response spectrum of this earthquake in all frequency bands. But it should be noted that the spectrum value of the earthquake along the river with a period of 0.6s corresponding to the dam's fundamental frequency, is relatively close to the spectrum value of the design earthquake. The first-order mode of vibration causes the maximum response at the dam foundation, which may lead to a large seismic response of the dam.

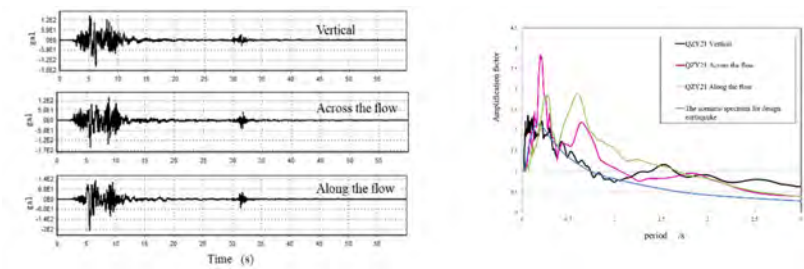

Fig. 2
Time-history curve and spectrum of amplification factors of acceleration in each direction at point 21 (bedrock free field).

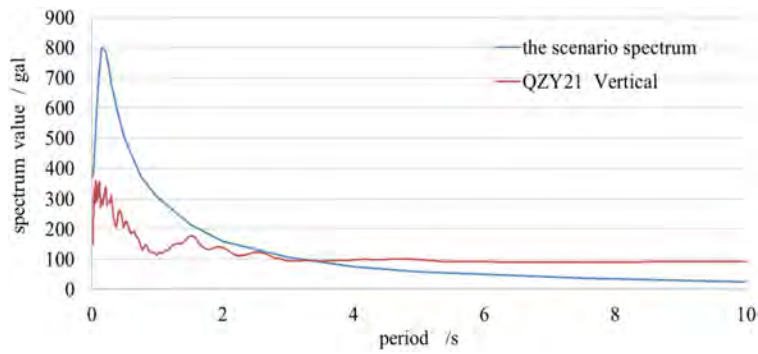

Fig. 3
Comparison of acceleration response spectrum of vertical direction at measuring point 21# and the scenario spectrum of the design earthquake

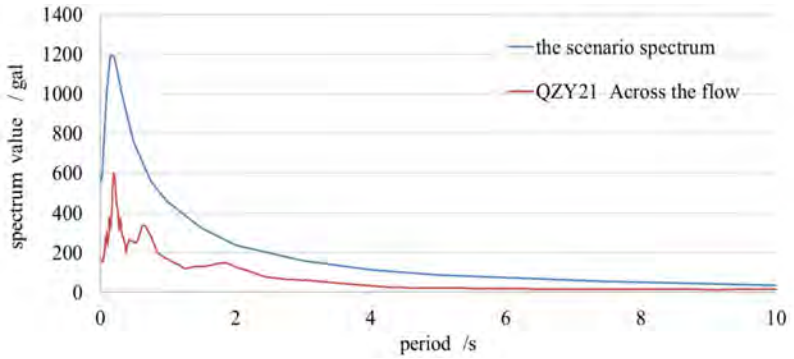

Fig. 4
Comparison of acceleration response spectrum of across the flow direction of measuring point 21# with the set earthquake spectrum of the design earthquake

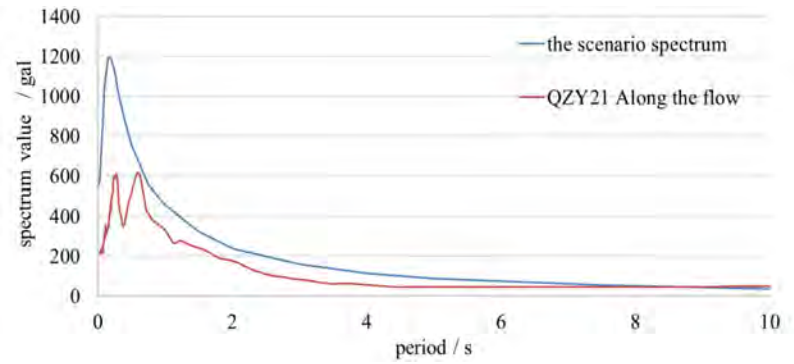

Fig. 5
Comparison of acceleration response spectrum of along the flow direction of measuring point 21# with the set earthquake spectrum of the design earthquake

4. PARAMETER VALUES OF DAM CONCRETE AND BEDROCK MATERIALS

Another key factor affecting the dynamic response of the dam is the selection of the main dynamic parameters of the dam concrete and bedrock soil materials. The concrete material parameters in the study are based on the dynamic performance test results of fully-graded concrete for the Dagangshan arch dam, and are

combined with the material parameters provided by the design to obtain values; The parameters of bedrock materials are mainly based on the design data provided.

4.1. Parameters of dam concrete materials

The concrete density of the dam is 2400kg/m^3.

The static elastic modulus of dam concrete is taken as the design value of 24GPa, and the Poisson's ratio is taken as the design value of 0.17.

The dynamic elastic modulus of dam concrete is based on the test value of fully-graded concrete. Considering that the variable amplitude cyclic loading method is more in line with the actual stress state of the dam under earthquake action, the test results of concrete specimens under dynamic cyclic loading should be used as the basis for determining its dynamic parameters.According to the test results, the average elastic modulus of fully-graded flexural-tensile specimens under variable amplitude cyclic dynamic loading is 35.2GPa. According to the provisions of the "Hydraulic Engineering Standard", the standard value of the elastic modulus of dam concrete can be taken as the 0.5 quantile value (i.e., the average value) of its probability distribution. Therefore, the dynamic elastic modulus is taken as 35.2GPa. The test gives an average value of 0.15 for the Poisson's ratio of fully-graded concrete. Considering that this value is close to the static Poisson's ratio of concrete provided by the design, which is 0.17, the dynamic value of Poisson's ratio is taken as 0.17. The average dynamic flexural-tensile strength of the dam's fully-graded concrete under variable-amplitude triangular wave loading is 3.97 MPa when the pre-static load is 40%, and the standard value is 3.37 MPa when the 80% quantile is taken.

4.2. Parameters of bedrock materials

For bedrock, the rock mass of the dam foundation is divided into four categories: II, III1, III2, and IV based on lithological characteristics, rock mass structure, degree of interlocking, weathering characteristics, and acoustic parameters. The parameters for the remote foundation are taken from the II category of rock mass parameters. Table 1 provides information for reference design to obtain the physical and mechanical parameters of bedrock materials.

The values of the stiffness coefficient and damping coefficient for the viscoelastic artificial boundary are determined by the following formula:

Table 1
Physical and mechanical parameters of rock mass in dam foundation

	DRY DENSITY	DEFORMATION MODULUS	POISSON'S RATIO
	ρ	E0	μ
	G/CM^3	GPA	
II	2.65	19.25	0.25
III 1	2.62	8.25	0.27
III 2	2.62	7.25	0.30
IV	2.58	2.25	0.35

Normal boundary:

$$K_n = \frac{E}{2r_b}, C_n = \rho c_p \tag{1}$$

Tangential boundary:

$$K_b = \frac{G}{2r_b}, C_b = \rho c_s \tag{2}$$

Wave velocity:

$$c_s = \sqrt{\frac{G}{\rho}} = \sqrt{\frac{E}{2(1+\nu)\rho}} \tag{3}$$

$$c_p = \sqrt{\frac{\lambda + 2G}{\rho}} = \sqrt{\frac{2(1-\nu)}{1-2\nu}} c_s \tag{4}$$

In the formula: r_b represents the distance from the bottom to the top of the foundation boundary; E represents the elastic modulus of the remote foundation medium; G represents the shear modulus of the medium; c_p represents the density of the medium; c_s is the compressional wave velocity of the medium outside the finite element model; λ, μ is the shear wave velocity of the medium outside the finite element modelis the Lame constant; ν is Poisson's ratio.

From the formula above, it can be seen that the energy absorption effect of viscoelastic boundaries and the calculation of free-field input are closely related to the value of the material parameters of the remote foundation.

5. ANALYSIS OF THE SEISMIC RESPONSE OF DAGANGSHAN ARCH DAM IN LUDING EARTHQUAKE

5.1. Calculating model

This study uses an explicit finite element method combined with a viscoelastic artificial boundary to analyze the seismic response of the Dagangshan arch dam. The overall finite element modeling of the dam-foundation is shown in Figure 6. Based on the dam shape and transverse joint location, the dam grid model and jointing are shown also.In the division of the finite element mesh of the bedrock, four categories of rock material zoning are considered.The near-field foundation of the entire finite element model includes a range of 1320 meters in the transverse direction, 920 meters in the longitudinal direction, and 320 meters vertically below the dam bottom, including artificial boundaries and contact boundaries with 28 transverse joints. The total number of nodes is 130,979, and the total number of elements is 120,925, including 4,722 nodes and 2,030 elements for the dam body.

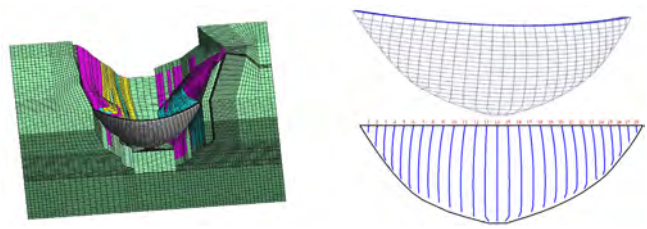

Fig. 6
Finite element model of the dam-foundation system

During the calculation process, static loads are applied based on the water level and other load conditions during the earthquake. After the static calculation is stable, seismic wave input is considered and seismic dynamic loads are applied. Rayleigh damping is used in the dynamic calculation, with a damping ratio of 0.05.

5.2. Acceleration response ratio comparison

Figure 7 shows the comparison between the calculated and measured values of acceleration vectors and maximum values at different locations on the dam surface. Figure 8 shows the comparison between the calculated and measured

acceleration time histories along the river direction for measuring points QZY14 and QZY16 after time synchronization.

From the comparison of the maximum acceleration values at different locations on the dam surface, it can be seen that except for the calculated values of the maximum acceleration values at the measuring points QZY6, QZY10, and QZY15 in the middle and upper elevations of the arch crown beam, which are slightly higher, the acceleration values at other locations are comparable to a certain extent, especially the maximum acceleration values at the measuring points QZY14 and QZY16 in the left and right 1/4 arch positions of the top arch and the measuring points QZY03, QZY05, and QZY07 at lower elevations, which are in good agreement.By comparing the time-history diagrams of QZY14 and QZY16 measuring points, it can be seen that in the calculated and measured acceleration time-history at the direction along the flow, the amplitude, frequency, and waveform are basically equivalent.

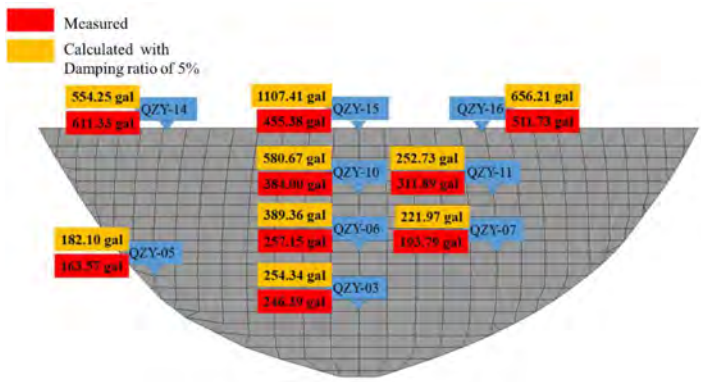

Fig. 7
Comparison of calculated and measured values of maximum acceleration vector at each measuring point

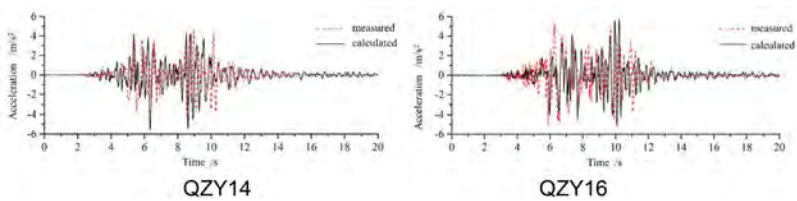

Fig. 8
Comparison of calculated and measured acceleration time history along the flow of measuring point QZY14 and QZY16

5.3. Comparison and analysis of transverse joint opening

Figure 9 shows the distribution of the maximum opening of each transverse joint at the top arch of the upstream and downstream surfaces during the earthquake. Figure 10 shows the time-history curve of the upstream and downstream opening of the No.12 transverse joint with the maximum opening.

The maximum opening of the transverse joints of the Dagangshan arch dam is not large, and the maximum opening of the upstream face of the No.12 transverse joint arch near the center of the dam is 2.96 mm. From the time history of the transverse joint opening, it can be seen that during the earthquake, there were only several instantaneous opening and closing processes between 13s and 20s when the seismic energy was concentrated. The maximum duration of a single opening of the transverse joint was only about 0.2s, with a large opening at the upstream and more open times at the downstream and a long total open duration. After the earthquake, both the upstream and downstream faces of the transverse joint arch were in a closed state.

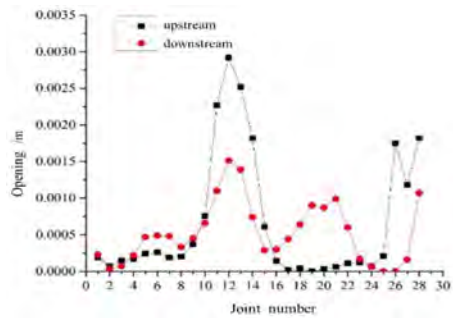

Fig. 9
Distribution of maximum opening of each transverse joint along the top arch

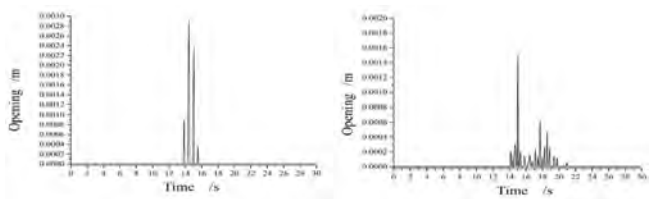

Fig.10
Time history of opening of upstream and downstream of 12# joint during earthquake

A set of joint meters is arranged in each irrigation area corresponding to the transverse joints of dams No.3, 5, 7, 9, 14, 18, 21, and 23 to monitor the change in the opening of the transverse joints. However, the joint meters can only provide information on the change in the opening of the transverse joints before and after the earthquake, and cannot track the opening of the transverse joints during the earthquake process, nor can they capture the maximum value of the opening of the transverse joints.The distribution of the maximum opening of the transverse joints during the earthquake process given by numerical analysis is shown in Figure 11, but the numerical analysis results show that the transverse joints were in a closed state before and after the earthquake, which is also consistent with the general rule of the static opening and closing of the transverse joints in arch dams.Figure 12 shows the distribution of the opening increment values before and after the earthquake given by the joint meter on the upstream face of the dam body.

The high frequency of opening and closing of transverse joints during an earthquake may cause partial stripping and blocking of grouting materials between joints, which in turn may lead to the failure of the joint meter to fully reset, resulting in minor post-earthquake residual opening. This phenomenon cannot be simulated by numerical calculations, and the observed residual opening of transverse joints indicates that there was an opening and closing phenomenon at the corresponding location of the transverse joints during the earthquake.As shown in the comparison between Figure 11 and Figure 12, the calculated positions of the low elevation of the left and right bank slope dam sections overlap with the measured positions of the residual opening of the transverse joints, and both exhibit a characteristic of large values near the bottom of the joints, indicating that the numerical calculation of the opening and closing of the transverse joints basically reflects the actual situation of this earthquake.

Fig. 11
Cloud map of the maximum opening distribution of transverse joints during the earthquake (calculation results)

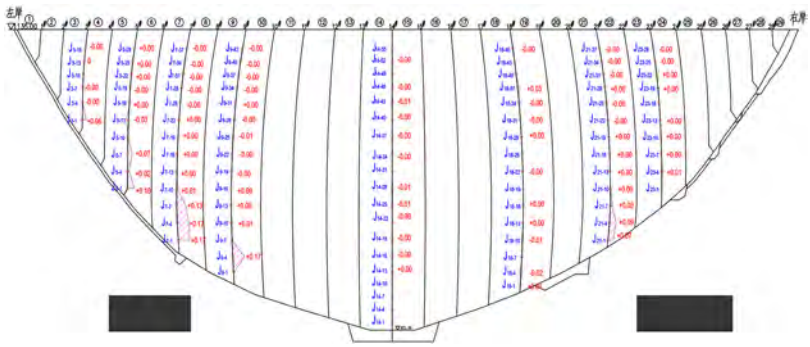

Fig. 12
Distribution of the post-earthquake increase in the opening of the transverse joint on the upstream face (monitoring results)

5.4. Static and dynamic comprehensive stress response

Figure 13 shows the maximum values of the static and dynamic maximum principal stresses on the upstream and downstream faces of the dam under the combination of static load and the main shock of this earthquake. From the perspective of the static and dynamic stress of the dam, except for the stress concentration area at the dam heel, the tensile stress values of other parts are not large. In the middle and upper regions of the dam, the maximum tensile stress on the upstream face is below 1 MPa, and the maximum tensile stress on the downstream face is below 1.5 MPa. This is within the dynamic allowable tensile strength (3.37 MPa) range of the dam concrete, which is consistent with the aseismic performance of the dam without damage.

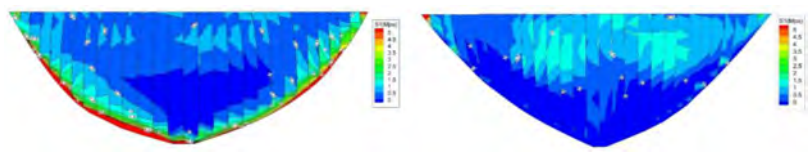

Fig. 13
The Maximum Static and Dynamic Comprehensive Principal Stress on the upstream and downstream dam surfaces (MPa)

6. CONCLUSION

This study is based on the strong motion monitoring records and seismic performance of the Dagangshan arch dam-foundation system during the 6.8-magnitude Luding earthquake, and the calculation and verification show that:

1. The records of the free-field measurement points on the bedrock indicate that the seismic ground motion input along the river direction at the Dagangshan arch dam site during this earthquake has a large acceleration response spectrum value near the dam's fundamental frequency of 1.65 Hz, which may cause a relatively large dynamic response of the dam during this earthquake.
2. Considering the radiation damping effect of the infinite foundation and the seismic wave response analysis of the dam-foundation system with the transverse joints of the dam, the acceleration response of the dam given by the analysis is in good agreement with the amplitude and waveform at most measuring points of the dam.
3. Although the calculated transverse joint opening cannot be compared with the time history and maximum value due to the lack of time history records of transverse joint opening, the observed significant opening position are consistent with the calculated position with large opening.
4. The maximum static and dynamic tensile stress of the dam body, as calculated and analyzed, does not exceed the tensile strength value obtained from the dynamic performance test of fully graded concrete specimens for the dam, which is consistent with the condition of no damage to the dam body after the earthquake.
5. The calculation and analysis results and the actual seismic performance indicate that the Dagangshan arch dam withstood the test of a strong earthquake in the 6.8-magnitude Luding earthquake, and there was no damage to the dam body after the earthquake, and the seismic safety performance of the dam body-foundation system remained unchanged.At the same time, it also verifies that the dam-foundation system seismic wave response analysis method applied during the design and construction phase of Dagangshan arch dam can reasonably simulate the seismic response of the dam.

ACKNOWLEDGMENTS

The authors are grateful for the financial support from China Huaneng Group Co., Ltd. (HNKJ22-H108), Power Construction Corporation of China (DJ-ZDXM-2021-03).

REFERENCES

[1] ZHU B.F., Damages to hydraulic structures caused by 921 Earthquake of Taiwan in 1999. *Journal of hydroelectric engineering*, Vol.22, no.3, pp. 21–33, 2003.

[2] CHEN H.Q., Analysis on damages of high concrete dams subjected to strong earthquake and lessons for learning. *Journal of hydraulic engineering*, Vol.40, no.1, pp. 10–18, 2009.

[3] WANG R.K., SHAO J.D., Shapai arch dam has withstood Wenchuan earthquake beyond fortification level. *Journal of hydroelectric engineering*, Vol.28, no.5, pp. 92–96, 2009.

[4] ZHANG C.R., YU Y.X., CHEN H.Q., LI M., Study on earthquake ground motion inputs for Shapai arch dam based on Wenchuan and Lushan earthquakes. *Journal of hydroelectric engineering*, Vol.33, no.3, pp. 210–215, 2014.

[5] FEMA, Earthquake Analyses and Design of Dams, Federal Guidelines for Dam Safety, 2005

[6] Bureau of Reclamation U.S, State-of-Practice for Nonlinear Analysis of Concrete Dams, 2006

[7] Federal Energy Regulatory Commission Division of Dam Safety and Inspections, Engineering Guidelines for the Evaluation of Hydropower Projects, Chapter 11-Arch Dams, 1999

[8] JEROME M. RAPHAEL, Tensile Strength of Concrete. *ACI JOURNAL, Proceedings*, Vol.81, no.17, pp. 158–165, 1984.

[9] WU S.X., ZHOU J.K., SHEN D.J., CHEN H.Q. Test technique and data processing method for dynamic flexural-tensile test of concrete. *Journal of hydraulic engineering*, Vol. 40, no. 5, pp. 569–575, 2009.

[10] CHEN H.Q., GUO S.S., Seismic damage analysis of high concrete dam-foundation system. *Journal of hydraulic engineering*, Vol.43, Suppl.1,pp. 2–7, 2012.

[11] TU J., LI D.Y., CHEN H.Q., OUYANG J.H., Study on integral seismic safety of Dagangshan Arch dam-foundation system. *Journal of hydraulic engineering*, Vol.42, no.2, pp. 152–159, 2011.

[12] TU J., *Aseismic anlysis of concrete dam with numerical method: theory and engineering practice. China Water & Power Press*, Beijing, 2007.

[13] TU J., LI D.Y., ZHANG C.R., WANG H.B., Study on the Seismic Verification of Shapai Arch Dam during the Wenchuan Earthquake. *Journal of hydraulic engineering*, Vol.47, no.5, pp. 656–662, 2016.

[14] HUANG H.B., CHEN G., JIANG D.J., Deformation characteristics analysis of Dagangshan super high arch dam in Sichuang Luding Ms6.8 earthquake. *Journal of hydraulic engineering*, Vol. 54, no. 5, pp. 599–609, 2023.

[15] JIANG D.J., HUANG H.B., QI S.G., Dynamic response analysis of Dagangshan arch dam under the Sichuan Luding Ms 6.8 earthquake. *Chinese Journal of Rock Mechanics and Engineering*, Vol.43, no.1, pp. 59–74, 2024.

Q.111 - R.33

COMMISSION INTERNATIONALE DES
GRANDS BARRAGES

VINGT-HUITIEME CONGRES DES
GRANDS BARRAGES
CHENGDU, MAI 2025

PREDICTION OF LIQUEFACTION LATERAL DISPLACEMENT LEVELS BASED ON GA-CART ALGORITHM (*)

Yifan ZHANG, Jixue TIAN, Yusheng YANG, Shu YU & Penghai YIN
State Key Laboratory of Simulation and Regulation of Water Cycle in River Basin, China Institute of Water Resources and Hydropower Research, Beijing

Zerui WU
China Power Construction Yili Construction Development Co., LTD, Xinjiang Yili state

Gang DENG
State Key Laboratory of Simulation and Regulation of Water Cycle in River Basin, China Institute of Water Resources and Hydropower Research, Beijing

CHINA

SUMMARY

With the development of geotechnical engineering towards digitalization and intelligence, artificial intelligence and machine learning are gradually used to assist in solving complex geotechnical engineering problems. Based on liquefaction case history, a GA-CART model for liquefaction lateral displacement prediction is developed in this paper. In this model, genetic algorithm (GA) is used to determine the calculation parameters of CART decision tree model, and the liquefaction lateral displacement is divided into four levels. The thickness of equivalent liquefaction layer (T_{15}), fine particle content (F_{15}),peak surface acceleration (a_{max} or *PGA*) and topographic influencing factors—free space ratio *W* (in the case of free space) or

**Détermination des déplacements latéraux par liquéfaction par l'algorythme GA-CART*

 DOI: 10.1201/9781003642428-134

slope *S*(in the case of gentlely slope ground) were considered, and on this basis, the practical chart for predicting liquefaction lateral displacement levels was proposed. The GA-CART model for liquefaction lateral displacement prediction established in this paper is simple, easy to apply and update, and the overall prediction success rate is increased by 5%-8% compared with the traditional method. Finally, the sensitivity analysis of liquefaction lateral displacement influencing factors by GA-CART model is carried out. The research shows that the free space ratio *W* and slope *S* are the most sensitive factors affecting the lateral deformation of liquefaction site, followed by equivalent layer thickness T_{15}, fine particle content F_{15} and peak surface acceleration a_{max}.

RÉSUMÉ

Avec le développement de l'ingénierie géotechnique vers la numérisation, l'intelligence artificielle et l'apprentissage automatique sont progressivement utilisés pour aider à résoudre des problèmes complexes. Sur la base de l'histoire de la liquéfaction, un modèle GA-CART pour la prévision du déplacement latéral est développé dans cet article. L'algorithme génétique (GA) est utilisé pour déterminer les paramètres de calcul du modèle d'arbre de décision CART, et le déplacement latéral de liquéfaction est divisé en quatre niveaux. L'épaisseur de la couche équivalente de liquéfaction (T_{15}), la teneur en particules fines (F_{15}), l'accélération de pointe de surface (a_{max} ou *PGA*) et les facteurs d'influence topographiques, le rapport d'espace libre *W* (dans le cas de l'espace libre) ou la pente *S* (dans le cas de terrains à pente douce) ont été pris en considération. Sur cette base, le schéma pratique de prévision des niveaux de déplacement latéral de liquéfaction a été proposé. Le modèle GA-CART pour la prévision du déplacement latéral de liquéfaction est simple, facile à appliquer et à mettre à jour, et le taux global de succès de la prévision est augmenté de 5 à 8% par rapport à la méthode traditionnelle. Enfin, l'analyse de sensibilité des facteurs influençant le déplacement latéral de la liquéfaction par modèle GA-CART est effectuée. La recherche montre que le rapport d'espace libre *W* et la pente *S* sont les facteurs les plus sensibles de la déformation latérale du site de liquéfaction, suivis de l'épaisseur de couche équivalente T_{15}, de la teneur en particules fines F_{15} et de l'accélération de pointe de surface a_{max}.

1. INTRODUCTION

The saturated sand layer may be liquefied under the action of ground motion, and the liquefaction lateral displacement will be driven by the static shear stress and the seismic cyclic shear stress exceeding the strength of the liquefied soil [1].

The liquefaction lateral displacement can cause serious damage to structures and infrastructure during and shortly after an earthquake [2].

At present, great progress has been made in the research of practical methods for soil liquefaction assessment [3,4]. For the prediction of liquefaction lateral displacement, in addition to relatively complex dynamic calculation methods [5–7], empirical and semi-empirical models based on liquefaction case history are widely used in engineering [8–14]. Based on the liquefaction horizontal deformation data of Niigata and Noshiro earthquakes in Japan and San Fernando earthquakes in the United States, Hamada et al. [11] developed the first empirical formula for predicting the liquefaction lateral displacement, taking into account the two influencing factors of the thickness and slope of the liquefied layer. Subsequently, Bartlett and Youd [12] collected 467 liquefaction case histories from eight earthquakes in Japan, the United States, etc. Furthermore, they developed two site types of empirical methods whether in the case of free face or not. Youd et al. [13] modified and added part of the data on the basis of Bartlett and Youd's research [12], and developed a multiple linear regression formula (MLR) that took into account eight parameters: earthquake magnitude, epicenter distance, slope, free face ratio, liquefied layer thickness, fine particle content and average particle size. Youd [14] proposed two problems in the practical engineering application of the Youd et al. [13] method, and both the minimum thickness of liquefied layer causing liquefation lateral displacement and the dilatancy parameter ψ were introduced in order to extend the method to the static penetration (CPT) database.

The above empirical methods were mainly developed based on Youd et al. [12,13] database, and the applicability to liquefaction case histories in recent earthquakes needs to be further verified. Meanwhile, the above empirical methods were mainly developed by multiple linear regression (MLR) method. With the development of computer technology and data science, data-driven methods based on machine learning have emerged [15–17]. Zhang et al. [16] established a constrained back propagation neural network (C-BPNN) model for soil liquefation assessment which combined the prior knowledge with neural network model. Shi Xuchao and Han Yang [17] established a multi-classification model for soil liquefaction assessment based on support vector machine classification algorithm. Zhang et al. [18] explored the effectiveness and the applicability of different machine learning methods for predicting liquefaction lateral displacement. Indeed, machine learning methods have been applied in the field of soil liquefaction assessment and predicting liquefaction lateral displacement.

However, due to data limitation, some liquefaction case histories only contain part of the required data used for liquefaction lateral displacement prediction. Such as in the 2010 Chile earthquake [19] and 2010 Haiti earthquake [20], some liquefaction case histories lack the information of epicenter distance and average particle size. The intelligent prediction method for liquefaction lateral displacement established by Zhang et al. [18] cannot be used for prediction of such cases. Moreover,

it may be difficult for some engineers to predict liquefaction lateral displacement by using machine learning method directly in practical application.

In order to increase the simplicity and practicability of the liquefaction lateral displacement prediction method, based on liquefaction case history, a GA-CART model for liquefaction lateral displacement prediction is developed in this paper. In this method, the liquefaction lateral displacement was divided into four levels, and the genetic algorithm (GA) was used to determine the calculation parameters of CART decision tree model. The thickness of equivalent liquefaction layer (T_{15}), fine particle content (F_{15}), peak surface acceleration (a_{max} or PGA) and topographic influencing factors—free space ratio W (in the case of free space) or slope S(in the case of gentlely slope ground) were considered, and on this basis, the practical chart for predicting liquefaction lateral displacement levels was proposed. Finally, the sensitivity analysis of liquefaction lateral displacement influencing factors by GA-CART model was carried out.

2. DATA SOURCE AND DATA PREPROCESSING

Currently, the commonly used liquefacion data sets include Rauch et al. [21], Bardet et al. [22], Youd et al. [12,13] and Faris et al. [23], which cover a total number of 484 liquefaction case histories from more than 10 earthquakes in the United States, Japan, etc. On this basis, liquefaction case histories from five recent earthquakes are collected and sorted out, including 1999 Chi-chi Earthquake [24], 1999 Turkey Earthquake [25], 2010 Chile earthquake [19], 2010 Haiti earthquake [20], 2011 Christchurch earthquake [26].

In order to increase the simplicity and practicability of the prediction method, this paper divides the liquefaction lateral displacement into four levels: the lateral displacement in the range of 0-0.5m ($0<D_H \leq 0.5$m) is a slight deformation (low level); the lateral displacement in the range of 0.5-1.0m ($0.5<D_H \leq 1.0$m) is a moderate deformation(moderate level); the lateral displacement in the range of 1.0-2.0m ($1.0<D_H \leq 2.0$m) is a sever deformation(high level) and the lateral displacement exceeding 2.0m ($D_H>2.0$m) is a very sever deformation(very high level). The liquefaction dataset of Zhang et al. [18] was used to establish the GA-CART model for the prediction of liquefaction lateral displacement, including Youd et al. 2002 data set, and liquefaction case histories from 1999 Chi-chi earthquake, 1999 Turkey earthquake, 2010 Chile earthquake, 2010 Haiti earthquake, 2011 Christchurch earthquake. 80% of the dataset were used as training and validation sets, and 20% of the dataset were used as test sets. The input parameters of GA-CART model mainly consider the influence factors of geological conditions—equivalent layer thickness (T_{15}), soil conditions—fine particle content (F_{15}), ground motion conditions—peak surface acceleration (a_{max} or PGA), and topographic conditions—free face ratio (W)(in the case of free face) or slope (S)(in the case of

gently slope ground). The output parameters are four levels of liquefaction lateral displacement.

It is necessary to preprocess the data before establishing the GA-CART model, including abnormal data processing and data normalization. In this paper, the statistical distribution diagram of data analysis adopts the 3σ principle[15–18], and the data exceeding $\pm 3\sigma$ is deleted. In addition, the data is normalized to the interval [0,1] for calculation as Leng et al. [15] and Zhang et al. [18].

3. ESTABLISHMENT OF GA-CART MODEL

The CART algorithm is divided into two processes: branching and pruning. Categorical variables and categorical variable thresholds are established through branching, and redundant categorical variable information is deleted by pruning. In the branching process of CART algorithm, an optimal branching variable and the optimal branching threshold corresponding to the variable need to be determined for a specific node. The research objects with the same properties are classified into the same child node, while the objects with significant differences in properties are classified into another child node.

For a particular node T, the GINI index of that node is:

$$\boldsymbol{gini}(\boldsymbol{T}) = \mathbf{1} - \sum_{\boldsymbol{j}=\mathbf{1}}^{\boldsymbol{J}} \boldsymbol{P}[\boldsymbol{j}|\boldsymbol{T}] \tag{1}$$

Where T is a specific node, J is the total number of categories, and $\boldsymbol{P}[\boldsymbol{j}|\boldsymbol{T}]$ is the probability of occurrence of the Jth category at node T.

For node T, the split GINI index of this node is:

$$\boldsymbol{GI}(\boldsymbol{T}, \boldsymbol{X}, \boldsymbol{Q}) = \boldsymbol{gini}(\boldsymbol{T}) - \sum_{\boldsymbol{k}=\mathbf{1}}^{\boldsymbol{K}} \{\boldsymbol{P}[\boldsymbol{q_k}(\boldsymbol{X})|, \boldsymbol{T}] \cdot \boldsymbol{gini}(\boldsymbol{T_k})\} \tag{2}$$

Where X is the split attribution, Q is the branching data set at the split attribution of node T, K is the number of child nodes contained in node T, T_k is the Kth child node, and $\{\boldsymbol{P}[\boldsymbol{q_k}(\boldsymbol{X})|, \boldsymbol{T}]\}$ is the probability of splitting from T node to kth child node.

The pruning process adopts the principle of minimum cost complexity:

$$\boldsymbol{R}_{\alpha}(\boldsymbol{T}) = \boldsymbol{R}(\boldsymbol{T}) + \alpha|\tilde{\boldsymbol{T}}| \tag{3}$$

Where $\alpha|\tilde{T}|$ is the classification error rate at node T, $|\tilde{T}|$ is the number of child nodes which reflects the size of the decision tree, and α is the complexity cost.

To build a classification decision tree model using CART algorithm, three important calculation parameters need to be determined: maximum tree depth (max_depth), minimum sample number (mini_samples_leaf) and minimum number of nodes (max_leaf_nodes). GA algorithm is used for paramter optimization, in order to obtain the optimal calculation parameters of CART algorithm. The calculation process of GA-CART model (Fig. 1) can be expressed as follows:

STEP1: The initialization population is randomly generated by binary coding.
STEP2: The branching and pruning process is carried out according to CART algorithm, and the CART classification decision tree model is established according to the maximum tree depth (max_depth), minimum sample number (mini_samples_leaf) and minimum number of nodes (max_leaf_nodes).
STEP3: The fitness of the calculation parameters was evaluated and the convergence was judged. Fitness function is the function of classification accuracy and cost complexity function. Classification accuracy refers to the percentage of correctly classified samples in the total number of samples, which is determined by 5-fold cross-validation. In this paper, convergence standard is set as classification accuracy greater than 80%.
STEP4: If the convergence condition is not met, GA algorithm is used to optimize the calculate parameters, and a new parameter population is generated through selection, crossover and mutation. This part is realized by Matlab Genetic Algorithm toolbox solver.
STEP5: Repeat the above STEP2-4 process until the convergence condition is met or the maximum number of iterations (10000) is reached.
STEP6: When the convergence condition is satisfied, the optimal calculation parameters of GA-CART model are obtained, and the GA-CART model is established and tested.

Before determining the calculation parameters of GA-CART model, it is necessary to determine the influence of population size on the prediction accuracy of GA-CART model. In this paper, GA-CART models with population size of 10, 20, 50, 100, 150 and 200 were established to explore their influence on the prediction accuracy. Table 1 and Table 2 show the effects of population size of GA-CART model on prediction accuracy in the case of free face and in the case of gentlely slope grpund respectively. The results show that with the increase of the initial population, the number of iterations in the final convergence decreases at first and then increases, and the prediction accuracy increases at first and then decreases. Overfitting phenomenon exists when the initial population is too large. Therefore, there is an optimal value of population size in the GA-CART model, which is 100 population size in the case of free face and 50 population size in the case of gentlely slope ground. Finally, the calculation parameters of the GA-CART model established in this paper are shown in Table 3.

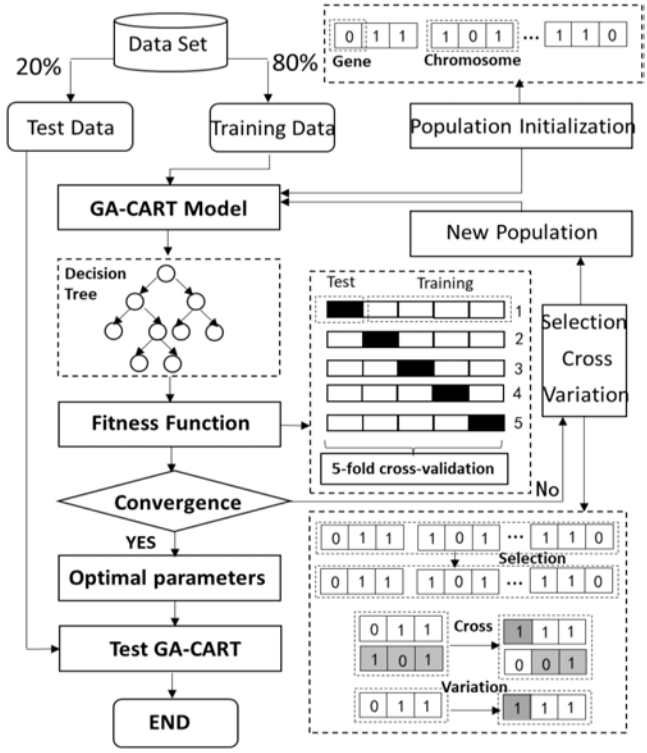

Fig. 1
Flow chart of GA-CART model for predicting liquefaction lateral displacement levels.

Table 1
Effect of population size on prediction accuracy of GA-CART model (Free Face)

POPULATION SIZE	RANK	ITERATIONS	ACCURACY	
			TRAINING SET	TEST SET
10	6	258	0.7953	0.7322
20	5	112	0.8145	0.7478
50	3	90	0.8329	0.7602
100	1	84	0.8404	0.7834
150	2	88	0.8402	0.7831
200	4	96	0.8244	0.7805

Table 2
Effect of population size on prediction accuracy of GA-CART model (Gently Slope Ground)

POPULATION SIZE	RANK	ITERATIONS	ACCURACY	
			TRAINING SET	TEST SET
10	6	196	0.8065	0.7103
20	5	112	0.8156	0.7169
50	1	65	0.8392	0.7302
100	2	67	0.8275	0.7386
150	3	79	0.8157	0.7299
200	4	74	0.8245	0.7164

Table 3
Calculation parameters of GA-CART model

CALCULATION PARAMETERS	FREE FACE	GENTLY SLOPE GROUND
The optimal population size	100	50
max_depth	5	5
mini_samples_leaf	8	10
max_leaf_nodes	55	65

4. GA-CART MODEL AND PRACTICAL CHART FOR PREDICTING LIQUEFACTION LATERAL DISPLACEMENT

4.1. GA-CART MODEL FOR PREDICTING LIQUEFACTION LATERAL DISPLACEMENT

The GA-CART model for liquefaction lateral displacement prediction in the case of free face (Fig. 2) or gently slope ground (Fig. 3) was established by using the calculation parameters in Table 3. In the figure, the four liquefaction lateral displacement levels are represented by different colors, and the categorical variables and thresholds of each node are shown, as well as the sample number and proportion of each liquefaction lateral displacement level according to the GA-CART model. Finally, a GA-CART model with 11 nodes and 12 terminal nodes was established for the prediction of liquefaction lateral displacement in the case of free face, and a GA-CART model with 10 nodes and 11 terminal nodes was established for the prediction of liquefaction lateral displacement in the case of gently slope ground.

4.2. Practical chart for predicting liquefaction lateral displacement

The practical chart (Table 4 and Table 5) for predicting liquefaction lateral displacement can be obtained from the terminal node to node 1 according to the branch node variables and threshold values in the GA-CART model for liquefaction lateral displacement prediction in the case of free face (Fig. 2) or gently slope ground (Fig. 3).

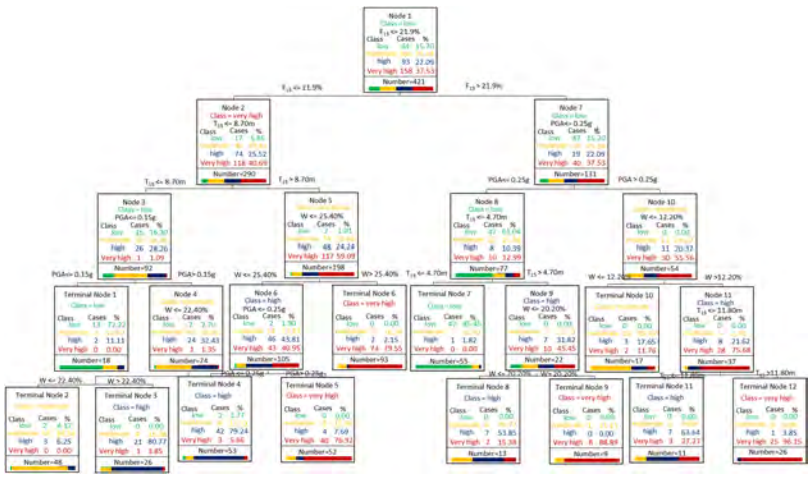

Fig. 2
GA-CART model for predicting liquefaction lateral displacement levels in the case of free face.

4.3. Reliability assessment of the GA-CART model and the practical chart

In order to test the reliability of the GA-CART model and the practical chart, the correlation analysis between the input parameters and the liquefaction lateral displacement was conducted by the GA-CART model. Moreover, the sensitivity analysis of liquefaction lateral displacement influencing factors by GA-CART model was carried out. Finally, the comparison of the predicting results of the GA-CART model with the existing methods were evaluated.

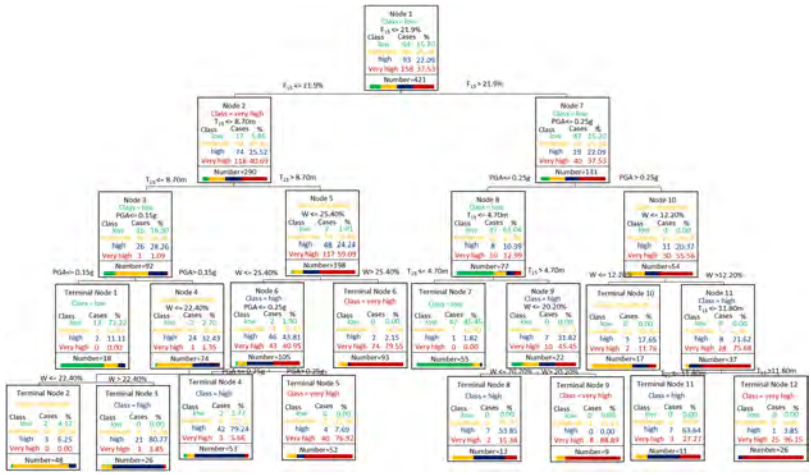

Fig. 3
GA-CART model for predicting liquefaction lateral displacement levels in the case of gently slope ground.

Table 4
Practical chart for predicting liquefaction lateral displacement levels in the case of free face

LEVELS OF LIQUEFACTION LATERAL DEFORMATION	CRITERION
Slight deformation(0-0.5m)	F15 ≤ 21.9%,T15 ≤ 8.70m,PGA ≤ 0.15g; F15>21.9%,T15 ≤ 4.70m,PGA ≤ 0.25g
Moderate deformation (0.5-1.0m)	F15 ≤ 21.9%,T15 ≤ 8.70m,PGA>0.15g,W ≤ 22.40%; F15>21.9%,PGA>0.25g,W ≤ 8.20%
Severe deformation (1.0-2.0m)	F15 ≤ 21.9%,T15 ≤ 8.70m,PGA>0.15g,W>22.40%; F15 ≤ 21.9%,T15>8.70m,W ≤ 25.4%,PGA ≤ 0.25g; F15>21.9%,PGA ≤ 0.25g,T15>4.70m,W ≤ 20.20%; F15>21.9%,PGA>0.25g,W>12.20%,T15 ≤ 11.80m
Very severe deformation (>2m)	F15 ≤ 21.9%,T15>8.70m,W ≤ 25.4%,PGA>0.25g; F15 ≤ 21.9%,T15>8.70m,W>25.4%; F15>21.9%,PGA ≤ 0.25g,T15>4.70m,W>20.20%; F15>21.9%,PGA>0.25g,W>12.20%,T15>11.80m

Table 5
Practical chart for predicting liquefaction lateral displacement levels in the case of gently slope ground

LEVELS OF LIQUEFACTION LATERAL DEFORMATION	CRITERION
Slight deformation(0-0.5m)	T15 $\leq$ 4.75m,F15 $\leq$ 16.70%,S $\leq$ 5.40%; T15 $\leq$ 8.75m,F15$>$16.70%,PGA $\leq$ 0.15g; T15$>$8.75m,S $\leq$ 3.60%
Moderate deformation (0.5-1.0m)	F15 $\leq$ 16.70%,4.75m $<$T15 $\leq$ 8.75m,S $\leq$ 5.40%; F15$>$16.70%,PGA$>$0.15g,T15 $\leq$ 8.75m
Severe deformation (1.0-2.0m)	F15 $\leq$ 16.70%,T15 $\leq$ 8.75m,5.40%$<$S $\leq$ 8.20%; 8.75 m $<$T15 $\leq$ 10.05m,S$>$3.60%,PGA $\leq$ 0.28g; T15$>$10.05m,S$>$3.60%,PGA $\leq$ 0.21g
Very severe deformation ($>$2m)	F15 $\leq$ 16.70%,T15 $\leq$ 8.75m,S$>$5.40%; 8.75m $<$T15 $\leq$ 10.05m,S$>$3.60%,PGA$>$0.28g; T15$>$10.05m, S$>$3.60%,PGA$>$0.21g

4.3.1. *Reliability assessment of the GA-CART model and the practical chart*

By analyzing the GA-CART model for predicting liquefaction lateral displacement (Fig. 2 and Fig. 3), it can be seen that: in the case of free face, with free face ratio W as the branch node variable, the larger W is, the higher the liquefaction lateral displacement level will be. Taking T_{15} as the branch node variable, the thicker the T_{15} is, the higher the liquefaction lateral displacement level will be. Taking PGA as the branch node variable, the larger the PGA is, the higher the level of liquefaction lateral displacement will be. Taking fine content F_{15} as the branch node variable, the higher the F_{15} is, the lower the level of liquefaction lateral displacement will be.In the case of gently slope ground, taking slope S as the branch node variable, the larger S is, the higher the liquefaction lateral displacement level will be. Taking T_{15} as the branch node variable, the higher the T_{15} is, the higher the liquefaction lateral displacement level will be. Taking PGA as the branch node variable, the larger the PGA is, the higher the level of liquefaction lateral displacement will be. With fine content F_{15} as the branch node variable, the higher the F_{15} is, the lower the liquefaction lateral displacement level will be. It can be concluded that: in the case of free face, W, T_{15} and PGA are positively correlated with liquefaction lateral displacement, while F_{15} is negatively correlated with liquefaction lateral displacement. In the case of gently slope ground, S, T_{15} and PGA are positively correlated with the level of liquefaction lateral displacement, while F_{15} is negatively correlated with the level of liquefaction lateral displacement.

4.3.2. *Influence weight analysis of input parameters*

Based on the GA-CART liquefaction lateral displacement model established above, the importance of the influence of GA-CART model input parameters on the level of liquefaction lateral displacement was analyzed, and the sensitivity of the influencing factors in predicting the liquefaction lateral displacement was explored. In this paper, the method used by Yang et al. [27] was used to evaluate the effects of input parameters of GA-CART model, such as peak surface acceleration a_{max}, free face ratio W, slope S, equivalent liquefied layer thickness T_{15}, fine particle content F_{15}. In this method, r_{ij} is used to reflect the influence of model input parameters on output results, and its expression can be expressed as:

$$r_{ij} = \sum_{k=1}^{n} (x_{ik} \times y_{ik}) / \sqrt{\sum_{k=1}^{n} x_{ik}^2 \sum_{k=1}^{n} y_{ik}^2} \tag{4}$$

Where n is the data sample size, x_{ik} and y_{ik} are the input parameters and output results of the model respectively. For each input parameter, r_{ij} ranges from 0 to 1 [0,1]. The higher the r_{ij} value, the more important the corresponding input parameter is to the output result. We assume that the sum of the importance of all parameters on the liquefaction lateral displacement is 1, and a quantitative expression of the percentage of the importance of each parameter can be obtained. The results (Fig. 4) show that in the case of free face, the most important factor affecting the level of liquefaction lateral displacement is the free face ratio W (influence weight of 31.37%), followed by equivalent layer thickness T_{15} (influence weight of 28.30%), fine particle content F_{15} (influence weight of 21.43%) and peak surface acceleration PGA (influence weight of 18.90%). In the case of gently slope ground, the most important factor affecting the level of liquefaction lateral displacement is slope S (influence weight of 30.19%), followed by equivalent layer thickness T_{15}(influence weight of 26.84%), peak surface acceleration PGA(influence weight of 21.92%) and fine particle content F_{15}(influence weight of 21.05%).

4.3.3. *Comparison of prediction effect between GA-CART model and existing methods*

In order to test the validity of the GA-CART model and the practical chart for predicting liquefaction lateral displacement, the prediction success rate in the case of free face and gently slope ground was compared with existing methods (Li et al., 2016[28]; Youd, 2018[14]) seperately in Table 6 and Table 7. The results show that the success rate of GA-CART model presented in this paper (82.90% in the case of free face, 81.74% in the case of gently slope ground) is superior to Youd (2018) method (77.91% in the case of free face, 77.61% in the case of gently slope ground) and Li et al. (2016) method (74.82% in the case of free face, 72.01% in the case of gently slope ground). It is worth noting that the prediction success rate of several methods for liquefaction lateral displacement of moderate level is low. The analysis

of GA-CART model shows that many liquefaction sites with moderate deformation level are misjudged as severe deformation level or very severe deformation level, which indicates that the threshold of liquefaction level deformation in GA-CART model needs to be further optimized.

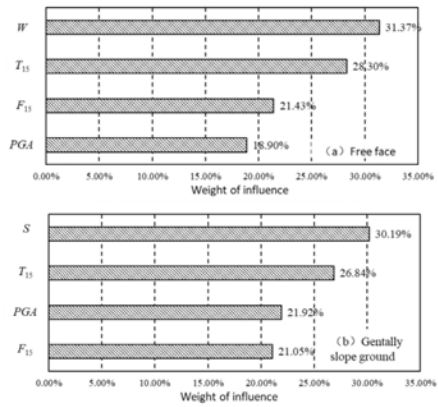

Fig. 4
Input parameters influence of GA-CART model for predicting liquefaction lateral displacement.

Table 6
Comparison of prediction success rate between GA-CART model and existing methods (free face)

LEVELS OF LIQUE-FACTION LATERAL DISPALCEMENT	IN THE CASE OF FREE FACE						
	THE NUMBER OF CASES	THE NUMBER OF CASES CORRECTLY PREDICTED			THE SUCCESSFUL RATE/%		
		IN THIS PAPER	LI ET AL. (2016)	YOUD (2018)	IN THIS PAPER	LI ET AL. (2016)	YOUD (2018)
Slight deformation (0-0.5m)	64	60	51	49	93.75	79.69	76.56
Moderate deformation (0.5-1.0m)	106	65	59	65	61.32	55.67	61.32
Severe deformation (1.0-2.0m)	93	77	68	78	82.79	73.12	83.87
Very severe deformation (>2m)	158	147	137	136	93.04	82.71	86.07
Average success rate					82.90	74.82	77.91

Table 7
Comparison of prediction success rate between GA-CART model and existing methods (gently slope ground)

LEVELS OF LIQUE-FACTION LATERAL DISPALCEMENT	IN THE CASE OF FREE FACE						
	THE NUMBER OF CASES	THE NUMBER OF CASES CORRECTLY PREDICTED			THE SUCCESSFUL RATE/%		
		IN THIS PAPER	LI ET AL. (2016)	YOUD (2018)	IN THIS PAPER	LI ET AL. (2016)	YOUD (2018)
Slight deformation (0-0.5m)	37	30	21	25	81.08	56.76	67.57
Moderate deformation (0.5-1.0m)	42	23	22	29	54.76	52.38	69.05
Severe deformation (1.0-2.0m)	76	59	49	54	77.63	64.47	71.05
Very severe deformation (>2m)	113	106	101	100	93.81	89.38	88.50
Average success rate					81.74	72.01	77.61

5. CONCLUSIONS

Based on liquefaction case history, a GA-CART model for liquefaction lateral displacement prediction is developed in this paper. The GA genetic algorithm is used to determine the optimal calculation parameters of CART algorithm. The results show that the proposed method is superior to the existing standard methods in terms of calculation efficiency and prediction success rate. The main conclusions are as follows:

1. The GA-CART model and pratical chart for liquefaction lateral displacement prediction were established, which divided liquefaction lateral displacement into four levels. This method mainly considered the influence factors such as equivalent liquefaction layer thickness (T_{15}), fine particle content (F_{15}), peak surface acceleration (a_{max} or PGA), free face ratio (W)(in the case of free face) and slope (S)(in the case of gently slope ground). The method has strong data scalability and practicability, and provides a new idea for the development of liquefaction lateral displacement prediction.
2. GA genetic algorithm was used to determine the optimal calculation parameters of CART decision tree model, and the GA-CART established by this method greatly improved the success rate of predicting liquefaction lateral displacement. The average prediction success rate of the GA-CART model for liquefaction lateral displacement is 82.90% in the case of free face and

81.74% in the case of gently slope ground respectively. Compared with the existing methods, the overall prediction success rate is increased by 5%-8%.

3. The sensitivity of influencing factors in predicting liquefaction lateral displacement by GA-CART model was investigated. The free face ratio W(influence weight of 31.37%) and slope S(influence weight of 30.19%) are the most sensitive factors affecting the liquefaction lateral displacement, followed by equivalent layer thickness T_{15}(influence weight of 28.30% in the case of free face and 26.84% in the case of gently slope ground),and then followed by fine particle content F_{15}(influence weight of 21.43% in the case of free face and 21.05% in the case of gently slope ground) and peak surface acceleration a_{max}(influence weight of 18.90% in the case of free face and 21.92% in the case of gently slope ground).
4. The pratical chart developed by GA-CART model for liquefaction lateral displacement prediction can be directly applied in engineering. With the further accumulation of liquefaction case histories, the pratical chart for liquefaction lateral displacement prediction can be updated by the GA-CART model established in this paper, which is easy to update and has a guiding significance for the development of liquefaction specification.

ACKNOWLEDGMENTS

The authors are grateful for the financial support from the National Natural Science Foundation of China (No. 42330719), the Natural Science Foundation of Heilongjiang Province (No. JQ2023E009), and the Scientific and Technological Achievements Transformation Fund of China Institute of Water Resources and Hydropower Research (Nos. GE121003A0072024 and GE121003A0042022).

REFERENCES

[1] KRAMER S. L. *Geotechnical earthquake engineering*. Prentice Hall, pp.1–653, 1996.

[2] BARTLETT S. F., YOUD T. L.. Empirical analysis of horizontal ground displacement generated by liquefaction-induced lateral spread. Tech. Rep. No. NCEER-92-0021. Buffalo, NY, USA: National Center for Earthquake Engineering Research, 1-114, 1992.

[3] ZHANG X., LI X., DU X.. Hyperbolic model for estimating liquefaction potential of sand considering the influences of fine grains. *Chinese Journal of Geotechnical Engineering*, vol. 43(3), pp. 448–455, 2021.

[4] YUAN X., FEI Y., CHEN L., *ET AL.* An unified formula for predicting sand liquefaction in different buried depths under severe seismic ground motion. *Chinese Journal of Rock Mechanics and Engineering*, vol. 40(10), pp. 2101–2012, 2021.

[5] WANG R., ZHANG J M, WANG G. A unified plasticity model for large post-liquefaction shear deformation of sand. *Computers and Geotechnics*, vol. 59, pp. 54–66, 2014.

[6] WANG G., WEI X. Liquefaction potential evaluation of dam foundation soil considering influence of overlying structures. *Journal of Hydroelectric Engineering*, vol. 33(4), pp. 220–226, 2014.

[7] AN Z., LI J.. Liquefaction properties and dynamic FEM analysis of the dam foundation of reservoir under seismic loa. *Journal of Hydroelectric Engineering*, vol. 25 (6), pp. 45–33, 2006.

[8] ZHANG J. Practical prediction method for large deformation of ground after earthquake liquefaction/In Proceedings of the 8th International Conference on Soil Mechanics and Geotechnical Engineering. Beijing: International Academic Press, 1999.

[9] CHEN Y., GAO X., LIU H. Simplified method of flow deformation induced by liquefied san. *Rock and Soil Mechanics*, vol. 34(6), pp. 1567–73, 2013.

[10] LIU F., LI Z. Probit model for exceedance of liquefaction-induced lateral deformation over a given threshold value due to earthquakes. *Chinese Journal of Geotechnical Engineering*, vol. 35(zk1), pp. 425–429, 2013.

[11] HAMADA M., YASUDA S., ISOYAMA R., *ET AL.* Study on liquefaction-induced permanent ground displacements and earthquake damage. *Doboku Gakkai Ronbunshu*, vol. 376, pp. 221–229, 1986.

[12] BARTLETT S. F., YOUD T. L. Empirical prediction of liquefaction-induced lateral spread. *Journal of Geotechnical and Geoenvironmental Engineering*, vol. 121(4), pp. 316–329, 1995.

[13] YOUD T. L., HANSEN C. M., BARTLETT S. F.. Revised multilinear regression equations for prediction of lateral spread displacement. *Journal of Geotechnical and Geoenvironmental Engineering*, vol. 128(2), pp. 1007–1017, 2002.

[14] YOUD T. L. Application of MLR procedure for prediction of liquefaction-induced lateral spread displacement. *Journal of Geotechnical and Geoenvironmental Engineering*, vol.144(6), 2018.

[15] LENG Y., ZHANG H., ZHANG W. *Introduction to Machine Learning (Practical application of MATLAB)*. Beijing: Tsinghua University Press, 2022.

[16] ZHANG Y., WANG R., ZHANG J. M., *ET AL.* A constrained neural network model for soil liquefaction assessment with global applicabilit. *Frontiers of Structural and Civil Engineering*, vol. 14, pp. 1066–1082, 2020.

[17] SHI X., HAN Y. Model of multi-class support vector machine on identifying sand seismic liquefaction. *Journal of Hydroelectric Engineering*, vol. 29(3), 6–12, 2010.

[18] ZHANG Y., WANG R., ZHANG J., *ET AL.* Study of data-driven methods for predicting soil liquefaction-induced lateral displacement. *Journal of Hydroelectric Engineering*, vol. 42(3), pp. 103–117, 2023.

[19] ARAUJO W., LEDEZMA C. Factors that affect liquefaction-induced lateral spreading in large subduction earthquakes. *Applied Science*, vol. 10(18), pp. 1–6503, 2020.

[20] OLSON S. M., GREEN R. A., LASLEY S., *ET AL.* Documenting liquefaction and lateral spreading triggered by the 12 January 2010 Haiti Earthquake. *Earthquake Spectra*, vol. 27(S1), pp. S93–S116, 2011.

[21] RAUCH A. F., MARTIN II J. R. Epolls model for predicting average displacements on lateral spreads. *Journal of Geotechnical and Geoenvironmental Engineering*, vol. 126(4), pp. 360–371, 2000.

[22] BARDET J. P., TOBITA T., MACE N., *ET AL.* Regional modeling of liquefaction-induced ground deformation. *Earthquake Spectra*, vol. 18(1), pp. 19–46, 2002.

[23] FAIRS A. T., SEED R. B., KAYEN R. E., *ET AL.* A semi-empirical model for the estimation of maximum horizontal displacement due to liquefaction-induced lateral spreading[C]/ In Proceedings of the 8th U.S. National Conference on Earthquake Engineering April 18–22, San Francisco, California, USA, 2006.

[24] CHU D. B., STEWART J. P., YOUD T. L., *ET AL.* Liquefaction-induced lateral spreading in near-fault regions during the 1999 Chi-Chi, Taiwan Earthquake. *Journal of Geotechnical and Geoenvironmental Engineering*, vol. 132(12), pp. 1549–1565, 2006.

[25] CETIN K. O., YOUD T. L., SEED R. B., *ET AL.* Liquefaction-induced lateral spreading at izmit bay during the Kocaeli (Izmit)-Turkey Earthquake. *Journal of Geotechnical and Geoenvironmental Engineering*, vol. 130(12), pp. 1300–1313, 2004.

[26] RATHJE E., MARTIN J., DETERLING O. Lateral spreading deformations from satellite images and optical image correlation for the 2011 Christchurch earthquake [DB]. Network Earthquake Eng. Simulation (NEES), 2015. Accessed June 22, 2024. https://doi.org/10.4231/D3MW28F9X.

[27] YANG Y., ZHANG Q. A hierarchical analysis for rock engineering using artificial neural networks. *Rock mechanics and rock engineering*, vol. 30, pp. 207–222, 1997.

[28] LI C., CAO Z., LI R. Assessment criterion for level of liquefaction-induced lateral spread and its reliability analysis. *Chinese Journal of Geotechnical Engineering*, vol 38(9), pp. 1668–1677, 2016.

Q.111 - R.34

COMMISSION INTERNATIONALE DES
GRANDS BARRAGES

VINGT-HUITIEME CONGRES DES
GRANDS BARRAGES
CHENGDU, MAI 2025

BROADBAND GROUND-MOTION SIMULATION: SENSITIVITY TO PULSE DURATION OF SOURCE SLIP-RATE FUNCTION (*)

Shaoqing WANG, Lijun ZHAO & Cuiran ZHANG
Earthquake Engineering Research Center, China Institute of Water Resources and Hydropower Research, Beijing

CHINA

SUMMARY

The slip-rate function is one of the most critical factors in strong-motion simulation using kinematic source model. In this paper, we propose a multi-Gaussian slip-rate function composed of Gaussian functions with different band-width and beginning time. Then, using spectral element method, we simulate an aftershock of Luding earthquake on 7 September 2022 using both the new proposed slip-rate function and Liu et al. (2006) function to investigate the influence of initial velocity pulse duration of in the slip-rate function on ground-motion simulation. By comparing the results, we show that, (1) the new slip-rate function can approximate other slip-rate functions (e.g. Liu et al 2006 model) by adopting proper parameters. (2) If the total rise time of the rupture process is the same, the duration of initial velocity pulse has significant influence on the median and high frequency content of simulated ground motion. The shorter is the pulse duration, the higher is the median- and high-frequency intensity. However, the pulse duration has only limited influence on low-frequency content. (3) The new proposed multi-Gaussian slip rate function is

Simulation de mouvements de terrain – sensibilité à la durée de l'impulsion de la fonction de taux de glissement de la source

 DOI: 10.1201/9781003642428-135

more flexible than Liu et al. (2006) model, and the simulation results using our new model may be closer with the record by setting proper parameters. This preliminary study may bring new insight to broadband simulation of ground motion using spectral element method.

RÉSUMÉ

La fonction de taux de glissement est l'un des facteurs les plus critiques dans la simulation de mouvements forts à l'aide d'un modèle de source cinématique. Dans cet article, nous proposons une fonction de taux de glissement multi-gaussienne composée de fonctions gaussiennes avec une largeur de bande et un temps de départ différents. Ensuite, en utilisant la méthode des éléments spectraux, nous simulons une réplique du tremblement de terre de Luding le 7 septembre 2022 en utilisant à la fois la nouvelle fonction de taux de glissement proposée et la fonction de Liu et al. (2006) pour étudier l'influence de la durée de l'impulsion de la vitesse initiale dans la fonction de taux de glissement sur la simulation du mouvement du sol. En comparant les résultats, nous montrons que (1) la nouvelle fonction de taux de glissement peut approximer d'autres fonctions de taux de glissement (par exemple le modèle de Liu et al 2006) en adoptant les paramètres appropriés. (2) Si le temps de montée total du processus de rupture est le même, la durée de l'impulsion de vitesse initiale a une influence significative sur le contenu médian et haute fréquence du mouvement du sol simulé. Plus la durée de l'impulsion est courte, plus l'intensité de la médiane et de la haute fréquence est élevée. Cependant, la durée de l'impulsion n'a qu'une influence limitée sur le contenu des basses fréquences. (3) La nouvelle fonction de taux de glissement multi-gaussienne proposée est plus flexible que le modèle de Liu et al. (2006), et les résultats de la simulation utilisant notre nouveau modèle peuvent être plus proches de l'enregistrement en définissant des paramètres appropriés. Cette étude préliminaire peut apporter un nouvel éclairage sur la simulation à large bande du mouvement du sol à l'aide de la méthode des éléments spectraux.

1. INTRODUCTION

In physical-based ground-motion simulation method using kinematic source models, the slip rate function of source is one of the most critical factors. Recent research using spectral-element code SPECFEM3D [1], such as He et al. [2] and

Wang et al. [3], utilize build-in Gaussian function as the slip rate function. However, pseudo-dynamic simulation [4,5], laboratory earthquake experiment [6], and related strong-motion simulations all show that, the strong energy of earthquake wave originates behind the rupture front during propagation, and the high-frequency content of ground motion radiates during a very short time just after the rupture starting. Therefore, the duration of initial slip-velocity pulse may represents the strong-motion energy radiated by earthquake sources better than rise time.

Many studies try to mimic the pulse-like initial slip velocity. On one hand, researchers proximately consider this phenomena by given shorter rise time. Wirth et al. [7] studies rationality of different rupture velocity and shows a shorter rise time produces better results in strong-motion simulation. Wang et al. [3] proposes an muti-dimension source model in which the rise time is half for an additioal layer, which indeed shortens the rise time. One the other hand, many source model use Kostrov-type slip-rate function directly modeling the pulse in the front of the time-velocity function. Those kinds of models are composed of a short initial pulse with high peak and a flat tail with long duration, which have a closer form with the results indicated by pseudo-dynamic simulations and laboratory experiments. For example. Guatteri et al. [5] defines a slip-rate function composed of two triangulars. Tinti & Cocco [8] and Liu et al. [13], on the other hand, define two smoother models. The model of Tinti & Cocco [8] incorporates the time of peak velocity in slip-rate function as a parameter, while the model of Liu et al. [13] has non-zero first and second derivatives at the start of rupture process, so that the initial phase of the simulated rupture process will radiate high-frequency energy.

In the model of Liu et al. [13], the initial pulse duration is fixed as 0.1267 times of the rise time. Thus, the slip velocity of the rupture is also fixed given a magnitude. However, research show that the pulse proportion is not the same, and the shape of the entire slip-rate function is also different. Therefore, in this paper, we propose a new slip-rate function composed with multiple Gaussian-type function to mimic different (pseudo-) real rupture time velocity process. We show that the new function is also a generalization of the model in Liu et al. [13] if adopting proper parameters. Based on this new method, we simulate ground motion of one of the Luding aftershocks, and then investigate the influence of initial pulse duration of time-velocity function on the ground-motion simulation. If properly truncated, this Guassian super-positioned model will also have non-zero first and second derivate at the beginning, like the model in Liu et al. Moreover, because SPECFEM3D has a build-in Gaussian source-time function, this new model can be directly used in finite source simulation using this software without any modification. Thus, it may bring new insight to the broadband simulation of strong motion using spectral element method.

2. SOURCE SLIP-RATE FUNCTION

2.1. Liu et al. (2006) model

Enlighted by the pseudo-dynamic simulation of works of Guatteri et al. [4∼5], Liu et al. proposed a slip rate function to simulate broadband ground motion. The form of Liu 2006 is

$$\dot{s}(t) = \begin{cases} C_N[0.7 - 0.7\ \cos\left(\dfrac{\pi t}{\tau_1}\right) + 0.6\ \sin\left(0.5\pi t/\tau_1\right)] & 0 \le t < \tau_1 \\ C_N[1 - 0.7\ \cos\left(\dfrac{\pi t}{\tau_1}\right) + 0.3\ \cos\left(\pi(t-\tau_1)/\tau_2\right)] & \tau_1 \le t < 2\tau_1 \\ C_N\left[0.3 + 0.3\ \cos\left(\dfrac{\pi t - \tau_1}{\tau_2}\right)\right] & 2\tau_1 \le t < \tau \end{cases} \quad (1)$$

where $C_N = \pi/(1.4\pi\tau_1 + 1.2\tau_1 + 0.3\pi\tau_2)$ and τ is rise time, $\tau_1 = 0.1267\tau$, $\tau_2 = \tau - \tau_1$. This model is also used in other studies such as Graves & Pitarka [9∼10] and Pitarka et al. [11]. In this paper, this model is adopted as a benchmark model, named as Liu 2006. An example of Liu 2006 model is plot in Fig. 1, as the gray solid line shows.

2.2. Multi-Gaussian slip-rate function

The model of Liu 2006 can be treated as a composition of two parts: a short initial velocity pulse with high peak and a slower flat tail with long duration. The duration of initial pulse is fixed, that is, $T_p = 0.1267$. However, the real rupture process may not obey this proportion. If using multi-Gaussian functions, the entire source-time process with any arbitrary shape may be represented approximately. For example, we can mimic a Kostrov-type slip-rate function, such as Liu et al. (2006) model or Tin et al. (2005) model, by using two Gaussian functions, the first has a narrow bandwidth but high peak and the second conversely has a wide bandwidth but lower peak.

The multi-Gaussian slip-rate function can be described as following:

$$s_r(t) = \sum_{j=1}^{n} C_j \quad \frac{A_j}{\pi}\exp\left\{-\left[\left(t - t0_j\right)A_j\right]^2\right\} \quad (2)$$

where C_j denotes the energy proportion of the jth Gaussian function; $A_j = \frac{\alpha}{\tau_j}$, and α is the decay rate of source; τ_j and $t0_j$ is the rise time and beginning time of the jth Gaussian function, which can be described by the rise time τ of the entire rupture

process,

$$\tau_j = K_j^{\tau}\tau \tag{3}$$

$$t0_j = K_j^{t0}\tau \tag{4}$$

where $\boldsymbol{C_j}$,$\boldsymbol{K_j^{\tau}}$ and $\boldsymbol{K_j^{t0}}$ are all model parameters, which can be calibrated using ground-motion records or be fitted by other slip-rate function. Using above functions, we can also obtain the beginning time $\boldsymbol{T_{F,j}}$ and slip distance $\boldsymbol{u_j}$ of each Gaussian function, given the entire slip of the rupture $\boldsymbol{u}$:

$$T_{F,j} = \left(K_{i,j}^{t0} - \frac{K_{i,j}^{\tau}}{2}\right)\tau_i \tag{5}$$

$$u_j = C_j u \tag{6}$$

Fig. 1 shows an approximation of Liu 2006 model using two Gaussian slip functions G1 and G2. The black solid line G1+G2 indicates the multi-Gaussian curve is very close to the original Liu 2006 model.

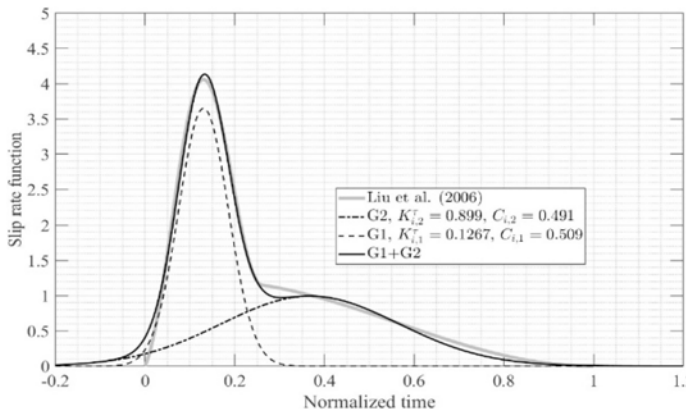

Fig. 1
Approximate Liu et al. (2006) model using two Gaussian slip functions. (G1 and G2 are both normalized Gaussian functions)

Approximate Liu et al. (2006) model using two Gaussian slip functions. (G1 and G2 are both normalized Gaussian functions)

3. SENSITIVITY OF INITIAL PULSE DURATION TO GROUND-MOTION SIMULATION

In this section, we simulate an aftershock of Luding earthquake using both our new proposed multi-Gaussian slip rate function with different parameters and Liu 2006 slip rate function. The objective is to show the influence of initial pulse duration to ground-motion simulation results. To eliminate other disturbances of other factors, we adopt a point source in our simulation.

3.1. EARTHQUAKE EVENT

We adopt an slip-type aftershock of Luding earthquake occurred on 02:42:15, 7 September 2022. According to Yang et al. [12], the mechanism of the source is Strike330/Dip70/Rake0, with a focal depth of 8 km. According to the website of Global CSMT, the source rise time of this aftershock is $\tau = \mathbf{2.4}$ s. The event is recorded by a station $\sim$5 km away, located on bedrock site near a reservoir dam. This gives us opportunity to validate our simulation results. Fig. 2 show the relative position of the source and site. We use a 15 km *13 km* 25 km cube for the simulation and consider topography in this region and a simplified crustal model. The final spectral element model have 893,000 elements and around 22.56 million degree of freedoms, as shown in Fig. 3. The highest effective frequency is $\sim$ 5.5 Hz.

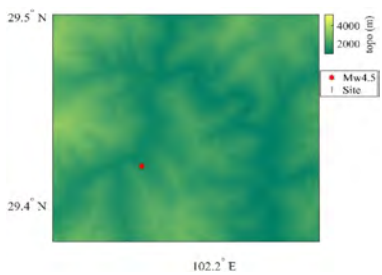

Fig. 2
Earthquake source of Luding aftershock occurred at 02:42:15, 7 September 2022 and the site

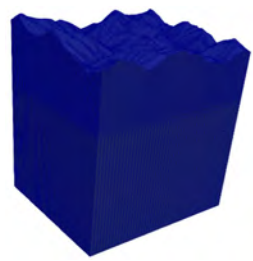

Fig. 3
Spectral element model

3.2. Slip-rate functions

In this section, we adopt 7 different slip-rate functions to show their influence on the ground-motion simulation, the slip-rate functions listed in Fig. 4b. Fig. 4a shows the benchmark slip-rate function, i.e. Liu 2006 model and the approximation of it using two Gaussian functions. Among those 7 functions, S1 is the Liu 2006 model, that is, the benchmark model. S2∼S6 are all superposition of two Gaussian functions, that is G.1 and G.2, but with different parameters, indicating different initial pulse durations. S7 is a single Gaussian slip-rate function. Because our objective is to study the effects of duration of initial pulses, we set S2 $\sim$ S6 have the same G2 ($\boldsymbol{T_p = 0.9\tau_r}$), but different G.1. The width of G.1 in S2 $\sim$ S6 are respective 0.08, 0.1267, 0.1, 0.15, and 0.2 times of τ_r. It is worth to note that S4 ($\boldsymbol{T_p = 0.1267\tau_r}$) approximates S1 (Liu 2006) using two Gaussian functions.

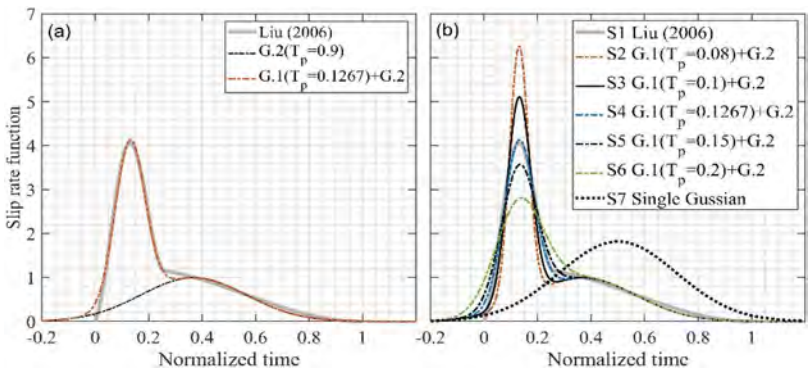

Fig. 4
(a) S1 (Liu 2006 model) and how to approximate S1 in S4 (two Gaussian function): (b) 7 slip-rate functions

4. RESULTS

We simulate the ground motion using the abovementioned 7 slip-rate functions, respectively. Fig. 5 shows the comparison of ground-motion velocity time histories among simulations and the record. The results show that, first, if adopting single Gaussian slip rate function model S7 (i.e. no initial velocity pulse), the simulated radiation energy of ground motion is significantly lower that records, indicating this slip function totally cannot represent the real intensity and frequency feature of real earthquake. Second, among S2 $\sim$ S7, S4 and S1 (Liu 2006 model) has the

closest results with the record, because the time-velocity functions of S1 and S4 are almost identical. Third, among S2 $\sim$ S6, the shorter is the pulse duration T_p, the higher is the amplitude of velocity time history.

Meanwhile, we also calculate the RotD50 of the response spectral acceleration (RSA) of both record and simulated ground accelerations, as shown in Fig. 6. RotD50 is the 50 percentiles of the two horizontal response spectral acceleration component rotated to all directions. The results show that, the initial pulse velocity duration mainly influence the high-frequency content of RSA. Among S2 $\sim$ S6, we can also see that the shorter is the pulse duration T_p, the higher is the amplitude. However, unlike the result in velocity time history that S4 ($T_p = 0.1267\tau_r$) and S1 (Liu et al 2006) are most close to the record, S3 ($T_p = 0.1\tau_r$) shows best results compared with the record. We can also see that S7 (single Gaussian) is lower that the record significantly. On the other hand, the second component of two-Gaussian slip rate function G.2 has almost none attribution to the high-frequency content of RSA. The results indicate the strong motion energy is mainly results of the short initial velocity, and is affected significantly by its duration.

To better illustrated the influence of short velocity pulses on RSA, we calculated the amplification coefficients of RSA to the case that $T_p/\tau_r = 0.2$, shown in Fig. 6. When T_p is lower, the RSA in all period range increase exponentially. The shorter is the period, more significant is the increase. T_p has little influence on low-frequency content. Therefore, T_p has influences on all frequency range, but mainly on high-frequency content.

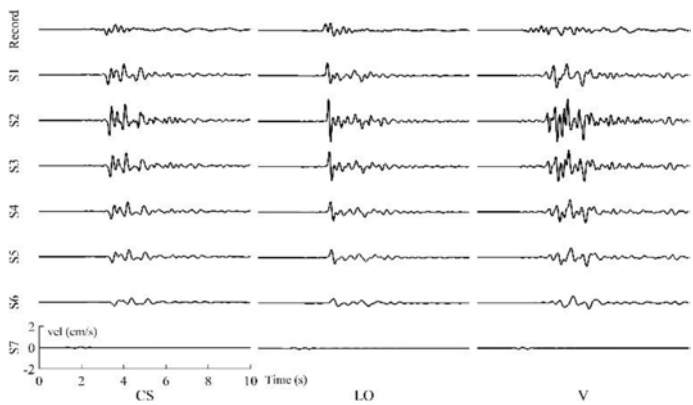

Fig. 5
Ground velocity time historied of both simulations and records filtered from 0.1 to 5.5Hz

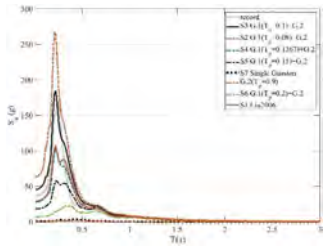

Fig. 6
Ground response spectral acceleration of both simulations and record (filtered from 0.1 to 5.5Hz)

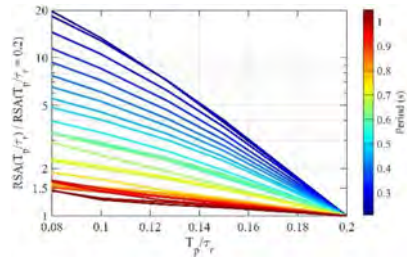

Fig. 7
RSA amplification coefficient to the case $T_p/\tau_r = 0.2$ for different T_p/τ_r

5. CONCLUSION

In this paper, we propose a new slip-rate function composed with multiple Gaussian-type function to mimic different (pseudo-) real rupture time velocity process. Then, using spectral element method, we simulate an aftershock of Luding earthquake on 7 September 2022 using both the new proposed slip-rate function and Liu et al. (2006) function to investigate the influence of initial velocity pulse duration on ground-motion simulation. By comparing the results, we show that:

1. The new slip-rate function can approximate other slip-rate function (e.g. Liu et al 2006 model) by adopting proper parameters.
2. If the total rise time of the rupture process is the same, the duration of initial velocity pulse has significant influence on the median and high frequency content of simulated ground motion. The shorter is the pulse duration, the higher is the median- and high-frequency intensity.
3. The new proposed multi-Gaussian slip rate function is more flexible than [13] model, and the simulation results using our new model may be closer with the recorded motion. This preliminary study may bring new insight to broadband simulation of ground motion using spectral element method.

REFERENCES

[1] KOMATITSCH D., TROMP J. Introduction to the spectral element method for three-dimensional seismic wave propagation. *Geophys J Int*; 139:806–22, 1999. https://doi.org/10.1046/j.1365-246X.1999.00967.x.

[2] HE C.H., WANG J.T., ZHANG C.H., JIN F. Simulation of broadband seismic ground motions at dam canyons by using a deterministic numerical approach. *Soil Dyn Earthq Eng*;76:136–44, 2015. https://doi.org/10.1016/j.soildyn.2014.12.004.

[3] WANG X.C., WANG J.T., ZHANG L., LI S., ZHANG C.H. A multidimension source model for generating broadband ground motions with deterministic 3d numerical simulations. *Bull Seismol Soc Am*;111:989–1013, 2021. https://doi.org/10.1785/0120200221.

[4] GUATTERI M, MAI P.M., BEROZA G.C., BOATWRIGHT J. Strong ground-motion prediction from Stochastic-dynamic source models. *Bull Seismol Soc Am*;93:301–13, 2003.

[5] GUATTERI M., MAI P.M., BEROZA G.C. A pseudo-dynamic approximation to dynamic rupture models for strong ground motion prediction. *Bull Seismol Soc Am*;94:2051–63, 2004. https://doi.org/10.1785/0120040037.

[6] MARTY S., PASSELEGUE F.X., AUBRY J., BHAT H.S., SCHUBNEL A, MADARIAGA R. Origin of High-Frequency Radiation During Laboratory Earthquakes. *Geophys Res Lett*;46:3755–63, 2019. https://doi.org/10.1029/2018GL080519.

[7] WIRTH E.A., FRANKEL A.D., VIDALE J.E. Evaluating a kinematic method for generating broadband ground motions for great subduction zone earthquakes: Application to the 2003 Mw 8.3 Tokachi-Oki earthquake. *Bull Seismol Soc Am*;107:1737–53, 2017. https://doi.org/10.1785/0120170065.

[8] TINTI E., COCCO M. Earthquake fracture energy inferred from kinematic rupture models on extended faults;110:1–25, 2005. https://doi.org/10.1029/2005JB003644.

[9] GRAVES R., PITARKA A. Broadband ground-motion simulation using a hybrid approach. *Bull Seismol Soc Am*;100:2095–123, 2010. https://doi.org/10.1785/0120100057.

[10] GRAVES R., PITARKA A. Refinements to the Graves and Pitarka (2010) broadband ground-motion simulation method. *Seismol Res Lett*;86:75–80, 2015. https://doi.org/10.1785/0220140101.

[11] PITARKA A., GRAVES R., IRIKURA K., MIYAKOSHI K., RODGERS A. Kinematic Rupture Modeling of Ground Motion from the M7 Kumamoto, Japan Earthquake. *Pure Appl Geophys*;177:2199–221, 2020. https://doi.org/10.1007/s00024-019-02220-5.

[12] YANG Z., DAI D., ZHANG Y., ZHANG X., LIU J. Rupture process and aftershock focal mechanisms of the 2022 M6. 8 Luding earthquake in Sichuan Related articles that may interest you M6. 8 Luding earthquake in Sichuan. *Earthq Sci 2022*;36:1–12, 2022. https://doi.org/10.1016/j.eqs.2022.12.005.

[13] LIU P., ARCHULETA R.J., HARTZELL S.H. Prediction of broadband ground-motion time histories: Hybrid low/high-frequency method with correlated random source parameters. *Bull Seismol Soc Am*;96:2118–30, 2006. https://doi.org/10.1785/0120060036

COMMISSION INTERNATIONALE DES
GRANDS BARRAGES

VINGT-HUITIEME CONGRES DES
GRANDS BARRAGES
CHENGDU, MAI 2025

EFFECTS OF ORIFICES AND SLUICE PIERS ON SEIMSIC RESPONSE OF A HIGH ARCH DAM (*)

Hui LIANG, Chunli YAN, Shengshan GUO & Jin TU
State Key Laboratory of Simulation and Regulation of Water Cycle in River Basin, China Institute of Water Resources and Hydropower Research, Beijing

CHINA

SUMMARY

A high arch dam is taken as an example. Seismic analysis of the dam with and without orifice and sluices piers is conducted considering the infinite foundation radiation damping effect and the contact nonlinearity of contraction joints. The static and dynamic displacement, stress, and contraction joint opening under the two schemes are compared and analyzed to demonstrate the influence of the multi-layered flood discharge orifices arrangement on the seismic performance of the arch dam. It is obtained that the effects of the orifices and sluice piers on the static and dynamic response are not significant overall. The relatively obvious difference appears mainly around the orifices and piers.

RÉSUMÉ

Ce rapport prend l'exemple un grand barrage-voûte. Une analyse sismique a été effectuée pour les barrages avec et sans orifices et piliers, en tenant compte de

**Effets des pertuis et des piles d'évacuateurs sur la réponse sismique d'un grand barrage-voûte*

DOI: 10.1201/9781003642428-136

l'effet d'amortissement infini du rayonnement de la fondation et de la non-linéarité de contact des joints de contraction. On a comparé et analysé les déplacements statiques et dynamiques, les contraintes et les ouvertures de joints selon les deux protocoles afin de démontrer l'influence de la disposition des pertuis sur la résistance sismique des barrages-voûtes. Les résultats montrent que l'influence des orifices et des piliers sur la réponse statique et dynamique n'est pas significative dans l'ensemble. Des différences relativement évidentes apparaissent principalement autour des orifices et des piles.

1. INTRODUCTION

Due to the common characteristics such as high water head, large flow rate, and narrow river valleys in high arch dam projects in western China, the way of simultaneously arranging multiple layers of spillway facilities such as surface holes, medium (deep) holes, etc. in the dam body is adopted preferentially on the premise of ensuring the safety of energy dissipation in the design of flood discharge and energy dissipation. However, the multi-layered flood discharge outlets objectively weaken the integrity of the arch dam, especially the orifice structures are often located at the upper elevation of the dam body where seismic dynamic amplification effects are more significant, and its stress condition is very complex. Meanwhile, the influence of the presence of orifices and piers on the static and dynamic response of the dam body is also a concern in engineering. Most of the existing research focuses on seismic analysis of dams without orifices and piers considering factors such as the infinite foundation radiation damping, contact nonlinearity of contraction joints and material nonlinearity of mass concrete[1]-[8]. The orifices and piers shall be separately calculated and analyzed in the local structural design [9]–[15]. Deyu LI, Jin Tu, et.al. [16] conduct a research on the influence of the presence or absence of orifices and piers on the static and dynamic stress response of the Xiluodu arch dam. Gong Yaqi, Jie Zhiqiang et al. [17] perform a comparative analysis of the effects of the upper structure and the arrangement of piers on the seismic performance of a dam. It is found that increasing the stiffness of piers and reducing the mass near the overflow weir show a significant shock-absorbing effect. Xiong Kun, Wang Weihao et al. [18] compare and analyze the effects of two schemes, namely the arrangement of flood discharge outlets and the absence of flood discharge outlets, on the overall stress, deformation, damage and the ultimate seismic capacity of an arch dam.

Generally, few research on seismic analysis of dams that consider both the orifice and the gate pier simultaneously is found. Hence, this study takes a high arch dam as an example. The infinite foundation radiation damping effect and the

contact nonlinearity of contraction joints are considered. The seismic analysis of the dam with and without orifice and sluices piers is conducted. The static and dynamic displacement, stress, and contraction joint opening under the two schemes are compared and analyzed to demonstrate the influence of the multi-layered flood discharge orifices arrangement on the seismic performance of the arch dam.

2. MODEL, MATERIAL PARAMETERS AND LOADS

2.1. Model configuration

Fig. 1 shows the finite element meshes of the dam foundation systems with and without orifices and piers. Fig. 2 are the meshes of the dams. Fig. 3 shows the layout of contraction joints. All 20 contraction joints are simulated according to the actual layout of the dam.

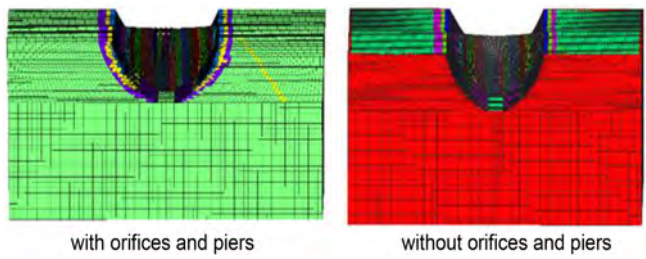

Fig. 1
The finite element meshes of the dam foundation systems

Fig. 2
The finite element meshes of the dams

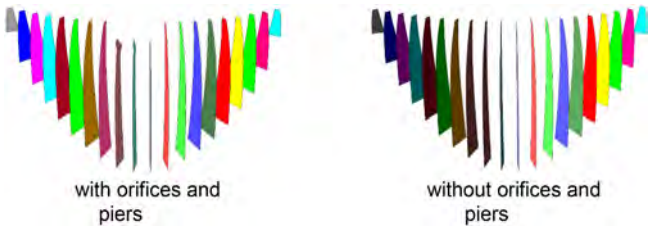

Fig. 3
The contraction joints

2.2. Material parameters

The bulk density of the dam concrete is 24.0 KN/m^3, the elastic modulus of the dam concrete is 24.0 GPa, the Poisson's ratio is 0.167, and the coefficient of linear expansion is 10-5/℃. In the dynamic analysis, the concrete elastic modulus is increased by 50% compared to the static elastic modulus according to the Chinese specifications. The rock types include granite and granodiorite. The dam foundation rock mass mechanical parameters are provided by the designer.

2.3. Load conditions

The upstream normal water level and its corresponding downstream water level are 2535.00 m and 2345.00 m. The floating bulk density and the internal friction angle of the silt are 8kN/m3 and 12º. Its elevation in front of the dam is 2420.00 m.

The generated normalized input earthquake motions in three directions i.e. cross-river direction, stream-river direction and vertical direction based on the site-related design response spectrum related to the scenario earthquake are shown in Fig. 4. The Westergaard added mass method is adopted to simulate the hydrodynamic water pressure. The viscoelastic artificial boundary[20] is adopted to consider the radiation damping effect. The dynamic contact model[19] is used to model the opening and sliding of the contraction joints.

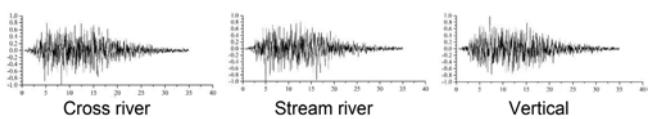

Fig. 4
The normalized artificial earthquake motions

3. RESULT AND DISCUSSION

3.1. Effects on static stress and displacement

Fig. 5 shows the upstream displacement of the arch crown cantilever varying with the elevation under the normal water condition. Fig. 6 displays the upstream and downstream minimum principal stress of the arch crown cantilever varying with the elevation under the normal water condition. Fig. 7 presents the upstream and downstream minimum principal stress at ▽2500 m arch ring varying with the distance to the left bank under the normal water condition. The maximum displacements at the arch crown cantilever with and without the orifices and piers are 11.14 cm and 10.27 cm, respectively, which are relatively close. It can be seen that except for the stress concentration regions such as the dam heel, dam toe, and the junction between the gate pier and the dam, compared with the dam without orifices and piers, slight difference of the upstream and downstream minimum principle stress located around the orifices and piers is observed under the normal water condition.

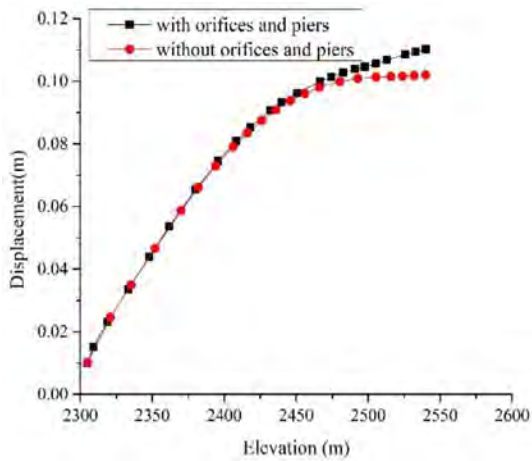

Fig. 5
The upstream displacement of the arch crown cantilever varying with the elevation under the normal water condition

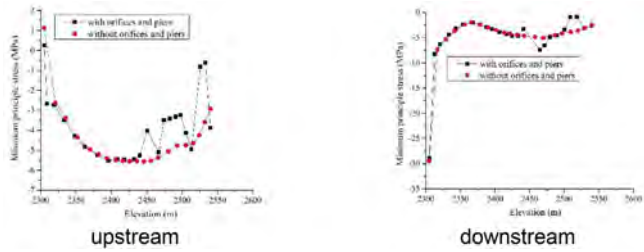

Fig. 6
The upstream and downstream minimum principal stress of the arch crown cantilever varying with the elevation under the normal water condition

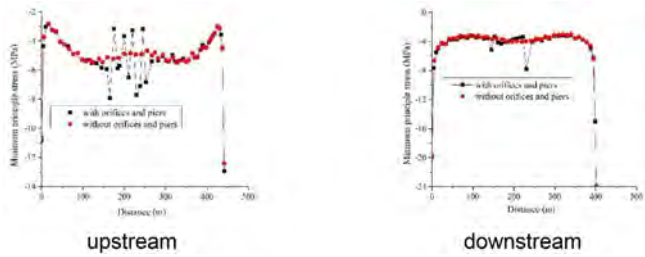

Fig. 7
The upstream and downstream minimum principal stress at ▽2500 m arch ring varying with the distance to the left bank under the normal water condition

3.2. Effects on the static and dynamic comprehensive stress and contraction joints

The maximum opening of the contraction joints at the dam crest are about 8.85 mm and 9.90 mm without and with orifices and piers under the normal water condition and artificial earthquake motions, respectively. The maximum opening at the dam crest with orifices and piers is greater than that without orifices and piers.

Fig. 8 and Fig. 9 show the maximum and minimum principal stress of the dam with and without orifices and piers. Fig. 10 shows the maximum and minimum principal stress of the arch crown cantilever varying with the elevation under the normal water condition and artificial earthquake motions. Except for the dam heel and toe, a slight difference in the upstream maximum principal stress varying with the elevation with and without orifices and piers is found. While, the difference in the

upstream minimum principal stress is relatively obvious. The upstream minimum principal stress with orifices and piers is slightly lower than that without orifices and piers below ▽2450 m. While above ▽2450 m, it is greater than that without orifices and piers as a whole. There is only a slight difference in the downstream maximum and minimum principal stress with and without orifices and piers.

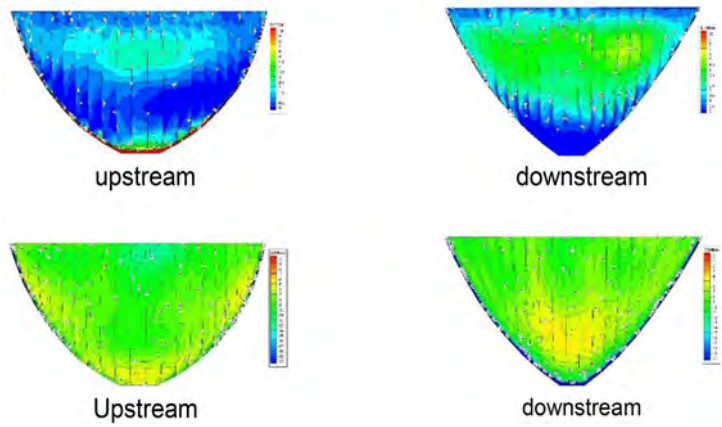

Fig. 8
The maximum and minimum principal stress of the dam under the normal water condition and artificial earthquake motions (without orifices and piers)

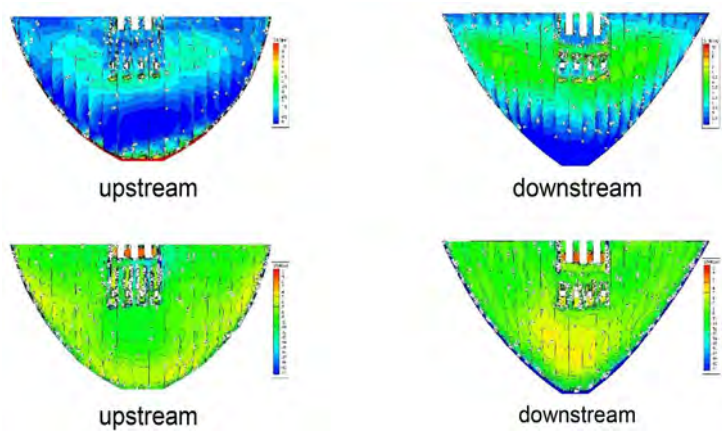

Fig. 9
The maximum and minimum principal stress of the dam under the normal water condition and artificial earthquake motions (with orifices and piers)

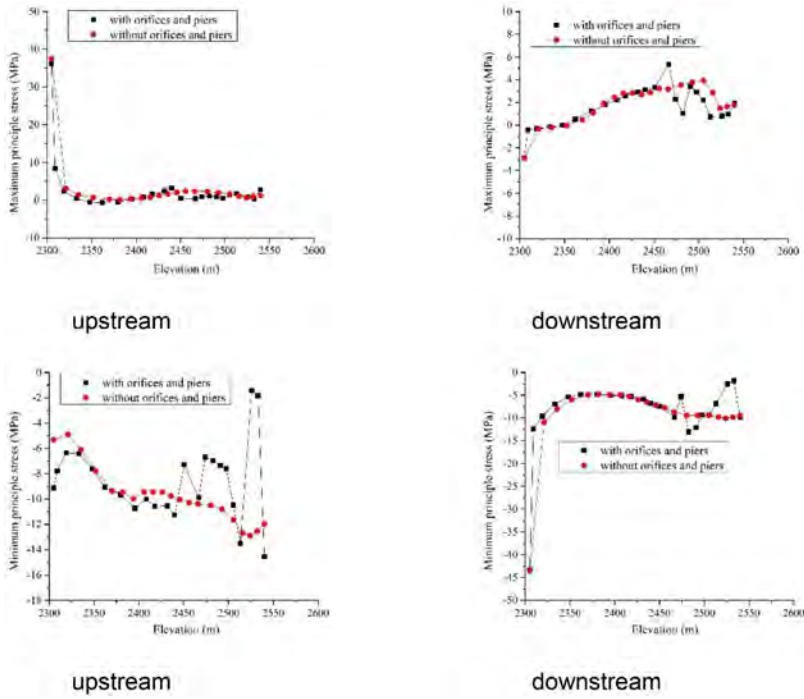

Fig. 10
The maximum and minimum principal stress of the arch crown cantilever varying with the elevation under the normal water condition and artificial earthquake motions

4. CONCLUSIONS

In this paper, the infinite foundation radiation damping effect and the contact nonlinearity of contraction joints are considered. The seismic analysis of the dam with and without orifice and sluices piers is conducted. The main conclusions are as follows:

1. The maximum displacements at the arch crown cantilever with and without the orifices and piers are 11.14 cm and 10.27 cm, respectively, which are relatively close. Except for the stress concentration regions, compared with the dam without orifices and piers, slight difference of the upstream and downstream minimum principal stress located around the orifices and piers is observed under the normal water condition. The maximum opening at the dam crest with orifices and piers is greater than that without orifices and piers.

2. Except for the dam heel and toe, a slight difference in the upstream maximum principal stress varying with the elevation with and without orifices and piers is found. The difference in the upstream minimum principal stress is relatively obvious. The upstream minimum principal stress with orifices and piers is slightly lower than that without orifices and piers below ▽2450 m. While above ▽2450 m, it is greater than that without orifices and piers as a whole. There is only a slight difference in the downstream maximum and minimum principal stress with and without orifices and piers.

ACKNOWLEDGMENTS

The authors are grateful for the financial support from the technology project i.e. Major technical research on a high-altitude long negative temperature period high roller compacted concrete dam supported by China Huaneng Group Co., Ltd. (HNKJ22-H108) and the technology project i.e. Research on the Theoretical and Technical System of Seismic Resistance for Ultra High Dam Projects in High Seismic Zones supported by supported by China Electric Power Construction Corporation (DJ-ZDXM-2021-03).

REFERENCES

[1] HARIRI-ARDEBILI M A, MIRZABOZORG H. Reservoir Fluctuation Effects on Seismic Response of High Concrete Arch Dams Considering Material Nonlinearity [J]. *Journal of Civil Engineering Research*, 2011, 1(1): 9–20.

[2] CHEN D H, CHENG-BIN D U, YUAN J W, *ET AL.* An Investigation into the Influence of Damping on the Earthquake Response Analysis of a High Arch Dam [J]. *Journal of Earthquake Engineering*, 2012, 16(3-4): 329–349.

[3] CHENG H, ZHANG L. Study on Ultimate Anti-Seismic Capacity of High Arch Dam [J]. *Journal of Aerospace Engineering*, 2013, 26(4): 648–656.

[4] YUE J, ZHANG X, YE L. Seismic Affection Analysis of Weir Dam based on 3-D FEM [J]. *Applied Mechanics and Materials*, 2013, 438-439: 1546–1550.

[5] WANG JIN-TING, JIN, *ET AL.* Scatter of dynamic response and damage of an arch dam subjected to artificial earthquake accelerograms [J]. *Soil Dynamics & Earthquake Engineering*, 2016, 87: 93–100.

[6] OMIDI O, LOTFI V. Seismic plastic–damage analysis of mass concrete blocks in arch dams including contraction and peripheral joints [J]. *Soil Dynamics & Earthquake Engineering*, 2017, 95: 118–137.

[7] GUO S, LIANG H, WU S, *ET AL.* Seismic damage investigation of arch dams under different water levels based on massively parallel computation[J]. *Soil Dynamics and Earthquake Engineering*, 2020, 129: 105917–1-8.

[8] MENG-ZHONG ZHANG, XIANG-CHAO WANG, JIN-TING WANG, JIAN-WEN PAN, FENG JIN, HUI-BAO HUANG. Seismic response analysis of Dagangshan arch dam during 2022 Luding Ms 6.8 earthquake using source-to-structure simulation [J]. *Soil Dynamics and Earthquake Engineering*, 2024, 178: 108492–1-11.

[9] WANG YIFENG. Seismic analysis of the spillway surface outlet piers of Ertan Arch Dam [J]. *Hydropower Station Design*, 1990 (02): 11–18. (In Chinese)

[10] CHEN PING, CUI GUANGTAO. Influence of Sluice Piers on Flood Discharge Vibration of High Arch Dams [J]. *Hydroelectric Power*, 1999 (4): 20–23. (In Chinese)

[11] JANG B S, LIM J Y, LEE M K, *ET AL.* Static Behavior Analysis of Spillway Pier for Dam Safety Evaluation [J]. *Journal of the Korea Concrete Institute*, 2007, 19(1): 11–18.

[12] ZHAO XIAOLIAN, ZHANG ZHONGQING. Stress analysis of horizontal beams and gate piers in a hyperbolic arch dam with dam crest openings [J]. *Journal of Water Resources and Water Transport Engineering*, 2004, 4 (4): 46–49. (In Chinese)

[13] SONG L, WU M, WANG J, *ET AL.* Seismic damage analysis of the outlet piers of arch dams using the finite element sub-model method [J]. *Earthquake Engineering and Engineering Vibration*, 2016, 15: 617–626.

[14] FUJITA M, SATO N, TOMIDA N, *ET AL.* Non-linear Dynamic Analysis of a 3D Solid Model for Safety Evaluation of Seismic Resistance of Dam Gate Piers [J]. *Journal of Japan Society of Dam Engineers*, 2017, 27(3): 185–194.

[15] KANTHAKASIKAM R, CHARATPANGOON B, HANSAPINYO C, *ET AL.* Seismic Safety Analysis of Dam Appurtenant Structures in Northern Thailand [J]. *KSCE Journal of Civil Engineering*, 2024, 28(7): 2885–2896.

[16] DE-YU LI, JIN T U, JIN-HUI O. Nonlinear seismic response analysis on Xiluodu arch dam with orifices and piers [J]. *Journal of Hydraulic Engineering*, 2013, 44(11): 1366–1371.

[17] GONG YAQI, JIE ZHIQIANG, *ET AL.* Seismic characteristics analysis of high gate piers in gravity dams [J]. *Hydroelectric Power*, 2014, 40 (4): 42–45. (In Chinese)

[18] XIONG KUN, WANG WEIHAO, HUANG HONGFEI. Study on the influence of two-layer spillway openings on the seismic performance of ultra-high arch dams [J]. *Journal of China Academy of Water Resources and Hydropower Research (Chinese and English)*, 2024, 22 (1): 63–72. (In Chinese)

[19] GUO S, LIANG H, LI D, *ET AL.* A comparative study of cantilever- and integral-type dead loads on the seismic response of high arch dams. *Int J Struct Stab Dyn* 2019; 19(3):1–21.

[20] JINGBO LIU, YIXIN DU, XIULI DU, *ET AL.* 3D viscous-spring artificial boundary in time domain [J]. *Earthquake Engineering and Engineering Vibration*, 2006, 5(1): 93–102.

Q.111 - R.36

COMMISSION INTERNATIONALE DES
GRANDS BARRAGES

VINGT-HUITIEME CONGRES DES
GRANDS BARRAGES
CHENGDU, MAI 2025

SEISMIC SAFETY ANALYSIS OF ASPHALT CONCRETE FACE ROCKFILL DAMS UNDER HIGH SEISMIC INTENSITY (*)

Gao DONGHONG & Zhu RUIHENG
Shanghai Investigation, Design & Research Institute Co., Ltd.

CHINA

SUMMARY

A proposed pumped storage power station is located in a strong earthquake area in China, with an upper reservoir asphalt concrete face rockfill dam and a maximum dam height of 101 m. The three-dimensional nonlinear finite element method is used to carry out the static and dynamic stress and deformation calculations of the dam and analyze the seismic stability of the dam. The results show that the deformation law of the dam under static conditions is in accordance with the general law, and the extreme values of the horizontal displacement and settlement of the dam body during the full storage period are 3.1 cm and 40 cm, respectively; Under the 100-year 1% exceeding probability check earthquake (seismic acceleration of 0.897 g), the dynamic response of the dam body and the panels are distributed in a reasonable pattern. The extreme values of the acceleration of the dam body in the down-river direction, the dam axis and the vertical direction are 10.649, 9.824 and 11.497 m/s^2, respectively. Considering the superposition of the seismic effect and the static force, the maximum tensile strain of the asphalt concrete panels occurs in the intersection of the panels and the reservoir basin close to

Analyse sismique d'un barrage en enrochement à masque en béton bitumineux sous l'effet d'un séisme majeur

 DOI: 10.1201/9781003642428-137

the side of the dam as 0.441%, which is smaller than the general permissible value of the tensile strength of the modified asphalt concrete.

RÉSUMÉ

Un projet de centrale de pompage-turbinage est situé dans une zone très sismique en Chine, avec un barrage supérieur en enrochement et parement en béton bitumineux et une hauteur maximale de 101 m. La méthode tridimensionnelle non linéaire des éléments finis est utilisée pour effectuer les calculs de contraintes et de déformations statiques et dynamiques du barrage et analyser la stabilité sismique du barrage. Les résultats montrent que la loi de déformation du barrage dans des conditions statiques est conforme à la loi générale, et que les valeurs extrêmes du déplacement horizontal et du tassement du corps du barrage pendant toute la vie de l'ouvrage sont respectivement de 3,1 cm et 40 cm. Pour le séisme de contrôle de probabilité supérieur de 1 % de 100 ans (accélération sismique de 0,897 g), la réponse dynamique du corps du barrage et du masque est répartie selon un schéma raisonnable. Les valeurs extrêmes de l'accélération du corps du barrage dans le sens aval du barrage, dans l'axe du barrage et dans la direction verticale sont respectivement de 10,649, 9,824 et 11,497 m/s^2. Compte tenu de la superposition de l'effet sismique et de la force statique, la déformation de traction maximale des dalles de béton bitumineux se produit à l'intersection des dalles et du réservoir près du côté du barrage à 0,441%, ce qui est inférieur à la valeur généralement admissible de la résistance à la traction du béton bitumineux modifié.

1. INTRODUCTION

In recent years, to achieve the goal of "carbon peaking and carbon neutrality", it is essential to build a new-type power system with large proportion of new energy. Taking the factors as the natural conditions of energy resources in China into consideration, pumped storage power station is considered to be a green, low-carbon, clean and flexible power source to the power system in terms of technology readiness level, economic efficiency, and potential of large-scaled development.

The dam type of the pumped storage power station was chosen based on the topographic and geological conditions of the dam site, and rockfill dam and gravity dam are the two options. Rockfill dam, especially the core dam and faced dam, is the first choice because of the features of its adaptation to the sudden drawdown and proven technologies[1]. In recent years, asphalt face is widely used in pumped

storage power projects because of the outstanding merits as its remarkable permeability, good adaptability to deformation, strong resistance to acid- and alkaline-corrosion and no pollution to water quality. All these make asphalt concrete face rockfill dam one of the optimal dam types[2]-[3]. However, there are various crucial technology issues to be solved for asphalt concrete faced-rockfill dams higher than 100 m[4]. Especially in West China, a region with high seismic intensity, the dams in service are probable facing with the hazards of extreme earthquake; therefore, the seismic safety during operation of the dams is one of the vital design researches [5]-[6]. For which, many scholars have conducted relevant studies. Zhi Bingcheng and others[7] considered the changes of factors as the dynamic characteristics of soil and analyzed the impacts of overburden on the dynamic response of asphalt core dam. He Jianxin and others[8], took Niya Reservoir in Xinjiang as an example, conducted the analysis of anti-seismic capacity of asphalt concrete core dams using equivalent linear viscoelastic model and hyperbolic residual deformation model. Zhao Jianming and others[9] conducted the analysis of maximum aseismic capability of a concrete face rockfill dam higher than 250 m by focusing on the stability, earthquake-induced residual deformation, unit aseismic safety, aseismic safety of impervious system, etc. and proposed the standards of seismic safety evaluation. Fang Huolang and others[10] conducted 3D FEM dynamic analyses on the reservoir faced wholly with asphalt concrete under construction, which was the largest in Japan for this type of reservoir and analyzed the earthquake response characteristics based on the geological and topographic conditions as well as the embankment condition of the reservoir. Wang Hui and others[11]-[12] conducted static stress deformation calculation using 3D FEM for the upper reservoir high asphalt concrete face rockfill dam of a proposed pumped storage power station located in the region with VIII degree of seismic intensity. Zou Degao and others[13] conducted 2D dynamic calculation on the typical section of upper reservoir asphalt concrete faced dam of a pumped storage power station, analyzed the deformation rules and patterns of the dam after earthquake and discussed the ultimate seismic capability. Although the research are focused on the projects with dams lower than 100 m, they also provide methods and thoughts for the dams of this type higher than 100 m, especially for those located in the regions with high seismic intensity, and instruct the in-depth research.

To further study the seismic safety analysis of asphalt concrete face rockfill dams under high seismic intensity, the upper reservoir asphalt concrete face rockfill dam of a pumped storage power station located in Northwest China is taken as an example. The upper reservoir has a full-supply storage level of 2505.00 m and a dead level of 2470.00 m, the dam is of an asphalt concrete face rockfill dam with the crest at the elevation of 2509.00 m in a width of 12.00 m and the dam height of 101.00 m. The dam zoning is of crushed stone cushion zone, transition zone, upstream rockfill zone, downstream rockfill zone, etc. below the impervious face; and a counterweight mass is placed downstream of the dam and the slope protection is of concrete frame vegetation. The reservoir impermeability adopts the structure of simple asphalt concrete face. The thickness of asphalt concrete impervious face is 20.2 cm for reservoir bank and 18.2 cm for reservoir basin. The aseismic

design standard adopts an exceeding probability of 2% within 100 years of the reference period and the corresponding bedrock peak ground acceleration is 724 gal (0.739 g); the aseismic check standard adopts an exceeding probability of 1% within 100 years of the reference period and the corresponding bedrock peak ground acceleration is 879 gal (0.897 g).

2. RESEARCH MODELS AND CONDITIONS

2.1. FEM MODEL AND STAGED LOADING SIMULATION

Build the 3D FEM model of the dam based on the geological information and design typical sections of the dam and the foundation. The element grids of FEM model are shown in Figure 1, for which, the down-river direction is X, and perpendicular to the dam axis pointing to outside of reservoir is positive; vertical direction is Y, and vertically upward is positive; dam axis direction is Z, and pointing to the right bank is positive. The calculation and analysis simulates the filling in 38 steps by referencing the filling scheme is the basic design of the project. The calculation simulates the impoundment (in 13 steps) in two stages, one is the construction of dam and the other is the initial impoundment to the full storage level (2505.00 m).

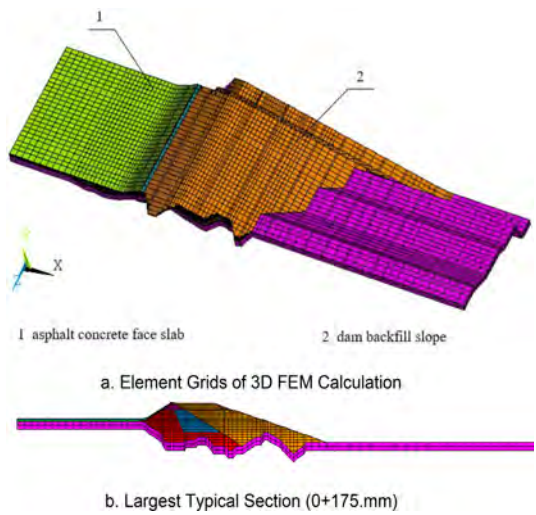

Fig. 1
Model of Asphalt Concrete Face Rockfill Dam

2.2. Static and dynamic calculation parameters

The static calculation adopts Dunan-Chang E-B Model and the rheological property analysis adopts Shen Zhujiang six-parameter rheological model, in which the impacts of surrounding compression and shear stress on particles broken are considered. The dynamic calculation adopts equivalent non-linear viscoelastic model and seismic permanent deformation adopts Shen Zhujiang permanent deformation model. The static and dynamic parameters of dam-building materials and asphalt concrete adopt laboratory large-sized three axial test results, refer to tables 1, 2 and 3.

Table 1
Calculation parameter table

DAM ZONING	ρ/(G/CM^3)	φ_0/(°)	$\Delta\varphi$/(°)	C/KPA	K	N	R_F	K_B	M
Asphalt concrete (10°C)	2.401	29.5		410	249	0.27	0.54	2072	0.40
Cushion	2.29	54.7	9.9		1322.1	0.26	0.70	743.5	0.14
Transition	2.26	54.6	10.3		1318.9	0.25	0.72	731.8	0.09
Upstream rockfill zone	2.23	53.7	10.2		1236.4	0.24	0.74	612.6	0.06
Downstream rockfill zone	2.20	52.4	9.7		1044.7	0.25	0.73	416.5	0.09
Reservoir basin backfilled material	2.15	51.7	9.5		905.5	0.25	0.70	353.0	0.10
Slope counterweight mass	2.04	38.6	5.4		292.2	0.40	0.84	162.6	0.28

Table 2
Calculation parameter table

DAM ZONING	φ/(%)	ρ/(G/CM^3)	B/(%)	C/(%)	D/(%)	M_1	M_2	M_3
Cushion	17	2.29	0.115	0.024	0.327	0.376	0.502	0.647
Transition	18	2.26	0.117	0.025	0.329	0.379	0.508	0.652
Upstream rockfill zone	19	2.23	0.127	0.027	0.346	0.384	0.512	0.669
Downstream rockfill zone	20	2.20	0.145	0.031	0.385	0.393	0.523	0.682
Reservoir basin backfilled material	20	2.15	0.201	0.045	0.535	0.413	0.561	0.735
Slope counterweight downstream of dam	24	2.04	0.450	0.108	1.105	0.466	0.638	0.783

Table 3
Calculation parameter table

DAM ZONING	K'_2	N	K_2	K'_1	K_1	λ
Cushion	17	0.354	2740	52.7	23.2	0.18
Transition	18	0.354	2740	52.7	23.2	0.18
Upstream rockfill zone	19	0.335	2626	50.5	38.0	0.19
Downstream rockfill zone	20	0.346	2229	46.5	35.0	0.20
Reservoir basin backfilled material	20	0.376	1949	37.1	27.9	0.22
Slope counterweight downstream of dam	24	0.457	820	18.4	13.9	0.27

2.3. Input of ground motion

Dynamic response analysis is conducted based on three sets of acceleration time-duration curves and according to the calculation results Figure 2 shows the time-duration curve fitting for relevant response spectrum at the typical sites set for seismic safety evaluation. The input of ground motion is uniform and even, i.e. takes the dam body above the slightly weathered bedrock as the calculated object. The input adopts three directions, i.e. down-river, vertical and dam axis, and the vertical peak acceleration uses the horizontal peak acceleration, the calculation time-step takes 0.02 seconds with a duration of 45 seconds.

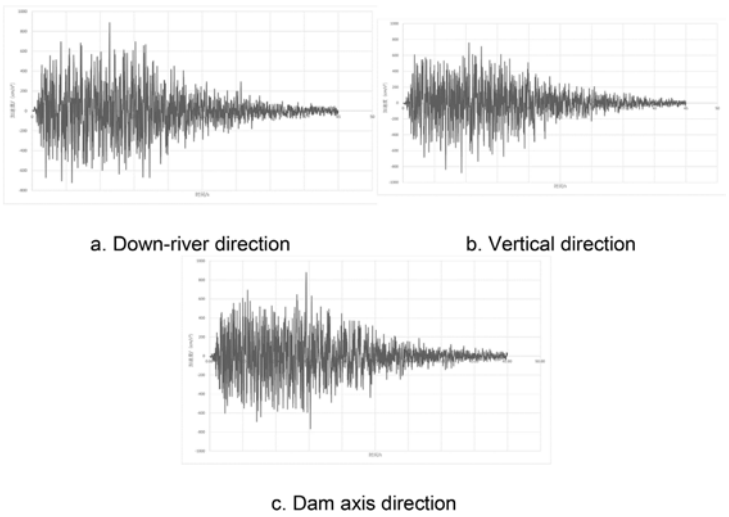

Fig. 2
Time-duration chart of bedrock seismic acceleration under check earthquake

3. DAM DEFORMATION CHARACTERISTICS

3.1. Dam deformation

Figure 3 is of the distributed deformation of typical dam section in the completion period. The maximum settlement of main dam in completion period occurs inside the downstream slope counterweight mass and the maximum value is 1.06 m accounting for 1.03% of the dam height. The maximum settlement inside the dam is about 0.4 m and the maximum up- and down-stream deformation is 0.03 m in dam shell and 0.38 m in slope counterweight, respectively.

In the completion period, the stress distribution of dam is even with significant self-weight effect and consistent with the general laws of earth-rock dam. The maximum primary stress of the dam is about 1.93 MPa at the bottom of the dam and the minimum is 0.64 MPa. In view of the stress level of the dam, the stress of most of the dam in the completion period is between 0.2 and 0.7 MPa, which means it has a rather high safety margin and static shear failure will not occur.

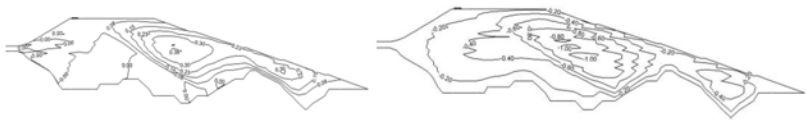

a. Horizontal displacement distribution in down-river direction

b. Settlement distribution in down-river direction

Fig. 3
Deformation distribution of typical dam section in completion period

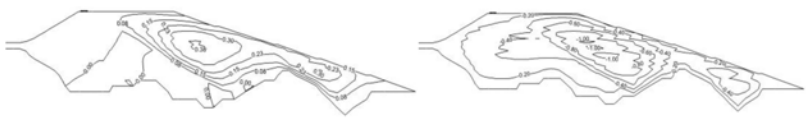

a. Horizontal displacement distribution in down-river direction

b. Settlement distribution in down-river direction

Fig. 4
Deformation distribution of typical dam section in full-storage period

Figure 4 is of the distributed deformation of typical dam section in the full-storage period. The maximum settlement of main dam in full-storage period occurs inside the slope counterweight mass and the maximum value is 1.06 m accounting for 1.03% of the dam height. The largest up- and down-stream deformation is 0.01 m in dam shell and 0.39 m in slope counterweight, respectively.

In the full-storage period, the stress distribution of dam is even with significant self-weight effect and consistent with the general laws of earth-rock dam. The maximum primary stress of the dam is about 1.95 MPa at the bottom of the dam and the minimum is 0.64 MPa. In view of the stress level of the dam, the stress of most of the dam in the full-storage period is between 0.2 and 0.7 MPa, which means it has rather high safety margin and the static shear failure will hardly occur.

3.2. Panel deformation and strain

The autogenous deformation of asphalt concrete face is rather small when the construction is finished. In the completion period, along the slope direction, the maximum compression stress is about 0.002 MPa at the intersection transition between the panel and reservoir basin and the maximum tensile stress is about 0.005 MPa at the top of the panel. The maximum axial compression stress of the panel is 0.002 MPa at the intersection transition between the panel and the reservoir basin and the maximum axial tensile stress is 0.004 MPa at the top of the panel.

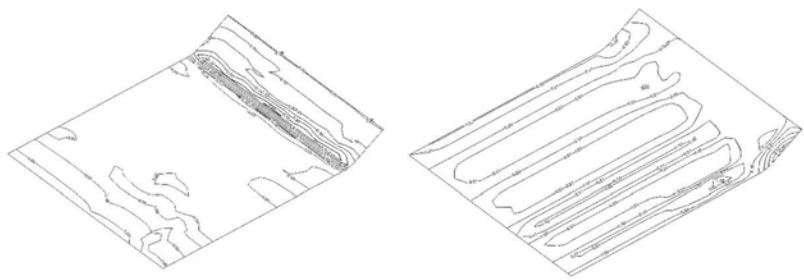

a. Strain distribution along the slope direction

b. Strain distribution in dam axis direction

Fig. 5
Strain distribution in full-storage period

In the full-storage period, along the slope direction, the maximum compression stress is about 0.283 MPa at the intersection transition between the panel and reservoir basin and the maximum tensile stress is about 0.011 MPa at the top of the panel. The maximum axial compression stress of the panel is 0.257 MPa at the intersection transition between the panel and the reservoir basin and the maximum axial tensile stress is 0.009 MPa at the top of the panel.

In the full-storage period, along the slope direction, the maximum compression strain is 0.645% at the intersection transition between the panel and reservoir basin and the maximum tensile strain is 0.013% at the intersection of the panel and reservoir basin close to the reservoir basin. The maximum axial compression strain of the panel is 0.025% at the intersection transition between the panel and the reservoir basin and the maximum axial tensile strain is about 0.05% at the right bank slope in the middle part of the panel.

Figure 5 shows the strain distribution of asphalt concrete face in the full-storage period.

4. SEISMIC DYNAMIC RESPONSE OF DAM

4.1. Dynamic response of dam

The analysis and calculation results indicate that the earthquake-induced seismic response acceleration and dynamic displacement are rather large and the under the seismic action. Refer to Figure 6 for the distribution of acceleration, in down-river direction and in vertical direction, of the typical cross-sectional and longitudinal sections in the central part of the dam.

The vertical acceleration response of the dam is rather strong and reaches the maximum value at the place close to the contact between the dam crest and slope counterweight mass in the middle part of the valley. The maximum response acceleration in vertical direction is 11.497 m/s2 and the amplification coefficient is 1.31. Above the foundation surface the acceleration response decreases first along the dam body elevations and then gradually increases to the maximum at the dam crest. The maximum response acceleration in down-river direction is 10.649 m/s2 and the amplification coefficient is 1.21 close to downstream slope of the counterweight mass in the middle part of the valley; the maximum acceleration in dam axis direction is 9.824 m/s2 and the amplification coefficient is 1.12. Overall, the acceleration response at the dam crest and the downstream dam slope area near the counterweight mass is rather large, hence, the possibility of loose rockfill and

collapse exist and the concrete frame vegetation slope protection adopted in the design scheme can effectively prevent the loose rockfill and collapse.

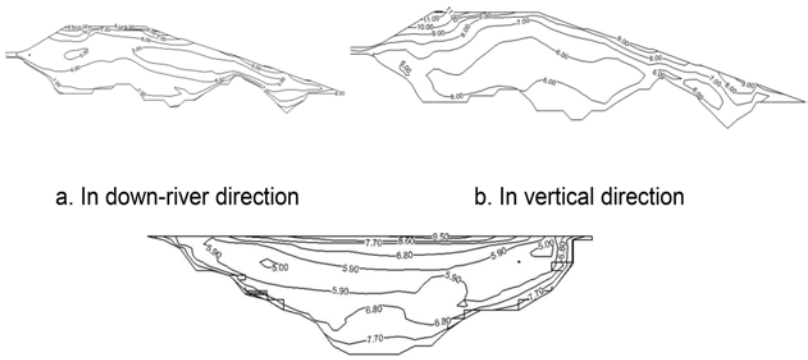

a. In down-river direction b. In vertical direction

c. In dam axis direction

Fig. 6
Seismic acceleration distribution of dam

The dynamic displacement response in down-river direction is rather strong and reaches the maximum value at the place close to the downstream of slope counterweight mass in the middle part of the valley. The maximum dynamic displacement in the down-river direction is 0.471 m. Above the foundation surface the dynamic displacement response increases gradually along the dam body elevations and reaches the maximum value at the dam crest. The maximum dynamic displacement of the dam in vertical direction is 0.179 m at the place close to the downstream of slope counterweight mass in the middle part of the valley; the maximum dynamic displacement in dam axis direction is 0.372 m. Overall, the dynamic displacement response at the dam crest and the downstream dam slope area near the counterweight mass is rather large, hence, the possibility of loose rockfill and collapse exist and the concrete frame vegetation slope protection adopted in the design scheme can effectively prevent the loose rockfill and collapse.

Figure 7 is the distribution of residual deformation of typical dam section. The vertical residual deformation reaches the maximum value at the place downstream of the dam crest slope counterweight mass in the central part of the valley, the maximum settlement is about 1.01 m and that of the dam body is about 0.5 m, which is far less than the freeboard for subsidence due to earthquake at the dam crest; hence the seismic deformation has less impact on the dam stability. After earthquake the dam body sinks downward and shrinks inward from the two sides, which

is consistent with the general law and the maximum subsidence due to earthquake accounts for 1.0% of the dam height. The distribution law of deformation after earthquake is consistent with the general law of faced rockfill dam. The residual deformation of dam body in dam axis direction is small.

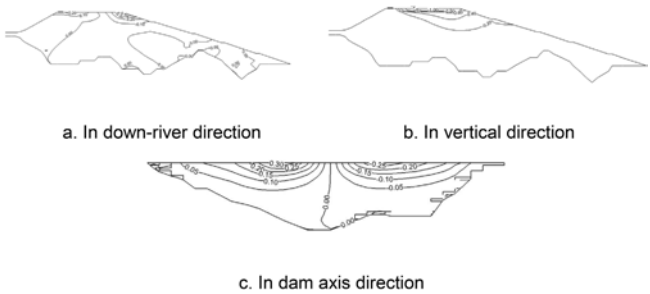

Fig. 7
Residual deformation distribution of dam body typical section

Overall, the residual deformation of dam body in vertical direction reaches the maximum value at the place close to the downstream slope of dam crest at the central part of the valley, far less than the freeboard of subsidence due to earthquake at the dam crest. The seismic deformation has less impact on the dam body stability, after earthquake, the dam body sinks downward and shrinks inward from the two sides, which is consistent with the general law. The residual deformation of dam body in dam axis direction is small.

4.2. Dynamic response of panel

Considering the superposition of earthquake action and static force, the distribution of major and minor primary strains of the panel is shown in Figure 8. For the asphalt concrete face (earthquake action + static force), the maximum major primary compression strain is 0.558% and the maximum major primary tensile strain is 0.437%, both occur at the intersection between the panel and reservoir basin close to the dam; the maximum compression strain along the slope direction is 0.617% occurs at the intersection between the panel and reservoir basin and the maximum tensile strain is 0.211% occurs at the intersection between the panel and reservoir basin close to the reservoir basin; the maximum compression strain in the dam axis direction is 0.115% and the maximum tensile strain is 0.150%, both occur at upper part of left bank of the panel. The tensile strains are less than the generally

permissible value, 0.5%; hence the strains of asphalt impervious face meet the dynamic safety requirements.

After earthquake, for the asphalt concrete face, the maximum major primary strain is 0.578% and the maximum minor primary strain is 0.441%, both occur at the intersection between the panel and reservoir basin close to the dam; the maximum compression strain along the slope direction is 0.652% occurs at the intersection between the panel and reservoir basin close to the dam, and the maximum tensile strain is 0.201% occurs at the dam crest close to the left bank slope; the maximum compression strain in dam axis direction is 0.055% occurs at middle part of the panel and the maximum tensile strain is 0.115% occurs in the middle part of left bank slope of the panel. After earthquake, the compression and tensile strains of asphalt face of reservoir banks and the asphalt of reservoir basin fall in the allowable range.

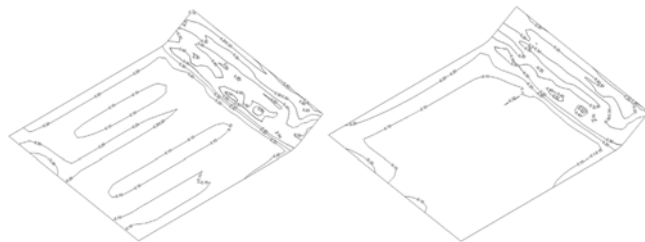

a. Distribution of major primary strain b. Distribution of minor primary strain

Fig. 8
(earthquake action + static force) Contour of primary strain distribution

5. DYNAMIC STABILITY ANALYSIS OF DAM SLOPE

The dynamic stability of the dead water level and the normal storage level in the reservoir under the action of design earthquake and check earthquake were calculated by using the dynamic finite element time history stability analysis method. The calculation results of the dynamic stability of the dam slope are shown in Figure 9.

The calculation results show that the minimum safety factor of seismic stability of the dam slope is less than 1.0 in individual instantaneous times during the earthquake process. Considering that the minimum safety factor occurs at a certain momentary moment, the safety factor is restored at the next moment due to the change in the direction of the seismic acceleration. Therefore, if the accumulation

time of the stability safety factor is less than 1.0, it can be considered that it is not enough to cause the instability of the dam slope. It is generally believed that in the process of earthquake, if the time of the stability safety factor is accumulated for more than 2s, the dam slope is close to the state of instability.

According to the calculation results, the minimum safety factor of the frontal dam slope is 0.977 and the accumulation time of less than 1.0 is 0.1s, respectively, and the minimum safety factor of the backwater dam slope is 1.380, and the accumulation time of less than 1.0 is 0.0s. In the case of the dead water level and the seismic condition, the minimum safety coefficients of the front and back dam slopes are 0.913 and 1.277, respectively, and the accumulation time of less than 1.0 is 0.4s and 0.0s, respectively. Under the normal water storage level and the design and verification of seismic work, the minimum safety factor of the frontal and back dam slopes is greater than 1.0.

It can be seen that under the action of design and verification earthquake, the accumulation time of the minimum safety factor of the dam facing and back dam slopes is less than 1.0 is less than 2s, and the dam slope can be considered to be stable during the earthquake.

Figure 10 shows the sliding surface corresponding to the minimum safety factor of dam slope stability. It can be seen that the most dangerous sliding surface is located at the top of the dam. This is due to the large reciprocating seismic inertia force at the top of the dam, which produces an obvious “whiplash” effect, resulting in the loosening of the rockfill body in the dam crest area, and the loss of the occlusion force between the rockfill particles, resulting in the sliding of the rockfill body on both sides of the dam crest and downstream. This is in line with the general law of the actual seismic damage and model test of the earth-rock dam, so special attention should be paid to the stability of the soil in the dam crest area in the seismic design of the earth-rock dam.

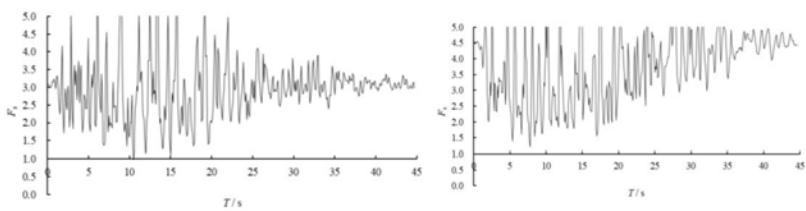

a. Upstream Dam Slope b. Downstream Dam Slope

Fig. 9
Time-history curve of safety factor of dam slope against sliding

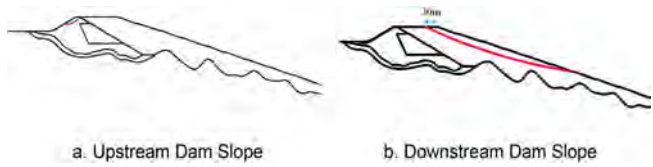

Fig. 10
Time-history curve of safety factor of dam slope against sliding

6. CONCLUSIONS AND SUGGESTIONS

1. The laboratory three-axial test parameters and the static and dynamic analysis results indicate that the recommended design scheme for the upper reservoir main dam and subsidiary dam of the pumped storage power station can meet the safety requirements during the periods of construction, impoundment, and operation, as well as under the given earthquake working conditions.
2. The stability safety coefficient of the up- and downstream slopes of the upper reservoir dam meet the requirements of specifications during the periods of construction and operation as well as under the earthquake working condition encountered during operation. However, under the working conditions of design earthquake and check earthquake, at different water levels the response acceleration at the dam crest and downstream slope area close to the dam crest is rather large, and the moments when the minimum value of time-duration curve of slope seismic stability safety coefficient is less than 1 exist, hence, the local dynamic shear failure at the slope close to the dam crest and local instantaneous slip in shallow layer may occur under the action of earthquake. The dam crest width, slope counterweight mass (concrete frame vegetation and dry-laid stone slope protection) adopted in the design scheme can effectively improve the local and overall stability against earthquake and decrease the risk of dam failure under the action of earthquake with unusual high intensity.
3. Under various working conditions, the tensile and compression stresses and strains of the asphalt concrete face of the dam and reservoir basin meet the requirements and the asphalt in different locations can effectively guarantee the safety under the action of earthquake.
4. The subsidence due to earthquake at the dam crest meets the freeboard design and the dam body has the capability of resisting seismic deformation. While, attention should be paid to the large deformation of downstream slope counterweight mass. The aseismic reinforcing measures to be adopted in the aseismic design of dam body are reasonable and effective and can increase the safety margin of the dam body, it is suggested that shaking table model test can be conducted to further verify the effectiveness of the aseismic reinforcing measures.

REFERENCES

[1] ZHU RUIHENG, CEN WEIJUN, XUE YANG, AND OTHERS. Influence analysis of dam foundation gallery cracks on seepage characteristics of core dam [J]. *Journal of Hohai University (Natural Sciences)*,2024,52(4):22–28.

[2] ZHANG CHUNSHENG, JIANG ZHONGJIAN. *Pumped Storage Power Station Design [M]*. Beijing: China Electric Power Press,2012.

[3] YE JIANCHUN, LU ZHONGMIN, CAI JINHUA, AND OTHERS. Salient features of Shahe Pumped Storage Power Station[J]. *WATER POWER*,2004, (5):41–43.

[4] WANG YINGJUN, ZHAO LIN, LEI XIANYANG, AND OTHERS. Design of High asphalt concrete face rockfill dam for pumped storage power station [J]. *YANGTZE RIVER*,2022,53(1):148–153.

[5] GU GANCHEN, SHEN CHANGSONG, CEN WEIJUN. *Earthquake engineering for earth-rock dams[M]*. Beijing: China Water & Power Press.2009.

[6] WANG WEIBIAO, HÖEG K, ZHANG YINBO. Design and performance of the Yele asphalt-core rockfill dam[J]. *Canadian Geotechnical Journal*, 2010, 47(12):1365–1381.

[7] ZHI BINGCHENG, SONG ZHIQIANG, WANG FEI. Dynamic response of asphalt concrete core wall dam to the variations of deep overburden layers.[J]. *Journal of water resources and water engineering*,2020,31(5):189–194.

[8] HE JIANXIN, WANG JING, YANG HAIHUA. Dynamic characteristics of dam materials and three-dimensional seismic response analysis of Niya Reservoir Advances in Science and Technology of Water Resources[J]. *Advances in Science and Technology of Water Resources*,2021,41(5):53–61.

[9] ZHAO JIANMING, LIU XIAOSHENG, YANG YUSHENG, AND OTHERS. Seismic safety assessment standard and ultimate aseismic capability of high faced rockfill dams[J]. *Chinese Journal of Geotechnical Engineering*,2015,37 (12):2254–2261. Criteria for seismic safety evaluation and maximum aseismic capability of high concrete face rockfill dams.

[10] FANG HUOLANG, TASHIRO YUKIE, 田代幸英,大内周, AND OTHERS. Aseismic Design of Reservoir Faced Wholly with Asphalt Concrete (English) [J]. *Chinese Journal of Rock Mechanics and Engineering*,2006,(8):1550–1562. ASEISMIC DESIGN OF RESERVOIR FACED WHOLLY WITH ASPHALT CONCRETE.

[11] WANG HUI, CEN WEIJUN, WANG DONGLIANG, AND OTHERS. Seismic safety analysis of a high asphalt concrete face rockfill dam in region with high seismic intensity[J]. *Journal of Water Resources and Water Engineering*,2023,34 (5):165–171.

[12] WANG DONGLIANG, TANG JIE, WANG HUI. Seismic Stability Analysis of Asphalt Concrete Face Rockfill Dam of Pumped Storage Power Station in Strong Earthquake Area[J]. *Water Resources and Power*,2024,42(1): 102–105.

[13] ZOU DEGAO, PENG JUN, LI JUNCHAO, AND OTHERS. Seismic Deformation and Ultimate Seismic Capacity Analysis of Asphalt Concrete Face Rockfill Dams[J]. *Hydropower and Pumped Storage*,2022,8(6):15–20.

Q.111 - R.37

COMMISSION INTERNATIONALE DES
GRANDS BARRAGES

VINGT-HUITIEME CONGRES DES
GRANDS BARRAGES
CHENGDU, MAI 2025

ANALYSIS ON INFLUENCE FACTOR OF INDUCED MODERATE RESERVOIR EARTHQUAKE (*)

Tinggai CHANG & Yanhong ZHANG
China Institute of Water Resources and Hydropower Research, Beijing

CHINA

SUMMARY

The problem of reservoir-induced earthquake is not only a key technical problem in the academic field, but also a focus of social concern. Especially when the earthquake with moderate intensity or above occurs in the reservoir area, there is a great controversy among different scholars about the discrimination of seismic attributes. In this paper, starting from the representative typical earthquake cases in China, the background of medium-intensity reservoir earthquakes after reservoir impoundment is comprehensively analyzed, and the common characteristics of induced medium-intensity reservoir earthquakes are summarized. It has important reference significance for the discrimination of reservoir-induced earthquakes and the risk prediction of reservoir-induced earthquakes, and provides technical support for exploring the mechanism of reservoir-induced earthquakes.

RÉSUMÉ

Le problème des séismes induits par les réservoirs de stockage d'eau n'est pas seulement un problème technique théorique, mais aussi une préoccupation générale. Les séismes d'intensité significative se sont surtout produits dans les

Analyse du facteur d'influence d'un séisme induit modéré dans un réservoir

 DOI: 10.1201/9781003642428-138

zones où se trouvaient des réservoirs et la discrimination des propriétés sismiques est très controversée entre les différents spécialistes. Dans cet article, à partir de cas représentatifs de tremblements de terre typiques en Chine, le contexte des tremblements de terre de moyenne intensité dans les réservoirs après la mise en eau des réservoirs est analysé en détail, et les caractéristiques communes des tremblements de terre induits de moyenne intensité dans les réservoirs sont résumées. Cette étude est une référence importante pour la discrimination des tremblements de terre induits par les réservoirs et la prédiction des risques de tremblements de terre induits par les réservoirs. Il fournit un soutien technique pour l'exploration du mécanisme des tremblements de terre induits par les réservoirs.

1. INTRODUCTION

At present, China's hydropower development is mainly located in the central and western regions where moderate and strong earthquakes occur frequently and regional active fault zones are widely distributed. Reservoir induced earthquake is an unavoidable problem in the construction of high dams and large reservoirs. According to the current standard, the fault activity and seismic activity background play a key role in predicting the intensity of induced earthquake in the risk prediction of reservoir induced earthquake. Because Holocene active fault zones are widely distributed in the central and western regions, it is more likely for each high dam and large reservoir to touch the active fault zones within the influence range of reservoir water, so only considering the activity of faults, the possibility of inducing earthquakes of moderate intensity or above can be given. In this paper, the common characteristics of lithology, structure, regional tectonic stress field and the relationship between reservoir and earthquake source are analyzed in depth based on the examples of moderate and strong earthquakes in several representative reservoirs in China after impoundment, which is of practical significance for the risk prediction and discrimination of reservoir-induced earthquakes in the future.

2. ANALYSIS OF TYPICAL EARTHQUAKE EXAMPLES

In this paper, the geological structural conditions of the epicentral area of the strongest earthquake occurred in the affected area of the reservoir water after the impoundment of the Xinfengjiang, Danjiangkou, Shanxi, Xiluodu and Three Gorges reservoirs in China are analyzed.

2.1. XINFENGJIANG RESERVOIR

Xinfeng River is located in Heyuan County, Guangdong Province. The normal high-water level of the reservoir is 116 m, the maximum working head is 81 m, and the total storage capacity is 13.9 billion m^3. The dam began to store water in October 1959. On March 19, 1962, when the water level of the reservoir reached 110.5 m, an earthquake of magnitude Ms6.1 occurred (Fig. 1 [1]), and the epicentral intensity was VIII. The epicenter location of the earthquake is shown in Fig. 2.

According to the correlation between the earthquake and the reservoir water level, the earthquake occurred at the stage when the reservoir water level dropped from the high point of 113 m, and the water level dropped by about 2.5 m. The stratum exposed on the surface of the epicentral area is K-N sandstone [2], and according to the drilling results, below 300 m is the massive rock mass of mixed granite. Tectonically, the earthquake occurred at the intersection of two sets of NNE and NNW faults. The NE Heyuan fault is in NNE trend in the epicentral area. According to the trigonometric and leveling survey, the horizontal movement reached 18.7 mm (counterclockwise) from 1964 to 1972.

The focal fault plane A of the Xinfengjiang Ms6.1 earthquake strikes N62 ° E, inclines NW, and dips 80 °, B strikes N28 ° W, dips SW, and dips 88 ° [1]. It is considered that the NNE direction is the focal dislocation surface. The focal parameters of Xinfengjiang Ms6.1 earthquake given by Wang et al.[4], show that the fault plane is NNW nodal plane, and the fault dislocation is mainly strike-slip. The fault of the main shock, whether nee or NNW, is not the strike of the Heyuan fault, and the focal dislocation plane is oblique to the Heyuan fault. According to the NW direction of the regional tectonic stress field in Xinfengjiang and the spatial distribution characteristics of the hypocenters [5], it is considered that the NNW Xingang-Baitian fault is more likely to produce sinistral dislocation under the action of the regional tectonic stress field. The fault has a steep dip and dips to the northeast.

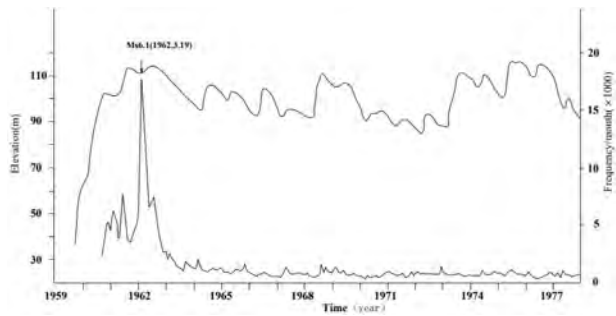

Fig. 1
The relationship between the monthly frequency of earthquakes in Xinfengjiang Reservoir and the water storage process of the reservoir

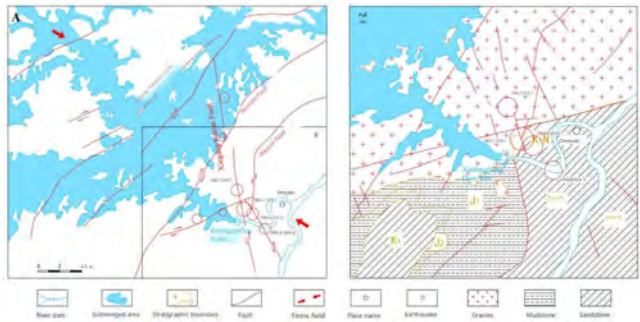

Fig. 2
The epicenter location and geological structure [2][3] of the Ms6.1 earthquake in Xinfengjiang Reservoir

2.2. Danjiangkou reservoir

Danjiangkou Reservoir is divided into two reservoir areas, Danjiang and Hanjiang. The first phase of the project, with a dam height of 97 m, a storage capacity of 16 billion m^3 and a normal water level elevation of 155 m, was completed in November 1976. In the second phase of the project, the water level elevation reaches 170 m and the storage capacity reaches 31.8 billion m^3.

The Danjiangkou Reservoir was impounded in November 1967. Until January 1970, there were obvious seismic activities in the reservoir area. Before 1973, the largest earthquake in the reservoir area was Ms3.5, located near Linmao Mountain. On November 29, 1973, when the reservoir water level dropped rapidly from 157 m [6] (Fig. 3), three felt earthquakes of magnitude 4 or above occurred in Songwan, with magnitudes of Ms4.7, 4.2 and 4.6, respectively. The focal depth was generally 4 to 9 km, and the maximum intensity of the epicenter was VII. The epicenter location is shown in Fig. 4 [7].

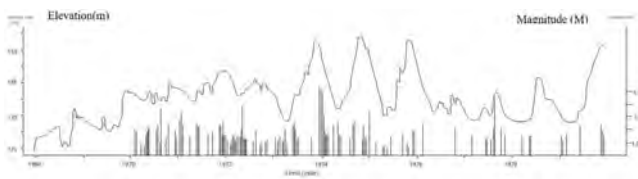

Fig. 3
Relationship between earthquake time sequence and reservoir water level in Danjiangkou Reservoir area (1968-1980)

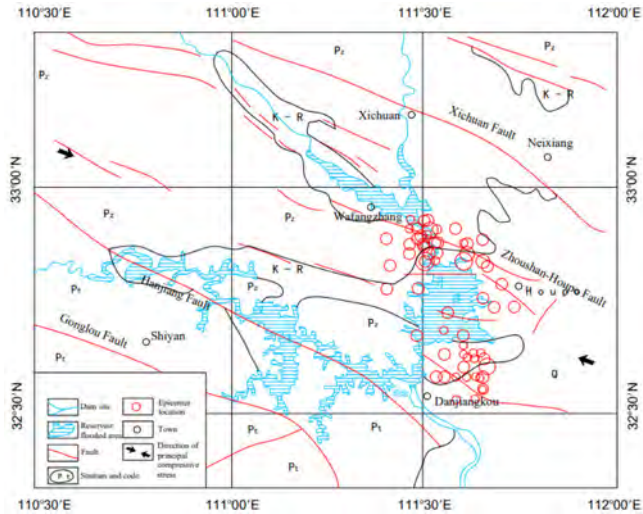

Fig. 4
Distribution of main active faults and epicenters of Danjiangkou Reservoir (1970-1980)

It can be seen from Fig. 4 that the lithology of the epicenter is mainly Proterozoic schist, sandstone and magmatic rock. Danku is located on the Paleozoic limestone and Cretaceous-Tertiary red beds, and the lithology of the epicenter area and its surrounding areas is relatively complex. The structure in this area is the Zhoushan-Houpo fault in NWW direction, which inclines to the northeast with a large dip angle. The fault zone is in the near future Still has strong activity [7]. The direction of the principal stress in Danjiangkou reservoir area is about N70 °W [8]. The focal mechanism solution of the Songwan mainshock is that the nodal plane A strikes N32 ° W, dipping SE, with a dip of 68 °, and the nodal plane B strikes N50 ° E, dipping NW, with a dip of 70 °.

2.3. Shanxi reservoir

Shanxi Reservoir is located in the upstream of Feiyun River in Wenzhou City, southern Zhejiang Province. The dam site is located in the canyon section 1 km upstream of Shanxi Town, Wencheng County, on the Jiuxi River in Feiyun River Basin. The maximum dam height is 132.5 m, the total reservoir capacity is 1.824 billion m^3, and the normal pool level is 142 m. The project was started in June 1997 and impounded in May 2000.

From May 2000 to June 30, 2017, the seismic activities in the reservoir area were mainly concentrated in four periods: January 1, 2002 to December 31, 2003; January, 1 2005 to December 31, 2007; January 1, 2010 to December 31, 2012; and January 1, 2014 to December 31, 2016. Among them, the earthquake sequences occurred in February 2006 and September 2014 were the strongest. According to the relationship between the earthquake occurrence and the reservoir water level, the four periods all occur in the descending stage of the reservoir water level, as shown in Fig. 5. The statistics of earthquake intensity of different earthquake sequences are shown in Table 1, the epicenter location is shown in Fig. 6, and the maximum intensity is VI.

Table 1
Seismic intensity statistics of different earthquake sequences since the impoundment of Shanxi Reservoir

EARTHQUAKE SEQUENCE	MAGNITUDE FILE					TOTAL	MAXIMUM MAGNITUDE
	ML $\frac{C}{a}$1.0	1.0∼1.9	2.0∼2.9	3.0∼3.9	4.0∼4.9		
2001∼2003		3	20	4		27	3.9
2005∼2007	346	427	215	42	13	1043	4.6
2010∼2012	101	30	1			132	2.0
2014∼2017	3086	755	132	34	5	4012	4.2

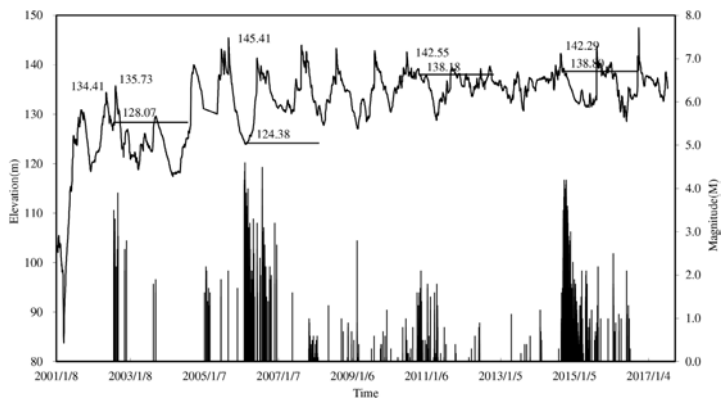

Fig. 5
Relationship between water level of Shanxi Reservoir and earthquake sequence (2001-2017)

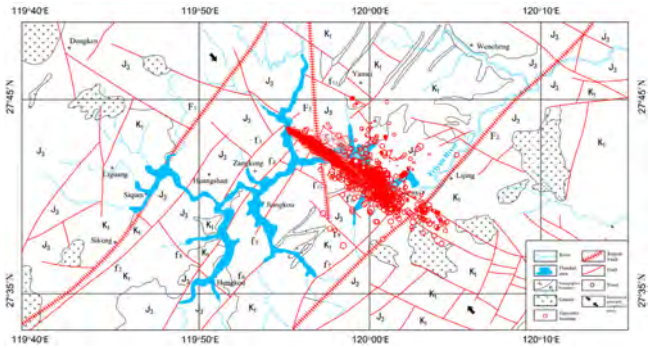

Fig. 6
Distribution of earthquake epicenters since the impoundment of the reservoir (2001-2017)

The lithology exposed in Shanxi reservoir area is mainly Jurassic rhyolite. From the relationship between the epicenter of the earthquake and the structure, the occurrence of the earthquake is mainly controlled by the northwest Shuangxi-Jiaoxi fault (f_{11}), which dips to the southwest with a dip angle of 80 ◦ The fault was formed in the late Yanshanian movement, with obvious or relatively obvious linear negative topographic features, straight and deep valley topography, and long extension. No dislocation of the drainage system by the NW fault is found. The Shanxi tectonic stress field is mainly controlled by the westward compression of the Pacific plate and the NWW compression of the Philippine plate, and the principal compressive stress in the reservoir area and its adjacent areas is in the NNW direction [10]. The Shuangxi-Jiaoxi fault in the NNW direction is easy to produce stress concentration at the intersection of the faults in other directions under the action of the main pressure in the NNW direction, which leads to the occurrence of earthquakes under the action of the reservoir water. Shanxi reservoir area and its adjacent areas belong to the weak seismic area. Since 1970, there has been no earthquake greater than magnitude 2 in this area. The felt earthquake occurred after the impoundment of the reservoir caused panic to the local residents and affected the normal operation of the reservoir.

2.4. Three gorges reservoir

The Three Gorges Project is located in Sandouping, Zigui County, in the Xiling Gorge of the Three Gorges. The dam is a concrete gravity dam, with a maximum dam height of 181m, a dam crest elevation of 185 m, a normal pool level of 175 m, and a total reservoir capacity of 39.3 billion m^3, of which the flood regulation capacity is about 22 billion m^3. On May 6, 2003, the Three Gorges Hydropower Station began

to impound water, and the earthquake in the reservoir area increased significantly after the impoundment of the reservoir. Until December 16, 2013, a M5.0 earthquake occurred at the east entrance of Badong County in the reservoir area. The earthquake occurred on the 38th day after the reservoir water level reached 175 m. On that day, the reservoir water level was 173.87m, and the cumulative drop of the water level from the high point was less than 1.2 m (Fig. 7). From March to May 2014, four earthquakes of M3.0 and above occurred during the fall of the reservoir water level. The maximum magnitude is M3.8, and the epicenter location is equivalent to that of M5.0. See Fig. 8 for the epicenter location of the earthquake.

The Three Gorges dam area is located in the west between the Qinling and Nanling complex latitudinal tectonic belts, and is the composite part [11] of the southern segment of the third uplift break belt of the Neocathaysian system and the reflex arc of the western wing of the Huaiyang epsilon-type. The fault direction is mainly NE and NNE. The epicentral area is clamped by the Gaoqiao fault (F_1) and the Zhoujiashan-Niukou fault (F_4), and the nearly east-west and north-west-west faults are developed between the two faults. The Gaoqiao fault was obviously active in the early Late Pleistocene and is still active today [12]. The Badong earthquake sequence is mainly controlled by nearly east-west faults. The focal mechanism solution of the main shock is that the nodal plane A strikes N74 ° E, dips NW, and dips 61 °, and the nodal plane B strikes N15 ° W, dips NE, and dips 88 °.

The principal compressive stress direction in the Three Gorges Reservoir Area is NE ∼ NEE [14], as shown in Fig. 8. The lithology of the epicentral area is mainly Triassic Badong Formation, Jurassic clastic rocks and Middle and Lower Triassic limestone, and the earthquakes are mainly distributed in the exposed limestone area. The tectonic background of the earthquake is mainly caused by the NWW fault under the combined action of the principal compressive stress and the reservoir water.

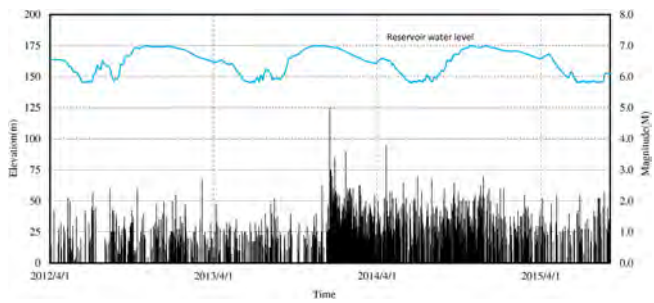

Fig. 7
Relation curve between water level of Three Gorges Reservoir and earthquake time sequence

2.5. XILUODU RESERVOIR

Xiluodu Hydropower Station is the backbone project of the national “West-to-East Power Transmission” project, located at the junction of Sichuan and Yunnan Jinsha River Go. The dam crest elevation is 610 m, the dam height is 285.5 m, the normal pool level of the reservoir is 600 m, the total capacity is 12.8 billion m^3, and the total installed capacity is 13860 MW. In April 2007, the main project of the dam was started, and on November 16, 2012, the diversion tunnel was closed and the cofferdam began to retain water. On May 4, 2013, the sluice gate was officially impounded.

After the formal impoundment of Xiluodu Reservoir, the seismic activity in the reservoir area has increased significantly, especially from the dam site to Huanghua section. The relationship between the monthly earthquake frequency and the reservoir water level is shown in Fig. 9. It can be seen from the figure that the monthly earthquake frequency has changed significantly after the impoundment of the reservoir.

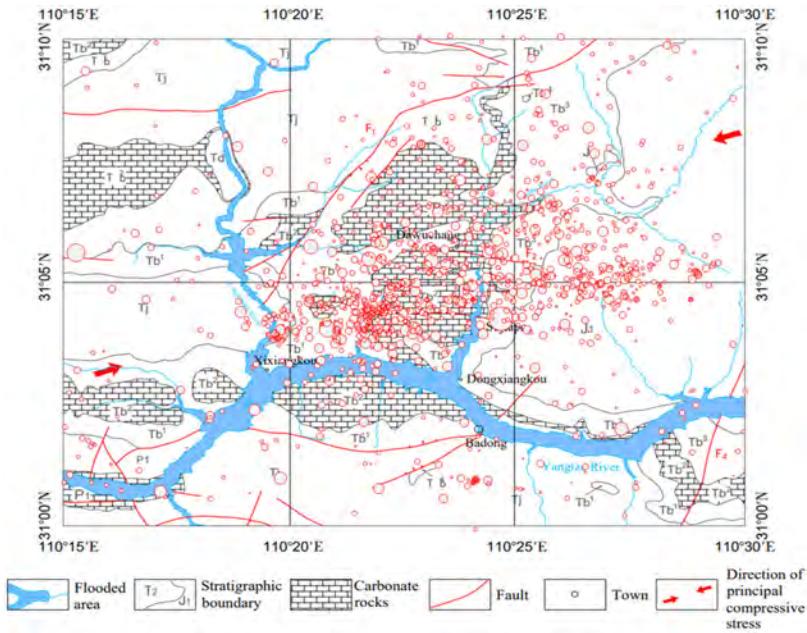

Fig. 8
Distribution of the epicenter of the Badong M5.0 earthquake and aftershocks on December 16, 2013

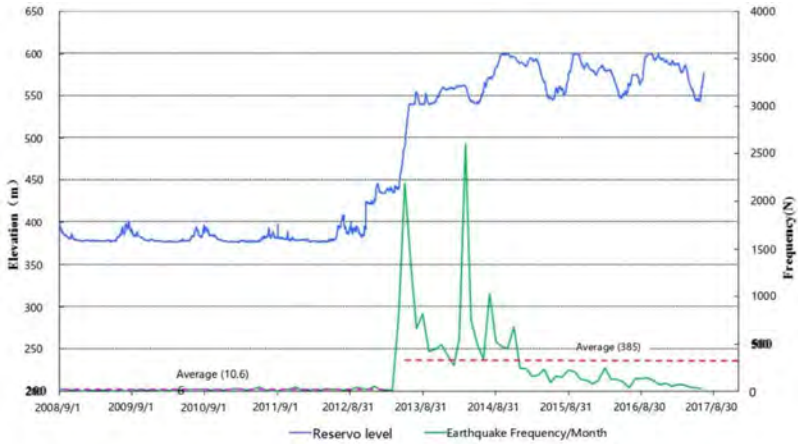

Fig. 9
The correlation between the monthly frequency of earthquakes in the Xiluodu reservoir area and the reservoir water level (2008.8-2017.12)

After the reservoir of Xiluodu Hydropower Station was impounded, M5.3 and M5.0 earthquakes occurred in Baisheng and Wuji on April 5 and August 17, 2014, respectively. The epicenter distribution of the main shock and aftershocks is shown in Fig. 10, and the maximum intensity reaches VII. The lithology of the strata exposed in the epicentral area is mainly limestone and dolomite of the Ordovician, Cambrian and Sinian systems of the Paleozoic. The main faults are the Majinzi fault (F_1), the Shangtianba fault (F_2) and the Xiaotan fault (F_3), all of which are thrust eastward. These three faults are accompanied by secondary transverse faults in NW and nearly EW directions. Under the action of regional principal pressure stress (the direction of the maximum horizontal principal stress is N40 ° ～ 60 °W [15]), the transverse faults are offset to the faults in nearly NS direction. There is about 2 mm thick fault gouge on the secondary fault plane at the mountain ridge, and the age of the sample is 21.83 ± 1.79 thousand years. The thickness of fault gouge on the main section is about 20 cm, and the age test result is 12.70 ± 0.99 million years. This indicates that the activity of the fault has not been strong [16] since the late Q_2. The focal mechanism solution shows that the controlling fault of the M5.3 earthquake strikes NNW, dips SW, with a dip angle of 30 °, and is of thrust nature. The M5.0 earthquake strikes northwest, dips northeast, and is left-lateral strike-slip nature.

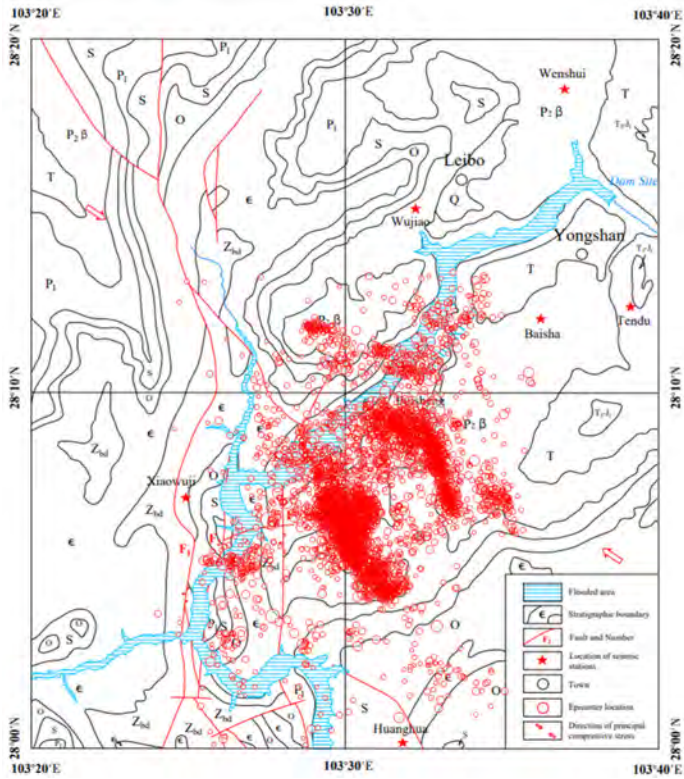

Fig. 10
Distribution map of the earthquake epicenter after the reservoir of Xiluodu Hydropower Station is impounded (2008.8-2017.12)

3. INFLUENTIAL FACTORS OF INDUCED MODERATE RESERVOIR EARTHQUAKE

Based on the analysis of the geological lithology, tectonic activity, focal mechanism solution, regional tectonic principal compressive stress direction and the relative position between the epicentral area and the reservoir of the induced earthquakes in Xinfengjiang, Danjiangkou, Shanxi, Three Gorges and Xiluodu reservoirs, the basic factors of the induced moderate reservoir earthquakes and the changes of the reservoir water level during the earthquake are shown in Table 2.

Table 2
Influential factors of typical induced moderate reservoir earthquakes in China

INFLUENTIAL FACTORS OF MODERATE RESERVOIR-INDUCED EARTHQUAKE	NAME OF THE RESERVOIR				
	XINFENGJIANG	DANJIANGKOU	SHANXI	THREE GORGES	XI LUO DU
Lithology of epicentral area	Mixed granite	Pre-Sinian metamorphic rock, Cambrian-Ordovician limestone, Cenozoic sandstone	Rhyolite	Upper Triassic Badong Formation limestone	Cambrian and Ordovician limestone, Sinian dolomite
Seismo-controlling structure	Xingang-Baitian fault: strike NNW, nearly vertical	Zhoushan-Houpo fault: strike N65°W, nearly vertical	Shuangxi-Jiaoxi fault: strike N60 °W, dip SW, dip angle 80°	NWW-trending fault, dipping northeast, dip angle 40 ～ 60°	N30 (W strike-slip fault, dipping NE, dip angle 62 °
Direction of principal compressive stress	NW	N70—W	NW	NE—NEE	NW
Angle of intersection between structure and principal compressive stress	17 (left and right)	5 (or so)	15 (or so)	25 (or so)	15 (or so)
Relative position of reservoir and fault	The footwall of a fault	The footwall of a fault	The footwall of a fault	The footwall of a fault	The footwall of a fault
Relationship between structure and reservoir water	Indirect	Direct	Direct	Indirect	Direct
Reservoir decline	113→110.5(2.5)	157→155(2)	145.4→124.4 (21)	175→173.9 (1.1)	562.85→559.3 (3.5)
Earthquake background	Weak earthquake	Weak earthquake	No shock	Weak earthquake	Strong earthquake
Fracture activity	The Heyuan and Renzishi faults are Holocene active faults.	Zhoushan-Houpo fault is a Holocene active fault.	No dislocation of the drainage system by the NW fault is found.	Inactivity since late Pleistocene	There was activity in the Middle Pleistocene
Maximum earthquake within 30km of epicentral area before impoundment	Three earthquakes of Ms 2 ～ 4	Impact intensity is less than V	Magnitude less than 2.0	5.1 （1979.5.22） Padang	5 ¼ (1948, Huang Hua)
Maximum earthquake in the reservoir area after impoundment	6.1	4.7	4.6	5.1	5.3
Focal depth	5.0	9.0	6.0	5.0	3.5

Based on the comprehensive comparison and analysis of five typical cases of induced earthquakes with magnitude M (4.5) in China, the common characteristics are as follows: (1) The lithological characteristics of the epicenter area are brittle rock mass, including igneous rock, Paleozoic limestone and pre-Sinian metamorphic rock. (2) The crossing angle between the spreading direction of the earthquake-controlling structure and the direction of the regional principal compressive stress is small, generally less than 20°. When the dip angle of the fault is steep, it shows the nature of strike-slip. When it is less than 35°, it shows the nature of thrusting (Xiluodu earthquake with M = 5.3). (3) All earthquakes occur at the stage of reservoir water level decline, but the magnitude of the decline is not related to the intensity of the earthquake. (4) The main reservoir body is located in the footwall of the fault. (5) There is a direct or indirect hydraulic connection between the fault zone and the reservoir water (the epicentral area is not beyond the influence range of the reservoir water 10 km).

4. CONCLUSION

1. The activity of seismic background in the reservoir area and its adjacent areas before the impoundment of the reservoir has no effect on the intensity of induced earthquakes (the intensity of induced earthquakes in the background of weak earthquakes often exceeds the background value).
2. The activity of the fault itself, there is no obvious correlation between the activity of the fault and the intensity of the induced earthquake. Therefore, in the prediction and evaluation of reservoir-induced earthquakes, the activity of the fault itself should not be taken as an important indicator of whether to induce tectonic reservoir-induced earthquakes [18].
3. The conditions of structural type reservoir-induced earthquake with moderate intensity are as follows: (1) brittle rock mass; (2) The fault intersects the regional principal compressive stress field at a small angle, and the dip angle of the fault is large (the intersection angle is generally less than 20 °, and the dip angle of the fault is greater than 60 °; (3) The reservoir body is located in the footwall of the fault; (4) There is a direct or indirect hydraulic connection between the fault zone and the reservoir.
4. After the impoundment of the reservoir, the common characteristics of the five typical earthquake cases in China have important reference value for whether to induce the medium-intensity tectonic reservoir earthquake. At the same time, the study on the risk prediction of reservoir-induced earthquake can reduce the risk of reservoir-induced earthquake.

REFERENCES

[1] SHEN C. G. *ET AL*. Xinfengjiang Reservoir Earthquake and Its Impact on the Dam, *Science in China*, vol. 17, 1974.

[2] DING Y. Z. *ET AL*. Tectonic condition of induced earthquake in Xinfengjiang reservoir.*Seismology and Geology*, vol.5, no. 3, pp. 63–74, 1983.

[3] PAN J. X. *ET AL*. Preliminary Study on Seismotectonics and Its Activity Characteristics in Xinfengjiang Reservoir Area, *Seismology and Geology*, vol. 4, no. 2, 1982.

[4] WANG M. Y. *ET AL*. l976, Preliminary Discussion on the Focal Mechanism and Origin of the Earthquake in the Xinfengjiang Reservoir, *Science in China*, vol. 1.

[5] CHENG H. H. *ET AL*. Finite Element Simulation of Seismic Poroelastic Coupling in Xinfengjiang Reservoir, *Science in China, Earth Sciences* vol. 42, no.6, 2012.

[6] GAO S. J. *ET AL*. Characteristics of Zhoujiangkou Reservoir Earthquake Sequence, *Crustal Deformation and Earthquakes*, pp. 86–93, 1983.

[7] YU P. Q. Geological Structure Conditions of Danjiangkou Reservoir Earthquake, *Journal of Northwest Seismology*, vol. 2, no. 4, pp. 40–49.

[8] LI J. H. Influence of tectonic stress field in reservoir area on reservoir-induced earthquakes, *Journal of Wuhan University (Engineering Edition)*, vol. 40, no. 6, pp. 51–55, 2007.

[9] LU F. M. Preliminary Discussion on Zhoujiangkou Reservoir Earthquake, *Earthquake Research*, vol. 3, no. 4, pp. 155–164, 1980.

[10] ZHONG Y. Y. *ET AL*. Precise Location and Seismogenic Structure of Shanxi Reservoir M4.6 Earthquake Swarm, *Earthquake Research*, vol. 34, no. 2, 2011.

[11] China Institute of Water Resources and Hydropower Research, Preliminary Assessment Report on Reservoir Induced Seismicity of the Three Gorges Project on the Yangtze River (Internal Report), 1986.

[12] XIA J. W. *ET AL*. Study on the Characteristics and Seismicity of the Gaoqiao Fault in the Head Area of the Three Gorges Reservoir, *Geodesy and Geodynamics*, vol. 28, no. 2, pp. 8–15, 2008.

[13] ZHANG L. F. *ET AL*. Analysis of the Badong M5.1 Earthquake Sequence and Seismogenic Structure on December 16, 2013, *Seismology and Geology*, vol. 38, no. 3, pp. 747–759, 2016.

[14] ZENG X. P. Focal Mechanism and Crustal Stress Field of Small Earthquakes in the Three Gorges Area of the Yangtze River, *South China Earthquake*, vol. 5, no. 3, pp. 71–75, 1985.

[15] DING L. F. *ET AL*. Hydrofracturing In-situ Stress Measurement and Analysis of Xiluodu Hydropower Station on Jinsha River, *China Earthquake*, vol. 20, no. 1, pp. 95–100 , 2004.

[16] Research on Reservoir Induced Earthquake Risk Prediction of Xiluodu Project in Jinsha River, China Institute of Water Resources and Hydropower Research, 2000.

[17] XIAO B. F., QI Y. P., LONG F., *ET AL*. Focal mechanism and seismogenic structure of M $\geq$ 4.7 earthquakes in Yongshan area of Yunnan since 2014. *North China Seismological Science*, vol. 38, no. 3, pp. 13–18, 2020.

[18] Risk Assessment of Reservoir-induced Seismicity[S] (GB 21075-2007);

COMMISSION INTERNATIONALE DES
GRANDS BARRAGES

VINGT-HUITIEME CONGRES DES
GRANDS BARRAGES
CHENGDU, MAI 2025

EXPERIMENTAL STUDY ON DYNAMIC PERFORMANCE OF CONCRETE SAMPLE OF BDA DAM (*)

Lijun ZHAO & Shaoqing WANG
State Key Laboratory of Simulation and Regulation of Water Cycle in River Basin, China Institute of Water Resources and Hydropower Research (IWHR), Beijing

CHINA

SUMMARY

The BDa Hydropower Station's dam, located in the Tibet Autonomous Region, is subject to a high seismic intensity classified as VIII degree. This study presents an experimental investigation into the uniaxial dynamic performance of concrete specimens from the BDa Dam. Utilizing a 15MN large-scale material testing machine, a series of static and dynamic tests were conducted on fully-graded and wet-screened concrete specimens. These tests aimed to determine the dynamic compressive strength, splitting tensile strength, and bending strength under various strain rates, simulating different seismic events. The experimental results demonstrate a significant increase in both compressive and tensile strength with the rise in strain rate, highlighting the concrete's dynamic response sensitivity to loading conditions. Notably, the wet-screened specimens exhibited higher strength values under quasi-static conditions, underscoring the importance of replicating in-situ conditions for accurate mechanical property assessment. The findings provide essential parameters for seismic numerical simulation and analysis, contributing to the current understanding of concrete behavior under seismic loading and offering a scientific basis for enhancing the safety and reliability of hydraulic structures. The results

**Etude expérimentale de la performance dynamique d'échantillons de béton du barrage de Bda*

DOI: 10.1201/9781003642428-139

have implications for future seismic design practices, particularly for hydraulic structures in seismically active regions.

RÉSUMÉ

Le barrage de la station hydroélectrique BDa, situé dans la région autonome du Tibet, est soumis à une intensité sismique élevée classée en degré VIII. Cette étude présente une enquête expérimentale sur la performance dynamique uniaxiale d'échantillons de béton du barrage BDa. En utilisant une machine d'essai des matériaux à grande échelle de 15MN, une série de tests statiques et dynamiques ont été effectués sur des échantillons de béton à granulat complet et tamisés à l'eau. Ces tests visent à déterminer la résistance à la compression dynamique, la résistance à la traction scindage et la résistance à la flexion sous divers taux d'écartement, simulant différents événements sismiques. Les résultats expérimentaux montrent une augmentation significative de la résistance à la compression et à la traction avec la hausse du taux d'écartement, mettant en évidence la sensibilité de la réponse dynamique du béton aux conditions de chargement. Notamment, les échantillons tamisés à l'eau ont présenté des valeurs de résistance plus élevées en conditions quasi-statiques, soulignant l'importance de reproduire les conditions in situ pour une évaluation précise des propriétés mécaniques. Les résultats fournissent des paramètres essentiels pour la simulation numérique et l'analyse sismique, contribuant à la compréhension actuelle du comportement du béton sous chargement sismique et offrant une base scientifique pour améliorer la sécurité et la fiabilité des structures hydrauliques. Les résultats ont des implications pour les pratiques de conception sismique futures, en particulier pour les structures hydrauliques dans les régions sismiquement actives.

1. INTRODUCTION

The dam of BDa Hydropower Station is situated in the Chaya County of Chamdo City, within the Tibet Autonomous Region. The dam site features steep terrain and complex geological conditions, and the basic seismic intensity of the site is classified as VIII degree. According to the Code for seismic design of hydraulic structures of hydropower project [1], the dam is categorized as Class A for seismic fortification, with a design seismic acceleration of 0.43g and a verification seismic acceleration of 0.53g. The prevailing seismic design criteria for hydraulic structures [2] dictate that the dynamic characteristics of concrete must be ascertained through specialized material testing procedures specifically tailored for Class A concrete dams. Consequently, it is imperative to conduct static and dynamic material tests on the BDa to provide essential parameters for subsequent seismic numerical simulation and analysis.

Internationally, significant advancements have been made in the field of concrete material dynamics, particularly in response to seismic events. Abrams D A[3]

initially introduced the concept of concrete compressive strength's sensitivity to the rate of application in 1917. Subsequently, a multitude of researchers globally have delved into the correlation between the peak strength and the strain rate at which concrete is loaded. The findings consistently indicate that concrete's mechanical characteristics exhibit a pronounced size and rate dependency [4–9].

This paper presents an experimental study aimed at evaluating the uniaxial dynamic performance of concrete specimens from the BDa Dam. A series of tests were conducted, including static and dynamic material tests, provide essential parameters for seismic numerical simulation and analysis, which are vital for ensuring the safety and structural integrity of the dam.

2. TEST SCHEME

The 15MN large-scale material testing machine built by China Institute of Water Resources and Hydropower Research (Fig. 1) is the main equipment for dynamic performance testing of concrete materials in China. The various raw materials used for the preparation of fully-graded concrete specimens are the actual materials used in the BDa Dam project. A representative $C_{90}20$ concrete from the dam is selected, and the specimens are cast and cured in the laboratory according to the actual mix ratio of the dam's concrete, as shown in Fig. 2. The specimens are transported to the laboratory shortly before the test age is reached. The concrete test of BDa dam includes static and dynamic compressive strength test, splitting tensile strength test and bending test [3]. The strain rate of tensile failure of concrete is about 5.6×10^{-4}/s, and the strain rate of compressive failure is about 5.6×10^{-3}/s. In order to study the variation of dynamic characteristics of concrete with loading strain rate, quasi-static (10^{-6}/s). Three different dynamic monotonic loading strain rates for fully-graded concrete specimens were selected for the three types of tests. The loading conditions for each test are shown in Table 1.

Fig. 1
The 15MN Large-scale Material Testing Machine

Fig. 2
The samples of BDa

Table 1
The Loading Conditions for Each Group

NO.	GROUP	LOADING CONDITIONS
1	Compressive strength test of fully-graded concrete specimens (Specimen C1)	Quasi-static (10^{-6}/s)
2		Dynamic strain rate (5×10^{-4}/s)
3		Dynamic strain rate (5.6×10^{-3}/s)
4		Dynamic strain rate (2×10^{-2}/s)
5	Compressive strength test of wet-screened concrete specimens (Specimen C2)	Quasi-static (10^{-6}/s)
6		Dynamic strain rate (5.6×10^{-3}/s)
7	Splitting tensile strength test of fully-graded concrete specimens (Specimen S1)	Quasi-static (10^{-6}/s)
8		Dynamic strain rate (10^{-4}/s)
9		Dynamic strain rate (5.6×10^{-4}/s)
10		Dynamic strain rate (2×10^{-3}/s)
11	Splitting tensile strength test of wet-screened concrete specimens (Specimen S2)	Quasi-static (10^{-6}/s)
12		Dynamic strain rate (5.6×10^{-4}/s)
13	Bending test of fully-graded concrete specimens (Specimen B1)	Quasi-static (10^{-6}/s)
14		Dynamic strain rate (10^{-4}/s)
15		Dynamic strain rate (5.6×10^{-4}/s)
16		Dynamic strain rate (2×10^{-3}/s)
17	Bending test of wet-screened concrete specimens (Specimen B2)	Quasi-static (10^{-6}/s)
18		Dynamic strain rate (5.6×10^{-4}/s)

3. TEST RESULTS

3.1. Results and analysis of compression test

The edge length of the fully-graded concrete cubic specimens for compression test is 300mm. There are a total of 12 strain gauges on the four lateral surfaces. The wet-screened cubic specimens have an edge length of 150mm, with a total of 4 strain gauges on the four lateral surfaces. Each set consists of at least 3 specimens, and a total of 18 sets of specimens have been completed for the compressive strength tests.

The quasi-static compression induces the emergence of numerous minor vertical fissures within the specimen. Some areas of the concrete on the specimen's exterior experience delamination. Essentially, the specimen retains its original form once the testing is halted, with no occurrences of rupture or significant block disintegration. As the rate of loading accelerates, the specimen's fragmentation becomes more pronounced. The compressive strength increases with the loading rate's increase (as depicted in Fig. 3). The average compression strength values of fully-graded concrete specimens for quasi-static and dynamic with the strain rate 5×10^{-4}/s, 5.6×10^{-3}/s and 2×10^{-2}/s were 31.1 MPa, 40.8MPa, 41.1MPa and 41.7MPa, respectively. The maximum dynamic factor of compressive strength is 1.34 for fully-graded concrete specimens and 1.15 for wet-screened concrete specimens, respectively.

Under quasi-static conditions, the compressive strength of the wet-screened specimens (35.4MPa) is greater than that of the fully-graded concrete specimens (31.1MPa). However, the compressive strength for the wet-screened specimens (40.9MPa) and the fully-graded specimens (41.1MPa) corresponding to the strain rate of the dam's fundamental frequency are essentially equal.

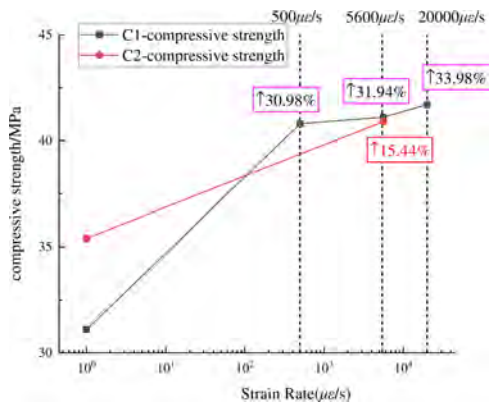

Fig. 3
Compressive strength of fully-graded concrete specimens and wet-screened concrete specimens

3.2. Results and analysis of splitting test

The edge length of the fully-graded concrete cubic specimens for splitting test is 300mm. The wet-screened cubic specimens have an edge length of 150mm. The splitting test utilizes steel spacers, with the fully-graded specimens having a cross-section of 15x15mm and the wet-sieved specimens having a cross-section of 5×7mm (with a loading surface width of 5mm). And there are a total of 6 strain gauges on the four lateral surfaces for both fully-graded concrete specimens and wet-screened specimens. Each set consists of at least 3 specimens, and a total of 13 specimens have been completed for the fully-graded concrete specimens and 8 for the wet-screened specimens.

The splitting tensile strength changes with the changing of the strain rate (Fig. 4). The average quasi-static splitting tensile strength of the fully-graded concrete specimens was 2.25MPa, which was 7.23 % of the quasi-static compressive strength of fully-graded concrete specimens(31.1MPa). The average dynamic splitting tensile strength values of fully-graded concrete specimens with the strain rate of 10^{-4}/s, 5.6×10^{-4}/s and 2×10^{-3}/s were 2.82MPa, 2.92MPa and 3.31MPa, respectively. The maximum dynamic factor of splitting tensile strength is 1.47 for fully-graded concrete specimens and 1.35 for wet-screened concrete specimens, respectively.

Unlike the compressive tests, the splitting tensile strength values of the wet-screened specimens are higher than those of the fully-graded concrete specimens at the same strain rate. Under quasi-static conditions, the splitting tensile strength of the wet-screened specimens (2.38MPa) is higher than that of the fully-graded concrete specimens (2.25MPa). The splitting tensile strength corresponding to the strain rate of the dam's fundamental frequency for the wet-screened specimens (3.21MPa) is also higher than the value of the fully-graded specimens (2.92MPa).

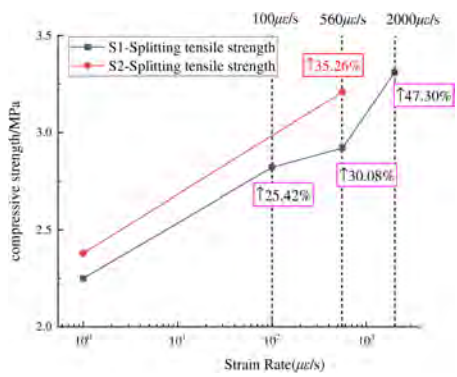

Fig. 4
Splitting tensile strength of fully-graded concrete specimens and wet-screened concrete specimens

3.3. Results and analysis of bending test

The bending strength is assessed using the three points loading method a simply- supported beam (Fig. 5). For the fully graded concrete specimens, the specimens are cubical in shape with dimensions of 300mm by 300mm by 1200mm, equipped with a total of 30 strain gauges distributed across the four lateral faces. And the wet-screened specimens are also cubical, measuring 150mm by 150mm by 550mm, and feature 4 strain gauges on the upper and lower faces. Each set consists of at least 3 specimens, and a total of 16 specimens have been completed for the fully-graded concrete specimens and 8 for the wet-screened specimens.

Fig. 5
Bending Test Specimen Installation Diagram (left for fully-graded concrete specimens, right for wet-screened concrete specimens)

The bending strength correlates with the strain rate (Fig. 6). The average quasi-static bending strength of the fully-graded concrete specimens was 2.63MPa, which was 8.46 % of the quasi-static compressive strength of fully-graded concrete specimens (31.1MPa). The average bending strength values of fully-graded concrete specimens with the strain rate of 10^{-4}/s, 5.6×10^{-4}/s and 2×10^{-3}/s were 3.29MPa, 4.09MPa and 3.43MPa, respectively. The maximum dynamic factor of bending strength is 1.56 for fully-graded concrete specimens and 1.32 for wet-screened concrete specimens, respectively.

The bending strength values of the wet-screened specimens are higher than those of the fully-graded concrete specimens at the same strain rate. Under quasi-static conditions, the bending strength of the wet-screened specimens (3.48MPa) is higher than that of the fully-graded concrete specimens (2.63MPa). The bending strength corresponding to the strain rate of the dam's fundamental frequency for the wet-screened specimens (4.59MPa) is also higher than the value of the fully-graded specimens (4.09MPa).

It should be noted that at a strain rate of 2×10^{-3}/s, the bending strength of fully-graded concrete specimens has decreased compared to when the strain rate was 5.6×10^{-4}/s, but it is still higher than the bending strength under quasi-static conditions. The difference in bending strength of the specimens is influenced not

only by the increase in compressive strength of the dam concrete in the later stages but also by the differences between the on-site mixing, casting, and curing conditions of the dam concrete and the laboratory molding and curing conditions. Therefore, specialized concrete material performance tests are of significant importance for obtaining the true mechanical properties of large-volume hydraulic concrete structures.

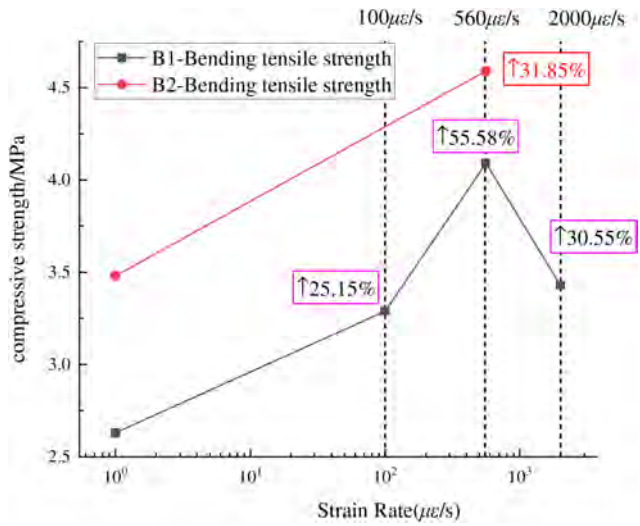

Fig. 6
Bending strength of fully-graded concrete specimens and wet-screened concrete specimens

4. CONCLUSIONS

The experimental study on the uniaxial dynamic performance of concrete specimens of the BDa Dam has provided valuable insights into the behavior of concrete under various strain rates. The compressive, splitting tensile tests and bending tensile tests of BDa specimens were carried out, and compared with the test results of fully-graded concrete specimens and wet-screened concrete specimens prepared in the laboratory. The research results reveal the tensile and compressive characteristics of BDa dam. The main conclusions are as follows.

1. The results indicate a clear trend of increasing compressive and tensile strength with the rise in strain rate for both fully-graded and wet-screened concrete specimens. This suggests that the concrete's dynamic response is significantly influenced by the strain rate.

2. The comparison between fully-graded and wet-screened concrete specimens under quasi-static condition reveals that the wet-screened concrete exhibits higher strength values. This phenomenon emphasizes the significance in capturing the true mechanical properties of large-volume hydraulic concrete structures. The discrepancies between laboratory-molded specimens and large-volume concrete specimens highlight the necessity for specialized concrete material performance tests.
3. The results underscore the importance of considering dynamic material properties in the context of seismic fortification and provide a scientific basis for enhancing the safety and reliability of such structures.

REFERENCES

[1] NB 35047-2015 Code for seismic design of hydraulic structures of hydropower project:[S]. 2015.

[2] GB 51247-2018 Standard for seismic design of hydraulic structures[S]. 2018.

[3] SL/T 352-2020 Test code for hydraulic concrete:.[S]. 2020.

[4] ABRMAS D A. Effeet of Rate of Application of Load on the Compressive Strength of Concrete[A]. Proc.20th Annu. Meeting, ASTM[C]. West Conshohoeken, Pa.,1917:366-374.

[5] CAVERZAN A. Compressive behaviour of dam concrete at higher strain rates[J]. *The European Physical Journal Special Topics*, 2016, 225(2):283–293.

[6] SOLOMOS G, BERRA M. Compressive behaviour of recycled aggregate concrete under impact loading[J]. *Cement and Concrete Research*, 2015 (71):46–55.

[7] GANG PENG. Study on dynamic compressive properties of concrete under pore water pressure environment[J]. *China Civil Engineering Journal*, 2015, 48(1):11–18.

[8] DONGMING YAN. Experimental and Theoretical Study on the Dynamic Properties of Concrcte[D]. *Dalian University of Technology*. 2006.

[9] FUJIN QU. Effect of strain rate on dynamic behavior of high-performance fiber reinforced concrete[J]. *Construction technology*,1997(05):5–7.

[10] MALVAR L J AND CRAWFORD J. *Dynamic Increase Factors for Concrete, Twenty-Eighth DDESB Seminar*, Orlando, FL, August 1998.

Q.111 - R.39

COMMISSION INTERNATIONALE DES
GRANDS BARRAGES

VINGT-HUITIEME CONGRES DES
GRANDS BARRAGES
CHENGDU, MAI 2025

SEISMIC FRAGILITY ANALYSIS OF GRAVITY DAM BASED ON MSA (*)

Maohua WANG
State Key Laboratory of Simulation and Regulation of Water Cycle in River Basin
China Institute of Water Resources and Hydropower Research, Beijing

Kai ZHANG
China Institute of Water Resources and Hydropower Research, Beijing

Yanhong ZHANG
State Key Laboratory of Simulation and Regulation of Water Cycle in River Basin
China Institute of Water Resources and Hydropower Research, Beijing

CHINA

SUMMARY

MSA is a fragility analysis analysis method for discrete strength factors, which provides an effective path for structural safety assessment, but is currently less applied in the field of gravity dam engineering. In this paper, for a concrete gravity dam project, the down-river displacement of the dam crest of the spillway dam section is selected as a performance index, the randomness of ground vibration is considered, and the radiation damping effect of the foundation is considered with viscoelastic boundaries, and then nonlinear fluctuating finite element analysis is carried out based on the plastic damage mechanics model of the concrete, and finally the susceptibility study is carried out by the MSA method, and the susceptibility curves and probabilities of the dams with different damage levels are obtained,

**Analyse de la fragilité sismique d'un barrage-poids basé sur MSA*

 DOI: 10.1201/9781003642428-140

so as to provide guidelines for the dam's strong seismic performance evaluation to provide guidelines and references.

RÉSUMÉ

MSA est une méthode d'analyse de fragilité pour les facteurs de résistance discrets, qui fournit une voie efficace pour l'évaluation de la sécurité structurelle. Elle est actuellement moins appliquée dans le domaine de l'ingénierie des barrages-poids. Dans ce rapport, pour un projet de barrage-poids en béton, le déplacement en aval de la crête du barrage de la section du barrage déversoir est choisi comme indice de performance ; le caractère aléatoire des vibrations du sol est pris en compte, et également l'amortissement des radiations de la fondation avec des limites viscoélastiques, L'étude de susceptibilité est réalisée par la méthode MSA, et les courbes de susceptibilité et les probabilités avec différents niveaux de dommages sont obtenues, de manière à fournir des lignes directrices pour l'évaluation de la performance sismique du barrage et à fournir des références.

1. INTRODUCTION

China's southwest strong earthquake area has about 80% of China's hydraulic energy resources, it is difficult to construct high dams and large reservoirs in these areas to avoid the problem of seismic safety of the dam structure, high dams in the earthquake once the dam breaks will be a serious secondary disaster to the downstream area [1]. High dams constructed in strong earthquake zones have high defense intensities, complex foundation conditions, and face the challenge of many major key technical problems, so it is necessary to use a reasonable method to evaluate the seismic safety performance of high dams [2]. The seismic fragility analysis of dams can predict the probability of different grades of dam breakage under different intensities of earthquakes, and thus can provide a scientific basis for performance-based seismic safety evaluation and decision-making of dams [3]. Therefore, the study of seismic fragility analysis is of great significance for the seismic design of high dams in strong earthquake zones and the reasonable judgment of their seismic capacity.

Ellingwood et al [4,5] introduced the susceptibility analysis method to the field of hydraulic structures, and analyzed the susceptibility of a concrete gravity dam in the United States under different flood levels as well as under different seismic levels. The Incremental Dynamic Analysis (IDA) method, which was elaborated and summarized by Vamvatsikos [6], has been widely used in the seismic fragility

analysis evaluation of gravity dams [7–9]. Based on the IDA, Amirpour et al. [10] found that the dam roof displacement is more suitable as a damage indicator than the peak stress in the upstream and downstream overstress zones. However, the IDA method requires a sufficient number of seismic waves and repeated amplitude adjustments of the selected seismic recordings so that the seismic intensity of each seismic wave reaches the required value for structural damage calculation, which makes the calculation more work and time-consuming [11]. The Multiple Stripe Analysis method (MSA) proposed by Jalayer [12] can evaluate the fragility analysis of discrete the Intensity Measure (IM) without adjusting the IM of ground motion to make the structural response exceed the limit state. Baker [13] found that MSA method was more effective than IDA method in estimating the parameters of the fragility analysis equation under a certain number of structural analyses. Pang et al [14] used the MSA method to carry out a dam fragility analysis study and showed that the appropriate reduction of the number of horizontal strips had little impact on the fragility analysis results, which was conducive to the reduction of calculation conditions. Therefore, MSA method, as a fragility analysis method for discrete strength factors, provides an effective path for structural safety assessment, but it is rarely used in the field of gravity dam engineering. In addition, in fragility analysis and research, the interaction between dam body and foundation is mostly based on the massless foundation method [7–10], which exaggerates the response of the dam to earthquake to a certain extent and cannot accurately reflect the actual seismic capacity of the dam.

In view of this, this paper first establishes the viscoelastic boundary considering the radiation damping effect of the foundation, and then conducts nonlinear wave finite element analysis based on the plastic damage mechanics model of concrete. The river-bound displacement of the dam top relative to the dam heel (hereinafter referred to as the river-bound displacement of the dam top) is adopted as the main performance index. This paper analyzes the fragility analysis curve and failure probability of concrete gravity dam, evaluates the seismic performance of the dam, and provides reference for seismic risk assessment and decision making of the dam.

2. RESEARCH METHOD

2.1. MSA METHOD

The seismic fragility analysis of a structure refers to the conditional probability that the structure exceeds a certain failure state under a certain intensity earthquake. The fragility analysis curve is used to describe the probability of the system reaction exceeding a certain failure state at the corresponding ground motion intensity (IM). The peak acceleration (PGA) of ground motion and the spectral

acceleration (Sa) corresponding to the fundamental period of the structure are often used as IMs. In this paper, PGA is selected as IM. It is generally assumed that the ground motion intensity IM that leads to structural failure conforms to a lognormal distribution, so the fragility analysis equation can be expressed as [15]:

$$P_f(C|IM = x) = \Phi\left(\frac{\ln(x/\theta)}{\beta}\right) \tag{1}$$

where, $P_f(C|IM = x)$ is the probability that the structure will reach the failure state when the ground motion intensity $IM = x$, Φ is the standard normal distribution function, θ is the median of the fragility analysis equation, and β is standard deviation of$\ln(IM)$.

For each ground motion intensity x_i, the number of seismic waves that exceed the limit state in all seismic waves can be calculated. Assuming that each observed seismic wave does not exceed or exceed the structural damage state is independent of other seismic waves [16], when $IM=x_i$, the probability of structural damage caused by z_i seismic waves in n_i groups is as follows:

$$P_f = \binom{n_i}{z_i} P_i^{z_i}(1 - P_i)^{n_i - z_i} \tag{2}$$

where, P_i is the probability of structural failure under ground motion when $IM=x_i$. To be able to estimate the fragility analysis parameter, the likelihood function can be expressed as:

$$L = \prod_{i=1}^{m} \binom{n_i}{z_i} \Phi\left(\frac{\ln(x_i/\theta)}{\beta}\right)^{z_i} \left[1 - \Phi\left(\frac{\ln(x_i/\theta)}{\beta}\right)\right]^{n_i - z_i} \tag{3}$$

where m is the number of IM levels, $\Pi$is the conjunction symbol, n_i and z_i are the number of overlimit states and the number of time seismic waves, respectively.

Parameters θ and β of the fragility analysis equation can be obtained by maximum likelihood estimation, and the corresponding equation is shown in equation (3):

$$\left\{\widehat{\theta}, \widehat{\beta}\right\} = \arg\max_{\theta,\beta} \sum_{i=1}^{m} \left\{ \ln\binom{n_i}{z_i} + z_i \ln \Phi\left(\frac{\ln(x_i/\theta)}{\beta}\right) + (n_i - z_i)\ln\left[1 - \Phi\left(\frac{\ln(x_i/\theta)}{\beta}\right)\right] \right\} \tag{4}$$

The main steps of MSA method for gravity dam fragility analysis are shown in Fig. 1.

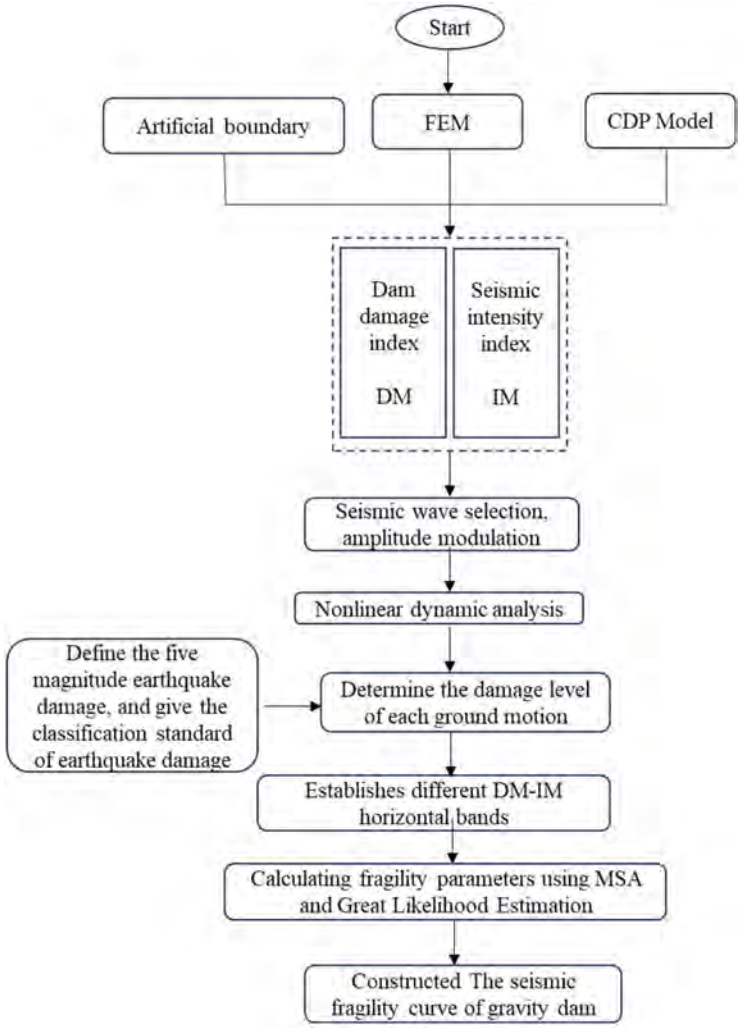

Fig. 1
Seismic fragility analysis flow chart of gravity dam

2.2. Viscoelastic artificial boundary

The viscoelastic artificial boundary simulates the stress condition on the artificial boundary, which is a kind of continuous distribution artificial boundary condition. When finite element method or other discrete methods are used to discretize the artificial boundary and the computational region surrounded by it, the viscoelastic artificial boundary is discretized at the same time, and then the decoupling artificial boundary can be formed simply by the centralized processing method, which is called the centralized viscoelastic artificial boundary. The centralized viscoelastic artificial boundary is simulated by the spring and the dashpot in ABAQUS, where the normal and tangential stiffness coefficients are:

$$\begin{cases} K_{BN} = \alpha_N \dfrac{G}{R}, C_{BN} = \rho c_p \\ K_{BT} = \alpha_T \dfrac{G}{R}, C_{BT} = \rho c_s \end{cases} \tag{5}$$

where, K_{BN} and K_{BT} are the normal and tangential stiffness coefficients of the spring respectively. C_{BN} and C_{BT} are the normal and tangential damping coefficients of the damper respectively.

The input seismic motion is converted into the equivalent node load directly acting on the artificial boundary element [17], and the equivalent node load of a certain node b on the boundary can be expressed as:

$$\begin{cases} F_{bn} = \left(R_{bn}^{ef} + C_{bn}\dot{u}_{bn}^{ef} + K_{bn}u_{bn}^{ef}\right)A_b \\ F_{bt} = \left(R_{bt}^{ef} + C_{bt}\dot{u}_{bt}^{ef} + K_{bt}u_{bt}^{ef}\right)A_b \end{cases} \tag{6}$$

where, F_{bt} and F_{bn} are tangential and normal equivalent node loads on the boundary element respectively. A_b is the influence area of node b; Damping coefficient C_b and spring stiffness coefficient K_b can be determined by equation (5). $\dot{u}_b^{ef}$ 、 u_b^{ef} and R_b^{ef} represent velocity, displacement and stress at artificial boundary nodes in free field analysis, respectively, and are solved by local wave field decomposition method [18].

3. FRAGILITY ANALYSIS OF GRAVITY DAM

3.1. FEM

The object of this paper is a concrete gravity dam in the west of China, which is a Class I (I) project and the water retaining structure is a Class 1 building. The overflow section of the dam is selected for fragility analysis. The height of the section is 144 m and the width of the crest is 52 m. The concrete strength of the dam body is relatively

high, and the main materials are C30, C40 and C55 concrete. The dam body is reasonably simplified, and the finite element model is shown in Fig. 2, in which the upper and lower reaches of the dam body and the bottom of the dam are intercepted as the finite element calculation range, and the fault zone is considered in the foundation.

Considering that the dam is subjected to loads such as self-weight, hydrostatic pressure, silt pressure, bidirectional seismic action and dynamic water pressure, the dynamic water pressure is simulated by Westergard additional mass model, and viscoelastic artificial boundary is established to simulate the radiation damping effect of foundation. Moreover, the concrete damage plasticity (CDP) constitutive model is used to describe the complex mechanical behavior of concrete materials under earthquake conditions. The large finite element software ABAQUS is used to calculate the nonlinear wave seismic response of gravity dam, and the dam fragility analysis is completed according to the steps of fragility analysis in Section 2.1.

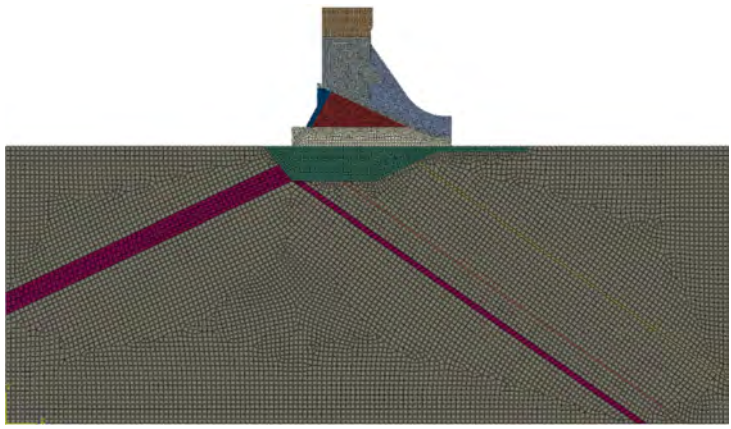

Fig. 2
Finite element model of overflow dam

3.2. Selection and standardization of seismic waves

Considering the uncertainty of earthquake action, different types of seismic waves that meet the requirements should be selected. In order to meet the conditions of near and shallow earthquakes required by seismic risk analysis, and also meet the conditions of rocks close to the dam site, 12 seismic waves in Table 1 are selected, where the magnitude M is 5.0∼7.0, and the epicenter is 10∼30 km away from R. Fig. 3 shows the magnification factor response spectrum of each seismic wave when the damping ratio is 5%, where the black line is the average value of the

above seismic wave response spectrum, and the red line is the standard response spectrum based on the seismic design standard. It can be seen from the figure that the average response spectrum of 12 seismic records is basically consistent with the standard spectrum, which can be well applied to the fragility analysis of gravity dams.

Table 1
Seismic wave information

ID	INCIDENT	YEAR	STATION	*M*	*R*(KM)
1	Santa Barbara	1978	Cachuma Dam Toe	5.92	23.75
2	Imperial Valley-05	1955	El Centro Array #9	5.40	13.78
3	Chi-Chi_ Taiwan-06	1999	CHY075	6.30	24.34
4	Taiwan SMART1(5)	1981	SMART1 O10	5.21	26.66
5	L'Aquila_ Italy	2009	Celano	6.30	17.82
6	L'Aquila_ Italy	2009	L'Aquila - Parking	5.40	13.97
7	Chuetsu-oki_ Japan	2007	Kawaguchi	6.80	23.63
8	Chuetsu-oki_ Japan	2007	NIGH11	6.80	21.19
9	Chalfant Valley-02	1986	Long Valley Dam (L Abut)	6.19	18.30
10	Iwate_ Japan	2008	IWT010	6.90	15.16
11	Darfield_ New Zeal-and	2010	RKAC	7.00	13.37
12	Landers	1992	Mission Creek Fault	5.38	26.96

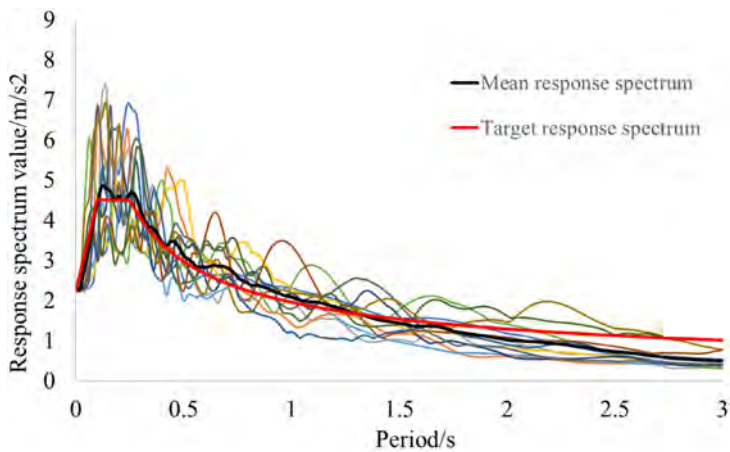

（a）Horizontal seismic wave

Fig. 3 Comparison of standard response spectrum with PEER response spectrum

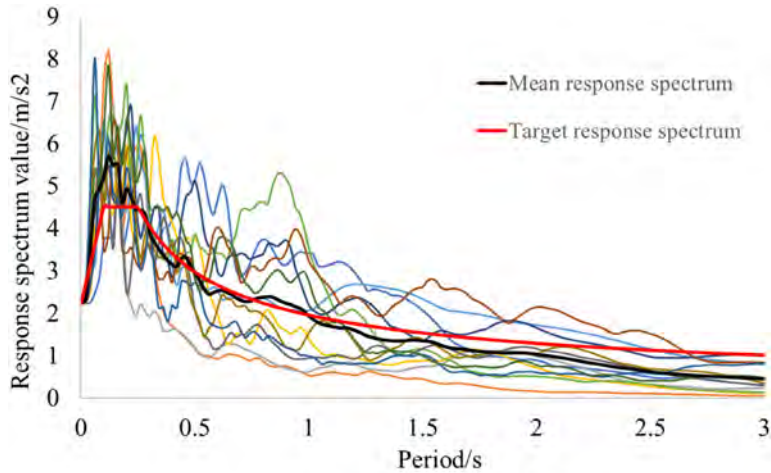

（b）Vertical seismic wave

Fig. 3
(Continued)

3.3. Classification of earthquake damage

There are also different damage states of gravity dams under different levels of earthquake action. Fragility analysis needs to determine the classification standard of earthquake damage under various seismic actions, that is, the value of displacement performance level LS. According to the previous earthquake damage investigation and test analysis, the damage and failure states of concrete dams subjected to earthquake loads can be divided into five levels, namely, basically intact, slight damage, moderate damage, serious damage, and dam failure. The detailed definitions are shown in Table 2. According to the classification criteria of dam body performance under earthquake action and related literature [9] in Table 2, and combined with the statistics of numerical calculation results, the damage index of dam top displacement along river direction is given in Table 2 to determine the earthquake damage grade of gravity dam, where H is the maximum dam height of the selected gravity dam section, which is 144 m.

Table 2
Definition of earthquake damage grade of gravity dam

MAGNITUDE	SPECIFIC DESCRIPTION	THE CREST OF THE DAM MOVES ALONG THE RIVER DM/MM
Level one, basically intact	The gravity dam remains basically intact, and there is a small amount of minor damage in the local area, which does not hinder the normal operation of the gravity dam.	0∼0.035% 0<DM ≤ 50
Level two, minor damage	The auxiliary structure of the gravity dam is slightly damaged, and the dam body can be restored to normal operation after some repair.	0.035%∼0.055% 50<DM ≤ 80
Level three, moderate damage	Most areas of the gravity dam have obvious cracks, and some places have begun to leak slightly. The gravity dam can continue to be used normally after repair if the auxiliary structure is moderately damaged.	0.055%∼0.076% 80<DM ≤ 110
Level four, serious damage	Most of the gravity dam appeared through cracks, serious leakage. It is difficult to repair the dam body because of serious damage to the attached structure.	0.076%∼0.097% 110<DM ≤ 140
Level five, dam failure	The gravity dam broke beyond repair.	>0.097% 140<DM

3.4. Seismic MSA fragility analysis

In this paper, the seismic peak acceleration PGA is selected as the seismic intensity parameter IM, and the amplitude modulation step is 0.1 g. The finite element calculation shows that the dam is seriously damaged when PGA=1.0 g. Therefore, the amplitude modulation range is 0.1∼1.0 g. According to the dynamic analysis of the selected seismic waves, the river-bound displacement of the dam top is obtained. Then, the MSA method is used to analyze the seismic fragility analysis, and the relationship between the peak acceleration of seismic waves PGA and the top displacement along the river can be obtained, as shown in Fig. 4. The data in Fig. 4 can be put into MSA fragility analysis formula (2) and (4) to obtain the corresponding fragility analysis parameter sum. The calculation results are shown in Table 3. LS1∼LS4 correspond to the four displacement performance levels of slight damage, moderate damage, severe damage and dam break in Table 2 respectively, and then combine with formula (2) to obtain the exceedance probability under different performance levels. Then, the fragility analysis curve of gravity dam is drawn, as shown in Fig. 5.

Table 3
Seismic fragility analysis parameters

ID	LS1	LS2	LS3	LS4
θ	0.399	0.641	0.869	1.038
β	0.179	0.199	0.198	0.132

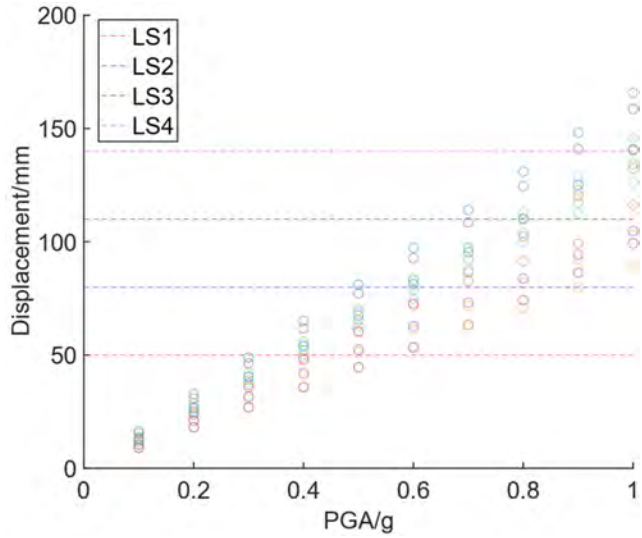

Fig. 4
Scatter diagram of PGA and dam crest displacement along river direction

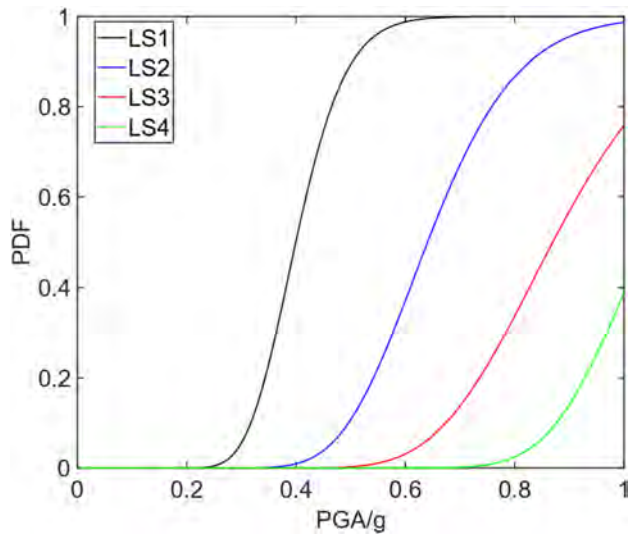

Fig. 5
Fragility analysis probability curve of gravity dam

According to the fragility analysis curves of four levels of gravity dam under different ground motion intensities, it can be seen that: (1) When the peak acceleration of ground motion input is 0.3g, the probability of slight damage is 5.5%, and moderate damage and severe damage are not easy to occur; When the peak acceleration is 0.5 g, the probability of slight damage is 89.3%, the probability of moderate damage is 10.7%, and it is not easy to cause serious damage. (2) When the peak acceleration is 0.7g, the dam body is completely capable of mild damage, the probability of moderate damage is 67.1%, and the probability of serious damage is 13.7%. (3) When the peak acceleration is 0.9g, the probability of moderate damage is 95.6%, the probability of serious damage is 56.8%, and the probability of dam break is 14.1%. (4) When the peak acceleration is 1.0g, the dam body is fully capable of moderate damage, the probability of serious damage is 75.8%, and the probability of dam break is 38.9%.

It can be seen from the slope of the curve that the slope of the LS1 state and LS2 state curves of the dam is large, which indicates that once the dam is slightly damaged or moderately damaged under the earthquake, the dam will quickly reach these two damage limit states with the increase of the small amplitude of the ground motion intensity. The slope of LS3 state and LS4 state curves is small, and with the increase of ground motion intensity, the possibility of dam serious damage and dam failure is small, which indicates that the dam has a large margin when resisting the ultimate seismic capacity.

From the above analysis, it can be seen that when the dam fragility analysis is conducted with the overflow dam section, the dam has a large safety margin below the peak acceleration value of 0.5 g, and a certain degree of serious damage occurs only at the peak value of 0.7 g. This is due to the fact that most of the concrete materials in the overflow dam section are high-strength concrete, which is less likely to be damaged under seismic action and is safer compared to the susceptibility analyses using non-overflow dam sections [7–9].

4. CONCLUSIONS

Considering the randomness of ground motion input, the MSA method is applied to the seismic performance evaluation of concrete gravity dams. The nonlinear wave finite element analysis is carried out with viscoelastic artificial boundary considering infinite foundation radiation damping effect and concrete plastic damage model. Based on the seismic fragility analysis of the dam roof displacement in river direction, the fragility analysis curves and probabilities of different grades of failure under strong earthquakes are obtained, which provides criteria and references for the evaluation of the dam’s strong seismic performance.

The results show that under the earthquake intensity of 0.3g, a certain probability of slight damage will occur in the overflow dam section, and moderate damage and severe damage will not occur. At the earthquake intensity of 0.5 g, the probability of slight damage is already very large, but the probability of moderate damage is still small, which indicates that the overflow dam section has a strong earthquake resistance. At 0.7 g earthquake intensity, the probability of moderate damage is higher. Under the ground motion intensity of 1.0g, the dam body has been completely capable of moderate damage, resulting in a high probability of serious damage, and a certain degree of dam break risk.

Due to the complexity of the problem, this paper selects the topside displacement of the overflow dam section as the evaluation index. It is necessary to add other performance evaluation indexes in subsequent studies, such as damage energy dissipation, damage volume ratio or area ratio, or other appropriate parameters or indexes reflecting strength or stability, and comprehensively evaluate the seismic performance of the dam according to the fragility analysis of different dam section types.

REFERENCES

[1] ZHANG C. H., JIN F., WANG J. T. Key issues and developments on seismic safety evaluation of high *concrete* dams. *Journal of Hydraulic Engineering*, vol. 47, no. 3, pp. 253–264, 2016.

[2] WANG H. B., LI D. Y，CHEN H. Q. Challenge in study of ultimate capacity of high arch dams against *earthquakes*. *Journal of Hydroelectric Engineering*, volu.33, no. 6, pp. 168–173, 2014.

[3] HARIRI-ARDEBILI MA, SAOUMAVE. Seismic fragility analysis of concrete dams：a state-of-the-art *review*. *Engineering Structures*, 2016, vol. 128, pp. 374–399.

[4] ELLINGWOOD B R, TEKIE P B. Fragility analysis of concrete gravity dams. *Journal of Infrastructure Systems*, vol. 7, no. 2, pp. 41–48, 2001.

[5] TEKIE P. B.，ELLINGWOOD B. R. Seismic fragility assessment of concrete gravity dams. *Earthquake Engineering and Structural Dynamics*, vol. 32, no. 14, pp. 2221–2240, 2003.

[6] VAMVATSIKOS D. Incremental dynamic analysis. *Earthquake Engineering and Structural Dynamics*, vol. 31, no. 3, pp. 491–514, 2002.

[7] WANG G., WANG Y., LU W. XFEM based seismic potential failure mode analysis of concrete gravity dam-water-foundation systems through incremental dynamic analysis. *Engineering Structures*, vol. 98, no. 1, pp. 81–94, 2015.

[8] HE L. X., CHEN D. H., YANG Z. H. Study on seismic performance of three-dimensional concrete *gravity* dam system based on IDA. *Journal of Natural Disasters*, vol. 28, no. 4, pp. 159–168, 2019.

[9] MA Z. Y., ZHANG W., ZHOU Q. A deformation-based method for seismic fragility analysis of gravity dam. *Journal of Vibration and Shock*, vol. 36, no. 22, pp. 51–58, 2017.

[10] AMIRPOUR A., MIRZABOZORG H. Quantifying the qualitative limit-states using IDA approach in concrete arch dams. *Arabian Journal for Science and Engineering*, vol. 39, no. 11, pp. 7729–7740, 2014.

[11] HUAN W. C. Seismic Fragility Analysis of Steel-concrete Tower Based on IDA MSA Method [D]. North China University of Water Resources and Electric Power, 2023.

[12] JALAYER F. *Direct probabilistic seismic analysis: implementing non-linear dynamic assessments[M]*. Stanford, CA: Stanford University, 2003.

[13] BAKER J W. Efficient analytical fragility function fitting using dynamic structural analysis [J]. *Earthquake Spectra*, 2015, 31, no. 1, pp. 579–599.

[14] PANG R., KONG X. J, ZOU D. G. Seismic subsidence fragility analysis of high CRFDs based on MSA [J]. *Journal of Hydraulic Engineering*, vol. 48, no. 7, pp. 866–873, 2017.

[15] KARIM K R，YAMAZAKI F. Effect of earthquake ground motions on fragility curves of highway bridge piers based on numerical simulation[J]. *Earthquake Engineering and Structural Dynamics*, vol. 30, no. 12, pp. 1839–1856, 2001.

[16] ACKNER M A, ROTEA M A. Structural control of floating wind turbines. *Mechatronics*, vol. 21, no. 4, pp. 704–719, 2011.

[17] HE J. T., MA H. F., ZHANG B. Y. Method and realization of seismic motion input of viscous-spring boundary. *Journal of Hydraulic Engineering*, vol. 41, no. 8, pp. 960–969, 2010.

[18] DU X. L. *Theories and Methods of Wave Motin for Engineering [M]*. Beijing: Sciences Publishing，2009.

Q.111 - R.40

COMMISSION INTERNATIONALE DES
GRANDS BARRAGES

VINGT-HUITIEME CONGRES DES
GRANDS BARRAGES
CHENGDU, MAI 2025

RESEARCH AND APPLICATION OF KEY TECHNOLOGIES FOR THE ULTRA-HIGH ARCH DAM OF THE BAIHETAN HYDROPOWER STATION (*)

Jianrong XU, Jianjun XU, Hua JI & Jianxin WANG
PowerChina Huadong Engineering Corporation Limited, Hangzhou

CHINA

SUMMARY

The Baihetan Hydropower Station is the second-largest hydropower station in the world, with a total installed capacity of 16 million kW and a maximum dam height of 289 m. The dam site is situated in a typical hot and dry valley of the Jinsha River, characterized by asymmetrical topographical and geological conditions on both abutments. Approximately 40% of the dam foundation area is exposed to easily weathered columnar jointed basalt, and the seismic intensity at the construction site reaches a basic level of VIII, presenting significant challenges to the project. To ensure the successful construction of the project, engineers and researchers undertake a series of studies addressing these issues, including the treatment and utilization of the columnar jointed basalt in the dam foundation, stability against sliding of the dam abutments, temperature control and crack prevention in low-heat cement concrete, and seismic resistance of high arch dams. These efforts result in key technological breakthroughs and provide invaluable experience for the construction of future high arch dam projects.

**Recherches et mise en oeuvre de technologies clés pour le très grand barrage-voûte de l'aménagement de Baihetan*

 DOI: 10.1201/9781003642428-141

RÉSUMÉ

La centrale hydroélectrique de Baihetan est la deuxième plus grande centrale hydroélectrique au monde, avec une capacité installée totale de 16 millions de kW et une hauteur de barrage maximale de 289 m. Le site du barrage est situé dans une vallée chaude et sèche typique de la rivière Jinsha, caractérisée par des conditions topographiques et géologiques asymétriques sur les deux culées. Environ 40 % de la zone de fondation du barrage est composée de basalte à joints colonnaires facilement altéré. L'intensité sismique sur le site de construction atteint un niveau de base de VIII, ce qui représente des défis importants pour le projet. Pour assurer la réussite de la construction, les ingénieurs et les chercheurs entreprennent une série d'études sur ces questions, notamment sur le traitement et l'utilisation du basalte à joints colonnaires dans les fondations du barrage, la stabilité contre le glissement des culées du barrage, le contrôle de la température et la prévention des fissures dans le béton de ciment à basse température, et la résistance sismique des grands barrages-voûtes. Ces efforts aboutissent à des percées technologiques clés et fournissent une expérience inestimable pour la construction de futurs projets de très grands barrages-voûtes.

1. INTRODUCTION

The Baihetan Hydropower Station is located on the lower reaches of the Jinsha River, spanning the border between Ningnan County in Sichuan Province and Qiaojia County in Yunnan Province. It serves as the second tier of four hydropower stages on the lower Jinsha River. The dam site controls a drainage area of 430,300 km^2, which accounts for 91% of the upstream drainage area of the Jinsha River. The primary development objectives of the station are power generation, along with flood control, navigation, and the promotion of local economic and social development. The station has installed 16 generators, each with a capacity of 1,000 MW, resulting in a total installed capacity of 16,000 MW. The average annual electricity generation is 62.443 billion kWh. The normal water level of the reservoir is 825 m, with a total storage capacity of 20.627 billion m^3.

The hub of the Baihetan hydropower station consists of several key structures, including a concrete hyperbolic arch dam, spillway tunnel, intake, underground powerhouse, pressure regulating shaft, tailrace tunnel, and diversion tunnels, as shown in Fig. 1. The hub structures have multiple world-leading indicators, including a single-unit capacity of 1 million kilowatts for the hydroelectric turbines, the scale of the underground cavern group, the size of the cylindrical tailrace regulation chamber, advanced seismic parameters for the high arch dam, the scale of the spillway tunnel group, and the first use of low-heat cement concrete throughout the entire dam. The construction of the arch dam commenced on April 12, 2017. The diversion tunnel was closed for water storage on April 6, 2021. The first batch of units was put

into operation for power generation on June 28, 2021. By December 20, 2022, all 16 units of the power station had been commissioned and were generating electricity.

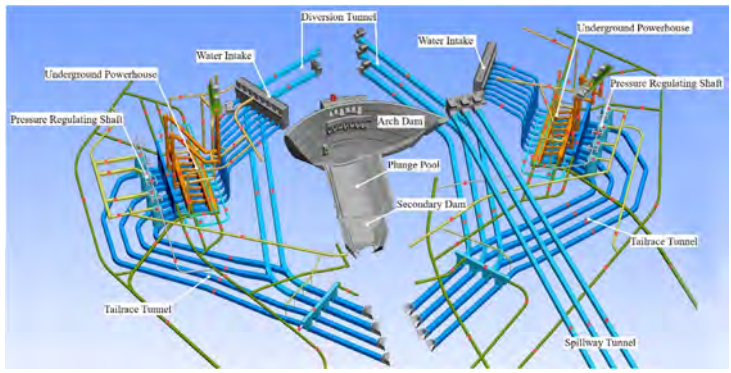

Fig. 1
Project layout of Baihetan Hydropower Station.

The design and construction of the Baihetan arch dam have encountered numerous challenges. The asymmetry of the valley's topography and geological conditions is evident. The exposed columnar jointed basalt in the middle and lower sections of the dam foundation is susceptible to relaxation after excavation, which can lead to a deterioration in rock mass quality [1]. Shear deformations exist along the fault zones within the gently inclined layers of the dam foundation, and weak structural features in the rock mass have an adverse impact on the stability of the dam's abutments [2,3]. Under the arid and hot valley climate, there is a risk of cracking in the large volume concrete of the arch dam. Additionally, the seismic safety issues of super-high arch dams under high seismic intensity require comprehensive research and design improvements [4,5]. In response to the above issues, this paper presents research on the foundation treatment, dam shoulder stability, temperature control design, and seismic safety of the super-high arch dam at the Baihetan Hydropower Station, along with its application and practice in engineering construction.

2. THE STRUCTURAL DESIGN OF THE BAIHETAN ARCH DAM

The Baihetan arch dam has a maximum height of 289 m and a total water thrust of up to 165 million kN. The foundation exposes the Upper Permian Emei Mountain Group basalt, with the selected foundation rock primarily consisting of slightly weathered to moderately fresh hard rock, mainly classified as categories II to III_1. The high-elevation dam foundations on both banks, as well as certain

localized areas, can utilize treated slightly weathered and low-load bearing category III_2 rock. The geological conditions on both banks exhibit significant asymmetry, which affects the arch dam's stress and strain, arch thrust, failure characteristics, and overload capacity. To mitigate these impacts, an adaptable elliptical profile was employed, and the dam's centreline was appropriately translated and rotated. Additionally, a concrete seat was established at the crest of the left bank, and an enlarged foundation was set at the toe of the arch dam's middle-lower section. These comprehensive measures improved the structural safety of the arch dam against the effects of geological asymmetry.

The Baihetan arch dam is an elliptical-shaped concrete double-curvature arch dam, as shown in Figure 2. The elevation of the riverbed foundation is 545 m, while the crest elevation is 834 m, resulting in a maximum dam height of 289 m. The thickness of the arch crown beam at the base is 63.5 m, and the width at the top of the dam is 14 m. The maximum thickness at the arch ends is 83.91 m, and the arc length of the centreline at the dam crest is 708.7 m. The thickness-to-height ratio is 0.22, and the arch height-to-span ratio is 2.45. The total concrete volume of the dam is 8.03 million m^3.

The dam body is equipped with six overflow surface outlets and seven overflow deep outlets, symmetrically arranged along the spillway centerline from sections 15 to 21 of the arch dam (Fig. 2). The elevation of the overflow surface outlets' crest is 810 m, with a net width of 14 m for each outlet. The outlets of the six surface flow holes utilize a layered large differential continuous weir and tongue-shaped weir design. A total of seven deep outlets are arranged in the dam body, with an opening size of 5.5 m $\times$ 8 m (width $\times$ height). To dissipate energy behind the dam, a stilling basin is employed, with a cross-sectional profile designed as a reverse arch-type bottom slab with a composite trapezoidal section. The lowest elevation of the bottom slab is 560.00 m, the top elevation is 635.00 m, and its length is 360 m, with a top width of 210 m. The secondary dam is a bidirectional overflow dam of gravity dam type, with a crest elevation of 608 m and a maximum height of 58 m.

Fig. 2
Dam structure of Baihetan Hydropower Station.

3. THE MAIN TECHNOLOGICAL INNOVATION OF BAIHETAN ULTRA-HIGH ARCH DAM

3.1. Reinforcement treatment for columnar jointed basalt dam foundation to prevent unload relaxation

Columnar jointed basalt is mainly found in the layers $P_2\beta_3^3$, $P_2\beta_2$, and $P_2\beta_3^{2\text{-}2}$, with the $P_2\beta_3^3$ layer being the most developed, reaching an approximate thickness of 55 m [Fig. 3(a)]. The block size of the cut rock mass is approximately 5 cm [Fig. 3 (b)(c)]. Without any treatment measures, the relaxation effect of the rock mass becomes evident after excavation and unloading [6,7]. The relaxation depth generally ranges from 2 to 3 m and can reach about 4 m in some areas influenced by structural surfaces. Therefore, targeted treatment of the columnar jointed basalt rock mass is essential for the foundation of the high arch dam.

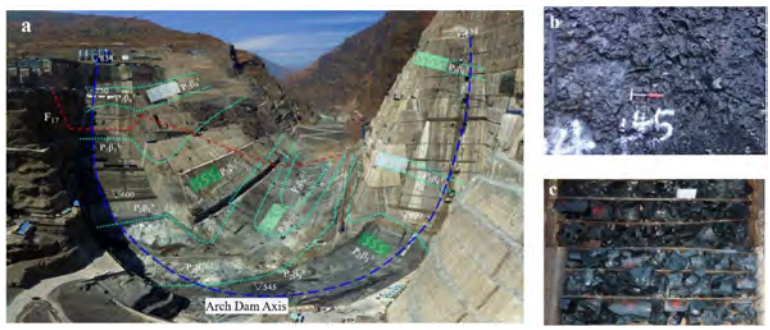

Fig. 3
Columnar jointed basalt of the Baihetan dam foundation. (a) distribution of the bedrock layers at the foundation of the arch dam, (b) columnar jointed basalt in the $P_2\beta_3^3$ layer, (c) core drilling of the columnar jointed basalt in the $P_2\beta_3^3$ layer.

The relaxation of the rock mass in the dam foundation is mainly affected by the rock mass structure, degree of unloading, excavation support methods, and timing of support. The relaxation of the rock mass due to unloading is controlled by its own structure. As shown in Fig. 4, intact rock has high deformation modulus and strength, resulting in smaller deformation and relaxation depths caused by excavation. The deformation and strength of jointed rock masses are controlled by structural surfaces. Excavation and unloading can easily lead to discontinuous deformation and shear yield failure along these surfaces, which may even result in relative movement between rock blocks, thereby damaging the integrity of the rock mass and exacerbating its relaxation. Therefore, the poorer the integrity of the rock mass, the more significant the relaxation caused by excavation and unloading will be.

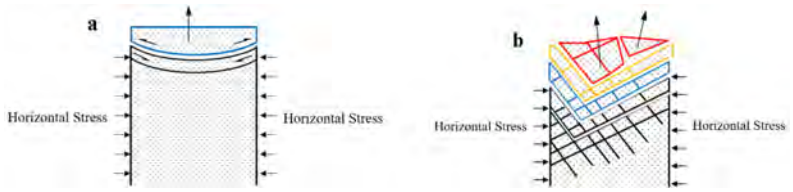

Fig. 4
Unloading relaxation characteristics of intact rock and jointed rock mass. (a) intact rock, (b) jointed rock mass.

The Baihetan hydropower station is the world's first hydropower project to use columnar jointed basalt as the foundation for an arch dam. Extensive geological investigations, experimental studies, and theoretical analyses were conducted on the unloading relaxation characteristics of columnar jointed basalt. This led to the development of a comprehensive technical system for preventing relaxation, which mainly includes: foundation reinforcement techniques such as rock protective layer cover re-consolidation grouting and shallow concrete cover reinforcement grouting, as well as excavation protection methods involving precise unloading control and timely restoration of confining pressure. As shown in Fig. 5, consolidation grouting is performed before the excavation of the protective layer rock mass to enhance its resistance to deformation. Based on the unloading characteristics of the easily relaxed rock mass under different excavation procedures, precise control of the unloading process is implemented. Rational support is applied to timely restore confining pressure before the rock mass relaxes. Shallow pipe grouting is conducted after the concrete is poured.

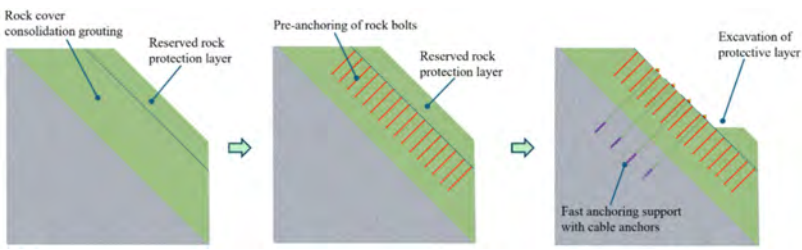

Fig. 5
Anti-relaxation technology system for the columnar jointed basalt

The excavation protection technology for easily relaxed rock masses significantly reduces the depth of relaxation in large areas of foundation excavation. The typical thickness of relaxation during excavation is generally between 1.2 and 1.4 m, achieving excellent protective results. The effectiveness of relaxation control is comparable to that of block basalt, which has a relaxation thickness of 1.3 to 1.5 m. The wave velocity of the relaxed layer of columnar jointed basalt is between 3500 and 4000 m/s, representing a reduction of approximately 24% to 30% compared to non-relaxed rock masses. The original columnar jointed structure is maintained, and no disintegration has occurred, ensuring that the excavated rock mass meets the foundation requirements for the high arch dam.

3.2. Stability of the dam abutment

In the site area of the Baihetan Dam, low-angle interlayer shear zones and steep faults are developed. The stability of the dam abutment sliding blocks formed by the combination of weak structural surfaces, along with the overall safety of the arch dam and its foundation, are crucial factors for evaluating the safe operation of the dam [8].

The sliding blocks that may occur on the dam shoulder can be categorized into several types: single-sided large blocks with fissures, double-sided large blocks with fissures, large blocks with multiple sliding surfaces, and local blocks. An analysis was conducted using the rigid body limit equilibrium method on the block composed of the left bank fault F17 and the internal slip zone LS331 [Fig. 6(a)]. The results indicate that this block does not meet the limit state of shear bearing capacity in its natural condition. At the normal reservoir water level, the safety factor for shear resistance ranges from 2.30 to 3.24, which does not satisfy the requirement for a sliding stability factor greater than 3.50. The overload model tests indicated that, with the increase in load, cracks appeared near the elevation of 700 m at the left abutment of F17. Ultimately, these cracks propagated along the structural surface down to the elevation of 680 m. Additionally, rock mass damage was observed in the vicinity of the F17 fault [Fig. 6(b)]. When the load exceeds a certain threshold, cracks may develop in the upper and middle sections of the dam abutments due to the exposure of structural surfaces such as interlayer shear zones C3-1, C3, and fault F14. This indicates that these weak structural planes are unfavorable locations for stress distribution in the dam abutments.

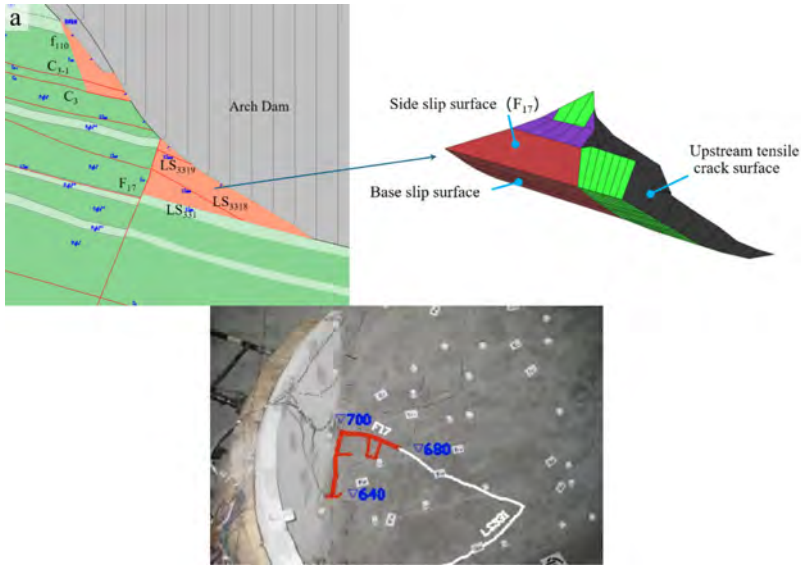

Fig. 6
Stability of the Structural Surface of the Left Abutment. (a) schematic diagram of the block on the Left abutment, (b) failure mode of the block on the Left abutment

To address the issue of low anti-sliding capacity of the left bank block, as shown in Fig. 7, two replacement wells were installed at fault F17, and replacement tunnels were constructed at the interlayer shear zones LS3318, LS3319, and LS331. Additionally, a drainage tunnel was established at interlayer shear zone LS331 for improved management. After reinforcement, the shear strength safety factor of the left bank partial block under normal water level conditions increased to 3.50–3.67, and under accidental conditions, it increased to 3.38–3.60, meeting the requirements of current standards. A comprehensive treatment was conducted for the weak structural planes in the upper middle section of the dam shoulder and the surrounding rock mass deformation trends. Concrete replacement tunnels were arranged in the interlayer shear zones C3-1 and C3 on the left bank, which are influenced by the arch dam's stress. Additionally, cutoff measures were implemented for the primary weak structural planes of the dam foundation. To strengthen the exposure and impact of unfavorable structural planes on both banks, pre-stressed anchoring treatments were applied to the slopes. These measures have proven effective in improving the overall stability of the dam abutment.

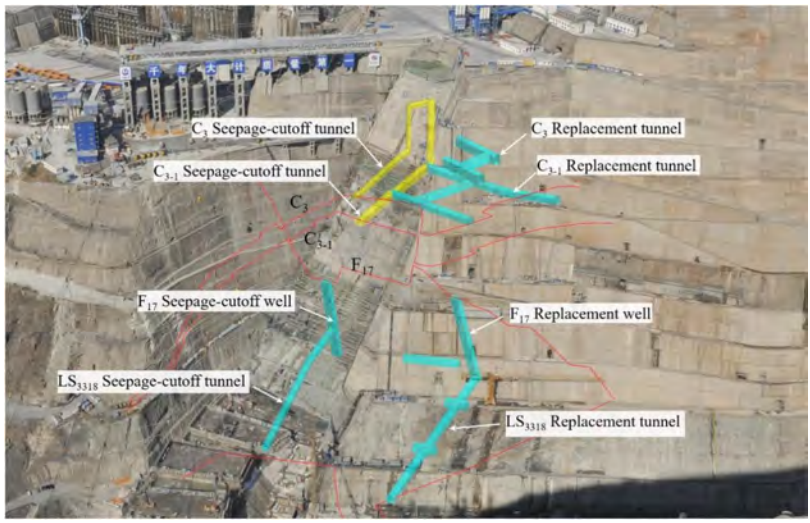

Fig. 7
Schematic diagram of reinforcement measures for the structural planes of the left bank abutment

3.3. Temperature control and crack prevention of low heat cement concrete

The Baihetan arch dam has a total concrete volume of 8.03 million m^3 and a maximum casting surface area of 2,200 m^2. The dam is located in the dry hot valley region of the Jinsha River, where sudden temperature drops frequently occur during the cold season. Additionally, strong winds of level 7 or above can last for up to 240 days each year. These factors collectively increase the risk of cracking in the dam's concrete.

According to existing dam construction experience, using moderate heat cement concrete as the material for ultra-high arch dams can reduce the risk of cracking [9,10]. However, due to the specific climate and engineering background at Baihetan, the crack resistance safety factor of the arch dam is set at 1.8, which is still insufficient in some areas. The use of low heat cement can help improve the crack resistance safety factor to 2.0, thereby providing strong support for the stability and durability of the project.

The primary advantage of low heat cement is that it generates less heat during the hydration process, which helps to reduce the increase in internal temperature of

the concrete, thereby lowering the risk of cracking due to temperature differentials. However, on the other hand, the slower hydration reaction of low heat cement results in lower early strength, which is detrimental to rapid construction and early load-bearing capacity of the dam. As shown in Fig. 8, the early strength of low heat cement concrete is lower than that of moderate heat cement concrete. However, after 90 days, the strength of low heat cement concrete exceeds that of moderate heat cement concrete.

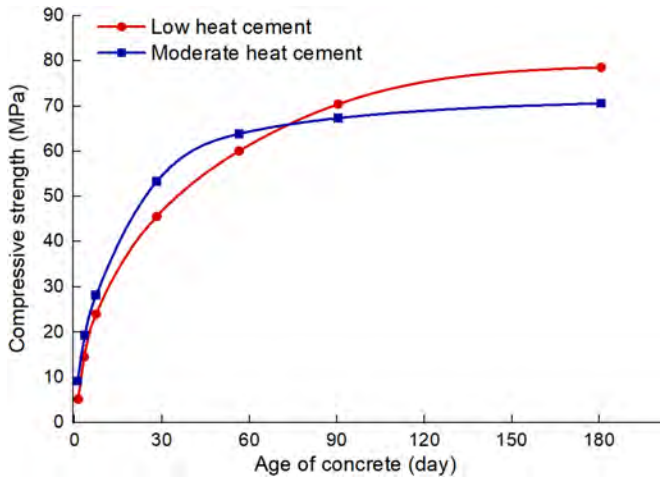

Fig. 8
Variation of compressive strength of low-heat and medium-heat cement concrete with age

Finding the optimal balance between sufficient strength and lower temperature rise is an important research direction in the field of materials science and engineering. To address this issue, one approach is to improve the quality of low heat cement concrete by optimizing the mix design and selecting appropriate supplementary materials. On the other hand, it is essential to develop temperature control methods that are suitable for the strength development process of low heat cement concrete. In temperature control for arch dam projects, traditional cooling has been divided into two phases. Standards require the incorporation of a mid-term cooling phase before winter to avoid temperature rebound after initial cooling, which can lead to excessive internal and external temperature differentials and result in cracking. Subsequently, the traditional two-phase cooling model gradually evolved into a three-phase, nine-stage cooling approach. It is particularly emphasized that in ultra-high arch dams, the mid-term cooling phase should be added for effective

control of temperature differentials during the concrete cooling process from both temporal and spatial perspectives. This facilitates the full play of creep and reduces thermal stress. This cooling model has been widely recognized in the engineering community as a successful experience for the water-cooling temperature reduction of high arch dam concrete.

The Baihetan Project adopted the optimized temperature control curve of the three phases and nine stages, with the full-cycle cooling model for low heat cement concrete shown in Fig. 9. The main concept is to set a lower limit for the maximum temperature of the concrete, which avoids excessive restrictions during the early temperature rise phase of low heat cement concrete. This is beneficial for the early hydration reaction of low heat cement and can accelerate the development of early strength in the concrete, partially compensating for the deficiency of low early strength in low heat cement concrete. On the other hand, minimizing the temperature gradient during the cooling process significantly reduces tensile stress in the concrete, thereby increasing the overall crack resistance and safety of the concrete.

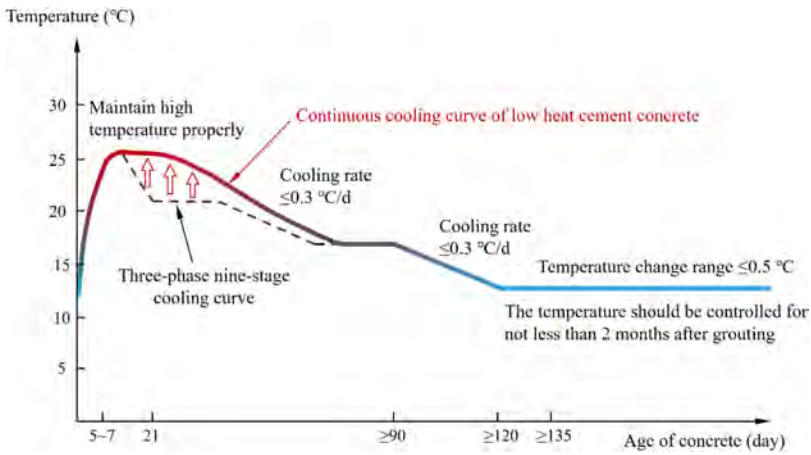

Fig. 9
Full-cycle continuous cooling model for low-heat cement concrete

3.4. The seismic safety of ultra-high arch dams in strong earthquake zones

The Baihetan Hydropower Station is located near the eastern edge of the Sichuan-Yunnan rhombic block, an area characterized by relatively high regional seismic activity. The basic seismic intensity of the project site is rated at level VIII,

and the peak ground acceleration for a 100-year return period with a 2% exceedance probability is 451 gal. The high seismic motion parameters impose stringent demands on the seismic resistance of the arch dam.

The dynamic response of the Baihetan Dam is investigated using a three-dimensional nonlinear finite element method. The effects of arch dam transverse joint opening and the radiation damping effect of an infinite foundation are considered. Additionally, artificial seismic waves generated based on a specified seismic spectrum are applied. The results indicate that the natural vibration frequency of the dam under normal reservoir conditions is 1.10 Hz, and the mode shape reflects the characteristics of an asymmetric arch dam. Under the design earthquake, the maximum opening of the transverse joint is approximately 40 mm. Considering the damage to the concrete material of the dam and the elastoplasticity of the foundation rock, slight damage is observed on the downstream face near the left abutment, while the upstream face remains intact. The crack range in the heel area is about 10% of the dam's base thickness and does not reach the dam curtain. The distribution pattern under the checked earthquake remains unchanged, with the dynamic response increasing by approximately 10-20%. The ultimate bearing capacity is not reached, and the dam-foundation system can maintain stability after the earthquake. The seismic overload capacity of the arch dam is predominantly controlled by the stability of the slide blocks on both sides, allowing it to withstand an overload factor of approximately 1.7 relative to the design seismic motion.

The spillway centerline of the Baihetan arch dam deviates both horizontally and angularly from its geometric centerline, significantly increasing the cantilever length of the pier structure at the dam's opening. This further complicates the seismic resistance of the cantilever structure of the dam under dynamic amplification effects. To address these issues, the Baihetan project employs a reinforcement design method that includes static design, dynamic adjustment, and nonlinear verification (Fig. 10), thereby enhancing the reinforcement system of the dam's opening structure and ensuring the safety of the engineering structure.

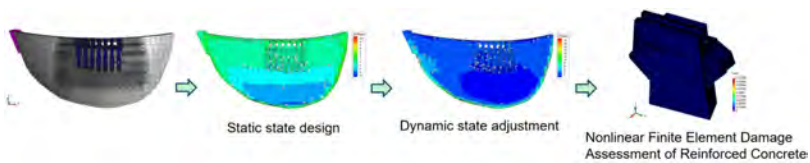

Fig. 10
Reinforcement design of cantilevered pier.

Considering the significant seismic loads and strong seismic response of the dam, the comprehensive seismic measures implemented include the use of C18040 strength grade concrete, the arrangement of seismic reinforcement on both

the upstream and downstream faces, enhanced design of transverse joints and waterstops, strengthened anchorage of the buttresses, reinforced upper connections of the dam body, and smooth transitions in the structural form.

4. OPERATIONAL STATUS OF THE ARCH DAM AFTER WATER STORAGE

The Baihetan Project has experienced three flood seasons since the water storage phase, and no thermal cracks have been detected in the concrete of the dam. At the end of October 2022, a hydraulic model test was conducted at normal water storage levels, with a maximum discharge of 11,383 m^3/s from the dam body and 11,344 m^3/s from the spillway. The flow in the piezometric holes was stable, and the pressure distribution in the flow channel was reasonable. The maximum impact pressure measured at the bottom slab of the tailwater pool was 4.37×9.81 kPa, observed under the condition of solo discharge from the No. 1 surface orifice, which is less than 15×9.8 kPa. The operation of the flood discharge and energy dissipation structures is satisfactory.

Monitoring results indicate that the deformation of the arch dam is positively correlated with the operating water level. During the water storage phase, the maximum radial displacement increment was 64.42 mm. The temperature rise of the arch dam and the nonlinear time-dependent deformation exhibited a slow variation characteristic, which aligns with the change patterns observed after water storage. The wave velocity of the treated columnar joint basalt in the dam foundation remained stable. Deformations of the concrete after casting and during water storage were continuous, and the seepage flow in the dam foundation showed a gradually decreasing trend. Overall, all monitoring results of the dam demonstrated stability.

5. CONCLUDING REMARKS

The Baihetan Hydropower Station is the second largest hydropower project in the world, situated in a region with complex topographical and geological conditions. The construction of the project has undergone a challenging journey, progressing from technological exploration to breakthroughs. Through continuous engineering practice, it has accumulated rich experience and innovative achievements, successfully realizing the construction of a seamless dam and achieving remarkable results that ensure the stable and safe operation of the project. This has important guiding significance for the safe operation of existing ultra-high arch dams and for future similar projects.

The high arch dam project has played a crucial role in promoting the development and utilization of hydropower resources in western China. The 14th Five-Year Plan proposes that by 2030, the installed capacity of hydropower should reach 420 million kilowatts, while the total exploitable hydropower resources in China amount to 687 million kilowatts. As the focus of hydropower resource development shifts to high-altitude and cold regions, the construction of high concrete dams in China will continue to face numerous challenges and require intensive efforts in practice.

REFERENCES

[1] JIANG, Q., FENG X. T., HATZOR Y. H., HAO X. J., LI S. J. Mechanical anisotropy of columnar jointed basalts: An example from the Baihetan hydropower station, China. *Engineering Geology*, 2014. 175: p. 35–45.

[2] SONG, Z. H., LIU Y. R., YANG Q. Experimental and numerical investigation on the stability of a high arch dam with typical problems of nonsymmetry: Baihetan Dam, China. *Bulletin of Engineering Geology and the Environment*, 2016. 75(4): p. 1555–1570.

[3] XU N. W., WU J. Y., DAI F., FAN Y. L., LI T., LI B. Comprehensive evaluation of the stability of the left-bank slope at the Baihetan hydropower station in southwest China. *Bulletin of Engineering Geology and the Environment*, 2018. 77(4): p. 1567–1588.

[4] ALEMBAGHERI A., GHAEMIAN M. Damage assessment of a concrete arch dam through nonlinear incremental dynamic analysis. *Soil Dynamics and Earthquake Engineering*, 2013. 44: p. 127–137.

[5] CHEN, J., QIN L. J., XU Q., LI J. Seismic Damage Indexes of a High Arch Dam Based on the Monolith. *KSCE Journal of Civil Engineering*, 2020. 24(7): p. 2063–2077.

[6] FAN, Q. X., WANG Z. L., XU J. R., ZHOU M. X., JIANG Q., LI G. Study on Deformation and Control Measures of Columnar Jointed Basalt for Baihetan Super-High Arch Dam Foundation. *Rock Mechanics and Rock Engineering*, 2018. 51(8): p. 2569–2595.

[7] SHI, A. C., WEI Y. F., ZHANG Y. H., TANG M. F. Study on the Strength Characteristics of Columnar Jointed Basalt with a True Triaxial Apparatus at the Baihetan Hydropower Station. *Rock Mechanics and Rock Engineering*, 2020. 53(11): p. 4947–4965.

[8] CHEN, Y., ZHANG L., YANG B. Q., DONG J. H., CHEN J. Y. Geomechanical model test on dam stability and application to Jinping High arch dam. *International Journal of Rock Mechanics and Mining Sciences*, 2015. 76: p. 1–9.

[9] XIN, J.D., ZHANG G. X., LIU Y., WANG Z. H., WU Z. Effect of temperature history and restraint degree on cracking behavior of early-age concrete. *Construction and Building Materials*, 2018. 192: p. 381–390.

[10] ZHANG, G.X., LUO X. Y., LIU Y., ZHU Z. Y. Influence of Aggregates on Shrinkage-Induced Damage in Concrete. *Journal of Materials in Civil Engineering*, 2018. 30(11).

COMMISSION INTERNATIONALE DES
GRANDS BARRAGES

VINGT-HUITIEME CONGRES DES
GRANDS BARRAGES
CHENGDU, MAI 2025

EXPLORATION OF PRE-EARTHQUAKE EARLY WARNING AND POST-EARTHQUAKE MONITORING MODE OF RESERVOIR DAM BASED ON INTELLIGENT SAFETY MONITORING MANAGEMENT PLATFORM (*)

MA LONG, Jian CHEN, Jun ZHOU & Bo JIANG
Baihetan Power Plant, Ningnan

CHINA

SUMMARY

In recent years, the frequent occurrence of extreme weather has led to the frequent occurrence of various geological disasters, and it is urgent to carry out effective pre-earthquake early warning and post-earthquake emergency monitoring and disposal of reservoir dams. Then the pre-earthquake early warning and post-earthquake monitoring of reservoir dams based on the intelligent management platform for safety monitoring may become a way to solve this problem. The digital twin model and knowledge platform functions on the platform are used to carry out earthquake early warning timely, predict the possible danger parts of the reservoir and dam after the earthquake, and make sufficient plans and drill preparations in advance. After an earthquake occurs, the accurate information of the site can be fed back in time through automatic monitoring and inspection of key parts, and the post-earthquake disposal plan provided by the knowledge platform function can be used to speed up the response speed of post-earthquake emergency work and provide reliable data support for safe and effective post-earthquake rescue and disaster relief.

Exploration du mode d'alerte précoce avant un séisme et de surveillance après un tremblement de terre d'un barrage-réservoir sur la base d'une plate-forme intelligente de gestion de la surveillance de la sécurité

DOI: 10.1201/9781003642428-142

RÉSUMÉ

Au cours des dernières années, des conditions météorologiques extrêmes ont été fréquentes, entraînant diverses catastrophes géologiques, et il est imminent de savoir comment procéder efficacement à l'alerte pré-barrage et à la surveillance et à l'élimination des urgences post-sismiques, tandis que l'approche de l'alerte précoce et de la surveillance post-séisme des barrages de réservoir basée sur une plate - forme de gestion intelligente de la surveillance de la sécurité peut être une solution au problème. Utilisez les fonctionnalités du jumeau numérique sur la plate-forme et de la plate-forme de connaissances pour effectuer des alertes sismiques en temps opportun, prévoir les zones potentiellement dangereuses après les barrages sismiques et planifier et faire des exercices adéquats à l'avance. Après un tremblement de terre, grâce à la surveillance et à l'inspection automatisées des sites clés et à la rétroaction rapide d'informations précises sur le site, les options d'élimination post-sismique fournies par la fonction de plate-forme de connaissances peuvent accélérer la réponse aux efforts d'urgence post-sismique, fournissant un support de données solide pour un sauvetage post-sismique sûr et efficace.

1. SITUATION AND PROBLEMS

With the rapid development of new monitoring technology, China's monitoring system platform has transformed from the automated monitoring stage, which utilizes advanced sensors, collection devices, and data analysis technologies to the digital stage which is based on modern information technology to convert information into digital formats[1], monitoring instruments and equipment are also gradually diversified and specialized, and many important monitoring points can be effectively monitored, so that problems can be found and solved timely, but for the reservoir dam the pre-earthquake early-warning and post-earthquake monitoring still exist many problems[2].

1. The pre-earthquake early-warning mechanism is not perfect. For example, there is a lack of targeted earthquake emergency plans and drills for on-site staff, and earthquake warning information cannot be pushed to all on-site personnel in time due to various reasons.
2. Post-earthquake emergency response is not professional, and the best opportunities to solve is often missed due to insufficient preparation of emergency plans and measures or incorrect on-site emergency command and disposal, resulting in further expansion of the disaster and losses[3].

3. The update and iteration of the monitoring system is relatively lagging behind, and the degree of integration and application with the AI model is low, which cannot give full play to its advantages in quickly generating post-earthquake reports, providing post-earthquake emergency response solutions through interactive dialogue and multi-modal learning and training capabilities, and there is still a big gap between the realization of intelligence and intelligence of the monitoring system.

Based on the above problems, a solution for pre-earthquake early warning and post-earthquake monitoring of reservoir dams based on the safety monitoring intelligent management platform is proposed, and the full integration and application of digital twins, AI models, knowledge platforms and other functions with the earthquake monitoring are promoted by building a safety monitoring intelligent management platform, so as to help realize timely pre-earthquake early warning and post-earthquake effective disposal.

2. CONSTRUCTION SCHEME OF THE PLATFORM

2.1. General thinking

The intelligent management platform for safety monitoring adopts a modular design, which mainly integrates three modular applications, such as security monitoring, intelligent service and business management. Each modular application is relatively independent but interrelated. The application of the safety monitoring module mainly takes the monitoring instrument as the management object, and provides managers with functions such as automatic collection of monitoring data, systematic management of measurement points, real-time monitoring and alarm of measurement points and data, robot and video patrol inspection, and so on[4]. The intelligent service module applies the monitoring data collected by the security monitoring module as the management object, and provides managers with functions such as digital twin model simulation, deep learning of large language model, and solutions for water conservancy knowledge platform. On the basis of the intelligent service module, the application of the business collaboration module takes all the monitoring data as the management object, and provides managers with functions such as sorting out design results, settling construction contracts, and processing comprehensive transactions[5]. The main line of the three modular applications is layered and progressive to jointly promote the construction of the intelligent management platform for safety monitoring. Fig. 1 shows the construction framework.

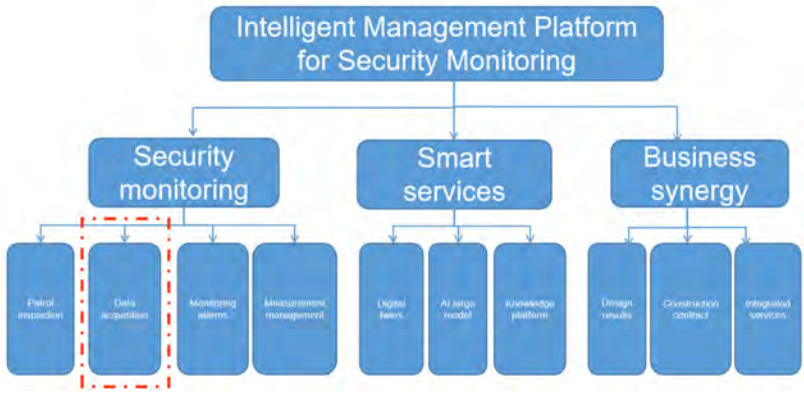

Fig. 1
Construction framework of the intelligent management platform for safety monitoring

2.2. Hierarchy of data acquisition functions

The data collection function shall include the following two parts: ① for the location that has the conditions and ability to adopt the automatic monitoring data collection method, an automatic measurement point or station should be built to speed up the collection of monitoring data and save a lot of manpower and material resources. ② For some relatively remote locations without construction conditions and capabilities, manual collection method can be used to achieve full coverage of monitoring surface without omission. The hierarchical structure of data collection function is shown in Fig. 2 below. The main hierarchical structure can be divided into the following two layers: automatic collection and manual collection, in which automatic collection can be divided into three parts: internal monitoring, external monitoring and strong earthquake monitoring, and strong earthquake monitoring includes pre-earthquake warning and post-earthquake monitoring.

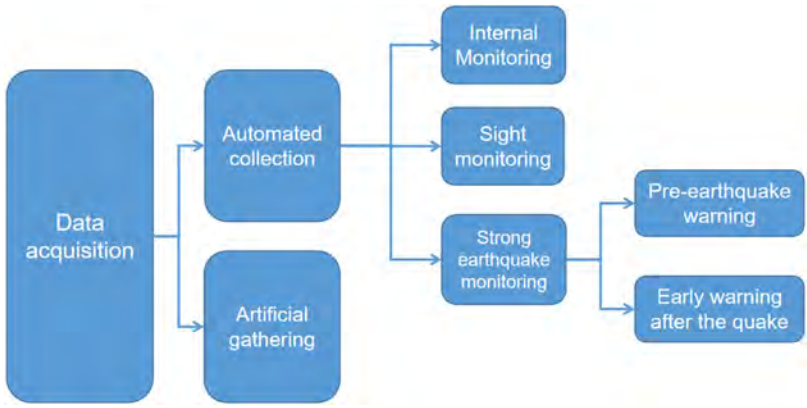

Fig. 2
The hierarchy diagram of the data acquisition application

3. PRE-EARTHQUAKE WARNING AND POST-EARTHQUAKE MONITORING

3.1. Pre-earthquake warning

The main workflow of pre-earthquake warning should be: digital simulation→pushing earthquake early warning information→case analysis and learning.

According to the relevant national regulations, project does not have the qualification to forecast the earthquake, so the earthquake early warning information is mainly based on the information released by official platforms such as the China Earthquake Network. However, on the one hand, the digital twin model in the application of intelligent services can be used to deduce future development trends, such as the creep of bank slope landslides, crustal deformation and fault activity that may cause earthquakes, so as to make theoretical trend analysis and prediction judgments on induced earthquakes in reservoir areas, and the results can provide a theoretical reference for earthquake prediction by China Earthquake Administration. On the other hand, the official earthquake information released by the China Earthquake Network is used to compare and analyze the theoretical value and the actual value, and the digital twin model is constantly optimized and improved, so as to complete the accurate and timely push of the early warning information.

The relevant earthquake early warning information is pushed in various ways, such as: ① automatically forward the earthquake early warning text messages to authorized users through the intelligent safety monitoring management platform and other official platforms such as the China Earthquake Network. ② Download the

“National Emergency Broadcasting” APP developed by the National Emergency Management Headquarters or the “Earthquake Early Warning” APP developed by the Chengdu High-tech Disaster Reduction Research Institute, and use the seismic wave propagation time difference when the earthquake occurs to give early warning, and the early warning information will provide the countdown and estimated intensity of the earthquake shear wave arrival.③ Use the earthquake early warning function of the mobile phone or pay attention to the “China Earthquake Network” applet to push early warning information, and the information sources of this push method are from the China Earthquake Early Warning Network and Chengdu High-tech Disaster Reduction Institute. The first method can provide corresponding emergency plan processing for authorized users, and the latter two methods can realize the push reminder and mandatory alarm of early warning information by customizing the estimated intensity.

Combining the digital twin model with the knowledge platform in the application of intelligent services, the abnormal behavior of the dam that may occur after a strong earthquake can be intelligently predicted through the learning of relevant accidents and cases, and the preliminary plan can be given by using the knowledge platform. Then the specific processes and steps of the implementation are continuously optimized and improved after the preliminary plan drill, and the final plan is uploaded to the knowledge platform for the platform to learn and accumulate, so as to realize the closed-loop management of problem discovery, reporting, solution and learning.

3.2. Post-earthquake monitoring

The main workflow of post-earthquake monitoring should be: the earthquake level exceeds the threshold→the monitoring system is triggered→ automatic monitoring→manual inspection→emergency response→report generation. When an earthquake occurs and reaches the seismic signal trigger conditions, the safety monitoring application should be launched in combination with the real-time information released by the China Earthquake Network, which will simultaneously carry out automatic data collection of internal and external monitoring instruments and on-site inspection of information notification personnel[6]. After receiving the alarm message, on-site inspectors and relevant management personnel should go to the inspection according to the actual situation of the site, and upload the inspection results to the platform in time. Then the intelligent service application will process the collected internal and external monitoring data and manual inspection reports, and complete the preliminary analysis to judge whether there is a danger or disaster, and provide a reference emergency plan or disposal plan. Relevant management personnel should review the post-earthquake dam inspection report generated by the AI model function timely according to the corresponding time limit and report it on time.

3.2.1. *The seismic response*

The instruments that can timely and effectively monitor and reflect the seismic acceleration mainly include: strong seismic meters, seismographs, force-balanced accelerometers, ultra-low frequency vibrometers and so on[7]. In order to monitor the magnitude and intensity of different parts of the dam, seismographs and strong seismic meters should be set at different elevation measuring points, and also shall be arranged in the far area at a certain distance from the dam site to observe the seismic reflection of the free field in the dam site area. At the same time, in order to monitor the free field vibration of the dam site, a force balance acceleration sensor should be set inside the dam body. A three-component ultra-low frequency vibrometer can be installed inside the dam body to monitor the dynamic characteristics of the main structure of the reservoir dam and its seismic response.

For the seismic monitoring instruments installed in different parts, there may be different interference factors on the site, which will affect the normal trigger of the seismic monitoring instruments, so these interference factors should be eliminated as much as possible to achieve the accurate triggering of the instrument. The main disturbance factors on the site are including: the vibration caused by the passage of vehicles at the dam crest, the vibration caused by the power generated by the unit, non-professional accidental collision, the influence of mountain rock falling interference, and so on. The main ways to eliminate interference are: ① installs video surveillance around the monitoring instrument and set a reasonable trigger threshold, ② prevails the real-time message released by China Earthquake Network, ③uses the knowledge platform of intelligent service application to analyze and evaluate the trigger records to determine whether a non-inductive earthquake occurs.

3.2.2. *Automated monitoring*

When the seismic monitoring instrument successfully triggers the seismic signal and starts the safety monitoring application, the internal and external monitoring function will automatically collect the post-earthquake monitoring data according to the content required in Table 1 below, and automatically upload the collected data to the intelligent service application for original data analysis and process line drawing. The original data analysis should compare the value of the latest monitoring results before the earthquake event with the value of the encrypted monitoring results after the earthquake event, and analyze whether it exceeds the corresponding design warning value, monitoring value or experience value[8]. The process line drawing is to show the development trend of the monitoring data more intuitively and facilitate decision-making personnel to understand and judge.

Table 1
Automated monitoring sites and contents

MONITORING SITE	MEASURING TIME	MONITORING METHOD	MONITORING INSTRUMENT
Internal monitoring	Within 5 minutes	Monitoring of settlement, displacement and deformation	Multi-point shift meter bedrock shift meter inverted vertical system
		Crack monitoring	Surface gauge transverse seam gauge
		Sewing monitoring	Sewing gauge
		Permetry monitoring	Measure water weir drainage hole pressure measuring pipe
		Stress and strain monitoring	Compressive stress gauge strain gauge
		temperature monitoring	thermometer
External monitoring	Within an hour	Transforming monitoring network	GNSS observation station

3.2.3. *Inspection and inspection*

After the earthquake, the platform will send alarm messages to the on-site inspectors and relevant management personnel to ensure that the earthquake information and processing methods are accurately and quickly conveyed to the relevant personnel as far as possible. Relevant personnel should rush to the scene as soon as possible after receiving the alarm message, carry out inspection and record of key parts on the premise of ensuring their own safety, and upload the manual inspection results to the platform in time for generating post-earthquake reports[9]. The key parts and contents of the dam inspection after the earthquake are shown in Table 2 below.

Table 2
Inspection parts and contents of key parts of the dam after the earthquake

CHECKPOINT	SCOPE OF EXAMINATION	DESCRIPTION OF THE DEFECTS OR ANOMALIES
Concrete dam	The crest wave wall of the dam collapsed, staggered and cracked	
	Dam shoulder, arch seat and dam body dislocation, damage and cracks	
Sluice structure	Uneven deformation, cracks, concrete damage and water seepage of the water retaining structure of the working gate room and control section	
Water transmission and power generation buildings	Foundation deformation of open channel and open compress pressure pipes and their supporting structures	

(Continued)

Table 2
Continued

CHECKPOINT	SCOPE OF EXAMINATION	DESCRIPTION OF THE DEFECTS OR ANOMALIES
	Deformation, damage, crack and leakage of exposed concrete structure of inlet tower (rack), trench bridge and open channel	
	Deformation and leakage of open compress pressure pipe (expansion section)	
	Deformation, cracks and damage of the plant support structure, etc	
	Damage of the supporting structure of the underground workshop	
Metal construction	Deformation and crack of working gate structure in water retaining state and the connection of supporting structure with door blade and foundation embedded parts of working gate	
	The connection between the frame and the frame and between the frame and the foundation; the deformation of the door (bridge) frame, the connecting bolts of the door (bridge) frame, and the relative position between the wheels and the track	
	The connection between the oil cylinder and the supporting structure and between the supporting structure and the foundation embedded parts	
Reservoir and basin	Basin cracks, collapse situation	
	The reservoir has an abnormal vortex situation	
	The structure of the bottom corridor of the reservoir is damaged, and the leakage amount is increased	
Slope of hub area and near dam bank	The stability, damage and anomaly of the slope near the dam	
Block the head and other	Deformation, water seepage and crack of the concrete structure of the plug head	
Monitoring facilities	Damage of exposed monitoring facilities such as vertical line, tension line, surface deformation observation pier and pressure measuring pipe	
Other related parts	Other anomalies	

3.2.4. *Emergency response*

After an earthquake accident or disaster occurs, on-site emergency treatment shall be carried out in accordance with the preplan formulated in advance, which can deal with most of the dangers or accidents, and for occasional and sudden secondary accidents, the following two treatment methods can be adopted: ①use the experience of technicians or relevant operating procedures, to carry out the pre-treatment of

the accident, and prepare the on-site special plan for organization and implementation after discussion, ② after the pre-treatment of the accident, using the reference solution provided by the AI model and knowledge platform function in intelligent service applications to deal with the on-site complex problem, then uploading the specific process and plan to the knowledge platform for learning and training after discussion, modification and processing, so as to continuously improve its accuracy and relevance of answering and dealing with complex water conservancy problems.

3.2.5. *Generate the post-earthquake report*

The AI model function combines the results of manual inspection and automatic monitoring to verify each other. At the same time, intelligently generates a report on the post-earthquake dam inspection according to certain rules and templates, and reports it for review according to the process. The post-earthquake dam inspection report generated by this function can be divided into quick report, express report, detailed report, continuation report and final report according to the report content and report time. The specific requirements are shown in Table 3 below. This function can also customize report generation rules based on parameters such as earthquake magnitude, seismic intensity, hypocenter depth, and epicenter distance, for example, after a inductive earthquake of M4.0 or higher and the epicenter is within 100 kilometers of the dam site, or an earthquake outside the dam site area is obviously felt and may affect the dam, the large model will generate a quick report, an express report, and a detailed report, and only a flash report will be generated in the event of an earthquake below M4.0.

Table 3
Type and content of earthquake reports

REPORT TALE	REPORTING TIME LIMIT	REPORT CONTENT
quick report	After an earthquake occurs or after the system triggers the earthquake signal	Time, location, type, name, and circumstances where the dam may be affected
express report	Within an hour after the earthquake	Quick report content, monitoring and inspection of affected parts, impact on production and emergency response
Detailed report	The total reporting time limit shall not exceed 12h	The contents of the report, the monitoring situation of the reservoir seismic network and the dam strong seismic instrument, the inspection of key parts of the dam, the key monitoring points of the dam with automatic monitoring, and the progress of the emergency response and the development trend of earthquake events
continuation report	If any new situation occurs after the detailed report, the first continuation report shall be reported within 72h	The weekly progress of earthquake emergency response after detailed report and the monitoring and inspection of the affected parts
final report	If a new situation occurs after the detailed report, within one week after the earthquake emergency response is completed	The summary and evaluation of the emergency disposal process after the end of the emergency disposal, and the impact of earthquake events on the dam safety is mainly analyzed and judged

4. CONCLUSION

By making full use of the modular application on the platform, the pre-earthquake early warning and post-earthquake monitoring based on the safety monitoring intelligent management platform can timely warn the occurrence of earthquakes, predict the possible dangerous parts of reservoir dams after the earthquake, and make sufficient plans and drill preparations in advance to improve the ability to deal with earthquake risks. After the earthquake occurs, the accurate information of the site after the disaster is fed back in time through automatic monitoring and patrol inspection, and the emergency plan and post-earthquake disposal plan provided by the knowledge platform function can be used to speed up the response speed of the post-earthquake emergency work, and can provide reliable data support for safe and effective post-earthquake rescue and disaster relief.

In the future work, it is still necessary to accelerate the integration of artificial intelligence and various modular applications in the platform, such as promoting the collaboration between generative artificial intelligence and digital twin model function to improve the accuracy and practicability of model and enhance model prediction accuracy[10]. accelerating the integration of large language model and knowledge platform function, so that they can greatly improve accuracy and relevance when answering complex water conservancy problems, and provide corresponding case support and complete solutions.

REFERENCES

[1] HUANG Y.W., NIU G.LI., LI D.Y., *ET AL.* Research and application of intelligent perception and management technology for dam safety monitoring. *Journal of Yangtze River Academy of Sciences*, 2021, 38 (10): 30–32.

[2] SU K.Z., ZHANG L.F., *ET AL.* Monitoring of strong earthquake safety in dams. *China Water Resources and Hydropower Press*, 1996.

[3] WANG H., ZHANG X.H. Situation of earthquake damaged reservoirs and post disaster recovery and reconstruction strategies.*Water Resources and Hydropower Technology*, 2009 (1).

[4] HUANG Y., REN X.J., LI A.Q., *ET AL.* Overall framework and application benefits of digital twin Three Gorges construction. *China Water Resources*, 2023 (19): 17–22+9.

[5] LU J.H., LIU X.L., ZHANG Y.B., XU K. Research and application of cloud service platform for reservoir dam safety management based on digital twin. *Water Resources and Hydropower Express*, 2022, 43 (01): 81–86.

[6] MA Y.X.,YU Z.Q. Feasibility study on the application of internet monitoring platform in post earthquake emergency monitoring. *Water Resources and Hydropower Engineering*,2022,53(S1): 186- 190.

[7] GUO Y.G. Strong earthquake monitoring and instruments for water conservancy and hydropower engineering. *Advances in Geophysics*, 2005, Volume 20, Issue 2.

[8] CHEN H.Q., SU K.Z., *ET AL.* Important Strong Earthquake Data and Analysis of Chinese Hydraulic Structures. *Earthquake Press*, 2000.

[9] WANG S.J., GU Y.C., NI X.R., LONG W.F. *ET AL.* Emergency inspection of reservoir dams after earthquakes. *China Water Resources*, 2012 (6): 35–37.

[10] SUN L., WANG R.G., YUAN R., *ET AL.* Application and Prospect of Artificial Intelligence Technology in intelligent Water Conservancy. *China Water Resources*, 2024 (3): 44–51.

COMMISSION INTERNATIONALE DES
GRANDS BARRAGES

VINGT-HUITIEME CONGRES DES
GRANDS BARRAGES
CHENGDU, MAI 2025

SEISMIC SAFETY ANALYSIS AND EVALUATION OF THE HIGH ARCH DAM OF YANGFANGGOU HYDROPOWER STATION IN YALONG RIVER, SICHUAN PROVINCE (*)

Jianjun XU
PowerChina Huadong Engineering Corporation Limited，Hangzhou, Zhejiang

Xinhua ZENG
Yalong River Hydropower Development Company, Ltd., Chengdu, Sichuan

Yihui HUANG & Haining WEI
PowerChina Huadong Engineering Corporation Limited，Hangzhou, Zhejiang

Deyu LI & Boyan ZHANG
China Institute of Water Resources and Hydropower Research, Beijing

CHINA

SUMMARY

The maximum height of Concrete Double-Curvature Arch Dam of Yangfanggou Hydropower Station is 155 meters, and its aseismatic fortification category is Class A. According to the provisions of the current Code for Seismic Design, the site-specific design response spectrum of dam site and the time history of artificial ground motion is studied. Subsequently, the shape of the arch dam is optimized and adjusted in the detailed design phase, and the three-dimensional non-linear finite element analysis considering opening and closing of the transverse joints under strong earthquake and the radiation damping effect of the infinite foundation is

Analyse et évaluation de la sûreté sismique du barrage-voûte de Yangfanggou sur la rovière Yalong, province de Sichuan

DOI: 10.1201/9781003642428-143

carried out. For potential sliding blocks of abutments of arch dams, rigid body limit equilibrium method based on mode decomposition response spectrum analysis and time-domain rigid body limit equilibrium method based on time history analysis are used to check dynamic stability. Finally, the seismic safety of the Yangfanggou arch dam is comprehensively evaluated. It can be seen that the optimized shape of Yangfanggou arch dam is safe and reliable under the design basic earthquake.

RÉSUMÉ

La hauteur maximale du barrage en béton à double courbure de la centrale hydroélectrique de Yangfanggou est de 155 m, et sa catégorie de vérification parasismique est de classe A. Conformément aux dispositions du Code actuel de conception sismique, le spectre de réponse de conception spécifique au site du barrage et l'historique du mouvement du sol artificiel sont étudiés. Par la suite, la forme du barrage-voûte est optimisée et ajustée dans la phase de conception détaillée, et l'analyse tridimensionnelle non linéaire par éléments finis prenant en compte l'ouverture et la fermeture des joints transversaux sous un fort tremblement de terre et l'effet d'amortissement par rayonnement de la fondation infinie est effectuée. Pour les blocs de glissement potentiels des culées des barrages-voûtes, la méthode d'équilibre limite des corps rigides basée sur l'analyse du spectre de réponse par décomposition de mode et la méthode d'équilibre limite des corps rigides dans le domaine temporel basée sur l'analyse de l'évolution temporelle sont utilisées pour vérifier la stabilité dynamique. Enfin, la sécurité sismique du barrage-voûte de Yangfanggou est évaluée de manière exhaustive. On peut constater que la forme optimisée du barrage-voûte de Yangfanggou est sûre et fiable dans le cadre du tremblement de terre de base.

1. INTRODUCTION

Yangfanggou Hydropower Station is the first large hydropower project of million kilowatts constructed in EPC mode in China. The Project is located in the middle reaches of Yalong River in Muli County, Liangshan Yi Autonomous Prefecture, Sichuan Province. The development task of the Project is to generate electricity. Yangfanggou Hydropower Station is a first-class large (1) project according to Chinese standard with total storage capacity of 512.5 million m^3 and total installed capacity of 1500MW. The project layout is composed of water retaining structures, flood release and energy dissipation structures, diversion and power generation systems, etc. The main hydraulic structures are Grade 1 structures. The project officially commenced on July 13, 2015, and all four units were put into operation in October 2021.

The water retaining structure adopts parabolic double-curvature thickened concrete arch dam. The maximum dam height is 155m, with riverbed foundation at

EL.1947m and dam crest at EL.2102m. The crown cantilever is 9m thick at top and 32m thick at bottom. The ratio of thickness to height is 0.206. The arc length of dam crest centerline is 362.17m. The ratio of arc length of height is 2.34. In detailed design phase, optimization and adjustment have been made in foundation interface, central angle of the arch and arc abutment. After optimization, the maximum arc abutment is 34.90m thick, the maximum central angle is 86.84°, the concrete quantity of basic dam shape is 758,100 m^3 and the slenderness coefficient is 13.2.

According to Code for seismic design of hydraulic structures of hydropower project [1] (NB 35047—2015) (hereinafter referred to as the "current Seismic Code"), the seismic analysis is carried out on the optimized arch dam shape in detailed design phase. By revealing the dam dynamic characteristics, seismic response and dynamic anti-sliding stability of dam abutment, the seismic safety of arch dam and dam abutment of the Project is comprehensively evaluated.

2. SITE-SPECIFIC RESPONSE SPECTRUM AND ARTIFICIAL SEISMIC WAVES OF SCENARIO EARTHQUAKE

In current Seismic Code, the design response spectrum is determined differently depending on the importance of project. For project with aseismatic fortification Class A that should be subject to special seismic safety evaluation, the site-specific response spectrum should be determined based on the scenario earthquake method as the design response spectrum according to the specific seismic and geological conditions of the site.

The aseismatic fortification class of this Project is Class A and its design ground motion parameters should be determined based on the results of special seismic safety evaluation. According to Seismic Safety Evaluation Report of Yangfanggou Hydropower Station site in Sichuan Province submitted by Institute of Earthquake Forecasting, CEA in March 2006 [2], the horizontal earthquake peak ground acceleration (PGA) of bedrock with a probability of exceedance 2% in 100 years is 0.309g, corresponding to the design basic earthquake (DBE) of the Project. According to Supplementary report on the design ground motion parameters of Yangfanggou Hydropower Station dam site[3] in April 2009, the horizontal PGA of bedrock with a probability of exceedance 1% in 100 years is 0.386g, corresponding to the maximum credible earthquake (MCE) of the Project. According to GB18306—2015 Seismic peak ground acceleration zonation map of China[4], the dam site of the Project belongs to Zone 0.15g, the characteristic period of the seismic response spectrum is 0.45s. According to the adjustment of characteristic period required in current Seismic Code, the characteristic period of standard response spectrum at Yangfanggou dam site is adjusted as 0.3s.

The design response spectrum of the Project should be determined by the scenario earthquake method, which lays a foundation for seismic design of the arch dam.

2.1. Determination of scenario earthquake and site-specific response spectrum

According to the contribution value of each potential seismic source area to the seismic risk of Yangfanggou dam site, the maximum contribution with a probability of exceedance both 2% and 1% in 100 years to the seismic risk of the dam site is from the potential seismic source area of No.10 Level 7.0 Qianbobei. Combining the principle of the maximum occurrence probability, the main steps to determine the scenario earthquake and the potential influence of No.10 Level 7.0 Qianbobei to the dam site, the earthquake magnitude and epicentral distance of the scenario earthquake at Yangfanggou dam site are obtained as shown in Table 1.

Table 1
Scenario earthquake of Project Yangfanggou Hydropower Station

PROBABILITY OF EXCEEDANCE	PGA		EARTHQUAKE MAGNITUDE M	EPICENTRAL DISTANCE/ KM	OCCURRENCE PROBABILITY/ \times $10-5$
	BEFORE CORRECTION	AFTER CORRECTION			
2% in 100 years	0.183*g*	0.309*g*	6.9	18.9	0.39035
1% in 100 years	0.202*g*	0.386*g*	7.0	15.4	0.30831

For safety consideration, the amplification coefficient spectrum β (T) based on hanging wall of reverse fault is taken as the site-specific response spectrum of Yangfanggou dam site determined by the scenario earthquake, as shown in Figure 1. By multiplying the spectral value β (T) by the seismic risk probability to calculate the PGA at corresponding probability levels after uncertainty calibration, the acceleration response spectrum of Yangfanggou Dam site is obtained, as shown in Figure. 2.

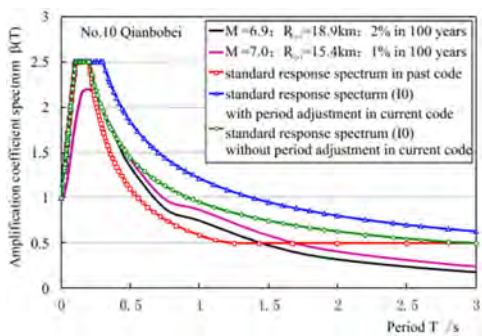

Fig. 1
Amplification coefficient spectrum of scenario earthquake at Yangfanggou Dam site

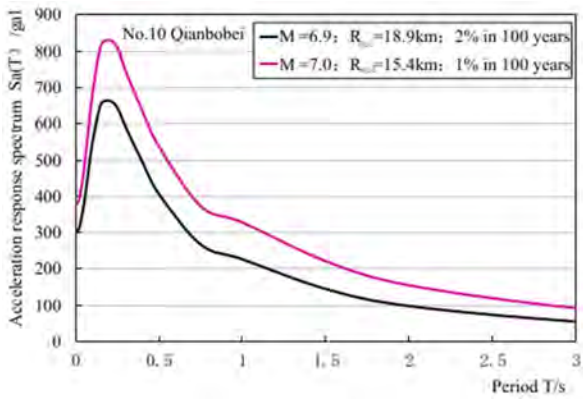

Fig. 2
Acceleration response spectrum of scenario earthquake at Yangfanggou Dam site

2.2. Artificial seismic waves based on site-specific response spectrum

According to the target spectrum from the determined site-specific response spectrum under DBE and MCE, 3 groups of ground motion time history with 3 components are generated corresponding to DBE and MCE respectively by using artificial ground motion technology based on current Seismic Code.

3. STATIC AND DYNAMIC ANALYSIS OF ARCH DAM

3.1. Overall dynamic analysis of arch dam based on trial-load method and linear elastic finite element method

Through the analysis of the arch dam with trial-load method (TLM) and linear elastic finite element method (FEM), it can be found that:

1. The natural frequencies of dam under two upstream water levels (fully supply level FSL and dead water level DWL) obtained by TLM and FEM are in good agreement with each other. The basic vibration mode of the dam is antisymmetric (transverse to the river), reflecting the general characteristics of high double-curvature arch dam.
2. Under static load combination of fully supply level (FSL), the maximum radial displacement of the dam is 4～5cm, which occurs at the middle and upper arch crown at EL. 2060～ 2080m. Under DBE, the maximum radial displacement is 7.81cm (TLM) and 7.21cm (FEM), respectively, which occurs at the arch crown of the dam crest.

3. The temperature drop condition under FSL with DBE standard response spectrum is studied. For TLM considering both static and dynamic effects, the principal tensile and compressive stress of upstream surface are 8.16 MPa and 11.97 MPa, respectively, while the ones of downstream surface are 5.56MPa and 8.96MPa, respectively. The maximum principal tensile stress and compressive stress occur near the upper arch crown. Compared with temperature drop condition, the principal tensile stress decreases and the principal compressive stress increases slightly under temperature rise condition. For FEM, the results show a roughly same stress distribution pattern as those in TLM. There are high tensile stress zones of more than 5MPa near the upstream arch crown of the dam crest and the left and right 1/4 downstream arch of the upper elevation. There are high compressive stress zones of more than 10MPa near the upstream arch crown of upper elevation. In addition, a small range of high tensile and compressive stress concentration zones occur at dam heel and toe.

3.2. Non-linear dynamic analysis considering the effect of foundation radiation damping and transverse joint opening

The conventional analysis shows that the dynamic amplification effect in the middle and upper part of the dam is obvious. By drawing on similar engineering experience, the infinite foundation radiation damping is simulated by viscoelastic boundary absorbing scattered waves, the non-linear opening of transverse joints is simulated by dynamic contact with Lagrange Discontinous Deformation Analysis (LDDA). Finally, the dam structure dynamic finite element simulation is carried out with model shown as in Figure 3. The layout and number of dam transverse joints are shown in Figure 4.

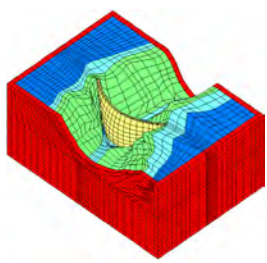

Fig. 3
Finite element model of dam-foundation system

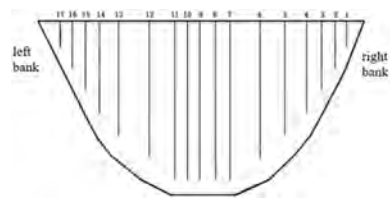

Fig. 4
Layout and number of dam transverse joints

Under static load combination, the principal tensile and compressive stress are not large, the maximum principal tensile stress is 1.18MPa, which only appears in the local area of the upstream arch abutment at the left bank at EL.1955m, the maximum principal compressive stress is 7.15MPa, which appears in the downstream arch crown at the right side at EL.1953m; the maximum displacement along the river is 4.86cm, which is close to the calculation result of TLM.

The DBE action with combination of radiation damping, transverse joints, various load conditions and seismic waves is studied. Considering both static and dynamic effects, the maximum principal tensile stress of upstream surface is 4.35MPa (relatively small compared with similar arch dam projects), which occurs at the left arch abutment at EL. 1955m. The range exceeding the 2.6MPa tensile stress control standard is the 10m thickness range near the dam heel below the dam foundation at EL.1980m, which is close to the curtain grouting line. However, due to the stress concentration effect of finite element at the dam- foundation interface, the stress value can not be used as a basis for seismic design. In view of the non-linearity of concrete materials, damage analysis and engineering experience of similar arch dams, the tensile stress value and distribution range can be reduced and not lead to adverse effect on the curtain grouting of dam foundation. The maximum principal compressive stress of downstream surface is 9.41MPa (less than the stress control standard), which occurs at the left arch abutment at EL. 2013m.

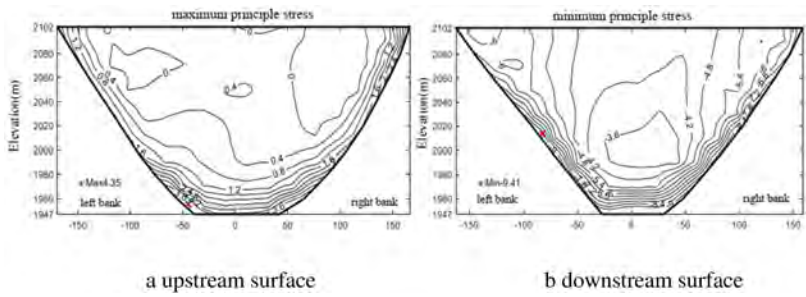

Fig. 5
principle stress isopleth under DBE (temperature drop in FSL)

The maximum opening of transverse joint under DBE is about 8.7mm, as shown in Figure 6. The opening range is above upstream surface at EL.2020m and downstream surface at EL.2060m. The degree of transverse joint opening under earthquake is at a medium level among similar arch dam projects. The opening and closing of transverse joint will not damage the waterstop facilities.

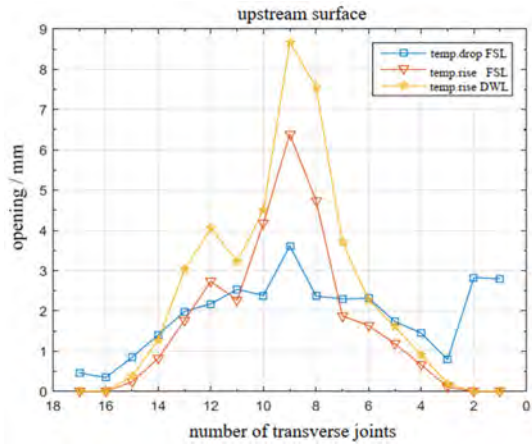

Fig. 6
Distribution of transverse joint opening along top arch under DBE

Under MCE action, the transverse joint opening and dam stress have all increased. The maximum transverse joint opening is 13mm, which will not destroy the waterstop facilities. The maximum principal tensile stress of dam body is 5.85MPa (slightly larger than the dynamic concrete tensile strength), which occurs at the upstream arch abutment of left side at EL.1955m. The maximum principal compressive stress is 10.36MPa (less than the dynamic concrete compressive strength), which occurs at the downstream arch abutment of left side at EL. 2013m.

4. DYNAMIC ANTI-SLIDING STABILITY ANALYSIS OF ABUTMENT

4.1. Rigid body limit equilibrium method based on mode decomposition response spectrum analysis

Using the three-dimensional rigid body limit equilibrium method based on mode decomposition response spectrum analysis, the anti-sliding stability analysis of the potential sliding blocks on the left and right arch dam abutment is carried out under FSL. It can be found that:

1. The safety factor of anti-sliding stability of the abutment under static condition is large, which is greater than the 3.5 specified in Design specification for

concrete arch dams [5] (SL 282-2018) (according to the shear friction formula of rigid body limit equilibrium).

2. Under DBE action with various combinations, the dynamic anti-sliding safety factors of sliding blocks at right bank are all greater than the 1.31 specified in the current Seismic Code. The dynamic anti-sliding safety factors of sliding blocks 1,3,6 at left bank are 1.14, 1.27, 1.20, which are less than the required 1.31. The safety factors of rest sliding blocks at left bank are all greater than 1.31. Compared with the standard design response spectrum from past seismic code, the site-specific response spectrum of scenario earthquake from current Seismic Code applied in detailed design phase shows a large increase in the range of the main vibration period, resulting in a significant increase in the dynamic thrust of the arch abutment and a decrease in the dynamic stability safety factor of each sliding block.

4.2. Time-domain rigid body limit equilibrium method based on time-history analysis

When using the thrust force by TLM based on mode decomposition response spectrum analysis to calculate abutment anti-sliding stability, the results show that the dynamic anti-sliding safety factors of partial blocks at left bank under DBE is relatively low. In this case, according to current Seismic Code 8.1.10, time-domain rigid body limit equilibrium method based on time-history analysis is further adopted to analyze block 1,3,6 at left bank. The anti-sliding stability of the potential sliding blocks of the abutment and its impact on the overall safety of the dam are comprehensively evaluated according to the duration and degree of the stability index exceeding the standard. In the time-history analysis method, the time-history of thrust at abutment is obtained by FEM time-history analysis. The inertial force time-history of rock mass is the product of three groups of artificial seismic acceleration waves and mass of sliding block.

The calculation results of the time-domain rigid body limit equilibrium method based on time-history analysis for block 1,3,6 at left bank are shown in Table 2. It can be seen that for these three blocks, the ratio of the total time when the safety factor less than 1.31 to the total duration of earthquake is very small, with a maximum duration no more than 0.7%. Moreover, the actual duration of each exceeding section is shorter. The residual deformation accumulated by such a short instantaneous sliding is not enough to cause the abutment instability. Comparing the results of similar arch dam projects in China with the same method, the ratio when the safety factor less than 1.31 of this Project is in the middle level.

Table 2
The minimum safety factor and ratio of unacceptable duration to total earthquake duration under DBE

SEISMIC WAVES	MINIMUM SAFETY FACTOR			TIME RATIO WHEN SAFETY FACTOR LESS THAN 1.31/%		
	BLOCK 1	BLOCK 3	BLOCK 6	BLOCK 1	BLOCK 3	BLOCK 6
Group 1	1.22	1.46	1.25	0.23	0.00	0.30
Group 2	1.12	1.25	1.11	0.66	0.10	0.57
Group 3	1.19	1.30	1.13	0.33	0.07	0.30

5. SEISMIC MONITORING

By May 20, 2024, the earthquake intensity around the dam has not reached the trigger value Degree III since the seismic monitoring system put into operation. According to the seismic waves recorded from surrounding seismic monitoring systems, the manual calculated earthquake intensity is between Degree I and II. The monitoring data of Yangfanggou Project during multiple earthquakes in surrounding areas show that: the displacement of dam, the opening of transverse joints and foundation joints, and the rebar stress meter of dam structure and anchor cable dynamometer, the amount of leakage, the displacement of dam abutment slope and the force of supporting structure all have very little changes. The monitoring data are normal.

6. CONCLUSION

As required in current Seismic Code, when applying site-specific response spectrum and artificial seismic waves based on scenario earthquake method and considering the effect of foundation radiation damping and transverse joint opening, the seismic dynamic response of Yangfanggou arch dam has a significant decrease. The large-scale high tensile stress zone near the middle and upper arch crown by conventional linear elastic analysis no longer exists, and the stress state of the arch dam under earthquake can meet the design requirements. The opening of transverse joints is not large and within the allowable range of waterstop deformation. The dynamic anti-sliding stability of abutment under DBE can meet the code requirements. Therefore, the seismic safety of Yangfanggou arch dam can be guaranteed under DBE.

REFERENCES

[1] NB 35047—2015, *Code for seismic design of hydraulic structures of hydropower project[S]* Beijing: National energy administration, 2015

[2] Institute of Earthquake Forecasting CEA . *Seismic Safety Evaluation Report of Yangfanggou Hydropower Station site in Sichuan Province[R]* Beijing: Institute of Earthquake Forecasting CEA, 2006

[3] *China earthquake disaster prevention center. Supplementary report on the design ground motion parameters of Yangfanggou Hydropower Station dam site[R]* Beijing: China earthquake disaster prevention center,2009

[4] GB18306—2015, *Seismic peak ground acceleration zonation map of China[S]* Beijing: Documentation Committee of seismic zonation of China

[5] SL 282—2018, *Design specification for concrete arch dams[S]* Beijing: Ministry of water resources of the People's Republic of China, 2018.

Q.111 - R.44

COMMISSION INTERNATIONALE DES
GRANDS BARRAGES

VINGT-HUITIEME CONGRES DES
GRANDS BARRAGES
CHENGDU, MAI 2025

CHILEAN PRACTICE ON LARGE TAILINGS DAMS CONSTRUCTED ON HIGH SEISMIC ENVIRONMENT (*)

José CAMPAÑA MSC
ARCADIS Chile, Senior Geotechnical Consultant, Santiago

Luis VALENZUELA MSC
Independent Tailings Dam Consultant, Santiago

Ramón VERDUGO PHD
CMGI, Partner and General Manager, Santiago

CHILE

SUMMARY

Due to the important annual production of Chilean copper, the mining operations must manage large volumes of tailings, which most of them are deposited in huge reservoirs confined by dams, either embankment dams or tailings sand dams. Experience in Chile until 1965 showed that the failure of tailings dams during earthquakes is a catastrophic event that has to be avoided by all means. Accordingly, to achieve both cost-efficient and safe tailings deposits, a high-end geotechnical engineering practice is required, including an appropriate seismic response when these tailings disposals are subjected to strong ground motions, frequent in the Chilean territory. This article presents the main aspects of the Chilean engineering practice associated with the seismic design of large tailings sand dams. Additionally, the observed seismic performance of existing Chilean tailings dams is presented.

**Pratique Chilienne sur les grands barrages de stériles construits dans une zône à forte sismicité*

 DOI: 10.1201/9781003642428-144

RÉSUMÉ

En raison de l'importante production annuelle de cuivre chilien, les opérations minières doivent gérer de grands volumes de résidus, la plupart étant stockés dans d'énormes réservoirs confinés par des barrages, qu'il s'agisse de barrages en remblai ou de barrages de sable de résidus. L'expérience au Chili jusqu'en 1965 a montré que la défaillance des barrages de résidus lors des tremblements de terre est un événement catastrophique qui doit être évité par tous les moyens. Par conséquent, pour réaliser à la fois des dépôts de résidus rentables et sûrs, une pratique de génie géotechnique de haut niveau est nécessaire, comprenant une réponse sismique appropriée lorsque ces rejets de résidus sont soumis à de forts mouvements de terrain, fréquents dans le territoire chilien. Cet article présente les principaux aspects de la pratique de génie chilienne associée à la conception sismique de grands barrages de sable de résidus. De plus, la performance sismique observée des barrages de résidus chiliens existants est présentée.

1. INTRODUCTION

The Chilean annual production of copper is quite relevant in the world market. For instance, it was around 5.5 million metric tons in 2023, representing 24,7% of the world production. Copper content in mineralized rocks is in general less than 1% and in Chile about 70% of extracted rock is processed by concentration producing about 1,6 million tons of tailings per day which must be properly managed and safely stored. To recover the minerals by concentration, the extracted ore is crushed to the size of fine sand to clay. From a geotechnical perspective, copper tailings classify as silty sands or sandy silts of low to null plasticity. Considering the important annual production of Chilean copper, the mining operations must manage large volumes of tailings, which most of them are deposited in huge reservoirs confined by dams, either embankment dams or tailings sand dams.

Experience in Chile until 1965 showed that the failure of tailings dams during earthquakes is a catastrophic event that must be avoided. Accordingly, to achieve both cost-efficient and safe tailings deposits, a high-end geotechnical engineering practice is required, including an appropriate seismic response when these tailings disposals are subjected to strong ground motions, frequent in the Chilean territory. Among the different types of tailings deposits, retained by embankment dams or tailings sand dams, the most vulnerable to the impact of earthquakes could be tailings sand dams.

2. SEISMIC FAILURES EXPERIENCED BY TAILINGS DAMS IN CHILE

The seismic failure of Barahona tailings dam is the first reported in Chile. It occurred after the Talca earthquake of October 1, 1928, Ms=8.3. This tailings dam, constructed using the upstream method, contained the residues from El Teniente copper mine. It had a maximum height of 65 m, and its failure involved 4 million tons of material that flowed down the valley, killing 54 people [1] [2]. Fig. 1-a shows a panoramic view of the failure after four days [3] and Fig. 1-b [4] illustrates the cross section of the remaining tailings post-failure. There are several almost-horizontal terraces that can be attributed to low post liquefaction strength in the weaker layers of the tailings disposed in the reservoir. It should be noted that the failed Barahona tailings dam was rebuilt in 1929 (named Barahona 1), with upstream construction and stay in operation until 1936, when the tailings starting to be deposit in a new reservoir (Barahona 2). Currently Barahona 2 is used as an emergency tailings deposit.

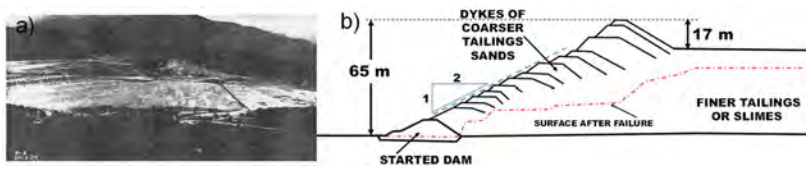

Fig. 1
Seismic failure of Barahona tailings dam, in 1928 [3][4].

El Cobre tailings dam that retained the tailings of El Soldado mine failed during the earthquake of March 28, 1965, Ms=7.4, with epicentre only 40 km away from the dam. The tailings dam failed catastrophically when more than 2 million tons of tailings flowed downstream about 12km in few seconds, burying the town of El Cobre, killing more than 200 people. At the time of failure, the dam was close to 33 m high, with a downstream slope of 35º to 40º [2].

Fig. 2 shows a cross section of the tailings dam before and after the failure. The final profile of the tailings consists of several terraces with 1º slope towards the valley [2].

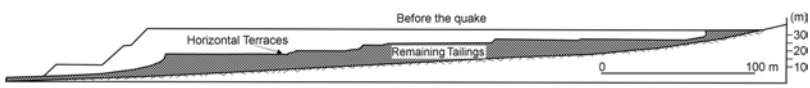

Fig. 2
Failure of El Cobre tailings dam, adapted from [2].

It was after the El Cobre failure in 1965 that the Chilean government banned by law in 1970 the upstream construction of tailings dams except under specific authorization of the government mining agency. Chile was the first country in banning upstream construction of tailings dams in consideration to the extremely high seismicity in the country. Since 1970 no new tailings dam built by upstream construction has been approved. Nevertheless, before 1970 there were other are existing relatively small upstream tailings dams that continued their operation and some of which have failed later under the impact of strong earthquakes.

N.M. Rana et al. [5] indicated that tailings flows triggered by seismic activity have steadily reduced in frequency over time. A majority of early seismic liquefaction failure cases were in Chile and Japan [2][6][7][8]; since then, both nations have advanced the state of operational practice such that tailings facilities have withstood powerful earthquakes [9][10][10][12][13]. A novel concern, however, is the potential role of sequential seismic tremors in accelerating the failure of marginally stable facilities [14][15].

Because of the Valparaíso earthquake occurred in 1985, of magnitude Ms=7.8, two tailing dams suffered seismic failure by liquefaction: Cerro Negro and Veta del Agua. The first one, Cerro Negro, 30 m high, was constructed with the upstream and centreline methods. Its failure involved 130,000 tons of tailings material that flowed down, covering a distance close to 8 km. Veta del Agua, maximum height of 15 m, failed - according to a witness- in the central part shortly after the earthquake shaking finished. The tailings material stored in the pond flowed along the El Sauce creek for 5 km [16].

The 2010 Maule earthquake, Mw=8.8, triggered seismic failures of five relatively small tailings dams: Chancón, Veta del Agua dike N°5 (both upstream), and Alhué (downstream) developed limited seismic displacements, whereas the Bellavista dike N°1 collapsed, and a significant volume of tailings flowed into the dike N°2, which worked as a buffer, stopping the tailings flow. During the same 2010 earthquake Las Palmas tailings dam underwent a catastrophic failure; the tailings flowed down for about 1 km, killing four people. The Fig. 3 shows a plant view of the situations before and after the failure of Las Palmas. The tailings liquefied again (less severely) during the aftershocks of M$>$5.0[17]. The upper dike that provoked the failure was settled over and upstream of lower dike in a configuration that could be consider an upstream construction.

Main tailings sand dams constructed with the downstream, or centreline methods designed respecting the restrictions of regulatory agency and recommendations of best practice have presented a stable seismic behaviour during strong earthquakes. It is important to mention that the in the last 50 years a significant number of large earthquakes have hit the Chilean territory where most of the tailings disposals are located. In Table 1 are listed the major earthquakes occurred in the last 50 years in Chile.

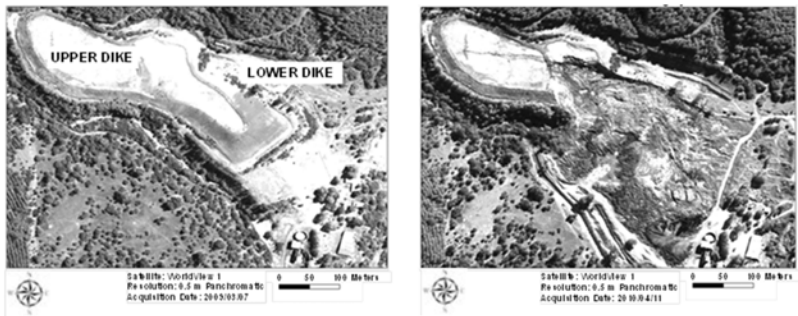

Fig. 3
Pre and Post failure, Las Palmas tailings dam [17]

Table 1
Mayor earthquakes in the last 50 years with epicentres near existing tailings disposals

EPICENTER	DATE	MAGNITUDE
La Ligua	December 28, 1966	7.8
Illapel	July 8, 1971	7.5
Algarrobo	March 3, 1985	8.0
Antofagasta	July 30, 1995	8.0
Punitaqui	October 15, 1997	7.1
Tarapacá	June 13, 2005	7.8
Tocopilla	November 14, 2007	7.7
Maule	February 27, 2010	8.8
Iquique	April 1, 2014	8.2
Illapel	September 16, 2015	8.3

3. EXAMPLES OF SUCCESSFUL SEISMIC PERFORMANCE OF TAILINGS SAND DAM

In Chile there are several tailings sand dams that corresponds to the retaining structures of large tailings deposits, a list of which is shown in Fig. 4. All of them are using the downstream construction method. In Chile there is only one tailings sand dam constructed by center line method (El Torito dam). It follows the example of 2 of these dams that have been subjected relatively recently to the impact of very strong earthquakes: Las Tórtolas and Quillayes tailings dams.

Table 2
Main downstream tailings sand dams in Chile

NAME	MAX HEIGHT (§) (M)	DAM LENGTH (M)	CAPACITY (MM^3) (+)	OPERATION START	TYPE	OPERATION END
El Cobre 4	68	1,140	31	1969	DS	1992
Piuquenes	58	500	20.5	1970	DS	1980
Pérez C. 2	115-135	500	84	1978	DS	1992
Talabre	40	5,300	1451	1985 (*)	EF/ DS	OP
El Chinche	110	470	14.5	1992	DS	1999
Las Tórto-las	150-170	1,700 (-)	690	1992	DS	OP
Torito	78	2,190 (+)	122	1992	DS/ CL	OP
Quillayes	175-198	1,600 (+)	360	1999	DS	2008
Ovejería	58-120	3,600 (+)	235	1999	DS	OP
El Mauro	237	1,450 (+)	1088	2008	DS	OP

Note: The data shown are approximated, obtained from different sources. Some of the deposits have been expanded, not all them registered in this table.
(-) Only main dam; (§) Approximate final height; (+) Approximately; (*) Deposition began in 1952, just in 1985 was necessary confinement walls. EF: Earthfill; DS: Downstream sand dam; CL: Centerline sand Dam

Las Tórtolas Tailings Storage Facility (TSF) is located at an elevation of 700 masl, 45 km North of Santiago, in Chile's central valley. In this dam, cross section shown in Fig. 4, initial conservative design criteria considered a maximum height of 150 m and a double cyclone station to guarantee 10% maximum fines content (FC) in the sand. The design considered also the implementation of a network of instruments, including piezometers and accelerometers. This is the first TSF in which a dynamic stability and deformational analysis was applied using the finite differences method. Satisfactory performance of this TSF, which began operating in 1992, made it possible to increase FC to 15% a few years later and to define a new maximum height of 170 m. The current height of this dam is near 130 m. Design of this deposit initially set a maximum capacity of 1,000 million tons of tailings, and recent estimates increased that capacity to 1,900 million tons. The deposit has two others smaller cyclone sand dams, all constructed using the downstream method, and one smaller earth dam. The dam is equipped with generous basal drains that were built in stages. The dam is constructed with cyclone sands compacted to 95% Proctor Standard. The sand was initially deposited forming a slope of 1:4 (V:H). After a few years of operation, and after verification of very satisfactory dam performance confirmed by density controls and piezometric level records, the deposition slope

was changed to 1:3.5 (V:H). A final slope of 1:3 (V:H) is considered for the closure stage [18].

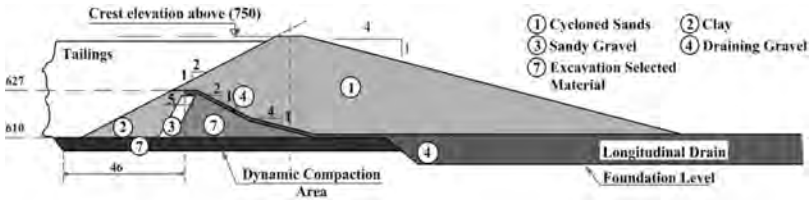

Fig. 4
Cross section Las Tórtolas dam [18]

Although this dam had not yet been built at the time of the Valparaíso earthquake of 1985, there were already accelerometers installed in rock at the dam site and the registers of this strong and relatively close earthquake were considered later in the dam dynamic stability analysis. Two large earthquakes have been registered during the operation of the TSF: the February 27, 2010 EQ Mw=8.8 and the September 16, 2015 earthquake Mw=8.4. In both seismic events, no-significant damage or deformation was observed. The instrument located in hard soil, associated with the main dam, recorded the data show in Table 3 [19].

Table 3
Recordings of large Earthquakes in Las Tórtolas Main Dam(1)[19].

DATE	M	DIST. (KM)	D (KM)	LOC.	PGA (G)	PGA (G)	VERT. PGA (G)
March 5, 1985 (2)	Ms = 7.8	~105	33	Basal soil Downstream	0,172 N64°E	0,144 N26°W	0,106
Feb 27, 2010	Mw = 8.8	~420	30	Basal soil Downstream	0,18 N64°E	0,18 N26°W	0,129
Sept 16, 2015	Mw = 8.4	~190	23	Basal soil Downstream	0,066 N64°E	0,064 N26°W	0,045
M= Magnitude according to U. de ChileDist.= Distance from epicenter to the dam D= Depth of earthquake				Loc = Location site of the accelerographPGA= Peak Ground Acceleration (Horizontal)Vert. PGA= Vert acceleration in g's			

Note: (1) Baseline corrected (2) Epicenter data according to USGS. https://www.usgs.gov/

The Quillayes Tailings Storage Facility (TSF) is of special interest, due to a series of conditions that resulted in severe design, construction, and operating

restrictions. Los Pelambres mine project is located 300 km North of Santiago with the TSF located near the other mining facilities. The site is in the foothills of the Andes Mountains, at an average elevation of 1,400 masl, distant some 85 km from the Pacific Ocean. The operation of the TSF started with a planned maximum capacity of 257 million tons of dry tailings, but a final capacity of 360 million tons was achieved with the final height of 198m of the tailings sand dam [18].

The main dam is a tailings sand dam, constructed by hydraulic deposition of sands obtained from the cycloning of the produced tailings, originally designed to have a maximum height of 175 m after 7 years of operation. The starter dam was a 70 m-high compacted earth embankment. The dam foundation consists of fluvial deposits in the central area of the dam, colluvial deposits, and / or alluvial terraced deposits in the right abutment and intrusive rock (granodiorite type) in the left abutment. The dam was raised following the downstream construction method, through continuous hydraulic deposition of tailings sands containing no more than 18% fines (material passing ASTM 200 mesh). The inclined deposition surfaces were compacted by tandem bulldozers and smooth vibratory rollers, with 1: 3.5 (V:H) to 1:4 (V:H) downstream slopes. Tailings placement stopped at the end of 2008.

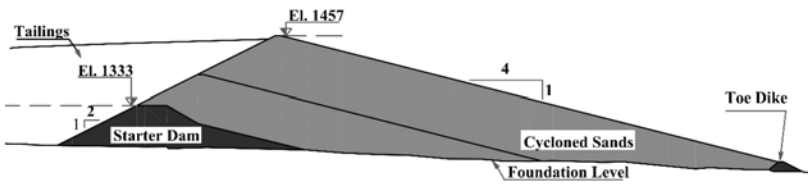

Fig. 5
Cross-Section of the Quillayes Dam [17].

Static and pseudo-static stability analysis using limit equilibrium methods were performed. The deformations under seismic loads were estimated carried out different methods: pseudo-dynamic analysis proposed by Makdisi and Seed [20] and formal numerical analysis with FLAC2D and FLAC3D. Both numerical analysis (2D, 3D) did not show evidence of failure by shear resistance or excess of deformation that could affect the global stability. The design earthquake (MCE) was of Ms = 8.3, with epicenter 123 km from dam an 23km of depth, with PGA of 0,37g (horizontal) and 0,25g (vertical) is hard soil. The September 16, 2015 earthquake of Mw = 8.4 was at the same depth and remarkably close to the epicenter of the design earthquake. According to the post-earthquake inspection by the Engineer of Record, non-significant deformations or instability was detected [18]. The final height of the dam after completing its operation is 198 m.

4. KEY ASPECTS CONSIDERED IN THE TAILINGS DAM DESIGN

4.1. Earthquakes to be considered in the seismic stability

In the subductive seismic environment of Chile, there are four potential seismic sources as shown in Fig. 6; interplate (thrust), intraplate (intermediate depth in-slab earthquakes caused by down-dip tension in the subducting plate), cortical (shallow crustal earthquake) and outer rise (beyond the trench) earthquakes. The latter from an engineering point of view is not important, so they are usually neglected.

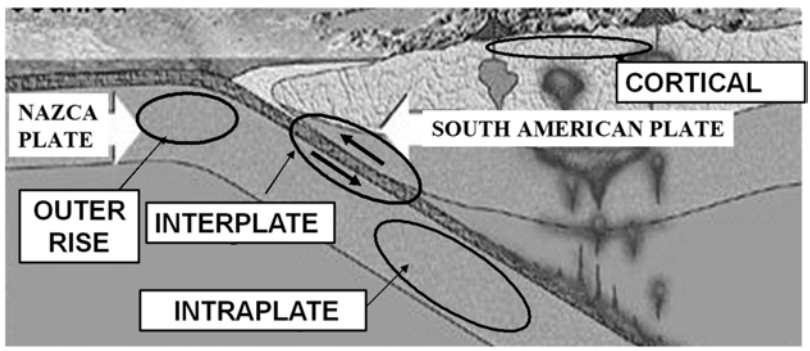

Fig. 6
Seismic sources in the Chilean subductive seismic environment

In the selection of the earthquakes, or acceleration records to be used in the seismic stability analyses, three criteria must be considered: 1) maximum peak ground acceleration, 2) Frequency content like the first or second mode of vibration of the dam, and 3) maximum duration. It should be noted that commonly, the criteria to define the design earthquake are exclusively focused on the maximum peak ground acceleration. However, the frequency content of the earthquake could be a more relevant criterion, especially in very high dams where the predominant frequency tends to be very low (large natural vibration period). To select the worst possible scenario, the natural period of the tailings dam must be estimated, and then, the seismic hazard analysis must identify those potential earthquakes that contain energy close to the natural frequency of the dam. Also, in seismic stability analysis the duration of the applied acceleration records is important, especially when some permanent displacements are indicated by the numerical analyses.

In the subductive seismic environmental of Chile, it is possible to expect intraplate earthquakes of Magnitude close to 8 and interplate earthquakes of Magnitude close to 9. In Fig. 7 are shown acceleration records of both intraplate and interplate Chilean earthquakes. The records obtained in Pica are associated with an intraplate earthquake (Tarapacá earthquake, M_w=7.8, June 13, 2005) and the recorded accelerations at Talca are associated with an interplate earthquake (Maule earthquake, M_w=8.8, February 27, 2010). As it can be observed, the intraplate earthquake presents a high value of peak acceleration, it contains high frequencies (low period), and it is of short duration. On the other hand, the interpolate earthquake has lower peak acceleration, a broad frequency band, and a long duration.

The Chilean practice considers at least these two seismic sources as inputs for the dynamic seismic stability analyses, considering in each case the Maximum Credible Earthquake (MCE), which is the largest possible earthquake that could hit the area of the project. The MCE is established using the deterministic approach. This earthquake is associated with the abandon condition of the tailings disposal and represents the ultimate possible seismic loading under which the tailings facility must remain in place without collapsing.

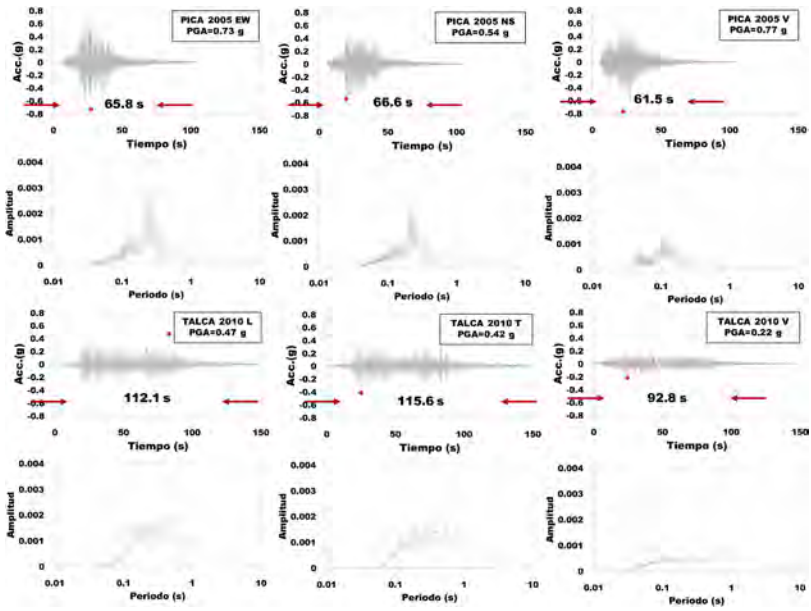

Fig. 7
Examples of acceleration records of Intraplate and Interplate earthquakes

4.2. Tailings sands with low fines content

The effect of low plastic fines content on the cyclic strength of copper tailings has been studied Troncoso and Verdugo [22] using reconstituted samples compacted at the same initial void ratio. Test results associated with the number of cycles required to develop 100% of pore water pressure build-up are shown in Fig. 8, where a clear degradation of cyclic strength exhibited by the tailing sands with the presence of low plastic tailings fines is observed. These results are indicative of the significant increase in liquefaction potential caused by the presence of low plastic fines in the sandy soil tailings, which have been confirmed by other reported data [23].

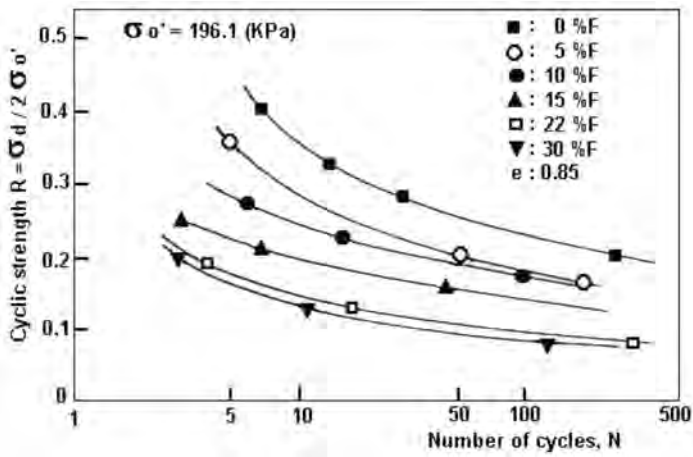

Fig. 8
Effect of low-plastic fines on the cyclic strength of tailings sandy soils under medium stress level [22]

According to these experimental results it is possible to conclude that the low plastic fines reduce the cyclic resistance of the tailings sands. The Chilean practice usually considers cycloned tailings sands with fines contents lower than 20%. However, under high confining pressure the effect of the fines content on the cyclic resistance is less pronounced. In fact, experimental results obtained by Campaña et. al.[24] and presented in Fig. 9, show that the cyclic resistance ratio (CSR) is practically constant for the four-copper tailing sand that were tested under confining pressures greater than 0.5 MPa.

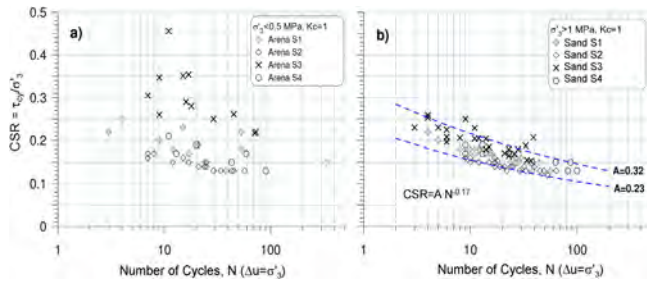

Fig. 9
Test results: a) $\sigma_o' \leq$ 0.5 MPa, b) $\sigma o' \geq$ 1 MPa [24]

4.3. Phreatic level in tailings sand dam body

An extremely important issue in the seismic stability of a tailings sand dam is associated with the level of the phreatic surface in the sand body of the dam. The requirement of maintaining a low level of the phreatic surface is to guarantee a low saturation of the compacted sand to avoid the possibility of liquefaction. This important requirement can be fulfilled by means of the two following conditions: 1) to maintain a large contrast of permeability between the finer tailings stored in the reservoir (slimes) and the tailings sands of the dam, 2) the design and construction of a generous basal drainage system. The first condition is achieved without difficulty when the cyclone tailings sands used to build the dam have fines contents less than 20 to 25%. In this case the horizontal permeability of the tailings sands is typically in the order of $5x10^{-3}$ to $5x10^{-4}$ cm/s. On the other hand, the permeability of the finer tailings stored in the pond (slimes) is in the order of 10^{-6} cm/s or even less. Therefore, the permeability of the dam body is two to three orders of magnitude higher than the permeability of the stored slimes or tailings. Thus, the reduced amount of water releases from the stored tailings is immediately transmitted throughout the dam as a moisture front, generating a phreatic level close to the base of the dam. The second condition is fulfilled with the design and construction of a generous network of basal drains that should be able to drain all water coming from the dam sand during the dam construction, operation and closure. The use of a generous drain system at the base of the tailings dams is a common practice in Chile.

4.4. Geotechnical considerations due to high confining pressures

The copper industry in the world has experienced a remarkable growth since year 2000, which has generated the need for higher tailings sand dams. In this

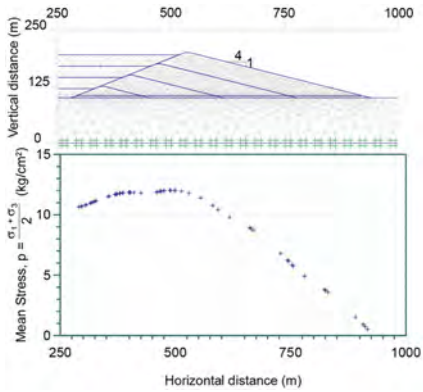

Fig. 10
Mean stress along the base of a tailings dam of 100 m in height.

context some of the largest dams recently constructed in Chile are, El Mauro with a height of 237 m, Quillayes with 198m, Las Tórtolas with 170 m, and Ovejeria with a height of 130 m [17]. New projects under development follow the same pattern with very high tailings dams. This situation makes it imperative to assess the effect of high confining pressures on the geotechnical properties of the tailings sands such as permeability, compressibility, static shear resistance and liquefaction resistance. The mean stress along the base of a typical tailings dam of 100 m in height is presented in Fig. 10. The mean stress reaches a maximum value close to 1.2 MPa, but for higher tailings dams, this value can be duplicated, which is well beyond the common capacity of available triaxial, or simple shear equipment. Considering this fact, the geotechnical laboratory of University of Chile developed a triaxial equipment for a maximum confining pressure of 6 MPa [25].

In Fig. 11 is presented (normalized by the initial void ratio before loading) the variation of the void ratio with the isotropic confining stress [26]. It is observed that tailings sands are more compressible than natural sands. This can be explained by the fact that tailings sands are extremely angular in shape, which causes crushing of the sharp contacts.

Fig. 12 shows experimental results of permeability as a function of void ratio and confining pressure σ'_3, for several tailings sands with various contents of fines [18]. As can be observed, a variation of the confining pressure from 1 to 3 MPa may cause a reduction in almost one order of magnitude in the permeability of the tailings sands. This is an important issue that has to be considered in the analyses because it may impact in the phreatic level within the dams.

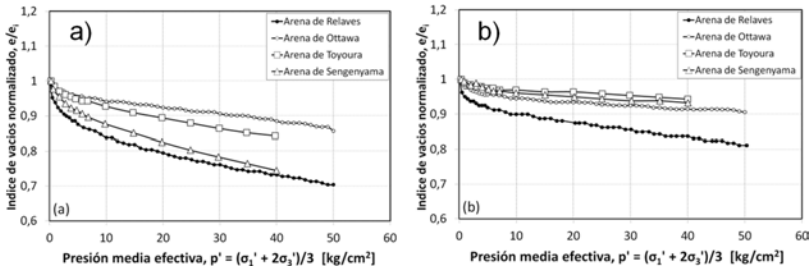

Fig. 11
Compressibility of tailings and natural sands, a) loose state and b) dense state [26].

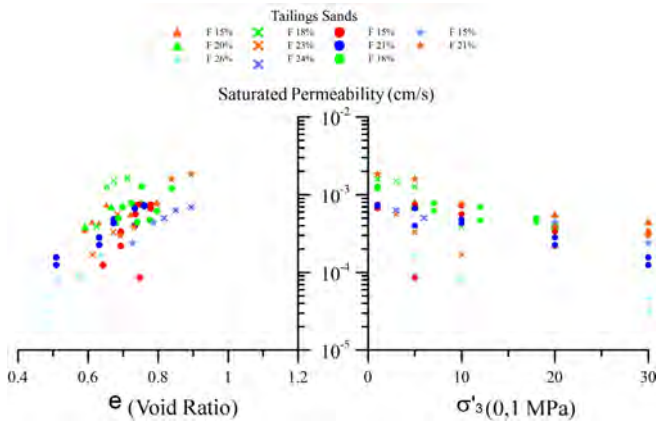

Fig. 12
Permeability as a function of void ratio and confining pressure σ'_3, for several tailings sands with various contents of fines [18] [21]

A well-designed tailings sand dam could develop a saturated zone, if any, right at its bottom, compromising only a few meters above its base. Thus, any analysis of liquefaction should be concentrated along this saturated zone and therefore, the pressure effect on the cyclic strength must be considered (K_σ). Different research have reported test results carried out in copper tailings sands under confining pressures greater than 0.5 MPa [24].

Fig. 13 shows values of experimentally obtained by several authors. These experimental data show that the reduction of K_σ with the level of confining pressure is significantly less important for tailings sands than natural sands.

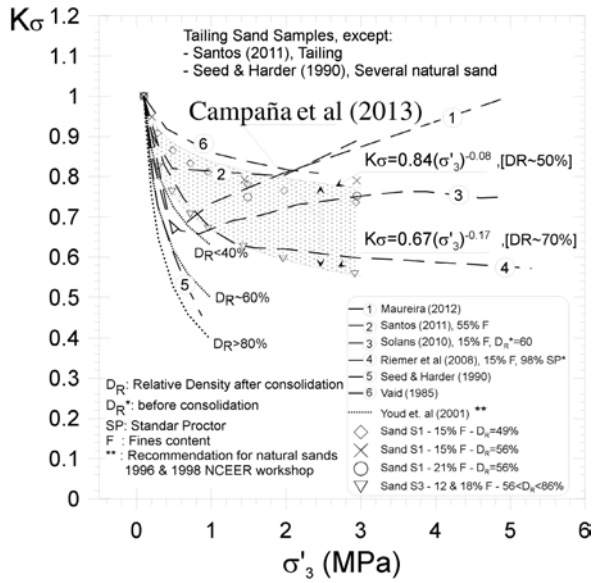

Fig. 13
Variation of factor Ks with the level of confining pressure, σ'_3. [24]

4.5. Seismic design process

Seismic dam design is part of a complex process that it is not limited to stability analyses. Analysis of failure experiences as well as successful experiences are important initial steps in this process as well as a detailed analysis and investigation of geological, hydrogeological and environmental characteristics of the site where the dam will be located. The early identification of possible areas prone to have landslides or the existence of liquefiable soils or soils with brittle behaviour in the dam area could be determining factors for the design. Geochemical characteristics of tailings and of tailings sands and the possibility of acid generation could represent a serious challenge for design. The designer must try to identify all possible vulnerabilities in front of a seismic loading on it predesigns, modifying those predesigns to mitigate the impact of the design earthquake.

Being the earthquake a dynamic loading, an initial consideration must be to the analysis of probable differential deformations among the dam, abutments, starter dam and ancillary structures in order to include these aspects in the design to eliminate or mitigate possible risks of inadequate performance. Foundation is probably one of the important aspects that must be studied in detail at early stages of the project. It is interesting to note that many tailings dam failures are related to

failure of their foundation. There are not many world cases of downstream slope failures either under static or seismic conditions apart from failure by liquefaction, static or seismic. This fact makes necessary to give special attention to the identification of liquefiable soils and to the solutions required to eliminate or to mitigate their effect.

4.6. Stability analyses of tailings dams

Independently that there not too many cases of downstream slope failures under static or seismic conditions, except when conditions are too extreme such as in the case of very strong cortical earthquakes, most of the stability analyses that are used are dedicated to verifying the stability of dam downstream slope. Some of these methods look for the determination of a Factor of Safety (FS) in terms of stresses or look for the determination of the degree of acceptance of deformations produced by the effect of an earthquake.

4.6.1. *Limit equilibrium methods and pseudo static stability analysis*

Limit equilibrium methods consider the stresses induced in a dam or cut slope due to the own weight of the soil over a potentially sliding surface or to the combined effect of own weight and an inertia force representing the earthquake loading. This is a very simple model that for static conditions has been calibrated with several actual cases as reported in the bibliography. This is not the case for seismic loadings where the main difficult is presented by the selection of the seismic coefficient (Kh and Kv). Although there are numerous proposals for their selection, none of them could represent the dynamic nature of earthquake shaking. Nevertheless, pseudo static stability analyses are widely used because of its simplicity and because most of regulator's agencies require a factor of safety for seismic conditions be submitted.

Independently that design would be verified by a truly dynamic analysis, the pseudo static stability analysis is still used during the design process to study different alternatives of predesigns. The knowledge of seismic coefficients Kh and FS of different projects in operation or that have failed could provide a mean of reference for designers and has proved to be an important tool for preliminary designs despite that a dynamic stability is finally applied.

In Chile in the 60´s a Kh=0,12 was used in important projects. At present Kh commonly adopted in the country has values varying from 0,15 to 0,20. Also, in Chile the required Safety of Factor is 1.4 (static), 1,2 (pseudo-static) and 1,0 (post-seismic).

4.6.2. *Pseudo dynamic stability analysis*

First proposal of simplified deformation analysis (performance based seismic analysis) goes back to 1965 (Newmark) based on a simple model of a rigid block sliding on an inclined plane. It was introduced the concept of critical or yielding acceleration (Ky or Ay) at which a FS =1.0 is obtained. The method accumulated slope movements along the slope (dam deformation) occurred during periods when the acceleration imposed by the earthquake is greater than Ky.

Many simplified seismic deformation analyses followed the Newmark concept. Among others: Sarma [27]; Makdisi and Seed [20]; Bray and Travasarou [28]; Urzua and Christian [29][30]; Bray, Macedo and Travasarou [31]; Bray and Macedo [32]; Macedo, Bray and Liu [33]. These simplified methods have been used frequently in the last 10 years to verify if the adopted seismic coefficient is compatible with an acceptable maximum deformation of the dam. Bray & Travasarou [34] and Macedo, Bray & Liu [33] has used this method also to estimate the value of seismic coefficient and to estimate dam deformations applying a seismic loading that could be representing a set of real earthquake registers.

4.6.3. *Dynamic analysis of dams*

Numerical analyses of dams have been in use for more than 50 years in dams of different types. Numerical analyses are generally used as a verification of a proposed design but also could be used as part of the design process if at that stage there is enough adequate information to define the different parameters required by the analysis. These analyses use a numerical method (finite elements, finite differences) and constitutive laws of the soils. The wide variety of numerical analyses are due to the relatively large number of proposed constitutive laws that are looking to "model" the behaviour of the soil under certain loading conditions (static or seismic). These methods provide the stress – strain response of a dam to static or seismic loading conditions.

Numerical analyses of dams (and other structures) require the selection of constitutive laws that better represent the actual behaviour of the soils. The physical properties of the soil, that would allow to define the parameters needed by the selected constitutive law, should be based on laboratory and field tests in sufficient number and high quality. Numerical analyses that are not based on adequate information, could create a risk if important decisions depend on the results of the analysis.

Numerical analyses are not easily understood in detail and experienced engineers should be involved in its conception and development. Many constitutive laws of soils have been defined considering some specific soil and because of this,

a careful study is necessary to verify which is the constitutive law that best represent the soil in a particular analysis. Most of the time the model needs to be calibrated or verified applying it for instance to simple problems where the result could be easily predicted. The case of constitutive laws for loose and contractive soils (as most of tailings are) are especially complex and a much caution must be taken to obtain reliable results.

The present Chilean practice include the use of : a) pseudo static stability analyses, as a value of factor of safety is required by regulators but also by practitioners in pre design stages; b) pseudo dynamic stability analyses are also applied in the study of new dams, although not officially recognized by regulators; c) numerical dynamic stability analyses have been in use in Chile in the design of large water and tailings dams for more than 40 years and lately also required by official regulators.

Unfortunately, despite the large number of earthquakes that occurs frequently in Chile and despite the number of accelerographs installed in many of the large tailings dams, there are no public registers of the response of those dams, except Las Tortolas, that could have allowed an adequate calibration of the numerical methods used.

4.6.5. *Acceptability criteria – physical stability*

The numerical stress-strain analyses are widely used to evaluate the physical stability of a mining facility, since they allow estimating the displacements it could experience due to an earthquake and help to identify possible failure mechanisms or zones with a concentration of deformations. To assess if the performance of dam was satisfactory or not in a numerical model, the Chilean practice consider [35]:

- Verify that the settlements in the dam crest are not capable of inducing the uncontrolled release tailings.
- Ensure that the potential landslide zone does not compromise more than 30% of the crest width for the Operational Seismic Earthquake (OBE) and 50% of the crest width for the Maximum Credible Earthquake (MCE), while considering potential landslides on the downstream and upstream slopes.
- Confirm that the remaining vertical deformation, measured at the center of the portion of the crest not affected by potential sliding surfaces, is less than 1% of the height, for the OBE and less than 3% of the dam height for MCE.
- Establish a maximum limit value of shear strain in potential slip surfaces based on laboratory test result conduced on representative material of dam affected by the potential slip surface. The laboratory test could be triaxial test, simple shear test, or similar.
- Verify the operational continuity or non-collapse of the dam components, such as drains, filters, geomembranes, and impermeable cores for OBE, and corroborate that this component could be reparable for MCE.

- Check that the deformations in the areas not affected by potential landslides have stabilized at the end of the seismic movement.
- Conduct stability analysis using Limit Equilibrium Methods (LEM) and Numerical Analysis. The key requirement is to ensure consistency in the potential slip surfaces obtained by LEM and dynamic analysis; any inconsistency would indicate that adjustments are needed.

5. CONCLUDING REMARKS

In active seismic regions there is sufficient evidence showing that tailings dams are sensitive to suffer seismic failures. However, in highly seismic countries such as Chile and Japan most of these seismic failures have been associated with upstream constructed tailings dams. It is worth to mention that properly designed tailings dams constructed in both downstream and center-line methods have shown a stable seismic behavior. Hence any of these two methods of construction should be used in seismic areas, avoiding the upstream method.

The case of Chile is quite remarkable. During almost 60 years there have not occurred a major failure even though Chile is subject quite frequently to strong earthquakes, except for Las Palmas failure in 2010 a particular case where design and operation were not in agreement with legal technical requirements. The Chilean practice is represented not only by conventional embankment or rockfill tailings dams but notably by large downstream tailings sand dams with heights of 200 m and more.

The Chilean practice applied local and international standards and in terms of stability verification analyses uses pseudo static and pseudo dynamic methods, with final verification through numerical stress – strain method. The key requirement is to ensure consistency in the potential slip surfaces obtained by limit equilibrium methods and dynamic analysis; any inconsistency would indicate that adjustments are needed. Maximum Credible Earthquake (MCE) is established using the deterministic approach corresponding to the largest possible earthquake that could hit the area of the project.

ACKNOWLEDGEMENTS

The authors wish to acknowledge the Engineer Claudio Scognamillo for your valuable comments.

REFERENCES

[1] AGÜERO G. (1929): “Formación de Depósitos de Relaves en el Mineral de El Teniente”. *Anales del Instituto de Ingenieros de Chile*, 5(1929), 164–187 (in Spanish).

[2] DOBRY R. AND ALVAREZ L. (1967): “Seismic Failure of Chilean tailings Dams”. *Journal of the Soil Mechanics and Foundations Division, ASCE, SM6*, 237–259.

[3] TRONCOSO, J.H., VERGARA, A., AVENDAÑO, A., (1993). Seismic failure of Barahona tailings dam. *Proceedings of the 3rd International Conference on Case Histories in Geotechnical Engineering 34*, St. Louis, USA.

[4] VERDUGO, R. (2022). The concept of static liquefaction and its application in the stability analysis of tailings dams. *Proc. of the 20th ICSMGE*, Sydney, Australia.

[5] RANA, N.M., GHAHRAMANI, N., EVANS, S.G., MCDOUGALL, S., SMALL, A., TAKE, A.W. (2021). Catastrophic mass flows resulting from tailings impoundment failures. *Engineering Geology*, V292.

[6] TORRES, N.A., BRITO, A.M., (1966). Effects of the March 1965 earthquake on the tailings dams of El Soldado mine, *Province of Valparaiso (in Spanish). Bull. Inst. Geol. Investig. Chile* 20, 21–42.

[7] OKUSA, S., ANMA, S., MAIKUMA, H., (1980). Liquefaction of mine tailings in the 1978 Izu- Ohshima-Kinkai earthquake, Central Japan. In: *Proceedings of the 7th World Conference on Earthquake Engineering 3*, Istanbul, Turkey.

[8] ISHIHARA, K., (1984). Post-earthquake failure of a tailings dam due to liquefaction of pond deposit. In: *Proceedings of the 1st International Conference on Case Histories in Geotechnical Engineering*, Missouri, USA.

[9] YASUDA, S., TOWHATA, I., ISHII, I., SATO, S., UCHIMURA, T., (2013). Liquefaction-induced damage to structures during the 2011 great East Japan *earthquake. J. Jpn. Soc. Civ. Eng.* 1 (1), 181–193.

[10] VILLAVICENCIO, G., ESPINACE, R., PALMA, J., FOURIE, A., VALENZUELA, P., (2014). Failures of sand tailings dams in a highly seismic country. *Can. Geotech. J.* 51 (4), 449–464.

[11] ISHIHARA, K., UENO, K., YAMADA, S., YASUDA, S., YONEOKA, T., (2015). *Breach of a tailings dam in the 2011 earthquake in Japan. Soil Dyn. Earthq. Eng*. 68, 3–22.

[12] VALENZUELA, L., (2016). Design, *construction, operation and the effect of fines content and permeability on the seismic performance of tailings sand dams in Chile. Obras y Proy*. 19 (6–22).

[13] TRONCOSO, J.H., VERDUGO, R., VALENZUELA, L., (2017). Seismic performance of tailings sand dams in Chile. In: *Proceedings of the 16th World Conference in Earthquake Engineering*, Santiago, Chile.

[14] AGURTO-DETZEL, H., BIANCHI, M., ASSUMPÇ˜AO, M., SCHIMMEL, M., COLLAÇO, B., CIARDELLI, C., BARBOSA, J.R., CALHAU, J., (2016). The tailings dam failure of 5 November 2015 in SE Brazil and its preceding seismic sequence. *Geophys. Res. Lett.* 43 (10), 4929–4936.

[15] MORGENSTERN, N.R., VICK, S.G., VIOTTI, C.B., WATTS, B.D., (2016). *Fund˜ao Tailings Dam Review Panel: Report on the Immediate Causes of the Failure of the Fund˜ao Dam*.

[16] CASTRO G. AND TRONCOSO J.H. (1989): "Seismic Behavior of Three Tailings Dams During the March 3, 1985 Earthquake". *5th Chilean Conference on Seismology and Earthquake Engineering.*

[17] BRAY J., FROST D., RATHJE E. (2013): "Geotechnical Lessons Learned From Earthquakes". *Seventh International Conference on Case Histories in Geotechnical Engineering..*

[18] VALENZUELA L. (2015): "Tailings Dams and Hydraulic Fills. The 2015 Casagrande Lecture". *16th International Conference on Soil Mechanics and Geotechnical Engineering*. Buenos Aires, Argentina.

[19] CAMPAÑA, J., BARD E., CANO, C., VALENZUELA, L., (2015). Registro Sísmico en Depósito de Relaves. IX Congreso Chileno de Geotecnia, *Valdivia-Chile*.

[20] MAKDISI, F., AND SEED, H. B. *(1978). "Simplified procedure for estimating dam and embankment earthquake-induced deformations." J. Geotech. Eng.*

[21] VALENZUELA L. (2016): "Design, *construction, operation and the effect of fines content and permeability on the seismic performance of tailings sand dams in Chile," Obras y Proyectos, June*, No.19

[22] TRONCOSO, J. AND VERDUGO, R. (1985): "Silt Content and Dynamic Behavior of Tailings Sands". *XI Int. Conf. on Soil Mechanics and Foundation Engineering*. Vol. 3. pp. 1311–1314.

[23] VERDUGO R. (2009): "Seismic performance based-design of large earth and tailings dams," Keynote Lecture, *International Conference on Performance-Based Design in Earthquake Geotechnical Engineering – from case history to practice*. Tsukuba, Japan.

[24] CAMPAÑA J., BARD E., AND VERDUGO R. (2013): “Shear Strength and Deformation Modulus of Tailing Sands under High Pressures”. *Proc. of the 18th Conf. on Soil Mechanics and Geotechnical Engineering*, Paris.

[25] SOLANS, D., (2010): “Equipo Triaxial Monótono y Cíclico de Altas Presiones y su Aplicación en Arenas de Relaves”. Tesis Magister en Cs. de la Ing., mención Ing. Geotécnica, *U. de Chile*. (In Spanish).

[26] MAUREIRA S. AND VERDUGO R. (2012): “Cyclic response of tailings sands subjected to high pressure,” *Proceedings VII Chilean Geotechnical Conference. Concepcion*. (In Spanish)

[27] SARMA, S. K. 1975. Seismic Stability of Earth Dams and Embankments, *Geo techpique*, Vol 25, No.4

[28] BRAY, J. D., AND TRAVASAROU, T. (2007). “Simplified procedure for estimating earthquake-induced deviatoric slope displacements.” *J. Geotech. Geoenviron. Eng*.

[29] URZÚA, A., AND CHRISTIAN, J. T. (2013). Sliding Displacements due to Subduction-Zone Earthquakes, *Engineering Geology*.

[30] URZÚA, A., AND CHRISTIAN, J. T. (2014). Displacements from the 2014 Iquique M8.2 Earthquake and M7.7 Aftershock Added to a Sliding Displacement Model, *Journal of Geotechnical and Geoenvironmental Engineering, ASCE)*.

[31] BRAY, J. D., MACEDO, J., & TRAVASAROU, T. (2018). Simplified procedure for estimating seismic slope displacements for subduction zone earthquakes. *Journal of Geotechnical and Geoenvironmental Engineering*.

[32] BRAY JD, MACEDO J. (2019). Procedure for estimating shear-induced seismic slope displacement for shallow crustal earthquakes. *J Geotech Geoenviron Eng*.

[33] MACEDO J., BRAY J. D., AND LIU C. 2023. Seismic Slope Displacement Procedure for Interface and Intraslab Subduction Zone *Earthquakes. J. Geotech. Geoenviron. Eng.,* 2023, 149(11): 04023104.

[34] BRAY J. D. & TRAVASAROU T. 2011. *Pseudostatic Slope Stability Procedure. 5th International Conference on Earthquake Geotechnical Engineering*.

[35] LEAL, F., BARRUETO, C., SANTOS, E., & CAMPAÑA, J. (2024). *Acceptability Criteria of Physical Stability of Taiings Dam Based on Numerical Analysis. 92nd ICOLD Annual Meeting and Symposium*, New Delhi.

Q.111 - R.47

COMMISSION INTERNATIONALE DES
GRANDS BARRAGES

VINGT-HUITIEME CONGRES DES
GRANDS BARRAGES
CHENGDU, MAI 2025

A NOVEL METHOD OF SEISMIC REINFORCEMENT FOR HIGH ROCKFILL DAMS SITUATED ON DEEP OVERBURDEN (*)

Li HONGJUN, Tian JIXUE & Xu ZEPING
Senior Engineer, China Institute of Water Resources and Hydropower Research, West Chegongzhuang Rd., Beijing

Lang ZIFAN
Doctor of Philosophy, China Institute of Water Resources and Hydropower Research, West Chegongzhuang Rd., Beijing

Yan ZUWEN
Senior Engineer, China Institute of Water Resources and Hydropower Research, West Chegongzhuang Rd., Beijing

CHINA

SUMMARY

For high rockfill dams situated on deep overburden in strong earthquake area, there is an urgent need to solve the problem of deep slip stability. In particular, when a weak soil layer exists in the overburden, the most dangerous slip surface safety coefficient of the deep slip arc is likely to be smaller than that of the shallow slip arc. This paper proposes a new seismic reinforcement measure by laying geogrid at the connection between the dam foundation and the overburden layer, aiming at solving the problem of deep slip stability of high rockfill dams on the deep overburden in a more economical way, and providing a reference for engineering practice.

**Une nouvelle méthode de renforcement sismique pour les barrages en enrochement de grande hauteur situés sur des terrains de couverture profonds*

 DOI: 10.1201/9781003642428-145

RÉSUMÉ

Pour les barrages en enrochement de grande hauteur situés sur des terrains de couverture profonds dans les zones de forts tremblements de terre, il est fondamental de résoudre le problème de la stabilité du glissement en profondeur. En particulier, lorsqu'une couche de sol faible existe dans les morts-terrains, le coefficient de sécurité de la surface de glissement la plus dangereuse de la courbe de glissement profond est susceptible d'être plus petit que celui de la ligne de glissement peu profond. Ce rapport propose une nouvelle mesure de renforcement sismique par la pose d'une géogrille à la connexion entre la fondation du barrage et la couche de couverture, afin de résoudre de manière plus économique le problème de la stabilité au glissement profond des barrages en enrochement sur couverture profonde, et de fournir une référence pour la pratique de l'ingénierie.

1. INTRODUCTION

As China's water conservancy and hydro-power industry has developed, the centre of hydro-power building has shifted to the southwestern region of China [1], which is rich in hydro-power resource but has complex geological conditions. The region in the southwestern of China are characterized by high strong earthquake and complex topography, with the dam site itself situated with a deep overburden. In light of the relatively weak load-bearing capacity of the overburden, it is necessary to consider the stability of the dam foundation when constructing a dam on it. The seismic safety of dams located on deep overburden is also of great importance, given that the majority of the southwestern region is situated within a strong earthquake area. It can be observed that the seismic inertia force generated by the earthquake will have a significant impact on the structure itself. Additionally, the amplification of seismic ground motion through the overburden and the dam body will obviously vary upon reaching the top of the dam, which may potentially affect the structural safety of the dam body. Accordingly, the primary objective of seismic design is to ascertain the dam's seismic stability based on the findings of the quasi static method stability analysis[2]. Quasi static method is based on the gravity, seismic peak ground acceleration of design earthquake and the ratio of acceleration to gravity, seismic effect reduction factor and the dynamic distribution coefficient of seismic inertia force, which is the product of the design of the seismic force and the static analysis method. The dynamic distribution coefficient of the horizontal seismic inertia force along the dam base to the top of the dam is of pivotal importance when calculating seismic effects and performing seismic stability calculations for rockfill dams using the quasi static method.

As a reinforcing material, geogrid has the capacity to enhance the deformation and strength characteristics of the soil body, and markedly augment the shear strength and overall stability of the soil body. This type of reinforcement can

effectively enhance the bearing capacity of the foundation soil layer and mitigate the potential for slip and uneven settlement caused by seismic activity, thereby enhancing the seismic safety of the dam body [3]. Additionally, geogrids can disperse seismic loads, reduce stress concentration, and promote the uniform distribution of forces within the dam body. As we know,it is common practice to place geogrids at the top of the dam, as this is the area of the dam body that experiences the most intense dynamic response [4]. This placement is intended to improve the seismic stability of the dam body. However, the formation of weak interlayers with small shear strength in the context of complex geological conditions in the deep overburden inevitably affects the deep slip stability of the dam. Consequently, the safety coefficient of the deep sliding body may be smaller than that of the shallow sliding body [5]. This paper builds on the concept of reinforcing the upper portion of the dam, as seen in an actual project model. It employs geogrid reinforcement at the base of the dam and the upper part of the building foundation. Using numerical simulations, it calculates the stability and safety coefficient of the dam slope. It then compares these results with those of the stability and safety coefficient of the dam slope after vibrating crushed stone pile reinforcement. Based on these findings, it draws conclusions that will provide a scientific basis for the subsequent construction of dams on deep overburden and seismic reinforcement of the dam body.

2. COMPUTATIONAL THEORY AND METHODS

2.1. Quasi static method

China's Standard for seismic design of hydraulic structures[2] uses the quasi static method to calculate the effect of seismic action, the representative value of the horizontal seismic inertia force acting on a single mass point along the height of the dam shall be calculated in accordance with the following equation:

$$\mathrm{E_i} = \mathrm{a_h}\xi\mathrm{G_{Ei}}\alpha_\mathrm{i}/\mathrm{g} \tag{1}$$

Where E_i is the representative value of the horizontal seismic inertia force acting on the mass; a_h is seismic peak ground acceleration of design earthquake; ξ is seismic effect reduction factor; G_{Ei} is the standard value of gravity action concentrated in the mass; α_i is the dynamic distribution coefficient of the seismic inertia force of the mass; and g is the gravitational acceleration. It can be seen from the formula that the determination of the dynamic distribution coefficient of the seismic inertia force of the mass point is the key to calculate the effect of seismic action using the quasi static method，while it's also the main object of research in this paper. The following figure illustrates the proposed distribution curves of the dynamic distribution coefficients of seismic inertia forces corresponding to different dam heights as outlined in the China's seismic design standard for hydraulic buildings.

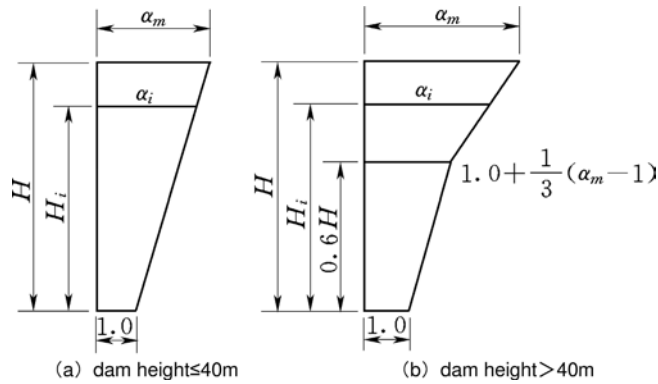

Fig. 1
Dynamic distribution coefficients of seismic inertia forces in the China's seismic design standard for rockfill dams

It can be observed from Fig. 1 that the presented curves in the specification fail to account for the impact of the deep overburden at dam base on the dynamic distribution coefficient of seismic inertia force. On the basis of Chinese standard, Lang [6] gave curves for dynamic distribution coefficients of seismic inertial forces considering deep overburden and geogrid reinforcement, as Fig. 2 show. In this paper, based on the conclusion of the research in Fig. 2, a computational study is carried out on an engineering case to give a new method of seismic reinforcement of high rockfill dam situated on deep overburden.

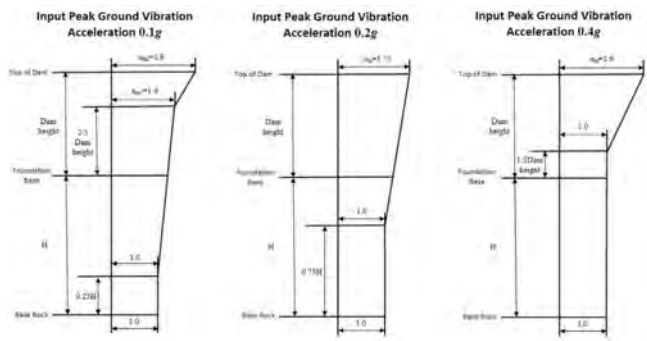

Fig. 2
Distribution curves of horizontal seismic inertia force coefficients of high rockfill dam situated on overburden with geogrid reinforcement

2.2. Seismic reinforcement of rockfill dams

At the present time, two typical types of foundation reinforcement are common in use: stone column reinforcement and geogrid reinforcement. In comparison to stone column reinforcement, geogrid reinforcement is a more cost-effective approach. Typically, geogrid reinforcement is positioned at the upper position of the dam to mitigate deformation and stress concentration in the area of the dam exhibiting the greatest dynamic response to seismic activity, thereby enhancing the stress distribution at the top of the dam. The two reinforcement techniques are illustrated in Fig. 3.

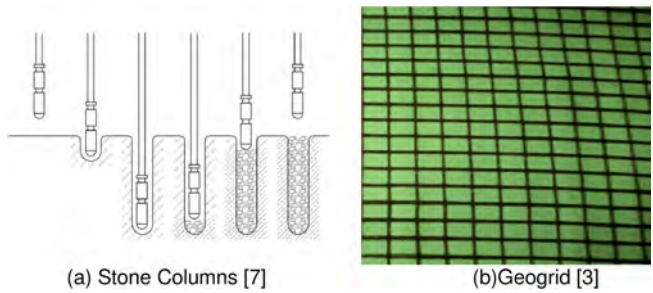

Fig. 3
Two typical reinforcement methods

However, the issue of deep-seated sliding stability of the dam body over deep overburden, due to the presence of deep overburden and weak soil layer in overburden, requires immediate attention. This paper proposes a novel seismic reinforcement measure involving the use of geogrid at the interface between the dam base and overburden. This approach aims to enhance the seismic resilience of the dam on the deep overburden in a cost-effective manner, while also laying the foundation for subsequent seismic reinforcement research. Fig. 4 illustrates the proposed reinforcement of the dam base.

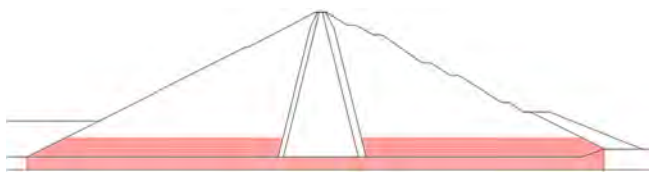

Fig. 4
Reinforcement with geogrid at the bottom of dam situated on deep overburden

2.3. Numerical simulation of geogrid reinforcement

There are three principal numerical calculation methods for the geogrid reinforcement of rockfill dams. The first is to regard the geogrid-reinforced soil body as consisting of two materials with different properties, namely soil and reinforcement. In this approach, the two materials transfer stresses to each other at the interface. The second method is to regard the reinforced composite material as a macroscopically homogeneous and anisotropic composite material, with the interaction between the soil and the reinforcement expressed as an internal force. This force affects the overall properties of the composite material but does not appear directly in the calculation of stresses and strains. The third method is to consider the geogrid-reinforced structure as a composite structure comprising geogrid and soil. Furthermore, it is assumed that the surrounding soil exerts a uniform pressure distribution, which is equivalent to the surrounding pressure[8]. This method neglects the interaction between the soil body and the geogrid, as well as the non-linear characteristics of the geogrid component. However, it can effectively streamline the calculation process. In particular, the calculation of equivalent surrounding pressure requires the determination of the size and distribution form of the equivalent surrounding pressure, based on the strength parameters of the soil body itself, the laying method of the reinforcement and the mechanical properties of the reinforcement. Subsequently, the aforementioned pressure is applied to the structure as a load, and a static analysis is conducted in order to obtain crucial parameters, including the displacement and stress of the structure. Subsequently, the results are validated to ascertain whether the structure complies with the specified design criteria. This method allows for a concise calculation of the stress-strain relationship in geogrid-reinforced soil bodies, while also accounting for the anisotropy inherent to these structures. Accordingly, this paper is founded upon the concept of equivalent surrounding pressure, with the objective of determining the value of the geogrid-reinforced soil parameter Δc in the static and dynamic calculation of the model. In order to simulate the effect of geogrid reinforcement measures on the dynamic characteristics of the soil body, the dynamic shear modulus of the geogrid-reinforced soil body is increased by 10% at least.

3. ENGINEERING CASE

In accordance with the dynamic coefficient distribution curve of horizontal inertia force recommended in this paper, static and dynamic calculations are conducted for the water-retaining building of the ML project. The water-retaining building of the typical project employs an clay core rockfill dam, with a maximum height of 150m. Geogrid reinforcement were incorporated within the upstream and downstream rock pile area within the bottom 1/5 of the dam height. The finite element

calculation grid of the dam body is illustrated in Fig. 5. The calculation parameters are presented in Table 1, Table 2, Table 3, Table 4.

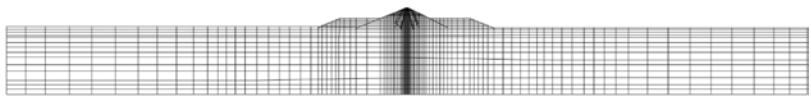

Fig. 5
Calculation mesh of engineering case

Table 1
Static parameters of overburden materials

SOIL LAYER NUMBER	BUOYANT UNIT WEIGHT (G/CM^3)	LINEAR PARAMETER		NONLINEAR PARAMETER	
		C(KPA)	$\varphi(^\circ)$	$\varphi o(^\circ)$	$\Delta\varphi(^\circ)$
③-3	1.08	46	34		
③-2	0.99	40	32		
③-1	1.13	50	34		
②	1.40			52	6
①	1.45			54	6

Table 2
Static parameters of dam materials

DAM MATERIAL	CONSTRUCTION UNIT WEIGHT	SATURATED UNIT WEIGHT	*C*(KPA)	$\varphi(^\circ)$
	(G/CM^3)	(G/CM^3)		
Core	2.1	2.2	35	33
Filter material	2.09	2.25	0	39
Transition material	2.12	2.3	0	42
Dam rockfill	2.18	2.3	0	45

Table 3
Dynamic parameters of major materials

TYPES OF SOIL MATERIALS	*C*	*N*
Overburden	2677.71	0.51
Dam rockfill	3272.78	0.46
Core	1275.97	0.55

Table 4
Dynamic parameters of major materials

TYPES OF SOIL MATERIALS	OVERBURDEN		DAM ROCKFILL		CORE	
SHEAR STRAIN	G/G_{MAX}		G/G_{MAX}	λ	G/G_{MAX}	λ
5.00E-06	0.9933	0.0085	0.9938	0.0096	0.9906	0.0204
1.00E-05	0.9718	0.0100	0.9817	0.0112	0.9830	0.0224
5.00E-05	0.8514	0.0223	0.8812	0.0204	0.9322	0.0315
1.00E-04	0.7780	0.0377	0.8115	0.0287	0.8822	0.0396
5.00E-04	0.5760	0.0793	0.6078	0.0634	0.6649	0.0855
1.00E-03	0.4656	0.1014	0.4985	0.0875	0.5324	0.1182
5.00E-03	0.2299	0.1641	0.2401	0.1682	0.3028	0.2183
1.00E-02	0.1455	0.2059	0.2193	0.2305	0.2402	0.2871

The impact of geogrid reinforcement was evaluated in comparison to stone columns reinforcement（seismic peak ground acceleration of design earthquake 0.535*g*）, as illustrated in Table 5 and Table 6 below.

Table 5
The factor of safety for the most dangerous slip of downstream (with stone columns reinforcement)

CASE	NORMAL STORAGE LEVEL +DESIGN EARTHQUAKE（DOWNSTREAM）
No reinforcement	1.032
50m stone columns reinforcement	1.470
60m stone columns reinforcement	1.482
70m stone columns reinforcement	1.494

Table 6
The factor of safety for the most dangerous slip of downstream (with geogrid reinforcement)

CASE	NORMAL STORAGE LEVEL +DESIGN EARTHQUAKE（DOWNSTREAM）
No reinforcement + Distribution according to Chinese standard	1.032
Geogrid reinforcement + Distribution according to Chinese standard	1.399
Geogrid reinforcement + Distribution according to proposed curves of horizontal inertial force	1.412

Based on the calculation results, it can be seen that the dynamic distribution coefficients suggested by the Chinese standard overestimate the seismic ground motion response and are not consistent with the actual results. With regard to the reinforcement effect, geogrid reinforcement at the bottom of the dam increased the safety factor of the most dangerous slip of the deep slip of the dam by 47.9%, while the reinforcement of the 70m stone columns had 44.8%, and from the point of view of the stability of the deep slide resistance, the reinforcement effect of the above-mentioned methods was consistent. It can be observed that under identical operational conditions, the geogrid reinforcement range of 30 metres at the base of the dam (within one-fifth of the dam height) is comparable to the reinforcement effect of 70-metre stone columns. Furthermore, the geogrid reinforcement is a more cost-effective alternative to stone columns and easy to place.

4. CONCLUSIONS

Geogrid reinforcement at the top of the dam is a common approach of seismic reinforcement of dams, but due to the increased depth of the overburden layer underneath the dam and the presence of weak soil layers in the overburden layer in the existing projects, it poses a great challenge to the deep-seated sliding stability of high core rockfill dams on deep overburden. In this paper, the geogrid reinforcement is carried out at the bottom 1/5 of the dam height range of the high core rockfill dams on the gravel overburden. On the basis of the results of research on the dynamic distribution coefficients of seismic inertia forces in high core rockfill dams on deep overburden, based on the domestic project example of a typical deep overburden of the high core rockfill dams, the safety coefficient of the most dangerous slip surface of the deep slip arc was calculated based on the seismic stability analysis and compared with the results of the stone columns calculation. The results of the analyses show that geogrid reinforcement at dam bottom improves the overall stiffness of the dam body, enhances its seismic bearing capacity and especially enhances the deep slip stability of the dam body, while is more cost-effective alternative to stone columns. Overall, this new seismic reinforcement technique can provide theoretical support for subsequent seismic reinforcement design of high rockfill dams on deep overburden.

ACKNOWLEDGEMENTS

The authors are grateful for the financial support from Tibet Autonomous Region Science and Technology Programme Project: Research on Seismic Safety of High Rockfill Dams on Deep Overburden (Project Number:XZ202101ZY0002G)

REFERENCES

[1] Office of the Leading Group for Western Regional Development of the State Council. *Outline of Water Conservancy Development Plan for Western Regions [M]*. China Water&Power Press, 2002.

[2] GB_51247-2018_STANDARD for seismic design of hydraulic structures[S]. Beijing: China Planning Press. 2018

[3] LI HONGJUN. *Study on Permanent Deformation and Safety Evaluation of High Rock-fill Dams Under Strong Earthquakes[D]*. Dalian University of Technology, 2008. DOI:10.7666/d.y1248659.

[4] KONG XIANJING, ZOU DEGAO, DENG XUEJING, *ET AL.* Comprehensive Earthquake Resistant Measure of High Earth-rockfill Dams and Effectiveness Verification [C]// *Journel of Hydraulic Engineering*, 2006:7.

[5] ZOU DEGAO, YU XIANG, YU TING, *ET AL.* Study on the Dynamic Stability Analysis Method for High Earth Built on Deep Overburden [J]. Hydropower and Pumped Storage, 2020, 6(01):22-27+2.

[6] LANG ZIFAN, LI HONGJUN, YAN ZUWEN, *ET AL.* Study on the distribution of coefficient of seismic inertia force of high core rockfill dam located on the deep overburden [J]. *Journal of China Institute of Water Resources and Hydropower. Research*, 2023, 21(03):254-265+276. DOI:10.13244/j.cnki.jiwhr.20220404.

[7] JIANG DAHUANG. Gravel Columns of Underwater Composite Foundation Settlement Calculation Method and Case Analysis [D]. Dalian University of Technology, 2016.

[8] YANG Z. Strength and deformation characteristic of reinforced sand[D]. Los Angeles, California: University of California, 1972.

Q.111 - R.48

COMMISSION INTERNATIONALE DES
GRANDS BARRAGES

VINGT-HUITIEME CONGRES DES
GRANDS BARRAGES
CHENGDU, MAI 2025

RESEARCH ON THE DYNAMIC RESIDUAL DEFORMATION MODEL FOR COARSE GRAINED SOIL (*)

Kai-bin ZHU, Jing-jun LI, Xiao-sheng LIU, Jian-ming ZHAO & Zheng-quan YANG
State Key Laboratory of Simulation and Regulation of Water Cycle in River Basin, China Institute of Water Resources and Hydropower Research, Beijing

CHINA

SUMMARY

The residual deformation of earth-rock dams under design earthquake conditions is a critical indicator for assessing their seismic safety. The primary methods for calculating earthquake residual deformation of earth-rock dams include sliding displacement analysis, integral deformation analysis, and elastoplastic analysis. The global analysis method, based on experimental results of earth-rock material residual deformation characteristics, is the predominant method in engineering analysis. Global deformation analysis encompasses two main models: dynamic stress-residual strain and cycle-residual strain. This paper reviews the deficiencies of the two major model categories and their enhanced versions, and proposes a new residual deformation calculation model based on an analysis of influencing factors and mechanisms, achieving promising results through experimental data.

RÉSUMÉ

La déformation résiduelle des barrages en remblai dans des conditions de séisme de conception est un indicateur critique pour évaluer leur sécurité sismique.

Recherche sur le modèle de déformation résiduelle dynamique de sol à gros grains

 DOI: 10.1201/9781003642428-146

Les principales méthodes de calcul de la déformation résiduelle des barrages en remblai en cas de tremblement de terre comprennent l'analyse des déplacements par glissement, l'analyse de la déformation intégrale et l'analyse élastoplastique. La méthode d'analyse globale, basée sur les résultats expérimentaux des caractéristiques de déformation résiduelle du matériau, est la méthode prédominante dans l'analyse technique. L'analyse globale de la déformation englobe deux modèles principaux : la contrainte dynamique-déformation résiduelle et le cycle-déformation résiduelle. Ce rapport examine les lacunes des deux principales catégories de modèles et de leurs versions améliorées, et propose un nouveau modèle de calcul de la déformation résiduelle basé sur une analyse des facteurs et des mécanismes d'influence, obtenant des résultats prometteurs grâce aux données expérimentales.

1. INTRODUCTION

Earth-rock dams are highly adaptable to geological conditions and are extensively employed in hydraulic engineering [1]. China's southwest and northwest high mountain and canyon regions are rich in hydropower resources, yet geological conditions are complex, and disasters occur frequently. To ensure the safety of earth-rock dams in high-seismic-risk areas, their seismic design and safety evaluation are critical. In particular, the residual deformation of earth-rock dams during earthquakes serves as a critical indicator of their seismic safety. Therefore, research into the residual deformation of coarse gravel is vitally important.

Methods for residual deformation in earth-rock dams after earthquakes primarily include sliding displacement analysis, integral deformation analysis, true-nonlinear analysis [2], and elastoplastic analysis. According to sliding displacement analysis, permanent deformation is seen as the accumulation of sliding displacement that occurs when the earth-rock dam's sliding soil experiences transient instability along the most dangerous sliding surface under seismic loads [3]. Global deformation analysis considers the soil as a continuous medium, employing the soil's dynamic constitutive behavior and combining it with experimental research using the finite element method for determination [3]. This includes the modified modulus method, strain potential method, and equivalent nodal force method. The elastoplastic model analysis method directly calculates residual deformation using the material's elastoplastic model. However, the elastoplastic analysis method often faces challenges with loading and unloading judgments and convergence issues during its calculation process, and due to the model's complexity, it is less frequently employed in engineering applications. Currently, the residual deformation of soil and rock materials continues to be analyzed using the global deformation analysis method derived from experimental results [4]. Earth-rock dams' residual deformation during earthquakes encompasses both volume and shear deformations. Currently, the global deformation analysis process predominantly employs the following two approaches for residual deformation analysis.

The dynamic stress-residual strain model described the relationship between dynamic stress and residual strain at a certain vibration cycle. The cycle dependent-residual strain model provides a comprehensive description of the relationship between residual stress and the number of vibration cycles. Currently, several models are widely used in engineering, such as the Taniguchi Eiji Model [5], the Water Science Institute Model [6,7], and the Shen Zhu-jiang Model [8]. These computational models are continually refined to more accurately capture the residual deformation characteristics of earth-rock dams during earthquakes.

This paper evaluates two existing models and introduces a new residual deformation model based on the mechanisms of permanent earthquake deformation, addressing the shortcomings of the current models. It begins with an analysis of the existing models, describing their strengths and weaknesses and suggesting directions for modification. Subsequently, by integrating tests of residual deformation characteristics from actual engineering projects and an analysis of key influencing factors from the existing literature, the new model is developed, and its principles are identified. Finally, the paper summarizes and comments on the newly revised model, offering suggestions for further refinement.

2. INTRODUCTION TO EXISTING MODELS

2.1. THE DYNAMIC STRESS-RESIDUAL STRAIN MODEL

In the 1980s, Rongyi Taniguchi and colleagues [5] investigated the residual deformation behavior of sandy soil using vibratory triaxial tests and introduced a residual shear strain model.

$$\frac{\tau}{\sigma_0} = \frac{\tau_d}{a + b\gamma_r} + \frac{\tau_s}{\sigma_0} \tag{1}$$

In the formula, τ is the sum of static and dynamic shear stresses on the 45 ° plane of the specimen, that is $\tau = \tau_s + \tau_d$. $\tau_s = (\sigma_1 - \sigma_3)/2$ is the initial static shear stress. $\tau_d = \sigma_d/2$ is the dynamic shear stress. $\sigma_0 = (\sigma_1 + \sigma_3)/2$ is the initial average effective stress. γ_r is the residual shear strain. a, b are the model parameter.

In early 2000, Wang et al.[7] discovered through large-scale dynamic triaxial tests on sand and gravel at the Zi Ping-pu dam foundation that the residual strain behavior under cyclic loads resembled that of sandy soil. Following the insights of Rongyi Taniguchi [5], it is recommended to apply the findings from sandy soil research to calculate the residual strain in sand and gravel for a given number of cycles.

$$\frac{\tau_{fsd}}{\sigma'_{f0}} = \frac{\gamma_p}{a + b\gamma_p} + \frac{\tau_{f0}}{\sigma'_{f0}} \tag{2}$$

In the formula, τ_{fds} is the total shear stress on the potential failure surface, τ_{f0} represents the static shear stress, σ'_{f0} is the normal effective stress; γ_p is the residual shear strain; *a* and *b* are experimental constants, related to the number of cycles *N*, stress state, and soil properties. Wang et al. [7] also proposed a power function expression for residual volumetric strain ε_{dv}, as follows:

$$\varepsilon_{dv} = K_v\left(\Delta\tau/\sigma'_0\right)^{n_v} \tag{3}$$

Based on the results of large-scale dynamic triaxial tests on the material of the Long-shou second-level concrete-faced rockfill dam, Zhao et al. [6] suggested that the residual shear strain could be more conveniently expressed in a power

$$\varepsilon_{da} = K_a\left(\Delta\tau/\sigma'_0\right)^{n_a} \tag{4}$$

$$\gamma_p = (1+\mu)\varepsilon_{da} \tag{5}$$

In the formula, ε_{da} represents residual axial strain; $\Delta\tau$ represents dynamic shear stress; σ'_0 represents effective normal stress on the 45° plane; K_v, K_a, n_v and n_a are the coefficients and indices of the residual strain model, determined based on experimental results; μ represents dynamic Poisson's ratio. The model from the Water Science Research Institute uses the dynamic shear stress ratio $\left(\Delta\tau/\sigma'_0\right)$ as the independent variable, with confining pressure, consolidation ratio, and vibration count as reference variables.

According to existing research, the dynamic stress-strain (residual) model shows a high degree of agreement between the experimental characterization and results at the selected cycle [6,9], effectively reflecting the residual strain characteristics of specific soils under varying dynamic stresses at that cycle. Besides simulating the calculation of residual shear strain, the model from the Water Science Institute also captures the shear contraction behaviors observed in the tests on the residual deformation characteristics of soil and rock materials.

According to existing research, the dynamic stress-strain (residual) model shows a high degree of agreement between the experimental characterization and results at the selected cycle [6,9], effectively reflecting the residual strain characteristics of specific soils under varying dynamic stresses at that cycle. Besides simulating the calculation of residual shear strain, the model from the Water Science Institute also captures the shear contraction behaviors observed in the tests on the residual deformation characteristics of soil and rock materials.

After the models of Taniguchi and the Water Conservancy and Hydropower Research Institute were proposed, Jia, Kong [10], Chi [9] and others, based on the residual strain characteristics of different soil materials in triaxial tests, added the influence of dynamic stress level (τ_d/σ_m) and consolidation stress state (σ_3 and S_l) on the residual strain characteristics on the basis of considering the influence of

dynamic stress ratio on the residual strain characteristics, and improved the degree of description of the experimental characteristics of dynamic residual deformation characteristics to a certain extent.

However, there are still shortcomings in this type of model. The regularity of model parameters with the number of vibrations is poor, which can easily lead to interpolation errors and affect the understanding of patterns. The China Institute of Water Resources and Hydropower Research (abbreviation IWHR) model considers the relationship between dynamic stress ratio $\left(\Delta\tau/\sigma_0'\right)$ and residual strain $\varepsilon_r$under a certain number of vibrations. Confining pressure, consolidation ratio, and vibration frequency are only reflected as reference variables in the experimental parameters and are described through multiple differences. However, in literature [6], there is no obvious regularity in the parameters. Although the improved model considers the influence of confining pressure and consolidation stress state (τ_d/σ_m) based on the level of dynamic stress, the parameter regularity in literature [9] is still poor, and both models still need to be improved.

2.2. Cycle-residual strain model

The analysis idea of the cycle-residual strain model is by observing the change law of the whole vibration process of a certain soil material under the experimental conditions of residual deformation characteristics, the relationship between the vibration cycle and the residual strain is determined, and the relationship between the influencing factors and the parameters of the relationship is established. This kind of model is mainly represented by Shen model [8], and its formula for calculating residual shear strain and residual volumetric strain is as follows:

$$\varepsilon_{vr} = c_{vr} log(1+N) \tag{6}$$

$$\gamma_r = c_{dr} log(1+N) \tag{7}$$

$$c_{vr} = c_1 \gamma_d^{c_2} exp(-c_3 s_l^2) \tag{8}$$

$$c_{dr} = c_4 \gamma_d^{c_5} s_l^2 \tag{9}$$

In the formula, ε_{vr} and γ_r represent the residual volumetric strain and residual shear strain, respectively. c_{vr} and c_{dr} represent respectively the residual volumetric strain parameter and residual shear strain parameter. γ_d represents the amplitude of dynamic shear strain. c_1,c_2,c_3,c_4 and c_5 are model parameters determined by fitting the experimental results. The model takes dynamic shear strain γ_d and vibration frequency N as independent variables, considers the influence of shear stress level s_l, and only requires one set of parameters to obtain the residual strain under different confining pressures and consolidation ratios.

The cycle-residual strain model considers the effects of dynamic shear strain γ_d and stress level S_l. It utilizes a semi-logarithmic relationship to describe the relationship between residual shear strain, residual volumetric strain, and vibration cycles. Ling [11] uses consolidation ratio K_c instead of stress level; Wang [12] considers both the effects of stress level and consolidation ratio; Zhu [13] uses dynamic stress level τ_d/σ_m, average principal stress σ_m, and stress level S_l to describe residual deformation characteristics. Zhu [14] and others propose using relative deviatoric stress level D^* to comprehensively describe the state of dynamic stress and consolidation stress.

However, the regularity of this type of model is relatively poor compared to the dynamic stress-(residual) strain model. Shen Zhujiang model, in literature [8,15], although the simulation results have a high degree of consistency with the experimental results when describing coarse-grained materials and rockfill materials, there is a significant deviation when describing coarse-grained materials containing fine materials, at a small number of vibration cycles or when the number of vibration cycles is greater than 25; although literature [11,12] has made corrections to the Shen model, there is still significant dispersion at high vibration cycles.

A review of the descriptions of the two major types of models in the above literature indicates that enhancing the key influencing factors can effectively elevate simulation accuracy. Integrating consolidation stress considerations into models that only account for dynamic stress conditions significantly enhances the representation of experimental residual deformation characteristics [9]. Ling [11], Wang [12], Zhu [13], Zhu [14], among others, all enhanced the representation of residual strain characteristics in different soils by expanding the range of influencing factors considered, thereby improving the responsiveness of experimental features. Therefore, before proposing a new model, it is essential to first analyze the mechanisms of action of various influencing factors and determine how parameters affect residual strain. Ultimately, by utilizing soil test results from actual engineering projects, a new residual strain model is formulated.

3. MECHANISM ANALYSIS AND ESTABLISHMENT OF NEW MODEL

This section integrates existing research with the findings from indoor tests on the residual deformation characteristics of an actual deep overburden layer to analyze the mechanisms of various factors and deduce a new model. The site's overburden has a maximum thickness exceeding 500 meters and is divided into four major layers and six sub-layers based on its material composition, hierarchical structure, cause of formation, age, and distribution. The third layer consists of sand, while the second layer is composed of coarse gravel.

3.1. Cycle-residual strain model

Studies have shown that the residual deformation characteristics of coarse-grained soils are influenced by multiple factors, namely: (1) soil properties, including soil type, density, particle size distribution, and water content. (2) consolidation stress state, encompassing confining pressure and consolidation stress ratio. (3) applied dynamic load and drainage conditions, including dynamic stress amplitude, number of vibration cycles, dynamic load waveform and frequency, and drainage conditions. This paper primarily analyzes the consolidation stress state and dynamic load conditions featured in the model from the IWHR and its subsequent improvements.

3.1.1. *Dynamic stress ratio*

The dynamic stress ratio represents the ratio between the amplitude of cyclic dynamic load and the confining pressure. A higher dynamic stress ratio corresponds to a larger vibration load, more significant disturbance of soil and rock materials, and greater residual strain [4]. Based on the model from the IWHR, the indoor test data for coarse gravel material in overburden layer ② are organized, as depicted in Fig. 1 and Fig. 2. Fig. 1 presents the axial residual strain test curve for sand-gravel material in layer ② under effective confining pressure $\sigma_3' = 1000\,kPa$ and a fixed consolidation ratio $K_c = 1.5$. The findings indicate that for the same soil material and consolidation stress state, a higher dynamic stress ratio leads to greater residual shear strain. Similarly, Fig. 2 illustrates the residual volumetric strain test curve for sand-gravel material in layer ② under effective confining pressure $\sigma_3' = 1000\,kPa$ and consolidation ratio $K_c = 2.5$, corroborating the results presented in Fig. 1.

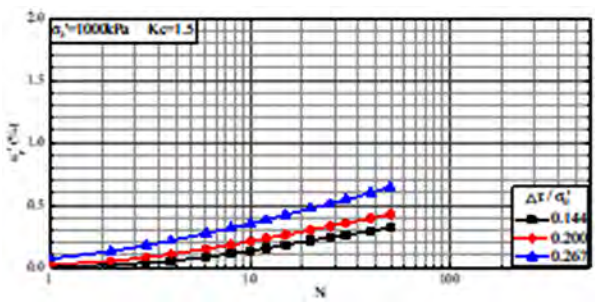

Fig. 1
Residual Shear Strain Test Curve for Sand-Gravel Material in Layer ②

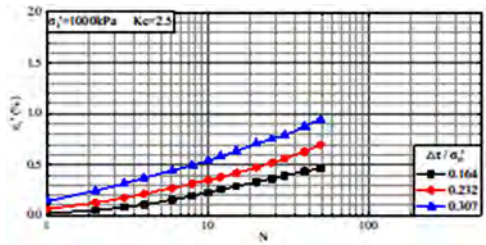

Fig. 2
Residual Volume Change Test Curve for Sand-Gravel Material in Layer ②

3.1.2. *Consolidation stress ratio*

Numerous studies and practical engineering experiences have demonstrated that the consolidation stress ratio significantly influences the development of residual shear and volumetric strains in soil and rock materials. Under specific conditions, as the consolidation stress ratio rises, the axial strain of soil and rock materials increases, while the volumetric strain slightly decreases. As the consolidation ratio increases, both residual axial and volumetric strains increase. The results are presented in Fig. 3 and Fig. 4.

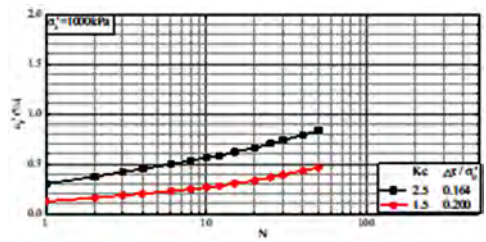

Fig. 3
The relationship between residual shear strain and consolidation ratio of layer ②

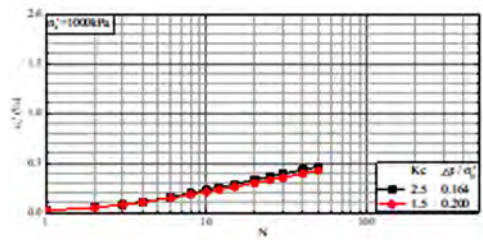

Fig. 4
The relationship between residual body strain and consolidation ratio of layer ②

3.1.3. *Confining pressure*

The higher the confining pressure before dynamic load application, the denser the specimen becomes, making the soil and rock particles less prone to overturning, thereby leading to smaller residual strains under certain conditions. For specific numbers of vibrations and various confining pressures, patterns in residual axial and volumetric strains of sand-gravel materials with dynamic shear stress show that with a fixed consolidation ratio, number of vibrations, and dynamic load, higher confining pressure leads to smaller residual strains in coarse-grained materials [4]. Fig. 5 and 6 depict the residual strain curves for layer ② sand-gravel materials with a consolidation ratio of 2.5 under various confining pressures. With roughly the same dynamic stress, higher confining pressure results in smaller residual strains. The close residual axial strain results at confining pressures of 2000 kPa and 3000 kPa in Fig. 5 primarily stem from the fact that high confining pressure corresponds to high dynamic stress, leading to substantial overlap without compromising the overall understanding of the trends.

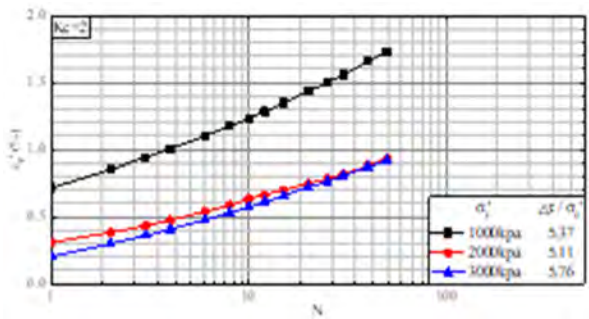

Fig. 5
The relationship between residual shear strain and confining pressure in layer ②

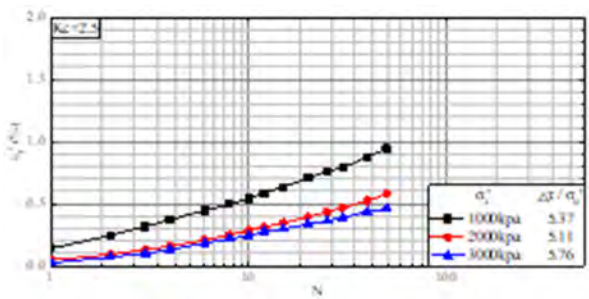

Fig. 6
The relationship between residual body deformation and confining pressure in layer ②

3.2. Derivation process of the new model

For uniform soil with consistent properties, the dynamic stress ratio and confining pressure are the primary factors influencing the residual shear and volumetric strains in sand-gravel materials. The consolidation ratio notably affects the residual shear strain of sand-gravel materials. Thus, the new model is deduced based on the following two aspects:

As illustrated in Fig. 1 and Fig. 2, under specific vibration cycles, the dynamic stress ratio or dynamic stress demonstrates a significant power index relationship with the axial residual strain or residual volumetric strain, as presented in Fig. 7. The data in this figure were organized based on formula (3), highlighting a positive correlation between residual strain and dynamic stress. However, Fig. 5 and Fig. 6 show an opposite trend, revealing a negative correlation between residual strain and confining pressure. The greater the confining pressure, the lower the residual strain. Consequently, an analysis of influencing factors reveals that dynamic stress and consolidation stress conditions (confining pressure) must be distinguished to enhance the model description and ensure greater parameter consistency.

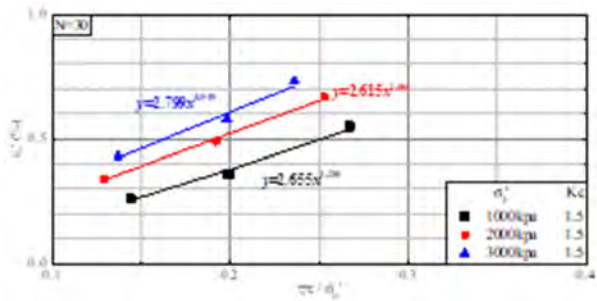

Fig. 7
The model relationship of the original water science and technology for layer ② sand and gravel material

As shown in Fig. 3 and 4, for layer ② sand-gravel material, the consolidation ratio significantly affects residual axial strain, while its impact on residual volumetric strain is negligible. In triaxial tests, the relationship between static shear stress levels and consolidation ratio can be determined using formula (10).

$$S_l = \frac{\tau}{\tau_f} = \frac{\frac{1}{2}(K_c - 1)\sigma_3}{\sigma_3 \tan \varphi} = \frac{K_c - 1}{2 \tan \varphi} \tag{10}$$

$$\varepsilon_p = f\left(S_l^a\right) \tag{11}$$

$$\varepsilon_v = f\left(S_l^a\right) \tag{12}$$

3.3. Introduction of a new model and analysis of its principles

In light of the aforementioned points, the new model can be represented in the format of equations (13) and (14):

$$\varepsilon_p = K_p \frac{(\Delta\tau/P_a)^{n_p}}{I_1/P_a} S_l^a \tag{13}$$

$$\varepsilon_v = K_v \frac{(\Delta\tau/P_a)^{n_v}}{I_1/P_a} S_l^a \tag{14}$$

In the formula, ε_p and ε_v respectively denote axial residual strain and residual volumetric strain; $\Delta\tau$ denotes dynamic stress; I_1 denotes the first stress invariant; S_l represents the level of static shear stress; P_a represents atmospheric pressure; K_p,n_p,K_v and n_v are model parameters derived from experimental results, and the coefficient a is obtained through correlation coefficients.

1. Model Law

   With I_1 and S_l remaining constant, the residual strain demonstrates a power-law relationship with dynamic stress, aligning with the patterns depicted in Fig. 1 and Fig. 2. When $\Delta\tau$ and I_1 remain constant, there is a positive correlation between residual strain and static shear stress levels. For $\Delta\tau$ and S_l, the residual strain demonstrates an inverse proportional relationship with the first stress invariant, mirroring the confining pressure characteristics shown in Fig. 5 and Fig. 6. Thus, the formula can theoretically capture all the characteristics of the experimental curves mentioned above.

   However, in equations (13) and (14), the coefficient a requires determination via correlation coefficients and is directly linked to the consolidation ratio. Different consolidation ratios result in varying values of a, significantly complicating the model's use. Normalization could be applied to establish a relationship between coefficient a and the consolidation ratio, as illustrated in the following equation:

$$a = f(Kc) \tag{15}$$

2. Model Correction

   Fig. 8 illustrates the residual strain behavior of layer ② sand-gravel material at 12 vibration cycles, as per formula (13). Test points are positioned on either side of the characteristic curve based on the consolidation ratio, with higher ratios above and lower ratios below. To enhance fitting accuracy and develop relationships across various consolidation ratios, the data must be realigned, necessitating revisions to formulas (13) and (14).

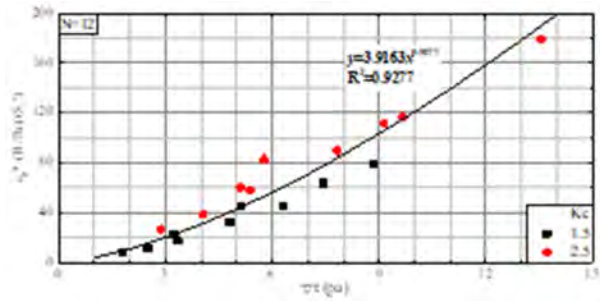

Fig. 8
The axial residual strain test characteristics of layer ② sand-gravel material are described by equation (13)

To normalize various consolidation ratios, we must establish the relationship outlined in equation (15). Choose the inverse proportional function from among the basic functions, and adjust equations (13) and (14) to (16) and (17):

$$\varepsilon_p = K_p \frac{(\Delta\tau/P_a)^{n_p}}{I_1/P_a} S_l^{a/Kc} \tag{16}$$

$$\varepsilon_v = K_v \frac{(\Delta\tau/P_a)^{n_v}}{I_1/P_a} S_l^{a/Kc} \tag{17}$$

4. MODEL APPLICATION AND ANALYSIS

4.1. Data foundation

The experimental protocol is presented in Table 1. To ensure consistent experimental conditions, the soil materials selected are all characterized by good drainage properties.

Table 1
The test soil and experiment scheme

SAMPLE NUMBER	SOIL TYPE	CONSOLIDATION RATIO Kc	CONFINING PRESSURE (kPa)	
②	coarse gravel	1.5/2.5	1000/2000/ 3000	Each set of tests should include at least three sets of dynamic stress results.
③-1	Medium coarse sand	1.5/2.0	800/1300	
			1900/2500	

4.2. Analysis of correlation coefficient

Initially, this model necessitates correlation coefficient analysis to standardize the tests across various consolidation ratios. Initially, determine the suitable number of vibration cycles for the correlation coefficient analysis (refer to reference [6] in this article). Subsequently, organize the test data corresponding to the selected cycles. Lastly, make an informed choice based on the correlation coefficient for subsequent in-depth analysis. The analysis outcomes are depicted in Fig. 9.

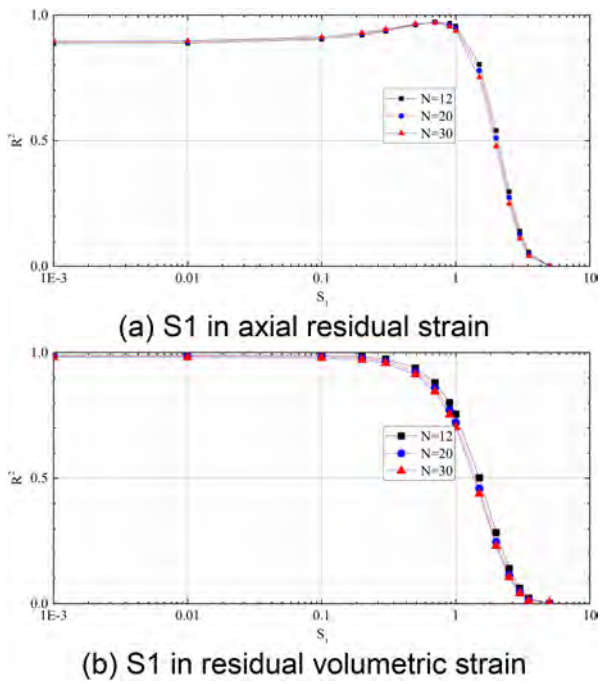

Fig. 9
Residual strain characteristics of layer ② sandy gravel material

The model results exhibit a high degree of alignment with the experimental findings and conclusions. (1) The consolidation ratio or static shear stress level significantly affects the axial residual strain of layer ② sand-gravel material, with a=0.7; (2) The impact of the consolidation ratio or static shear stress level on the residual volumetric strain of layer ② sand-gravel material can be largely disregarded. The value of a remains relatively stable within the range of 0.001 to 0.1, and it is suggested to a=0.01 for volumetric strain, based on 12 cycles as an example.

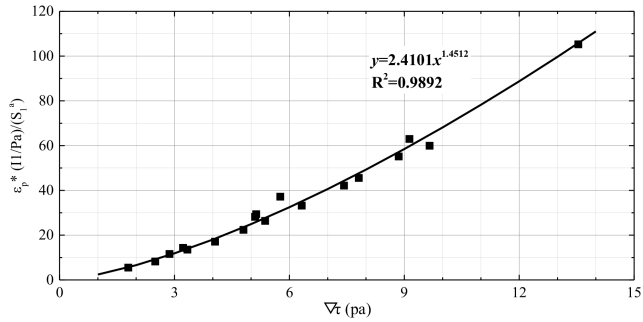

（a）*a*=0.001

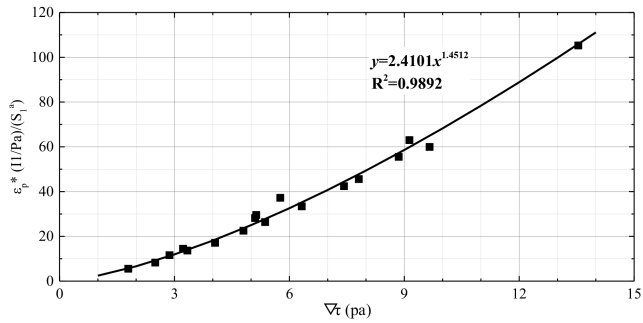

（b）*a*=0.01

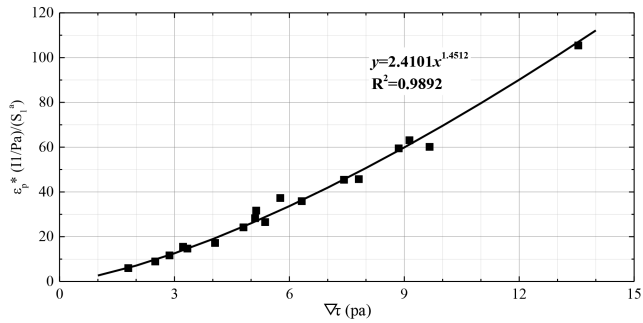

（c）*a*=0.1

Fig. 10
Characteristic description of residual volumetric strain tests for sand-gravel materials in layer ② at different a values

4.3. Analysis of the patterns for coefficient K and exponent n

Based on the Selected Value of *a*, the Residual Strain Parameters are Calculated at a Certain Number of Vibration Cycles. These include Axial Strain Parameters K_p and n_p, as well as Volumetric Strain Parameters K_v and n_v. The Results are Shown in Fig. 11.

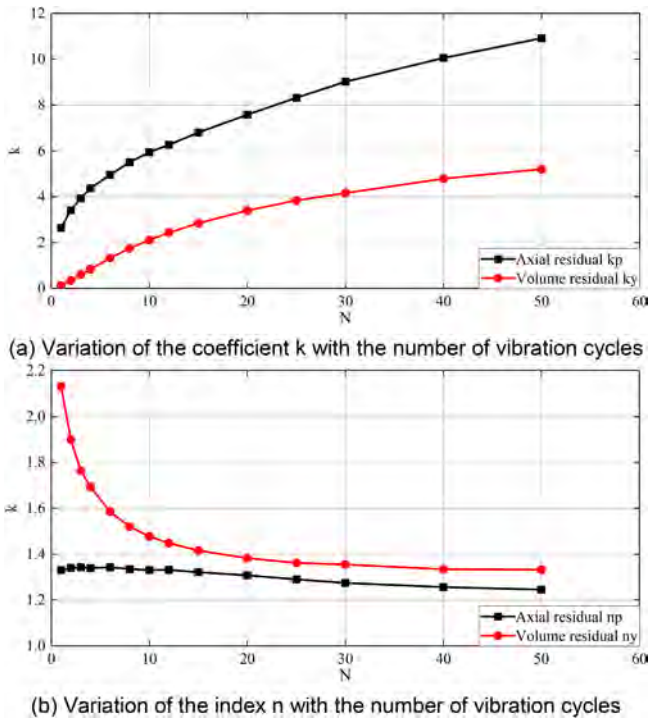

Fig. 11
Variation curves of coefficient k and index n for sand-gravel material in layer ② with the number of vibration cycles

Both the coefficient *K* and the index *n* demonstrate monotonic changes. The value of the coefficient k changes relatively gently. At the same number of cycles, the coefficient K_p for residual axial strain is significantly larger than that for residual volumetric strain K_v, adhering to the principle that axial strain is greater than volumetric strain. Both the index n for residual axial strain and residual volumetric strain

decrease monotonically. The initial change in residual volumetric strain is large, followed by a smaller change. This is because during the test, the residual volumetric strain changes dramatically at the beginning. As the number of vibration cycles increases, the soil sample gradually becomes denser. Due to the occlusive phenomenon between soil particles, structural properties emerge, leading to smaller volume changes and a gradual stabilization of the index n_p for residual axial strain. During the triaxial vibration process, there was no sudden instability in this experiment.

The variations of coefficient K and exponent n accurately describe the specimen's changes during vibration, thereby further clarifying the significance of the model parameters in this study. All parameters mentioned above were determined using the gravel material from layer ②. This study also simulated the medium-coarse sand in layer ③-1 using the same method, determining the axial variation coefficient a=0.3 and the volumetric variation coefficient a=0.1 through the correlation coefficient method. The variations of coefficient k and exponent n are illustrated in Fig. 12.

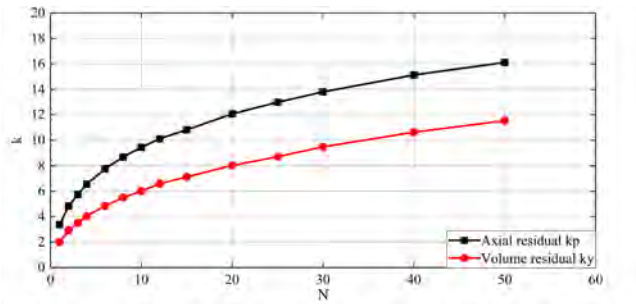

(a) Variation of the coefficient k with the number of vibration cycles

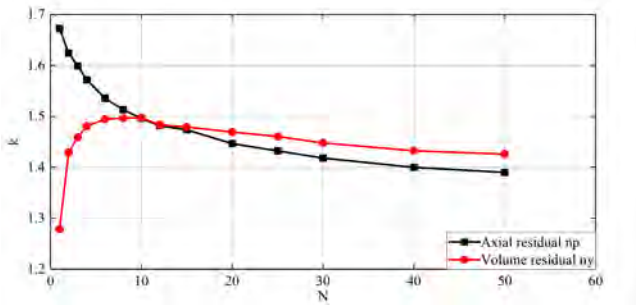

(b) Variation of the index n with the number of vibration cycles

Fig. 12
Variation curves of coefficient k and index n for sand-gravel material in layer ③ with the number of vibration cycles

The trend in coefficient k closely mirrors that of the sand-gravel material, aligning with the general pattern where axial strain exceeds volumetric strain throughout the testing. The exponent n for residual volumetric strain exhibits anomalies during the first 5 vibration cycles. Following the onset of axial strain, both volumetric and axial strains stabilize after 5 cycles.

5. RESULTS AND DISCUSSION

The model presented herein demonstrates optimal performance when applied to sandy gravel and medium-coarse sand. This enhanced model exhibits robust applicability to soil materials under well-drained conditions. Considering the aforementioned simulation outcomes, this model possesses the following advantages: (1) This model precisely defines the significance of each parameter, incorporating dynamic and consolidation stress state parameters in the analysis of soil sample variations during residual deformation tests, thereby enhancing physical clarity. The relationship between parameters and vibration cycles is more pronounced, enhancing the model's overall comprehensibility and providing more reliable data for interpolation calculations.

ACKNOWLEDGMENTS

The authors are grateful for the financial support from the the scientific achievement transformation foundation of China Institute of Water Resources and Hydropower Research (GE121003A0032022, GE121003A0032024) ; The Independent Research Project of State Key Laboratory of Simulation and Regulation of Water Cycle in River Basin (SKL2022ZD05).

REFERENCES

[1] JIA J.S. Construction of dams in China and the world in 2005[C]. Yunnan, Kunming, China, 2006:5.

[2] ZHAO J.M., WANG W.S., CHANG Y.P. 3-D authentic nonlinear method for dynamic analysis of high CFRD[J]. *Journal of Hydraulic Engineering*, 2003 (09): 12–18.

[3] LIU H.L. The permanent deformation of soil [J]. *Advances in Science and Technology of Water Resources*, 1995, 15(4): 23–29.

[4] WANG T.B., FU Z.Z., CHEN S.S., HAN HUA-QIANG. Residual deformation model for rock-fill materials[J]. *Chinese Journal of Geotechnical Engineering*, 2016, 38(08): 1399–1406.

[5] TANIGUCHI E.W.R.V.M. Prediction of earthquake-induced deformation of earth dams[J]. *Soils and Foundations*, 1983,23(4):126–132.

[6] ZHAO J.M., CHEN N., CHANG Y.P., LIU Y.L. Study on earthquake-induced permanent deformation of Longshou CFRD[J]. *World Earthquake Engineering*, 2003, 19(04): 57–62.

[7] WANG K.Y., CHANG Y.P., CHEN N. Residual deformation characteristics of coarse-grained soils under cyclic loading[J]. *China Civil Engineering Journal*, 2000, 33(03): 48–53.

[8] SHEN Z.J., XU G. Deformation behavior of rock materials under cyclic loading [J]. *Journal of Nanjing Hydraulic Research Institute*, 1996(02): 143–150.

[9] CHI S.C., LV X.L. A study of size effect and boundary effect in centrifugal tests [J]. *Chinese Journal of Geotechnical Engineering*, 2016, 38(02): 370–376.

[10] JIA G.X., KONG X.J. Study on residual deformation characteristics of coarse-grained soils[J]. *Chinese Journal of Geotechnical Engineering*, 2004, 26(01): 26–30.

[11] LING H, FU H, CAI Z.Y., LIU H.L. Experimental study on dynamic residual deformation characteristics of dam materials[J]. *Journal of Hohai University (Natural Sciences)*, 2010, 38(5): 532–537.

[12] WANG Y.Z., CHI S.C., SHAO LEI, YANG XIN-GUANG. Residual deformation behavior of rockfill materials and sensitivity analysis of parameters[J]. *Rock and Soil Mechanics*, 2013, 34(3): 856–862.

[13] ZHU S, ZHOU J.B. Deformation behavior of coarse-grained materials under cyclic loading[J]. *Rock and Soil Mechanics*, 2010, 31(05): 1375–1380.

[14] WANG L, ZHU B, LAI X.H. Cyclic accumulative deformation of sand and its explicit model[J]. *Chinese Journal of Geotechnical Engineering*, 2015, 37(11): 2024–2029.

[15] ZOU D.G., MENG FW., KONG X.J., XU B. Residual deformation behavior of rock-fill materials[J]. *Chinese Journal of Geotechnical Engineering*, 2008, 30 (6): 807–812.

Q.111 - R.50

COMMISSION INTERNATIONALE DES
GRANDS BARRAGES

VINGT-HUITIEME CONGRES DES
GRANDS BARRAGES
CHENGDU, MAI 2025

SEISMIC ANALYSIS OF THE HORKA DAM: LOAD ESTIMATION FOR EARTHQUAKE SWARMS (*)

Miroslav BROU EK
Assistant professor, CTU in Prague, Faculty of Civil Engineering

Petra SUCHOÁRKOVÁ
Head of the Dpt. of Dam Surveillance, Povodí Ohře, State Enterprise

Ondřej ŠVARC
Head of the Dpt. of Earthfill Dams and Tailings Dams, VODNÍ DÍLA – TBD, JSCo

CZECH REPUBLIC

SUMMARY

The Horka Dam is the closest among the large dams suited in western Bohemia to the epicentres of earthquake swarms. To improve the dam safety supervision programme, a cooperation with the Institute of Geophysics of the Czech Academy of Sciences (GFÚ) was established in 1998, consisting of transferring information about seismic events. The Horka dam gradually became an important object of the applied research in the seismic area of western Bohemia/Vogtalnd carried out by the GFÚ as the mechanics of the origins of the earthquake swarms are not fully comprehended. Despite nearly constant activity at the intersection of faults, the earthquakes observed during the 20th century were of small magnitudes and intensities. A paleoseismic study, however, revealed significant soil deformation attributed to an earthquake with a local magnitude over 6.5. The Horka dam is located approximately 20km from the centre of the most active part of the fault so a new seismograph was installed in the lowest part of the grouting gallery in 2017 and

Analyse seismique du barrage Horka – Estimation des charges pour les essaims sismiques

 DOI: 10.1201/9781003642428-147

4 new accelerometers were installed in 2019-2020 as part of the development of the WEBNET monitoring network. In 2021, the dam operator introduced continuous monitoring of the levels in hydrogeological boreholes that have proven to respond to earthquakes in the past. The results of the seismic measurements were statistically evaluated in 2023 and together with accelerograms from the course of actual earthquakes and available European PSHA models provide the input data for the deformation and stability analysis of the Horka dam, which is carried out by the Department of Hydraulic Structures at the Faculty of Civil Engineering of the Czech Technical University in Prague. The paper focuses on the selection process of applied seismic loading with an abundance of the available PSHA with respect to the limited historical information and lack of understanding about the mechanics of the earthquake swarms. Dam behaviour during recent earthquakes as well as measured response of the dam to natural seismic background and liquefiable potential resulting from the soil characteristics is presented.

RÉSUMÉ

Parmi les grands barrages de l'ouest de la Bohême, le barrage Horka est, en raison de sa position, le plus proche des épicentres des essaims sismiques. Le barrage est formé d'une massif en terre avec un corroi central en argile. Pour une meilleure performance du contrôle technique et de la sécurité, une collaboration a été nouée en 1998 avec l'Institut de géophysique (GFÚ) de l'Académie des sciences de la République tchèque, consistant dans un échange d'informations sur les événements de caractère sismique. Le barrage de l'ouvrage hydraulique Horka a progressivement été placé au centre d'intérêt des spécialistes du GFÚ en tant qu'ouvrage important pour la recherche appliquée dans la zone d'activité sismique de Bohême de l'Ouest, car le mécanisme de naissance des essaims sismiques n'est pas encore bien expliqué. Malgré une activité quasi-continue au contact des failles, la magnitude et les intensités de tous les séismes observés au 20^{e} siècle ont été faibles. Cependant, une récente étude paléo-sismique a mis à jour des déformations de la terre dues à un séisme d'une magnitude supérieure à 6,5. Le barrage se trouve approximativement à 20 km du centre de la partie la plus active de la faille et c'est pourquoi un sismographe a été installé en 2017, dans le cadre du développement du réseau de contrôle WEBNET, dans la partie la plus basse de la galerie d'injection, 4 accéléromètres ayant été placés en 2019-2020. L'exploitant de l'ouvrage hydraulique a mis en place en 2021 un contrôle continu des niveaux dans les forages hydrogéologiques pour lesquels une réaction aux séismes a été enregistrée dans le passé. Les résultats des mesures sismiques ont été traités de manière statistique en 2023, évalués et, avec les accélérogrammes au cours des séismes réels et les modèles européens disponibles de menace sismique, ils servent de base pour l'élaboration d'une analyse de la déformation et de la stabilité de l'ouvrage hydraulique de Horka, réalisée au sein de la Chaire d'hydrotechnique de la Faculté de génie civil de l'Université polytechnique de Prague (ČVUT). L'article

traite de la détermination de la charge sismique en cas de surabondance de modèles disponibles de menace sismique, eu égard aux informations historiques limitées et à la compréhension des mécanismes de naissance des essaims sismiques. En outre, il présente une mesure de la réaction du barrage aux vibrations sismiques naturelles, le potentiel de liquéfaction des terres du barrage et le comportement du barrage au cours des séismes récents.

1. INTRODUCTION

The Horka Dam was built in the second half of the 1960s in the “close” vicinity of the Mariánské Lázn Fault, one of the few significantly seismically active areas in the Czech Republic. The active part of the fault, which is oriented SSW-SSE and is therefore almost parallel to the axis of the Horka dam, is approximately 20 km long and the location of the epicentres of the earthquakes recorded between 1995 and 2022 relative to the Horka dam are visible on the following map (Fig. 1). Although the map of seismically active areas according to the outdated ČSN 73 0036 Seismic loads on structures [1] assumes for the area the 7th intensity degree of earthquakes

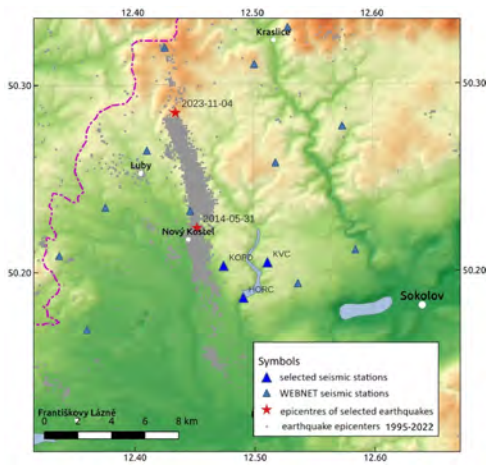

Fig. 1
Position of the Horka dam (HORC station) to the epicentres of earthquakes and seismic stations - the active extent of the Mariánské Lázn fault [3].
Position du barrage de Horka (station HORC) par rapport aux épicentres des tremblements de terre et aux stations sismiques - l'étendue active de la faille de Mariánské Lázn [*3*].

according to the Mercalli-Cancani-Sieber scale (M.C.S). According to a recent paleo-seismic study [2], earthquakes greater than M_L = 6.5 have been identified around the location between the years 792 CE and 1020 CE with soil displacements of 29-39 cm. The strongest tremor recorded by the WEBNET seismic station network, initiated after a significant earthquake swarm in late 1985 and early 1986, occurred in May 2014 with a local magnitude of M_L = 4.3.

2. IMPACTS OF EARTHQUAKES ON EARTHFILL DAMS AND HISTORICAL EXPERIENCE N

Historical records of earthquake-related failures and failures of earthfill embankments contain several failure mechanisms for which current methods can be used to validate them through theoretical procedures and modelling or analysis of experimental data. The following table (Table 1) provides an overview of the observed effects of earthquakes on earthfill embankments. Note: For rockfill dams, issues dealing with the liquefaction of the dam or parts of the dam due to an increase in pore pressures can be excluded from the assessment. The number of earthquake-related accidents and failures of rockfill dams is generally significantly lower compared to earthfill dams [4].

Table 1
Consequences of the earthquake and Horka Dam
Conséquences du séisme et du barrage de Horka

DESCRIPTION OF THE IMPACT ON THE DAM	APPLICABILITY AT HORKA DAM	VERIFICATION METHOD
Loss of stability (sliding) of an upstream or downstream slope or its part, including foundation, if applicable	YES	PSA, NM
Unacceptable settlement leading to overtopping and/or cracks with uncontrolled seepage	YES	SMDA, NM
Liquefaction or sliding due to pore pressure increase	YES	EM
differential deformations near fault under the dam body	NO	IGP, PS
Overtopping due to impact waves resulting from sliding or avalanches into the reservoir area	YES	NM, EM
Damage of the outlet structures or excessive seepage through the impervious element/core	YES	SMDA, NM

Legend: PSA … pseudo-static analysis, NM … numerical methods, SMDA … simplified methods of dynamic analysis, EM … empirical methods, IGP … geotechnical survey, PS … paleoseismic studies

While for earthquake-induced accidents, the most common damage mechanism cannot be easily determined, the most common damage mechanism for failures is liquefaction, which is particularly relevant for saturated sandy and gravelly soils [5]. For example, in the 1939 Ojika earthquake in Japan, 12 failures of earthfill dams made of sandy soils occurred due to liquefaction, and another 40 embankments made of similar material experienced slope failures, while dams made of clayey soils that were even closer to the epicentre were not significantly damaged [6].

The effect on the surface of an earthquake generally depends on the nature of the fault [7]. Typical tectonic earthquakes are manifested by a mainshock, which causes most of the damage, followed for months to years by so-called aftershocks, a series of weaker tremors [8]. However, in the subject area affecting the Horka VD, so-called earthquake swarms occur, for which the physical processes of their formation are not fully understood, which introduces some uncertainty in the determination of the design characteristics of the seismic load. Swarms are characterized by the generation of hundreds to thousands of tremors over days to months of activity [9].

3. DESIGN SEISMIC LOAD

As in the case of other loads and dam response (uplifts, seepage pressures through the dam body, etc.), there has been a gradual evolution in the determination of design values of seismic loads and the methods of determining the structural response in the case of earthfill dams. Due to the expansion of monitoring networks, in the Erzgebirge area of the WEBNET network, there is a significant reduction of epistemic uncertainty in determining the probability of exceedance of the studied phenomena. The increasing requirements for dam safety, to which we have become accustomed in the area of flood safety, are now being applied also to the design and especially the assessment concerning seismic loads. At the same time, a longer series of observed earthquakes, and thus directly measured accelerograms, are available for use in calibrating structural response models and a broader knowledge base in assessing the risk of liquefaction.

3.1. Czech republic – historical development

The seismic activity in the Cheb region did not represent a significant challenge for dam construction in the territory of the present-day Czech Republic until the beginning of the second half of the twentieth century when the construction of

three major dams began. These were the Jesenice Dam, built in 1957-1961, the Skalka Dam (1962-1964) and the Horka Dam (1966-1970). While the Skalka dam is an asphalt-facing rockfill dam (AFRD), the other two dams are earthfill dams with fine-grained soil cores. However, during the implementation of the Horka Dam, neither the requirements for shear or strength characteristics of the soils were specified (only the grading curve range, compaction and saturated hydraulic conductivity), nor were stability calculations [10] performed to deal with the potential seismic loading, although limit equilibrium methods still in use today were available. After 1970, publications on dam design started to work with the seismic coefficient (k_h - horizontal), which is defined as the ratio of seismic and gravitational acceleration. The values of k_h recommended for the territory of the Czech Republic are in the range of 0.08 - 0.1, i.e. a = 0.8 to 1.0 $m.s^{-2}$, which corresponded to the basic seismic coefficient K according to [1] for 8 to 9 degrees of earthquake intensity according to the M.C.S. scale.

3.2. Current standards in CR and ICOLD recommendations

According to the valid Czech standard ČSN 75 2310 Embankment dams [11], the load from an earthquake up to 8° MSK 64 (Medvedev-Sponheuer-Kárník) must be considered in the stability assessment. However, this is a degree of earthquake intensity that can only be converted to ground acceleration at the dam site using approximate tables, e.g. according to [12], 8° MSK 64 would correspond to a peak acceleration of 2.0 $m.s^{-2}$, i.e. a factor k_h=0.2.

The current international practice [13] in selecting design values of seismic loads uses two design values for the analysis concerning the probability of their occurrence during the design lifetime of the dam and the allowable damage. Thus, using the analogy to the Czech approach to the flood safety of dams, these are the “design” (Operating Basis Earthquake - OBE) and “control/evaluation” (Safety Evaluation Earthquake - SEE) earthquakes. For OBE, the requirement for a 50% probability of exceedance over 100 years has been established, corresponding to a 145-year return period and an annual exceedance probability of 6.9‰. The OBE-level earthquake must not cause significant damage to the dam or appurtenant structures. Methods for SEE determination vary in different countries mainly depending on the assessment of the potential damage due to failure or allowable risk. An analogy with floods due to breach waves in the Czech Republic would mean using earthquake values with a recurrence period of 10,000 years for Class I and II dams from the perspective of potential damage and dam safety monitoring and 1,000 years for Class III dams using a deterministic approach in the assessment. The loads due to the SEE must not cause the failure of the dam body, i.e. the occurrence of a Type 1 special flood (Breach wave due to complete dam failure in Czech terminology). In the case of earthfill embankments, this requires additional slope stability requirements at potential slip surfaces that threaten the overall

stability of the dam, limits in deformations that would result in overtopping at normal water level or cracking accompanied by uncontrolled seepage, liquefaction of the entire dam body, or part of the embankment or subsoil, and damage to appurtenant structures which would endanger the embankment.

3.3. Seismic hazard models for Horka dam

Available probabilistic seismic hazard analysis (PSHA) models, including the national annexe to Eurocode 8, were used to determine the design peak ground accelerations (PGA) for the Horka Dam. Their comparison can be seen in the following figure and the values from the table below.

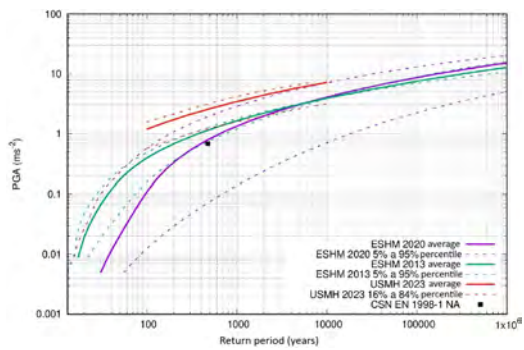

Fig. 2
Available PSHA for Horka Dam – for final assessment the ESHM 2013 (green curve) was used [3].
PSHA disponible pour le barrage de Horka - pour l'évaluation finale, l'ESHM 2013 (courbe verte) a été utilisé [*3*].

Table 2
Values of peak ground accelerations (PGA v $m.s^{-2}$) according to the available PSHA for Horka Dam and selected recurrence intervals in years – values used for the assessment are in bold.
Valeurs des accélérations maximales du sol (PGA v $m.s^{-2}$) selon le PSHA disponible pour le barrage de Horka et les intervalles de récurrence sélectionnés en années - les valeurs utilisées pour l'évaluation sont en gras.

RETURN PERIOD	ESHM 2013	ESHM 2020	USMH 2023
100	0,40	0,11	1,19
1000	1,65	1,34	3,44
10000	3,90	4,10	7,25

4. HORKA DAM EARTHQUAKE RESPONSE – MEASURED DATA

In April 2022, with the help of 23 seismic probes, the Geophysical Department of the Academy of Sciences of the Czech Republic measured the natural seismic vibrations of the body. The figure below (Fig. 3) shows the amplification of the motions relative to reference stations located on the right abutment 110 m upstream and 250 m downstream of the dam. The scale is plotted for a frequency of 3.12 Hz, which is also the first fundamental resonance frequency of the dam. The amplification of the motions/shocks is up to 20 times in the crest - the direction of the motions is perpendicular to the dam. At the second fundamental resonance frequency (3.46 Hz) in the direction parallel to the axis of the dam, the maximum amplification in the central part of the dam crest is tenfold. The strongest event observed since the installation of accelerometers at the Horka Dam occurred on 4.11.2023 with a local magnitude of 3.1 and a PGA perpendicular to the dam of 0.08 $m.s^{-2}$, which corresponds to an average recurrence time of 34 years.

Fig. 3
Relative amplification of the Horka Dam motions for the basic resonance mode with a frequency of 3.12 Hz [14].
Amplification relative des mouvements du barrage de Horka pour le mode de résonance de base avec une fréquence de 3,12 Hz [*14*].

4.1. Risk of liquefaction and characteristics of the soils in the embankment

Since the end of the 20th century, there have been major revisions in the approach to the risk of soil liquefaction due to dynamic stresses. The original criteria for the risk of liquefaction, plotted in the following figure (Fig. 4) against the grading curves of the soils used in the Horka Dam, are now considered too narrow, based on laboratory experiments and failure and accident analyses. Nevertheless, the soils used in the dam meet these criteria.

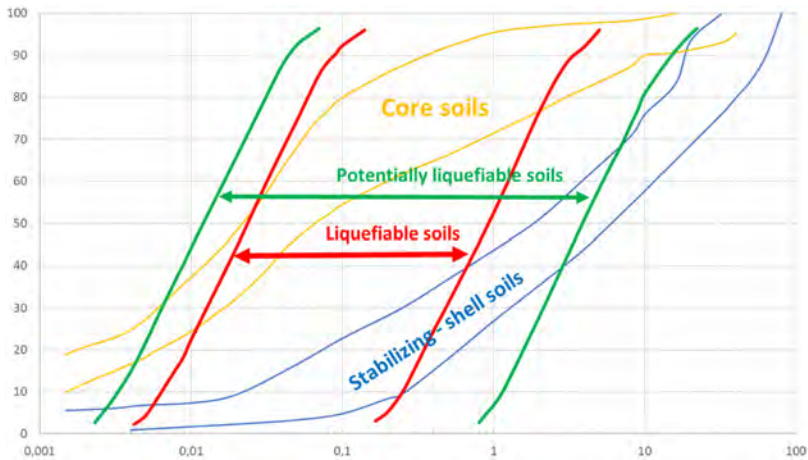

Fig. 4
Grading curves of the soils used for Horka Dam [10] and areas of soils subject to liquefaction (red) or threatened by liquefaction (green) [6].
Courbes granulométriques des sols utilisés pour le barrage de Horka [*10*] *et zones de sols sujets à la liquéfaction (rouge) ou menacés par la liquéfaction (vert)* [*6*].

5. CONCLUSION

The Horka Dam was constructed in a seismically active area in a way that corresponded to the then-current level of knowledge in terms of the dynamic loading on earth-filled dams, potential earthquake intensity and dam safety requirements. In all three aspects, there has been a significant development in understanding as well as assessment approach and safety requirements since the dam construction. Recent paleoseismic studies have confirmed the occurrence of extreme loads near the Horka Dam site and probabilistic seismic hazard analyses, using current levels

of knowledge, allow the determination of design seismic loads in line with the safety requirements of modern society. This paper presents information obtained from measurements directly on the dam during natural vibrations and during earthquakes.

REFERENCES

[1] CZECH STANDARD ČSN 73 0036 Seismic loads on structures (1975): Prague. The Czech Office for Standards, Metrology and Testing, 1975, 45 s. (In Czech language only).

[2] ŠT PANčÍKOVÁ, P., FISCHER, T., STEMBERK, J., NOVÁKOVÁ, L., HARTVICH, F., FIGUEIREDO, P.M. (2019): Active tectonics in the Cheb Basin: youngest documented Holocene surface faulting in central Europe? *Geomorphology*. 327 (2019). pp. 472–488.

[3] DOUBRAVOVÁ, J., BURJÁNEK, J. (2023): Seismic data for deformation and stability analysis of Horka Dam. Institute of Geophysics of the Czech Academy of Sciences Praha. 13 s. (In Czech language only)

[4] ICOLD BULLETIN 99 UPDATE (2019): Statistical analysis of dam failures. Paris: ICOLD – CIGB (preprint – ICOLD members only), 65 s.

[5] FELL, R., MACGREGOR, P., STAPLEDON, D., BELL, G. (2005): *Geotechnical Engineering of Dams*. London: Taylor & Francis Group plc., 912 s.

[6] TANCHEV, L. (2005): *Dams and Appurtenant Hydraulic Structures* 2nd Ed., London: Taylor & Francis Group plc., 1097 s.

[7] SHERARD, J.L., CLUFF, L.S., ALLEN, C.R. (1974): Potentially active faults in dam foundations. *Geotechnique.* 24(3). pp. 367–428.

[8] REITER, L. (1990): *Earthquake Hazard Analysis*, New York: Columbia University Press. 254 s.

[9] HORÁLEK J., FISCHER T., BOUŠKOVÁ A., MICHÁLEK J., HRUBCOVÁ P. (2009): The West Bohemian 2008-earthquake swarm: When, where, what size and data, *Stud. Geophys. Geod* (53), pp. 351–358.

[10] BARVÍNEK, R. (1969): SOKOLOVSKO Zeminy hráze 7273 - IN, Praha: Stavební geologie n.p., 24 s.(In Czech language only)

[11] CZECH STANDARD ČSN 75 2310 Embankment dams (2006): Prague. The Czech Office for Standards, Metrology and Testing, 2006, 36 s. (In Czech language only)

[12] NEWMARK, N., ROSENBLUETH, E. (1971): *Fundamentals of earthquake engineering*, New Jersey: Prentice-Hall. 640 s.

[13] ICOLD BULLETIN 72 Revised (2010): Selecting seismic parameters for large dams Guidelines. Paris: ICOLD – CIGB, 37 s.

[14] BURJÁNEK, J. (2023): Estimation of resonance characteristics of the dam body of the Horka Dam. Institute of Geophysics of the Czech Academy of Sciences. Prague. 2 s. (In Czech language only)

COMMISSION INTERNATIONALE DES
GRANDS BARRAGES

VINGT-HUITIEME CONGRES DES
GRANDS BARRAGES
CHENGDU, MAI 2025

AN OVERVIEW OF THE SAFETY SEISMIC ASSESSMENT OF 50+ LARGE DAMS ACCORDING TO THE NEW ITALIAN DESIGN STANDARDS (*)

Gianluca GATTO
Head of Dams and Geotechnics Department, Speri, Italy

Andrea ABATI
Head of Structures and Modelling Department, Gruner Stucky, Switzerland

Edoardo COSTANTINI, Federico BISCI & Alessandro SCHERINO
Civil engineers, Speri, Italy

Alban KITA
Civil engineer, Gruner Stucky, Switzerland

ITALY

SUMMARY

The Italian technical Standard for the Design and Construction of Dams was updated in 2014, replacing the previous one dated 1982. The updated Standard triggered the necessity to reassess their performance. The Authors have carried out the seismic assessment of more than 50 dams in Italy, geographically distributed throughout the whole country: spanning from the Alps in the North, in the Apennines along the peninsula and Sicily. Most of them were built in the first half of the 20th century, designed with a Service Life of more than 50 years and often with no specific seismic requirement.

**Une vue d'ensemble de l'évaluation de la sécurité de plus de 50 grands barrages selon les nouvelles normes de conception italiennes*

DOI: 10.1201/9781003642428-148

This paper provides an overview of the safety seismic assessment of the set of dams in Italy. A step-by-step methodology is developed to this aim. At first, the distinct types of dams are identified, from gravity to embankment, to multiple-arch, mixed, etc, while most of the construction materials are considered, from granular materials to dry masonry, masonry, cyclopean and conventional concrete, etc. An accurate survey is carried out for each dam, including the acquisition of historical and archival information. Also, vast investigation campaigns are considered case by case for enhanced material characterization of dam body materials and foundation, the latter a crucial knowledge task in the case of existing dams. The seismic input is defined based on the Italian seismic hazard maps. Also, a site-specific probabilistic seismic hazard study is considered for the analyses where required. The overall relevant information is widely illustrated for the set of dams under investigation. The analyses carried out encompass from simple 2D pseudo-static analysis with linear constitutive models of materials to advanced full 3D time-history (with site-specific natural accelerograms) analyses with non-linear materials, modeling of joints, etc. The obtained results are comparatively summarized for the whole set of dams with reference to Ultimate and Serviceability Limit States. Despite the very old design, typically aseismic, and some natural ageing of material, most of the assessed dams comply with the national Standards and generally exhibit satisfactory behavior in seismic conditions.

RÉSUMÉ

La norme technique Italienne pour la Conception et la Construction des Barrages a été mise à jour en 2014, remplaçant la précédente version de 1982. La norme mise à jour a déclenché la nécessité de réévaluer la performance des barrages. Les auteurs ont réalisé l'évaluation sismique de plus de 50 barrages en Italie, répartis géographiquement dans tout le pays: des Alpes au nord, aux Apennins le long de la péninsule et à la Sicile. La plupart de ces barrages ont été construits dans la première moitié du XX^{e} siècle, conçus pour une durée de vie de plus de 50 ans et souvent sans exigence sismique spécifique.

Cet article présente un aperçu de l'évaluation de la sécurité sismique de cet ensemble de barrages en Italie. Une méthodologie pas-à-pas a été développée à cette fin. Dans un premier temps, les différents types de barrages sont identifiés : barrage-poids, barrages en remblai, barrages voûtes multiples, barrages mixtes, etc., en prenant en compte la plupart des matériaux de construction, des matériaux granulaires à la maçonnerie sèche, la maçonnerie traditionnelle, le béton cyclopéen et le béton conventionnel, etc. Une étude minutieuse est réalisée pour chaque barrage, y compris l'acquisition d'informations historiques et d'archives. En outre,

des campagnes d'investigation approfondies sont menées au cas par cas pour améliorer la caractérisation des matériaux du corps du barrage et de la fondation, cette dernière étant une tâche de connaissance cruciale dans le cas des barrages existants. La charge sismique est définie sur la base des cartes de l'aléa sismique italien. En outre, une étude probabiliste de l'aléa sismique spécifique au site est envisagée pour les analyses lorsque cela est nécessaire. Les informations pertinentes sont largement illustrées pour l'ensemble des barrages examinés. Les| analyses réalisées comprennent de simples analyses pseudo-statiques en 2D avec des modèles constitutifs linéaires de matériaux à des analyses avancées en 3D complète dans le domaine du temps (avec des accélérogrammes naturels spécifiques au site), incluant des matériaux non linéaires, la modélisation des joints, etc. Les résultats obtenus sont résumés de manière comparative pour l'ensemble des barrages, en référence aux États Limites Ultimes et de Service. Malgré leur conception ancienne, typiquement antisismique, et un certain vieillissement naturel des matériaux, la plupart des barrages évalués sont conformes aux normes nationales et présentent un comportement globalement satisfaisant en conditions sismiques.

1. INTRODUCTION

The majority of the more than 500 large existing dams in Italy were built in the first half of the 20th century. No specific seismic requirements and design criteria were considered at the time. Most of such dams, which retain large reservoirs and constitute strategic assets for national energy production, are located in moderate-to-high seismic hazard zones. During the past century, the national regulations for the safety assessment of hydraulic structures evolved simultaneously with the increase of knowledge on the national seismic hazard, together with worldwide observed dams behavior and the evolution of the numerical capabilities to predict the dam performances under static and dynamic loading conditions.

The increased knowledge and awareness posed questions about the resilience of old existing dams designed relying mainly on static loading conditions. The latest update of the national standards dates to 2014, with the release of the New Italian Technical Standard for the Design and Construction of Dams [1]. This document, which is inspired by the National Building Code [2], the Eurocodes [3] and International Standards applicable to dams, replaces the previous regulation from 1982 [4], which had the merit to explicitly introduce the seismic input, following major seismic events occurred in Italy. This recent major update in the national standard triggered the necessity to reassess the performances of many existing large dams under operation. In this framework, the Authors have been engaged to carry out the seismic assessment of 53 existing dams of different ages and

typologies, spread all over the country from the Alps in the North, across the Apennines in the Centre, down to Sicily in the South. Dam types range from concrete gravity and masonry structures to embankments, zoned or with upstream facing. A 100-year-old mixed structure, consisting of two cyclopean concrete lateral gravity abutments and one multiple-arch central block was also assessed [5]. The dams are all located in medium-to-high seismic hazard areas, identified by the most recent Italian regulations. The present paper aims to present the step-by-step methodology followed in the studies, as well as a general overview of the assessed dams and the performances under seismic loading conditions that have been foreseen with numerical analyses.

2. THE NEW ITALIAN STANDARDS FOR SEISMIC ASSESSMENT

2.1. History of italian standards for dams

After the disaster of the Gleno Dam in 1923, the first Italian dam design standards were published [6] aiming at introducing a regulation and guaranteeing a high level of safety for these important hydraulic structures, with a connected intrinsic high level of risk. At the time, already 100 dams were built or under construction without specific guidelines. However, the first standards containing specific guidelines for seismic design were published only in 1982. Several earthquakes occurred in Italy from the 80s to the present day [7]; therefore, the attention to seismic design criteria has constantly increased during this period and the standards have been updated several times. Finally, this process led to the publication of the actual new National Building Code [2] in 2018 and the New Italian Technical Standard for the Design and Construction of Dams [1] in 2014, with the related Seismic Guidelines in 2019 [8].

2.2. The new italian seismic code for dams

This framework of regulations introduced several innovations in seismic analysis and earthquake-resistant design of large dams in Italy. An important change concerns the request for a multiperformance design approach, developed through different levels of damage accepted for different seismic actions: two Serviceability Limit States SLS (OLS – Operational Limit State, and DLS – Damage Limit State) and two Ultimate Limit States ULS (LLS – Life-Safety Limit State, and CLS – Collapse Limit State) (Table 1). In particular, the performances to be achieved may be often focused on only 2 limit states, DSL and CSL.

Table 1
Limit States and performance requirements for gravity dams according to the New Italian Technical Standards [1].
États limites et exigences de performance pour les barrage-poids selon les nouvelles normes techniques Italiennes [*1*].

LIMIT STATE	SERVICEABILITY LIMIT STATE (SLS)				ULTIMATE LIMIT STATE (ULS)			
	OPERATIONAL (OLS)		DAMAGE (DLS)		LIFE SAFETY (LLS)		COLLAPSE (CLS)	
Condition: Lost (L) Attained (A)	L	A	L	A	L	A	L	A
	No damage occurs at the dam and appurtenant structures (normal operating condition).	Occurrence of repairable damages without uncontrolled release of water.		Occurrence of irreparable damages without uncontrolled release of water.		Occurrence of irreparable damages producing uncontrolled release of water and/or risk of loss of life.		Collapse with uncontrolled release of all or a relevant part of the reservoir water.
Requests for gravity dams	Stresses lower than elastic limits: $\sigma'_{t,max} < f_{ctk}$ and $\sigma'_{c,max} < 0.2 \cdot f_{ck}$ [(1)(2)] If exceeded, use Ghanaat criterion[(3)]:				Sliding criterion FS $_{sliding} < 1.15$. If exceeded, non-linear time-history dynamic analyses with engineering judgment on stresses, cracks and permanent displacements.			
	1. Area ($1.0 < DCR < 2.0$) < 15% Atot;							
	1. time ($DCR > 1.0$) < limited (Figure 1); $DCR < 2.0$							
Requests for embankment dams	No damages occur		Dam maintains substantially its elastic behavior		No damages to the impervious system		No collapse occurrence.	
	$w_c/H_d < 0.1$ % [(4)].		$w_c/H_d < 0.4$ % [(4)].		$w_c/H_d <$ 1.0% [(4)].		$w_c/H_d < 2.5$% [(4)].	

[(1)] $\sigma'_{t,max}$ and $\sigma'_{c,max}$ are the maximum principal effective tensile and compressive stresses, respectively. [(2)] f_{ctk} is the characteristic tensile strength and f_{ck} is the characteristic cylindrical compressive strength. [(3)] DCR = $\sigma_{t,max} / f_{ct}$ is the demand capacity ratio, $\sigma_{t,max}$ is the principal tensile stress and f_{ct} is the static tensile strength obtained from the uniaxial splitting tension test [9]. (4) w_c is the crest permanent settlement and H_d is the dam height; the limits are defined according to the literature [9]

Another important innovation is the progressively increasing complexity-based approach that is compulsory for dam safety assessment. Each dam is scrutinized firstly according to simplified procedures, such as pseudo-static two-dimensional limit equilibrium analyses for gravity dams or Newmark displacement assessments based on linear equivalent analyses for embankments. If, based on the outcomes of

the first simplified assessment, the performance requirements for all the Limit States are satisfied, the assessment can be considered positively concluded; otherwise, an increasing level of complexity is introduced in the analysis.

2.3. The methodology for seismic assessment of existing dams

Dams are classified by their typology at first, which dictates the specific procedure to assess compliance with the safety requirements. A particular case is represented by dry-masonry dams: conceived at the very beginning of the last century as gravity dams, designed to not undergo tensile stresses and base sliding, they may be assimilated to embankments, according to the New Italian Standards [1]. Then, each dam is duly scrutinized, starting from the acquisition of historical and archival information, up to dedicated site inspections. The behavior under operation conditions is analyzed for each dam by the collection and analysis of the monitoring system dataset. Additional investigation campaigns are specified case-by-case for each dam. The information obtained both from in-situ investigations and laboratory tests on concrete, soil and rock, is synthesized to define or enhance the mechanical characterization of the dam body and its foundation. Based on the seismic input defined in the Italian seismic hazard maps, a site-specific probabilistic seismic hazard study is performed when the Peak Ground Acceleration at 475 years of return period exceeds 0.15 g. The main features and properties of the assessed dams are described hereafter.

Once the base data for the analyses is collected, the seismic safety assessment is carried out following methodologies specific for concrete (gravity and arch dams) and embankment dams.

Gravity dams are assessed with a first step of verification for the SLS through a pseudo-static analysis, followed by a pseudo-dynamic analysis [11] [12]. If the strength of the concrete is exceeded (most typically in the tensile direction), a linear time-history dynamic analysis must be carried out, progressively removing conservative assumptions and increasing the analysis complexity (soil-structure interaction with mass in foundation and fluid-structure interaction with acoustic elements). If the strength is still exceeded, the level of damage shall be evaluated to be acceptable or not with the criterion proposed by Ghanaat [13]. The criterion is based on the computation of the demand capacity ratio (DCR), predicting the acceptability of the expected cracking criteria based on the extent of the overstressed area and the duration of strength excursion during the time-history.

The performance of a gravity dam for the ULS is satisfactory if the sliding safety factor is higher than 1.15. The sliding safety factor is first computed with

pseudo-static analysis. In case the minimum safety factor is not met, a linear time-history analysis is conducted. If the criterion is still not accomplished, non-linearities concentrated in the weakest and most stressed zones of the structure, or within the whole structure are introduced in the analysis. The results of the non-linear time-history analysis require sound engineering judgment on cracks extension and permanent displacements of the structure [14], together with an evaluation of post-seismic conditions.

Embankment dams are assessed with the first level of analysis consisting of a time-history analysis, with a visco-elastic model for the dam and foundation. The cyclic behavior of the soil (stiffness degradation and damping cyclically increasing with deformations) is taken into consideration with the simplified equivalent linear elastic method [15]. Permanent displacements are subsequently estimated with the modified Newmark sliding block method [16].

It is important to remark that the traditional pseudo-static approach, worldwide used as a preliminary simplified analysis for slope seismic stability, is not considered anymore sufficient in Italy, for any level of seismic analysis of the embankment dams.

The SLS is verified if the dam undergoes only limited damages. This performance is considered accomplished whether the peak dynamic deformations remain within the range of medium shear strain ($\approx 10^{-4}$-10^{-3} [-]). For this level of strain, the dynamic linear equivalent method is justified and the number of cyclic load repetitions can be disregarded because the volumetric threshold shear strain is not exceeded and there is no build-up of pore water pressure [17]. The estimated permanent settlements of the crest are almost null.

During the strongest seismic events for the ULS, the volumetric threshold is probably exceeded; therefore, the stability of the dam will be challenged by the loss of shear strength and excess pore water pressure build-up. Relevant permanent displacements are expected and then the equivalent linear elastic method shall be replaced by a non-linear analysis with direct integration in the time domain of the elasto-plastic constitutive models.

The ULS is verified if the collapse of the dam is excluded. Guidelines specify four possible collapse mechanisms to be investigated: crest overtopping, global instability, liquefaction and internal erosion for the seepage process after the earthquake.

The global instability is excluded by checking the final settlement of the dam crest. This index is considered representative of the overall seismic response of the dam [18]. A correlation between the crest settlement and the related damages in existing dams has been studied and threshold values have been established for different Italian limit states [9]. Crest overtopping is excluded based on the residual

freeboard at the end of the seismic event. Liquefaction triggering analysis is carried out according to grading and density requirements for every material, according to the Italian Building Code [2].

A procedure to assess the risk for internal erosion is not strictly regulated in the Italian code and is left to the engineering judgment of the designer. The Authors have assumed the ICOLD recommendations [20] to assess the erosion risk in case of failure of the impervious barrier due to the earthquake. The timing for lowering the reservoir also plays a crucial role in the assessment of this risk.

3. MAIN FEATURES OF THE INVESTIGATED DAMS

3.1. Large dams classification according to Italian standards

The New Italian Standard [1] classifies the dams into the following types:

(a) Concrete dams
a1 Gravity (a.1.1 ordinary and a.1.2 buttress)
a2 Arch (a.2.1 simple; a.2.2 arch-gravity and a.2.3 double curvature)
(b) Embankment dams (b.1 homogeneous; b.2 with internal impervious barrier and b.3 with upstream facing)
(c) Barrages
(d) Mixed type and other (older type) dams.

Three importance levels are defined for the calculation of seismic load: A - strategic dams (structure for civil protection, hydroelectric or potable purposes); B - relevant dams (large dams with height $>$ 15 m or reservoir volume $>$1 Mm^3) and C - normal dams (all the dams not belonging to categories A and B; small dams only).

3.2. Main characteristics of the dams

Fig. 1 and Table 2 synthesize the main characteristics of the 53 investigated dams: more than half (59%) belong to high-seismicity regions ($PGA_{Tr=475\ years} > 0.15$ g) while the majority (87%) were built before the '80s with no specific seismic standard. The tallest is the dam ID 47 (89 m), the largest fill volume is the dam ID 29 (11.6 Mm^3 – the largest in Europe!), having also the highest reservoir (482 Mm^3).

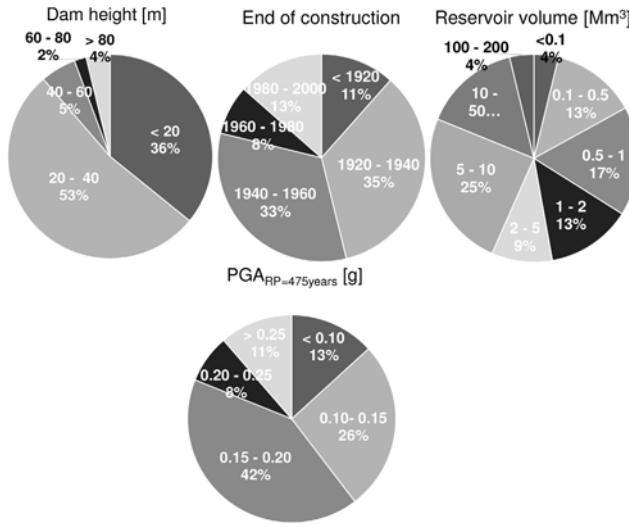

Fig. 1
Main characteristics of the investigated dams
Principales caractéristiques des barrages étudiés

Table 2
Main characteristics of the investigated dams.
Caractéristiques principales des barrages étudiés.

ID	TYPE	H [M]	DAM VOL. [M^3]	RES. VOL. [MM^3]	YEAR	TYPE	IMP.	PGA_{475YRS} [G]
1	Gravity	16.5	-	5.70E-01	1930	c	A	0.197
2	CCED	16.5	7.98E+04	5.70E-01	1930	b.2	A	0.197
3	Dry masonry	33.0	1.20E+05	8.50E+00	1926	b.3	A	0.097
4	Gravity	26.4	2.40E+04	5.05E+00	1955	a.1.1	A	0.179
5	CCED	10.5	2.90E+04	5.05E+00	1955	b.2	A	0.179
6	CCED	49.4	4.40E+06	1.56E+02	1993	b.2	A	0.264
7	CCED	32.0	4.00E+05	5.60E+00	1958	b.2	A	0.271
8	Gravity	24.3	1.75E+04	2.50E+00	1948	a.1.1	A	0.085
9	BFRD	45.4	4.19E+05	6.23E+00	1987	b.3	A	0.170
10	CCED	39.0	1.40E+06	1.00E+01	1980	b.2	B	0.124
11	Dry masonry	24.5	5.33E+04	1.60E+01	1912	b.3	A	0.13
12	Dry masonry	19.2	1.37E+04	7.10E-02	1954	b.3	A	0.254
13	CCED	21.7	1.20E+05	6.25E-01	1928	b.2	A	0.177

(Continued)

Table 2
Continued

ID	TYPE	H [M]	DAM VOL. [M^3]	RES. VOL. [MM^3]	YEAR	TYPE	IMP.	PGA_{475YRS} [G]
14	CFED	23.9	1.20E+06	1.32E+00	1982	b.3	A	0.059
15	Multiple-arch	40.0	6.30E+04	2.70E+00	1928	d	A	0.19
16	CFED	11.3	1.35E+04	1.60E+01	1912	b.3	A	0.129
17	Gravity	19.3	2.20E+04	8.55E+00	1965	a.1.1	A	0.248
18	Gravity	20.2	1.36E+04	1.66E-01	1939	a.1.1	A	0.110
19	CCED	4.7	0.00E+00	1.66E-01	1939	b.2	A	0.110
20	CCED	18.9	1.40E+05	1.04E+00	1960	b.2	A	0.174
21	CCED	28.9	7.00E+05	1.04E+00	1960	b.2	A	0.174
22	Gravity	38.0	3.60E+04	7.90E-01	1950	a.1.1	A	0.181
23	Dry masonry	21.0	1.00E+04	2.40E-01	1929	b.3	A	0.065
24	Dry masonry	19.6	3.30E+04	5.00E+00	1913	b.3	A	0.149
25	Dry masonry	23.6	9.00E+04	9.45E+00	1921	b.3	A	0.106
26	CFED	19.2	3.00E+03	1.40E-01	1922	b.3	A	0.197
27	BFRD	31.5	1.65E+06	5.68E+00	1988	b.3	A	0.259
28	CFED	17.5	1.21E+05	1.67E+01	1958	b.3	A	0.075
29	BFED	65.5	1.16E+07	4.82E+02	1983	b.3	A	0.115
30	Gravity	13.7	8.36E+04	1.80E+01	1955	c	A	0.144
31	CFED	20.5	7.00E+04	3.37E+00	1911	b.3	A	0.203
32	Dry masonry	38.0	1.80E+05	3.28E+01	1923	b.3	A	0.176
33	BFRD	25.1	2.40E+06	7.45E+00	1986	b.3	A	0.257
34	Gravity	12.9	4.40E+04	6.00E+00	1959	c	A	0.142
35	Gravity	19.0	2.00E+04	1.93E+00	1925	c	A	0.162
36	CFED	18.0	2.92E+04	4.47E-02	1958	b.3	A	0.138
37	BFRD	20.0	1.40E+06	7.18E+00	1987	b.3	A	0.172
38	Gravity	25.5	1.16E+04	5.30E-01	1958	a.1.1	A	0.144
39	CCED	16.5	1.79E+05	3.34E+00	1958	b.2	A	0.124
40	Gravity	16.5	8.50E+03	2.90E-01	1927	a.1.1	A	0.139
41	Gravity	14.9	1.20E+04	1.05E+00	1958	c	A	0.177
42	Gravity*	20.0	7.00E+03	2.10E-01	1917	d	A	0.188
43	Gravity*	38.0	4.00E+04	6.28E+00	1911	d	A	0.195
44	CCED	32.8	3.82E+05	2.15E+00	1958	b.2	A	0.265
45	Gravity	23.0	1.65E+04	5.80E-01	1923	a.1.1	A	0.065
46	Dry masonry	23.0	1.65E+04	5.80E-01	1923	b.3	A	0.065
47	Gravity	89.0	2.88E+05	4.39E+01	1932	a.1.1	A	0.195

(Continued)

Table 2
Continued

ID	TYPE	H [M]	DAM VOL. [M^3]	RES. VOL. [MM^3]	YEAR	TYPE	IMP.	PGA_{475YRS} [G]
48	Gravity	13.0	1.25E+04	1.88E+00	1965	c	A	0.186
49	Gravity*	28.5	2.00E+04	5.70E-01	1928	a.1.1	A	0.200
50	Gravity*	35.4	1.80E+04	1.38E+00	1941	a.1.1	A	0.187
51	Gravity	88.0	1.80E+05	3.40E+01	1953	a.1.1	A	0.196
52	Dry masonry	27.4	5.00E+04	1.12E-01	1939	b.3	A	0.200
53	Gravity	22.5	2.46E+04	6.90E-01	1955	a.1.1	A	0.180

CFED = Concrete Face Earthfill Dam; CCED = Central Core Earthfill Dam; BFRD = Bituminous Face Rockfill Dam; CFRD = Concrete Face Rockfill Dam and Gravity* = Masonry gravity dam

4. MATERIALS PROPERTIES AND INVESTIGATIONS

4.1. Concrete materials

The concrete database has been prepared compiling the information from 20 gravity dams and 2 stone masonry gravity dams with concrete mortar. Almost half of the dams (11) needed additional investigations. The (average) compressive strength is generally satisfactory, around 25 MPa (Table 3 and Fig. 2). Only 2 dams, with stone masonry structures, have shown moderately low values (10-15 MPa). The (average) tensile strength is quite low compared to the compressive one (less than the typical 1/10 f_{cm}) (Table 3 and Fig. 2). This lower bound value is mainly due to conservative assumptions considered for the characterization of the tensile strength, because of the limited number of tests. Lift joints, which are generally assumed to be weak planes in the analyses [12], [22], [23]) are barely distinguishable from parent concrete for the investigated dams. Moreover, the core samples and the camera inspections have always shown fully bonded lift joints. However, the tensile strength of the joints has been conservatively estimated as a ratio of the parent concrete strength, generally between 50 and 65% [24]. Shear strength has been assumed equal to the lower bound envelope of bonded lift joints from the literature [25], resulting in a cohesion of 0.97 MPa and a friction angle of 57°. For some dams, a further conservative reduction of the strength parameters has been considered to cover uncertainties in the material characterization and consequently, a cohesion of 0.30 MPa and a friction angle of 45° has been adopted in the analysis [26]. The same conservative approach has been considered for the concrete-to-rock joints characterization, considering the lower bound of the peak strength from the literature [25]. In one case, it has been possible to collect intact samples at the concrete-to-rock contact and to perform direct shear tests enabling the direct determination of peak and residual strengths [14].

Table 3
Average properties of the investigated dams.
Propriétés moyennes des barrages étudiés.

PROPERTIES	SYMBOL	UNIT	AVERAGE	ST. DEV.
Compressive strength	f_{cm}	MPa	25.05	8.46
Tensile strength	f_{ctm}	MPa	1.76	0.88
Dynamic Young's modulus	E_d	GPa	31.41	10.72

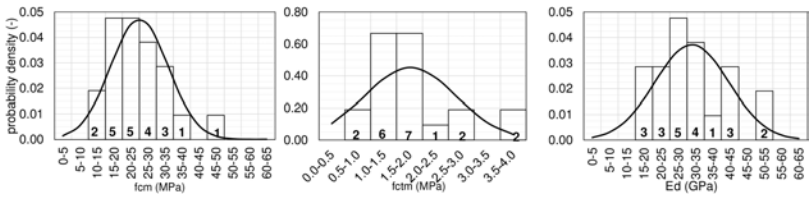

Fig. 2
Statistical distribution of compressive strength (left), tensile strength (center) and dynamic Young's modulus (right) of concrete
Distribution statistique de la résistance à la compression (gauche), celle à la traction (centre) et du module du Young dynamique (droite) du béton.

4.2. EMBANKMENT MATERIALS

This chapter presents the main results of the mechanical characterization of materials for embankment dams (rockfill, earthfill and core materials).

Table 4 summarises the classes of the three material types. The earthfill material is mainly constituted of gravel and sand, with an average fine content of 23% (Fig. 3). Rockfill materials (Fig. 4) are generally constituted of coarser material (85% gravel and cobbles), with $<$5% fine content. Earthfill curves are broadly distributed: in some cases, approaching rockfill distributions (ID 6, 7, 14 and 28), while in others they approach core materials (ID 2, 10 and 39). Grain size distributions of the core materials present a fine content generally greater than 35% and an average of 50% (Fig. 5) guaranteeing the watertightness of the impervious barrier. However, even the coarser material with 23% fine content (ID 7) has demonstrated excellent behavior during the last 70 years of operation.

Table 5 summarizes the values of the dry specific weight according to the information source. For most of the shell materials, such values are provided from in-situ tests performed during the construction period (7 out of 18) and from recent investigations (7 out of 18) where, in this last case, in-situ density tests for 6 cases

(ID 7, 20, 21, 29, 31 and 44) have been performed. The average values calculated for the three materials are typical: rockfill 20.2 kN/m^3, earthfill 18.8 kN/m^3, core 16.6 kN/m^3. The differences are mainly due to the grain size distributions apart from the compaction effort and the specific gravity of the grains: ID 29 (classified as earthfill) has a unit weight equal to 23 kN/m^3, quite above the average for this type of material, because of its grain size distribution similar to rockfill with almost null fine content.

Table 5 also summarizes the friction angles assumed for the seismic assessments. For coarse-grained materials, large-diameter triaxial tests were used (11 cases). The seismic analysis is conducted with the available resistance under critical state conditions. All the materials are cohesionless. In five cases, mostly rockfill materials, a curvilinear strength envelope curve, according to *de Mello* equation [28], was needed to improve the experimental results. For rockfill, friction angles ranged from 39° to 52°, with an average value of 47°. The average value for the earthfill group is significantly lower at 37°, due to the higher fine content. The core material, as expected, has an even lower average value of 31°. The absolute minimum, 23°, is represented by ID 2 showing also the higher fine content of the set (87%) and a lower bound unit weight (15.6 kN/m^3). Finally, Table 5 shows the average shear wave velocities representative of the entire group of dams. The results are closely linked to the degree of compaction and the grain size composition of the materials. Some very old structures (ID 2, 13, 16 and 31) show limited velocity ($<$300 m/s) due to the outdated compaction technology adopted at the time of construction. The highest bound value is recorded in ID 7 (400 m/s) where the core material is the coarser of the set (23% of fine content) and more similar to the earthfill size distribution. Materials in the earthfill group have an average Vs of 410 m/s. Excluding the lower values, the average approaches that of rockfill materials, which stand at 540 m/s. The high velocity recorded in ID 29 earthfill (617 m/s) confirms again the similarity with (higher bound) rockfill values.

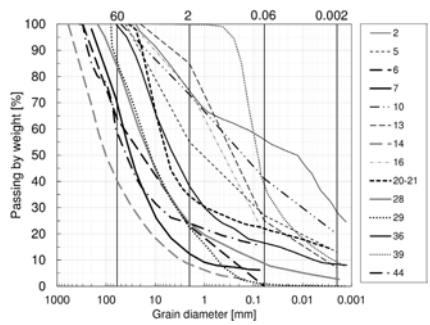

Fig. 3
Grain size distributions for Earthfill materials
Distribution granulométrique des matériaux de remblai.

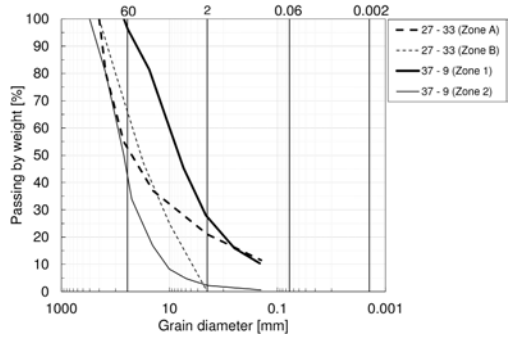

Fig. 4
Grain size distributions for Rockfill materials
Distribution granulométrique des matériaux d'enrochement.

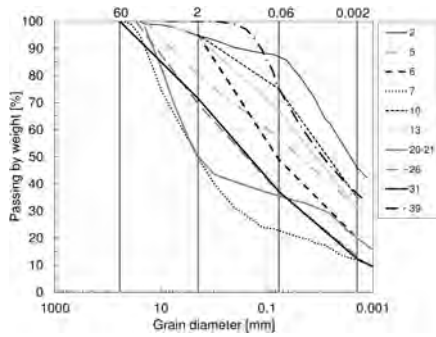

Fig. 5
Grain size distributions for Core materials.
Distribution granulométrique des matériaux de noyau.

Table 4
Grain size classes according to AGI [27]. St. dev. in parentheses.
Classes granulométriques selon AGI 1977 [*27*] *pour les matériaux de barrage en remblai. Écart-type entre parenthèses.*

DIAMETER D	**D > 60 MM**	**60 > D > 2 MM**	**2 > D > 0.06 MM**	**D < 0.06 MM**
Class	Cobbles	Gravel	Sand	Silt+Clay
Rockfill	33 (23)	53 (17)	11 (10)	4 (5)
Earthfill	14 (21)	38 (20)	26 (19)	23 (17)
Core	0	22 (19)	25 (11)	53 (13)

Table 5

Dry unit weight, friction angle and Vs of embankment materials.

Poids unitaire sec, angle de frottement et Vs des matériaux de barrage en remblai.

ID	MATERIAL	γ DRY (KN/M^3)			FRICTION ANGLE (°)					VS (M/S)		
		A	B	C	D	E	F	G		J	K	L
44	Earthfill			19		43				524		
27 – 33 (Zone A)	Rockfill	18.9			39					551		
27 – 33 (Zone B)	Rockfill	17.8			45					551		
28	Earthfill		22.7					44	X		450	
14	Earthfill		23.8					50	X		540	
7	Core			18.1				37		403		
7	Earthfill			19.1				44		571		
26	Core			15.3		35			X	257		
5	Core			16.8		33				315		
5	Earthfill			18.9		35					395	
20 - 21	Core			19			32			413		
20 - 21	Earthfill			19.8				44		445		
37 – 9 (Zone 1)	Rockfill		20.6					50		514		
37 – 9 (Zone 2)	Rockfill		20.6					50		514		
31	Core			15.0				35		295		
13	Core			16.3		30				179		
13	Earthfill			15.7		32				288		
6	Core		17.4				24			329		
6	Earthfill		21.3					42	X		750	
39	Core		16			30				237		
39	Earthfill		16.3			33				222		
2	Core			15.6			23				250	
2	Earthfill			15.6			23				250	
10	Core		16.3			29						300
10	Earthfill		17			27				449		
29	Earthfill			23				52	X	617		
36	Earthfill	18						38		268		
16	Earthfill	17.2				32				200		

A and D original technical specifications; B field density tests during the construction; C new laboratory tests and/or new field density tests; E TX tests on full specimen; F TX tests on scalped specimen; G large diameter TX tests; X Curvilinear envelope; J cross-hole test; K surface geophysic in situ tests; L literature

4.3. Dry-stone masonry

Dry-stone masonry dams were commonly built in Italy during the early decades of the 20th century. The blocks (up to 50-70 cm large) within the masonry were arranged by hand trying to minimize the porosity of the material ($< 35\%$) or dumping on site small coal-type wagons. The watertight barrier was always on the upstream face, made of different types: concrete, bituminous concrete or steel lining. After the 1950s, this type of structure was abandoned in favor of rockfill dams. Given the size of the blocks, the measure of the porosity on-site requires the excavation of a pit of about 2 to 3 cubic meters. This type of test was conducted only for one dam, the tallest of this type in Italy: ID 32 (h= 38 m). In the other cases, the dry weight was estimated equal to 17-19 kN/m^3 based on the specific weight of the blocks and the porosity available from construction information.

The shear wave velocity in the material (Fig. 6) was investigated using cross-hole or down-hole geophysical tests. The hand-placed materials show values consistently higher than the dumped materials (average Vs of 1007 vs 341 m/s). The dumped material values are similar to the lower bound of rockfill or average earthfill. Therefore, the behavior of this peculiar material has been assimilated to the rockfill material strength evaluated through Leps [29] regression.

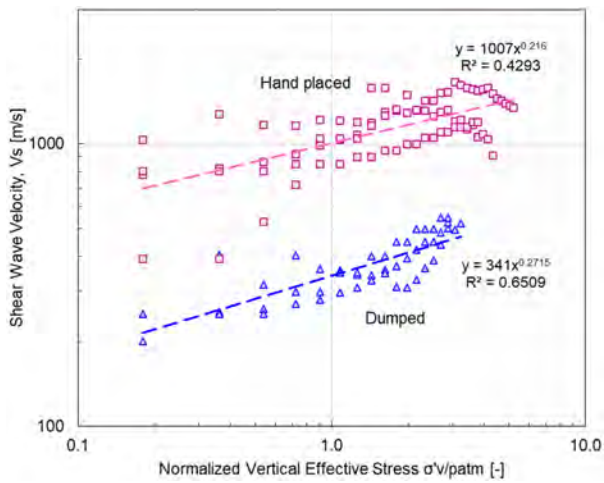

Fig. 6
Shear wave velocities of the dry masonry materials.
Vitesse de propagation des ondes de cisaillement des matériaux de maçonnerie sèche.

5. RESULTS OF SEISMIC ASSESSMENTS

5.1. EMBANKMENTS

The obtained results are synthesized in terms of normalized-to-height crest settlements versus peak ground acceleration for both limit states, DLS and CLS. In particular, the embankments under investigation are subdivided into three main groups with reference to Table 2 (Dry masonry with upstream face, Earthfill/rockfill with upstream face and Earthfill with zones and core).

Regarding DLS (Fig. 7), the following observations can be drawn:

- PGAs are always lower than 0.2 g;
- All dams comply with the limit of 0.4% [9] of normalized crest settlement and therefore the expected damages are “minor” or “none”;
- Results are not scattered;
- Results are consistent with the data observed in the literature [18][19].

Regarding CLS (Fig. 8), the following observations can be drawn:

- PGAs are in the range of 0.15-0.85 g;
- All dams comply with the limit of 2.5% [9] of crest settlement and therefore the expected damages are “moderate” to “serious”, without any collapse;
- Results are a little scattered;
- Results are consistent with the data observed in the literature [18][19];
- Only 4 cases need to be investigated with dynamic non-linear analysis (illustrated in full red symbols);
- The use of non-linear analysis is not dependent on the PGA level.

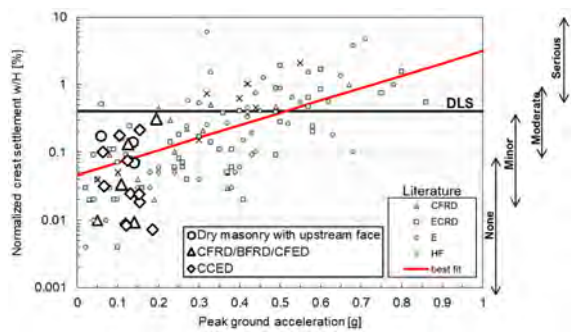

Fig. 7
DLS results for embankments.
Résultats ELS (état limite de service) pour les barrages en remblais.

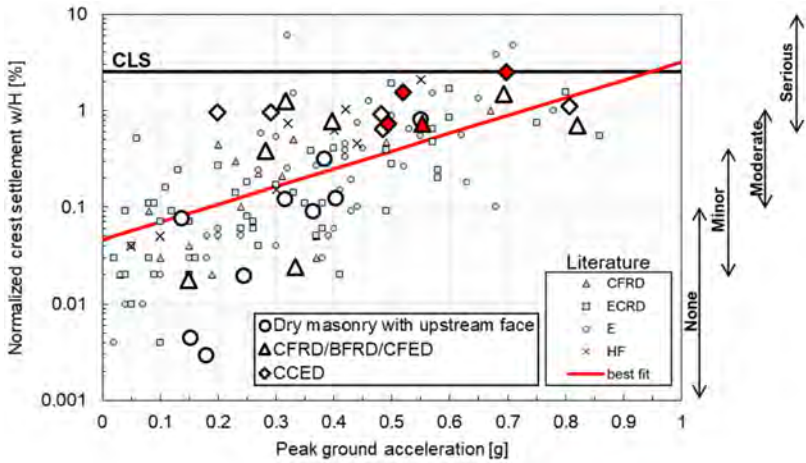

Fig. 8
CLS results for embankments.
Résultats ELU (état limite ultime) pour les barrages en remblais.

5.2. GRAVITY DAMS

The obtained results are synthesized in terms of the stress-to-strength ratio for the DLS and the Sliding Safety Factor SSF for the CLS. The following observations can be drawn:

- DLS (see Fig. 9). All dams have been verified with the pseudo-static (or pseudo-dynamic) approach, except for ID 47 assessed with linear dynamic time-history analysis and Ghanaat criterion.
- Results of stress-to-strength ratios are plotted vs the first period of vibration Sa (T1) and the dam's height H, whereby for both there is a good correlation (an increasing seismic input and/or height yields higher values of stress-to-strength ratios).
- CLS (see Fig. 10). All dams have been verified. For ID 4, 17 and 47, the limit state is verified with the introduction of one or multiple non-linear lift joints and post-seismic stability analysis.
- Results of SSF are plotted vs the first period of vibration Sa(T1), whereby a good correlation can be observed (progressively increasing seismic input yields lower values of SSF).

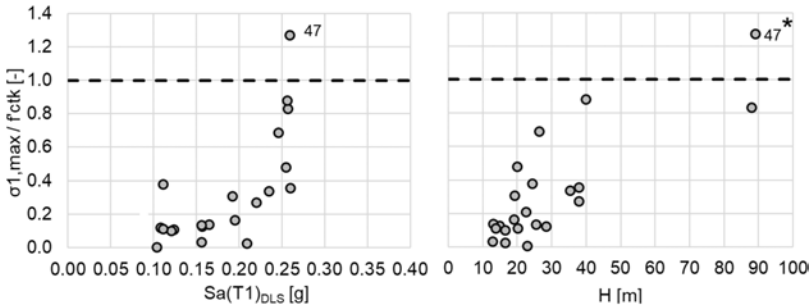

Fig. 9
DLS results for concrete dams (* verified with Ghaanat criterion).
Résultats ELS (état limite de service) pour les barrages en béton (vérifié avec le critère de Ghaanat).*

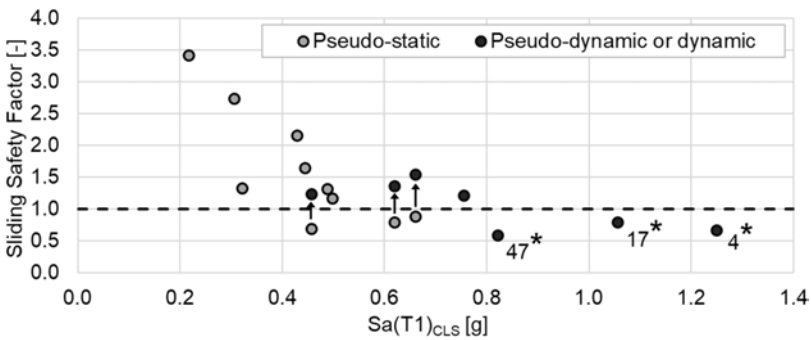

Fig. 10
CLS results for concrete dams (* one or multiple non-linear lift joints).
Résultats ELU (état limite ultime) pour les barrages en béton (un ou plusieurs joints non linéaires).*

In addition, Fig. 11 shows the progressive levels of complexity adopted in the analysis for the safety assessment of the dams. Noteworthy, only 6 cases needed a level of analysis with FEM time-history analyses. In particular:

- When the pseudo-acceleration at the first period of vibration Sa(T1) is lower than 0.35g, the pseudo-static approach (Level 1) is sufficient for the DLS verification of the dam. Only for the specific cases of ID 43, an arch-gravity masonry dam, and ID 15, a multiple-arch dam, additional / further levels of analysis are adopted. In particular, ID 15 has shown some vulnerability for CLS and called for seismic retrofit with a progressive intervention strategy [5].

- In the range 0.35g $\leq$ Sa(T1) $\leq$ 0.70g there is no DLS case with a pseudo-dynamic analysis (Level 2).
- For Sa(T1) $\geq$ 0.70g, the pseudo approach is never sufficient and a higher level of complexity is required (Levels 3 and 4). Once the time-history analysis was required, a model with mass in the foundation was necessary (Level 4).
- For Sa(T1) $\geq$ 0.80g, the linear analyses are not anymore sufficient, whereby FEM non-linear are needed (Level 5).

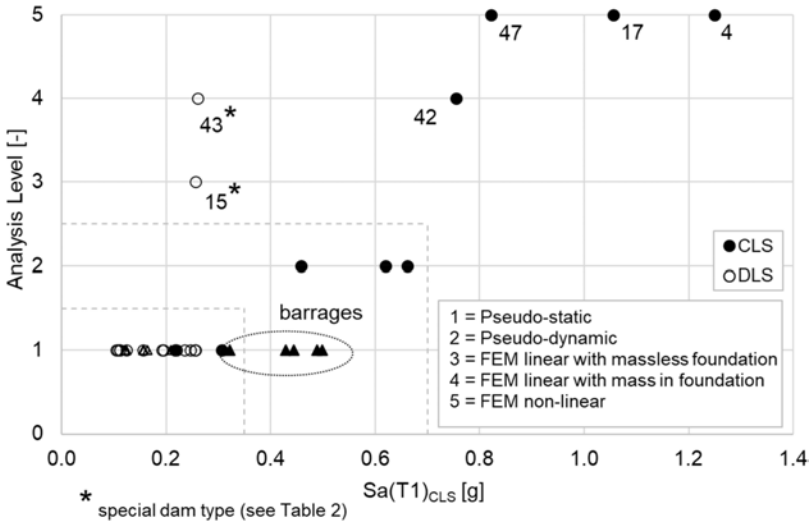

Fig. 11
Level of complexity attained for the concrete dams.
Niveau de complexité atteint pour les barrages en béton

6. CONCLUSIONS

This paper presented the safety seismic assessment of a set of 53 existing large dams in Italy, following the introduction of the New Italian Technical Standard for the Design and Construction of Dams in 2014 which requested a deep reanalysis in terms of the level of earthquake and performance required. One of the results of this study is the possibility of anticipating the case for which more complex analysis will be required. The main conclusion of the conducted studies is that, despite the relevant age and the lack of seismic considerations during the design and construction, all the investigated dams have shown a satisfactory performance complying with the requirements specified by the most recent national standards, confirming a certain degree of resilience of these structures against the seismic hazard.

The paper provided a general overview of all types of conducted analyses, showing how more complex analyses were required in a limited number of cases, 4 for embankments (dynamic non-linear analysis for ID 5, 7, 27 and 44) and 3 for concrete dams (ID 4, 17 and 47, by introducing non-linear lift joints and post-seismic stability analysis), notwithstanding the significant seismic hazard.

For embankment dams, it was not possible to establish a PGA value clearly indicating the need for advanced non-linear analysis, as this level of complexity is more influenced by the construction and specific dam typology and material characteristics. For gravity dams, a Sa(T1) higher than 0.80g is a good indicator that the highest level of complexity foreseen by the Italian standards, i.e. non-linear time-history analysis, may be required. Finally, ID 15, a peculiar multiple-arch dam, has shown some vulnerability for CLS and called for seismic retrofit with a progressive intervention strategy.

REFERENCES

[1] NTD14. D.M. 26 giugno 2014. “Norme tecniche per la progettazione e la costruzione degli sbarramenti di ritenuta (dighe e traverse)”. (in Italian), 2014.

[2] NTC18. D.M. 17 gennaio 2018. Aggiornamento delle Norme tecniche per le costruzioni (in Italian), 2018.

[3] Eurocode EN 1998-1. Design of structures for earthquake resistance. Part 1: General rules, seismic action and rules for buildings., European Committee for Standardization, Brussels, Belgium, 2005.

[4] DM82. D. Min. LL.PP. 24/03/1982. Norme tecniche per la progettazione e la costruzione delle dighe di sbarramento. (in Italian), 1982.

[5] ABATI A., GATTO G., FREZZA A., SPARNACCI R. Seismic safety assessment of an old multiple arch gravity dam - 91st Annual ICOLD Meeting – Gothenburg 13-14 June 2023.

[6] PILOTTI M., MARANZONI A., TOMIROTTI M., VALERIO G., Gleno dam break: Case study and numerical modeling. *Journal of Hydraulic Engineering*, 2011, 137.4: 480–492.

[7] ROVIDA A., LOCATI M., CAMASSI R., LOLLI B., GASPERINI P. CPTI15, the 2015 version of the parametric catalogue of Italian earthquakes. Istituto Nazionale di Geofisica e Vulcanologia, 2016.

[8] MIT-DGD19. (2019). Istruzioni per l'applicazione della normativa tecnica di cui al D.M. 26 giugno 2014 (NTD14) e del D.M. 17 gennaio 2018 (NTC18). Direzione generale per le dighe e infrastrutture idriche ed elettriche. 2019. (in Italian).

[9] ALIBERTI D., BIONDI G., CASCONE E. Performance indexes for seismic analyses of earth dams. In Earthquake Geotechnical Engineering for Protection and Development of Environment and Constructions. Silvestri e Moraci. Associazione Geotecnica Italiana, 2019.

[10] RAPHAEL J. M. Tensile strength of concrete. In: Journal Proceedings, 1984, p. 158-165.

[11] CHOPRA A. K. Earthquake response analysis of concrete dams. In: *Advanced dam engineering for design, construction, and rehabilitation*. Boston, MA: Springer US, 1988, p. 416–465.

[12] CHOPRA A. K. Earthquake Engineering for Concrete Dams: Analysis, Design, and Evaluation, 2020.

[13] GHANAAT, Y. Seismic performance and damage criteria for concrete dams. In: Proceedings of the 3rd US-Japan Workshop on Advanced Research on Earthquake Engineering for Dams. United States Society for Dams San Diego, 2002.

[14] GATTO G., BISCI F., ABATI A., CARUANA R. Non-linear seismic analysis of a concrete gravity dam according to new Italian regulation, International Symposium on Dams and Earthquakes 7th Meeting of the EWG, Athens, 2024.

[15] KRAMER S.L. *Geotechnical Earthquake Engineering*. Prentice-Hall, New Jersey, 1996.

[16] KRAMER S. L., SMITH, M. W. Modified Newmark model for seismic displacements of compliant slopes. *Journal of Geotechnical and Geoenvironmental Engineering*, 1997, 123.7: 635–644.

[17] ISHIHARA, K. Soil behaviour in earthquake geotechnics. 1996.

[18] SWAISGOOD J. R. Embankment dam deformations caused by earthquakes. 2003 Pacific Conference on Earthquake Engineering, 2003.

[19] BUFFI G., CARUANA R., BALSAMO A., CANCI M., FARRONATO G., FIGINI R., PALMIERI M., PREVITALI R., TAFFINI E., ZACCHEI E. Seismic Behaviour of Earth Dams: World Relevant Cases, International Symposium on Dams and Earthquakes 7th Meeting of the EWG, 2024.

[20] ICOLD. Internal erosion of existing dams, levees and dikes, and their foundations, 2015.

[21] ICOLD. The physical properties of hardener conventional concrete in dams, 2009.

[22] LEGER P., LECLERC M., LARIVIERE R. Seismic safety evaluation of concrete dams in Québec. *Int. J. Hydropower Dams* 10 (2), 2003.

[23] KITA A., LUPATTELLI A., VENANZI I., SALCIARINI D., UBERTINI F. The role of seismic hazard modeling on the simplified structural assessment of an existing concrete gravity dam. *Structures* 34: 4560–4573, 2021.

[24] PACELLI W. A., ANDRIOLO F. R., SARKARIA G.S. Treatment and performance of construction joints in concrete dams. *International Water Power and Dam Construction* 45(11): 26–31, 1993.

[25] Electrical Power and Research Institute (EPRI). Uplift Pressures, Shear Strengths and Tensile Strengths for Stability Analysis of Concrete Gravity Dams" Volume I Report No. EPRI TR-1 00345. Prepared by Stone and Webster Engineering Corp, Denver, Colorado, 1992.

[26] Canadian Dam Safety Association. Dam Safety Guidelines, 1999.

[27] Associazione Geotecnica Italiana (AGI). Raccomandazioni sulla programmazione ed esecuzione delle indagini geotecniche (in italian), 1977.

[28] DE MELLO V.F.B. Reflection on design decisions of practical significance to embankment dams, 17th Rankine Lecture. Géotechnique, v. 27, n. 3, pp. 279-355, 1977.

[29] LEPS T. M. Review of shearing strength of rockfill. *Journal of the Soil Mechanics and Foundations Division*, 1970, 96.4: 1159–1170.

Q.111 - R.52

COMMISSION INTERNATIONALE DES
GRANDS BARRAGES

VINGT-HUITIEME CONGRES DES
GRANDS BARRAGES
CHENGDU, MAI 2025

RECENT STUDIES ON ADVANCED FINITE ELEMENT SIMULATION METHODS FOR SAFETY ASSESSMENT OF CONCRETE DAMS (*)

Giorgia FAGGIANI, Martina COLOMBO, Antonella FRIGERIO & Piero MASARATI
Ricerca sul Sistema Energetico – RSE S.p.A

ITALY

SUMMARY

The evaluation of the structural response of concrete dams is carried out by means of numerical simulations generally with the finite element method (FEM). Currently, the hydroelectric infrastructures need to operate outside the conditions for which they were originally designed, considering on the one hand the aging of the assets and on the other hand the high performances required by the new regulations. In order to accurately and realistically represent their structural behaviour, there is a strong need to adopt advanced numerical analysis methods. The latest studies performed by RSE in the field of dam safety are mainly aimed at modelling the seismic response and the cracking behaviour of concrete dams. Regarding the first topic, an advanced approach, to be adopted in the frame of time-history linear or non-linear analyses, was recently implemented and tested by RSE: this approach, indicated by the acronym SAM-4D (Seismic Advanced Model for Dams), allows to appropriately simulate the propagation of seismic waves in a realistic massed foundation, considering its semi-unbounded extent. Regarding the second topic, two modelling approaches for the description of the cracking behaviour of concrete were tested and compared: the Concrete Damaged Plasticity model (CDP) and the

**Études récentes sur les méthodes avancées de simultation par éléments finis pour l'évaluation de la sécurité des barrages en béton*

 DOI: 10.1201/9781003642428-149

eXtended Finite Element Method (XFEM), both available in the commercial FEM code Abaqus. The case study of Pine Flat Dam was adopted to try out these advanced methods.

Pine Flat Dam was considered as a case study by several authors and was also proposed in the frame of ICOLD and USSD Workshops, because of its simple geometry that allows to obtain fast and easily comprehensible results. The ICOLD Technical Committee A (TC-A) “Computational Aspects of Analysis and Design of Dams” is evaluating to propose this case study to test and validate simulation methods and approaches. For years, the TC-A has been working to offer the analysts suitable tools for the verification and validation of their analyses, also considering the frequent lack of measured data.

RÉSUMÉ

L’évaluation de la réponse structurelle des barrages en béton est réalisée au moyen de simulations numériques, généralement avec la méthode des éléments finis (FEM). Actuellement, les infrastructures hydroélectriques doivent fonctionner en dehors des conditions pour lesquelles elles ont été conçues à l’origine, en raison du vieillissement des structures d’une part et des performances élevées requises par les nouvelles réglementations de l’autre. Afin de représenter avec précision et réalisme leur comportement structurel, il est indispensable d’adopter des méthodes d’analyse numérique avancées. Les dernières études réalisées par RSE dans le domaine de la sécurité des barrages visent principalement à modéliser la réponse sismique et le comportement de fissuration des barrages en béton. En ce qui concerne le premier thème, une approche avancée, à adopter dans le cadre d’analyses linéaires ou non linéaires de l’évolution temporelle, a été récemment mise en œuvre et testée par RSE : cette approche, désignée par l’acronyme SAM-4D (Seismic Advanced Model for Dams), permet de simuler de manière appropriée la propagation des ondes sismiques dans une fondation massive, en tenant compte de son étendue semi-illimitée. En ce qui concerne le deuxième thème, deux approches de modélisation pour la description du comportement de fissuration du béton ont été testées et comparées: le modèle Concrete Damaged Plasticity (CDP) et le modèle eXtended Finite Element Method (XFEM), tous deux disponibles dans le code commercial d’éléments finis Abaqus. L’étude de cas du barrage de Pine Flat a été adoptée pour tester ces méthodes avancées.

Le barrage de Pine Flat a été considéré comme une étude de cas par plusieurs auteurs et a également été proposé dans le cadre des ateliers de la CIGB et de l’USSD, en raison de sa géométrie simple qui permet d’obtenir des résultats rapides et facilement compréhensibles. Le Comité technique A (CT-A) de l’ICOLD “Computational Aspects of Analysis and Design of Dams” évalue la possibilité de proposer cette étude de cas pour tester et valider les méthodes et approches de

simulation. Depuis des années, le TC-A s'efforce d'offrir aux analystes des outils appropriés pour la vérification et la validation de leurs analyses, en tenant compte également du manque fréquent de données mesurées.

1. INTRODUCTION

Since its establishment in 1988, the ICOLD Technical Committee A (TC-A) "Computational Aspects of Analysis and Design of Dams" have been aimed to spread the use of numerical modelling in dam engineering and to transfer experience, skill and knowledge across generations. Numerical modelling can help to address particularly complex issues in both the design and safety assessment of large dams, which are currently called upon to play a key role in supporting the climate and energy policies of the European Green Deal. However, using advanced and complex numerical methods and increasingly user-friendly computational codes requires knowledge, experience and competence whether to set up sound models or to understand the reliability of the results, especially when few measurements are available either to calibrate the material parameters of the constitutive laws or to verify that the numerical structural response accurately matches the observed dam behaviour. For this reason, since 1991 the TC-A has been promoting Benchmark Workshops (BWs), at the beginning to validate the numerical codes in their initial development phase, and now to improve the rational use of mathematical models in addressing safety-related problems that are not yet satisfactorily analysed at present.

Referring to concrete dams, in past BWs several Themes have focused on the response to seismic events and aging phenomena, with particular attention to modelling the non-linear behaviour of structures under different loading and boundary conditions. These BWs have offered the analysts suitable tools for the verification of their analyses and the validation of their methods and codes, also considering the frequent lack of available measurements. Therefore, the TC-A is evaluating to propose some BWs Themes as reference case studies for dam engineers, such as the one devoted to the seismic analysis of Pine Flat Dam, included in the 15th BW held in 2019 in Milan (Italy) and adopted in this paper to try out the advanced numerical methods recently studied in the frame of RSE's research activity on dam safety.

Section 2 briefly introduces the methods adopted in the frame of seismic and non-linear analyses: the SAM-4D (Seismic Advanced Model for Dams) model (§ 2.1), able to simulate the propagation of seismic waves in a semi-unbounded massed foundation, and the two modelling approaches for the description of the cracking behaviour of concrete (§ 2.2), the Concrete Damaged Plasticity model (CDP) and the eXtended Finite Element Method (XFEM). Section 0 describes the

case study, detailing the numerical model (§ 3.1), the loadings (§ 3.2) and the results (§ 3.3). The main outcomes are summed up in Section 4.

2. ADVANCED SIMULATION METHODS FOR THE SAFETY ASSESSMENT OF CONCRETE DAMS

Numerical simulations, generally carried out by means of the finite element method (FEM), are nowadays the most widely used and effective tool for assessing the structural safety of complex structures such as concrete dams. In order to appropriately meet the high performances required by the current regulations and provide a reliable, accurate and realistic structural response, the adoption of advanced numerical analysis methods is strongly needed.

In the frame of seismic analyses, the time-history analysis based on the direct integration of the equations of motion is to date the most powerful method available for evaluating the response of the dams to earthquakes: it can be used for both linear and non-linear analyses and it can properly consider the dynamic interactions of the dam with the reservoir and the foundation. SAM-4D (Seismic Advanced Model for Dams), an advanced model in the context of time-history analyses, recently implemented and tested by RSE [1] [2] [3] [4] to simulate the propagation of seismic waves in a semi-unbounded massed foundation, is summarized in Section 2.1.

Due to high-intensity actions (not only in case of extreme events such as earthquakes and landslides, but also in case of significant thermal variations, aging and/or degradation processes), the structural behaviour of concrete dams can be characterized by strong non-linearities, either for the opening and sliding of construction joints and interfaces or for the triggering of cracking phenomena. To model the cracking behaviour of concrete, the two approaches (Concrete Damaged Plasticity model, CDP [5] [6] and eXtended Finite Element Method, XFEM [7] [8]) briefly described in Section 2.2 are studied in RSE.

2.1. The seismic wave propagation model SAM-4D

The seismic wave propagation model SAM-4D (Seismic Advanced Model for Dams) allows to ideally reproduce the behaviour of the actual semi-unbounded foundation, representing the wave propagation in a computational domain delimited by appropriate artificial boundaries and realistically provided with mass. The model, whose main characteristics were deduced from [9] [10] [11] [12] [13], was adopted to overcome the main deficiencies (above all the excessive conservativeness of the results) of traditional and simplified methods (mainly the massless

approach [14], proved to significantly overestimate the seismic response of dams [15] [16] [17]). The artificial boundaries (absorbing or non-reflecting) consist in a layer of normal and tangential dampers and springs, that allow the entrance into the foundation of the incoming seismic waves as well as the exit of the outgoing waves scattered by the dam-reservoir system, that propagate towards infinity. If only dampers are used, the classic non-reflecting boundaries are obtained [18]. The incoming seismic waves are specified by means of effective earthquake forces, applied on both the bottom and the side boundaries of the foundation and computed, starting from the free-field ground motion, using the theoretical solution of the vertically propagating elastic wave problem in a half-space; in case the half-space is homogeneous and undamped, the incident motion at the bottom boundary is equal to one-half the free surface motion: this simplification is appropriate if the rock is assumed homogeneous and with no or little (up to 2%) material damping [13].

The model has been implemented in both the FEM codes used by RSE for the simulation of the structural behaviour of concrete dams: the commercial code Abaqus [19], able to reliably simulate the non-linear behaviour of the concrete, and the in-house code CANT-SD [20], specifically designed for the analysis of dam-reservoir systems and particularly suitable in modelling the structural discontinuities (contraction joints and interfaces) in concrete dams. To simulate the non-reflecting boundaries in the frame of a FEM model, two alternative solutions were experienced: the infinite elements and the orthotropic elements. The infinite elements provide non-reflecting boundaries to the finite element model through the effect of just a damping matrix [19]; this can be a practical solution if the FEM code is equipped with such type of elements. If infinite elements are not available in the FEM code or the stiffness behaviour of the non-reflecting boundaries is considered important, the orthotropic elements can be introduced: these elements must be characterized by massless material with orthotropic linear behaviour where stiffness and damping characteristics are defined independently. The orthotropic elements can be easily obtained provided that the FEM code is able to simulate both the orthotropic material behaviour and the Rayleigh damping behaviour. The calculation and assignment of the effective earthquake forces are not straightforward tasks and require specific pre-processing tools. Since in FEM codes the forces are usually expressed as sum of products of space and time functions, two pre-processors were developed: the one aimed at writing the set of files with the space information (face of element and direction of the applied force), the other devoted to writing the set of the corresponding files with the time information (time-history). The validation of the model included the reproduction of the theoretical solution of the vertically propagating elastic wave problem for a flat foundation box (half-space) subject to impulsive or seismic excitation [21] and the reproduction of the analytical or numerical solutions available in literature for a semi-cylindrical canyon cut in a foundation half-space subject to sinusoidal excitation [13] [22] [23].

2.2. Modelling of the cracking behaviour of concrete

In the assessment of the structural behaviour of concrete dams, it is important to properly account the non-linearities caused by the cracking phenomena that could occur in quasi-brittle materials as concrete. Due to their low tensile strength, materials made up of matrix and aggregates (such as concrete) can be subject to cracking even under low loads. Concrete dams usually experience cracking both in the construction phase, in the ordinary operations and under severe and extreme loads (i.e. caused by earthquakes, floods, landslides, significant thermal variations, aging and degradation processes). These cracking phenomena generally lead to stiffness reduction and modify the distribution of internal stresses, but they do not necessarily cause a worsening of the structural performances and safety.

To numerically simulate the cracking behaviour of concrete, two alternative approaches based on the finite element method (FEM) are mainly used: the smeared crack approach, in which the damaged areas are identified by assigning appropriate constitutive equations to the continuous medium, and the discrete crack approach, based on fracture mechanics which describes the localized formation of cracks, considered as geometric discontinuities that cross the continuous medium [24]. The discrete crack approach is supposed to better represent the physical reality of cracking phenomena, since cracks are described as geometric (displacement) discontinuities. On the other hand, the smeared crack approach is perhaps more intuitive in the FEM context, since it allows the cracked material to be considered as a degraded continuum: the discontinuity caused by the crack is spread over the finite elements. In the frame of the smeared crack approach, a plastic-damage constitutive model was specifically developed by Lee and Fenves [5] to deal with concrete structures subjected to cyclic loading: it is therefore particularly suitable for addressing seismic analysis of concrete dams [6]. The model is available in the commercial FEM code Abaqus, named Concrete Damaged Plasticity (CDP). According to this model, under uniaxial tensile loading the stress-strain response of concrete is linear-elastic until the tensile strength is attained; subsequent increases of strain cause the progressive damage of the material, characterized by loss of stress for increasing strain (softening) and by reduction of stiffness in the unloading phase. In the frame of the discrete approach, in the late ‘90s the eXtended Finite Element Method (XFEM) was introduced [7] [8]: it represents a development of the classical FEM formulation that allows cracks to propagate through the finite elements (and not only along the elements edges as in the traditional discrete approaches). In the XFEM model the standard displacement-based finite element approximation is enriched by adding local functions, in conjunction with additional degrees of freedom, to model cracks: this technique allows simulating the crack path independently of the mesh. Even the XFEM model is available in the commercial FEM code Abaqus.

3. THE CASE STUDY OF PINE FLAT DAM

The case study was recently proposed in the frame of the 15th ICOLD International Benchmark Workshop on Numerical Analysis of Dams [25] and before in the USSD Workshop "Evaluation of Numerical Models and Input Parameters in the Analysis of Concrete Dams" [21]. Pine Flat Dam (Fresno, California, USA) is a large concrete gravity dam consisting of thirty-six 15.25 m wide monoliths and one 12.2 m wide monolith. The case study just concerns the tallest 15.25 m wide dam monolith no. 16 (about 122 m high): it can be represented as a 2D problem, particularly suitable to carry out complex analyses in a reasonable computation time. For this reason, Pine Flat Dam was considered as a case study by several authors.

In this paper, the case study of Pine Flat Dam is adopted to try out the advanced numerical methods recently examined in the frame of RSE's research activity on dam safety. The analyses reported in this section are referred to the comparison between the massless approach and the SAM-4D model and between the CDP and the XFEM models.

3.1. Geometrical and physical model

Fig. 1 shows the 3D FEM model including the dam monolith and the relevant portions of the foundation and of the reservoir. The structural problem is schematized as a 2D (plane strain) problem applying appropriate symmetry conditions at the side boundaries of the model. A quite fine mesh, with element size of about 1.5 m, is used to model the dam monolith to comply with non-linear models. The model of the foundation is characterized by elements of uniform height equal to about 6 m that allows to describe with good accuracy frequencies up to about 15 Hz (for the time-history analyses with the SAM-4D model). The case study was approached with the commercial FEM code Abaqus.

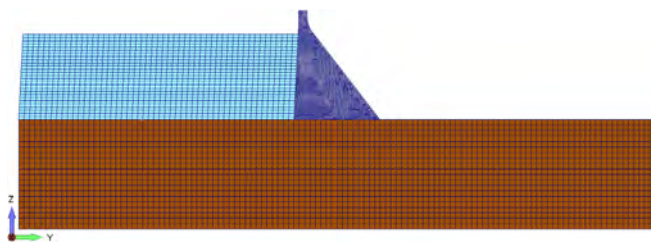

Fig. 1
FEM model of the dam monolith, the foundation and the reservoir.
Modèle FEM du monolithe du barrage, de la fondation et du réservoir.

Foundation rock is assumed to behave linear-elastically; the non-linear behaviour of dam concrete is simulated with the CDP or the XFEM models. As explained in Section 2.2, the CDP model allows to represent the brittle tensile failure of the material through a progressive loss of stress and a progressive degradation of elastic stiffness: the loss of stress and the growth of damage are assigned as functions of the progressive opening of the crack (Fig. 2). The damage variable can take values from zero, representing the undamaged material, to one, which represents total loss of strength. The area below the curve showed in Fig. 2, left, is equal to the fracture energy.

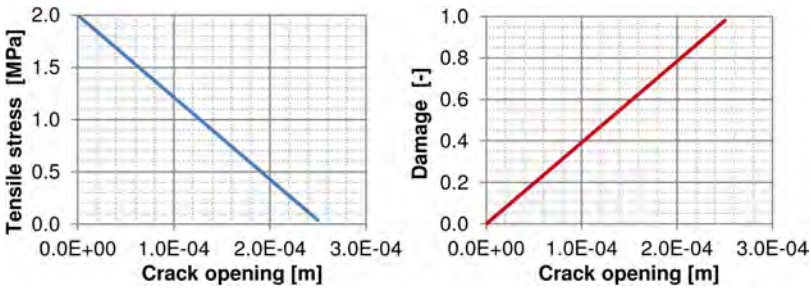

Fig. 2
Concrete Damaged Plasticity model (CDP). Tensile stress (left) and damage variable (right) versus crack opening.
Modèle Concrete Damaged Plasticity (CDP). Contrainte de traction (à gauche) et variable d'endommagement (à droite) en fonction de l'ouverture de la fissure.

Regarding the XFEM model, the evolution of the crack is described using the cohesive approach, which specifies damage properties as material characteristics. The tensile strength and the fracture energy are assigned to respectively define the initiation and propagation of the cracks, whose position is normal to the direction of the maximum principal stress. The behaviour of the continuum is assumed to be linear elastic until the maximum principal stress reaches the tensile strength: in the elements where this condition is reached a geometric discontinuity (crack) is created. Depending on the type of simulation (monolithic or considering interface non-linearity), dam-foundation interface is either ignored or supplied with friction no-tension behaviour: normal contact stress can be either zero (in open state) or compressive with a constitutive law reproducing the Coulomb friction behaviour (in closed state).

The dynamic interaction between the dam and the reservoir is achieved through the classic structural-acoustic coupling [26]; no dynamic interaction is considered between the foundation and the reservoir, while the upstream truncation of

the reservoir is provided with non-reflecting acoustic condition. The dynamic interaction between the dam and the foundation is approached either with the massless approach or with the SAM-4D model, depending on the type of analysis (foundation without or with mass). The principal physical-mechanical properties of the materials are summarized in Table 1. The viscous damping, assumed equal to 2% for both the dam and the foundation, is defined using the classic Rayleigh modelling.

Table 1
Material properties.
Propriétés du matériau.

PARAMETER	CONCRETE	ROCK	INTERFACE	WATER
Density [kg/m^3]	2483	2483 (0)		1000
Elastic modulus [MPa]	22410	22410		
Poisson's ratio [-]	0.2	0.2		
Compressive strength [MPa]	28.0			
Tensile strength [MPa]	2.0			
Fracture energy [N/m]	250			
Friction angle [°]			45	
Cohesion [MPa]			0	
Shear wave velocity [m/s]		1939		
Compressional wave velocity [m/s]		3167		
Sound velocity [m/s]				1439

3.2. Loadings

The static loads are the self-weight of the dam and the hydrostatic pressure at winter reservoir water level (268.21 m a.s.l.), applied both on the upstream face of the dam and on the surface of the foundation. The seismic action is the Taft horizontal acceleration time-history record of the M 7.3 Kern County, California, earthquake (peak ground acceleration of 1.77 m/s2), showed in Fig. 3 and considered as a free field ground motion at the surface of the foundation.

In the time-history analyses with the massless approach, the acceleration is uniformly applied at the base and at the side boundaries of the foundation. In the time-history analyses with the SAM-4D model, the seismic action is applied at the base and at the side boundaries of the foundation, provided with damper and spring elements to model the semi-unbounded extent of the foundation, by means of effective earthquake forces computed using the theoretical solution of the vertically propagating elastic wave problem in a half-space, considering the incident motion at the bottom foundation boundary ½ the surface motion.

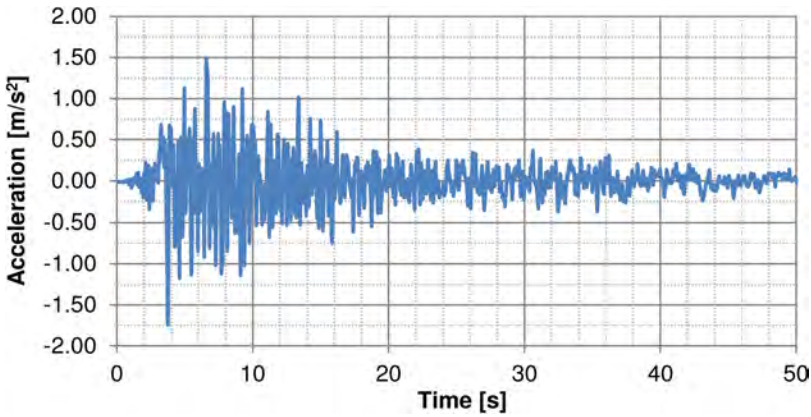

Fig. 3
Taft earthquake horizontal record: acceleration time-history.
Enregistrement horizontal de Taft séisme: évolution temporelle de l'accélération.

The dynamic coupled problem is solved using the implicit direct time integration method HHT [27], with integration time step of 0.005 s that well represents frequencies up to 10 Hz.

3.3. Results

The results of the analyses are reported in terms of damage evolution† and of horizontal dynamic relative (with respect to dam heel) displacement at dam crest.

Fig. 4 reports the tensile damage variable resulting from the non-linear (CDP model) time-history analyses either with the massless approach (left) or with the SAM-4D model (right). In the case with the massless approach, at the end of the analysis several damaged areas occur at dam-foundation interface (triggering both from dam heel and toe) and in the dam body (triggering from the downstream face near and below the slope change and propagating up to or towards the upstream face). The case with the SAM-4D model shows a dramatically less severe response:

†*Damage evolution is reported in terms of tensile damage variable (DAMAGET) in the case of the CDP model and of status of the enriched element (XFEMSTATUS) in the case of the XFEM model. Both these variables can take values in the range from zero (undamaged material) to one (fully damaged material).*

a small, damaged area occurs at dam-foundation interface in the nearby of dam heel, but the overall behaviour of the structure is almost linear [28] [29].

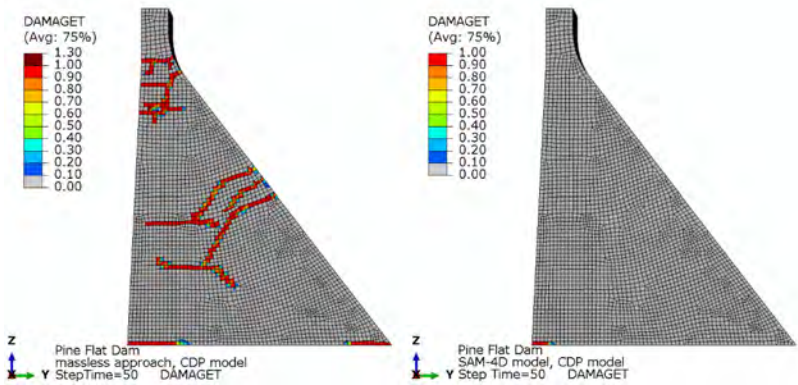

Fig. 4
Non-linear (CDP model) time-history analyses with the massless approach (left) and with the SAM-4D model (right): tensile damage variable (DAMAGET).
Analyses non linéaires (modèle CDP) avec l'approche sans masse (à gauche) et avec le modèle SAM-4D (à droite): variable d'endommagement par traction (DAMAGET).

Fig. 5 shows the status of the enriched element resulting from the non-linear (XFEM model) time-history analyses either with the massless approach (left) or with the SAM-4D model (right). In case with the massless approach, the simulation stops at 6.92 s (about 13% of the total run time) with level set errors, that seem to be related to the presence of multiple cracks (Fig. 6) that could have intersected if the analysis had continued and/or to an incorrect path of the crack (not uniform in the cross-stream direction). On the other hand, in the case with the SAM-4D model, the simulation correctly runs up to the end providing the same structural response of the corresponding case (time-history analysis with SAM-4D model) in which the non-linearities are modelled with CDP model, in terms both of damage evolution and of dynamic displacement at dam crest reported in Fig. 7 (maximum value of about 5 cm both towards downstream and upstream, without any residual displacement). In the same Fig. 7 also the results of the analyses with massless approach, for both CDP and XFEM models, are depicted: in the first 6.92 s (i.e. until both simulations exist) the trend of displacements is quite similar for the two non-linear models; afterwards, starting just after 7 s, the CDP massless case exhibits a significant drift towards upstream, up to a residual displacement of about 19 cm.

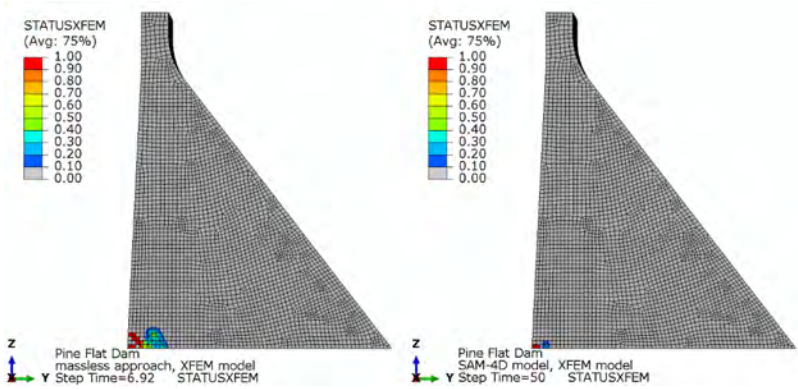

Fig. 5

Non-linear (XFEM model) time-history analyses with the massless approach (left) and with the SAM-4D model (right): status of the enriched element (STATUSXFEM).

Analyses non linéaires (modèle XFEM) avec l'approche sans masse (à gauche) et avec le modèle SAM-4D (à droite): statut de l'élément enrichi (STATUSXFEM).

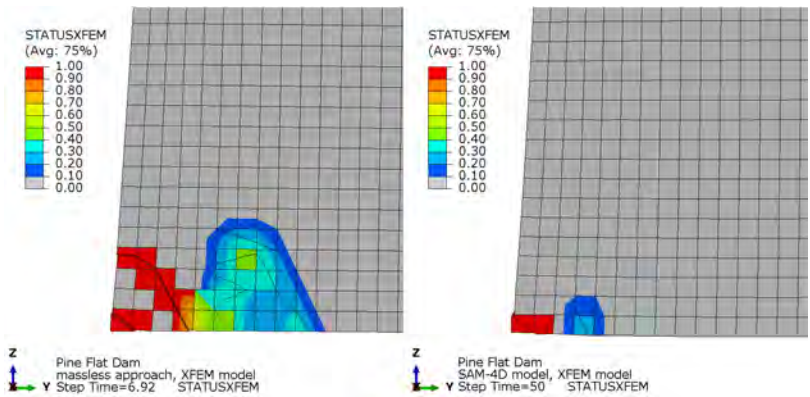

Fig. 6

Non-linear (XFEM model) time-history analyses with the massless approach (left) and with the SAM-4D model (right): status of the enriched element (STATUSXFEM), detail on dam heel.

Analyses non linéaires (modèle XFEM) avec l'approche sans masse (à gauche) et avec le modèle SAM-4D (à droite) : état de l'élément enrichi (STATUSXFEM), détail sur le pied aval du barrage.

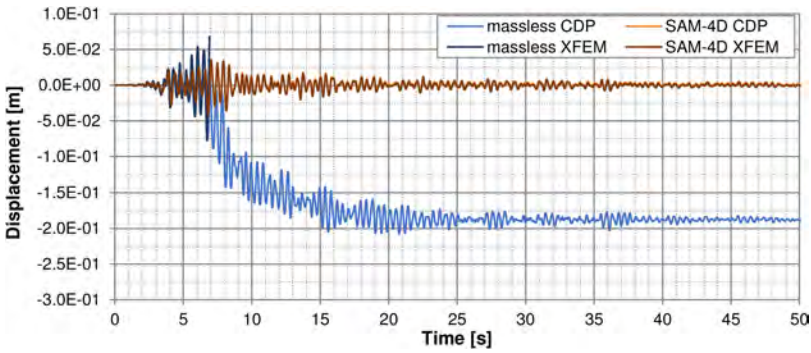

Fig. 7
Horizontal dynamic displacement time-history at dam crest: comparison among the non-linear time-history analyses (CDP or XFEM models, massless approach or SAM-4D model).
Évolution temporelle des déplacements dynamiques horizontaux en crête de barrage : comparaison entre les analyses non linéaires (modèles CDP ou XFEM, approche sans masse ou modèle SAM-4D).

In Fig. 8 the tensile damage variable (left) and the status of the enriched element (right) resulting from the non-linear (CDP or XFEM model and dam-foundation interface) time-history analyses with the massless approach are compared. The analyses with dam-foundation interface have been carried out to deepen the case with the XFEM model that seems to meet problems when the crack is near the boundary between two different materials. Both the analyses run up to the end, but they provide quite different results in terms both of damage/crack and of displacement at dam crest (Fig. 9). In the analysis with the CDP model several damaged areas occur in the dam body (triggering from the downstream face near and below the slope change and propagating up to or towards the upstream face): the damage state is quite comparable to that observed in Fig. 4, a little bit more severe. Even the trend of the dynamic displacement at dam crest is comparable to that observed in the case without dam-foundation interface, with a slightly higher residual displacement (about 27 cm). In the analysis with the XFEM model just a single crack can be observed, triggering from the downstream face in the lower half of the dam and propagating towards the upstream face: yet still, the maximum principal stress (Fig. 10) shows that other cracks should have formed as the tensile strength of the concrete is greatly exceeded in other significantly extended areas of the dam body. As a consequence of the significantly less severe damage state with respect to CDP case, the dynamic displacement at dam crest varies between 5 cm towards downstream and 10 cm towards upstream, without any residual displacement. Again, the simulation of multiple cracks seems to be a challenging and unresolved topic in the XFEM [30] [31].

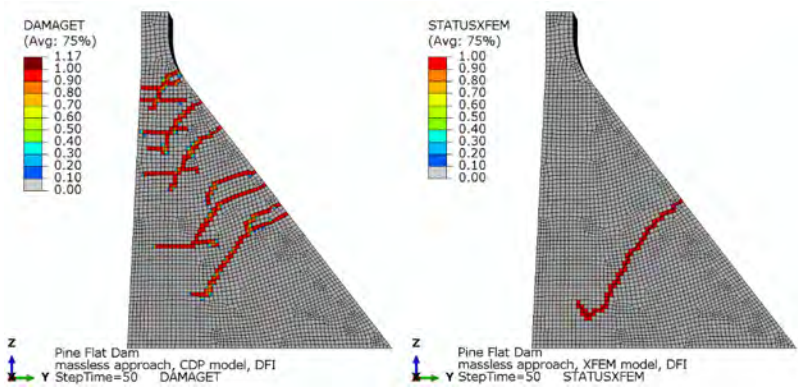

Fig. 8

Non-linear (CPD or XFEM model and dam-foundation interface) time-history analyses with the massless approach: DAMAGET (left) and STATUSXFEM (right).

Analyses non linéaires (modèle CPD ou XFEM et interface barrage-fondation) avec l'approche sans masse : DAMAGET (à gauche) et STATUSXFEM (à droite).

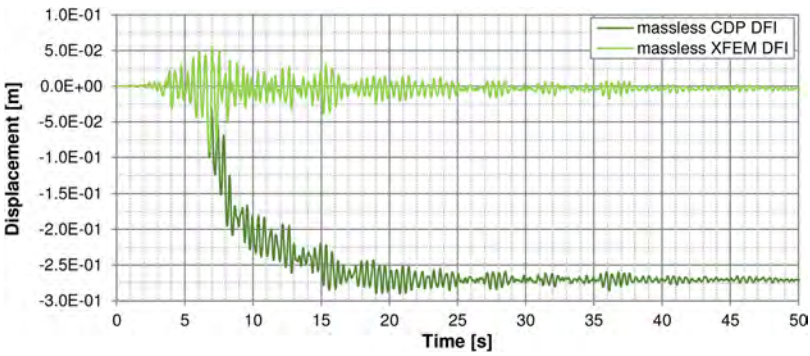

Fig. 9

Horizontal dynamic displacement time-history at dam crest: comparison between the non-linear time-history analyses (CDP or XFEM models and dam-foundation interface, massless approach).

Évolution temporelle des déplacements dynamiques horizontaux à la crête du barrage : comparaison entre les analyses non linéaires de l'historique (modèles CDP ou XFEM et interface barrage-fondation, approche sans masse).

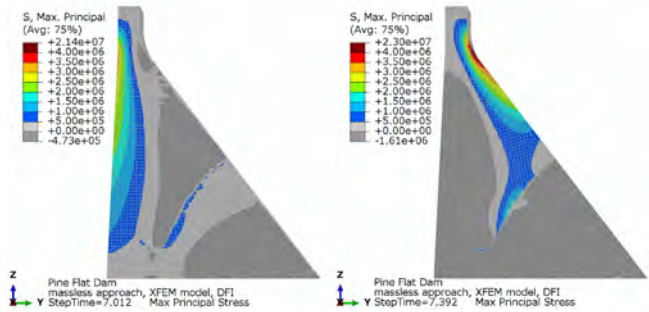

Fig. 10
Non-linear (XFEM model and dam-foundation interface) time-history analysis with the massless approach: maximum principal stress at step times 7.012 (left) and 7.392 (right).
Analyse non linéaire (modèle XFEM et interface barrage-fondation) avec l'approche sans masse : contrainte principale maximale au temps 7.012 (gauche) et 7.392 (droite).

4. CONCLUSIONS

The case study of Pine Flat Dam was adopted to try out the advanced numerical methods recently examined in the frame of RSE's research activity on dam safety: the SAM-4D (Seismic Advanced Model for Dams) model, recently implemented in the frame of the structural FEM codes used by RSE to simulate the propagation of seismic waves in a semi-unbounded massed foundation, and the two modelling approaches, the Concrete Damaged Plasticity model (CDP) and the eXtended Finite Element Method (XFEM), for the description of the cracking behaviour of concrete, both available in the commercial FEM code Abaqus.

Several case studies were carried out to compare the SAM-4D model and the traditional and consolidated massless approach and the two models that allow to simulate the cracking behaviour of concrete. The strong conservativity of the massless approach was highlighted by the results of all the performed analyses: in the cases with the SAM-4D model only a small damaged area occurs at dam-foundation interface in the nearby of dam heel, but the overall behaviour of the structure is almost linear, while in the cases with the massless approach and CDP model, the dam behaves in a strongly non-linear way.

The analyses performed with the XFEM model (and the massless approach, as in the SAM-4D cases the non-linear behaviour is actually not engaged) have brought to light many problems and difficulties: in the monolithic case the simulation stops abruptly at about the 13% of the total run time, after generating cracks with a

strange and incorrect path; in the case with the dam-foundation interface a single crack occurred despite the stress state would indicate that other cracks should trigger. As confirmed in some literature references, the simulation of multiple cracks seems to be a challenging and unresolved topic in the XFEM.

Due to the uncertainties and the complexity in their use, advanced methods benefit greatly from Benchmark Workshops that offer the analysts adequate tools and data for the verification and validation of their analyses and codes, also considering the frequent lack of available measurements.

REFERENCES

[1] FAGGIANI G., MASARATI P., POLIDORO F., BRUNO G. Modellazione dell'interazione diga-fondazione nell'analisi sismica delle dighe. Applicazione a casi bi-dimensionali. Ricerca di Sistema, RSE, n. 19012845, Milano, 2019.

[2] FAGGIANI G., MASARATI P., POLIDORO F., BRUNO G. Analisi sismica dei sistemi tridimensionali diga-bacino-fondazione con modelli di interazione avanzata. Ricerca di Sistema, RSE, n. 20010749. Milano, 2020.

[3] FAGGIANI G., MASARATI P., POLIDORO F., BRUNO G. Analisi sismica dei sistemi tridimensionali diga-bacino-fondazione, con modelli di interazione avanzata: applicazioni e confronti numerico-sperimentali. Ricerca di Sistema, RSE, n. 21010320, Milano, 2021.

[4] FAGGIANI G., MASARATI P., BRUNO G. Metodi avanzati per la modellazione dell'interazione struttura-fondazione nell'analisi sismica delle dighe: implementazione del modello di propagazione delle onde SAM-4D nel codice proprietario CANT-SD. Ricerca di Sistema, RSE, n. 22014055, Milano, 2022.

[5] LEE J., FENVES G.L. A plastic-damage model for cyclic loading of concrete structures. *Journal of Engineering Mechanics*, 124(8), 1998.

[6] LEE J., FENVES G.L. A Plastic-Damage Concrete Model for Earthquake Analysis of Dams. *Earthquake Engineering & Structural Dynamics*, 27(9): 937–956, 1998.

[7] BELYTSCHKO T., BLACK T. Elastic crack growth in finite elements with minimal remeshing. *International Journal for Numerical Methods in Engineering*, 45(5): 601–620, 1999.

[8] MOËS N., DOLBOW J., BELYTSCHKO T. A finite element method for crack growth without remeshing. *International Journal for Numerical Methods in Engineering*, 46: 131–150, 1999.

[9] CHEN D.H., DU C.B., YUAN J.W., HONG Y.W. An investigation into the Influence of Damping on the Earthquake Response Analysis of a High Arch Dam. *Journal of Earthquake Engineering*, 16(3): 329–349, 2012.

[10] LIU J., DU Y., DU X., WANG Z., WU J. 3D viscous-spring artificial boundary in time domain. *Earthquake Engineering and Engineering Vibration*, 5(1): 93–102, 2006.

[11] LIU Y.S., CHEN D.H. *Earthquake Response Analysis of a Gravity Dam Considering the Radiation Damping of Infinite Foundation*. APCOM & ISCM, Singapore, 2013.

[12] ZHANG C., PAN J., WANG J. Influence of seismic input mechanisms and radiation damping on arch dam response. *Soil Dynamics and Earthquake Engineering*, 29(9): 1282–1293, 2009.

[13] LØKKE A., CHOPRA A.K. Direct-Finite-Element Method for Nonlinear Earthquake Analysis of Concrete Dams Including Dam–Water–Foundation Rock Interaction. PEER Report No. 2019/02, Pacific Earthquake Engineering Research Center, Headquarters at the University of California, Berkeley, 2019.

[14] CLOUGH R.W. Non-linear mechanisms in the seismic response of arch dams, Proceedings of the International Research Conference Earthquake Engineering, Skopje, Yugoslavia, 1980.

[15] CHOPRA A.K. Earthquake Analysis of Concrete Dams: Factors To Be Considered, Proceedings of the 10th U.S. National Conference in Earthquake Engineering, Anchorage, Alaska, 2014.

[16] HANSEN K.D., NUSS L.K. Seismic Upgrades for Concrete Dams - Then and Now, *The Journal of Dam Safety*, 11(4): 21–35, 2013.

[17] ZHANG C., JIN F. Seismic Safety Evaluation Of High Concrete Dams Part I: State Of The Art Design And Research, The 14th World Conference on Earthquake Engineering, Beijing, China, 2008.

[18] LYSMER J., KUHLEMEYER R.L. Finite dynamic model for infinite media. *Journal of the Engineering Mechanics Division*, 95(4): 859–878, 1969.

[19] DASSAULT SYSTÈMES S.A. SIMULIA Abaqus Unified FEA. 2021.

[20] MASARATI P., MEGHELLA M. The FEM computer code CANT-SD for non-linear static and dynamic analysis of dams. Enel.Hydro PIS n. 6045, Milano, 2000.

[21] SALAMON, J.W. Evaluation of numerical models and input parameters in the analysis of concrete dams – A summary report of the USSD Workshop. USBR DSO-19-132018, Miami, 2018.

[22] TRIFUNAC, M.D. Scattering of plane SH waves by a semi-cylindrical canyon. *Earthquake Engineering & Structural Dynamics*, 1(3): 267–281, 1972.

[23] WONG, H.L. Effect of surface topography on the diffraction of P, SV, and Rayleigh waves. *Bulletin of the Seismologycal Society of America*, 72(4): 1167–1183, 1982.

[24] ROTS J.G., BLAAUWENDRAAD J. Crack Models for Concrete: Discrete or Smeared? Fixed, Multidirectional or Rotating? HERON, Delft, 1989.

[25] SALAMON J.W., WOOD C., HARIRI-ARDEBILI M.A., MALM R., FAGGIANI G. Seismic analysis of Pine Flat Concrete Dam. Theme A – Formulation and Synthesis of Results, Proceedings of the 15th ICOLD International Benchmark Workshop, Cham: Springer, Milano, 2020.

[26] ZIENKIEWICZ O.C. *The Finite Element Method*. 3rd Edition, McGraw-Hill, 1977.

[27] HILBER H.M., HUGHES T.J.R., TAYLOR R.L. Improved numerical dissipation for time integration algorithms in structural dynamics. *Earthquake Engineering & Structural Dynamics*, 5(9): 283–292, 1977.

[28] FAGGIANI G., MASARATI P., FRIGERIO A. Assessment of the Dynamic Response of Pine Flat Concrete Gravity Dam. FEM Simulation of Dam-Foundation Interaction. Proceedings of the 15th ICOLD International Benchmark Workshop, Cham: Springer, Milano, 2020.

[29] FAGGIANI G., MASARATI P. Assessment of the seismic behaviour of concrete dams: from simplified to advanced methods. Proceedings of the 18th World Conference on Earthquake Engineering (online), Milano, 2024.

[30] WEN L.F., TIAN R., WANG L.X., FENG C. Improved XFEM for multiple crack analysis: Accurate and efficient implementations for stress intensity factors. *Computer Methods in Applied Mechanics and Engineering*, 411: 116045, 2023.

[31] LØKKE A., CHOPRA A.K. Direct finite element method for nonlinear earthquake analysis of concrete dams: Simplification, modelling and practical application. *Earthquake Engineering & Structural Dynamics*, 48: 818–842, 2019.

Taylor & Francis
Taylor & Francis Group
http://taylorandfrancis.com

GENERAL REPORT ON QUESTION 111

RAPPORT GÉNÉRAL SUR LA QUESTION 111

Taylor & Francis
Taylor & Francis Group
http://taylorandfrancis.com

COMMISSION INTERNATIONALE DES
GRANDS BARRAGES

VINGT-HUITIEME CONGRES DES
GRANDS BARRAGES
CHENGDU, MAI 2025

QUESTION 111

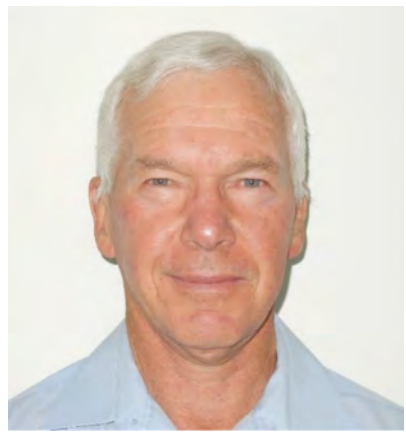

EARTHQUAKE PERFORMANCE AND SAFETY OF DAMS

DOI: 10.1201/9781003642428-150

GR Q.111

Trevor MATUSCHKA
Vice-Chair, ICOLD Committee on Seismic Aspects of Dam Design. Director, ENGINEERING GEOLOGY LIMITED

NEW ZEALAND

GENERAL REPORTER

TABLE OF CONTENTS

(*continued*)

Continued

1. INTRODUCTION

Dams generally have a good record of performance in earthquakes. However, although they only represent a small percentage of the causes of all dam failures, their consequences can be much more significant because there is generally no warning, so that affected people have little to no time to evacuate.

The subject of the present report "Question 111 – Earthquake Performance and Safety of Dams" was proposed by the Committee on Seismic Aspects of Dam Design. There are five themes

1. Static, seismic and post-seismic monitoring of dams
2. Feedback from earthquake failures, including tailings dams and levees
3. Importance of multiple features of earthquake hazard (e.g., ground shaking, surface fault movements, mass movements)
4. Seismic design and performance criteria for dam structure, reservoir rim and impacted area
5. Earthquake safety evaluation of all types of dams and safety-critical elements (e.g., spillway, low-level outlets)

Previous ICOLD Questions dealing with seismic aspects of dams were as follows:

- Question 18, 5th Congress in Paris, France in 1955
  Settlement of earth dams due to compressibility of the dam materials or of the foundation, effect of earthquakes on the design of dams
- Question 29, 8th Congress in Edinburgh, United Kingdom in 1964
  Results and interpretation of measurements made on large dams of all types, including earthquake observations
- Question 35, 9th Congress in Istanbul, Turkey in 1967
  Dams in earthquake zones or other unfavourable situations
- Question 51, 13th Congress in New Delhi, India in 1979
  Seismicity and aseismic design of dams
- Question 83, 21st Congress in Monreal, Canada, 2003
  Seismic aspects of dams

Several other Questions discussed at ICOLD Congresses have also dealt with earthquake hazard and the seismic vulnerability of dams.

The earthquake performance and safety of dams covers the full lifecycle; planning, design, construction, operation, decommissioning/closure. At a more detailed level it involves understanding the seismic hazards, siting to minimize risks, understanding potential failure modes, developing design concepts and details to mitigate the risks, constructing to high quality, independent peer review, good dam safe safety management and operational procedures, regular dam safety reviews

including periodic independent comprehensive safety reviews, and emergency preparedness and response plans. Many of these elements are covered in Q.111.

2. OVERVIEW OF REPORTS RECEIVED

A total of 52 papers from 12 countries were submitted. Seven were not related to Q.111 and are not discussed in this report. The largest number of contributions was from China (16) followed by Canada (3), Japan (3), France (3), Switzerland (3), Australia (2), Italy (2), and USA (2). The large number of papers submitted by China reflects the number of large dams that have been and are being built in China and because of the high seismicity in parts of the country where many dams are located.

A summary of the submitted papers related to the different themes (sub-questions) associated with Q.111 is provided below. It is noted that some papers covered more than one topic.

1. Theme 1: Static, seismic and post-seismic monitoring of dams: Addressed in the following 5 papers (R1, R5, R24, R41, and R50)
2. Theme 2: Feedback from earthquake failures, including tailings dams and levees: Addressed in paper R32
3. Theme 3: Importance of multiple features of earthquake hazard (e.g., ground shaking, surface fault movements, mass movements): Addressed in the following 6 papers (R10, R25, R26, R34, R37, and R45)
4. Theme 4: Seismic design and performance criteria for dam structure, reservoir rim and impacted area: Addressed in the following 25 papers (R2, R3, R6, R12, R13, R14, R15, R15, R18, R21, R22, R23, R27, R31, R35, R36, R38, R40, R42, R44, R47, R48, and R52)
5. Theme 5: Earthquake safety evaluation of all types of dams and safety-critical elements (e.g., spillway, low-level outlets): Addressed in the following 8 papers (R8, R9, R11, R19, R20, R30, R39, and R51)

Most papers submitted were associated with Theme 4 (design and performance criteria).

3. EARTHQUAKE PUBLICATIONS AND ONGOING WORK OF THE COMMITTEE ON SEISMIC ASPECTS OF DAM DESIGN

The Committee on Seismic Aspects of Dam Design, which at present comprises dam and earthquake experts from about 35 different countries, has prepared the following ICOLD Bulletins:

- Bulletin 27 (1975): A review of earthquake resistant design of dams
- Bulletin 46 (1983): Seismicity and dam design
- Bulletin 52 (1986): Earthquake analysis procedures for dams (Report prepared on behalf of the Committee on analysis and design of dams of ICOLD, O. C. Zienkiewicz, R, W. Clough, H. B. Seed)
- Bulletin 62 (1988): Inspection of dams following earthquakes - guidelines
- Bulletin 72 (1989): Selecting seismic parameters for large dams
- Bulletin 112 (1998): Neotectonics and dams
- Bulletin 113 (1999): Seismic observation of dams
- Bulletin 120 (2001): Design features of dams to effectively resist seismic ground motion
- Bulletin 123 (2002): Earthquake design and evaluation of structures appurtenant to dams
- Bulletin 137 (2011) Reservoirs and seismicity
- Bulletin 148 (2016) Selecting seismic parameters for large dams
- Bulletin 166 (2016) Inspection of dams following earthquake guidelines
- Position Paper (2021) Dam safety and earthquakes.

Three Bulletins have been published since Q.83 in 2003 (Bulletins 137, 148, and 2016). Bulletin 137 is about the topic of reservoir triggered seismicity. These are earthquakes that are triggered by the impoundment of large depths and volumes of water. They are normally associated with very large dams. Bulletin 148 provides recommendations for selecting seismic design parameters. The design criteria are dependent on the risk or consequences of failure. Many seismic guideline documents published by country members of ICOLD have adopted or adapted the recommendations in Bulletin 148. More details of Bulletin 148 are covered in Section 4.4 of this General Report. Bulletin 166 provides practical advice on undertaking safety inspections of dams following earthquakes.

The terms of reference of the current Committee on Seismic Aspects of Dam Design (2023-2026) were approved at the ICOLD General Assembly in Gothenburg, Sweden in 2023. They are:

1. Seismic design aspects of CFRD dams, dams with asphalt core and other types of liners.
2. Interpretation of seismic data obtained from dams.
3. Seismic deformation analysis of embankment dams.

4. Seismic aspects of safety-critical electro-mechanical and hydro-mechanical equipment
5. Dissemination of information on (i) seismic safety of existing dams, (ii) the updated design criteria for large dam projects, and (iii) the multiple hazards caused by strong earthquakes.

A summary of progress on these topics follows:

- ToR 1: A document is under preparation by a sub-working group.
- ToR 2: A significant number of strong motion records from dams have been collected from the March 11, 2011 Tohoku earthquake and its aftershocks, compiled by JCOLD. The acceleration records have been analysed by different organisations in Japan, Korea, Austria and France. The draft document is available and shall be finalised.
- ToR 3: For the design and safety evaluation of new types of embankment dams such as CFRDs and asphalt core rockfill dams, and dams located in highly seismic areas, more reliable methods of inelastic seismic analyses are required than the present methods, which are still based on the 50 years old linear equivalent method. A document was prepared by USSD in 2022, which shall serve as basis for a new ICOLD bulletin. A sub-working group was formed to prepare this bulletin.
- ToR 4: The seismic design of safety-critical electro-mechanical and hydro-mechanical equipment (spillway gates, low-level outlets) has not yet been covered by any ICOLD guidelines and is a requirement based on ICOLD Bulletin 148 “Selecting seismic parameters for large dams”. A sub-working group was formed to prepare this bulletin.
- ToR 5: The current seismic design and safety criteria of large storage dams (ICOLD Bulletin 148) were presented in workshops, seminars and conferences in a number of countries, mainly in Asia. Also, the fact that the earthquake hazard is a multi-hazard for large dam projects, must be disseminated as most of the seismic design guidelines focus on ground shaking only. Moreover, there is a need for the reassessment of the earthquake safety of existing dams as all dams should satisfy the same minimum seismic safety criteria. This is an ongoing activity, which is of main importance for “earthquake countries” and countries which are developing their water resources but are not able to participate regularly in ICOLD events.

Some of the previous terms of reference have not resulted in bulletins, but the issues have been discussed in several workshops in different countries with a significant number of dam engineers, academics and students participating in these events.

4. MAIN CHANGES AND DEVELOPMENTS IN THE SEISMIC DESIGN AND SAFETY EVALUATION OF LARGE DAMS SINCE 2003 Q.83

This section summarises new information and changes to the state-of-practice since the General Report (Q.83) in 2003.

4.1. Seismic hazard is a multi-hazard

It is very important to note that the seismic hazard is a multi-hazard and does not only include ground shaking. The main earthquake-related hazards that must be considered in large dam projects are as follows:

- Ground shaking causing vibrations in dams, appurtenant structures and equipment, and their foundations (most earthquake regulations are concerned with this hazard only). Ground shaking can result in deformations and cracking of dams, failure of appurtenant structures electro-mechanical equipment, softening or liquefaction of embankment and foundation materials, and waves in reservoirs;
- Fault movements in dam foundation or discontinuities in dam foundation near major faults which can be activated causing structural distortions and cracking of embankments;
- Fault movement in reservoir causing water waves in the reservoir (seiches) or loss of freeboard;
- Mass movements (rockfalls) causing damage to gates, spillway piers, retaining walls, powerhouses, electro-mechanical equipment, penstocks, transmission lines, access roads to dams, etc;
- Other site-specific and project-specific hazards.
- Reservoir-triggered seismicity (RTS) is another type of earthquake hazard, which must be considered in new dam projects. RTS is mainly causes ground shaking and mass movements. However, as most RTS events are relatively small, fault movements are not a major concern.

4.2. Significant earthquakes since 2003, which have caused important damage to dams and new lessons learnt from these events

There are always lessons to be learnt from dams subject to earthquakes. This covers all aspects of dam safety (planning, design, construction, operation, dam safety inspections, and emergency preparedness and response planning). Our knowledge can be considerably enhanced by observing and documenting the performance of dams subjected to earthquakes, comparing performance against

existing design methods and then amending existing or developing new design methods, and we can learn how to better prepare for and respond to earthquakes. Dam engineers are encouraged to read reports documenting the performance of dams subjected to earthquakes.

Several significant earthquakes have occurred since Q.83 in 2003. They include some very large earthquakes with Mw 8 or greater that had very long durations of shaking. Observations and some lessons learnt are summarised below. More details can be found in published papers and reports. The USSD has compiled reports on the observed performance of dams during earthquakes. Volume III covers earthquakes in the period 2000 to 2014 (Ref.3) and this is a useful resource.

1. **June 14, 2008 Mw 6.9 Iwate-Miyagi Nairku, Japan**
   134 dams were inspected after the earthquake. 12 were found to have been damaged but not seriously enough to result in uncontrolled release of water.
2. **May 12, 2008 Mw 7.9 Wenchuan, China**
   The Wenchuan earthquake was one of the most costly and damaging earthquakes in history. The earthquake damaged over 2,200 dams and reservoirs of all sizes and types in 8 provinces in China. Damage to dams included cracks in 1,425 dams, collapse and settlement in 687 dams, slides in 354 dams, leaks and seepage in 428 dams, mechanical hoisting equipment damage in 161 dams, and outlet works, spillway, and office building damage to 422 dams. This earthquake demonstrated that earthquakes have multiple hazards, not just ground shaking. Large rockfalls associated with this earthquake affected access to dam sites and caused substantial damage to powerhouses, gates, piers, and appurtenant structures. The Wenchuan earthquake provided a unique opportunity to evaluate the performance of dams subjected to significant earthquake loading. Many papers have been published on the learnings from this earthquake.
3. **February 7, 2010 Mw 8.8 Maule, Chile**
   At least 16 dams were moderately to severely shaken, with no reported failures.
4. **March 11, 2011 Mw 9.0-9.1 Tohoku, Japan**
   400 dams were inspected by the Japan Dam Engineering Center. Generally, dams performed well with minor or moderate cracking occurring at embankment dams. A 76 m high concrete gravity dam and a 48 m high RCC dam subjected to base PGA of between about 0.3 and 0.4 g suffered no damage. One embankment dam (approximately 18 m high) failed and 8 people were killed in the flood wave. The dam was constructed in 1949 and a preliminary report indicated that there may have been some flaws.
5. **April 16, 2016 Kumamoto, Japan (M = 7.0)**
   153 dams were inspected after the earthquake, 4 dams suffered some damage. This included a horizontal crack near the crest of the upstream concrete face of Jizoubara earthfill dam and fault rupture damage to the spillway of the Oh-Kirihata earth dam.
6. **November 14, 2016 Mw 7.8 Kaikoura, New Zealand**

Several small embankment irrigation dams (up to 25 m high) were located within 30 km of the fault rupture. PGAs of greater than 0.7 g were inferred at some dam sites. In general, there was very minor or no damage. Some minor longitudinal cracking on or near the dam crest and movement of riprap was observed in some cases. Seich waves were apparent in two reservoirs. The runup was estimated to be 1 m vertical. 196 landslide dams occurred. Monitoring was instituted at 12 locations that were considered hazardous. None resulted in breaches that put people at risk downstream.

7. **February 6, 2023 Mw7.8 Kahramanmaras, Turkey**

Two large shallow earthquakes with magnitudes of 7.8 and 7.7 occurred within the same day at two different locations in southeastern Turkey. They were associated with strike-slip faulting affected an area spanning several hundred kilometres. In this area there are approximately 140 dams. Seventeen dams of various types including zoned earthfill, earth core rockfill, earth core sand gravel, earthfill, and concrete-faced rockfill were damaged. The acceleration at the crest levels of the damaged dams was approximately 4 times greater than those at the foundations. It has provided a unique opportunity to evaluate the performance of large embankment dams that were subjected to significant earthquake loading.

The main feature of the 2008 Wenchuan and the Kaikoura earthquakes was the large number of mass movements, which exceeded 100,000 in both earthquakes. Therefore, more attention must be paid to mass movements in the safety evaluation of large dams, especially those located in mountainous regions. These mass movements created many landslide dams, most of them washed away within a short period, but some of them created risks to the downstream region. Mass movements may create impulse waves in the reservoirs, which can overtop dams. These impulse waves are most critical for embankment dams.

In the high mountains, earthquakes may trigger GLOFs (glacial lake outflow floods) or large mass movements in the catchment of reservoirs that can create large inflows into reservoirs.

4.3. Dam safety and seismic safety criteria

Safety includes the following elements, which must be considered in the seismic safety evaluation of large dams:

- Structural Safety: Design of dam according to state-of-practice (codes, regulations, guidelines) (earthquake and flood design criteria, methods of seismic analysis)
- Dam Safety Monitoring: Dam instrumentation, visual inspections, data analysis and interpretation, annual reports, etc.

- Operational Safety: Guidelines for reservoir operation under usual and unusual conditions, qualified staff, maintenance
- Emergency Planning: Emergency preparedness and response plans, water alarm systems, dam breach analysis, evacuation plans, engineering back-up, etc.

The general seismic safety performance criteria for the Safety Evaluation Earthquake (SEE) are as follows:

- To retain water in the reservoir,
- To control the water level in the reservoir after a SEE, and
- To lower the reservoir for (i) repair of damage, and (ii) to increase the dam safety if there are doubts about its static or seismic safety.

For controlling the water level and lowering of the reservoir the spillway and low-level outlets must be used and, therefore, must function after the SEE. As reservoirs can only be lowered to below the spillway sill after a strong earthquake, low-level outlets are highly recommended for all storage dams.

4.4. Dam risk classification and seismic design criteria

In the ICOLD Bulletin 148, the following recommendations are provided for determining seismic parameters. The seismic parameters are dependent on the risk (governed by the consequence of a dam failure) classification of the dam.

- For extreme or high consequence dams the SEE ground motion parameters should be estimated at the 84th percentile level if developed by a deterministic approach and need not have a mean annual exceedance probability (AEP) smaller than 1/10,000 if developed by a probabilistic approach.
- For moderate consequence dams the SEE ground motion parameters should be estimated at the 50th to 84th percentile level if developed by a deterministic approach and need not have a mean AEP smaller than 1/3,000 if developed by a probabilistic approach.
- For low consequence dams the SEE ground motion parameters should be estimated at the 50th percentile level if developed by a deterministic approach and need not have a mean AEP smaller than 1/1,000 if developed by a probabilistic approach.
- The ground motions for the OBE will usually have a mean AEP of about 1/145.

Dams with a height of less than 15 m, and small reservoir volume, may have to be designed for earthquakes with recurrence periods of 3,000 or 1,000 years.

Many seismic design guidelines have similar criteria as above but with variations in the definitions of the consequence classification and the seismic loading.

4.5. Seismic design criteria and definition of the different types of design earthquakes for dams

The main structures and elements of large hydropower projects are as follows:

- Main dam and saddle dams; the safety-critical elements like bottom outlets and spillways (including hydro-mechanical and electro-mechanical equipment, etc.), which must be operable after a strong earthquake, critical slopes at the dam site, the reservoir region and the catchment,
- Appurtenant structures such as powerhouse, penstocks, power waterways with intake and outlet structures, surge chambers, desilting facilities, tailrace structures, switchyard, non-safety critical hydro-mechanical and electro-mechanical equipment, access roads, etc. and
- Temporary structures such as cofferdams, diversion facilities, and retaining structures. In addition, critical construction stages of the dam and appurtenant structures must also be checked.

The following design earthquakes are recommended by ICOLD Bulletin 148 for the seismic design of the different structures and elements of a large dam project:

1. Safety Evaluation Earthquake (SEE): The SEE is the earthquake ground motion a dam must be able to resist without uncontrolled release of the reservoir. The SEE is the governing earthquake ground motion for the safety assessment and seismic design of the dam and safety-critical components, which must be functioning after the SEE.
2. Operating Basis Earthquake (OBE): The OBE may be expected to occur during the lifetime of the dam. No damage or loss of service must happen. It has a probability of occurrence of about 50% during the service life of 100 years. The return period is taken as 145 years. Dam owners sometimes adopt more stringent criteria for the OBE depending on their assessment of risks and consideration of economic impacts. This is especially the case for hydropower facilities. The OBE ground motion parameters are estimated based on a probabilistic seismic hazard analysis (PSHA). The mean values of the ground motion parameters of the OBE can be taken.
3. Design Basis Earthquake (DBE) for Appurtenant Structures: The DBE with a return period of 475 years is the recommended design earthquake for appurtenant structures that have no dam-safety critical role. The DBE ground motion parameters are estimated based on a PSHA. The mean values of the ground motion parameters of the DBE can be taken. (Note: The return period of the DBE may be determined in accordance with the earthquake codes and regulations for buildings and bridges in the project region if no seismic codes are available for these structures.)
4. Construction Earthquake (CE): The CE is to be used for the design of temporary structures such as coffer dams and considers the service life of the

temporary structure, seismic vulnerability and the consequences of its failure. There are different methods to calculate this design earthquake. For the temporary diversion facilities, a probability of exceedance of 10% is sometimes assumed for the design life span of the diversion facilities. Risk assessments may also be used to assist with assessing the CE. Alternatively, the return period of the CE of the diversion facilities may be taken as that of the design flood of the river diversion

The SEE ground motion parameters can be obtained from a probabilistic and/or a deterministic seismic hazard analysis as summarized below.

- Maximum Credible Earthquake (MCE): The MCE is the event, which produces the largest ground motion expected at the dam site on the basis of the seismic history and the seismotectonic setting in the region. It is estimated based on deterministic earthquake scenarios. According to ICOLD Bulletin 148 the ground motion parameters of the MCE shall be taken as the 84 percentile (mean plus one standard deviation).
- Maximum Design Earthquake (MDE): For large dams and those that have high consequences of failure the return period of the MDE is taken as 10,000 years. For dams with small or limited damage potential shorter return periods can be specified. The MDE ground motion parameters are estimated based on a probabilistic seismic hazard analysis (PSHA). According to ICOLD the mean values of the ground motion parameters of the MDE shall be taken. This is almost universally adopted but there are some differences. For example, ANCOLD (2019) requires consideration of the 85th fractile of the 1 in 10,000 AEP ground motion for Extreme Consequence dams. The justification is to make it more likely that a dam designed for this ground motion would satisfy ANCOLD's (2003) tolerable risk criteria. Australia is a country of generally low seismic hazard and the adoption of 85th fractile ground motions is not as onerous as in countries of high seismic hazard. In the case where a single seismic source (fault) is the main contributor to the seismic hazard, uniform hazard spectra can be used for the seismic design. Otherwise, based on the disaggregation of the seismic hazard (magnitude versus focal distance) different scenario earthquakes may be defined.

For high consequence dams the SEE ground motion parameters are taken as the maximum value of the MCE and MDE ground motion parameters if both earthquakes are determined, which is the normal case. However, if due to the prevailing seismotectonic setting there are no known active or potentially active faults, only the MDE may be determined. However, it is observed that in some earthquake guidelines a different definition of the SEE is given, which deviates from the above recommendation and the recommendations given in ICOLD Bulletin 148.

There are different definitions of active faults and where it is conservative (i.e., very long return period), and the fault is close to the site, the adoption of the MCE can be conservative compared to the MDE. For this reason, some guidelines define

the SEE as the MCE, but the ground motion need not exceed the MDE. If it is not possible to make a realistic assessment of the MCE, then the SEE should be taken equal to the MDE.

Site-specific seismic hazard studies are recommended for high consequence dams. The results of existing seismic studies may be considered for low consequence dams. Country or dam owner guidelines may provide specific advice on assessing seismic hazards and design criteria.

4.6. List of structures and elements of large dam projects, which have to be checked for the safety evaluation earthquake

The safety of the following elements of a large dam project must be checked for the SEE:

- Dam body (including saddle dams),
- Appurtenant structures with a safety-critical function (e.g., intake structures, walls or tunnels of ungated spillways)
- Safety-critical elements (gated spillways, low-level outlets),
- Dam abutments (abutment stability is most important for arch dams),
- Reservoir slopes (rockslides or landslides may plug intakes of safety-critical elements or may create large impulse waves in reservoir causing overtopping of a dam).

The safety-critical elements of dams are:

- Gates of gated spillways (gate systems including motors, oil hydraulic systems, power supply, control units, emergency power supply, cranes for lifting spillway gates, etc.), and
- Gates and valves of low-level outlets (sometimes called bottom outlets, irrigation outlets, sediment flushing outlets etc.) and their operational systems.

The safety-critical elements are used to control and lower the reservoir level in the case of emergencies; thus, the same safety standards apply as for the dam body. In the case of ungated spillways there are no concerns about controlling the reservoir level after a strong earthquake, provided the spillway chute and walls are undamaged.

4.7. Seismic safety evaluation of existing dams and procedure for periodic seismic safety checks of dams

Due to the following reasons the seismic safety of existing dams must be reassessed:

- New information on seismic hazard (multi-hazard) or seismotectonics is available;
- A dam has been subjected to strong earthquake shaking;
- New seismic design criteria are introduced;
- New seismic performance and safety criteria are introduced;
- New dynamic methods of analysis are introduced, such as nonlinear dynamic analysis methods;
- The seismic vulnerability of a dam has increased due to modifications, ageing etc.,
- Changes in risk or consequence classification of dams;
- The seismic risk has increased, e.g., due to the number of people living downstream of a dam having increased and due to economic development, etc.

At this time, the main reason for the reassessment of the seismic safety of large dams is the fact that there are dams, which were either not designed against earthquakes or that were designed against earthquakes with the pseudo-static analysis method in which the seismic hazard was characterized by a seismic coefficient of 0.1 (or a similarly low number). This method is considered obsolete today. This was already known since the 1971 San Fernando earthquake in California.

Seismic safety evaluations are also required for the reasons listed above. In order that all dams satisfy the current seismic safety criteria, periodic safety checks are required, for example, every five years, in which it is checked if important changes in the design and safety criteria, etc. have taken place. If this is the case, then a safety evaluation would be required. This may be necessary every 20 to 40 years. The term “important changes” is mentioned, because a lot of new developments are under way, especially in the field of seismic hazard analysis and new results may be published frequently. This does not mean that a seismic safety evaluation would be needed every time new seismic hazard results are announced. A substantial change in the response spectra would be required before a seismic analysis should be done, e.g., an increase in the PGA-value of more than 0.2 to 0.3 g is suggested.

4.8. Dynamic properties of mass concrete and rockfill

The study of dynamic material properties and constitutive models for concrete, soils and rock has evolved over time. Most available information is related to the dynamic material properties of concrete and rock, the shear strength of joints, and

the shear strain dependent shear moduli and damping ratios of soils, which are required in the different types of constitutive models and dynamic analyses of embankment dams. The uncertainties in material properties or even lack of them require extensive sensitivity analyses. New results for mass concrete, RCC and soils are expected. For concrete dams the main interest is in the damping ratio, which controls the dynamic response.

There is an increase in the compressive strength of concrete under dynamic loading. The Dynamic Increase Factor (DIF) is usually about 1.3 for the compressive strength of mass concrete but can be more than 1.5 for the tensile strength under seismic strain rate. The elastic modulus of mass concrete shows little increase under seismic strain rate. In the numerical analyses of nonlinear responses of concrete dams, the constitutive relationship after cracking is important, which is closely related to the fracture energy of the mass concrete. This influences the damage process under strong destructive earthquakes.

4.9. Shaking table tests of concrete dams

Shaking table tests are an important way to investigate seismic responses as well as the possible failure modes of concrete dams. The China Institute of Water Resources and Hydropower Research (IWHR) has carried out large scale experiments for large dam projects. In the shaking table tests, the dynamic dam-foundation-reservoir interaction, dynamic energy emission from near field to far field, opening and closing of contraction joints of arch dams, sliding of abutment wedges of arch dams, uplift pressure on the shear planes of the wedges and the overstressing of dam materials must been carefully simulated.

Besides the similarity in geometry, the scaled physical model must meet the similarity in the material properties and all the loads on a dam system. As water is used in the model reservoir, it is required that the density scale of material and the scale of acceleration must be unity so that the hydrostatic pressure in a normal gravitational field can be correctly represented.

For all the concrete dams tested at IHWR China in recent years, most seismic cracks were found on the upper part of the dam bodies as well as the dam-rock interfaces. The dynamic cracks may run through the dam body and form detached blocks with contraction joints. Very strong impact at horizontal cracks repeated during seismic overloading is observed, which results in dynamic crushing of concrete locally, displaying a potential failure mode.

4.10. Numerical analysis

There have been significant advances and application of numerical analysis since Q.83 in 2003. The seismic performance of dams is closely related to the earthquake induced deformations. Numerical analysis allows for modeling of the stress-strain characteristics of materials and estimation of the deformation when subject to earthquake ground motion. The analyses are performed using finite element or finite difference programs. Soils, in particular, behave in a nonlinear manner when subject to large stresses such as imposed by an earthquake. Constitutive models have been developed to simulate this behavior. The models have been developed in parallel with dynamic laboratory testing. Nonlinear deformation analyses can provide significantly greater insight into the anticipated response of a dam. They are valuable when the uncertainty in estimated performance resulting from the use of simpler analyses may sway the outcome of a dam safety evaluation or when a better understanding of seismic deformation patterns could improve the evaluation of dam performance. Persons undertaking numerical analyses should be aware of the assumptions, theory, limitations, and uncertainties associated with such analyses.

USSD (Ref.2) recently published a guideline document on the analysis of seismic deformations of embankment dams. A phased analysis approach that begins with simple evaluations and adds sophistication as needed is usually considered an effective approach to seismic deformation analysis of embankment dams. This approach also applies to other types of dams.

There are significant uncertainties associated with numerical analyses (associated with the numerical procedures, characterization of site conditions, ability of constitutive models to simulate soil behavior, the input seismic ground motion, and critical parameters such as liquefied or residual strength). Sensitivity studies are always recommended to understand the effects of various assumptions and to properly consider uncertainty. The main sources of uncertainty with numerical modeling are the earthquake ground motions and especially the characterization of embankment and foundation properties.

4.11. New types of dams

Traditional types of dams (concrete gravity, concrete arch and embankment dams) continue to be popular. There are new types of dams, which are being built in increasing number, i.e.

- Roller compacted concrete (RCC) dams,
- Concrete-faced rockfill dams (CFRD),
- Asphalt core rockfill dams,

- Rock-filled concrete dams (RFC), and
- Cemented material dams (CMD).

Very few of these dams have been exposed to strong ground shaking similar to the SEE, therefore, very few observations of their seismic behavior is available. These dams are built in seismic regions. There may be problems with dams with relatively thin waterproofing elements, when a dam is undergoing significant seismic deformations.

4.12. Developments for tailings dams

There is no accurate database of tailings dams in the world. Estimates of more than 30,000 have been published with more than 3,500 currently active. There are three main types of construction (upstream, centreline and downstream). Upstream construction is of particular risk when subject to earthquake ground shaking because tailings are partly relied upon to provide retention of the contents. Typically, tailings are placed as a slurry and are in a loose state. As such they are vulnerable to liquefaction. Breaches of tailings dam can have extreme consequences. The awareness of risks posed by tailings dams, including earthquake hazards, has increased significantly since Q.83, 2003. There is increased technical knowledge associated with seismic loading, the characterization and the behaviour of embankment materials, foundations and tailings, and application of this knowledge to the design of new tailings dams and when assessing the safety of existing tailings dams. In addition, some notable failures of large tailings dams in Brazil (Brumadinho and Fundao) resulted in a new Global Industry Standard for Tailings Management (GISTM). It covers six major topics:

- Topic I: Project-affected people,
- Topic II: Knowledge about the social, environmental and local economic context of a proposed or existing tailings facility,
- Topic III: Designing, constructing, operating, maintaining, monitoring, and closing tailings facilities,
- Topic IV: Management and governance of a tailings facility,
- Topic V: Emergency preparedness and response in the event of a tailings facility failure, and
- Topic VI: Public disclosure of information about tailings facilities to support public accountability

Topic III includes requires consideration of earthquake effects and provides recommendations for seismic design based on the consequence classification of the tailings storage facility.

Tailings are often susceptible to liquefaction and for upstream construction dams the assessment of liquefaction triggering and liquefied strength is vitally

important for assessing stability. The post-earthquake stability case often governs design. This requires assessment of the liquefied strength of the tailings. In some cases, it is advisable to undertake numerical modelling to assess deformations. The existence of foundations that are liquefiable or subject to softening under seismic loading adds to the complication of assessing stability.

In 2022 ICOLD published Bulletin 194 (2022) Tailings Dam Safety as a pre-print. It includes guidance on design for earthquakes covering seismic hazard, seismic design criteria, liquefaction assessment including liquefied shear strength, earthquake stability and deformation analysis. There is much research and regular conferences and workshops that are focused on the characterisation of tailings and tailings dam safety including seismic aspects.

4.13. Outlook on future developments

In future new developments may be expected in different areas that will affect the seismic analysis and design of new dams and the safety assessment of existing dams. In the assessment of future developments, the current ICOLD guidelines documented in several bulletins serve as benchmarks. As these guidelines, which represent the state-of-the-practice, have not yet been implemented by all dam owners or dam safety authorities, the first steps in the future will be to follow the recommendations made in these guidelines. The seismic safety standards used in some countries may be ahead of that of ICOLD and what is considered as new or future development may not be the case everywhere. It is also important to note that future development does not mean new research results but new methods and guidelines that are suitable for practical application. Several problems in the seismic safety evaluation of dams have been discussed, which may be considered as the subjects where future developments are needed. Accordingly, the following developments may be expected in the future:

- Seismic hazard evaluation of dam site:

  There are four important aspects:

  (a) besides ground shaking the earthquake hazard includes fault displacement, mass movements and others,
  (b) the dam engineer does not need real earthquake records as analysis input but models of the earthquake ground motion,
  (c) for the safety check of dams, spectrum-matched acceleration time histories of the safety evaluation earthquake are required, and
  (d) improvements in ground motion models, especially for ground motion parameters with very long return periods.

- The main future developments in the ground shaking hazard relevant for large dams include the following items:
  (a) evaluation of ground motion parameters of strong near-field earthquakes,
  (b) evaluation of site-specific geological and topographic effects on ground motion parameters,
  (c) evaluation of directivity effects on ground motion parameters at dam sites,
  (d) definition of duration of strong ground shaking of different design earthquakes,
  (e) development of site-specific (spectrum-matched) acceleration time histories used for the seismic safety assessment of dams,
  (f) development of non-uniform ground motion models for dams, and
  (g) use of recorded ground motions to calibrate theoretical estimates of seismic hazard and models that predict the response of dams.
- Seismic design criteria: Changes are related to
  (a) the seismic design of hydro-mechanical end electro-mechanical components of spillways and low-level outlets,
  (b) the seismic load combinations, and
  (c) the design criteria for dam cascades along rivers and very large reservoirs.
- Seismic performance criteria: The general criteria may remain, but there is a need for low-level outlets in storage dams.
- Dynamic material properties: New material models are expected for embankment dam materials. The deformational characteristics of rockfill are required as input for advanced deformation analyses of embankment dams.
- Methods of seismic analyses of dams: Nonlinear seismic analysis methods need further development. New types of embankment dams need reliable estimates of inelastic seismic deformations, e.g. asphalt core rockfill dams.
- Tailings dams: Tailings dams should satisfy the same safety criteria as water dams. Periodic safety checks are required even after decommissioning.
- Seismic instrumentation of dams: Seismic instrumentation should be installed in all large dams.

5. DISCUSSION OF PAPERS

5.1. GENERAL

A total of 52 papers were submitted. Seven papers were not related to the five themes associated with Q.111. A summary of the papers associated with each theme is provided below.

1. Theme 1: Static, seismic and post-seismic monitoring of dams: 5 papers
2. Theme 2: Feedback from earthquake failures, including tailings dams and levees: 1 paper

3. Theme 3: Importance of multiple features of earthquake hazard (e.g., ground shaking, surface fault movements, mass movements): 6 papers
4. Theme 4: Seismic design and performance criteria for dam structure, reservoir rim and impacted area: 25 papers
5. Theme 5: Earthquake safety evaluation of all types of dams and safety-critical elements (e.g., spillway, low-level outlets): 8 papers

Some papers submitted cover more than one subject. The papers have been reviewed and comments are provided in the following sections in accordance with the five main themes.

5.2. Static, seismic and post-seismic monitoring of dams

Most dams are monitored for deformation and seepage flows under static load conditions. Post earthquake monitoring of these parameters can provide useful information on a dam's performance. Monitoring of vibrations is also becoming more common and is encouraged by ICOLD Committee B. Papers associated with this theme covered monitoring of forced vibration tests and small seismic events to determine elastic stiffness and natural periods and assist with calibration of analytical models of dams. They also covered measurement of strong ground motions associated with larger earthquakes. Measurements of strong ground motions can be used to validate and calibrate models (analytical and empirical) that are used for design.

Paper R1 presents a statistical analysis of strong motion data recorded on existing embankment dams utilizing the JCOLD 2014 strong motion database that comprises190 shaking events from 54 earthquakes recorded on 60 dams. The strong motion data was recorded at dam foundations and crests from earthquakes occurring from 1978 to 2012. Multivariate analysis and linear/nonlinear fit modelling were employed to investigate seismic response characteristics and their pairwise correlations. The focus was on seismic amplification and fundamental periods, and their relationships with shaking intensity, dam geometry, and input motion frequency content. The range in PGA is large with the maximum up to close to 1.0 g, however, most data are less than 0.1 g. Correlations between the dam crest and foundation PGA (for earthfill and rockfill embankments), between the natural period of the dam and the foundation PGA, and between the natural period of the dam and dam height were determined. Correlations were developed for three directions (accelerations parallel and perpendicular to the dam crest and vertically). There is considerable scattering in the data and associated uncertainty with the correlations. However, they are helpful for estimating seismic response at a preliminary stage of design. Users need to be aware of the limitations (height of dam and limited number of recordings at high accelerations) when using the correlations. These types of studies are useful and should be repeated as further data becomes available.

Paper R5 describes the seismic monitoring systems and continuous dynamic monitoring system and forced vibration tests on concrete dams in Portugal. The dam heights are from 41.0 to 136.0m. Numerical models for dynamic analyses of the dams were developed, with the dam-foundation-reservoir system. The discontinuities related to the dam's contraction joints, the dam-foundation joint, and the dam-reservoir interface were represented, while the rock mass was assumed to be an equivalent continuum. The reservoir was discretized with macro-elements in the software 3DEC. The dam-reservoir interface was represented by an elastic joint with zero tangential stiffness. The models were initially calibrated with the results of forced vibration tests, considering a linear elastic behavior of the dam concrete. The purpose was to monitor the evolution of dam behaviour during the different phases of their life.

Paper R24 is an example that demonstrates the benefits of having accelerometers installed to monitor the performance of dams. It discusses the Paltinu dam, a symmetrical double curvature arch dam, located in Romania. Over time it has been subjected to an intensive monitoring program using in situ ambient vibration measurements. As part of this program, a finite element mathematical model was developed and calibrated using data from the initial measurement campaigns and employed to evaluate the structure's safety at each monitoring stage. If there is no change in the fundamental period of the structure over time it can be concluded that the dam has not suffered structural degradation.

A new system to enhance seismic monitoring capabilities was installed in 2022. It comprises six strong motion accelerometers and one broadband seismometer. The accelerometers are installed at the following locations: one in the free field, one on each abutment, one on the foundations, and two on the crest. The new system has recorded a series of low-intensity events. The enhanced monitoring program improves the capacity to detect seismic events and the reliability of assessing any structural degradation.

Paper R50 describes the measured response of the Horka dam located in western Bohemia in the Czech Republic. It is in area where there is historic seismicity including an estimated magnitude 6.5 earthquake inferred from a paleoseismic study. The Horka Dam is an earth embankment constructed in the period 1966-1970. No stability analyses for seismic loading were undertaken as part of the design. Requirements for seismic design were implemented after 1970. The paper summarises current seismic design requirements in the Czech standard CSN 75 2310 and compares it to estimates of PGA from probabilistic seismic hazard studies annexed to Eurocode 8.

A seismograph was installed in the lowest part of the grouting gallery in 2017, and four accelerometers were installed in 2019-2020. In April 2022 the Geophysical Department of Academy of Sciences of the Czech Republic installed 23 seismic probes and measured the natural vibrations of the dam. The first fundamental period of the dam was determined to be 3.12 Hz. The amplification of the crest motions was

20 times that measured at the base. The amplification would be expected to be smaller when subjected to earthquake ground motions representative of the SEE level due to the non-linear response of the earthfill.

Paper R41 presents recommendations for improving the safety of dams by better utilisation of monitoring data and preparedness before and post-earthquake events. It relies on full automation of monitoring information, and speedy interpretation of monitoring information and dissemination of recommendations and actions to parties responsible for dam safety and other stakeholders. The proposed system relies on an intelligent management platform with full integration and application of digital twins, AI models, and knowledge platforms. The concept has potential significant benefits but would require considerable effort to develop into a practical tool.

5.3. Feedback from observed performance, including tailings dams and levees

Observations and feedback on the performance of dams subjected to earthquake effects is vitally important to advancing the seismic resilience and safety of dams located in areas where seismic hazards exist. They provide insight into the behavior and consequences which can have implications for design, assessing the safety of existing dams and for preparing and managing emergency response to dam incidents and failures.

It is very useful if dams are instrumented with strong motion recorders at the base and crest as a minimum but also ideally in the free-field, on the abutments and at mid-height on the downstream shoulder. In some countries, some strong motion recorders are mandatory. ICOLD Committee B encourages dam owners to install such instrumentation. It allows assessment of fundamental dynamic characteristics, provides information for development and refinement of simplified empirical design methods and allows calibration of more advanced design methods.

Paper R32 is an important paper. It describes the seismic behaviour of the 210 m high Dagangshan arch dam，which was subjected to the magnitude Ms 6.8 Luding earthquake in China on September 5, 2022. The epicentral distance was 21 km. There are 21 strong motion instruments in the dam body and the foundation rock. The highest recorded PGA in the rock foundation was 0.22 g in river direction. With a horizontal PGA of 0.57 g, Dagangshan dam is the dam that was designed for the strongest ground shaking in China. The recorded peak acceleration on the dam crest was 0.51 g. A dynamic analysis of the dam-reservoir-foundation system was carried out using the recorded acceleration time histories in the dam foundation as input. The numerical analysis results were then compared with the measured ones during the Luding earthquake. It can be observed that the amplification of the peak acceleration at the base to the crest is about 2.4, which is quite small for a large arch dam. The analysis showed that the dynamic tensile strength of mass concrete was not exceeded during

the Luding earthquake, and the dam was undamaged. Contraction joint opening was analysed but no instruments were provided to measure joint openings during earthquakes. Dynamic joint meters are not yet in use and would only be of interest for research purposes, but not as standard instrumentation in large dams.

5.4. Importance of multiple features of earthquake hazard (e.g., ground shaking, surface fault movements, mass movements)

Seismic hazard is a multiple hazard. It includes ground shaking, fault displacement, hydrodynamic pressures, liquefaction, landslides (above the reservoir and submarine), rockfalls, and seiches. All these hazards need to be considered in the design of new dams and assessing the safety of existing dams.

5.4.1. *Earthquake ground motion*

The most important earthquake hazard is ground shaking. Large earthquakes can generate strong ground motions that can be felt over a wide area. There is increasing sophistication with methods for estimating ground shaking hazard that allow for aleatory and epistemic uncertainty. A wide range of possibilities for earthquake sources and ground motion models can be incorporated through a logic tree approach.

The effects of earthquake aftershocks are often underestimated or neglected in the design or retrofit of dams. Large earthquakes are typically accompanied by many aftershocks, and they can occur a short time after the mainshock. This is a potential concern for soils that are prone to softening or liquefaction effects and needs consideration. This arises because the pore pressures generated during the mainshock changes the effective stress state and alters how the material behaves during the subsequent aftershock events.

Paper R10 presents a numerical study investigating the effects of an initial earthquake, followed by aftershocks, on an idealized embankment system. The analysis is based on a 20 m high hypothetical embankment comprised of dense sand shoulders and a clay core with foundations consisting of 20 m of medium dense sand over bedrock. The analysis was conducted using FLAC 8.1 (finite difference program) which allows estimation of the embankment deformations (vertical and horizontal). The soils were modelled using PM4Sand (shoulders and foundation) or PM4Silt (core) and the bedrock was assumed to be linear elastic. The analyses considered different possibilities for the main and aftershock events and considered three different degrees of consolidation between the main and

aftershock events (as a proxy for different time intervals between the mainshocks and aftershocks).

The analyses provide an insight into how aftershocks can affect the deformations in an embankment. Aftershocks were shown to result in greater dam crest settlements. Interestingly the analyses showed greater settlements for higher reconsolidation between the mainshock and aftershock events. This may seem counter intuitive. The authors provide a possible explanation; the reestablished stiffness after higher reconsolidation decreases the dam's natural period, aligning better with ground motion frequency and energy. A limitation of the analyses is the lack of direct modelling of seepage during reconsolidation. This can be difficult to estimate with accuracy and is dependent on the time between the mainshock and aftershock which is not predictable. Designers should consider the effects of aftershocks on the performance of embankment dams where the embankment fill materials and/or the foundations are susceptible to softening or liquefaction. The analyses presented in Paper R10 provide insight. However, there will always be considerable uncertainty associated with any analyses and so sensitivity analyses and the use of judgement will be required in practice.

R34 present new slip-rate functions for modelling fault rupture time for use in simulations of earthquake ground motions. It is applied to an aftershock of the Luding earthquake and the predicted ground motions are compared with the recorded ground motions.

5.4.2. *Fault movement*

The identification of active faults is important when assessing the seismic hazard for dams. Fault rupture near a dam site can result in multiple hazards with ground shaking the moist prominent. If the fault underlies the site it can result in ground deformation that can severely damage a dam. Various methods can be used to identify active faults. ICOLD Bulletin 148 provides the following definition for an active fault for the purposes of dam design: "there is evidence of movement (earthquake events) during the Holocene Period (from 11,000 years ago), or for large faults showing evidence of movement during the Late Pleistocene Age (from 35,000 years ago), or for major faults main lines showing evidence of movement in the Quaternary Age (from 1.8 million years ago)." This definition is not universally adopted and there is some confusion as to what constitutes a large or major fault. In probabilistic seismic hazard analyses, it is best to err on the side of conservatism and include faults with long recurrence intervals. Faults with very long recurrence intervals generally have small influence on the SEE as the maximum recurrence interval for the highest dam consequence classification is generally 10,000 years. However, in deterministic analyses faults with very long recurrence intervals can result in much higher ground motions than from probabilistic analyses. Determining whether a probabilistic or deterministic approach is more appropriate for a given

dam site requires judgement. Designers may opt for the higher of the deterministic or probabilistic ground motion estimates where in doubt. In the cases where there are significant differences between deterministic and probabilistic estimates it is recommended to limit the reduction in seismic demand parameters to not less than 80% of the higher estimates.

Paper R25 refers to electric resistivity tomography, geo-radar, seismic refraction and seismic reflection as well as paleoseismic trenching and carbon dating on specific soil layers. The paper includes an example of identifying the active Sumatra Fault and different segments. Recommendations and examples are provided for the scale of maps depicting the locations of faults, for undertaking various types of geophysical surveys, for paleoseismic trenching and for carbon dating.

5.4.3. *Seismic hazard studies*

Indonesia is a country with very high seismic hazard. There are four major subduction zones and many large shallow crustal faults that are all capable of producing major earthquakes. Paper R26 discusses the current practice of seismic hazard assessment for dams in Indonesia with reference to a new guideline document on undertaking seismic hazard studies for dam projects in Indonesia (Guidelines of Seismic Study for Determination the Earthquake Design Parameters, Volume I, Seismic Hazard Assessment). The guideline is awaiting review before being published by the Indonesian Ministry of Public Works and Housing. It covers guidance required for feasibility studies and detailed design. It also covers evaluation during construction where excavations for the dam foundation and appurtenant structures may reveal the existence of faults which were not previously identified. The scope and details of seismic hazard studies are dependent on the consequences of failure of the dam. The level of detail and requirements for the seismic hazard study are dependent on risk factors that are related to reservoir volume, height of dam, number of people that require evacuation and downstream damage factor. These four factors are summed to obtain a Total Risk Factor. There are four Risk Classes (I, II, III, and IV). Seismic hazard studies are required for all dams during the feasibility study. They use the latest Indonesian Earthquake Source and Hazard Map published by PuSGeN/Ministry of PUPR to obtain an indication of the PGA. The dam risk level is assessed using this estimate of PGA. If the dam is assessed as Class III or Class IV risk class, then more detailed studies (regional and near-field) are required to identify and characterize earthquake sources and nearby earthquake faults. The paper outlines the details of the studies required to identify and characterize active faults. The paper recommends that where parallel fault segments are separated by less than 4 km then then the segments should be combined and treated as a single fault. Estimates of the SEE ground motion are based on deterministic estimates considering the active faults that are identified.

5.4.4. *Reservoir-triggered seismicity*

Reservoir-triggered seismicity commonly is associated with high dams with large reservoirs. Paper R37 presents the results of a study of the geological structural conditions of the epicentral areas of the strongest earthquakes occurring at five large dams in China (Xinfengjiang, Danjiangkou, Shanxi, Xiluodu and Three Gorges) to determine how they affect reservoir triggered seismicity. Conditions found to be important factors include (1) Brittle rock mass; (2) The fault intersects the regional principal compressive stress field at a small angle, and the dip angle of the fault is large (the intersection angle is generally less than 20 °, and the dip angle of the fault is greater than 60 °; (3) The reservoir body is located in the footwall of the fault; (4) There is a direct or indirect hydraulic connection between the fault zone and the reservoir. Other conclusions were that the background seismicity in the reservoir area and adjacent to the reservoir prior to impoundment has no effect on the intensity of reservoir triggered seismicity. There was no obvious correlation between the activity of existing faults prior to impoundment of the reservoir and the intensity of reservoir triggered seismicity.

Paper R45 presents the results of a study to determine details of seismogenic structures from analysis of digitised waves recorded by a network of 35 seismographs located in the Xiangjiaba and Xiluodu reservoir areas over four years. The Xiangjiaba and Xiluodu hydropower stations are large with installed capacities of 6.4 million kW and 13.86 million kW, respectively. They have reservoir storage capacities of 5.19 billion m3 and 13.9 billion m3, respectively. Following impoundment of water in the reservoirs there was a significant increase in seismicity. The two largest are reported as magnitude 5.1 and 5.2. This phenomenon is a well-known feature associated with large reservoirs. It is attributed to the increased loading and stresses resulting in deformations in the underlying earth's crust. Normally a combination of analysis of earthquake focal mechanisms and earthquake aftershock distributions is used to determine the location and geometry of seismogenic structures. This paper presents the results of using the theory of double-difference tomography which can simultaneously solve the problems of 3D velocity structure inversion and allows more accurate location of earthquakes. The paper explains the methodology and presents the results when applied to the Xiangjiaba and Xiluodu reservoirs.

5.5. Seismic design and performance criteria for dam structure, reservoir rim and impacted area

This theme of Q.111 had the most papers. There is steady evolution and development of country statutory requirements that require consideration of seismic loads and effects in the design of dams and when undertaking dam safety reviews. New and updated guideline documents continue to be published. They include:

- ICOLD Bulletin 148 (2016) Selecting seismic parameters for large dams

- ICOLD Bulletin 166 (2016) Inspection of dams following earthquake guidelines
- ICOLD Bulletin 194 (2022) Tailings Dam Safety, preprint- final version submitted for publishing
- ANCOLD Guidelines for Design of Dams and Appurtenant Structures for Earthquakes (May 2019)
- USSD Analysis of Seismic Deformations of Embankment Dams (2022)
- NZSOLD New Zealand Dam Safety Guidelines 2024

In addition, there is ongoing research, development of performance criteria and design methods that have been published and presented at various technical conferences and workshops. This includes development and advancement of design methods, especially related to numerical modelling. There is also development in simplified methods that have their place in design and safety assessments of existing dams.

Practitioners are reminded that earthquake safety of dams is much more than estimating seismic hazard and advanced dynamic analyses. It is about understanding potential failure modes and the development of mitigation measures (design concepts and details), quality of construction, independent peer review, dam safety management including safe operational procedures, surveillance and monitoring (focused on potential failure modes), maintenance, regular dam safety reviews including periodic independent comprehensive safety reviews, and emergency preparedness and response plans.

The papers submitted for this theme cover many types of dams and different aspects of performance criteria and design.

5.5.1. *General guidelines*

The issue of the challenges with ongoing progress in the field of probabilistic seismic hazard analysis often resulting in increases in seismic hazard is discussed in paper R7. It is a challenging issue for dam owners and regulators, both for new dams and for safety assessments of existing dams. It may normally be assumed that a seismic re-evaluation is required where there has been a change in estimates of seismic hazard. Paper R7 notes that one should be aware of the fact that the seismic safety analysis of dams includes various uncertainties which are comparable with those of the seismic hazard and simply improving the seismic hazard analyses will not improve the quality of the seismic safety assessment if the other uncertainties remain unchanged. The main conclusions and recommendations are:

1. Minor changes in the seismic hazard in the order of 0.1-0.2 g in regions of moderate to strong seismicity do not require any re-analysis of well-designed, well-constructed and well-maintained dams.

2. A “beyond the SEE ground motion” load combination, in which the ground motion of the safety evaluation earthquake is multiplied by a factor of 1.5 or 2.0, is recommended as an additional seismic load combination. This load combination can be used to determine the seismic safety reserves of a dam project. At the same time, there will be no need for a seismic re-analysis of dams, when the increased seismic hazard is less than that of this extreme load combination.
3. It is expected that a comprehensive seismic safety evaluation of a dam may only be required approximately every 20 to 40 or even 50 years, unless a dam shows signs of unusual behavior, or its risk classification is increased.

Paper R23 presents new rules on seismic hazard in dams in Albania. Albania is a country that has a high level of seismic hazard. It has almost 650 dams of which 350 are classified as large dams. Most are embankment dams. The original seismic design of most dams was based on a pseudo-static approach with a seismic coefficient of 0.1. Albania Committee on Large Dams (ALBCOLD) is planning to prepare National Standards and Guidelines for the design and monitoring of dams where the methodology for the assessment of seismic hazard will be described in detail. ALBCOLD proposes three dam risk classifications (Small, Moderate and High Potential risk). The level of ground shaking hazard is proposed to be related to the dam risk classification. For irrigation dams the design PGA is obtained by factoring existing 475-year return period estimates of PGA prepared by the National Institute of Geosciences (IGEO). The scaling factors are 1, 1.2, and 1.4 for Small, Moderate, and High potential risk dams, respectively. For large dams with hydropower generation, water supply and urban purposes, the importance parameters have to be applied on the same return period of PGA parameters on rock condition that are given in the original designs of them or ICOLD Bulletin No. 148, dated 2016.

5.5.2. *Embankment dams*

Papers were received on a range of topics related to the design of embankment dams and with some papers focused on particular types of dams (CFRD, CSG, and tailings dams).

Paper R3 presents the dynamic analysis of the Santa Rita Dam in Colombia as a case history where the potential for liquefaction is considered in the assessment of the performance of embankment dams. The analysis is undertaken using FLAC2D software. Two soil constitutive models are used: 1) Mohr-Coulomb and a more advanced model 2) PM4Sand/Silt constitutive model. Analyses are run for four different return periods (475, 2,500, 5,000, and 10,000 years). The estimated deformations using the different constitutive models are compared. Greater deformations are estimated with the PM4Sand/Silt constitutive model. The paper provides a good summary of the steps to follow including guidance on setting up the

model, selection and scaling of accelerograms, and selection of soil model parameters when undertaking dynamic analyses using an advanced constitutive soil model like PM4Sand/Silt.

Paper R13 introduces a three-dimensional (3D) formulation of a simple and practical constitutive model designed to capture the nonlinear hysteretic damping characteristics of non-liquefiable materials under earthquake loading. This model is a 3D extension of the two-dimensional (2D) UBCHyst model, developed at the University of British Columbia, which has been extensively employed for modelling of soils typically used in embankment dams such as compacted clays, dense and unsaturated rockfill, or stiff foundation and weathered bedrock. The 2D model was formulated and implemented in the 2D space, taking into consideration the hysteretic nature of the material, the shear modulus variation as a function of the stress ratio, limiting this ratio by a Mohr-Coulomb yield surface criterion. The 3D model uses the Mohr-Coulomb yield surface generalized in 3D principal stress space but also addresses some limitations with the original 2D model. The paper takes the reader through the formulation of the 3D model including the improvements to the model. The 3D formulation has been implemented as a user-defined model in FLAC2D/3D version 9.0 for application in boundary value problems.

Paper R13 presents the results of a comparison of the new 3D model with the original 2D model for monotonic and cyclic direct simple shear tests. The model is then verified against experimental data for rockfill and gravelly materials in both static and cyclic triaxial stress paths. A key improvement in the 3D model is its capability to capture the shear modulus reduction that occurs in the cyclic triaxial stress paths. Finally, a seismic response analysis is carried out by applying a seismic record at the base of a one-dimensional (1D) column. The results of the conventional UBCHyst model are compared to the 3D extended UBCHyst model. For isotropic stress conditions the results are identical. For K_0 stress conditions the 3D model predicts higher cyclic stresses and displacements.

The work in extending the original 2D UBCHyst model to 3D and the improvements to the model represent an advancement in this constitutive model. The authors note that UBCHyst has been developed to simulate shear induced deformation of rockfills, gravelly materials and dilative cohesive soils under cyclic loading. In its current form the model is not capable of capturing other mechanisms that may cause permanent deformations such us particle degradation causing a reduction of the effective strength properties, and seismic compaction, among others. Future updates of the model will be implemented focusing on these limitations.

Paper R22 presents a simplified and graded approach for assessing the seismic behaviour of embankment structures. It begins by describing a linearization method that considers the effects of pore pressure on the equivalent linear shear modulus. This approach is applied to the Aratozawa dam (PGA 1.04 g). Subsequently, a graded approach (static, simplified dynamic, nonlinear time response) is implemented on an

embankment dam similar in height to Aratozawa and subjected to very strong seismic loading (PGA 1.22 g). Finally, a new simplified method for evaluating the seismic behaviour of levees, embankments, and medium-sized dams is presented. This method accounts for the specific geometries and foundation properties of these works in the assessment of their seismic behaviour. More instrumental data obtained from earthquakes will allow validation and calibration of the proposed methods.

Estimates of deformations in earth-rock dams resulting from earthquake loading are critical to assessing their performance and seismic safety. There are different methods that can be used. One is global deformation analysis. It considers the soil as a continuous medium with its dynamic constitutive behaviour based on experimental testing combined with finite element modelling. Paper R48 evaluates two existing models and introduces a new residual deformation model based on the mechanisms of permanent earthquake deformation, addressing the shortcomings of the current models. The first existing model is the dynamic stress-residual strain model. It describes the relationship between dynamic stress and residual strain at a certain vibration cycle. The second existing model is the cycle dependent-residual strain model. It provides a comprehensive description of the relationship between residual stress and the number of vibration cycles. The new model that is introduced in paper R48 has the advantage that it precisely defines the significance of each parameter, incorporating dynamic and consolidation stress state parameters in the analysis of soil sample variations during residual deformation tests, thereby enhancing physical clarity. The relationship between parameters and vibration cycles is more pronounced, enhancing the model's overall comprehensibility and providing more reliable data for interpolation calculations. The model is suitable to be applied to sandy gravel and medium-coarse sand under well-drained conditions. It requires running dynamic tests with different shear stress ratios on samples at different consolidation ratios and confining pressures.

Paper R47 presents the concept of using geogrids to reinforce and improve the strength of fill at the base of high rockfill dams and in the upper part of the foundations. The improvement in the factor safety for stability with geogrid reinforcement is demonstrated by way of an example.

Paper R12 presents a summary of the design of a new 52 m high Concrete Faced Rockfill dam (CFRD) in New Zealand (Waimea Community Dam). The primary purpose is for irrigation. The SEE earthquake is a 1:10,000 annual exceedance probability (AEP) probabilistic ground motion from an earthquake with a moment magnitude of 7.1, a peak ground acceleration (PGA) of 0.64 g and maximum spectral acceleration of approximately 1.65 g. The NZ Dam Safety Guidelines require that the design must include one aftershock within a day following the mainshock. The design aftershock for Waimea Dam has a moment magnitude of 6.5 and PGA of 0.58 g.

Key elements of the design include:

- An erosion-resistant and flexible rockfill embankment, allowing controlled movement during earthquakes. The overarching embankment design performance requirements were the accommodation of earthquake deformations and conveyance of post-earthquake leakage which would have reduced embankment stability to an unsafe level.
- A reinforced concrete facing slab with appropriate slab dimensions, joint details and reinforcing.
- Flexible waterproofing elements connecting the facing slab to the crest walls, as well as between wall elements with appropriate capability for accommodating large movements, and post-seismic flooding.

Dynamic 2D numerical analyses were undertaken to estimate the deformations of the embankment under the design seismic loads. Maximum vertical deformations of the crest of 1.1 m occur with the reservoir at the normal minimum operating level. The design aftershock results in another 0.35 m of vertical deformation. The amount of deformation is expected to result in joint opening and cracking of the concrete facing. A flexible external waterstop system was adopted to accommodate the expected movement between the parapet wall and the face slab.

The paper outlines the seismic potential failure modes and discusses the design concepts adopted to mitigate the effects. Post-earthquake damage to the concrete facing is anticipated and failure modes include leakage discharge resulting in unravelling of the downstream toe progressing to backward erosion towards the reservoir and seepage pressures resulting in global instability. Design mitigation features include a cohesionless sandy transition zone and inclined drain downstream of the concrete facing that is contiguous with a blanket drain that extends from behind the upstream plinth to the downstream toe of the embankment dam. Paper R12 is a useful reference that documents design issues and mitigation features for a CFRD located in a high seismic environment.

Asphalt concrete face rockfill dams are used in China in pumped storage power projects due to its low permeability, ability to accommodate deformations, strong resistance to acid- and alkaline-corrosion and no pollution to water quality. Paper R36 presents the design analyses for earthquake loading for a 101 m high asphalt concrete face rockfill dam associated with a pumped storage reservoir located in northwest China. The design thickness of the asphalt lining is 20.2 cm. The analysis uses a 3D finite element model. Details of the modelling and design assumptions are provided in the paper. The 1 in 5,000 and 1 in 10,000 AEP bedrock PGA values at the site are 0.74 g and 0.90 g, respectively. The analyses demonstrate that the design can meet the safety requirements during the periods of construction, impoundment and operation, as well as under the given earthquake working conditions. During the earthquake loading the slope stability safety coefficient is less than 1.0 for only very short periods of time and the resulting deformations are acceptably small. Tensile and compression stresses in the asphalt concrete face and reservoir basin meet the design requirements and it is concluded

that the asphalt liner can safely retain the water. The post-earthquake settlement at the crest is about 1 m and meets the freeboard performance criteria.

Cemented sand and gravel (CSG) dams are a relatively new type of dam that was developed in Japan. They are constructed from mixing a small amount of cement with unprocessed gravel and sand obtained from riverbeds or alluvial plains or excavated weak rock. It is an economical type of construction that has environmental advantages. The Apporo Dam, a 47.2 m high CSG dam located in Japan, was subjected to a peak acceleration of approximately 0.45 g measured in the bottom inspection gallery during an earthquake in 2018. It was undamaged providing evidence of the successful seismic performance of this type of dam.

Paper R15 presents the results of a study on the effects of the elastic modulus and of the upstream and downstream slopes of a hypothetical 50 m high CSG dam on the seismic performance. Seismic response analyses were undertaken with different upstream and downstream slopes and with different cement contents to determine the most economical design. Numerical analyses used with an input acceleration time history with a peak acceleration of 320 cm/s^2. Details of the assumptions and results are provided in the paper. It was concluded that the dam volume and the total amount of cement used may be reduced while ensuring the seismic stability of the dam by flexibly adjusting the slope and the arrangement of the unit cement content. It was demonstrated that the dam volume could be reduced by 10%, and the total amount of cement could be reduced by 11%.

Paper R2 presents an example of raising of an existing tailings dam in the Republic of North Macedonia by upstream construction where the SEE PGA for the site is 0.36 g. The paper discusses the evolution of the design informed by application of design methods that recognize the potential for liquefaction of the tailings and the need to consider both the deformations that can arise during and post the design earthquake and consideration of the post-earthquake stability Factor of Safety. The design evolved considerably from the initial concept and eventually included buttressing of the existing starter dam and a widened upstream embankment. The peak and liquefied strengths of the tailings were determined from empirical relationships using the results from SPTs and CPTs conducted at two locations. The dynamic response was modelled using an equivalent linear analysis method (SIGMA/W, GeoStudio). There is now some good advice available on assessing the performance of liquefiable soils and the effects on tailings dams. This includes ICOLD Bulletin 194 “Tailings Dam Safety” [1] and a publication by the USSD “Analysis of Seismic Deformations of Embankment Dams” [2].

Paper R44 summarises Chilean practice for the design of large tailings dams in a high seismic environment. Mining is a large industry in Chile, e.g., approximately 25 % of the world’s copper production was from Chile in 2023. There are large volumes of tailings that need to be managed and contained in reservoirs formed by

dams. Many are very large dams (the largest over 200 m high). Chile is in an area of high seismic hazard due to its location on the boundary between the Nazca and South American tectonic plates. The experience and practice for design of tailings dams in Chile is of interest because of the high number of large tailings dams and high seismic hazard. Paper R44 summarises the performance of tailings dams subjected to large earthquakes in Chile, provides examples of downstream and centreline dams constructed from cyclone tailings sands that have withstood very high levels of earthquake ground motion, and provides a summary of key aspects that are considered in the design of tailings dams in Chile.

A notable failure of the El Cobre tailing dam in 1965 led to the Chilean government banning upstream tailings dams in 1970. Since then, there have been some further failures of upstream construction dams due to liquefaction of tailings initiated by strong earthquake ground motion. However, dams constructed by downstream or centreline methods have performed well when subjected to strong ground motion. Key aspects of design covered in the paper include the assessment of seismic hazard, properties of cyclone tailings used in the construction of many tailings dams in Chile, control of the phreatic surface, considerations of high confining pressures on geotechnical properties (compressibility, permeability, cyclic strength), design process, stability analyses (pseudo-static, pseudo dynamic, dynamic), and acceptable performance criteria. Pseudo-static stability analyses to assess seismic stability are a statutory requirement in Chile even though it is well understood that such analyses are not considered appropriate. However, other design methods that are considered state of practice are undertaken. Sometimes it can take time for statutory requirements to be amended to reflect current practice.

5.5.3. *Concrete gravity dams*

Paper R18 introduces several important aspects in the seismic design of concrete dams: (1) select design earthquakes; (2) define design ground motions; (3) compute stress and deformation demands by dynamic analysis of the dam-water-foundation system.

Paper R18 notes the service life of many dam projects is taken as 100 years; however, many important dams have already existed in service for more than 100 years or very close to 100 years and will most likely remain functional for many more years to come. The paper makes the point that if a service life of 200 years is considered, then for the same probability of exceedance, the ground motion will now be more intense.

The paper states that the uniform hazard spectrum (UHS) is not an appropriate target for selecting ground motions to be used in dynamic analysis of concrete dams. It has been demonstrated to be over-conservative. The conditional mean

spectrum (CMS), that overcomes the drawbacks of the uniform hazard spectrum (UHS) derived from probabilistic seismic hazard analysis (PSHA), may be appropriate as a target spectrum (TS) for dynamic analysis of structures. Disaggregation of the results from a UHS can also provide insight into the scenario earthquakes that should be considered in the selection of ground motions.

Paper R18 also provides comments on some essential factors to consider in earthquake analysis of concrete dams. If the mass of the foundation rock is ignored it will result in stresses being overestimated. If the compressibility of water is ignored it can result in either underestimation or overestimation of earthquake-induced stresses compared to the assumption that water is incompressible.

Paper R17 reports on the seismic evaluation of dam gated piers. Using beam elements to model the dam gate piers may be applicable for some low dams. In the evaluation of the contact behavior between the dam gated pier and spillway gate, setting the foundation spring as a constraint condition at the base of the M-φ model of the dam gated pier enables a reasonable evaluation, considering the effects of the overflow shape and stiffness of the dam body.

Paper R52 is concerned with the seismic analysis of Pine Flat Dam, for which advanced numerical methods were used, that simulate the propagation of seismic waves in a semi-unbounded massed foundation, and the modelling of the cracking behaviour of concrete that can be modelled by the smeared crack approach or by discrete cracks. For the smeared crack approach, the Concrete Damaged Plasticity (CDP) constitutive model, and for the discrete crack approach the eXtended Finite Element Method (XFEM) was used that allows cracks to propagate through the finite elements (and not only along the element edges). This technique allows simulating the crack path independently of the finite element mesh.

For the seismic analyses, the time-history analysis based on the direct integration of the equations of motion was used, which is the most powerful method for evaluating the response of the dams to earthquakes: it can be used for both linear and non-linear analyses and it can properly consider the dynamic interactions of the dam with the reservoir and the foundation. Both smeared and discrete crack models are available in the commercial FEM code ABAQUS.

A two-dimensional model of the Pine Flat gravity dam with the reservoir and the foundation was analysed. Several analyses were carried out for massless and massed foundation using the smeared and discrete crack models of mass concrete. These advanced seismic analysis methods are still in the research and development phase and must be used with great care.

Paper R16 presents the example of a 16 m high concrete gravity dam that has been in operation for more than 100 years. The dam was considered to have

developed horizontal cracks due to deterioration of horizontal joints. A two-dimensional FEM model is developed modeling the continuous horizontal cracks as joint elements.

Paper R16 shows the impact of the cracks on the earthquake behavior of the dam and the effectiveness of prestressed (PS) anchor reinforcement. The upper block generated extremely high accelerations during separation and impact caused by rocking motion. Introducing compressive stress into the horizontal cracks by PS anchors effectively suppresses upstream separation, resulting in minimal crack displacement.

There is very little observational data on the behaviour of large dams subjected to very strong ground shaking similar to that expected for the safety evaluation earthquake. There are two options to determine the seismic safety of dams, first, by dynamic analysis of dam-reservoir-foundation systems, and second, by shaking table tests. Paper R31 is concerned with shaking table tests of a 200 m high RCC gravity dam. Shaking table test is the most straightforward and robust approach to investigate the performance of concrete dams under strong earthquake shocks. A three-dimensional model of the gravity dam, consisting of 16 blocks, the crest spillway and the power intake was tested. All the blocks including the contraction joints were modelled. The horizontal peak ground acceleration of the safety evaluation earthquake (SEE) with a return period of 10,000 years was 0.53 g. The tests were carried out for all three earthquake components acting simultaneously. It is important to note that this dam-reservoir-foundation model was tested for the SEE up to 4 times the design basis earthquake ground motion (horizontal PGA of 0.43 g for return period of 5000 years), i.e. 1.72 g. The amplification of the peak acceleration in river direction from the base to the crest of the different blocks ranged from 1.8 to 2.5, which is rather small compared to the values obtained from the dynamic analysis of gravity dams, which may be of the order of 5 depending on the PGA-value.

Almost all high arch dams built in seismic-active zones in China have been tested on shaking tables. Seismic safety checks for ground motions exceeding the SEE ground motion are very important and are highly recommended for both shaking table tests and dynamic analysis, because if there are any future changes in the SEE ground motion, it will not be necessary to carry out a reassessment of the seismic safety of the dam.

Paper R38 presents an experimental study on the dynamic strength properties of mass concrete of Bda Dam, which is located in a highly seismic region in Tibet in China. The concrete tests include static and dynamic compressive strength tests, splitting tensile strength tests and flexural tensile tests which provide the main parameters for the seismic analysis and safety assessment of the dam. The tests were carried out for quasi-static and three different dynamic strain rates.

The average compression strength values of fully-graded cubic concrete specimens (30 cm edge length) for quasi-static and dynamic strain rates of 5×10-4/s, 5.6×10-3/s and 2×10-2/s were 31.1 MPa, 40.8 MPa, 41.1 MPa and 41.7 MPa, respectively. The maximum dynamic factor of compressive strength is 1.34. For the fully-graded concrete specimens the actual materials used in the Bda Dam were used.

The average dynamic splitting tensile strength values of fully-graded concrete specimens for quasi-static and dynamic strain rates of 10-4/s, 5.6×10-4/s and 2×10-3/s were 2.25 MPa, 2.82 MPa, 2.92 MPa and 3.31 MPa, respectively. The maximum dynamic factor of splitting tensile strength is 1.47.

The average flexural tensile strength values of fully-graded concrete specimens (beam specimens with cross section of 30x30 cm and a length of 120 cm) for quasi-static and dynamic strain rates of 10-4/s, 5.6×10-4/s and 2×10-3/s were 2.63 MPa, 3.29 MPa, 4.09 MPa and 3.43 MPa, respectively. The dynamic factor of bending strength is 1.56 for a strain rate of 2×10-3/s.

The test results confirm the increase in the strength properties of mass concrete with increasing strain rates. However, rather than splitting and flexural tensile tests, which overestimate the tensile strength, it would be more appropriate to carry out uniaxial tensile tests.

Paper R27 is about the seismic design of Batang Toru dam in Indonesia, a roller compacted concrete (RCC) curved gravity dam. The PGA with a return period of 145 years is 0.402 g and with a return period of 10,000 years is 0.648 g by DSHA.

With 3D finite element models of both the dam and foundation the linear response spectrum analyses and nonlinear time-history analyses are carried out to assess the dam behaviors and dam safety for seismic load cases. Reinforcement is arranged in the dam face and some defensive measures are taken to improve the earthquake-resistant performance of the Batang Toru dam. Paper R27 presents ways to improve the seismic performance of concrete dams founded on soft rock and can provide a useful reference for the seismic design of concrete dams in high seismic regions.

5.5.4. *Concrete arch dams*

Paper R6 compares the variations in the dynamic responses of an arch dam subjected to linearly scaled (with respect to PGA) and spectrally matched recorded acceleration time histories for three earthquake zones in Switzerland. The 150 m high arch dam is located in a narrow V-shaped valley. The calculation includes six sets of three component ground motions, with each set composed of 11 records.

The maximum horizontal acceleration at the crest and the maximum tensile stresses within the dam body were used for comparison. The average maximum responses of the dam were slightly larger for the linearly scaled records than for the spectrum-matched records. The modelled dam was a linear elastic structure with a massless foundation, monolithic structure with rigid contact surfaces and hydrodynamic loads were as defined by the Westergaard method. The authors note that a more accurate assessment of the dynamic performance of concrete arch dams may necessitate revising these assumptions.

Many existing arch dams were designed before 1990. Their design often considers only a fixed seismic coefficient (pseudo-static) approach without any site-specific seismic hazard assessment. Paper R21 presents the seismic analyses of Enguri dam in a highly seismic region.

The seismic analysis of Enguri dam, one of the highest arch dams, which needs to be verified for an earthquake with a PGA close to 1.0 g, revealed high shear stresses within the concrete. The main conclusions from the seismic analysis are as follows:

- Amplification of the acceleration from the base of the dam to the crest varies from 6 to 12,
- The maximum dynamic crest displacement toward downstream can reach twice the static displacement due to water load.
- The maximum static and dynamic compression stresses are 1.5 MPa and 5 MPa, respectively.
- It seems difficult to trigger any failure mechanisms in the upper part of the dam due to the SEE ground motion. Overturning mechanism of a detached block toward upstream is not possible.

In large dams with large safety floods several flood discharge openings may have to be provided in the body of concrete dams, which may weaken the dam body during strong earthquakes. Paper R35 is concerned with this problem. A comparison of the dynamic response of a large arch dam with and without flood discharge openings is made. Artificially generated acceleration time histories were use as input. As expected, the stresses in the zone of the orifices and crest spillway vary most compared to the case of a monolithic dam. The maximum crest displacement increases by about 8.5% when the effects of the flood opening are considered. If major flood openings are provided, then they should be modelled in the finite element model of the dam; this applies in particular to the crest spillway.

Paper R40 is concerned with the design and construction of the 289 m high Baihetan arch dam at the Jinsha River in Yunnan Province of China. Several key technologies were used for the design and construction of this large dam project. The review, however, is focused on the seismic analysis and design aspects of the dam located in an asymmetric valley. The special design features include

the treatment of the jointed basalt and the stability of potential wedges along the abutments, which are important for the seismic safety of the dam. The dam is located in a seismic region. The horizontal PGA-value of the design earthquake with a return period of 5000 years is 0.45 g.

For the dynamic analysis of Baihetan Dam a three-dimensional nonlinear finite element model was used in which the block joints and the radiation damping of the infinite foundation are considered. Artificially generated acceleration time histories were used in the dynamic analysis. The lowest eigenfrequency of the dam with full reservoir is 1.1 Hz. The maximum block joint opening for the design earthquake is about 40 mm. Based on the results of the nonlinear dynamic analysis it is concluded that slight damage is possible on the downstream face near the left abutment, while the upstream face remains intact, which is different from other large arch dams, where stress concentrations occur along the upstream face at the dam-foundation contact. Special seismic reinforcement was provided in the piers of the crest spillway, where the dynamic amplification effects are the largest.

The seismic overload capacity of the arch dam is approximately 1.7 with respect to the PGA of the design earthquake. The check of the seismic overload factor is essential and should be determined for all large dams. This is the rational response to claims for frequent seismic safety reassessment of dams, whenever the seismic hazard is increased because of frequent updates of the seismic hazard analysis required by new developments and new earthquake data.

Paper R42 is concerned with the seismic safety evaluation of the 155 m high Yangfanggou arch dam on the Yalong River in China. The thickness of the dam at the crest and the base is 9 m and 32 m, respectively. The horizontal PGA of the safety evaluation earthquake with a return period of 10,000 years is 0.386 g. Rather than uniform hazard spectra recommended by ICOLD, so-called scenario earthquake response spectra were used. Artificially generated acceleration time histories according to the current seismic code in China were used as input for the dynamic analysis of the dam-reservoir-foundation system. In the nonlinear dynamic analysis, the effect of wave radiation in the dam foundation and opening of the block joints were considered. In addition, the dynamic stability of wedges at both abutments was analysed for the design basis earthquake with a recurrence period of 5000 years. All abutment wedges remain stable under this earthquake.

The maximum dynamic opening of the block joints during the design basis earthquake with a horizontal PGA of 0.309 g is 8.7 mm, which is within the allowable range of waterstop deformations. This is a special performance criterion given in the Chinese code. According to ICOLD damage of waterstops would be acceptable under the safety evaluation earthquake (SEE), if the water pressure in the block joints does not affect the stability of the dam. If a dam is damaged during a strong earthquake, then the reservoir may have to be lowered, depending on the type of damage. Repair

of damaged waterstops would be a problem in concrete dams; therefore, it is of advantage that waterstops can withstand seismic deformations.

5.5.5. *Appurtenant structures*

Appurtenant structures are safety-critical if their function is to retain water and to manage the inflow or outflow from a reservoir after a strong earthquake. Structures that support safety-critical electro- and hydro-mechanical equipment must perform such that any attached safety-critical equipment is still operable after the SEE.

Paper R17 reports on the seismic evaluation of dam gated piers. Using beam elements to model the dam gate piers may be applicable for some low dams as presented in the paper. In the evaluation of the contact behavior between the dam gated pier and spillway gate, setting the foundation spring as a constraint condition at the base of the M-φ model of the dam gated pier enables a reasonable evaluation, taking into account the effects of the overflow shape and stiffness of the dam body.

5.6. Earthquake safety evaluation of all types of dams and safety-critical elements (e.g., spillway, low-level outlets)

5.6.1. *General*

The safety evaluation of existing dams and associated safety-critical elements is important to provide assurance to dam owners and stakeholders that dams are maintained in a safe condition such that the risks associated with potential failure are at an acceptable level. Several papers associated with this theme were submitted. One was related to the assessment of the safety of a portfolio of dams in Italy (R51). Others were associated with specific dam types or dams.

5.6.2. *Portfolios of dams*

The Italian Technical Standard for the Design and Construction of Dams was updated in 2014, replacing the previous one dated 1982. Paper R51 presents the results of the seismic assessment of 53 dams of many different types (concrete face earthfill, central core earthfill, bituminous face rockfill, concrete face rockfill, concrete gravity, stone masonry, and multiple arch). The dams are located throughout Italy. The assessment was undertaken in accordance with the 2014 Technical Standard and the related Seismic Guidelines published in 2019. The paper presents the methodology followed to assess their seismic safety and the design seismic loads

and performance requirements stipulated by the Italian Technical Standard. This standard requires consideration of performance under two Serviceability Limit States (OLS – Operational Limit State, and DLS – Damage Limit State) and two Ultimate Limit States ULS (LLS – Life-Safety Limit State, and CLS – Collapse Limit State).

Paper R51 explains the approach taken. A step-by-step approach was developed. The basic steps were identification of dam type, survey of dam, acquisition of historical and archival information, material characterisation including additional investigations, seismic design loads from Italian seismic hazard maps or site specific probabilistic seismic hazard studies and analyses. A pseudo-static approach was used for assessing the performance of most dams. More complex analyses were adopted for some dams. This involved dynamic non-linear analysis for four embankment and introducing non-linear lift joints and post-seismic stability analysis for three concrete dams.

The study concluded that although the designs of most dams did not originally consider seismic loads and some natural ageing of material, most of the assessed dams comply with the national Standards and generally exhibit satisfactory behaviour in seismic conditions.

5.6.3. *Embankment dams*

Paper R8 provides a comparison of the methodologies considered for earthquake dam safety evaluation of five large embankment dams with earthfill core, located in different countries (Philippines, Mexico, Switzerland, Armenia, and Colombia). The comparison focuses on the determination of the seismic loads and highlights the importance of national guidelines to reach consistency regarding the level of safety. It also studies the analysis methods used (pseudo-static method, simplified deformation analyses, sliding block analyses, non-linear deformation analyses, post-earthquake stability analyses) and the performance criteria applied. Each method is evaluated in terms of advantages, limitations and disadvantages regarding the accuracy and reliability of the analyses results. Additionally, the requirements for budget, time and computational resources are discussed. Explanation is given why analyses methods developed in the 1960s are still attractive compared to sophisticated non-linear analyses.

The paper concludes that that the most commonly applied method to calculate the earthquake response of large earth core embankment dams is still the equivalent-linear method and that sophisticated non-linear dynamic analysis is rarely used. Simplified methods are still widely used but it is warned that it is of great importance to evaluate whether the selected method is suitable and within the limits of applicability. The paper also comments that it seems to be generally accepted that the pseudo-static analysis method is outdated, at least for embankment dams with earthfill core.

Paper R19 presents the results of applying a process that allows for incorporating aleatory and epistemic uncertainties into a seismic fragility (likelihood of failure) assessment of the Left Embankment of the Wanapum Dam. The process included adaptation and implementation of a process recommended by the Senior Seismic Hazard Analysis Committee (SSHAC) for the Nuclear Regulatory Commission. The Wanapum Dam is part of the Priest Rapids Hydroelectric Project located on the Columbia River (Washington State, USA). The study reported on in the paper is part of the dam owners (Grant County Public Utility District) risk-informed approach to the seismic safety evaluation of the Left Embankment.

The SSHAC process provides a structure to make a detailed assessment of the sources of aleatory and epistemic uncertainty in the characterization of the embankment. The sources of epistemic uncertainty that were identified were incorporated in a logic tree format that provides the structure for estimating the uncertainty in the seismic fragility. The two main types of epistemic uncertainty that were considered in the Wanapum Dam were uncertainty in the estimation of seismic deformations of the embankment in response to earthquake ground motions and the uncertainty in modelling the progression of embankment deformations (damage) to failure for individual failure modes. The variability in seismic loading (earthquake time histories for the same magnitude earthquake and ground motion level) is a substantial contributor to the aleatory uncertainty in the estimated embankment deformations. The process allowed the aggregate impact of uncertainties in the embankment characteristics and seismic loading on the estimate of embankment deformations and potential for uncontrolled release of water to be estimated.

Paper R19 provides an example of the state of practice for assessing the probability of embankment failure of an existing embankment. The results reveal there is considerable uncertainty in estimating the seismic fragility of the Left Embankment. The SSHAC process is rigorous, and the results provide a good basis for making decisions on whether risks are acceptable or if measures are required to mitigate risks.

5.6.4. *Concrete gravity*

Paper R9 presents the results of a study to evaluate the seismic vulnerability of concrete dams, with a particular focus on the critical failure mode of base sliding. A coupled 2D dam-foundation-reservoir (DFR) model that considered both material and contact non-linearity, was used to better understand the interactions between the dam, foundation, and reservoir. The choice of contact interaction i.e., tied versus cohesive, incorporation of uplift, and variations of ground motions within and across the return periods significantly influence the system response, introducing variations in the dam's response that impact the dam's seismic

vulnerability assessment. The key findings and implications that emerge from the study are listed below.

1. Tied models generally overestimate failure probabilities compared to models with cohesive interaction at the dam foundation interface. This overestimation is especially pronounced in crest displacement-based fragility (NCD). The tied models present a more conservative failure probability estimation. This difference underscores the importance of accurately modeling the dam-foundation interface to avoid over-conservative safety assessments.
2. Incorporating uplift affects the outcome of the analysis significantly impacting the base sliding-based fragility (NBD). The failure probability increases markedly when uplift is taken into account, highlighting the critical role of uplift forces in the seismic stability of dams. This finding emphasizes the necessity of including uplift in comprehensive seismic assessments.
3. Employing multiple damage indices (NBD and NCD) in fragility assessments offers a more detailed and nuanced understanding of the dam's seismic performance. This approach enables a better evaluation of different failure modes and their associated risks, providing a holistic view of potential vulnerabilities.
4. Considering multiple return periods (475, 975, 2475, 5000, and 10,000 years) and a range of ground motions helps account for record-to-record (RTR) variability. This comprehensive approach ensures that the analysis captures the variations in seismic demand across different scenarios, thereby offering a robust probabilistic assessment framework.
5. This research addresses some of the limitations of previous studies by incorporating non-reflecting boundary conditions and a probabilistic assessment framework.

Paper R11 presents the original approach to optimize the shear strength parameters of dam joints and corresponding seismic stability analyses of the Isle-Maligne monoliths. It highlights the importance of properly defining shear parameters, field investigation and the impact of rehabilitation work of old dams.

The seismic parameters were derived from a site-specific probabilistic seismic hazard assessment, the spectral accelerations on the rock for the Isle-Maligne site for the 5,000 year return period were greater than 0.9 g for the horizontal component, for 5% damping.

Seismic stability of old dams was checked by the gravity method and temporal dynamic rigid body analyses, with the Newmark sliding block method, residual sliding displacement were obtained.

Paper R30 is concerned with the rapid post-earthquake assessment of the safety of large dams:

- The rapid determination of seismic input at the dam site;
- The quick calculation of the seismic response of the dam structure;
- The assessment of the overall seismic safety of the dam structure, in order to determine what actions such as lowering of the reservoir and emergency measures have to be taken. Speed is a crucial factor in the safety assessment of a dam after an earthquake.

The methods and steps for rapid assessment of seismic safety of a concrete dam after an earthquake are given. The rapid safety assessment procedure proposed in the report is applicable in the case that no up-to-date seismic safety assessment of a large dam project exists. Hopefully this should be the exception as it is a basic long-time objective that all dams satisfy the current seismic safety criteria specified by ICOLD. If this is not the case the dam owners and dam safety authorities make sure that such seismic safety evaluations exist. It must be pointed out that seismic safety assessments form part of emergency planning, which is more comprehensive than dam breach flood wave analyses and/or emergency action plans.

An important aspect is the check of the seismic safety of concrete dams for seismic overload factors. It is understood from the reports on very large concrete dams, prepared by Chinese dam engineers that the seismic reserves of dams must be checked. These reserves are characterized by overload factors. This is an excellent concept, which should also be applied to large dams in all other countries as this concept would protect the dam owners from frequent requests for the seismic safety re-assessment of their dams (R.31, R.40).

Paper R39 is concerned with the seismic fragility analysis of gravity dams using the Multiple Stripe Analysis method (MSA), a method which is hardly known for the seismic safety assessment of dams. Fragility curves were mainly used in the probabilistic seismic safety assessment of components of nuclear power plants. The fragility curve based safety assessment of dams is basically an outdated concept and should only be used as a screening method of gravity dams, where the concrete blocks have a similar shape. For the detailed safety analysis of large gravity dams, these methods shall not be used as seismic failure modes, dam failure, or earthquake damage or seismic vulnerability of dams are terms, which are hard to quantify. As dam failure and damage are related to the seismic vulnerability of a dam and since the vulnerability depends mainly on the number of relevant load cycles, i.e. the duration of strong ground shaking, which is a key parameter.

In Paper R39 a nonlinear dynamic analysis of a 144 m high concrete block of a gravity dam is analyzed, considering the concrete damage plasticity constitutive model for mass concrete. Twelve earthquakes are analyzed and the earthquake damage of the concrete block is quantified based on the seismic crest displacement. The classification of the damage in different categories from no damage to failure is

rather subjective. The fragility curves are presented for each damage category as a function of the PGA.

It is obvious that the characterization of the earthquake ground motion by the PGA is much too simplistic. In this paper the damage is characterized by the crest displacement. The authors mentioned that other damage indices should also be considered. The fact remains that both the damage and the earthquake ground motion cannot be represented by a single parameter. Moreover, earthquake observations and shaking table tests of concrete dams show that the damage is of discrete nature and cannot be represented by plastic damage models.

5.6.5. *Levees*

Paper R20 presents the approach used by the main hydropower companies in France (EDF and CNR) to evaluate the seismic safety of levees associated with their power projects. The levees are several hundred kilometres in length. The evaluation of the safety of large dams based on the assessment of stability has been mandatory in France since 2018 by a ministerial decree. It is a challenge to undertake meaningful assessment of the stability over the full length of the levees. The way to demonstrate earthquake stability or the calculation methods are defined in French recommendations published by the French profession. A graduated approach is recommended. It consists of increasing the level of complexity of the studies by stage when the previous stage does not justify the work studied. This type of approach has been adopted by CNR for the two main risks, which are liquefaction and dynamic shear. EDF has developed a simplified transitional dynamic method for the risk of dynamic shear. It excludes liquefaction issues. The paper describes the development and application of the methods. CNR report that almost all their embankments are not sensitive to liquefaction due to favourable construction provisions (nature and compaction of fills) and the presence of materials that are not or only slightly susceptible to liquefaction. The graduated approach for assessing dynamic shear stability involves initially using the pseudo-static method, and then the pseudo-dynamic method (Newmark sliding block approach). EDF has developed a further gradation in the analyses of dynamic shear stability (simplified transient dynamic analysis). Application of these methods to their levees has generally demonstrated compliance with statutory requirements.

6. CONCLUDING REMARKS

The seismic safety of dams is important because earthquakes can result in catastrophic effects on people, property, infrastructure, historical and cultural sites, and the environment if they fail. To prevent uncontrolled release of water a dam

must be able to withstand the seismic hazards, including ground shaking, associated with an extreme earthquake which is referred to as the Safety Evaluation Earthquake (SEE).

The subject of the seismic safety of dams and levees continues to evolve. The awareness of the importance of seismic safety and the technical knowledge base has expanded considerably since Q.83 in 2003.

Going forward the following recommendations are provided:

1. Large dams should be instrumented with strong motion recorders (free-field, base, mid-crest and abutments) to measure accelerations. Deformation monitoring is also important. Measurements of response during earthquake events allows calibrating estimates of seismic hazard (ground shaking) as well as models that predict response of the dam to earthquakes. The information can also add to the body of knowledge for all dams.
2. Monitoring and observations of dam and safety-critical equipment behavior during earthquakes should continue and be carefully interpreted. Observations should be shared to allow benefit to all stakeholders. People with responsibility for dam safety should study the lessons learnt and apply them to their work.
3. There are multiple features of earthquake hazards (i.e., ground shaking, surface fault movement, mass movements, waves in reservoirs, etc.). They all need to be considered.
4. The seismic safety of dams needs regular review because of the evolving understanding of seismic hazards, changes in the risks associated with potential failure of a dam, deterioration of the dam, the understanding of potential failure modes and the measures available to mitigate risks.
5. There is continuing evolvement of the dynamic properties and constitutive models for dam materials and foundations and advances in numerical modeling of the stress-strain characteristics of materials and estimation of the deformation of dams when subject to earthquake ground motion. However, there are still significant uncertainties associated with numerical analyses. Sensitivity studies are always recommended to understand the effects of various assumptions and to properly consider uncertainty.

7. ABBREVIATIONS

The following abbreviations are used in the General Report and in some of the papers associated with Q.111:

CFRD: Concrete faced rockfill dam

Commission Internationale des Grands Barrages

Vingt-Huitieme Congres des Grands Barrages
Chengdu, Mai 2025

CMD: Cemented material dam

CSG: Cemented sand gravel

DBE: Design basis earthquake

MCE: Maximum credible earthquake (term used in deterministic seismic hazard analysis of high consequence dams)

OBE: Operating basis earthquake (term used in probabilistic seismic hazard analysis of dams)

PGA: Peak ground acceleration

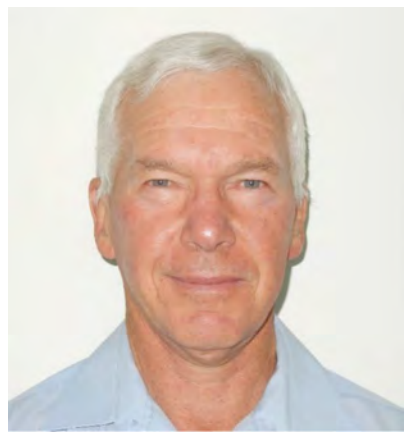

RCC: Roller compacted concrete

RFC: Rock-filled concrete

RTS: Reservoir-triggered seismicity (in the past the term reservoir-induced seismicity was used to describe earthquakes triggered by the reservoir, but the correct term used today is RTS)

SEE: Safety evaluation earthquake (return period of up to 10,000 years depending on seismic risk of a dam project)

DOI: 10.1201/9781003642428-150

ACKNOWLEDGEMENTS

I would like to thank Dr. Martin Wieland for his advice and assistance with review of the papers submitted for Q.111 and the discussion of Chapter 4 on the Main Changes and Developments in the Seismic Design and Safety Evaluation of Large Dams since 2003. I would also like to thank Dr. Haibo Wang for the review of papers related to concrete dams and for the valuable comments and suggestions on this General Report.

REFERENCES

[1] ANCOLD. *Guidelines for Design of dams and Appurtenant Structures for Earthquake*. 2019

[2] ICOLD. *Bulletin 137. Reservoirs and Seismicity*. 2011.

[3] ICOLD. *Bulletin 148. Selecting Seismic Parameters for Large Dams*. 2016.

[4] ICOLD. *Bulletin 166. Inspection of Dams following earthquake*. 2016.

[5] ICOLD. *Bulletin 194. Tailings Dam Safety. Preprint* 2022.

[6] ICOLD. *Position paper. Dam safety and earthquakes*. 2021

[7] NZSOLD. *New Zealand Dam Safety Guidelines*. 2024

[8] USSD. *Analysis of Seismic Deformation of Embankment Dams*. 2022.

[9] USSD. *Observed Performance of Dams During Earthquakes*, Vol. III. 2014.

QUESTION 111

PERFORMANCE SISMIQUE ET SÉCURITÉ DES BARRAGES

Trevor MATUSCHKA
Vice-président du comité de la CIGB sur les aspects sismiques de la conception des barrages. Directeur, ENGINEERING GEOLOGY LIMITED

NOUVELLE-ZÉLANDE

RAPPORTEUR GÉNÉRAL

TABLE DES MATIÉRES

(*continued*)

Continued

1. INTRODUCTION

Les barrages ont généralement un bon comportement en cas de tremblement de terre. Cependant, bien qu'ils ne représentent qu'un faible pourcentage des causes de rupture des barrages, leurs conséquences peuvent être beaucoup plus importantes car il n'y a généralement pas d'avertissement, de sorte que les personnes touchées n'ont que peu ou pas de temps pour évacuer.

Le sujet du présent rapport "Question 111 - Performance sismique et sécurité des barrages" a été proposé par le Comité sur les aspects sismiques de la conception des barrages. Il y a cinq thèmes

1. Surveillance statique, sismique et post-sismique des barrages
2. Retour d'information sur les défaillances dues aux tremblements de terre, y compris les digues à stériles et les levées de terre
3. Importance des multiples caractéristiques de l'aléa sismique (par exemple, secousses du sol, mouvements des failles de surface, mouvements de masse)
4. Critères de conception et de performance sismiques pour la structure du barrage, le bord du réservoir et la zone touchée
5. Évaluation de la sécurité sismique de tous les types de barrages et d'éléments critiques pour la sécurité (par exemple, déversoir, sorties à faible niveau)

Les questions précédentes de la CIGB traitant des aspects sismiques des barrages étaient les suivantes :

- Question 18, 5ème Congrès à Paris, France en 1955
  Tassement des barrages en terre dû à la compressibilité des matériaux du barrage ou de la fondation, effet des tremblements de terre sur la conception des barrages
- Question 29, 8ème Congrès à Edimbourg, Royaume-Uni en 1964
  Résultats et interprétation des mesures effectuées sur les grands barrages de tous types, y compris les observations des tremblements de terre
- Question 35, 9ème Congrès à Istanbul, Turquie en 1967
  Barrages dans les zones sismiques ou autres situations défavorables
- Question 51, 13e Congrès à New Delhi, Inde, en 1979
  Sismicité et conception asismique des barrages
- Question 83, 21ème Congrès à Monreal, Canada, 2003
  Aspects sismiques des barrages

Plusieurs autres questions débattues lors des congrès de la CIGB ont également porté sur les risques sismiques et la vulnérabilité sismique des barrages.

La performance et la sécurité des barrages face aux tremblements de terre couvrent l'ensemble du cycle de vie : planification, conception, construction,

exploitation, déclassement/fermeture. À un niveau plus détaillé, il s'agit de comprendre les risques sismiques, de choisir les sites pour minimiser les risques, de comprendre les modes de défaillance potentiels, de développer des concepts et des détails de conception pour atténuer les risques, de construire avec une qualité élevée, de procéder à un examen indépendant par les pairs, d'appliquer de bonnes procédures opérationnelles et de gestion de la sécurité des barrages, de procéder à des examens réguliers de la sécurité des barrages, y compris des examens périodiques complets et indépendants de la sécurité, et d'élaborer des plans de préparation et d'intervention en cas de situation d'urgence. Bon nombre de ces éléments sont couverts par la question Q.111.

2. APERÇU DES RAPPORTS REÇUS

Au total, 52 documents provenant de 12 pays ont été soumis. Sept d'entre eux n'étaient pas liés à la question Q.111 et ne sont pas abordés dans le présent rapport. Le plus grand nombre de contributions provient de la Chine (16), suivie du Canada (3), du Japon (3), de la France (3), de la Suisse (3), de l'Australie (2), de l'Italie (2) et des États-Unis (2). Le grand nombre d'articles soumis par la Chine s'explique par le nombre de grands barrages qui ont été construits et sont en cours de construction en Chine et par la forte sismicité des régions du pays où se trouvent de nombreux barrages.

Un résumé des documents soumis relatifs aux différents thèmes (sous-questions) associés à la question Q.111 est fourni ci-dessous. Il est à noter que certains documents couvrent plus d'un sujet.

1. Thème 1 : Surveillance statique, sismique et post-sismique des barrages : Abordé dans les 5 articles suivants (R1, R5, R24, R41, et R50)
2. Thème 2 : Retour d'expérience sur les défaillances dues aux tremblements de terre, y compris les digues à stériles et les digues : Abordé dans le document R32
3. Thème 3 : Importance des caractéristiques multiples du risque sismique (par exemple, secousses du sol, mouvements des failles de surface, mouvements de masse) : Abordé dans les 6 articles suivants (R10, R25, R26, R34, R37, et R45)
4. Thème 4 : Conception sismique et critères de performance pour la structure du barrage, le bord du réservoir et la zone impactée : Abordé dans les 25 articles suivants (R2, R3, R6, R12, R13, R14, R15, R18, R21, R22, R23, R27, R31, R35, R36, R38, R40, R42, R44, R47, R48, et R52)
5. Thème 5 : Évaluation de la sécurité sismique de tous les types de barrages et d'éléments critiques pour la sécurité (par exemple, déversoir, sorties à faible niveau) : Abordé dans les 8 articles suivants (R8, R9, R11, R19, R20, R30, R39, et R51)

La plupart des documents soumis étaient associés au thème 4 (critères de conception et de performance).

3. EARTHQUAKE PUBLICATIONS ET TRAVAUX EN COURS DU COMITÉ SUR LES ASPECTS SISMIQUES DE LA CONCEPTION DES BARRAGES

Le comité sur les aspects sismiques de la conception des barrages, qui comprend actuellement des experts en barrages et en tremblements de terre d'environ 35 pays différents, a préparé les bulletins suivants de la CIGB :

- Bulletin 27 (1975) : Une revue de la conception des barrages résistants aux tremblements de terre
- Bulletin 46 (1983) : Sismicité et conception des barrages
- Bulletin 52 (1986) : Earthquake analysis procedures for dams (Rapport préparé au nom du Comité d'analyse et de conception des barrages de la CIGB, O. C. Zienkiewicz, R, W. Clough, H. B. Seed).
- Bulletin 62 (1988) : Inspection des barrages à la suite de tremblements de terre - lignes directrices
- Bulletin 72 (1989) : Choix des paramètres sismiques pour les grands barrages
- Bulletin 112 (1998) : Néotectonique et barrages
- Bulletin 113 (1999) : Observation sismique des barrages
- Bulletin 120 (2001) : Caractéristiques de conception des barrages pour résister efficacement aux mouvements sismiques du sol
- Bulletin 123 (2002) : Conception et évaluation parasismiques des ouvrages annexes aux barrages
- Bulletin 137 (2011) Réservoirs et sismicité
- Bulletin 148 (2016) Sélection des paramètres sismiques pour les grands barrages
- Bulletin 166 (2016) Inspection des barrages selon les directives relatives aux tremblements de terre
- Position Paper (2021) Sécurité des barrages et tremblements de terre.

Trois Bulletins ont été publiés depuis Q.83 en 2003 (Bulletins 137, 148, et 2016). Le bulletin 137 traite de la sismicité déclenchée par les réservoirs. Il s'agit de tremblements de terre déclenchés par la retenue de grandes profondeurs et de grands volumes d'eau. Ils sont généralement associés à de très grands barrages. Le Bulletin 148 fournit des recommandations pour la sélection des paramètres de conception sismique. Les critères de conception dépendent du risque ou des conséquences d'une défaillance. De nombreux documents d'orientation sismique publiés par les pays membres de la CIGB ont adopté ou adapté les recommandations du Bulletin 148. Plus de détails sur le Bulletin 148 sont couverts dans la section 4.4 de ce rapport général. Le Bulletin 166 fournit des conseils pratiques sur la

réalisation d'inspections de sécurité des barrages à la suite de tremblements de terre.

Le mandat de l'actuel Comité sur les aspects sismiques de la conception des barrages (2023-2026) a été approuvé lors de l'Assemblée générale de la CIGB à Göteborg (Suède) en 2023. Il s'agit de :

1. Aspects de la conception sismique des barrages CFRD, des barrages à noyau d'asphalte et d'autres types de revêtements.
2. Interprétation des données sismiques obtenues à partir des barrages.
3. Analyse de la déformation sismique des barrages en remblai.
4. Aspects sismiques des équipements électromécaniques et hydromécaniques critiques pour la sécurité
5. Diffusion d'informations sur (i) la sécurité sismique des barrages existants, (ii) les critères de conception actualisés pour les projets de grands barrages, et (iii) les risques multiples causés par les forts tremblements de terre.

Voici un résumé des progrès réalisés dans ces domaines :

- TdR 1 : Un document est en cours de préparation par un sous-groupe de travail
- TdR 2 : Un nombre important d'enregistrements de mouvements forts provenant de barrages a été collecté lors du tremblement de terre de Tohoku du 11 mars 2011 et de ses répliques, compilés par le JCOLD. Les enregistrements d'accélération ont été analysés par différentes organisations au Japon, en Corée, en Autriche et en France. Le projet de document est disponible et doit être finalisé.
- TdR 3 : Pour la conception et l'évaluation de la sécurité des nouveaux types de barrages en remblai tels que les barrages CFRD et les barrages en enrochement à noyau d'asphalte, et les barrages situés dans des zones fortement sismiques, des méthodes plus fiables d'analyses sismiques inélastiques sont nécessaires que les méthodes actuelles, qui sont toujours basées sur la méthode de l'équivalent linéaire vieille de 50 ans. Un document a été préparé par l'USSD en 2022, qui servira de base à un nouveau bulletin de la CIGB. Un sous-groupe de travail a été formé pour préparer ce bulletin.
- TdR 4 : La conception sismique des équipements électromécaniques et hydromécaniques critiques pour la sécurité (vannes de déversoir, sorties de bas niveau) n'a pas encore été couverte par des directives de la CIGB et est une exigence basée sur le bulletin 148 de la CIGB "Sélection des paramètres sismiques pour les grands barrages". Un sous-groupe de travail a été formé pour préparer ce bulletin.
- TdR 5 : Les critères actuels de conception et de sécurité sismiques des grands barrages de stockage (Bulletin 148 de la CIGB) ont été présentés lors d'ateliers, de séminaires et de conférences dans un certain nombre de pays, principalement en Asie. En outre, le fait que le risque sismique est un risque multiple pour les projets de grands barrages doit être diffusé, car la plupart des

directives de conception sismique se concentrent uniquement sur les secousses du sol. En outre, il est nécessaire de réévaluer la sécurité sismique des barrages existants, car tous les barrages devraient satisfaire aux mêmes critères minimaux de sécurité sismique. Il s'agit d'une activité permanente, qui revêt une importance capitale pour les "pays à tremblement de terre" et les pays qui développent leurs ressources en eau mais ne sont pas en mesure de participer régulièrement aux événements de la CIGB.

Certains des mandats précédents n'ont pas donné lieu à des bulletins, mais les questions ont été débattues lors de plusieurs ateliers organisés dans différents pays, avec la participation d'un nombre important d'ingénieurs des barrages, d'universitaires et d'étudiants ( ).

4. PRINCIPAUX CHANGEMENTS ET DÉVELOPPEMENTS DANS LA CONCEPTION SISMIQUE ET L'ÉVALUATION DE LA SÉCURITÉ DES GRANDS BARRAGES DEPUIS 2003 Q.83

Cette section résume les nouvelles informations et les changements intervenus dans l'état des pratiques depuis le rapport général (Q.83) de 2003.

4.1. Le risque sismique est un risque multiple

Il est très important de noter que le risque sismique est un risque multiple et ne comprend pas seulement les secousses du sol. Les principaux risques liés aux tremblements de terre qui doivent être pris en compte dans les projets de grands barrages sont les suivants:

- Les secousses du sol provoquent des vibrations dans les barrages, les structures et équipements annexes, et leurs fondations (la plupart des réglementations relatives aux tremblements de terre ne concernent que ce risque). Les secousses du sol peuvent entraîner des déformations et des fissures dans les barrages, la défaillance des structures annexes et des équipements électromécaniques, le ramollissement ou la liquéfaction des matériaux de remblai et de fondation, ainsi que des vagues dans les réservoirs ;
- Mouvements de faille dans la fondation du barrage ou discontinuités dans la fondation du barrage à proximité de failles majeures qui peuvent être activées et provoquer des distorsions structurelles et des fissures dans les remblais ;
- Mouvement de faille dans le réservoir provoquant des vagues d'eau dans le réservoir (seiches) ou une perte de franc-bord

- Mouvements de masse (éboulements) causant des dommages aux vannes, aux piliers des déversoirs, aux murs de soutènement, aux centrales électriques, aux équipements électromécaniques, aux conduites forcées, aux lignes de transmission, aux routes d'accès aux barrages, etc ;
- Autres risques spécifiques au site et au projet.
- La sismicité déclenchée par le réservoir (RTS) est un autre type de risque de tremblement de terre, qui doit être pris en compte dans les nouveaux projets de barrage. La sismicité déclenchée par les réservoirs est principalement et provoque des secousses du sol et des mouvements de masse. Cependant, comme la plupart des événements RTS sont relativement faibles, les mouvements de faille ne sont pas une préoccupation majeure.

4.2. Les tremblements de terre importants survenus depuis 2003, qui ont causé d'importants dommages aux barrages, et les nouvelles leçons tirées de ces événements

Il y a toujours des leçons à tirer des barrages soumis à des tremblements de terre. Cela concerne tous les aspects de la sécurité des barrages (planification, conception, construction, exploitation, inspections de la sécurité des barrages, préparation aux situations d'urgence et planification des interventions). Nos connaissances peuvent être considérablement améliorées en observant et en documentant la performance des barrages soumis à des tremblements de terre, en comparant cette performance aux méthodes de conception existantes, puis en modifiant les méthodes de conception existantes ou en en développant de nouvelles, et nous pouvons apprendre à mieux nous préparer et à mieux réagir aux tremblements de terre. Les ingénieurs des barrages sont encouragés à lire les rapports documentant la performance des barrages soumis à des tremblements de terre.

Plusieurs tremblements de terre importants se sont produits depuis Q.83 en 2003. Il s'agit notamment de très grands tremblements de terre, d'une magnitude de 8 ou plus, qui ont duré très longtemps. Les observations et les leçons tirées sont résumées ci-dessous. De plus amples détails peuvent être trouvés dans les documents et rapports publiés. L'USSD a compilé des rapports sur la performance observée des barrages pendant les tremblements de terre. Le volume III couvre les tremblements de terre survenus entre 2000 et 2014 (Ref.3) et constitue une ressource utile.

1. **14 juin 2008 Mw 6.9 Iwate-Miyagi Nairku, Japon**
   134 barrages ont été inspectés après le tremblement de terre. 12 d'entre eux ont été endommagés, mais pas suffisamment gravement pour entraîner un déversement incontrôlé d'eau.
2. **12 mai 2008 Mw 7.9 Wenchuan, Chine**

Le tremblement de terre de Wenchuan a été l'un des plus coûteux et des plus destructeurs de l'histoire. Il a endommagé plus de 2 200 barrages et réservoirs de toutes tailles et de tous types dans 8 provinces chinoises. Les dommages causés aux barrages comprennent des fissures dans 1 425 barrages, des effondrements et des tassements dans 687 barrages, des glissements dans 354 barrages, des fuites et des infiltrations dans 428 barrages, des dommages aux équipements de levage mécanique dans 161 barrages, et des dommages aux ouvrages de décharge, aux déversoirs et aux bâtiments administratifs dans 422 barrages. Ce tremblement de terre a démontré que les tremblements de terre ne sont pas les seuls à présenter des risques multiples. D'importants éboulements associés à ce tremblement de terre ont affecté l'accès aux sites des barrages et ont causé des dommages substantiels aux centrales électriques, aux vannes, aux piliers et aux structures annexes. Le tremblement de terre de Wenchuan a fourni une occasion unique d'évaluer, à l'adresse , la performance des barrages soumis à des charges sismiques importantes. De nombreux articles ont été publiés sur les enseignements tirés de ce tremblement de terre.

3. **7 février 2010 Mw 8.8 Maule, Chili**
   Au moins 16 barrages ont été modérément ou fortement secoués, mais aucune rupture n'a été signalée.
4. **11 mars 2011 Mw 9.0-9.1 Tohoku, Japon**
   400 barrages ont été inspectés par le Centre japonais d'ingénierie des barrages. En général, les barrages se sont bien comportés, des fissures mineures ou modérées apparaissant sur les barrages en remblai. Un barrage-poids en béton de 76 m de haut et un barrage en béton armé de 48 m de haut soumis à une PGA de base comprise entre 0,3 et 0,4 g n'ont subi aucun dommage. Un barrage en remblai (d'environ 18 m de haut) s'est rompu et 8 personnes ont été tuées dans l'onde de crue. Le barrage avait été construit en 1949 et un rapport préliminaire indiquait qu'il pouvait y avoir des défauts.
5. 1**6 avril 2016 Kumamoto, Japon (M = 7.0)**
   153 barrages ont été inspectés après le tremblement de terre, 4 barrages ont subi des dommages. Il s'agit d'une fissure horizontale près de la crête du parement en béton en amont du barrage en terre de Jizoubara et d'une rupture de faille sur le déversoir du barrage en terre d'Oh-Kirihata.
6. **14 novembre 2016 Mw 7.8 Kaikoura, Nouvelle-Zélande**
   Plusieurs petits barrages d'irrigation en remblai (jusqu'à 25 m de haut) étaient situés dans un rayon de 30 km autour de la rupture de la faille. Des PGA supérieurs à 0,7 g ont été déduits sur certains sites de barrage. En général, les dommages sont très limités, voire inexistants. Quelques fissures longitudinales mineures sur ou près de la crête du barrage et des mouvements d'enrochement ont été observés dans certains cas. Des ondes de Seich ont été observées dans deux réservoirs. Le runup a été estimé à 1 m vertical. 196 barrages de glissement de terrain se sont produits. Une surveillance a été mise en place à 12 endroits considérés comme dangereux. Aucun n'a donné lieu à des ruptures mettant en danger les personnes en aval.
7. **6 février 2023 Mw7.8 Kahramanmaras, Turquie**

Deux grands tremblements de terre superficiels d'une magnitude de 7,8 et 7,7 se sont produits le même jour en deux endroits différents du sud-est de la Turquie. Ils ont été associés à des failles de décrochement qui ont affecté une zone s'étendant sur plusieurs centaines de kilomètres. Cette zone compte environ 140 barrages. Dix-sept barrages de différents types, notamment des barrages en remblai zoné, des barrages en enrochement à noyau de terre, des barrages en gravier sableux à noyau de terre, des barrages en remblai et des barrages en enrochement revêtus de béton, ont été endommagés. L'accélération au niveau de la crête des barrages endommagés était environ 4 fois supérieure à celle des fondations. Cette catastrophe a fourni à une occasion unique d'évaluer la performance de grands barrages en remblai soumis à une charge sismique importante.

La principale caractéristique des tremblements de terre de Wenchuan et de Kaikoura en 2008 était le grand nombre de mouvements de masse, qui ont dépassé les 100 000 dans les deux cas. Par conséquent, il convient d'accorder une plus grande attention aux mouvements de masse dans l'évaluation de la sécurité des grands barrages, en particulier ceux situés dans les régions montagneuses. Ces mouvements de masse ont créé de nombreux barrages de glissement de terrain, dont la plupart ont été emportés en peu de temps, mais dont certains ont créé des risques pour la région en aval. Les mouvements de masse peuvent créer des vagues d'impulsion dans les réservoirs, qui peuvent faire déborder les barrages. Ces ondes de choc sont particulièrement critiques pour les barrages en remblai.

En haute montagne, les tremblements de terre peuvent déclencher des inondations de type GLOF (glacial lake outflow floods) ou de grands mouvements de masse dans le bassin versant des réservoirs qui peuvent créer d'importants apports d'eau dans les réservoirs.

4.3. Critères de sécurité des barrages et de sécurité sismique

La sécurité comprend les éléments suivants, qui doivent être pris en compte dans l'évaluation de la sécurité sismique des grands barrages :

- Sécurité structurelle : Conception du barrage conformément à l'état de la pratique (codes, réglementations, lignes directrices) (critères de conception en cas de tremblement de terre et d'inondation, méthodes d'analyse sismique).
- Surveillance de la sécurité des barrages : Instrumentation des barrages, inspections visuelles, analyse et interprétation des données, rapports annuels, etc.
- Sécurité d'exploitation : Lignes directrices pour l'exploitation du réservoir dans des conditions normales et inhabituelles, personnel qualifié, entretien, etc.

- Planification des urgences : Plans de préparation et d'intervention en cas d'urgence, systèmes d'alarme pour l'eau, analyse des ruptures de barrage, plans d'évacuation, moyens techniques de secours, etc.

Les critères généraux de performance en matière de sécurité sismique pour l'évaluation de la sécurité en cas de tremblement de terre (SEE) sont les suivants :

- Pour retenir l'eau dans le réservoir,
- Contrôler le niveau d'eau dans le réservoir après une ESE, et
- Abaisser le réservoir pour (i) réparer les dommages, et (ii) augmenter la sécurité du barrage en cas de doute sur sa sécurité statique ou sismique.

Pour contrôler le niveau de l'eau et l'abaissement du réservoir, il faut utiliser le déversoir et les évacuations à basse altitude, qui doivent donc fonctionner après le séisme. Comme les réservoirs ne peuvent être abaissés en dessous du seuil de l'évacuateur de crues qu'après un fort tremblement de terre, il est fortement recommandé d'utiliser des déversoirs de faible hauteur pour tous les barrages de stockage.

4.4. Classification des risques liés aux barrages et conception sismique

Dans le bulletin 148 de la CIGB, les recommandations suivantes sont fournies pour la détermination des paramètres sismiques. Les paramètres sismiques dépendent de la classification du risque (régi par les conséquences d'une défaillance du barrage) du barrage.

- Pour les barrages à conséquences extrêmes ou élevées, les paramètres du mouvement du sol SEE doivent être estimés au niveau du 84e percentile s'ils sont élaborés par une approche déterministe et ne doivent pas avoir une probabilité de dépassement annuel moyen (AEP) inférieure à 1/10 000 s'ils sont élaborés par une approche probabiliste.
- Pour les barrages à conséquences modérées, les paramètres du mouvement du sol SEE doivent être estimés au niveau du 50e à 84e percentile s'ils sont élaborés par une approche déterministe et ne doivent pas avoir une PEA moyenne inférieure à 1/3 000 s'ils sont élaborés par une approche probabiliste.
- Pour les barrages à faibles conséquences, les paramètres du mouvement du sol SEE doivent être estimés au niveau du 50e percentile s'ils sont développés par une approche déterministe et n'ont pas besoin d'avoir une PEA moyenne inférieure à 1/1 000 s'ils sont développés par une approche probabiliste.
- Les mouvements du sol pour l'OBE ont généralement une PEA moyenne d'environ 1/145.

Les barrages d'une hauteur inférieure à 15 m et d'un faible volume de réservoir peuvent devoir être conçus pour des tremblements de terre dont la période de récurrence est de 3 000 ou 1 000 ans.

De nombreuses directives de conception sismique présentent des critères similaires à ceux mentionnés ci-dessus, mais avec des variations dans les définitions de la classification des conséquences et de la charge sismique.

4.5. Critères de conception sismique et définition des différents types de séismes de conception pour les barrages

Les principales structures et les principaux éléments des grands projets hydroélectriques sont les suivants :

- Le barrage principal et les barrages annexes ; les éléments critiques pour la sécurité tels que les évacuations de fond et les déversoirs (y compris les équipements hydromécaniques et électromécaniques, etc.), qui doivent être opérationnels après un fort tremblement de terre, les pentes critiques sur le site du barrage, la région du réservoir et le bassin hydrographique,
- les structures annexes telles que la centrale électrique, les conduites forcées, les voies d'eau avec les structures d'entrée et de sortie, les chambres d'équilibre, les installations de désensablement, les structures du canal de fuite, le poste de commutation, les équipements hydromécaniques et électromécaniques non critiques pour la sécurité, les routes d'accès, etc. et
- Les structures temporaires telles que les batardeaux, les installations de dérivation et les structures de retenue. En outre, les étapes critiques de la construction du barrage et des structures annexes doivent également être vérifiées.

Le Bulletin 148 de la CIGB recommande les séismes de conception suivants pour la conception sismique des différentes structures et éléments d'un grand projet de barrage :

1. Évaluation de la sécurité en cas de tremblement de terre (SEE) : L'ESE est le mouvement sismique du sol auquel un barrage doit pouvoir résister sans que le réservoir ne se libère de manière incontrôlée. Le SEE est le mouvement du sol qui régit l'évaluation de la sécurité et la conception sismique du barrage et des composants critiques pour la sécurité, qui doivent fonctionner après le SEE.
2. Séisme de référence (OBE) : On peut s'attendre à ce que l'OBE se produise pendant la durée de vie du barrage. Aucun dommage ou perte de service ne doit se produire. Sa probabilité d'occurrence est d'environ 50 % pendant la durée de vie de 100 ans. La période de retour est de 145 ans. Les propriétaires

de barrages adoptent parfois des critères plus stricts pour l'OBE en fonction de leur évaluation des risques et de la prise en compte des impacts économiques. C'est notamment le cas pour les installations hydroélectriques. Les paramètres du mouvement du sol de l'OBE sont estimés sur la base d'une analyse probabiliste des risques sismiques (PSHA). Les valeurs moyennes des paramètres de mouvement du sol de l'OBE peuvent être prises.

3. Séisme de référence (DBE) pour les structures annexes : Le DBE avec une période de retour de 475 ans est le séisme de conception recommandé pour les structures annexes qui n'ont pas de rôle critique pour la sécurité des barrages. Les paramètres du mouvement du sol du DBE sont estimés sur la base d'un PSHA. Les valeurs moyennes des paramètres de mouvement du sol du DBE peuvent être prises. (Remarque : la période de retour du DBE peut être déterminée conformément aux codes et réglementations parasismiques pour les bâtiments et les ponts dans la région du projet si aucun code sismique n'est disponible pour ces structures).
4. Construction Earthquake (CE) : Le séisme de construction est utilisé pour la conception de structures temporaires telles que les batardeaux et prend en compte la durée de vie de la structure temporaire, la vulnérabilité sismique et les conséquences de sa défaillance. Il existe différentes méthodes pour calculer ce séisme de conception. Pour les installations de dérivation temporaires, une probabilité de dépassement de 10 % est parfois supposée pour la durée de vie des installations de dérivation. L'évaluation des risques peut également être utilisée pour faciliter l'évaluation de l'EC. La période de retour de l'EC des ouvrages de dérivation peut également être considérée comme celle de la crue de conception de la dérivation fluviale.

Les paramètres du mouvement du sol SEE peuvent être obtenus à partir d'une analyse probabiliste et/ou déterministe de l'aléa sismique, comme résumé ci-dessous.

- Séisme maximal crédible (SMCC) : Le MCE est l'événement qui produit le plus grand mouvement du sol attendu sur le site du barrage sur la base de l'histoire sismique et du contexte sismotectonique de la région. Il est estimé sur la base de scénarios déterministes de tremblement de terre. Selon le bulletin 148 de la CIGB, les paramètres du mouvement du sol du MCE doivent être considérés comme le percentile 84 (moyenne plus un écart type)
- Séisme maximal de conception (SMD) : Pour les grands barrages et ceux dont les conséquences d'une défaillance sont importantes, la période de retour du séisme maximal de conception est de 10 000 ans. Pour les barrages dont les dommages potentiels sont faibles ou limités, des périodes de retour plus courtes peuvent être spécifiées. Les paramètres du mouvement du sol de la MDE sont estimés sur la base d'une analyse probabiliste des risques sismiques (PSHA). Selon la CIGB, les valeurs moyennes des paramètres de mouvement du sol de la MDE doivent être prises. Cette méthode est presque universellement adoptée, mais il existe quelques différences. Par exemple, l'ANCOLD (2019) exige la prise en compte du 85e fractile du mouvement du sol AEP de 1 sur 10 000 pour les barrages à conséquences extrêmes. La justification est

qu'il est plus probable qu'un barrage conçu pour ce mouvement de sol satisfasse les critères de risque tolérable de l'ANCOLD (2003). L'Australie est un pays où l'aléa sismique est généralement faible et l'adoption de mouvements du sol du 85ème fractile n'est pas aussi onéreuse que dans les pays où l'aléa sismique est élevé. Dans le cas où une source sismique unique (faille) est le principal contributeur à l'aléa sismique, des spectres d'aléa uniformes peuvent être utilisés pour la conception sismique. Sinon, en fonction de la désagrégation de l'aléa sismique (magnitude en fonction de la distance focale), différents scénarios de tremblement de terre peuvent être définis.

Pour les barrages à conséquences élevées, les paramètres de mouvement du sol SEE sont pris comme la valeur maximale des paramètres de mouvement du sol MCE et MDE si les deux tremblements de terre sont déterminés, ce qui est le cas normal. Cependant, si, en raison du contexte sismotectonique dominant, il n'y a pas de failles actives ou potentiellement actives connues, seul le MDE peut être déterminé. Cependant, on observe que certaines directives relatives aux tremblements de terre donnent une définition différente de la SEE, qui s'écarte de la recommandation ci-dessus et des recommandations données dans le bulletin 148 de la CIGB.

Il existe différentes définitions des failles actives et lorsqu'elles sont conservatrices (c'est-à-dire avec une période de retour très longue) et que la faille est proche du site, l'adoption de l'EEM peut être conservatrice par rapport à l'EDM. Pour cette raison, certaines lignes directrices définissent l'ESE comme étant l'ECM, mais le mouvement du sol ne doit pas nécessairement dépasser l'EDM. S'il n'est pas possible de procéder à une évaluation réaliste du MCE, la SEE doit être considérée comme égale à la MDE.

Les études de risque sismique spécifiques au site sont recommandées pour les barrages à conséquences élevées. Les résultats des études sismiques existantes peuvent être pris en compte pour les barrages à faible impact. Les directives du pays ou du propriétaire du barrage peuvent fournir des conseils spécifiques sur l'évaluation des risques sismiques et les critères de conception.

4.6. Liste des structures et des éléments des projets de grands barrages qui doivent être vérifiés pour l'évaluation de la sécurité en cas de tremblement de terre

La sécurité des éléments suivants d'un projet de grand barrage doit être vérifiée pour le SEE:

- Corps de la mère (y compris les mères à selle),
- Structures annexes ayant une fonction critique pour la sécurité (par exemple, structures de prise d'eau, murs ou tunnels des déversoirs non obturés

- Éléments critiques pour la sécurité (déversoirs à vannes, sorties à faible niveau),
- Les culées de barrage (la stabilité des culées est particulièrement importante pour les barrages-voûtes),
- Pentes des réservoirs (les éboulements ou les glissements de terrain peuvent boucher les prises d'eau des éléments critiques pour la sécurité ou créer de grandes vagues d'impulsion dans le réservoir, entraînant le débordement d'un barrage).

Les éléments critiques pour la sécurité des barrages sont les suivants :

- les vannes des déversoirs à vannes (systèmes de vannes comprenant les moteurs, les systèmes hydrauliques à huile, l'alimentation électrique, les unités de contrôle, l'alimentation électrique de secours, les grues pour soulever les vannes du déversoir, etc.
- Vannes et soupapes des exutoires de bas niveau (parfois appelés exutoires de fond, exutoires d'irrigation, exutoires d'évacuation des sédiments, etc.

Les éléments critiques pour la sécurité sont utilisés pour contrôler et abaisser le niveau du réservoir en cas d'urgence ; par conséquent, les mêmes normes de sécurité s'appliquent que pour le corps du barrage. Dans le cas des déversoirs sans vannes, il n'y a pas de problème de contrôle du niveau du réservoir après un fort tremblement de terre, à condition que la goulotte et les murs du déversoir ne soient pas endommagés.

4.7. Évaluation de la sécurité sismique des barrages existants et procédure de vérification périodique de la sécurité sismique des barrages

Pour les raisons suivantes, la sécurité sismique des barrages existants doit être réévaluée :

- De nouvelles informations sur les risques sismiques (multirisques) ou la sismotectonique sont disponibles ;
- Un barrage a été soumis à de fortes secousses sismiques ;
- De nouveaux critères de conception sismique sont introduits ;
- De nouveaux critères de performance et de sécurité sismiques sont introduits ;
- De nouvelles méthodes d'analyse dynamique sont introduites, telles que les méthodes d'analyse dynamique non linéaire ;
- La vulnérabilité sismique d'un barrage a augmenté en raison de modifications, du vieillissement, etc,
- Changements dans la classification des risques ou des conséquences des barrages;

- Le risque sismique a augmenté, par exemple en raison de l'augmentation du nombre de personnes vivant en aval d'un barrage, du développement économique, etc.

À l'heure actuelle, la principale raison de la réévaluation de la sécurité sismique des grands barrages est le fait qu'il existe des barrages qui n'ont pas été conçus pour résister aux tremblements de terre ou qui ont été conçus pour résister aux tremblements de terre avec la méthode d'analyse pseudo-statique dans laquelle le risque sismique était caractérisé par un coefficient sismique de 0,1 (ou un chiffre tout aussi faible). Cette méthode est aujourd'hui considérée comme obsolète. On le savait déjà depuis le tremblement de terre de San Fernando en Californie en 1971.

Des évaluations de la sécurité sismique sont également nécessaires pour les raisons susmentionnées. Afin que tous les barrages satisfassent aux critères de sécurité sismique en vigueur, des contrôles de sécurité périodiques sont requis, par exemple tous les cinq ans , au cours desquels on vérifie si des changements importants ont été apportés à la conception, aux critères de sécurité, etc. Si c'est le cas, une évaluation de la sécurité s'impose. Cela peut être nécessaire tous les 20 à 40 ans. L'expression "changements importants" est mentionnée parce qu'un grand nombre de nouveaux développements sont en cours, en particulier dans le domaine de l'analyse des risques sismiques, et que de nouveaux résultats peuvent être publiés fréquemment. Cela ne signifie pas qu'une évaluation de la sécurité sismique serait nécessaire chaque fois que de nouveaux résultats concernant les risques sismiques sont annoncés. Une modification substantielle des spectres de réponse serait nécessaire avant qu'une analyse sismique ne soit effectuée, par exemple, une augmentation de la valeur PGA de plus de 0,2 à 0,3 g est suggérée.

4.8. Propriétés dynamiques du béton de masse et des enrochements

L'étude des propriétés dynamiques des matériaux et des modèles constitutifs pour le béton, les sols et les roches a évolué au fil du temps. La plupart des informations disponibles concernent les propriétés dynamiques du béton et de la roche, la résistance au cisaillement des joints, les modules de cisaillement dépendant de la déformation et les coefficients d'amortissement des sols, qui sont nécessaires dans les différents types de modèles constitutifs et d'analyses dynamiques des barrages en remblai. Les incertitudes concernant les propriétés des matériaux, voire l'absence de propriétés, nécessitent des analyses de sensibilité approfondies. De nouveaux résultats pour le béton de masse, le RCC et les sols sont attendus. Pour les barrages en béton, l'intérêt principal porte sur le taux d'amortissement, qui contrôle la réponse dynamique.

La résistance à la compression du béton augmente sous l'effet d'une charge dynamique. Le facteur d'augmentation dynamique (FAD) est généralement d'environ 1,3 pour la résistance à la compression du béton de masse, mais il peut être supérieur à 1,5 pour la résistance à la traction sous l'effet de la déformation sismique. Le module d'élasticité du béton de masse augmente peu sous l'effet des déformations sismiques. Dans les analyses numériques des réponses non linéaires des barrages en béton, la relation constitutive après la fissuration est importante, car elle est étroitement liée à l'énergie de rupture du béton de masse. Cela influe sur le processus d'endommagement lors de forts tremblements de terre destructeurs.

4.9. Essais des barrages en béton à l'aide d'une table vibrante

Les essais sur table de secousses sont un moyen important d'étudier les réponses sismiques ainsi que les modes de défaillance possibles des barrages en béton. L'Institut chinois de recherche sur les ressources en eau et l'hydroélectricité (IWHR) a réalisé des expériences à grande échelle pour de grands projets de barrages. Dans les essais sur table vibrante, l'interaction dynamique barrage-fondation-réservoir, l'émission dynamique d'énergie du champ proche au champ lointain, l'ouverture et la fermeture des joints de contraction des barrages-voûtes, le glissement des coins de culée des barrages-voûtes , la pression de soulèvement sur les plans de cisaillement des coins et la surcontrainte des matériaux du barrage doivent être soigneusement simulés.

Outre la similitude de la géométrie, le modèle physique à l'échelle doit répondre à la similitude des propriétés des matériaux et à toutes les charges qui s'exercent sur un système de barrage. L'eau étant utilisée dans le réservoir modèle, il est nécessaire que l'échelle de densité du matériau et l'échelle d'accélération soient identiques afin que la pression hydrostatique dans un champ gravitationnel normal puisse être correctement représentée.

Pour tous les barrages en béton testés à l'IHWR en Chine ces dernières années, la plupart des fissures sismiques ont été trouvées sur la partie supérieure du corps du barrage ainsi que sur les interfaces barrage-roche. Les fissures dynamiques peuvent traverser le corps du barrage et former des blocs détachés avec des joints de contraction. Un impact très fort sur les fissures horizontales répétées pendant la surcharge sismique est observé, ce qui entraîne un écrasement dynamique du béton localement, ce qui constitue un mode de défaillance potentiel.

4.10. Analyse numérique

L'analyse numérique a connu des avancées et des applications significatives depuis Q.83 en 2003. La performance sismique des barrages est étroitement liée aux déformations induites par les tremblements de terre. L'analyse numérique permet de modéliser les caractéristiques de contrainte et de déformation des matériaux et d'estimer la déformation lorsqu'ils sont soumis à un tremblement de terre. Les analyses sont effectuées à l'aide de programmes d'éléments finis ou de différences finies. Les sols, en particulier, se comportent de manière non linéaire lorsqu'ils sont soumis à des contraintes importantes telles que celles imposées par un tremblement de terre. Des modèles constitutifs ont été développés pour simuler ce comportement. Ces modèles ont été développés parallèlement à des essais dynamiques en laboratoire. Les analyses de déformation non linéaire permettent de mieux comprendre la réponse attendue d'un barrage. Elles sont précieuses lorsque l'incertitude de la performance estimée résultant de l'utilisation d'analyses plus simples peut influencer le résultat d'une évaluation de la sécurité d'un barrage ou lorsqu'une meilleure compréhension des modèles de déformation sismique peut améliorer l'évaluation de la performance d'un barrage. Les personnes qui entreprennent des analyses numériques doivent être conscientes des hypothèses, de la théorie, des limites et des incertitudes associées à ces analyses.

L'USSD (Ref.2) a récemment publié un document d'orientation sur l'analyse des déformations sismiques des barrages en remblai. Une approche d'analyse progressive qui commence par des évaluations simples et qui se perfectionne au fur et à mesure des besoins est généralement considérée comme une approche efficace de l'analyse des déformations sismiques des barrages en remblai. Cette approche s'applique également à d'autres types de barrages.

Il existe des incertitudes significatives associées aux analyses numériques (associées aux procédures numériques, à la caractérisation des conditions du site, à la capacité des modèles constitutifs à simuler le comportement du sol, au mouvement sismique du sol d'entrée et aux paramètres critiques tels que la résistance liquéfiée ou résiduelle). Les études de sensibilité sont toujours recommandées pour comprendre les effets des différentes hypothèses et pour prendre en compte correctement l'incertitude. Les principales sources d'incertitude de la modélisation numérique sont les mouvements sismiques du sol et en particulier la caractérisation des propriétés des remblais et des fondations.

4.11. Nouveaux types de barrages

Les types traditionnels de barrages (barrages-poids en béton, barrages-voûtes en béton et barrages en remblai) continuent d'être populaires. Il existe de nouveaux types de barrages, qui sont construits en nombre croissant, à savoir

- Barrages en béton compacté au rouleau (RCC),
- Barrages en enrochement bétonné (CFRD),
- Barrages en enrochement à noyau d'asphalte,
- les barrages en béton enroché (RFC), et
- Barrages en matériaux cimentés (CMD).

Très peu de ces barrages ont été exposés à de fortes secousses similaires à celles de l'ESE, et par conséquent, très peu d'observations de leur comportement sismique sont disponibles. Ces barrages sont construits dans des régions sismiques. Les barrages dont les éléments d'étanchéité sont relativement minces peuvent poser des problèmes lorsqu'ils subissent des déformations sismiques importantes.

4.12. Développements pour les digues à stériles

Il n'existe pas de base de données précise sur les digues à stériles dans le monde. Des estimations de plus de 30 000 barrages ont été publiées, dont plus de 3 500 sont actuellement en activité. Il existe trois principaux types de construction (en amont, dans l'axe et en aval). Les constructions en amont présentent un risque particulier lorsqu'elles sont soumises à des secousses sismiques, car on compte en partie sur les résidus pour retenir le contenu. Généralement, les résidus sont placés sous forme de boue et sont en vrac. Ils sont donc vulnérables à la liquéfaction. Les ruptures de digues à résidus peuvent avoir des conséquences extrêmes. La prise de conscience des risques posés par les digues à stériles, y compris les risques de tremblement de terre, a augmenté de manière significative depuis Q.83, 2003. Les connaissances techniques associées à la charge sismique, à la caractérisation et au comportement des matériaux de remblai, des fondations et des résidus se sont accrues, et ces connaissances sont appliquées à la conception de nouvelles digues à résidus et à l'évaluation de la sécurité des digues à résidus existantes. En outre, certaines défaillances notables ( ) de grandes digues à stériles au Brésil (Brumadinho et Fundao) ont donné lieu à une nouvelle norme industrielle mondiale pour la gestion des stériles (GISTM). Cette norme couvre six sujets principaux:

- Thème I : Personnes affectées par le projet,
- Thème II : Connaissance du contexte social, environnemental et économique local d'un parc à résidus proposé ou existant,

- Thème III : Conception, construction, exploitation, entretien, surveillance et fermeture des parcs à résidus miniers,
- Thème IV : Gestion et gouvernance d'un parc à résidus,
- Thème V : Préparation et réponse aux situations d'urgence en cas de défaillance d'un parc à résidus, et
- Thème VI : Publication d'informations sur les installations de traitement des résidus miniers afin de soutenir la responsabilité publique

Le thème III exige la prise en compte des effets des tremblements de terre et fournit des recommandations pour la conception sismique en fonction de la classification des conséquences de l'installation de stockage de résidus.

Les résidus sont souvent sensibles à la liquéfaction et, pour les barrages construits en amont, l'évaluation du déclenchement de la liquéfaction et de la résistance à la liquéfaction est d'une importance vitale pour l'évaluation de la stabilité. Le cas de stabilité post-séisme régit souvent la conception. Cela nécessite une évaluation de la résistance à la liquéfaction des résidus. Dans certains cas, il est conseillé d'entreprendre une modélisation numérique pour évaluer les déformations. L'existence de fondations liquéfiables ou susceptibles de se ramollir sous l'effet d'une charge sismique complique encore l'évaluation de la stabilité.

En 2022, la CIGB a publié le Bulletin 194 (2022) Tailings Dam Safety (Sécurité des digues à stériles) sous forme de prépublication. Il comprend des conseils sur la conception pour les tremblements de terre couvrant le risque sismique, les critères de conception sismique, l'évaluation de la liquéfaction, y compris la résistance au cisaillement liquéfié, la stabilité sismique et l'analyse de la déformation. La caractérisation des résidus et la sécurité des digues à stériles, y compris les aspects sismiques, font l'objet de nombreuses recherches et de conférences et d'ateliers réguliers.

4.13. Perspectives d'évolution

À l'avenir, on peut s'attendre à de nouveaux développements dans différents domaines qui affecteront l'analyse et la conception sismiques des nouveaux barrages et l'évaluation de la sécurité des barrages existants. Dans l'évaluation des développements futurs, les lignes directrices actuelles de la CIGB documentées dans plusieurs bulletins servent de référence. Comme ces lignes directrices, qui représentent l'état de la pratique ( ), n'ont pas encore été mises en œuvre par tous les propriétaires de barrages ou les autorités chargées de la sécurité des barrages, les premières étapes consisteront à suivre les recommandations formulées dans ces lignes directrices. Les normes de sécurité sismique utilisées dans certains pays peuvent être en avance sur celles de la CIGB et ce qui est considéré comme un développement nouveau ou futur peut ne pas être le cas partout. Il est également

important de noter que le développement futur ne signifie pas de nouveaux résultats de recherche, mais de nouvelles méthodes et lignes directrices adaptées à l'application pratique. Plusieurs problèmes liés à l'évaluation de la sécurité sismique des barrages ont été discutés et peuvent être considérés comme des sujets nécessitant des développements futurs. En conséquence, les développements suivants peuvent être attendus à l'avenir :

- Évaluation des risques sismiques sur le site d'un barrage :
  Il y a quatre aspects importants :
  (a) outre les secousses du sol, le risque de tremblement de terre comprend le déplacement des failles, les mouvements de masse et autres,
  (b) l'ingénieur en charge des barrages n'a pas besoin de données réelles sur les tremblements de terre comme données d'entrée de l'analyse, mais de modèles du mouvement du sol en cas de tremblement de terre,
  (c) pour la vérification de la sécurité des barrages, des historiques temporels d'accélération correspondant au spectre du tremblement de terre d'évaluation de la sécurité sont nécessaires, et
  (d) l'amélioration des modèles de mouvement du sol, en particulier pour les paramètres de mouvement du sol avec des périodes de retour très longues.
- Les principaux développements futurs dans le domaine des risques de secousses telluriques pour les grands barrages sont les suivants :
  (a) l'évaluation des paramètres du mouvement du sol pour les tremblements de terre de forte intensité dans un champ proche,
  (b) l'évaluation des effets géologiques et topographiques spécifiques au site sur les paramètres du mouvement du sol,
  (c) évaluation des effets de la directivité sur les paramètres du mouvement du sol sur les sites des barrages,
  (d) la définition de la durée des fortes secousses du sol pour différents séismes de conception,
  (e) l'élaboration d'historiques d'accélération spécifiques au site (adaptés au spectre) utilisés pour l'évaluation de la sécurité sismique des barrages,
  (f) le développement de modèles de mouvements de terrain non uniformes pour les barrages, et
  (g) l'utilisation des mouvements du sol enregistrés pour calibrer les estimations théoriques de l'aléa sismique et les modèles qui prédisent la réponse des barrages.
- Critères de conception sismique : Les changements concernent
  (a) la conception sismique des composants hydromécaniques et électromécaniques des déversoirs et des évacuations de faible hauteur,
  (b) les combinaisons de charges sismiques, et
  (c) les critères de conception des cascades de barrages le long des rivières et des très grands réservoirs.

- Critères de performance sismique : Les critères généraux peuvent être maintenus, mais il est nécessaire de prévoir des sorties à faible niveau dans les barrages de stockage.
- Propriétés dynamiques des matériaux : De nouveaux modèles de matériaux sont attendus pour les matériaux des barrages en remblai. Les caractéristiques de déformation des enrochements sont nécessaires pour les analyses de déformation avancées des barrages en remblai.
- Méthodes d'analyse sismique des barrages : Les méthodes d'analyse sismique non linéaire doivent être développées davantage. Les nouveaux types de barrages en remblai nécessitent des estimations fiables des déformations sismiques inélastiques, par exemple les barrages en enrochement à noyau d'asphalte.
- Barrages de retenue : Les digues à stériles doivent répondre aux mêmes critères de sécurité que les digues à eau. Des contrôles de sécurité périodiques sont nécessaires, même après la mise hors service.
- Instrumentation sismique des barrages : Des instruments sismiques devraient être installés dans tous les grands barrages.

5. DISCUSSION DES DOCUMENTS

5.1. GÉNÉRAL

Au total, 52 articles ont été soumis. Sept documents n'étaient pas liés aux cinq thèmes associés à la question Q.111. Un résumé des documents associés à chaque thème est fourni ci-dessous.

1. Thème 1 : Surveillance statique, sismique et post-sismique des barrages : 5 documents
2. Thème 2 : Retour d'expérience sur les défaillances dues aux tremblements de terre, y compris les digues à stériles et les digues : 1 document
3. Thème 3 : Importance des caractéristiques multiples du risque sismique (par exemple, secousses du sol, mouvements des failles de surface, mouvements de masse) : 6 articles
4. Thème 4 : Conception sismique et critères de performance pour la structure du barrage, le bord du réservoir et la zone touchée : 25 articles
5. Thème 5 : Évaluation de la sécurité sismique de tous les types de barrages et d'éléments critiques pour la sécurité (par exemple, déversoir, sorties à faible niveau) : 8 articles

Certains documents soumis couvrent plus d'un sujet. Les documents ont été

examinés et des commentaires sont fournis dans les sections suivantes en fonction des cinq thèmes principaux.

5.2. Surveillance statique, sismique et post-sismique des barrages

La plupart des barrages font l'objet d'une surveillance des déformations et des flux d'infiltration dans des conditions de charge statique. La surveillance de ces paramètres après un tremblement de terre peut fournir des informations utiles sur la performance d'un barrage. Le contrôle des vibrations est également de plus en plus courant et est encouragé par le Comité B de la CIGB. Les communications associées à ce thème couvrent le contrôle des essais de vibration forcée et des petits événements sismiques afin de déterminer la rigidité élastique et les périodes naturelles et d'aider à l'étalonnage des modèles analytiques des barrages. Elles ont également porté sur la mesure des forts mouvements du sol associés à des tremblements de terre plus importants. Les mesures de fortes secousses peuvent être utilisées pour valider et calibrer les modèles (analytiques et empiriques) utilisés pour la conception.

L'article R1 présente une analyse statistique des données de mouvement fort enregistrées sur les barrages en remblai existants en utilisant la base de données de mouvement fort JCOLD 2014 qui comprend 190 événements de secousses provenant de 54 tremblements de terre enregistrés sur 60 barrages. Les données de mouvement fort ont été enregistrées au niveau des fondations et des crêtes des barrages lors de tremblements de terre survenus entre 1978 et 2012. L'analyse multivariée et la modélisation linéaire/non linéaire ont été utilisées pour étudier les caractéristiques de la réponse sismique et leurs corrélations par paire. L'accent a été mis sur l'amplification sismique et les périodes fondamentales, ainsi que sur leurs relations avec l'intensité des secousses, la géométrie du barrage et le contenu de la fréquence du mouvement d'entrée. La gamme des PGA est large, avec un maximum proche de 1,0 g, mais la plupart des données sont inférieures à 0,1 g. Des corrélations entre la crête du barrage et la PGA de la fondation (pour les remblais et les enrochements), entre la période naturelle du barrage et la PGA de la fondation, et entre la période naturelle du barrage et la hauteur du barrage ont été déterminées. Des corrélations ont été développées pour trois directions (accélérations parallèles et perpendiculaires à la crête du barrage et verticales). Les données sont très dispersées et les corrélations sont entachées d'incertitude. Cependant, elles sont utiles pour estimer la réponse sismique à un stade préliminaire de la conception. Les utilisateurs doivent être conscients des limites (hauteur du barrage et nombre limité d'enregistrements à des accélérations élevées) lorsqu'ils utilisent les corrélations. Ces types d'études sont utiles et devraient être répétés lorsque des données supplémentaires sont disponibles.

L'article R5 décrit les systèmes de surveillance sismique, le système de

surveillance dynamique continue et les essais de vibration forcée sur des barrages en béton au Portugal. Les hauteurs des barrages sont comprises entre 41,0 et 136,0 m. Des modèles numériques pour les analyses dynamiques des barrages ont été développés, avec le système barrage-fondation-réservoir. Les discontinuités liées aux joints de contraction du barrage, au joint barrage-fondation et à l'interface barrage-réservoir ont été représentées, tandis que la masse rocheuse a été supposée être un continuum équivalent. Le réservoir a été discrétisé avec des macro-éléments dans le logiciel 3DEC. L'interface barrage-réservoir a été représentée par un joint élastique avec une rigidité tangentielle nulle. Les modèles ont été initialement calibrés avec les résultats des essais de vibration forcée, en considérant un comportement élastique linéaire du béton du barrage. L'objectif était de suivre l'évolution du comportement des barrages au cours des différentes phases de leur vie.

L'article R24 est un exemple qui démontre les avantages de l'installation d'accéléromètres pour surveiller la performance des barrages. Il traite du barrage de Paltinu, un barrage-voûte symétrique à double courbure, situé en Roumanie. Au fil du temps, il a fait l'objet d'un programme de surveillance intensif utilisant des mesures de vibrations ambiantes in situ. Dans le cadre de ce programme, un modèle mathématique à éléments finis a été développé et calibré à l'aide des données des campagnes de mesure initiales et utilisé pour évaluer la sécurité de la structure à chaque étape de la surveillance. Si la période fondamentale de la structure ne change pas au fil du temps, on peut conclure que le barrage n'a pas subi de dégradation structurelle.

Un nouveau système destiné à améliorer les capacités de surveillance sismique a été installé en 2022. Il comprend six accéléromètres à mouvement fort et un sismomètre à large bande. Les accéléromètres sont installés aux endroits suivants : un dans le champ libre, un sur chaque culée, un sur les fondations et deux sur la crête. Le nouveau système a enregistré une série d'événements de faible intensité. Le programme de surveillance renforcé améliore la capacité de détection des événements sismiques et la fiabilité de l'évaluation de toute dégradation structurelle.

L'article R50 décrit la réponse mesurée du barrage de Horka, situé dans l'ouest de la Bohême, en République tchèque. Il s'agit d'une zone où il y a une sismicité historique, y compris un tremblement de terre de magnitude 6,5 déduit d'une étude paléosismique. Le barrage de Horka est une digue en terre construite entre 1966 et 1970. Aucune analyse de stabilité pour les charges sismiques n'a été entreprise dans le cadre de la conception. Les exigences en matière de conception sismique ont été mises en œuvre après 1970. L'article résume les exigences actuelles en matière de conception sismique dans la norme tchèque CSN 75 2310 et les compare aux estimations de l'AGP provenant des études probabilistes des risques sismiques annexées à l'Eurocode 8.

Un sismographe a été installé dans la partie la plus basse de la galerie

d'injection en 2017, et quatre accéléromètres ont été installés en 2019-2020. En avril 2022, le département géophysique de l'Académie des sciences de la République tchèque a installé 23 sondes sismiques et mesuré les vibrations naturelles du barrage. La première période fondamentale du barrage a été déterminée comme étant de 3,12 Hz. L'amplification des mouvements de la crête était 20 fois supérieure à celle mesurée à la base. On s'attend à ce que l'amplification soit plus faible lorsqu'elle est soumise à des mouvements du sol représentatifs du niveau SEE en raison de la réponse non linéaire du remblai.

Le document R41 présente des recommandations visant à améliorer la sécurité des barrages grâce à une meilleure utilisation des données de surveillance et à une meilleure préparation avant et après les tremblements de terre. Il s'appuie sur l'automatisation complète des informations de surveillance, l'interprétation rapide de ces informations et la diffusion de recommandations et d'actions aux parties responsables de la sécurité des barrages et aux autres parties prenantes. Le système proposé à l'adresse repose sur une plateforme de gestion intelligente avec une intégration et une application complètes des jumeaux numériques, des modèles d'intelligence artificielle et des plateformes de connaissances. Le concept présente des avantages potentiels importants, mais son développement en un outil pratique nécessiterait des efforts considérables.

5.3. Retour d'information sur les performances observées, y compris les digues à stériles et les de terre

Les observations et le retour d'information sur la performance des barrages soumis aux effets des tremblements de terre sont d'une importance vitale pour faire progresser la résilience et la sécurité sismiques des barrages situés dans des zones où il existe des risques sismiques. Elles permettent de comprendre le comportement et les conséquences qui peuvent avoir des implications pour la conception, l'évaluation de la sécurité des barrages existants et pour la préparation et la gestion des interventions d'urgence en cas d'incidents ou de ruptures de barrages.

Il est très utile que les barrages soient équipés d'enregistreurs de mouvements forts au niveau de la base et de la crête au minimum, mais aussi idéalement dans le champ libre, sur les culées et à mi-hauteur sur l'épaulement aval. Dans certains pays, certains enregistreurs de mouvements forts sont obligatoires. Le Comité B de la CIGB encourage les propriétaires de barrages à installer de tels instruments. Cela permet d'évaluer les caractéristiques dynamiques fondamentales, de fournir des informations pour le développement et l'affinement des méthodes de conception empiriques simplifiées et de permettre l'étalonnage de méthodes de conception plus avancées.

L'article R32 est un article important. Il décrit le comportement sismique du

barrage-voûte de Dagangshan, haut de 210 m, qui a été soumis au tremblement de terre de Luding de magnitude Ms 6,8, en Chine, le 5 septembre 2022. La distance épicentrale était de 21 km. Il existe 21 instruments de mesure des mouvements forts dans le corps du barrage et dans la roche de fondation. Le PGA le plus élevé enregistré dans la fondation rocheuse était de 0,22 g dans la direction de la rivière. Avec une PGA horizontale de 0,57 g, le barrage de Dagangshan est le barrage conçu pour les plus fortes secousses en Chine. L'accélération maximale enregistrée sur la crête du barrage était de 0,51 g. Une analyse dynamique du système barrage-réservoir-fondation a été réalisée en utilisant les historiques temporels d'accélération enregistrés dans la fondation du barrage comme données d'entrée. Les résultats de l'analyse numérique ont ensuite été comparés aux résultats mesurés lors du tremblement de terre de Luding. On peut observer que l'amplification de l'accélération maximale de la base à la crête est d'environ 2,4, ce qui est assez faible pour un grand barrage-voûte. L'analyse a montré que la résistance dynamique à la traction du béton de masse n'a pas été dépassée pendant le tremblement de terre de Luding et que le barrage n'a pas été endommagé. L'ouverture des joints de contraction a été analysée, mais aucun instrument n'a été fourni pour mesurer l'ouverture des joints pendant les tremblements de terre. Les appareils de mesure des joints dynamiques ne sont pas encore utilisés et ne seraient intéressants qu'à des fins de recherche, mais pas en tant qu'instrument standard dans les grands barrages.

5.4. Importance des multiples caractéristiques de l'aléa sismique (par exemple, secousses du sol, mouvements des failles de surface, mouvements de masse)

Le risque sismique est un risque multiple. Il comprend les secousses du sol, le déplacement des failles, les pressions hydrodynamiques, la liquéfaction, les glissements de terrain (au-dessus du réservoir et sous-marins), les éboulements et les seiches. Tous ces risques doivent être pris en compte lors de la conception de nouveaux barrages et de l'évaluation de la sécurité des barrages existants.

5.4.1. *Mouvement du sol en cas de tremblement de terre*

Le risque de tremblement de terre le plus important est la secousse du sol. Les grands tremblements de terre peuvent générer de fortes secousses du sol qui peuvent être ressenties sur une large zone. Les méthodes d'estimation des risques de secousses sismiques sont de plus en plus sophistiquées et tiennent compte de l'incertitude aléatoire et épistémique. Un large éventail de possibilités de sources de tremblements de terre et de modèles de mouvements du sol peut être incorporé par le biais d'une approche par arbre logique.

Les effets des répliques des tremblements de terre sont souvent sous-estimés

ou négligés lors de la conception ou de la modernisation des barrages. Les grands tremblements de terre s'accompagnent généralement de nombreuses répliques, qui peuvent se produire peu de temps après la secousse principale. Il s'agit d'une préoccupation potentielle pour les sols qui sont sujets à des effets de ramollissement ou de liquéfaction et qui doivent être pris en compte. Cela est dû au fait que les pressions interstitielles générées pendant la secousse principale modifient l'état de contrainte effective et altèrent le comportement du matériau pendant les répliques ultérieures.

L'article R10 présente une étude numérique des effets d'un tremblement de terre initial, suivi de répliques, sur un système de remblai idéalisé. L'analyse est basée sur un remblai hypothétique de 20 m de haut composé d'épaulements de sable dense et d'un noyau d'argile avec des fondations composées de 20 m de sable moyennement dense sur un substratum rocheux. L'analyse a été réalisée à l'aide de FLAC 8.1 (programme de différences finies) qui permet d'estimer les déformations du remblai (verticales et horizontales). Les sols ont été modélisés à l'aide de PM4Sand (épaulements et fondation) ou PM4Silt (noyau) et le substratum rocheux a été supposé élastique linéaire. Les analyses ont pris en compte différentes possibilités pour les événements principaux et les répliques et ont considéré trois degrés différents de consolidation entre les événements principaux et les répliques (en tant que proxy pour les différents intervalles de temps entre les chocs principaux et les répliques).

Les analyses donnent un aperçu de la manière dont les répliques peuvent affecter les déformations d'une digue. Il a été démontré que les répliques entraînent des tassements plus importants de la crête du barrage. Il est intéressant de noter que les analyses ont montré des tassements plus importants pour une reconsolidation plus élevée entre le choc principal et les répliques. Cela peut sembler contraire à l'intuition. Les auteurs fournissent une explication possible : la rigidité rétablie après une reconsolidation plus importante diminue la période naturelle du barrage, s'alignant mieux sur la fréquence et l'énergie du mouvement du sol. L'une des limites des analyses est l'absence de modélisation directe de l'infiltration pendant la reconsolidation. Ce phénomène peut être difficile à estimer avec précision et dépend du temps écoulé entre la secousse principale et la réplique, qui n'est pas prévisible. Les concepteurs doivent prendre en compte les effets des répliques sur la performance des barrages en remblai lorsque les matériaux de remblai et/ou les fondations sont susceptibles de se ramollir ou de se liquéfier. Les analyses présentées dans le document R10 donnent un aperçu de la situation. Cependant, il y aura toujours une incertitude considérable associée à toute analyse et donc des analyses de sensibilité et l'utilisation du jugement seront nécessaires dans la pratique.

R34 présente de nouvelles fonctions de taux de glissement pour modéliser le temps de rupture des failles et les utiliser dans les simulations des mouvements du

sol des tremblements de terre. Elles sont appliquées à une réplique du tremblement de terre de Luding et les mouvements du sol prédits sont comparés aux mouvements du sol enregistrés.

5.4.2. *Mouvement de la faille*

L'identification des failles actives est importante lors de l'évaluation du risque sismique pour les barrages. La rupture d'une faille à proximité d'un barrage peut entraîner de multiples risques, les secousses du sol étant les plus importantes. Si la faille est sous-jacente au site, elle peut entraîner une déformation du sol susceptible d'endommager gravement un barrage. Diverses méthodes peuvent être utilisées pour identifier les failles actives. Le bulletin 148 de la CIGB donne la définition suivante d'une faille active dans le cadre de la conception d'un barrage : "Il existe des preuves de mouvement (séismes) au cours de la période holocène (il y a 11 000 ans), ou pour les grandes failles des preuves de mouvement au cours de la fin du pléistocène (il y a 35 000 ans), ou pour les lignes principales des grandes failles des preuves de mouvement au cours du quaternaire (il y a 1,8 million d'années). Cette définition n'est pas universellement adoptée et il existe une certaine confusion quant à la définition d'une grande faille ou d'une faille majeure. Dans les analyses probabilistes de l'aléa sismique, il est préférable de pécher par excès de conservatisme et d'inclure les failles ayant de longs intervalles de récurrence. Les failles avec des intervalles de récurrence très longs ont généralement peu d'influence sur l'ESE car l'intervalle de récurrence maximum pour la classification la plus élevée des conséquences sur les barrages est généralement de 10 000 ans. Cependant, dans les analyses déterministes, les failles avec de très longs intervalles de récurrence peuvent donner lieu à des mouvements de terrain beaucoup plus élevés que dans les analyses probabilistes. Déterminer si une approche probabiliste ou déterministe est plus appropriée pour un site de barrage donné demande du discernement. En cas de doute, les concepteurs peuvent opter pour la plus élevée des estimations déterministes ou probabilistes des mouvements du sol. Dans les cas où il existe des différences significatives entre les estimations déterministes et probabilistes, il est recommandé de limiter la réduction des paramètres de la demande sismique à au moins 80 % des estimations les plus élevées.

L'article R25 fait référence à la tomographie par résistivité électrique, au géoradar, à la sismique réfraction et à la sismique réflexion, ainsi qu'aux tranchées paléosismiques et à la datation au carbone de certaines couches de sol. Le document comprend un exemple d'identification de la faille active de Sumatra et de ses différents segments. Des recommandations et des exemples sont fournis pour l'échelle des cartes décrivant l'emplacement des failles, pour la réalisation de différents types de levés géophysiques, pour les tranchées paléosismiques et pour la datation au carbone.

5.4.3. *Études des risques sismiques*

L'Indonésie est un pays où le risque sismique est très élevé. Il existe quatre zones de subduction majeures et de nombreuses failles importantes dans la croûte terrestre qui sont toutes capables de produire des tremblements de terre importants. Le document R26 examine la pratique actuelle de l'évaluation des risques sismiques pour les barrages en Indonésie en se référant à un nouveau document d'orientation sur la réalisation d'études des risques sismiques pour les projets de barrages en Indonésie (Guidelines of Seismic Study for Determination the Earthquake Design Parameters, Volume I, Seismic Hazard Assessment). Ce document est en cours d'examen avant d'être publié par le ministère indonésien des travaux publics et du logement. Elle couvre les orientations requises pour les études de faisabilité et la conception détaillée. Elle couvre également l'évaluation pendant la construction, lorsque les excavations pour la fondation du barrage et les structures annexes peuvent révéler l'existence de failles qui n'avaient pas été identifiées auparavant. La portée et les détails des études de risques sismiques dépendent des conséquences de la rupture du barrage. Le niveau de détail et les exigences de l'étude de danger sismique dépendent des facteurs de risque liés au volume du réservoir, à la hauteur du barrage, au nombre de personnes devant être évacuées et au facteur de dommage en aval. Ces quatre facteurs sont additionnés pour obtenir un facteur de risque total. Il existe quatre classes de risque (I, II, III et IV). Des études de risque sismique sont requises pour tous les barrages lors de l'étude de faisabilité. Elles utilisent la dernière carte indonésienne des sources et des risques sismiques publiée par PuSGeN/Ministère de la PUPR pour obtenir une indication de l'AGP. Le niveau de risque du barrage est évalué à l'aide de cette estimation du PGA. Si le barrage est évalué comme une classe de risque III ou IV, des études plus détaillées (régionales et de champ proche) sont nécessaires pour identifier et caractériser les sources de tremblement de terre et les failles sismiques à proximité. Le document décrit les détails des études requises pour identifier et caractériser les failles actives. Le document recommande que lorsque des segments de failles parallèles sont séparés par moins de 4 km, les segments soient combinés et traités comme une seule faille. Les estimations du mouvement du sol SEE sont basées sur des estimations déterministes tenant compte des failles actives identifiées.

5.4.4. *Sismicité déclenchée par les réservoirs*

La sismicité déclenchée par les réservoirs est souvent associée à des barrages de grande hauteur avec de grands réservoirs. L'article R37 présente les résultats d'une étude des conditions structurelles géologiques des zones épicentrales des plus forts tremblements de terre survenus sur cinq grands barrages en Chine (Xinfengjiang, Danjiangkou, Shanxi, Xiluodu et Trois Gorges) afin de déterminer comment elles affectent la sismicité déclenchée par les réservoirs. Les conditions qui se sont avérées être des facteurs importants sont les suivantes : (1) masse rocheuse fragile ; (2) la faille croise le champ de contraintes de compression

principal régional à un angle faible et l'angle de pendage de la faille est important (l'angle d'intersection est généralement inférieur à 20° et l'angle de pendage de la faille est supérieur à 60°) ; (3) le corps du réservoir est situé dans le mur de pied de la faille ; (4) il existe une connexion hydraulique directe ou indirecte entre la zone de la faille et le réservoir. D'autres conclusions sont que la sismicité de fond dans la zone du réservoir et à proximité du réservoir avant la mise en eau n'a pas d'effet sur l'intensité de la sismicité déclenchée par le réservoir. Il n'y a pas de corrélation évidente entre l'activité des failles existantes avant la mise en eau du réservoir et l'intensité de la sismicité déclenchée par le réservoir.

L'article R45 présente les résultats d'une étude visant à déterminer les détails des structures sismogéniques à partir de l'analyse des ondes numérisées enregistrées par un réseau de 35 sismographes situés dans les zones des réservoirs de Xiangjiaba et de Xiluodu sur une période de quatre ans. Les centrales hydroélectriques de Xiangjiaba et de Xiluodu sont importantes, avec des capacités installées de 6,4 millions de kW et de 13,86 millions de kW, respectivement. Les capacités de stockage des réservoirs sont respectivement de 5,19 milliards de m3 et de 13,9 milliards de m3. L'accumulation d'eau dans les réservoirs a entraîné une augmentation significative de la sismicité. Les deux plus importantes sont de magnitude 5,1 et 5,2. Ce phénomène est une caractéristique bien connue des grands réservoirs. Il est attribué à l'augmentation des charges et des contraintes entraînant des déformations de la croûte terrestre sous-jacente. Normalement, une combinaison d'analyses des mécanismes de focalisation des tremblements de terre et des distributions des répliques sismiques est utilisée pour déterminer l'emplacement et la géométrie des structures sismogènes. Cet article présente les résultats de l'utilisation de la théorie de la tomographie à double différence, qui permet de résoudre simultanément les problèmes d'inversion de la structure de vitesse 3D et de localiser plus précisément les tremblements de terre. Il explique la méthodologie et présente les résultats obtenus pour les réservoirs de Xiangjiaba et de Xiluodu.

5.5. Critères de conception et de performance sismiques pour la structure du barrage, le bord du réservoir et la zone touchée

Ce thème de Q.111 a fait l'objet du plus grand nombre d'articles. Il y a une évolution et un développement constants des exigences statutaires nationales qui requièrent la prise en compte des charges et des effets sismiques dans la conception des barrages et lors de la réalisation d'études de sécurité des barrages. Des documents d'orientation nouveaux et mis à jour continuent d'être publiés. Il s'agit notamment des documents suivants

- Bulletin ICIGB 148 (2016) Sélection des paramètres sismiques pour les grands barrages
- Bulletin 166 de la CIGB (2016) Inspection des barrages selon les directives relatives aux tremblements de terre

- Bulletin CIGB 194 (2022) Sécurité des digues à stériles, version préliminaire - version finale soumise pour publication
- Lignes directrices de l'ANCOLD pour le dimensionnement des barrages et des structures annexes pour les tremblements de terre (mai 2019)
- Analyse USSD des déformations sismiques des barrages en remblai (2022)
- NZSOLD Directives néo-zélandaises pour la sécurité des barrages 2024

En outre, des recherches sont en cours, des critères de performance et des méthodes de conception sont développés et ont été publiés et présentés lors de diverses conférences et ateliers techniques. Cela comprend le développement et l'avancement des méthodes de conception, en particulier en ce qui concerne la modélisation numérique. On trouve également sur le site des méthodes simplifiées qui ont leur place dans la conception et l'évaluation de la sécurité des barrages existants.

Il est rappelé aux praticiens que la sécurité sismique des barrages va bien au-delà de l'estimation des risques sismiques et des analyses dynamiques avancées. Il s'agit de comprendre les modes de défaillance potentiels et d'élaborer des mesures d'atténuation (concepts et détails de conception), la qualité de la construction, l'examen indépendant par les pairs, la gestion de la sécurité des barrages, y compris les procédures opérationnelles sûres, la surveillance et le contrôle (axés sur les modes de défaillance potentiels), la maintenance, les examens réguliers de la sécurité des barrages, y compris les examens périodiques indépendants de la sécurité globale, et les plans de préparation et d'intervention en cas d'urgence.

Les documents soumis pour ce thème couvrent de nombreux types de barrages et différents aspects des critères de performance et de la conception.

5.5.1. *Lignes directrices générales*

La question des défis posés par les progrès continus dans le domaine de l'analyse probabiliste des risques sismiques, qui se traduisent souvent par une augmentation des risques sismiques, est abordée dans le document R7. Il s'agit d'une question difficile pour les propriétaires de barrages et les régulateurs, à la fois pour les nouveaux barrages et pour les évaluations de sécurité des barrages existants. On peut normalement supposer qu'une réévaluation sismique est nécessaire lorsqu'il y a eu un changement dans les estimations de l'aléa sismique. Le document R7 note qu'il faut être conscient du fait que l'analyse de la sécurité sismique des barrages comprend diverses incertitudes qui sont comparables à celles du risque sismique et que le simple fait d'améliorer les analyses du risque sismique n'améliorera pas la qualité de l'évaluation de la sécurité sismique si les autres incertitudes restent inchangées. Les principales conclusions et recommandations sont les suivantes :

1. Des changements mineurs dans le risque sismique de l'ordre de 0,1-0,2 g dans des régions de sismicité modérée à forte ne nécessitent pas une nouvelle analyse des barrages bien conçus, bien construits et bien entretenus.
2. Une combinaison de charges "au-delà du mouvement du sol SEE", dans laquelle le mouvement du sol du tremblement de terre d'évaluation de la sécurité est multiplié par un facteur de 1,5 ou 2,0, est recommandée comme combinaison de charges sismiques supplémentaire. Cette combinaison de charges peut être utilisée pour déterminer les réserves de sécurité sismique d'un projet de barrage. En même temps, il ne sera pas nécessaire de procéder à une nouvelle analyse sismique des barrages, lorsque l'augmentation du risque sismique est inférieure à celle de cette combinaison de charges extrêmes.
3. On s'attend à ce qu'une évaluation complète de la sécurité sismique d'un barrage ne soit nécessaire que tous les 20 à 40 ans, voire tous les 50 ans, à moins que le barrage ne montre des signes de comportement inhabituel ou que sa classification de risque ne soit augmentée.

Le document R23 présente de nouvelles règles sur les risques sismiques dans les barrages en Albanie. L'Albanie est un pays où le risque sismique est élevé. Elle compte près de 650 barrages, dont 350 sont classés comme grands barrages. La plupart sont des barrages en remblai. La conception sismique originale de la plupart des barrages était basée sur une approche pseudo-statique avec un coefficient sismique de 0,1. Le comité albanais sur les grands barrages (ALBCOLD) prévoit de préparer des normes et des lignes directrices nationales pour la conception et la surveillance des barrages, dans lesquelles la méthodologie d'évaluation du risque sismique sera décrite en détail. L'ALBCOLD propose trois classifications du risque des barrages (risque potentiel faible, modéré et élevé). Il est proposé de relier le niveau de risque de secousse du sol à la classification du risque des barrages. Pour les barrages d'irrigation, l'AGP de conception est obtenue en factorisant les estimations existantes de l'AGP pour une période de retour de 475 ans, préparées par l'Institut national des géosciences (IGEO). Les facteurs d'échelle sont de 1, 1,2 et 1,4 pour les barrages à risque potentiel faible, modéré et élevé, respectivement. Pour les grands barrages destinés à la production d'énergie hydroélectrique, à l'approvisionnement en eau et à des fins urbaines, les paramètres d'importance doivent être appliqués à la même période de retour des paramètres PGA sur l'état des roches qui sont donnés dans les conceptions originales de ces barrages ou dans le Bulletin de la CIGB No. 148, daté de 2016.

5.5.2. *Barrages en remblai*

Des documents ont été reçus sur un éventail de sujets liés à la conception des barrages en remblai et certains documents se sont concentrés sur des types particuliers de barrages (CFRD, CSG, et barrages de résidus).

L'article R3 présente l'analyse dynamique du barrage de Santa Rita en

Colombie comme un cas d'étude où le potentiel de liquéfaction est pris en compte dans l'évaluation de la performance des barrages en remblai. L'analyse est réalisée à l'aide du logiciel FLAC2D. Deux modèles constitutifs du sol sont utilisés : 1) Mohr-Coulomb et un modèle plus avancé 2) PM4Sand/Silt constitutive model. Les analyses sont effectuées pour quatre périodes de retour différentes (475, 2 500, 5 000 et 10 000 ans). Les déformations estimées à l'aide des différents modèles constitutifs sont comparées. Les déformations les plus importantes sont estimées avec le modèle constitutif PM4Sand/Silt. L'article fournit un bon résumé des étapes à suivre, y compris des conseils sur la configuration du modèle, la sélection et la mise à l'échelle des accélérogrammes, et la sélection des paramètres du modèle de sol lors de la réalisation d'analyses dynamiques à l'aide d'un modèle constitutif de sol avancé comme PM4Sand/Silt.

L'article R13 présente une formulation tridimensionnelle (3D) d'un modèle constitutif simple et pratique conçu pour capturer les caractéristiques d'amortissement hystérétique non linéaire des matériaux non liquéfiables sous l'effet d'une charge sismique. Ce modèle est une extension 3D du modèle bidimensionnel (2D) UBCHyst, développé à l'Université de Colombie Britannique, qui a été largement utilisé pour la modélisation des sols typiquement utilisés dans les barrages en remblai tels que les argiles compactées, les enrochements denses et non saturés, ou les fondations rigides et le substratum rocheux altéré par les intempéries. Le modèle 2D a été formulé et mis en œuvre dans l'espace 2D, en tenant compte de la nature hystérétique du matériau, de la variation du module de cisaillement en fonction du rapport de contrainte, en limitant ce rapport par un critère de surface de rendement de Mohr-Coulomb. Le modèle 3D utilise la surface d'écoulement de Mohr-Coulomb généralisée dans l'espace des contraintes principales 3D, mais aborde également certaines limitations du modèle 2D original. Le document présente au lecteur la formulation du modèle 3D, y compris les améliorations apportées au modèle. La formulation 3D a été mise en œuvre en tant que modèle défini par l'utilisateur dans la version 9.0 de FLAC2D/3D pour une application dans les problèmes de valeurs limites.

L'article R13 présente les résultats d'une comparaison entre le nouveau modèle 3D et le modèle 2D original pour les essais de cisaillement simple direct monotone et cyclique. Le modèle est ensuite vérifié par rapport à des données expérimentales pour des enrochements et des matériaux graveleux dans des trajectoires de contraintes triaxiales statiques et cycliques. Une amélioration clé du modèle 3D est sa capacité à capturer la réduction du module de cisaillement qui se produit dans les trajectoires de contraintes triaxiales cycliques. Enfin, une analyse de la réponse sismique est effectuée en appliquant un enregistrement sismique à la base d'une colonne unidimensionnelle (1D). Les résultats du modèle UBCHyst conventionnel sont comparés au modèle UBCHyst étendu en 3D. Pour des conditions de contraintes isotropes, les résultats sont identiques. Pour des conditions de contrainte K_0, le modèle 3D prédit des contraintes et des déplacements cycliques plus élevés.

Le travail d'extension du modèle 2D original d'UBCHyst à la 3D et les améliorations apportées au modèle représentent un progrès pour ce modèle constitutif. Les auteurs notent qu'UBCHyst a été développé pour simuler la déformation induite par le cisaillement des enrochements, des matériaux graveleux et des sols cohésifs dilatifs sous charge cyclique. Dans sa forme actuelle, le modèle n'est pas capable de capturer d'autres mécanismes susceptibles de provoquer des déformations permanentes, tels que la dégradation des particules entraînant une réduction des propriétés de résistance effective, et le compactage sismique, entre autres. Les futures mises à jour du modèle seront axées sur ces limitations.

Le document R22 présente une approche simplifiée et graduelle pour évaluer le comportement sismique des structures de remblai. Il commence par décrire une méthode de linéarisation qui prend en compte les effets de la pression interstitielle sur le module de cisaillement linéaire équivalent. Cette approche est appliquée au barrage d'Aratozawa (PGA 1,04 g). Ensuite, une approche graduelle (statique, dynamique simplifiée, réponse temporelle non linéaire) est mise en œuvre sur un barrage en remblai d'une hauteur similaire à celle d'Aratozawa et soumis à une très forte charge sismique (PGA 1,22 g). Enfin, une nouvelle méthode simplifiée d'évaluation du comportement sismique des digues, des remblais et des barrages de taille moyenne est présentée. Cette méthode tient compte des géométries spécifiques et des propriétés des fondations de ces ouvrages dans l'évaluation de leur comportement sismique. Des données plus instrumentales obtenues à partir de tremblements de terre permettront de valider et d'étalonner les méthodes proposées.

L'estimation des déformations des barrages en terre-roche résultant d'une charge sismique est essentielle pour évaluer leur performance et leur sécurité sismique. Différentes méthodes peuvent être utilisées. L'une d'entre elles est l'analyse des déformations globales. Elle considère le sol comme un milieu continu dont le comportement constitutif dynamique est basé sur des essais expérimentaux combinés à une modélisation par éléments finis. L'article R48 évalue deux modèles existants et introduit un nouveau modèle de déformation résiduelle basé sur les mécanismes de déformation permanente des tremblements de terre, afin de remédier aux lacunes des modèles actuels. Le premier modèle existant est le modèle de contrainte dynamique-déformation résiduelle. Il décrit la relation entre la contrainte dynamique et la déformation résiduelle à un certain cycle de vibration. Le deuxième modèle existant est le modèle de déformation résiduelle dépendant du cycle. Il fournit une description complète de la relation entre la contrainte résiduelle et le nombre de cycles de vibration. Le nouveau modèle présenté dans le document R48 présente l'avantage de définir précisément la signification de chaque paramètre, en incorporant les paramètres de l'état de contrainte dynamique et de consolidation dans l'analyse des variations de l'échantillon de sol pendant les essais de déformation résiduelle, améliorant ainsi la clarté physique. La relation entre les paramètres et les cycles de vibration est plus prononcée, ce qui améliore la compréhensibilité globale du modèle et fournit des données plus fiables pour les

calculs d'interpolation. Le modèle peut être appliqué au gravier sableux et au sable moyennement grossier dans des conditions bien drainées. Il nécessite la réalisation d'essais dynamiques avec différents rapports de contrainte de cisaillement sur des échantillons à différents rapports de consolidation et pressions de confinement.

L'article R47 présente le concept d'utilisation de géogrilles pour renforcer et améliorer la résistance des remblais à la base des hauts barrages en enrochement et dans la partie supérieure des fondations. L'amélioration du facteur de sécurité pour la stabilité grâce au renforcement par géogrilles est démontrée à l'aide d'un exemple.

L'article R12 présente un résumé de la conception d'un nouveau barrage en enrochement à parement de béton (CFRD) de 52 m de haut en Nouvelle-Zélande (Waimea Community Dam). L'objectif principal est l'irrigation. Le tremblement de terre SEE est un mouvement probabiliste du sol avec une probabilité de dépassement annuel (AEP) de 1:10 000 d'un tremblement de terre avec un moment de magnitude de 7,1, une accélération maximale du sol (PGA) de 0,64 g et une accélération spectrale maximale d'environ 1,65 g. Les directives de sécurité des barrages néo-zélandais exigent que la conception comprenne une réplique dans le jour qui suit la réplique principale. La réplique prévue pour le barrage de Waimea a un moment d'une magnitude de 6,5 et une accélération spectrale maximale de 0,58 g.

Les éléments clés de la conception sont les suivants :

- Une digue en enrochement flexible et résistante à l'érosion, permettant un mouvement contrôlé pendant les tremblements de terre. Les exigences primordiales en matière de performance de la conception du remblai étaient l'absorption des déformations dues aux tremblements de terre et le transport des fuites après le tremblement de terre, ce qui aurait réduit la stabilité du remblai à un niveau dangereux.
- Une dalle de parement en béton armé avec les dimensions de la dalle, les détails des joints et l'armature appropriés.
- Des éléments d'étanchéité flexibles reliant la dalle de parement aux murs de crête, ainsi qu'entre les éléments de mur, avec une capacité appropriée pour faire face aux mouvements importants et aux inondations post-sismiques.

Des analyses numériques dynamiques en 2D ont été entreprises pour estimer les déformations du remblai sous les charges sismiques de conception. Les déformations verticales maximales de la crête de 1,1 m se produisent lorsque le réservoir est au niveau d'exploitation minimal normal. La réplique sismique de conception entraîne une déformation verticale supplémentaire de 0,35 m. L'ampleur de la déformation devrait entraîner l'ouverture des joints et la fissuration du revêtement en béton. Un système d'arrêt d'eau externe flexible a été adopté pour tenir compte du mouvement prévu entre le mur de parapet et la dalle de parement.

Le document décrit les modes de défaillance sismique potentiels et discute des concepts de conception adoptés pour atténuer les effets. Des dommages post-séisme au parement en béton sont prévus et les modes de défaillance comprennent l'écoulement de fuites entraînant l'effilochage du pied aval progressant vers l'érosion vers le réservoir et les pressions d'infiltration entraînant une instabilité globale. Les caractéristiques d'atténuation de la conception comprennent une zone de transition sableuse sans cohésion et un drain incliné en aval du parement en béton qui est contigu à un drain de couverture qui s'étend de l'arrière du socle en amont jusqu'au pied en aval du barrage en remblai. Le document R12 est une référence utile qui documente les problèmes de conception et les mesures d'atténuation pour une digue en béton armé située dans un environnement fortement sismique.

Les barrages en enrochement à parement en béton bitumineux sont utilisés en Chine dans les projets de pompage-turbinage en raison de leur faible perméabilité, de leur capacité à supporter les déformations, de leur forte résistance à la corrosion acide et alcaline et de l'absence de pollution de la qualité de l'eau. L'article R36 présente les analyses de conception pour la charge sismique d'un barrage en enrochement à parement en béton bitumineux de 101 m de haut associé à un réservoir de pompage-turbinage situé dans le nord-ouest de la Chine. L'épaisseur du revêtement en asphalte est de 20,2 cm. L'analyse utilise un modèle d'éléments finis en 3D. Les détails de la modélisation et des hypothèses de conception sont fournis dans l'article. Les valeurs PGA du substratum rocheux de 1 sur 5 000 et 1 sur 10 000 AEP sur le site sont de 0,74 g et 0,90 g, respectivement. Les analyses démontrent que la conception peut répondre aux exigences de sécurité pendant les périodes de construction, de retenue et d'exploitation, ainsi que dans les conditions de travail en cas de tremblement de terre. Pendant la charge sismique, le coefficient de sécurité de la stabilité de la pente n'est inférieur à 1,0 que pendant de très courtes périodes et les déformations résultantes sont acceptablement faibles. Les contraintes de traction et de compression dans le parement en béton bitumineux et le bassin du réservoir répondent aux exigences de conception et il est conclu que le revêtement bitumineux peut retenir l'eau en toute sécurité. Le tassement post-séisme au niveau de la crête est d'environ 1 m et répond aux critères de performance du franc-bord.

Les barrages en sable et gravier cimentés (CSG) sont un type de barrage relativement nouveau qui a été développé au Japon. Ils sont construits en mélangeant une petite quantité de ciment avec du gravier et du sable non traités provenant du lit de rivières, de plaines alluviales ou de roches fragiles excavées. Il s'agit d'un type de construction économique qui présente des avantages environnementaux. Le barrage d'Apporo, un barrage CSG de 47,2 m de haut situé à au Japon, a été soumis à une accélération maximale d'environ 0,45 g mesurée dans la galerie d'inspection inférieure lors d'un tremblement de terre en 2018. Il n'a pas été endommagé, ce qui prouve la bonne performance sismique de ce type de barrage.

L'article R15 présente les résultats d'une étude sur les effets du module d'élasticité et des pentes en amont et en aval d'un barrage CSG hypothétique de 50 m de haut sur la performance sismique. Des analyses de la réponse sismique ont été entreprises avec différentes pentes en amont et en aval et avec différentes teneurs en ciment afin de déterminer la conception la plus économique. Des analyses numériques ont été utilisées avec un historique d'accélération d'entrée avec une accélération de pointe de 320 cm/s^2. Les détails des hypothèses et des résultats sont fournis dans l'article. Il a été conclu que le volume du barrage et la quantité totale de ciment utilisée peuvent être réduits tout en assurant la stabilité sismique du barrage en ajustant de manière flexible la pente et la disposition de la teneur en ciment unitaire. Il a été démontré que le volume du barrage pouvait être réduit de 10 % et que la quantité totale de ciment pouvait être réduite de 11 %.

L'article R2 présente un exemple de rehaussement d'un barrage de résidus existant dans la République de Macédoine du Nord par une construction en amont où le PGA SEE pour le site est de 0,36 g. L'article discute de l'évolution de la conception éclairée par l'application de méthodes de conception qui reconnaissent le potentiel de liquéfaction des résidus et la nécessité de prendre en compte à la fois les déformations qui peuvent survenir pendant et après le tremblement de terre de conception et la prise en compte du facteur de sécurité de la stabilité après le tremblement de terre. La conception a considérablement évolué par rapport au concept initial et a finalement inclus un contrefort de la digue de départ existante et un élargissement du remblai en amont. Les résistances maximales et liquéfiées des résidus ont été déterminées à partir de relations empiriques en utilisant les résultats des essais SPT et CPT effectués à deux endroits. La réponse dynamique a été modélisée en utilisant une méthode d'analyse linéaire équivalente (SIGMA/W, GeoStudio). Il existe aujourd'hui de bons conseils sur l'évaluation de la performance des sols liquéfiables et les effets sur les digues à stériles. Il s'agit notamment du Bulletin 194 de la CIGB "Tailings Dam Safety" [1] et d'une publication de l'USSD "Analysis of Seismic Deformations of Embankment Dams" [2].

Le document R44 résume la pratique chilienne en matière de conception de grandes digues à stériles dans un environnement fortement sismique. L'exploitation minière est une industrie importante au Chili. Par exemple, environ 25 % de la production mondiale de cuivre proviendra du Chili en 2023. D'importants volumes de résidus doivent être gérés et contenus dans des réservoirs formés par des barrages. Il s'agit souvent de très grands barrages (les plus grands mesurent plus de 200 m de haut). Le Chili se trouve dans une zone à haut risque sismique en raison de sa situation à la limite entre les plaques tectoniques de Nazca et d'Amérique du Sud. L'expérience et la pratique de la conception des digues à stériles au Chili sont intéressantes en raison du nombre élevé de grandes digues à stériles et du risque sismique élevé. Le document R44 résume la performance des digues à stériles soumises à de grands tremblements de terre au Chili, fournit des exemples de digues en aval et dans l'axe construites à partir de sables de stériles cycloniques qui ont résisté à des niveaux très élevés de mouvements du sol dus à

des tremblements de terre, et fournit un résumé des aspects clés qui sont pris en compte dans la conception des digues à stériles au Chili.

La rupture notable du barrage à résidus d'El Cobre en 1965 a conduit le gouvernement chilien à interdire les barrages à résidus en amont en 1970. Depuis lors, il y a eu d'autres ruptures de barrages construits en amont en raison de la liquéfaction des résidus provoquée par de forts mouvements de terrain dus à des tremblements de terre. Cependant, les barrages construits en aval ou selon la méthode de l'axe central se sont bien comportés lorsqu'ils ont été soumis à de forts mouvements de terrain. Les principaux aspects de la conception abordés dans l'article comprennent l'évaluation du risque sismique, les propriétés des résidus cycloniques utilisés dans la construction de nombreux barrages de résidus au Chili, le contrôle de la surface phréatique, les considérations relatives aux pressions de confinement élevées sur les propriétés géotechniques (compressibilité, perméabilité, résistance cyclique), le processus de conception, les analyses de stabilité (pseudo-statique, pseudo-dynamique, dynamique), et les critères de performance acceptables. Les analyses de stabilité pseudo-statiques pour évaluer la stabilité sismique sont une exigence légale au Chili, même s'il est bien connu que ces analyses ne sont pas considérées comme appropriées. Toutefois, d'autres méthodes de conception considérées comme conformes à l'état de la pratique sont utilisées. Il faut parfois du temps pour que les exigences légales soient modifiées afin de refléter les pratiques actuelles.

5.5.3. *Barrages à gravité en béton*

Le document R18 présente plusieurs aspects importants de la conception sismique des barrages en béton : (1) sélectionner les séismes de conception ; (2) définir les mouvements du sol de conception ; (3) calculer les contraintes et les déformations requises par l'analyse dynamique du système barrage-eau-fondation.

Le document R18 note que la durée de vie de nombreux projets de barrages est de 100 ans ; cependant, de nombreux barrages importants sont déjà en service depuis plus de 100 ans ou très près de 100 ans et resteront très probablement fonctionnels pendant encore de nombreuses années. Le document souligne que si l'on considère une durée de vie de 200 ans, pour une même probabilité de dépassement, le mouvement du sol sera plus intense.

Le document indique que le spectre de risque uniforme (UHS) n'est pas une cible appropriée pour sélectionner les mouvements du sol à utiliser dans l'analyse dynamique des barrages en béton. Il a été démontré qu'il était trop conservateur. Le spectre moyen conditionnel (CMS), qui surmonte les inconvénients du spectre de risque uniforme (UHS) dérivé de l'analyse probabiliste des risques sismiques (PSHA), peut être approprié comme spectre cible (TS) pour l'analyse dynamique des structures. La désagrégation des résultats d'un UHS peut également donner un

aperçu des scénarios de séismes qui devraient être pris en compte dans la sélection des mouvements du sol.

Le document R18 fournit également des commentaires sur certains facteurs essentiels à prendre en compte dans l'analyse sismique des barrages en béton. Si la masse de la roche de fondation est ignorée, les contraintes seront surestimées. Si la compressibilité de l'eau est ignorée ( ), il peut en résulter une sous-estimation ou une surestimation des contraintes induites par les tremblements de terre par rapport à l'hypothèse que l'eau est incompressible.

Le document R17 fait état de l'évaluation sismique des piliers des vannes de barrage. L'utilisation d'éléments de poutre pour modéliser les piliers des vannes de barrage peut être applicable pour certains barrages de faible hauteur. Dans l'évaluation du comportement de contact entre la pile de la vanne du barrage et la vanne du déversoir, la mise en place du ressort de fondation comme condition de contrainte à la base du modèle M-φ de la pile de la vanne du barrage permet une évaluation raisonnable, compte tenu des effets de la forme du déversoir et de la rigidité du corps du barrage.

L'article R52 concerne l'analyse sismique du barrage de Pine Flat, pour laquelle des méthodes numériques avancées ont été utilisées, qui simulent la propagation des ondes sismiques dans une fondation massive semi-unie, et la modélisation du comportement de fissuration du béton qui peut être modélisé par l'approche des fissures étalées ou par des fissures discrètes. Pour l'approche des fissures étalées, le modèle constitutif de la plasticité du béton endommagé (CDP) a été utilisé, et pour l'approche des fissures discrètes, la méthode des éléments finis étendue (XFEM) a été utilisée, qui permet aux fissures de se propager à travers les éléments finis (et pas seulement le long des bords de l'élément). Cette technique permet de simuler la trajectoire des fissures indépendamment du maillage des éléments finis.

Pour les analyses sismiques, l'analyse de l'évolution temporelle basée sur l'intégration directe des équations du mouvement a été utilisée. Il s'agit de la méthode la plus puissante pour évaluer la réponse des barrages aux tremblements de terre : elle peut être utilisée pour des analyses linéaires et non linéaires et elle peut prendre en compte de manière appropriée les interactions dynamiques du barrage avec le réservoir et la fondation. Les modèles de fissures étalées et discrètes sont disponibles dans le code FEM commercial ABAQUS.

Un modèle bidimensionnel du barrage-poids de Pine Flat avec le réservoir et la fondation a été analysé. Plusieurs analyses ont été effectuées pour des fondations sans masse et avec masse, en utilisant les modèles de fissures étalées et discrètes du béton de masse. Ces méthodes d'analyse sismique avancées sont encore en phase de recherche et de développement et doivent être utilisées avec beaucoup de précautions.

L'article R16 présente l'exemple d'un barrage-poids en béton de 16 m de haut, en service depuis plus de 100 ans. On considère que le barrage a développé des fissures horizontales dues à la détérioration des joints horizontaux. Un modèle FEM bidimensionnel est développé, modélisant les fissures horizontales continues comme des éléments de joint.

L'article R16 montre l'impact des fissures sur le comportement sismique du barrage et l'efficacité du renforcement par ancrage précontraint (PS). Le bloc supérieur a généré des accélérations extrêmement élevées lors de la séparation et de l'impact causés par le mouvement de basculement. L'introduction d'une contrainte de compression dans les fissures horizontales par des ancrages précontraints supprime efficacement la séparation en amont, ce qui entraîne un déplacement minimal des fissures.

Il existe très peu de données d'observation sur le comportement des grands barrages soumis à de très fortes secousses du sol semblables à celles attendues pour le tremblement de terre d'évaluation de la sécurité. Il existe deux options pour déterminer la sécurité sismique des barrages : premièrement, l'analyse dynamique des systèmes barrage-réservoir-fondation et deuxièmement, les essais sur table vibrante. Le document R31 traite des essais sur table de secousses d'un barrage-poids en béton armé d'une hauteur de 200 m. Les essais sur table de secousses sont les plus simples et les plus efficaces. Les essais sur table vibrante constituent l'approche la plus simple et la plus robuste pour étudier la performance des barrages en béton sous l'effet de fortes secousses sismiques. Un modèle tridimensionnel du barrage-poids, composé de 16 blocs, du déversoir de crête et de la prise d'eau, a été testé. Tous les blocs, y compris les joints de contraction, ont été modélisés. L'accélération horizontale maximale du sol du séisme d'évaluation de la sécurité (SEE) avec une période de retour de 10 000 ans était de 0,53 g. Les tests ont été effectués pour les trois composantes du séisme agissant simultanément. Il est important de noter que ce modèle de barrage-réservoir-fondation a été testé pour le SEE jusqu'à 4 fois le mouvement du sol du tremblement de terre de référence (PGA horizontal de 0,43 g pour une période de retour de 5000 ans), soit 1,72 g. L'amplification de l'accélération maximale dans la direction de la rivière, de la base à la crête des différents blocs, allait de 1,8 à 2,5, ce qui est plutôt faible par rapport aux valeurs obtenues à partir de l'analyse dynamique des barrages-poids, qui peuvent être de l'ordre de 5 en fonction de la valeur du PGA.

Presque tous les barrages à voûte élevée construits dans des zones sismiques actives en Chine ont été testés sur des tables vibrantes. Les vérifications de la sécurité sismique pour les mouvements du sol dépassant le mouvement du sol SEE sont très importantes et sont fortement recommandées à la fois pour les tests sur table vibrante et pour l'analyse dynamique, car s'il y a des changements futurs dans le mouvement du sol SEE, il ne sera pas nécessaire de procéder à une réévaluation de la sécurité sismique du barrage.

L'article R38 présente une étude expérimentale sur les propriétés de résistance dynamique du béton de masse du barrage de Bda, situé dans une région hautement sismique du Tibet en Chine. Les essais de béton comprennent des essais de résistance à la compression statique et dynamique, des essais de résistance à la traction par fendage et des essais de résistance à la traction par flexion qui fournissent les principaux paramètres pour l'analyse sismique et l'évaluation de la sécurité du barrage. Les essais ont été réalisés pour des taux de déformation quasi-statiques et trois taux de déformation dynamiques différents.

Les valeurs moyennes de résistance à la compression d'éprouvettes de béton cubique entièrement calibrées (longueur d'arête de 30 cm) pour des taux de déformation quasi-statiques et dynamiques de 5×10-4/s, $5{,}6\times10$-3/s et 2×10-2/s étaient respectivement de 31,1 MPa, 40,8 MPa, 41,1 MPa et 41,7 MPa. Le facteur dynamique maximal de la résistance à la compression est de 1,34. Pour les spécimens de béton entièrement calibrés, les matériaux réels utilisés dans le barrage de Bda ont été utilisés.

Les valeurs moyennes de la résistance dynamique à la traction par fendage d'éprouvettes de béton entièrement calibré pour des taux de déformation quasi-statiques et dynamiques de 10-4/s, $5{,}6\times10$-4/s et 2×10-3/s étaient respectivement de 2,25 MPa, 2,82 MPa, 2,92 MPa et 3,31 MPa. Le facteur dynamique maximal de la résistance à la traction par fendage est de 1,47.

Les valeurs moyennes de résistance à la traction par flexion d'échantillons de béton entièrement calibrés (échantillons de poutre avec une section transversale de 30x30 cm et une longueur de 120 cm) pour des taux de déformation quasi-statiques et dynamiques de 10-4/s, $5{,}6\times10$-4/s et 2×10-3/s étaient respectivement de 2,63 MPa, 3,29 MPa, 4,09 MPa et 3,43 MPa. Le facteur dynamique de la résistance à la flexion est de 1,56 pour une vitesse de déformation de 2×10-3/s.

Les résultats des essais confirment l'augmentation des propriétés de résistance du béton de masse avec l'augmentation des taux de déformation. Cependant, plutôt que d'effectuer des essais de traction par fendage et par flexion, qui surestiment la résistance à la traction, il serait plus approprié d'effectuer des essais de traction uniaxiale.

L'article R27 porte sur la conception sismique du barrage de Batang Toru en Indonésie, un barrage-poids courbe en béton compacté au rouleau (RCC). Le PGA pour une période de retour de 145 ans est de 0,402 g et pour une période de retour de 10 000 ans de 0,648 g selon la DSHA.

Avec des modèles d'éléments finis 3D du barrage et de la fondation, des analyses linéaires du spectre de réponse et des analyses non linéaires de l'évolution dans le temps sont effectuées pour évaluer le comportement et la sécurité du barrage dans des cas de charge sismique. Des renforts sont disposés

sur la face du barrage et certaines mesures défensives sont prises pour améliorer la performance parasismique du barrage de Batang Toru. Le document R27 présente des moyens d'améliorer la performance sismique des barrages en béton fondés sur des roches tendres et peut constituer une référence utile pour la conception sismique des barrages en béton dans les régions fortement sismiques.

5.5.4. *Barrages voûtes en béton*

L'article R6 compare les variations des réponses dynamiques d'un barrage-voûte soumis à des historiques d'accélération enregistrés à échelle linéaire (par rapport au PGA) et à correspondance spectrale pour trois zones de tremblement de terre en Suisse. Le barrage-voûte de 150 m de haut est situé dans une vallée étroite en forme de V. Le calcul comprend six séries de trois séries d'ondes de choc. Le calcul comprend six séries de mouvements du sol à trois composantes, chaque série étant composée de 11 enregistrements. L'accélération horizontale maximale à la crête et les contraintes de traction maximales dans le corps du barrage ont été utilisées pour la comparaison. Les réponses maximales moyennes du barrage étaient légèrement plus importantes pour les enregistrements à échelle linéaire que pour les enregistrements à spectre adapté. Le barrage modélisé était une structure élastique linéaire avec une fondation sans masse, une structure monolithique avec des surfaces de contact rigides et des charges hydrodynamiques telles que définies par la méthode Westergaard. Les auteurs notent qu'une évaluation plus précise de la performance dynamique des barrages voûtes en béton pourrait nécessiter la révision de ces hypothèses.

De nombreux barrages-voûtes existants ont été conçus avant 1990. Leur conception ne prend souvent en compte qu'un coefficient sismique fixe (pseudo-statique) sans évaluation des risques sismiques spécifiques au site. L'article R21 présente les analyses sismiques du barrage d'Enguri dans une région fortement sismique.

L'analyse sismique du barrage d'Enguri, l'un des plus hauts barrages-voûtes, qui doit être vérifié pour un tremblement de terre avec un PGA proche de 1,0 g, a révélé des contraintes de cisaillement élevées dans le béton. Les principales conclusions de l'analyse sismique sont les suivantes

- L'amplification de l'accélération de la base du barrage à la crête varie de 6 à 12,
- Le déplacement dynamique maximal de la crête vers l'aval peut atteindre le double du déplacement statique dû à la charge d'eau.
- Les contraintes maximales de compression statique et dynamique sont respectivement de 1,5 MPa et 5 MPa.
- Il semble difficile de déclencher des mécanismes de rupture dans la partie supérieure du barrage en raison du mouvement du sol de l'ESE. Le mécanisme de renversement d'un bloc détaché vers l'amont n'est pas possible.

Dans les grands barrages avec des crues de sécurité importantes, plusieurs ouvertures d'évacuation des crues peuvent être prévues dans le corps des barrages en béton, ce qui peut affaiblir le corps du barrage lors de forts tremblements de terre. L'article R35 traite de ce problème. Une comparaison de la réponse dynamique d'un grand barrage voûte avec et sans ouvertures d'évacuation des crues est effectuée. Des historiques d'accélération générés artificiellement ont été utilisés comme données d'entrée. Comme prévu, les contraintes dans la zone des orifices et du déversoir de crête varient le plus par rapport au cas d'un barrage monolithique. Le déplacement maximal de la crête augmente d'environ 8,5 % lorsque les effets de l'ouverture de la crue sont pris en compte. Si des ouvertures de crue importantes sont prévues, elles doivent être modélisées dans le modèle d'éléments finis du barrage ; cela s'applique en particulier au déversoir de crête.

Le document R40 porte sur la conception et la construction du barrage-voûte de Baihetan, d'une hauteur de 289 m, sur la rivière Jinsha, dans la province chinoise du Yunnan. Plusieurs technologies clés ont été utilisées pour la conception et la construction de ce grand projet de barrage. L'étude se concentre toutefois sur l'analyse sismique et les aspects de conception du barrage situé dans une vallée asymétrique. Les caractéristiques particulières de la conception comprennent le traitement du basalte jointoyé et la stabilité des coins potentiels le long des culées, qui sont importants pour la sécurité sismique du barrage. Le barrage est situé dans une région sismique. La valeur PGA horizontale du tremblement de terre de conception avec une période de retour de 5000 ans est de 0,45 g.

Pour l'analyse dynamique du barrage de Baihetan, un modèle d'éléments finis non linéaire tridimensionnel a été utilisé, dans lequel les joints de blocs et l'amortissement par rayonnement de la fondation infinie sont pris en compte. Des historiques d'accélération générés artificiellement ont été utilisés dans l'analyse dynamique. La fréquence propre la plus basse du barrage avec un réservoir plein est de 1,1 Hz. L'ouverture maximale des joints de blocs pour le séisme de conception est d'environ 40 mm. Sur la base des résultats de l'analyse dynamique non linéaire, il est conclu que de légers dommages sont possibles sur la face aval près de la culée gauche, tandis que la face amont reste intacte, ce qui est différent des autres grands barrages-voûtes, où les concentrations de contraintes se produisent le long de la face amont au niveau du contact barrage-fondation. Un renforcement sismique spécial a été prévu dans les piles du déversoir de crête, où les effets d'amplification dynamique sont les plus importants.

La capacité de surcharge sismique du barrage-voûte est d'environ 1,7 par rapport au PGA du tremblement de terre de conception. La vérification du facteur de surcharge sismique est essentielle et devrait être déterminée pour tous les grands barrages. C'est la réponse rationnelle aux demandes de réévaluation fréquente de la sécurité sismique des barrages, chaque fois que le risque sismique augmente en raison des mises à jour fréquentes de l'analyse du risque sismique requises par de nouveaux développements et de nouvelles données sur les tremblements de terre.

Le document R42 porte sur l'évaluation de la sécurité sismique du barrage-voûte de Yangfanggou, d'une hauteur de 155 m, situé sur la rivière Yalong en Chine. L'épaisseur du barrage à la crête et à la base est de 9 m et 32 m, respectivement. Le PGA horizontal du tremblement de terre d'évaluation de la sécurité avec une période de retour de 10 000 ans est de 0,386 g. Plutôt que les spectres de danger uniformes recommandés par la CIGB, des spectres de réponse aux tremblements de terre dits de scénario ont été utilisés ( ). Des historiques d'accélération générés artificiellement conformément au code sismique en vigueur en Chine ont été utilisés comme données d'entrée pour l'analyse dynamique du système barrage-réservoir-fondation. Dans l'analyse dynamique non linéaire, l'effet du rayonnement des vagues dans la fondation du barrage et l'ouverture des joints de blocs ont été pris en compte. En outre, la stabilité dynamique des cales des deux culées a été analysée pour le tremblement de terre de référence avec une période de récurrence de 5000 ans. Toutes les cales des culées restent stables sous ce tremblement de terre.

L'ouverture dynamique maximale des joints de blocs pendant le tremblement de terre de référence avec un PGA horizontal de 0,309 g est de 8,7 mm, ce qui se situe dans la plage admissible des déformations des waterstops. Il s'agit d'un critère de performance spécial indiqué dans le code chinois. Selon la CIGB, l'endommagement des waterstops serait acceptable dans le cadre de l'évaluation de la sécurité en cas de tremblement de terre (SEE), si la pression de l'eau dans les joints des blocs n'affecte pas la stabilité du barrage. Si un barrage est endommagé lors d'un fort tremblement de terre, il se peut que le réservoir doive être abaissé, en fonction du type de dommage. La réparation des waterstops endommagés serait un problème dans les barrages en béton ; il est donc avantageux que les waterstops puissent résister aux déformations sismiques.

5.5.5. *Structures annexes*

Les structures annexes sont critiques pour la sécurité si leur fonction est de retenir l'eau et de gérer l'entrée ou la sortie d'un réservoir après un fort tremblement de terre. Les structures qui supportent des équipements électromécaniques et hydromécaniques essentiels à la sécurité doivent fonctionner de manière à ce que tout équipement essentiel à la sécurité qui y est rattaché soit encore opérationnel après l'ESE.

L'article R17 porte sur l'évaluation sismique des piliers des vannes de barrage. L'utilisation d'éléments de poutre pour modéliser les piliers des vannes de barrage peut être applicable pour certains barrages de faible hauteur, comme présenté dans l'article. Dans l'évaluation du comportement de contact entre la pile de la vanne du barrage et la vanne du déversoir, la mise en place du ressort de fondation comme condition de contrainte à la base du modèle M-φ de la pile de la

vanne du barrage permet une évaluation raisonnable, en tenant compte des effets de la forme du déversoir et de la rigidité du corps du barrage.

5.6. Évaluation de la sécurité sismique de tous les types de barrages et d'éléments critiques pour la sécurité (par exemple, déversoir, sorties à faible niveau)

5.6.1. *Général*

L'évaluation de la sécurité des barrages existants et des éléments critiques associés est importante pour garantir aux propriétaires de barrages et aux parties prenantes que les barrages sont maintenus dans un état de sécurité tel que les risques associés à une défaillance potentielle sont à un niveau acceptable. Plusieurs documents associés à ce thème ont été soumis. L'un d'entre eux concernait l'évaluation de la sécurité d'un portefeuille de barrages en Italie (R51). D'autres étaient associés à des types de barrages ou à des barrages spécifiques.

5.6.2. *Portefeuilles de barrages*

La norme technique italienne pour la conception et la construction des barrages a été mise à jour en 2014, remplaçant la précédente datant de 1982. Le document R51 présente les résultats de l'évaluation sismique de 53 barrages de différents types (enrochement de parement en béton, enrochement de noyau central, enrochement de parement bitumineux, enrochement de parement en béton, gravité en béton, maçonnerie de pierre et voûtes multiples). Les barrages sont situés dans toute l'Italie. L'évaluation a été entreprise conformément à la norme technique de 2014 et aux lignes directrices sismiques connexes publiées en 2019. Le document présente la méthodologie suivie pour évaluer leur sécurité sismique et les charges sismiques de conception et les exigences de performance stipulées par la norme technique italienne. Cette norme exige la prise en compte de la performance dans deux états limites d'aptitude au service (OLS - Operational Limit State, et DLS - Damage Limit State) et deux états limites ultimes ULS (LLS - Life-Safety Limit State, et CLS - Collapse Limit State).

Le document R51 explique l'approche adoptée. Une approche par étapes a été développée. Les étapes fondamentales ont été l'identification du type de barrage, l'étude du barrage, l'acquisition d'informations historiques et d'archives, la caractérisation des matériaux, y compris des investigations supplémentaires, les charges sismiques de conception à partir des cartes italiennes des risques sismiques ou des études et analyses probabilistes des risques sismiques spécifiques au site. Une approche pseudo-statique a été utilisée pour évaluer la performance de la

plupart des barrages. Des analyses plus complexes ont été adoptées pour certains barrages. Il s'agit d'analyses dynamiques non linéaires pour quatre digues et de l'introduction de joints de levage non linéaires et d'analyses de stabilité post-sismique pour trois barrages en béton.

L'étude a conclu que, bien que la conception de la plupart des barrages n'ait pas tenu compte à l'origine des charges sismiques et d'un certain vieillissement naturel des matériaux, la plupart des barrages évalués sont conformes aux normes nationales et présentent généralement un comportement satisfaisant dans des conditions sismiques.

5.6.3. *Barrages en remblai*

Le document R8 fournit une comparaison des méthodologies considérées pour l'évaluation de la sécurité des barrages en cas de tremblement de terre de cinq grands barrages en remblai, situés dans différents pays (Philippines, Mexique, Suisse, Arménie et Colombie). La comparaison se concentre sur la détermination des charges sismiques et souligne l'importance des directives nationales pour parvenir à une cohérence en ce qui concerne le niveau de sécurité. Elle étudie également les méthodes d'analyse utilisées (méthode pseudo-statique, analyses de déformation simplifiées, analyses de blocs coulissants, analyses de déformation non linéaires, analyses de stabilité post-séisme) et les critères de performance appliqués. Chaque méthode est évaluée en termes d'avantages, de limites et d'inconvénients en ce qui concerne la précision et la fiabilité des résultats des analyses. En outre, les exigences en matière de budget, de temps et de ressources informatiques sont discutées. Les raisons pour lesquelles les méthodes d'analyse développées dans les années 1960 sont encore attrayantes par rapport aux analyses non linéaires sophistiquées sont expliquées.

Le document conclut que la méthode la plus couramment appliquée pour calculer la réponse sismique des grands barrages en remblai à noyau de terre est encore la méthode linéaire équivalente et que l'analyse dynamique non linéaire sophistiquée est rarement utilisée. Les méthodes simplifiées sont encore largement utilisées, mais il est signalé qu'il est très important d'évaluer si la méthode choisie est appropriée et dans les limites de l'applicabilité. Le document indique également qu'il semble généralement admis que la méthode d'analyse pseudo-statique est dépassée, du moins pour les barrages en remblai.

L'article R19 présente les résultats de l'application d'un processus permettant d'incorporer des incertitudes aléatoires et épistémiques dans une évaluation de la fragilité sismique (probabilité de défaillance) du talus gauche du barrage de Wanapum. Le processus comprenait l'adaptation et la mise en œuvre d'un processus recommandé par le Senior Seismic Hazard Analysis Committee (SSHAC) pour la Nuclear Regulatory Commission. Le barrage de Wanapum fait partie du

projet hydroélectrique de Priest Rapids situé sur le fleuve Columbia (État de Washington, États-Unis). L'étude présentée dans ce document fait partie de l'approche fondée sur les risques adoptée par les propriétaires du barrage (Grant County Public Utility District) pour l'évaluation de la sécurité sismique de la digue gauche.

Le processus SSHAC fournit une structure pour faire une évaluation détaillée des sources d'incertitude aléatoire et épistémique dans la caractérisation du remblai. Les sources d'incertitude épistémique qui ont été identifiées ont été incorporées dans un format d'arbre logique qui fournit la structure pour l'estimation de l'incertitude dans la fragilité sismique. Les deux principaux types d'incertitude épistémique qui ont été pris en compte dans le cas du barrage de Wanapum étaient l'incertitude dans l'estimation des déformations sismiques du remblai en réponse aux mouvements du sol dus aux tremblements de terre et l'incertitude dans la modélisation de la progression des déformations du remblai (dommages) jusqu'à la défaillance pour les modes de défaillance individuels. La variabilité de la charge sismique (historique des tremblements de terre pour une même magnitude et un même niveau de mouvement du sol) contribue de manière substantielle à l'incertitude aléatoire dans les déformations estimées du remblai. Le processus a permis d'estimer l'impact global des incertitudes dans les caractéristiques du remblai et la charge sismique sur l'estimation des déformations du remblai et le potentiel de libération incontrôlée de l'eau.

Le document R19 fournit un exemple de l'état de la pratique pour l'évaluation de la probabilité de rupture d'un remblai existant. Les résultats révèlent une incertitude considérable dans l'estimation de la fragilité sismique du talus de gauche. Le processus SSHAC est rigoureux et les résultats fournissent une bonne base pour décider si les risques sont acceptables ou si des mesures sont nécessaires pour les atténuer.

5.6.4. *Gravité du béton*

L'article R9 présente les résultats d'une étude visant à évaluer la vulnérabilité sismique des barrages en béton, avec un accent particulier sur le mode de défaillance critique du glissement de la base. Un modèle 2D couplé barrage-fondation-réservoir (DFR) prenant en compte la non-linéarité des matériaux et des contacts a été utilisé pour mieux comprendre les interactions entre le barrage, la fondation et le réservoir. Le choix de l'interaction de contact (liée ou cohésive), l'incorporation du soulèvement et les variations des mouvements du sol à l'intérieur et entre les périodes de retour influencent de manière significative la réponse du système, introduisant des variations dans la réponse du barrage qui ont un impact sur l'évaluation de la vulnérabilité sismique du barrage. Les principales conclusions et implications qui ressortent de l'étude sont énumérées ci-dessous.

1. Les modèles liés surestiment généralement les probabilités de rupture par rapport aux modèles avec interaction cohésive à l'interface de la fondation du barrage. Cette surestimation est particulièrement prononcée pour la fragilité basée sur le déplacement de la crête (NCD). Les modèles liés présentent une estimation plus conservatrice de la probabilité de défaillance. Cette différence souligne l'importance d'une modélisation précise de l'interface barrage-fondation afin d'éviter des évaluations de sécurité trop conservatrices.
2. L'incorporation du soulèvement affecte le résultat de l'analyse de manière significative en influençant la fragilité de la base basée sur le glissement (NBD). La probabilité de défaillance augmente sensiblement lorsque le soulèvement est pris en compte, ce qui met en évidence le rôle critique des forces de soulèvement dans la stabilité sismique des barrages. Cette constatation souligne la nécessité d'inclure le soulèvement dans les évaluations sismiques globales.
3. L'utilisation de plusieurs indices de dommages (NBD et NCD) dans les évaluations de fragilité offre une compréhension plus détaillée et plus nuancée de la performance sismique du barrage. Cette approche permet une meilleure évaluation des différents modes de défaillance et des risques associés, offrant ainsi une vision holistique des vulnérabilités potentielles.
4. La prise en compte de périodes de retour multiples (475, 975, 2475, 5000 et 10 000 ans) et d'une gamme de mouvements du sol permet de tenir compte de la variabilité d'un record à l'autre (RTR). Cette approche globale garantit que l'analyse capture les variations de la demande sismique à travers différents scénarios, offrant ainsi un cadre d'évaluation probabiliste robuste.
5. Cette recherche aborde certaines des limites des études précédentes en incorporant des conditions limites non réfléchissantes et un cadre d'évaluation probabiliste.

L'article R11 présente l'approche originale visant à optimiser les paramètres de résistance au cisaillement des joints de barrage et les analyses de stabilité sismique correspondantes des monolithes de l'Isle-Maligne. Il souligne l'importance d'une définition correcte des paramètres de cisaillement, de l'enquête sur le terrain et de l'impact des travaux de réhabilitation des vieux barrages.

Les paramètres sismiques ont été dérivés d'une étude probabiliste des risques sismiques spécifique au site, les accélérations spectrales sur la roche pour le site de l'Isle-Maligne pour la période de retour de 5 000 ans étaient supérieures à 0,9 g pour la composante horizontale, pour un amortissement de 5 %.

La stabilité sismique des anciens barrages a été vérifiée par la méthode de la gravité et les analyses dynamiques temporelles des corps rigides, avec la méthode des blocs de glissement de Newmark, les déplacements résiduels de glissement ont été obtenus.

Le document R30 porte sur l'évaluation rapide de la sécurité des grands barrages après un tremblement de terre :

- La détermination rapide de l'apport sismique sur le site du barrage ;
- Le calcul rapide de la réponse sismique de la structure du barrage ;
- L'évaluation de la sécurité sismique globale de la structure du barrage, afin de déterminer les actions à entreprendre, telles que l'abaissement du réservoir et les mesures d'urgence. La vitesse est un facteur crucial dans l'évaluation de la sécurité d'un barrage après un tremblement de terre.

Les méthodes et les étapes de l'évaluation rapide de la sécurité sismique d'un barrage en béton après un tremblement de terre sont présentées. La procédure d'évaluation rapide de la sécurité proposée dans le rapport est applicable dans le cas où il n'existe pas d'évaluation actualisée de la sécurité sismique d'un grand projet de barrage. Il faut espérer que cela soit l'exception, car l'un des objectifs fondamentaux à long terme est que tous les barrages satisfassent aux critères actuels de sécurité sismique spécifiés par la CIGB. Si ce n'est pas le cas, les propriétaires de barrages et les autorités chargées de la sécurité des barrages veillent à ce que de telles évaluations de la sécurité sismique existent. Il convient de souligner que les évaluations de la sécurité sismique font partie des plans d'urgence, qui sont plus complets que les analyses de l'onde de crue en cas de rupture de barrage et/ou les plans d'action d'urgence.

Un aspect important est la vérification de la sécurité sismique des barrages en béton pour les facteurs de surcharge sismique. Les rapports sur les très grands barrages en béton, préparés par les ingénieurs chinois, montrent que les réserves sismiques des barrages doivent être vérifiées. Ces réserves sont caractérisées par des facteurs de surcharge. Il s'agit d'un excellent concept, qui devrait également être appliqué aux grands barrages dans tous les autres pays, car ce concept protégerait les propriétaires de barrages contre les demandes fréquentes de réévaluation de la sécurité sismique de leurs barrages (R.31, R.40).

L'article R39 porte sur l'analyse de la fragilité sismique des barrages-poids à l'aide de la méthode d'analyse des bandes multiples (MSA), une méthode peu connue pour l'évaluation de la sécurité sismique des barrages. Les courbes de fragilité ont été principalement utilisées dans l'évaluation probabiliste de la sécurité sismique des composants des centrales nucléaires. L'évaluation de la sécurité des barrages basée sur les courbes de fragilité est fondamentalement un concept dépassé et ne devrait être utilisée que comme méthode de sélection des barrages-poids, où les blocs de béton ont une forme similaire. Pour l'analyse détaillée de la sécurité des grands barrages-poids, ces méthodes ne doivent pas être utilisées car les modes de défaillance sismique, la défaillance des barrages, les dommages causés par les tremblements de terre ou la vulnérabilité sismique des barrages sont des termes difficiles à quantifier. La défaillance et l'endommagement d'un barrage étant liés à sa vulnérabilité sismique et cette dernière

dépendant principalement du nombre de cycles de charge pertinents, c'est-à-dire de la durée des fortes secousses du sol, qui est un paramètre clé, ces méthodes ne doivent pas être utilisées pour l'analyse détaillée de la sécurité des grands barrages-poids.

Dans l'article R39, une analyse dynamique non linéaire d'un bloc de béton de 144 m de haut d'un barrage-poids est analysée, en tenant compte du modèle constitutif de plasticité de l'endommagement du béton pour le béton de masse. Douze tremblements de terre sont analysés et les dommages causés par le tremblement de terre au bloc de béton sont quantifiés sur la base du déplacement de la crête sismique. La classification des dommages en différentes catégories, de l'absence de dommages à la rupture, est plutôt subjective. Les courbes de fragilité sont présentées pour chaque catégorie de dommages en fonction du PGA.

Il est évident que la caractérisation du mouvement du sol du tremblement de terre par le PGA est beaucoup trop simpliste. Dans cet article, les dommages sont caractérisés par le déplacement de la crête. Les auteurs mentionnent que d'autres indices de dommages devraient également être pris en compte. Il n'en reste pas moins que les dommages et le mouvement du sol ne peuvent pas être représentés par un seul paramètre. En outre, les observations des tremblements de terre et les essais sur table de secousses des barrages en béton montrent que les dommages sont de nature discrète et ne peuvent pas être représentés par des modèles de dommages plastiques.

5.6.5. *Levées*

Le document R20 présente l'approche utilisée par les principales compagnies hydroélectriques françaises (EDF et CNR) pour évaluer la sécurité sismique des digues associées à leurs projets de production d'énergie. Les digues ont une longueur de plusieurs centaines de kilomètres. L'évaluation de la sécurité des grands barrages basée sur l'évaluation de la stabilité est obligatoire en France depuis 2018 en vertu d'un décret ministériel. Il est difficile d'entreprendre une évaluation significative de la stabilité sur toute la longueur des digues. La manière de démontrer la stabilité sismique ou les méthodes de calcul sont définies dans les recommandations françaises publiées par la profession française. Une approche graduelle est recommandée. Elle consiste à augmenter le niveau de complexité des études par étape lorsque l'étape précédente ne justifie pas les travaux étudiés. Ce type d'approche a été adopté par la CNR pour les deux risques principaux que sont la liquéfaction et le cisaillement dynamique. EDF a développé une méthode dynamique transitoire simplifiée pour le risque de cisaillement dynamique. Elle exclut les problèmes de liquéfaction. Le document décrit le développement et l'application des méthodes. CNR indique que presque tous ses remblais ne sont pas sensibles à la liquéfaction en raison de dispositions de construction favorables (nature et compactage des remblais) et de la présence de matériaux qui ne sont pas ou peu sensibles à la liquéfaction. L'approche graduelle pour l'évaluation de la stabilité

dynamique au cisaillement implique d'abord l'utilisation de la méthode pseudo-statique, puis de la méthode pseudo-dynamique (approche par blocs coulissants de Newmark). EDF a développé une gradation supplémentaire dans les analyses de la stabilité au cisaillement dynamique (analyse dynamique transitoire simplifiée). L'application de ces méthodes à ses digues a généralement démontré la conformité avec les exigences réglementaires.

6. REMARQUES FINALES

La sécurité sismique des barrages est importante car les tremblements de terre peuvent avoir des effets catastrophiques sur les personnes, les biens, les infrastructures, les sites historiques et culturels et l'environnement en cas de défaillance. Pour éviter une libération incontrôlée de l'eau, un barrage doit pouvoir résister aux risques sismiques, y compris les secousses du sol, associés à un tremblement de terre extrême, que l'on appelle le séisme d'évaluation de la sécurité (SEE).

Le sujet de la sécurité sismique des barrages et des digues continue d'évoluer. La prise de conscience de l'importance de la sécurité sismique et la base de connaissances techniques se sont considérablement développées depuis la question 83 en 2003.

Les recommandations suivantes sont formulées pour l'avenir :

1. Les grands barrages doivent être équipés d'enregistreurs de mouvements puissants (champ libre, base, milieu de la crête et culées) pour mesurer les accélérations. La surveillance des déformations est également importante. Les mesures de la réponse pendant les tremblements de terre permettent de calibrer les estimations de l'aléa sismique (secousses du sol) ainsi que les modèles qui prédisent la réponse du barrage aux tremblements de terre. Ces informations peuvent également enrichir l'ensemble des connaissances relatives à tous les barrages.
2. La surveillance et l'observation du comportement des barrages et des équipements essentiels à la sécurité pendant les tremblements de terre doivent se poursuivre et être soigneusement interprétées. Les observations doivent être partagées afin que toutes les parties prenantes puissent en bénéficier. Les personnes responsables de la sécurité des barrages doivent étudier les enseignements tirés et les appliquer à leur travail.
3. Les risques sismiques présentent de multiples caractéristiques (secousses du sol, mouvements des failles superficielles, mouvements de masse, ondes dans les réservoirs, etc.)). Elles doivent toutes être prises en compte.
4. La sécurité sismique des barrages doit faire l'objet d'un examen régulier en raison de l'évolution de la compréhension des risques sismiques, des

changements dans les risques associés à la défaillance potentielle d'un barrage ( ), de la détérioration du barrage, de la compréhension des modes de défaillance potentiels et des mesures disponibles pour atténuer les risques.

5. Les propriétés dynamiques et les modèles constitutifs des matériaux et des fondations des barrages continuent d'évoluer, et des progrès ont été réalisés dans la modélisation numérique des caractéristiques de contrainte et de déformation des matériaux et dans l'estimation de la déformation des barrages lorsqu'ils sont soumis à des mouvements de terrain dus à des tremblements de terre. Cependant, les analyses numériques comportent encore des incertitudes significatives. Des études de sensibilité sont toujours recommandées pour comprendre les effets des différentes hypothèses et pour prendre en compte correctement l'incertitude

7. ABRÉVIATIONS

Les abréviations suivantes sont utilisées dans le rapport général et dans certains documents associés à Q.111 :

CFRD : Barrage en enrochement à parement de béton

CMD : Barrage en matériau cimenté

CSG : Gravier sableux cimenté

DBE : Séisme de référence

MCE : Séisme maximal crédible (terme utilisé dans l'analyse déterministe des risques sismiques des barrages à hautes conséquences).

OBE : Séisme de référence (terme utilisé dans l'analyse probabiliste de l'aléa sismique des barrages)

PGA : Accélération maximale du sol

RCC : Béton compacté au rouleau

RFC : Béton enroché

RTS : Sismicité déclenchée par le réservoir (dans le passé, le terme sismicité induite par le réservoir était utilisé pour décrire les tremblements de terre déclenchés par le réservoir, mais le terme correct utilisé aujourd'hui est RTS).